UNIVERSIDAD COMPLUTENSE DE MADRID

FACULTAD DE CIENCIAS GEOLÓGICAS

TESIS DOCTORAL

Las plataformas carbonatadas y sistemas deltaicos del Aptiense-Albiense inferior del noroeste de Cantabria: registro de cambios paleoambientales y eventos anóxicos

MEMORIA PARA OPTAR AL GRADO DE DOCTORA

PRESENTADA POR

María Najarro de la Parra

Directores

Idoia Rosales Franco
Jesús García Senz
Javier Martín Chivelet

Madrid, 2016

INSTITUTO GEOLÓGICO Y MINERO DE ESPAÑA-FACULTAD DE CIENCIAS GEOLÓGICAS. UNIVERSIDAD COMPLUTENSE DE MADRID

LAS PLATAFORMAS CARBONATADAS Y SISTEMAS DELTAICOS DEL APTIENSE-ALBIENSE INFERIOR DEL NOROESTE DE CANTABRIA: REGISTRO DE CAMBIOS PALEOAMBIENTALES Y EVENTOS ANÓXICOS

TESIS DOCTORAL

Mayo, 2015

MARÍA NAJARRO DE LA PARRA

INSTITUTO GEOLÓGICO Y MINERO DE ESPAÑA-FACULTAD DE CIENCIAS GEOLÓGICAS. UNIVERSIDAD COMPLUTENSE DE MADRID

LAS PLATAFORMAS CARBONATADAS Y SISTEMAS DELTAICOS DEL APTIENSE-ALBIENSE INFERIOR DEL NOROESTE DE CANTABRIA: REGISTRO DE CAMBIOS PALEOAMBIENTALES Y EVENTOS ANÓXICOS

TESIS DOCTORAL

Mayo, 2015

MARÍA NAJARRO DE LA PARRA

LAS PLATAFORMAS CARBONATADAS Y SISTEMAS DELTAICOS DEL APTIENSE-ALBIENSE INFERIOR DEL NOROESTE DE CANTABRIA: REGISTRO DE CAMBIOS PALEOAMBIENTALES Y EVENTOS ANÓXICOS

TESIS DOCTORAL

MARÍA NAJARRO DE LA PARRA

Memoria presentada para optar al grado de Doctora en Geología

Mayo, 2015

Esta Tesis Doctoral ha sido dirigida por los doctores Idoia Rosales Franco, Investigadora Titular del Área de Recursos y Geología Marina del Instituto Geológico y Minero de España; Jesús García Senz, Investigador Titular del Área de Geología, Geomorfología y Cartografía Geológica del Instituto Geológico y Minero de España; y Javier Martín Chivelet, Catedrático del Departamento de Estratigrafía de la Facultad de Ciencias Geológicas, Universidad Complutense de Madrid.

VºBº VºB VºBº

Fdo.: Idoia Rosales Franco Fdo.: Jesús García Senz Fdo.: Javier Martín Chivelet

A mis padres

AGRADECIMIENTOS

Me gustaría dedicar estas primeras líneas a todas aquellas personas que de una u otra forma han contribuido en la realización de esta memoria.

En primer lugar mi más sincero y profundo agradecimiento a la directora principal de esta Tesis, la Dra. Idoia Rosales. Millones de gracias por haberme guiado, enseñado ayudado, apoyado y contagiado tu motivación y amor por la geología. Haber disfrutado de tu compañía y entusiasmo en tantísimas campañas de campo ha sido realmente un lujo. Para mí ha sido un placer compartir todos estos años contigo tanto en el ámbito profesional como en el personal. Gracias de todo corazón.

También he tenido la fortuna de contar con otros dos directores excepcionales: El Dr. Jesus García Senz y el Dr. Javier Martín Chivelet. Jesu, muchas gracias por compartir todos tus conocimientos sobre la estructura regional de Cantabria, que sin duda han sido imprescindibles a la hora de realizar el capítulo de tectónica. A los dos, muchas gracias por vuestro tiempo, apoyo, y por todas vuestras aportaciones y sugerencias durante la corrección final del manuscrito.

Al Instituto Geológico y Minero de España (IGME) le agradezco la concesión de una beca Doctoral desde el año 2006 al 2010 y todas las ayudas para asistir a reuniones científicas y congresos.

Quisiera agradecer al convenio de colaboración entre el IGME, la Consejería de Cultura, Turismo y Deporte del Gobierno de Cantabria y la empresa SIEC S.A. (2008–2012) la dotación económica del proyecto "Investigación Científica y Técnica de la Cueva de El Soplao y su entorno Geológico", así como al Ministerio de Ciencia e Innovación por la dotación económica al proyecto "Variaciones seculares geoquímicas e isotópicas en facies carbonatadas marinas del Carbonífero, Jurásico y Cretácico en la Península Ibérica: Aplicación a la interpretación de crisis paleoclimáticas".

Agradezco especialmente al gran grupo científico multidisciplinar con el que he tenido el privilegio de trabajar y que sin él la elaboración de los artículos científicos hubiese sido inviable. Gracias a los Drs: Josep Anton Moreno-Bedmar, Miquel Company, Gines de Gea, José Manuel Castro, María Luisa Quijano, Richard Pancost, Cesar Menor-Salván, Fernando Tornos, Francisco Velasco, Felix Schlagintweit, Eduardo Barrón, Enrique Peñalver y a todo el grupo de Xavier Delclòs.

Me gustaría agradecer también toda la ayuda y apoyo a Fabio López y Manolo Montes, (con los que comencé en el IGME), Paqui y Rafael Martínez

A Antonio Barnolas, por haber sido el mejor de los jefes.

Mi más sentido agradecimiento a Antonio Bartolomé por la preparación de tantísimas láminas delgadas.

Asimismo, doy las gracias al Dr. Clemente Recio del Servicio General de Isótopos Estables de la Universidad de Salamanca quien realizó los análisis isotópicos de O y C.

Quisiera dedicar también un espacio en este apartado a mis directores de DEA los Drs. José Arribas, Ramón Mas y José Fernández Barrenechea, con los que empecé en esto de la investigación y aprendí tantísimo.

A mis colegas del IGME, que empezaron siendo compañeros de trabajo y han terminado siendo grandísimos amigos. Gracias a Javi, Laura, Mai, José, Fer, Raquel, Carmen, Nacho, Ricardo, Manu, Sara, Enrique, Gloria, Eva, Icíar, Rafa, Javi Cuarcis, Geles, Pilar, Irene, Ana, Juan Carlos, Paz, Laura S…Muchas gracias a todos por esos momentazos vividos en la sala de becarios y fuera de ella.

A mis compañeros de facultad, por todos sus ánimos e inyecciones de moral y por estar siempre que les he necesitado. Gracias a Fanny, María, Vane, Hugo, Paquito, Junma, Ruthy y Miguelón.

A mis amigas, que son mi gran tesoro: Ana, Chelo, Ali, Carmen, Gema, Ceci, Cris, María, Elena y Gaby. Y a mis amigas Adriana y Helena que, a pesar de estar lejos, siempre las siento tan cerca.

A Celia, Sandra, Riqui, Nacho, Lía, Dani y Laura (otra vez), mil gracias por vuestra amistad incondicional.

A mis amigos de Colmenar, por animarme y ayudarme siempre que os he necesitado. Sin duda lo mejor de mudarme a la aldea…

Quisiera agradecer también de manera especial a Jorge todo su apoyo, ayuda y compañía.

Y por último, me gustaría dar las gracias con todo mi corazón y dedicar esta memoria a mi GRAN FAMILIA (incluidos mis dos pequeñajos!) por ser mi luz, mi bastón y mi guía.

ÍNDICE

RESUMEN

LAS PLATAFORMAS CARBONATADAS Y SISTEMAS DELTAICOS DEL APTIENSE-ALBIENSE INFERIOR DEL NOROESTE DE CANTABRIA: REGISTRO DE CAMBIOS PALEOAMBIENTALES Y EVENTOS ANÓXICOS

INTRODUCCIÓN

En este trabajo se estudian los materiales del Aptiense-Albiense Inferior del sector occidental de la cuenca (sub-cuenca) Nor-Cantábrica (borde nor-occidental de la cuenca Vasco-Cantábrica), con especial énfasis en el estudio del reflejo sedimentario de los cambios paleoclimáticos acontecidos durante el intervalo de tiempo estudiado. El enfoque multidisciplinar de esta tesis, abarcando estudios estratigráficos, sedimentológicos, bioestratigráficos, paleontológicos, quimioestratigráficos, paleogeográficos y paleotectónicos, ha permitido abordar un análisis integral tanto del reflejo sedimentario que pudieron tener los cambios paleoclimáticos globales en los ambientes someros de plataforma carbonatada y terrígena, como del papel que tuvieron los factores globales, regionales y locales en el control de la sedimentación y del relevo de plataformas carbonatadas y sistemas deltaicos. Las perturbaciones ambientales y climáticas globales acaecidas durante el intervalo de estudio son: el calentamiento global relacionado con el Evento Anóxico Oceánico del Aptiense Inferior (OAE 1a), el interludio frío o *cold-snap* del Aptiense Superior, y el calentamiento global relacionado con el Evento Anóxico Oceánico del Albiense Inferior (OAE 1b).

OBJETIVOS

Los principales objetivos de esta Tesis son:

1) Mejorar el esquema estratigráfico y bioestratigráfico del área de estudio.
2) Caracterizar las facies sedimentarias, microfacies, ambientes deposicionales, e identificar los cambios paleoambientales en el espacio y en el tiempo.
3) Reconocer las discontinuidades estratigráficas y los patrones arquitecturales en la estratigrafía de las facies, con el fin de definir las secuencias deposicionales y sus límites.

4) Reconstruir la estructura extensiva de la cuenca Nor-Cantábrica durante el Cretácico Inferior, mediante correlación de columnas estratigráficas, análisis de facies y espesores, cortes geológicos y modelos de tectónica extensiva.
5) Identificar y caracterizar la repercusión de la crisis paleoclimática y paleoceonográfica del Aptiense Inferior, conocida como el Evento Anóxico Oceánico del Aptiense Inferior (OAE 1a) o Evento *Selli*, en la zona de estudio.
6) Prospectar y caracterizar los depósitos ambarígenos del Albiense Inferior del área de estudio, con el fin de definir el contexto paleogeográfico, sedimentario y paleoambiental de este tipo de depósitos y predecir su posible localización.

RESULTADOS

En conjunto se han estudiado 17 afloramientos y levantado un total de 15 secciones estratigráficas a escala métrica y decimétrica, que suman más de 3100 m de serie estratigráfica. Esto ha permitido diferenciar tres sectores sedimentarios (La Florida, sinclinal de Santillana y Cuchía) y 9 unidades litoestratigráficas, definiéndose una nueva unidad litoestratigráfica de carácter formal (Formación Rábago) para las áreas de La Florida y del sinclinal de Santillana. Las unidades litoestratigráficas han sido datadas con mayor precisión que la existente, a partir de biozonas de ammonites, de foraminíferos planctónicos y bentónicos y de nanofósiles calcáreos y con palinomorfos. Esto, junto con las correlaciones estratigráficas, ha permitido reconocer lagunas estratigráficas durante el Bedouliensey Gargasiense inferior en el área de La Florida y durante el Aptiense basal y el Albiense Inferior–Medio en el área de Cuchía.

El estilo estructural de la cuenca varía de una tectónica de basamento en el margen del *rift* cantábrico (Banda del Nansa) con una vergencia hacia el sur de las unidades cabalgantes, a un estilo de cobertera, desvinculada del basamento por el horizonte dúctil del Keuper, en el centro del graben (Bloque Costero de Santander). El análisis de cambios de espesores y facies ha permitido establecer para el sector occidental de la cuenca Nor-Cantábrica, la actuación de seis fallas principales con actividad sinsedimentaria, oblicuas a los márgenes de la cuenca: la falla N017 de Bustriguado, la falla E-O de Santibáñez y las fallas N060 de Peña Castillo, Santa Ana,

Torrelavega-Usgo y Rubárcena. Según su disposición en planta, para el Bloque Costero de Santander estas fallas se han agrupado en dos áreas genéticas que individualizan dos sub-cuencas: área de Treceño y área de Santander. Éstas se encuentran limitadas por una zona de acomodación (área de Reocín), siendo este tipo de disposición característico de un *rift* oblicuo con eje asimétrico, cuya dirección de extensión más propicia es N330, aunque existe un rango de variación compatible de unos 45º hacia el norte.

El registro sedimentario muestra la siguiente evolución de ambientes sedimentarios: 1) plataforma mixta terrígeno-carbonatada, de edad Bedouliense inferior (parte baja de la Zona *D. oglanlensis*, parte baja del Aptiense Inferior, Fm. Rábago); 2) calcarenitas de alta energía de rampa interna a media, de edad Bedouliense inferior (parte alta de la Zona *D. oglanlensis*, Aptiense Inferior, Fm. Umbrera); 3) sistema de cuenca marina abierta, prodelta y frente deltaico, de edad Bedouliense inferior (Zona *D. forbesi*, Aptiense Inferior, Fm. Patrocinio); 4) plataforma carbonatada somera con rudistas y corales, de edad Bedouliense superior (zonas *D. deshayesi* y *D. furcata*, parte alta del Aptiense Inferior, Fm. San Esteban); 5) plataforma carbonatada externa y abierta y plataforma terrígena (*shoreface* y *offshore*), de edad Gargasiense inferior (parte baja del Aptiense Superior, Fm. Rodezas); 6) plataforma carbonatada, en su mayoría de ambiente somero, aunque también se han identificado ambientes de plataforma externa y mar abierto, de edad Gargasiense-Clansayesiense (Aptiense Superior, entrando probablemente en la parte basal del Albiense Inferior, Fm. Reocín); 7) sistema deltaico-estuarino, distinguiéndose ambientes de bahía influenciada por marea y oleaje, de llanura deltaica y relleno de canal, de relleno de bahía interdistributaria y de frente deltaico con barras distributarias (Albiense Inferior-Medio, Fm. Las Peñosas).

Se ha establecido el modelo paleogeográfico de la zona, que muestra una polaridad general de los cinturones de facies desde áreas con menores espesores y facies más someras (paleo-alto) al norte y al oeste (áreas de La Florida y Comillas-Cuchía), a áreas de surco intraplataforma con mayores acumulaciones de sedimento y facies relativamente más profundas, al sur y este de la zona de estudio (área del sinclinal de Santillana), lo que encaja con el modelo extensional de la cuenca. Asimismo, las áreas de paleo-alto de La Florida y Comillas-Cuchía muestran varios hiatos deposicionales asociados a exposiciones subaéreas y a adelgazamiento o ausencia de algunas unidades

litoestratigráficas (i.e. Fms. Umbrera, San Esteban y Rodezas, en el área más occidental de La Florida; y Fms. Rábago, Rodezas y Las Peñosas en el área de Comillas-Cuchía).

Se han identificado 5 secuencias de depósito transgresivas-regresivas (T-R) principales, limitadas por discontinuidades. Éstas son: 1) SD1, Bedouliense basal, Fm. Rábago; 2) SD2, Bedouliense inferior-superior, Fms. Umbrera, Patrocinio y San Esteban; 3) SD3, Gargasiense inferior, Fm. Rodezas y parte inferior de la Fm. Reocín; 4) SD4, Gargasiense superior-base del Albiense Inferior, parte superior de la Fm. Reocín; 5) SD5, Albiense Inferior-Medio, Fm. Las Peñosas p.p.

Con respecto al Evento Anóxico Oceánico del Aptiense Inferior (OAE 1a), se han estudiados dos secciones de la Fm. Patrocinio en las áreas de La Florida y Cuchía. Para ello se han llevado a cabo análisis sedimentológicos, bioestratigráficos y quimioestratigráficos ($\delta^{13}C$, $\delta^{18}O$, TOC, $CaCO_3$) de alta resolución.

Como resultado de todos los estudios mencionados, esta Tesis aporta los siguientes artículos científicos, publicados en revistas internacionales indexadas (SCI):

- **Najarro, M**., Rosales, I. and Martín-Chivelet, J. (2011a). **Major palaeoenvironmental perturbation in an Early Aptian carbonate platform: prelude of the Oceanic Anoxic Event 1a?** *Sedimentary Geology*, 235, 50–71, doi:10.1016/j.sedgeo.2010.03.011.

- **Najarro, M**., Rosales, I., Moreno-Bedmar, J.A., de Gea, G.A., Barrón, E., Company, M. and Delanoy, G. (2011b). **High-resolution chemo- and biostratigraphic records of the Early Aptian Oceanic Anoxic Event in Cantabria (N Spain): Palaeoceanographic and palaeoclimatic implications**. *Palaeogeography, Palaeoclimatology, Palaeoecology*, 299, 137–158, doi: 10.1016/j.palaeo.2010.10.042.

- **Najarro, M**., Peñalver, E., Rosales, I., Pérez-de la Fuente, R., Daviero-Gomez, V., Gomez, B. and Delclòs, X. (2009). **Unusual concentration of Early Albian arthropod-bearing amber in the Basque-Cantabrian Basin (El Soplao, Cantabria, Northern Spain): Palaeoenvironmental and palaeobiological implications**. *Geologica Acta*, 7 (3), 363–387, doi: 10.1344/105.000001443.

- **Najarro, M**., Peñalver, E., Pérez-de La Fuente, R., Ortega-Blanco, J., Menor-

Salván, C., Barrón, E., Soriano, C., Rosales, I., López del Valle, R., Velasco, F., Tornos, F., Daviero-Gomez, V., Gomez, B. and Delclòs, X. (2010). **Review of the El Soplao amber outcrop, Early Cretaceous of Cantabria, Spain**. *Acta Geologica Sinica (English Edition)*, 84, 801–818, doi: 10.1111/j.1755-6724.2010.00258.x.

CONCLUSIONES

En la cuenca Nor-Cantábrica, el inicio del OAE 1a estuvo precedido por un cambio en el tipo de producción carbonatada en la zona nerítica, pasando de una composición de tipo fotozoan a una de tipo heterozoan, esta última presentando gran cantidad de partículas terrígenas. Este cambio composicional indica un estrés ambiental, inducido probablemente por el aumento del nivel trófico y turbidez en las aguas oceánicas debido al incremento del aporte de nutrientes y partículas terrígenas por escorrentía desde zonas continentales emergidas, precediendo el ahogamiento (*drowning*) de la plataforma durante el OAE 1a. Seguidamente, la sedimentación durante el OAE 1a se caracterizó por el depósito de margas y materiales siliciclásticos (Fm. Patrocinio). Los principales mecanismos que originaron el ahogamiento de la plataforma carbonatada durante el OAE 1a fueron el incremento del aporte de terrígenos desde el continente, aumento de nutrientes y subida del nivel del mar, inducidos por los elevados niveles de CO_2 atmosférico y calentamiento global durante el Aptiense Inferior.

Se han reconocido perturbaciones en el ciclo global del carbono que resultaron en una pronunciada excursión isotópica ($\delta^{13}C$) negativa, seguida de una excursión isotópica positiva, del carbono tanto de la fracción carbonatada como orgánica de los sedimentos, en consonancia con los estadios isotópicos (C2–C7) reconocidos en otras cuencas. Estos resultados apoyan el carácter global de estas excursiones isotópicas y de su mecanismo de inducción. Además, se ha refinado la edad y duración del OAE 1a con nuevos datos bioestratigráficos de alta resolución, acotándose la edad en el área de estudio del segmento C3 de la curva patrón de $\delta^{13}C$ del OAE 1a, a la parte media-alta de la zona de ammonites *Deshayesites forbesi* (antes denominada *D. weissi),* a la parte alta de la zona *Blowiella blowi* de foraminíferos planctónicos y la parte alta de la zona

Hayesites irregularis de nanofósiles calcáreos.

El cambio a condiciones climáticas globales relativamente más frías durante el Aptiense Inferior alto-Aptiense Superior (conocido como *cold-snap*), quedó registrado en el área de estudio por un cambio en la abundancia de algunos grupos de palinomorfos (descenso de *Classopollis* y aumento de polen tipo bisacado, indicativo de un cambio significativo en la flora terrestre), junto con un amplio desarrollo de la sedimentación carbonatada de plataforma. Este desarrollo de las plataformas carbonatadas estuvo jalonado por oscilaciones y caídas del nivel del mar, produciendo eventos mayores de emersión de la plataforma al final del Aptiense Inferior (techo de la Fm. San Esteban) y al final del Aptiense Superior–inicios del Albiense (techo de la Fm. Reocín).

Durante el Albiense Inferior, después del periodo de exposición subaérea a techo de la Fm. Reocín, la sedimentación carbonatada fue reemplazada por un sistema deltaico-estuarino (Fm. Las Peñosas). Este sistema, principalmente siliciclástico, aparece rellenando las zonas de surco intraplataforma, haciendo *on-lap* y disminuyendo de potencia, o incluso despareciendo hacia las zonas de alto (ej. área de Cuchía). Este sistema se interpreta en su conjunto como el relleno transgresivo de un amplio valle inciso de algunas decenas de kilómetros de extensión, controlado por tectónica. La evolución de la sucesión deltaico-estuarina de la Fm. Las Peñosas indica una tendencia transgresiva-regresiva-transgresiva, con una progresiva inundación de los ambientes continentales y de transición. Esto produjo la anegación y deterioro ambiental en las comunidades de bosques de medios continentales y transicionales, originando, junto con otros factores (ej. incendios), condiciones propicias para la proliferación de insectos y otros artrópodos y para la exudación masiva de resinas como mecanismo defensivo de las plantas. Como resultado, estos depósitos presentan una alta acumulación de masas de ámbar con bioinclusiones y su estudio ha llevado al descubrimiento del yacimiento de ámbar de El Soplao. En este trabajo se aporta el marco geológico y deposicional para comprender el origen de este tipo de depósitos, así como sus implicaciones paleambientales y su contexto paleogeográfico.

SUMMARY

APTIAN-LOWER ALBIAN CARBONATE PLATFORMS AND DELTA SYSTEMS OF THE NORTHWEST OF CANTABRIA: RECORD OF PALEOCLIMATIC CHANGES AND OCEANIC ANOXIC EVENTS

INTRODUCTION

This study focuses on the sedimentary, tectono-sedimentary and paleoenvironmental evolution of the Lower Cretaceous successions (Aptian-Lower Albian) deposited in the North-Cantabrian basin, which constitutes the northwestern margin of the Basque-Cantabrian basin (north of Spain), with accent on the paleoclimatic changes recorded in the stratigraphic succession. The multidisciplinary approach of this Thesis, including stratigraphical, sedimentological, biostratigraphical, paleontological, chemostratigraphical, paleogeographical and tectonic studies, has given a comprehensive analysis of the sedimentary expression of global paleoclimatic changes in shallow carbonate and siliciclastic environments within the studied interval, as well as the interplay between global, regional and local factors in controlling sedimentation. The frame of global environmental perturbations that occurred at this time are the global warming related to the Early Aptian Oceanic Anoxic Event (OAE 1a), the cold snap that followed the OAE 1a during the Late Aptian–earliest Albian and the global warming related to the Early Albian Oceanic Anoxic Event (OAE 1b).

OBJECTIVES

The main objectives of this study are to:

1) Upgrade the stratigraphic and biostratigraphic schema of the study area.
2) Describe the sedimentary facies, microfacies, depositional environments and paleoenvironmental changes.
3) Recognize stratigraphic discontinuities and the facies architecture via the stratigraphic correlation of unconformities, in order to define the depositional sequences and their limits.

4) Reconstruct the extensive structure of the North-Cantabrian basin during the Lower Cretaceous by means of stratigraphic correlation, changes of facies and sedimentary thicknesses, structural cross-sections and models of extensive tectonics.
5) Identify and characterize the impact in the study area, of the global paleoclimatic and paleoceanographic crisis known as the Oceanic Anoxic Event 1a (OAE 1a) or Selli event, which took place during the Lower Aptian.
6) Survey and characterize the amber deposits of the Lower Albian in the study area, with the aim of stablishing the paleogeographical, sedimentary and paleoenvironmental context of this type of deposits and criteria for predicting their possible location.

RESULTS

A total of 17 outcrops and 15 stratigraphic sections totalizing more than 3100 m of sedimentary thickness have been logged in metric and decimetric scale in the Aptian-Lower Albian succession. This allowed the identification of three sedimentary sectors (La Florida, Cuchía and Santillana synclinorium) and 9 lithostratigraphic units, establishing a new formal unit in the areas of La Florida and Santillana synclinorium, namely the Rábago Formation. The lithostratigraphic units have been dated with a better resolution than previously reported, by means of biozones of ammonites, benthic and planktonic foraminifera, calcareous nannofossils and palynomorphs. This, along with stratigraphic correlations, allowed the identification of major depositional hiatuses during the Bedoulian andlowermost Gargasian in La Florida area, and for the lowermost Aptian and Lower-Middle Albian in the Cuchía area.

The structural style of the North-Cantabrian basin varies from basement tectonics at the rift margin (Banda del Nansa), with an imbricate of south-vergent thrust units, to a detached cover at the graben center (Bloque Costero de Santander). The analysis of thicknesses and facies changes allows to identify the activity of six major syn-sedimentary faults oblique to the basin margins: the N017 Bustriguado fault, the E-W Santibañez fault and the N060 Peña Castillo, Santa Ana, Torrelavega-Usgo and Rubárcena faults. When examined in plan view, these faults are grouped in two genetic

areas by reasons of connectivity (Treceño and Santander areas), bounded by an accommodation zone (Reocín area). This pattern characterizes an oblique rift with axial asymmetry.

The studied sedimentary record shows the evolution of the following depositional systems: 1) mixed carbonate-siliciclastic platform for the lowermost Bedoulian (lower *D. oglanlensis* Zone, lowermost Aptian, Rábago Fm.); 2) high-energy, calcarenitic carbonate ramp for the lower Bedoulian (upper *D. oglanlensis* Zone, Lower Aptian, Umbrera Fm.); 3) basinal, prodelta and delta front system for the lower Bedoulian (*D. forbesi* Zone, Lower Aptian, Patrocinio Fm.); 4) rudist-coral-dominated shallow platform for the upper Bedoulian (*D. deshayesi* and *D. furcata* zones, Lower Aptian, San Esteban Fm.); 5) outer carbonate platform and siliciclastic platform (shoreface and offshore), for the lower Gargasian (lower Upper Aptian, Rodezas Fm.); 6) carbonate platform, mainly of shallow water environment, along with outer and open marine environments for the Gargasian–Clansayesian (Upper Aptian entering probably into the lowermost Albian, Reocín Fm.); and 7) estuarine-delta system, with wave- and tidal-influenced estuarine bay, delta plain interdistributary bay, delta plain distributary meandering channels and delta front distributary mouth bars environments (Lower-Middle Albian, Las Peñosas Fm.).

A paleogeographic model of the area has been established, showing an overall trend of facies belts from areas with shallower and thinner sedimentary successions (paleo-highs) to the north and west (areas of La Florida and Comillas-Cuchía) towards areas with deeper and thicker sedimentary successions (depocentral areas) to the south and east (area of Santillana synclinorium), in accordance with the extensional model of the basin. In addition, the paleo-high areas of La Florida and Comillas-Cuchía display frequent depositional hiatuses associated to subaerial exposure, with pinch-out or absence of several lithostratigraphic units (i.e. Umbrera, Rodezas and San Esteban Fms. in the western part of La Florida area, and Rábago, Rodezas and Las Peñosas Fms. in the Comillas-Cuchía area).

Five transgressive-regressive (T-R) depositional sequences bounded by unconformities have been identified for the lowermost Bedoulian (SD1, Rábago Fm.), lower-upper Bedoulian (SD2, Umbrera, Patrocinio and San Esteban Fms.), lower

Gargasian (SD3, Rodezas and lower Reocín Fms.), upper Gargasian–lowermost Albian (SD4, upper Reocín Fm.) and Lower-Middle Albian (SD5, Las Peñosas Fm.).

Regarding the OAE 1a event, two Lower Aptian sections of the Patrocinio Fm. (La Florida and Cuchía) have been investigated using high-resolution sedimentological, biostratigraphical and chemostratigraphical ($\delta^{13}C$, $\delta^{18}O$, TOC, $CaCO_3$) approaches.

As a result of the aforementioned studies, this Thesis has contributed with the following peer-reviewed articles (SCI papers):

- **Najarro, M**., Rosales, I. and Martín-Chivelet, J. (2011a). **Major palaeoenvironmental perturbation in an Early Aptian carbonate platform: prelude of the Oceanic Anoxic Event 1a?** *Sedimentary Geology*, 235, 50–71, doi:10.1016/j.sedgeo.2010.03.011.

- **Najarro, M**., Rosales, I., Moreno-Bedmar, J.A., de Gea, G.A., Barrón, E., Company, M. and Delanoy, G. (2011b). **High-resolution chemo- and biostratigraphic records of the Early Aptian Oceanic Anoxic Event in Cantabria (N Spain): Palaeoceanographic and palaeoclimatic implications**. *Palaeogeography, Palaeoclimatology, Palaeoecology*, 299, 137–158, doi: 10.1016/j.palaeo.2010.10.042.

- **Najarro, M**., Peñalver, E., Rosales, I., Pérez-de la Fuente, R., Daviero-Gomez, V., Gomez, B. and Delclòs, X. (2009). **Unusual concentration of Early Albian arthropod-bearing amber in the Basque-Cantabrian Basin (El Soplao, Cantabria, Northern Spain): Palaeoenvironmental and palaeobiological implications**. *Geologica Acta*, 7 (3), 363–387, doi: 10.1344/105.000001443.

- **Najarro, M**., Peñalver, E., Pérez-de La Fuente, R., Ortega-Blanco, J., Menor-Salván, C., Barrón, E., Soriano, C., Rosales, I., López del Valle, R., Velasco, F., Tornos, F., Daviero-Gomez, V., Gomez, B. and Delclòs, X. (2010). **Review of the El Soplao amber outcrop, Early Cretaceous of Cantabria, Spain**. *Acta Geologica Sinica (English Edition)*, 84, 801–818, doi: 10.1111/j.1755-6724.2010.00258.x.

CONCLUSIONS

In the North-Cantabrian basin, the onset of the OAE 1a was preceded by a change in the neritic carbonate factory from photozoan to heterozoan style, the later rich in terrigenous particles. This compositional change indicates environmental stress induced by high trophic level conditions and enhanced terrestrial runoff, preluding the platform drowning during the OAE 1a. Sedimentation during the OAE 1a was characterized by marly and siliciclastic deposition (Patrocinio Fm.). Increasing continental runoff, nutrient influx and a sea-level rise induced by high levels of CO_2 and global warming, are proposed as the main mechanism for platform drowning during the OAE 1a. The age and duration of the OAE 1a have been refined on the basis of new high-resolution biostratigraphic data provided in this study. In addition, carbon isotope perturbations (a sharp negative $\delta^{13}C$ excursion followed by a positive $\delta^{13}C$ excursion) in both bulk organic matter carbon and marine carbonate carbon have been recorded, in agreement with other $\delta^{13}C$ records of Lower Aptian deposits worldwide. These results support the global character of these isotopic excursions together with their triggering mechanisms.

The change to relatively cooler climate conditions after the OAE 1a, during the upper Early Aptian–Late Aptian (so-called "cold-snap"), is recorded in the study area by a change in the abundance of some particular groups of palynomorphs (decrease of *Classopollis* and increase of bisaccated pollen), indicative of significant changes in the terrestrial flora, and by the widespread development of carbonate deposition. Carbonate platform development was punctuated by sea-level oscillations and stages of sea-level fall, with major platform emersion at the end of the Lower Aptian (*D. furcata* Zone, top of San Esteban Fm.) and end of the Aptian–earliest Albian (top of the Reocín Fm.).

During the Lower Albian, and following subaerial exposure on top of the Reocín Fm., carbonate sedimentation was replaced by a siliciclastic estuarine-delta system (Las Peñosas Fm.). This delta-estuarine system filled intraplatform troughs, onlapping, thinning or disappearing toward the highs. It is interpreted as the transgressive infill of a kilometre-scale incised valley controlled by tectonics. The evolution of the Las Peñosas delta-estuarine succession indicates a transgressive-regressive-transgressive trend, with a progressive flooding of the continental and transitional marine environments. This

gave rise to the flooding and damage of the continental and transitional forests, producing, together with other possible factors such as fires, favorable conditions for the proliferation of insects and other arthropods and the massive exudation of resins as a protective mechanism of the plants. Consequently, these deposits yielded a high accumulation of amber pieces with abundant bioinclusions. The study of these deposits has resulted in the discovery of the amber-bearing deposit of the El Soplao. This study provides the geological and depositional framework for understanding the origin of these deposits, their paleoenvironmental implications and their paleogeographic context.

CAPÍTULO 1:

INTRODUCCIÓN

CAPÍTULO 1

1.- INTRODUCCIÓN

1.1.- NATURALEZA Y OBJETIVOS DE LA TESIS

Esta Tesis Doctoral se ha realizado dentro del marco de los proyectos: "Relación entre sedimentación, tectónica y flujo de fluidos durante la extensión del Cretácico Inferior en la Cuenca de Santander", financiado por Instituto Geológico y Minero de España (IGME 2005–2008); "Investigación Científica y Técnica de la Cueva de El Soplao y su entorno Geológico" surgido del Convenio de Colaboración entre el IGME, la Consejería de Cultura, Turismo y Deporte del Gobierno de Cantabria y la empresa SIEC S.A. (2008–2012) y el proyecto "Variaciones seculares geoquímicas e isotópicas en facies carbonatadas marinas del Carbonífero, Jurásico y Cretácico en la Península Ibérica: Aplicación a la interpretación de crisis paleoclimáticas", concedido por la DGI del Ministerio de Ciencia e Innovación (2009–2011, CGL2008-01237). En concreto, este trabajo se ha centrado en el estudio de la evolución sedimentaria, tectono-sedimentaria y paleoambiental de los materiales del Aptiense–Albiense Inferior del sector occidental de la cuenca Nor-Cantábrica (NO de Cantabria), con especial énfasis en el estudio del reflejo en estas sucesiones estratigráficas, de los cambios paleoclimáticos que se produjeron durante el intervalo Aptiense Inferior y del Albiense Inferior.

El estudio del Cretácico Inferior es de especial interés, ya que estuvo caracterizado por una intensa actividad volcánica con formación de "Grandes Provincias Ígneas" (Coffin y Eldhom, 1994; Larson y Erba, 1999), elevados niveles de CO_2 atmosférico, pronunciado aumento de las temperaturas medias (hasta 7ºC mayores que la actual), significativas fluctuaciones eustáticas, perturbaciones mayores en el ciclo global del carbono, y episodios de desarrollo de anoxia en los fondos marinos, crisis en la producción de carbonatos, acidificación de las aguas y extinciones en masa (e.j. Weissert y Lini, 1991; Erba, 1994; Föllmi *et al.*, 1994; Weissert *et al.*, 1998; Menegatti *et al.*, 1998; Jenkyns, 2003; Wissler *et al.*, 2003; Föllmi *et al.*, 2006; Dumitrescu *et al.*, 2006; Burla *et al.*, 2008). En resumen, toda una batería de efectos interrelacionados que

afectaron a las plataformas carbonatadas extendidas a lo largo del dominio del Tetis, y cuyo desencadenante inicial es aún poco conocido. Dentro de este marco general, en esta Tesis Doctoral se han llevado a cabo estudios enfocados a analizar cambios paleoambientales y paleoceanográficos durante el Aptiense–Albiense Inferior en el área de estudio, y comprobar hasta qué punto estuvieron condicionados por los cambios globales ocurridos durante el Cretácico Inferior.

La cuenca Nor-Cantábrica constituye el borde nor-occidental de la cuenca Vasco-Cantábrica, donde afloran, para el Aptiense–Albiense, depósitos de plataforma carbonatada (calizas urgonianas) interestratificados con depósitos siliciclásticos costeros. Estos sistemas de plataforma carbonatada ofrecían *a priori* gran potencial para abordar este tipo de estudios, ya que son sistemas particularmente sensibles a los cambios ambientales, climáticos y oceanográficos (incluidos cambios relativos del nivel del mar), en cuanto a que afectan el químismo del agua, temperatura, salinidad, turbidez, aporte de sedimento detrítico, actividad biológica, nutrientes, etc. Estos cambios pudieron ser rápidamente registrados en los sistemas de plataforma carbonatada del área de estudio como discontinuidades y cambios en la composición y producción de carbonato, así como en el estilo de sedimentación.

El área de estudio constituía también una zona prometedora desde el punto de vista paleontológico por contener indicios de ámbar en las unidades siliciclásticas albienses, si bien no se habían encontrado hasta el momento enclaves importantes con contenido fosilífero. Durante la realización de esta Tesis se ha llevado a cabo un trabajo detallado de prospección en busca de yacimientos paleontológicos que ha permitido el descubrimiento de nuevos enclaves y yacimientos de ámbar ricos en bioinclusiones fósiles (principalmente artrópodos), alguno de ellos de gran relevancia como es el caso del *Yacimiento de ámbar de El Soplao*, actualmente en estudio exhaustivo por parte de científicos especialistas nacionales e internacionales.

Por otro lado, si bien el Cretácico Inferior de la cuenca Vasco Cantábrica ha sido extensamente estudiado desde un punto de vista estratigráfico, sedimentológico y tectónico (ej. Rat, 1959; Aguilar, 1970; Floquet y Rat, 1975; Pujalte, 1977; García-Mondéjar, 1979a, 1979b; 1990; Pascal, 1985; Fernández-Mendiola, 1986; García-Garmilla, 1987; Rat, 1988; Robles *et al.*, 1988; Gómez-Pérez, 1994; Gräfe, 1994;

Rosales *et al.*, 1994, 2002; Rosales, 1995, 1999; Agirrezabala, 1996; Espina, 1996; García-Mondéjar *et al.*, 1996; Aranburu, 1998; López-Horgue, 2000; Quintanar-Soto, 2003, Iriarte, 2004; Soto *et al*, 2007; Millán *et al*., 2009; Quintana, 2012, entre otros), hasta la fecha el Cretácico Inferior de la cuenca Nor-Cantábrica había estado menos investigado, con escasos trabajos publicados en los años setenta (ej. Ramírez del Pozo, 1972; Ramírez del Pozo *et al*, 1976a; 1976b; Carreras *et al.*, 1978; 1979; Collignon *et al*., 1979) y principios de los ochenta (Martínez-García, 1980; Hines, 1985), o más recientemente (Wilmsen, 2005), lo que también justifica su estudio. Además, teniendo en cuenta que en los últimos años se ha producido un gran avance del conocimiento científico, tanto en lo referente al análisis de cuencas, como en el uso de trazadores paleoclimáticos y paleoambientales, esta tesis pretende contribuir, mediante un enfoque multidisciplinar, al conocimiento estratigráfico, sedimentológico, bioestratigráfico, paleontológico, quimioestratigráfico, paleogeográfico y paleotectónico del área de estudio durante el periodo considerado. En detalle, se han perseguido y alcanzado los siguientes objetivos:

1. Avanzar en el conocimiento estratigráfico del área de estudio, construyendo un esquema litoestratigráfico más preciso que el existente, mediante la redefinición y definición de unidades estratigráficas.

2. Mejorar la resolución bioestratigráfica de los materiales estudiados mediante la colaboración con especialistas en ammonites, foraminíferos planctónicos y bentónicos, nanofósiles calcáreos y palinomorfos. Con ello se ha conseguido datar con mejor precisión las unidades, revelar las lagunas estratigráficas existentes y usar la distribución bioestratigráfica de determinados grupos de nanofósiles calcáreos y palinomorfos para inferir los cambios ambientales y climáticos.

3. Identificar facies y microfacies sedimentarias, ambientes de depósito y cambios paleoambientales, a través del análisis sedimentológico de las unidades litostratigráficas, examinando la distribución en el espacio y en el tiempo de los sistemas

sedimentarios carbonatados y siliciclásticos y de su brusco relevo en secuencias de depósito.

4. Definir las secuencias de depósito y sus límites.

5. Reconstruir la estructura extensiva de la cuenca Nor-Cantábrica durante el Cretácico Inferior, mediante correlación de columnas estratigráficas, análisis de facies y espesores, cortes geológicos y modelos de tectónica extensiva.

6. Identificar y caracterizar la repercusión de la crisis paleoclimática y paleoceonográfica del Aptiense Inferior, conocida como el Evento Anóxico Oceánico del Aptiense Inferior (OAE 1a), en la zona de estudio. Está bien establecido que el OAE 1a produjo a escala global perturbaciones mayores en el ciclo del C, desarrollo de anoxia con acumulación de materia orgánica en los fondos marinos, crisis bióticas y de producción de carbonatos y acidificación de las aguas oceánicas (ej. Föllmi *et al.*, 1994; Weissert *et al.*, 1998; Menegatti *et al.*, 1998; Jenkyns, 2003), cuyos efectos en la zona de estudio se ha perseguido identificar.

7. Prospectar y estudiar geológicamente los depósitos ambarígenos del Albiense Inferior del área de estudio. La sedimentología detallada de la unidad ambarígena es prioritaria para establecer el contexto paleogeográfico y paleoambiental de este tipo excepcional de depósitos y predecir su localización.

Para la realización de esta Tesis Doctoral se ha optado por la presentación en la modalidad de **compendio de publicaciones**. Éstas se incluyen en el Capítulo 4 de esta Memoria. Las publicaciones internacionales aparecen acompañadas cada una de un resumen en castellano. La Tesis Doctoral está construida sobre 4 artículos científicos, publicados en revistas indexadas de reconocido prestigio internacional del ámbito de las Ciencias de la Tierra, siendo la autora de esta tesis la primera firmante de todos ellos. Estos trabajos son por orden cronológico:

(1) Najarro, M., Peñalver, E., Rosales, I., Pérez-de la Fuente, R., Daviero-Gomez, V., Gomez, B. and Delclòs, X. (2009). Unusual concentration of Early Albian arthropod-bearing amber in the Basque-Cantabrian Basin (El Soplao, Cantabria, Northern Spain): Palaeoenvironmental and palaeobiological implications. *Geologica Acta*, 7 (3), 363–387, doi: 10.1344/105.000001443. (**Factor de Impacto** en 2009: **1,226**).

(2) Najarro, M., Peñalver, E., Pérez-de La Fuente, R., Ortega-Blanco, J., Menor-Salván, C., Barrón, E., Soriano, C., Rosales, I., López del Valle, R., Velasco, F., Tornos, F., Daviero-Gomez, V., Gomez, B. and Delclòs, X. (2010). Review of the El Soplao amber outcrop, Early Cretaceous of Cantabria, Spain**.** *Acta Geologica Sinica (English Edition)*, 84, 801–818, doi: 10.1111/j.1755-6724.2010.00258.x. (**Factor de Impacto** en 2010: **1,408**).

(3) Najarro, M., Rosales, I. and Martín-Chivelet, J. (2011a). Major palaeoenvironmental perturbation in an Early Aptian carbonate platform: prelude of the Oceanic Anoxic Event 1a? *Sedimentary Geology*, 235, 50–71, doi:10.1016/j.sedgeo.2010.03.011. (**Factor de Impacto** en 2011: **1,537**).

(4) Najarro, M., Rosales, I., Moreno-Bedmar, J.A., de Gea, G.A., Barrón, E., Company, M. and Delanoy, G. (2011b). High-resolution chemo- and biostratigraphic records of the Early Aptian Oceanic Anoxic Event in Cantabria (N Spain): Palaeoceanographic and palaeoclimatic implications. *Palaegeography, Palaeoclimatology, Palaeoecology*, 299, 137–158, doi: 10.1016/j.palaeo.2010.10.042. (**Factor de Impacto** en 2011: **2,392**).

Además de estos artículos principales, se incluyen complementariamente como anexos otros dos artículos científicos surgidos como colaboraciones específicas relacionadas con el trabajo de la Tesis Doctoral:

(5) Menor-Salván, C., **Najarro, M**., Velasco, F., Rosales, I., Tornos, F. and Simoneit, B.R.T. (2010). Terpenoids in extracts of Lower Cretaceous ambers from the

Basque-Cantabrian basin (El Soplao, Cantabria, Spain): Paleochemotaxonomic aspects. *Organic Geochemistry*, 41, 1089–1103, doi: 10.1016/j.orggeochem.2010.06.013. (**Factor de Impacto** en 2010: **2,375**).

(6) Quijano, M.L., Castro, J.M., Pancost, R.D., de Gea, G.A., **Najarro, M**., Aguado, R., Rosales, I. and Martín-Chivelet, J. (2012). Organic geochemistry, stable isotopes, and facies analysis of the Early Aptian OAE: New records from Spain (western Tethys). *Palaegeography, Palaeoclimatology, Palaeoecology,* 365-366, 276–293, doi: 10.1016/j.palaeo.2012.09.033. (**Factor de Impacto** en 2012: **2,392**).

1.2.- MARCO GEOGRÁFICO

La zona de estudio se localiza en el extremo noroccidental de la Comunidad Autónoma de Cantabria, abarcando alrededor de 20 x 80 Km (Figura 1.1). Tiene como límites geográficos aproximados el río Nansa al oeste, la sierra del Escudo de Cabuérniga al sur, el mar Cantábrico al norte y el río Besaya al este. Esta área ocupa parte de las hojas del Mapa Topográfico Nacional de España del Instituto Geográfico Nacional a escala 1:50.000, números: 33 (Comillas), 34 (Torrelavega), 57 (Cabezón de la Sal) y el extremo norte de la hoja 58 (Los Corrales de Buelna). Las localidades más importantes son Torrelavega, Comillas, Cabezón de la Sal, San Vicente de la Barquera, Santillana del Mar y Suances.

La zona presenta un relieve de baja montaña, que culmina en los picos de Castro Rubio (682 m), Costalvío (304 m) y Pico de las Palomas (422 m). La red hidrográfica está estructurada en torno a tres ríos principales que discurren paralelos en una dirección N-S: el Nansa al oeste, que desemboca en la ría de Tina Menor y los ríos Saja y Besaya al este, que desembocan en la ría de San Martín de la Arena. La costa presenta numerosos acantilados como el de El Fraile y Los Caballos que ofrecen excelentes afloramientos, si bien en ocasiones no resultan de fácil acceso.

El clima es típicamente oceánico con precipitaciones anuales de unos 1000 l/m^2 y temperaturas medias que oscilan entre 12º y 17ºC. Este clima suave y húmedo condiciona el desarrollo de una densa cobertera vegetal, pudiendo llegar incluso a cubrir los afloramientos de calizas, normalmente resaltantes, lo que dificulta el trabajo del geólogo. Así se pueden observar robledales, plantaciones de eucaliptos y pinares en las zonas montañosas, mientras que las zonas calizas se encuentran bien descubiertas o bien tapizadas por formaciones arbustivas. Asimismo, los numerosos valles que atraviesan la zona de estudio se hallan tapizados por extensos prados y cultivos.

Los recursos naturales se centran hoy en día en la explotación de las rocas carbonatadas del Carbonífero, Jurásico y Cretácico Inferior para su utilización como áridos de construcción. Se explota también sal en el diapiro de Polanco. Sin embargo, el mayor recurso de la zona fue, hasta hace pocos años, las explotaciones mineras de Pb y

Zn enclavadas en los materiales carbonatados urgonianos, destacando las minas de Reocín, la Florida y Novales. Por otro lado cabe resaltar el uso creciente de los recursos geológicos y patrimonio minero de la zona como parte fundamental del atractivo turístico (ej. cueva de El Soplao).

Figura 1.1.- Mapa geográfico de la zona de estudio con localización aproximada de las secciones estratigráficas.

1.3.- MARCO GEOLÓGICO

El área de estudio se sitúa en el norte de la Cordillera Cantábrica, en el margen noroccidental de la cuenca Vasco-Cantábrica (CVC) (Figura 1.2). Ésta limita al oeste con el macizo Asturiano, al sur con las cuencas terciarias del Duero y del Ebro y el macizo de la Demanda, al este con los macizos Vascos de Cinco Villas y Quinto Real y al norte con el mar Cantábrico (Rat, 1988). Su historia geológica se encuentra estrechamente relacionada con la apertura del Golfo de Vizcaya durante el Mesozoico (Triásico-Cretácico Inferior) y con la convergencia de las placas Ibérica y Europea (final del Cretácico y Terciario) (ej. Boillot y Malod, 1988).

En la CVC afloran principalmente materiales del Mesozoico y Cenozoico Inferior. Los espesores totales acumulados pueden alcanzar en algunos sectores de la cuenca más de 15.000 m apilados en la lateral (ej. Quintana, 2012), si bien estos espesores varían considerablemente en cortas distancias debido a la subsidencia controlada por fallas y a la tectónica salina. Los materiales aflorantes en la CVC son principalmente del Cretácico y del Terciario, apareciendo los afloramientos de materiales jurásicos y triásicos principalmente en las áreas adyacentes a los macizos paleozoicos y a los domos diapíricos (Figura 1.2).

La historia geológica de la CVC comienza hace unos 200 millones de años con la extensión post-varisca de la corteza continental en el Pérmico (Rat, 1988) y termina con el cierre de la cuenca producida por el plegamiento alpino en el Eoceno tardío. La cuenca se formó durante la apertura del Golfo de Vizcaya, que separó el Macizo Ibérico del Macizo Armoricano durante la expansión mesozoica del Atlántico Norte. El proceso de oceanización en el Golfo de Vizcaya a partir del Cretácico Inferior hasta el Cretácico Superior, tiene asociada la rotación antihoraria de Iberia respecto a Europa (Sibuet y Collete, 1991). Durante esta etapa se han estimado desplazamientos relativos entre Europa e Iberia del orden de 300–400 km (Le Pichon *et al.*, 1971), 180 km (Roest y Srivastava, 1991) y 80 km (Sibuet y Collette, 1991).

El modelo de desplazamiento de la placa Ibérica con respecto a la Europea durante la apertura del Golfo de Vizcaya ha suscitado, y sigue suscitando, mucha controversia. Tradicionalmente se han considerado dos mecanismos principales de

apertura: rotación simple en "tijera" y desgarre sinestral (sintetizados en Ries, 1978). Boillot y Capdevilla (1977) y Boillot *et al.* (1979) defienden un modelo simple de extensión y posterior colisión. Le Pichon *et al.* (1971) y Choukrone y Mattauer, (1979) sugieren que la apertura del Golfo de Vizcaya se produjo por movimientos sinistrales a lo largo de grandes fallas transformantes (Aquitania, Norpirenaica, Vizcaína y Cantábrica). Boillot (1986) sugiere extensión por cizalla simple hasta el Aptiense y desplazamiento sinistro a lo largo del eje del *rift* a partir del Albiense y durante todo el Cretácico Superior. García-Mondéjar (1989, 1996) y García-Mondejar *et al.* (1996) explican la apertura de la cuenca y la subsidencia extensional durante el Aptiense-Albiense (episodio Urgoniano) por movimientos de desgarre sinistro relacionado a las fallas transformantes, además de extensión por cizalla simple. Recientemente, Quintana *et al.* (2009a, 2009b) y Quintana (2012) proponen que la formación y geometría rómbica de la CVC se pudo producir mediante régimen extensional a partir de: 1) zonas de transferencia extensional, desarrolladas entre fallas normales subparalelas; 2) a partir de sistemas de fallas normales ortorrómbicas; y 3) por coexistencia de fallas perpendiculares y oblicuas a la dirección de extensión principal, siendo estas últimas estructuras heredadas.

La formación preorogénica de la CVC puede explicarse mediante dos fases principales de extensión en el Pérmico–Triásico Inferior y Jurásico Superior–Cretácico Inferior, y dos fases de la subsidencia más uniforme y generalizada durante el Jurásico Inferior–Medio y Cretácico Superior–Paleógeno (ej. Rat, 1988; Martín-Chivelet *et al.*, 2002), aunque también existió subsidencia diferencial.

La segunda etapa de extensiva (Jurásico Superior–Cretácico Inferior) es una fase de *rifting* en relación a la apertura del Golfo de Vizcaya y fue la más importante, por la individualización de la CVC. Durante este episodio tuvo lugar el movimiento relativo de Iberia hacia el SO con respecto a Europa (Olivet, 1978; Olivet *et al.*, 1984; Grimaud *et al.*, 1982 y Boillot, 1984, entre otros). De acuerdo con los modelos cinemáticos existentes, este movimiento de rotación antihoraria de Iberia respecto a Europa, con una componente de movimiento de Europa hacia el SE (Montadert *et al.*, 1979; Sibuet *et al.*, 2004), estuvo en parte acomodado por fallas transformantes (Le Pichon *et al.*, 1971).

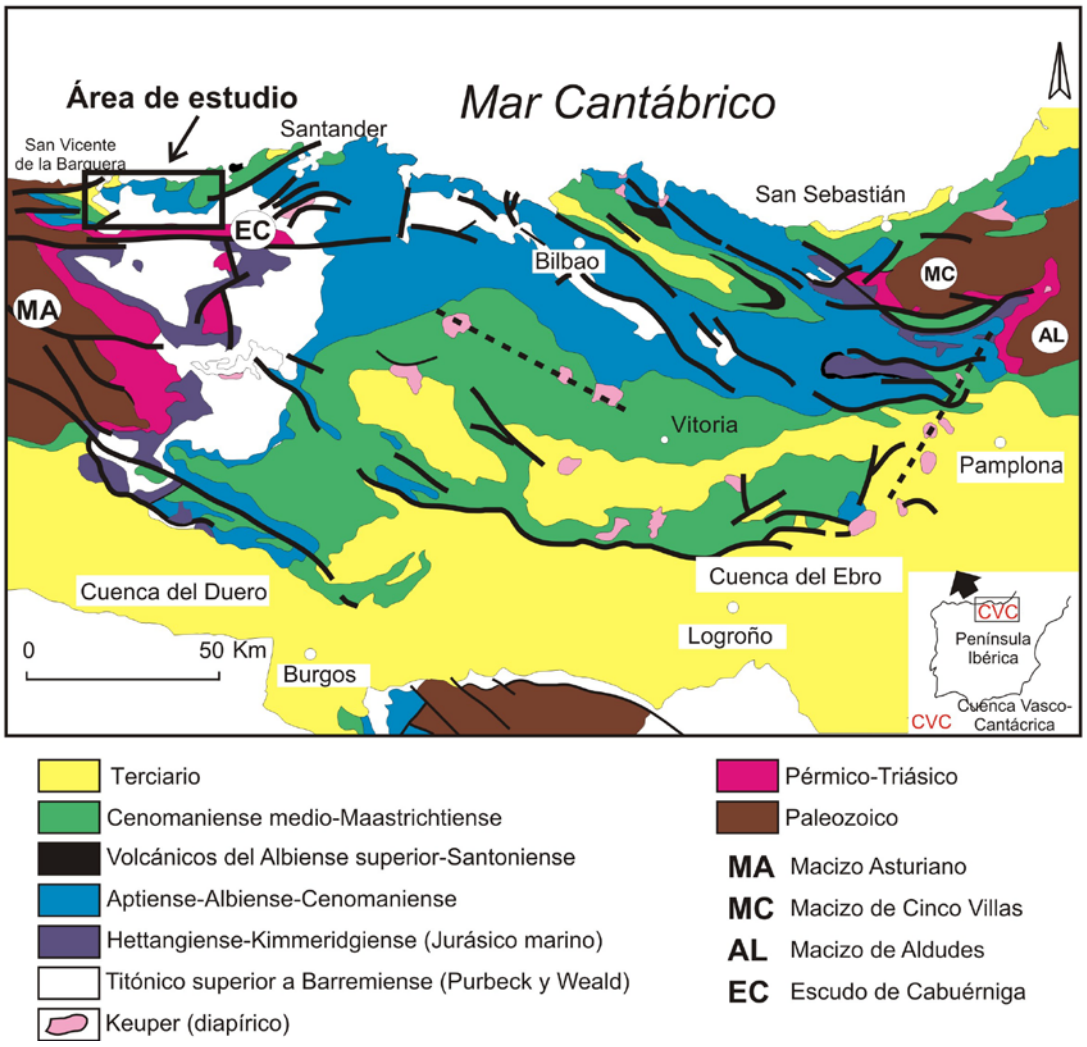

Figura 1.2.- Mapa geológico sintético de la cuenca Vasco-Cantábrica marcando la localización del área de estudio.

Durante la etapa inicial del *rifting* continental se produjeron las llamadas "cubetas wealdenses" (complejo Purbeck-Weald de Pujalte, 1977), limitadas por fallas extensionales. Estas cuencas se rellenaron con sedimentos siliciclásticos y carbonatados en ambientes continentales y transicionales (Ramírez del Pozo, 1971; Pujalte, 1977, 1981). A comienzos del Aptiense la velocidad de la subsidencia se incrementa (Rat, 1988) dando como respuesta una transgresión marina (transgresión urgoniana) coincidente aproximadamente con la base del Aptiense (Rat, 1959, 1988; García-Mondéjar, 1989, 1990), que a su vez coincidió en el tiempo con una transgresión marina global (Haq *et al*., 1988). Una de las consecuencias fue el recubrimiento de gran parte de la región por un mar somero epicontinental donde se desarrollaron amplias plataformas carbonatadas con rudistas y corales (calizas urgonianas) y plataformas mixtas terrígeno-carbonatadas, que en general persistieron hasta el Albiense (García-

Mondéjar, 1990; Martín-Chivelet *et al.*, 2002; García-Mondéjar *et al.*, 1996, 2004). A partir del Aptiense Superior la subsidencia diferencial se hizo más acusada, individualizándose subcuencas (interpretadas por algunos autores como de *pull-apart*; ej. Choukroune y Mattauer, 1978; García-Mondéjar *et al.*, 1996, 2004) y produciéndose la compartimentación de estas en altos y surcos, con la formación de calizas en las zonas más someras desprovistas de aportes terrígenos.

Durante el Albiense se incrementa la extensión, originándose un surco *flysch* en el norte de la cuenca (sinclinorio de Vizcaya), localizado, presumiblemente, en la zona de sutura entre Iberia y Europa (Rat, 1988). Este incremento de la subsidencia en la cuenca, junto al rejuvenecimiento de las áreas fuentes originó un aporte considerable de materiales terrígenos al área, lo que produjo el progresivo enterramiento de las plataformas urgonianas por sistemas siliciclásticos (Complejo Supraurgoniano, Rat, 1988). Estos procesos coincidieron con acreción oceánica en el Golfo de Vizcaya y con un importante adelgazamiento cortical en la CVC, lo que quedó reflejado en el volcanismo básico del Albiense Superior en el Sinclinorio de Vizcaya (Mathey, 1982, 1986). A partir de este momento, comienza una etapa de tipo post-rift con expansión oceánica en el Golfo de Vizcaya y deriva de la placa Ibérica. En los puntos donde sólo existía corteza continental ésta se adelgazó mucho, produciéndose una subsidencia más amplia y la profundización del surco *flysch*.

Por tanto, a lo largo del Cretácico Superior hasta el Santoniense, se produjo la flexión progresiva del margen cantábrico dando como resultado una transgresión marina generalizada con desarrollo, por una parte, de amplias plataformas carbonatadas al sur, centro y noroeste de la CVC, y por otra parte, depósitos de tipo *flysch* con intercalaciones de lavas basálticas en la zona noreste de la cuenca. A finales del Santoniense finaliza la expansión oceánica en el Golfo de Vizcaya y el volcanismo en el sinclinorio de Vizcaya, coincidiendo con el cambio de margen pasivo a margen activo y con la subducción parcial de la corteza ibérica hacia el norte (Alonso *et al.*, 2007).

Con la convergencia entre Iberia y Europa se produce la inversión de la cuenca por cabalgamientos. En la zona de estudio, la etapa de compresión esta registrada desde el Eoceno superior hasta el Oligoceno (Hines, 1985; Rat, 1988).

Dentro del contexto geodinámico general explicado anteriormente para la CVC, la zona de estudio se localiza en la denominada cuenca Nor-Cantábrica (por Wilmsen, 2000; Wilmsen 2005; Najarro *et al.*, 2007), también denominada Bloque Costero de Santander (por Barnolas y Pujalte, 2004), que constituye la terminación noroccidental de la CVC (Figura 1.3). Esta área se comportó durante la fase de extensión cretácica como un bloque poco subsidente, con orientación E–O y espesores comparativamente reducidos de los materiales cretácicos de varios cientos de metros a apenas 2500 metros, en contraste con los varios miles de metros que presentan otras áreas de la CVC, superponiéndose a la extensión triásica y enmascarando la geometría derivada de ella.

Paleogeográficamente, la cuenca Nor-Cantábrica estuvo limitada al sur por el alto y falla de Cabuérniga, al oeste por el macizo Asturiano (presumiblemente emergido durante parte del Cretácico), al norte por el alto estructural de Liencres, que hoy día está sumergido justo en frente de la actual línea de costa, y al este por una estructura extensional cretácica denominada Flexura del Río Miera (Feuillée y Rat, 1971) (Figura 1.4).

Durante la extensión cretácica la cuenca Nor-Cantábrica se compartimentó internamente en surcos y altos controlados por fallas sinsedimentarias de orientación principal E–O y secundariamente por fallas de orientación N–S y NE–SO. Entre las principales fallas extensivas que controlaron la subsidencia y la sedimentación en esta zona durante el Cretácico Inferior, cabe destacar la Falla de Bustriguado y la Falla de Santibáñez (Figura 1.3). La actuación conjugada de estas fallas condicionó la formación de tres dominios sedimentarios en función de su evolución tectónica y estratigráfica. Estas áreas han sido denominadas (de SO a NE, Figs. 1.3 y 1.5): área de La Florida, área del sinclinal de Santillana y área de Cuchía. Así las áreas de La Florida y Cuchía representan dos zonas de menor subsidencia o bloques elevados, mientras que el área del sinclinal de Santillana constituye un depocentro o bloque hundido dentro del área de estudio (Figura 1.5). A partir del Eoceno superior, durante la orogénia Alpina, se produjo la inversión de la Falla de Cabuérniga y el plegamiento de la serie principalmente mesozoica depositada en la cuenca Nor-Cantábrica, configurándose la estructura tectónica del área de estudio tal como se reconoce hoy en día.

A pesar de que la cuenca Nor-Cantábrica constituye el extremo noroccidental de la CVC, en ella se pueden distinguir dos dominios estructurales bien diferenciados: el primero de ellos (o dominio occidental), que coincide con el área de La Florida, se corresponde al extremo nororiental del macizo Asturiano que equivale a su vez al límite nororiental del basamento paleozoico de la Zona Cantábrica (Lotze, 1945; Espina, 1994). Uno de los rasgos más característicos de las estructuras tectónicas de este dominio es su llamativa orientación E–O, que, a su vez, impera en las alineaciones orientales paleozoicas del macizo Asturiano. El segundo dominio estructural (o dominio oriental), que engloba a las áreas del sinclinal de Santilla y Cuchía, pertenece al borde noroccidental de la cuenca Vasco-Cantábrica (o Bloque Costero de Santander, según Barnolas y Pujalte, 2004). Las orientaciones estructurales que presenta este dominio son poco frecuentes en el resto de la cuenca (Feuillé y Rat, 1971; Hines, 1985), destacando una orientación dominante NE–SO de los pliegues y fallas.

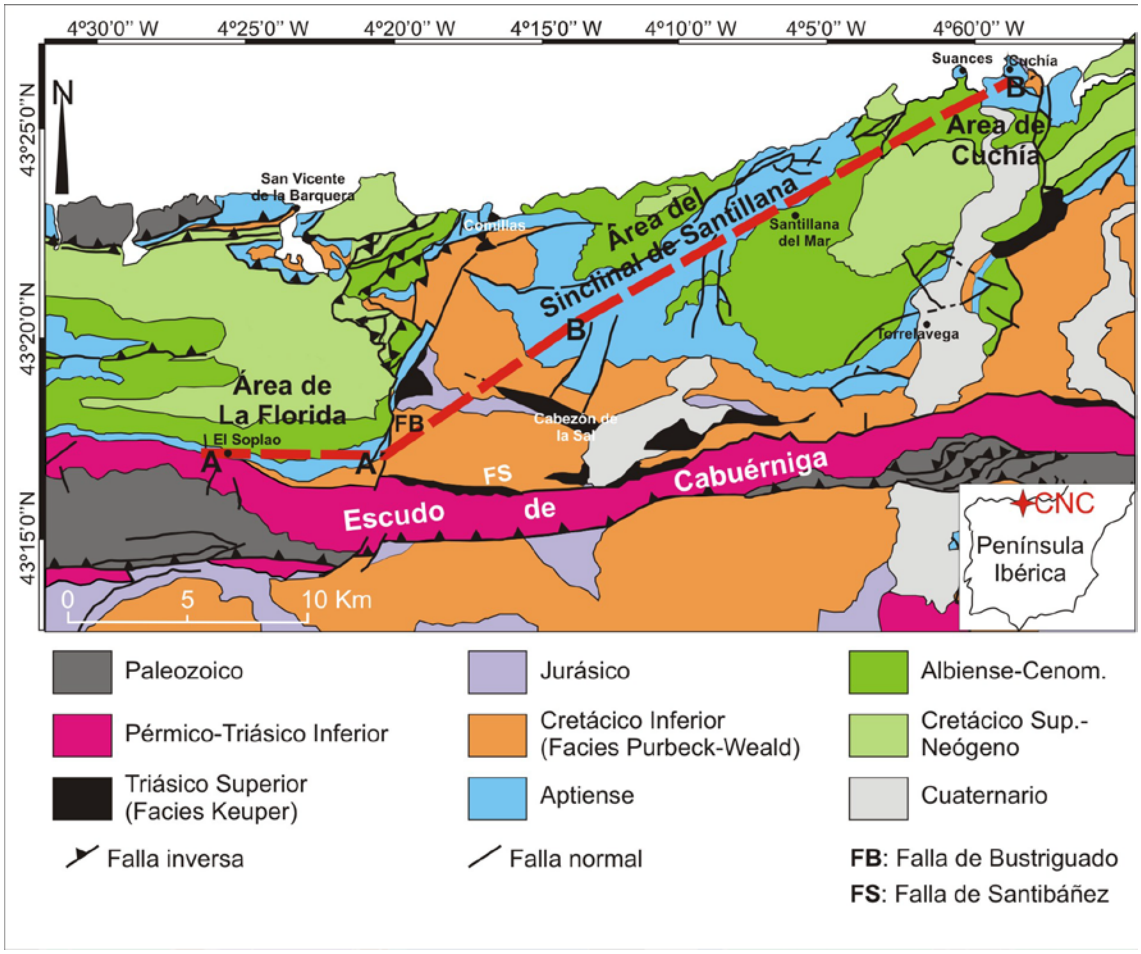

Figura 1.3.- Mapa geológico simplificado del área de estudio en la cuenca Nor-Cantábrica. Modificado de Hines (1985). La línea roja A-A´' a B-B' indica la dirección del corte de reconstrucción estratigráfica mostrada en la Figura 1.5.

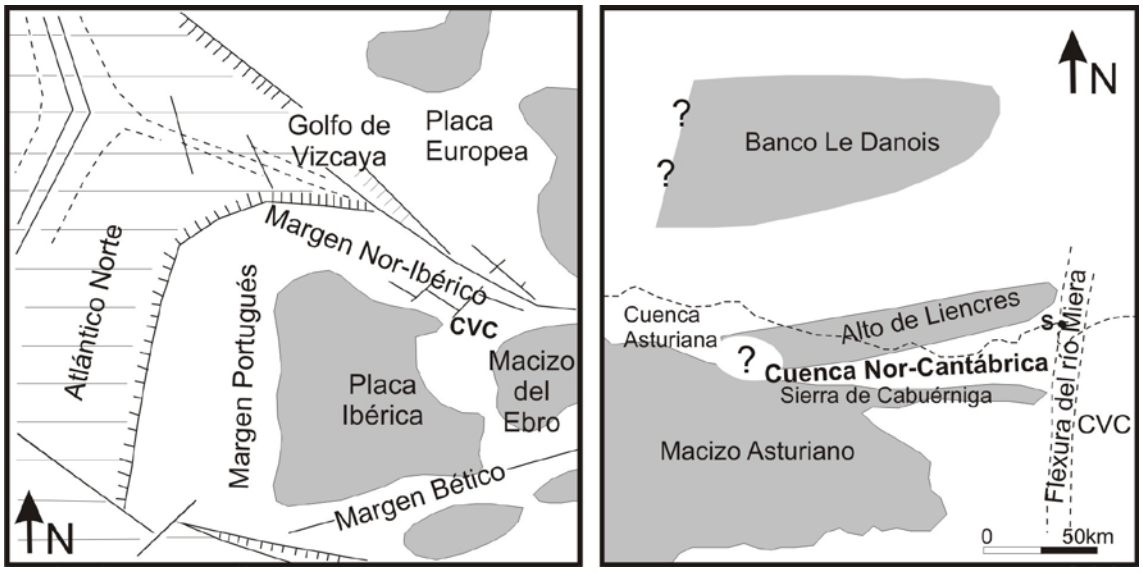

Figura 1.4.- Contexto paleogeográfico regional de la cuenca Nor-Cantábrica: **A**). Paleogeografía de la Península Ibérica durante el Cretácico Inferior. **B**). Esquema paleogeográfico de la zona de estudio durante el Cretácico Inferior. Las áreas en gris corresponden a zonas emergidas. S = Santander. Modificado de Wilmsen (2000).

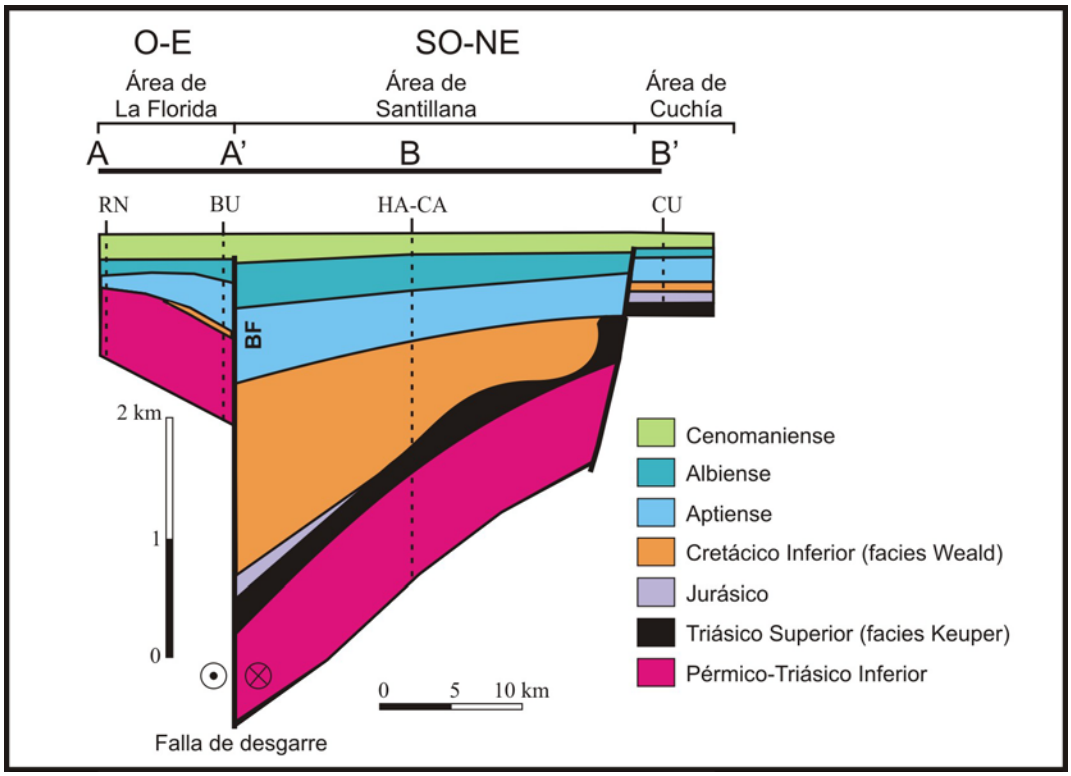

Figura 1.5.- Corte estratigráfico mostrando la geometría reconstruída de la cuenca Nor-Cantábrica durante el Cretácico Inferior y las diferencias de registro sedimentario y espesores entre los principales dominios o áreas, en base a la cartografía geológica y a las secciones de referencia indicadas. Tomado de Najarro *et al.* (2011a y 2011b). Consultar la Figura 1.3 para la localización del corte. RN: sección de río Nansa; BU: sección de Bustriguado, HA-CA: sección de Hayuela-Canales, CU: sección de Suances-Cuchía.

1.4.- ANTECEDENTES

1.4.1.- ESTRATIGRAFÍA

Los primeros antecedentes bibliográficos específicos de los materiales de edad Aptiense-Albiense de la zona de estudio se remontan a la segunda mitad del siglo XIX con los trabajos de Vernuill (1852), Maestre (1864), Carez (1881) y Puig y Sánchez (1888). Estos trabajos describen preferentemente los macrofósiles en un contexto estratigráfico de tiempo geológico y esbozan las primeras subdivisiones litostratigráficas.

El primer trabajo que detalla la estratigrafía del Cretácico Inferior en las zonas de Torrelavega-Reocín, Cuchía y La Florida es el de Mengaud (1920), quien, además de separar con cierta precisión el Aptiense del Albiense, realiza un estudio paleontológico detallado con ammonites. Posteriormente, Karrenberg (1934) revisa prácticamente los mismos cortes que Mengaud (1920); y Ciry (1940) describe la geología general en la zona de estudio y al sur de la misma.

En lo que puede considerarse como el inicio de una nueva etapa, Rat (1959) en su ya clásica Tesis Doctoral, describe y cartografía (mapa escala 1:200.000) los materiales mesozoicos y cenozoicos de gran parte de la cuenca Vasco-Cantábrica, centrando su estudio en las rocas de edad Aptiense y Albiense, con la definición de los complejos Urgoniano y Supraurgoniano. Aunque la presente zona de estudio queda fuera de los límites geográficos de la tesis de Rat, éste re-describió los afloramientos estudiados por Mengaud (1920) aportando nuevas dataciones.

Ciry y colaboradores (1967) realizan una descripción de las unidades litoestratigráficas de edad Aptiense-Albiense al oeste de Torrelavega, tomando como referencia para el Aptiense la división de Mengaud (1920).

Aguilar Tomás (1970) presenta un estudio general petrográfico y sedimentológico del Albiense en la zona de La Florida y dos años después Ramírez del

Pozo (1972) analiza la microfauna y revisa la estratigrafía del Aptiense-Albiense del mismo área.

Los mapas geológicos a escala 1:50.000 del Proyecto MAGNA (hojas de Comillas (33), Torrelavega (34), Cabezón de las Sal (57), Los Corrales de Buelna (58); por Ramírez del Pozo *et al.*, 1976a y 1976b; Carreras *et al.*, 1978, 1979), suponen un avance significativo en la precisión con que se definen los contactos de las unidades cartografiables, y como se verá más adelante, en la representación de la estructura geológica.

Collignon y colaboradores (1979) revisan de nuevo la paleontología y estratigrafía de los cortes estudiados por Mengaud en 1920, llegando prácticamente a las mismas conclusiones.

Las Tesis Doctorales de Pujalte (1977) y García-Mondéjar (1979), aunque realizadas fuera del área de este estudio, establecen un marco estratigráfico y sedimentológico del Cretácico Inferior del margen ibérico de la Cuenca Vasco-Cantábrica, que permite un reconocimiento más preciso de las facies continentales y marinas desde los dominios de plataforma a la cuenca. Es en este marco moderno donde se van a integrar tesis y trabajos estratigráficos posteriores en áreas vecinas (García-Garmilla, 1987; Gómez-Pérez, 1994; Rosales, 1995; Aranburu, 1998; López-Horgue, 2000). García-Mondéjar y Pujalte (1981) describen la sedimentológía del corte del Río Saja al oeste de Torrelavega, diferenciando las distintas unidades litoestratigráficas. Un año después, García-Mondéjar (1982) publica un trabajo de síntesis en el monográfico del Cretácico de España, donde se propone una clasificación litoestratigráfica formal de los materiales aptienses y albienses de la cuenca a partir de las unidades y toponimias de mayor uso en la bibliografía. De este modo, quedan establecidas formalmente algunas de las formaciones más conocidas de la zona de estudio.

Pascal (1985) supone una continuación de la línea de investigación emprendida por Rat (1959), abarcando exclusivamente los materiales del complejo urgoniano. Este autor diferencia cuatro sistemas biosedimentarios en la cuenca Vasco-Cantábrica. Concretamente, en los materiales aflorantes en las zonas de Torrelavega-Reocín y

Cuchía, realiza una breve descripción sedimentológica y aporta datos bioestratigráficos puntuales.

Hines (1985) presenta un estudio general sedimentológico de los materiales mesozoicos y cenozoicos al noroeste de Santander, que incluye dos columnas estratigráficas del Aptiense-Albiense en los afloramientos de Cuchía y de Comillas. La síntesis de Hines destaca por su claridad en la descripción de las unidades y las relaciones entre tectónica y sedimentación. En esta Tesis Doctoral se ha adoptado la terminología utilizada por este autor para la mayor parte de las formaciones litoestratigráficas de edad Aptiense–Albiense.

Robador y colaboradores (1990) realizan una cartografía a escala 1:100.000, publicada por el IGME, de toda la Comunidad Autónoma de Cantabria construida principalmente a partir de las cartografías 1:50.000 del plan MAGNA, pero usando también la información cartográfica contenida en tesis doctorales y trabajos precedentes sobre el macizo Asturiano y la cuenca Vasco-Cantábrica.

En esta última década, Wilmsen (2005) publica un estudio bioestratigráfico y sedimentológico del Aptiense Inferior en el corte de Cuchía apoyándose en los trabajos de Collignon *et al.* (1979) y Pascal (1985).

Finalmente, parte de los resultados de estratigrafía, quimioestratigrafía, bioestratigrafía y sedimentología obtenidos durante la realización de la presente Tesis Doctoral se han publicado previamente: Najarro y Rosales, (2008a, 2008b y 2008c); Najarro *et al.* (2007, 2009, 2010, 2011a, 2011b); Rosales *et al.* (2009).

1.4.2.- TECTÓNICA

Las primeras referencias significativas sobre la estructura tectónica de la zona de estudio se encuentran en las cartografías, dibujos panorámicos y cortes geológicos elaborados por Mengaud (1920), Karrenberg (1934), Lotze, (1945), Rat (1959), Pello, (1967); Ciry *et al.* (1967); Tosal (1968), Feuillée y Rat (1971) y Ramírez del Pozo (1971, 1972).

A mediados de los 70 el conocimiento estructural se acelera con la publicación de las cartografías geológicas a escala 1:50.000 de la serie MAGNA, mostrando los pliegues asociados a cabalgamientos característicos del macizo Asturiano en el área del Nansa, el imbricado del cabalgamiento de Comillas y los pliegues y fallas con elevación diapírica del Keuper que alcanzan gran desarrollo en el área de Santander. Estos mapas van acompañados de cortes geológicos poco profundos y un esquema de dominios estructurales.

Por otra parte, Hines (1985) además de realizar el estudio general sedimentológico de los materiales mesozoicos y terciarios, elabora una síntesis tectónica de la zona de estudio, invocando la tectónica salina sin-extensiva como una de las principales causas de la variación de espesores observada.

La cartografía a escala 1:100.000 de Robador y colaboradores (1990) publicada por el IGME es un mapa de síntesis que representa la estructura varisca y alpina de un área extensa como la Comunidad Autónoma de Cantabria, con un detalle comparable a los mapas 1:50.000 usados primordialmente para su elaboración.

Cámara Rupelo (1989) y Sánchez Ferrer (1991) interpretan la estructura tectónica de la zona, estableciendo un modelo estructural donde cobran gran importancia los despegues del *Keuper* y el desacoplamiento entre las estructuras despegadas suprayacentes y las extensionales infrayacentes.

La estructura de inversión alpina en el macizo Asturiano ha sido estudiada principalmente por el Grupo de Geofísica y Estructura de la Litosfera de la Universidad de Oviedo. Entre los múltiples trabajos publicados cabe destacar los de Martínez García (1981) y Marquínez (1989) donde definen al macizo Asturiano como un imbricado de cabalgamientos verticalizados de orientación E–O vergentes hacia el sur. Asimismo destacan los trabajos de Pulgar y Alonso (1993) y Alonso *et al.* (1996) donde establecen el primer modelo general sobre el significado estructural y el origen del relieve cantábrico en la transversal asturiana, confirmado posteriormente por la sísmica de reflexión profunda a través de la transición entre la Cordillera Cantábrica y la Cuenca del Duero (Pulgar *et al.*, 1996). Asimismo, la Tesis Doctoral de Espina (1997) muestra

la implicación del basamento varisco de la zona más noroccidental de la cuenca Vasco-Cantábria, tanto en los procesos extensivos que controlaron la sedimentación mesozoica, como en las estructuras contractivas generadas durante el acortamiento alpino. Como continuación en esta línea de trabajo, la Tesis Doctoral de Quintana (2012) se centra en la estructura de extensión e inversión tectónica del sector central de la cuenca Vasco-Cantábrica. Por otro lado, a la escala de la cordillera, los perfiles de sísmica de refracción y perfiles profundos de sísmica de reflexión llevados a cabo en el proyecto ESCI-N revelan la subducción parcial de la corteza ibérica hacia el norte, formando una raíz cortical continua en dirección E–O situada bajo los máximos relieves de la cordillera Pirenaico-Cantábrica (Gallástegui, 2000; Pedreira, 2005; Fernández-Viejo y Gallástegui, 2005).

La reconstrucción de la geometría extensiva de ciertos sectores de la cuenca Vasco-Cantábrica ha sido abordada en varias tesis doctorales y numerosos trabajos por un grupo del departamento de Estratigrafía y Paleontología de la Universidad del País Vasco, principalmente a partir de diagramas de correlación estratigráfica que muestran cambios de espesor y de facies de las series cretácicas en relación con flexiones y fallas. De interés para el presente estudio destaca el trabajo de García-Mondéjar y Pujalte (1981) que subdivide el dominio estructural periasturiano en cuatro sectores tectonoestratigráficos; Pujalte (1982) que interpreta la actividad de la falla de Cabuérniga desde el Jurásico Inferior y finalmente García-Mondéjar *et al.* (1996, 2004), que sintetiza la información estructural de las principales fallas sinsedimentarias, pliegues, diapiros y discordancias angulares durante el Aptiense–Albiense de la cuenca Vasco-Cantábrica, proponiendo un contexto tectónico regional de fallas en dirección discutido por Quintana *et al.* (2009a) y Quintana (2012).

Entre los avances recientes sobre la estructura de la zona de estudio destacan los trabajos de Najarro *et al.* (2007, 2009) obtenidos en la elaboración de esta Tesis Doctoral en relación con la tectónica-sedimentación, el de Lopez-Mir y Roca (2008) sobre la estructura de la Banda del Nansa, el de García-Senz y Robador (2009) sobre la relación de la deformación entre el macizo Asturiano y el Bloque Costero de Santander y la conclusión del proyecto de cartografía 1:25.000 de toda la Comunidad de Cantabria (http://mapas.cantabria.es). Finalmente los datos y conclusiones presentados en el

capítulo 2 sobre la tectónica del área de estudio están en curso de presentarse como artículo científico.

1.4.3.- METALOGENIA

Las zonas de La Florida, Reocín, y Novales han sido objeto de importantes explotaciones mineras de Zn (Pb) asociadas a las calizas dolomitizadas del Aptiense Superior. Los principales trabajos que estudian estas mineralizaciones son los de Bustillo y Ordoñez (1980; 1985, 1995), Vadala (1981), Vadala *et al.* (1981), Barbanson *et al.* (1983), Bustillo (1983, 1984, 1985), Saulas *et al.* (1986), Barbanson (1987), Herrero y Velasco (1988), Robador *et al.* (1990); Velasco *et al.* (2003), Grandia *et al.* (2003), Symons *et al.* (2009) entre otros. Recientemente se han publicado varios artículos sobre la petrografía de las dolomías que forman el encajante, entre los que destacan los de Essalhi *et al.* (2009) y López-Cilla *et al.* (2009, 2012, 2013).

1.5.- METODOLOGÍA

La metodología utilizada para alcanzar los objetivos planteados ha sido la propia de la geología sedimentaria y quimioestratigrafía. La descripción detallada de los métodos utilizados se encuentra descrita en los distintos artículos científicos, y se resume siguiendo los pasos que se exponen a continuación agrupados en: trabajo de campo, trabajo de laboratorio y trabajo de gabinete.

Trabajo de Campo:

- Reconocimiento y seguimiento cartográfico de las principales unidades estratigráficas previamente descritas en la bibliografía, comprobando su distribución espacial, cambios laterales de facies y espesores y su validez para los distintos sectores de la zona de estudio, así como método para la localización de nuevas secciones y descripción de unidades inéditas. Para ello se ha partido de trabajos cartográficos previos a escala 1:100.000 (Mapa Geológico de Cantabria, ITGE-Diputación Regional de Cantabria) y 1:50.000 (hojas 33-Comillas, 34-Torrelavega, 57-Cabezón de la Sal, 58-Los Corrales de Buelna del Mapa Geológico de España, serie Magna, IGME) y en la etapa final de esta Tesis se han consultado las recientes cartografías 1:25.000 de Cantabria del IGME-Gobierno de Cantabria. Además se ha utilizado como base de trabajo las ortofotografías aéreas de los vuelos a escala 1:10.000 de los años 2001 y 2004, y la topografía digital restituída a escala 1:5.000 de la Dirección General de Ordenación del Territorio y Urbanismo del Gobierno de Cantabria.
- Simultáneamente al estudio estratigráfico y seguimiento cartográfico de las unidades estratigráficas, se han llevado a cabo labores de prospección paleontológica para la búsqueda de fósiles datadores y de yacimientos fosilíferos. Ésta se ha basado en la observación de la riqueza paleontológica de las diferentes unidades estratigráficas.
- Levantamiento de columnas estratigráficas: se han levantado un total de 15 columnas estratigráficas generales a escala decimétrica y métrica (Figura 1.1), tomando observaciones de litología, espesor, estructuras sedimentarias y contenido paleontológico.

- Estudio centrado en el análisis de facies sedimentarias para la caracterización de ambientes de depósito y de su distribución espacial y temporal.
- Reconocimiento y seguimiento cartográfico de discontinuidades estratigráficas, secuencias de depósito y niveles guía de correlación estratigráfica.
- Reconocimiento de campo de fallas y pliegues sinextensivos y elaboración de cortes de correlación estratigráfica con el fin de reconstruir la cuenca de depósito.
- Muestreos litológicos y palentológicos. Según su finalidad se han realizado 7 tipos de muestreos diferentes: 1) recogida sistemática de muestras de mano de diferentes niveles estratigráficos para la realización de láminas delgadas y su posterior estudio de microfacies y fases diagenéticas; 2) recogida de muestras de marga y caliza a intervalos regulares métricos y decimétricos del intervalo Aptiense Inferior de tres secciones estratigráficas (Río Nansa, Rábago y Cuchía) para su posterior análisis quimioestratigráfico del contenido de carbonato cálcico, carbono orgánico total (TOC), isótopos estables de O y C en la fracción de carbonato ($\delta^{13}C_{carb}$ y $\delta^{18}O_{carb}$) e isótopos estables de C de la fracción de materia orgánica ($\delta^{13}C_{org}$); 3) recogida de muestras de margas a intervalos métricos para el posterior estudio del contenido de microfósiles (foraminíferos planctónicos y nanoplacton calcáreo), 4) recogida de muestras de lutitas y margas de diferentes unidades estratigráficas para su posterior estudio del contenido en palinomorfos; 5) donde ha sido posible, recolección de macrofósiles datadores, principalmente ammonoideos, con fines biostratigráficos; y 6) recolección de muestras de ámbar y restos carbonosos para estudios paleontológicos y biogeoquímicos y de madurez térmica.
- Organización y participación de excavaciones paleontológicas: a raíz del descubrimiento, como resultado de las labores de prospección de esta Tesis Doctoral, del yacimiento de ámbar con contenido fosilífero de El Soplao, se ha participado en las labores de organización y ejecución de 3 campañas de excavaciones paleontológicas en octubre de 2008, marzo de 2009 y julio de 2009. Las muestras más grandes (masas de hasta 30 cm de diámetro) fueron extraídas manualmente, mientras que para la extracción de muestras centimétricas se utilizó una retro-excavadora y un sistema de lavado y tamizado

del sedimento con agua a presión y ayuda de pequeñas hormigoneras, para separar el ámbar del sedimento por flotación. Con este procedimiento se recogieron varias decenas de kilos de fragmentos variados y grandes masas de ámbar y restos vegetales que han proporcionado una nutrida colección de muestras que dieron lugar a la exposición itinerante "El largo viaje del ámbar de El Soplao" organizada por el Gobierno de Cantabria, y cuyas bioinclusiones están siendo fruto de intensa investigación específica por especialistas paleoentomólogos fuera del ámbito de esta Tesis.

Trabajo de laboratorio:

Se han realizado métodos de estudio petrográfico, metódos analíticos y métodos de estudio paleontológico:

a) Métodos de estudio petrográfico:

- Estudio petrográfico bajo microscopio de luz reflejada y transmitida: se han estudiado más de 250 láminas delgadas pulidas bajo microscopio petrográfico para el estudio de microfacies (composición, textura y contenido fosilífero) y diagenético de las muestras de mano recogidas. Las láminas delgadas han sido realizadas en el Área de Laboratorios y Servicios del Instituto Geológico y Minero de España. Para el estudio petrográfico se ha utilizado un microscopio *Nikon Eclipse LV 100Pol*. El análisis petrográfico mediante microscopía de luz reflejada y de luz ultravioleta, se ha realizado con el mismo equipo al que se le acopló una lámpara *Power supply Nikon UN2-PSE100* mediante un adaptador *TE-AT Double Lamphouse*, y una fuente de luz *Super high pressure mercury lamp power Nikon C- SHG1*. Para la caracterización de las microfacies de rocas carbonatadas se ha seguido la clasificación textural de Dunham (1962) con las modificaciones de Embry y Klovan (1971).
- Análisis de láminas delgadas mediante microscopía de catodoluminiscencia (CL). El equipo empleado ha sido un microscopio *Nikon Eclipse E400 Pol* acoplado a una unidad *Technosyn Cold Cathodoluminescence CL8200 MK5* y a una bomba de vacío *Alcatel Pascal 2005 SD*. Los análisis se realizaron a 13 Kv, con corriente entre 400 y 500 μA y con una presión de vacío de

aproximadamente 0,005 Torr. El estudio se realizó en varias láminas delgadas seleccionadas entre las previamente estudiadas mediante métodos de análisis petrográfico. Su principal objetivo fue el estudio y caracterización de diferentes fases de disolución y precipitación de cementos, ayudando a establecer la historia diagenética temprana y a reconocer etapas de exposición subaérea para la caracterización de límites de secuencia. En ambos microscopios se tomaron imágenes fotomicrográficas con una cámara digital *Nikon Digital Sight DS-5m* y una pantalla *Nikon Digital Sight DS-L1*.

b) Métodos analíticos:

- Recolección de micromuestras para análisis geoquímicos mediante un microtaladro de dentista equipado con fresas de carburo de tungsteno, acoplado a una lupa binocular *Nikon SM7 1500*. Se extrajeron aproximadamente 50 mg por muestra.
- Molienda de muestras de marga de mayor tamaño para análisis geoquímicos mediante un molino de bolas.
- Los análisis de isótopos estables de C y O ($\delta^{13}C$ y $\delta^{18}O$) del carbonato fueron realizados en el Servicio General de Isótopos Estables de la Universidad de Salamanca, mediante un espectrómetro de masas de fuente gaseosa, modelo *SIRA-II*, equipado con un sistema automático "ISOCARB". Para recoger el CO_2, las muestras fueron atacadas con ácido ortofosfórico al 100% (H3PO4) siguiendo el método convencional de digestion de McCrea (1950). Los resultados se expresan usando la anotación usual δ, en ‰ en relación al estándar Viena Pee Dee Belemnite (V-PDB). La precisión derivada de múltiples análisis del estándar internacional NBS-19 (National Bureau of Standards; $\delta^{13}C$ = 1,95‰ y $\delta^{18}O$ = –2,20‰) fue de 0,01‰ para el $\delta^{13}C$ y 0,05‰ para el $\delta^{18}O$.
- Los análisis de isótopos estables de C ($\delta^{13}C_{org}$) de la materia orgánica contenida en las mismas muestras se realizaron en el Laboratorio de Isótopos Estables de la Universidad de East Anglia (GB). Para este estudio, la fracción carbonatada de las muestras fue removida previamente mediante digestión ácida repetida en una solución al 10% de ácido hidroclórico. Una vez lavados los residuos con agua destilada se secaron en un horno a 50–80ºC y se analizaron con un equipo

Finnigan Delta Plus XP en línea con un analizador elemental *Costech*. Para calibrar el equipo se utilizó un estándar interno con una precisión de 0,1‰ (n=12).

- Los análisis de contenido total de carbono orgánico (TOC) y carbonato cálcico ($CaCO_3$) se han determinado en los Servicios de Arsidad de La Coruña, mediante el uso de un analizador *Carbo Erba EA1108*.

- Estudio bioquímico comparativo de muestras de ámbar y restos vegetales en colaboración con el Dr. Cesar Menor-Salván (Centro de Astrobiología, CSIC-INTA). El estudio se llevó a cabo mediante la extracción durante 8 horas con un solvente orgánico (CH_2Cl_2:CH_3OH, 3:1) de 150 gramos de ámbar especialmente seleccionado por su homogeneidad y ausencia de inclusiones. El extracto orgánico se sometió a un fraccionamiento por cromatografía flash utilizando columnas de sílice polares, separándose cuatro fracciones mediante elución secuencial con n-hexano, n- hexano:diclorometano (3:1), diclorometano y metanol. Las dos primeras (A y B) contienen hidrocarburos saturados y aromáticos. La tercera (C) es una fracción polar formada por terpenoides fenólicos. La cuarta (D) contiene los terpenoides ácidos. Las fracciones C y D se derivaron por sililación con N, O-bis-(trimetilsilil) trifluoroacetamida conteniendo 1% de trimetilclorosilano. Los trimetilsilil esteres resultantes se analizaron mediante cromatografía de gases acoplada a espectrometría de masas (GC-MS) en las mismas condiciones. En paralelo se lleva a cabo el análisis de la fracción orgánica extraíble de hojas fósiles, especialmente de *Frenelopsis sp.,* conífera mayoritaria en el depósito de El Soplao y de azabache del yacimiento. En base a este método se han estudiado los terpenoides y otros biomarcadores específicos retenidos en las muestras. Dado que estas moléculas específicas son características de cada taxón biológico (quimiotaxonomía), el estudio ha permitiendo estimar su origen botánico mediante la comparación de los biomarcadores retenidos en el ámbar y en los otros restos vegetales fósiles.

- Estudio biogeoquímico de muestras de marga del Aptiense Inferior del área de estudio, llevado a cabo en colaboración con los Drs. María Luisa Quijano (Dpto. de Química Inorgánica y Orgánica) y José Manuel Castro (Dpto. de Geología) de la Universidad de Jaén, con el fin de caracterizar la naturaleza de la materia orgánica y realizar un estudio preliminar de su composición

molecular (biomarcadores). Para ello se ha realizado un proceso de extracción de la materia orgánica mediante una mezcla de diclorometano-metanol (80:20) durante 48 horas en un *Soxhlet*. El extracto obtenido se ha analizado mediante cromatografía de gases-espectrometría de masas (CG-MS) utilizando un cromatógrafo de gas *Thermo DSQ II* conectado a un espectrómetro de masas *Thermo Trace Ultra* en el Centro de Instrumentación Científica de la Universidad de Jaén. Los extractos se separaron en tres fracciones mediante columnas de sílice: hidrocarburos saturados, compuestos aromáticos y compuestos polares. Los biomarcadores de cada fracción fueron identificados por comparación de tiempos de retención y espectros de masas en bases de datos de compuestos bioquímicos.

c) Métodos de estudio paleontológico:

- Estudio y determinación de asociaciones de ammonites del Aptiense en colaboración con los Drs. Josep Anton Moreno-Bedmar (Universidad de Barcelona, actualmente en la Universidad Nacional Autónoma de México) y Dr. Miquel Company (Universidad de Granada). La colección de ammonites recolectados y determinados está actualmente depositada en las Colecciones de Paleontología de la Universidad Autónoma de Barcelona (PUAB) y en el Museo Geominero (IGME) de Madrid. Para este estudio se revisaron además algunos especímenes adicionales procedentes de las unidades estudiadas y pertenecientes al Museo Geológico del Seminario de Barcelona (MGSB) y a una colección particular (Manuel Díaz, Cantabria). Las muestras más representativas de ammonoideos se han fotografiado digitalmente, para lo cual se ha procedido a blanquearlas previamente con óxido de manganeso para acentuar el contraste de la ornamentación.
- Estudio y determinación de asociaciones de foraminíferos planctónicos y nanofósiles calcáreos de materiales del Aptiense Inferior en colaboración con el Dr. Gines de Gea (Universidad de Jaén). Las asociaciones de foraminíferos planctónicos se estudiaron a partir de 40 muestras de marga tomadas sistemáticamente a intervalos de 1 metro a lo largo de una sección (sección de Cuchía). En el resto de las secciones, los foraminíferos planctónicos fueron escasos o estaban muy mal preservados. Posteriormente las muestras fueron

disgregadas, lavadas y tamizadas en tres fracciones (> 200μm, 100-200 μm, 50-100 μm). Los foraminíferos obtenidos se determinaron mediante microscopio óptico y microscopio electrónico de barrido (SEM). Para el estudio de asociaciones de nanoplancton calcáreo se procesaron 55 muestras de margas procedentes de dos secciones (Cuchía y Río Nansa) mediante técnicas estándar y se estudiaron mediante microscopio de luz polarizada usando un aumento de 1250x. Para la determinación de biozonas y límites de zonas se usaron los eventos bioestratigráficos citados en Applegate y Bergen (1988) y en Aguado *et al.* (1999).

- Determinación de asociaciones de foraminíferos bentónicos en lámina delgada de materiales del Aptiense, en colaboración con los Drs. José Manuel Castro (Universidad de Jaén), Idoia Rosales (IGME) y Felix Schlagintweit (Universidad de Munich).

- Estudio y determinación de asociaciones de palinomorfos en materiales del Aptiense y Albiense en colaboración con el Dr. Eduardo Barrón (IGME). Para este estudio se han procesado y analizado un total de 20 muestras de diferentes unidades estratigráficas del Aptiense y Albiense. Las muestras fueron procesadas y preparadas bajo petición en el laboratorio ALICONTROL (Madrid) siguiendo la técnica de preparación palinológica estándar descrita en Batten (1999) que consiste en un ataque ácido con HCl, HF y HNO_3 a temperatura alta. A continuación se concentra y tamiza el residuo a través de matices con diferentes diámetros de malla y se montan las muestras en glicerina sobre soportes de cristal. Las muestras se estudiaron con un microscopio *Olympus BX51*. No todas las preparaciones de muestras dieron asociaciones bien preservadas e incluso algunas fueron estériles.

- Estudio del contenido de bioinclusiones fósiles en ámbar (principalmente artrópodos) en colaboración con el Dr. Enrique Peñalver (IGME), y el grupo del Dr. Xavier Delclòs (Universidad de Barcelona).

- Estudio taxonómico de macro restos paleobotánicos de las unidades ambarígenas en colaboración con los Drs. Bernard Gomez y Véronique Daviero-Gomez (Universidad de Lión).

Trabajo de Gabinete:

- Recopilación bibliográfica regional del Cretácico Inferior del sector noroccidental de la cuenca Vasco-Cantábrica y específica relativa a los diferentes temas de estudio tratados en la Tesis.
- Elaboración de columnas estratigráficas y cortes de correlación a partir de los datos de campo. Toda la información generada ha sido informatizada y redibujada con el programa gráfico *Corel Draw*.
- El contorneo de isopacas limitadas por fallas se ha realizado con los programas *GeoCap* y *3DField*.
- Elaboración de cortes estratigráficos con el programa *Move* (*Midland valley*).
- Los datos analíticos geoquímicos han sido tratados y representados gráficamente en la hoja de cálculo *Microsoft Excel*.
- Preparación de resultados y redacción de trabajos para su publicación y presentación en reuniones científicas.

1.6.- REFERENCIAS

Agirrezabala, L.M. (1996). El Aptiense-Albiense del Anticlinorio Nor-Vizcaíno entre Gernika y Azpitia. Tesis Doctoral, Universidad del País Vasco, 429 p.

Aguado, R., Castro, J.M., Company, M. & Gea de, G.A. (1999). Aptian bio-events –an integrated biostratigraphic analysis of the Almadich Formation, Inner Prebetic Domain, SE Spain. Cretaceous Research v. 20, p. 663-683.

Aguilar Tomás, M.J. (1970). Sedimentología y Paleogeografía del Albense de la Cuenca Cantábrica. Tesis Doctoral, Facultad de Ciencias, Universidad de Barcelona.

Alonso, J.L., Pulgar, J.A., García Ramos, J.C. & Barba, P. (1996). Tertiary basins and Alpine tectonics in the Cantabrian Mountains (NW Spain). En: P.F. Friend & C.J. Dabrio (ed.), Tertiary basins of Spain The stratigraphic records of crustal kinematics, Cambrige Univerity Press, Cambridge, p. 214-227.

Alonso, J.L., Pulgar, J.A. & Pedreira, D. (2007). El relieve de la Cordillera Cantábrica. Enseñanza de las Ciencias de la Tierra, v.15, n.2, p. 151-163.

Aranburu, A. (1998). El Aptiense-Albiense de Trucíos-Güeñes (oeste de Vizcaya). Tesis Doctoral, Universidad del País Vasco, 606 p.

Applegate, J.L. & Bergen, J.A. (1988). Cretaceous calcareous nannofossil biostratigraphy of sediments recovered from the Galicia Margin, ODP leg 103. En: G. Boillot, E.L. Winterer, et al. (ed.), Proceedings of the Ocean Drilling Program, Scientific Results v. 103, p. 293-348.

Barbanson, L. (1987). Les mineralizations Zn-Pb-Ba-Hg-Cu de socle et couverture carbonatés de la province de Santander (Nord de l'Espagne). Tesis Doctoral. Universidad de Orleans, 291 pp.

Barbason, L., TourayJ.C., Saulas, D. & Vadala, D. (1983). Distribution a differentes echelles et chronologie relative des carbonates de l'Aptien de la province de Santander: relation entre aureole ferrifere et mineralisations Zn-Pb dyu type Reocín. Chronique de la Recherche Miniere, v. 51 (473), p. 39-48.

Barnolas, A. & Pujalte, V. (2004). La Cordillera Pirenaica: Definición límites y división. En: Geología de España (J.A. Vera, ed.), SGE-IGME, p. 233-2241.

Batten, D.J. (1999). Chapter 20E. Upper Jurassic and Cretaceous Miospores. En: Palynology: Principles and Applications (Eds. J. Jansonius and D.C. McGregor).

American Association of Stratigraphic Palynologists Foundation, Salt Lake City, v. 2, p. 807–830.

Boillot, G. (1984). Some remarks on the continental margins in the Aquitaine and French pyrinees. Geological Magazine, v. 121, p. 407-412.

Boillot, G. (1986). Comparison between the Galicia and Aquitaine and French Pyrenees. Geological Magazine, v. 121, p. 407-412.

Boillot, G., Auxietre, J.L., Dunand, J.P., Dupeuble, P.A. & Mauffret, A. (1979). The northwestrn Iberian margin a Cretaceous passive margin deformed during Eocene. Maurice Ewing Ser. Am. Geophys. Union, v. 3, p. 138-153.

Boillot, G. & Capdevilla, R. (1977). The pyrénées: Subduction and Collision?. Earth and planetary Science Letters, v. 95, p. 151-160.

Biollot, G. & Malod, J. (1988). The north and northwest Spanish continental margin a review. Revista de la Sociedad Geologica de España, v. 1 (3-4), p. 296-316.

Burla, S., Heimhofer, U., Hochuli, P.A., Weissert, H. & Skelton, P. (2008). Changes in sedimentary patterns of coastal and deep-sea successions from the North Atlantic (Portugal) linked to Early Cretaceous environmental change. Palaeogeography, Palaeoclimatology, Palaeoecology, v. 257 (1-2), p. 38-57.

Bustillo, M. (1983). Breve síntesis delas texturas presentes en las mineralizaciones de Zn-(Pb) del yacimiento de Reocín (Cantabria). Revista de Materiales y Procesos Geológicos, v.1, p. 329-330.

Bustillo, M. (1984). Estudio petrológico y geoquímico de la smineralizaciones de Zn-Pb del Cretácico Inferior (Aptiense) de Cantabria (zona oeste). Tesis Doctral. Universidad Complutense de Madrid, 403 pp.

Bustillo, M. (1985). Contribución al conocimiento de las mineralizaciones Pb-Zn del tipo reocín en el sector oeste de Cantabria. Estudios Geológicos, v. 41, p. 127-138.

Bustillo, M. & Ordoñez, S. (1980). Posible origen diagenético de los sulfuros sedimentarios en facies carbonáticas (provincia metaogénetica de Cantabria). Revista del Instituto de Investigaciones Geológicas (Universidad de Barcelona), v. 34, p. 339-349.

Bustillo, M. & Ordoñez, S. (1985). Los yacimientos Pb-Zn del tipo Reocín en el sector oeste de Cantabria. Estudio comparativo y aspectos genéticos. Boletín del ITGE, v. XCVI-VI, p. 626-631.

Bustillo, M. & Ordoñez, S. (1995). Lower Cretaceous Pb-Zn ores of Cantabria, northern Spain. Transactions of the Institution of Mining and Metallurgy Section B. Applied Earth Sciences, v. 104, p. 55-65.

Cámara Rupelo, P. (1989). La terminación estructural occidental de la Cuenca Vasco-Cantábrica. Libro Homenaje a Rafael Soler. AGGEP, Madrid, p. 27-35.

Carez, L. (1881). Etude des terrains cretaces et Tertiares du Nord de l´Spagne. Tesis Doctoral. Paris, Francia, 323 pp.

Carreras, F.J., Aguilar, M.J., Ramírez del Pozo, J., Giannini, G. & Pujalte, V. (1978). Hoja geológica número 57. Cabezón de la Sal. Mapa geológico de España, escala 1:50.000, Serie MAGNA, IGME.

Carreras, F.J., del Olmo, P., Portero García, J.M., Ramírez del Pozo, J., Giannini, G. & Aguilar, M.J. (1979). Hoja geológica número 58. Los Corrales de Buelna. Mapa geológico de España, escala 1:50.000, Serie MAGNA, IGME.

Choukroune, P. & Mattauer (1978). Tectonique des plaques et Pyrénées: sur le fonctionnrmrnt de la faille transformante nord-pyrénéenne: comparisons avec des modèles actuels. Bull. Soc. Geol. France, v. 5, p 689-700.

Ciry, R. (1940). Etude géologique d'une partie des provinces de Burgos, Palencia, León et Santander. Thèse Fac. Sci. Paris, Bzrll. Soc. Ilist. Snt. Toulouse, T. 74.

Ciry, R., Rat, P., Mangin, J.P., Feuillee, P., Amiot, M., Colchen, M. & Delance J.H. (1967). Reunion Extroardinaire de la Societé Géologique de la France en Espagne, des Pyrinées aux Asturies. Compte Rendu Sommaire des Séances de la Societé Géologique de la France, v. 9, p. 389-444.

Coffin, M. F. & Eldhom, O. (1994). Large igneous provinces:crustal structures, dimensions and external consequences. Rev. Geophys, v. 32, p. 1-36.

Collignon, M., Pascal., A., Peybernès, B. & Rey J. (1979). Faunes d'ammonites de l'aptien de la Région de Santander (Espagne). Annales de Paléontologie, v. 65, fasc. 2, p. 139-156.

Dunham, J. (1962). Classication of carbonate rocks according to depositional texture. En: W.E. Ham (ed.), Classification of carbonate rocks. Am. Ass. Petrol. Geol. Mem., 1, p. 108-121.

Dumitrescu, M., Brassell, S.C., Schouten, S., Hopmans, E.C. & Damsté, J.S.S. (2006). Instability in tropical Pacific sea-surface temperatures during the Early Aptian. Geology v. 34, p. 833-836.

Embry, A.F. & Klovan, J.E. (1971). A Late Devonian reef tract on northeastern Banks Island, Northwest Territories. Bull. Can. Pet. Geol, v. 33, 730–781

Erba, E. (1994). Nannofossils and 'superplumes': the Early Aptian Nannoconid crisis. Paleoceanography, v. 3, p. 483-501.

Espina, R.G. (1994). Extensión mesozoica y acortamiento alpino en el borde occidental de la Cuenca Vasco Cantábrica. Cuadreno Lab. Xeolóxico de Laxe, v. 19, p. 137-150.

Espina, R.G. (1996). Tectónica extensional en el borde ocidental de la Cuenca Vasco-Cantábrica (Cordillera Cantábrica, NO de España). Geogaceta, v, 20 (4), p. 890-892.

Espina, R.G. (1997). La estructura y evolución tectonoestratigráfica del borde occidental de la Cuenca Vasco-Cantábrica (Cordillera Cantábrica, NO de España). Tesis Doctoral. Universidad de Oviedo. 230 p.

Essalhi, M., Sizaret, S., Barbason, L., Chen, Y., Branquet, Y., Panis, D., camps, P., Rochette, P. & Canals, A. (2009). Track of fluid paleocirculation in dolomite host rocks at regional scale by the anisotropy of magnetic susceptibility (AMS): an example from Aptian carbonates of La Florida, northern Spain. Earth and Planetary Sciences Letters, v. 277 (3-4), p. 501-513.

Fernández-Mendiola, P.A. (1986). El complejo urgoniano en el sector oriental del Anticlinorio de Bilbao. Tesis Doctoral, Universidad del País Vasco, 421 p.

Fernández-Viejo, G. & Gallástegui. J. (2005).The ESCI-N Project after a decade: a synthesis of the results and open questions. Trabajos de Geología, Univ. Oviedo, v. 25, p. 9-25.

Feuillée, P. & Rat, P. (1971). Structures et paléogéographies Pyrénéo-Cantabriques. En: Histoire Structurale du Golfe de Gascogne. Publication de l'Institute Français du Pétrole. Collection Colloque et Séminaires, ed. Technip, Paris, v. 22, p. 1-1 v. 1-48.

Floquet, M. & Rat, P. (1975). Un example de interrelation entre socle, paléogéographie et structures dans l'arc pyrénéen basque: La Sierra de Aralar. Rev. Geogr. Phys. Géol. Dyn., v. 17, p. 497-512.

Föllmi K.B., Godet, A., Bodin, S. & Linder, P. (2006). Interactions between environmental change and shallow water carbonate buildup along the northern Tethyan margin and their impact of the early Cretaceous carbon isotope record. Paleoceanography, v. 21, p. 4211-4226.

Föllmi, K.B., Weissert, H., Bisping, M. & Funk, H. (1994). Phosphogenesis, carbon-isotope stratigraphy and carbonate platform evolution along the Lower Cretaceous northern Tethyan margin. Geological Society of American Bulletin, v. 106 (6), p. 729-74.

Gallástegui, J. (2000). Estructura cortical de la cordillera y margen continental cantábricos.: Perfiles ESCI-N. Trabajos de Geología, Univ. Oviedo, v. 22, p. 9-234.

Garcia-Garmilla, F. (1987). Las formaciones terrígenas del weladense y del Aptiense Inferior en los anticlinorios de Bilbao y Ventoso (Bizcaia, Cantabria): Estratigrafía y sedimentación. Tesis Doctoral, Universidad del País Vasco. 340 pp.

García-Mondéjar, J. (1979a). Nueva interpretación estratigráfica de del Complejo Urgoniano en el área SW de la región Vasco-Cantábrica. Acta Geológica Hispánica, v. 4, p. 223-228.

García-Mondéjar, J. (1979b). "El Complejo Urgoniano del Sur de Santander". Ann. Arbor Michigan University Microfilms Intemational, 1980. 673 p.

García-Mondéjar, J. (1982). Aptiense y Albiense. Región Vasco-Cantábrica y Pirineo navarro. En: A. García (ed.), El Cretácico de España. Madrid, Universidad Complutense, p. 63-76.

García-Mondéjar, J. (1989). Strike-slip subsidence of the Basque-Cantabrian basin of northern Spain and its relationship to Aptian-Albian opening of Bay of Biscay. En: A.J. Tankard & H.R. Balkwill (ed.), Extensional tectonics and Stratigraphy of the north Atlantic Margins. Mem. Am. Ass. Petrol. Geol, v. 46. pp. 395-409.

García-Mondéjar, J. (1990). The Aptian-Albian carbonate episode of the Basque-Cantabrian Basin (northern Spain): general characteristics, controls and evolution. En: M.E. Tucker, J.L. Wilson, P.D. Crevello, J.F. Sarg & J.F. Read (ed.), Carbonate Platforms: Facies, Sequences and Evolution. Blackwell, IAS, Sp. Publ., v.9, p. 257-290.

García-Mondéjar, J. (1996). Plate reconstruction of the Bay of Biscay. Geology, v. 24, n. 7, p. 635-638.

García-Mondéjar, J., Agirrezabala, L.M., Aranburu, A., Fernández-Mendiola, P.A., Gómez-Pérez, I., López-Horgue, M. & Rosales, I. (1996). Aptian–Albian tectonic pattern of the Basque-Cantabrian Basin (northern Spain). Geological Journal, v. 31, p. 13-45.

García-Mondéjar, J., Fernández-Mendiola, P.A., Agirrezabala, L.M., Aramburu, A., López-Horgue, M.A., Iriarte, E. & Martinez de Rituerto, S. (2004). El Aptiense-Albiense de la Cuenca Vasco-Cantábrica. En: Geología de Espa.a (J.A. Vera, ed.), SGE-IGME, p. 291-296.

García-Mondéjar, J. & Pujalte, V. (1981). El Jurásico Superior y el Cretácico Inferior de la región Vasco-Cantábrica (parte occidental). Libro de guía de jornadas de campo, 9-12 septiembre 1982. Grupo español del Mesozoico. P.I.G.C. Mid Cretaceous Events. Dpto. de Geología, 133 pp.

García-Senz, J. & Cañas Pernández, V. (2013a). Hoja del Mapa Geológico 1:25.000 de la Comunidad Autónoma de Cantabria, nº 33-3 San Vicente de La Barquera. IGME y Gobierno de Cantabria.

García-Senz, J. & Cañas Pernández, V. (2013b). Hoja del Mapa Geológico 1:25.000 de la Comunidad Autónoma de Cantabria, nº 33-4 Comillas. IGME y Gobierno de Cantabria.

García-Senz, J. & Merino-Tomé, O. (2011). Hoja del Mapa Geológico 1:25.000 de la Comunidad Autónoma de Cantabria, nº 51-1 Puentenansa. IGME y Gobierno de Cantabria.

García-Senz, J. & Robador, A. (2009). Variation in structural style at a lateral termination of a basement-involved wedge: the margin of the West Cantabrian basin. 6º Simposio sobre el Margen Ibérico Atlántico, Oviedo, España, p. 61-64.

Gómez-Pérez, I. (1994). El modelo de la plataforma carbonatada-cuenca de Goebea (Aptiense Superior-Albiense). Tesis Doctoral, Universidad del País Vasco, 443 pp.

Gräfe, K.U. (1994). Sequence stratigraphy in the Cretaceous and Paleogene (Aptian to Eocene) of the Basque-Cantabrian Basin (N Spain). Tübinger Geowiss. Arb., v. 18, 418 p.

Grandia, F., Canals, A., Cardellach, E., Banks, D.A. & Perona, J. (2003). Origing of ore-forming brines in sediment hosted Zn-Pb deposits if the Basque-Cantabrian Basin, Northern Spain. Economy Geology, v. 98, p. 1397-1411.

Grimaud, S., Boillot, G., Collette, B.J., Mauffret, A., Miles, P.R. & Roberts, D.B. (1982). Western extensión of the Iberian-European plate Boundary during the Early Cenozoic (Pyrenean) convergence: a new model. Marine Geology, v. 45, p. 63-77.

Haq, B.U., Hardenbol, J. & Vail, P.R. (1988). Mesozoic and Cenozoic chronostratigraphy and cycles of sea-level change. En: C.K. Wilgus, B.S. Hastings, C.G.St.C. Kendall, H.W. Posamentier, C.A. Ross & J.C. Van Wagoner (ed), Sea-level Changes: An Integrated Approach. S.E.P.M. Special publication. n. 42, p. 71−108.

Herrero, J.M. & Velasco, F. (1988). Tipología de los yacimientos de Fe y Pb-Zn-F (Ba) de la Cuenca cretácica Vasco-Cantábrica. Bol. Soc. Española de Mineraloga, v. 11, p. 176-178.

Hines, F.M. (1985). Sedimentation and tectonics in north-west Santander. En: M.D. Milá & J. Rosell (ed.), 6th European Regional Meeting, Excursion Guidebook, International Association of Sedimentologists, p. 371−398.

Huerta Carmona, (2009). Hoja del Mapa Geológico 1:25.000 de la Comunidad Autónoma de Cantabria, nº 57-2 Cabezón de la Sal. IGME y Gobierno de Cantabria.

Iriarte, E. (2004). La depresión intermedia entre Leitza y Elizondo (Pirineos occidentales): esratirafía y relaciones tectónica-sedimentación durante el Cretácico. Tesis Doctoral. Universidad del País Vasco. pp. 310.

Jenkyns, H.C. (2003). Evidence for rapid climate change in the Mesozoic-Palaeogene greenhouse world. The Royal Society of London, v. 361, p. 1885–1961.

Karrenberg, H. (1934). Die postvariche entwicklung des Cantabro-Asturiche gebirees (Nordwestpanien). Publ. Extr. Geol. España (CSIC), v. 3, p. 103-225.

Larson, R.L. & Erba, E. (1999). Onset of the Mid-Cretaceous greenhouse in the Barremian–Aptian: igneous events and the biological, sedimentary and geochemical response. Paleoceonography, v. 14 (6), p. 663-678.

Larrondo Echevarria, E., Mediato Arribas, F.F. & Hernainz Huerta, P.P. (2008). Hoja del Mapa Geológico 1:25.000 de la Comunidad Autónoma de Cantabria, nº 34-4 Renedo. IGME y Gobierno de Cantabria.

Le Pichon, X., Bonnin, J., Francheteau, J. & Sibuet, J.C. (1971). Une hypothèse d'evolution tectonique du Golfe de Gascogne. En: J. Debycer, X. Le Pichon & L. Montardet (ed.), Histoire structurale du Golfe de Gascogne. Technip, Paris, v. 2, p. 11.1-11.44.

López-Cilla, I., Rosales, I., Gasparrini, M. & Martín-Chivelet, J. (22013). Diagenesis of Lower Cretaceous platform carbonates from the northwestern margin of the

Basque Cantabrian basin (northern Spain). 30th IAS Meeting of Sedimentology, Conference Abstracts Volume, Manchester, UK.

López-Cilla, I., Rosales, I., & Najarro, M. (2012). Diagenesis in Lower Cretaceous platform carbonates of northern Spain (NW Cantabria): An example of multistage dolomitization and calcite cementation. GEOFLUIDS VII-International Conference, 6-8 Junio, Proceedings of Geofluids VII, IFP Energies Nouvelles, Rueil-Malmaison (Francia). Extended abstracts book, pp. 205-208.

López-Cilla, I., Rosales, I., Najarro, M., Martín-Chivelet, J. Velasco, F. & Tornos, F. (2009). Etapas de formación de dolomías masivas del entorno de La Florida-El Soplao, Cantabria. Geogaceta, v. 47, p. 65-68.

López-Mir, B. & Roca, E. (2008). Estructura geológica de las secuencias cretácico-cenozoicas en el extremo noroccidental de la Cuenca Vasco-Cantábrica (Pirineos Occidentales). GeoTemas, v. 10, pp. 152.

López-Horgue, M.A. (2000). El Aptiense-Albiense de Karrantza-Lanestosa (Vizcaya y Cantabria). Tesis Doctoral, Universidad del País Vasco, 264 p.

Lotze, F. (1945). Zur gliederung der Varisziden der Iberichen Mesetas. Geot. Fors., v. 6, p. 78-92.

Maestre, A. (1864). Descripción física y geológica de la provincia de Santander. Junta General de Estadística. Madrid, 120 pp.

Marquínez, J. (1989). Síntesis cartográfica de la Región del Cuera y Los Picos de Europa. Trabajos de Geología, Universidad de Oviedo, v.18, p, 137-144.

Martín-Chivelet, J., Berasategui, X., Rosales, I., Vilas, L., Vera, J.A., Caus, E., Gráfe, K.U., Mas, R., Puig, C., Segura, M., Robles, S., Floquet, M., Quesada, S., Ruiz-Ortiz, P.A., Frenegal-Martínez, M.A., Salas, R., García, A., Martín-Algarra, A., Arias, C. & Mathey, B. (2002). El Cretácico Superior del Arco Vasco. En: A. García (ed.), El Cretácico de España. Universidad Complutense, Madrid, p. 111-136.

Martínez-García, E. (1980). Hoja geológica número 32. Llanes. Mapa geológico de España, escala 1:50.000, Serie MAGNA, IGME.

Martínez-García, E. (1981). El Paleozoico en la Zona Cantábrica Oriental (NW de España). Trabajos de Geología, Universidad de Oviedo, v. 11, p. 95-127.

Mathey, B. (1982). El Cretácico Superior del Arco Vasco. En: A. García (ed.), El Cretácico de España. Madrid, Universidad Complutense, p. 111-136.

Mathey, B. (1986). Les flychs du Crétace supérieur des pyrénées Basques. Tesis Doctoral. Universidad de Bourgogne, 403 pp.

Menegatti, A.P., Weissert, H., Brown, R.S., Tyson, R.V., Farimond, P., Strasser, A. & Caron, M. (1998). High-resolution $\delta^{13}C$ stratigraphy through the Early Aptian 'Livello Selli' of the Alpine Tethys. Paleoceonography, v.13, p. 530-545.

Menguad, L. (1920). Recherches geologiques Dans la region Cantabrique. Livr. Sc. J. Hermann, 1374 pp.

Millán, M.I. (2009). Palaeoceanographic changes record during the Early Aptian of Aralar (N Spain). Tesis Doctoral. Universidad del Pais Vasco. pp. 157.

Montardet, L., Roberts, D.G., De Charpal, O. & Guennoc, P. (1979). Rifting and subsidence of the northern continental margin of the Bay of Byscay. En: Initial Reports of the Deep Sea Drilling Project, v. 48, Washington, D.C., U.S. Government printing Office, p. 1025-1059.

Najarro, M., Peñalver, E., Rosales, I., Pérez-de la Fuente, R., Daviero-Gomez, V., Gomez, B. & Delclòs, X. (2009). Unusual concentration of Early Albian arthropod-bearing amber in the Basque-Cantabrian Basin (El Soplao, Cantabria, Northern Spain): Palaeoenvironmental and palaeobiological implications. Geologica Acta, v. 7 (3), p. 363-387.

Najarro, M., Peñalver, E., Pérez-de La Fuente, R., Ortega-Blanco, J., Menor-Salván, C., Barrón, E., Soriano, C., Rosales, I., López del Valle, R., Velasco, F., Tornos, F., Daviero-Gomez, V., Gomez, B. & Delclòs, X. (2010). Review of the El Soplao amber outcrop, Early Cretaceous of Cantabria, Spain. Acta Geologica Sinica (English Edition), v. 84, p. 801-818.

Najarro, M. & Rosales, I. (2008a). Disoluciones e Incrustaciones Ferruginosas asociadas al OAE 1a en la plataforma carbonatada de La Florida. Geogaceta, v. 44, p. 199-202.

Najarro, M. & Rosales, I. (2008b). Evidencias sedimentológica, diagenética y quimioestratigráfica del Evento Anóxico Oceánico del Aptiense Inferior (OAE 1a) en la plataforma carbonatada de La Florida (NO de Cantabria). Geotemas, v. 10, p. 163-166.

Najarro, M. & Rosales, I. (2008c). Facies evolution, diagenesis and isotope analyses in a carbonate platform related to the Lower Cretaceous Anoxic Event 1a. Abstract

Volume of the 26th Regional meeting of the International Association of Sedimentologists, Bochum, Germany, p. 194.

Najarro, M., Rosales, I. & Martín-Chivelet, J. (2007). Evolución de la plataforma carbonatada de la Florida durante el rifting del Cretácico Inferior (Aptiense, NO de Cantabria).En: D.D. Bermudez, M. Najarro & C. Quesada (ed.), II Semana de Jóvenes Investigadores del I.G.M.E., Instituto Geologico y Minero de España, Madrid, p. 123-128.

Najarro, M., Rosales, I., Moreno-Bedmar, J.A., de Gea, G.A., Barrón, E., Miquel Company, M., & Delanoy, G. (2011a). High-resolution chemo- and biostratigraphic records of the Early Aptian Oceanic Anoxic Event in Cantabria (N Spain): Palaeoceanographic and palaeoclimatic implications. Palaeogeography, Palaeoclimatology, Palaeoecology, v. 299, p. 137–158.

Najarro, M., Rosales, I. & Martín-Chivelet, J. (2011b). Major palaeoenvironmental perturbation in an Early Aptian carbonate platform: Prelude of the Oceanic Anoxic Event 1a? Sedimentary Geology, v. 235, p. 50–71.

Olivet, J.L. (1978). Noveau modèle d'évolution de l'Atlantique nord et central. Thèse. Univ. P. et M. Curie, 234 pp.

Olivet, J.L., Bonnin, J., Beuzard, P. & Auzende, J.M. (1984). Cinématique de l'Atlantique nord et central. Raport Sci. Techn. ; Paris CNEXO, 54, 5 planches, 108 pp.

Pascal, A. (1985). Les Systems biosédimentaires urgoniens (Aptien−Albien) sur la marge Nord Ibérique. Mémoires Géologiques de l'Úniversité de Dijon, v. 10, p. 1-569.

Pedreira, D. (2005). Estructura cortical de la zona de transición entre los Pirineos y la Cordillera Cantábrica. Ediciones de la Universidad de Oviedo, CD-ROM, 343 pp.

Pello, J. (1967). Estudio geológico de la prolongación del borde oriental de la Cuenca Minera Central de Asturias (NW de España). Trabajos de Geologia. Univ. de Oviedo, v.1, p. 27-38.

Puig, G. & Sanchez, R. (1888). Datos para la geología de la provincia de Santander. Mapa geológico de España, v. 15, p. 251-329.

Pujalte, V. (1977). El complejo Purberck-Weald de Santander: Estratigrafía y sedimentación. Tesis Doctoral. Universidad de Bilbao, 204 pp.

Pujalte, V. (1981). Sedimentary succesion and palaeonvironments within a fault controlled basEn: the Wealden of the Santander area, northern Spain. Sedimentary Geology, v. 28, p. 293-325.

Pujalte, V. (1982). La evolución paleogeográfica de la Cuenca "Wealdense" de Cantabria. Cuadernos de Geología Ibérica, v. 8, p. 65-83.

Pulgar, J.A. & Alonso, J.L. (1993). La estructura alpina de la Cordillera Cantábrica. En: Resúmenes XV Reunión de Xeología e Minería do NO Peninsular Lab. Xeol. Laxe, O Castro, Sada, La Coruña, p. 69-71.

Pulgar, J.A., Gallart, J., Fernández-Viejo, G., Pérez-Estaún, A., Álvarez-Marrón, J., & ESCI-N Group. (1996). Sesimic images of the Cantabrian Mountains in teh western extension of the Pyrinean Belt from integrated reflection and refraction data. Tectonophysics, v. 264, p. 1-19.

Quintana, L. (2012). Extensión e inversión tectónica en el sector central de la región vasco-cantábrica (Cantabria-Vizcaya, norte de España). Tesis Doctoral. Universidad de Oviedo. pp. 560.

Quintana, L., Pulgar, J.A., Alonso, J.L. & Rodríguez-Fernández, L.R. (2009a). Las cuencas rómbicas cantabríco-pirenaicas: ¿pull-apart o extensionales? 6º Simposio sobre el Margen Ibérico Atlántico, Oviedo, España, p.53-56.

Quintana, L., Alonso, J.L., Pulgar, J.A. & Rodríguez-Fernández, L.R. (2009b). Zonas de transferencia extensional en el sector central de la Zona Vasco-Cantábrica. 6º Simposio sobre el Margen Ibérico Atlántico, Oviedo, España, p. 57-60.

Quintanar-Soto, A. B. (2003). El Cretácico medio del extremo suroriental del Anticlinorio de Bilbao: Estratigrafía y sedimentología. Tesis Doctoral, Universidad del País Vasco, 217 p.

Ramírez del Pozo, J. (1971). Bioestratigrafía y microfacies del Jurásico y Cretácico del norte de de España (región Cantábrica). Memorias del Instituto Geológico y Minero de España, v. 78, p. 1-357.

Ramírez del Pozo, J. (1972). Algunos datos sobre la estratigrafía y micropaleontología del Aptense y Albense al oeste de Santander. Revista Española de Micropaleontología v. 15, p. 59–97.

Ramírez del Pozo, J., Portero García, M., Olivé Davó, A., Martín Alafont, J.M., Aguilar Tomás, M.J. & Giannini, G. (1976a). Hoja geológica número 33. Comillas. Mapa geológico de España, escala 1:50.000, Serie MAGNA, IGME.

Ramírez del Pozo, J., Portero García, M., Olivé Davó, A., Martín Alafont, J.M., Aguilar Tomás, M.J. & Giannini, G. (1976b). Hoja geológica número 34. Torrelavega. Mapa geológico de España, escala 1:50.000, Serie MAGNA, IGME.

Rat, P. (1959). Les pays crétacés basco-cantabriques (Espagne). Thèse. publ. Université de Dijon, v. XVIII, 525 pp.

Rat, P. (1988). The Basque-Cantabrian basin between the Iberian and European plates some facts but still many problems. Revista de la Sociedad Geológica de España, v.1 (3-4), p. 327-348.

Ries, A.C. (1978). The opening of the Bay of Biscay: a review. Earth Science Reviews, v. 14 (1), p. 35-63.

Robador, A., Heredia, N. & Rodríguez, L.R. (1990). Mapa geológico de Cantabria. E. 1: 100.000. ITGE-Diputación Regional de Cantabria.

Robles, S., Pujalte, V. & García-Mondéjar, J. (1988). Evolución de los sistemas sedimentarios del margen occidental cantábrico durante el Albiense y el Cenomaniense, en la transversal del litoral vizcaino. Revista de la Sociedad Geológica de España, v. 1, p. 409-441.

Roest, W.R. & Srivastava, S.P. (1991). Kinematics of the plate boundaries between Eurasia, Iberia and Africa in the north Atlantic from the Late Cretaceous to the present. Geology, v. 19, p. 613-616.

Rosales, I. (1995). La plataforma carbonatada de Castro-Urdiales (Aptiense-Albiense, Cantabria). Tesis Doctoral, Universidad del País Vasco, 496 p.

Rosales, I. (1999). Controls on carbonate-platform evolution on active fault blocks. The Lower Cretaceous Castro Urdiales platform (Aptian-Albian, Northern Spain). Journal of Sediemntary Research, v. 69, p. 447-465.

Rosales I., Fernandez-Mendiola, P. A. & García-Mondejar, J. (1994). Carbonate depositional sequence development on active fault blocks: the Albian in the Castro Urdiales area, northern Spain. Sedimentology, v. 41, p. 861-882.

Rosales, I. Gräfe, K.U., Robles, S. Quesada, S. & Floquet M. (2002). Cretaceous: the Basque-Cantabrian Basin. En: W. Gibbons & T. Moreno (ed.), Geological Society (London), p. 272-281.

Rosales, I., Najarro., M., Moreno-Bedmar, J., de Gea, G. & Company., M. (2009). High-resolution chemo- and biostratigraphic records of the Early Aptian

Oceanic Anoxic Event in Cantabria (northern Spain). Geochimica et Cosmochimica Acta, 73/13S, A1118-A1118.

Sánchez Ferrer, F. (1991). Evolución estructural post-kimmerica de la plataforma continental vasco-cantábrica. Tesis Doctora. Escuela Técnica superior de Ingenieros de Minas, Universidad Politécnica de Madrid, 224 p.

Saulas, D. Barbason, L. & Loredo-Pérez, J. (1986). Conditions de depot des minéralisations filoniennes á Zn-Pb (hg, Cu); mises en place en limite scole-couverture dans le sectour asturo-cantabrique; données de l'etude des inclusions fluids. Bulletin de la Société Géologique de France, v. 2 (3), p. 521-523.

Sibuet, J.C. & Collette, B.J. (1991). Triple junctions of Bay of Biscay and North Atlantic: new constraints on the kinematic evolution. Geology, v.19, p. 522-525.

Sibuet, J.C., Srivastava, S. P. & W. Spakman (2004), Pyrenean orogeny and plate kinematics, Journal of. Geophysical Research., v. 109, B08104, doi:10.1029/2003JB002514.

Solé Pont, F.J., Mediato Arribas, F.F., Larrondo Echevarria, E. & Hernainz Huerta, P.P. (2008a). Hoja del Mapa Geológico 1:25.000 de la Comunidad Autónoma de Cantabria, nº 34-3 Torrelavega. IGME y Gobierno de Cantabria.

Solé Pont, F.J., Mediato Arribas, F.F. & Hernainz Huerta, P.P. (2008b). Hoja del Mapa Geológico 1:25.000 de la Comunidad Autónoma de Cantabria, nº 34-1 Suances. IGME y Gobierno de Cantabria.

Solé Pont, F.J., Mediato Arribas, F.F., Larrondo Echevarria, E. & Hernainz Huerta, P.P. (2008c). Hoja del Mapa Geológico 1:25.000 de la Comunidad Autónoma de Cantabria, nº 34-2 Muriedas. IGME y Gobierno de Cantabria.

Soto, R., Casas-Sainz, A.M., Villalaín, J., Oliva-Urcía, B. (2007). Mesozoic extension in the Basque-Cantabrian Basin (N Spain): Contributions from AMS and brittle mesostructures. Tectonophysics, 373–394.

Symons, D.T.A., Lewchuk, M.T., Kawasaki, K., Velasco & F., Leach, D.L. (2009). The Reocín zinclead deposit, Spain: paleomagnetic dating of a late Tertiary ore body. Mineralium Deposita, v.44, p. 867-880.

Tosal, J.M. (1968). Relaciones zócalo-cobertera en el límite de las provincias de Oviedo y Santander. Brev. Geol. Astur., v. 19, p. 9-14.

Vadala, P. (1981). Le gite de ZnS-PbS a gangue ankeritique de Reocín (Santander, Espagne). Tectonique diapirique, phenomenes karstiques et mineralisations. Tesis Doctoral. Universidad de Orleans, 288 pp.

Vadala, P., Touray, J.C., García-Iglesias, J. & Ruiz, F. (1981). Nouvelles dones sur le gisement de Reocín (Santander, Espagne). Chron. Min., v. 462, p. 43-59.

Velasco, F., Herrero, J.M., Yusta, I., Alonso, J.A., Seebold, I. & Leach, D. (2003). Geology and geochemistry of the Reocín Zinc-Lead deposit, Basque-Cantabrian basin, northern Spain. Economic Geology, v. 98, p. 1371-1396.

Verneuil, E. (1852). El terreno cretáceo en España. Revista de Mineralogía, v. 3, p. 339-471.

Weissert, H. & Lini, A. (1991). Ice age interludes during the time of Cretaceous greenhouse climate. En: D.W. Müller, J. A. MacKencie, H. Weissert (ed.), Controversies in Modern Geology, Academic Press, London, p.173-191.

Weissert, H., Lini, A., Föllmi, K.B. & Kuhn, O. (1998). Correlation of Early Cretaceous carbon isotope stratigraphy and platform drowning events: a possible link?. Palaeogeography, Palaeoclimatology, Palaeoecology, v. 137 (3-4), p. 189-203.

Wilmsen, M. (2000). Evolution and demise of a mid Cretaceous carbonate shelf: the Altamira Limestones (Cenomanian) of northern Cantabria (Spain). Sedimentary Geology, v. 133, p. 195-226.

Wilmsen, M. (2005). Stratigraphy and biofacies of the Lower Aptian of Cuchía (Cantabria, northern Spain). Journal of Iberian Geology, v. 31 (2), p. 253-275.

Wissler, L., Funk, H. & Weissert, H. (2003). Response of Early Cretaceous carbonate platforms to changes in atmospheric carbon dioxide levels. Palaeogeography, Palaeoclimatology, Palaeoecology, v. 200, p. 187-205.

CAPÍTULO 2:

TECTÓNICA

CAPÍTULO 2

2.- TECTÓNICA

Además de las recientes publicaciones sobre tectónica-sedimentación en Najarro *et al*. (2007; 2009), durante la realización de esta Tesis se han concluido dos proyectos que han supuesto un gran avance al conocimiento de la tectónica de la zona de estudio. El primero ha sido la cartografía geológica a escala 1:25.000 de la Comunidad Autónoma de Cantabria (realizada por el IGME y el Gobierno de Cantabria). El segundo proyecto se enmarca dentro del programa ALGECO2 2012-2015 del IGME y ha tenido como objetivo la evaluación de potenciales almacenes geológicos de CO_2. Dentro de éste último, Najarro y García-Senz (2014) y García-Senz (2014) han realizado un estudio detallado de las estructuras cortadas por los sondeos MC-E1 y MC-J1 (Figura 1.1) en el margen cantábrico, mediante cortes geológicos seriados, líneas sísmicas y correlación estratigráfica, demostrando la existencia de una zona triangular entre una provincia salina despegada cabalgante hacia el norte (el Bloque Costero de Santander) y los cabalgamientos de basamento de la Banda del Nansa dirigidos hacia el sur. En este capítulo se sintetizan parte de los datos y conclusiones obtenidos a partir de la realización de estos dos proyectos, que a su vez están en curso de presentarse como artículos científicos.

2.1.- ESTRUCTURA REGIONAL

La Cordillera Cantábrica es un cinturón de pliegues y cabalgamientos adyacente a la costa del mar Cantábrico que constituye la continuación topográfica y geológica de los Pirineos al oeste de la falla de Pamplona (Figura 2.1A). Su elevación es consecuencia de la colisión entre las placas de Iberia y Europa ocurrida entre el final del Cretácico y el Cenozoico. Los perfiles de sísmica de reflexión y los perfiles profundos de sísmica de refracción muestran un orógeno bivergente (Figura. 2.1B) que cabalga hacia el sur a las cuencas de antepaís del Duero y del Ebro con subducción de la corteza inferior ibérica bajo la

corteza europea, mientras que hacia el norte desarrolla un prisma de acreción en el basamento oceánico del Golfo de Vizcaya (Gallástegui, 2000; Pedreira, 2005).

Al igual que ocurre en los Pirineos, los cabalgamientos alpinos de la Cordillera Cantábrica reactivan a los sistemas transtensivos-extensivos de edad Pérmica-Cretácica. Por esta razón el enfoque más adecuado para relacionar el relieve con la variación longitudinal de la estructura contractiva y con la estructura extensional heredada es la tectónica de inversión. En esta línea, Alonso *et al*. (2007) distinguen un sector occidental situado entre Asturias y Galicia con relieve medio y cobertera mesozoica inexistente; un sector central también denominado macizo Asturiano donde se encuentran las máximas elevaciones y puede estar preservada una cobertera mesozoica delgada, y finalmente un sector oriental o sector Vasco-Cantábrico (aquí denominado cuenca Vasco-Cantábrica) de elevaciones medias y espesores importantes de mesozoico.

La región que rodea al área de estudio forma parte del límite entre el macizo Asturiano y la cuenca Vasco-Cantábrica occidental (Figura 2.2). El macizo Asturiano es interpretado en esta región como un gran pliegue de acomodación sobre un cabalgamiento de basamento dirigido hacia el sur (Pulgar y Alonso, 1993). El relieve estructural que produce este pliegue permite observar en superficie el basamento paleozoico y permo-triásico que se sumerge hacia el este bajo el Mesozoico de la cuenca Vasco-Cantábrica. De forma similar, este sector de la cuenca Vasco-Cantábrica es interpretado por Espina (1997) como transportado sobre una rampa de basamento donde se entroncan fallas individuales reactivadas que limitan las cuencas mesozoicas invertidas de Polientes, Cabuérniga y del Bloque Costero de Santander (Figura 2.2).

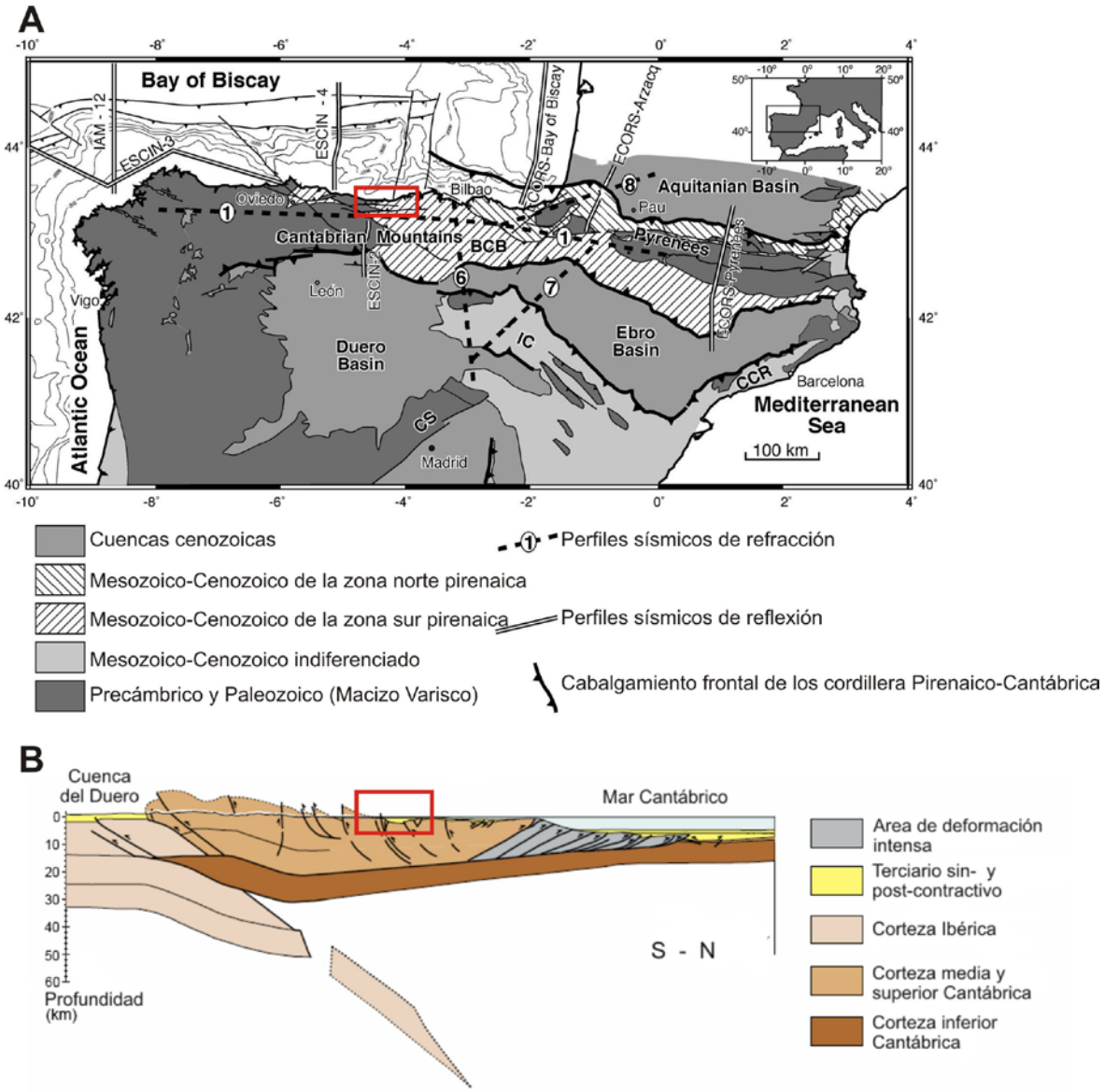

Figura 2.1.- **A**) Mapa estructural de la cordillera Pirenaico-Cantábrica con situación de los perfiles de sísmica de refracción (Pedreira, 2005); **B**) Modelo orogénico de colisión de la Cordillera Cantábrica interpretado de los perfiles ESCIN-2 y ESCIN-4 (Gallástegui, 2000). El rectángulo sitúa el área de estudio cerca del eje del orógeno, dentro de la Zona Surpirenaica con cabalgamientos dirigidos hacia el sur que se extienden profundamente en la corteza y que reactivan fallas extensivas mesozoicas y cabalgamientos variscos.

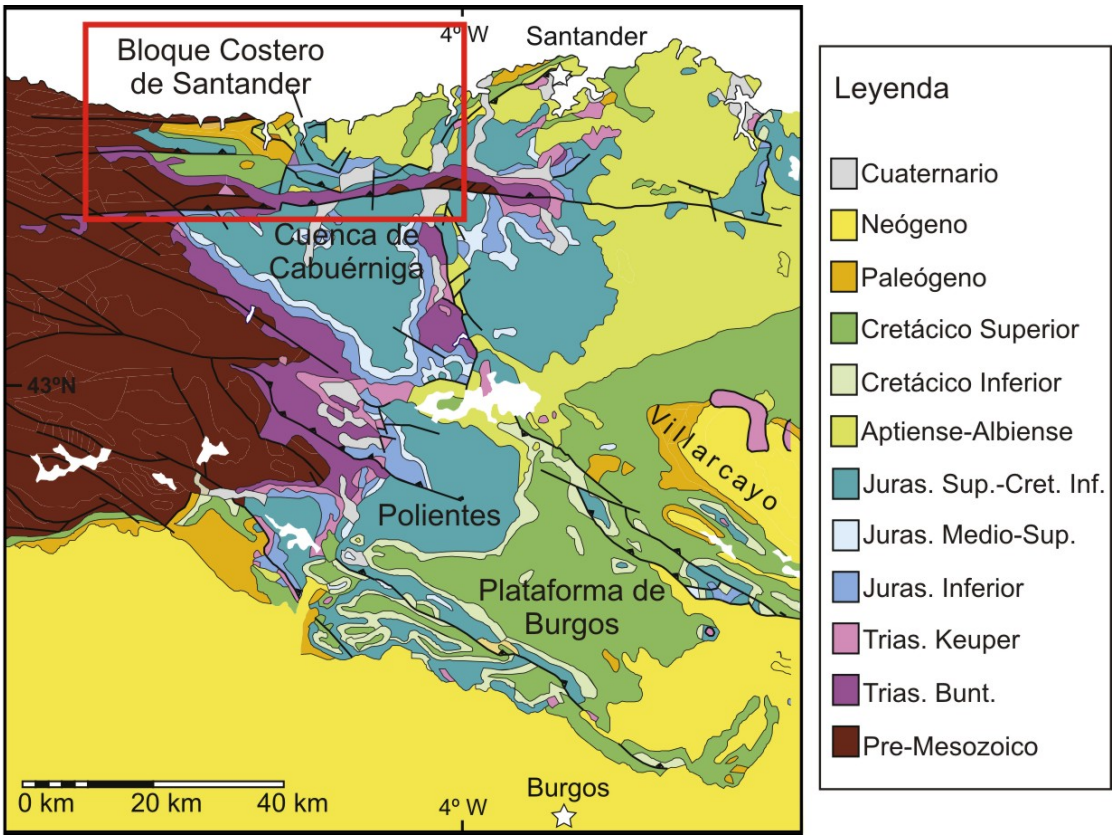

Figura 2.2.- Mapa geológico del límite entre el macizo Asturiano que expone el basamento paleozoico y permo-triásico y la cuenca Vasco-Cantábrica occidental dividida en subcuencas. El rectángulo rojo delimita la zona de estudio.

Finalmente, el área de estudio, denominada en los artículos que conforman esta Tesis como cuenca Nor-Cantábrica (Wilmsen, 2000; 2005; Najarro *et al*. 2009; 2010; 2011a y 2011b) abarca la porción del macizo Asturiano definida como Banda del Nansa (Espina, 1994; 1997) y la porción de la cuenca mesozoica definida como el Bloque Costero de Santander (Barnolas y Pujalte, 2004). Éstas son las dos áreas que se describen en detalle a continuación. Su descripción se beneficia de la información contenida en las recientes cartografías geológicas 1:25.000 de la Comunidad Autónoma de Cantabria, realizadas por el IGME y el Gobierno de Cantabria (García-Senz y Cañas Fernandez, 2013a; 2013b; García-Senz y Merino-Tomé, 2011; Huerta Carmona 2009; Solé-Pont *et al*., 2008a; 2008b; 2008c; Larrondo Echevarría *et al*., 2008).

2.2.- BANDA DEL NANSA

Está formada por un imbricado de cabalgamientos E-O verticalizados dirigidos hacia el sur que continúan la estructura de las regiones del Ponga y de los Picos de Europa en Asturias (Tosal, 1968; Martínez García, 1980; Marquínez, 1989; Espina, 1994; 1997).

Los cabalgamientos individuales de este imbricado pueden estar ya sea fosilizados por el Pérmico, el Buntsandstein o el Cretácico, lo que los define como cabalgamientos variscos, o pueden llegar a superponer rocas del Ordovícico sobre sedimentos sinorogénicos marinos del Priaboniense-Oligoceno (Mengaud, 1920) lo que los identifica como cabalgamientos variscos reactivados (Espina, 1997; Pulgar y Alonso, 1993). El desplazamiento varisco es siempre muy superior al alpino. El cabalgamiento dominante del sistema es el cabalgamiento frontal de Cabuérniga que limita por el sur la Banda del Nansa (Espina, 1997).

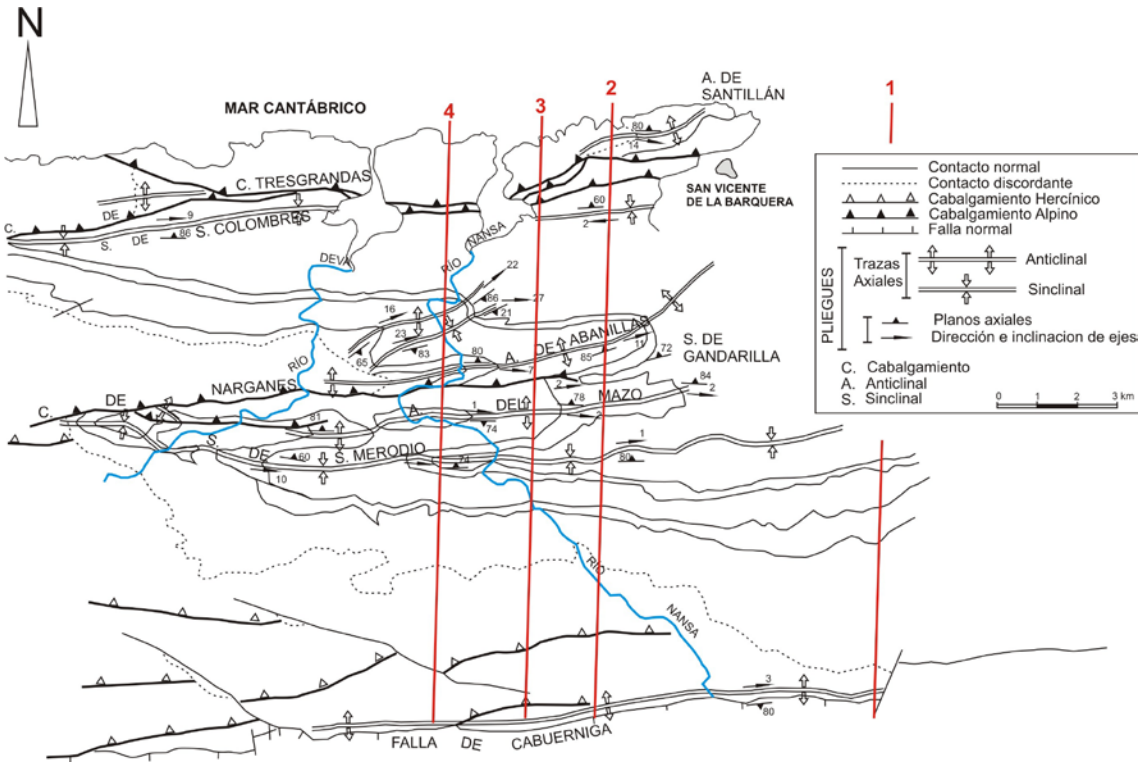

Figura 2.3.- Esquema estructural de la Banda del Nansa, modificado de Espina (1997) con situación de los cortes geológicos de la figura 2.4. Dichos cortes han sido tomados de García-Senz y Cañas Fernández (2013a) y García-Senz y Merino-Tomé (2011).

Los pliegues en la Banda del Nansa tienen una inmersión media de 08º hacia N088 que expone en superficie distintos niveles de la estructura y permite apreciar las relaciones entre fallas y pliegues. Se observa que los pliegues se hacen más anchos y pierden amplitud en la dirección de inmersión a la vez que sus trazas axiales se curvan hacia el noreste y los pliegues individuales se fusionan en una terminación periclinal común (García-Senz y Robador, 2009).

La descripción más detallada de las principales estructuras que componen la Banda del Nansa se debe a Espina (1997). Aquí se adapta la descripción similar pero más concisa de García-Senz y Robador (2009). De norte a sur se distinguen:

Cabalgamiento de Tresgrandas y anticlinal de Santillán

El cabalgamiento de Tresgrandas sitúa la Cuarcita de Barrios del Ordovícico sobre la Fm. Oyambre del Oligoceno con un desplazamiento de 3.5 km (cortes 3 y 4, Figura 2.4). La superficie principal de falla se divide hacia arriba en astillas que cortan, elevan y rotan a la vertical rocas eocenas del bloque inferior. El Paleozoico, bastante inclinado en el bloque superior cabalgante, está truncado por la Fm. Reocín del Aptiense Superior-Albiense basal, que se halla plegada a su vez en una charnela anticlinal suave, el anticlinal de Santillan, cuya forma no representa a la estructura varisca (corte 4, Figura 2.4).

Sinclinal de Colombres

Es un sinclinal asimétrico en el bloque inferior del cabalgamiento de Tresgrandas. Tiene un flanco sur largo y un flanco norte corto y rotado del que proceden las astillas de caliza eocena visibles en superficie. Sobre el techo de este sinclinal, está el cabalgamiento de Comillas, interpretado como un olistostroma sincontractivo que se adapta al relieve deprimido del valle sinclinal (corte 1, Figura 2.4) (García-Senz y Robador, 2009).

Cabalgamiento de Narganes y anticlinal de Abanillas

El cabalgamiento de Narganes con 1.5 km de desplazamiento superpone la caliza carbonífera sobre el Cretácico Inferior. El anticlinal de bloque superior asociado, anticlinal de Abanillas, es asimétrico con inclinación mayor en el flanco frontal. El cretácico del flanco dorsal está plegado por pliegues secundarios sobre niveles de despegue locales (corte 4, Figura 2.4).

Anticlinal de Mazo

Es un anticlinal de perfil abierto a suave en el bloque inferior del cabalgamiento de Narganes (corte 2, Figura 2.4). Su flanco sur es algo más inclinado y corto que el norte definiendo una ligera vergencia sur. De acuerdo con Espina (1997), este pliegue no se asocia a ningún cabalgamiento aflorante o ciego, aunque sí que existen pliegues secundarios y cabalgamientos que afectan a la cobertera cretácica cerca del río Deva.

Sinclinal de Merodio

Es un pliegue de perfil abierto a suave y ligera vergencia sur que comparte el flanco corto del anticlinal del Mazo y el flanco largo del anticlinal de Cabuérniga (cortes 2, Figura 2.4). En el sinclinal de Merodio, y posiblemente también en el anticlinal del Mazo, comienzan a aparecer bajo el Cretácico las areniscas del Buntsandstein discordantes sobre los materiales variscos.

Cabalgamiento y anticlinal de Cabuérniga

El cabalgamiento E-O de Cabuérniga es el cabalgamiento alpino frontal dominante del imbricado del Nansa. A semejanza del cabalgamiento de Tresgrandas, se trata de un cabalgamiento varisco reactivado. Su superficie casi vertical pone en contacto la cuarzo-arenita del Ordovícico con el Buntsandstein, o la caliza del Carbonífero con el Liásico. El cabalgamiento es parte de la estructura compresiva del anticlinal de Cabuérniga (Espina, 1997) cuyo flanco dorsal elevado en el borde fallado del basamento, cuelga sobre el flanco frontal verticalizado donde se concentra la deformación (corte 2, Figura 2.4). El desplazamiento del techo del Buntsandstein por la falla se estima en 700-800 m.

El modelo adoptado por Espina (1997) para los pliegues de la Banda del Nansa es el de pliegues de propagación de falla (Suppe y Medwedeff, 1984; Mitra 1990), caracterizados por la transferencia del desplazamiento del cabalgamiento al pliegue que se desarrolla en su extremidad. Sin embargo García-Senz y Robador (2009) también enfatizan que la cantidad de acortamiento disminuye hacia el este a lo largo de la dirección de los pliegues como prueban los cortes seriados (Figura 2.4) lo que implica una rotación levógira de eje vertical dentro de la Banda del Nansa.

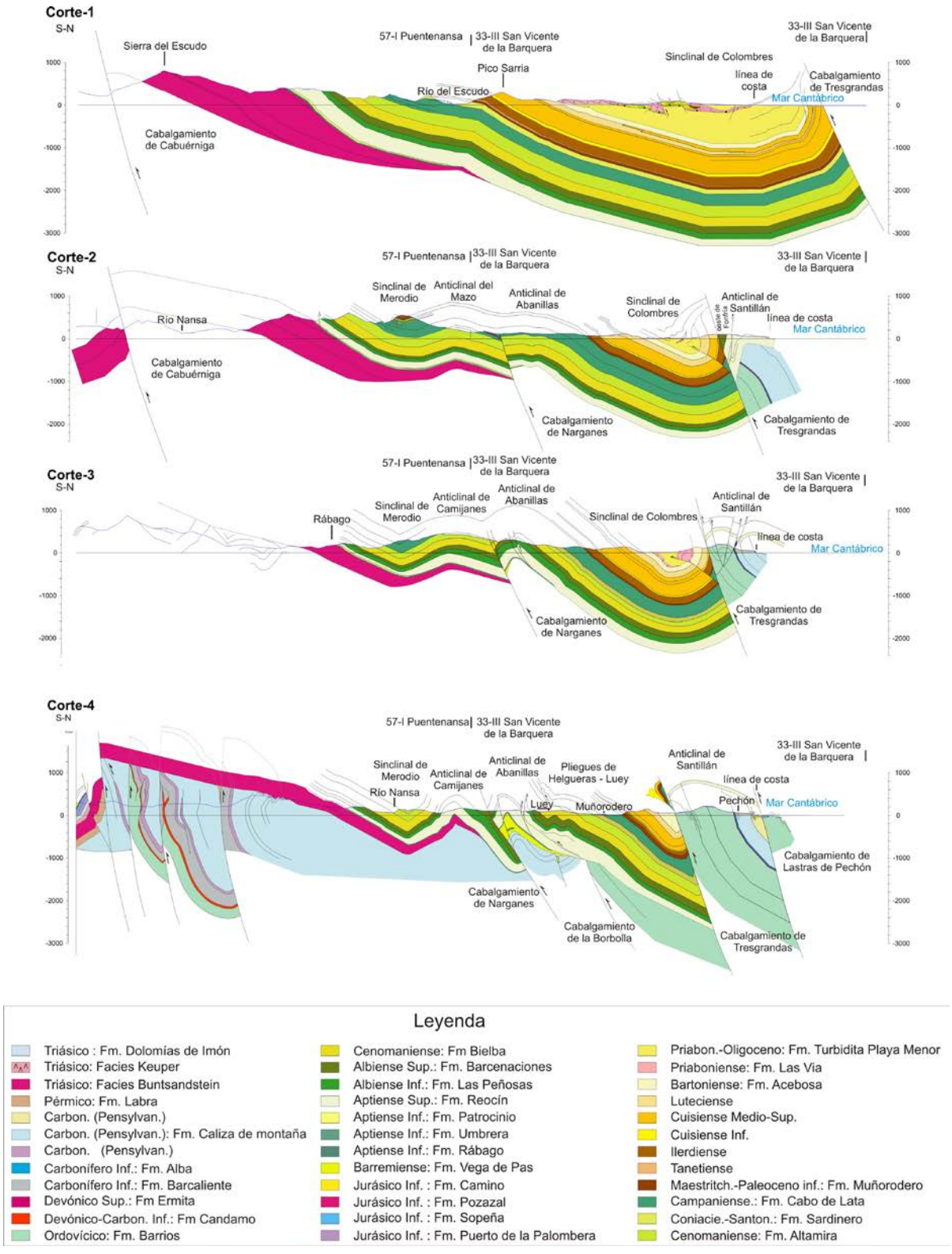

Figura 2.4.- Cortes geológicos seriados transversales al plegamiento de la Banda del Nansa (situación en Figura 2.3) tomados de García-Senz y Merino-Tomé (2011) que muestran cabalgamientos variscos reactivados y no reactivados. Se aprecia la relación entre pliegues y cabalgamientos que los identifica como pliegues de propagación de falla, y también la disminución progresiva del apretamiento de los pliegues y del desplazamiento de los cabalgamientos alpinos (García-Senz y Merino-Tomé, 2011).

2.3.- BLOQUE COSTERO DE SANTANDER

El Bloque Costero de Santander (Figura 2.5) es un extenso afloramiento de sedimentos del Mesozoico al Eoceno limitado al sur por el cabalgamiento de Cabuérniga, al oeste por la falla NNE-SSO de Bustriguado que la separa de la Banda del Nansa, al este por el cabalgamiento de Ramales que constituye la última estructura salina que mantiene la orientación NE-SO a N-S propia del interior del Bloque Costero de Santander, y al norte bajo el mar Cantábrico en la extremidad de un tren de pliegues despegados en la terminación de la cuenca del Keuper. El límite norte pasa junto al sondeo de petróleo MC-J1 frente a la costa de Suances, ya que este pozo corta una serie estratigráfica sin facies Keuper ni Fm. Vega de Pas, similar a la existente en la Banda del Nansa (Shell España, 1980; Cámara Rupelo, 1989).

Aunque se halla poco deformado, su arquitectura es compleja por la coexistencia de orientaciones N060, N017 y N097 de fallas y pliegues, que adicionalmente presentan una distribución poco simétrica lo que dificulta su descripción a lo largo de una única dirección. La mejor manera de describirla es agrupando genéticamente las fallas, pliegues y diapiros en dos áreas, Treceño y Santander, separadas por una zona de fallas dispersas sin diapiros, Reocín.

Zona de fallas de Treceño

Es un enrejado de fallas conectadas. La falla N017 de Bustriguado es una importante falla de basamento de alto ángulo con desplazamiento oblicuo inverso dirigido hacia el noroeste o hacia el norte, que llega a superponer el Keuper y el Jurásico Inferior sobre el Maastrichtiense y el Eoceno. Presenta características de falla extensiva reactivada ya que limita bloques con distinta serie estratigráfica, distinta cantidad de subsidencia y estilo de deformación. Separa esencialmente un área oriental diapírica con un Keuper y un Cretácico Inferior potente, en especial la Fm. Vega de Pas que puede alcanzar 1377 m de espesor; de un área occidental donde la Fm. Vega de Pas es inexistente o está reducida a escasos metros y el Keuper está ausente, al igual que el Jurásico (Najarro *et al*., 2007). Respecto a su estructura contractiva, tiene características de falla transversa que compartimenta el plegamiento, ya que pone en contacto el flanco meridional inclinado hacia el norte del sinclinal de Merodio (descrito en la Banda del Nansa) con el flanco frontal del anticlinal de Treceño (Huerta Carmona, 2009).

El anticlinal de Treceño deforma la depresión rectangular que limita el enrejado de fallas de Bustriguado, Santibañez y Peña Castillo (Figura 2.5). Visto en corte (corte 5, Figura 2.6A.) tiene vergencia sur y perfil abierto, con características de pliegue de acomodación de falla. Su zona de charnela está cortada por un cabalgamiento secundario dirigido también hacia el sur.

La falla E-O de Santibáñez (Figura 2.5) es una falla extensiva que conecta en una esquina con la falla de Bustriguado (Huerta Carmona, 2009; García-Senz y Robador, 2009) para perder desplazamiento desde este punto hasta su extremidad, situada al este de Cabezón de la Sal. En su bloque superior hay un ascenso diapírico de Keuper que alcanza la superficie en el diapiro de Cabezón.

Las fallas ENE-OSO de Peña Castillo, Santa Ana y Rubárcena se ramifican de la extremidad norte de la falla de Bustriguado (Figura 2.5). La falla de Peña Castillo es una importante falla extensiva de polaridad sur que mantiene una separación normal de hasta 1000 m en la serie pre-extensiva y produce un aumento de espesor estratigráfico de la Fm. Vega de Pas y de las plataformas del Aptiense para terminar fosilizada en la parte alta de la Fm. Reocín (Figura 2.6A). Esta fosilización favorece que en su trazado existan segmentos ciegos como el de Cóbreces y posiblemnte en Cuchía, donde la falla está enterrada bajo las secuencias del Aptiense Superior-Cenomaniense (Figura 2.5) y reapariciones en superficie como en el anticlinal de Oreña.

Finalmente, la falla de Rubárcena es una falla extensiva reactivada como inversa que junto con la falla de Santa Ana limita un diapiro contraído de Keuper que se halla extruido como *pop-up* (corte 6, Figura 2.6A). El bloque inferior de la falla de Rubárcena contiene numerosos pliegues ENE-OSO dispuestos en escalera con relevos dextros que forman la costa al este del cabo de Oyambre (Figura 2.5). Estos pliegues desarrollados sobre una suela de Keuper, cabalgan al Cenozoico plegado en sinclinal.

Zona sin fallas de Reocín

Es un área alargada NNO-SSE entre las localidades de Reocín y Oreña (Figura 2.5) delimitada por la terminación difusa de las dos agrupaciones de fallas y diapiros descritas anteriormente. La deformación se localiza únicamente en cabalgamientos de vergencia opuesta en los márgenes sur y norte, mientras que el área central está ocupada

por la terminación del sinclinal NE-SO de Santillana de perfil muy laxo y desprovisto de fallas (corte 7, Figura 2.6B). La Fm. Bielba es más potente en el flanco sur del sinclinal y se adelgaza hacia el flanco norte que enlaza con el anticlinal de Oreña en el área de costa.

El anticlinal N060 de Oreña (corte 7, Figura 2.6B) es de perfil abierto y vergente hacia el norte con el flanco largo dorsal tendido y el flanco frontal corto más inclinado sobre todo las capas internas que se disponen verticalizadas a invertidas en una banda de cizalla asociada a un cabalgamiento que reactiva la extremidad de la falla extensiva de Peña Castillo.

Zona de fallas de Santander

Es un área de solape de tres largas fallas N060 inclinadas hacia el sur, que limitan bloques rotados sobre diapiros y cuencas sinclinales (Figura 2.5). Algunos de estos rasgos se muestran en los cortes 7 y 8 de la figura 2.6 aunque estos no atraviesan la zona de mayor complejidad. De sur a norte se distingue una cuenca sinclinal en la Fm. Vega de Pas con una relación de *onlap* sobre el diapiro de Parbayón, seguida de un largo flanco monoclinal inclinado hacia la falla de Puente Arce. El bloque inferior de la falla de Puente Arce está plegado en el sinclinal N060 de San Román considerado como la prolongación del sinclinal de Santillana. Es un pliegue de perfil abierto, bastante simétrico y de eje inclinado 08º hacia el NE lo que favorece el afloramiento de Cenozoico. El flanco norte se caracteriza por una serie estratigráfica adelgazada que alcanza una fuerte inclinación en la línea de costa.

Relación entre basamento y cobertera en el Bloque Costero de Santander

La orientación N060 dominante en la cobertera del Bloque Costero de Santander tiene una oblicuidad de unos 30º respecto a la orientación E-O del basamento que aflora en la Banda del Nansa y en el anticlinal de Cabuérniga. Se constata asimismo que muchas de las fallas oblicuas que afectan a la cobertera terminan hacia el sur sin desplazar al Buntsandstein de la Sierra de Cabuérniga. Estas observaciones sugieren: (1) que la deformación de la cobertera se halla desvinculada del basamento tanto en la extensión como en la contracción por el horizonte del Keuper y (2) que la Sierra de Cabuérniga es un área de borde respecto a la deformación de la cobertera tanto en la extensión como en la contracción ya que los cabalgamientos principales se localizan en

los bordes y no en el interior del Bloque Costero de Santander. El resultado de la contracción es la delaminación de la cobertera hacia los márgenes del graben (García-Senz y Robador, 2009).

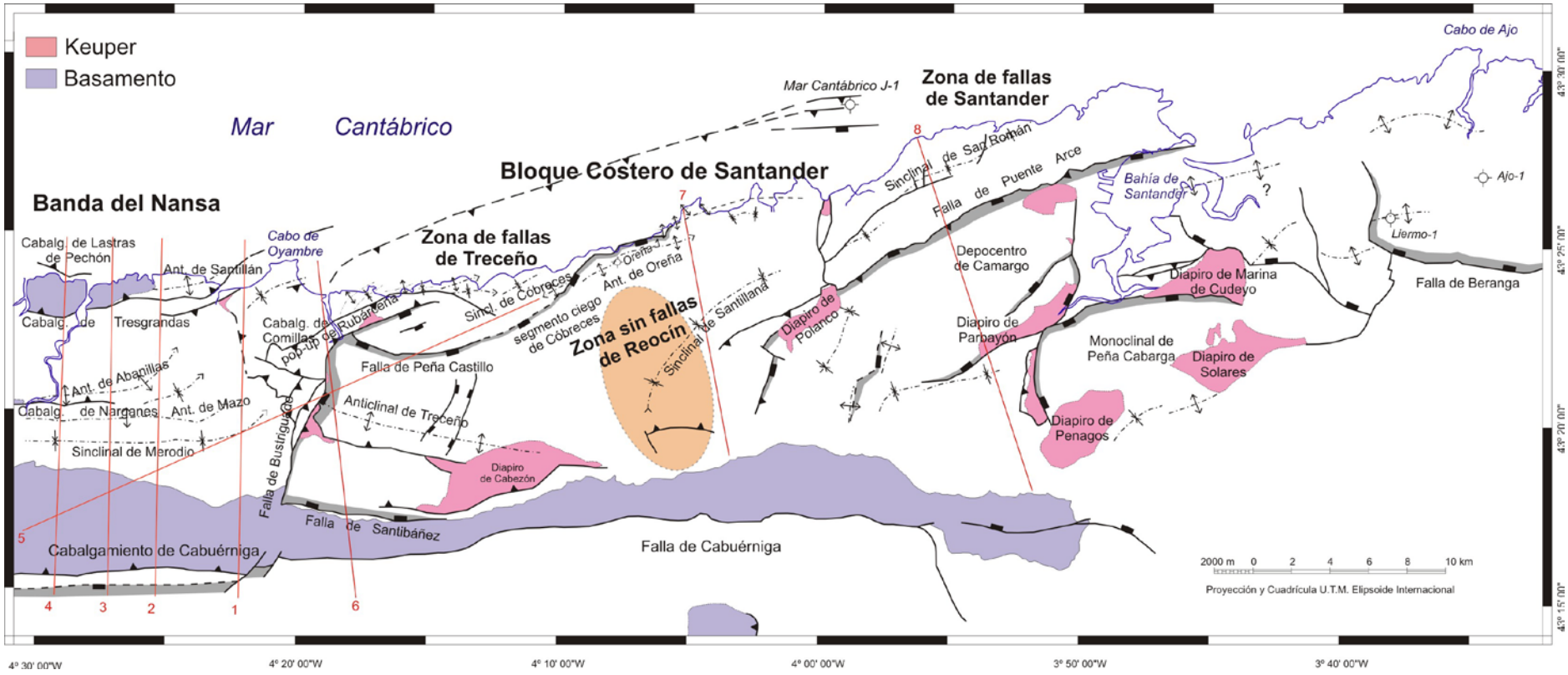

Figura 2.5.- Esquema estructural de la Banda del Nansa y del Bloque Costero de Santander con la posición de los cortes geológicos de las figuras 2.4 y 2.6 (basado en el mapa 1:100.000 de Cantabria). Se aprecia el patrón oblicuo dextral en escalera de las fallas de cobertera respecto a la orientación del basamento de Cabuérniga y del Nansa (áreas sombreadas) y la asociación de las fallas con los diapiros de Keuper. La mayoría son fallas extensivas poco o nada reactivadas. Los cabalgamientos se concentran en los márgenes oeste, norte y sur extruyendo a la cuenca extensiva. El cabalgamiento de Comillas se considera un olistostroma gravitatorio en la Fm. Oyambre.

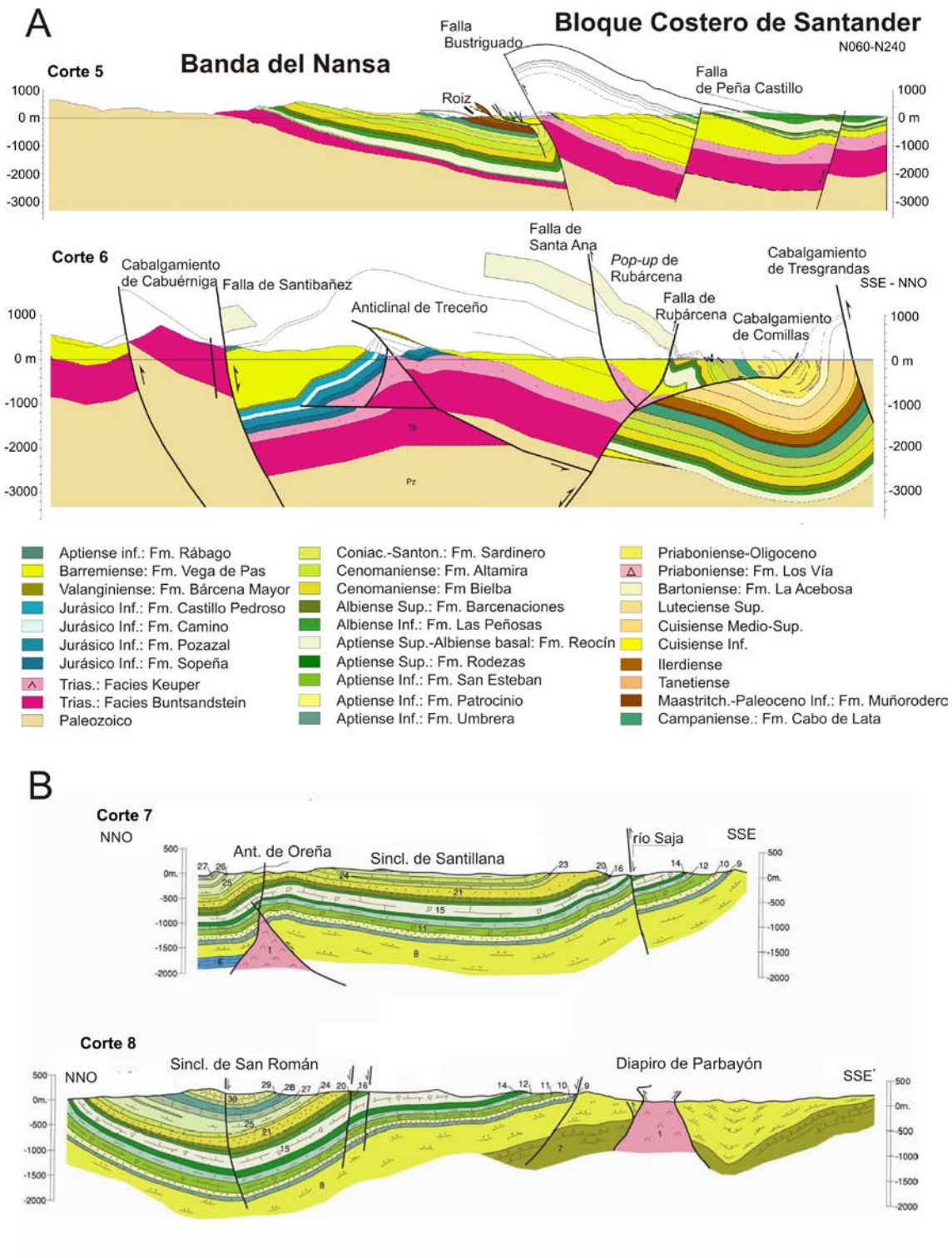

1-2, Triásico; 3-6, Triásico Superior-Jurásico; 7 y 8, Grupo Pas; 9 a 20, Complejo Urgoniano; 21 y 22, Complejo Supraurgoniano; 23 a 30, Cretácico Superior, 31 a 36, Paleógeno.

Figura 2.6.- Cortes geológicos seriados en el Bloque Costero de Santander. Cortes 5 y 6 tomados de García-Senz y Cañas Fernández (2013b); García-Senz y Merino-Tomé (2011) y Huera Carmona (2009). Cortes 7 y 8 tomados de Solé *et al*. (2008).

2.4.- ESTRUCTURA EXTENSIVA Y DISTRIBUCIÓN DE ESPESORES

La distribución de espesores de los sedimentos del Cretácico Inferior en relación con el sistema de fallas revela que la estructura contractiva está superimpuesta a una estructura extensiva previa. La estructura extensiva es muy patente en el Bloque Costero de Santander pero también se detecta en la Banda del Nansa donde Najarro *et al*. (2007) y García-Senz (2013) identifican respectivamente en columnas estratigráficas (Figura 2.7) y en cortes geológicos seriados (Figura 2.8) un cambio de espesor inusual de la Fm. Reocín que aflora en la sierra de Arnero, cambio que es relacionable *a priori* con una flexión en el bloque inferior de la falla de Bustriguado situada pocos kilómetros al este (Figura 2.8). Para averiguar si esta flexión es de eje paralelo a la dirección de la falla es necesario restituir la inclinación adquirida durante el plegamiento contractivo rotando a la horizontal los buzamientos de la Fm. Las Peñosas. Tras esta operación la Fm. Reocín buza de manera residual 117/06 (dirección de buzamiento) en el área de la flexión, es decir con una dirección de capa paralela a la falla de Bustriguado lo que confirma que se trata de una flexión asociada a esta falla (Figura 2.8).

En el Bloque Costero de Santander, la distribución de las fallas extensivas define una segmentación del terreno extendido en dos áreas espaciadas separadas por una zona menos deformada (Figura 2.9A). El segmento más occidental de Treceño se caracteriza por un enrejado ortogonal de fallas conectadas N017 y N097 que afectan al basamento del borde del terreno extendido (Figura 2.9A). Estas fallas terminan a lo largo de su dirección definiendo un graben con asimetría axial. Hacia su extremidad superior las fallas se imbrican en la cobertera y producen cambios de espesor en el Cretácico Inferior en asociación con el Keuper diapírico.

El segmento oriental de Santander está caracterizado por fallas sintéticas N060 inclinadas en el mismo sentido sur y con importante diapirismo asociado. El desplazamiento de las fallas disminuye hacia el suroeste a la vez que su traza se curva hacia la ortogonalidad con el basamento de Cabuérniga (Figura 2.9A). A diferencia con el segmento occidental no existen aquí fallas de borde.

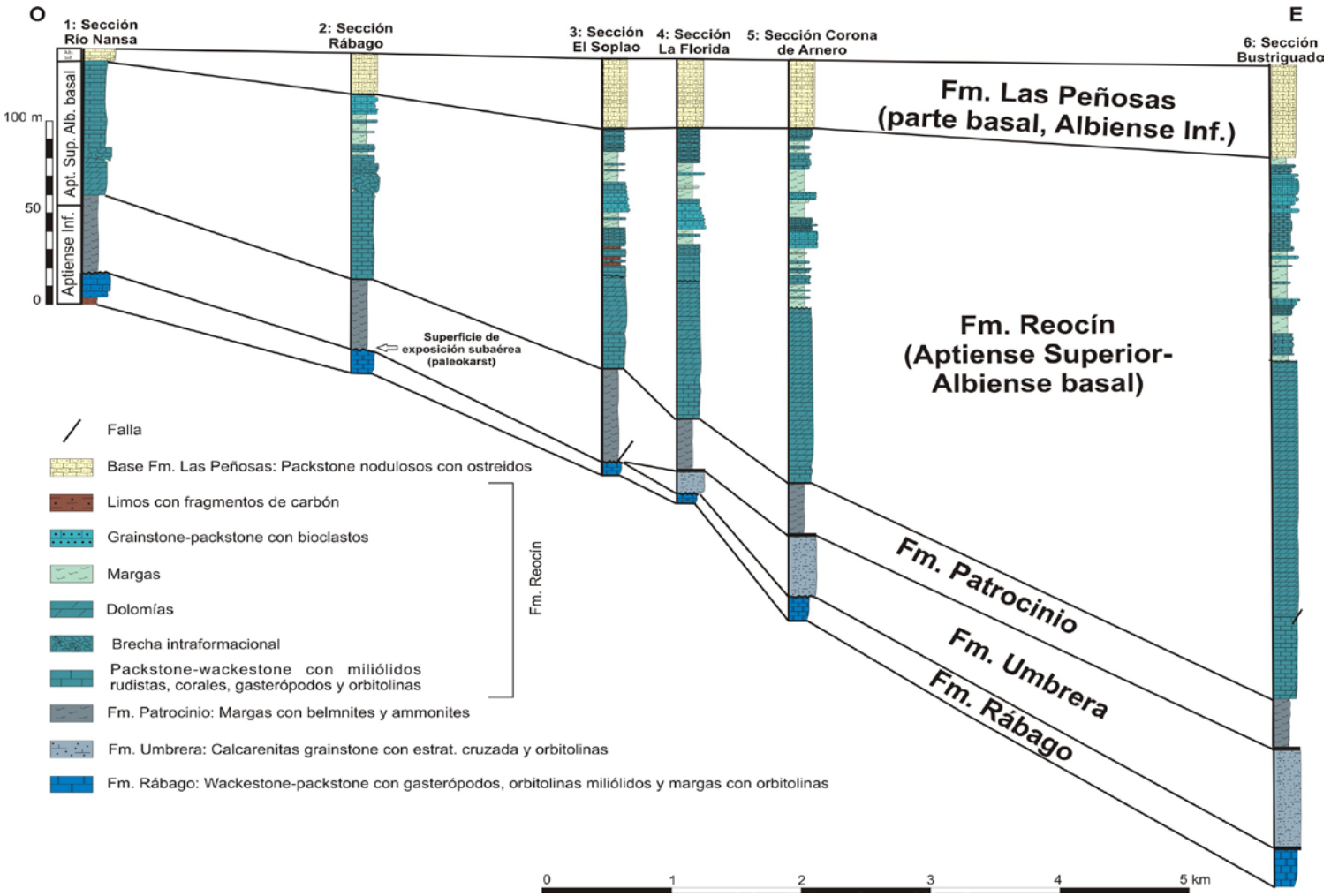

Figura 2.7.- Columnas estratigráficas levantadas en las calizas de la Sierra de Arnedo, motrando los tipos principales de facies sedimentarias El *datum* de base es la superficie transgresiva de la base del Aptiense y el *datum* de techo es el contacto de la Fm. Reocín (Aptiense Superior-Albiense basal) con la Fm. Las Peñosas (Albiense Inferior). La secciones 1 a 6 se localizan en la figura 2.8A.

Otra aproximación a la forma de la cuenca extensiva se obtiene por el contorneo del relleno sinextensivo realizado sobre una malla de puntos, usando como discontinuidades las líneas de las fallas (Figura 2.9B). El contorneo revela dos cuencas individuales separadas por un alto NNO-SSE en la zona de solape de los segmentos de falla. Las cuencas son asimétricas, la occidental más importante que la oriental, con rampas transversas formadas por la acomodación de los estratos a la alternancia de máximos y mínimos de desplazamiento que ocurre entre los centros y las extremidades de las fallas y por la elevación del bloque inferior y la transferencia del desplazamiento entre las fallas escalonadas (Faulds y Varga, 1998).

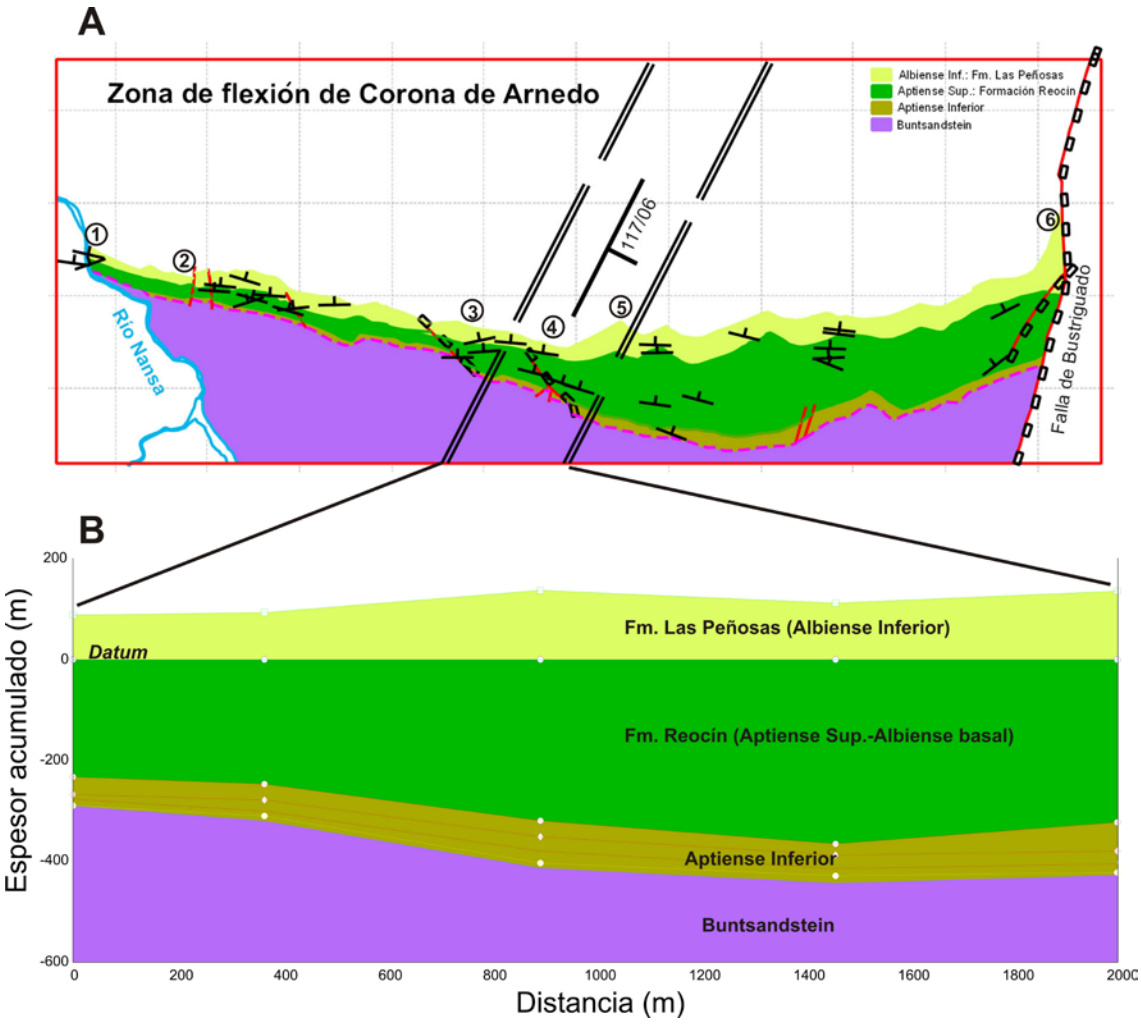

Figura 2.8.- **A**) Mapa de la sierra de Arnero. Malla UTM 1x1 km. La restitución a la horizontal de los buzamientos en la Fm. Peñosas deja un buzamiento residual de la Fm. Reocín hacia 117/06 en la corona de Arnedo. Este buzamiento implica una flexión paralela a la dirección de la falla de Bustriguado (análisis realizado en el programa *Move,* Midland Valley). Se muestra la posición de las secciones, 1 a 6 de la figura 2.7; **B**) Corte estratigráfico con el *datum* a techo de la Fm. Reocín que muestra el cambio de espesor de 233 a 366m que esta flexión produce en la Fm. Reocín, en la zona de la corona de Arnedo.

Modelo extensivo y paleoesfuerzos

Las zonas de *rift* pueden ser ortogonales u oblicuas e involucrar varios episodios superpuestos (ej. Bonini *et al*., 1997). En la cuenca Vasco-Cantábrica occidental varias de las fallas NO-SE principales del *rift* cretácico (Figura 2.2) se consideran fallas heredadas de la extensión edad pérmica y triásica (Pujalte, 1979; Espina, 1994; Hines 1985; Espina *et al*. 2004), incluyendo la larga falla E-O de Cabuérniga que determina el límite externo de la extensión cretácica del Bloque Costero de Santander.

La extensión dentro del Bloque Costero de Santander ocurre por fallas extensivas N060 con relevos en escalera destrales a 30º respecto a los límites externos orientados E-O lo que es característico de zonas de *rift* de baja oblicuidad (Corti, 2012) donde cabe esperar una cinemática combinada de desplazamiento normal, oblicuo y en dirección según sea la orientación de las fallas respecto a la dirección de extensión. Las áreas de mayor estiramiento de Treceño y de Santander indicarían una extensión más ortogonal mientras que una cinemática en dirección es previsible en el área de relevo menos extendida de Reocín. Con este patrón, la dirección de extensión más propicia es N330 aunque también es compatible un rango de variación de 45º hacia el norte.

Resulta interesante comparar el modelo extensivo obtenido para el Bloque Costero de Santander con la dirección de extensión cretácica dada por distintos autores en el resto de cuencas mesozoicas situadas al sur del Bloque Costero de Santander. Espina (1997) calcula una dirección de extensión NE-SO a NNE-SSO compatible con el plano de movimiento calculado en fallas normales y en dirección. Soto *et al*. (2007) determinan una dirección de extensión NE-SO a partir de lineaciones magnéticas, que interpretan producidas por un campo de esfuerzos próximo. Obtienen asimismo direcciones de extensión N-S a NE-SO y de forma secundaria NO-SE a partir de grietas de tensión y diaclasas; y una extensión dominante NO-SE a E-O calculada por cinemática de fallas, que interpretan debida a un campo de esfuerzos lejano. Finalmente Tavani y Muñoz (2011) también por criterios cinemáticos determinan una dirección regional de extensión entre N005 y N025.

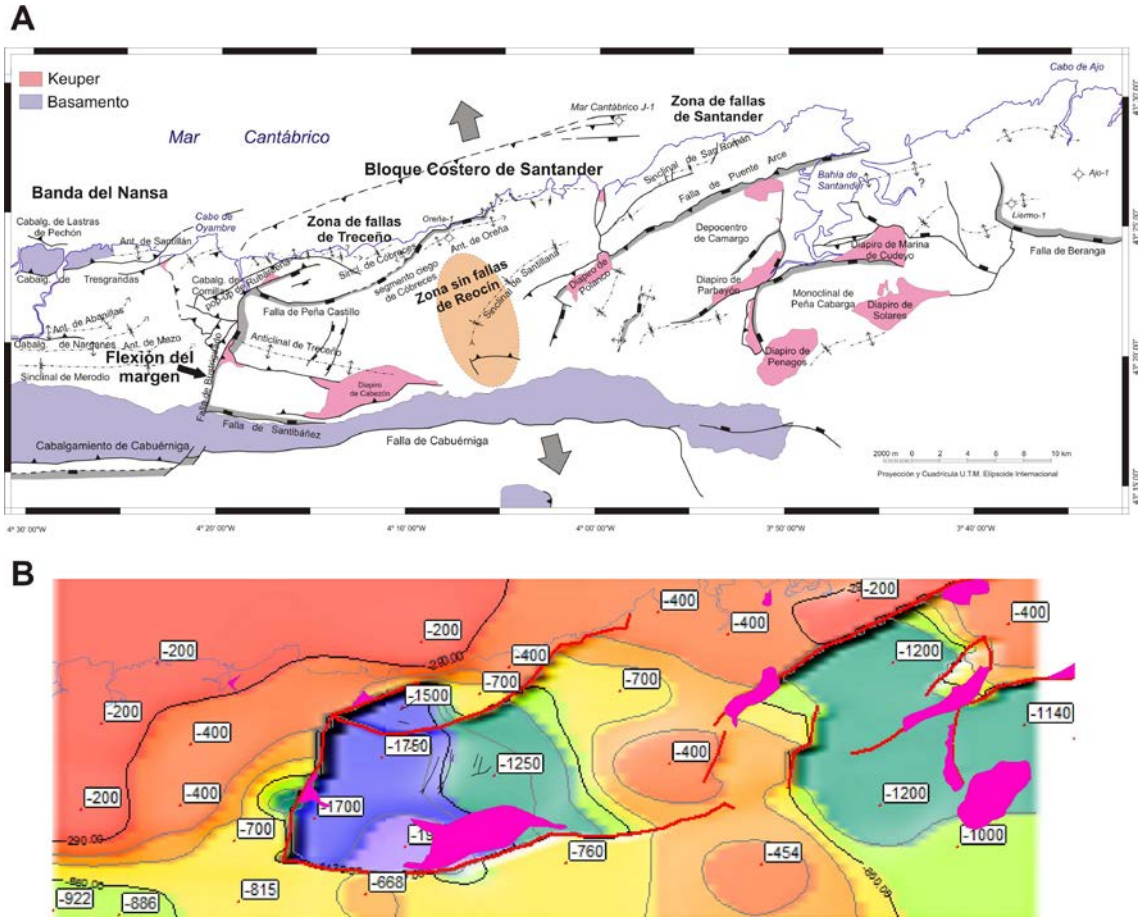

Figura 2.9.- **A**) Mapa estructural que representa la Corona de Arnedo y las dos zonas de concentración de fallas y diapiros de Treceño y de Santander separadas por la zona de relevo transversa de Reocín. Las flechas indican una de las posibles direcciones de extensión acordes con esta geometría. **B**) Contorneo con fallas del intervalo base Fm. Vega de Pas-techo Fm. Las Peñosas que define dos depocentros separados por un alto en la zona de transferencia de Reocín. El contorneo revela la asimetría de la subsidencia causada por la variación del desplazamiento de las fallas a lo largo de su dirección y por la transferencia del mismo a otras fallas**.**

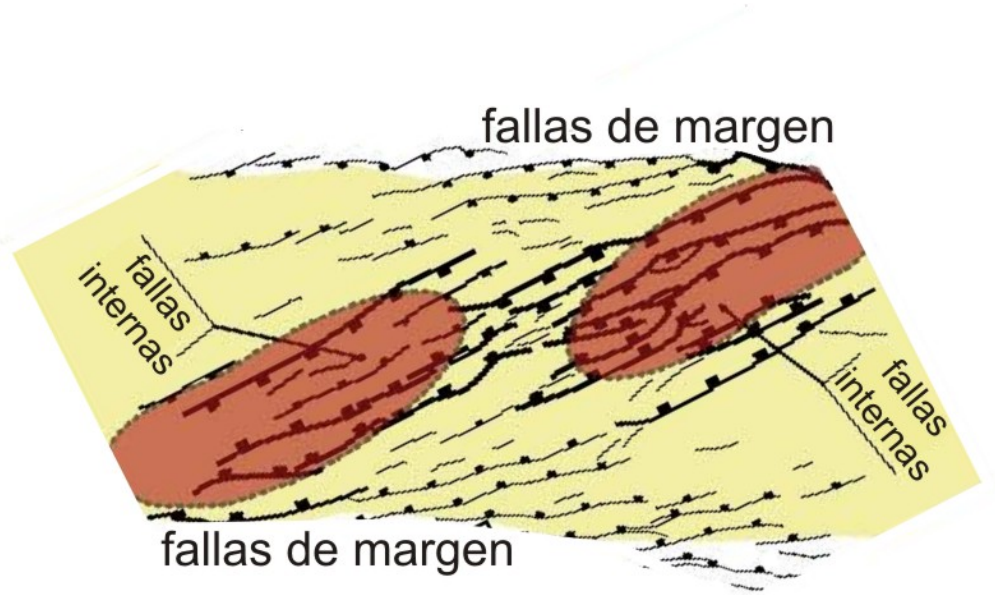

Figura 2.9.- Modelo analógico del adelgazamiento en un rift de oblicuidad moderada (30º) similar al descrito para el Bloque Costero de Santander (adaptado de Corti, 2012).

2.5.- REFERENCIAS

Alonso, J.L., Pulgar, J.A. & Pedreira, D. (2007). El relieve de la Cordillera Cantábrica. Enseñanza de las Ciencias de la Tierra, v.15, n.2, p. 151-163.

Barnolas, A. & Pujalte, V. (2004). La Cordillera Pirenaica: Definición límites y división. En: Geología de España (J.A. Vera, ed.), SGE-IGME, p. 233-2241.

Bonini, M., Souriot, Th., Boccaletti, M. & Brun, J.P. (1997). Successive orthogonal and oblique extension episodes in a rift zone: Laboratory experiments with application to the Ethiopian Rift. Tectonics, v. 16 (2), p. 347-362.

Cámara Rupelo, P. (1989). La terminación estructural occidental de la Cuenca Vasco-Cantábrica. Libro Homenaje a Rafael Soler. AGGEP, Madrid, p. 27-35.

Corti, G. (2012). Evolution and characteristics of continental rifting: Analog modeling-inspired view and comparison with examples from the East African Rift System. Tectonophysics, v. 522-523, p. 1-33.

Espina, R.G. (1994). Extensión mesozoica y acortamiento alpino en el borde occidental de la Cuenca Vasco Cantábrica. Cuadreno Lab. Xeolóxico de Laxe, v. 19, p. 137-150.

Espina, R.G. (1997). La estructura y evolución tectonoestratigráfica del borde occidental de la Cuenca Vasco-Cantábrica (Cordillera Cantábrica, NO de España). Tesis Doctoral. Universidad de Oviedo. 230 p.

Espina, R.G., Alonso, J.L. & Pulgar, J.A. (2004). Extensión Triásica en la Cuenca Vasco-Cantábrica. En: Geología de Espa.a (J.A. Vera, ed.), SGE-IGME, p. 338-339.

Faulds, J.E. & Varga, R.J. (1998). The role of accommodation zones and transfer zones in the regional segmentation of extended terranes. Geol. Soc. Of Am. Special Paper v. 323, p. 1-45.

Gallastegui, J. (2000). Estructura cortical de la cordillera y margen continental cantábricos.: Perfiles ESCI-N. Trabajos de Geología, Univ. Oviedo, v. 22, p. 9-234.

García-Senz. J. (2014). Sondeo Mar cantábrico E1. p. 72-82. En: Caracterización geológica del margen continental español para la determinación de estructuras susceptibles de constituir emplazamientos de almacenamiento de CO_2. Informe de los estudios realizados en el margen cantábrico y del Delta del Ebro. Proyecto ALGECO2 offshore. Instituto Geológico y Minero de España. (IGME). 196 pp.

García-Senz, J. (2013). Estructura Geológica del entorno de El Soplao. En: Avances de la investigación geológica de la cueva de El Soplao y su entorno (Rosales, I, coord.). Madrid, IGME. p. 17-29.

García-Senz, J. & Cañas Fernández, V. (2013a). Hoja del Mapa Geológico 1:25.000 de la Comunidad Autónoma de Cantabria, nº 33-3 San Vicente de La Barquera. IGME y Gobierno de Cantabria.

García-Senz, J. & Cañas Fernández, V. (2013b). Hoja del Mapa Geológico 1:25.000 de la Comunidad Autónoma de Cantabria, nº 33-4 Comillas. IGME y Gobierno de Cantabria.

García-Senz, J. & Merino-Tomé, O. (2011). Hoja del Mapa Geológico 1:25.000 de la Comunidad Autónoma de Cantabria, nº 51-1 Puentenansa. IGME y Gobierno de Cantabria.

García-Senz, J. & Robador, A. (2009). Variation in structural style at a lateral termination of a basement-involved wedge: the margin of the West Cantabrian basin. 6º Simposio sobre el Margen Ibérico Atlántico, Oviedo, España, p. 61-64.

Huerta Carmona, (2009). Hoja del Mapa Geológico 1:25.000 de la Comunidad Autónoma de Cantabria, nº 57-2 Cabezón de la Sal. IGME y Gobierno de Cantabria.

Larrondo Echevarria, E., Mediato Arribas, F.F. & Hernainz Huerta, P.P. (2008). Hoja del Mapa Geológico 1:25.000 de la Comunidad Autónoma de Cantabria, nº 34-4 Renedo. IGME y Gobierno de Cantabria.

Marquínez, J. (1989). Síntesis cartográfica de la Región del Cuera y Los Picos de Europa. Trabajos de Geología, Universidad de Oviedo, v.18, p, 137-144.

Martínez-García, E. (1980). Hoja geológica número 32. Llanes. Mapa geológico de España, escala 1:50.000, Serie MAGNA, IGME.

Menguad, L. (1920). Recherches geologiques Dans la region Cantabrique. Livr. Sc. J. Hermann, 1374 pp.

Mitra, S. (1990). Fault-Propagation Folds: Geometry, kinematic evolution, and hydrocarbon traps. The American Association of Petroleum Geologists Bulletin. v.74 (6), p. 921-945.

Najarro, M. & García-Senz, J. (2014). Sondeo Mar Cantábrico J1. p. 98-111. En: Caracterización geológica del margen continental español para la determinación de estructuras susceptibles de constituir emplazamientos de almacenamiento de CO_2. Informe de los estudios realizados en el margen cantábrico y del Delta del

Ebro. Proyecto ALGECO2 offshore. Instituto Geológico y Minero de España. (IGME). 196 pp.

Najarro, M., Rosales, I. & Martín-Chivelet, J. (2007). Evolución de la plataforma carbonatada de la Florida durante el rifting del Cretácico inferior (Aptiense, NO de Cantabria).En: D.D. Bermudez, M. Najarro & C. Quesada (ed.), II Semana de Jóvenes Investigadores del I.G.M.E., Instituto Geologico y Minero de España, Madrid, p. 123-128.

Pedreira, D. (2005). Estructura cortical de la zona de transición entre los Pirineos y la Cordillera Cantábrica. Ediciones de la Universidad de Oviedo, CD-ROM, 343 pp.

Pujalte, V. (1979). Control tectónico de la sedimentación "purbeck-weald" en las provincias de Santander y N. de Burgos. Acta Geológica Hispánica. v. 14, p. 216-222.

Pulgar, J.A. & Alonso, J.L. (1993). La estructura alpina de la Cordillera Cantábrica. En: Resúmenes XV Reunión de Xeología e Minería do NO Peninsular Lab. Xeol. Laxe, O Castro, Sada, La Coruña, p. 69-71.

Shell España (1980). Mar Cantábrico J1, Well Summary Sheet, NV.

Solé Pont, F.J., Mediato Arribas, F.F., Larrondo Echevarria, E. & Hernainz Huerta, P.P. (2008a). Hoja del Mapa Geológico 1:25.000 de la Comunidad Autónoma de Cantabria, nº 34-3 Torrelavega. IGME y Gobierno de Cantabria.

Solé Pont, F.J., Mediato Arribas, F.F. & Hernainz Huerta, P.P. (2008b). Hoja del Mapa Geológico 1:25.000 de la Comunidad Autónoma de Cantabria, nº 34-1 Suances. IGME y Gobierno de Cantabria.

Solé Pont, F.J., Mediato Arribas, F.F., Larrondo Echevarria, E. & Hernainz Huerta, P.P. (2008c). Hoja del Mapa Geológico 1:25.000 de la Comunidad Autónoma de Cantabria, nº 34-2 Muriedas. IGME y Gobierno de Cantabria.

Suppe, J. & Medwedeff, D.A. (1984). Fault-propagation folding. Geological Society of America. 1984 Annual Meeting Abstracts with Programs, v. 16, 670p.

Tavani, S. & Muñoz, J.A. (2011). Mesozoic rifting in the Basque-Cantabrian Basin (Spain): Inherited faults, transversal structures and stress perturbation. Terra Nova, v. 00, p. 1-7.

Tosal, J.M. (1968). Relaciones zócalo-cobertera en el límite de las provincias de Oviedo y Santander. Brev. Geol. Astur., v. 19, p. 9-14.

CAPÍTULO 3:

LITOESTRATIGRAFÍA Y BIOESTRATIGRAFÍA

CAPÍTULO 3

3.- LITOESTRATIGRAFÍA Y BIOESTRATIGRAFÍA

3.1.- SÍNTESIS DE LA ESTRATIGRAFÍA DE LA CUENCA NOR-CANTÁBRICA

Los materiales aflorantes en la cuenca Nor-Cantábrica (CNC) abarcan edades comprendidas entre el Ordovícico y el Cenozoico, aunque la gran mayoría de los sedimentos pertenecen al Cretácico. Además, localmente, se encuentran depósitos cuaternarios asociados a terrazas, rellenos de fondo de valle, desembocaduras de ríos y depósitos de playa. En las memorias de los mapas 1:50.000 del I.G.M.E de Comillas (33), Torrelavega (34) y Cabezón de la Sal (57) se puede encontrar información general de la estratigrafía de la zona, así como en la síntesis que realizó Hines (1985) donde aparece una descripción general de las principales unidades litoestratigráficas. A continuación se pasa a describir las principales características litológicas de los materiales aflorantes en la CNC, exceptuando los materiales de edad Aptiense-Albiense Superior pro parte y su bioestratigrafía, que serán descritos con mayor detalle en el siguiente apartado, al ser el objetivo fundamental de esta Tesis.

Los materiales ordovícicos corresponden a cuarcitas rosadas en la base y blanquecinas en el resto de la serie, con estratificación cruzada, laminación paralela y *ripples* de corriente (Formación Barrios, Martínez-García, 1981). Presentan alguna intercalación de pizarras y niveles muy delgados carbonosos. Los afloramientos de estos materiales se sitúan en la zona de Pechón (entre las rías Tina Mayor y Tina Menor) cabalgando sobre materiales cretácicos y terciarios.

Los materiales del Carbonífero del área de estudio pertenecen a la "Caliza Griotte" y a la "Caliza de Montaña" en sentido amplio, incluyéndose en esta última las Formaciones Barcaliente, Valdeteja y Picos de Europa (Martínez-García, 1971, 1981). La Caliza Griotte aflora en Pechón y está constituida por calizas tableadas y nodulosas, microcristalinas, de tonos rosados con abundantes restos de crinoideos, goniatítidos,

ostrácodos y radiolarios. La Caliza de Montaña aflora tanto en la zona de Pechón como en el borde SO de la zona de estudio, junto al río Nansa (entre Rábago y Celis). Ésta está constituida por calizas laminadas y masivas, bioesparíticas y micríticas, parcialmente dolomitizadas, de tonos grises y oscuros, depositadas en ambientes que varían desde talud y cuenca a plataforma carbonatada (Martínez-García, 1981). Fuertemente discordante sobre estas calizas, en la serie que aflora entre Rábago y el oeste del embalse de la Palombera, se puede distinguir un tramo discontínuo de brechas calcáreas rellenando paleorrelieves resultantes tras la orogenia Varisca, y cuyos cantos subangulosos a subredondeados recuerdan a las microfacies más frecuentes de la Caliza de Montaña. Culmina con un tramo de margas y lutitas de color gris y negro con restos carbonosos, que tienen algunas intercalaciones de brechas calcáreas semejantes a las del anterior tramo. La edad más probable de estos materiales es Pérmico Inferior (atribuibles a la Fm. Sotres en sus equivalentes laterales) (Martínez-García, 1981; Robles, 2004) y se interpretan como depósitos subaéreos de talud, abanico aluvial y lacustres (Robles *et al.*, 1987; López-Gómez *et al.*, 2002).

Los materiales triásicos que afloran en el área de estudio se presentan en facies germánicas. Las facies del Triásico Inferior-Medio (Buntsandstein) aflorantes en el margen SO de la zona de tesis (Sierra del Escudo de Cabuérniga) se apoyan en discordancia y solapamiento expansivo sobre las materiales plegados del basamento varisco (Carbonífero principalmente) (López-Gómez *et al*, 2002; Robles, 2004). Estas facies están representadas por lutitas rojas vinosas con intercalaciones de areniscas rojizas de grano fino a medio, lutitas rojas y verdes, areniscas y conglomerados, organizados en una sucesión compleja de carácter positivo (Robles y Pujalte, 2004). Los espesores de estos materiales son variables (100 a 600 metros) debido al relleno de espectaculares paleorrelieves del techo de las calizas carboníferas infrayacentes (García-Mondéjar *et al*, 1986). Las facies Keuper del Triásico Superior (Carniense; Robles y Pujalte, 2004) están constituidas por arcillas plásticas, de tonos abigarrados, con intercalaciones de yesos versicolores y sal en profundidad. Los afloramientos de estos materiales se sitúan principalmente en la zona sur-central y al NE del área de estudio y secundariamente como pequeñas áreas en los alrededores de San Vicente de la Barquera, Caviedes, Cuchía (playa de Usgo) y Comillas.

Los materiales del Jurásico presentes en la zona de estudio corresponden exclusivamente al Jurásico Inferior (Lías). Estos afloran de una manera dispersa generalmente a favor de estructuras tectónicas mayores y asociados a la extrusión diapírica de arcillas y evaporitas del Keuper. Así los afloramientos del Jurásico Inferior están limitados a la zona NE (área de Cuchía; Foto 3.1) y centro (área de Cabezón de la Sal) del área de estudio. Los materiales pertenecientes al Lías inferior (Hettangiense–Sinemuriense) están compuestos por brechas dolomíticas intraformacionales (carniolas), a las que siguen dolomías masivas y calizas microdolomíticas bandeadas, terminando la serie con dolomías bien estratificadas y calizas micríticas que contienen lamelibranquios, ostrácodos y *Lingulina*. Los materiales del Lías superior (Pliensbaquiense) están compuestos por una alternancia rítmica de margas hojosas ricas en materia orgánica y pirita y calizas tableadas o nodulosas (Robles *et al.*, 2004) (Foto 3.1). Estos materiales, que presentan belemnites, ammonites, crinoideos y bivalvos, se interpretan como depósitos hemipelágicos (Formación Camino; Quesada *et al.*, 2005).

Foto 3.1.- Discordancia angular entre la ritmita de calizas, margas y lutitas orgánicas hemipelágicas del Pliensbaquiense inferior (Fm. Camino) y areniscas fluviales del Hauteriviense-Barremiense (Fm. Vega de Pas). Acantilados de Cuchía entre la playa de Usgo y la playa de Los Caballos.

Los materiales del Jurásico Medio y Superior, así como los del Berriasiense y Valanginiense Inferior y Medio (en facies Purbeck) están ausentes en toda la zona de estudio, posiblemente debido a que durante la etapa de *rifting* del Jurásico Superior-Cretácico Inferior la zona estuvo sujeta a erosión y/o no deposición (Robles *et al.*, 2004).

Los materiales del Cretácico Inferior en facies wealdenses (Hauteriviense–Barremiense) se extienden por toda la zona de estudio, apoyándose en disconformidad o en discordancia angular sobre el Buntsandstein, Keuper (margen SO de la zona de estudio) y Lías (áreas de Cuchía, Cabezón de la Sal y Riocorvo) (Foto 3.1). Estas facies corresponden con el Grupo Pas (Pujalte, 1981) y se caracterizan por litologías predominantes de lutitas rojas con paleocaliches y paleosuelos, areniscas y arcillas limolíticas con intercalaciones de niveles de carbones y areniscas de carácter fluvial, asimilables a la Formación Vega de Pas (Pujalte, 1982; Pujalte *et al.*, 2004). Las facies wealdenses muestran una marcada variación lateral de potencia, disminuyendo los espesores regionales en el área de estudio hacia el oeste y norte. Esta variación de espesores puede atribuirse a un tectonismo activo asociable al inicio de la etapa de *rift* del Jurásico Superior–Cretácico Inferior (Pujalte *et al.*, 2004).

Estos sedimentos de naturaleza continental dan paso de forma gradual y rápida a los sedimentos del Aptiense y Albiense, de ambientes transicionales y marinos someros. Todos estos materiales forman la mayoría de los afloramientos cretácicos de la zona de estudio, y están constituidos principalmente por 8 unidades litoestratigráficas con rango de formación, una de ellas de nueva definición a partir de este estudio, que de más antigua a más moderna se han denominado: Fm. Rábago, Fm. Umbrera, Fm. Patrocinio, Fm. San Esteban, Fm. Rodezas, Fm. Reocín, Fm. Las Peñosas y Fm. Barcenaciones (síntesis de García-Mondéjar, 1982, con modificaciones de Hines, 1985 y Najarro *et al.*, 2011b). Estas unidades litoestratigráficas constituyen el denominado Complejo Urgoniano, donde se enmarcan los objetivos de este estudio, por lo que su descripción detallada será tratada en el siguiente apartado. Los materiales del Albiense Superior corresponden principalmente a la Formación Barcenaciones, de naturaleza carbonatada (García-Mondéjar, 1982) y a parte de la Formación Bielba (equivalente lateral hacia el noroeste de la Formación Valmaseda, García-Mondéjar, 1982), de naturaleza siliciclástica. El estudio de estas dos últimas unidades no se incluye entre los objetivos

de este trabajo de investigación. No obstante, el hecho de que la Fm. Barcenaciones represente el techo de la sucesión estudiada, junto con que aparezca en las tres áreas diferenciadas, hace que esta formación sea el *datum* de techo de referencia de este estudio. Así pues, se ha considerado oportuno incluir también una descripción litoestratigráfica más detallada de esta formación en el siguiente apartado, junto con el resto de las formaciones de edad Aptiense-Albiense, foco ya de este estudio.

Los materiales del Cretácico Superior afloran en el núcleo de los sinclinales de Merodio, Cóbreces y Santillana y se dividen en las siguientes unidades litoestratigráficas (García-Mondéjar y Pujalte, 1981): 1) Formación Bielba (parte alta del Albiense Superior–Cenomaniense Inferior, Wilmsen, 2000): de unos 250 metros de espesor, compuesta por un tramo inferior de arenas finas, limos y arcillas limolíticas, con restos carbonosos y por un tramo superior formado por limos y arcillas limolíticas con orbitolinas, ostreidos y foraminíferos, que se intercalan con bancos de caliza. 2) Formación Altamira (Cenomaniense Inferior-Medio): de unos 100–150 metros de espesor máximo en el área de estudio, está constituida por bancos de calcarenitas, gris-amarillentas, bioclásticas, con orbitolinas y algunos rudistas, intercalados con margas hojosas. 3) Formación Margas y Calizas del Sardinero (Turoniense-Campaniense Medio): de unos 500 metros de espesor en el área de estudio, está formada por una alternancia monótona de margas y calizas arcillosas de color gris verdoso. La parte baja de la serie contiene abundante glauconita, mientras que hacia el techo de la misma se observa desarrollo de dolomitización. 4) Formación de Cabo de Lata (Campaniense Superior-Maastrichtiense): de unos 150 metros de potencia, está constituida por calcarenitas, calizas arenosas y areniscas calcáreas que frecuentemente contienen glauconita. La parte alta de la unidad se presenta bastante dolomitizada. 5) Formación de Muñorrodero (Campaniense Superior-Maastrichtiense-Paleoceno): de unos 90–170 metros de potencia, es en parte equivalente lateral de la unidad anterior hacia el oeste y está formada principalmente por dolomías sacaroideas y arenosas.

Los materiales cenozoicos yacen concordantes sobre los materiales del Cretácico Superior, aflorando en el núcleo del sinclinal de Merodio, en el flanco norte del anticlinal de Abanillas y en el flanco sur cabalgado del anticlinal de Santillán.

Los sedimentos del Paleoceno están constituidos por dolomías anteriormente descritas de la Formación Muñorrodero.

Los materiales del Eoceno se caracterizan por su gran riqueza en alveolinas y nummulites. A grandes rasgos, se compone de unos 250 metros de calizas bioclásticas; arenas conglomeráticas con intercalaciones lenticulares de areniscas calcáreas; calcarenitas grises, con glauconita en algunos tramos; calcarenitas arenosas localmente dolomitizadas; margas arenosas de tonos grises y azulados con restos carbonosos en algunos niveles; y areniscas y conglomerados que pasan lateralmente a brechas calcáreas con olistolitos de calizas rosadas arrecifales, con intercalaciones de arcillas plásticas, pardo-rojizas (Hines, 1985).

Los afloramientos del Priaboniense-Oligoceno de carácter marino presentes en el NO de la CNC son los únicos conocidos en todo el norte de España, ya que en otras zonas el Oligoceno se presenta siempre en facies continentales. Estos materiales están constituidos por arcillas con abundantes microforaminíferos, calcarenitas turbidíticas y conglomerados calcáreos resedimentados con frecuentes intercalaciones de arcillas rojizas y arcillas grises (Hines, 1985).

3.2.- LITOESTRATIGRAFÍA Y BIOESTRATIGRAFÍA DEL APTIENSE-ALBIENSE DE LA CUENCA NOR-CANTÁBRICA

La estratigrafía y bioestratigrafía general del Aptiense-Albiense de la zona de estudio ha sido tratada con anterioridad por Mengaud (1920), Ramírez del Pozo (1972), Collignon *et al.* (1979), García-Mondéjar (1982), Pascal (1985), Hines (1985) y Wilmsen (2005). Sin embargo, hasta la fecha, no se había realizado un estudio detallado de la organización estratigráfica y de las características litológicas de los materiales de estas edades que afloran en las tres áreas diferenciadas en la zona de estudio (i.e. áreas de La Florida, sinclinal de Santillana y Cuchía, Figura 3.1). La primera denominación formal de las unidades litoestratigráficas del Aptiense-Albiense de la zona fue realizada por García-Mondéjar (1982), estableciendo los nombres, edad y equivalencias de las principales unidades estratigráficas. Este esquema fue posteriormente modificado por

Hines (1985), que cambió el nombre de algunas de las formaciones y subdividió otras en diferentes formaciones o en unidades menores a las que dió rango de miembro. En este trabajo se ha optado por adoptar la terminología utilizada por Hines (1985) para denominar las distintas formaciones, añadiendo algunas modificaciones. Esto ha llevado a la definición de una nueva unidad litoestratigráfica de carácter formal (Formación Rábago) en las áreas de La Florida y del sinclinal de Santillana y a la redefinición del esquema litoestratigráfico previamente establecido en el área (Figura 3.1) (García-Mondéjar, 1982; Hines 1985).

Desde el punto de vista bioestratigráfico, este trabajo de investigación aporta nuevas dataciones en base a ammonites, foraminíferos planctónicos y bentónicos, nanofósiles calcáreos y palinomorfos, sintetizados en el apartado 3.2.2 de este capítulo. De este modo, se ha podido determinar la existencia de una laguna estratigráfica que abarca al menos la parte alta del Aptiense Inferior en el área de La Florida, de otra laguna estratigráfica que abarca gran parte del Albiense Inferior y Medio en el área de Cuchía (Fm. Reocín), y se ha redefinido la edad de varias unidades en el área de Cuchía (Figuras 3.1, 3.2 y 3.3).

Para el resto de las dataciones se han utilizado datos de estudios previos de fauna de ammonites y de zonas de conjunto y de extensión de foraminíferos bentónicos, especialmente orbitolínidos, previamente definidas por distintos autores (ej. Mengaud, 1920; Rat, 1959; Ramírez del Pozo, 1972; Collignon *et al.*, 1979; Pascal, 1985, entre otros).

La correlación de las diferentes unidades litoestratigráficas se ha realizado fundamentalmente basándonos en el seguimiento cartográfico de las unidades y en el reconocimiento de niveles guía, y cuando ha sido posible, en base a datos bioestratigráficos. Una vez conocida la correlación entre las diferentes unidades, la edad de alguna de ellas, a falta de otros datos paleontológicos, ha sido inferida a partir de las unidades que son sus equivalentes laterales.

3.2.1. ESTUDIO LITOESTRATIGRAFICO

En este capítulo se describen las características principales de las unidades litoestratigráficas estudiadas, con indicación de las aportaciones y modificaciones que se proponen en este trabajo al esquema establecido. En esta descripción se incluyen aspectos generales regionales, sedimentológicos y de edad de las unidades, que se detallan con aportaciones propias de descripciones de facies y secuencias de las series tipo (estratotipo e hipoestratotipo) estudiadas, junto con su interpretación. También se establecen las diferencias de arquitectura litoestratigráfica a lo largo del área de estudio debido a la compartimentación del área en distintos bloques (llamados en este trabajo áreas o sectores). En orden cronológico, las distintas unidades litoestratigráficas que componen la serie del Aptiense-Albiense de la zona de estudio son las siguientes (Figura 3.1):

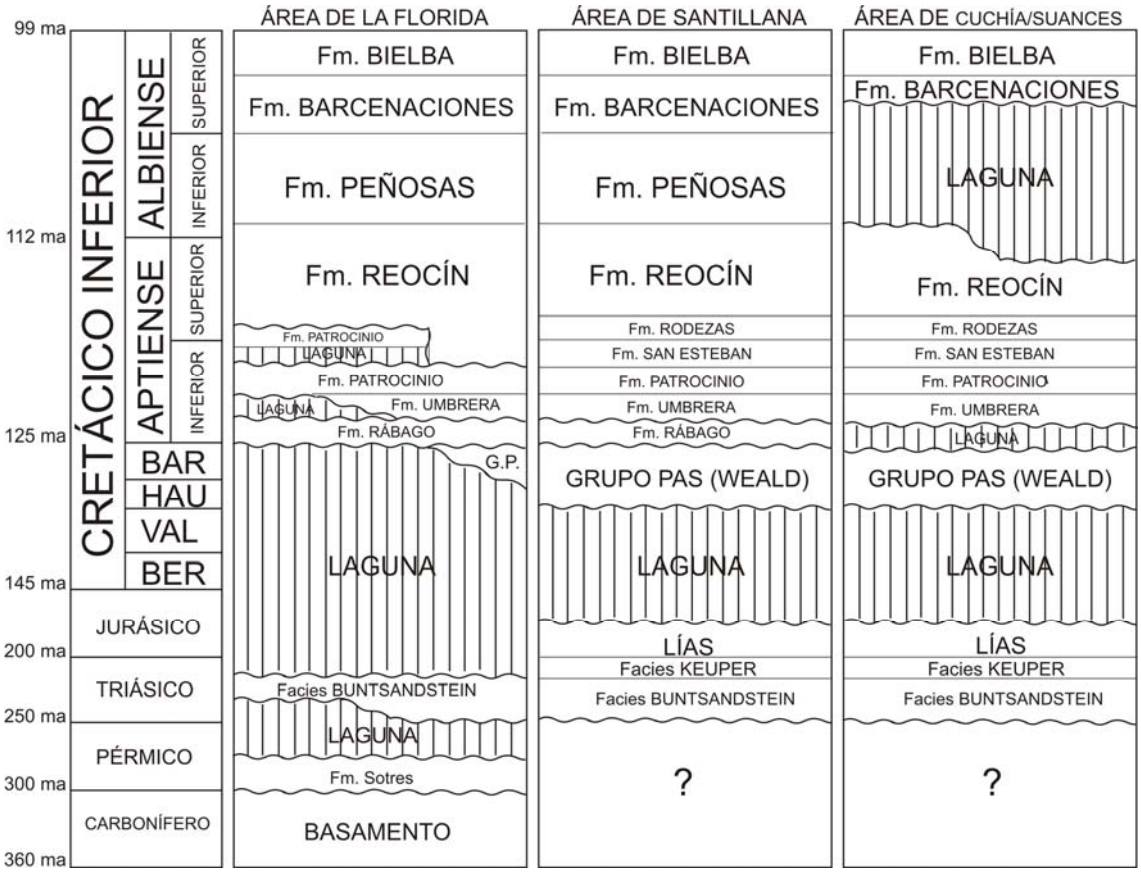

Figura 3.1.- Litoestratigrafía revisada del área de estudio (basado en García-Mondéjar, 1982; Hines, 1985 y en los datos de este trabajo).

3.2.1.1. FORMACIÓN RÁBAGO

Nombre de la Unidad: Rábago

Rango de la Unidad: Formación

Antecedentes: Unidad individualizada por primera vez por Najarro *et al.* (2011b) y definida formalmente para este trabajo de investigación. Anteriormente este litosoma era incluido en la unidad suprayacente, sin tener en cuenta la discontinuidad estratigráfica que lo separa del litosoma suprayacente, de esta forma García-Mondéjar (1982) incluyó esta unidad dentro de lo que denominó como Formación de Caranceja.

Secciones de referencia: La unidad aflora en las áreas de La Florida y sinclinal de Santillana. La sección tipo se localiza en el área de La Florida, concretamente junto al río Nansa a la altura de la pequeña localidad de Rábago y, pasado dicho pueblo, en un camino que corta la carretera de montaña que sube a la cueva de El Soplao. En el área del sinclinal de Santillana, la unidad se observa bien en la carretera que une las localidades de Hayuela y Canales. En el área de Cuchía, esta unidad está ausente.

Aspectos regionales: El límite inferior de esta unidad viene marcado por una discordancia angular sobre las facies Buntsandstein (Figura 3.1; Fotos 3.2 y 3.3), o bien sobre las facies wealdenses (Figura 3.1). El límite superior está representado por una discontinuidad estratigráfica que se manifiesta, según la zona, por una superficie de erosión (Foto 3.4), o por una superficie de disolución por exposición subaérea del techo de la unidad (Foto 3.5) y sobre la que se desarrolla una costra ferruginosa (Foto 3.6). Esta costra presenta varios milímetros de espesor y está compuesta por finas películas de óxido de hierro (*biofilms*), incrustaciones de foraminíferos aglutinantes, serpúlidos y microperforaciones (descrito en Najarro y Rosales, 2008a) (Foto 3.7). La potencia de la unidad varía entre 4 y 18 metros.

Foto 3.2.- Contacto discordante entre areniscas de la base de la Formación Rábago del Aptiense Inferior y lutitas rojas del Triasico (facies Buntsandstein) en las proximidades de Rábago (sección de Las Antenas en Rábago, área de La Florida).

Foto 3.3.- Afloramiento mostrando la discontinuidad sedimentaria del contacto entre areniscas ocres de la base de la Formación Rábago del Aptiense Inferior y lutitas rojas del Triasico (facies Buntsandstein) en las proximidades de Cades (corte de la carretera S-230, sección de río Nansa, área de La Florida).

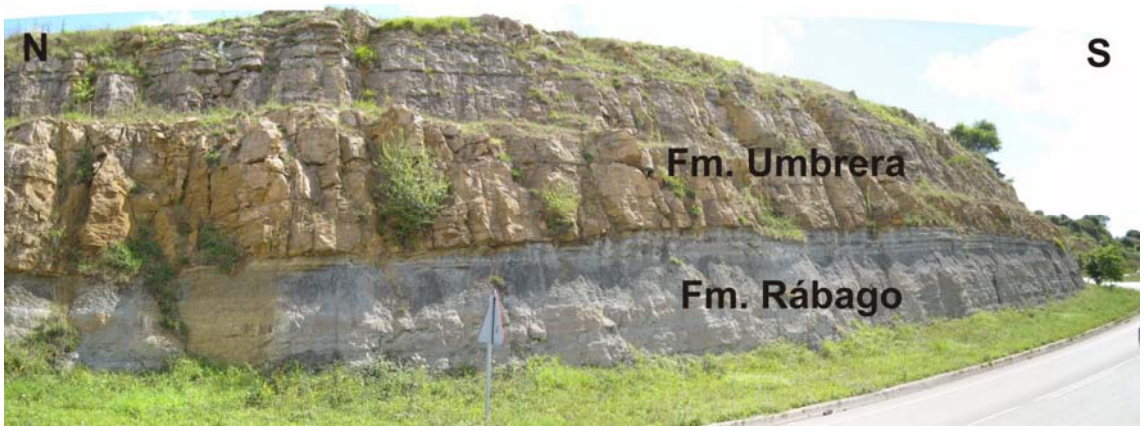

Foto 3.4.- Superficie de erosión entre el techo de la Formación Rábago y las calcarenitas de la Formación Umbrera en la carretera CA-135 a la altura de la localidad de La Hayuela. Sección Hayuela-Canales, área del sinclinal de Santillana.

Foto 3.5.- Aspecto de campo de la superficie irregular de disolución con cavidades de tamaño decimétrico, fisuras y macro y microrelieves, con superficies corrosivas que se rellenan con cantos calizos de la Fm. Rábago en una matriz de material calcarenítico de la unidad suprayacente (Fm. Umbrera). Sección Rábago, área de La Florida.

Foto 3.6.- Aspecto de campo de la costra ferruginosa que aparece tapizando la superficie de disolución por exposición subaérea a techo de la Fm. Rábago. Sección de Rábago, área de La Florida.

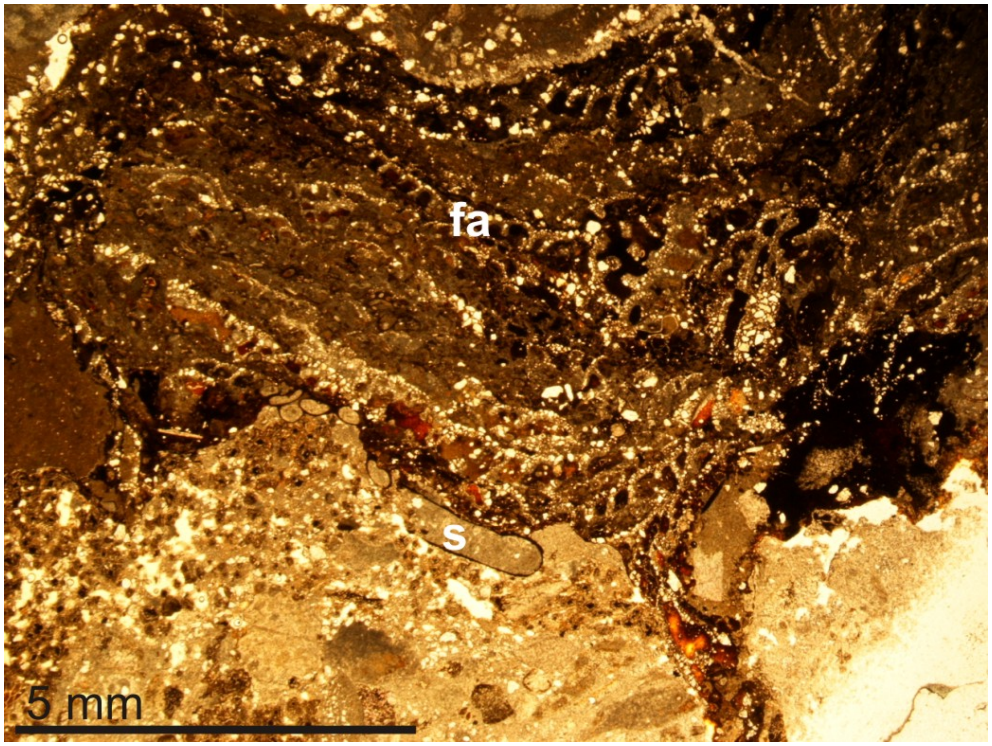

Foto 3.7.- Imagen con lupa binocular de la costra ferruginosa compuesta por películas de óxido de hierro (*biofilms*), incrustaciones de foraminíferos aglutinantes (fa), serpúlidos(s) y microperforaciones. Muestra LA-12, sección de Rábago, área de La Florida.

Edad: Aptiense Inferior, concretamente Bedouliense inferior, si se tiene en cuenta su posición estratigráfica. Mengaud (1920) y Ramírez del Pozo (1972) citan en materiales correspondientes a eta unidad *Palorbitolina lenticularis* (BLUMENBACH).

Descripción: La unidad presenta una naturaleza mixta terrígeno-carbonatada. En la localidad tipo la parte basal de la unidad es predominantemente siliciclástica (Fotos 3.8A y B), distinguiéndose una alternancia de areniscas micáceas de grano fino-medio con estratificación cruzada, lutitas carbonosas y limos con laminación lenticular, *flaser* y *ripples* de corriente. La parte media de la serie muestra una composición mixta terrígeno-carbonatada de arenas calcáreas con laminación ondulada y ocasionalmente *ripples* de oscilación que alternan con niveles de lutitas aleuríticas, calizas *packstone-grainstone* y margas con orbitolinas. El tramo superior de la unidad, más carbonatado, está compuesto por una alternancia de margas con orbitolinas, calizas margosas nodulosas y calizas *grainstone-packstone* en la parte inferior y calizas *wackestone-mudstone* con corales, gasterópodos y rudistas de pequeño tamaño en la parte superior (Foto 3.8C y D, Lámina 1). La unidad culmina con una superficie irregular de disolución con cavidades de tamaño decimétrico, fisuras y macro y micro relieves con superficies corrosivas que se rellenan con cantos calizos de la serie infrayacente en una matriz de material calcarenítico de la unidad suprayacente (Foto 3.6). Localmente la superficie de disolución se encuentra tapizada por una costra ferruginosa. En el área del sinclinal de Santillana la unidad es predominantemente margosa-limosa con orbitolinas. Aquí el techo de la unidad presenta una superficie de erosión que trunca los estratos infrayacentes (Foto 3.4).

Interpretación del medio sedimentario: Se interpreta esta unidad como un sistema de plataforma marina somera mixta terrígeno-carbonatada. La base de la unidad representa una transgresión rápida sobre materiales continentales cretácicos o triásicos (facies Weald o Buntsandstein) según las áreas. El techo se interpreta como una superficie de exposición subaérea.

Foto 3.8.- Formación Rábago. **A)** Aspecto general de la Formación Rábago en la sección de río Nansa, área de La Florida. **B)** Tramo inferior de la unidad compuesta por areniscas micáceas de grano fino-medio, lutitas carbonosas y limos con laminación lenticular, *flaser* y *ripples* de corriente. Sección Río Nansa, área de La Florida. **C)** Parte superior de la unidad formada por una alternancia de margas con orbitolinas, calizas margosas nodulosas y calizas *grainstone-packstone*. Sección Rábago, área de La Florida. **D)** Detalle de la parte superior de la unidad compuesta por caliza *mudstone*. Sección de río Nansa, área de La Florida.

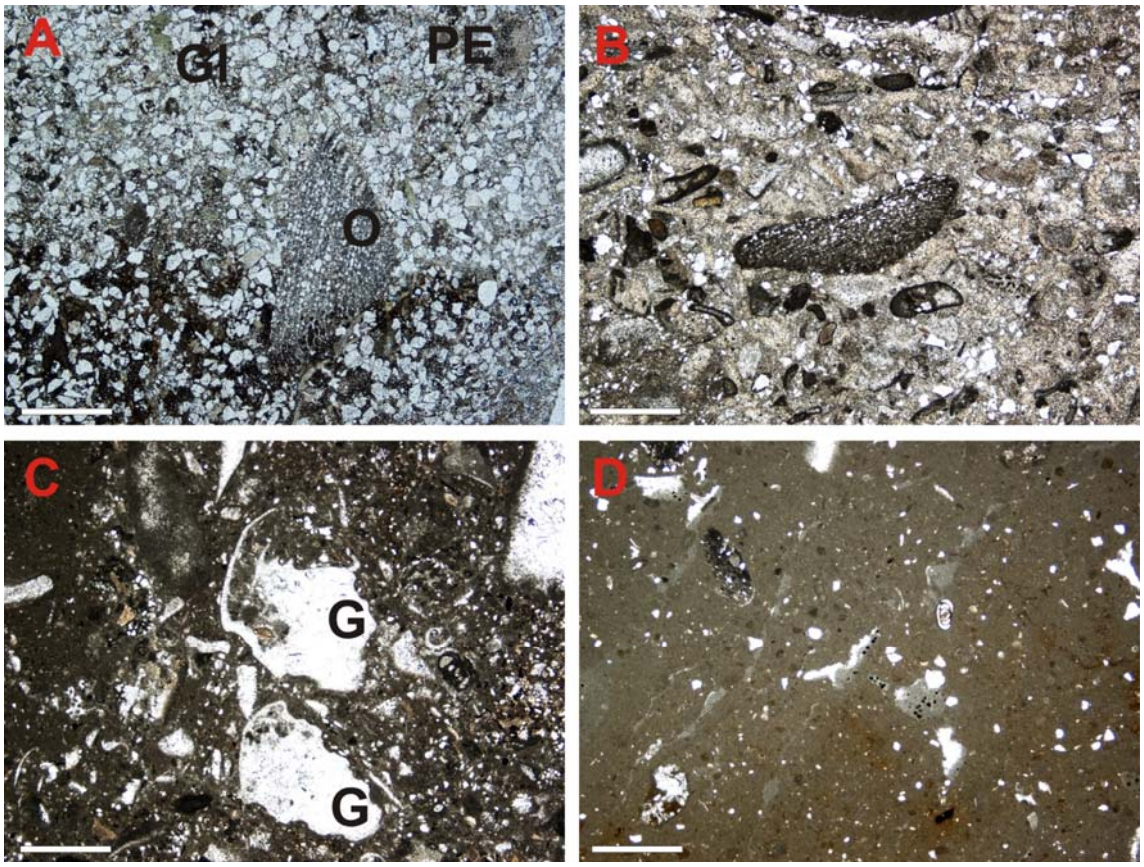

Lámina 1.- Microfacies de la Formación Rábago. La escala para todas las imágenes es de 1mm. **A)** Arenisca calcárea con orbitolinas (O), placas de equinodermo (PE) y granos de glauconita detrítica (Gl). Muestra PN-1, sección de río Nansa, área de La Florida. **B)** Calcarenita *grainstone-packstone* con orbitolinas y bioclastos. Muestra PN-7, sección de río Nansa, área de La Florida. **C)** Caliza *packstone* con gasterópodos, foraminíferos y bioclastos. Muestra PN-9B, sección de río Nansa, área de La Florida. **D)** Caliza *mudstone* con foraminíferos y porosidad fenestral rellena por *silt* vadoso. Muestra PN-10, sección de río Nansa, área de La Florida.

3.2.1.2. FORMACIÓN UMBRERA

Nombre de la Unidad: Umbrera

Rango de la Unidad: Formación

Antecedentes: Unidad definida por Hines (1985). Es equivalente en parte a: "nivel 3" del corte de Suances de Mengaud (1920), "Tramo 1" del corte de Saja realizado por Rat (en Ciry *et al.*, 1967), Unidad C_{151}[1] del MAGNA, Formación de Caranceja de García-Mondéjar (1982) y miembro calcarenítico de la Formación Caranceja de Wilmsen (2005).

Secciones de referencia: La sección tipo se localiza en Punta de Umbrera, en la costa de Cuchía (denominada Sección de Cuchía en la Figura 3.2), término municipal de Miengo.

Aspectos regionales: Presenta una potencia máxima de 50 metros en el sector de La Florida (sección de Bustriguado, Figuras 3.2 y 3.3), que disminuye gradualmente hasta desaparecer en la sección de El Soplao (Figuras 3.2 y 3.3). En esta zona, el límite inferior está definido por una relación de *onlap* sobre la superficie de disolución tapizada por una costra ferruginosa, a techo de la Formación Rábago (Najarro y Rosales, 2008a). En el área del sinclinal de Santillana la unidad presenta una potencia de unos 12 metros (sección de Hayuela-Canales, Figura 3.2) y su contacto con la unidad infrayacente está representado por una superficie erosiva (Foto 3.4). En el área de Cuchía, la unidad alcanza 20 metros de potencia, estando el límite inferior representado por una superficie de inundación, neta, ligeramente erosiva y bioturbada, sobre lutitas con paleosuelos de las facies Wealdenses infrayacentes (Fotos 3.9 y 3.10). El límite superior de la unidad viene marcado por una superficie de cambio brusco en el tipo de litología (i.e. a margas oscuras laminadas) o por una discontinuidad reconocible como una superficie ferruginizada, fuertemente bioturbada, incrustada con ostreidos y con desarrollo de glauconita autigénica (sección de Cuchía), sobre la que se produce el depósito de las margas oscuras de la siguiente unidad (Fm. Patrocinio).

Foto 3.9.- Vista panorámica del contacto entre las calcarenitas de la Formación Umbrera y las facies wealdenses (Fm. Vega de Pas) formadas por lutitas versicolores y paleosuelos, en el área de Cuchía.

Foto 3.10.- Detalle del contacto neto transgresivo entre lutitas versicolores con paleosuelos y signos de edafización de las facies Weald (Fm. Vega de Pas) y la base de las calcarenitas de la Fm. Umbrera. Sección de Cuchía (playa de Los Caballos), área de Cuchía.

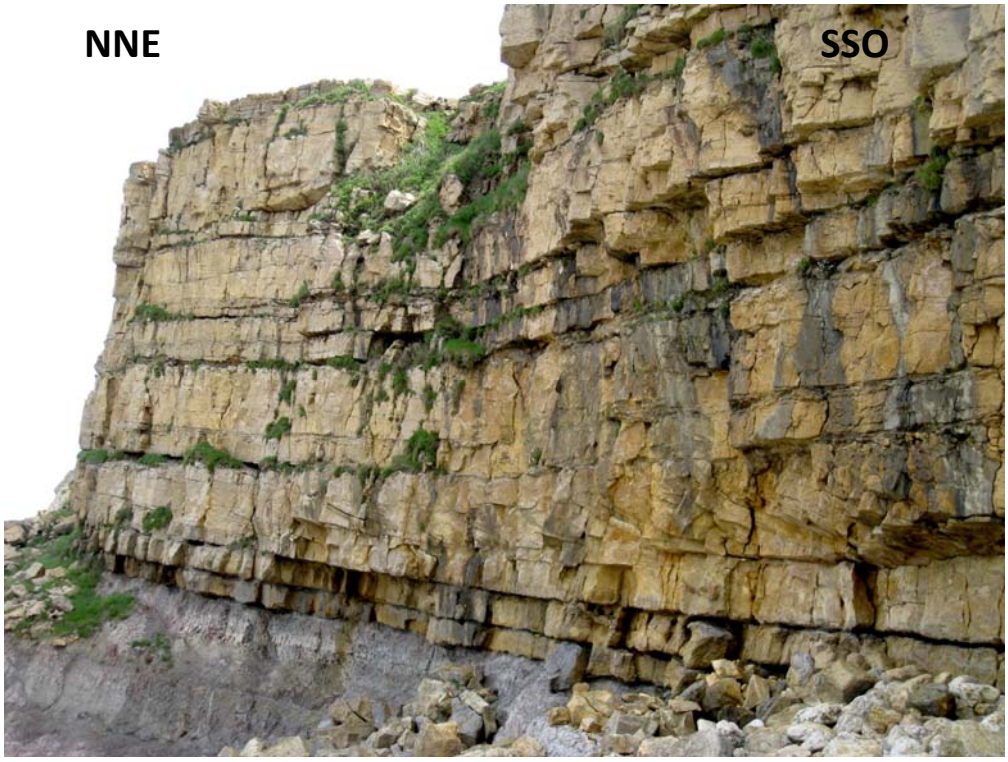

Foto 3.11.- Aspecto de la Formación Umbrera en el afloramiento anterior (área de Cuchía). La unidad está formada por bancos métricos tabulares de calcarenita con estratificación cruzada a escala métrica y decimétrica.

Edad: La edad de esta formación se ha asignado al Bedouliense inferior en base a su contenido paleontológico, caracterizado por la asociación de *Palorbitolina lenticularis* (BLUMENBACH) (Pascal, 1985) y *Choffatella decipiens* SCHLUMBERGER (Collignon *et al.*, 1979), así como a su posición estratigráfica.

Descripción: En el corte tipo de Punta de Umbrera (sección de Cuchía en la Figura 3.2), la unidad está compuesta por una sucesión de bancos decimétricos a métricos de calcarenitas *grainstone*, *packstone* y ocasionalmente *rudstone* con estratificación cruzada (Fotos 3.11 y 3.12A y B, Lámina 2). La parte basal de la serie presenta niveles continuos de calcarenitas bioclásticas arenosas y bancos de caliza *grainstone* con oolitos ferruginizados y estratificación cruzada en surco. En la parte inferior y media de la serie se identifican bancos de caliza *grainstone* con abundantes bioclastos y oolitos, con estratificación cruzada en surco de escala métrica y decimétrica. La parte superior de la unidad está formada por calizas *packstone* y *grainstone* con laminación cruzada que intercalan niveles discontinuos de margas con orbitolinas (Foto 3.12C). El techo de los bancos de caliza suelen presentar bioturbaciones de tipo *Thalassinoides* (Foto 3.12D) rellenas por margas con orbitolinas. El techo de la unidad está compuesto por un banco de calcarenita con ostreidos, glauconita e intensa bioturbación (Foto 3.12E).

Interpretación del medio sedimentario: Se interpreta esta unidad como barras de arena oolítico-bioclástica formando depósitos de bajíos o *shoals* en un medio de alta energía, localizado en la parte interna a media de una rampa carbonatada. La superficie bioturbada con glauconita e incrustada por ostreidos en el techo de la unidad en la sección de Cuchía indica un periodo de no-depósito o baja tasa de sedimentación (*firmground* incipiente) debido a un aumento rápido en la profundidad del medio, de modo que los bajíos fueron abandonados y colonizados por organismos cavadores y posteriormente cubiertos por margas. Todo ello sugiere que la Formación Umbrera se depositó durante un episodio transgresivo, produciéndose una profundización rápida del medio sedimentario hacia el techo de la unidad.

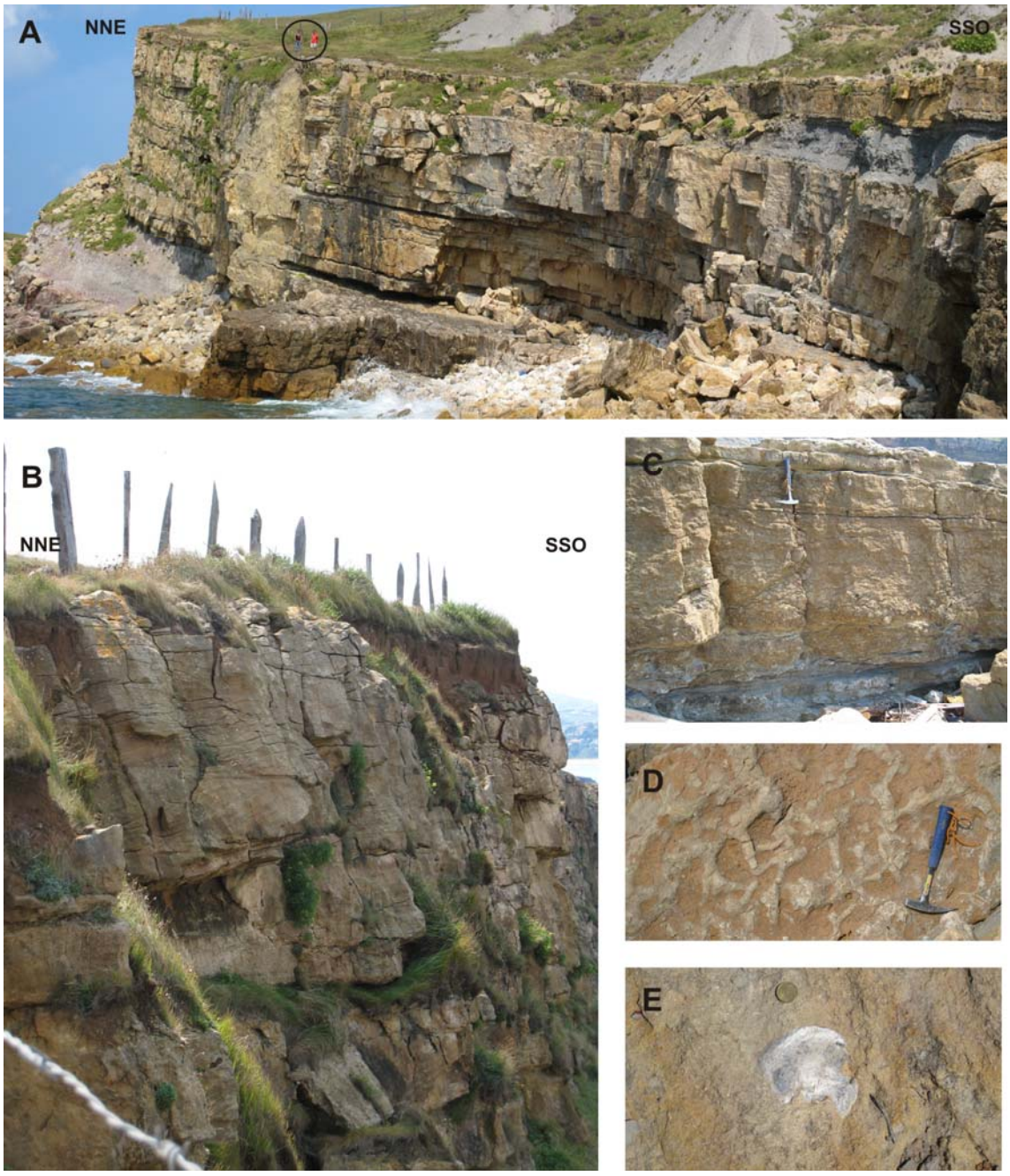

Foto 3.12.- Aspecto de la Formación Umbrera en el corte tipo de Punta Umbrera (área de Cuchía). **A)** Bancos métricos de calcarenita con estratificación cruzada en surco de escala métrica y decimétrica, sobre lutita roja de la Fm. Vega de Pas. **B)** Detalle de los bancos de calcarenita con estratificación cruzada. **C)** Parte superior de la unidad formada por calizas *packstone* y *grainstone* con laminación cruzada que intercalan niveles discontinuos de margas con orbitolinas. **D)** Bioturbaciones de tipo *Thalassinoides* al techo de los bancos de caliza. **E)** Techo de la unidad compuesto por calcarenitas con ostreidos, glauconita e intensa bioturbación.

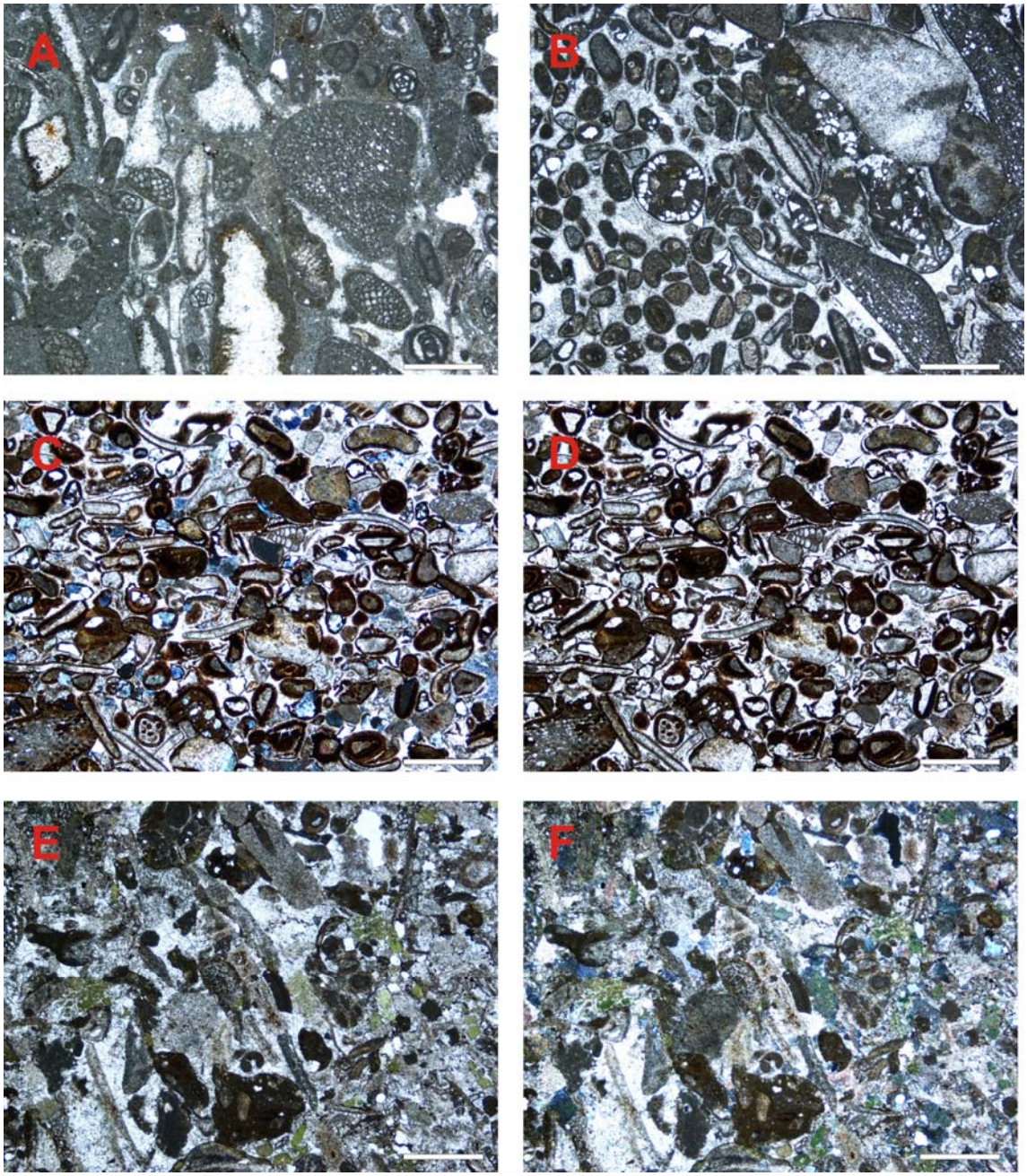

Lámina 2.- Microfacies de la Formación Umbrera. La escala para todas las imágenes es de 1 mm. **A)** Calcarenita *packstone* bioclástica (muestra CU-2, sección de Cuchía, área de Cuchía). **B**) *Grainstone* de oolitos y bioclastos (muestra LF-3, sección de La Florida, área de La Florida). **C**) *Grainstone* de oolitos y bioclastos ferruginizados (muestra LIG-caran, sección Bustriguado, área de La Florida). **D**) Misma imagen con nícoles paralelos. **E**) *Grainstone* bioclástico con glauconita (muestra CU-8, sección de Cuchía, área de Cuchía). **F**) Misma imagen con nícoles cruzados.

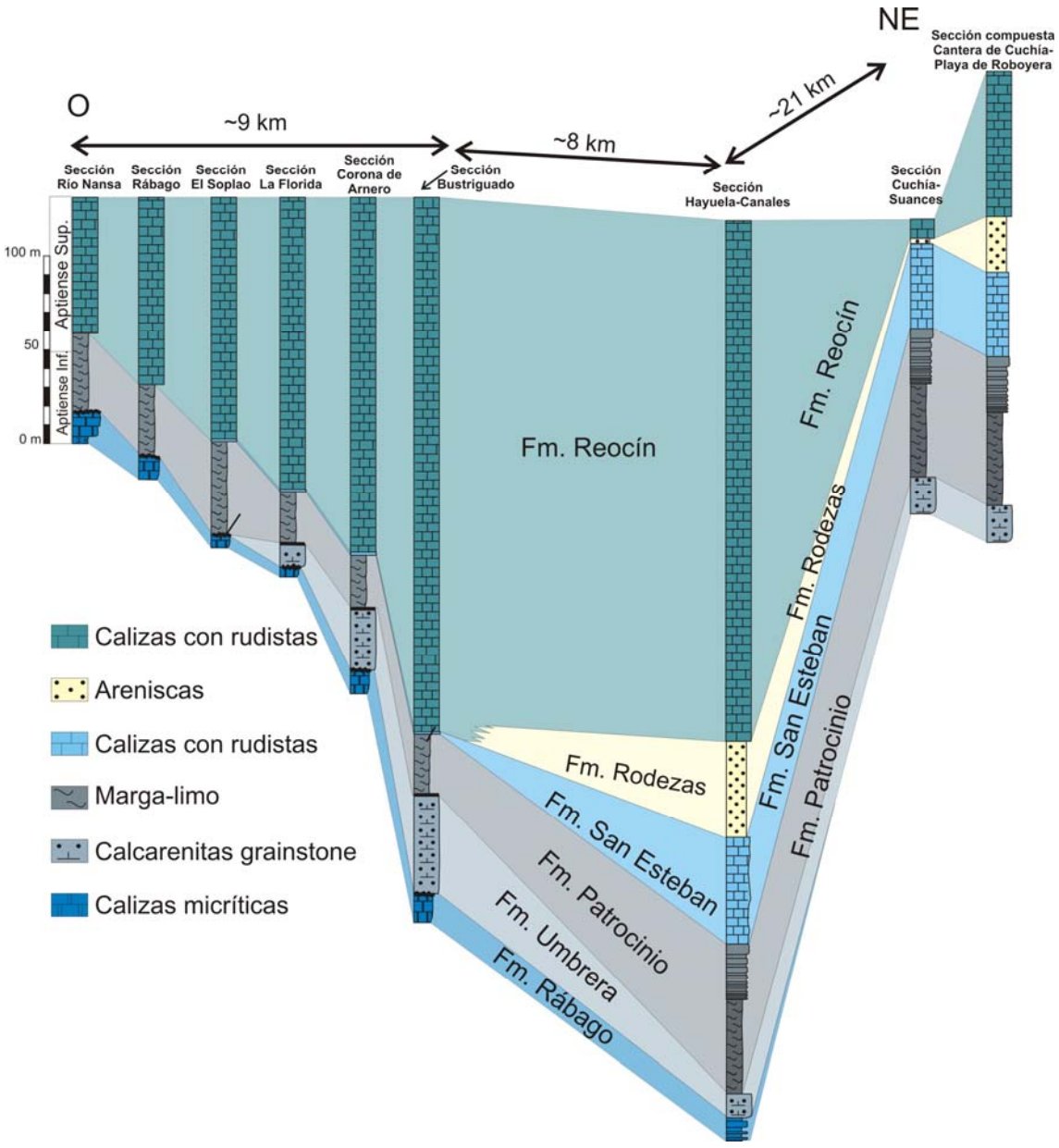

Figura 3.2.- Diagrama de correlación litoestratigráfica de las diferentes unidades del Aptiense del área de estudio, mostrando las principales facies, distribución de las formaciones y variaciones regionales de las potencias sedimentarias. Modificado de Najarro *et al.* (2011b).

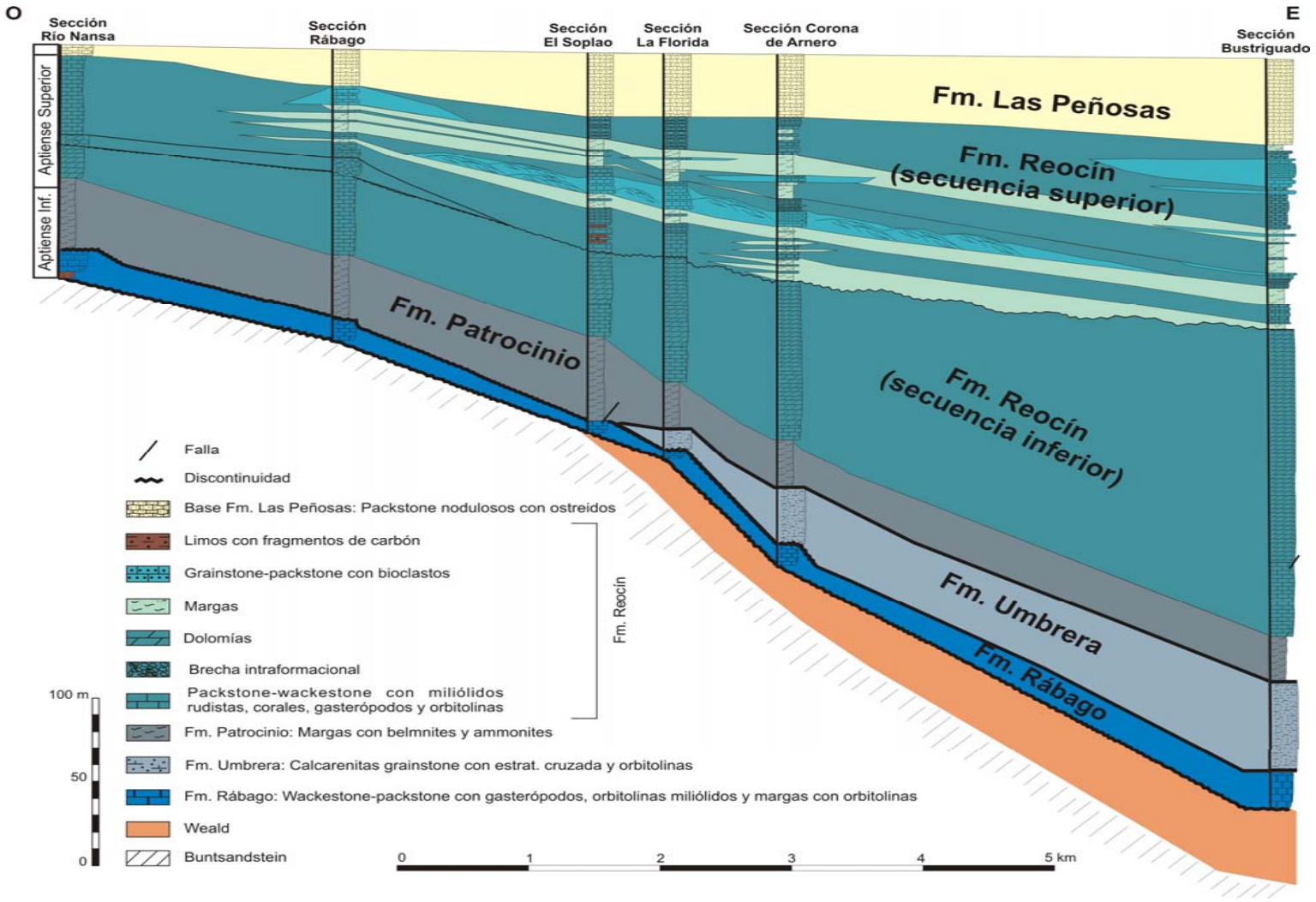

Figura 3.3.- Panel de correlación de facies y litoestratigráfica de las unidades del Aptiense en el área de La Florida. Modificado de Najarro *et al.* (2007).

3.2.1.3. FORMACIÓN PATROCINIO

Nombre de la Unidad: Patrocinio

Rango de la Unidad: Formación

Antecedentes: Unidad definida por Hines (1985). Es equivalente a los "niveles 4 y 5" del corte de Suances de Mengaud (1920), a las "margas con Parahoplites de Cuchía (margen este de la Ría de Suances)" de Rat (1959), al "Tramo 1" del corte de Saja de Rat (en Ciry *et al.*, 1967), a la Unidad C_{151}[1] del MAGNA, a la *"Formation terrigène à Ammonites*" de Collignon *et al.* (1979), a las "Areniscas 1" de García-Mondéjar y Pujalte (1981), a la Formación de Caranceja de García-Mondéjar (1982) (aunque mal contextualizada en edad en ese trabajo) y al "miembro margoso" de la Formación Caranceja de Wilmsen (2005).

Secciones de referencia: La sección tipo se localiza en la playa de los Caballos (sección de Cuchía), que ofrece un corte excepcional de esta unidad (Foto 3.13A). En el área de La Florida los mejores afloramientos se localizan en la sección del río Nansa y en la sección de Rábago (Figura 3.3; Foto 3.13F). En el área del sinclinal de Santillana la unidad aflora parcialmente cubierta, pudiéndose distinguir únicamente parte de la base y del techo de la unidad en la sección de Hayuela-Canales.

Aspectos regionales: La unidad aflora en las tres áreas de estudio y presenta una potencia de entre 30 y 80 metros. El límite inferior de la unidad está representado por la discontinuidad estratigráfica del techo de la Fm. Umbrera. El límite superior de la Fm. Patrocinio es concordante y viene marcado por un cambio transicional pero rápido de litología y de tipo de sedimentación a la unidad suprayacente la Formación San Esteban (Foto 3.13D).

Edad: La datación de esta formación se ha establecido anteriomente por Collignon *et al.* (1979) como Bedouliense en base a ammonites recolectados en la sección de Cuchía, y que dichos autores atribuyeron a las biozonas *P. fissicostatus* y *D. forbesi* para su nivel inferior y *D. deshayesi* y *T. bowerbanki* para su nivel superior, por lo que según estos autores estarían representadas en un tramo concreto de esta unidad todas las zonas del Aptiense Inferior. Posteriormente Najarro *et al.* (2011b) han

realizado, para esta Tesis, una revisión bioestratigráfica de la unidad en base a ammonites, nanofósiles calcáreos y foraminíferos planctónicos, modificándose y acotándose esta distribución bioestratigráfica, cuyos detalles serán tratados más adelante en otro apartado de este capítulo. En base a este estudio, se deduce que en el área occidental de La Florida la edad de la Fm. Patrocino comprende desde al menos la Zona *D. forbesi* (no basal) del Bedouliense inferior hasta como mínimo la parte alta de la Zona *D. furcata* (equivalente a *T. bowerbanki)* del Bedouliense superior, con la existencia de una importante laguna estratigráfica interna que abarca, al menos, el Bedouliense medio y la parte baja del Bedouliense superior (Figura 3.1). En la zona de Cuchía, y por extensión posiblemente también en el área del sinclinal de Santillana, la edad del tramo inferior de la unidad se restringe a la zona *D. forbesi* no basal, del Bedouliense inferior. La edad del tramo superior no ha podido ser estableciada aún con ammonites, pero Pascal (1985) reconoce en este tramo *Palorbitolina lenticularis* (BLUMENBACH), *Choffatella decipiens* SCHLUMBERGER, *Charentia* aff. *cuvillieri* NEUMANN y *Sabaudia minuta* (HOFKER), sugiriendo una edad Bedouliense superior, y que por correlación quiomiestratigráfica con otras cuencas (isótopos estables de C; Najarro *et al.*, 2011b) se atribuye tentativamente a la Zona *D. deshayesi*.

Recientemente, García-Mondéjar *et al*. (2015) han revisitado el afloramiento de la Formación Patrocinio en la playa de Los Caballos de Cuchía, desde el punto de vista de la bioestratigrafía de ammonites, concluyendo que la unidad abarca las biozonas *D. forbesi* y *D. deshayesi*, más una zona que ellos consideran como transicional entre *D. deshayesi* y *Dufrenoyia furcata*. Estos datos difieren de nuestras determinaciones (Najarro *et al*., 2011b), posiblemente debido a la dificultad en la identificación de algunas especies, en concreto de *Deshayesites deshayesi*.

Descripción: La sección tipo de esta formación, que aflora en la playa de los Caballos de Cuchía, presenta dos tramos claramente diferenciables: El tramo inferior está compuesto mayoritariamente por unos 50 metros de lutitas margosas oscuras con nódulos rojizos de siderita, pirita, y restos de materia orgánica. En su mitad inferior afloran los dos niveles previamente descritos por Collignon *et al.* (1979) de calizas nodulosas con gran cantidad de ammonites. Hacia la parte alta, el contenido en limos aumenta apareciendo niveles bioclásticos de base erosiva con fragmentos de braquiópodos, equinodermos, bivalvos, orbitolinas y restos carbonosos de troncos. El

tramo superior de la formación tiene una potencia de 30 metros y está formado por una secuencia estrato- y grano-creciente de facies heterolíticas compuestas por una alternancia de niveles de lutitas carbonosas y micáceas, limos y areniscas con estratificación cruzada, y laminación *convolute* (Foto 3.13B y C). Gradualmente, hacia el techo de la unidad aflora un nivel de areniscas calcáreas con gran cantidad de orbitolinas (Foto 3.13D), sobre el que se apoyan las calizas con corales y rudistas pertenecientes ya a la unidad suprayacente (Fm. San Esteban). En el área de La Florida, la Fm. Patrocinio está compuesta por una unidad de 30 a 45 metros de potencia de lutitas margosas grises, bastante homogénea, con escasos belemnites y orbitolinas en la parte superior de la unidad (Foto 3.13E).

Interpretación del medio sedimentario: El depósito de las lutitas margosas oscuras de la parte inferior de la Formación Patrocinio refleja el hundimiento rápido de la plataforma carbonatada, posiblemente debido a la acción conjunta de una rápida subida relativa del nivel del mar y al incremento en el aporte de terrígenos finos desde el continente. Esta parte de la unidad se depositó en un ambiente marino abierto, relativamente profundo y de baja energía, con condiciones de fondo deficientes en oxígeno, lo que favoreció la preservación de materia orgánica (Najarro *et al.*, 2011b; Quijano *et al.*, 2012). El aumento del contenido en limos hacia la parte alta sugiere un incremento del aporte de material terrígeno, mientras que los niveles bioclásticos esporádicos con base erosiva representan tempestitas e indican que fueron depositados por encima del nivel de base de las tormentas. Finalmente, los materiales heterolíticos de la parte superior de la Formación Patrocinio reflejan la progradación de un sistema deltaico (presente al menos en la sección de Cuchía). Por tanto, se sugiere para esta unidad primero una profundización rápida en el medio deposicional respecto a las unidades carbonatadas infrayacentes, junto con un aumento del aporte de terrígenos finos, seguido en su parte superior por una somerización y regresión rápida, con progradación localmente de un sistema deltaico.

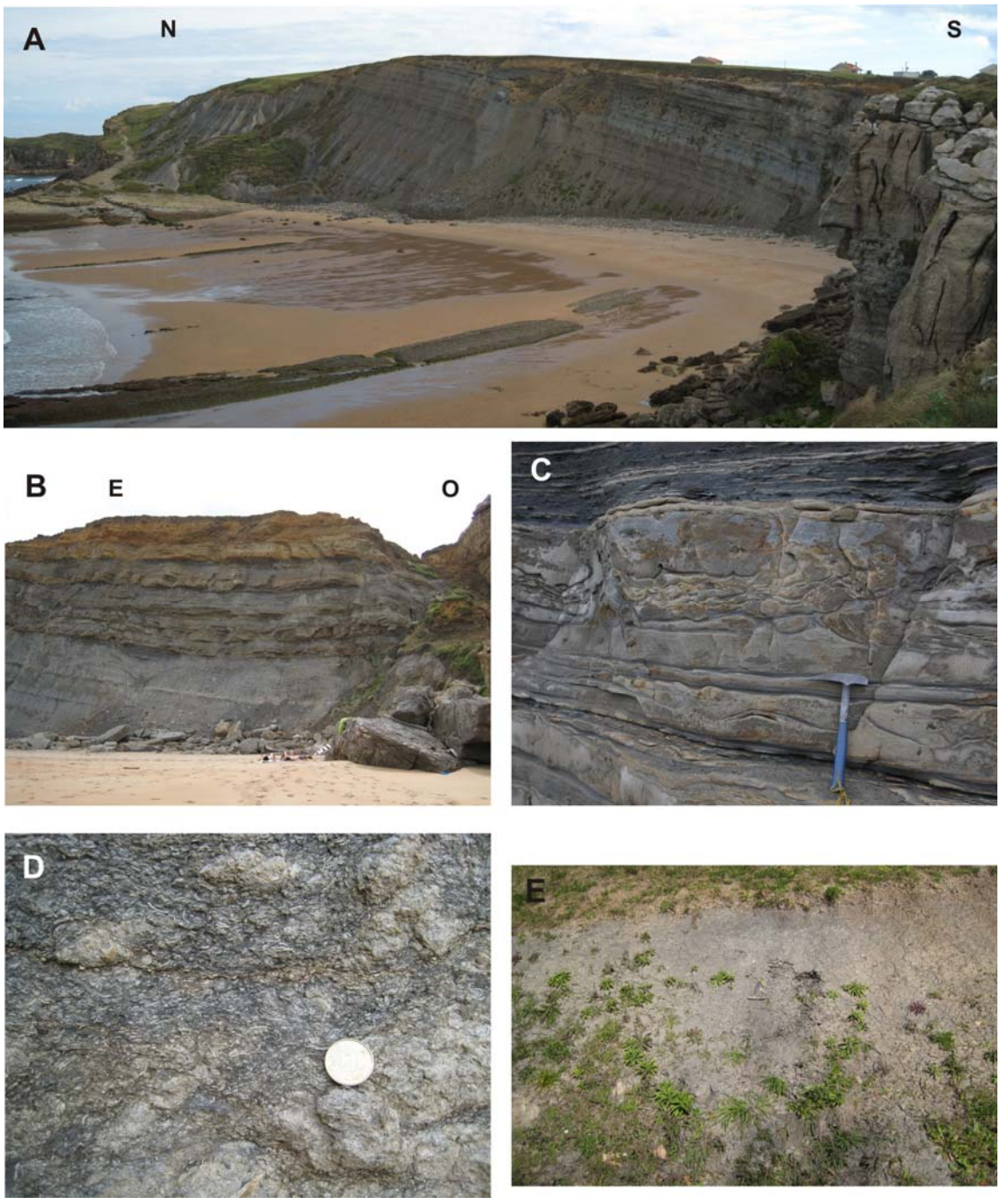

Foto 3.13.- **A)** Aspecto general de la Formación Patrocinio en la sección tipo de la playa de los Caballos (área de Cuchía). **B)** Detalle de la parte superior del tramo inferior y del tramo superior de la Formación Patrocinio. Nótese la secuencia estrato- y grano-creciente de facies heterolíticas del tramo superior de la formación. **C)** Detalle de facies heterolíticas compuestas por una alternancia de niveles de lutitas carbonosas y micáceas, limos y areniscas con estratificación cruzada, y laminación *convolute*. **D)** Detalle del nivel de areniscas calcáreas con gran cantidad de orbitolinas hacia el techo de la formación en la playa de los Caballos (área de Cuchía). **E)** Aspecto de la Formación Patrocinio en la sección de río Nansa (área de La Florida).

3.2.1.4. FORMACIÓN SAN ESTEBAN

Nombre de la Unidad: San Esteban

Rango de la Unidad: Formación

Antecedentes: Definida por García-Mondéjar (1982). Esta unidad corresponde al "Primer nivel de calizas con rudistas" de Mengaud (1920), al "tramo 2" del corte de Saja de Rat (en Ciry *et al.*, 1967), a la unidad C_{152}^{1} de las hojas del MAGNA, a la "barra urgoniana inferior" de Collignon *et al.* (1979), a las "calizas 1" (San Esteban) de García-Mondéjar y Pujalte (1981) y a las "Calizas de San Esteban" de García-Mondéjar (1982).

Secciones de referencia: La sección tipo se localiza en las proximidades de la localidad de San Esteban, en el área del sinclinal de Santillana. Aquí la formación presenta sus mejores afloramientos en el corte de la estación de ferrocarril de Casar de Periedo (Foto 3.14), así como en el corte de la carretera que une la localidad de Ruilobuca con Canales (sección de Ruilobuca). En el área de Cuchía, continuando la serie en la playa de los Caballos (sección de Cuchía), la unidad aflora a favor de pequeños acantilados y calas hasta llegar a la Punta de la Barra (Foto 3.15). Al otro lado de la ría de San Martín de la Arena, en la localidad de Suances, la parte alta de la Formación San Esteban presenta un buen afloramiento en la Punta del Dichoso, así como en la margen izquierda de la Ría de Mogro, entre la playa de Usgo y la Punta del Águila, en la playa de Robayera. Sin embargo, en estas dos últimas secciones, la base de la unidad está cubierta por el mar.

Aspectos regionales: La Formación San Esteban está presente en las áreas del sinclinal de Santillana y Cuchía y está ausente en el área occidental de La Florida, debido a la existencia en esta última zona de una laguna estratigráfica que afecta como mínimo a la parte alta del Aptiense Inferior (Najarro *et al.*, 2011b). En la zona oriental del área de La Florida la unidad aparece representada por unos pocos metros incluidos a la base de la Fm. Reocín, que se acuñan rápidamente hacia el oeste a la altura de El Soplao. La potencia media de la unidad es de unos 30-50 metros. El límite inferior de la unidad es transicional y viene marcado por un cambio gradual y rápido en el tipo de sedimentación, de areniscas o limos con orbitolinas de la unidad infrayacente a calizas

con corales y rudistas de plataforma somera. El límite superior es un diastema a techo de un nivel calizo fuertemente bioturbado, o localmente, un nivel de brechas calcáreas.

Foto 3.14.- Aspecto de la Formación San Esteban en en el corte de la estación de ferrocarril de Casar de Periedo.

Foto 3.15.- Vista panorámica del tránsito de la Fm. Patrocinio a la Fm. San Esteban y de la base de la Formación San Esteban en el corte de la playa de Los Caballos a la Punta de la Barra, área de Cuchía.

Edad: De acuerdo con Pascal (1985), esta formación se enmarca en el Bedouliense superior en base a la presencia de *Iraquia simplex* HENSON. Ramírez del Pozo (1972) cita también *Choffatella decipiens* SCHLUMBERGER y *Palorbitolina lenticularis* (BLUMENBACH).

Descripción: En general, la Formación San Esteban está compuesta por una sucesión de bancos decimétricos a métricos de calizas *mudstone*, *wackestone*, *floatstone* y *packstone* de tonos claros, con gran cantidad de rudistas requiénidos de pequeño tamaño (*Toucasia* y *Requienia*), corales ramosos, gasterópodos *Nerinea*, algas dasycladáceas, miliólidos, bivalvos, orbitolinas y oncoides de *Lithocodium aggregatum* ELLIOT y *Bacinella irregularis* RADOIČIĆ (Fotos 3.16A, 3.19 y Lámina 3), interestratificados con margas nodulosas con corales. En la sección de Ruilobuca la formación comienza con una serie de bancos de calizas y margocalizas con orbitolinas, seguido por una sucesión de bancos de calizas claras con requiénidos y *L. aggregatum*-*B. irregularis*, y finalizando, a techo de la unidad, con un nivel de calcarenita, algo ferruginizado, con intensa bioturbación y colonización de ostreidos, lo que se interpreta como un diastema.

En la sección de Cuchía la sucesión comienza con un nivel de calcarenitas con abundantes orbitolinas (Foto 3.13D), seguido de margas nodulosas con bioclastos, orbitolinas, esponjas y corales planares y masivos, que gradualmente pasan a bancos claros de caliza con pequeños requiénidos (Foto 3.20). Estos últimos paquetes aparecen organizados en ciclos métricos de somerización (de 1 a 3 metros de potencia) que culminan con niveles decimétricos de brechificación con cantos calcareos negros, interpretados como superficies de exposición subaérea (Foto 3.21A-C). En la sección de Cuchía, el techo de esta unidad se caracteriza por presentar una superficie irregular tapizada por un nivel de unos 50 cm de brechas con cantos calcáreos, entre los que se incluyen cantos de calizas de estromatolitos laminados y cantos calcáreos negros (Foto 3.22), interpretada también como una superficie mayor de exposición subaérea. Esta brecha aparece tapizada por un nivel de unos 30–50 cm de caliza de rudistas que incorporan también cantos negros y clastos de la brecha caliza infrayacente y que marca el techo de la unidad y de secuencia (Foto 3.23A y B).

Foto 3.16.- Caliza de tonos claros con gran cantidad de rudistas requiénidos de pequeño tamaño (*Toucasia* y *Requienia*) de la Formación San Esteban. Sección de Ruilobuca (área del sinclinal de Santillana).

Foto 3.17.- Caliza *packstone* con rudistas y corales ramosos de la Formación San Esteban. Sección de Ruilobuca (área del sinclinal de Santillana).

Foto 3.18.- Caliza con abundantes corales ramosos y gasterópodos *Nerinea* de la Formación San Esteban. Sección de Ruilobuca (área del sinclinal de Santillana).

Foto 3.19.- Caliza con abundantes oncoides de *Lithocodium aggregatum* ELLIOT y *Bacinella irregularis* RADOIČIĆ de la Formación San Esteban. Sección de Suances (área de Cuchía).

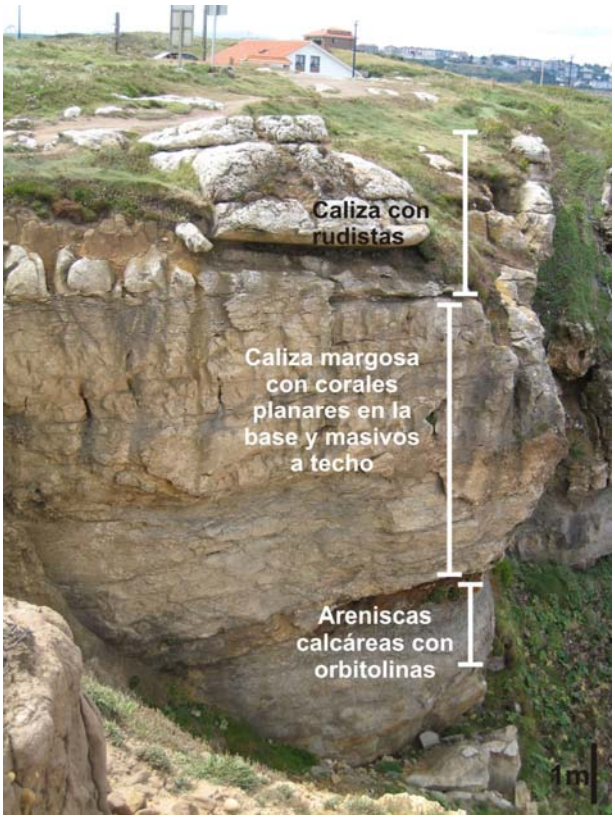

Foto 3.20.- Detalle de la base de la Formación San Esteban en la sección de Cuchía, mostrando la secuencia de implantación de las facies de plataforma de la Fm. San Esteban.

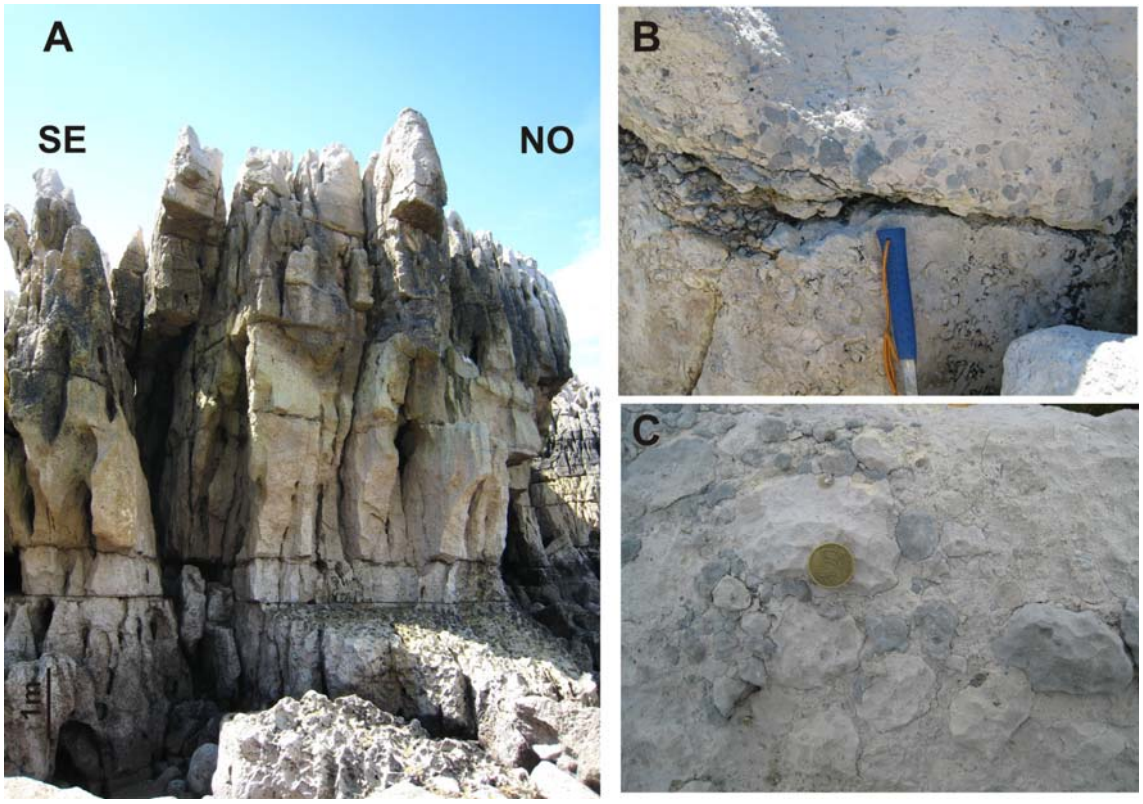

Foto 3.21.- **A)** Aspecto general de los ciclos de somerización de la Formación San Esteban en la sección de Cuchía. **B** y **C)** Detalle de niveles decimétricos de brechificación con cantos calcáreos negros a techo de los ciclos de somerización e interpretados como superficies de exposición subaérea.

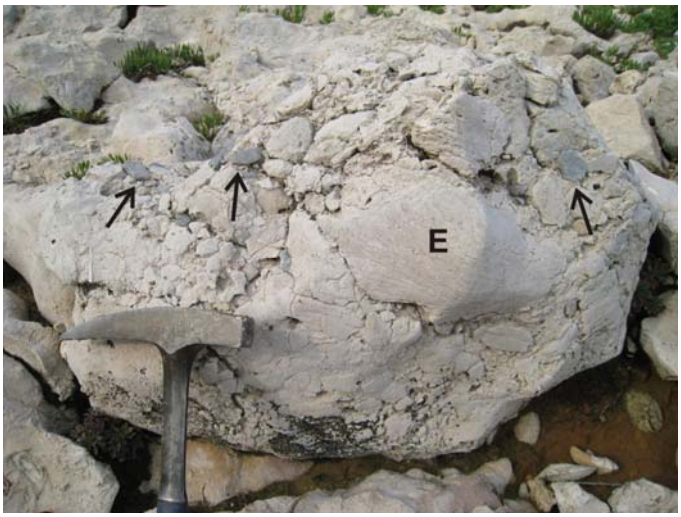

Foto 3.22.- Techo de la Formación San Esteban en la sección de Cuchía, compuesto por una superficie irregular tapizada por un nivel de unos 50 cm de brechas con cantos calcáreos, entre los que se incluyen cantos de calizas de estromatolitos laminados (E) y cantos calcáreos negros (flechas).

Foto 3.23.- **A** y **B**) Nivel de 30–50 cm de potencia de caliza de rudistas que incluye litoclatos calizos y cantos negros, que marca el techo de la Formación San Esteban y de secuencia en la sección de Cuchía.

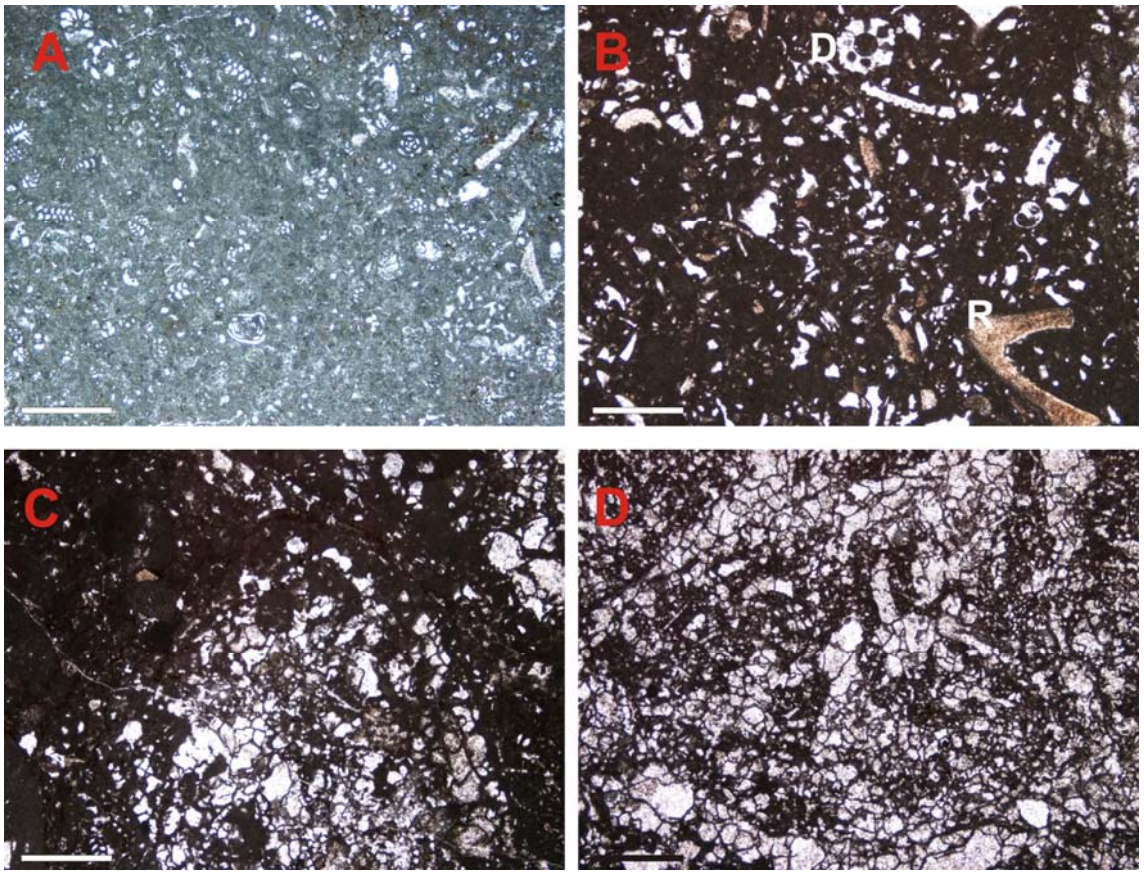

Lámina 3.- Microfacies de la Formación San Esteban. La escala para todas las imágenes es de 1 mm. **A)** Caliza *wackestone* con abundantes faraminíferos bentónicos de tipo miliólido, textulárido y lituólido. Muestra CU-13. Sección de Cuchía, área de Cuchía. **B)** Caliza *wackestone* con conchas de rudistas (R), algas dasycladáceas (D) y bioclastos. Muestra SU-11, sección de Suances, área de Cuchía). **C)** Oncoide de *Lithocodium aggregatum* y *Bacinella irregularis*. Muestra SU-9, sección de Suances, área de Cuchía. **D)** Masa de *Lithocodium aggregatum* y *Bacinella irregularis*. Muestra SU-10, sección de Suances, área de Cuchía.

En la sección de Suances se observan también ciclos de somerización (al menos 6) que culminan, al igual que en la sección de Cuchía, con desarrollo de brechas calcáreas con cantos negros, interpretadas como superficies de exposición subaérea. Aquí la secuencia termina con el desarrollo de un nivel decimétrico de estromatolitos laminados con huellas de desecación y parcialmente brechificado, a techo de calizas con rudistas y oncoides de *Lithocodium-Bacinella* (Foto 3.24).

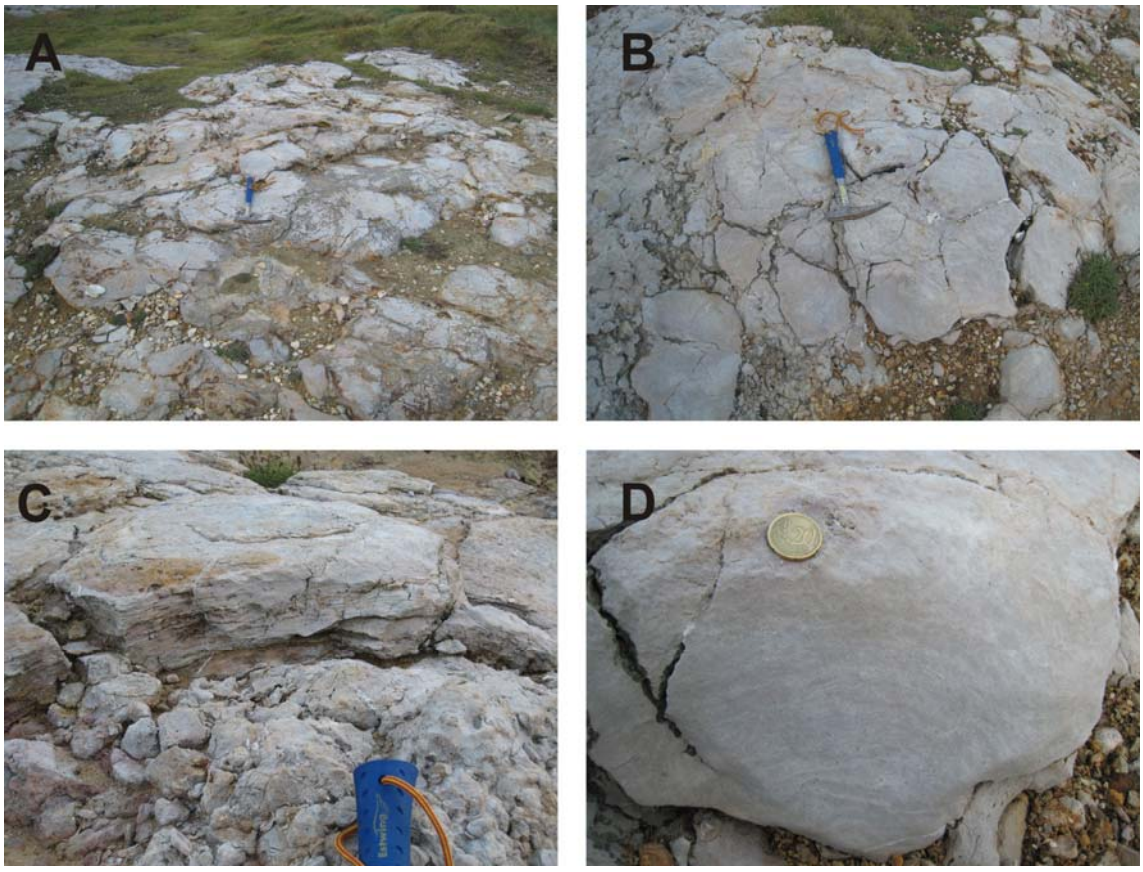

Foto 3.24.- Aspecto general y detalles de los estromatolitos laminados con huellas de desecación y parcialmente brechificados a techo de la Fm. San Esteban. Sección de Suances, área de Cuchía. **A** y **B)** Vista en planta de la superficie en domos del techo de los estromatolitos con presencia de fracturas poligonales e inicio de brechificación. **C)** Sección transversal del nivel de estromatolitos tapizando un nivel irregular de brecha calcárea. **D)** Detalle del nivel de estromatolitos.

Interpretación del medio sedimentario: Esta unidad se interpreta como la instaturación de una plataforma carbonatada somera y protegida, dominada por facies de baja energía ricas en fango carbonatado. El paso de la Fm. Patrocinio a la Formación San Esteban indica la recuperación de la producción carbonatada debido a la somerización del medio y a una drástica disminución del aporte de partículas terrígenas. Tal y como describe Vilas *et al.* (1995) en un caso similar en las Cordilleras Béticas de la Península Ibérica, en el comienzo de la sedimentación carbonatada los orbitolínidos son los primeros colonizadores, debido a su mayor tolerancia a condiciones adversas tales como la turbidez del agua, la escasez de luz y la presencia de partículas terrígenas. La evolución vertical desde las facies margosas con orbitolinas a las facies de calizas con rudistas y abundante fauna somera sugiere un cambio hacia condiciones medioambientales más favorables para la producción de carbonato y biodiversidad en un ambiente marino somero de plataforma interna relativamente restringida. Durante su

desarrollo, los carbonatos someros progradaron y colmataron el espacio de acomodación (bien por causas autocíclicas, alocíclicas o cambios climáticos globales) hasta, al menos localmente, alcanzar el nivel del mar, desarrollando ciclos de somerización que culminaron con la exposición subaérea de la plataforma. El techo de la unidad indica una etapa final de exposición subaérea seguido de un episodio de profundización rápida y de un cambio en el estilo de sedimentación.

3.2.1.5. FORMACIÓN RODEZAS

Nombre de la Unidad: Rodezas

Rango de la Unidad: Formación

Antecedentes: Unidad definida por Hines (1985). Corresponde con el "nivel 3" del corte de Reocín de Mengaud (1920); con los niveles 3-4 de "intercalación terrígena y margas" y "calizas margosas con *Exogyra latissima* y *Douvilleiceras*" de Puente Arce, Reocín y Udías de Rat (1959); con el "nivel 3" del corte de Saja de Rat (en Ciry *et al.*, 1967); la unidad C_{153}^{1} del MAGNA; la base de las "Calizas 2" (Golbardo) de García-Mondéjar y Pujalte (1981). Regionalmente es equivalente a las formaciónes del Puerto de las Estacas y del Río Trueba de García-Mondéjar (1982). Hacia el este de Cantabria, es equivalente a la unidad "Calizas nodulosas con ostreidos de Cérdigo" de Rosales (1995). García-Mondéjar (1982) denominó esta unidad como Formación Cuchía por un supuesto afloramiento en la playa de Cuhía. Sin embargo, esta unidad está mal identificada aquí, ya que estos afloramientos de areniscas en la playa de Cuchía correponden en realidad con la Fm. Bielba. Por lo que la Fm. Cuchía no existe por estar mal contextualizada en el trabajo de García-Mondéjar (1982).

Secciones de referencia: La Formación Rodezas está presente solo en las áreas del sinclinal de Santillana y Cuchía, aunque generalmente aparece cubierta de forma parcial debido a su carácter poco consistente. La sección tipo de esta unidad se localiza en la localidad de Rodezas, cerca de Udías (Hines, 1985). Debido a las malas condiciones de afloramiento, para este estudio la sección de referencia se ha establecido en la carretera que une las localidades de Ruilobuca y Canales (sección de Ruilobuca de este trabajo, área del sinclinal de Santillana). También se puede observar un corte

excepcional en los acantilados de la playa de Robayera (área de Cuchía), en la margen izquierda de la ría de Mogro.

Aspectos regionales: En la sección tipo, la unidad presenta una potencia de unos 80 metros, mientras que en la sección de playa de Robayera la potencia ronda los 60 metros. En las secciones de Cuchía (Punta de la Barra) y de Suances (Punta del Dichoso), la formación está muy reducida (pocos metros). En el área de La Florida, la Fm. Rodezas también está ausente o muy reducida. La interpretación en este trabajo en base a datos bioestratigráficos nuevos, es que en el área occidental de La Florida, la Fm. Rodezas es equivalente lateral de los últimos 10 metros de la Fm. Patrocinio, con una laguna estratigráfica interna que engloba a la Fm. San Esteban (Najarro *et al.*, 2011b, Figura 13), y presentando posiblemente hacia esta zona cambios laterales a facies de plataforma somera en el tránsito con la Fm. Reocín. El límite inferior de esta unidad está representando por la discontinuidad del techo de la Fm. San Esteban, con exposición subaérea en el área de Cuchía, y localmente discordancia angular abservada en el afloramiento de la playa de Robayera. El límite superior, en zonas de surco relativo, es transicional y rápido con la unidad suprayacente y viene marcado por la desaparición de la fauna oportunista de ostreidos, abundantes hacia la parte alta de la unidad, para dar paso a las calizas de plataforma somera de la Fm. Reocín. En zonas de umbral (i.e. paleoalto de Suances-Cuchía) su contacto con la unidad suprayacente de plataforma somera es una superficie erosiva y de remoción.

Edad: La edad de esta formación se atribuye al tránsito Bedouliense–Gargasiense y Gargasiense inferior en base a su contenido en ammonites. Mengaud (1920) describe en el corte de Reocín y en la parte alta de la Fm. Rodezas numerosos ejemplares de *Douvilleiceras* cf. *tschernyschewi* SINZOW, *D.* cf. *tschernyschewi* var. *laticosta* SINZOW, *Douvilleiceras* sp. y *Ammonitoceras* cf. *ucetiae* DUMAS. Recientemente esta colección ha sido revisada sistemáticamente por Moreno-Bedmar *et al.* (2009), que citan *Epicheloniceras gracile* CASEY, *Epicheloniceras* sp. y *Pseudoaustraliceras ramososeptatum* (ANTHULA), pertenecientes a la Subzona *Epicheloniceras gracile* de la Zona de *Epicheloniceras martini* del Gargasiense inferior. Igualmente, Collignon *et al.* (1979), nombran para la parte alta de la formación, en la localidad de Reocín, la existencia de *(Cheloniceras) mackesoni* CASEY y *Cheloniceras*

(Epicheloniceras) gracile CASEY, precisando también la Subzona *E. gracile* de la Zona de *E. martini* del Gargasiense inferior.

Descripción: En la sección de Ruilobuca, la Formación Rodezas muestra tres tramos claramente diferenciables. El tramo inferior, de unos 15 metros de potencia, está formado por calizas margosas con corales ramosos, fragmentos bioclásticos (rudistas y gasterópodos) y miliólidos, que alteran con margas limosas. El tramo medio, de unos 25 metros de potencia, es principalmente terrígeno-arenoso y está formado por intercalaciones de niveles de lutitas aleuríticas marrones-grisáceas con bioclastos, niveles de calcarenitas con pequeños ostreidos, gasterópodos y bioclastos, bancos métricos de areniscas micáceas anaranjadas de grano fino-medio con estratificación cruzada, areniscas calcáreas con gran cantidad de bioclastos y niveles de limo-arenisca de grano muy fino con *ripples* de oscilación, laminación ondulada y restos de carbón. Los últimos 15 metros del tramo presentan calizas limosas-arenosas anaranjadas con abundantes gasterópodos y ostreidos, para culminar con calcarenitas bioclásticas de grano medio (Foto 3.25). El tramo superior margoso de la Formación Rodezas, de unos 40 metros de potencia, está formado por margocalizas nodulosas con glauconita y restos vegetales, margas oscuras con finas pasadas de arenisca de grano muy fino (Foto 3.26), y calizas margosas y margas con orbitolinas, braquiópodos, ostreidos en posición de vida bien aislados o formando bancos monoespecíficos (*Exogyra latissima* SAY y *Plicatula placunea* LAMARCK) (Foto 3.27), ammonites y belemnites.

En la sección de la playa de Robayera la formación de unos 60 metros de potencia, es heterolítica y comienza con varios paquetes de calizas brechoides y calizas margosas con abundantes corales masivos, coloniales y ramosos (tramo 1), seguido sucesivamente de alternancias de caliza-marga nodulosas, margas con serpúlidos, margocalizas nodulosas bioturbadas (tramo 2), areniscas y limos heterolíticos con laminación lenticular y *flaser*, areniscas con estratificación cruzada en surco (tramo 3) y finalmente calizas nodulosas con ostreidos (*Exogyra latissima*) (tramo 4), pasando de forma transicional y rápida a calizas *grainstone* de la base de la Fm. Reocín suprayacente.

En las secciones de Cuchía (Punta de la Barra) y Suances (Punta del Dichoso) la unidad está representada por un tramo de tan solo 2,5 a 5 metros de margas con

braquiópodos y niveles margocalizos con corales planares y ramosos y de alternancia de margas con serpúlidos, glauconita y calizas nodulosas bioturbadas (Fotos 3.28, 3.29 y 3.30). Aquí los tramos siliciclásticos (tramo 3) y de calizas nodulosas con ostreidos (tramo 4) de la parte media y alta de la unidad observados en la playa de Robayera, no están representados, estando solo presentes y de forma muy reducida, los tramos inferiores de la unidad (tramo 2). Por tanto existe una laguna estratigráfica que abarca a los tramos 3 y 4 de la Fm. Rodezas en este sector.

Interpretación del medio sedimentario: Respecto del techo de la unidad infrayacente, esta unidad se interpreta como la respuesta a un episodio de profundización rápida seguido de regresión. La unidad se depositó en un medio de plataforma mixta terrígeno-carbonatada, depositándose en ambientes que varían desde plataforma carbonatada externa relativamente profunda con ammonites y belemnites, a talud arrecifal y hasta ambientes de plataforma fangosa submareal con abundantes bancos de ostreidos en posición de vida (similar al descrito para la misma edad en Asturias por Alonso-García y Bahamonde, 2006).

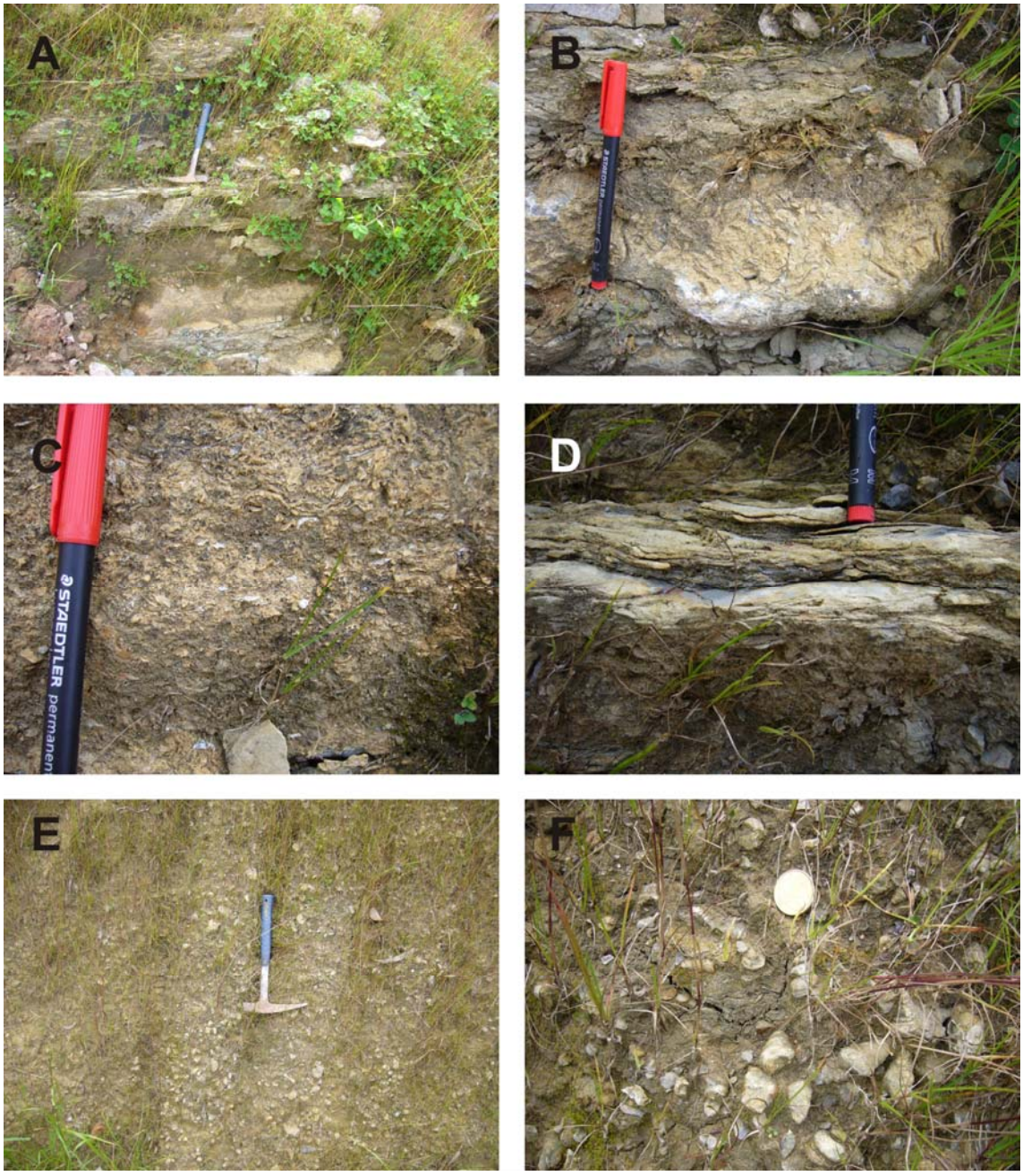

Foto 3.25.- Tramo inferior y medio de la Formación Rodezas en la sección de Ruilobuca (área del sinclinal de Santillana). **A)** Base de la Formación Rodezas formada por una alternancia de facies heterolíticas. **B)** Detalle de arenisca calcárea con ostreidos y bioclastos. **C)** Detalle de arenisca calcárea bioclástica. **D)** Detalle de limos-areniscas micáceas de grano muy fino-fino con *ripples* simétricos y laminación ondulada. **E)** Aspecto de limos margosos de tonos claros con abundantes gasterópodos y ostreidos. **F)** Detalle del nivel de limos margosos anterior donde se observan abundantes gasterópodos.

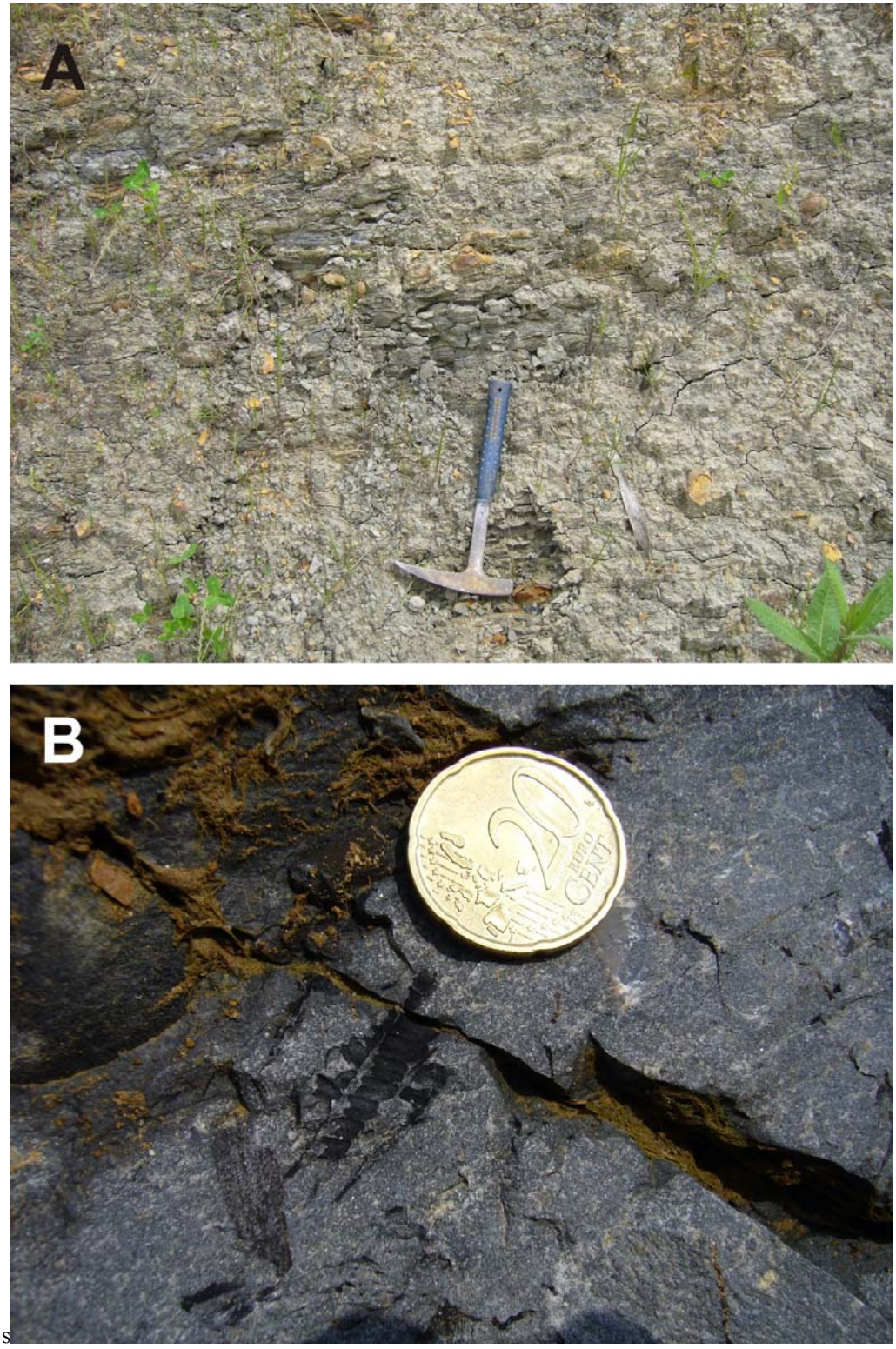

Foto 3.26.- Aspecto del tramo superior de la Formación Rodezas en la sección de Ruilobuca (área del sinclinal de Santillana). **A)** Margas oscuras con finas pasadas de arenisca de grano muy fino. **B)** Margocalizas nodulosas con glauconita y restos vegetales.

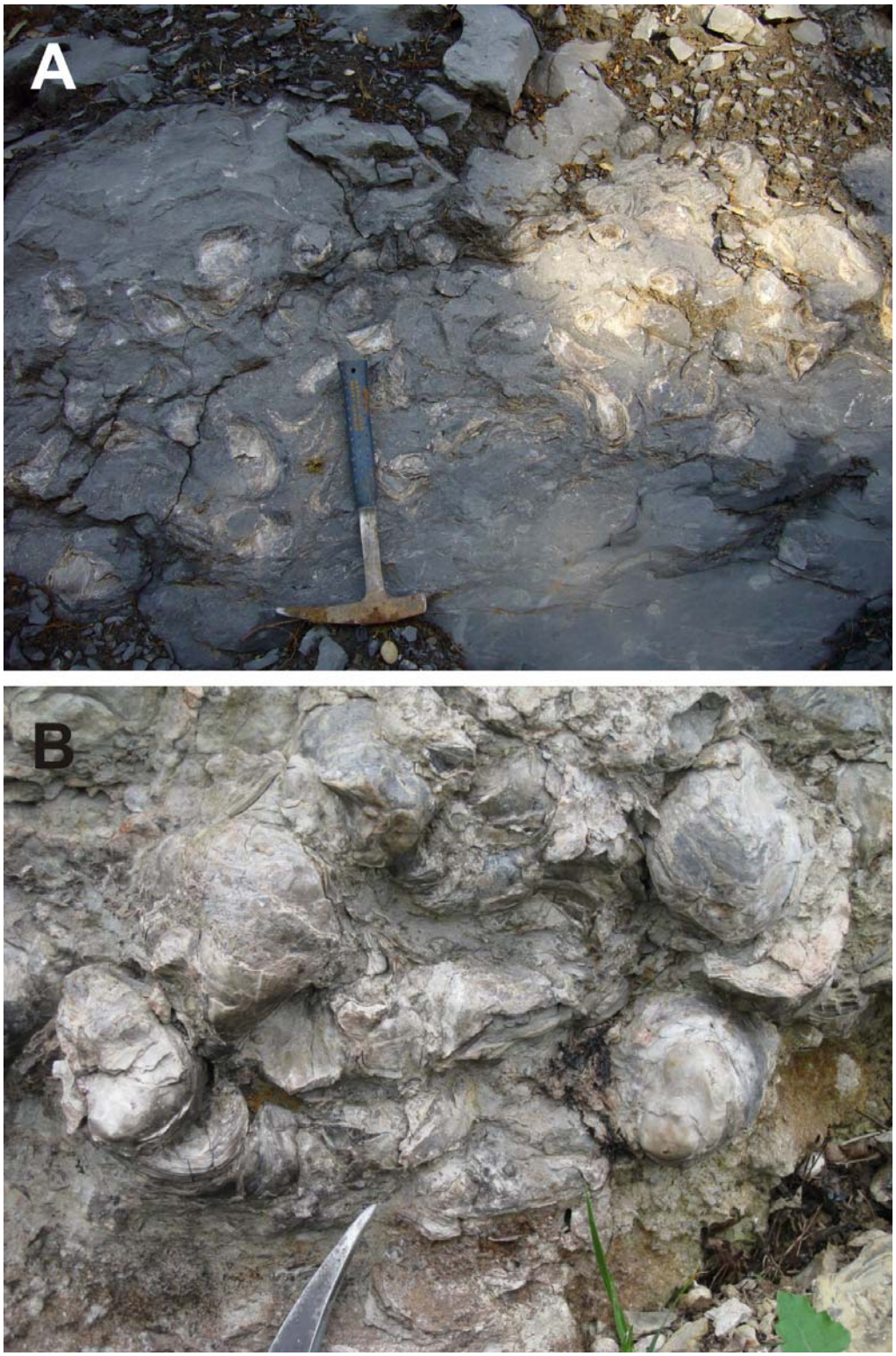

Foto 3.27.- Detalle del tramo superior de la Formación Rodezas. **A)** Calizas margosas y margas con ostreidos en posición de vida, aislados o formando bancos monoespecíficos (*Exogyra latissima* SAY y *Plicatula placunea* LAMARCK). Sección de Ruilobuca (área del sinclinal de Santillana). **B)** Detalle de banco de ostreidos (*Exogyra latissima* SAY) del techo de la Fm. Rodezas en las proximidades de Duña (área del sinclinal de Santillana).

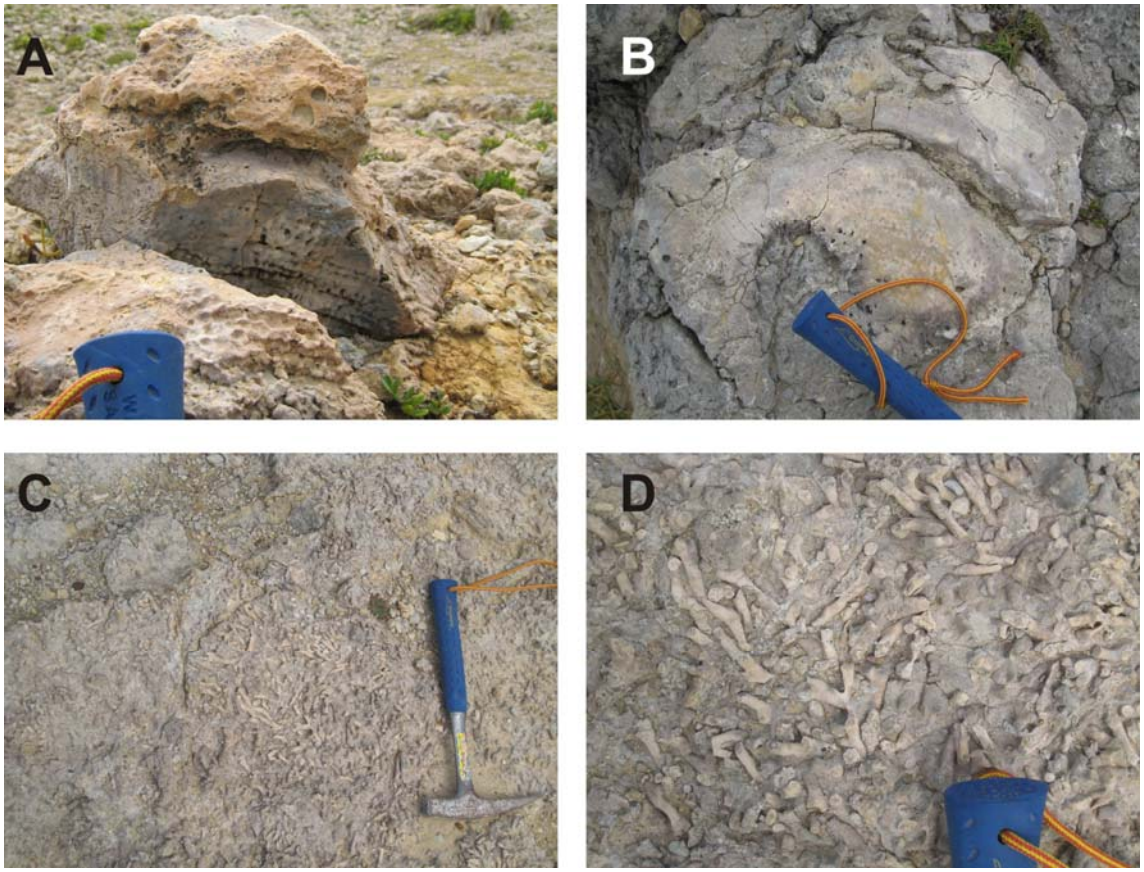

Foto 3.28.- Aspecto de niveles margocalizos con corales planares y ramosos de la base de la Formación Rodezas (tramo 1) en la sección de Suances (área de Cuchía). **A)** Coral masivo en posición de vida. **B)** Detalle de coral masivo **C)** Vista en planta de corales ramosos en posición de vida. **D)** Detalle de los corales ramosos de la imagen anterior.

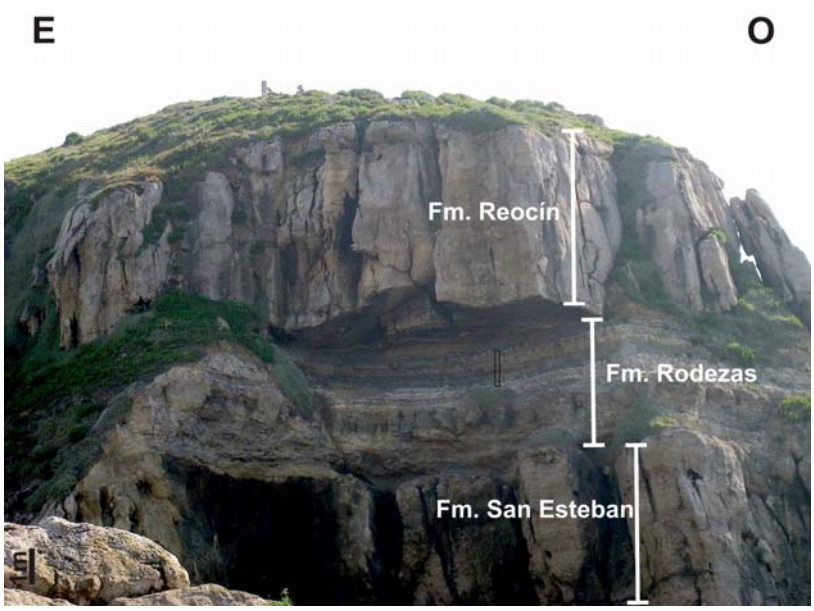

Foto 3.29.- Afloramiento mostrando el aspecto con fuerte reducción de potencias de las Fms. Rodezas (nivel margoso) y Reocín (nivel calizo superior) en la Punta del Dichoso (Suances). El nivel calizo inferior corresponde con el techo de la Fm. San Esteban.

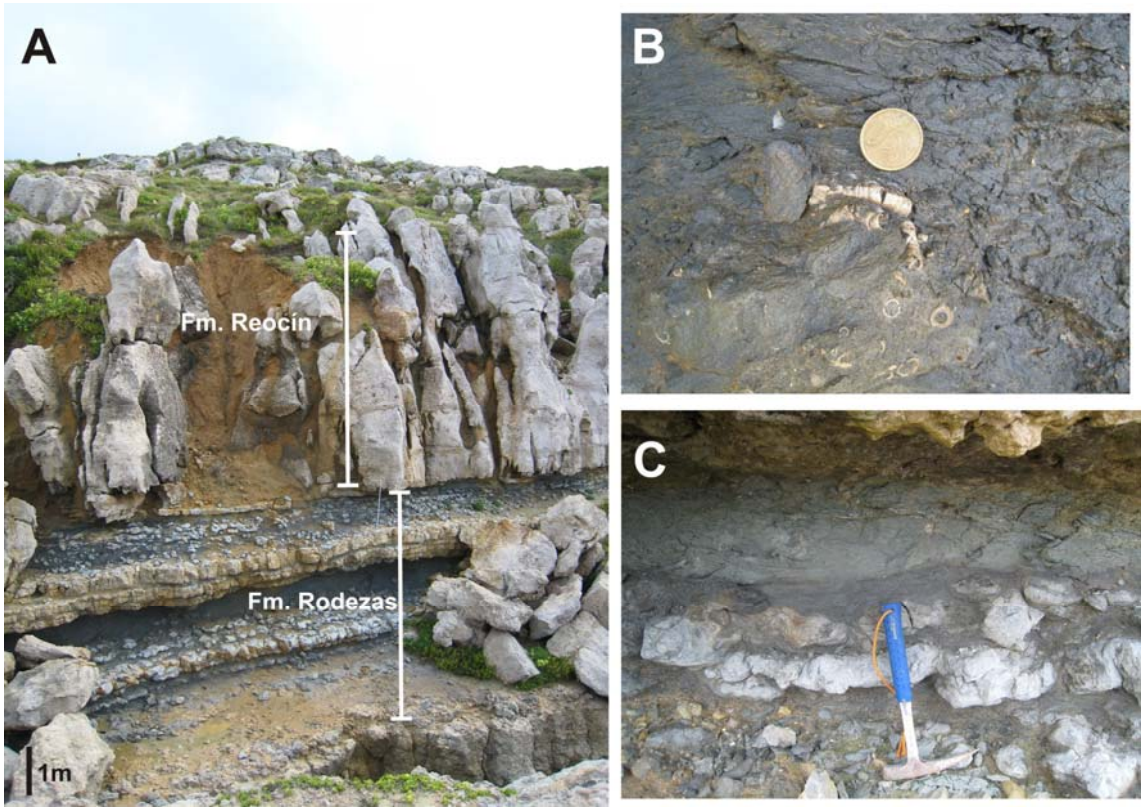

Foto 3.30.- **A)** Aspecto del afloramiento de la Fm. Rodezas (tramo inferior de margas y calizas nodulosas) en la Punta del Dichoso y el tránsito mediante contacto neto erosivo (regresión forzada) a la Fm. Reocín (tramo calizo superior) (sección de Suances, área de Cuchía). **B)** Detalle de margas oscuras con pequeña concentración de serpúlidos de la Fm. Rodezas. **C)** Detalle de margas oscuras nodulosas bioturbadas. Nótese el color verdoso por el contenido de glauconita.

3.2.1.6. FORMACIÓN REOCÍN

Nombre de la Unidad: Reocín

Rango de la Unidad: Formación

Antecedentes: Unidad definida por García-Mondéjar (1982). Es equivalente a las "Calizas de Reocín, Udías, Novales, Monte Berbecha, La Florida" de Mengaud (1920), Karremberg (1934) y Rat (1959); también corresponden al "tramo 4" del corte de Saja de Rat (en Ciry *et al.*, 1967), al nivel C_{15}^{23} del MAGNA; y a las "Calizas 2 (Golbardo)" de García-Mondéjar y Pujalte (1981). Hines (1985) denominó esta unidad como Formación Reocín con tres miembros: Miembro Barrio, para el tramo calizo inferior, Miembro Novales, para el tramo dolomítico medio y Miembro Sierra para el tramo calizo superior. Dado que la dolomitización que afecta a esta unidad es un rasgo diagenético tardío, no se considera esta subdivisión a este trabajo.

Secciones de referencia: La sección tipo de la unidad se encuentra definida en el valle del río Saja a la altura de Golbardo (García-Mondéjar, 1982), aunque la sección de referencia para nuestro estudio se ha establecido en el Cerro de Castrorubio, localizado entre Bustablado y la finca de Santa Eulalia (sección de Santa Eulalia en este trabajo, área del sinclinal de Santillana). En este corte la Formación Reocín origina un gran resalte, pudiéndose observar en detalle las características litoestratigráficas de la unidad (Foto 3.31A). Otra sección de referencia de la unidad en esta zona de estudio se localiza en la cantera de Las Lastrías, en Caranceja, cerca de Casar de Periedo (Foto 3.31B). En el área de La Florida, una sección representativa de la unidad se localiza entre la cueva El Soplao y el cerro de Corona de Arnero (Foto 3.31C). En la localidad de Cuchía la formación presenta un excelente afloramiento en la cantera de Solvay (Foto 3.31D), aunque no aflora su base.

Aspectos regionales: La formación aflora en las tres áreas de estudio. El límite inferior de la unidad viene marcado en el área del sinclinal de Santillana por un cambio gradual y rápido en la litología, de calizas margosas con ostreidos o calizas nodulosas con orbitolinas a calizas *grainstone* con orbitolinas y finalmente a calizas con rudistas de plataforma somera. En el área de Cuchía, en el afloramiento de playa de Robayera el tránsito es gradual con la Fm. Rodezas, sin embrago en Suances, el contacto de la Fm. Rodezas con la Fm. Reocín es erosivo. En Cuchía (playa y cantera) el contacto de la Fm. Rodezas con la Fm. Reocín no aflora. La potencia de la unidad y el límite superior es variable según el área. En el área de La Florida la unidad forma un litosoma carbonatado en cuña con un espesor máximo de 366 metros en el este (sección de Bustriguado) y mínimo de 70 metros en el oeste (sección de río Nansa) (Figuras 3.2 y 3.3). En esta zona la unidad se apoya directamente sobre la Fm. Patrocinio, si bien, como ya se ha explicado anteriormente, hacia el oeste, el último tramo de esta formación equivaldría en edad a parte de la Formación Rodezas. Mientras que hacia el este de La Florida, la base de la Fm. Reocín es equivalente en edad al menos a parte de la Fm. San Esteban (Zona de *Iraquia simplex*). Por tanto, el límite inferior es diacrónico. El límite superior es una superficie con rasgos microscópicos de disolución, que se intrepretan como exposición subaérea, sobre la que se deposita una unidad mixta de transición a depósitos deltaicos.

En el área del sinclinal de Santillana la unidad también presenta variaciones de espesor, pasando de unos 130 metros en el corte de la cantera de Las Lastrías y en el área costera de Comillas-Punta Calderón, a 209 metros en la sección tipo de Santa Eulalia, y a unos 350 metros en el corte de Novales. En esta área el límite superior de contacto con la Fm. Las Peñosas es neto y está marcado por un nivel de arcillas verde-rojas edáficas desarrollado sobre calizas de rudistas (Foto 3.32), indicando exposición subaérea y un diastema.

En la cantera de Cuchía, la formación presenta unos 80 metros de espesor mínimo, ya que el parte inferior de la unidad no aflora. Aquí el techo de la Fm. Reocín se caracteriza por presentar brechificación bajo una superficie irregular tapizada por un nivel decimétrico de areniscas y limos que incluyen clastos de la serie infrayacente (Fotos 3.33 y 3.34). Se intrepreta esta superficie irregular tapizada por brechas como una superficie de exposición subaérea. Sobre este nivel, la unidad suprayacente corresponde a la Fm. Barcenaciones del Albiense Superior, existiendo, por tanto, una laguna estratigráfica entre ambas unidades y un cambio brusco en el tipo de sedimentación.

En las secciones de Suances (Punta del Dichoso) y Cuchía (playa del Huevo), esta unidad está muy reducida de potencia, estando representada solo parte de ella por un nivel de 6–9 metros de potencia de calizas de plataforma somera con ostreidos, rudistas y oncoides de *Lithocodium-Bacinella* (Foto 3.35). Aquí la base de este nivel de calizas es ligeramente erosivo y presenta sobre la superficie de erosión un tramo irregular de hasta 0,3 m de parabrecha calcárea que incorpora cantos de los niveles infrayacentes en una matriz bioclástica (interpretado en esta tesis como una superficie de regresión forzada) (Fotos 3.30A y 3.36). El techo de la unidad es un nivel irregular decimétrico de brechas calcáreas que incorpora cantos negros, interpretado como una superficie de exposición subaérea, con el techo fuertemente bioturbado y nodulizado (Foto 3.37).

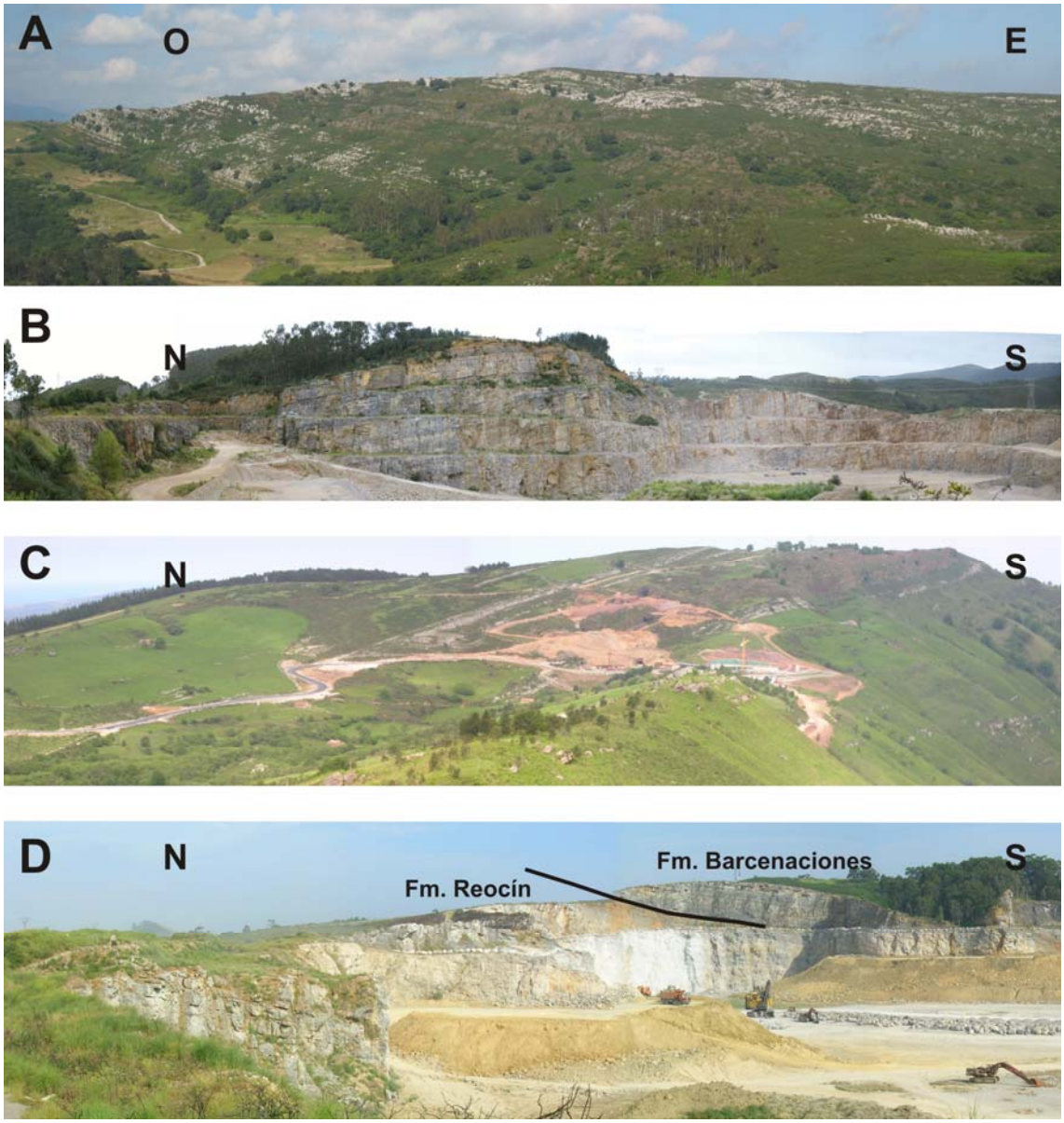

Foto 3.31.- Aspecto general de la Formación Reocín en las distintas secciones levantadas en este trabajo. Nótese como en las imágenes A y C esta formación está dolomitizada en su parte central (color ocre). **A)** Formación Reocín en el Cerro de Castrorubio, localizado entre Bustablado y la finca de Santa Eulalia (sección de Santa Eulalia, área del sinclinal de Santillana). **B)** Formación Reocín en la cantera de Las Lastrías, en Caranceja, cerca de Casar de Periedo, área del sinclinal de Santillana. **C)** Formación Reocín en el área de La Florida, entre la Cueva El Soplao y el cerro de Corona de Arnero. **D)** Formación Reocín en la cantera de Solvay, la parte superior de la cantera corresponde con la Fm. Barcenaciones. Sección de la cantera de Cuchía, área de Cuchía, en este trabajo.

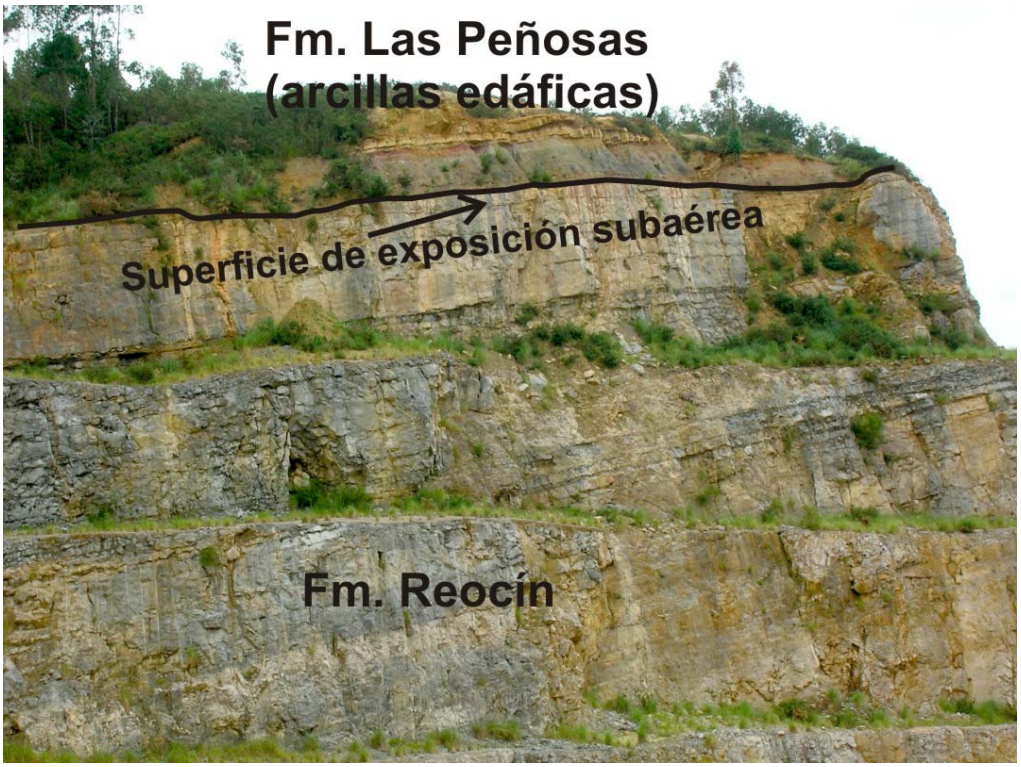

Foto 3.32.- Techo de la Fm. Reocín, con desarrollo de arcillas verde-rojas edáficas sobre el techo de la unidad (discontinuidad en el contacto con la Fm. Las Peñosas del Albiense Inferior), en el afloramiento de la cantera de La Lastrías (Caranceja).

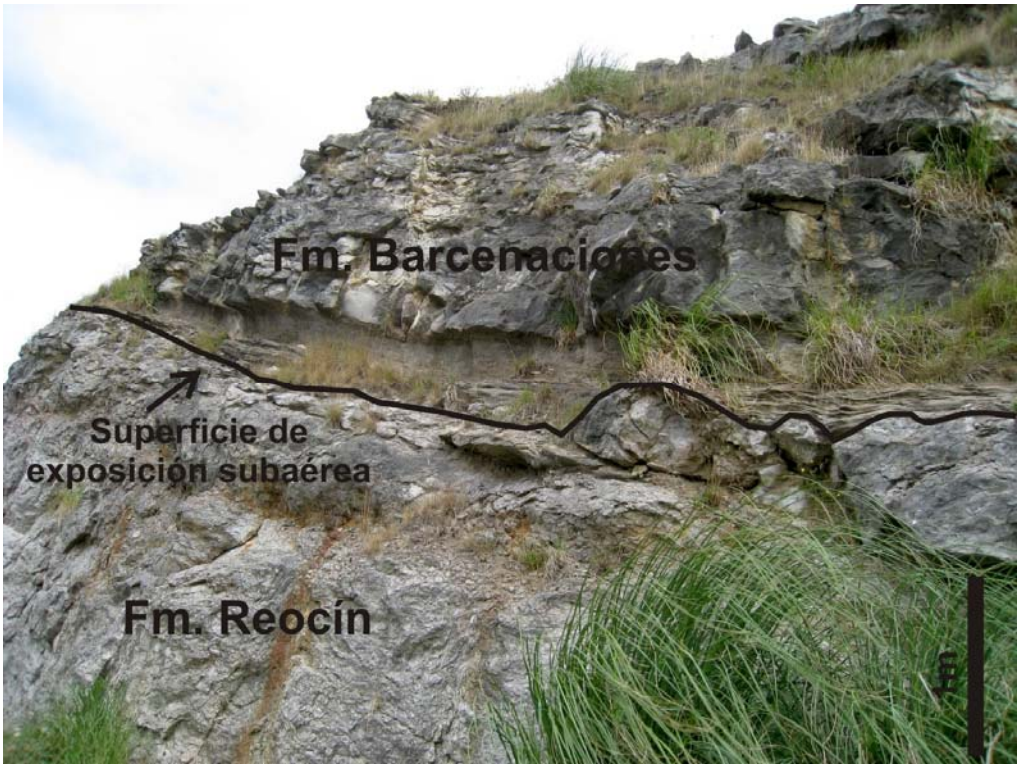

Foto 3.33.- Techo de la Fm. Reocín en la cantera de Cuchía, caracterizado por la presencia de brechificación y una superficie irregular tapizada por un nivel decimétrico de areniscas y limos laminados con cantos de la caliza infrayacente. Se interpreta como una superficie de exposición subaérea. Por encima de este nivel terrígeno se encuentra directamente la Fm. Barcenaciones del Albiense Superior.

Foto 3.34.- Detalle de la discontinuidad del techo de la Fm. Reocín en la cantera de Cuchía, mostrando brechificación a techo de la unidad, cubierta por un nivel decimétrico de limos que incorpora cantos de la caliza infrayacente.

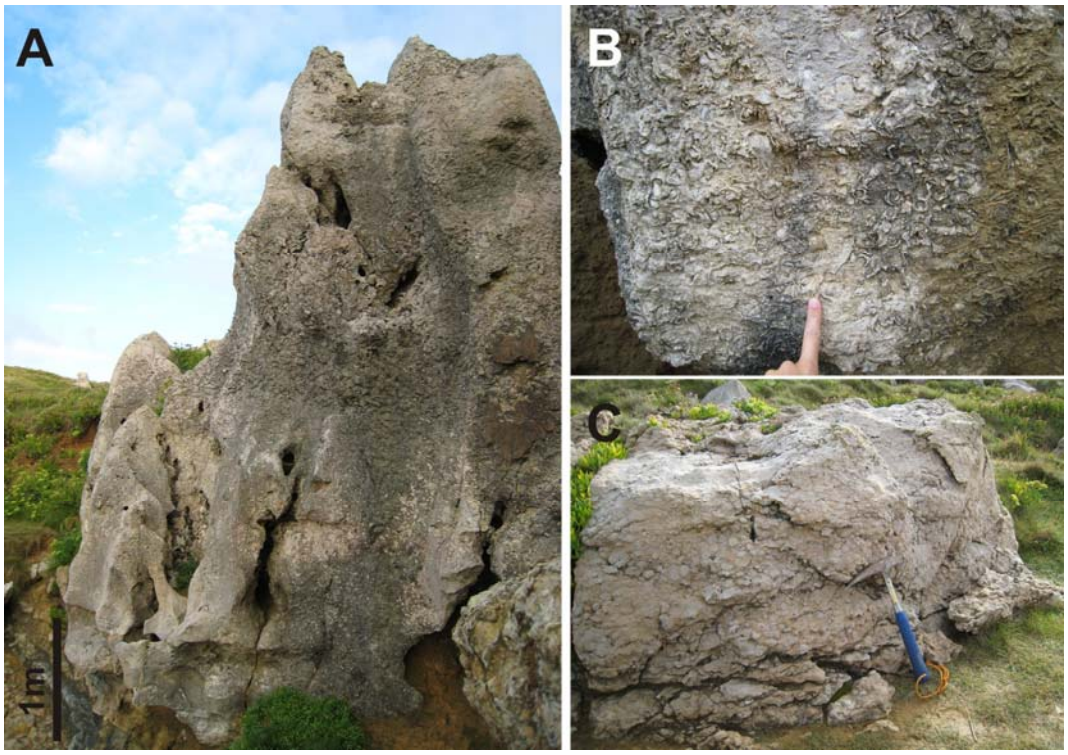

Foto 3.35.- **A)** Aspecto de campo de la Formación Reocín en la sección de Suances (Punta del Dichoso, área de Cuchía). Nótese la reducida potencia de la formación en esta localidad, estando sólo representada probablemente la parte alta de la unidad. **B)** Detalle de la caliza bioclástica de rudistas en la sección de Suances (Punta del Dichoso). **C)** Detalle de la caliza formada por oncoides de *Lithocodium-Bacinella* en la sección de Suances (Punta del Dichoso).

Foto 3.36.- Parabrecha calcárea sobre superficie erosiva a la base de la Fm. Reocín en la Punta del Dichoso (sección de Suances).

Foto 3.37.- Brecha calcárea desarrollada a techo de la Fm. Reocín en la Punta del Dichoso (sección de Suances), en la superficie de discontinuidad del límite entre la Fm. Reocín (Aptiense Superior-Albiense basal) y la Fm. Barcenaciones (Albiense Superior, Vraconiense). La parte basal consiste en una ortobrecha caótica con clastos calcáreos desorganizados, que grada hacia arriba a calcarenitas bioturbadas con incorporación de clastos de la brecha infrayacente.

Edad: Esta formación se asigna al Gargasiense superior-Clansayesiense, pudiendo llegar el techo hasta la base del Albiense Inferior, en base a su contenido en orbitolínidos y otros foraminíferos bentónicos y su posición estratigráfica. Así, Ramírez del Pozo (1972) describe la presencia de *Orbitolina* (*Mesorbitolina*) *texana texana* (ROEMER), *Sabaudia minuta* (HOFKER) y *Simplorbitolina manasi* CIRY y RAT. Collignon *et al.* (1979) citan también *Sabaudia minuta* (HOFKER), *Pseudochoffatella cuvillieri* DELOFFRE, *Orbitolina (Mesorbitolina) parva* DOUGLASS, *Orbitolina (Mesorbitolina) minuta* DOUGLASS, *Orbitolina (Mesorbitolina) texana* (ROEMER), y *Orbitolinopsis reticulada* MOULLADE y PEYBERNÈS para la parte media de la unidad en Reocín y para la parte baja del afloramiento de la cantera de Cuchía, sugiriendo una edad Gargasiense superior para este tramo. En la parte alta de la unidad citan *Simplorbitolina manasi* CIRY y RAT, *Orbitolinopsis* cf. *buccifer* ARNAUD VANNEAU y THIEULOY, *Coskinolinella daguini* DELMAS y DELOFFRE y *Cuneolina pavonia* D'ORBIGNY, indicando una edad Aptiense terminal (Clansayesiense), no descartando que incluya parte del Albiense Inferior, para el tramo final de la unidad. De igual modo, esta unidad presenta *Polyconites verneuili* (BAYLE) y *Pseudotoucasia santanderensis* (DOUVILLÉ) (Mengaud, 1920; Rat, 1959; Collignon *et al.*, 1979; Ramírez del Pozo, 1972), siendo ambos rudistas característicos a partir del Gargasiense (Masse, 1995).

Descripción: En general, la Formación Reocín está compuesta por una succesión de calizas bioclásticas, calizas micríticas con *B. irregularis-L. aggregatum,* calizas con miliólidos, rudistas y corales, y margocalizas con corales y orbitolinas, que aparecen parcialmente dolomitizadas. La unidad presenta dos tramos o secuencias claramente diferenciables. El tramo o secuencia inferior es más masivo y está constituido principalmente por alternacias de bancos métricos de calizas *grainstone* y *wackestone-packstone* con miliólidos, orbitolinas, gasterópodos y rudistas, y por paquetes decimétricos a métricos de caliza micrítica con *B. irregularis-L. aggregatum* formando masas irregulares o *lumps* (Foto 3.38D). El tramo o secuencia inferior se encuentra preferentemente dolomitizado en gran parte del área de estudio. El tramo o secuencia superior es más estratificado y está formado principalmente por una sucesión de bancos generalmente más cubiertos, constituidos por limos carbonosos, margas y calizas nodulosas con orbitolinas, esponjas y corales masivos y tabulares, que alternan con calizas *grainstone* y *packstone-wackestone* con miliólidos, orbitolinas,

gasterópodos y rudistas, formando secuencias métricas a decamétricas de somerización (Foto 3.39).

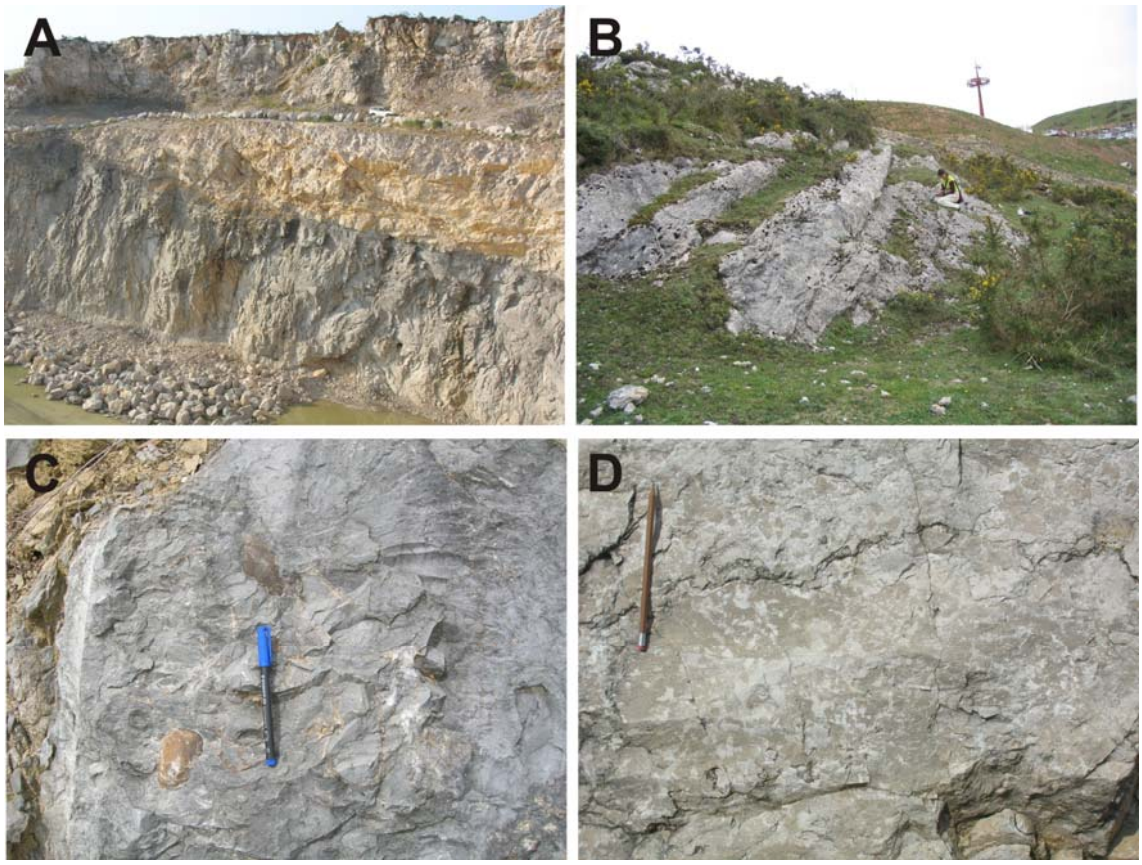

Foto 3.38.- Aspecto de campo del tramo o secuencia inferior de la Formación Reocín. **A)** Tramo inferior en la sección de la cantera de Cuchía, área de Cuchía. **B)** Tramo inferior no dolomitizado en la sección de El Soplao, área de La Florida. **C)** Detalle de banco de caliza con rudistas (sección El Soplao, área de La Florida). **D)** Detalle de caliza micrítica con *B. irregularis-L. aggregatum* (sección de la cantera de Cuchía, área de Cuchía).

Localmente (oeste del área de La Florida), el contacto entre los dos tramos que componen la Fm. Reocín es un nivel de brechificación (Foto 3.40), intepretado aquí como un límite de secuencia, que incorpora intraclastos de tamaño decimétrico de calizas con rudistas y gasterópodos y cantos negros de naturaleza micrítica y tamaño centimétrico. La matriz entre los clastos está compuesta por margas con orbitolinas y por calcarenitas *packstone* con bioclastos. Este nivel se ha observado solo en las zonas más occidentales de la plataforma del sector de La Florida (secciones de río Nansa y Rábago). En el resto de las zonas, el límite entre los dos tramos o secuencias de la Fm. Reocín se ha establecido en una superficie irregular bioturbada-nodulizada, tapizada por un nivel decimétrico a métrico de limos-arenas finas o margas (Foto 3.41), que

representa un episodio de rápida inundación de la plataforma. Sobre él se desarrolla un segundo episodio de plataforma carbonatada caracterizado por alternacia de bancos métricos de calizas margosas con orbitolinas y corales y calizas con miliolidos y rudistas.

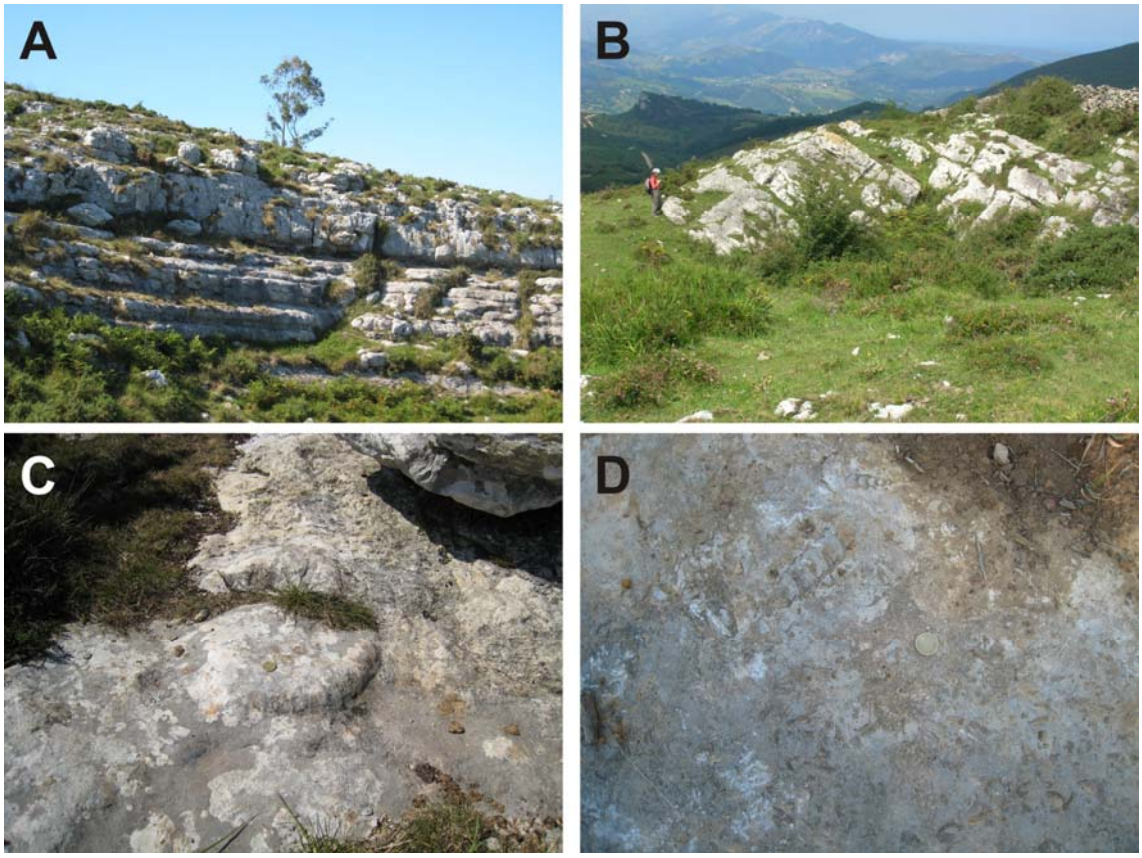

Foto 3.39.- Aspecto de campo del tramo o secuencia superior de la Formación Reocín. **A)** Tramo superior en la sección de Santa Eulalia, área del sinclinal de Santillana. **B)** Tramo superior de la Formación Reocín en la sección de Corona de Arnedo, área de La Florida). **C)** Caliza con coral masivo, sección Corona de Arnedo, área de La Florida. **D)** caliza con corales ramosos y gasterópodos del techo de la sección de Santa Eulalia, área del sinclinal de Santillana).

La Formación Reocín se presenta afectada extensamente por dolomitización de origen hidrotermal o geotermal (Foto 3.31A y C). La dolomitización muestra una distribución en masas y lentejones irregulares, pero que a grandes rasgos es subparalela a la estratificación de la caliza, afectando preferencialmente a su parte central, mientras que la parte superior e inferior se encuentran casi invariablemente no dolomitizadas. No obstante, existen variaciones sustanciales en la distribución de la dolomitización, y en según que zonas puede llegar a afectar al muro de la unidad (sección de río Nansa), mientras que en otras zonas, la Formación aparece sin dolomitizar en todo su espesor (secciones de Rábago, cantera de Las Lastrías, Cuchía y Suances) (Foto 3.31 B y D).

Estas dolomías encajan importantes mineralizaciones metálicas de Fe, Pb y Zn, que en la zona de estudio fueron explotadas intensamente en las minas de La Florida, Novales y Reocín.

Foto 3.40.- Nivel brechificado que separa los dos tramos de la Formación Reocín en la zona más occidental del área de La Florida. Sección Rábago.

Foto 3.41.- Nivel de limos-arenas de grano fino con restos de carbón que separa los dos tramos de la Formación Reocín en zonas más orientales del área de La Florida. Sección El Soplao.

Interpretación del medio sedimentario: En general el paso de la Formación Rodezas a la Formación Reocín representa una caída relativa del nivel mar, pasando gradualmente de un ambiente de plataforma carbonatada externa-cuenca relativamente pobre en oxígeno, con ammonites y belemnites, a un ambiente de plataforma carbonatada somera con variación de ambientes desde *lagoon* restringido a plataforma interna, plataforma media poco profunda y plataforma externa, formando variaciones laterales de facies y ciclos de plataforma.

3.2.1.7. FORMACIÓN LAS PEÑOSAS

Nombre de la Unidad: Las Peñosas

Rango de la Unidad: Formación

Antecedentes: Unidad definida por García-Mondéjar (1982) y admitida por Hines (1985). Esta unidad se ha identificado también anteriormente como "complejo areniscoso supraurgoniano" por Menguad (1920) y Rat (1959); "tramo 5" del corte de Saja por Rat (en Ciry *et al.*, 1967); también como la unidad C_{16} [1] del MAGNA; y como las "areniscas 3" por García-Mondéjar y Pujalte (1981).

Secciones de referencia: El corte tipo de la unidad se encuentra definido en la localidad de Las Peñosas, al este de Comillas (García-Mondéjar, 1982). Sin embargo, las mejores secciones de referencia de la unidad se localizan en el área de La Florida, donde los mejores afloramientos se hallan en las secciones del río Nansa, Rábago y Plaza del Monte. Otra sección de referencia muy bien aflorada se localiza en la ensenada de Fonfría, al este de Comillas.

Aspectos regionales: La Formación Las Peñosas suele aparecer cubierta en la mayor parte de las secciones debido a su carácter friable. Además, presenta variaciones laterales de espesor importantes, llegando incluso a desaparecer por acuñamiento a la altura de Torrelavega (Reocín). De esta forma, en las secciones de Cuchía y Suances (área de Cuchía) la unidad está ausente, existiendo en esta zona una laguna estratigráfica. Por tanto, contrario a algunas representaciones cartográficas previas a este trabajo, al oeste de Santander la extensión regional de la Fm. Las Peñosas se limita a los

sectores de La Florida, sinclinal de Santillana y Comillas. Debido a esto, en muchas cartografías y trabajos previos en las zonas donde la Fm. Las Peñosas está ausente, se ha confundido la Fm. Las Peñosas con la Fm. Bielba, también siliciclástica, del Albiense Superior-Cenomaniense Inferior, y la unidad caliza situada debajo de ella que corresponde con la Fm. Barcenaciones del Albiense Superior, se ha confundido con la Fm. Reocín. Sin embargo, en estas zonas, la presencia del caprinido *Caprina choffati* DOUVILLÉ en las calizas localizadas por debajo de la unidad siliciclástica confirma su edad Albiense Superior (Vraconiense) (por ejemplo, en la playa de Cuchía).

En el sector de La Florida, la Fm. Las Peñosas presenta su mayor potencia (alrededor de 100 metros) en la zona oriental (secciones de Bustriguado y de Plaza del Monte), y la menor (unos 47 metros) en la sección de Rábago (Figura 3.4). Aquí el límite superior con la unidad suprayacente es transicional y se caracterizan por un cambio gradual en el tipo de sedimentación.

En el sector de Comillas, la unidad aflora de forma excepcional en la ensenada de Fonfría (al este de Comillas) aunque en esta sección la base y el contacto inferior con la Fm. Reocín se encuentran cubiertos (Foto 3.42). Aquí el espesor de la unidad está bastante reducido (76 metros), y el contacto con la unidad suprayacente (Fm. Barcenaciones) es también transicional y rápido.

En el sector del sinclinal de Santillana, la Fm. Las Peñosas presenta su máxima potencia en el sinclinal de Cóbreces (200 metros). No obstante, en esta zona no fue posible el levantamiento de ninguna columna estratigráfica debido a la abundante vegetación que cubre la unidad, pudiéndose realizar exclusivamente observaciones puntuales. Debido a esto, en este área los límites inferior y superior con las unidades infrayacente y suprayacente son dificiles de observar. Un buen afloramiento del límite inferior y del contacto con la Fm. Reocín en esta zona, lo ofrece la cantera de Las Lastrías (Foto 3.32), donde el límite es una discontinuidad marcada por una superficie neta de exposición subaérea sobre la cual se depositan lutitas verde-rojas con signos de edafización.

Edad: A esta formación se le ha asignado una edad Albiense Inferior-Medio, en base a la presencia de *Orbitolina (Mesorbitolina) texana texana* (ROEMER) descrita en la sección de Bielba (área de La Florida) por Ramírez del Pozo (1972).

Foto 3.42.- Vista panorámica de la Formación Las Peñosas en la ensenada de Fonfría (este de Comillas).

Descripción: En el área de La Florida, dentro de la Formación Las Peñosas se han distinguido tres sub-unidades de carácter informal en base a sus características litológicas (Najarro *et al.*, 2009), denominadas de base a techo: Las Peñosas 1, Las Peñosas 2 y Las Peñosas 3 (Figura 3.4). La potencia de la sub-unidad inferior (Las Peñosas 1) varía entre 11 metros (sección de Rábago) y 40 metros (sección de Plaza del Monte), y se caracteriza por presentar una alternancia de calizas *grainstone* o calizas bioclásticas con abundantes ostreidos, calizas margosas-limosas nodulosas y bioturbadas, y limos con delgados niveles de arena muy fina y laminación cruzada. En conjunto, Las Peñosas 1 muestra una disminución del contenido en carbonato y un progresivo aumento del contenido en limo y arena fina hacia techo. La sub-unidad intermedia (Las Peñosas 2) presenta una potencia que varía lateralmente de 25 metros en la sección de Rábago a 60 metros en la sección de Plaza del Monte (Figura 3.4). Está formada por una alternancia de: i) facies heterolíticas de arenas y limos con laminación *wavy*, *linsen* y *flaser* y *mud drapes,* o con estratificación *hummocky* (HCS) de pequeña escala y *ripples* de oscilación y de corriente, ii) limos bioturbados (*Rhizocorallium*, *Teichichnus*) y lutitas oscuras sulfurosas con restos de carbón, fragmentos vegetales, moldes piritizados de pequeños gasterópodos y bivalvos marinos y abudantes piezas de ámbar, iii) areniscas de grano fino a grueso con estratificación cruzada organizadas en secuencias estrato- y granocrecientes, y iv) areniscas de grano medio-grueso con geometrias acanaladas intercaladas entre lutitas grises-rojas con rasgos de edafización,

moteado y localmente huellas de raíces (paleosuelos). Finalmente, la sub-unidad superior (Las Peñosas 3) presenta un espesor que varía entre 13 metros en la sección de Rábago y 40 metros en la sección de Plaza del Monte. Se caracteriza por una alternacia de limos margosos y arenas de grano muy fino y calizas *packstone* con ostreidos, gasterópodos y bivalvos, formando secuencias métricas terrígeno-carbonatadas que presentan un progresivo aumento en el contenido de carbonato hacia techo, pasando progresivamente a la unidad carbonatada suprayacente. El contacto con la unidad caliza suprayacente (Formación Barcenaciones) se ha establecido para este estudio en un nivel margoso noduloso con abundantes bivalvos megalodontos de gran tamaño y bioclastos (Foto 3.43), sobre el cual se recupera la sedimentación carbonatada.

En la sección de la ensenada de Fonfría, en el sector de Comillas, y en el sector del sinclinal de Santillana (ej. cantera de Las Lastrías) sólo se desarrollan las sub-unidades media y superior de la Fm. Las Peñosas. Al igual que en el área de La Florida, aquí el techo de la Fm. Las Peñosas viene marcado por el nivel margoso noduloso con los grandes bivalvos megalodontos.

Foto 3.43.- Nivel margoso noduloso con abundantes bivalvos megalodontos de gran tamaño que marca el techo de la Formación Las Peñosas y el inicio de la sedimentación carbonatada de la Fm. Barcenaciones.

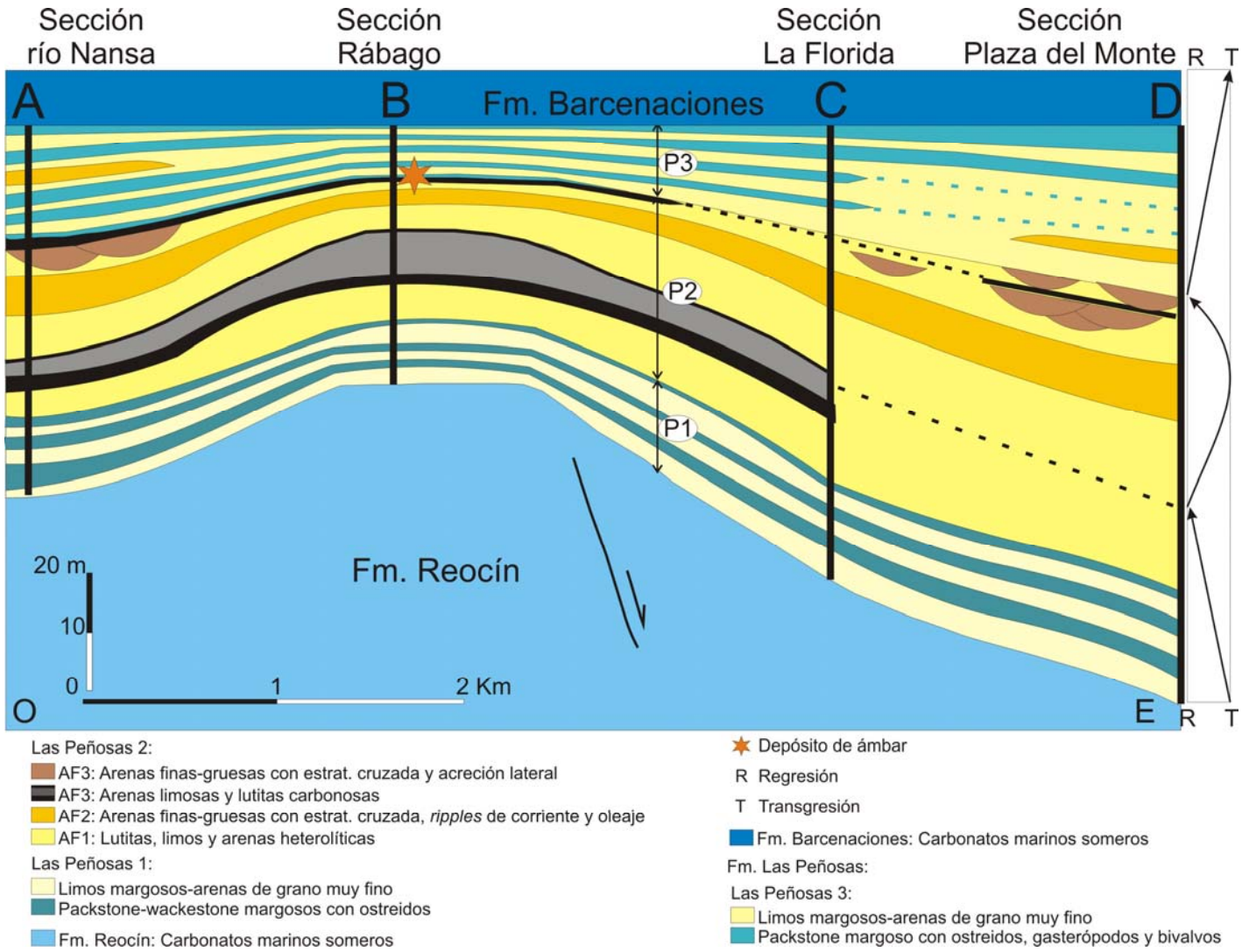

Figura 3.4.- Correlación litoestratigráfica de la Formación Las Peñosas (Albiense Inferior) en el área de La Florida. Modificado de Najarro *et al.* (2009).

Interpretación del medio sedimentario: La sub-unidad inferior (Las Peñosas 1), observada solo en el sector de La Florida, se interpreta como una unidad transicional depositada en un ambiente debahía con una progresiva influencia siliciclástica durante el inicio de un episodio transgresivo tras la exposición subaéra de la Fm. Reocín. La sub-unidad intermedia (Las Peñosas 2), es interpretada como la progradación de un sistema deltaico, con ambientes que varían desde frente deltaico, con progradación de barras deltaicas de desembocadura y barras distales, a llanura deltaica, con zonas emergidas con desarrollo de paleosuelos, surcadas por canales distribuitarios de ríos meandriformes y por bahías interdistributarias. El desbordamiento de los ríos durante grandes tormentas debió producir inundaciones que acumularon en las bahías interdistributarias arcillas y limos con abundantes hojas, fragmentos de troncos y eventualmente piezas de ámbar, provenientes de zonas boscosas más interiores (Najarro *et al.*, 2009). Estos ambientes evolucionan rápidamente en la vertical a ambientes litorales de llanura mareal y estuarinos con abundante bioturbación, y con influencia de mareas, oleaje y tormentas. Por último, la sub-unidad superior (Las Peñosas 3) se interpreta como una unidad transicional, depositada en un ambiente de plataforma mixta terrígeno-carbonatada durante un nuevo pulso transgresivo.

3.2.1.8. FORMACIÓN BARCENACIONES

Como se ha explicado anteriormente, el estudio de esta unidad queda fuera de los objetivos de este trabajo de investigación. Sin embargo, debido a que su base constituye el *datum* de techo referencia de la sucesión estudiada, se ha considerado oportuno incluir una descripción de la unidad en este apartado.

Nombre de la Unidad: Barcenaciones
Rango de la Unidad: Formación

Antecedentes: La Formación Barcenaciones fue definida por García-Mondéjar (1982) y admitida por Hines (1985). Es equivalente a la unidad "Calizas con Caprinidos" de Mengaud (1920) y Rat (1959); "Nivel 6" del corte de Saja de Rat (en Ciry *et al.*, 1967); "Niveles C_{16}^{12} y C_{16}^{23}" del MAGNA; y "Calizas 3 (Barcenaciones), areniscas 4 y calizas 4" de García-Mondéjar y Pujalte (1981).

Secciones de referencia: El corte tipo se establece en el valle del río Saja, a orillas de la carretera a su paso por la localidad de Barcenaciones (oeste de Torrelavega) (García-Mondéjar, 1982). Otras secciones de referencia en el área de estudio se localizan: para el área del sinclinal de Santillana, en el corte de la carretera que une las localidades de Novales y Fresnedo; para el área de La Florida, en la corte del río Nansa y en el corte de la carretera de Rábago a la cueva de El Soplao; y para el área de Cuchía, en la parte alta de la cantera de Solvay, en los afloramientos de costa entre la playa del Huevo y la playa de Cuchía, y en la parte alta de la Punta del Dichoso (Suances).

Aspectos regionales: La unidad aflora en las tres áreas de estudio. En el corte tipo la unidad presenta unos 100 metros de potencia. Este espesor se reduce progresivamente hacia el norte y noreste, presentando una potencia de 65 metros en el corte de la carretera de Novales a Fresnedo, mientras que en el sector de Cuchía presenta 20 metros de potencia en el corte de la cantera de Solvay y unos 13 metros en la sección de Suances (Punta del Dichoso). En el área de La Florida su potencia varía entre unos 44 metros en la sección de Rábago y unos 100 metros en la sección de Bustriguado.

En los sectores de La Florida y sinclinal de Santillana, el límite inferior con la Fm. Las Peñosas se caracteriza por un cambio gradual en el tipo de sedimentación, mientras que en el área de Cuchía, el contacto con la unidad infrayacente (Fm. Reocín) es una discontinuidad con laguna estratigráfica. Aquí la formación presenta una potencia bastante reducida respecto a las otras áreas, posiblemente debido a que la laguna estratigrafica a la base de la unidad abarca además del Albiense Inferior-Medio (Fm. Las Peñosas), también a la parte baja del Albiense Superior.

Edad: El contenido fósil de esta formación le otorga una edad Albiense Superior. Así, en las secciones estudiadas se han identificado, hacía la parte alta de la unidad, numerosos ejemplares de *Caprina Choffati* DOUVILLÉ (Foto 3.44), ya citados en los trabajos de Mengaud (1920) y Rat (1959), y cuya distribución estratigráfica se asigna a la parte alta del Albiense Superior (Vraconiense) (Masse *et al.*, 1998). Mengaud (1920) cita en los niveles margosos nodulosos con bivalvos de la parte basal de la unidad en la ensenada de Fonfría (Comillas), los ammonítidos *Parengonoceras ebrayi* DE LORIOL, *Cnemiceras (Placenticeras) uhligi* CHOFFAT sp. y *Cnemiceras*

(Placenticeras) ebrayi DE LORIOL sp., que indican una edad de Albiense Superior, posiblemente pre-Vraconiense (Zona *Mortoniceras inflatum*) (Breistroffer, 1936).

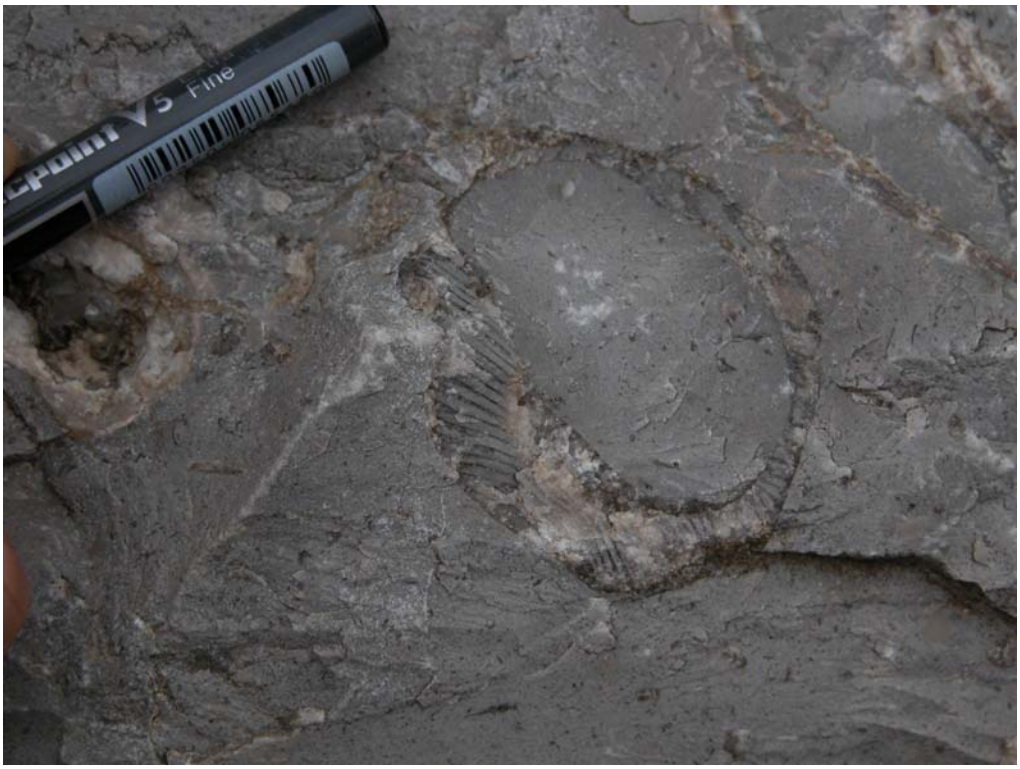

Foto 3.44.- Ejemplar de *Caprina choffati* DOUVILLÉ encontrado en la parte alta de la sección de la cantera de Cuchía.

Descripción: En el corte tipo de la Formación Barcenaciones, donde presenta su máxima potencia (área del sinclinal de Santillana), se pueden distinguir tres miembros (García-Mondéjar, 1982). El miembro inferior presenta unos 70 metros de potencia y está compuesto por: i) calizas *packstone-wackestone* nodulosas y laminadas con orbitolinas, miliólidos, gasterópodos, ostreidos y algas; ii) niveles de margas nodulosas con bioclastos y glauconita y iii) calcarenitas *packstone-grainstone* con estratificación cruzada en surco y *hummocky*, bioclastos y glauconita detrítica. El miembro medio consiste en unos 20 metros de: i) areniscas con estratificación cruzada y orbitolinas; y ii) limos-lutitas con *ripples* de corriente, bioclastos y restos de carbón. El miembro superior, de edad Vraconiense, está formado por unos 15 metros de: i) calizas *packstone-wackestone* nodulosas con corales ramosos y masivos, rudistas caprínidos (*Caprina choffati* DOUVILLÉ), requiénidos y radiolítidos, milólidos, orbitolinas y

Chondrodonta sp.; y ii) calcarenitas *grainstone-packstone* con estratificación cruzada en surco, ooides, orbitolinas, bioclastos y glauconita detrítica.

El seguimiento cartográfico y observación de la unidad en las diferentes secciones estudiadas permite determinar que en el área de La Florida, Cuchía y en el sector de Comillas está ausente el miembro medio (Fotos 3.45 y 3.46A-C), mientras que en el área de la costa al norte y este de Cuchía (secciones de Suances y Somocueva) solo se encuentra el miembro superior (Vraconiense), que se deposita directamente encima de la Fm. Reocín (Foto 3.46D-E).

En el área de La Florida, el miembro inferior de la Formación Barcenaciones, de unos 12 metros de potencia, está constituido por calizas margosas *packstone* y *wackestone*, algo nodulosas, con orbitolinas, ostreidos, gasterópodos, y corales, cuyo techo está representado por una superficie irregular de bioturbación con contenido importante de glauconita (Foto 3.45E, sección de río Nansa), interpretada como una discontinuidad asociada con inundación y condensación. El miembro superior de la Fm. Barcenaciones está constituído por una sucesión de 43 metros de tramos de 1 a 4 metros de margas limosas micáceas con niveles centimétricos a decimétricos de calizas con laminaciones estromatolíticas (Foto 3.45C-D) y tramos métricos a decamétricos de grainstone con estratificación cruzada, que alternan en secuencias métricas a decamétricas (Foto 3.45A, B, E).

Interpretación del medio sedimentario: Los miembros inferior y superior de la Formación Barcenaciones presentan facies características de ambientes abiertos de plataforma carbonatada media y externa de baja energía (calizas con corales y rudistas, calizas nodulosas bioturbadas, calizas margosas y margas con ammonites) y de bajíos o *shoals* depositados en ambientes de alta energía localizados en la parte media de una rampa carbonatada afectada por corrientes mareales y tormentas. Esto sugiere una alternancia de periodos más energéticos, caracterizados por el desarrollo y migración de barras de calcarenitas con estratificación cruzada, y de otros menos energéticos, caracterizados por la decantación de arcillas y margas, y por desarrollo de abundante bioturbación. Por otro lado el miembro medio de la formación presenta facies características de un ambiente siliciclástico marino costero.

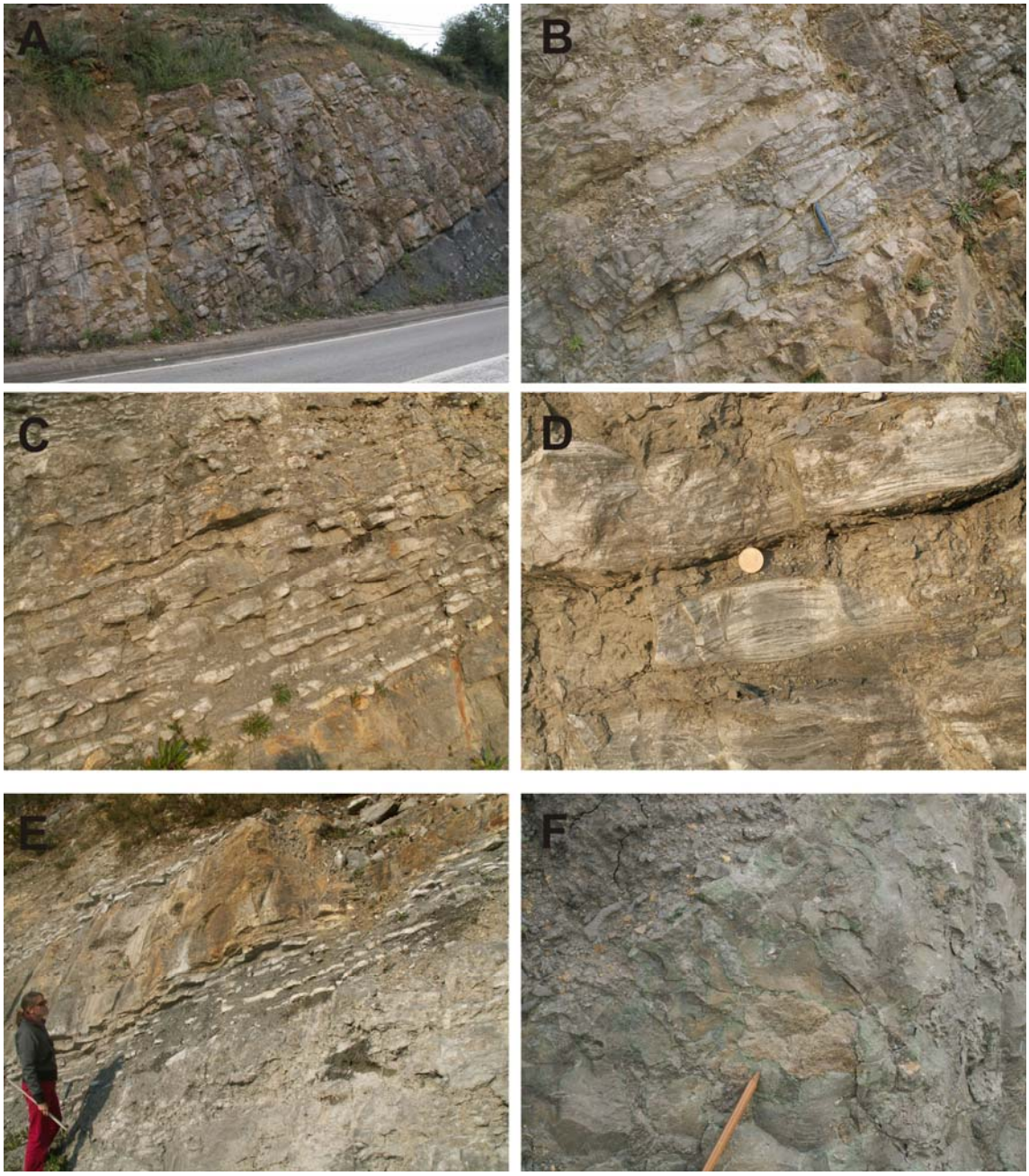

Foto 3.45.- Aspecto de las distintas facies que forman la Formación Barcenaciones en el área de La Florida (sección de río Nansa). **A)** Aspecto general de bancos de calcarenitas con estratificación cruzada que alternan con niveles margosos con glauconita. **B)** Detalle de estratificación cruzada en los bancos de calcarenita. **C)** Alternancia de margas con niveles centimétricos de calizas con laminación de estromatolitos. **D)** Detalle de los niveles de estromatolitos laminados. **E)** Aspecto de la caliza margosa con ostreidos y corales (parte inferior de la imagen), alternancia de margas y niveles de estromatolitos laminados (parte media) y banco de calcarenitas (parte superior de la imagen). **F)** Detalle del techo de nivel calizo con corales y ostreidos glauconitizado y bioturbado (superficie de inundación y condensación).

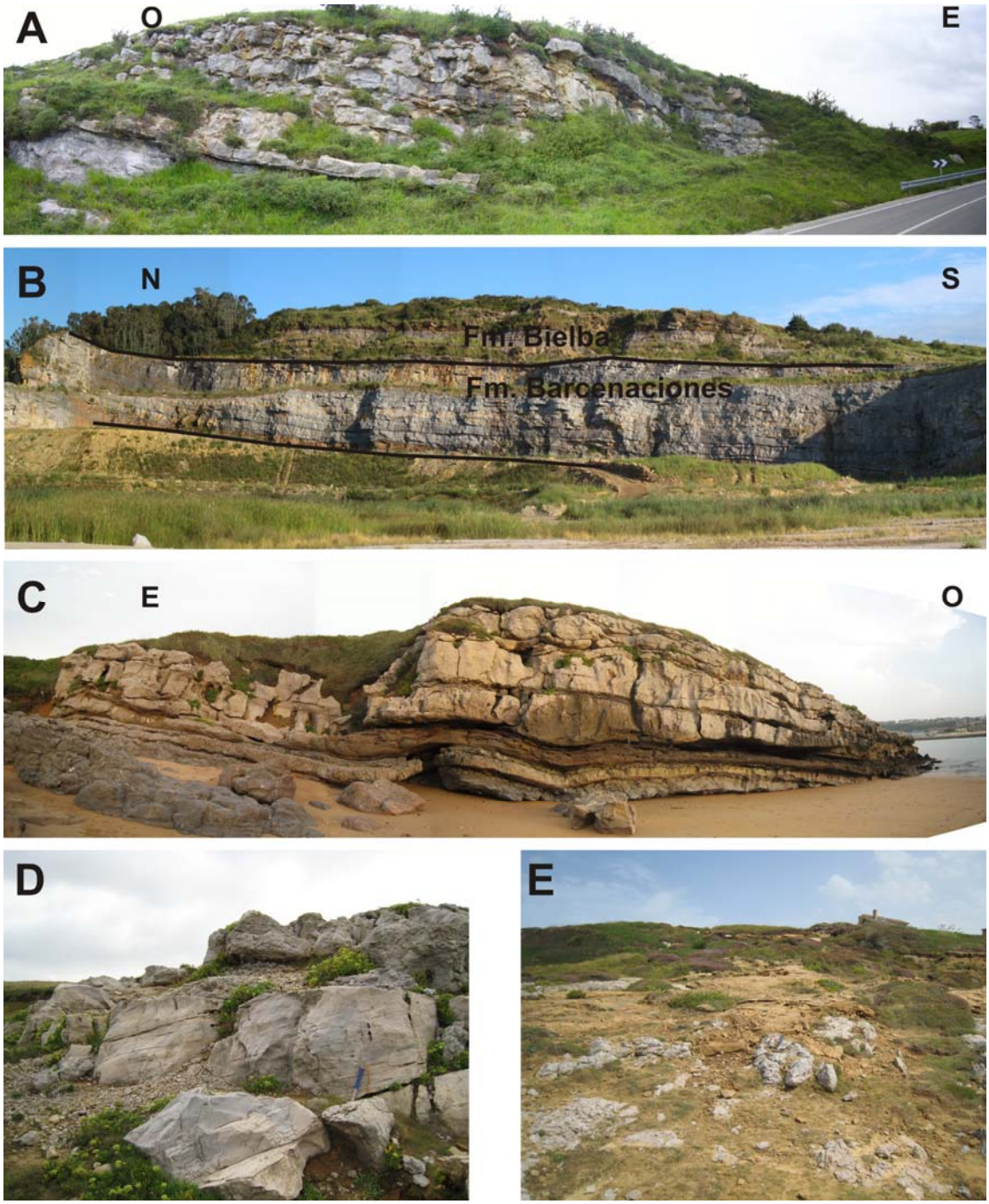

Foto 3.46.- Aspecto de la Formación Barcenaciones en las distintas áreas de estudio. **A)** Calizas margosas nodulosas y calcarenitas en la sección de Novales (área del sinclinal de Santillana). **B)** Aspecto general de los bancos de caliza y calcarenitas en la cantera de Cuchía, área de Cuchía. **C)** Formación Barcenaciones en la playa del Huevo (área de Cuchía). **D)** Calcarenitas y calizas margosas nodulosas que corresponden a la parte superior de Formación Barcenaciones en la Punta del Dichoso (sección de Suances, área de Cuchía). **E)** Contacto en planta entre la Formación Barcenaciones y la Formación Bielba en la Punta del Dichoso mostrando una superficie irregular kárstica (sección de Suances, área de Cuchía).

3.2.2. APORTACIONES A LA BIOESTRATIGRAFÍA

Se ha realizado un análisis bioestratigráfico basado en el estudio de diferentes grupos fósiles recolectados en varias secciones estratigráficas del área de estudio. En particular, los estudios bioestratigráficos se han centrado principalmente en las secciones de río Nansa-Rábago (área de La Florida) y Cuchía-Suances (área de Cuchía), localizadas en los extremos SO y NE respectivamente del área de estudio, con el fin de comprobar la extensión lateral y la fiabilidad de la correlación de las unidades litoestratigráficas, de precisar mejor el encuadre temporal de los eventos estudiados, y de poder determinar la posible existencia o no de discontinuidades significativas en estas zonas de paleoalto relativo y, en lo posible, la magnitud de las lagunas estratigráficas asociadas a éstas.

Según las unidades, los fósiles con valor bioestratigráfico recolectados o identificados, con ayuda de diferentes especialistas, son: ammonites, foraminíferos planctónicos, foraminíferos bentónicos, nanofósiles calcáreos, rudistas y palinomorfos. En particular, los nuevos datos bioestratigráficos aportados en este estudio han permitido redefinir algunas de las biozonas de ammonites definidas previamente para el Aptiense Inferior del área, y calibrar e integrar éstas junto con biozonas de foraminíferos planctónicos y nanofósiles calcáreos. También han permitido caracterizar mejor la asociación de foraminíferos bentónicos para las unidades calcáreas del Aptiense y Albiense, así como establecer por primera vez biozonas de nanofósiles calcáreos y de contenido de palinomorfos para las unidades margosas y terrígenas estudiadas (Formaciones Patrocinio y Las Peñosas).

En la figura 3.5 se muestra el esquema lito y bioestratigráfico propuesto para el Aptiense-Albiense del área de estudio, deducido a partir de los datos bioestratigráficos aportados en este trabajo, junto con la revisión de datos previos (Mengaud, 1920; Collignon *et al.*, 1979; Ramírez del Pozo, 1972; Najarro *et al.*, 2011b).

A continuación se detallan las aportaciones de esta Tesis al conocimiento bioestratigrafico del Aptiense-Albiense del área de estudio.

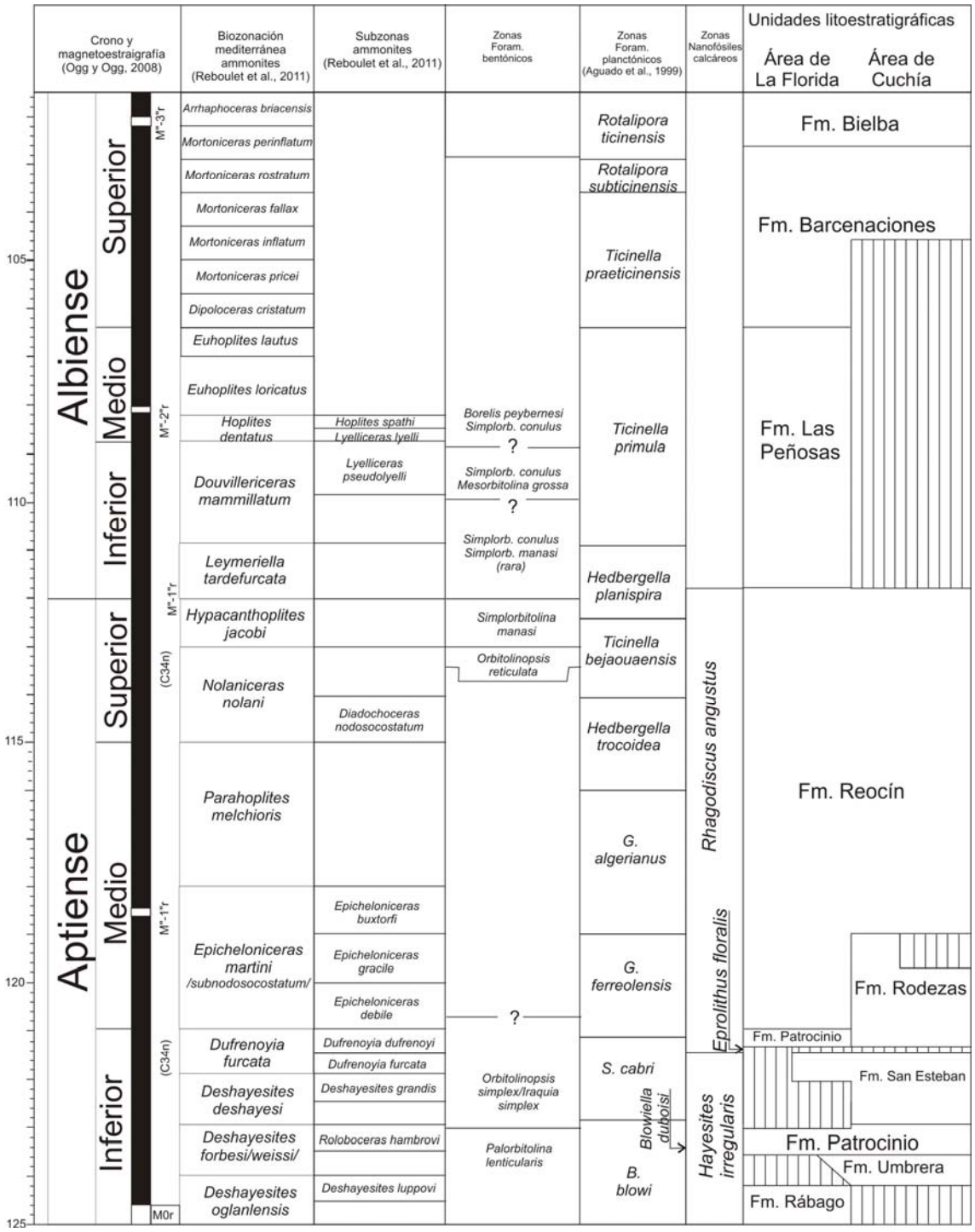

Figura 3.5.- Esquema bioestratigráfico y cronoestratigráfico propuesto para el Aptiense-Albiense del área de estudio (basado en Ramírez del Pozo, 1972; Reboulet *et al*., 2011; Cherchi y Schroeder, 1998 y en los datos de esta Tesis modificados de Najarro *et al.*, 2011b).

3.2.2.1. AMMONITES

Durante el desarrollo de las labores de campo de esta investigación, los hallazgos de ammonites han sido relativamente escasos en cuanto a niveles encontrados, limitándose a los depósitos margosos de plataforma abierta distal y cuenca de las Formaciones Patrocinio y Barcenaciones, del Aptiense Inferior y del Albiense Superior respectivamente**.**

De las diversas secciones estudiadas en la **Formación Patrocinio** (Aptiense Inferior), sólo ha aportado restos de ammonoideos la sección de la playa de los Caballos de Cuchía. La presencia de ammonites en esta sección se conoce desde los trabajos regionales de Mengaud (1920) y Rat (1959), que citan la presencia de varias especies de edad Aptiense. Posteriormente, Collignon *et al.* (1979) llevaron a cabo un estudio más detallado de estas faunas e identificaron dos niveles con ammonites en el corte de la playa de Los Caballos de Cuchía. En el inferior reconocieron *Prodeshayesites fissicostatus* (PHILLIPS), *P. bodei* (KOENEN), *P.* cf. *lestrangei* CASEY, *Deshayesites euglyphus* CASEY, *D. forbesi* CASEY, *D. fittoni* CASEY, *D. punfieldensis* SPATH y *D. callidiscus* CASEY. De acuerdo con el esquema de Casey (1961), estos ammonites caracterizarían las Zonas *Prodeshayesites fissicostatus* y *Deshayesites forbesi*. En el segundo nivel, localizado algunos metros por encima del anterior, reconocieron *Cheloniceras cornuelianum* (D'ORBIGNY), *Ch. crassum* SPATH, *Ch. royerianum* D'ORBIGNY y *Vectisites hispanicus* COLLIGNON, que atribuyeron a las Zonas de *Deshayesites deshayesi* y *Tropaeum bowerbanki* de Casey (1961). Por tanto, de acuerdo con estos autores, todas las zonas del Beduliense estarían representadas dentro de estos dos niveles con ammonites. Estas atribuciones estratigráficas han sido aceptadas como válidas en trabajos recientes (ej. Wilmsen, 2005).

En este estudio se han reconocido también los dos horizontes con ammonites de Collignon *et al.* (1979). Ambos niveles se localizan en la parte baja de las margas de la Formación Patrocinio, concretamente a 8 y 16 m respectivamente del techo de la Fm. Umbrera en la sección de la playa de los Caballos. Se han recolectado ejemplares nuevos procedentes de estos dos niveles y además se han revisado otros ejemplares procedentes también de estos niveles, pertenecientes al Museo Geológico del Seminario de Barcelona (los siglados MGSB) y a una colección particular. Los nuevos ejemplares recolectados se encuentran depositados en las Colecciones de Paleontología de la

Universidadt Autónoma de Barcelona (los ejemplares siglados PUAB) y en el Museo Geominero del IGME en Madrid (siglados IGME y MGM) (Lámina 4). Para el nivel inferior se han recolectado abundantes ejemplares de deshayesítidos (Lámina 4), casi todos identificados como *Deshayesites* cf. *forbesi* CASEY junto con algunos fragmentos de macroconchas atribuidas a *Deshayesites* cf. *callidiscus* CASEY. Junto a ellos se ha encontrado también ejemplares de *Pseudohaploceras liptoviensis* (ZEUSCHNER), *Pseudosaynella undulata* (SARASIN) y *Toxoceratoides* sp. En este primer nivel los cheloniceratidos son escasos y difícilmente identificables, aunque sí se han podido identificar dos fragmentos de *Roloboceras* cf. *hambrovi* (FORBES).

Para el segundo nivel, localizado 8 m por encima del anterior, se ha podido identificar varios ejemplares de *Deshayesites* cf. *forbesi* CASEY, *Deshayesites* cf. *consobrinus* (D'ORBIGNY), *Deshayesites planus* CASEY, *Deshayesites fittoni* CASEY, *Pseudosaynella bicurvata* (MICHELIN), *Toxoceratoides* sp. Los cheloniceratidos también son escasos, aunque se ha podido identificar también para este nivel un fragmento de *Roloboceras hambrovi* (FORBES) y un ejemplar juvenil de *Roloboceras* sp. (Lámina 4).

La revisión de los ammonites procedentes de la sección de Cuchía depositados en las colecciones del Museo Geológico del Seminario de Barcelona (MGSB) han permitido reconocer *Deshayesites* cf. *forbesi* CASEY, *Pseudosaynella undulata* (SARASIN), *Deshayesites* cf. *callidiscus* CASEY, *Roloboceras* cf. *hambrovi* (FORBES) y *Roloboceras* sp. La revisión de la colección particular ha permitido identificar *Deshayesites* cf. *forbesi* CASEY, *Deshayesites planus* CASEY, *Roloboceras hambrovi* (FORBES), *Roloboceras* sp. y *Toxoceratoides royerianus* (D'ORBIGNY). Se trata, por tanto, de los mismos taxones que han proporcionado los muestreos llevados a cabo para la realización de este trabajo.

Todas las especies de deshayesítidos identificadas en los dos niveles de ammonites de Cuchía (Figura 3.6) son características de la biozona *Deshayesites weissi* de la zonación estándar para el área mediterránea de Reboulet *et al.* (2009), renombrada, recientemente como *Deshayesites forbesi* por Reboulet *et al.* (2011), que es equivalente a la Zona de *Deshayesites forbesi* en el esquema de Casey (1961). Por tanto, de acuerdo con estos datos, ambos horizontes son inequívocamente atribuibles a la Zona de *Deshayesites forbesi* (antiguamente *D. weissi*). Además, la presencia de *Roloboceras* en

los dos niveles de ammonites indicaría que este intervalo corresponde concretamente a la parte media-alta de la Zona de *Deshayesites forbesi* (antiguamente *D. weissi*) (Casey, 1961, Casey *et al.* 1998, Moreno-Bedmar *et al.*, 2009). Por otra parte, la presencia de varios ejemplares de *Pseudosaynella* sugiere también la parte alta de la Zona *Deshayesites forbesi* (antiguamente *D. weissi*) ya que, aunque estas especies también están presentes en la Zona *Deshayesites deshayesi*, su registro en esta biozona suele ser mucho más escaso (Moreno-Bedmar *et al.*, 2009).

Estos resultados difieren en gran medida de los presentados por Collignon *et al.* (1979), que proponen que todas las biozonas del Bedouliense (Aptiense Inferior) están presentes en los dos horizontes de ammonites de Cuchía. El origen de esta diferente atribución de edad para los mismos horizontes se basa fundamentalmente en diferencias en la interpretación taxonómica de los ammonites. En concreto, los ejemplares procedentes del nivel inferior de Cuchía y atribuidos por Collignon *et al.* (1979) al género *Prodeshayesites*, característico de la Zona de *P. fissicostatus* del dominio boreal, corresponderían de acuerdo con nuestro estudio a individuos juveniles de *Deshayesites* cf. *forbesi*, la cual es una especie típica de la Zona de *D. forbesi* (antiguamente *D. weissi*) del dominio tetisiano (los representantes del género *Prodeshayesites* muestran secciones generalmente más comprimidas y una costulación más rígida y prominente que los deshayesítidos presentes en Cuchía; Moreno-Bedmar, com. per.). De igual manera, los ejemplares que Collignon *et al.* (1979) identificaron como pertenecientes a los géneros *Cheloniceras* y *Vectisites*, que indicarían las Zonas de *D. deshayesi* y *T. bowerbanki,* corresponderían, de acuerdo con nuestra interpretación, con individuos juveniles o microconchas de *Roloboceras (*Moreno-Bedmar, com. per.), un género también característico de la Zona de *D. forbesi* (antiguamente *D. weissi*) juntos con los deshayesítidos encontrados para este nivel. Esta nueva atribución de edad para la Fm. Patrocinio aparece confirmada además por las asociaciones de foraminíferos planctónicos y nanofósiles calcáreos reconocidos para la misma unidad, y que serán tratados a continuación.

Recientemente García-Mondéjar *et al*. (21015) han revisado la misma sección de la Fm. Patrocinio en la playa de Los Caballos de Cuchía, llegando a conclusiones que difieren de nuestros resultados. Según estos autores en este afloramiento la unidad comprende las biozonas de *D. forbesi*, *D. deshayesi*, y una zona que ellos definen aquí, al igual que en la sección de Igaratza (Aralar), como zona transicional *D. deshayesi-D.*

furcata (García-Mondéjar *et al*., 2009), y que no ha sido reconocida o adoptada por otros autores, ni por la revisión reciente del "Grupo Kilian" (Reboulet *et al*., 2011). Como ya se ha comentado, estas diferencias en la asignación bioestratigráfica de la Fm. Patrocinio en Cuchía se deben a los problemas con la identificación taxonómica de *D. desahesi*. Esta especie ha sido revisada recientemente por Moreno-Bedmar *et al*. (2014), poniendo de manifiesto la similitud de algunas formas que pertenecen a la familia Deshayesitidae, lo que lleva a muchos autores a determinar con el mismo nombre taxonómico diferentes especies. Esta dificultad en la diferenciación taxonómica está relacionada con cuestiones de variaciones ontogénicas, variabilidad o dimorfismo sexual, etc. En el caso que nos incumbe, las similitudes entre *D. forbesi* y *D. deshayesi* dificultan su asignación taxonómica y la correcta asignación de estas biozonas. Además, García-Mondéjar *et al* (2015) consideran las faunas de ammonites del Aptiense Inferior de la cuenca Vasco-Cantábrica como de afinidad Boreal principalmente, a diferencia de otros autores que los consideran de marcado carácter Tetisiano (ej. Gaona-Narvaez *et al*., 2013; Moreno-Bedmar *et al*., 2014).

Por otra parte, en cuanto a la **Formación Barcenaciones** (Albiense Superior), en la sección de la ensenada de Fonfría ha aparecido un ejemplar de ammonites de la especie *Engonohoplitoides* sp. (figurado en la Lámina 12D), que se asigna a la parte alta del Albiense Superior o Vraconiense (Zona *Stoloczkaia dispar*, parte alta de la subzona *Stoliczkaia blancheti*) (Moreno-Bedmar, com. per.).

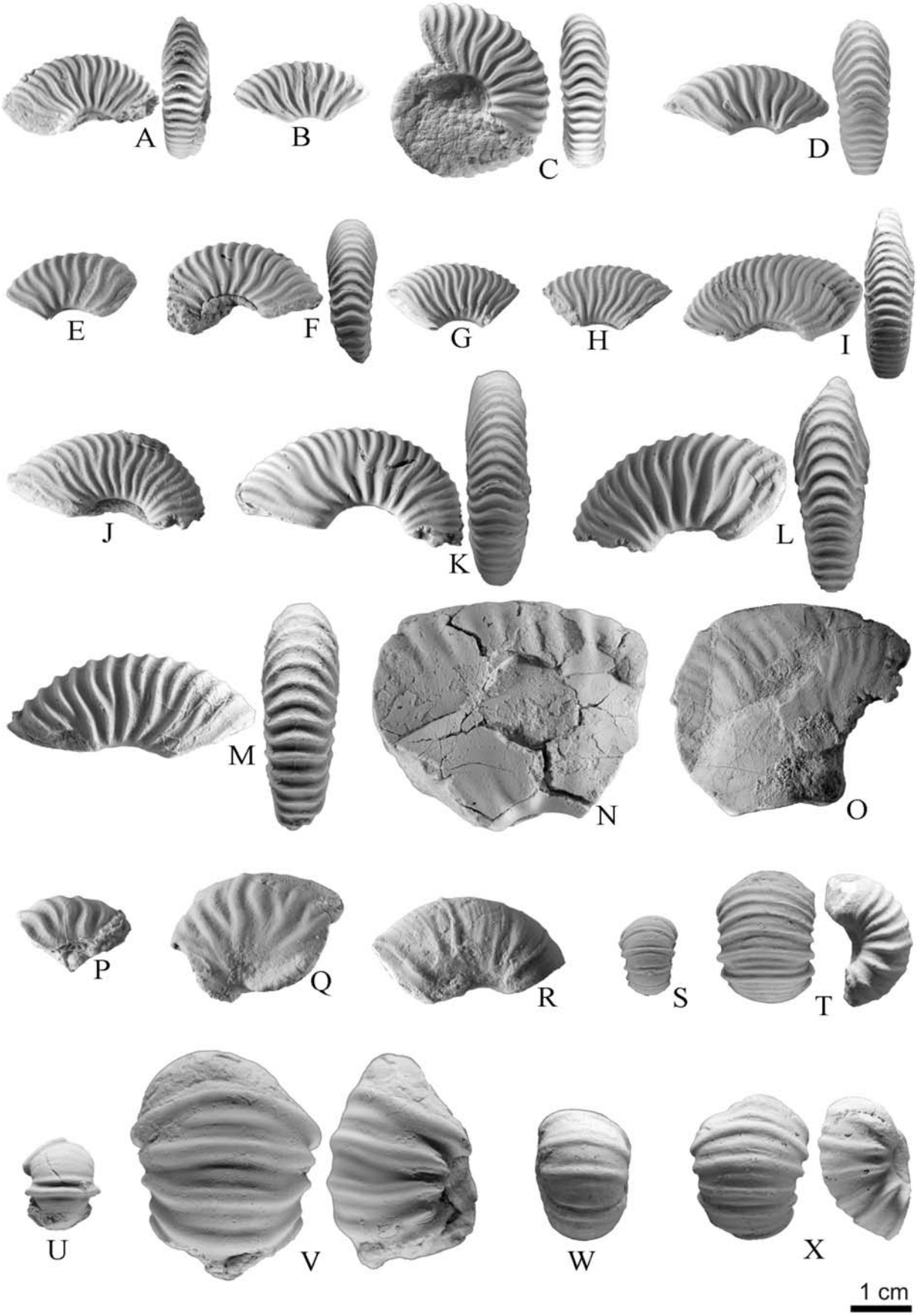
A
B
C
D
E
F
G
H
I
J
K
L
M
N
O
P
Q
R
S
T
U
V
W
X
1 cm

Lámina 4.- A: *Deshayesites* cf. *forbesi* vista lateral y ventral del ejemplar MGSB 18730-3. **B**: *Deshayesites* cf. *forbesi* vista lateral del ejemplar MGSB 1870-2. **C**: *Deshayesites* cf. *forbesi* vista lateral y ventral del ejemplar MGSB 18730-1. **D**: *Deshayesites* cf. *forbesi* vista lateral y ventral del ejemplar depositado en las Colecciones de Paleontología de la Universidad Autónoma de Barcelona, PUAB 68536, nivel inferior de Cuchía. **E**: *Deshayesites* cf. *forbesi* vista lateral del ejemplar PUAB 68533, nivel inferior de Cuchía. **F**: *Deshayesites* cf. *forbesi*, vista lateral y ventral del ejemplar PUAB 68545, nivel inferior de Cuchía. **G**: *Deshayesites planus* vista lateral del ejemplar PUAB 68554, nivel superior de Cuchía. **H**: *Deshayesites planus* vista lateral del ejemplar PUAB 68555, nivel superior de Cuchía. **I**: *Deshayesites planus* vista lateral y ventral del ejemplar PUAB 68557, nivel superior de Cuchía. **J**: *Deshayesites planus* vista lateral del ejemplar PUAB 68559, nivel superior de Cuchía. **K**: *Deshayesites fittoni* vista lateral y ventral del ejemplar PUAB 68562, nivel superior de Cuchía. **L**: *Deshayesites* cf. *consobrinus* vista lateral y ventral del ejemplar PUAB 68561, nivel superior de Cuchía. **M**: *Deshayesites* cf. *consobrinus* vista lateral y ventral del ejemplar PUAB 68563, nivel superior de Cuchía. **N**: *Deshayesites* sp. cf. *callidiscus* vista lateral del ejemplar MGSB 18730-4. **O**: *Pseudosaynella bicurvata* vista lateral del ejemplar PUAB 68564. **P**: *Pseudosaynella undulata* vista lateral del ejemplar PUAB 68538, nivel inferior de Cuchía. **Q**: *Pseudosaynella undulata* vista lateral del ejemplar MGSB 18730-5. **R**: *Pseudohaploceras liptoviensis* vista lateral del ejemplar PUAB 68534, nivel inferior de Cuchía. **S**: *Roloboceras* sp. vista ventral del ejemplar PUAB 68542, nivel inferior de Cuchía. **T**: *Roloboceras* sp. microconcha, vista lateral y ventral del ejemplar PUAB 68552, nivel inferior de Cuchía. **U**: *Roloboceras* sp. vista ventral del ejemplar PUAB 68532, nivel inferior de Cuchía. **V**: *Roloboceras* sp. macroconcha vista ventral y lateral del ejemplar MGSB 78706. **W**: *Roloboceras* sp. microconcha vista ventral del ejemplar MGM 10807C. **X**: *Roloboceras hambrovi*, macroconcha vista ventral y lateral del ejemplar MGM 10809C. La barra de escala es de 1 cm.

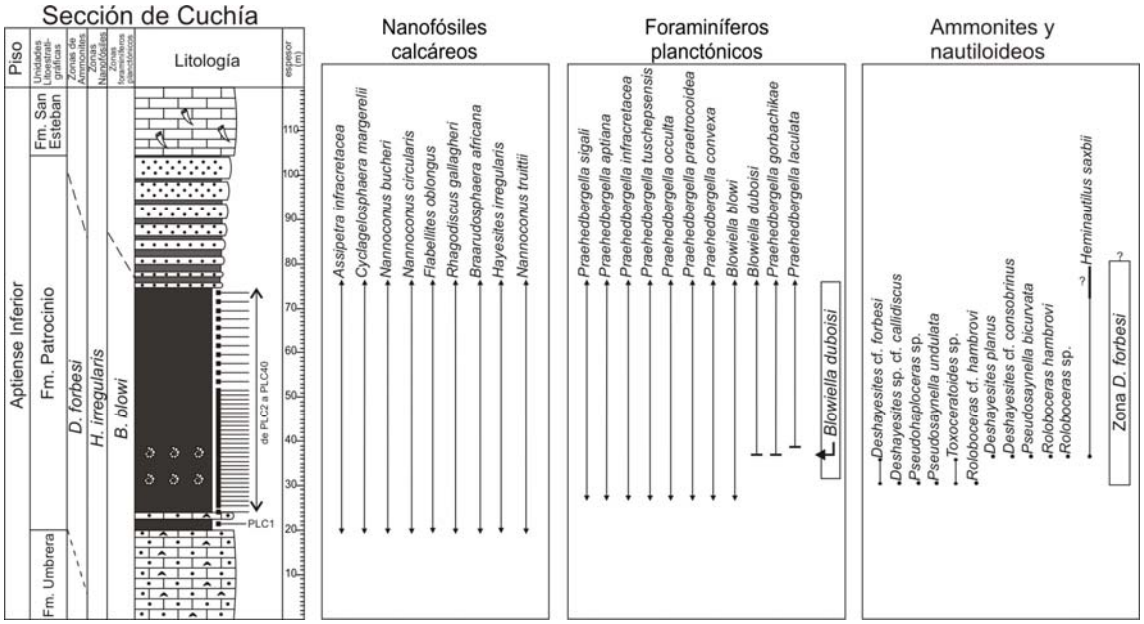

Figura 3.6.- Sección estratigráfica sintética del Aptiense Inferior en el afloramiento de la playa de los Caballos (área de Cuchía), mostrando la distribución de fósiles principales identificados con valor bioestratigráfico.

3.2.2.2. FORAMINÍFEROS PLANCTÓNICOS

Se ha estudiado la asociación de foraminíferos planctónicos del Aptiense Inferior presentes en la Formación Patrocinio. Para este estudio se recolectaron muestras de la Formación Patrocinio tanto en la sección de Cuchía (playa de los Caballos) como en la sección de río Nansa, aunque solo de la sección de Cuchía se obtuvieron ejemplares con suficiente calidad para poder ser clasificados.

En la sección de Cuchía se han estudiado 40 muestras localizadas a lo largo de la unidad a intervalos estratigráficos de aproximadamente 2 metros (muestras PLC-1 a PLC-40, Figura 3.6). De éstas, solo las muestras basales (PLC-1 a PLC-3) no han presentado foraminíferos planctónicos. El resto de las muestras arrojan una asociación de foraminíferos planctónicos caracterizados por formas con pared microperforada, con cuatro a cinco cámaras redondeadas. Se han reconocido principalmente formas pertenecientes a los géneros *Praehedbergella* y *Blowiella*, que incluyen las especies (Lámina 5): *Praehedbergella sigali* (MOULLADE), *Praehedbergella aptiana* (BARTENSTEIN) s.s., *Praehedbergella infracretacea* (GLAESSNER), *Praehedbergella occulta* (LONGORIA), *Praehedbergella convexa* (LONGORIA), *Praehedbergella praetrocoidea* (KRECHMAR y GORBACHIK), *Praehedbergella gorbachikae* (LONGORIA), *Praehedbergella tuschepsensis* (ANTONOVA), *Praehedbergella laculata* BANNER, COPESTAKE y WHITE, *Blowiella blowi* (BOLLI), *Blowiella duboisi* (CHEVALIER), *Blowiella maridalensis* (BOLLI). En la muestra PCL-14 se ha detectado la primera aparición de *B. duboisi* (CHEVALIER) y *P. gorbachikae* (LONGORIA). Estos bioeventos ocurren en la parte alta de la Zona *Blowiella blowi*, antes de la primera aparición de *Schackoina cabri* (Aguado *et al.*, 1999; Gea *et al.*, 2003). Por tanto, esta asociación permite datar la Fm. Patrocinio como parte alta de la Zona *Blowiella blowi* de foraminíferos planctónicos (Moullade, 1974; Moullade *et al.* 2002). Esta biozona se correlaciona con la mitad superior de la Zona *H. irregularis* de nanofósiles y con la parte media-superior de la Zona *D. forbesi* de ammonites (Figura 3.5).

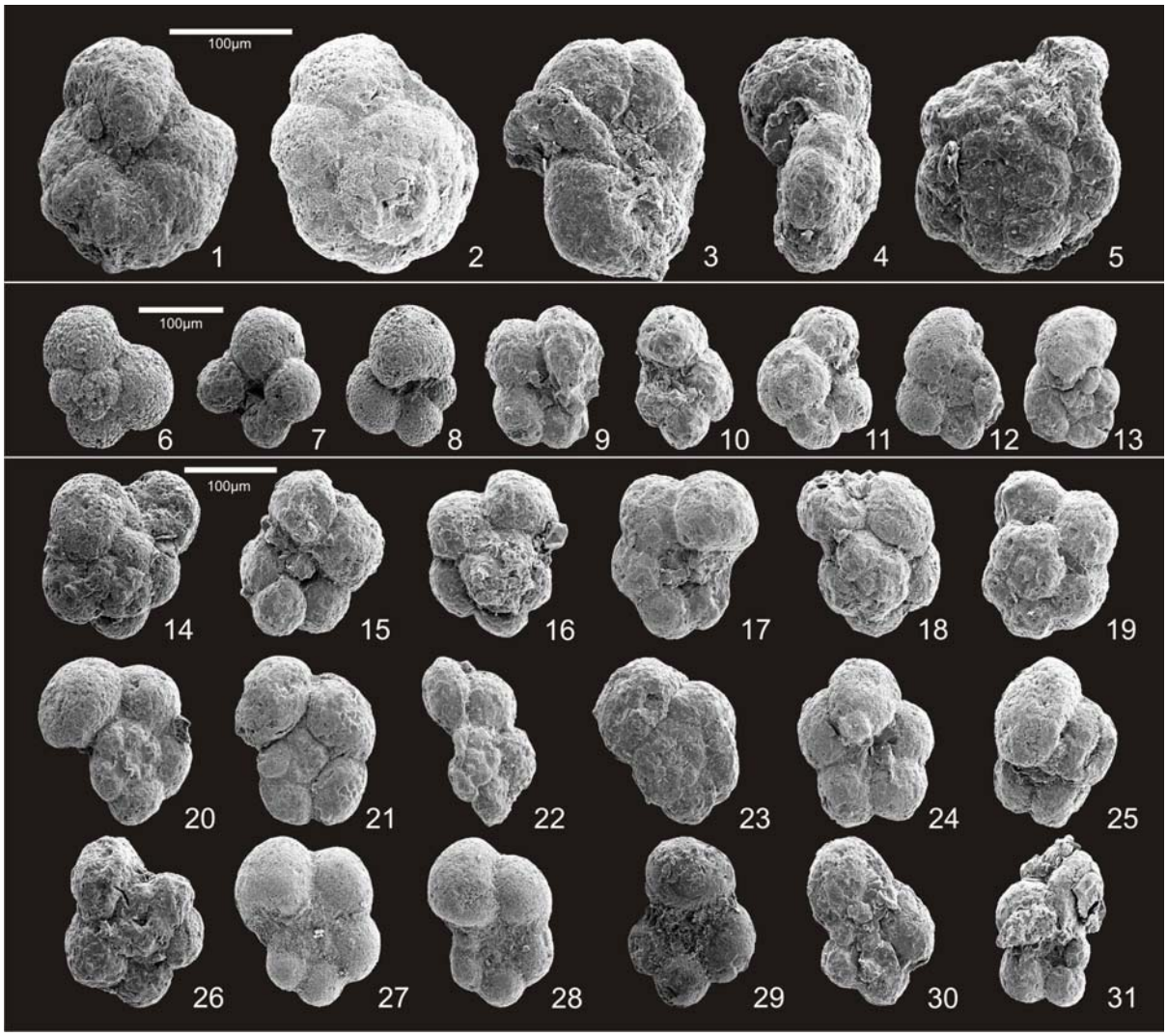

Lámina 5.- 1,2: *Praehedbergella praetrocoidea*. **3,4**: *Praehedbergella oculta*. **5**: *Praehedbergella convexa*. **6-11**: *Praehedbergella sigali*. **12,13**: *Praehedbergella tuschepsensis*. **14-19**: *Praehedbergella infracretacea*. **20-23**: *Praehedbergella aptiana*. **24,25**: *Praehedbergella gorbachikae*. **26-28**: *Blowiella blow*i. **29-31**: *Blowiella duboisi*. Escalas: Fotos 1–5 c x 300, Fotos 6–13 c x500, Fotos 14–31 c x400.

El listado de taxones de foraminíferos planctónicos identificados para las muestras estudiadas de la Formación Patrocinio es el siguiente:

- *Blowiella blowi* (Bolli, 1959)
- *Blowiella duboisi* (Chevalier, 1961)
- *Blowiella maridalensis* (Bolli, 1959)
- *Praehedbergella aptiana* (Bartenstein, 1965) *s.s.*
- *Praehedbergella convexa* (Longoria, 1974)
- *Praehedbergella gorbachikae* (Longoria, 1974)
- *Praehedbergella infracretacea* (Glaessner, 1936)

- *Praehedbergella laculata* Banner, (Copestake y White, 1993)
- *Praehedbergella occulta* (Longoria, 1974)
- *Praehedbergella praetrocoidea* (Krechmar y Gorbachik, 1986)
- *Praehedbergella sigali* (Moullade, 1966)
- *Praehedbergella tuschepsensis* (Antonova, 1964)
- *Schackoina cabri* Sigal, 1952

3.2.2.3. NANOFÓSILES CALCÁREOS

Se ha estudiado la asociación de nanofósiles calcáreos presentes en la Formación Patrocinio del Aptiense Inferior, a partir de muestras recolectadas en las áreas de Cuchía (playa de los Caballos) y de La Florida (río Nansa y Rábago) (Figuras 3.6 y 3.7).

En las muestras estudiadas de estas secciones los nanofósiles calcáreos no son muy abundantes, presentan un grado de preservación moderado y una escasa diversidad. Las asociaciones identificadas son de carácter marcadamente tetisiano, y están dominadas por los géneros *Watznaueria*, *Rhagodiscus* y *Nannoconus*, junto con otras especies como *Assipetra terebrodentaria*, *Hayesites irregularis*, *Zeugrhabdotus noeliae*, *Lithraphidites carniolensis*, *Biscutum ellipticum*, *Discorhabdus ignotus*, *Diazomatolithus lehmanii* y *Micrantholithus obtusus*. Otras formas presentes, también características aunque menos abundantes, son *Cyclagelosphaera margerelii*, *Braarudosphaera africana*, *Flabellites oblongus*, *Assipetra infracretacea* y *Helenea chiastia.* Las formas más características identificadas para la Formación Patrocinio aparecen representadas en las Figuras 3.6 y 3.7, con representación de su distribución estratigráfica a lo largo de la unidad. Como se refleja en las Figuras 3.6 y 3.7 y en la Lámina 6, la mayor parte de las muestras estudiadas contienen la asociación *Hayesites irregularis*, *Nannoconus truittii*, *Braarudosphaera africana* y *Conusphaera rothii*, que caracteriza la parte media/alta de la biozona de nanofósiles *Hayesites irregularis*, de acuerdo a la biozonación de Applegate y Bergen (1988) y Aguado (1994). Aguado *et al.* (1999) correlacionan esta asociación con la Zona *Deshayesites forbesi* de ammonites.

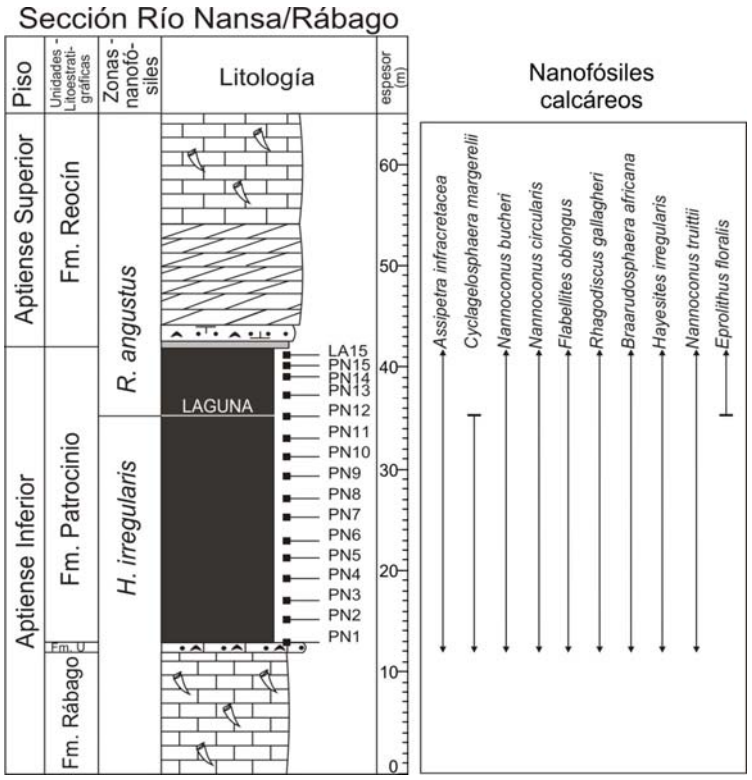

Figura 3.7.- Sección estratigráfica simplificada del Aptiense del sector occidental de La Florida (secciones de río Nansa-Rabago), mostrando la localización de las muestras estudiadas, la distribución de nanofósiles calcáreos y las biozonas de nanofósiles identificadas.

El análisis cuantitativo de la abundancia de nanofósiles (Najarro *et al.*, 2011a) ha revelado una ausencia generalizada de nanocónidos de canal estrecho (como *Nannoconus steinmannii*), lo que permite identificar este evento como la "crisis de los nanocónidos", que ha sido identificada en otras cuencas del Tetis para el mismo intervalo temporal (Erba, 1994). La "crisis de los nanocónidos" se registra en otras cuencas en la mitad superior de la Zona *H. irregularis* (Erba, 1994; Aguado *et al.*, 1999) y se ha correlacionado con condiciones paleoceanográficas de aumento de acidificación de los océanos durante un episodio anóxico oceánico global que ocurrió en el Aptiense Inferior, el denominado OAE 1a.

Estas observaciones permiten deducir que en la sección de Cuchía (Figura 3.6) las margas grises de la parte basal de la Fm. Patrocinio (muestras PLC-3 a PLC-40) pertenecen a la mitad superior de la Zona *Hayesites irregularis* de nanofósiles, la cual es equivalente a la parte media-superior de la Zona *Deshayesites forbesi* de ammonites.

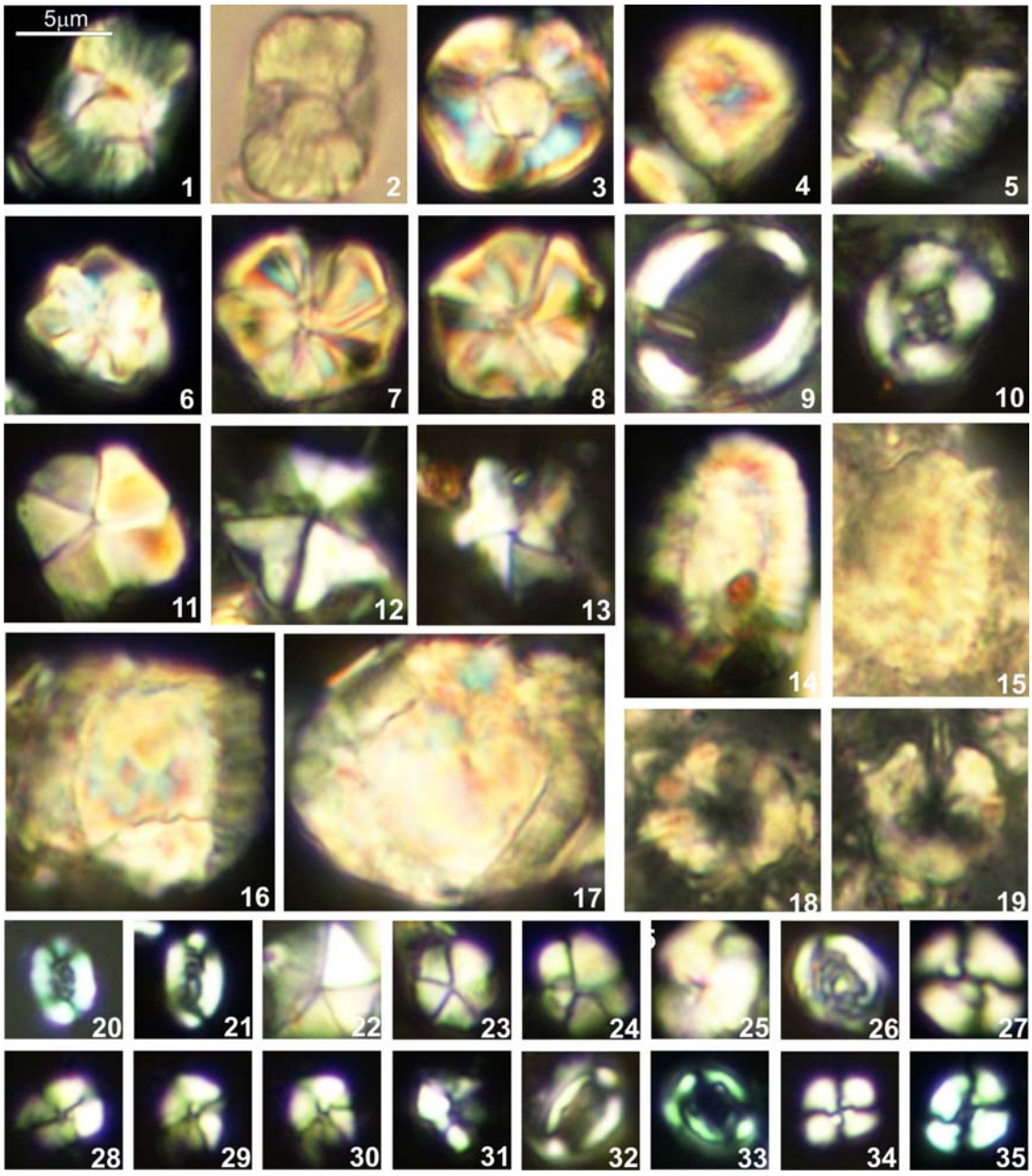

Lámina 6.- Nanofósiles calcáreos identificados para la Fm. Patrocinio. 1–5: *Nannoconus truittii* (foto 2 con nícoles paralelos). 6-8: *Assipetra infracretacea* (especimen grande). 9: *Manivitella pemmatoidea*. 10: *Helenea chiastia*. 11: *Braarudosphaera africana*.12: *Micrantholithus obtusus*. 13: *Micrantholithus stellatus*. 14: *Nannoconus kamptneri*. 15: *Nannoconus steinmannii*. 16: *Nannoconus bucheri*. 17: *Nannoconus circularis*. 18–19: *Eprolithus floralis*. 20–21: *Rhagodicus gallagheri*. 22: *Micrantholithus hoschulzii*. 23–24: *Braarudosphaera africana*. 25: *Assipetra infracretacea*. 26: *Rhagodiscus asper*. 27: *Watznaueria barnesae*. 28–31: *Hayesites irregularis*. 32–33: *Flabellites oblongus*. 34: *Cyclagelosphaera margerelii*. 35: *Watznaueria británica*. Todas las fotos c. x3000.

En la sección de río Nansa-Rábago (Figura 3.7), desde la base de la unidad hasta la muestra PN-12, la Formación Patrocinio, corresponde a la mitad superior de la Zona *H. irregularis*. En esta sección, la primera aparición de *Eprolithus floralis*, que define la Zona *Rhagodicus angustus* de nanofósiles, se registra a partir de la muestra PN-12 (Figura

3.7). Este evento bioestratigráfico permite asignar la parte alta de la Formación Patrocino a partir de la muestra PN-12, al menos en este sector occidental del área de La Florida, a la Zona *Rhagodiscus angustus* de nanofósiles. Según Aguado *et al.* (1999), la base de la Zona *R. angustus* cae dentro de la parte alta de Zona *Dufrenoyia furcata* de ammonites, cuya edad corresponde con la parte más alta del Aptiense Inferior. Esto implica que en la sección de río Nansa-Rábago existe una laguna estratigráfica que comprendería la parte alta de la Zona de *Hayesites irregularis* de nanofósiles, es decir, que afecta al menos a la parte alta del Aptiense Inferior y quizás la base del Aptiense Superior (Najarro *et al.*, 2011a). Esta laguna podría corresponder con la duración de la parte más alta de la Zona *D. forbesi*, con el total de la Zona *Deshayesites deshayesi* y con la parte baja de la Zona *D. furcata* de ammonites. Por tanto, en la sección de río Nansa, la parte más alta de la Formación Patrocinio correspondería en edad con la base de la Formación Rodezas (Figura 3.5), existiendo aquí una laguna entre los últimos 7 metros y el resto de la unidad.

El listado de taxones de nanofósiles calcareous identificados para las muestras estudiadas de la Formación Patrocinio es el siguiente:

- *Assipetra infracretacea* (Thierstein, 1973) Roth, 1973
- *Assipetra terebrodentaria* (Applegate *et al.* in Covington y Wise, 1987) Rutledge y Bergen, 1994
- *Biscutum ellipticum* (Gorka, 1957) Grün in Grün y Allemann, 1975
- *Braarudosphaera africana* Stradner, 1961
- *Conusphaera rothii* (Thierstein, 1971) Jakubowski, 1986
- *Cyclagelosphaera margerelii* Noël, 1965
- *Diazomatolithus lehmanii* Noël, 1965
- *Discorhabdus ignotus* (Gorka, 1957) Perch-Nielsen, 1968
- *Eprolithus floralis (Stradner, 1962)* Stover 1966
- *Flabellites oblongus* (Bukry, 1969) Crux, 1982
- *Hayesites irregularis* (Thierstein in Roth y Thierstein, 1972) Covington y Wise, 1987
- *Helenea chiastia* Worsley, 1971
- *Lithraphidites carniolensis* Deflandre, 1963
- *Manivitella pemmatoidea* (Deflandre ex Manivit, 1961) Thierstein, 1971
- *Micrantholithus hoschulzii* (Reinhardt, 1966) Thierstein, 1971

- *Micrantholithus obtusus* Stradner, 1963
- *Micrantholithus stellatus* Aguado, 1997
- *Nannoconus bucheri* Brönnimann, 1955
- *Nannoconus circularis* Déres y Achériteguy, 1980
- *Nannoconus kamptneri kamptneri* Brönnimann, 1955
- *Nannoconus steinmannii* Kamptner, 1931 ssp. *steinmannii*
- *Nannoconus truittii* Brönnimann, 1955
- *Prediscosphaera columnata* (Stover, 1966) Manivit, 1971
- *Rhagodiscus angustus* (Stradner, 1963) Reinhardt, 1971
- *Rhagodiscus asper* (Stradner, 1963) Reinhardt, 1967
- *Rhagodiscus gallagheri* Rutledge y Bown, 1996
- *Watznaueria barnesae* (Black in Black y Barnes, 1959) Perch-Nielsen, 1968
- *Watznaueria britannica* (Stradner, 1963) Reinhardt, 1964
- *Zeugrhabdotus noeliae* Rood, Hay y Barnard, 1971

3.2.2.4. FORAMINÍFEROS BENTÓNICOS

El estudio de microfacies en lámina delgada ha permitido identificar varias asociaciones de foraminíferos bentónicos encontrados en las secciones estudiadas (Figuras 3.8 a 3.22). Cuando ha sido posible, la identificación se ha realizado a nivel específico; en otros casos solo se ha podido llegar a determinaciones a nivel genérico debido a la falta de secciones idóneas en las láminas delgadas estudiadas y/o a la existencia de varias especies cuya separación hubiera requerido estudios mas especializados, fuera del objetivo de esta tesis. La precisión bioestratigráfica que ofrecen las asociaciones de foraminíferos bentónicos es en general inferior a la obtenida con los planctónicos, no obstante, se han podido caracterizar con foraminíferos bentónicos varias de las unidades litoestratigráficas del Aptiense-Albiense definidas en las diferentes áreas.

El género *Mesorbitolina* SCHROERER fue originalmente definido como un subgénero, siendo elevado a género por Loeblich y Tappan (1987) y por lo que en este estudio es considerado como género.

En el área de **La Florida** se han identificado, a partir de estudios de láminas delgadas procedentes de las secciones de río Nansa, Rábago, El Soplao y Bustriguado (ver localización de las secciones entre sí en la Figura 3.3 y detalles de las secciones estratigráficas con posición de las muestras de lámina delgada en las figuras 3.8, 3.9, 3.10 y 3.13), las siguientes asociaciones de foraminíferos bentónicos por unidades:

- **Formación Rábago**: Para esta unidad se ha identificado la asociación formada por *Palorbitolina lenticularis* (BLUMENBACH) y *Choffatella decipiens* SCHLUMBERGER (Lámina 7A y 7B respectivamente), junto con *Sabaudia* sp. Esta asociación permite asignar a la unidad una edad Bedouliense, correspondiente a la biozona del Aptiense Inferior *P. lenticularis* (Figura 3.5).

- **Formación Reocín**: Debido a los procesos de dolomitización que afectan a esta unidad y que han destruido parcialmente las texturas originales de las calizas precursoras, solo se han podido estudiar las asociaciones de foraminíferos presentes en muestras de las partes basal y alta de la Fm Reocín, ya que la parte media de la unidad se encuentra dolomitizada en prácticamente toda la zona. En la sección de río Nansa (Figura 3.8), la parte basal de la unidad también aparece dolomitizada. En la sección de Rábago (Figura 3.9), donde la unidad aparece sin dolomitizar, la parte basal de la Fm. Reocín presenta *Pseudochoffattela cuvillieri* DELOFFRE (Lámina 8A), lo que permite atribuir una edad Gargasiense superior-Clansayesiense (Moullade & Peybernès, 1975) para este tramo en esta sección. Esta edad es consistente con las dataciones aportadas por las asociaciones de nanofósiles calcáreos en el extremo O del área de estudio. Por el contrario, en la sección de El Soplao (Figura 3.10), localizada aproximadamente 2 km al E de la sección de Rábago (Figura 3.3), la base de las calizas (sin dolomitizar) que forman aquí la base de la formación Reocín, presenta *Iraquia simplex* HENSON (Lámina 8 E), lo que indica una edad de Aptiense Inferior parte alta a base del Aptiense Superior (Zona de *Iraquia simplex*, Figura 3.5) para la base de la unidad en esta sección. Esta biozona corresponde con el techo del Bedouliense-base del Gargasiense, equivalente a la zona de ammonites *D. furcata* y base de *Epicheloniceras martini* (Figura 3.5).

Por tanto, estos datos indican una diacronía en la edad de la base de la Fm. Reocín entre las secciones localizadas al O y al E del área de La Florida, sugiriendo que la base de la unidad es más antigua en el sector oriental y más moderna en el sector occidental

del entorno de El Soplao. Esto podría indicar, apoyado también en los datos de nanofósiles calcáreos, que la laguna estratigráfica existente aquí dentro de la Fm. Patrocinio abarca un lapso de tiempo mucho mayor en el sector occidental (secciones de río Nansa a Rábago) que en el sector oriental del área de estudio (secciones de El Soplao a Bustriguado). Otra implicación de estos datos es que la base de la Fm. Reocín, solo en el sector oriental del área de La Florida, podría ser equivalente lateral en parte de la Fm. San Esteban del Bedouliense superior (García-Mondéjar, 1982), definida para el sector del sinclinal de Santillana. Esta unidad desaparece en el sector occidental del área de estudio bien por acuñamiento, bien por erosión, o por ambas cosas.

En todas las secciones estudiadas de este área, la parte media de la Fm. Reocín, justo por encima de la dolomitización, presenta abundantes ejemplares de *Sabaudia sp*., *Sabaudia capitata* ARNAUD-VANNEAU y *Sabaudia minuta* (HOFKER) (niveles de *Sabaudia*, Lámina 7C), junto con *Pseudochoffattela cuvillieri* DELOFFRE (Lámina 8B), *Nautiloculina* sp. y *Cuneolina* sp. Hacia la parte alta de la Fm. Reocín, todas las secciones de esta área muestran la asociación formada por *Coskinolinella daguini* DELMAS y DELOFFRE (Lámina 7D y 7E), *Pseudochoffattela cuvillieri* DELOFFRE (Lámina 8B), *Mesorbitolina texana* (ROEMER), *Sabaudia minuta* (HOFKER), *Sabaudia sp*., *Simplorbitolina manasi* CIRY y RAT (Lámina 8 C-D), *Orbitolinopsis* sp., *Charentia cuvillieri* NEUMANN (Lámina 8F) y *Cuneolina* sp. Esta asociación indica una edad correspondiente al intervalo Aptiense alto (Gargasiense no basal)-Albiense basal.

- **Formación Barcenaciones**: Se ha encontrado una asociación de foraminíferos caracterizada por la presencia de *Hensonina lenticularis* HENSON (Lámina 7F) y *Cuneolina pavonia* D'ORBIGNY, que caracteriza el Albiense.

En el área del **sinclinal de Santillana** se han identificado también, a partir de estudios de láminas delgadas procedentes de las secciones de Novales, Ruilobuca, Santa Eulalia, Hayuela-Canales y cantera de Las Lastrías (ver localización de las secciones en la Figura 1.1 y detalles de las secciones estratigráficas con posición de las muestras de lámina delgada en las Figuras 3.14, 3.15, 3.16, 3.17 y 3.18) las siguientes asociaciones de foraminíferos bentónicos para las siguientes unidades:

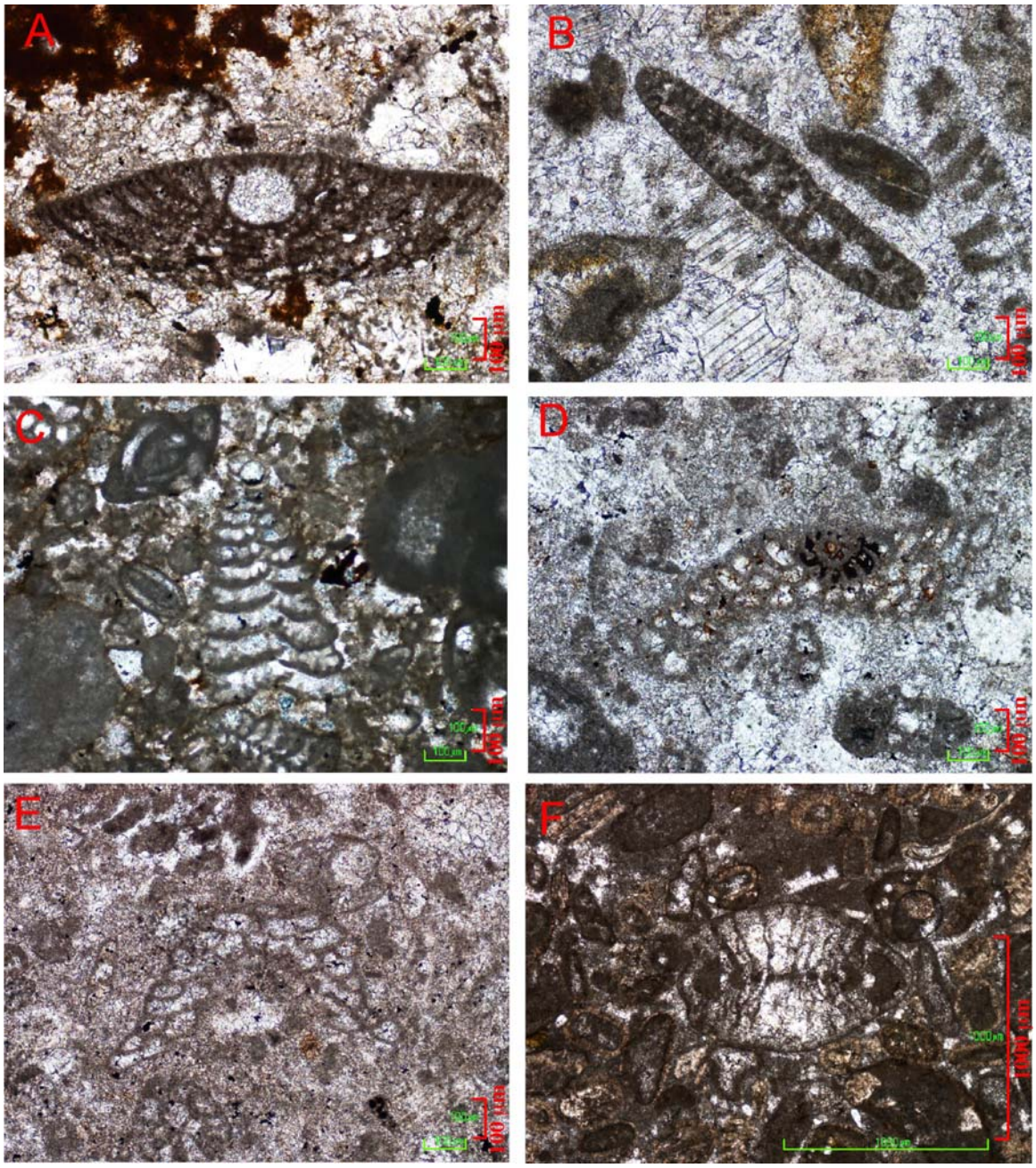

Lámina 7.- Foraminíferos bentónicos con valor bioestratigráfico, del Aptiense y Albiense del área de **La Florida**, secciones de río Nansa, Rábago y El Soplao. **A**) *Palorbitolina lenticularis* (BLUMENBACH), muestra SOP-1 (sección de El Soplao), Formación Rábago, Aptiense Inferior. **B**) *Choffatella decipiens* SCHLUMBERGER, muestra PN-2 (sección de río Nansa). Formación Rábago, Aptiense Inferior. **C**) *Sabaudia capitata* ARNAUD-VANNEAU (arriba) y *Sabaudia minuta* (HOFKER) (abajo). Parte media de la Formación Reocín, muestra PN-13 (sección de río Nansa). **D**) *Coskinolinella daguini* DELMAS y DELOFFRE. Parte alta de la Formación Reocín. Aptiense Superior-Albiense basal. **E**) *Coskinolinella daguini* DELMAS y DELOFFRE. Parte alta de la Formación Reocín, muestra LA-25 (sección de Rábago), Aptiense Superior-Albiense basal. **F**) *Hensonina lenticularis* HENSON, muestra PN-BAR-1 (sección de río Nansa). Formación Barcenaciones. Albiense Superior.

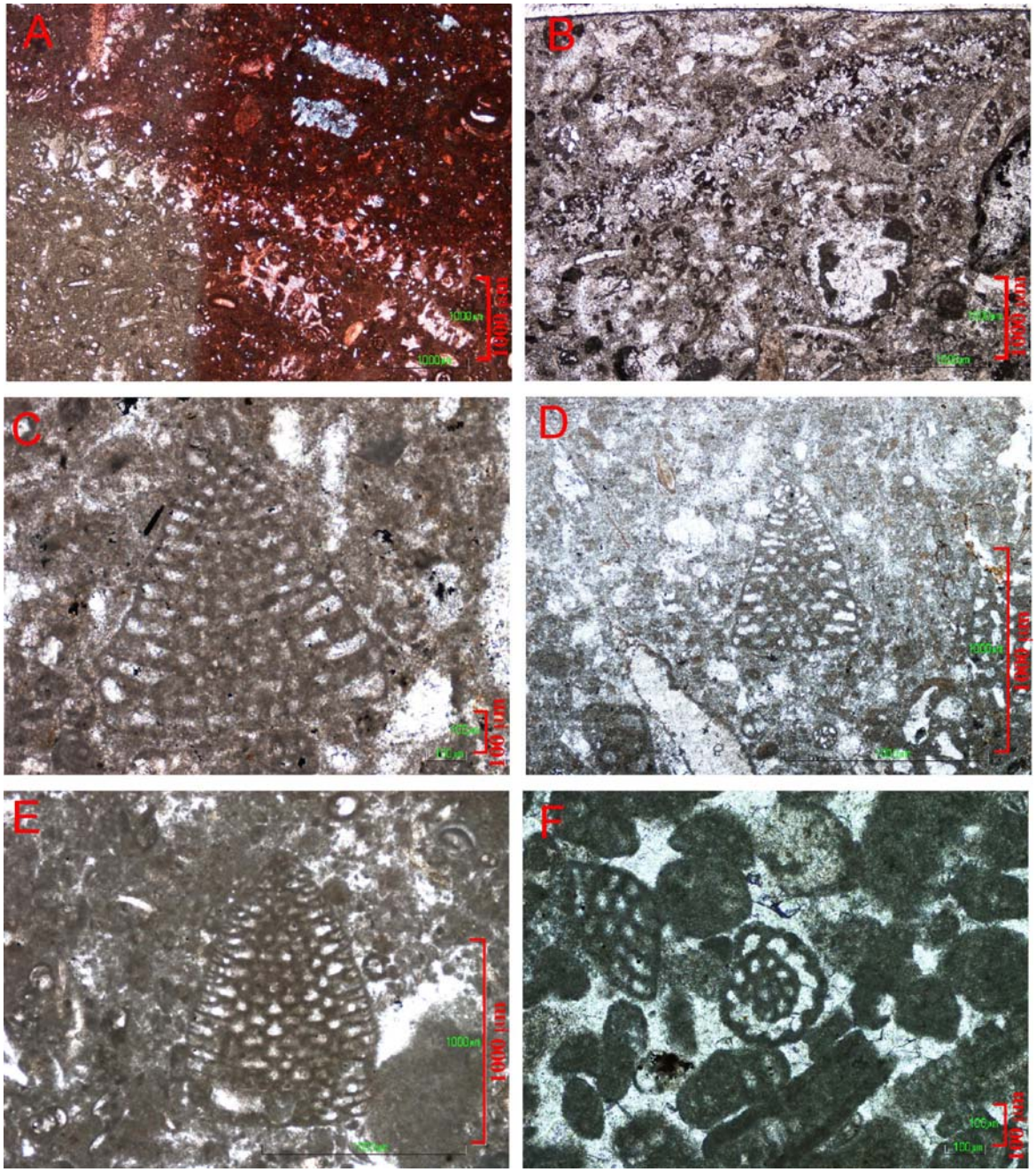

Lámina 8.- Foraminíferos bentónicos con valor bioestratigráfico del Aptiense y Albiense del área de **La Florida**, secciones de Rábago y El Soplao. **A**) *Pseudochoffattela cuvillieri* DELOFFRE, muestra LA-11 (sección de Rábago-Las Antenas), Formación Reocín, Aptiense Superior. **B**) *Pseudochoffattela cuvillieri* DELOFFRE, muestra LA-25 (sección de Rábago-Las Antenas), Formación Reocín, Aptiense Superior. **C**) *Simplorbitolina manasi* CIRY y RAT, Aptiense terminal-Albiense basal, Formación Reocín, muestra CS-1 (sección de Rábago-carretera de El Soplao). **D**) *Simplorbitolina manasi* CIRY y RAT, Aptiense terminal-Albiense basal, Formación Reocín, muestra LI-27 (sección de El Soplao). **E**) *Iraquia simplex* HENSON. Parte basal de la Formación Reocín en el sector oriental de La Florida, muestra SOP-3 (sección de El Soplao). Parte alta del Aptiense Inferior. **F**) *Charentia cuvillieri* NEUMANN. Parte alta de la Formación Reocín, muestra CON-2 (sección de Bustriguado). Parte alta del Aptiense Superior-Albiense Inferior.

- **Formación Rábago** y **Formación Umbrera**: Las muestras analizadas de estas dos unidades para este sector presentan abundantes secciones de *Palorbitolina lenticularis* (BLUMENBACH), correspondiente a la Zona *P. lenticularis* del Aptiense Inferior (Figura 3.5).

- **Formación San Esteban:** El estudio de láminas delgadas de esta unidad procedentes de la sección de Ruilobuca (Figura 3.15) presentan una asociación compuesta por *Iraquia simplex* HENSON, *Orbitolinopsis* sp., *Sabaudia* sp. y *Choffatella decipiens* SCHLUMBERGER (Lámina 9 A-C), lo que indica un intervalo de edad de Bedouliense superior a base del Gargasiense (Zona de *Iraquia simplex*), siendo la edad más probable Bedouliense superior.

- **Formación Rodezas:** La asociación de foraminiferos bentónicos para esta unidad se ha estudiado a partir de láminas delgadas procedentes de la sección de Ruilobuca (Figura 3.15). En ellas se ha reconocido *Mesorbitolina parva* DOUGLASS, junto con *Mesorbitolina texana* (ROEMER) en la parte superior (Lámina 9 D-E). Esta asociación indica un intervalo de edad desde Aptiense Superior (Gargasiense) hasta el Albiense Medio, siendo la edad más probable Gargasiense.

- **Formación Reocín**: A partir del estudio de láminas delgadas de esta unidad, procedentes de las secciones de Santa Eulalia, Novales y cantera de Las Lastrías (Figuras 3.16, 3.17 y 3.18), se ha reconocido una asociación de foraminíferos bentónicos que presenta, en la parte baja de la unidad, *Mesorbitolina parva* DOUGLASS y *Mesorbitolina texana* (ROEMER) (Lámina 9F, Lámina 10A). Hacia la parte media de la unidad, junto con ésta última presenta además abundantes ejemplares de *Sabaudia minuta* (HOFKER) (Lámina 10B), y hacia la parte alta de la unidad presenta *Sabaudia minuta* (HOFKER), *Coskinolinella daguini* DELMAS y DELOFFRE (Lámina 10C), *Cuneolina* sp., *Simplorbitolina manasi* CIRY y RAT y *Mesorbitolina birmanica* (SAHNI) (Lámina 10D). Esta última especie se reconoce aquí por primera vez en la cuenca y aparece ampliamente descrita en Schlagintweit y Wilmsen (2014). *M. birmanica* aparece descrita por Ramírez del Pozo (1971) como *Orbitolina* (*Mesorbitolina*) *texana melendezi* nov. subsp., exclusia del Gargasian superior. Esta asociación sugiere para esta unidad una edad, en este sector, de Aptiense Superior no basal, no descartándose el Albiense basal hacia la parte alta de la unidad.

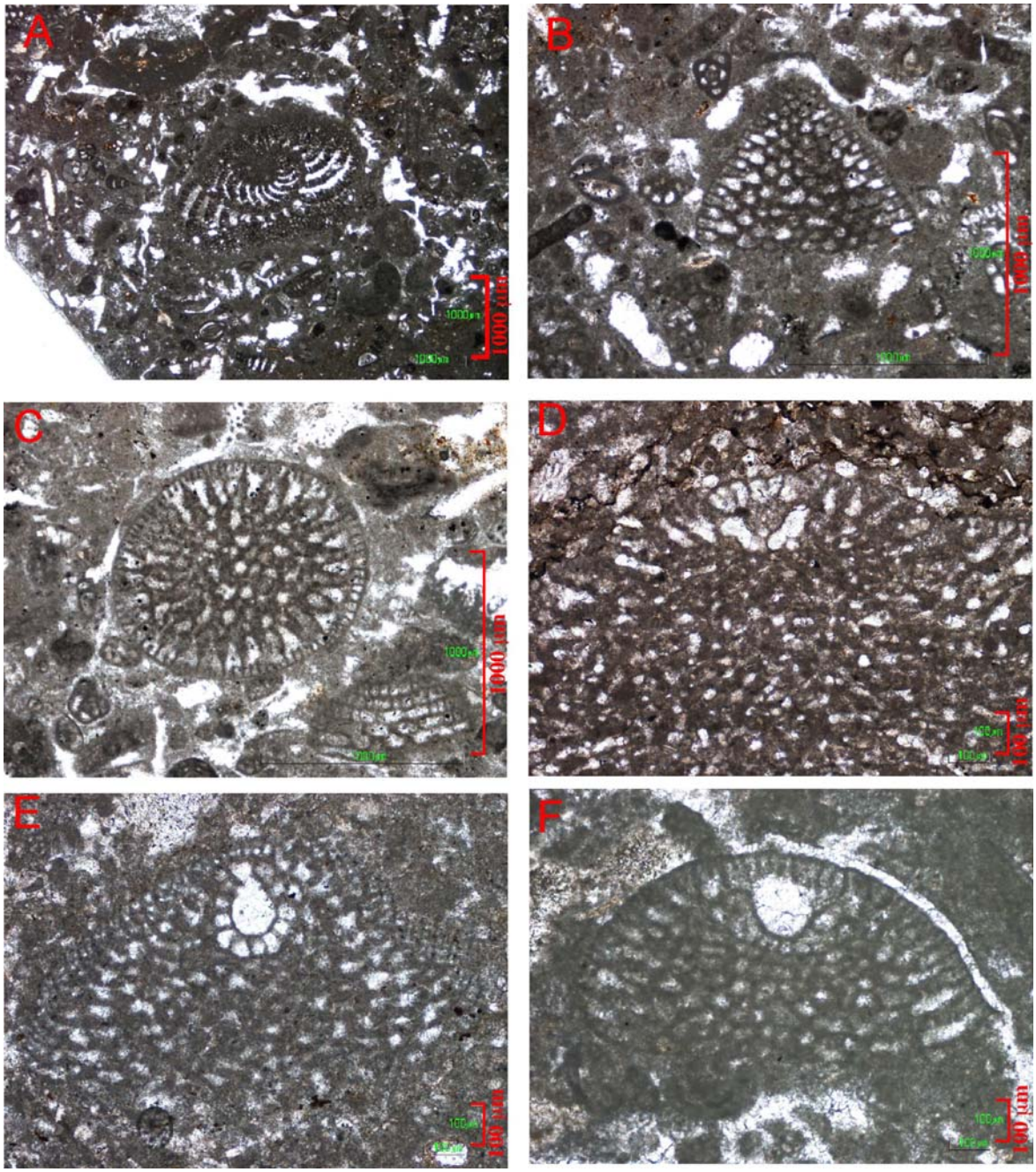

Lámina 9.- Foraminíferos bentónicos con valor bioestratigráfico del Aptiense del área del **sinclinal de Santillana**, secciones de Ruilobuca y Santa Eulalia. **A**) *Choffatella decipiens* SCHLUMBERGER, muestra RU-6, sección Ruilobuca, Formación San Esteban, Aptiense Inferior. **B**) *Iraquia simplex* HENSON, muestra RU-6, sección Ruilobuca, Formación San Esteban, Aptiense Inferior. **C**) *Iraquia simplex* HENSON, sección horizontal, muestra RU-6, sección Ruilobuca, Formación San Esteban, Aptiense Inferior **D**) *Mesorbitolina texana* (ROEMER), muestra RU-69, sección Ruilobuca, Formación Rodezas, Aptiense Superior. **E**) *Mesorbitolina texana* (ROEMER), muestra RU-61', sección Ruilobuca, Formación Rodezas, Aptiense Superior. **F**) *Mesorbitolina texana* (ROEMER), muestra SE2-7, sección Santa Eulalia, Formación Reocín, Aptiense Superior.

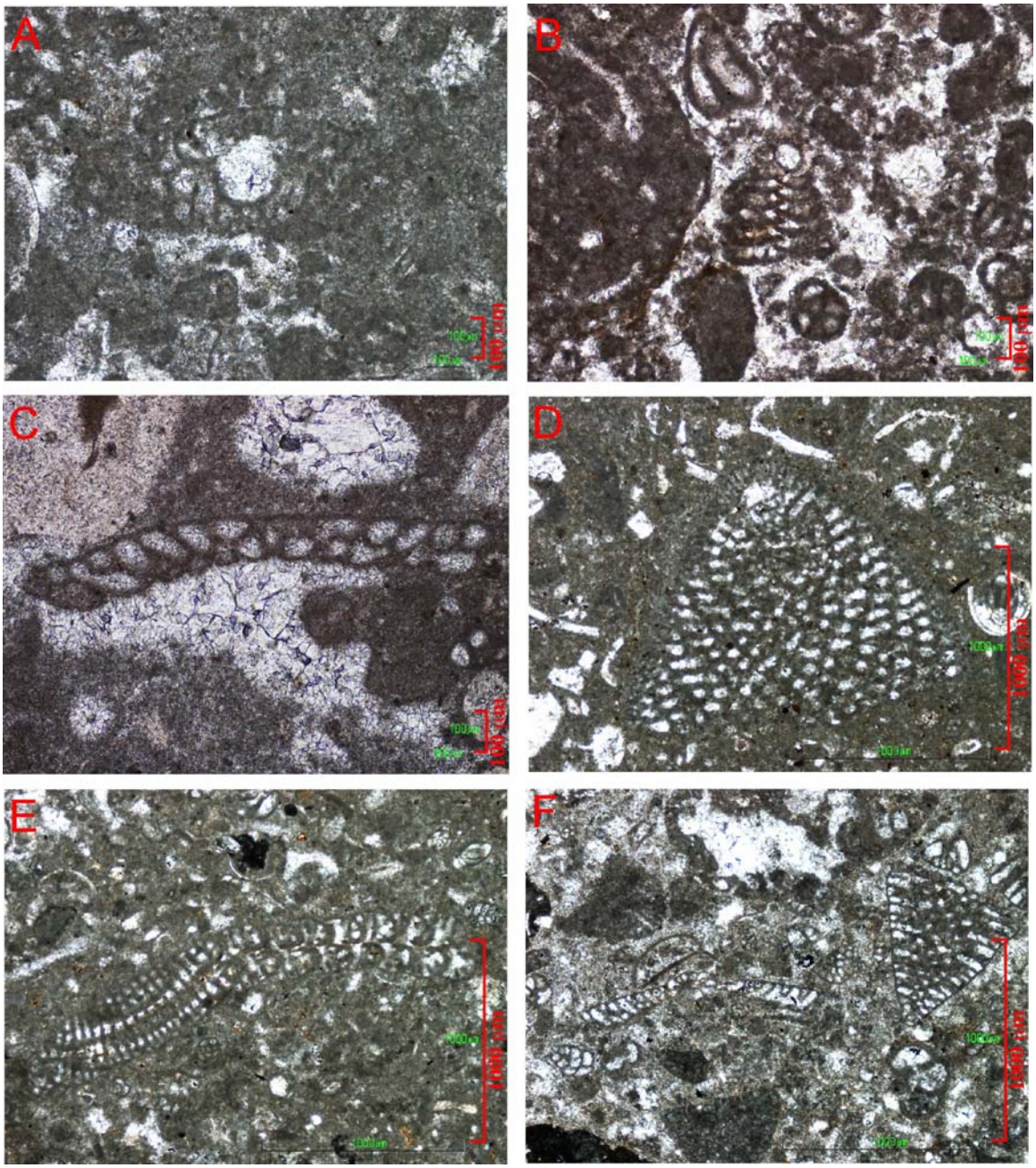

Lámina 10.- Foraminíferos bentónicos con valor bioestratigráfico del Aptiense y Albiense del **sinclinal de Santillana**, secciones de Santa Eulalia, Novales y cantera de Las Lastrías. **A**) *Mesorbitolina texana* (ROEMER), muestra SE-7', sección Santa Eulalia 2, Formación Reocín, Aptiense Superior. **B**) *Sabaudia minuta* (HOFKER), muestra NO-5, sección de Novales, parte media de la Formación Reocín. **C**) *Coskinolinella daguini* DELMAS y DELOFFRE, muestra NO-29, sección de Novales, parte alta de la Formación Reocín. **D**) *Mesorbitolina birmanica* (SAHNI), muestra NO-23, sección de Novales, parte alta de la Formación Reocín. **E**) *Cuneolina pavonia* D'ORBIGNY, muestra NO-33, sección de Novales, Formación Las Peñosas. **F**) *Coskinolinella daguini* DELMAS y DELOFFRE junto con *Simplorbitolina manasi* CIRY y RAT, muestra NO-34, sección de Novales, Formación Las Peñosas, Albiense Inferior.

- **Formación Las Peñosas**: El estudio en la sección de Novales, de láminas delgadas procedentes de los niveles carbonatados intercalados entre las facies siliciclásticas de la parte baja de esta unidad (Figura 3.18), ha permitido reconocer *Cuneolina pavonia* D'ORBIGNY (Lámina 10E), junto con *Cuneolina* sp., *Sabaudia minuta* (HOFKER), *Sabaudia* sp., *Coskinolinella daguini* DELMAS y DELOFFRE y *Simplorbitolina manasi* CIRY y RAT (Lámina 10F). Esta asociación sugiere una edad Albiense Inferior, al menos para la parte baja de la unidad.

- **Formación Barcenaciones**: El estudio de láminas delgadas procedentes de la sección de Novales (Figura 3.18), ha permitido reconocer para esta unidad una asociación de foraminíferos bentónicos que contiene abundantes ejemplares de *Hensonina lenticularis* HENSON, junto con *Cuneolina pavonia* D'ORBIGNY.

En el área de **Cuchía**, a partir de estudios de láminas delgadas procedentes de las secciones de Cuchía (playa de Los Caballos-playa del Huevo), cantera de Cuchía, y Suances (ver localización de las secciones en la Figura 1.1 y detalles de las secciones estratigráficas con posición de las muestras de lámina delgada en las Figuras 3.20, 3.21 y 3.22), se han reconocido las siguientes asociaciones de foraminíferos bentónicos por unidades:

- **Formación San Esteban**: El estudio de láminas delgadas de esta unidad aflorante en la sección de Punta del Cuerno (acantilado de Cuchía) ha permitido reconocer abundantes secciones de *Iraquia simplex* HENSON, junto con secciones de *Palorbitolina lenticularis* (BLUMENBACH), lo que indica una edad de Bedouliense superior.

- **Formación Reocín**: Los foraminíferos bentónicos de esta unidad se han estudiado a partir de láminas delgadas procedentes de la sección de la cantera de Cuchía, donde la unidad presenta un espesor mayor, ya que en los acantilados de Cuchía (playa del Huevo) y de Suances (Punta del Dichoso) la unidad se encuentra muy reducida de potencia (ca. 9-11 metros para toda la unidad). En la cantera de Cuchía no aflora la base de la unidad. En esta sección se ha reconocido, para la parte media y alta de la unidad, *Recteodictyoconus giganteus* SCHROEDER, *Dictyoconus? pachymarginalis* SCHROEDER, *Sabaudia minuta* (HOFKER), *Sabaudia* sp. (Lámina 11C),

Mesorbitolina texana (ROEMER) y *Mesorbitolina birmanica* (SAHNI) (Schlagintweit per. com.), junto con secciones de *Polyconites verneuili* (BAYLE) (Lámina 11A), lo que sugiere una edad de Aptiense Superior.

- **Formación Barcenaciones**: En el área de Cuchía, en las calcarenitas de la base de esta unidad aflorantes en la sección de Cuchía (playa del Huevo) (Foto 3.46C) se ha reconocido *Hensonina lenticularis* HENSON (Lámina 11F), *Cuneolina pavonia* D'ORBIGNY, junto con abundantes secciones de *Caprina choffati* DOUVILLÉ, lo que permiten atribuir este afloramiento al Albiense Superior. Igualmente, en la sección de la cantera de Cuchía, en su parte alta, se ha reconocido también *Cuneolina pavonia* D'ORBIGNY (Lámina 11 D-E) y *Caprina choffati* DOUVILLÉ (Lámina 11B), lo que permite atribuir la parte alta de las calizas en esta sección al Albiense Superior, y por tanto a la Formación Barcenaciones. En la sección de Suances (Punta del Dichoso) se ha reconocido también para esta unidad *Hensonina lenticularis* HENSON (Lámina 12F), *Cuneolina pavonia* D'ORBIGNY (Lámina 12E) y *Cuneolina* sp., junto con abundantes secciones de *Caprina choffati* DOUVILLÉ (Lámina 12 A-C), lo que le confiere también una edad de Albiense Superior.

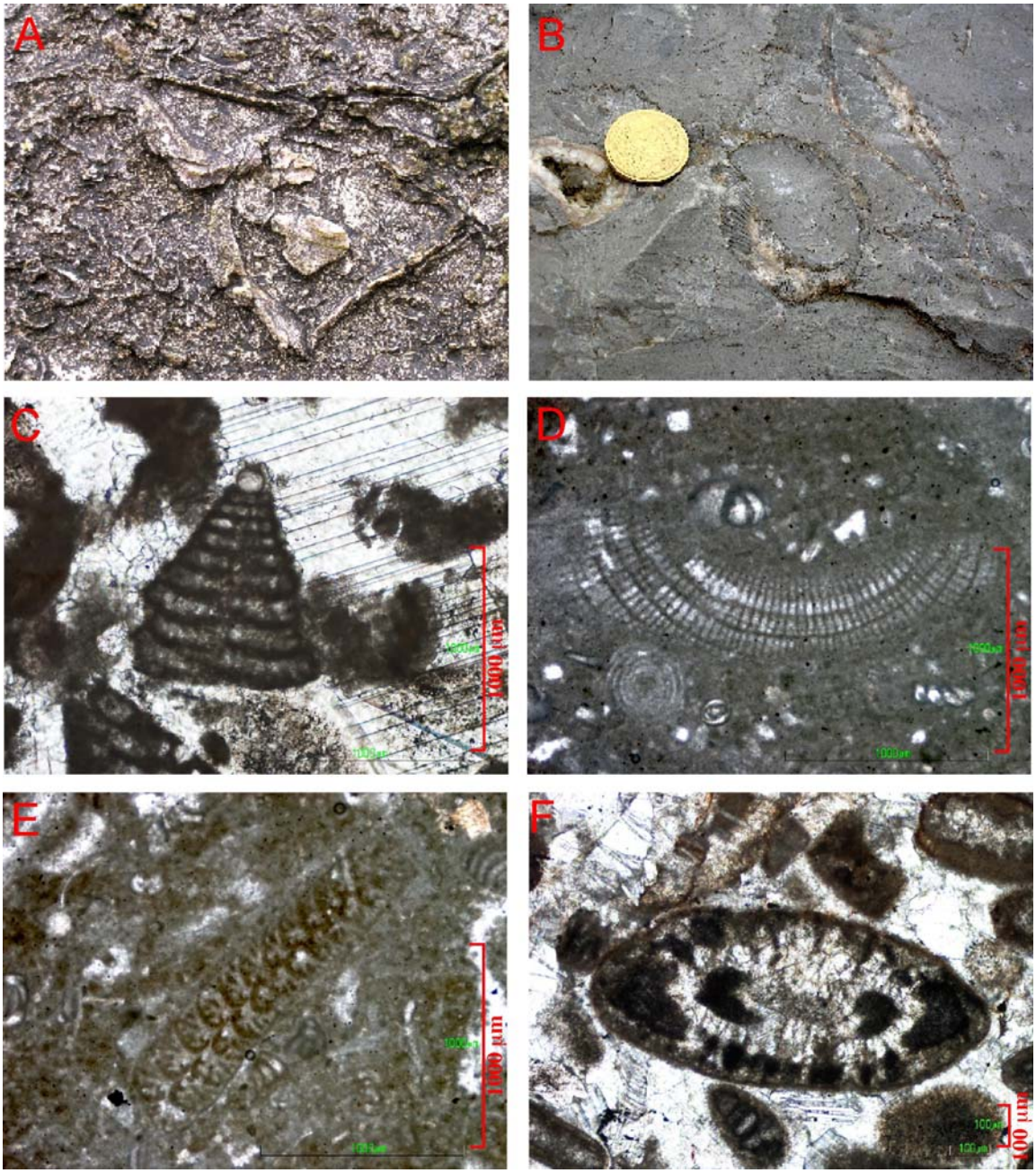

Lámina 11.- Fósiles con valor bioestratigráfico del Aptiense y Albiense del área de **Cuchía**. **A**) *Polyconites verneuili* (BAYLE), sección de Suances (Punta del Dichoso), Formación Reocín, Aptiense Superior. **B**) *Caprina choffati* DOUVILLÉ, sección de la cantera de Cuchía (parte alta), Formación Barcenaciones, Albiense Superior. **C**) *Sabaudia* sp., muestra CCU-3, sección de la cantera de Cuchía, Formación Reocín. **D**) *Cuneolina pavonia* D'ORBIGNY, muestra CCU-106, sección de la cantera de Cuchía, Formación Barcenaciones. **E**) *Cuneolina pavonia* D'ORBIGNY, muestra CCU-111, sección de la cantera de Cuchía, Formación Barcenaciones. **F**) *Hensonina lenticularis* HENSON, muestra CU-26 sección de Cuchía (playa del Huevo-playa de Cuchía), Formación Barcenaciones, Albiense Superior.

Lámina 12.- Fósiles con valor bioestratigráfico de la Formación Barcenaciones (Albiense Superior): **A**), **B**) y **C**) Diferentes secciones de *Caprina choffati* DOUVILLÉ de la sección de Suances (Punta del Dichoso), que indican el Albiense Superior (Scott, 2010). **D**) Ejemplar de *Engonohoplitoides* sp., recolectado en la ensenada de Fonfría (Comillas). Marca la Zona *Stoloczkaia dispar*, parte alta de la subzona *Stoliczkaia blancheti* (Moreno-Bedmar, com. per.). **E**) *Cuneolina pavonia* D'ORBIGNY, muestra SU-33, sección de Suances (Punta del Dichoso). **F**) *Hensonina lenticularis* HENSON, muestra SU-30, sección de Suances (Punta del Dichoso).

3.2.2.5. PALINOMORFOS

Durante el desarrollo de este trabajo se han recolectado y procesado para el estudio del contenido palinológico, un total de 21 muestras procedentes de las unidades estratigráficas Formación Patrocinio, Formación Rodezas, Formación Reocín y Formación Las Peñosas, según los métodos descritos en el anterior apartado metodológico de esta memoria (Capítulo 1.2). De las 21 muestras recogidas, no todas presentaron asociaciones bien preservadas e incluso cinco fueron estériles. En este trabajo solo se indicarán los resultados de las muestras más fértiles que, además, fueron las que presentaron los ejemplares mejor preservados.

Para la determinación de los palinomorfos y la datación estratigráfica se han utilizado los textos de Groot y Groot (1962), Burger (1966), Norris (1969), Kemp (1970), Dörhöfer (1977), Arias y Doubinger (1980), Hochuli (1981), Leereveld *et al.* (1989), Trincão (1990), Hughes *et al.* (1991), Hughes y McDougall (1990), Batten (1999), Vajda (2001), Dejax *et al.* (2007).

De las 16 muestras con contenido palinológico, dos pertenecen a la Formación Patrocinio del Aptiense Inferior (secciones de Hayuela-Canales y El Soplao, muestras Canales-Patrocinio y Sop-Patrocinio respectivamente, Tabla 1), una a la Formación Rodezas del Aptiense Superior (sección de Ruilobuca, muestra Ru-Cuchía, Tabla 1), una a la Formación Reocín del Aptiense Superior (sección de Ruilobuca, muestra Ru-Reocín, Tabla 1) y el resto a la unidad ambarígena o Formación Las Peñosas del Albiense Inferior (secciones de Cóbreces y El Soplao, muestras Peñosas-Cóbreces y Sop-Peñosas, Tabla 2; y muestras P-1 a P-11, Tabla 3). Todas las muestras estudiadas están dominadas por miosporas, encontrándose los palinomorfos acuáticos escasamente representados.

Muestras	Canales-Patrocinio	(%)	Sop-Patrocinio	(%)	Ru-Cuchía	(%)	Ru-Reocín	(%)
Esporas de pteridofitas								
Appendicisporites spp.	0	0.0	0	0.0	2	0.4	0	0.0
Cicatricosisporites venustus Deák 1963	0	0.0	0	0.0	0	0.0	1	0.3
Cicatricosisporites spp.	20	2.6	2	0.5	11	2.3	6	1.6
Cingutriletes sp.	2	0.3	0	0.0	0	0.0	0	0.0
Concavissimisporites verrucosus (Delcourt & Sprumont) Delcourt, Dettmann & Hughes	0	0.0	0	0.0	1	0.2	0	0.0
Converrucosisporites sp.	1	0.1	1	0.2	0	0.0	0	0.0
Costatoperforosporites spp.	0	0.0	0	0.0	0	0.0	1	0.3
Deltoidospora australis (Couper 1953) Srivastava 1975	0	0.0	1	0.2	4	0.8	5	1.3
Deltoidospora minor (Couper 1953) Pocock 1970	13	1.7	3	0.7	3	0.6	3	0.8
Deltoidospora sp.	1	0.1	0	0.0	22	4.6	4	1.0
Distaltriangulisporites sp.	0	0.0	0	0.0	4	0.8	0	0.0
Gleicheniidites senonicus Ross 1949	0	0.0	0	0.0	1	0.2	1	0.3
Ischyosporites sp.	0	0.0	0	0.0	3	0.6	1	0.3
Laevigatosporites sp.	1	0.1	0	0.0	0	0.0	0	0.0
Leptolepidites macroverrucosus Schulz 1967	1	0.1	0	0.0	0	0.0	1	0.3
Leptolepidites sp.	8	1.0	0	0.0	0	0.0	0	0.0
Maculatisporites sp.	0	0.0	0	0.0	1	0.2	0	0.0
Neoraistrickia truncata (Cookson 1953) Potonié 1956	1	0.1	0	0.0	0	0.0	0	0.0
Neoraistrickia sp.	0	0.0	0	0.0	1	0.2	0	0.0
Patellasporites tavaredensis Groot & Groot 1962	2	0.3	0	0.0	0	0.0	2	0.5
Punctatisporites sp.	0	0.0	0	0.0	1	0.2	0	0.0
Rubinella major (Couper 1958) Norris 1968	3	0.4	0	0.0	0	0.0	0	0.0
Todisporites major Couper 1958	0	0.0	0	0.0	1	0.2	0	0.0
Undulatisporites sp.	1	0.1	0	0.0	0	0.0	0	0.0
Granos de polen (gimnospermas)						0.0		
Alisporites bilateralis Rouse 1959	2	0.3	2	0.5	24	5.0	11	2.8
Alisporites grandis (Cookson 1947) Dettmann 1963	0	0.0	0	0.0	2	0.4	0	0.0
Alisporites spp.	8	1.0	5	1.2	103	21.6	58	15.0
Araucariacites australis Cookson 1947	3	0.4	1	0.2	6	1.3	5	1.3
Callialasporites dampieri Dev 1961	1	0.1	0	0.0	1	0.2	1	0.3
Cedripites sp.	0	0.0	0	0.0	0	0.0	1	0.3
Classopollis classoides Pflug 1953 emend. Pocock and Jansonius 1961	118	15.3	46	10.7	23	4.8	9	2.3
Classopollis spp.	163	21.1	319	74.2	113	23.7	38	9.8
Ephedripites zaklinskainae Azéma et Boltenhagen 1974	2	0.3	0	0.0	0	0.0	0	0.0
Ephedripites multicostatus Brenner 1963	3	0.4	0	0.0	0	0.0	0	0.0
Ephedripites spp.	61	7.9	2	0.5	0	0.0	0	0.0
Eucommiidites troedsonii Erdtman 1948	2	0.3	0	0.0	0	0.0	1	0.3
Eucommiidites minor Groot & Penny 1960	1	0.1	0	0.0	0	0.0	2	0.5
Exesipollenites tumulus Balme 1957	261	33.9	19	4.4	0	0.0	4	1.0
Ginkgocycadophytus nitididus (Balme 1957) de Jersey 1962	5	0.6	0	0.0	0	0.0	3	0.8
Inaperturopollenites dubius (Potonié et Venitz 1932) Thompson et Pflug 1953	0	0.0	14	3.3	5	1.1	25	6.5
Inaperturopollenites spp.	12	1.6	7	1.6	11	2.3	7	1.8
Monosulcites chaloneri Brenner 1963	1	0.1	0	0.0	0	0.0	0	0.0
Monosulcites minimus Cookson 1947 ex. Couper 1953	21	2.7	0	0.0	0	0.0	0	0.0
Monosulcites spp.	6	0.8	2	0.5	1	0.2	1	0.3
Perinopollenites elatoides Couper 1958	8	1.0	1	0.2	1	0.2	0	0.0
Pinuspollenites sp.	0	0.0	1	0.2	3	0.6	3	0.8
Podocarpidites sp.	0	0.0	0	0.0	3	0.6	1	0.3
Spheripollenites sp.	8	1.0	0	0.0	0	0.0	0	0.0
Vitreisporites pallidus (Reissinger 1950) Nilsson 1958	0	0.0	0	0.0	2	0.4	0	0.0
Granos de polen bisacados de coníferas ideterminados	2	0.3	4	0.9	121	25.4	188	48.7
Granos de polen (angiospermas)								
Afropollis sp.	4	0.5	0	0.0	1	0.2	0	0.0
Clavatipollenites hughesii Couper 1958	4	0.5	0	0.0	0	0.0	1	0.3
Clavatipollenites minutus Brenner, 1963	3	0.4	0	0.0	0	0.0	0	0.0
Clavatipollenites sp. (Trichotomosulcate)	1	0.1	0	0.0	0	0.0	0	0.0
Clavatipollenites spp.	4	0.5	0	0.0	0	0.0	0	0.0
Retimonocolpites sp.	1	0.1	0	0.0	0	0.0	0	0.0
Tricolpites sp.	1	0.1	0	0.0	0	0.0	0	0.0
Granos de polen de angiospermas indeterminados	11	1.4	0	0.0	1	0.2	2	0.5
TOTAL	771	100.0	430	100.0	476	100.0	386	100.0

Tabla 1.- Diagrama de palinomorfos identificados para el Aptiense del área de estudio, con indicación de porcentajes de los representantes presentes.

- **Formación Patrocinio**: Las muestras que proceden de la Formación Patrocinio están caracterizadas por la abundancia de *Classopollis* (Lámina 13e) y *Exesipollenites tumulus*. El género *Classopollis* era producido por coníferas hoy extinguidas de la familia Cheirolepidiaceae (Taylor y Alvin, 1984; Watson, 1988), mientras que *E. tumulus* está relacionado tanto con coníferas taxodioides como con plantas del orden Bennettitales (Balme, 1995). Le siguen en abundancia los granos de polen del género *Ephedripites* (Lámina 13f). Este género está relacionado con el orden Ephedrales (Azéma y Boltenhagen, 1974). También se observan en bajas proporciones esporas de *Cicatricosisporites* spp. y de *Deltoidospora australis* (Lámina 13b). Los granos de polen de angiospermas primitivas están presentes en estas muestras aunque son escasos. Particularmente, se ha identificado un ejemplar atribuible al género *Tricolpites* en una de las muestras (Lámina 13c). La importancia de este descubrimiento es doble: por una parte, se trata del registro más antiguo hasta el momento de este tipo polínico en la península Ibérica (Najarro *et al.*, 2011b); por otra, relaciona esta asociación del Aptiense Inferior con otras de Portugal, sur de Inglaterra, Egipto, Israel, oeste de África y Norte América (Friis *et al.*, 2011).

- **Formación Rodezas:** Se ha estudiado una muestra procedente del afloramiento de la Fm. Rodezas en la sección de Ruilobuca (muestra Ru-Cuchía; Tabla 1). La muestra de esta unidad se diferencia de la asociación de pólenes del Aptiense Inferior (Fm. Patrocinio) por presentar una disminución en la proporción de representantes del género *Classopollis* (28,5%, Tabla 1), la desaparición de *Exesipollinites* (0%) y el aumento de la proporción de representantes de pólenes bisacados relacionados con coníferas; de *Alisporites* (~27%, Tabla 1) (Najarro *et al.*, 2011b), relacionados estos últimos con "helechos con semillas" del orden Peltaspermales (Balme, 1995) y de *Deltoidospora* (~6%).

- **Formación Reocín**: La muestra estudiada procedente de la Formación Reocín, está dominada por bisacados indeterminados, lo que parece señalar un medio de sedimentación de plataforma marina al que llegaron gran cantidad de palinomorfos continentales alóctonos a causa de un proceso de anemofilia. Los 30 taxones que se han determinado en esta muestra a partir de miosporas no arrojan ninguna información desde un punto de vista bioestratigráfico. Tampoco lo hace la presencia de dinoquistes indeterminados del género *Spiniferites*.

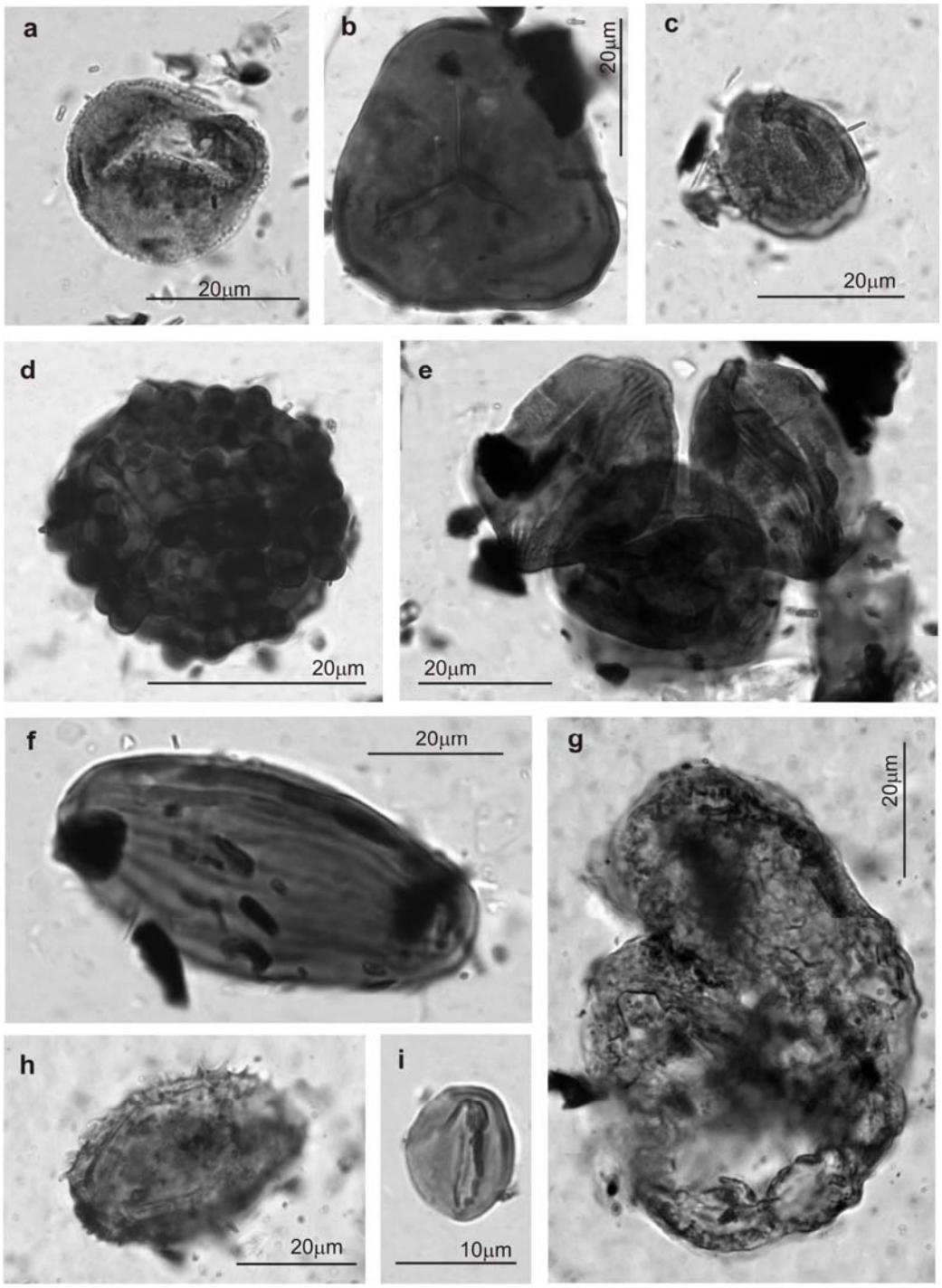

Lámina 13.- Palinomorfos seleccionados del Aptiense del área de estudio (tomado de Najarro *et al.*, 2011b). **a**: grano de polen de *Clavatipollenites* sp., de la Fm. Patrocinio; **b**: espora de la especie *Deltoidospora australis* (Couper) Pocock, de la Fm. Patrocinio; **c**: grano de polen de *Tricolpites* sp. (*T.* aff. *parvus* Stanley), de la Fm. Patrocinio; **d**: espora *Rubinella major* (Couper) Norris, de la Fm. Patrocinio; **e**: *Classopollis classoides* Pflug emend. Pocock and Jansonius, de la Fm. Patrocinio; **f**: grano de polen *Ephedripites multicostatus* Brenner, de la Fm. Patrocinio; **g**: grano de polen biscado mal preservado de *Alisporites* sp., Fm. Reocín; **h**: quiste de dinoflagelado de aff. *Criboperidinium* sp., de la Fm. Reocín; **i**: grano de polen de *Ginkgocycadophytus nitidus* (Balme) de Jersey Cookson ex. Couper, de la Fm. Patrocinio. Escala gráfica 20 µm, excepto para i: 10 µm.

La aparición del dinoflagelado *Aptea histrix* indica una edad no más antigua del Hauteriviense, mientras que la presencia de *Pseudoceratium polymorphum* señala un registro que comienza en el Aptiense.

Si comparamos esta muestra con la del Aptiense Inferior (Fm. Patrocinio), la asociación de la Fm. Reocín del Aptiense Superior muestra también una clara disminución en la abundancia de *Classopollis* y la casi desaparición de *Exesipollenites*, acompañado de un gran incremento de granos de polen bisacados relacionados con coníferas (48,7%). Así mismo, aparecen granos de polen cupresoides de *Inaperturopollenites dubius* (6,5%); y aumenta la presencia de granos, también bisacados, del género *Alisporites* (Lámina 13g). Este tipo de polen se relaciona con "helechos con semilla" del orden Peltaspermales (Balme, 1995). La aparición de quistes de dinoflagelados (*Tenua histrix* Eisenak emend Sarjeant, *Pseudoceratium polymorphum* (Eisenak) Bint y *Spiniferites* sp.) en la muestra de la Fm. Reocín, junto con algunos rellenos orgánicos de caparazones de foraminíferos confirman el ambiente de sedimentación marina para esta unidad.

- **Formación Las Peñosas**: De las muestras procedentes de la Fm. Peñosas, 12 proceden del enclave del yacimiento del ámbar de El Soplao (muestra Sop-Peñosas, Tabla 1 y muestras de P1 a P11, Tabla 2) y otra procede de la sección de Cóbreces (muestra Peñosas-Cobreces). Esta última (Najarro *et al.*, 2010) es muy rica desde un punto de vista palinológico (52 tipos de miosporas), y además presenta dinoflagelados y *lining* de foraminíferos indeterminados (Tabla 2). Esta asociación se parece mucho a las identificadas en los yacimientos ambarígenos de la subcuenca de Oliete, en la Cordillera Ibérica (Peyrot *et al.*, 2007). En este caso, la especie mejor representada fue *Inaperturopollenites dubius* que se relaciona con coníferas de la familia Cupressaceae. La aparición en la Fm. Las Peñosas de las especies *Appendicisporites robustus*, *Cicatricosisporites patapscoensis* y *Asteropollis* sp., indica para esta muestra una edad dentro del intervalo Aptiense Superior-Albiense Medio, aunque la presencia de *Retimonocolpites dividuus* Pierce (Lámina 14-1) junto con la escasa aparición de *Tricolpites* sp. parecen señalar una edad Albiense Inferior (Doyle y Robbins, 1977).

	Peñosas-Cóbreces	%	Sop-Peñosas	%
Esporas				
Appendicisporites robustus Kemp 1970	1	0.147	0	0
Appendicisporites dentimarginatus Brenner 1963	0	0	2	0.410
Appendicisporites tricornitatus Weyland & Greifeld 1953	1	0.147	0	0
Appendicisporites spp.	2	0.290	1	0.205
Baculatisporites sp.	0	0	1	0.205
Biretisporites potoniaei Delcourt & Sprumont 1955	3	0.440	3	0.615
Ceratosporites sp.	1	0.147	0	0
Cibotiumspora jurienensis (Balme 1957) Filatoff 1975	0	0	1	0.205
Cicatricosisporites apicanalis Phillips & Felix 1971	1	0.147	0	0
Cicatricosisporites apitereus Phillips & Felix 1971	1	0.147	0	0
Cicatricosisporites patapscoensis Brenner 1963	1	0.147	0	0
Cicatricosisporites recticicatricosus Döring 1965	1	0.147	0	0
Cicatricosisporites venustus Deák 1963	2	0.290	1	0.205
Cicatricosisporites spp.	13	1.908	6	1.230
Cingutriletes sp.	1	0.147	1	0.205
Contignisporites spp.	1	0.147	0	0
Crybelosporites sp.	0	0	1	0.205
Deltoidospora australis (Couper 1953) Srivastava 1975	4	0.587	13	2.664
Deltoidospora minor (Couper 1953) Pocock 1970	8	1.174	27	5.533
Deltoidospora sp.	4	0.587	8	1.640
Densoisporites velatus Weyland & Krieger 1953	1	0.147	1	0.205
Dictyophyllidites harrisii Couper 1958	2	0.290	1	0.205
Echinatisporis sp.	1	0.147	0	0
Gleicheniidites senonicus Ross 1949	0	0	4	0.819
Laevigatosporites sp.	0	0	7	1.434
Leptolepidites sp.	0	0	1	0.205
Patellasporites tavaredensis Groot & Groot 1962	1	0.147	0	0
Retitriletes sp.	0	0	1	0.205
Stereisporites sp.	0	0	1	0.205
Taurucosporites segmentatus Stover 1962	1	0.147	0	0
Trachysporites sp.	1	0.147	0	0
Triporoletes reticulatus (Pocock 1962) Playford 1971	1	0.147	1	0.205
Todisporites major Couper 1958	1	0.147	0	0
Granos de polen (gimnospermas)				
Alisporites bilateralis Rouse 1959	5	0.734	8	1.640
Alisporites spp.	20	2.937	12	2.460
Araucariacites australis Cookson 1947	12	1.762	25	5.123
Callialasporites dampieri Dev 1961	1	0.147	0	0
Cedripites sp.	1	0.147	0	0
Classopollis classoides Pflug 1953 emend. Pocock & Jansonius 1961	213	31.277	46	9.426
Classopollis spp.	58	8.517	9	1.844
Cycadopites spp.	8	1.174	2	0.410
Eucommiidites minor Groot & Penny 1960	4	0.587	2	0.410
Exesipollenites tumulus Balme 1957	6	0.881	3	0.615
Ginkgocycadophytus nitididus (Balme 1957) de Jersey 1962	1	0.147	3	0.615
Inaperturopollenites dubius (Potonié & Venitz 1932) Thompson & Pflug 1953	205	30.102	249	51.024
Inaperturopollenites spp.	21	3.084	9	1.844
Monosulcites chaloneri Brenner 1963	22	3.230	8	1.640
Monosulcites sp.	4	0.587	3	0.615
Pinuspollenites sp.	2	0.290	2	0.410
Podocarpidites sp.	0	0	2	0.410
Spheripollenites sp.	12	1.762	5	1.024
Vitreisporites pallidus (Reissinger 1950) Nilsson 1958	2	0.300	1	0.205
Granos de polen bisacados ideterminados	1	0.147	6	1.230
Granos de polen (angiospermas)				
Afropollis sp.	2	0.300	1	0.205
Clavatipollenites hughesii Couper 1958	2	0.300	3	0.615
Clavatipollenites minutus Brenner 1963	5	0.734	1	0.205
Clavatipollenites sp. (trichomosulcate)	4	0.587	0	0
Clavatipollenites spp.	5	0.734	4	0.819
Liliacidites dividus (Pierce 1961) Brenner 1963	3	0.440	0	0
Pennipollis peroreticulatus Brenner 1963	1	0.147	1	0.205
Tricolpites sp.	1	0.147	0	0
Granos de polen de angiospermas indeterminados	6	0.881	1	0.205
TOTAL	681	100	488	100

Tabla 2.- Diagrama de palinomorfos identificados para el Albiense Inferior (Fm. Las Peñosas) del área de estudio, muestras procedentes de Cóbreces y del yacimiento de ámbar de El Soplao, con indicación de porcentajes de los representantes presentes (tomado de Najarro *et al.*, 2010).

Muestras	P1	P2	P3	P4	P5	P6	P7	P8	P9	P10	P11
Esporas de criptógamas vasculares											
Antuslporites sp.											*
Appendicisporites bilateralis					*					*	*
Appendicisporites problematicus		*									
Appendicisporites pseudomacrorhyza/dentimarginatus								*			
Appendicisporites spp.			*							*	
Baculatisporites comaumensis	*						*	*			*
Biretisporites sp.		*	*		*		*	*		*	
Cicatricosisporites patapscoensis							*				
Cicatricosisporites pseudotripartitus		*									
Cicatricosisporites sternum					*						
Cicatricosisporites venustus				*				*			*
Cicatricosisporites spp.	*	*	*	*	*	*	*	*		*	*
Clavifera sp.						*					
Concavissimisporites subgranulatus				*	*						
Concavissimisporites verrucosus						*	*			*	*
Contignisporites sp.	*										
Costatoperforosporites triangulatus											*
Costatoperforosporites sp.											
Deltoidospora australis	*	*	*	*	*	*	*	*	*	*	*
Deltoidospora minor	*	*	*	*	*	*	*	*	*	*	*
Deltoidospora sp.	*	*	*	*	*	*	*	*	*	*	*
Densoisporites velatus											*
Dictyophyllidites sp.										*	
Echinatisporis sp.			*								
Foveotrioletes sp.				*							
Gleicheniidites senonicus	*	*	*	*	*	*	*	*		*	*
Gregussosporites orientalis									*		
Ischyosporites pseudoreticulatus .	*										
Laevigatosporites sp.			*	*	*					*	*
Leptolepidites macroverrucosus										*	
cf. Leptolepidites sp.		*									
Maculatisporites sp.										*	*
Microfoveolatisporites subtriangularis	*										
Neoraistrickia sp.	*						*	*			
Ornamentifera peregrina		*	*	*	*						
Osmundacidites wellmanii	*						*			*	
Patellasporites tavaredensis		*					*	*	*	*	
Retitriletes austroclavatidites	*	*	*	*	*		*	*		*	*
Rotverrusporites sp.	*							*			
Stereisporites sp.	*	*	*	*							
Trachysporites sp.	*				*		*		*		
Triporoletes reticulatus					*						
Tuberositriletes sp.		*									
Todisporites major											*
Undulatisporites sp.			*		*						*
cf. *Vallizonosporites* sp.	*										
Trilete indet.	*	*	*	*	*					*	
Granos de polen (Gimnospermas)											
Afropollis sp.			*								
Alisporites bilateralis	*	*	*	*	*	*	*	*	*	*	*
Alisporites grandis					*			*			*
Alisporites microsaccus											*
Alisporites spp.	*	*	*	*	*	*	*	*	*	*	*
Araucariacites australis	*	*	*	*	*	*	*	*	*	*	*
Bisacados indeterminados	*	*	*	*	*	*	*	*	*	*	*
Callialasporites dampieri	*			*				*		*	*
Callialasporites segmentatus			*								
Cerebropollenites macroverrucosus			*	*	*	*	*	*	*		*
Classopollis major	*	*	*	*	*	*	*	*	*	*	*
Classopollis spp.	*	*	*	*	*	*	*	*	*	*	*
Cycadopites maximus				*		*		*			*
Cycadopites follicularis	*	*		*	*	*	*	*	*	*	*
Cycadopites sp. (con verrugas)						*					
Cycadopites spp.	*	*	*	*	*	*	*	*	*	*	*
Ephedripites multicostatus					*			*			
Equisetosporites sp.					*			*			
Eucommiidites minor	*	*					*		*		*
Eucommiidites troedsonii			*	*	*	*	*	*	*	*	*
Exesipollenites tumulus	*	*	*	*	*	*	*	*	*	*	*
Inaperturopollenites dubius	*	*	*	*	*	*	*	*	*	*	*
Inaperturopollenites spp.	*	*	*	*	*	*	*	*	*	*	
Monosulcites chaloneri	*	*	*	*	*	*	*	*	*	*	*
Monosulcites minimus	*	*	*	*	*	*		*			
Monosulcites spp.	*	*		*	*	*	*			*	*
Parvisaccites sp.	*										
Parvisaccites cf. *similis*											*
Perinopollenites elatoides											*
Piceapollenites sp.			*		*						
Pinuspollenites sp.	*	*	*	*	*	*	*			*	
Podocarpidites sp.		*	*	*	*		*			*	*
Spheripollenites sp.	*	*	*	*	*	*	*	*	*	*	*
Vitreisporites pallidus	*	*	*	*	*	*		*	*	*	*

Granos de polen (Angiospermas)											
Asteropollis asteroides							*				
Asteropollis trichotomosulcatus	*		*		*	*					*
Clavatipollenites hughesii	*	*	*	*		*		*		*	*
Clavatipollenites minutus		*								*	
Clavatipollenites tenellis	*	*	*							*	
Clavatipollenites spp.	*		*	*	*	*	*	*	*	*	*
Doyleipollenites robbinsiae	*										
Pennipollis peroreticulatus	*	*	*	*	*						*
Pennipollis reticulatus	*	*	*	*	*		*				*
Pennipollis spp.	*										
Retimonocolpites spp.		*					*				
Transitoripollis similis	*			*	*	*	*	*		*	
Transitoripollis sp. A			*	*	*	*	*	*	*	*	*
Tricolpites spp.	*	*			*		*				*
granos de polen indeterminables de angiosp.	*	*	*	*	*	*	*	*	*	*	*
Otros palinomorfos											
Dinocistes indeterminables	*	*	*	*	*	*	*	*		*	
Oligosphaeridium complex	*			*			*				
Cyclonepehlium distinctum								*		*	
Cyclonepehlium cf. *distinctum*					*						
Cyclonepehlium hirtellum							*	*		*	
Cyclonepehlium cf. *hirtellum*							*				
Cyclonephelium sp.	*						*	*			
Cyclonephelium-Aptea											*
Gonyoulacacean indet.					*						
aff. *Impletosphaeridium* sp.	*	*									
Kallaiosphaeridium assymetricum											
Kallosphaeridium sp.					*		*	*		*	*
Ovoidinium sp.											
Palaeohystrichosphaera cheit											
cf. *Palaeoperidinium cretaceum*											
Subtilisphaera terrula											
Subtilisphaera sp.											
Tenua histrix											
Tenua cf. *histrix*		*	*		*	*			*		*
aff. *Trichidinium castanea*			*								
Spiniferites ramosus			*				*			*	
Spiniferites sp.					*						
Acritarcos indeterminables			*	*	*	*	*	*	*	*	*
Michrystridium sp.	*	*	*			*				*	
Veryhachium sp.								*	*		
Tasmanites sp.											
Lining de foraminíferos		*	*		*	*			*		

Tabla 3.- Relación de palinomorfos identificados en la Formación Las Peñosas del Albiense Inferior (muestras procedentes de la cata del yacimiento del ámbar de El Soplao). Las estrellas indican la presencia o no presencia de los diferentes taxones para cada muestra.

La muestra Sop-Peñosas, con 44 taxones identificados, tiene una asociación similar a la anterior (Najarro *et al.*, 2010), pero en ella no se han encontrado los taxones que indican la edad mencionada. Lo único que se puede concluir es que la presencia de *Pennipollis* spp. y de *Densoisporites velatus* señalan al intervalo Aptiense-Albiense.

Las muestras P1-P11 fueron recogidas en la cata del yacimiento de ámbar de Rábago-El Soplao con intervalos estratigráficos de unos 15 cm. Todas ellas son ricas en miosporas, si bien las asociaciones obtenidas fueron muy similares excepto en las muestras P10 y P11, tomadas a techo del yacimiento (Tabla 3). Además, todas ellas presentan palinomorfos marinos. En conjunto, se han identificado 46 tipos de esporas de criptógamas vasculares y 52 de granos de polen (33 de gimnospermas y 19 de angiospermas primitivas) (Tabla 3).

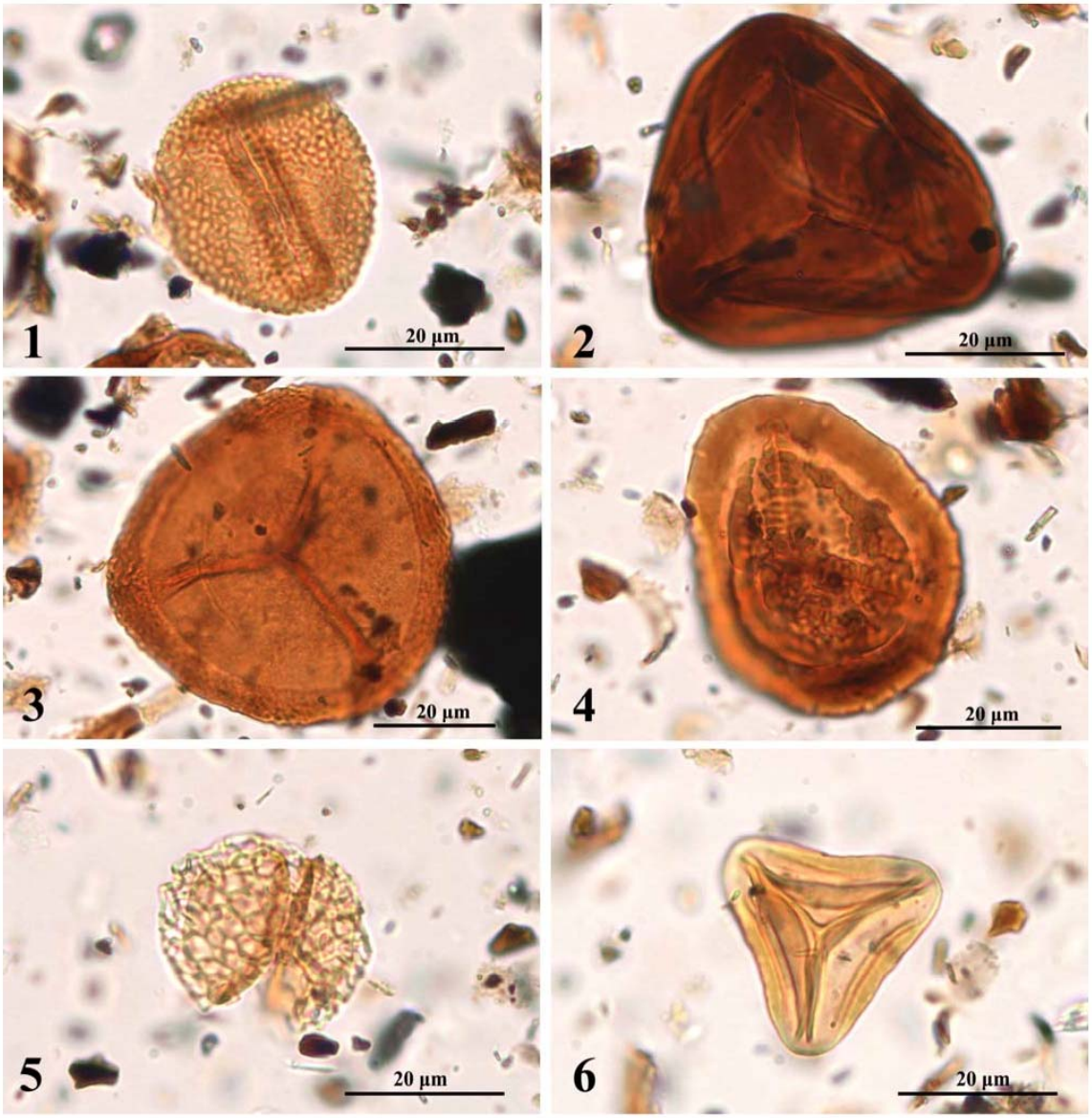

Lámina 14.- Miosporas seleccionadas de la Formación Las Peñosas del Albiense (tomada de Najarro *et al.*, 2010). **1**: *Retimonocolpites dividuus* Pierce; **2**: *Cicatricosisporites patapscoensis* Brenner; **3**: *Densoisporites velatus* Weyland y Krieger; **4**: *Taurocosporites segmentatus* Stover; **5**: *Pennipollis peroreticulatus* Brenner; **6**: *Gleicheniidites senonicus* Ross.

Las asociaciones de las muestras de la Formación Las Peñosas están siempre dominadas por *Inaperturopollenites dubius* y *Classopollis* spp., mostrando estos dos taxones porcentajes similares en torno al 30% de abundancia (Tabla 2). Le siguen en importancia con alrededor de un 5% de presencia *Exesipollenites tumulus*, *Araucariacites australis*, *Monosulcites chaloneri*, *Cycadopites* spp. y las esporas de cryptógamas vasculares (principalmente *Deltoidospora* spp.) (Tabla 2). Los granos de

polen de angiospermas primitivas están presentes en todas las muestras aunque de forma muy escasa (~1%), siendo frecuentes especies de los géneros *Clavatipollenites*, *Brenneripollis* y *Transitoripollis* (Tabla 2). Los granos tricolpados son raros y aparecen esporádicamente. Concretamente, las especies identificadas han sido *Retitricolpites maximus*, *Tricolpites vulgaris* y *Tricolpites* sp. Las muestras P10 y P11 se diferencian del resto por mostrar una menor abundancia de *Inaperturopollenites dubius* y *Exesipollenites tumulus* y presentar un pequeño incremento respecto a las muestras inferiores de *Araucariacites australis*, *Monosulcites* sp. y *Transitoripollis* spp.

Desde un punto de vista bioestratigráfico, la presencia de *Cicatricosisporites patapscoensis* y *Gregussisporites orientalis* en las muestras de la Formación Las Peñosas del yacimiento de ámbar de El Soplao (muestras de la cata), indican una edad de Aptiense Superior-Albiense (Arias y Doubinger, 1980; Leereveld *et al.*, 1989), siendo la edad más probable Albiense Inferior, ya que el techo de la unidad infrayacente (Fm. Reocín) ha sido datada con foraminíferos bentónicos como Aptiense terminal-Albiense basal.

3.3.- SECCIONES ESTRATIGRÁFICAS

Los datos estratigráficos adquiridos durante el desarrollo de esta investigación se basan fundamentalmente en el levantamiento de columnas estratigráficas de detalle, cuya representación se expone de forma sintética en este apartado. Se han levantado 15 columnas estratigráficas a lo largo de los tres sectores de estudio (áreas de La Florida, sinclinal de Santillana y Cuchía), que en conjunto suman más de 3.100 metros de series estratigráficas. Estas secciones estratigráficas han servido como base principal para los estudios llevados a cabo en esta tesis, para el reconocimento de secuencias deposicionales y límites de secuencia y para ayudar a establecer la geometría de la cuenca extensiva y los rasgos paleogeográficos principales. A patir de ellas se han caracterizado los tipos de facies sedimentarias y sus cambios laterales a escala de afloramiento, con especial atención en la geometría de los depósitos, litología, textura, contenido fósil y presencia de estructuras sedimentarias. La evolución vertical de las facies y su organización en secuencias, así como el reconocimiento de las discontinuidades estratigráficas principales han permitido organizar la sucesión estudiada en secuencias deposicionales transgresivo-regresivas (T-R). La correlación lateral de las diferentes unidades litoestratigráficas, discontinuidades y secuencias deposicionales distinguidas en cada una de las secciónes estudiadas, junto con su seguimiento cartográfico, ha permitido observar variaciones laterales de facies y espesores sedimentarios a escala regional y reconocer en el campo las fallas principales con actividad sinsedimentaria que controlaron estos cambios, lo que ha constituido la base para ayudar en la reconstrucción de la geometría *sinrift* de la cuenca de estudio.

La localización de los afloramientos donde se han levantado estas columnas se representa en la Figura 1.1 y las coordenadas geográficas del techo y base de cada una de ellas se muestran en la Tabla 4. Se ha utilizado en todas ellas una simbología común mostrada en la figura 3.7, que incluye litología, textura, contenido fósil y estructuras sedimentarias, con un detalle suficiente para permitir la lectura de todas ellas directamente a partir de la representación gráfica. Además de esto, cada sección estratigráfica incluye, junto a la representación de las facies, una columna descriptiva de cada uno de los tramos distinguidos y su interpretación y ambiente deposicional. Por

tanto, no se ha considerado necesario incluir una descripción detallada de cada tipo de facies o una descripción por tramos de cada una de las secciones.

El análisis de facies de los materiales que componen las secciones estratigráficas estudiadas del Aptiense y Albiense muestran asociaciones de facies de medios que varían desde ambientes litorales transicionales deltaico-estuarinos a bahía estuarina, plataforma terrígena (*nearshore*), plataforma carbonatada interna-*lagoon*, plataforma carbonatada abierta o media energética, plataforma externa proximal, talud carbonatado y plataforma distal (*offshore*).

Los ambientes **transicionales deltaico-estuarinos** se cararerizan por presentar litologías siliciclásticas, compuestas por las siguientes asociaciones de facies: a) lutitas y limos con estratificación lenticular de finos niveles de arena con *ripples* y gradación positiva y areniscas bioclásticas, depositados en un medio de prodelta; b) areniscas de grano fino a medio con estratificación cruzada de surco a media escala, organizadas en secuencias grano y estratocrecientes formando barras métricas a decamétricas con *ripples* de oscilación a techo, interpretadas como barras submareales distributarias depositadas en medio de frente deltaico; c) lutitas y limos sulfurosos y facies heterolíticas bioturbadas de lutita-arena con laminación lenticular, con abundantes macrorestos vegetales y ámbar, depositados en subambientes de bahía interdistributaria; d) areniscas de grano medio a grueso con estratificación cruzada, base erosiva y forma acanalada con *lag* basal, interpretados como depósitos de canales fluvio-deltaicos y e) lutitas y arenas finas versicolores con tonos rojos y huellas de raíces, interpretados como niveles de paleosuelos en medios de llanura deltaica.

Los ambientes de **bahía estuarina** se caracterizan por presentar facies mixtas terrígeno-carbonatadas compuestas por areniscas calcáreas, calizas bioclásticas margosas o arenosas con ostreidos y *grainstone* y areniscas bioclásticas con estratificación cruzada sigmoidal y *ripples* de oscilación, interestratificados con limos, facies heterolíticas de limo-arena y margas limosas. Estas facies son interpretadas como el relleno de bahías estuarinas afectadas por correintes de marea y oleaje.

Los ambientes de **plataforma terrígena** están caracterizados por presentar limos y areniscas finas bioturbadas con orbitolinas.

Los ambientes de **plataforma carbonatada interna y *lagoon*** se caracterizan por la presencia de facies someras de baja energía compuestas por calizas micríticas con abundante *Bacinella irregularis-Lithocodium aggregatum* formando masas irregulares trombolíticas, *lumps* y oncoides, calizas *floatstone* a *rudstone* de rudistas, principalmente requiénidos y polyconites, y calizas *wackestone* a *packstone* con miliólidos, peloides y algas.

Los ambientes de **plataforma carbonatada abierta o media energética** presentan facies de calizas *packstone* y *grainstone* bioclásticas o bioclásticas-oolíticas, con fragmentos de colares ramosos, fragmentos de rudistas, equinodermos, orbitolinas, etc. Se organizan en paquetes decimétricos a métricos, masivos o con estratificación cruzada, formando bancos tabulares y *shoals* interestratificados con niveles de margas, calizas margosas o limos con restos de carbón. También presentan, en menor medida, calizas bioclásticas con corales y rudistas radiolítidos, caprínidos y caprotínidos.

Los ambientes de **plataforma externa proximal** se caracterizan por la presencia de calizas nodulosas, calizas margosas y margas con corales masivos y tabulares o esponjas, o bien margas bioclásticas o limosas, normalmente bioturbadas, con orbitolinas.

Los ambientes de **plataforma distal** (*offshore*) se caracterizan por presentar sucesiones monótonas de lutitas oscuras y margas grises limosas, con nódulos de pirita, glauconita, restos carbonosos, belemnites y niveles de ammonites.

El estudio de las facies sedimentarias y su evolución temporal a lo largo de las series estudiadas (Figura 3.7 a 3.22) sugieren una alternancia de sistemas de plataforma carbonatada que alternan con sistemas deltaicos y de plataforma siliciclástica o mixta, como respuesta a variaciones relativas del nivel del mar, tectónica sinsedimentaria, y cambios en el tipo dominante de aporte sedimentario. La organización de las unidades litoestratigráficas y sistemas deposicionales en secuencias deposicionales (T-R), será tratada a continuación en el siguiente capítulo.

Situación de las columnas estratigráficas. Coordenadas UTM (30 N, en ETRS89)		
Sección río Nansa	Base	Techo
	X= 381302,5 Y= 4795774,3	X= 380703,4 Y= 4796446,4
Sección Rábago	Base	Techo
	X= 383482,6 Y= 4795245,2	X= 382586,1 Y= 4795809,2
Sección El Soplao	Base	Techo
	X= 385453,7 Y= 4794714,9	X= 385261,1 Y= 4795250,4
Sección La Florida	Base	Techo
	X= 385896,6 Y= 4794474,5	X= 385913,2 Y= 4794875,7
Sección Corona de Arnedo	Base	Techo
	X= 386818,9 Y= 4794176,0	X= 386784,7 Y= 4794956,8
Sección Bustriguado	Base	Techo
	X= 390493,6 Y= 4794768,7	X= 390153,3 Y= 4796044,5
Sección Fonfría	Base	Techo
	X= 397501,3 Y= 4805038,0	X= 397460,1 Y= 4805113,1
Sección Hayuela-Canales	Base	Techo
	X= 396995,3 Y= 4799074,1	X= 397041,9 Y= 4799886,9
Sección Ruilobuca	Base	Techo
	X= 397682,9 Y= 4802572,2	X= 398248,1 Y= 4803279,1
Sección Santa Eulalia	Base	Techo
	X= 402689,5 Y= 4798783,7	X= 403036,7 Y= 4800146,8
Sección Novales	Base	Techo
	X= 405123,7 Y= 4803991,8	X= 405676,2 Y= 4803725,1
Sección cantera de Las Lastrías	Base	Techo
	X= 406635,0 Y= 4798825,0	X= 406681,6 Y= 4798899,0
Sección Cuchía	Base	Techo
	X= 417453,3 Y= 4810836,0	X= 416441,6 Y= 4810048,6
Sección cantera de Cuchía	Base	Techo
	X= 417883,0 Y= 4809208,3	X= 417711,6 Y= 4808905,6
Sección Suances	Base	Techo
	X= 415375,0 Y= 4810678,4	X= 415244,9 Y= 4810381,0

Tabla 4.- Coordenadas proyectadas UTM del techo y base de las columnas estratigráficas.

Leyenda

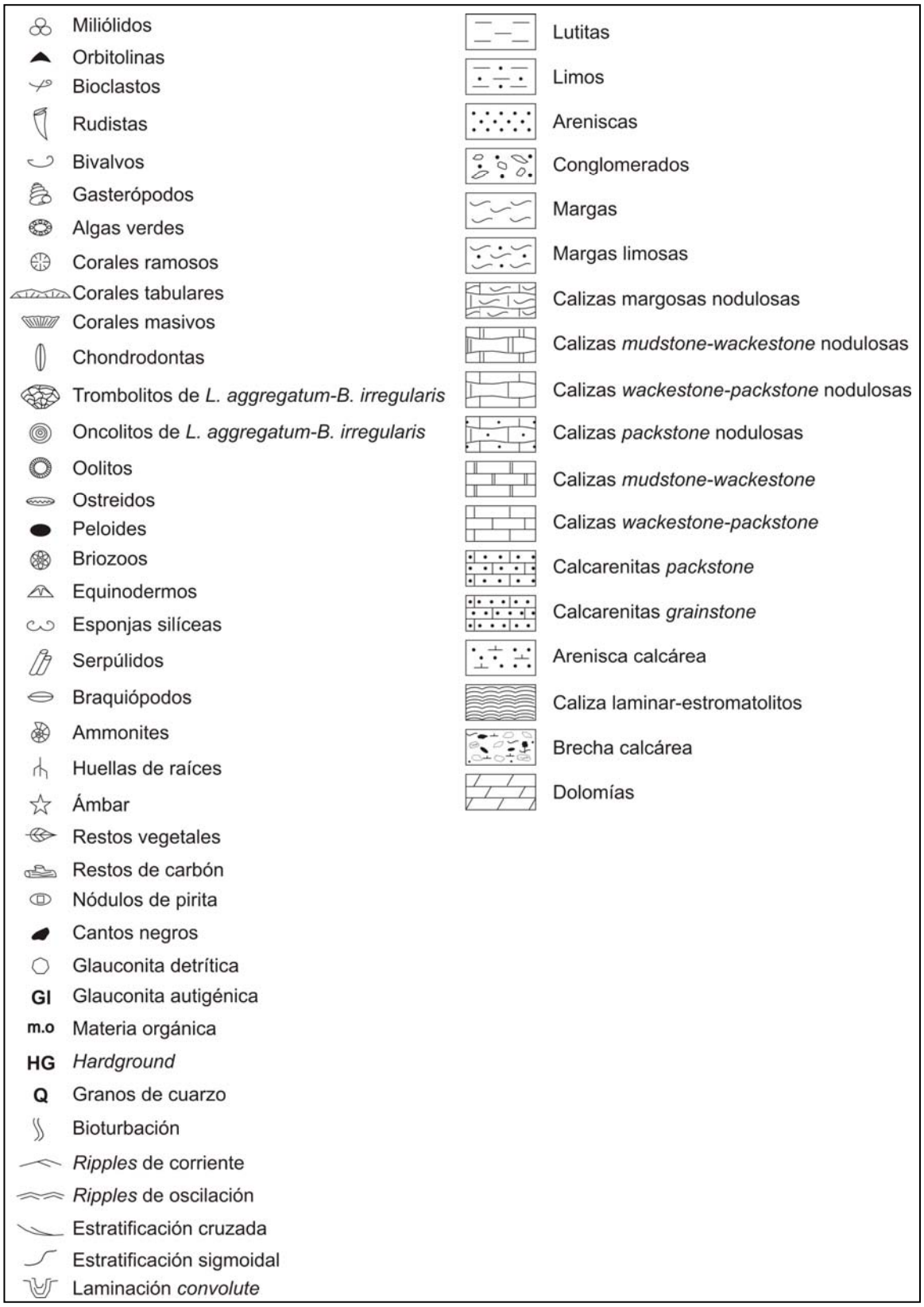

Figura 3.7.- Simbología utilizada en todas las columnas estratigráficas.

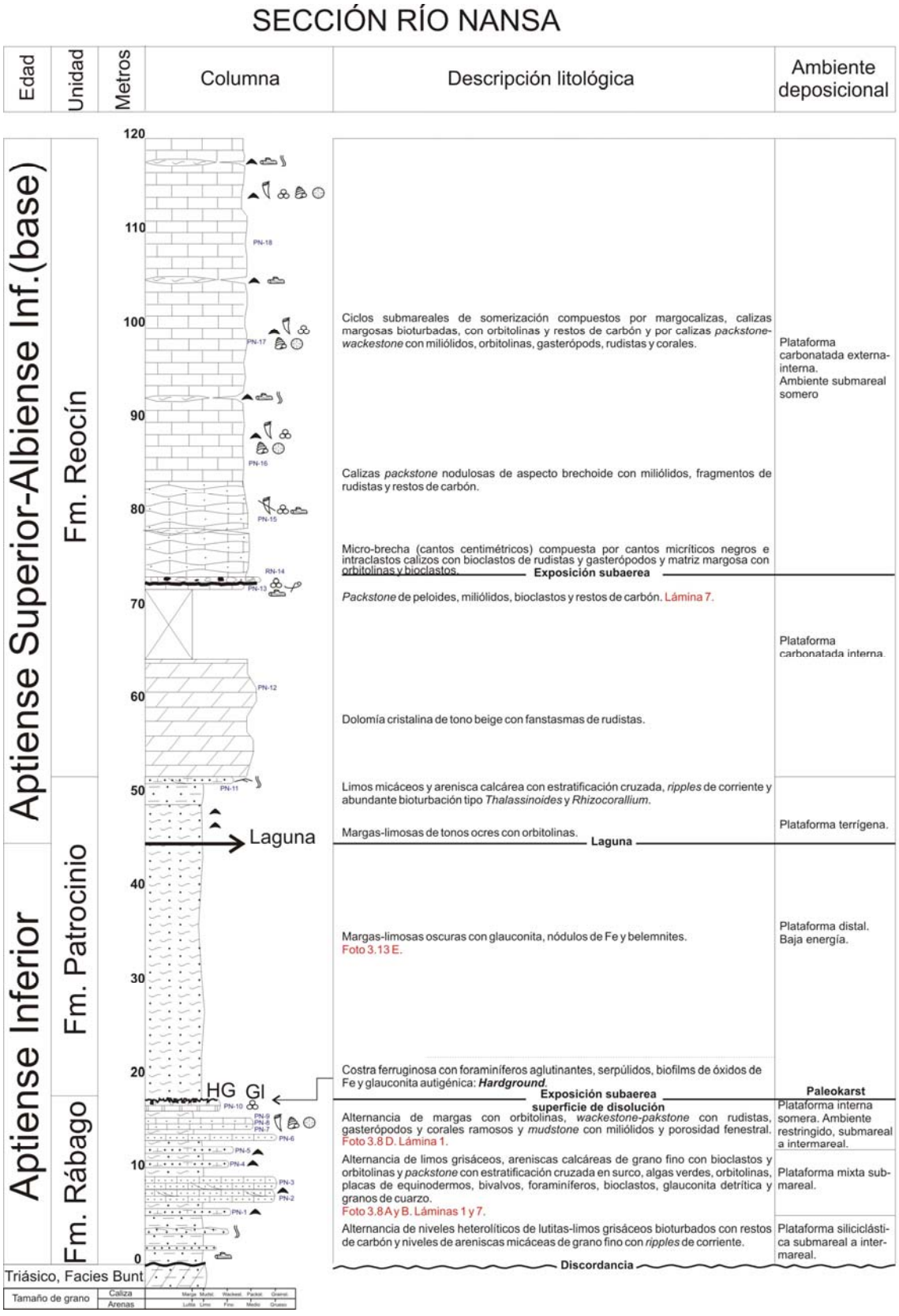

Figura 3.8.- Sección sintética de Río Nansa (área de La Florida).

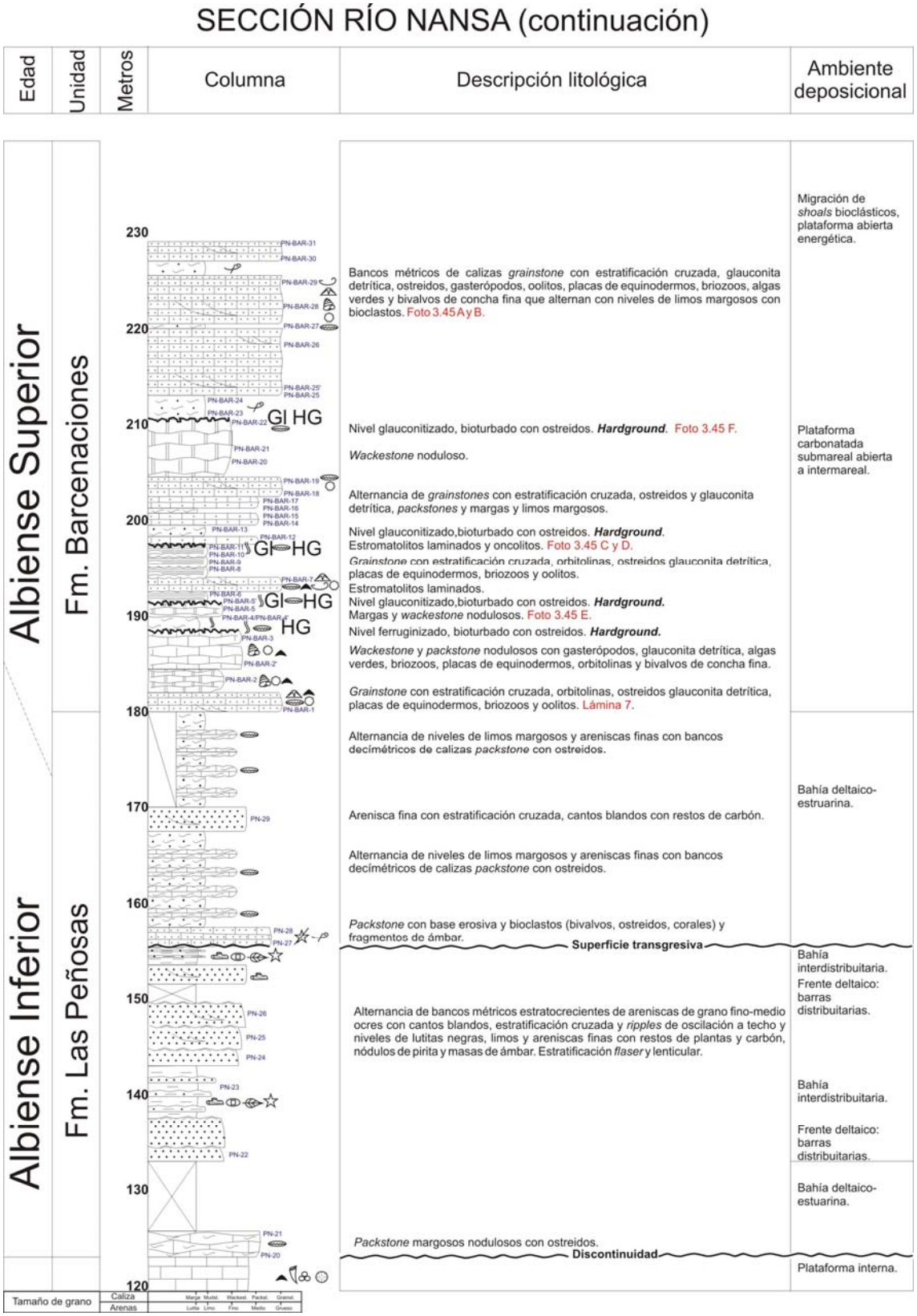

Figura 3.8.- Sección sintética de Río Nansa (área de La Florida). Continuación.

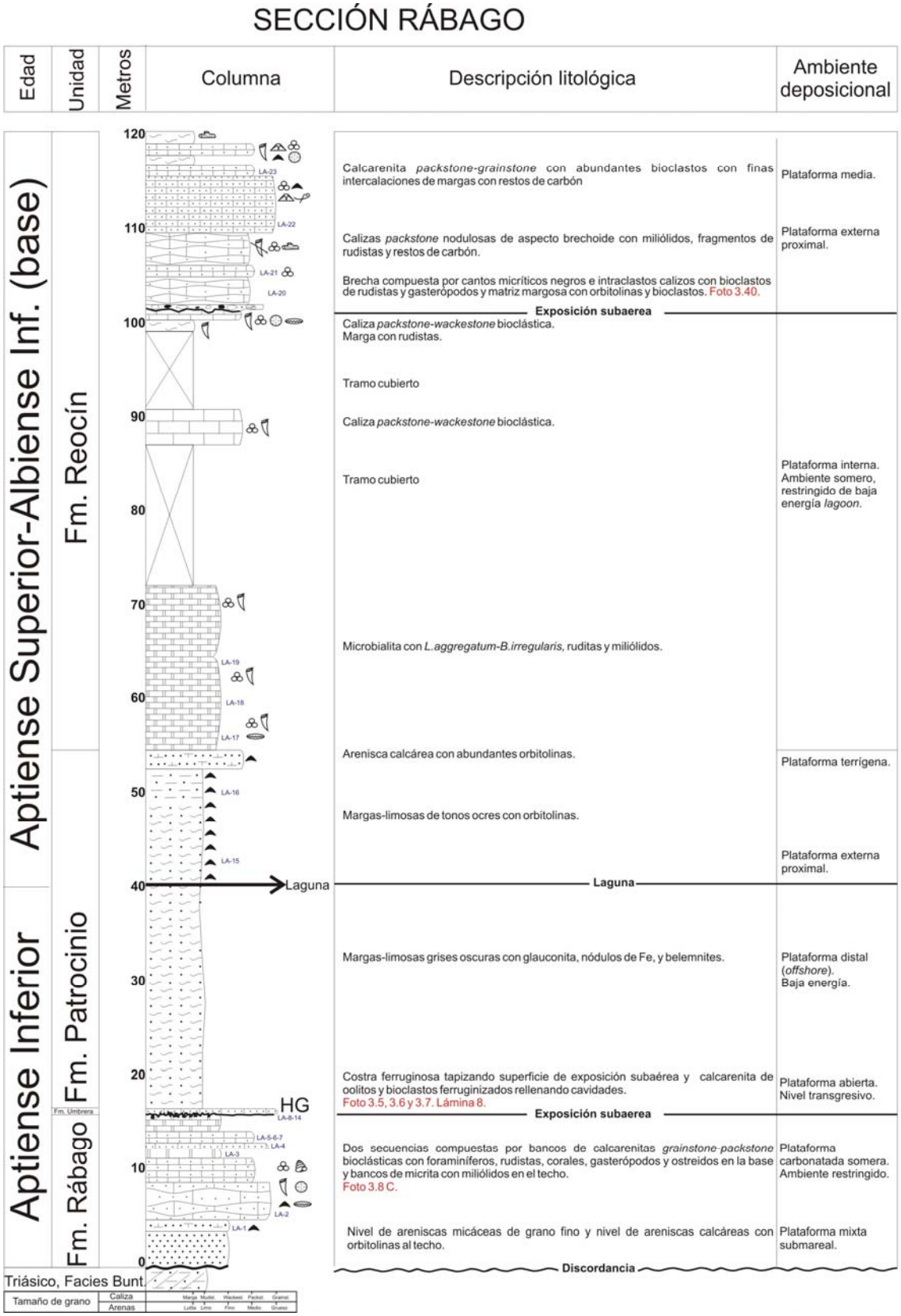

Figura 3.9.- Sección sintética de Rábago (área de La Florida).

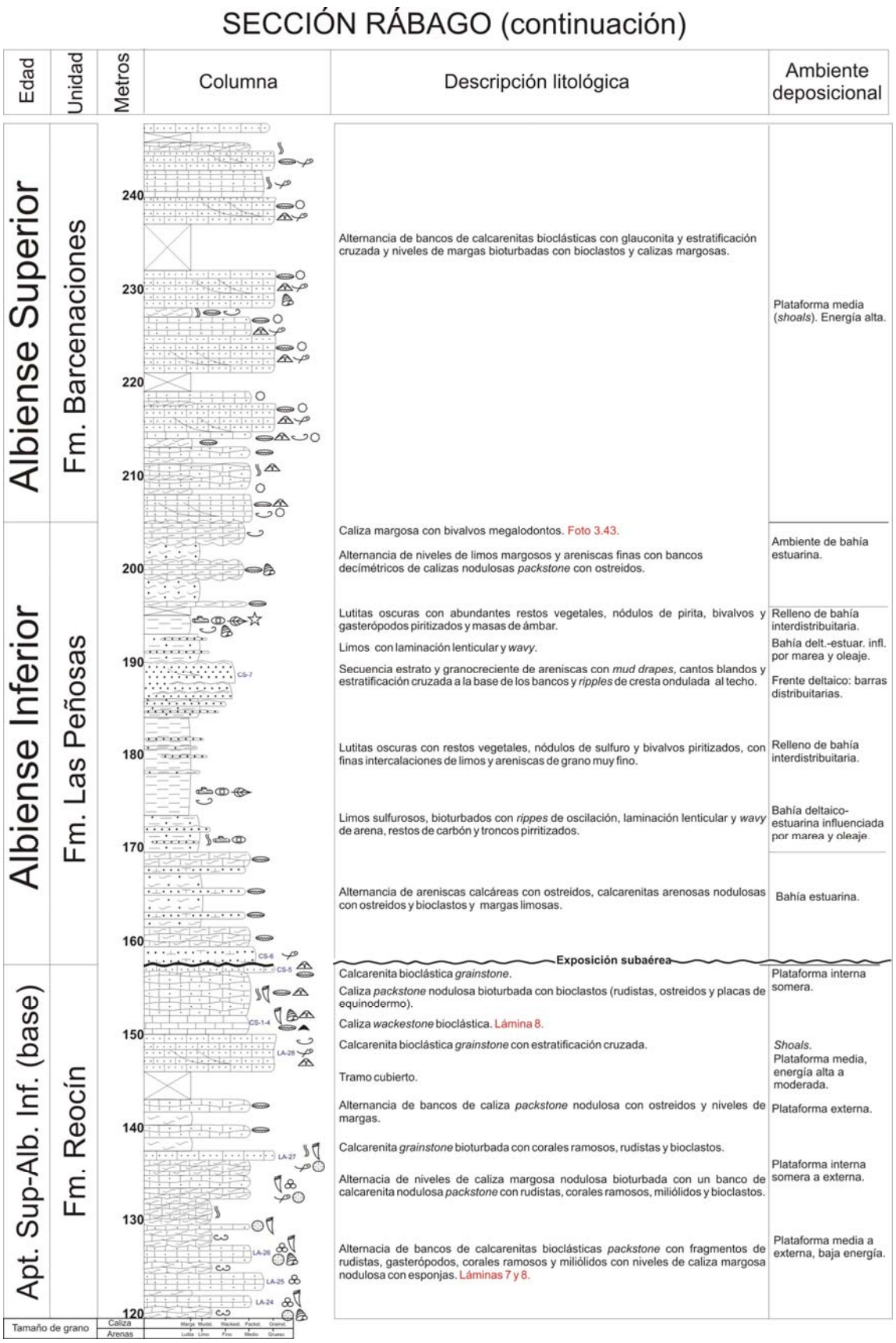

Figura 3.9.- Sección sintética de Rábago (área de La Florida). Continuación.

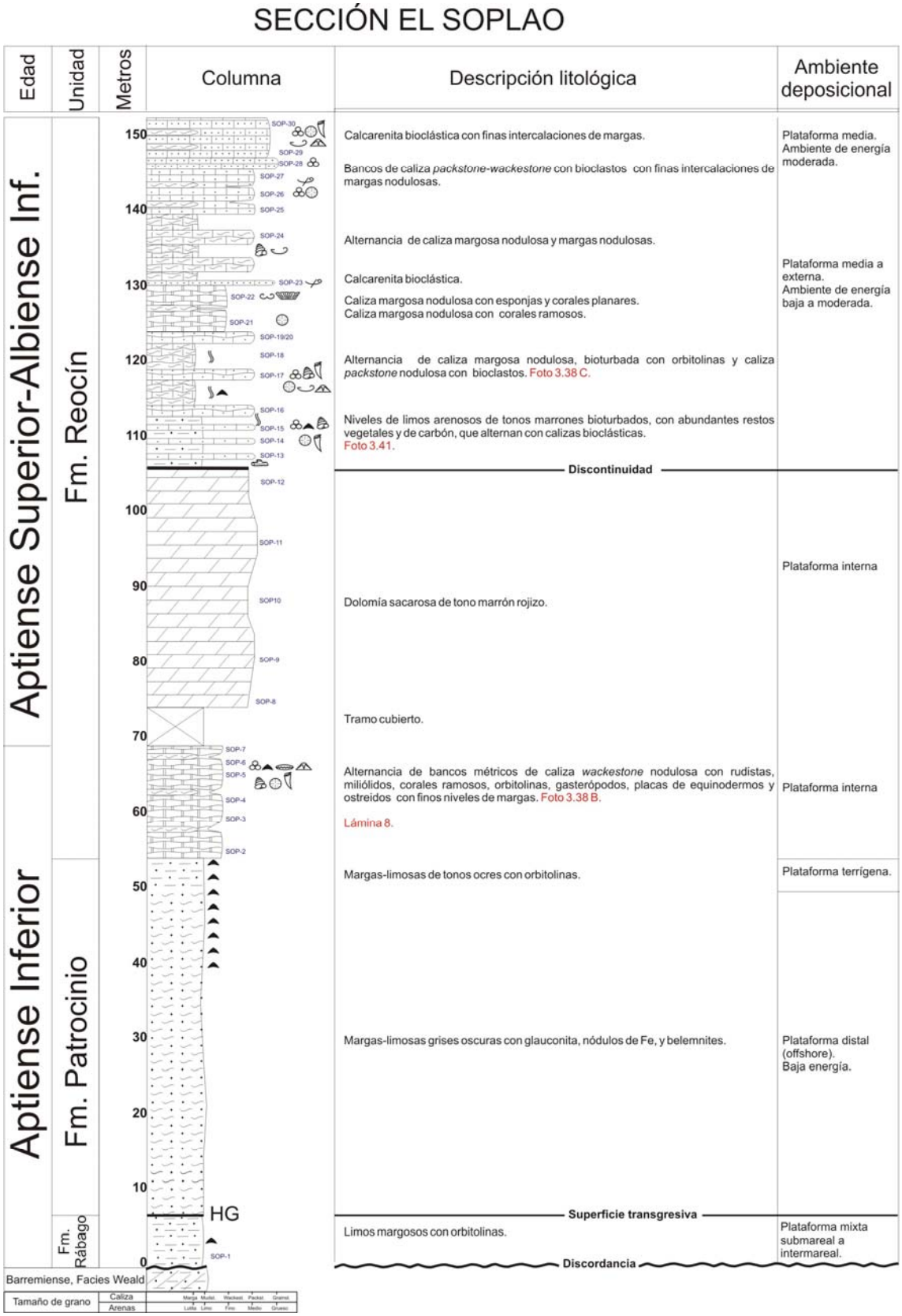

Figura 3.10.- Sección sintética de El Soplao (área de La Florida).

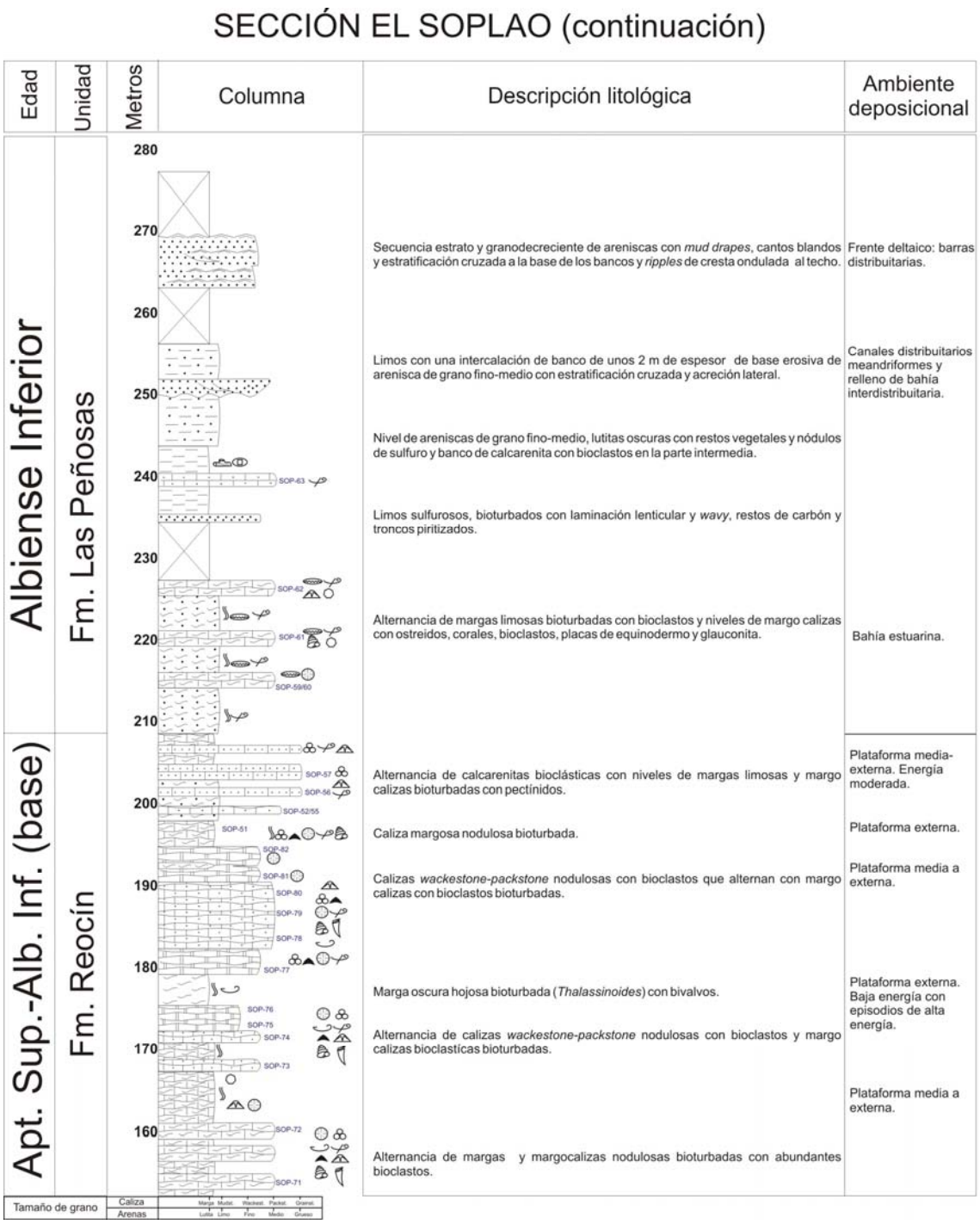

Figura 3.10.- Sección sintética de El Soplao (área de La Florida). Continuación.

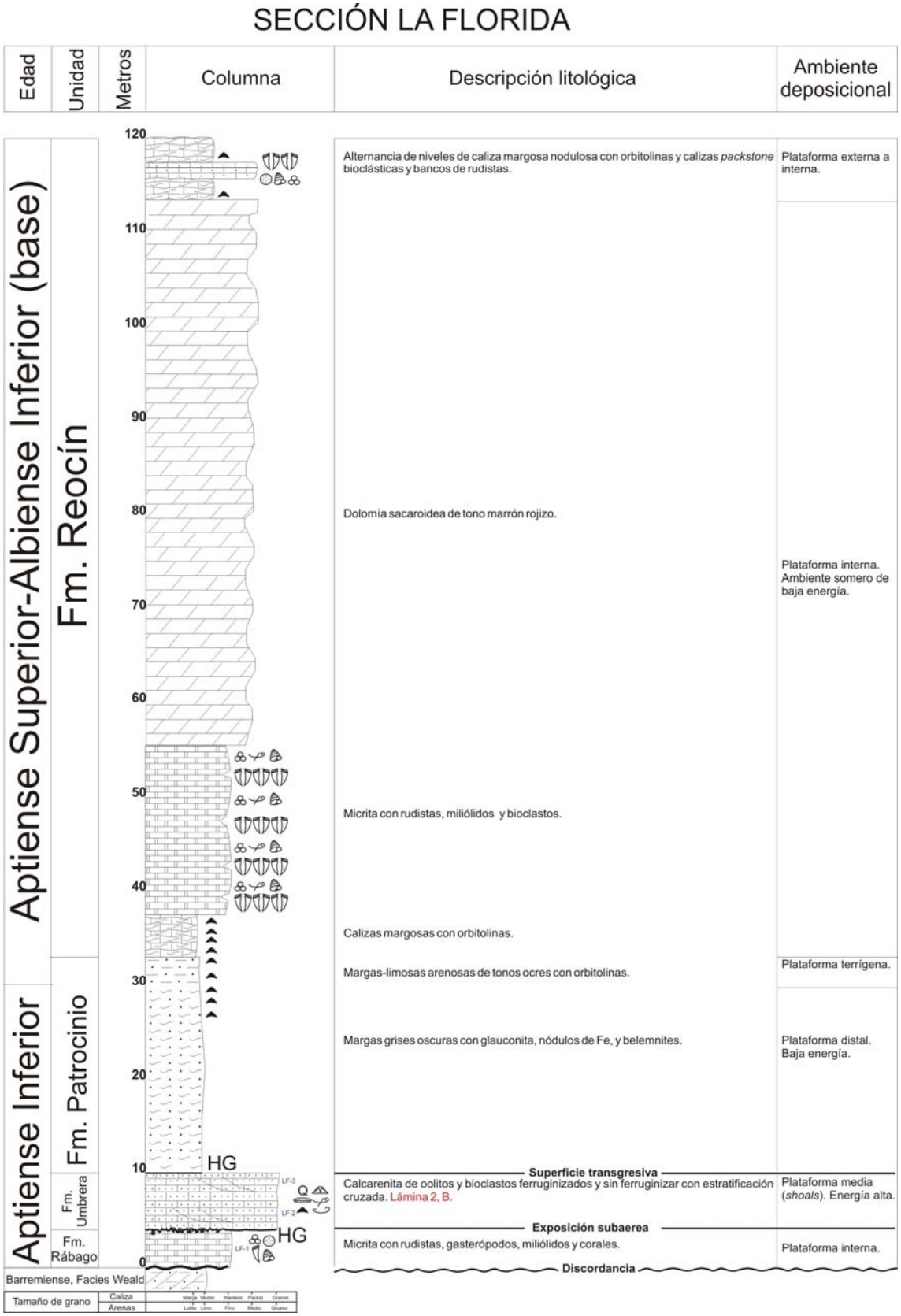

Figura 3.11.- Sección sintética de La Florida (área de La Florida).

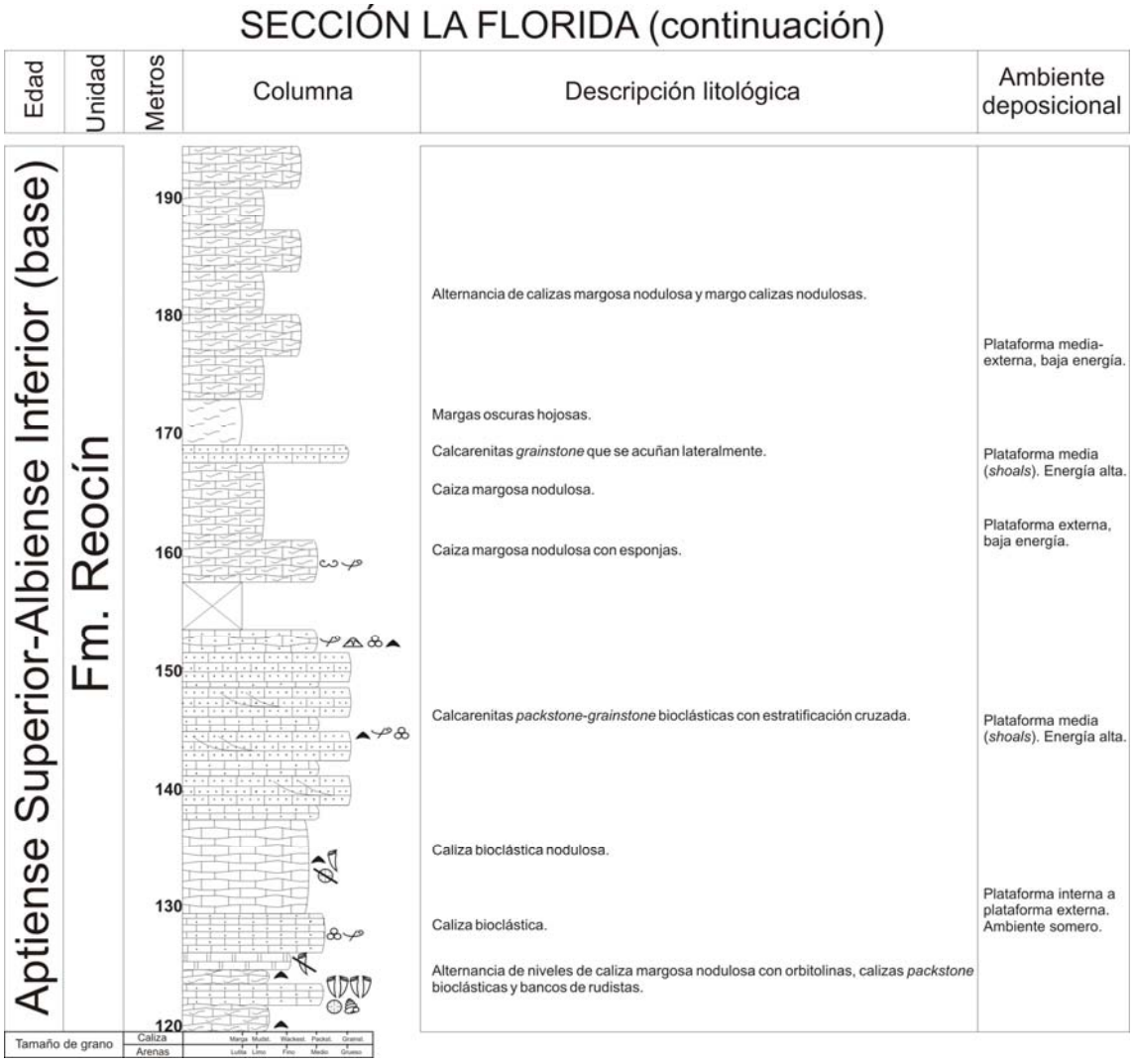

Figura 3.11.- Sección sintética de La Florida (área de La Florida). Continuación.

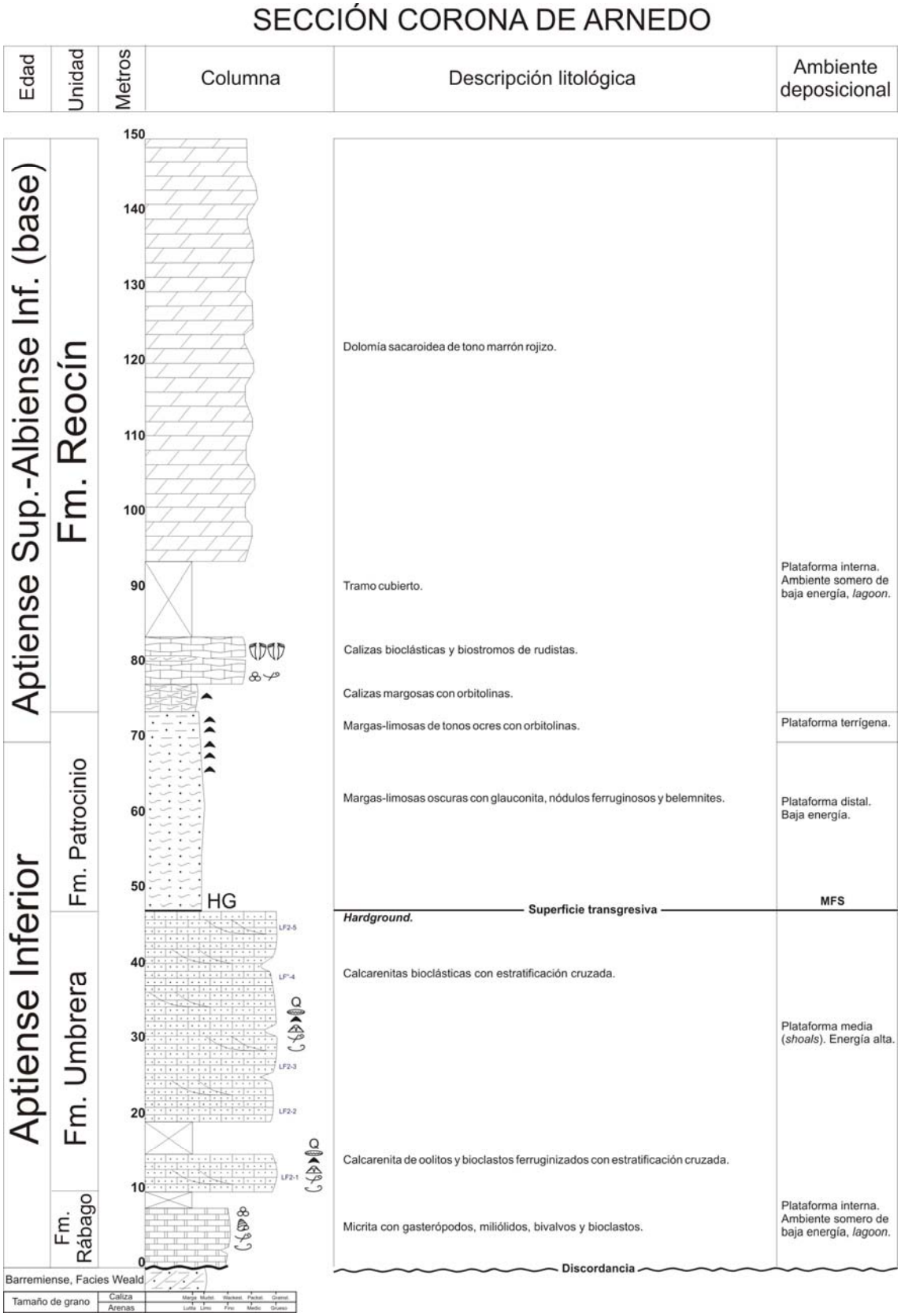

Figura 3.12.- Sección sintética de Corona de Arnedo (área de La Florida).

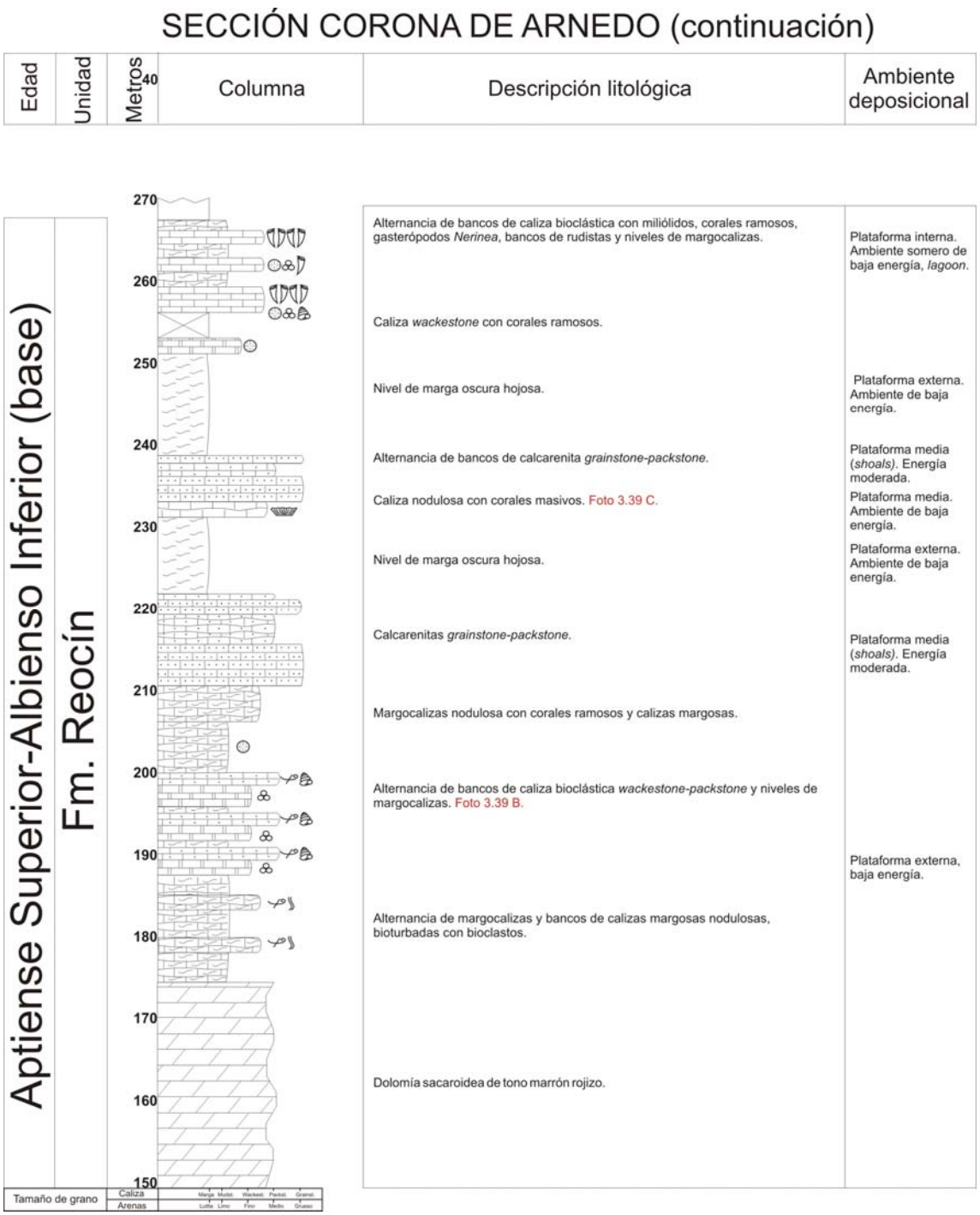

Figura 3.12.- Sección sintética de Corona de Arnedo (área de La Florida). Continuación.

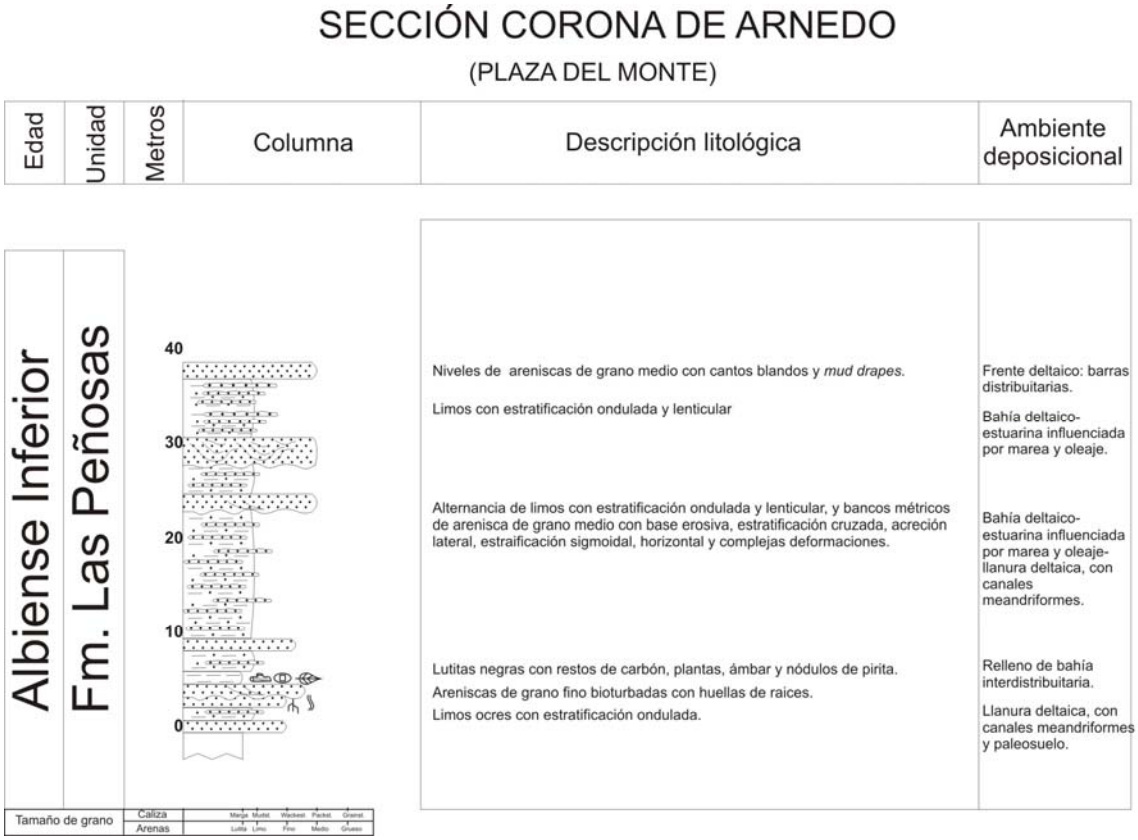

Figura 3.12.- Sección sintética de Corona de Arnedo, Plaza del Monte (área de La Florida). Continuación.

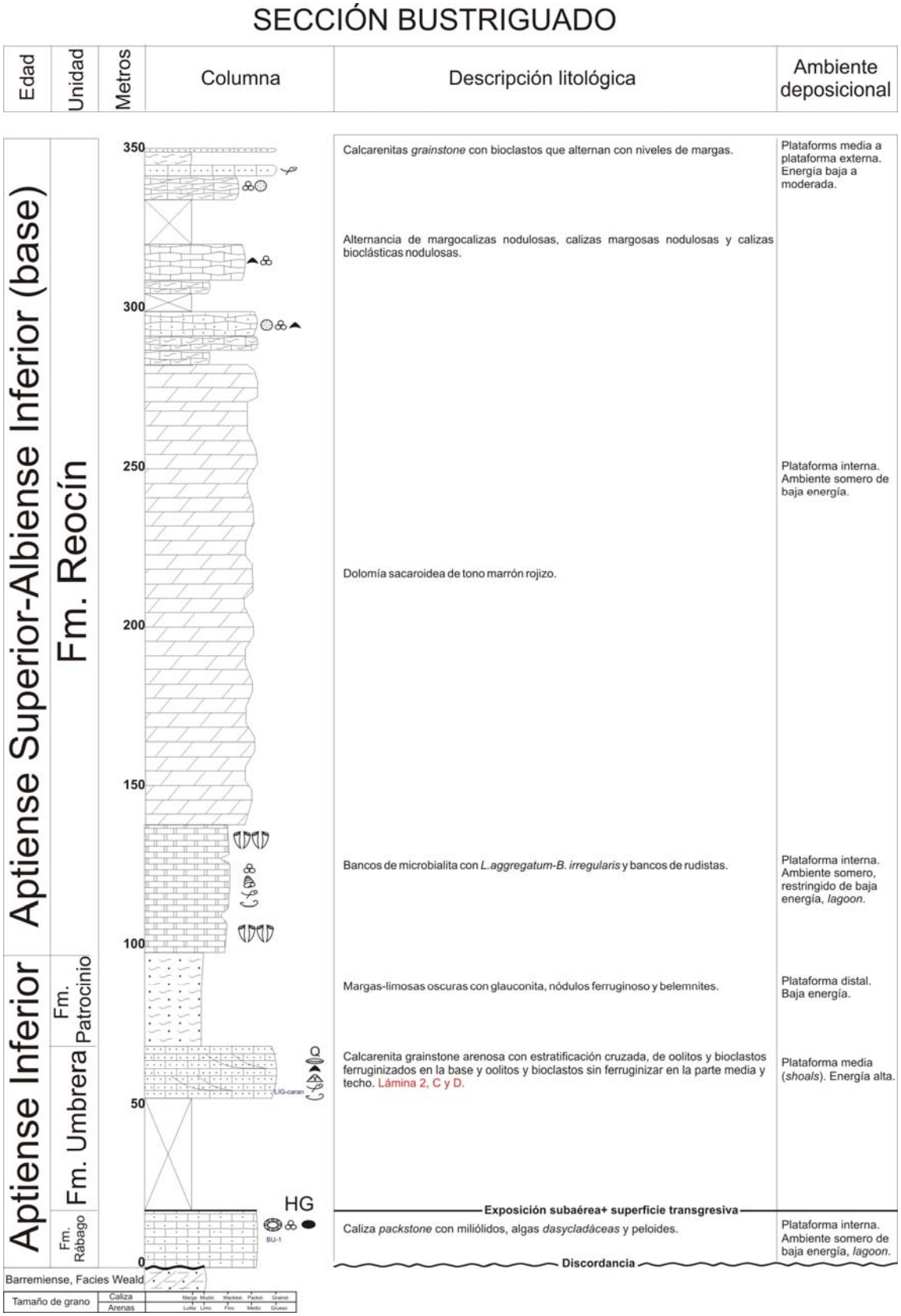

Figura 3.13.- Sección sintética de Bustriaguado (área de La Florida).

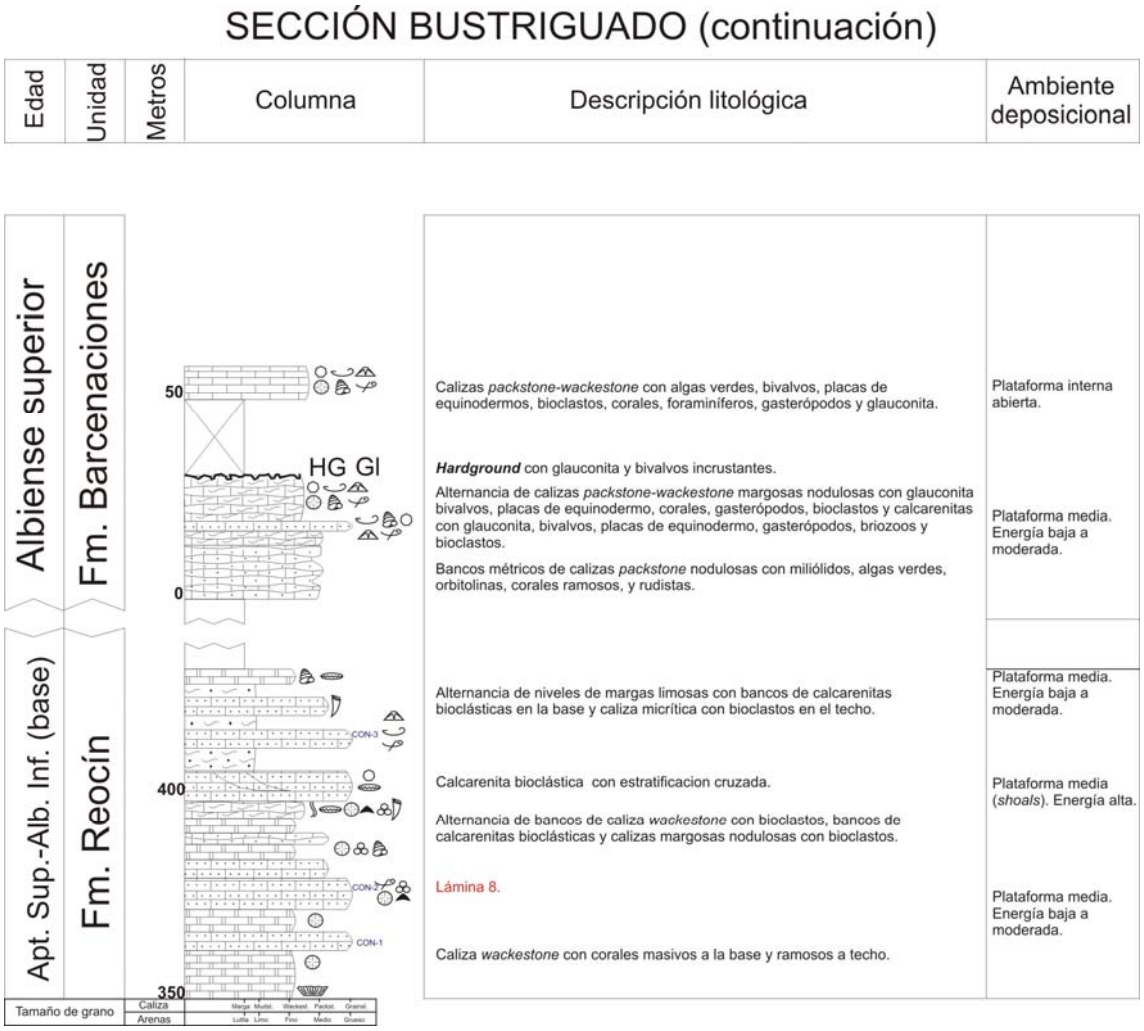

Figura 3.13.- Sección sintética de Bustriaguado (área de La Florida). Continuación.

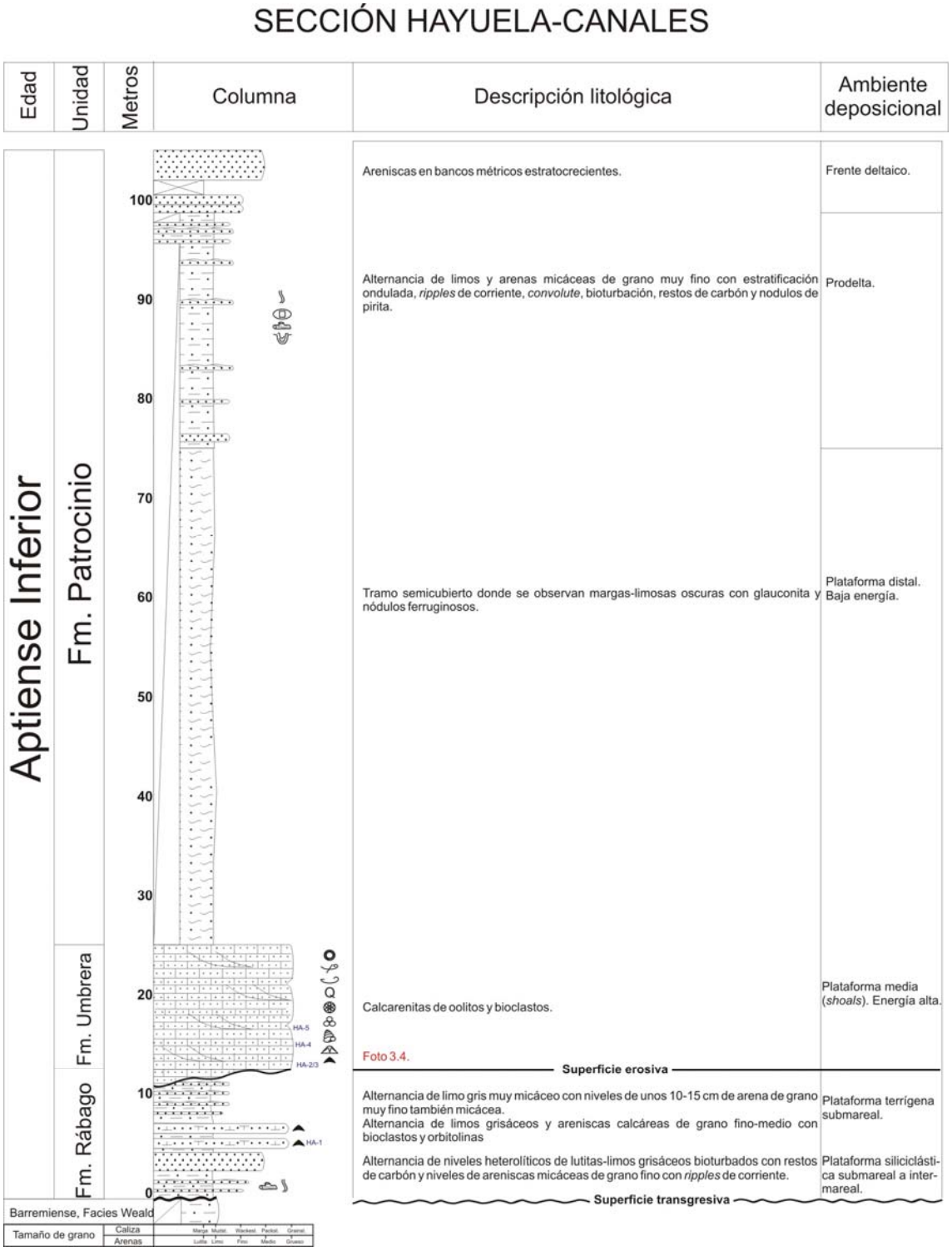

Figura 3.14.- Sección sintética de Hayuela-Canales (área del sinclinal de Santillana).

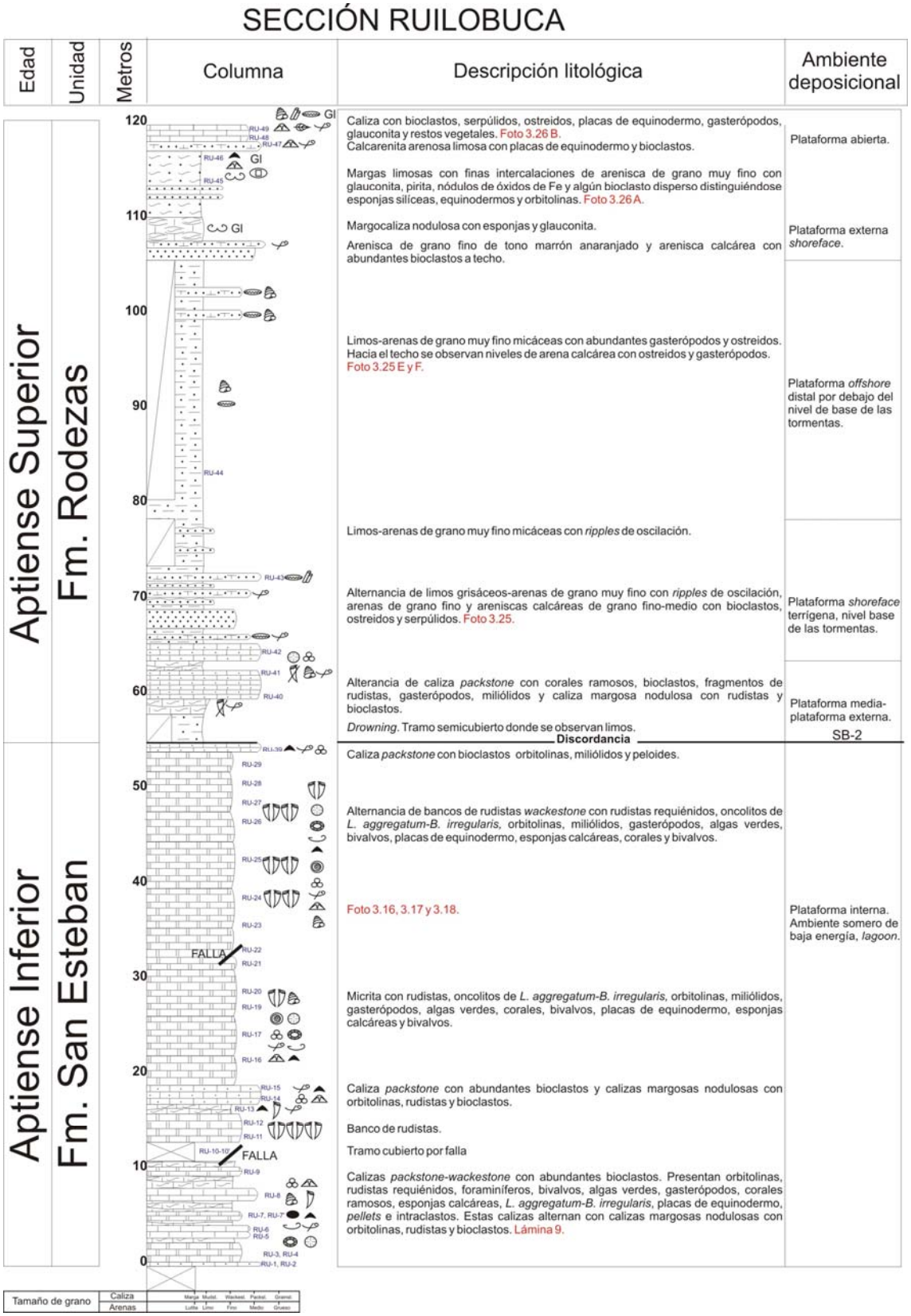

Figura 3.15.- Sección sintética de Ruilobuca (área del sinclinal de Santillana).

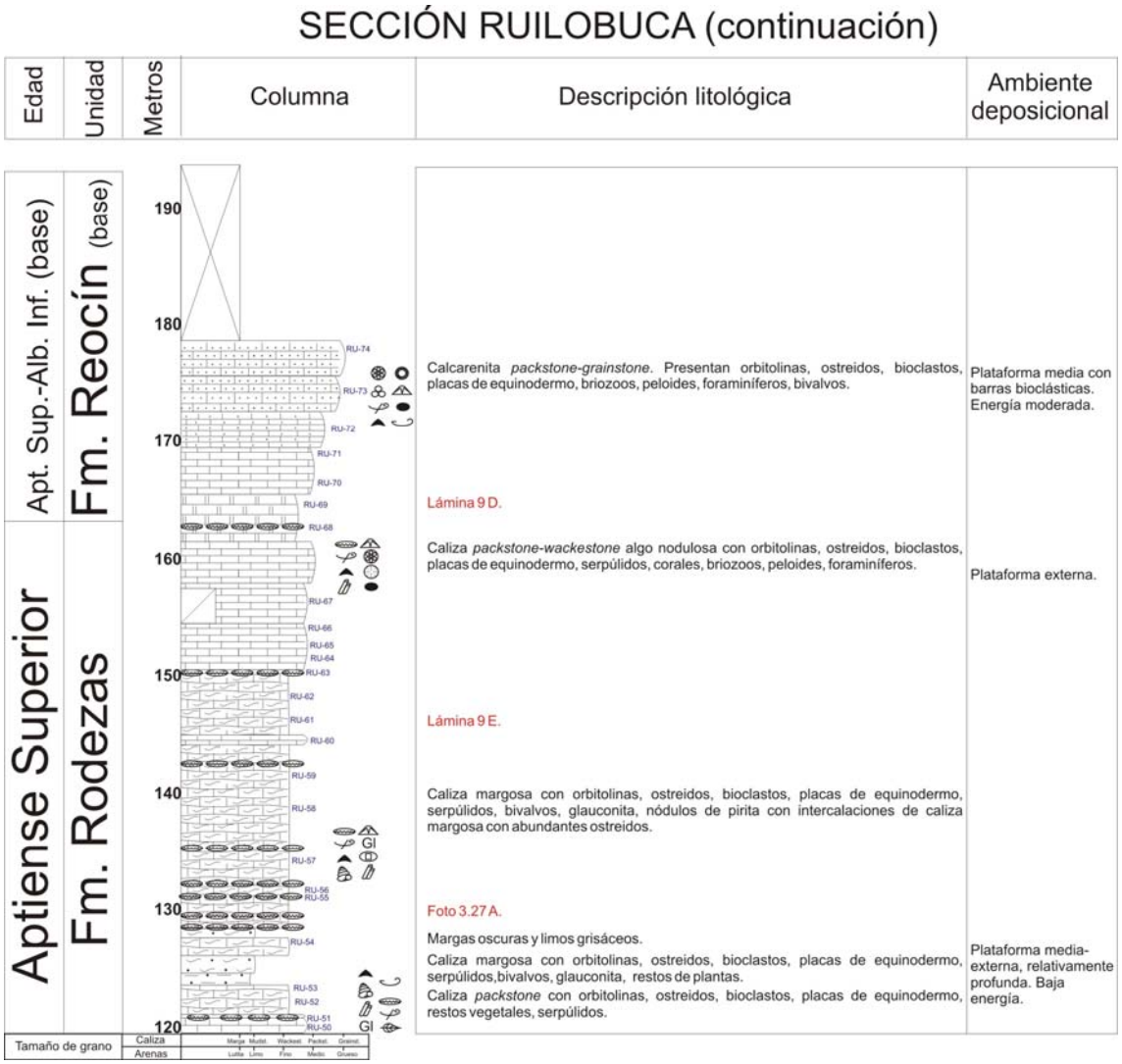

Figura 3.15.- Sección sintética de Ruilobuca (área del sinclinal de Santillana). Continuación.

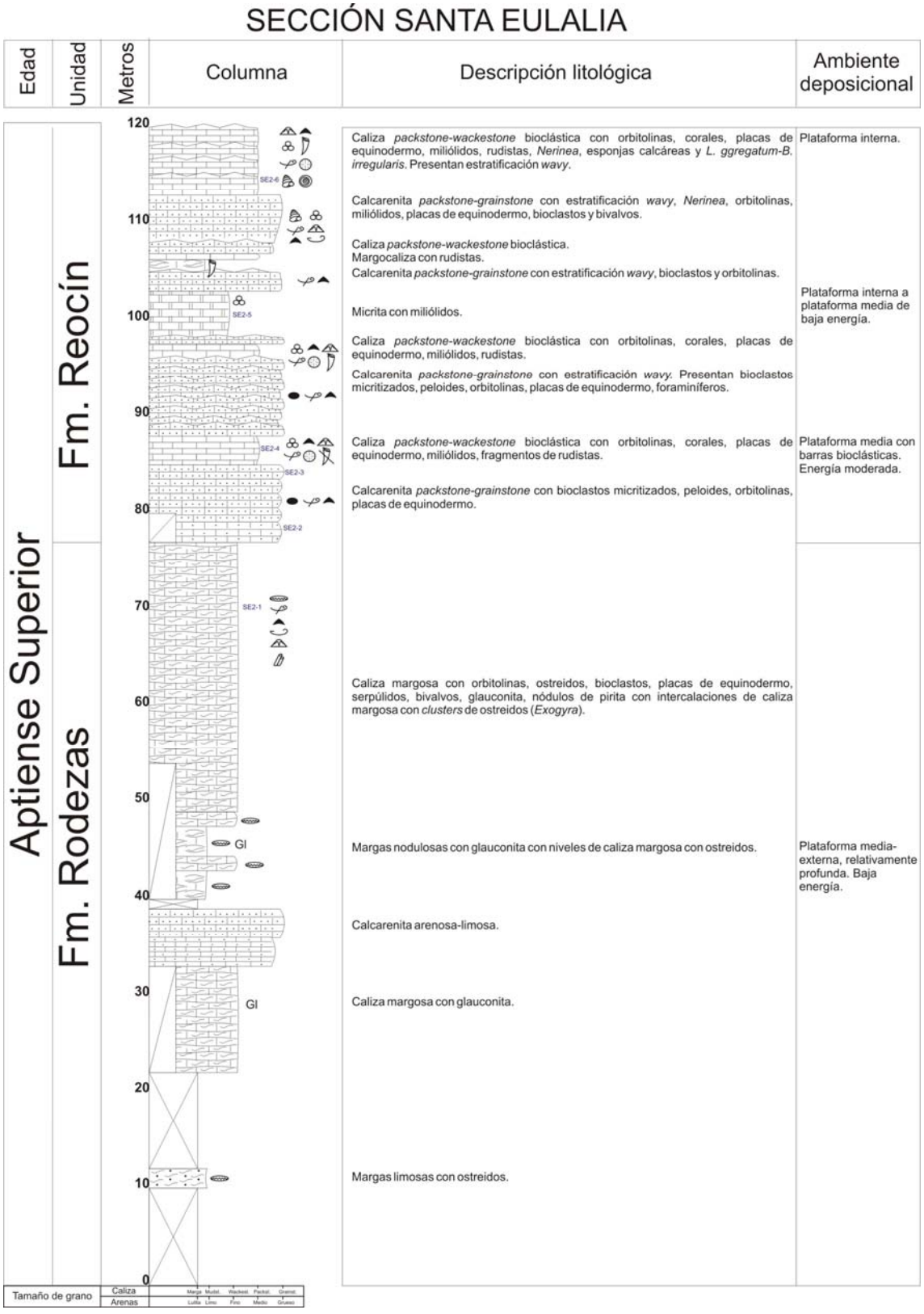

Figura 3.16.- Sección sintética de Santa Eulalia (área del sinclinal de Santillana).

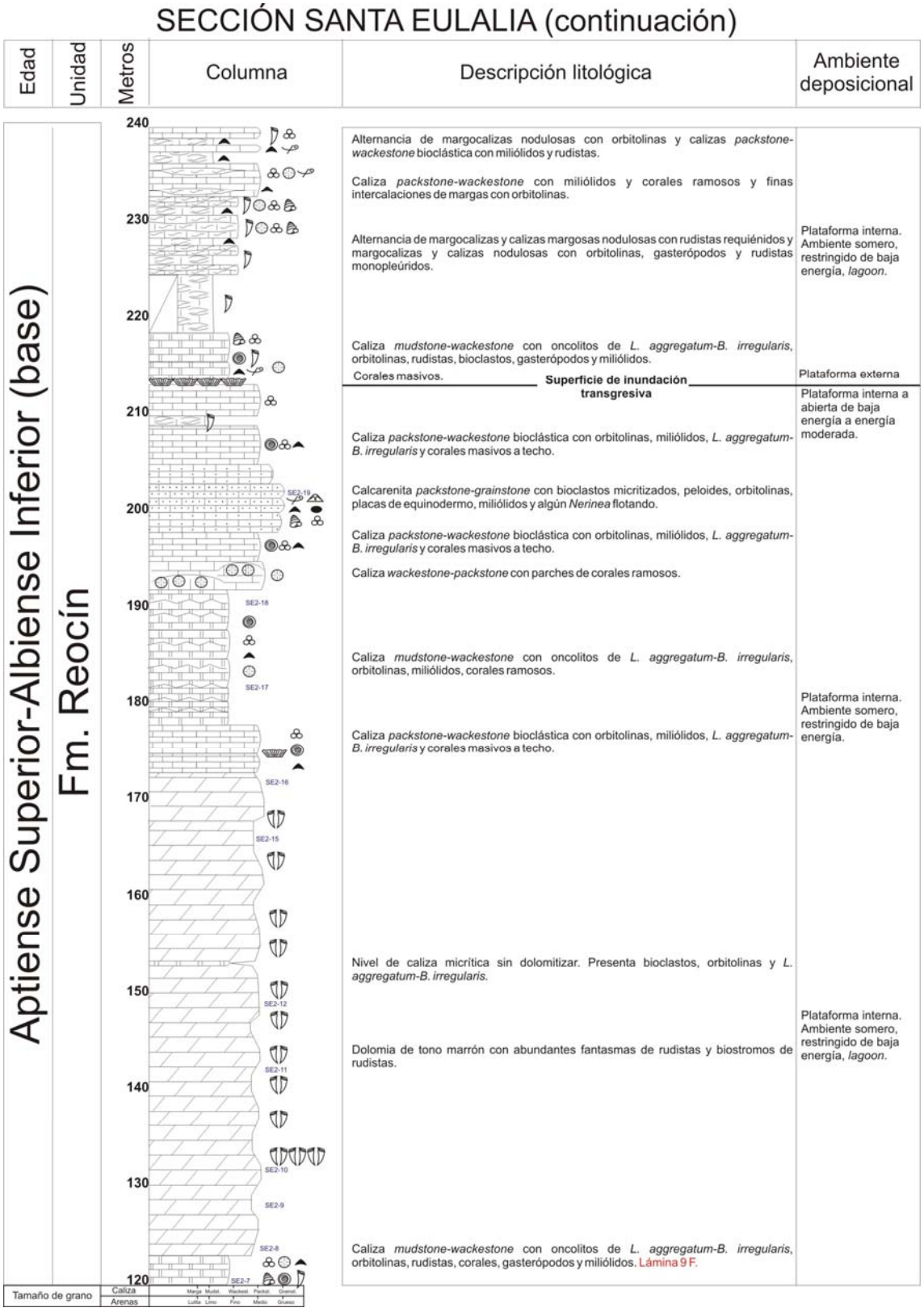

Figura 3.16.- Sección sintética de Santa Eulalia (área del sinclinal de Santillana). Continuación.

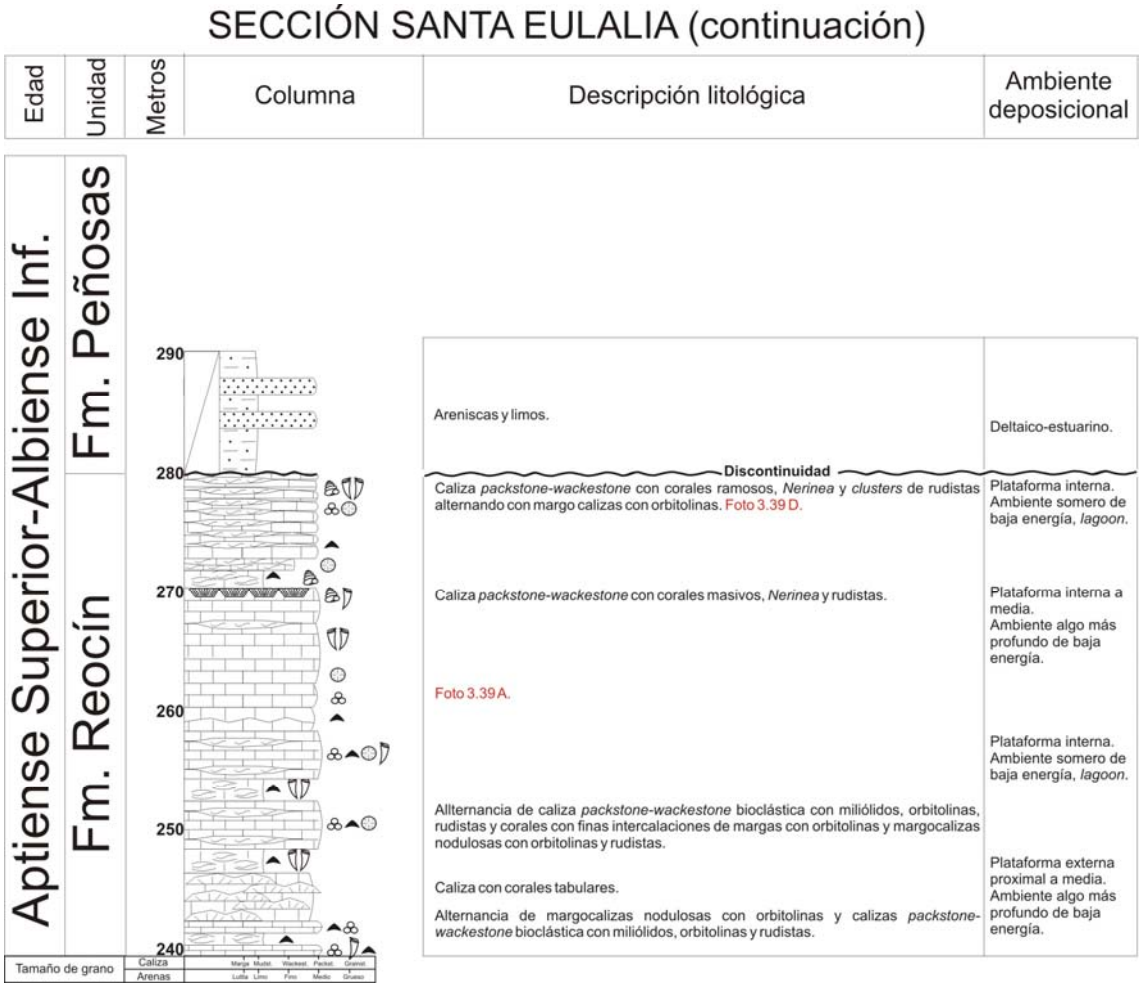

Figura 3.16.- Sección sintética de Santa Eulalia (área del sinclinal de Santillana). Continuación.

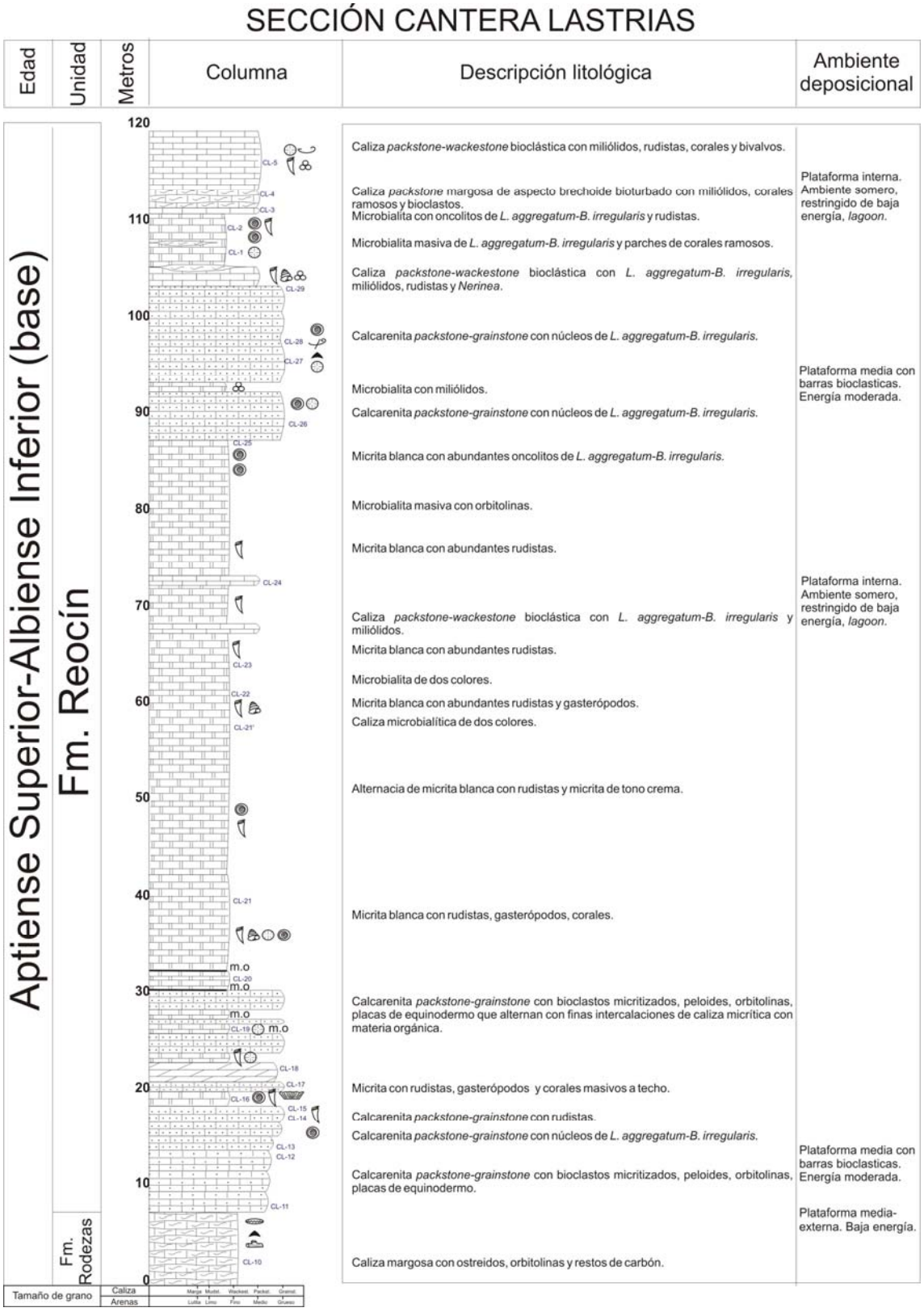

Figura 3.17.- Sección sintética de Cantera Lastrías (área del sinclinal de Santillana). Continuación.

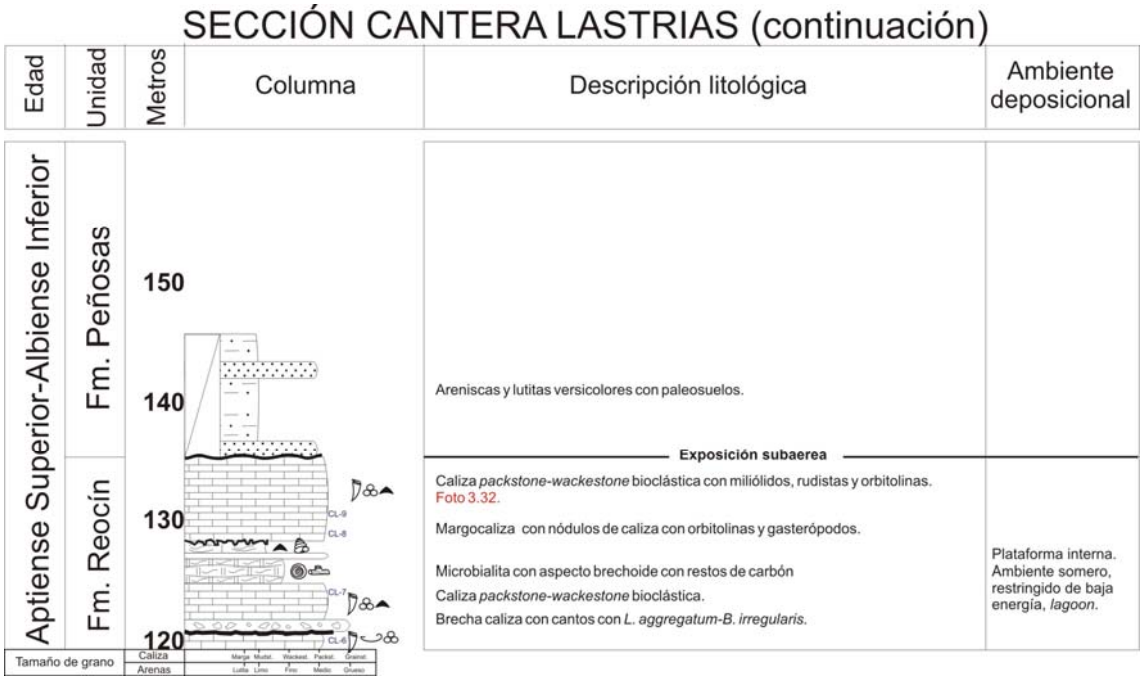

Figura 3.17.- Sección sintética de Cantera Lastrías (área del sinclinal de Santillana). Continuación.

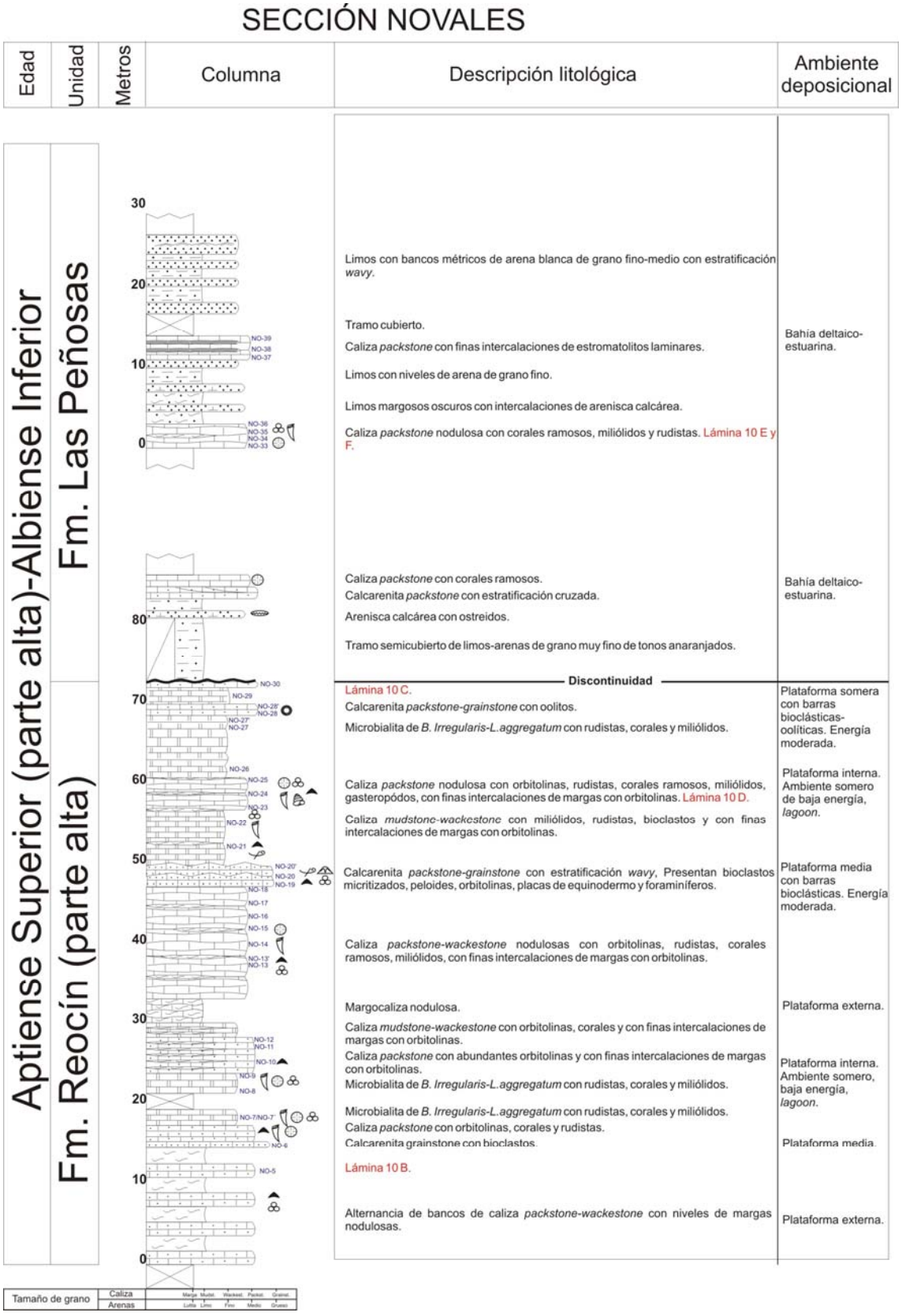

Figura 3.18.- Sección sintética de Novales (área del sinclinal de Santillana).

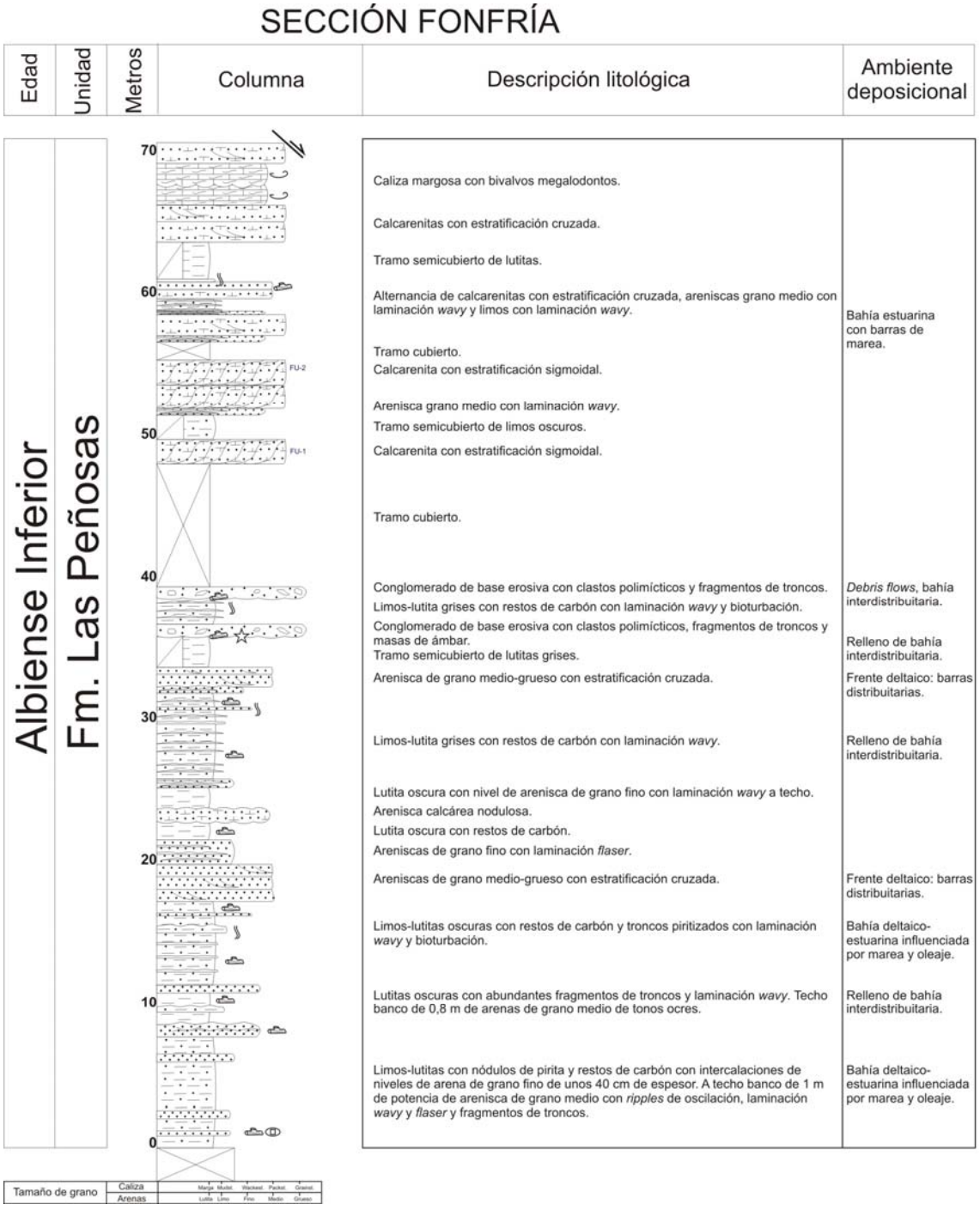

Figura 3.19.- Sección sintética de Fonfría (área del sinclinal de Santillana).

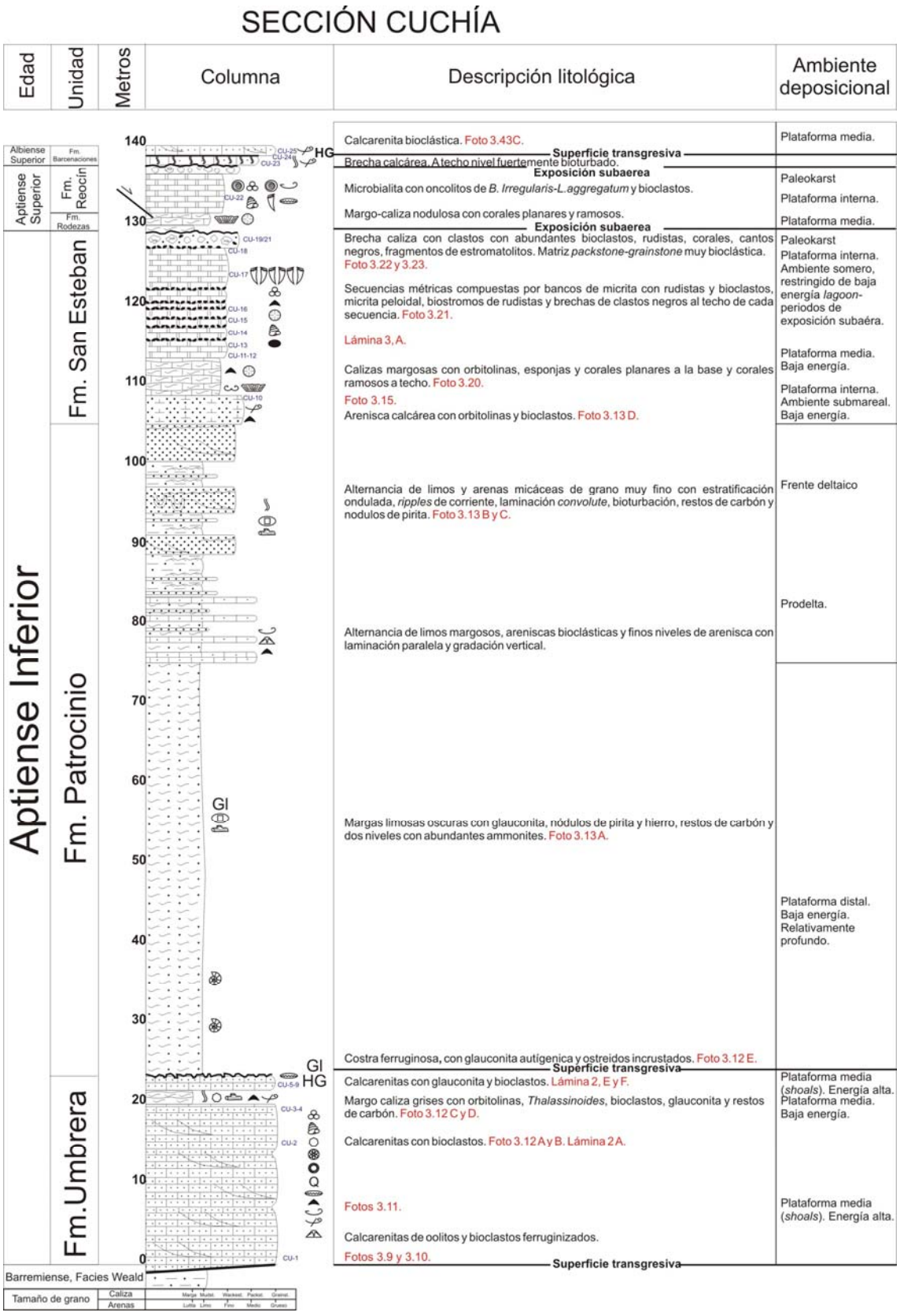

Figura 3.20.- Sección sintética de Cuchía (área de Cuchía).

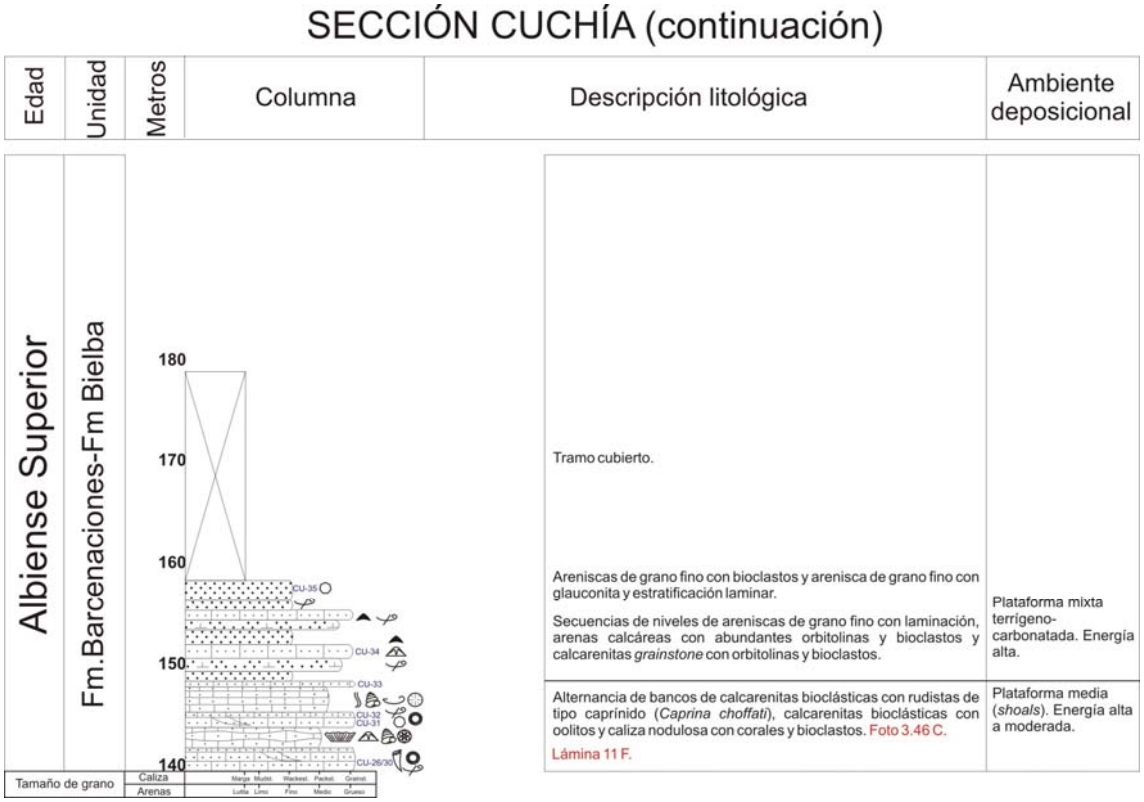

Figura 3.20.- Sección sintética de Cuchía (área de Cuchía). Continuación.

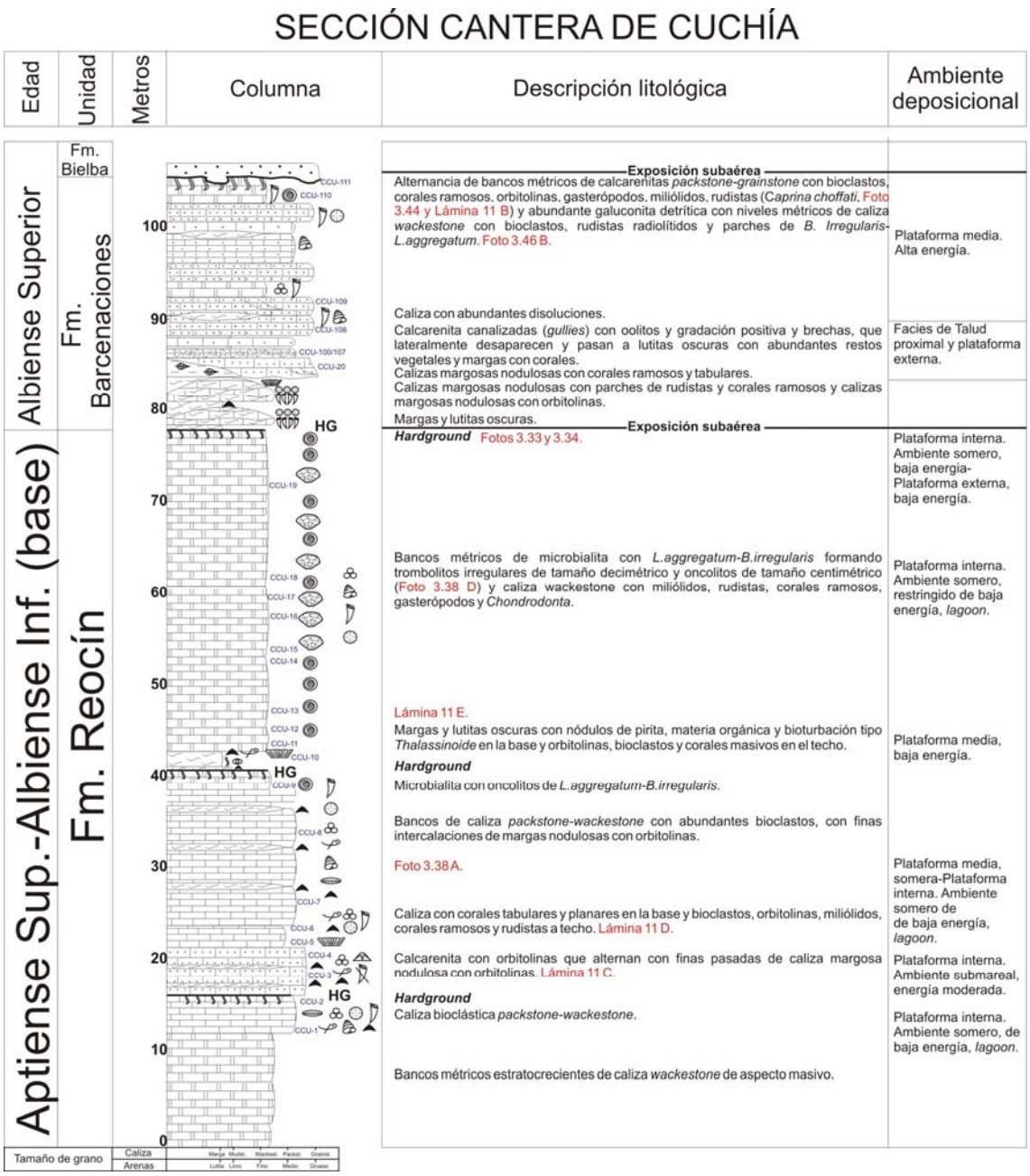

Figura 3.21.- Sección sintética de Cantera de Cuchía (área de Cuchía).

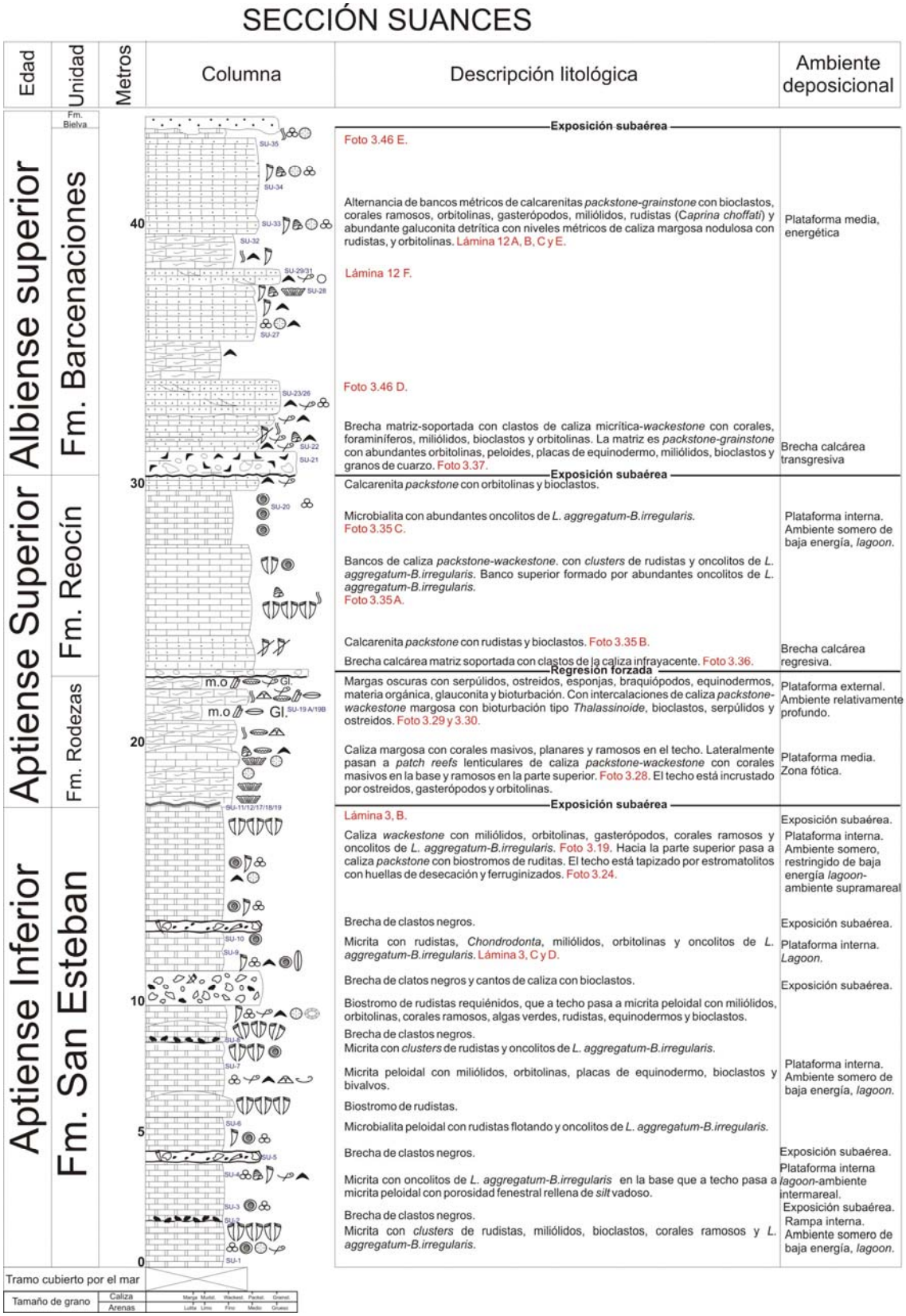

Figura 3.22.- Sección sintética de Suances (área de Cuchía).

3.4.- DISCUSIÓN: SECUENCIAS DEPOSICIONALES

Se han distinguido 5 secuencias de depósito (SD1 a SD5), para el intervalo Aptiense Inferior-Albiense Inferior del noroeste de Cantabria. La organización en secuencias fundamentales de los sistemas sedimentarios estudiados se ha realizado siguiendo tendencias de facies organizadas en secuencias transgresivo-regresivas (T-R). La caracterización de secuencias T-R constituye en este caso la opción más adecuada para subdividir la sucesión estudiada, dada la dificultad existente en el reconocimiento de cortejos sedimentarios de los esquemas basados en estratigrafía secuencial clásica. En este caso las secuencias se subdividen en dos tramos principales reconocibles a escala de afloramiento: una parte basal transgresiva y una parte superior regresiva. Siguiendo los criterios de Embry (2002), las secuencias deposicionales se han definido a partir de cuatro tipos de límites: 1) superficies de exposición subaérea; 2) superficies de *ravinement*; 3) superficies de regresión máxima, que marcan el cambio de tendencia de progradante a retrogradante y 4) superficies de inundación máxima, que marcan el pico de la transgresión.

Si bien una superficie de exposición subaérea es evidencia de un límite de secuencia elemental, en algunas ocasiones este tipo de discontinuidades no han podido arrastrarse lateralmente más allá del afloramiento en el que aparecen y por ello no se ha individualizado como límites de una correspondiente secuencia de depósito.
Siguiendo este criterio, se han distinguido en el área de estudio 5 secuencias deposicionales principales (SD1 a SD5, ver Figura 3.23). A continuación se describen las secuencias de depósito en orden correlativo, describiendo las discontinuidades que las limitan, las unidades litoestratigráficas que las componen y su evolución interna junto con los rasgos sedimentarios principales.

Secuencia Deposicional 1 (SD1)

Litoestratigrafía

Esta secuencia de depósito comprende la Formación Rábago de edad Aptiense Inferior, concretamente Bedouliense inferior.

Límites de secuencia

Límite inferior: base de la Fm. Rábago, límite superior: techo de la Fm. Rábago. La base de esta secuencia (LS0) es una superficie de transgresión rápida sobre materiales continentales del Weald o sobre materiales del basamento (Triásico). El techo de esta secuencia (LS1), está marcado por la discontinuidad de techo de la Fm. Rábago. Esto es, según las zonas, una superficie de truncamiento erosivo que bisela estratos del techo de la Fm. Rábago erosionando y formando paleorelieves laxos de hasta 2 m en algunos puntos (área del sinclinal de Santillana); o bien está representado por una superficie de disolución con formación de cavidades de tamaño decimétrico y brechas, interpretada como una superficie de exposición subaérea (área oeste de La Florida).

Evolución vertical de facies y ambientes sedimentarios

La secuencia presenta la evolución vertical de los siguientes ambientes deposicionales y facies sedimentarias: 1) estadio 1: plataforma siliciclástica submareal a intermareal. Formada por una alternancia de areniscas micáceas de grano fino-medio con estratificación cruzada, lutitas carbonosas y limos con laminación lenticular*, flaser* y *ripples* de corriente, representando la primera implantación de la sedimentación marina somera en el área de estudio (transgresión del Aptiense Inferior); 2) estadio 2: plataforma abierta mixta submareal terrígeno carbonatada. Formada por arenas calcáreas con laminación ondulada y ocasionalmente *ripples* de oscilación que alternan con niveles de lutitas aleuríticas, calizas *packstone-grainstone* y margas con orbitolinas; y 3) estadio 3: plataforma carbonatada interna somera restringuida. Formada por una alternancia de margas con orbitolinas, calizas margosas nodulosas y calizas *grainstone-packstone* en la parte inferior y calizas *wackestone-mudstone* con porosidad fenestral, corales, gasterópodos y rudistas en la parte superior. Este sistema culmina con el límite LS1.

Interpretación

Esta secuencia representa un ciclo transgresivo-regresivo, en el que el límite inferior de la secuencia viene marcado por una superficie transgresiva (LS0). El estadio 1 representa las facies transgresivas de la base del ciclo, con la implantación de un ambiente terrígeno transicional a marino somero. El paso al estadio 2, indicaría una

disminución gradual del aporte de terrígenos al medio como consecuencia de un aumento relativo del nivel del mar durante el máximo transgresivo, resultando en la instauración de ambientes de *offshore* y de plataforma carbonatada abierta (máxima inundación). La parte superior regresiva del ciclo está representada por la instauración de ambientes de plataforma carbonatada somera restringida (Estadio 3). Finalmente, la presencia en el techo del estadio 3, bien de una superficie de truncamiento erosivo (área del sinclinal de Santillana), o bien de una superficie de exposición subaérea (aréa de La Florida) indicaría una caída relativa del nivel del mar con erosión de paleorelieves y paleokarst. Esta secuencia solo tiene representación en las áreas del sinclinal de Santillana y de La Florida, no apareciendo sus equivalentes en el área de Cuchía (bien por falta de depósito o bien por erosión). Las potencias sedimentarias, de los estadios 1 y 2 fueron relativamente constantes por lo que se deduce un periodo tectónico relativamente tranquilo durante su desarrollo. Sin embargo, al final del estadio 3 se deduce una actividad tectónica de fallas extensivas (Bustriguado y Santibañez), causando un pulso de la actividad tectónica, que produjo una elevación y exposición subaérea de la plataforma. Este pulso tectónico con elevación de bloques y exposición subaérea pudo ser responsable de su completa erosión en el área de Cuchía.

Secuencia Deposicional 2 (SD2)

Litoestratigrafía

La secuencia de depósito 2 abarca las Formaciones Umbrera, Patrocinio y San Esteban, comprendiendo una edad de Bedouliense inferior-Bedouliense superior.

Límites de secuencia

El límite inferior de esta secuencia corresponde con el techo de la Fm. Rábago y el límite superior de la secuencia SD1 (LS1). En el área de La Florida el contacto de los depósitos de la base del ciclo SD2 con el límite inferior de secuencia está definido por una relación de *onlap* sobre la superficie de disolución por exposición subaérea. La superficie aparece tapizada por una costra ferruginosa con tapices microbianos y con incrustación de serpúlidos y foraminíferos, desarrollada durante la subsiguiente fase de inundación marina (Najarro y Rosales, 2008a). En el área del sinclinal de Santillana el límite inferior de secuencia (LS1) está representado por una superficie erosiva, mientras

que en el área de Cuchía, el límite inferior viene marcado por una superficie de inundación, neta, ligeramente erosiva y bioturbada, sobre lutitas con paleosuelos de las facies wealdenses infrayacentes.

El límite superior (LS2) está al techo de la Fm. San Esteban. En el área del sinclinal de Santillana, este límite de secuencia está representado por un diastema a techo de un nivel calizo fuertemente bioturbado, mientras que en el área de Cuchía este límite está formado por un nivel de brechas con cantos calcáreos interpretado como una superficie mayor de exposición subaérea. En el área de La Florida, el límite superior está marcado por una laguna estratigráfica a techo de la Fm Patrocionio (discutido en el capítulo anterior), faltando la parte regresiva del ciclo y estando representada solo la parte transgresiva del ciclo T-R.

Evolución vertical de facies y ambientes sedimentarios

La evolución vertical de facies y ambientes sedimentarios de esta secuencia comprende 4 estadios evolutivos. 1) El estadio 1, coincide con el depósito de la Fm. Umbrera y está formado por barras decimétricas a métricas de calcarenitas *grainstone-packstone* de arenas oolítico-bioclásticas con estratificación cruzada. Se interpretan como depósitos de bajíos o *shoals* en un medio de alta energía, localizado en la parte interna a media de una rampa carbonatada. El techo del estadio 1 viene marcado bien por un cambio brusco en el tipo de sedimentación (áreas de La Florida y sinclinal de Santillana) o bien por una superficie bioturbada con glauconita e incrustada por ostreidos (área de Cuchía). 2) El estadio 2, que comprende el tramo inferior de la Fm. Patrocinio, se caracteriza por el depósito de lutitas margosas oscuras con nódulos de siderita, pirita, ammonites y restos de materia orgánica. Hacia la parte alta, el contenido en limos aumenta apareciendo niveles bioclásticos de base erosiva (tempestitas) con fragmentos de braquiópodos, equinodermos, bivalvos, orbitolinas y restos carbonosos de troncos. Este tipo de depósito se formó en un ambiente marino abierto, relativamente profundo y de baja energía, con condiciones de fondo deficientes en oxígeno (Najarro *et al.*, 2011b; Quijano *et al.*, 2012). 3) El paso al estadio 3, que abarca al tramo superior de la Fm. Patrocinio, es gradual y se caracteriza por una secuencia estrato- y grano-creciente de facies heterolíticas de alternancia de lutitas carbonosas y micáceas, limos y finalmente areniscas con estratificación cruzada y laminación *convolute*, depositadas por progradación de un ambiente deltaico. 4) A base del estadio 4 disminuye el

contenido en terrígenos, depositándose bien calizas y margocalizas con abundantes orbitolinas (área del sinclinal de Santillana) o bien areniscas calcáreas con gran cantidad de orbitolinas (área de Cuchía), nivel sobre el que se apoyan las calizas con corales y rudistas pertenecientes ya al estadio 4. Así pues el paso al estadio 4 viene marcado por un cambio transicional pero rápido de litología y de ambiente de sedimentación pasando de un ambiente de frente deltaico a un ambiente de plataforma carbonatada somera, representado por la Fm. San Esteban. Tanto el estadio 3 como el 4 no están registrados en el área de La Florida (por la presencia de una laguna estratigráfica). En el área del sinclinal de Santillana el cuarto estadio se caracteriza por el depósito de bancos de calizas y margocalizas con orbitolinas, seguido por una sucesión de bancos de calizas claras con requiénidos y *L. aggregatum-B. irregularis*. Aquí el límite de secuencia 2 (LS2) lo constituye un nivel de calcarenita, algo ferruginizado, con intensa bioturbación y colonización de ostreidos, que se interpreta como un diastema. En el área de Cuchía el estadio 4 comienza con un nivel de calcarenitas con abundantes orbitolinas, seguido de margas nodulosas con bioclastos, orbitolinas, esponjas y corales planares y masivos, que gradualmente pasan a bancos claros de caliza con pequeños requiénidos. Estos últimos paquetes aparecen organizados en ciclos métricos de somerización (de 1 a 3 metros de potencia) que culminan con niveles decimétricos de brechificación con cantos calcareos negros, interpretados como superficies locales de exposición subaérea. Aquí el techo de este estadio, que equivale al límite de secuencia 2 (LS2) viene marcado bien por una superficie irregular tapizada por un nivel de unos 50 cm de brechas con cantos calcáreos, entre los que se incluyen cantos de calizas de estromatolitos laminados y cantos negros (afloramiento de Punta de Afuera), o bien por un nivel decimétrico de estromatolitos laminados con huellas de desecación y parcialmente brechificado (afloramiento de Punta del Dichoso).

Interpretación

Esta secuencia representa un ciclo transgresivo-regresivo mayor, que incluye dos secuencias menores. El estadio 1 marca el inicio de la nueva transgresión marina. Constituye la parte basal (transgresiva) del primer ciclo de la secuencia, con el depósito de bajíos o *shoals* calcareniticos en la parte interna a media de una rampa carbonatada. Hacia el final de este estadio, se produce una profundización rápida del medio sedimentario, dando lugar a una superficie bioturbada con glauconita e incrustada por ostreidos que indica un periodo de no-depósito o baja tasa de sedimentación

(*firmground* incipiente), de modo que los bajíos fueron abandonados y colonizados por organismos cavadores. Estos fueron posteriormente cubiertos por lutitas margosas oscuras durante el estadio 2, según avanzó la transgresión marina. De esta manera, el depósito de estas lutitas margosas de la Fm. Patrocinio refleja el periodo de máxima transgresión o inundación del ciclo principal T-R (Figura 3.23), posiblemente debido a la acción conjunta de una rápida subida relativa del nivel del mar y a un incremento en el aporte de terrígenos finos desde el continente en relación a unas condiciones climáticas más húmedas (Najarro et al., 2011a, 2011b). A partir del estadio 3 se produce una somerización progresiva del medio de depósito y el comienzo de una regresión rápida, con progradación localmente de un sistema deltaico (parte regresiva del primer ciclo). Finalmente el estadio 4, que tuvo lugar durante el máximo regresivo de la secuencia principal, constituye internamente un ciclo transgresivo-regresivo menor. La parte transgresiva del ciclo menor está constituida por margas y arenas orbitolínicas (a techo del sistema deltaico inferior) mientras que la parte regresiva del ciclo está marcada por la instauración de la plataforma carbonatada somera y protegida, en la que su evolución vertical indica la recuperación rápida de la producción carbonatada debido a la somerización del medio y a una drástica disminución del aporte de partículas terrígenas. Durante su desarrollo, los carbonatos someros progradaron y colmataron el espacio de acomodación (bien por causas autocíclicas, alocíclicas o cambios climáticos globales) hasta, al menos localmente, alcanzar el nivel del mar, desarrollando ciclos de somerización que culminaron con la exposición subaérea de la plataforma.

Secuencia Deposicional 3 (SD3)

Litoestratigrafía

Esta secuencia de depósito comprende la Formación Rodezas y la mitad inferior de la Formación Reocín. Su edad abarca desde el techo del Bedouliense superior hasta el Gargasiense inferior.

Límites de secuencia

El límite inferior de esta secuencia (LS2) coincide con el techo de la Formación San Esteban. En el área del sinclinal de Santillana se caracteriza por un cambio rápido

en el tipo de sedimentación que es reemplazada por un sistema terrígeno, mientras que en el área de Cuchía viene marcado por un periodo de exposición subaérea.

El límite superior de la secuencia 3 (LS3), en la zona de estudio más occidental (secciones de río Nansa y Rábago), está marcado por un nivel de brechas intraformacionales cuyo origen se interpreta con una nueva fase de exposición subaérea de la plataforma y posterior retrabajamiento erosivo durante la siguiente transgresión marina. Este nivel incorpora a la base de la secuencia siguiente, intraclastos de tamaño decimétrico de calizas con rudistas y gasterópodos y cantos negros de naturaleza micrítica y tamaño centimétrico. La matriz entre los clastos está compuesta por margas con orbitolinas y por calcarenitas *packstone* con bioclastos. En la zona de umbral del paleoalto de Suances-Cuchía el límite de secuencia es una superficie erosiva y de remoción. Sobre la superficie de erosión se observa un tramo irregular de hasta 0,3 m de parabrecha calcárea que incorpora cantos de los niveles infrayacentes en una matriz bioclástica, interpretada como una superficie de regresión forzada. En el resto de las zonas, el límite de secuencia 3 se ha establecido en una superficie irregular bioturbada-nodulizada, tapizada por un nivel decimétrico a métrico de limos-arenas finas o margas con abundantes restos vegetales, que representa un episodio de rápida inundación de la plataforma.

Evolución vertical de facies y ambientes sedimentarios

A lo largo de esta secuencia se han distinguido 5 estadios evolutivos, estando formados de manera consecutiva por los siguientes ambientes deposicionales y litologías: Estadio 1) ambiente de plataforma externa-media, compuesto por limos y calizas *packstone* con bioclastos, fragmentos de rudistas, corales ramosos y gasterópodos, que alternan con finos niveles de caliza margosa y nodulosa con bioclastos y corales. Estadio 2): ambiente de plataforma terrígena que varía desde primero *shoreface*, por encima del nivel de base de tormentas, a *offshore* por debajo del nivel base de tormentas. Esta formado por intercalaciones de niveles de lutitas marrones-grisáceas con bioclastos, niveles de calcarenitas con pequeños ostreidos, gasterópodos y bioclastos, bancos métricos de areniscas micáceas anaranjadas de grano fino-medio con estratificación cruzada, areniscas calcáreas con gran cantidad de bioclastos y niveles de limo-arenisca de grano muy fino con *ripples* de oscilación, laminación *hummocky* y restos de carbón, con un aumento de los niveles lutíticos hacia la parte alta del estadio. Estadio 3) ambiente de plataforma externa-media, compuesta

por calizas limosas-arenosas con abundantes gasterópodos y ostreidos, con calcarenitas bioclásticas de grano medio al techo. Estadio 4) ambiente de plataforma abierta, formada por margocalizas nodulosas con glauconita y restos vegetales, margas oscuras con finas pasadas de arenisca de grano muy fino y calizas margosas y margas con orbitolinas, braquiópodos, ostreidos en posición de vida bien aislados o formando bancos monoespecíficos de *Exogyra latissima* y/o *Plicatula placunea*, ammonites y belemnites. Estos depósitos se localizan solo en el sector central y oriental del área de estudio y gradan lateralmente hacia el sector occidental (área de La Florida) a calizas con rudistas y corales de plataforma somera. Estadio 5 ambiente de plataforma carbonatada interna a *lagoon*. Está formado principalmente por alternancia de bancos métricos de calizas *wackestone-packstone* con miliólidos, orbitolinas, gasterópodos y rudistas, y por paquetes decimétricos a métricos de caliza micrítica con *B. irregularis*-*L. aggregatum* formando masas irregulares o *lumps*. En su conjunto, este último estadio presenta un crecimiento progradacional en la base, seguido de una rápida agradación hacia el techo. Sus espesores varían entre 26 m en las zonas más occidentales (sección de río Nansa) a 180–90 m de potencia en las zonas más orientales (secciones de Bustriguado, Santa Eulalia).

Interpretación

Esta secuencia representa de nuevo otro ciclo transgresivo-regresivo. Así el estadio 1 marcaría la inundación rápida del medio y comienzo de la transgresión después del periodo de exposición subaérea marcada por el límite de secuencia 2. El estadio 2 indicarían la implantación de una plataforma terrígena con una profundización gradual del medio indicada por la sedimentación de materiales depositados primero en un medio de *shoreface* por encima del nivel de base de las tormentas y posteriormente, en un medio de *offshore* por debajo del nivel base de tormentas que representaría la máxima inundación. Los estadios 3, 4 y 5 representarían la parte regresiva del ciclo con implantación gradual de un nuevo sistema de plataforma carbonatada., desarrollándose primero ambientes de plataforma abierta seguido de ambientes de plataforma somera. Finalmente, el depósito tanto de las brechas intraformacionales, como de los limos-arenas finas con abundantes restos vegetales a techo de este episodio, está relacionado con una nueva fase de caída relativa del nivel del mar con exposición subaérea al menos a nivel local. Los cambios eustáticos ocurridos durante el Aptiense Inferior (Inmenhauser, 2005), junto con la actividad tectónica distensiva de la falla de

Bustriguado (Najarro *et al*., 2007; 2009), cuya actividad creo en el área de La Florida un pliegue de propagación de falla, se interpretan como los responsables del desarrollo de esta secuencia y su límite superior con exposición subaérea en el área de La Florida.

Secuencia Deposicional 4 (SD4)

Litoestratigrafía

Esta secuencia de depósito comprende el tramo superior de la Formación Reocín, presentando una edad comprendida entre el Gargasiense superior hasta la base del Albiense Inferior.

Límites de secuencia

El límite inferior (LS3) se caracteriza por el nivel de brechas intraformacionales (secciones de río Nansa y Rábago), por la superficie erosiva y de remoción de regresión forzada (paleoalto de Suances-Cuchía) o por el nivel bioturbado cubierto de limos-arenas con restos vegetales y margas (resto de las secciones) del techo de la secuencia anterior.

En el área de La Florida, el límite de secuencia superior (LS4) es una superficie con rasgos microscópicos de disolución, que se intrepretan como de exposición subaérea, sobre la que se deposita una unidad mixta de transición a depósitos deltaicos. En el área del sinclinal de Santillana el límite de secuencia LS4 es neto y se caracteriza por desarrollo de arcillas verde-rojas con rasgos edáficos sobre calizas de rudistas, indicando exposición subaérea y un diastema. Finalmente, en el área de Cuchía, el límite de secuencia superior viene marcado bien por un nivel de brechificación bajo una superficie irregular tapizada por un nivel decimétrico de areniscas y limos, que incluyen clastos de la serie infrayacente (sección cantera de Cuchía), o bien por un nivel irregular decimétrico de brechas calcáreas que incorpora cantos negros (secciones de Suances y Cuchía). En ambos casos el límite de secuencia se interpreta como superficies de exposición subaérea.

Evolución vertical de facies y ambientes sedimentarios

En esta secuencia se han reconocido dos estadios evolutivos. El estadio 1 está constituido principalmente por alternacias de bancos métricos de calizas *grainstone* y

wackestone-packstone con miliólidos, orbitolinas, gasterópodos, corales ramosos y en menor medida rudistas, y por paquetes decimétricos a métricos de caliza micrítica con *B. irregularis-L. aggregatum* formando masas irregulares trombolíticas, oncoides y *lumps*. El paso al estadio 2 está marcado por una superficie de bioturbación cubierta de un nivel decimétrico a métrico de margas y margocalizas nodulosas bioturbadas. El estadio 2 está formado principalmente por una sucesión de bancos estratificados, constituidos por limos carbonosos, margas y calizas nodulosas con orbitolinas, esponjas y corales masivos y tabulares, que alternan con calizas *grainstone* y *packstone-wackestone* con miliólidos, orbitolinas, gasterópodos y rudistas, formando secuencias métricas a decamétricas de somerización.

Esta secuencia muestra marcados cambios de potencia y facies en toda la zona de estudio. Así, en el área de La Florida la secuencia forma un litosoma carbonatado en cuña. Los menores espesores (44 m) aparecen en el área más occidental, donde la secuencia está constituida principalmente por calizas packstone-wackestone con miliólidos, orbitolinas, gasterópodos y rudistas, con finas intercalaciones de niveles margosos con orbitolinas y fragmentos de carbón (sección de río Nansa). Hacia zonas más orientales, el espesor de la secuencia aumenta progresivamente alcanzando hasta 186 m (sección de Bustriguado) y 115 m (sinclinal de Santillana). En estas zonas se han diferenciado cuatro tipos de facies, que se suceden formando secuencias menores de profundización-somerización: i) limos y arenas de grano fino con abundantes fragmentos vegetales; ii) margas y margocalizas grisáceas con corales masivos y esponjas; iii) packstone-wackestone con miliólidos, orbitolinas, corales y rudistas; y iv) bancos de calcarenitas packstone-grainstone bioclásticas.

En el área del sinclinal de Santillana también se aprecian cambios de espesores, pasando de unos 53 metros en el corte de la cantera de Las Lastrías a 115 metros en la sección tipo de Santa Eulalia.

Finalmente en el área de Cuchía esta secuencia está muy reducida, presentando 54 m en la sección de la cantera de Cuchía, formados por calizas masivas con masas trombolíticas y oncoides de *B. irregularis-L. aggregatum*, y solo 6-9 m de potencia en la sección de Cuchía y Suances, formados por calizas con rudistas y oncoides de *B. irregularis-L. aggregatum*, no distinguiéndose aquí los estadios 1 y 2.

Interpretación

Esta secuencia deposicional se originó en un ambiente de plataforma carbonatada somera con variación de ambientes desde plataforma interna, plataforma media poco profunda y plataforma externa.

El primer estadio de la secuencia deposicional SD4 representa un cambio gradual desde ambientes de plataforma interna a plataforma media poco profunda y finalmente plataforma externa (margas y margocalizas bioturbadas), que representa la parte de máxima transgresión del ciclo. El estadio 2, con variaciones laterales de facies y ciclos de profundización-somerización, representaría la parte regresiva del ciclo. El techo de la secuencia viene marcado por un periodo de exposición subaérea, al que le sigue una nueva subida relativa del nivel del mar.

El marcado cambio de potencias y de facies en a lo largo del depósito de esta secuencia indica la acción conjunta de la actividad sinsedimentaria de las fallas distensivas de Bustriguado, Santibañez y Peña Castillo, junto a los cambios eustáticos, que tuvieron lugar durante el Aptiense Inferior (Inmenhauser, 2005).

Secuencia Deposicional 5 (SD5)

Litoestratigrafía

Esta secuencia de depósito abarca la Formación Las Peñosas, presentando una edad de Albiense Inferior-Medio.

Límites de secuencia

Esta secuencia solo se registra en el área de La Florida, sinclinal de Santillana y zona de Comillas. En el sector de Cuchía está ausente y su equivalente lateral es una superficie de exposición subaérea a techo de la Fm Reocín y sequencia SD4 (límite de secuencia LS4). Su límite inferior (LS4) viene marcado por una superficie de exposición subaérea. En el área de La Florida se trata de una superficie con rasgos microscópicos de disolución, mientras que en el área del sinclinal de Santillana el límite se caracteriza por un nivel de arcillas verde-rojas edáficas.

El límite de secuencia superior (LS5), está marcado por un nivel bioturbado, margoso y noduloso, con abundantes bivalvos megalodontos de gran tamaño, sobre el cual se recupera la sedimentación carbonatada de la Formación Barcenaciones.

Evolución vertical de facies y ambientes sedimentarios

A lo largo de esta secuencia de depósito se han distinguido 3 estadios evolutivos. El estadio 1 se depositó en un ambiente de plataforma mixta terrígeno-carbonatada, que se caracteriza por presentar una alternancia de calizas *grainstone* o calizas bioclásticas con abundantes ostreidos, calizas margosas-limosas nodulosas y bioturbadas, y limos con delgados niveles de arena muy fina y laminación cruzada. En conjunto, este estadio muestra una disminución del contenido en carbonato y un progresivo aumento del contenido en limo y arena fina hacia techo. En el estadio 2 las facies están fortmadas por una sucesión de: i) facies heterolíticas de arenas y limos con laminación *wavy*, *linsen* y *flaser* y *mud drapes,* o con estratificación *hummocky* (HCS) de pequeña escala y *ripples* de oscilación y de corriente, ii) limos bioturbados (*Rhizocorallium*, *Teichichnus*) y lutitas oscuras sulfurosas con restos de carbón, fragmentos vegetales, moldes piritizados de pequeños gasterópodos y bivalvos marinos y abundantes piezas de ámbar, iii) areniscas de grano fino a grueso con estratificación cruzada organizadas en secuencias estrato- y granocrecientes, y iv) areniscas de grano medio-grueso con geometrías acanaladas intercaladas entre lutitas grises-rojas con rasgos de edafización, moteado y localmente huellas de raíces (paleosuelos). El estadio 2 se depositó en un ambiente deltaico, con subambientes que varían desde frente deltaico, con progradación de barras deltaicas de desembocadura y barras distales, a llanura deltaica, con zonas emergidas con desarrollo de paleosuelos, surcadas por canales distribuitarios de ríos meandriformes y por bahías interdistributarios. Finalmente el estadio 3 se depositó en un ambiente de plataforma mixta terrígeno-carbonatada, y está formado por una alternancia de limos margosos y arenas de grano muy fino y calizas *packstone* con ostreidos, gasterópodos y bivalvos, formando secuencias métricas terrígeno-carbonatadas que presentan un progresivo aumento en el contenido de carbonato hacia techo, pasando progresivamente a la secuencia carbonatada suprayacente.

Esta secuencia también muestra notables cambios de espesor en cortas distancias. Así, por ejemplo, en el área de La Florida, el episodio 1 varía entre 11 metros (sección de Rábago) y 40 metros (sección de Plaza del Monte); el episodio 2 presenta

una potencia que pasa lateralmente de 25 metros en la sección de Rábago a 60 metros en la sección de Plaza del Monte y el episodio 3 presenta un espesor que varía entre 13 metros en la sección de Rábago y 40 metros en la sección de Plaza del Monte.

Interpretación

En esta secuencia se ha distinguido un ciclo transgresivo-regresivo-transgresivo. Así, el primer estadio del ciclo tuvo lugar durante el inicio de un episodio transgresivo tras la exposición subaérea del techo de la secuencia de depósito 4 (LS4), desarrollándose un ambiente de plataforma mixta terrígeno-carbonatada, con un aumento progresivo del material terríegeno hacia el techo del episodio. Seguidamente, tuvo lugar una fase de regresión, dando lugar al desarrollo del episodio 2, implantándose un sistema deltaico. Por último (estadio 3), tuvo lugar un nuevo episodio transgresivo, dando lugar al desarrollo de un ambiente de plataforma mixta terrígeno-carbonatada, con un aumento del contenido en carbonatos hacia techo, culminando con la total recuperación de la sedimentación carbonatada en la siguiente secuencia de depósito.

El marcado cambio de espesores en el área de La Florida registrado en esta secuencia de depósito refleja la flexión en el bloque inferior (*footwall*) de la falla de Bustriguado.

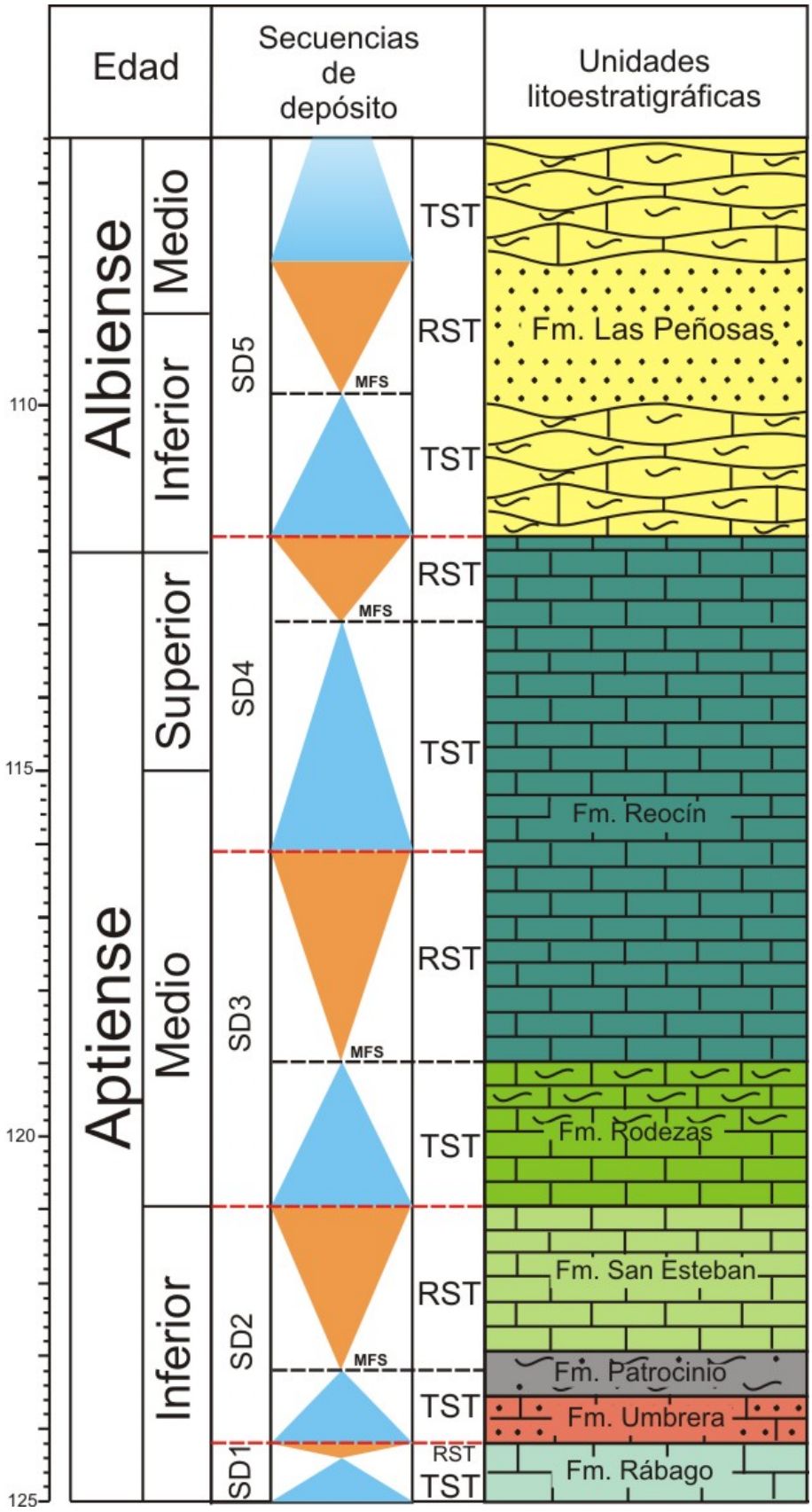

Figura 3.23.- Secuencias de depósito, SD1 a SD5 reconocidas en la zona de estudio. TST: *Transgressive System Tract*. RST: *Regressive System Tract*. MFS: *Maximum Flooding Surface.*

3.5.- REFERENCIAS

Aguado, R. (1994). Nannofósiles del Cretácico de la Cordillera Bética (sur de España). Bioestratigrafía. Tesis Doctoral, Universidad de Granada, 413 pp.

Aguado, R., Castro, J.M., Company, M. & Gea de, G.A. (1999). Aptian bio-events –an integrated biostratigraphic analysis of the Almadich Formation, Inner Prebetic Domain, SE Spain. Cretaceous Research v. 20, p. 663-683.

Alonso-García, M. & Bahamonde, J.R. (2006). Sedimentología y caracterización paleoambiental de la serie cretácica inferior de Antromero-Luanco (Asturias). Geogaceta, v. 40, p. 247-250.

Applegate, J.L. & Bergen, J.A. (1988). Cretaceous calcareous nannofossil biostratigraphy of sediments recovered from the Galicia Margin, ODP leg 103. En: G. Boillot, E.L. Winterer, et al. (ed.), Proceedings of the Ocean Drilling Program, Scientific Results v. 103, p. 293-348.

Arias, C. & Doubinger, J. (1980). La limite Aptien-Albien dans le Secteur de Mompichel (Albacete). Cretaceous Research, v. 1, p. 235–251.

Azéma, C. & Boltenhagen, E. (1974). Pollen du Crétacé Moyen du Gabon attribué aux Ephedrales. Paléobiologie continentale, v. 5(1), p. 1-37.

Balme, B.E. (1995). Fossil in situ spores and pollen grains: an annotated catalogue. Review of Palaeobotany and Palynology, v. 87, p. 81-323.

Batten, D.J. (1999). Chapter 20E. Upper Jurassic and Cretaceous Miospores. En: Palynology: Principles and Applications (Eds. J. Jansonius and D.C. McGregor). American Association of Stratigraphic Palynologists Foundation, Salt Lake City, v. 2, p. 807–830.

Breistroffer, M. (1936).- Les subdivisions du Vraconien dans le Sud-Est de la France.- Bulletin de la Société Géologique de France, Paris, (5° série), t. VI, n 1-3, 63-68.

Burger, D. (1966). Palynology of uppermost Jurassic and lowermost Cretaceous strata in the eastern Netherlands. Leidse Geologische Mededelingen, v. 35, 209–276.

Carreras, F.J., Aguilar, M.J., Ramírez del Pozo, J., Giannini, G. & Pujalte, V. (1978). Hoja geológica número 57. Cabezón de la Sal. Mapa geológico de España, escala 1:50.000, Serie MAGNA, IGME.

Carreras, F.J., del Olmo, P., Portero García, J.M., Ramírez del Pozo, J., Giannini, G. & Aguilar, M.J. (1979). Hoja geológica número 58. Los Corrales de Buelna. Mapa geológico de España, escala 1:50.000, Serie MAGNA, IGME.

Casey, R. (1961). A monograph of the Ammonoidea of the Lower Greensand, part III. Monographs of the Palaeontographical Society, London v. 114, p. 119-216.

Casey, R., Bayliss, H.M. & Simpson, M.I. (1998). Observations on the lithostratigraphy and ammonite succession of the Aptian (Lower Cretaceous) Lower Greensand of Chale Bay, Isle of Wight, UK. Cretaceous Research, v. 19, p. 511-535.

Cherchi & Schroeder (1998). Aptian and Albian large foraminifera at Madoz. En: Lamolda, M.A. (ed.), 24° Coloquio Europeo de Micropaleontología, pp. 71–73. Libro Guía.

Ciry, R., Rat, P., Mangin, J.P., Feuillee, P., Amiot, M., Colchen, M. & Delance J.H. (1967). Reunion Extroardinaire de la Societé Géologique de la France en Espagne, des Pyrinées aux Asturies. Compte Rendu Sommaire des Séances de la Societé Géologique de la France, v. 9, p. 389-444.

Collignon, M., Pascal., A., Peybernès, B. & Rey J. (1979). Faunes d'ammonites de l'aptien de la Région de Santander (Espagne). Annales de Paléontologie, v. 65, fasc. 2, p. 139-156.

Dejax, J., Pons, D. & Yans, J. (2007). Palynology of the dinosaur-bearing Wealden facies in the natural pit of Bernissart (Belgium). Review of Palaeobotany and Palynology, v. 144, p. 25–38.

Dörhöfer, G. (1977). Palynologie und Stratigraphie der Bückeberg-Formation (Berriasium-Valanginium) in der Hilsmulde (NW- Deutschland). Geologisches Jahrbuch Reihe A, v. 42, p. 3–122.

Doyle, J.A. & Robbins, E.I. (1977). Angiosperm pollen zonation of the Continental Cretaceous of the atlantic coastal plain and its application to deep wells in the Salisbury embayment. Palynology, v. 1, p. 43-78.

Erba, E. (1994). Nannofossils and 'superplumes': the Early Aptian Nannoconid crisis. Paleoceanography, v. 3, p. 483-501.

Embry, A.F. (2002). Transgressive-Regressive (T-R) Sequence Straigraphy. 22nd Annual Gulf Coast Section SEPM Foundation Bob F. Perkins Research Conference–2002. p. 151–172.

Friis, E.M. Crane, P.R. & Pedersen, K.R. (2011). Early flowers and angiosperm evolution. Cambridge University Press, Cambridge, 585 pp.

Gaona-Narvaez, T., Maurrasse, F.J-M. R. & Moreno Bedmar, J.A. (2013). Stable carbon-isotope stratigraphy and ammonite biochronology at Madotz, Navarra,

northern Spain: implications for the timing and duration of oxygen depletion during OAE 1a.

García-Mondéjar, J. (1982). Aptiense y Albiense. Región Vasco-Cantábrica y Pirineo navarro. En: A. García (ed.), El Cretácico de España. Madrid, Universidad Complutense, p. 63-76.

García-Mondéjar, J. & Pujalte, V. (1981). El Jurásico Superior y el Cretácico Inferior de la región Vasco-Cantábrica (parte occidental). Libro de guía de jornadas de campo, 9-12 septiembre 1982. Grupo español del Mesozoico. P.I.G.C. Mid Cretaceous Events. Dpto. de Geología, 133 pp.

García-Mondéjar, J., Pujalte, V. & Robles, S. (1986). Características sedimentológicas, secuenciales y tectoestratigráficas del Triásico de Cantabria y norte de Palencia. Cuadernos de Geología Ibérica, v. 10. p. 151-172.

García-Mondéjar, J., Fernández Mendiola, P.A., Millán, M.I. & Mendicoa, J. (2009). La plataforma urgoniana aptiense del sur de Bilbao (valle de Bolintxu): organización estratigráfica y evolución. Geogaceta, v. 47, p. 77-80.

García-Mondéjar, J., Hugh, G.O. & Fernández-Mendiola, P.A. (2015). Early Aptian sedimentary record and OAE1a in Cuchía (northern Spain): new data on facies and ammonite dating. N. Jb. Geol. Paläont. Abh. Doi: 10.1127/njgpa/2015/0466.

Gea de, G.A., Castro, J.M., Aguado, R., Ruiz-Ortiz, P.A. & Company, M. (2003). Lower Aptian carbon isotope stratigraphy from a distal carbonate shelf setting: the Cau section, Prebetic zone, SE Spain. Palaeogeography, Palaeoclimatology, Palaeoecology v. 200, p. 207–219.

Groot, J.J., & Groot, C.R. (1962). Plant microfossils from Aptian, Albian and Cenomanian deposits of Portugal. Comunicações dos Serviços Geologicos de Portugal, v. 46, p. 133–176.

Hines, F.M. (1985). Sedimentation and tectonics in north-west Santander. En: M.D. Milá & J. Rosell (ed.), 6th European Regional Meeting, Excursion Guidebook, International Association of Sedimentologists, p. 371−398.

Hochuli, P.A. (1981). North Gondwanan floral elements in lower to middle Cretaceous sediments of the Southern Alps (Southern Switzerland, Northern Italy). Review of Palaeobotany and Palynology, v. 35, p. 337–358.

Hughes, N.F. & McDougall, A.B. (1990). Barremian-Aptian angiospermid pollen records from southern England. Review of Palaeobotany and Palynology, v. 65, p. 145–151.

Hughes, N. F., McDougall, A. B. & Chapman, J. L. (1991). Exceptional new record of cretaceous hauterivian angiospermid pollen from Southern England. Journal of micropalaeontology, v. 10(1), p. 75-82.

Immenhauser, A. (2005). High-rate sea-level change during the Mesozoic: New approaches to an old problem. Sedimentary Geology, v. 175, p. 277-296.

Karrenberg, H. (1934). Die postvariche entwicklung des Cantabro-Asturiche gebirees (Nordwestpanien). Publ. Extr. Geol. España (CSIC), v. 3, p. 103-225.

Kemp, E.M. (1970). Aptian and Albian miospores from southern England. Palaeontographica Abteilung B, v. 131, p. 73–143.

Leereveld, H., de Haan, P.J. & Juhász, M. (1989). Stratigraphic evaluation of spore/pollen assemblages from the Lower Cretaceous of the Alpine-Mediterranean Realm. LPP Contributions series, v.89/07, p. 1-253+251-298.

Loeblich, A.R. Jr. & Tappan, H. (1987). Foraminiferal genera and their classification. Van Nostrand Reinhold, New York, x +970, viii+1059 p.

López-Gómez, J., Arche, A. & Pérez-López, A. (2002). Permian and Triassic. En: W. Gibbons, T. Moreno (eds), The Geology of Spain. Published, London: 185-212.

López-Horgue, M.A., Aramburu, A., Fernández-Mendiola, P.A. & García-Mondejar, J. (2001): Facies estuarinas en el Albiense Superior de Cabo Quintres (Cantabria, región Vasco-Cantábrica occidental). Geogaceta, v. 30, p. 75-78.

Martínez-García, E. (1971). The age of the Caliza de Montaña in the Eastern Cantabrian Mountains. Trabajos de Geología, Universidad de Oviedo, v., p. 267-276.

Martínez-García, E. (1981). El Paleozoico en la Zona Cantábrica Oriental (NW de España). Trabajos de Geología, Universidad de Oviedo, v. 11, p. 95-127.

Masse, J.P. (1995). Lower Cretaceous rudist biostratigraphy of southern France –a reference of Mesogean correlations. Revista Mexicana de Ciencias Geológicas, v. 12 (2), p. 236-256.

Masse, J.P., Arias, C. & Vilas, L. (1998). Lower Cretaceous Rudists faunas of Southeast SpaEn: an overview. Geobios, v. 22, p. 193-210.

Menguad, L. (1920). Recherches geologiques Dans la region Cantabrique. Livr. Sc. J. Hermann, 1374 pp.

Moreno-Bedmar, J.A., Company, M., Bover-Arnal, T., Salas, R., Delanoy, G., Martínez, R. & Grauges, A. (2009). Biostratigraphic characterization by means of ammonoids of the lower Aptian Oceanic Anoxic Event (OAE 1a) in the

eastern Iberian Chain (Maestrat Basin, eastern Spain). Cretaceous Research, v. 30, p. 864-872.

Moreno-Bedmar, J.A., Barragán, R., Delanoy G., Company, M & Salas, R. (2014). Review of the early Aptian (Early Cretaceous) ammonoid species Deshayesites deshayesi (d'Orbigny, 1841). Cretaceous Research. v. 51, p. 341-

Moullade, M. (1974). Zones de foraminiféres du Crétacé Inférieur mésogéen. Comptes Rendus Hebdomadaires des Séances de l'Académie des Sciences de Paris, Serie D 278, p. 1813-1816.

Moullade, M. & Peybernès, B. (1975). Biozonation par Orbitolinidés du Clansayesian et de l´Albien calacaires des Pyrénées franco-espagnoles. Comptes Rendus de l´Académie des Sciences, Sér. D, 280, 2529-2532.

Moullade, M., Bellier, J.P. & Tronchetti, G. (2002). Hierarchy of criteria, evolutionary processes and taxonomic simplification in the classification of Lower Cretaceous planktonic foraminifera. Cretaceous Research v. 23, p. 111-148.

Najarro, M., Peñalver, E., Rosales, I., Pérez-de la Fuente, R., Daviero-Gomez, V., Gomez, B. & Delclòs, X. (2009). Unusual concentration of Early Albian arthropod-bearing amber in the Basque-Cantabrian Basin (El Soplao, Cantabria, Northern Spain): Palaeoenvironmental and palaeobiological implications. Geologica Acta, v. 7 (3), p. 363-387.

Najarro, M., Peñalver, E., Pérez-de La Fuente, R., Ortega-Blanco, J., Menor-Salván, C., Barrón, E., Soriano, C., Rosales, I., López del Valle, R., Velasco, F., Tornos, F., Daviero-Gomez, V., Gomez, B. & Delclòs, X. (2010). Review of the El Soplao amber outcrop, Early Cretaceous of Cantabria, Spain. Acta Geologica Sinica (English Edition), v. 84, p. 801-818.

Najarro, M. & Rosales, I. (2008a). Disoluciones e Incrustaciones Ferruginosas asociadas al OAE 1a en la plataforma carbonatada de La Florida. Geogaceta, v. 44, p. 199-202.

Najarro, M., Rosales, I. & Martín-Chivelet, J. (2007). Evolución de la plataforma carbonatada de la Florida durante el rifting del Cretácico inferior (Aptiense, NO de Cantabria).En: D.D. Bermudez, M. Najarro & C. Quesada (ed.), II Semana de Jóvenes Investigadores del I.G.M.E., Instituto Geologico y Minero de España, Madrid, p. 123-128.Najarro, M., Rosales, I. & Martín-Chivelet, J. (2011b). Major palaeoenvironmental perturbation in an Early Aptian carbonate platform: Prelude of the Oceanic Anoxic Event 1a? Sedimentary Geology, 235, p. 50–71.

Najarro, M., Rosales, I., Moreno-Bedmar, J.A., de Gea, G.A., Barrón, E., Miquel Company, M., & Delanoy, G. (2011a). High-resolution chemo- and biostratigraphic records of the Early Aptian Oceanic Anoxic Event in Cantabria (N Spain): Palaeoceanographic and palaeoclimatic implications. Palaeogeography, Palaeoclimatology, Palaeoecology, v. 299, p. 137–158.

Najarro, M., Rosales, I. & Martín-Chivelet, J. (2011b). Major palaeoenvironmental perturbation in an Early Aptian carbonate platform: Prelude of the Oceanic Anoxic Event 1a? Sedimentary Geology, v. 235, p. 50–71.

Norris, G. (1969). Miospores from the Purbeck beds and marine Upper Jurassic of Southern England. Palaeontology, v 12 (4), p. 574-620.

Ogg, J.G. & Ogg, G. (2008). Early Cretaceous (103–138 Ma time-slice). Update to Geological Time Scale 2004 (Gradstein, F.M., Ogg, J.G., Smith, A.G., et. al., Cambridge Univ. Press) and The Concise Geologic Time Scale (Ogg, J.G., Ogg, G.,Gradstein,F.M.,2008).URL:https://engineering.purdue.edu/Stratigraphy/charts/Timeslices/4_Mid-Cret.pdf.

Pascal, A. (1985). Les Systems biosédimentaires urgoniens (Aptien−Albien) sur la marge Nord Ibérique. Mémoires Géologiques de l'Úniversité de Dijon, v. 10, p. 1-569.

Peyrot, D., Rodríguez-López, J.P., Lassaletta, L., Meléndez-Hevia, N. & Barrón, E. (2007). Contributions to the palaeoenvironmental knowledge of the Escucha Formation in the Lower Cretaceous Oliete Sub-basin, Teruel, Spain. Comptes Rendus Palevol., v. 6, p. 469–481.

Pujalte, V. (1981). Sedimentary succesion and palaeonvironments within a fault controlled basEn: the Wealden of the Santander area, northern Spain. Sedimentary Geology, v. 28, p. 293-325.

Pujalte, V. (1982). La evolución paleogeográfica de la Cuenca "Wealdense" de Cantabria. Cuadernos de Geología Ibérica, v. 8, p. 65-83.

Pujalte, V., Robles, S., García-Ramos, J.C., Hernández, J.M. (2004). El Malm-Barremiense no marinos de la Cordillera Cantábrica. En: Geología de Espa.a (J.A. Vera, ed.), SGE-IGME, p. 288-291.

Quesada, S. Robles, S. & Rosales, I. (2005). Depositional architecture and transgressive-regressive cycles within Liassic backstepping carbonate ramps in the Basque-Cantabrian Basin, northern Spain. Journal of the Geological Society of London, v. 162, p. 531-548.

Quijano, M.L., Castro, J.M., Pancost, R.D., de Gea, G.A., Najarro, M., Aguado, R., Rosales, I. and Martín-Chivelet, J. (2012). Organic geochemistry, stable isotopes, and facies analysis of the Early Aptian OAE: New records from Spain (western Tethys). Palaegeography, Palaeoclimatology, Palaeoecology, 365-366, 276–293, doi: 10.1016/j.palaeo.2012.09.033.

Ramírez del Pozo, J. (1971). Bioestratigrafia y microfacies del Jurásico y Cretácico del Norte de España (region cantábrica). Mémoria del Instituto Geológico y Minero de España, 78, 1-357.

Ramírez del Pozo, J. (1972). Algunos datos sobre la estratigrafía y micropaleontología del Aptense y Albense al oeste de Santander. Revista Española de Micropaleontología v. 15, p. 59–97.

Ramírez del Pozo, J., Portero García, M., Olivé Davó, A., Martín Alafont, J.M., Aguilar Tomás, M.J. & Giannini, G. (1976a). Hoja geológica número 33. Comillas. Mapa geológico de España, escala 1:50.000, Serie MAGNA, IGME.

Ramírez del Pozo, J., Portero García, M., Olivé Davó, A., Martín Alafont, J.M., Aguilar Tomás, M.J. & Giannini, G. (1976b). Hoja geológica número 34. Torrelavega. Mapa geológico de España, escala 1:50.000, Serie MAGNA, IGME.

Rat, P. (1959). Les pays crétacés basco-cantabriques (Espagne). Thèse. publ. Université de Dijon, v. XVIII, 525 pp.

Reboulet, S., Klein, J., Barragán, R., Company, M., González-Arreola, C., Lukeneder, A., Raisossadat, S.N., Sandoval, J., Szives, O., Tavera, J.M., Vasicek, Z., Vermeulen, J. (2009). Report on the 3rd International Meeting of the IUGS Lower Cretaceous Ammonite Working Group, the "Kilian Group" (Vienna, Austria, 15th April, 2008). Cretaceous Research 30, 496–502.

Reboulet, S., Rawson, P. F, Moreno-Bedmar, J. A., Aguirre-Urreta, M. B., Barragán, R., Bogomolov, Y., Company, M., González-Arreola, C., Stoyanova I., Lukeneder, A., Matrion, B., Mitta, V., Randrianaly, H., Va_si_cek, Z., Baraboshkin, E. J., Bert, D., Bersac, S., N. Bogdanova, T.N., Bulot, L. G., Latil, J-L., Mikhailova, I. A., Ropolo, P. & Szives, O. (2011). Report on the 4th International Meeting of the IUGS Lower Cretaceous Ammonite Working Group, the "Kilian Group" (Dijon, France, 30th August 2010). Cretaceous Research, v. 32, p. 786-793.

Robles, S. (2004). El Pérmico de la Cuenca Vasco-Cantábrica. En: Geología de España (J.A. Vera, ed.), SGE-IGME, p. 269-271.

Robles, S. & Pujalte, V. (2004). El Triásico de la Cordillera Cantábrica. En: Geología de Espa.a (J.A. Vera, ed.), SGE-IGME, p. 274-276.

Robles, S., Pujalte, V. & García-Mondéjar, J. (1987). Sistemas aluviales pérmicos del área de Peña Labra-Peña Sagra (Cantabria y Palencia). Cuadernos de Geología Ibérica, v. 11, p. 5-21.

Robles, S., Quesada, S. Rosales, I., Aurell, M., & García-ramos, J.C. (2004). El Jurásico marino de la Cordillera Cantábrica. En: Geología de Espa.a (J.A. Vera, ed.), SGE-IGME, p. 279-285.

Rosales, I. (1995). La plataforma carbonatada de Castro-Urdiales (Aptiense-Albiense, Cantabria). Tesis Doctoral, Universidad del País Vasco, 496 p.

Schlagintweit, F. & Wilmsen, M. (2014). Orbitolinid biostratigraphy of the top Taft Formation (Lower Cretaceous of the Yazd Block, Central Iran). Cretaceus Research. v. 49, 125–133.

Scott, R.W. (2010). Numerical ages of selected rudist bivalvia: Preliminary results. Turkish Journal of Earth Sciences, v. 19, 769–790.

Taylor, T.N. & Alvin, K.L. (1984). Ultrastructure and development of Mesozoic pollen Classopollis. American Journal of Botany. v. 71, p. 575–587.

Trincão, P.R. (1990). Esporos e granos de polen do Cretácico Inferior (Berriasiano-Aptiano) de Portugal: Paleontología e Biostratigrafia. Ph. D. thesis, Univ. Nova, Lisboa, Portugal, 312 pp.

Vajda, V. (2001). Aalenian to Cenomanian terrestrial palynofloras of SW Scania, Sweden. Acta Paleontologica Polonica, v. 46, p. 403–426.

Vilas, L., Masse, J.P. & Arias, C. (1995). Orbitolina episodes in carbonate platform evolution: the Early Aptian model from SE Spain. Palaeogeography, Palaeoclimatology, Palaeoecology, v. 119, p. 35-45.

Watson, J. (1988). The Cheirolepidiaceae. En: Beck, C.B. (ed.), Origin and evolution of Gymnosperms. Columbia University Press, NY, pp. 382–447.

Wilmsen, M. (2000). Evolution and demise of a mid Cretaceous carbonate shelf: the Altamira Limestones (Cenomanian) of northern Cantabria (Spain). Sedimentary Geology, v. 133, p. 195-226.

Wilmsen, M. (2005). Stratigraphy and biofacies of the Lower Aptian of Cuchía (Cantabria, northern Spain). Journal of Iberian Geology, v. 31 (2), p. 253-275.

CAPÍTULO 4:

ARTÍCULOS CIENTÍFICOS

4.1.- Major palaeoenvironmental perturbation in an Early Aptian carbonate platform: prelude of the Oceanic Anoxic Event 1a?

M. NAJARRO[(1))], I. ROSALES[(1)], J. MARTÍN-CHIVELET[(2)]

(1) Instituto Geológico y Minero de España.

(2) Departamento de Estratigrafía, Instituto de Geología Económica (CSIC-UCM), Facultad de Ciencias Geológicas. Universidad Complutense.

Doi: 10.1016/j.sedgeo.2010.03.011

Sedimentary Geology 2011a, Vol. 235, p. 50-71.

RESUMEN

El Evento Anóxico Oceánico del Aptiense Inferior (OAE 1a) tuvo lugar en un contexto global de elevado efecto invernadero, acumulación generalizada de depósitos orgánicos en los ambientes marinos abiertos, perturbaciones mayores en el ciclo del C y un incremento generalizado de la cantidad de aportes procedentes del continente a los océanos. Este trabajo muestra el impacto regional y los efectos que tuvo el OAE 1a en carbonatos de plataforma de aguas someras depositados durante el Aptiense Inferior en la cuenca Nor-Cantábrica (Norte de España) a partir de un análisis sedimentológico, diagenético y quimioestratigráfico. La sucesión vertical de facies sedimentarias presenta cuatro estadios en la evolución de la plataforma. El estadio 1 (Bedouliense inferior) representa el inicio de una rápida transgresión marina en la zona, que dio lugar al depósito de carbonato micrítico con comunidades de tipo photozoan, características de condiciones oligotróficas en aguas tropicales, compuestas por rudistas, corales hermatípicos, algas dasicladáceas y miliólidos, que posteriormente se vio afectado por un intervalo de exposición subaérea. El estadio 2 (Bedouliense inferior) registra una rápida transgresión, depositándose grainstones compuestos por asociaciones de partículas de tipo heterozoan, características de condiciones ambientales mesotróficas, junto con oolitos ferruginizados. El estadio 3 (Bedouliense inferior) se caracteriza por el hundimiento de la plataforma y el depósito en ambiente de mar abierto, de margas oscuras, que son consideradas como la representación sedimentaria local del OAE 1a. Finalmente, en el estadio 4 se reanuda la sedimentación de carbonatos de aguas someras compuestos por comunidades de tipo photozoan. El estudio quimiestratigráfico del $\delta^{18}O$ y $\delta\ ^{13}C$ ha revelado marcadas excursiones negativas coincidiendo con el depósito de las margas oscuras del estadio 3, lo cual estaría asociado a los importantes cambios globales que tuvieron lugar al inicio del OAE 1a. El claro cambio composicional de los carbonatos que preceden las excursiones isotópicas, así como el hundimiento de la plataforma, indican condiciones de estrés ambiental, causadas por la combinación tanto de factores locales como globales. Así, los cambios globales relacionados al OAE 1a, unidos a un aumento de la subsidencia en la cuenca, dieron lugar al hundimiento de la plataforma carbonatada (drowning) debido a la reducción progresiva y anegamiento de la fábrica de carbonatos.

ABSTRACT

The Early Aptian Oceanic Anoxic Event (OAE 1a) was characterized by intensified greenhouse climate conditions, widespread accumulation of organic deposits in open-marine settings, major perturbations in the C cycle and a generalized increase in terrestrial runoff. Sedimentological, diagenetic and chemostratigraphic analyses of Lower Aptian platform carbonates from the North Cantabrian basin (N Spain) illustrate the regional impact and effects of those global conditions on shallow marine environments. The studied interval outlines four stages of platform evolution. Stage 1 (earliest Bedoulian) is defined by an initial rapid marine transgression that led to deposition of shallow water oligotrophic photozoan skeletal assemblages, and by a later interval of subaerial exposure. Stage 2 (early Bedoulian) starts with a rapid transgression followed by deposition of grainstones that yield heterozoan assemblages, more typical of mesotrophic conditions, along with ferruginized oolites. Stage 3 (early Bedoulian) is defined by the drowning of the carbonate platform and subsequent deposition of open-marine marls, which are thought to represent the local expression of the OAE 1a. Finally, stage 4 shows the return of shallow water photozoan carbonate sedimentation. The carbonate O and C stable isotope records have revealed prominent negative excursions during deposition of the marly interval of the stage 3, which may be associated with the important global changes that occurred at the onset of the OAE 1a. The change in skeletal assemblages that preceded the isotopic excursions and the platform drowning documents conditions of environmental stress caused by a combination of local and global factors. The global change, coupled with increased basin subsidence, triggered the drowning of the platform by progressive reduction of the growth potential of the carbonate factory.

***Keywords*: Carbonate platform; OAE 1a; heterozoan facies; meteoric diagenesis; Early Aptian; Cantabria.**

INTRODUCTION

The Cretaceous shallow carbonate platforms of the northern Tethys domain are typically characterized by rudist-dominated facies with corals and green algae, which are considered as an oligotrophic, photozoan style of carbonate production (e.g. Carannante et al., 1995; James, 1997; Philip and Gari, 2005; Föllmi et al., 2006; Burla et al., 2008). Their evolution is however punctuated by some stages of dominance of heterozoan communities as well as several phases of platform demise (e.g. Föllmi et al., 1994, 2006; Philip and Gari, 2005; Weissert et al., 1998). One of the best known stage of platform growth crisis occurred during the Early Aptian linked to a global oceanic anoxic event, the so-called OAE 1a. This event was characterized by widespread distribution of organic-rich deposits, and was associated to extreme greenhouse conditions and significant changes in the ocean-climate system (Schlanger and Jenkyns, 1976; Spicer and Corfield, 1992; Jenkyns, 2003). During this time, widespread drowning of shallow water carbonate platforms appears to have been synchronous at a global scale, defining a correlation between the OAE 1a and these drowning incidents (e.g. Arnaud-Vanneau and Arnaud, 1990; Hunt and Tucker, 1993; Jansa, 1993; Masse, 1993; Scott, 1993; Föllmi et al., 1994; Lehmann et al., 1998; Ruiz-Ortiz and Castro, 1998; Weissert et al., 1998; Bosellini et al., 1999; Wissler et al., 2003). One indicator of the influence upon the platform carbonates of environmental change associated to this event is the occurrence of significant variations in styles of carbonate production and diagenesis. In fact, the anoxic event is not other than the effect of a battery of interrelated palaeoclimatic and palaeoceanographic changes that converge at this time and whose triggering mechanisms are still poorly understood. Under such situation of environmental collapse, carbonate sedimentation is expected to suffer strong modifications. One important consequence is that heterozoan associations become dominant in the platforms (Simone and Carannante, 1988; James, 1997). However, there are still few references to heterozoan style of carbonate production during this period, and a timing correspondence between rising of heterozoan facies and the anoxic episode has not yet been clearly established.

This study examines the effects of the OAE 1a on the style of carbonate sedimentation and early diagenesis of a Lower Aptian carbonate platform from northwest Cantabria, in northern Spain. The area exhibits a well-exposed and continuous succession of Aptian shallow water platform carbonates that include a

Lower Aptian openmarine marly unit (Patrocinio Formation). The latter is thought to represent a short-lived episode of platform drowning and the local expression of the OAE 1a (Wilmsen, 2005; Najarro and Rosales, 2008a, b). The carbonate platform turned from photozoan to heterozoan biogenic assemblages before experiencing platform drowning. In attempts to explain the change of carbonate production and the drowning event, several questions arise: (I) which factors determined the carbonate factory shutdown and the drowning of the Cantabrian platform?, (II) to which extent all those changes could be induced or enhanced by regional mechanisms (e.g., local tectonics) rather than global forcings?. Sedimentological, geochemical, and diagenetic data are evaluated here in order to address those questions and to discriminate the effects of the OAE 1a on shallow carbonate deposition.

GEOLOGICAL SETTING

The studied area is located in the northwestern margin of the Basque-Cantabrian Basin (BCB; Fig. 1). During the Cretaceous, this part of the BCB belonged to the northern margin of the Iberian plate and was subjected to extension. The BCB evolution and its current structure are the result of a complex kinematics between the European and Iberian plates (Malod and Mauffret, 1990; Olivet, 1996). After a first extensional phase during the Permian–Triassic, a second rifting phase linked to the opening of the Bay of Biscay and North Atlantic ocean took place during the Late Jurassic–Early Cretaceous (e.g. Le Pichon and Sibuet, 1971; Rat, 1988; García-Mondéjar et al., 1996; Martín-Chivelet et al., 2002). Renewed extension and perhaps left-lateral strike slip movement along NW–SE faults occurred in theAptian–Cenomanian, during the last rifting phases (e.g.Malod and Mauffret, 1990; García-Mondéjar et al., 1996; Soto et al., 2007). Due to these tectonic events, numerous extensional basins and sub-basins bounded by active synsedimentary faults developed in theNorth Iberian plate margin (Fig. 1A).

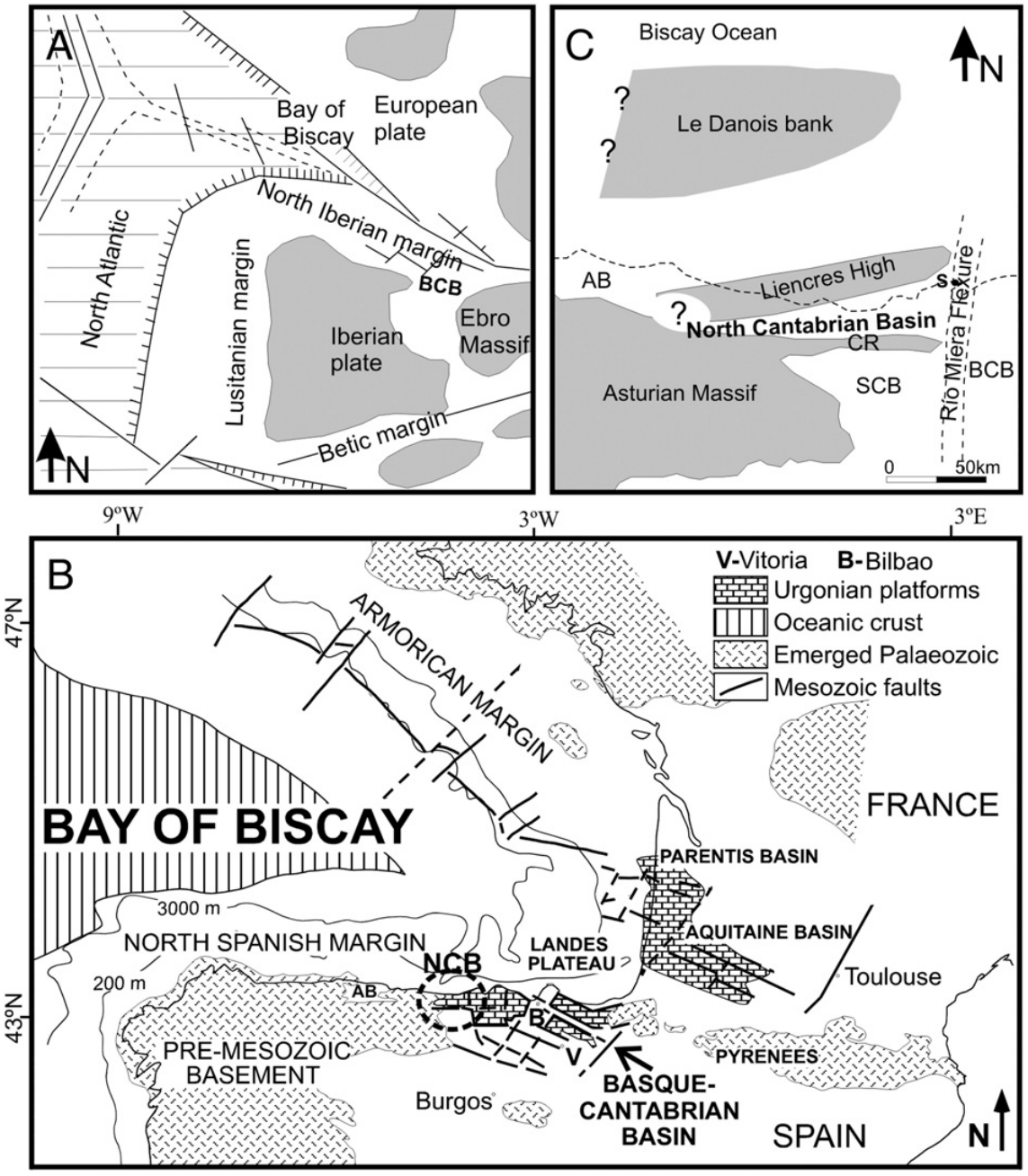

Figure 1.- (A) Palaeogeography and plate tectonics setting of Iberia during the Early Cretaceous (modified from Wilmsen, 2000). (B) Palaeotectonic map during the Early Cretaceous of the Bay of Biscay, showing the location of the North Cantabrian sub-basin (NCB) and major palaeotectonic features (modified from García-Mondéjar and Fernández-Mendiola, 1993). (C) Palaeogeography of the NCB in the Lower Cretaceous (modified from Wilmsen, 2000). BCB: Basque-Cantabrian basin; CR: Cabuérniga Ridge; SCB: South Cantabrian sub-basin; AB: Asturian basin.

The studied succession was deposited in one of these sub-basins, the North Cantabrian basin (NCB; Fig. 1B). This area developed as a relatively small (20×80 km), E–W elongated sub-basin, that behaved independently for most of the Cretaceous time (Fig. 1C). The NCB was separated from the more strongly subsiding rest of the BCB to the east, by a N–S extensional structure (Río Miera Flexure; Feuillée and Rat, 1971)

(Fig. 1C). To the south it was limited by the Cabuérniga Ridge (Figs. 1C and 2), an E–W trending palaeo-high which represents a previous Variscan tectonic structure reactivated as extensional faults during the Mesozoic (Rat, 1988; García-Espina, 1997). To the west, the NCB was bounded by the Asturian Massif and, to the north, by the Liencres High, an ENE–WSW trending swell now situated mostly offshore in the Bay of Biscay (Wilmsen, 2000) (Fig. 1C). Internally, the NCB was configured into swells and troughs controlled by the presence of N–S and E–W oriented synsedimentary faults and secondarily by NE–SW oriented faults (Najarro et al., 2009). Among the principal synsedimentary faults, it is worth mentioning the important role that played the North Cabuérniga and Bustriguado faults (Fig. 2A), which controlled subsidence patterns during the Early Cretaceous and determined strong local changes in sedimentary accumulation (Fig. 2B) (Najarro et al., 2007, 2009). As shown in the SW–NE cross-section of Fig. 2, the NCB can be divided into three main areas according to their tectonic evolution and stratigraphy, from SW to NE: La Florida, Santillana, and Cuchía. The areas of La Florida and Cuchía represent respectively two low-subsiding blocks. Between them, the Santillana area formed a sedimentary trough and the main depocentre of the NCB during the Early Cretaceous (Fig. 2).

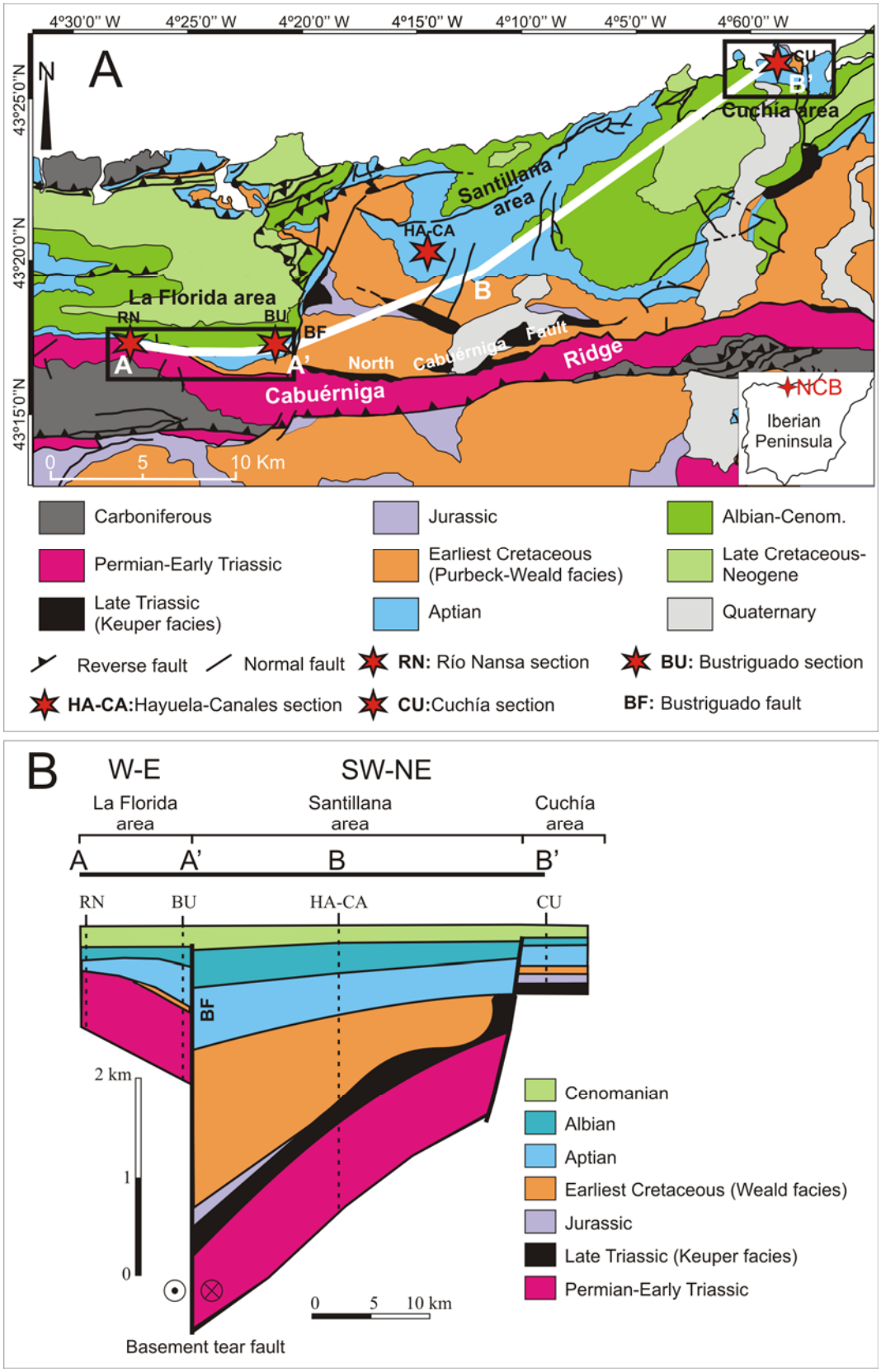

Figure 2.- (A) Geological map of the NCB. White line A–A′–B–B′ shows the location of the stratigraphic cross-section in B. (B) Cross-section showing the restored geometry of the NCB during the Cretaceous and the sedimentary record in the three principal areas (La Florida, Santillana and Cuchía).

STRATIGRAPHY

The general stratigraphic and biostratigraphic frameworks of the Aptian successions of the NCB were established by Ramírez del Pozo (1972), Collignon et al. (1979) and Hines (1985). More recently, the main depositional systems and sequences have been revised, establishing a new lithostratigraphic unit (Rábago Formation) and updating the stratigraphic and biostratigraphic schemes (Figs. 3 and 4) (Najarro and Rosales, 2008c; Najarro et al., 2009; Rosales et al., 2009). The Aptian lithostratigraphy of the NCB is composed of six formations, named from oldest to youngest (Fig. 3): 1) Rábago Formation (early Bedoulian, Palorbitolina lenticularis zone), which consists of shallow platform sandstones, orbitolinid marls and rudists limestones. 2) Umbrera Formation (early Bedoulian*, P. lenticularis* zone), composed of shallow platform cross-bedded grainstones. 3) Patrocinio Formation (mostly early Bedoulian, *Deshayesites weissi* ammonite zone and middle upper part of the *Hayesites irregularis* nannofossil zone; Rosales et al., 2009), made of open-marine marls. 4) San Esteban Formation (late Bedoulian), characterized by shallow platform rudist-bearing limestones, with *Iraquia simplex* (Pascal, 1985). 5) Rodezas Formation (latest Bedoulian–early Gargasian, according to Collignon et al., 1979), made of shallow marine sandstones, marly limestones and marls; and finally 6) Reocín Formation (Gargasian–Clansayesian, *Orbitolina (Mesorbitolina) texana texana* and *Simplorbitolina manasi* zones; Ramírez del Pozo, 1972), composed of shallow water coral and rudist-bearing limestones.

In the La Florida area, the Aptian succession consists of an E–W elongate lithosome, 9 km long, with wedge-shaped geometry deepening and thickening eastward, on the slope of a tilted block active during this time (Najarro et al., 2007) (Fig. 2B). In this area, the initial Early Aptian marine transgression led to deposition of the Rábago and Umbrera formations (Figs. 3 and 4). Continued transgression during the early Bedoulian caused platform drowning and resulted in deposition of the Patrocinio Formation, which completely covered the former carbonate platform. Subsequent regression during the Late Aptian originated the deposition of the Reocín Formation (Figs. 3 and 4). New biostratigraphic data based on calcareous nannofossils (Rosales et al., 2009) reveal the existence of a stratigraphic gap (paraconformity) in this area that comprises at least the late Early Aptian (late Bedoulian). This stratigraphic gap is time-equivalent to the San Esteban Formation, which is missed in this area (Fig. 4). In

contrast, in the Santillana area the Aptian succession is essentially complete without major hiatuses and the lithological units show their largest thicknesses (Fig. 3).

Finally, in the Cuchía area, the first recorded Aptian unit is the Umbrera Formation, which rests unconformably on continental Wealdean facies (Fig. 3). Remarkably, the Rábago unit is missing here (Figs. 3 and 4), probably because it was eroded before the deposition of Umbrera Formation, or alternatively because it pinched out in this area. Subsequent transgression produced deposition of the marly Patrocinio Formation. The upper part of this unit shows in this area an upward increase in the content of siliciclastic siltstones and sandstones which resulted of a local delta progradation (Wilmsen, 2005). The siliciclastic deltaic deposits grade upwards to the San Esteban Formation. Like in the previous area, the Late Aptian stratigraphy is represented by the Rodezas and Reocín Formations, except in the Suances section where these two units are absent; indicative of a depositional and/or erosive hiatus that comprises at least the entire Late Aptian (Fig. 3).

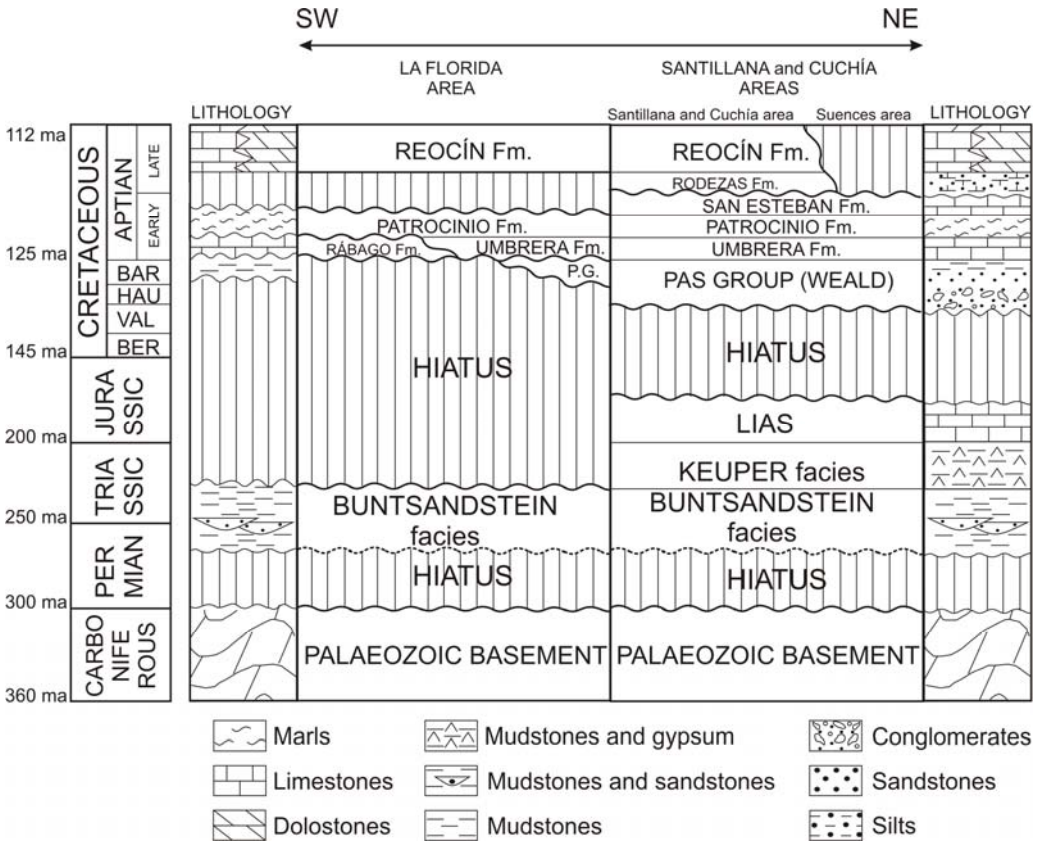

Figure 3.- Lithostratigraphy of the La Florida, Santillana and Cuchía areas. P.G. is Pass Group (Weald). Chronostratigraphy after Gradstein (2004).

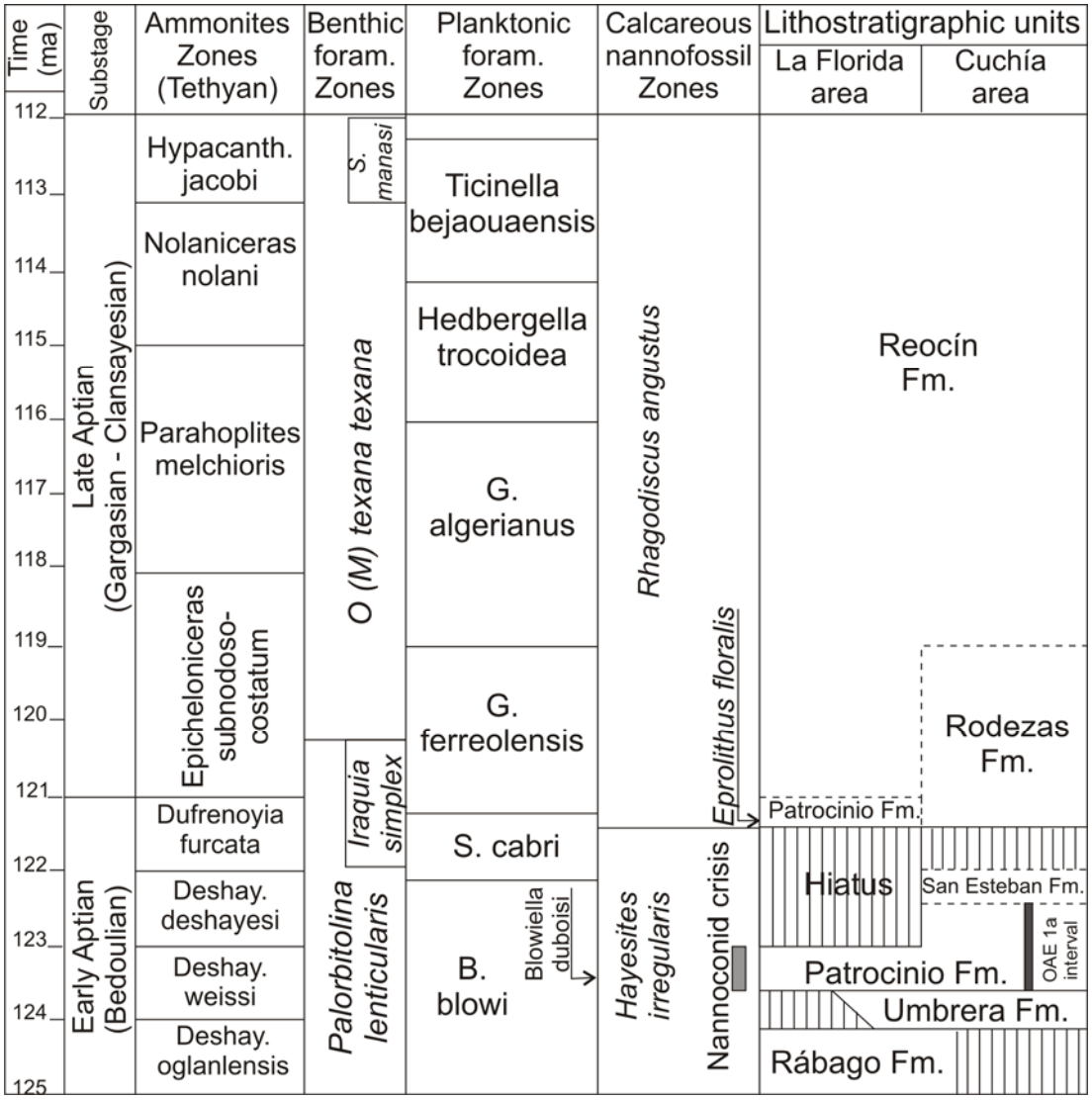

Figure 4.- Chrono-biostratigraphic scheme for the Aptian succession of the NCB.Ammonoid data based on Collignon et al. (1979), Rosales et al. (2009), and Moreno-Bedmar (pers. com.). Benthic foraminifera data based on Ramírez del Pozo (1972), Pascal (1985), and Castro (pers. com.). Planktonic foraminifera and nannofossil data based on Rosales et al. (2009), and de Gea (pers. com.). The OAE 1a interval is equivalent to the "Selli level" defined by Menegatti et al. (1998). Chronostratigraphy after Gradstein (2004).

METHODOLOGY AND STUDIED SECTIONS

A total of eight laterally correlative stratigraphic sections were measured and analyzed through the NCB for this work (Fig. 5). Six of them belong to the La Florida area (from W to E: Río Nansa, Rábago, El Soplao, La Florida, Corona de Arnero, and Bustriguado, Fig. 6). The other two are considered to be representative of the Santillana

and Cuchía areas respectively: the first one logged between the villages of Hayuela and Canales, and the second at the Los Caballos beach near the village of Cuchía (Fig. 2A).

When outcrop conditions were favourable, sedimentological features and macrofossil content were documented in detail in the field and sampling formicrofacies analysis was conducted systematically (at least 1 sample per 2 m, often at a smaller scale). Uncovered and polished thin sections were investigated with an optical microscope and cold cathodoluminescence (CL), and then classified according to microfabrics and mineral composition. Thin sections were stained with a mixture of Alizarin Red S and potassium ferricyanide (Dickson, 1966) to aid in the identification of ferroan and non-ferroan phases of calcite and dolomite. Cathodoluminescence (CL) analyses were obtained from a Technosyn cold cathodoluminescence operator model CL8200 MK5, operating at 15 kVwith a current of 500–600 μA. Oxygen and carbon stable isotope analyses were performed on limestone and marl samples throughout two selected stratigraphic sections (Río Nansa and Rábago), which may be easily correlated and combined to conform a composite complete section. Powders for isotope analyses were retrieved by using a microdrill on micrites and marls, and avoiding diagenetic calcite and dolomite from crack fillings, replaced fossils or matrix irregularities, especially in limestone samples. The sample material was treated with 100% orthophosphoric acid using the conventional digestion method (McCrea, 1950) and the $\delta^{13}C$ and $\delta^{18}O$ composition of the evolving CO_2 gas was analyzed in a SIRA-II doted with an "ISOCARB" automatic systemat the University of Salamanca (Spain). The results are expressed in the common δ-notation in per mil (‰) relative toVPDB-standard. The international carbonate standard NBS-19 (National Bureau of Standards; $\delta^{13}C$=1.95‰ and $\delta^{18}O$=−2.20‰) was used to calibrate the PDB, with an average precision of 0.01‰ for $\delta^{13}C$ and 0.05‰ for $\delta^{18}O$.

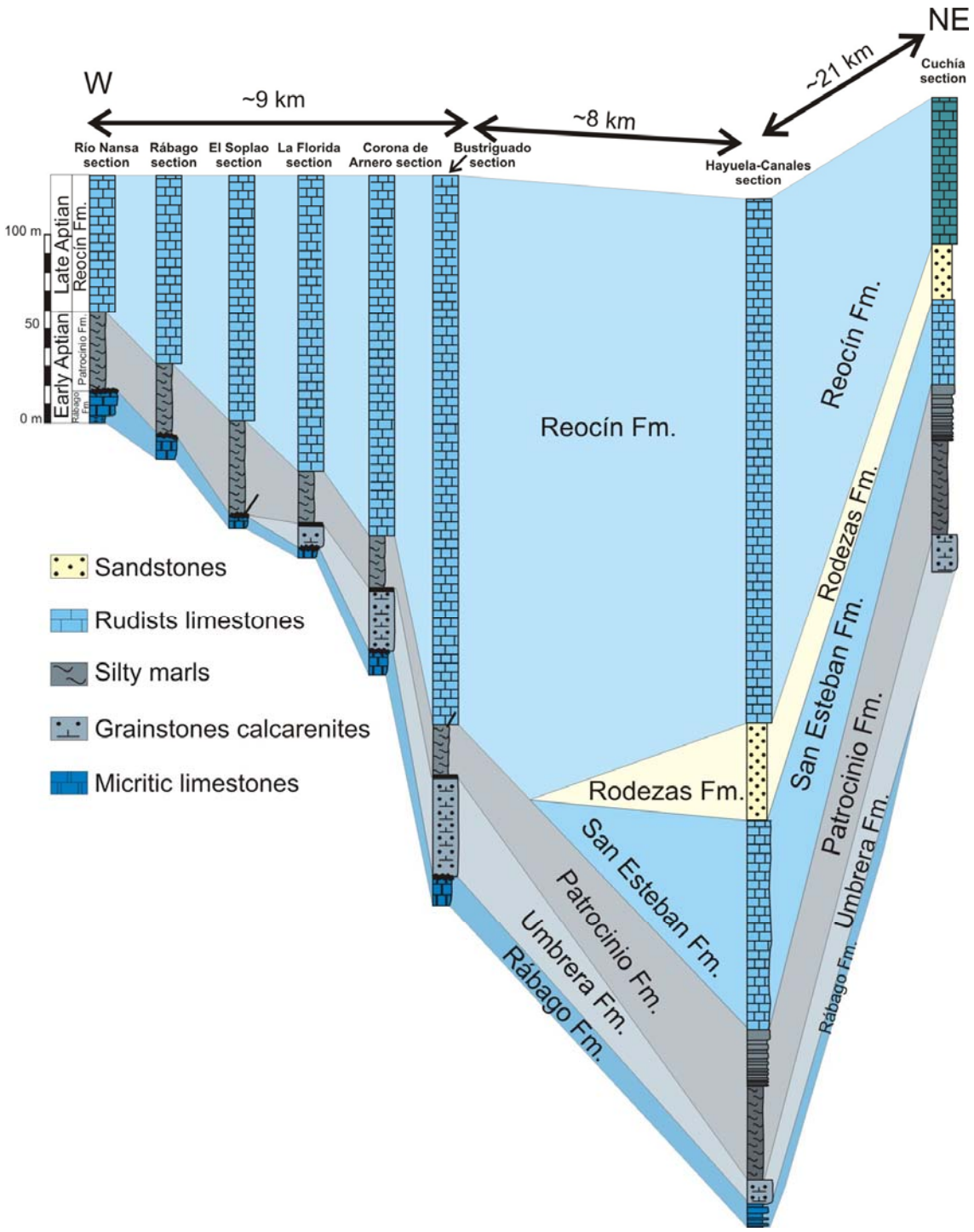

Figure 5.- Lithostratigraphic correlation of logged sections through the NCB, showing the main units, depositional facies and lateral thickness variation.

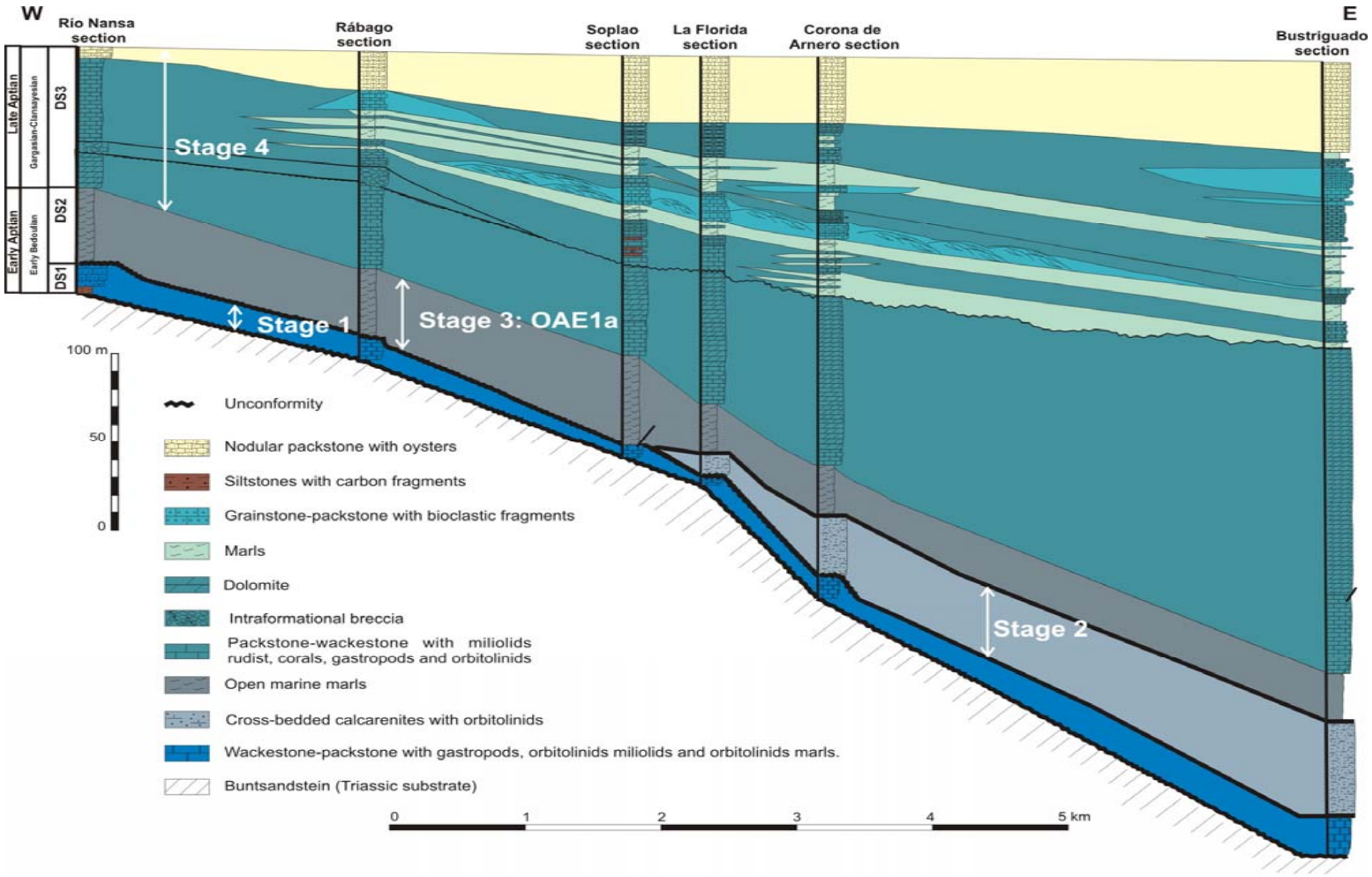

Figure 6.- Detailed stratigraphic correlation of the sections logged in La Florida area, showing the main stages of carbonate production and changes in sedimentary thickness and facies. Note the lateral thickness variation from west to east.

STAGES OF PLATFORM EVOLUTION

During the Early Aptian, the shallow water carbonate succession of the NCB presents four distinctive stages of platform evolution, which have been differentiated on the basis of facies and stratal patterns, with special emphasis in vertical changes in facies, skeletal composition and particle associations, and correlation of particular sedimentary surfaces (Figs. 5 and 6). Lithological description and interpretation of the four stages are summarized in Table 1, which show the following principal aspects from base to top:

Stage 1: Initial transgression and carbonate platform development

Description

It corresponds to the Rábago Formation. In the studied sections it presents a maximum thickness of 12–17 m. Its basal part is predominantly siliciclastic or mixed carbonate–siliciclastic, whereas the upper part is mostly carbonate alternating with some orbitolinid-rich marls (Fig. 7). Vertical stacking patterns of facies show three main facies associations, which from base to top are: i) siliciclastic platform, ii) mixed carbonate– siliciclastic platform, and iii) carbonate platform (Fig. 7 and Table 1).

Siliciclastic platform facies are present at the base of Río Nansa and Rábago sections (Fig. 7). They consist of a 5 to 7 m thick interval of interbedded, carbonaceous and laminated claystones, siltstones and fine to medium-grained micaceous sandstones, typically with lenticular and flaser bedding, and current ripples at the tops of the sandstones beds.

Mixed carbonate–siliciclastic platform facies mainly consist of sandy limestones with variable amount of quartz sand and other terrigenous grains. They are organized in tabular beds 20 cm to 1 m thick (Fig. 8A), which often show wavy lamination and occasionally wave ripples at the bed tops. These sandy limestones are interbedded with claystones–siltstones, packstone–grainstones, and orbitolinid-rich marls (Fig. 7).

Carbonate platform facies consist of alternations of orbitolinid-rich marls and nodular marly limestones, grainstones, packstones, wackestones and mudstones with corals and rudists of small size (Figs. 7 and 8B). They are organized in planar to nodular, massive beds ranging from 0.3 to 1 m thick. These facies are arranged in a

finingupward succession. Hence, packstone and grainstone are the most frequent textures in the lower terms of the succession, whereas coral rudist wackestone and microbialite mudstone with fenestral fabrics developed on the upper part (Fig. 7 and Table 1).

In the La Florida area, the succession culminates with a dissolution surface displaying irregular cavities of decimetre size, fissures and macro and micro topographic relief with corrosive surfaces and indents. Interestingly, a thin Fe-rich crust appears in places coating the dissolution surface (Fig. 8D). This crust is several millimetres thick and is made of very thin films (biofilms) of iron oxides with encrustations of agglutinated foraminifera, serpulids and microborings. Above this surface, the depressed zones of the palaeo relief and the cavities are filled with carbonate breccias made of centimetre- to decimetre-size sub-angular clasts of the underlying limestone (Fig. 8E) and small broken (reworked) pieces of the Fe-crust. The matrix of the breccia consists of red-stained crinoid-rich calcarenite infiltrated of the overlaying stage 2.

In the Santillana area, the end of the stage 1 is recorded as an erosive surface that truncates strata below (Fig. 9A). In the Cuchía area, the stage 1 is not recorded.

Interpretation

As a whole, the stage 1 reflects an initial transgressive event followed by a shallowing-upward succession with gradual upward decrease in siliciclastic content in conjunction with increment of carbonate production. The platform evolves from a siliciclastic or mixed carbonate–siliciclastic platform to a restricted inner fossiliferous carbonate platform under low-energy and photic zone conditions, and finally to peritidal facies. The dissolution surface at the top suggests emersion with small-scale karst morphologies (kamenitzas, as described in Di Stefano and Mindszenty, 2000) (Fig. 8C). The presence of the marine Fe-rich crust (hardground) coating the dissolution surface is interpreted to form during the following transgression at the onset of the stage 2.

Characteristics	Stage 1			Stage 2	Stage 3		Stage 4
Lithology	Interbedded, carbonaceous and laminated claystones, siltstones and micaceous sandstones	Sandy limestone with quartz sand	Marls, marly limestones, grainstones, packstones, wackestones, and mudstones	Grainstones and packstones, rarely rudstones. Orbitolinid marls upsection	Silty marls to dark-grey, soft clayed marls	Siltstones and mica-rich sandstones	Wackestones, packstones and marly limestones
Primary structures, vertical stacking and bioturbation	Lenticular and flaser bedding; current ripples	Wavy lamination; current ripples	Planar to nodular massive beds. Fining-upward	High –amplitud wavy lamination; planar–oblique and high-angle cross-stratification; internal erosive surfaces, bi-directional and sigmoidal cross- stratification. Thinning- and fining-upward. *Thalassinoides* up section.	–	Ripple trough cross-bedding, flaser and lenticular bedding. Coarsening-upward and *Ophiomorpha nodosa*	Fining-upward
Particle composition	Wood fragments, fine- to medium grained quartz, clay minerals and mica	Orbitolinids, echinoderms plates and thin shelled bivalves. Clay minerals (<5%)	Photozoan: Rudist and coral lithosomes, *L.aggregatum-B. irregularis*, miliolids, nerineid gastropods, *Chondrodonta* , dasycladacean green algae, orbitolinids, peloids, intraclasts and micritized grains.	Heterozoan: Large agglutinated benthic foraminifera, bryozoans, plates and spines of echinoderms, crinoid ossicles, red algae, oysters, bivalves, gastropods, quartz grains, glauconite, calcite ooids, ferruginized ooids and coated grains, extraclasts, and plant fragments	Ammonites, belemnites, planktonic foraminifera nannofossils, glauconite, and Fe-nodules	Bivalves, brachiopods, echinoids, orbitolinids, and wood fragments	Photozoan: Rudists and corals lithosomes, miliolids, orbitolinids, calcareous algae, *L.aggregatum-B. irregularis* , peloids, and bioclasts
Depositional environment	Siliciclastic platform	Mixed carbonate-siliciclastic platform	Restricted inner carbonate platform. Low energy and shallow water conditions. Shallowing upward and emersion at the top	Inner to mid carbonate shelf. High-energy shallow bars and shoals	Open marine	Delta progradation	Restricted inner carbonate platform. Low energy and shallow water conditions
Nutrient levels	–	–	Oligotrophic	Meso-eutrophic	–	–	Oligotrophic
Cement C1	–	–	Scarce	High	–	–	Scarce
Cement C2	–	–	High	Only in reworked bioclasts	–	–	–
Glauconite	–	–	–	High	High	–	–
Ferruginization	–	–	–	High	–	–	–
$\delta^{13}C$ values	–	–	Stable and positive values. Mean: 2.2‰	Progressive decrease of ~1‰. Positive values. Mean: 1.1‰	Negative excursion from -0.41‰ to -4.53‰		Positive excursion. Mean 2.8‰

Table 1.- Main characteristics of the different stages of the carbonate platform.

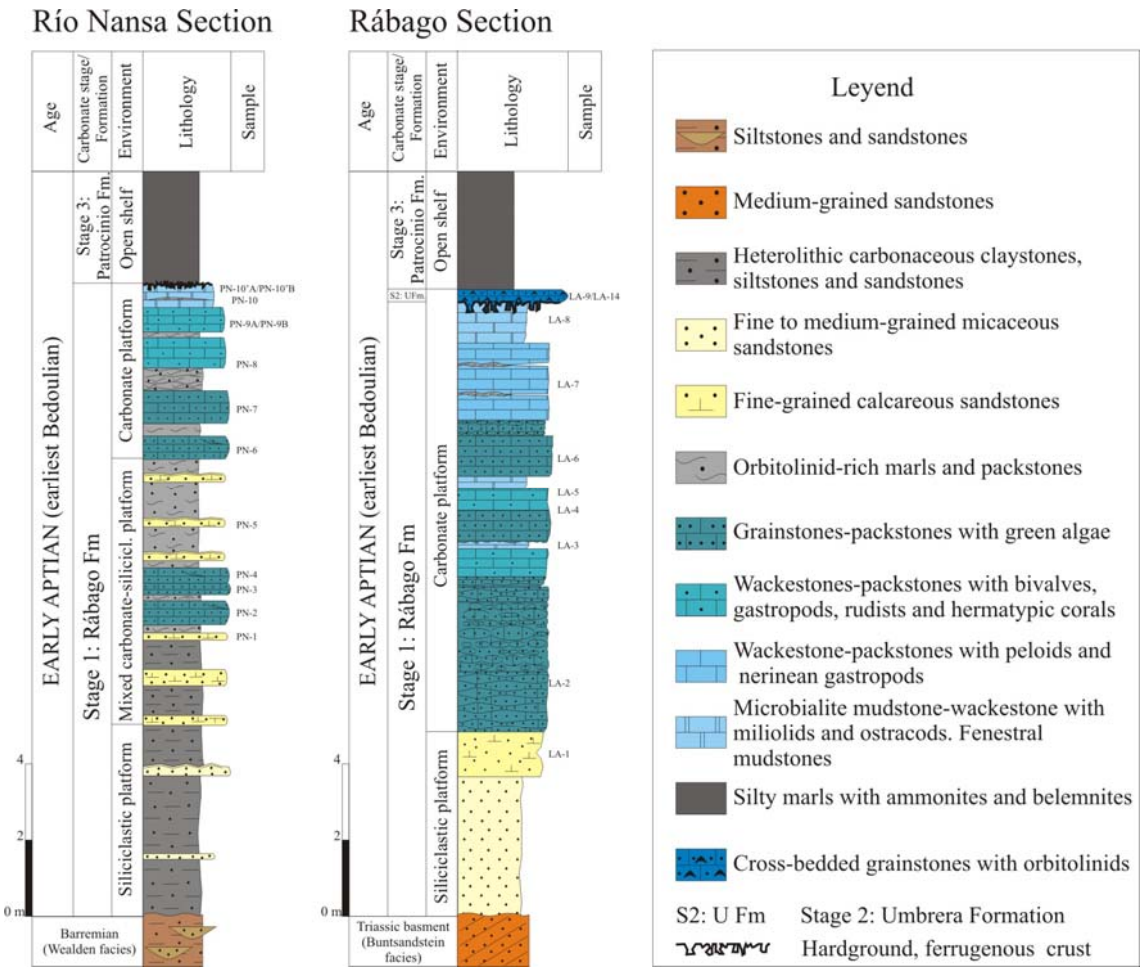

Figure 7.- Stratigraphic sections of stage 1 (Rábago Formation) at Río Nansa and Rábago localities, showing the main depositional environments and facies associations.

Stage 2: Carbonate production – deepening phase

Description

Stage 2 is represented by the Umbrera Formation (Fig. 9), which consists mostly of cross-bedded bioclastic grainstone and packstone, rarely rudstone, arranged in a thinning- and fining-upward succession. Coarser bioclastic sands are concentrated in the lower part of the succession in beds up to 1–2 m thick. Red to tan coloured ferruginized oolitic grainstones with trough cross-bedding characterize the base of the succession. The lower–middle part of the succession is made of bioclastic–oolitic grainstones organized in massive and metre- to decimetre-thick cross-bedded sets (Fig. 9C). The upper part of the succession is made of packstones and fine-grained grainstones that alternate with orbitolinid-rich marls. The top of the limestone beds is frequently

bioturbated by *Thalassinoides* burrows (Fig. 9D), which are filled with the overlying orbitolinid marls.

The maximum thickness of the calcarenite deposits of stage 2 is 52m in the eastern part of La Florida area (Bustriguado section; Fig. 6). Here, these deposits pinch out and disappear westward (Río Nansa section, Fig. 6), onlapping progressively on the underlying dissolution Surface coated by the Fe-rich crust. The end of the carbonate stage 2 is marked by a discontinuity on top of a bioturbated and reddish calcarenite bed, which is covered by marls of the Patrocinio Formation (Fig. 10A).

Interpretation

Sedimentary lithofacies and structures suggest that high-energy tidal and coastal currents controlled deposition of these carbonate sands (sand waves). They represent high-energy shallow bars and shoals deposited in an open-marine, inner to mid carbonate shelf environment. At the upper part of the succession, abandoned bars were rapidly colonized by burrowing organisms (*Thalassinoides*) and then buried by marls. This suggests an overall deepening trend of the succession linked to a transgressive episode.

Stage 3: Carbonate platform drowning at the onset of OAE 1a

Description

The stage is represented by the Patrocinio Formation (Fig. 10A). Open-marine marls of this unit abruptly overlie the shallow water carbonates of stage 2. Lithofacies are formed by silty marls to darkgrey, soft clayed marls with glauconite and ironstone nodules. These yield ammonites, belemnites, and microfossils including planktonic foraminifera and nannoplankton. Up-section, the silt content of the marls increases and appear bioclastic beds with erosional surfaces, and debris of bivalves, brachiopods, echinoids and orbitolinids as well as wood fragments. Bioturbation also becomes intense upwards. In the Cuchía area (Fig. 10A), the upper part of the stage 3 records an upward increase in the content of siltstones and mica-rich, bioturbated sandstones with *Ophiomorpha nodosa*, ripple trough crossbedded sandstones, and heterolithic facies with flaser and lenticular bedding, organized in a thickening and coarsening-upward sequence.

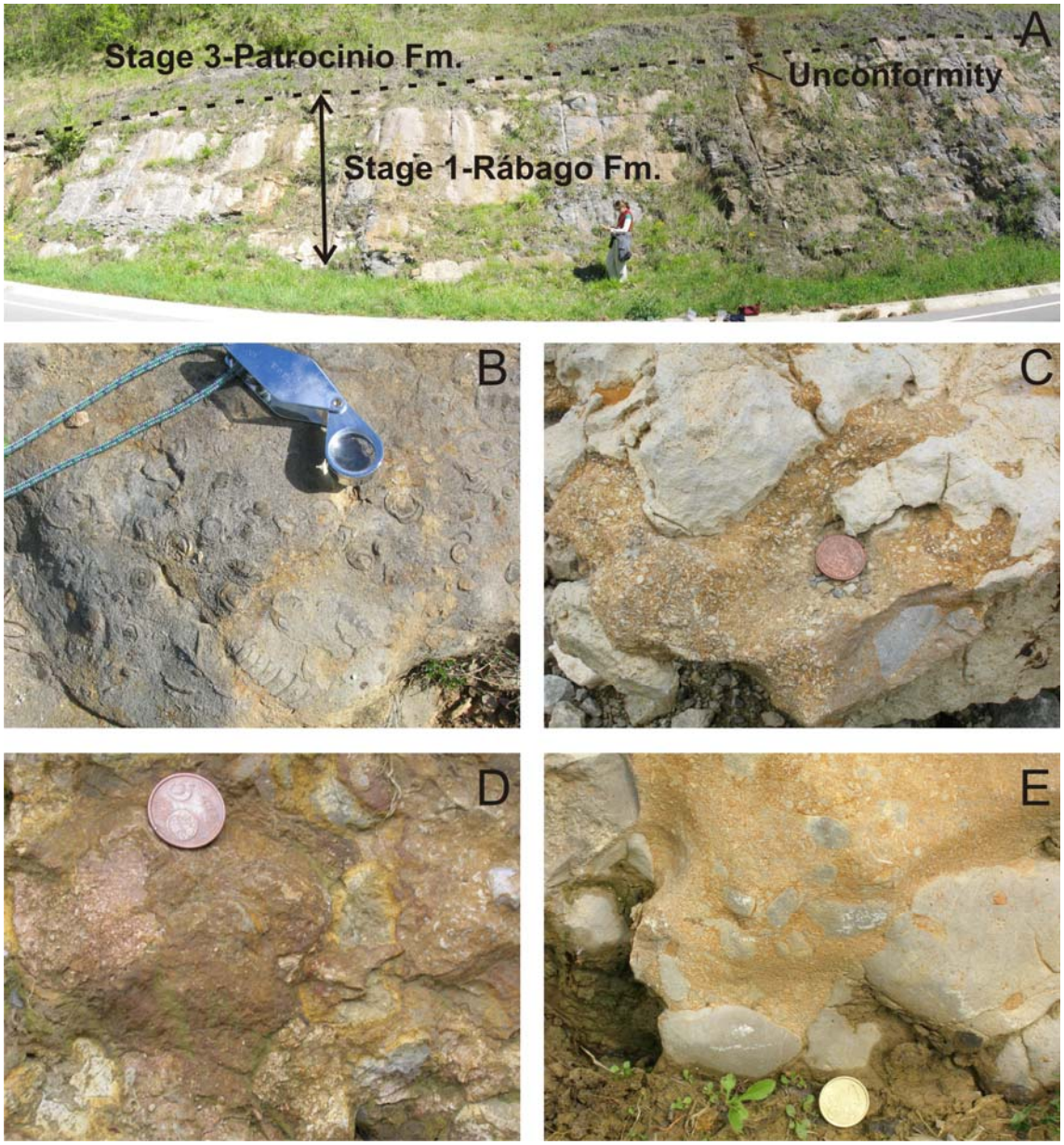

Figure 8.- Field pictures of the stage 1 (Rábago Formation) at La Florida area. (A) Field view of the stage 1 at Río Nansa section. (B) Detailed picture of a wackestone–packstone with gastropods and corals at Río Nansa section. (C) Detail of the dissolution surface at the top of stage 1, showing irregular cavities and fissures filled by red-stained bioclastic grainstones of the stage 2 at Rábago section. (D) Fe-rich crust coating the dissolution surface of the stage 1 at Rábago section. (E) Irregular cavity filled by carbonate breccia made of cm-size subangular clasts and a matrix of red-stained bioclastic calcarenite from the stage 2 at Rábago section.

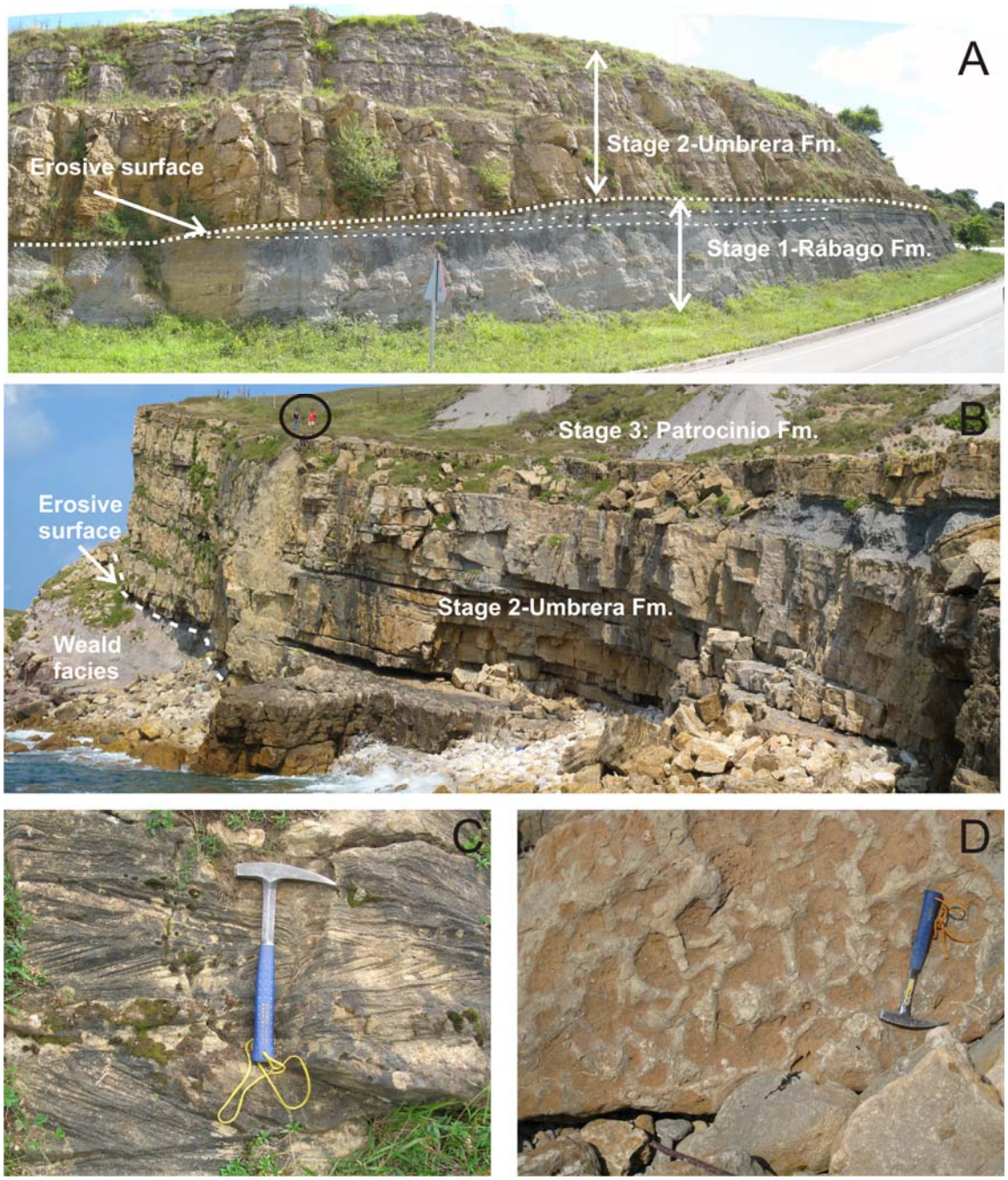

Figure 9.- Field pictures of the stage 2 (Umbrera Formation). (A) Contact between the stage 1 (orbitolinid marls and marly limestones) and the stage 2 (cross-bedded grainstones) at Santillana area. An erosive surface truncates the top of stage 1; traffic sign for scale is 2 m. (B) Cross-bedded bioclastic grainstone of the stage 2 at Cuchía. In this area the stage 1 is not recorded and the stage 2 rests directly on Wealden facies. The end of stage 2 is marked by deposition of the dark marls of the Patrocinio Formation; people for scale. (C) Detail of cross-bedding of bioclastic–oolitic grainstones at the lower part of the Umbrera Formation (Corona de Arnero section, La Florida area). (D) Large *Thalassinoides* burrows at the top of the Umbrera Formation in the Cuchía area.

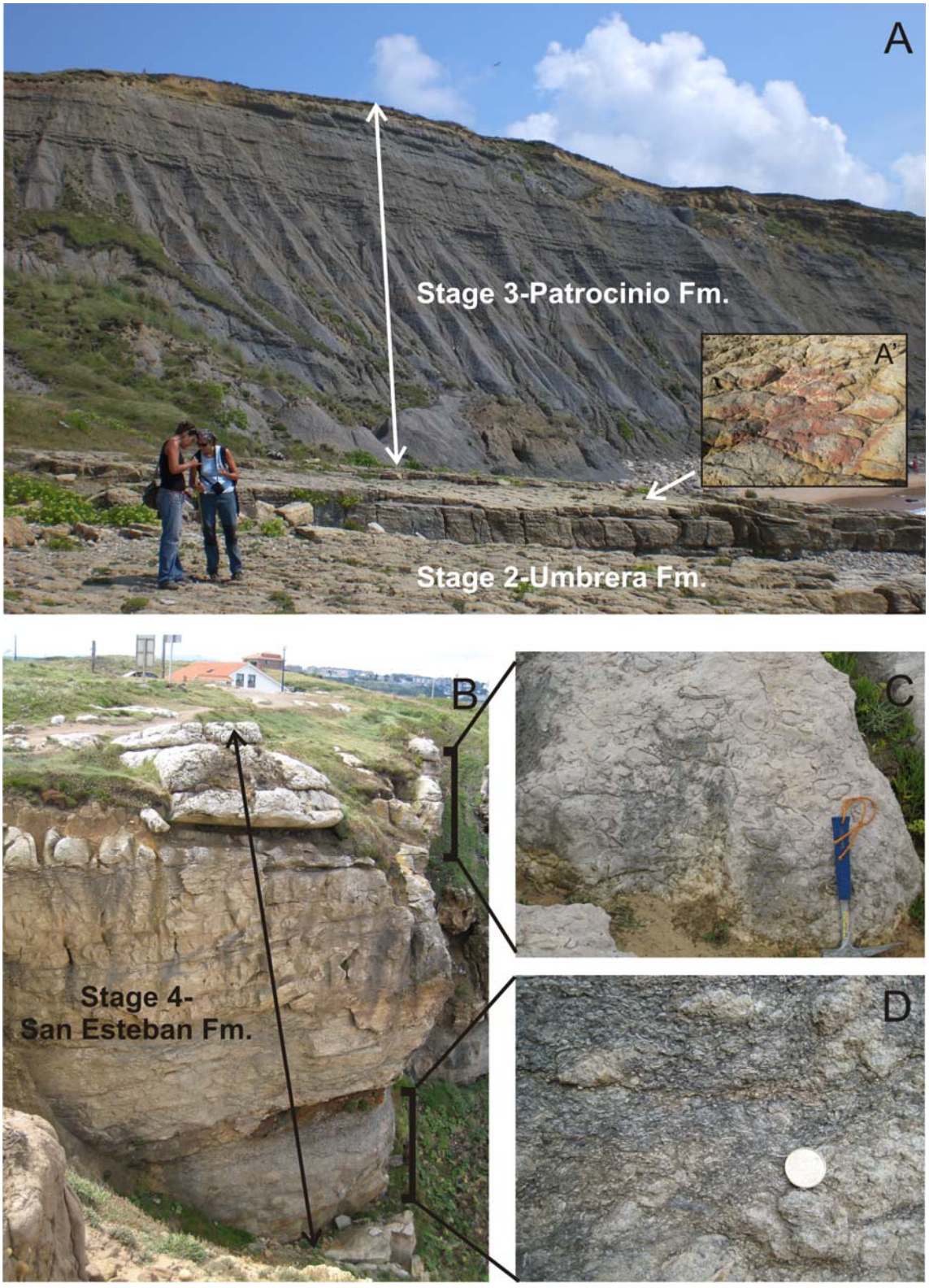

Figure 10.- Field aspects of the stage 3 (Patrocinio Formation) and the stage 4 (San Esteban Formation) at Cuchía area. (A–A′) Bioturbated and reddish surface at the top of stage 2 covered by dark marls of the Patrocinio Formation. (B) General view of shallow water limestones of the stage 4 (San Esteban Formation). (C) Limestones with requiniid rudists at the upper part of the unit. (D) Orbitolinid marls at the lower part of the unit.

Interpretation

These deposits reflect the shutdown of the shallow water carbonate factory in the area and the drowning of carbonate platform stage 2, likely as the result of a combined action of a relative sea-level rise and poisoning by siliciclastic particles. The lower marly interval is interpreted as formed by fall of fine carbonate particles mixed with fine-grained terrigenous material, under low-energy conditions below storm wave base. Up-section, the increment of silt content suggests input of coarser siliciclastic material from continent. The bioclastic erosive layers suggest storm beds deposited above the storm wave base, and finally, the sandstone lithofacies at the top represents progradation of deltaic facies (Wilmsen, 2005). This whole succession indicates a net shallowing-upward trend and rapid regression towards the end of the stage.

Stage 4: Carbonate platform recovering

Description

The shallow water carbonate production and deposition recovered during the late Early Aptian (late Bedoulian) and dominated until the Late Aptian. The interval is represented by decimetre- to metre-scale beds of wackestones and packstones with rudist–coral assemblages and L. aggregatum–B. irregularis oncoids. The succession starts with up to 4 m of orbitolinid-rich, marly to nodular limestone beds (Fig. 10B–D), that are usually followed by marly limestones with orbitolinids, bioclasts, sponges and corals; these grading upward to well-bedded limestones with abundant requieniid rudists (Toucasia and Requienia) (Fig. 10C).

Interpretation

The instauration of stage 4 indicates the recovery in the effectiveness of the carbonate factory, favoured by the progressive shallowing of the depositional system and by the decontamination of terrigenous particles. When the carbonate sedimentation was reestablished, the orbitolinids were the first colonizers, due to their higher tolerance to adverse conditions such as water turbidity, terrigenous poisoning and limited light (as described in a similar case by Vilas et al., 1995). The vertical evolution from marly orbitolinid facies to micrite rudist facies may indicate a gradual environmental change to more favourable ecological conditions for carbonate secretion and biodiversity. The

micritic limestones with miliolids, rudists and benthic foraminifera indicate a shallow water, restricted lagoonal environment with low terrigenous influence.

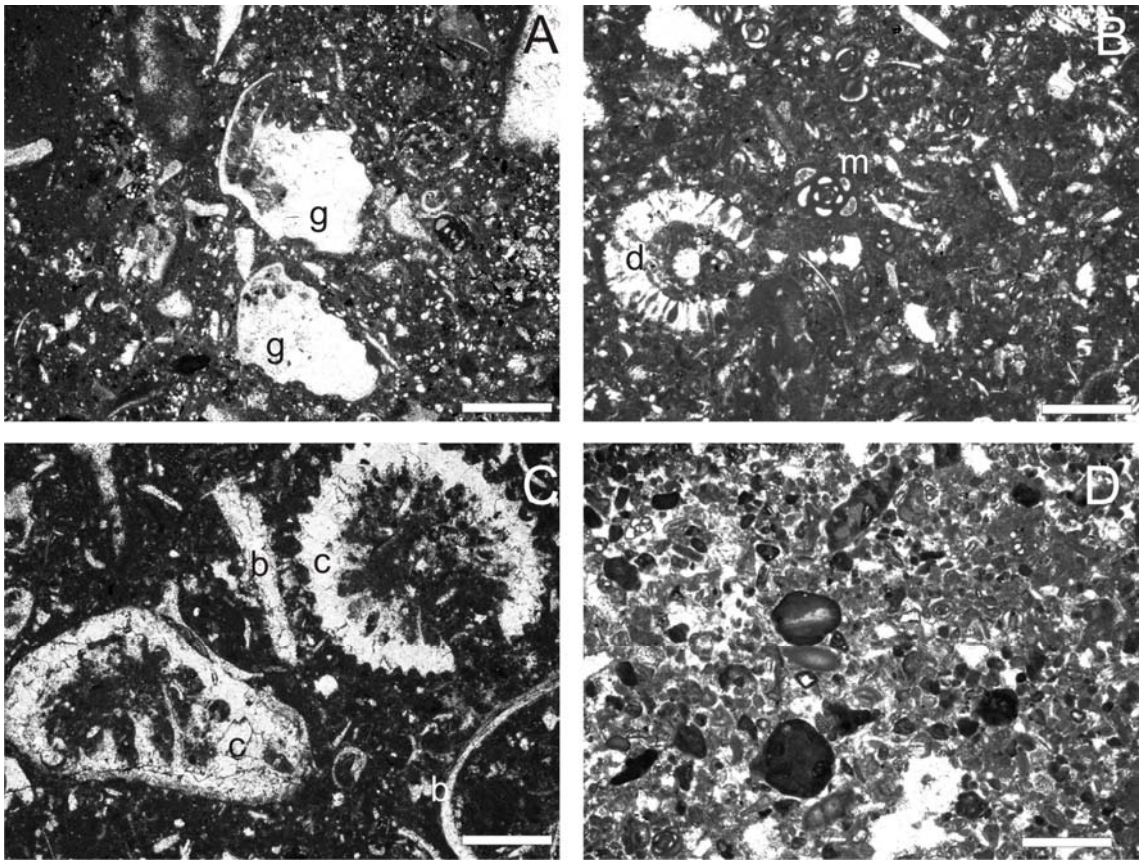

Figure 11. Microfacies of the stages 1 and 4; scale bar for all plane-light photomicrographs is 1 mm. (A) Packstone with dissolved gastropods (g), bioclasts and miliolids. Sample PN-9, Río Nansa section, La Florida area, Rábago Formation. (B) Packstone–wackestone with micritized grains, miliolids (m) and dasycladacean green algae (d); Bustriguado section, La Florida area, Rábago Formation. (C) Wackestone with hermatypic corals (c) and thin shelled bivalves (b); Rábago section, La Florida area, Reocín Formation. (D) Peloidal packstone with intraclasts formed by micritic limestones, foraminiferans and bioclasts. Sample LA-7, Rábago section, La Florida area, Rábago Formation.

PARTICLE COMPOSITION

Skeletal carbonate components of stages 1 and 4

Carbonate platform lithofacies of stages 1 and 4 display comparable assemblages of skeletal components. In grainstone and packstone lithofacies, well-rounded fragments of green algae (dasycladacean, codiacean), coralline sponges, lumps of cyanobacteria, benthic arenaceous foraminifera, orbitolinids, and fragments of rudists and other bivalves are the most common carbonate components, with a minor

contribution of plates and spines of echinoderms, gastropods, and fragments of branching corals, brachiopods and oysters. Microfacies of wackestone beds are dominated by intact and fragmented skeletons of rudists (mostly requieniids and monopleurids), nerineid gastropods, branching and colonial corals, dasycladacean green algae and thin shelled bivalves, with variable contributions of *L. aggregatum– B. irregularis* oncoids, Chondrodonta, miliolids, orbitolinids and benthic agglutinated foraminifera (Fig. 11A–C). In minor proportion, coralline algae, brachiopods, echinoderm plates, oysters and ostracods are also found.

Non-skeletal components of stages 1 and 4

Intraclasts, peloids and micritized grains represent the most common non-skeletal particles in the carbonate platform lithofacies of stages 1 and 4. Intraclasts (<5%) are small and well rounded, and derived from facies of micrite matrix with foraminifera and bioclasts (Fig. 11D). Peloids are small in size, subspherical to ovoidal in shape, conspicuously rounded, and well sorted. They don't exhibit any evident structure or organization such as gradation or lamination. Silt-size grains of quartz (<1%) and opaque minerals are also present.

Skeletal carbonate components of stage 2

During the carbonate stage 2, the principal skeletal components of the microfacies are large agglutinated benthic foraminifera (orbitolinids and large lituolids), bryozoans, plates and spines of echinoderms, crinoid ossicles, red algae and mollusc debris (bivalves, gastropods, and oysters) (Fig. 12A). No intact rudist shells, corals and green algae have been observed. These appear as minor components preferentially concentrated in the basal beds of the calcarenite interval, immediately above the basal unconformity, and correspond to well-rounded to subrounded, abraded fragments, generally about 1 mm in size or less (Fig. 12B). These reworked fragments of rudists and corals are recrystallized and commonly constitute the nucleus of ooids (Fig. 12C). Occasionally miliolids are present and may appear broken as well (Fig. 12B).

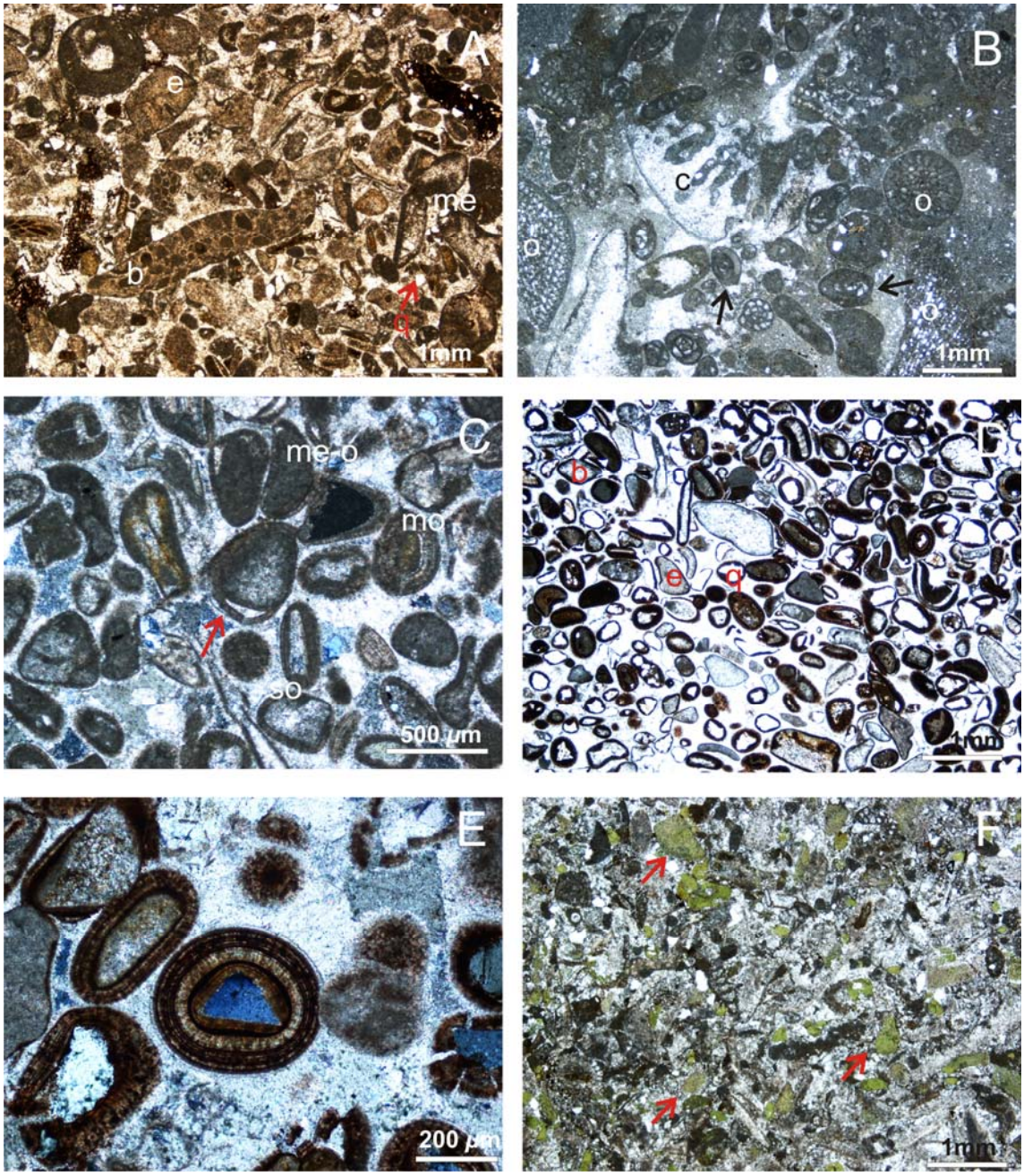

Figure 12.- Photomicrographs showing microfacies of the stage 2 (Umbrera Formation.). (A) Bioclastic grainstonewith bryozoans (b), plates of echinoderms (e), micritized bioclasts (me) and quartz grains (q); Bustriguado section, La Florida area. (B) Packstone with orbitolinids (o) and abraded fragments of corals (c) and miliolids (arrows); Cuchía section, Cuchía area. (C)Oolitic grainstone with mixed ooids (mo), superficial ooids (so) and micritized ooids (me-o). Note the broken ooid cortex separated from the nucleus by thin calcite cement (arrow); crossed polarized-light; La Florida section, La Florida area. (D) Ferruginized oolites with different types of nucleus such as quartz grains (q), echinoderm (e) and dissolved bioclast (b), and iron oxide or iron-stained cortices; Bustriguado section, La Florida area. (E) Detail of a mixed ooid whose nucleus is composed by a quartz-grain and the cortex by layers of iron oxides and calcite; Bustriguado section, La Florida area; crossed polarized-light. (F) Glauconite-rich grainstone with quartz grains and bioclasts. Glauconite appears as detrital grains and replacing echinoderm plates (arrow); Cuchía section, Cuchía area.

Non-skeletal components of stage 2

Non-skeletal components of stage 2 are represented by fine to medium sand-sized quartz grains, glauconite grains, calcite ooids, ferruginized ooids and coated grains, and extraclasts (reworked fragments of previously lithified rocks). The latter include rock fragments derived from the underlying Fe-rich crust, from limestones deposited during the stage 1, and from older sandstone units. Quartz grains may represent 5 to 30% of the whole components, are sub-angular to subrounded in shape, and show moderate sorting. Plant fragments are a minor but ubiquitous component.

Ooids and coated grains are fine to medium-grained, moderately to poorly sorted and well-rounded (Fig. 12C–E). The nuclei consist of quartz grains, chert, extraclasts, echinoid plates, and abraded fragments of corals and bioclasts that generally appear dissolved and replaced by calcite (Fig. 12C). It has been distinguished both superficial and well-developed (normal) ooids with thick mixed cortices. Irregular concentric cortices of one or two layers form superficial ooids. Mixed ooids are common and result from the superposition of cortices made of both tangential calcite and micrite layers (Fig. 12E). In addition, ooids formed entirely by layers of tangential arrangement of tightly packed radial calcite crystals, and micritic ooids made of concentric micrite layered structures have been observed. Some composed ooids with two or more nuclei also occur. Some ooid cortices appear broken and separated from the nucleus or other cortices by thin calcite cement (Fig. 12C). Cracked ooids also occur, which may develop new cortices in discordance with the broken ones.

Glauconite beds occur in the upper part of the calcarenite succession, appearing as detrital grains, filling pore spaces, or replacing skeletal particles (Fig. 12F).

EARLY DIAGENESIS

The study of thin sections under optical and CL microscopy allows differentiation of a series of diagenetic features which reveal essential aspects of early diagenesis. These notably complete the environmental information given by facies and fossils, and contribute to reconstruct the evolution of the platform, especially during the stages 1 and 2, that preceded the OAE 1a.

Micritization

During the stage 1, bioclasts commonly present micrite rims or appear completely micritized. Both destructive and constructive micrite envelops are observed. Micrite envelops and micritization also occurred during the stage 2 affecting to skeletal particles and ooids.

Destructive micrite envelopes are formed by microboring produced by microendolithic organism and infilling of the tiny little voids by microcrystalline Mg calcite or aragonite cements (Bathurst, 1966; Perry, 1999). Constructive micrite envelopes may result from the growth of externally calcified filamentous algae on the surface of the carbonate grains (e.g. Calvet, 1982). Both modes are interpreted to be connected with the activity of microbes, algae and fungi (Perry, 1999; Flügel, 2004; Chacón et al., 2006) and represent microbial development on the bioclastic debris. The micritized ooids are considered as the result of intense micritization of radial calcite ooids, caused by microboring by algae or fungi (Margolis and Rex, 1971).

Ferruginization

Concentration of iron oxide occurred on the ferruginous crust that coated the palaeokarst surface on top of the stage 1. It is made by serpulid worm tubes and encrusting agglutinated foraminifera (nubeculariids) embedded in a matrix of iron-oxide films (Fig. 13A). In addition, red to brown grainstone beds with abundant iron-stained components occurred in the first metres above this surface. Iron staining affects to echinoderm fragments, foraminifera and bryozoan chambers and ooids. In these reddish beds, the cortex and nucleus of the majority of the ooids are strongly ferruginized and present abundant microborings and microfilaments (Fig. 13B–D), which may have destroyed completely the original textural patterns. The iron oxides may replace the external calcite cortices only or may form mixed ooids. Mixed ooids are formed by tangential calcite or fine micrite layers that alternate with thin Fe-rich coatings (Fig. 13B, C).

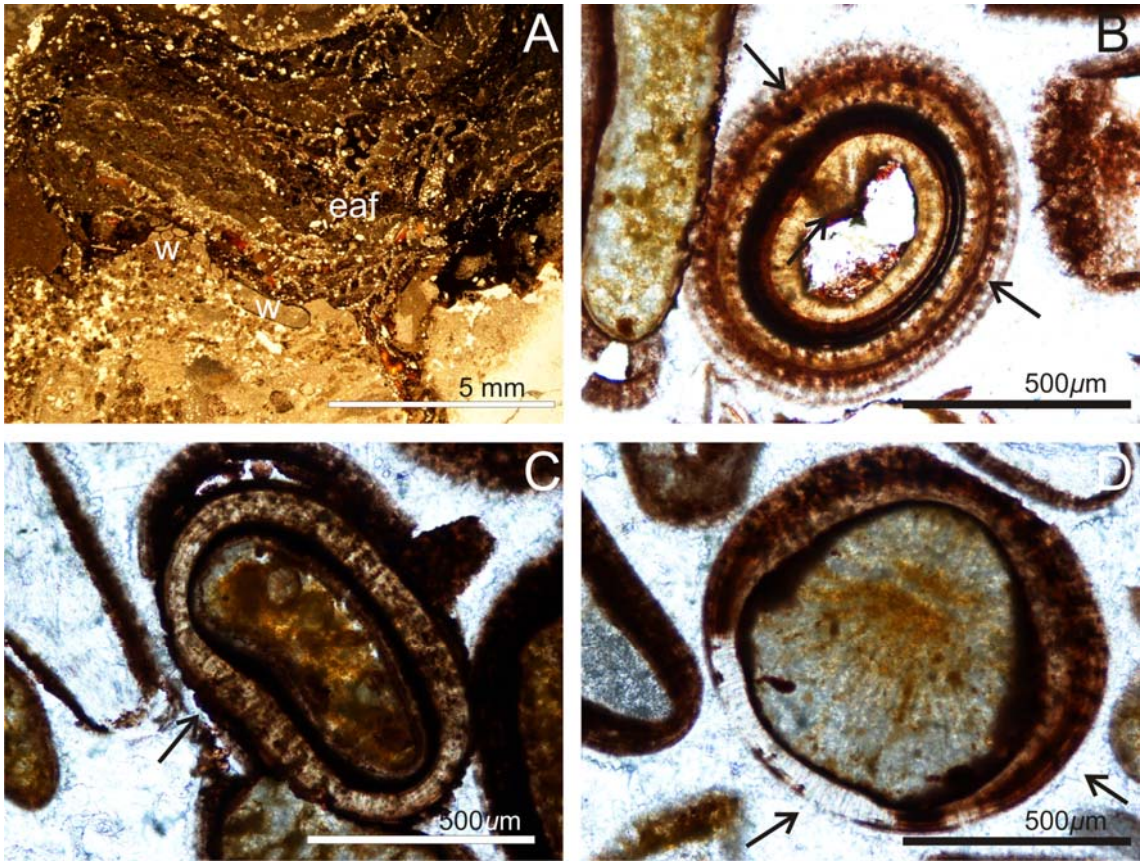

Figure 13.- Detailed plane-light photomicrographs of the hardground that appears coating the palaeokarst surface of the stage 1, and of the ferruginized oolites at the first metres above this surface. (A) Fe-rich crust composed by worm tubes (w), encrusting agglutinated foraminifera (eaf) embedded in a matrix of iron-oxide films. Sample LA-12, Rábago section, La Florida area. (B) Detail of mixed iron ooid with microborings (arrow); Bustriguado section, La Florida area. (C) Mixed iron ooid with microborings (arrow) resulted from reworking of previously deposited ooid and formation of new carbonate cortex on previous ferruginous layers; Bustriguado section, La Florida area. (D) Fine-radial calcite cortex is replaced by submicrometre-scale iron oxides. Note the isopachous, fibrous-to-bladed calcite cement (C1) around the ferruginized ooid (arrows).

Ferruginized ooids and crusts similar to those described above are frequent in Jurassic hardgrounds and condensed sections of the Tethyan basins (e.g. Di Stefano and Mindszenty, 2000; Préat et al., 2000; Ramajo et al., 2002; Gradzinski et al., 2004; Mamet and Préat, 2006; Reolid et al., 2008), but are identified throughout the whole stratigraphic record since the Proterozoic. Their genesis has been interpreted in diverse ways that include subaerial and submarine environments, with the iron being supplied from volcanic to hydrothermal, lateritic or continental sources (e.g. Jenkyns, 1970; Nahon et al., 1980; Kearsley, 1989; Aurell et al. 1994; Sturesson et al., 2000). In this study, the presence of serpulids and ooid nuclei indicate a definitive marine origin for the iron crust and ooids. The fact that the iron staining is related to bioclast and ooid

portions which have lost the original texture suggests the presence of microbes that oxidized the ferrous iron. This may have occurred at the sediment–water interface (Préat et al., 2000), but implies that water energy at the sea bottom varied intermittently. Once the calcite ooids were formed, they rested on the sea-floor during a time interval long enough to allow that the original calcite surfaces of the ooids provide substratum for colonization of iron-oxidizing bacteria and fungi, forming colonies within the carbonate cortex. The microbial activity led to precipitation and replacement of the carbonate support by submicrometric iron oxides, and the ooids became reddish (Fig. 13D). This is an early marine diagenetic process that occurred at slow rates and that requires a relatively large exposition of the ooids near the sediment–water interface. After that, the ferruginized ooids may be reworked during subsequent episodes of high energy, or may be latterly transported to the high-energy depositional settings of stage 2. Mixed ooids may result from reworking of previously deposited and ferruginized ooids affected by later formation of a new carbonate cortex on old ferruginous layers (Fig. 13C).

Glauconite authigenesis

Glauconite cement has been observed in the stage 2, filling primary intraparticle voids, particularly within echinoderms and orbitolinids.

This authigenic glauconite is considered to have been precipitated from marine pore waters during early marine diagenesis, under low sedimentary rates and partially reducing conditions (Odin and Matter, 1981), and indicates primary mineralization in condensed marine sediments (Odin, 1988; Glenn et al., 1994).

Carbonate cementation

Carbonate cementation affects all the analyzed samples froma variety of diagenetic processes extending from early marine diagenesis on the sea-floor to meteoric and burial environments. Only the sea-floor and meteoric diagenetic stages are discussed in this paper. These carbonate cements appear as pore-lining and pore-filling cements in primary cavities, intergranular pore space, and in secondary mouldic porosity.

Early marine cement

Isopachous, fibrous-to-bladed calcite cement (C1) appears aroun ferruginized ooids, skeletal grains, quartz particles and extraclasts associated preferably to the grainstone of the stage 2 of carbonate production. Isopachous fringing cement is also observed on samples from the stages 1 and 4, although it occurs more scarcely. This cement stains pink (non-ferroan) and fills primary intergranular porosity. Under cathodoluminescence (CL), it is bright to dull orange (Fig. 14A–B).

This calcite cement appears to have formed early, in the marine phreatic or near sea-floor environment as high-Mg calcite or fibrous aragonite, and later transformed to low-Mg calcite (Moore, 1989; James and Choquette, 1990). The luminescence bright-dull orange suggests recrystallization or primary precipitation under slightly reducing conditions (Barbin, 2000). However, the regular pattern and homogeneous intensity of luminescence point to a rather primary precipitation.

Shallow burial meteoric cement

Blocky equant calcite spar (C2) occurs as pore-lining and pore filling cement in primary inter- and intraparticle pores as well as in secondary mouldic porosity. This cement commonly occurs as scalenohedral (dogtooth) spar around pores or as drusy to equant calcite when occluding pore spaces. It is non-ferroan and probably low-Mg, and is rich in Fe-oxide solid inclusions. In CL this cement presents three cements zones (Z1 to Z3; Fig. 14C–D). Z1 is nonluminescent. Z2 is mainly orange- to yellow bright luminescent, and may occur as one single bright zone or as several bright luminescent/non-luminescent multizones (Fig. 14D). Z3 zone is dark-dull luminescent.

Spar crystals of calcite C2 have been observed in all the carbonate stages. However, there is a significant difference in how calcite C2 appears through the succession, especially through the stages 1 and 2. Beneath the unconformity at the top of stage 1, this calcite spar occurs extensively in intergranular, shelter, intraskeletal and mouldic pores, the later generated after leaching of aragonite skeletons. In contrast, above the unconformity, C2 calcite does not cement grainstones of the stage 2 (Fig. 14E–F). In this case, it is observed only in some abraded skeletal grains, eroded and reworked from the previous stage 1 (Fig. 14E–F).

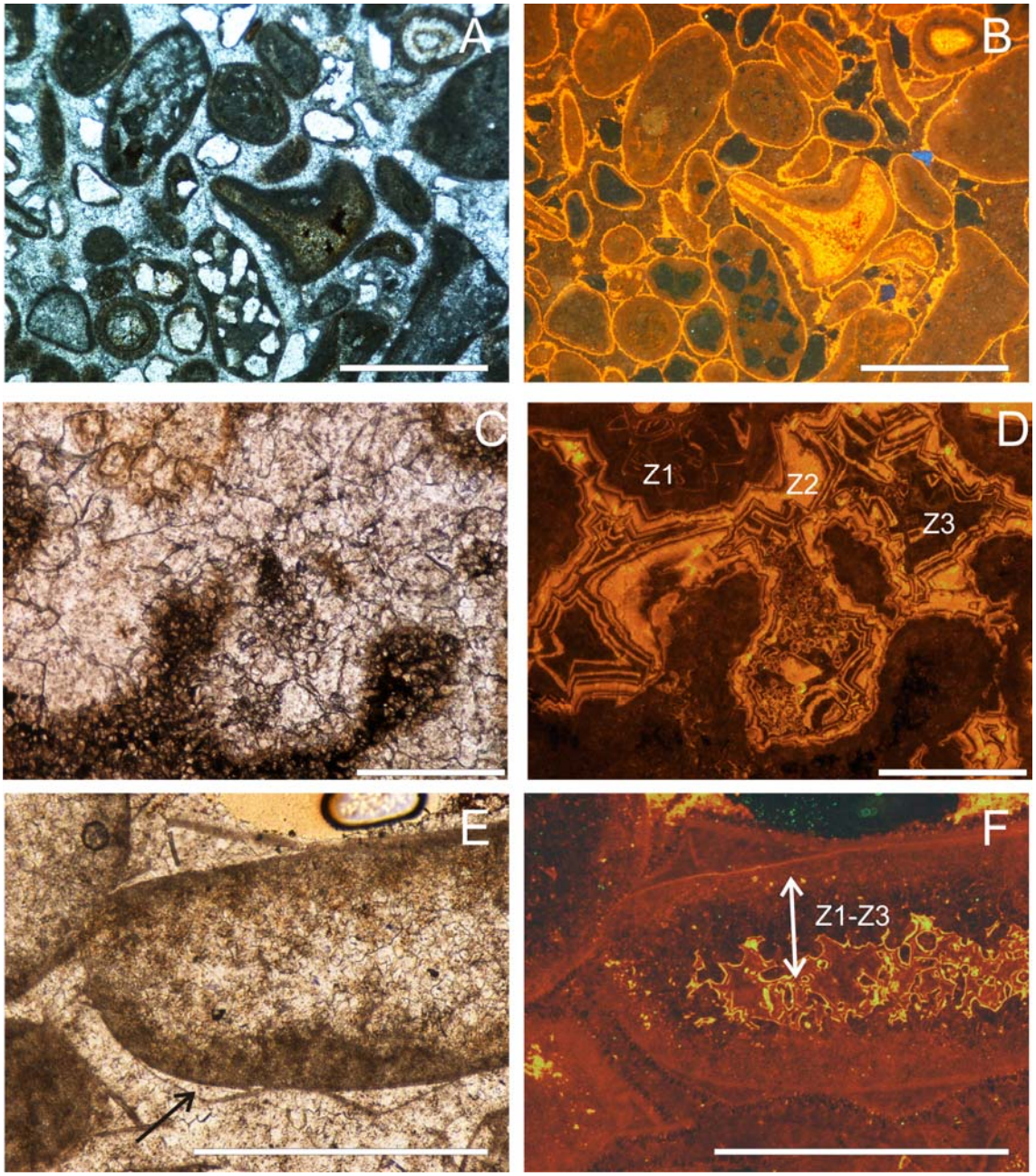

Figure 14.- Photomicrographs of paired plane-light (left) and CL (right) images; scale bar in each case is 500 µm. (A–B) Isopachous, fibrous-to-bladed calcite cement (C1) fringing primary intergranular porosity in grainstones of the stage 2. Under CL the fringing cement is bright orange; Hayuela-Canales section, Santillana area. (C–D) Pore filling, low-Mg, nonferroan calcite cement (C2) precipitated in the mould porosity of a dissolved coral of the stage 1. In CL, C2 presents three cements zones (Z1–Z3). Z1 is non-luminescent. Z2 is mainly multizoned non-luminescent and orange bright luminescent and Z3 is dark-dull luminescent; sample LA-6, Rábago section, La Florida area. (E–F) Reworked bioclast of stage 2 replaced by equant calcite cement (C2) that in CL shows the Z1–Z3 cement zones. Note the micrite envelope separated from the bioclast due to early mechanical compaction (arrow); Sample LA-12, Rábago section, La Florida area.

Calcite spar C2 is considered to indicate freshwater shallow burial (meteoric) cementation from oxidizing (non-luminescent) to moderate reducing (bright

luminescent) pore fluids (Moore, 1989; Muchez et al., 1998; Dickson and Saller, 1995; Mutti, 1995). This process is well documented in modern aquifers (Champ et al., 1979). Leaching of the aragonite skeletons and subsequent replacement by calcite spar C2 occurred during emersion at the end of stage 1. During the following transgression, with erosion of the previous stage, they were eroded and recycled in the grainstones of the stage 2.

STABLE ISOTOPES

Stable carbon isotopic composition ($\delta^{13}C$) throughout the studied succession in La Florida area (Fig. 15), varies from +3.6‰ to −4.5‰, recording a noticeable range of variability, which exceeds 8‰. In that succession, the $\delta^{13}C$ record can be subdivided into three successive intervals (Fig. 15). The basal interval matches with stages 1 and 2 of carbonate production. It shows relatively homogeneous and positive $\delta^{13}C$ values during the stage 1 (mean of +2.2‰), and a significant and progressive decrease (of about 1‰) in the record of the stage 2 (but still within positive values). The second interval of the $\delta^{13}C$ curve correlates with the Patrocinio Formation (stage 3). This interval is characterized by a notable negative excursion from values of −0.4‰ at the base of the interval to −4.5‰ at the top. The decrease in the values is not gradual but shows three negative peaks (−2.9‰, −4.1‰ and −4.5‰ respectively; Fig. 15). Finally, the third interval in the $\delta^{13}C$ record shows the return to positive values. This change occurs during the re-instauration of carbonate production in the stage 4. During this interval the $\delta^{13}C$ values range from +2.5‰ to +3.6‰, and are, in average, more positive than those of the first interval.

The oxygen-isotope record ($\delta^{18}O$) also shows a remarkable variability, with values varying from −2.7‰ to −13.8‰ (Fig. 15). It reveals comparable patterns to those of the carbon-isotope curve, and three main intervals can be also differentiated along the section. The first interval coincides with the stages 1 and 2, and presents relatively constant values (mean of −3.5‰). A sharp negative excursion is recorded during deposition of the marly Patrocinio Formation. Here the values range from −5.7‰ to −13.8‰. The third interval of the $\delta^{18}O$ curve shows a return to less negative values (mean of −4.3‰), which are correlated with deposition of the stage 4 (Fig. 15).

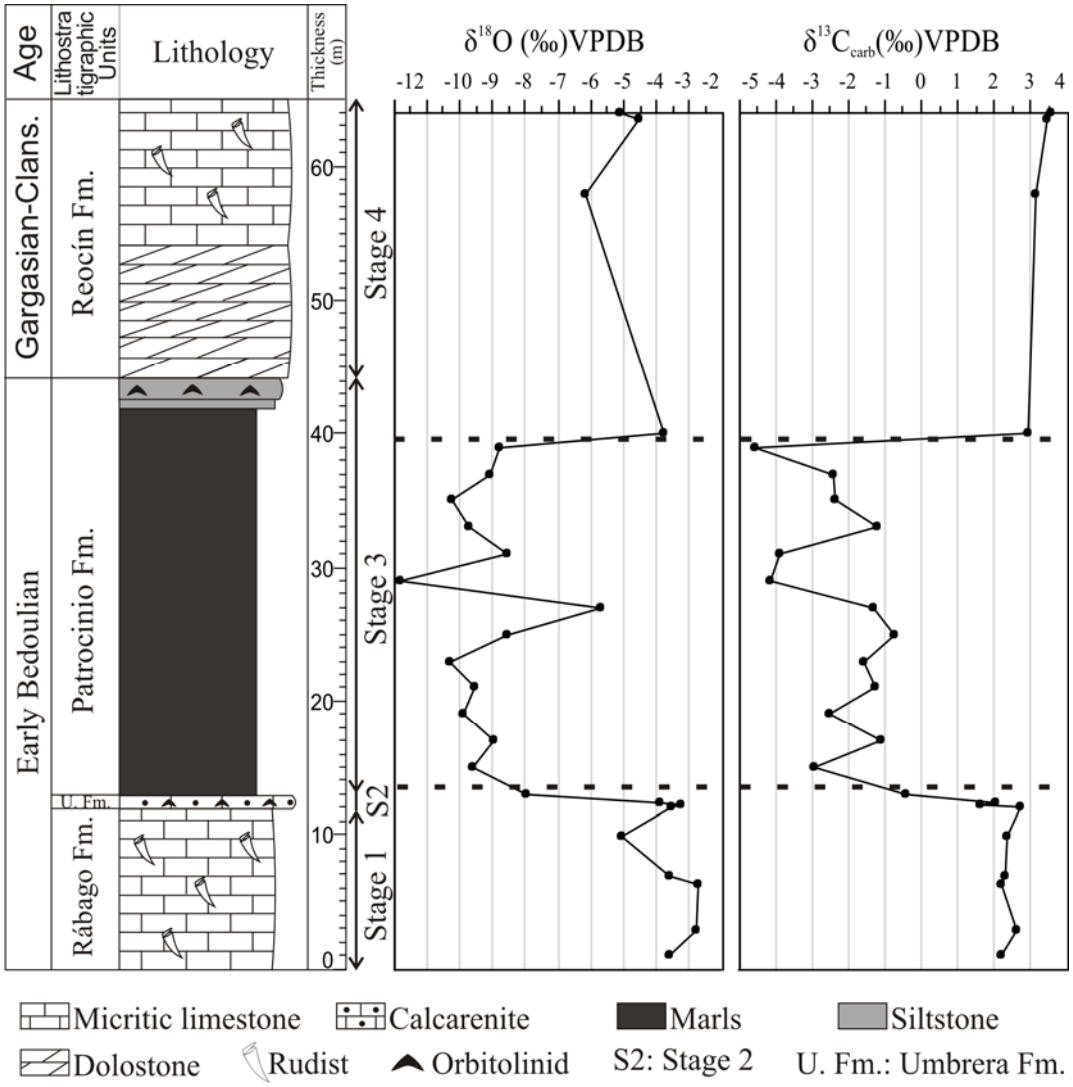

Figure 15.- Carbonate carbon and oxygen stable isotope records of the Aptian carbonate succession from La Florida area. The isotopic records are plotted against stratigraphic thickness, lithology and stratigraphic units. Dotted lines mark isotopic intervals.

DISCUSSION

Understanding the effects of the OAEs in the deep oceans has become a major objective of a large number of works in the last years. However, little is still known about the effects of these events on shallow marine platform carbonates and the interaction of their effects with local tectonic factors. The studied shallow platform succession was affected during the Aptian by the OAE 1a and by extensional tectonics. During the Aptian and immediately preceding the anoxic event, the platform evolved from stage 1 (photozoan assemblages) to stage 2 (heterozoan assemblages) of carbonate production. Later, a rapid drowning of the platform and deposition of open-marine shales (stage 3) occurred at the onset of the OAE 1a. Finally, the recovering of shallow water carbonate deposition with photozoan assemblages took place during the stage 4, at the end and after the anoxic event. The data indicate that the stratigraphic, sedimentological, diagenetic and chemostratigraphic shifts that affected the platform carbonates during this time were abrupt, and all of them point to rapid environmental changes accompanying the platform evolution.

Photozoan versus heterozoan styles of carbonate production

The predominance during the carbonate stages 1 and 4 of light dependent benthic organisms and skeletal grain types (corals, dasycladacean algae, etc.) indicates a photozoan style of carbonate production (Table 1). Comparing with modern carbonate sediments, this photozoan assemblage reflects favourable platform growth conditions in seawaters that are shallow, transparent, warm, euhaline, and oligotrophic (Hallock, 1988; Föllmi et al., 1994; James, 1997). The photozoan textures (wackestone and packstone) of stages 1 and 4 suggest that the depositional energy was predominantly low. The presence of miliolids, monopleurid and requieniid rudist banks, *L. aggregatum–B. irregularis*, and fenestral microbialites suggests shallow water with stable bottom conditions and deposition in protected lagoons with weak bottom currents (e.g. Ross and Skelton, 1993; Gómez-Pérez et al., 1998), only occasionally affected by high energy episodes. The low amount of non-skeletal grains and the minor contribution of siliciclastic particles, except for the mixed carbonate–siliciclastic facies at the transgressive bases of the carbonate stages, suggest low contribution of terrigenous runoff during these stages of carbonate growth.

In contrast, during the stage 2, the platform sedimentation was dominated by a heterozoan style of carbonate production, with predominance of calcite components, absence of organic build-ups, and abundance of suspension feedings such as crinoids and bryozoans. The substantial amount of orbitolinids indicates conditions of high nutrient input, since these asexually reproducing benthic foraminifera thrive in such conditions (Birkeland, 1988; Vilas et al., 1995). The heterozoan skeletal grains of the stage 2 (e.g. echinoids, coralline algae and molluscs) are ubiquitous elements present in a wide range of shallow marine systems and latitudes, although they became predominant only when other organisms are inhibited by environmental conditions such as light availability, temperature, salinity and nutrients (Hallock, 1988). In modern platform analogues, this heterozoan association typifies sedimentation in cool waters, or alternatively, sedimentation below the photic zone (James, 1997). However, nutrient poisoning (excess) can produce enough environmental stress to radically alter the platform benthos and eventually led to platform drowning (Hallock and Schlager, 1986; Hallock, 1988; Jenkyns, 1995). During the Aptian, sedimentation in the Basque-Cantabrian basin occurred in warm, sub-tropical climatic regions (e.g. Scotesse et al., 1998), and the data indicate that both the photozoan and heterozoan stages of carbonate deposition took place in shallow water conditions. The presence of light-dependent organisms in the photozoan stages implies deposition within the photic zone. In the heterozoan stage 2, the overall lack of carbonate mud, the common high-energy traction current structures, and the presence of oolites suggest deposition under agitated bottom waters, likely within the photic zone as well. Therefore, depth seems not to have played a major role in the compositional shifting to heterozoan carbonate sedimentation during the stage 2. The presence of substantial amounts of sand-sized siliciclastic particles accompanying the heterozoan stage 2 may be considered as an indicator of higher nutrient influx levels accompanying the import of detrital particles in this stage that preceded the OAE 1a (Föllmi et al., 1994; Burla et al., 2008).

Recently, there is an open debate about a possible causal relationship between the presence of *Lithocodium–Bacinella* communities in shallow epicontinental seas and the OAE 1a (Immenhauser et al., 2005). According to these authors, the *Lithocodium–Bacinella* consortium may represent an out-of-balance facies, flourished under rising nutrient levels, which are time-equivalent in shallow water platforms to the black shales deposited in hemipelagic and pelagic environments during the OAE 1a (Immenhauser et

al., 2005). However, in this study the presence of *Lithocodium–Bacinella* communities is not related with the OAE 1a. In fact, this facies appears indistinctly before and after the OAE 1a, (stages 1 and 4) with the maximum bloom taking place during the Late Aptian (Reocín Formation), which is not time-equivalent with the OAE 1a. On the contrary, the time-equivalent facies at the onset of the OAE 1a are represented by the black marls of the stage 3 (Patrocinio Formation) deposited during transgression and drowning of the platform.

Ferruginization, glauconite, and environmental stress

The shifting from the photozoan stage 1 to the heterozoan stage 2 was marked by a subaerial exposure surface coated by a later submarine iron crust; and the heterozoan skeletal association of stage 2 was accompanied by formation of ferruginized oolites. The ferruginous crust indicates early sea-floor cementation resulting in a hardground-capped unconformity, likely related to iron bacteria and microbe activity. This is suggested by the existence of microborings filled with iron oxides. The presence of nubeculariid foraminifers may suggest relatively shallow warm waters (Gradzinski et al., 2004).

Ferruginization of previous calcite oolites resulting in the formation of ferruginized oolites took place also under the influence of iron-oxidizing bacteria. This process can be produced by a variety of both phototrophic and non-phototrophic microorganisms. Due to the lack of light dependence of these organisms, they probably formed under dim conditions and required slow sedimentation rates, the presence of low-oxygen water masses and a source of iron (Mamet and Préat, 2006; Préat et al., 2008). Such conditions were likely associated with dysaerobic sediment–water interfaces (Mamet and Préat, 2006). Under such conditions the stability of the soluble reduced state of iron is higher and the metabolic activity of Feoxidizing bacteria can induce ferric oxide and hydroxide precipitation as a secondary by-product (Konhauser, 1998; Mamet and Préat, 2006). Therefore, these ferruginized oolites suggest the existence of long periods with dysaerobic bottom conditions that would alternate with high-energy conditions where the cross-stratified grainstones were formed. As indicated by the presence of some oolites with mixed layers of iron oxides and calcite, iron precipitation occurred probably very early, just after formation of oolite calcite cortices and fragmentation of skeletons and their immediate deposition, although they were still susceptible of periodic reworking. The source of the iron mineral can be explained by a

terrigenous origin, with the iron derived from enhanced continental weathering during sedimentation.

The formation of both hardground surfaces coated with iron oxide and glauconite-bearing sediments is frequent in the geological record related to condensed series and submarine hiatuses, and their genesis appear to be directly related to rapid sea-level rises, carbonate platform destruction and eutrophication (Hallock and Schlager, 1986; Hallock, 1988; Föllmi et al., 1994). The data suggest that enhanced terrestrial runoff during the stage 2 of carbonate production probably brought iron and nutrients to the North Cantabrian platform, resulting in water-column eutrophication and environmental stress. These particular trophic conditions may explain the proliferation of heterotrophic Fe-oxidizing bacteria and suspension-feeding benthic organisms, such as crinoids and other heterozoan skeletal components of the stage 2 (James, 1997; Föllmi et al., 2006).

Early calcite cements and environmental conditions of stages 1 and 2

The analysis of diagenetic features in the carbonates has been of great value to recognize meteoric alteration of the platform carbonates and to provide an additional record of changes in relative sea-level and environmental conditions. The occurrence of precompaction, calcite spar C2 is interpreted to precipitate from oxidized to slightly reduced meteoric waters in the phreatic zone (e.g. Benito et al., 2005; Bishop et al., 2009). Early meteoric cements have been exclusively observed on samples from the stage 1, accompanying medium-scale karstic features that occur at the top of this stage. The meteoric fluids entered the platform as a result of a combination of both subaerial exposure and acceleration of the hydrological cycle, which induced increased rainfall, fluvial discharge, and continental runoff. The interaction of meteoric waters with exposed marine carbonates during platform emersion caused dissolution and favoured the circulation of freshwater lenses through the carbonate mass, which acted as an unconfined aquifer. This resulted in further dissolution and precipitation of the non-luminescent to bright luminescent (Z1–Z2) blocky spar, filling all available porosity (primary cavities and secondary mouldic porosity). It should be noted that the occurrence of these type of cements recognized in some of the basal samples of the stage 2 is only apparent, as they are always found in recycled and reworked lithoclasts from the previous stage.

Primary intergranular porosity in grainstones from the stage 2 was filled with rinds of marine isopachous calcite cements, which precipitated primary most likely as luminescent cements. Manganese is the most common activator of the luminescence in natural calcites (Marshall, 1988) and its incorporation in marine cements may suggest changes in the trace element concentration of the seawater or changes in the redox environmental conditions of precipitation (Barbin, 2000). Besides, the influx of freshwater may increase the Mn content of seawater and, therefore, of the calcite precipitated under such environmental conditions. For example, cathodoluminescence studies carried out on recent biogenic calcites have revealed an increase of luminescence and Mn contents of the shell calcites with decreasing salinity (Barbin et al., 1991).

Platform drowning and negative C and O-isotope excursions of stage 3

The platform drowned during the evolutionary stage 3. The age of the drowning episode is well constrained with ammonites, planktonic foraminifers and nannofossils (Fig. 4), confirming that the marly interval (Patrocinio Formation) corresponds unequivocally to the OAE 1a (Gea et al., 2003; Rosales et al., 2009; Moreno-Bedmar et al., 2009). The chemostratigraphic analyses have revealed a prominent negative shift (~6‰) in the carbon-isotope record during deposition of these open-marine black marls. This negative shift is very similar to those reported from other coeval sections from adjacent basins (e.g. Moreno-Bedmar et al., 2009) and other basins from Europe, North America, Japan and the Pacific Ocean (Menegatti et al., 1998; Erba et al., 1999; Gröcke et al., 1999; Jenkyns and Wilson, 1999; Luciani et al., 2001; Ando et al., 2002; Bellanca et al., 2002; Jenkyns, 2003; Weissert and Erba, 2004, Burla et al., 2008), and is defined as a distinctive feature of the onset of the OAE 1a. Although the possible causal mechanisms of this carbon-isotope negative excursion are under a controversial debate (Jahren et al., 2001; Beerling et al., 2002; Jenkyns, 2003; Milkov, 2004), the massive release of isotopically light carbon to the atmosphere/hydrosphere reservoirs from methane hydrate dissociation is regarded as the most plausible hypothesis. This release was probably triggered by intensive volcanism and formation of large igneous provinces (Larson and Erba, 1999).

There is a good correlation between the $\delta^{13}C$ record of the studied Aptian carbonates and the main changes occurring in the evolution of the platform. The photozoan stages 1 and 4 are characterized by $\delta^{13}C$ values typical of micritic limestones

from carbonate platforms of this period (Menegatti et al., 1998; Burla et al., 2008). The installation of the heterozoan stage 2 is correlated with a slight shift to more negative $\delta^{13}C$ values before the sharp negative spike that characterize the stage 3 of platform drowning and the onset of the OAE 1a. Similar correlations of $\delta^{13}C$ negative shifts and phases of heterozoan carbonate growth have been also described for other Early Cretaceous Tethyan platforms (Föllmi et al., 2006). The cause of this correlation is unclear but may be influenced in some degree by the input to the basin of continental water rich in dissolved isotopically light carbon derived from soil erosion.

The oxygen-isotope record during the stage 3 of platform drowning shows also a prominent shift (up to 11‰) to more negative values accompanying the C-isotope negative spike. Generally, relative low $\delta^{18}O$ values in pristine marine calcites are explained as reflecting elevated seawater temperatures (e.g. Marshall, 1992). However, the negative $\delta^{18}O$ values registered during the stage 3 are incompatible with any reasonable palaeotemperature reconstruction since, if interpreted only in terms of palaeotemperature, would give unrealistic extremely high seawater temperatures. New $\delta^{18}O$ data on pelagic carbonates from ODP survey in the central Pacific (Ando et al., 2008) has revealed extreme warming at the onset of the OAE 1a, with $\delta^{18}O$ pelagic values as low as −4.5‰ departing from background values of about −2‰. By comparison, only a small portion (~2–3‰) of the isotopic shift recorded in the samples across the marly interval of stage 3 may have been caused by this warming episode.

Other possible mechanism to explain isotopically light values of both $\delta^{18}O$ and $\delta^{13}C$ records in shallow platform carbonates can be found in early diagenetic processes associated with platform exposure (Immenhauser et al., 2002, 2003, 2008). These authors propose that low C and O isotope values in platforms tops are usually related to the combination of two processes. One is the influence of ^{18}O-depleted early meteoric fluids and the other is the influence of ^{13}C-depleted soil-zone CO_2 during carbonate recrystallization. However, in this study the negative shifts in C and O isotopes are not recorded in the shallow platform carbonates but in the open-marine marls of the Patrocinio Formation, which deposited during widespread transgression under water-depth conditions far from subaerial exposure.

More plausible, secondary changes in the isotope ratios could occur with carbonate recrystallization during burial diagenesis, and could explain at least the anomalous low $\delta^{18}O$ values. Early precipitation of diagenetic isotopically light calcite in the marly interval as a consequence of bacterial organic matter decomposition in the

sulphate-reducing zone is likely a mechanism that operated in many organic-rich rocks (Sass et al., 1991). However, the scarcity of organic matter present in our samples (0.5% or less; Rosales et al., 2009) may compromise this interpretation. Alternatively, depletion in the $\delta^{18}O$ and $\delta^{13}C$ composition of the seawater may have been caused by an influx of terrestrial runoff into the platform during the stage 3 as a consequence of acceleration of the hydrological cycle (e.g. as described in the Early Toarcian OAE by Sælen et al., 1996). The change in the isotope composition of the platform seawater during this stage may have acted in combination with the warming episode (Ando et al., 2008) to cause the low $\delta^{18}O$ values detected in the samples.

Climate (global) versus tectonic (local) controls on the platform evolution

Beyond the influence of the OAE 1a, the described patterns of platform evolution in the NCB are also influenced by regional factors such as local tectonics and differential subsidence or runoff changes. Eustacy also should play a significant role in the evolution of the platform.

Regionally, rift tectonism occurred during the Tithonian–Cenomanian (e.g. Martín-Chivelet et al., 2002). The syn-rift nature of the carbonate succession deposited during the Aptian in the NCB is indicated by the fact that strata thicken and fan out into hangingwall areas and thin onto footwall areas (Figs. 2B and 5). Therefore, it can be assumed that the accommodation space for platform growth was created from a combination of sea-level change, local block movements, and regional subsidence from crustal thinning and sediment loading.

The contact between the carbonate platform stage 1 and the next stage 2, which is marked by an unconformity with evidence of erosion, dissolution and meteoric diagenesis on footwall crests, points to local uplift and a brief period of subaerial exposure. The stage 2 was a carbonate sequence developed initially only on the more subsiding parts of the basin. The unit shows pronounced onlap at the base and is interpreted as the passive fill of a wedge-shape accommodation space during a phase of relative sea-level rise. This stratigraphic pattern closely resembles the depositional architecture predicted by the models of Bosence (2005) and Gardner et al. (2009) for fault-block carbonate platforms, and suggests that local tectonics was the major cause of this unconformity that produced hangingwall subsidence and footwall uplift. The flooding and onlapping on this surface were accompanied by the change to a heterozoan style of carbonate production with influx of siliciclastic particles. The predominance of

such type of grains, and the rest of evidences presented in this study, all suggest environmental perturbation by continental waters charged in siliciclastic particles and nutrients, resulting in a mesotrophic habitat in the stage that preceded the OAE 1a. The carbonate factory changed to a less-effective mode of sedimentation that occurred at slow rates, as indicated by the presence of glauconite, and the high rates of microbial activity and ferruginization. This sedimentary response may have been induced by the tectonic uplift and fluvial erosion of the southern and western margins of the NCB. However, deterioration of the shallow water carbonate systems occurred almost simultaneously worldwide, such in the Pacific (Jenkyns, 1995), France (Masse et al., 1999), Switzerland (Wissler et al., 2003), Helvetic Alps (Föllmi et al., 2006), and Portugal (Burla et al., 2008) among others, suggesting that this was an inter-regional phenomenon.

The shallow water carbonate platform deterioration took place during a rapid rise in relative sea-level. The weakened production rate of the carbonate stage 2 could not keep-up with the rising sea-level, with the consequent drowning of the platform and deposition of open-marine marls of the stage 3. Although this event was influenced by tectonic subsidence, the early Aptian flooding should be considered as a major eustatic transgressive event. It is well recorded in other rifted-basins of both the Tethys and the North Atlantic, and remarkably, it has been also reported from cratonic areas, such as the East African craton, which are considered as geologically more stable (Bosellini et al., 1999). Because this transgression correlates well with similar events around the world and within different tectonostratigraphic settings (Somalia, Arabian Peninsula, Ethiopia, southern Italy, France, Spain, Portugal, north-eastern Mexico, Pacific realm, etc.) (e.g. Lehmann et al., 1999; Bosellini et al., 1999; Rosales, 1999; Burla et al., 2008; Föllmi, 2008), it is considered as a global phenomenon linked to the OAE 1a. Therefore, and in summary, in the NCB, the proximity of emerged land areas to the south of the Cabuérniga Ridge and in the Asturian Massif (see Fig. 1C for location) along with a combination of tectonic movements and more humid climate conditions, would have increased continental erosion, river drainage and runoff, which ultimately would have been responsible for the local/regional platform eutrophication and the subsequent drowning that accompany the OAE 1a.

CONCLUSIONS

The following conclusions from the study of the Early Aptia carbonate succession of the North Cantabrian basin can be drawn:

1) Four successive stages of carbonate production (1 to 4) outline the evolution of the platform, from which stage 3 corresponds to the local expression of the OAE 1a.

2) The carbonate stages that preceded the OAE 1a exhibit compositional shifting from photozoan (stage 1) to heterozoa (stage 2) skeletal grains. These two stages of carbonate production are separated by an unconformity. This surface exhibits evidence of erosion, karstic dissolution and meteoric diagenesis, and is capped by a submarine ferruginous crust during the following transgressive event.

3) Tectonic activity favoured the influx of terrigenous particles from terrestrial runoff that accompanied the observed biotic changes. Besides, an accelerated hydrological cycle increased the input o freshwater and nutrients into the platform, causing the change from oligotrophic (stage 1) to mesotrophic (stage 2) conditions.

4) This event in the evolution of the carbonate platform correlates well with worldwide environmental deterioration of benthic environments. The combination of water freshening, nutrient poisoning, tectonic activity and rising eustatic sea-level may have acted together resulting in the progressive destabilisation of the marine environments and the change to less-effective carbonate factories (heterozoan), which may be the cause of the demise of many carbonate platforms worldwide previous to the instauration of the OAE.

5) Finally, the integration of sedimentological, diagenetic and chemostratigraphic analysis has been proven as a useful tool to identify and characterize global palaeoclimatic perturbations in shallow water carbonate platform environments.

ACKNOWLEDGEMENTS

This work is part of the Ph.D. Thesis of the first author (M.N.), who is supported by a scholarship from the Instituto Geológico y Minero de España (IGME). The study is a contribution to the DGI project CGL2008-01237/BTE (MICINN, Spanish Government), and to the UJA- 07-16-41 project (Jaén University, Spain). Many thanks

are due to A. Immenhauser and D. Sanders for valuable scientific comments and suggestions to improve the original manuscript.

REFERENCES

Ando, A., Kakegawa, T., Takashima, R., Saito, T., 2002. New perspective on Aptian carbon isotope stratigraphy: data from $\delta^{13}C$ records of terrestrial organic matter. Geology 30, 227–230.

Ando, A., Kaiho, K., Kawahata, H., Kakegawa, T., 2008. Timing and magnitude of Early Aptian extreme warming: Unraveling primary $\delta^{18}O$ variation in indurated pelagic carbonates at Deep Sea Drilling Project Site 463, central Pacific Ocean. Palaeogeography, Palaeoclimatology, Palaeoecology 260, 463–476.

Arnaud-Vanneau, A., Arnaud, H., 1990. Hauterivian to Lower Aptian carbonate shelf sedimentation and sequence stratigraphy in the Jura and northern subalpine chains (southeastern France and Swiss Jura). In: Tucker, M.E. Wilson, J.L., Crevello, P.D., Sarg F.J. Read, F.J. (Eds.), Carbonate Platforms, Facies, Sequences, and Evolution. IAS Special Publication 9, pp. 203–234.

Aurell, M., Fernández-López, S., Meléndez, G., 1994. The Middle-Upper Jurassic oolitic ironstone level in the Iberian Range (Spain). Eustatic implications. Geobios Mem. Spec. 17, 549−561.

Barbin, V., 2000. Cathodoluminescence of carbonate shells: Biochemical vs diagenetic process. In: Pagel, M., Barbin, V., Blanc, Ph., Ohnenstetter (Eds.), Cathodoluminescence in Geosciences. Springer Verlag, 12, pp. 303–329.

Barbin, V., Ramseyer, K., Debena, J.P., Schein, E., Roux, M., Decrouez, D., 1991. Cathodoluminescence of recent biogenic carbonates: an environmental and ontogenetic fingerprint. Geological Magazine 128, 19–26.

Bathurst, R.G.G., 1966. Boring algae, micrite envelops and lithification of molluscan biosparites. Geological Journal 5, 15–32.

Beerling, D.J., Lomas, M.R., Gröcke, D., 2002. On the nature of methane gas-hydrate dissociation during the Toarcian and Aptian oceanic anoxic events. American Journal of Sciences 302, 28–49.

Bellanca, A., Erba, E., Ner, R., Premoli-Silva, I., Sprovieri, M., Tremolada, F., Verga, D., 2002. Palaeoceanography significance of the Tethyan 'Livello Selli' (Early

Aptian) from the Hybla Formation, Northwestern Sicily: biostratigraphy and high-resolution chemostratigraphy records. Palaeogeography, Palaeoclimatology, Palaeoecology 185, 175–196.

Benito, M.I., Lohmann, K.C., Mas, R., 2005. Late Jurassic palaeogeography and palaeoclimate in the Northern Iberian Basin of Spain: Constraints from diagenetic records in reefal and continental carbonates. Journal of Sedimentary Research 75, 82−96.

Birkeland, C., 1988. Second-order ecological effects of nutrient input into coral communities. Galaxea 7 (2), 91−100.

Bishop, J.W., Montañez, I.P., Gulbranson, E.L., Brenkle, P.L., 2009. The onset of mid-Carboniferous glacio-eustasy: Sedimentologic and diagenetic constrains, Arrow Canyon, Nevada. Palaeogeography, Palaeoclimatology, Palaeoecology 276, 217–243.

Bosence, D., 2005. A genetic classification of carbonate platforms based on their basinal and tectonic setting in the Cenozoic. Sedimentary Geology 175, 49–72.

Bosellini, A., Russo, A., Schroeder, R., 1999. Stratigraphic evidence for an Early Aptian sea-level fluctuation: the Graua Limestone of south-eastern Ethiopia. Cretaceous Research 20, 783–791.

Burla, S., Heimhofer, U., Hochuli, P.A., Weissert, H., Skelton, P., 2008. Changes in sedimentary patterns of coastal and deep-sea successions from the North Atlantic (Portugal) linked to Early Cretaceous environmental change. Palaeogeography, Palaeoclimatology, Palaeoecology 257 (1-2), 38–57.

Calvet, F., 1982. Constructive marine envelope developed in vadose continental environment in Pleistocene eolianites of Mallorca (Spain). Acta Geológica Hispánica 17, 169–178.

Carannante, G., Cherchi, A., Simone, L., 1995. Chlorozoan versus foramol lithofacies in Upper Cretaceous rudists limestones. Palaeogeography, Palaeoclimatology, Palaeoecology 199 (1-2), 137–154.

Chacón, E., Barrendero, E., García-Pichel, F., 2006. Biogeological signatures of microboring cyanobacterial communities in marine carbonates from Cabo Rojo, Puerto Rico. Sedimentary Geology 185, 215−228.

Champ, D.R., Gulens, J., Jackson, R.E., 1979. Oxidation-reduction sequences in ground water flow systems. Canadian Journal of Earth Sciences 16, 12−23.

Collignon, M., Pascal., A., Peybernès, B., Rey J., 1979. Faunes d'ámmonites de l'Aptien de la Région de Santander (Espagne). Annales de Paléontologie 65 (2), 139– 156.

Di Stefano, P., Mindszenty, A., 2000. Fe-Mn-encrusted "Kamenitza" and associated features in the Jurassic of Monte Kumeta (Sicily): subaerial and/or submarine dissolution?. Sedimentary Geology 132, 37–68.

Dickson, J.A.D., 1966. Carbonate identification and genesis as revealed by staining. Journal of Sedimentary Petrology 36, 491−505.

Dickson J.A.D., Saller, A.H., 1995. Identification of subaerial exposure surfaces and porosity preservation in Pennylvanian and Lower Permian shelf limestones, eastern Central basin Platform, Texas. In: Budd, D.A., Saller, A.H., Harris, P.M. (Eds.), Unconformities and porosity in carbonate strata. American Association of Petroleum Geologists, Memory 63, pp. 239−257.

Erba, E., Channell, J., Claps, M., Larson, R., Opdyke, B., Premoli-Silva, I., Riva, A., Salvini, G., Torricelli, S., 1999. Integrated stratigraphy of the Cismon APTICORE (Southern Alps, Italy): A 'reference section' for the Barremian–Aptian interval at low latitudes. Journal of Foraminiferal Research 29, 371–391.

Feuillée, P., Rat, P., 1971. Structures et paléogéographies Pyrénéo-Cantabriques. In: Histoire Structurale du Golfe de Gascogne. Publication de l'Institute Français du Pétrole. Collection Colloque et Séminaires, Technip, Paris 22, pp. 1−48.

Flügel, E., 2004. Microfacies of carbonate rocks: Analysis, interpretation and application. Springer-Verlag Berlin Heidelberg, 976 pp.

Föllmi, K.B., 2008. A synchronous, middle Early Aptian age for the demise of the Helvetic Urgonian platform related to the unfolding oceanic anoxic events 1a ("Selli event"). Revue de Paléobiologie 27, 461–468.

Föllmi, K.B., Weissert, H., Bisping, M., Funk, H., 1994. Phosphogenesis, carbon-isotope stratigraphy and carbonate platform evolution along the Lower Cretaceous northern Tethyan margin. Geological Society of American Bulletin 106 (6), 729–74.

Föllmi, K.B., Godet, A., Bodin, S., Linder, P., 2006. Interactions between environmental change and shallow water carbonate buildup along the northern Tethyan margin and their impact of the early Cretaceous carbon isotope record. Paleoceanography 21, 4211–4226.

García-Espina, R., 1997. La estructura y evolución tectonoestratigráfica del borde occidental de la Cuenca Vasco-Cantábrica (Cordillera Cantábrica, NO de España). Ph. D. Thesis, Oviedo University, Spain.

García-Mondéjar, J., Fernández-Mendiola, P.A., 1993. Sequence stratigraphy and systems tracts of a mixed carbonate and siliciclastics platform-basin setting: The Albian of Lunada and Soba, Northern Spain. American Association of Petroleum Geologists, Memory 77, 245−275.

García-Mondéjar, J., Agirrezabala, L.M., Aranburu, A., Fernández-Mendiola, P.A., Gómez-Pérez, I., López-Horgue, M., Rosales, I., 1996. Aptian–Albian tectonic pattern of the Basque-Cantabrian Basin (northern Spain). Geological Journal 31, 13–45.

Gardner, J.A., Bosence, D., Burgess, P.M., and Waltham, D., 2009. Tectono-stratigraphic models for Phanerozoic platforms. AAPG Search and Discovery Article #90090. AAPG Annual Convention and Exhibition, Denver, Colorado, June 2009.

Gea, G.A., Castro, J.M., Aguado, R., Ruiz-Ortiz, P.A., Company, M., 2003. Lower Aptian carbon isotope stratigraphy from a distal carbonate shelf setting: the Cau section, Prebetic Zone SE Spain. Palaeogeography, Palaeoclimatology, Palaeoecology 200, 207–219.

Glenn C.R., Föllmi, K.B., Riggs, S.R., Baturin, G.N., Grim, K.A., Trappe, J., Abed, A.M., Galli-Olivier, C., Garrison, R.E., Ilyin A.V., Jehl, C., Rorhlich, V., Sadaqah, R.M.Y., Schidlowski, M., Sheldon, R.E., Siegmund, H., 1994. Phosphorous and phosphorites: Sedimentology and environments of formation. Ecologae Geologicae Helvetiae 87, 747–788.

Gómez-Pérez, I., Fernández-Mendiola, P.A., García-Mondéjar, J., 1998. Constructional dynamics for a Lower Cretaceous carbonate ramp (Gorbea Massif, north Iberia). In: Wright V.P., Burchette, T.P. (Eds.), Carbonate ramps. Geological Society, London, Special Publications 149, pp. 229−252.

Gradstein, F.M., 2004. A Geologic Time Scale 2004. Cambrige University Press.

Gradzinski, M., Tyszca, J., Uchman, A., Jach, R., 2004. Large microbial-foraminiferal oncoids from condensed Lower-Middle Jurassic deposits : a case study from The Tatra Mountains, Polan. Palaeogeography, Palaeoclimatology, Palaeoecology 213, 133−151.

Gröcke, D., Hesselbo, S.P., Jenkyns, H.C., 1999. Carbon-isotope composition of Lower Cretaceous fossil wood: ocean–atmosphere chemistry and relation to sea level change. Geology 27, 155–158.

Hallock, P., 1988. The role of nutrient availability in bioerosion: consequences to carbonate buildups. Palaeogeography, Palaeoclimatology, Palaeoecology 63, 275–291.

Hallock, P., Schlager, W., 1986. Nutrient excess and the demise of coral reefs and carbonate platforms. Palaios 1, 389–398.

Hesselbo, S.P., Gröcke, D.R., Jenkyns, H.C., Bjerrum, C.J., Farrimond, P., Morgans Bell, H.S., Green, O.R., 2000. Massive dissociation of gas hydrate during a Jurassic oceanic anoxic event. Nature 406, 392–395.

Hines, F.M., 1985. Sedimentation and tectonics in north-west Santander. In: 6th European Regional Meeting, Excursion Guidebook. Milá, M.D. and Rosell, J. (Eds.), International Association of Sedimentologists, 371−398.

Hunt, D., Tucker, M.E., 1993. The Middle Cretaceous urgonian platform of southeastern France. In: Simo., T., Scott, R.W., Masse, J.P. (Eds.), Cretaceous Carbonate Platforms. American Association of Petroleum Geologists Memory 56, pp. 409–453.

Immenhahuser, A., Kenter, J.A.M., Ganssen, G., Bahamonde, J.R., van Vliet, A., Saher, M.H., 2002. Origin and significance of isotope shifts in Penssylvanian carbonates (Asturias, NW Spain). Journal of Sedimentary Research 72 (1), 82–94.

Immenhauser, A., Della Porta, G., Kenter, J.A.M., Bahamonde, J.R., 2003. An alternative model for positives shifts in shallow marine carbonate δ13C and δ18O. Sedimentology 50 (5), 953–959.

Immenhauser, A., Hillgartner H., van Bentum, E., 2005. Microbial foraminiferal episodes in the Early Aptian of the southern Tethyan margin: ecological significance and possible relation to Oceanic Anoxic Event 1a. Sedimentology 52 (1), 77–99.

Immenhauser A., Holmden C., Patterson, W.P., 2008. Interpreting the carbonate isotope record of ancient shallow epeiric seas: Lessons from the recent. In: Pratt, B.R. Holmden, C. (Eds.), Dynamics of Epeiric Seas. Geological Association of Canada, Special Publication 48, pp. 135–174.

Jahren, A.H., Arens, N.C., Sarmiento, G., Guerrero, J., Amundson, R., 2001. Terrestrial record of methane hydrate dissociation in the Early Cretaceous. Geology, 29 (2), 159–1662.

James, N.P., 1997. The cool-water carbonate depositional realm. In: James, N.P., Clarke, J.A.D. (Eds.), Cool-water carbonates. SEPM Special Publication 56, pp. 1–20.

James N.P., Choquette, P.W., 1990. Limestones: the meteoric diagenetic environment. In: Macillreath, I.A., Morrow, D.W. (Eds.), Diagenesis. Geosciences Canada, pp. 161–194.

Jansa, L.F., 1993. Early Cretaceous carbonate platforms of the northeastern North American margin. In: Simo., T., Scott, R.W., Masse, J.P. (Eds.), Cretaceous Carbonate Platforms. American Association of Petroleum Geologists Memory 56, pp. 111–126

Jenkyns, H.C., 1970. Submarine volcanism and the Toarcian iron pisolites of western Sicily. Ecologae Geologicae Helvetiae 63, 741–774.

Jenkyns, H.C., 1995. Carbon isotope stratigraphy and paleoceanographic significance of the Lower Cretaceous shallow-water carbonates of Resolution Guyot, Mid Pacific Mountains. In: Winterer, E.L., Sager, W.W., Firth, J.V., Arnaud, H.M., Baker, P.E., Baudin, F., Bralower, T.J., Castillo, P.R., Cooper, P.A., Flood, P.G., Golovchenko, X., Iryu, Y., Ivanov, M.K., Jenkyns, H.C., Kenter, J.A.M., Murdmaa, I.O., Mutterlose, J., Nogi, Y., Paull, C.K., Polgreen, E.L., Roehl, U., Sliter, W.V., Strasser, S.K. (Eds.), Proceedings of the Ocean Drilling Program. Scientific Results. Texas A & M University, Ocean Drilling Program, Collage Station, Texas, United States 143, pp. 99−104.

Jenkyns, H.C., 2003. Evidence for rapid climate change in the Mesozoic-Palaeogene greenhouse world. The Royal Society of London 361, 1885–1961.

Jenkyns, H.C., Wilson, P.A., 1999. Stratigraphy, paleoceanography, and evolution of Cretaceous Pacific guyots: relics from a greenhouse Earth. American Journal of Science 299, 341–392.

Kearsley, A.T., 1989. Iron-rich ooids, their mineralogy and microfabrics: clues to their origin and evolution. In: Young, T.P., Taylor, W.E.G. (Eds.), Geological Society. Special Publication 46, 141−163.

Konhauser, K.O., 1998. Diversity of bacterial iron mineralization. Earth Science Reviews 43, 91−121.

Larson, R.L., Erba, E., 1999. Onset of the Mid-Cretaceous greenhouse in the Barremian–Aptian: igneous events and the biological, sedimentary and geochemical response. Paleoceanography 14 (6), 663–678.

Le Pichon, X., Sibuet, J.C., 1971. Western extension of the boundary between European and Iberian plates during the Pyrenean orogeny. Earth and Planetary Science Letters 12, 83−88.

Lehmann, Ch., Osleger, D.A., Montañez, I.P., 1998. Controls of cyclostratigraphy of Lower Cretaceous carbonates and evaporites, Cupido and Coahuila platforms, northeastern Mexico. Journal of Sedimentary Research 68, 1109–1130.

Lehmann, Ch., Osleger, D.A., Montañez, I.P., Arnaud-Vanneau, A., Banner, J., 1999. Evolution of Cupido and Coahuila carbonate platforms, Early Cretaceous, north-eastern Mexico. Geological Society of America Bulletin 111, 1010–1029.

Luciani, V., Cobianchi, M., Jenkyns, H.C., 2001. Biotic and geochemical response to anoxic events: the Aptian pelagic succession of the Gargano promontory (southern Italy). Geological Magazine 137, 277–298.

Malod, J.A., Mauffret, A., 1990. Iberian plate motions during the Mesozoic. Tectonophysics 184, 261–278.

Mamet, B., Préat, A., 2006. Iron-bacterial mediation in Phanerozoic red limestones: State of the art. Sedimentary Geology 185, 147–157.

Margolis, S., Rex, R.W., 1971. Endolithic algae and micritic envelop formation in Bahaman oolites as revealed by scanning electron microscopy. Geological Society of American Bulletin 82, 843–852.

Marshall, D.J., 1988. Cathodoluminescence of Geological Materials. Boston: Unwin Hyman. 149 pp.

Marshall, D.J., 1992. Climatic and oceanographic isotopic signals from the carbonate rock record and their preservation. Geological Magazine 129 (2), 143–160.

Martín-Chivelet, J., Berasategui, X., Rosales, I., Vilas, L., Vera, J.A., Caus, E., Gráfe, K.U., Mas, R., Puig, C., Segura, M., Robles, S., Floquet, M., Quesada, S., Ruiz-Ortiz, P.A., Frenegal-Martínez, M.A., Salas, R., García, A., Martín-Algarra, A., Arias, C., Meléndez, M., Chacón, B., Molina, J.M., Sanz, J.L., Castro, J.M., García-Hernández, M., Carenas, B., García-Hidalgo, J., Gil, J., Ortega, F., 2002. Cretaceous. In: Gibbons, W. and Moreno, T. (Eds.), The Geology of Spain. The Geological Society, London, pp. 255–292.

Masse, J.P., 1993. Valanginian−Early Aptian carbonate platforms from Provence, southeastern France. In: Simo., T., Scott, R.W., Masse, J.P. (Eds.), Cretaceous Carbonate Platforms. American Association of Petroleum Geologists Memory 56, pp. 363–374.

Masse, J.P., El Albani, A., Erlenkeuser, H., 1999. Stratigraphie isotopique (δ13C) de l'Aptien inférieur de Provence (SE France); applications aux corrélations plateforme/bassin. Eclogae Geologicae Helvetiae 92 (2), 259−263.

McCrea, J.M., 1950. On the isotopic chemistry of carbonates and a paleotemperature scale. Journal of Chemical Physics 18, 849−857.

Menegatti, A.P., Weissert, H., Brown, R.S., Tyson, R.V., Farimond, P., Strasser, A., Caron, M., 1998. High-resolution δ13C stratigraphy through the Early Aptian 'Livello Selli' of the Alpine Tethys. Paleoceanography 13, 530–545.

Milkov, A.V., 2004. Global estimates of hydrate-bound gas in marine sediments: how much is really out there? Earth Sciences Reviews 66, 183–197.

Moore, C.H., 1989. Carbonate diagenesis and porosity. Developments in Sedimentology. Elsevier, Amsterdam.

Moreno-Bedmar, J.A., Company, M., Bover-Arnal, T., Salas, R., Delanoy, G., Martínez, R., Grauges, A., 2009. Biostratigraphic characterization by means of ammonoids of Lower Aptian Oceanic Anoxic Event (OAE1a) in the eastern Iberian Chain (Maestrat Basin, eastern Spain). Cretaceous Research 30 (4), 1–9.

Muchez, P., Nielsen, P., Sintubin, M., Lagrau, D., 1998. Conditions of meteoric calcite formation along a Variscan fault and their possible relation to climatic evolution during the Jurassic−Cretaceous. Sedimentology 45, 845−854.

Mutti, M., 1995. Porosity development and diagenesis in the Orfento Supersequence and its bounding unconformities (upper Cretaceous, Montagna Della Maiella, Italy). In: Budd, D.A., Saller, A.H., Harris, P.M. (Eds.), Unconformities and porosity in carbonate strata. American Association of Petroleum Geologists, Memory 63, 141–158.

Nahon, D., Carozzi, A.V., Parron C., 1980. Lateritic weathering as a mechanism for the generation of ferruginous ooids. Journal of Sedimentary Petrology 50, 1287–1289.

Najarro, M., Rosales, I., 2008a. Disoluciones e incrustaciones ferruginosas asociadas al OAE 1a en la plataforma carbonatada de La Florida (NO de Cantabria). Geogaceta 44, 199–202.

Najarro, M., Rosales, I., 2008b. Evidencias sedimentológica, diagenética y quimioestratigráfica del Evento Anóxico Oceánico del Aptiense Inferior (OAE 1a) en la plataforma carbonatada de La Florida (NO de Cantabria). Geotemas 10, 163–166.

Najarro, M., Rosales, I., 2008c. Facies evolution, diagenesis and isotope analyses in a carbonate platform related to the Lower Cretaceous Anoxic Event 1a. SDGG 58. Abstract Volume of the 26th Regional meeting of the International Association of Sedimentologists, Bochum, Germany, pp. 194.

Najarro, M., Rosales, I., Martín-Chivelet, J., 2007. Evolución de la plataforma carbonatada de la Florida durante el rifting del Cretácico Inferior (Aptiense, NO de Cantabria). In: Bermúdez, D.D., Najarro, M., Quesada, C. (Eds.), Volumen Monográfico de la II Semana de Jóvenes Investigadores del IGME. Publicaciones del IGME, pp. 123–128.

Najarro, M., Peñalver, E., Rosales, I., Pérez-de la Fuente, R., Daviero-Gomez, V., Gomez, B., Delclòs, X., 2009. Unusual concentration of Early Albian arthropod-bearing amber in the Basque-Cantabrian Basin (El Soplao, Cantabria, Northern Spain): Palaeoenvironmental and palaeobiological implications. Geologica Acta 7 (3), 363−387.

Odin, G.S., 1988. Green Marine Clays. Development in Sedimentology. Elsevier, Amsterdam.

Odin, G.S., Matter, A., 1981. De glauconarium origine. Sedimentology 28, 611–641.

Olivet, J.M., 1996. La cinématique de la plaque Ibérique. Bulletin des Centres de Recherches Exploration-Production Elf-Aquitaine 20, 131–195.

Pascal, A., 1985. Les Systems biosédimentaires urgoniens (Aptien−Albien) sur la marge Nord Ibérique. Mémoires Géologiques de l'Úniversité de Dijon 10, 1–569.

Perry, C.T., 2002. Biofilm-related calcification, sediment trapping and constructive micrite envelops: a criterion for the recognition of ancient grass-bed environments? Sedimentology 46 (81), 33–45.

Philip, J.M., Gari, J., 2005. Late Cretaceous heterozoan carbonates: palaeoenvironmental setting, relationship with rudist carbonates (Provence, south-east France). Sedimentary Geology 175 (1-4), 315–337.

Préat, A., Mamet, B., De Ridder, C., Boulvain, F., Gillan, D., 2000. Iron bacterial and fungal mats, Bajocian stratotype (Mid-Jurassic, northern Normandy, France). Sedimentary Geology 137, 107-126.

Préat, A., El Hassani, A., Mamet, B., 2008. Iron bacteria in Devonian carbonates (Tafilat, Anti-Atlas, Marocco). Facies 54, 107−120.

Ramajo, J., Aurell, M., Cepría, J., 2002. Facies analysis of the Arroyofrío ferruginous oolitic bed in Sierra de Arcos (Jurassic, northern Iberian Change). Journal of Iberian Geology 28, 45−64.

Ramírez del Pozo, J., 1972. Algunos datos sobre la estratigrafía y micropaleontología del Aptense y Albense al oeste de Santander. Revista Española de Micropaleontología 15, 59–97.

Rat, P., 1988. The Basque-Cantabrian basin between the Iberian and European plates some facts but still many problems. Revista de la Sociedad Geológica de España 1, 327–348.

Reolid, M., Abad, I., Martín-García, J.M., 2008. Palaeoenvironmental implications of ferruginous deposits related to a Middle-Late Jurassic discontinuity (Prebetic Zone, Betic Cordillera, Southern Spain). Sedimentary Geology 203, 1−16.

Rosales, I., 1999. Controls on carbonate-platform evolution on active fault blocks: the Lower Cretaceous Castro Urdiales platform (Aptian–Albian, northern Spain). Journal of Sedimentary Research 69, 447–465.

Rosales, I., Najarro, M., Moreno-Bedmar, J.A., Gea, G.A., Company, M., 2009. High resolution chemo and biostratigraphy records of the Early Aptian Oceanic Anoxic Event in Cantabria (northern Spain). Geochimica et Cosmochimica Acta, Special Suplement 73, pp. 1118.

Ross, D.J., Skelton, P.W., 1993. Rudists formation of the Cretaceous: a palaeoecological, sedimentological and stratigraphical review. In: Wright, V.P. (Eds.), Sedimentology Review. Blackwell Scientific publications, pp. 73−91.

Ruiz-Ortiz, P.A., Castro, J.M., 1998. Carbonate depositional sequences in shallow to hemipelagic platform deposits; Aptian, Prebetic of Alicante (SE Spain). Bulletin de la Société Géologique de France 169, 21–33.

Sass, E., Bein, A., Almogi-Labin, A., 1991. Oxygen-isotope composition of diagenetic calcite in organic-rich rocks: Evidence for 18O depletion in marine anaerobic pore water. Geology 19, 839–842.

Sælen, G., Doyle, P., Talbot, M.R., 1996. Stable-isotope analyses of belemnite rostra from the Whitby Mudstone Formation, England: Surface water conditions during deposition of a marine black shale. Palaios 11, 97–117.

Schlanger, S.O., Jenkyns, H.C., 1976. Cretaceous oceanic anoxic events: causes and consequences. Geologie en Mijnbouw 55 (3-4), 179–184.

Scotesse, C.R., Gahagan, L.M., Larson, R.L., 1998. Plate tectonic reconstructions of the Cretaceous and Cenozoic Ocean Basins. Tectonophysics 155 (1-4), 27–48.

Scott, R.W., 1993. Cretaceous carbonate platform, U.S. Gulf Coast. In: Simo, T., Scott, R.W., Masse, J.P. (Eds.), Cretaceous Carbonate Platforms. American Association of Petroleum Geologists Memory 56, pp. 97–109.

Simone, L., Carannante, G., 1988. The fate of foramol ('temperate-type') carbonate platforms. Sedimentary Geology 60, 347–354.

Soto, R., Casas-Sainz, A., Villalaín, J.J., Oliva-Urcia, B., 2007. Mesozoic extension in the Basque-Cantabrian basin (N Spain): Contributions from AMS and brittle mesostructures. Tectonophysics 445, 373−394.

Spicer, R.A., Corfield, R.M., 1992. A review of terrestrial and marine climates in the Cretaceous with implications for modelling the "Greenhouse Earth". Geological Magazine 129, 169–180.

Sturesson, U., Heikoop, J.M., Risk, M.J., 2000. Modern and Palaeozoic iron ooids: a similar volcanic origin. Sedimentary Geology 136, 137–146.

Vilas, L., Masse, J.P., Arias, C., 1995. Orbitolina episodes in carbonate platform evolution: the Early Aptian model from SE Spain. Palaeogeography, Palaeoclimatology, Palaeoecology 119, 35–45

Weissert, H., Erba, E., 2004. Volcanism, CO2 and palaeoclimate: a Late Jurassic–Early Cretaceous carbon and oxygen isotope record. In: Morgans Bell, H.S., Cohen, A.S. (Eds.), Organic-Carbon Burial, Climate Change and Ocean Chemistry (Mesozoic−Palaeogene). Geological Society of London, Special Publication, United Kingdom.

Weissert, H., Lini, A., Föllmi, K.B., Kuhn, O., 1998. Correlation of Early Cretaceous carbon isotope stratigraphy and platform drowning events: a possible link?. Palaeogeography, Palaeoclimatology, Palaeoecology 137 (3-4), 189–203.

Wilmsen, M., 2000. Evolution and demise of a Mid-Cretaceous carbonate shelf : the Altamira Limestones (Cenomanian) of northern Cantabria (Spain). Sedimentary Geology 133, 195−226.

Wilmsen, M., 2005. Stratigraphy and biofacies of the Lower Aptian of Cuchía (Cantabria, northern Spain). Journal of Iberian Geology 31 (2), 253−275.

Wissler, L., Funk, H., Weissert, H., 2003. Response of Early Cretaceous carbonate platforms to changes in atmospheric carbon dioxide levels. Palaeogeography, Palaeoclimatology, Palaeoecology 200, 187–205.

4.2.- High-resolution chemo- and biostratigraphic records of the Early Aptian Oceanic Anoxic Event in Cantabria (N Spain): palaeoceanographic and palaeoclimatic implications

M. NAJARRO[(1))], I. ROSALES[(1)], J.A. MORENO-BEDMAR[(2)], G.A. DE GEA[(3)], E. BARRÓN[(1)], M. COMPANY[(4)], G. DELENOY[(5)].

(1) Instituto Geológico y Minero de España.

(2) Departament de Geoquímica, Petrología i Prospecció Geológica. Facultat de Geologia. Universitat de Barcelona.

(3) Departamento de Geología. Facultad de Ciencias Experimentales. Universidad de Jaén.

(4) Departamento de Estratigrafía y Paleontología, Universidad de Granada

(5) Département des Sciences de la Terre, Université de Nice-Sophia Antipolis (France).

Doi: 10.1016/j.palaeo.2010.10.042.

Palaeogeography, Palaeoclimatology, Palaeoecology, 2011b, Vol. 299, p. 137-158.

RESUMEN

Los cambios paleoambientales a escala global que se produjeron durante el Aptiense Inferior dieron lugar a un Evento Anóxico Oceánico (OAE 1a) y a una perturbación global del ciclo del C. La obtención de nuevos registros de detalle de tipo lito-, bio- y quimioestratigráfico (TOC, $\delta^{13}C_{carb}$, $\delta^{13}C_{org}$) en dos secciones excepcionalmente expuestas y expandidas del Aptiense Inferior de Cantabria (La Florida y Cuchía), ha permitido reconocer la expresión del OAE 1a en ambientes de plataforma marina somera del norte de España. La sucesión está formada por calizas de plataforma somera que contienen una unidad margosa (Formación Patrocinio) cuyo depósito se produjo al comienzo del OAE 1a (120,5 Ma). Este trabajo presenta la integración de nuevos datos bioestratigráficos en base a ammonites, foraminíferos planctónicos, nanofósiles calcáreos y palinomorfos, que han permitido datar con gran precisión ambas secciones. La unidad margosa registra una excursión negativa del $\delta^{13}C$ muy marcada, tanto en el C_{org} (hasta el 5‰) como en el C_{carb} (hasta el 6‰, media del 3‰), tal y como ha sido documentada al inicio del OAE 1a en otras secciones del mundo. En detalle, esta excursión presenta dos mínimos en las secciones estudiadas. Esta doble excursión negativa ha sido datada con gran exactitud, produciéndose durante la mitad superior de la zona de nanofósiles de *Hayesites irregularis*, en la parte superior de la zona de foraminíferos de *Blowiella blowi* y en la parte media-alta de la zona de ammonites de *Deshayesites weissi*. Un tercer pico negativo ocurrió a la base de la zona de nanofósiles de *Rhagodiscus angustus*, la cual se correlaciona con la zona de ammonites de *Dufrenoyia furcata*. Estos nuevos datos definen perfectamente la edad del inicio del OAE 1a en la zona de estudio, así como la existencia de una laguna estratigráfica en el margen más occidental de la cuenca Vasco-Cantábrica, que abarcaría hasta la parte alta del Aptiense Inferior. El estudio de las facies sedimentarias y el análisis cuantitativo de palinomorfos y nanofósiles calcáreos evidencia importantes cambios ambientales asociados al OAE 1a. Así, los cambios composicionales de los carbonatos neríticos y los datos de nanofósiles calcáreos indican una crisis en la biocalcificación, interpretada como producida por una acidificación de las aguas relacionada con cambios en el quimismo del agua y en la concentración de CO_2. Los datos de palinomorfos indican un máximo térmico seguido de una fase de enfriamiento, con una presencia máxima de *Classopollis* durante el OAE 1a, seguido de un descenso en este tipo de polen y un aumento de polen de tipo bisacado después del evento anóxico oceánico.

ABSTRACT

During the Early Aptian, major palaeoenvironmental changes occurred leading to an oceanic anoxic event (OAE 1a) and a perturbation of the global carbon cycle. New detailed litho-, bio-, and chemostratigraphic (TOC, $\delta^{13}C_{carb}$, $\delta^{13}C_{org}$) records of two superbly exposed and expanded Lower Aptian sections in Cantabria (La Florida and Cuchía) allow to recognize the expression of the OAE 1a in shallow shelf environments of northern Spain. The succession consists of shallow platform limestones that include a marly unit (Patrocinio Formation), the deposition of which occurred mostly at the onset of the OAE 1a (~120.5 Ma). This study presents a new integrated biostratigraphy based on ammonites, planktonic foraminifera, calcareous nannofossils and palynomorphs that allows an accurate age resolution of the succession. The marly unit records an abrupt negative $\delta^{13}C$ excursion in both bulk organic matter (up to 5‰) and carbonate (up to 6‰, mean 3‰), as has been already observed at the onset of the OAE 1a in other Lower Aptian deposits worldwide. In detail, however, the negative excursion presents two minima in the studied sections. This negative spike is confidently attributed to the upper half of the *Hayesites irregularis* nannofossil Zone, to the upper part of the *Blowiella blowi* foraminiferal Zone, and to the middle–upper part of the *Deshayesites weissi* ammonite Zone. A third negative excursion occurs at the base of the *Rhagodiscus angustus* nannofossil Zone, which may be correlatable with the *Dufrenoyia furcata* ammonite Zone. This data set refines the age of the OAE 1a and reveals the existence of a stratigraphic gap in the westernmost margin of the Basque Cantabrian Basin that covers at least a portion of the upper part of the Early Aptian. Sedimentary facies and quantitative analysis of palynomorphs and nannofossils document significant environmental changes associated with the OAE 1a: compositional changes of neritic carbonates and calcareous nannofossils data indicate the occurrence of a biocalcification crisis inferred to have been related to CO_2-induced changes in seawater chemistry, and palynomorphs identify a thermal maximum followed by a cooling phase. The latter show a *Classopollis* maximum during the OAE 1a, which is followed by a decrease in *Classopollis* and an increase of bisaccate pollen after the event.

***Keywords*: Early Aptian, OAE 1a, C-isotopes, high-resolution biostratigraphy, biocalcification crisis, Basque Cantabrian Basin.**

INTRODUCTION

The Early Aptian is recognised as an interval of significant, widespread environmental change generated by a battery of interrelated palaeogeographic and palaeoceanographic events. It is marked by a geologically brief (≤1 Myr; Bralower et al., 1994) episode known as the oceanic anoxic event 1a (OAE 1a) (Arthur et al., 1990; Jenkyns, 1980, 1999; Schlanger and Jenkyns, 1976), which is characterized by global rise in sea level (Haq et al., 1988), extreme greenhouse conditions (Dumitrescu et al., 2006; Frakes, 1979; Herman and Spicer, 1996; Larson, 1991; Vakhrameyev, 1982), global distribution of organic-rich deposits (so-called "Selli Event"; Coccioni et al., 1989; Jenkyns, 2003; Schlanger and Jenkyns, 1976), increase in continental weathering and runoff (Erba, 1994; Föllmi et al., 1994; Najarro et al., 2010), a biocalcification crisis with strong impact on planktonic microfauna and nannoflora (Erba, 1994, 2004; Erba and Tremolada, 2004; Gea et al., 2003; Larson and Erba, 1999; Weissert and Erba, 2004), and major perturbations in global carbon cycling (e.g. Menegatti et al., 1998; Weissert and Erba, 2004). The triggering mechanisms for the OAE 1a are not well known yet. It has been postulated that the emplacement of the large igneous provinces of Ontong Java Plateau and Kerguelen Plateau initially sparked this event (e.g. Jahren, 2002; Larson and Erba, 1999; Leckie et al., 2002; Méhay et al., 2009; Tejada et al., 2009).

The onset of the OAE 1a coincides with a pronounced, sharp and short-lived negative $\delta^{13}C$ excursion in both organic matter and marine carbonate. This isotopic shift is considered to be global because it has been identified in several localities around the world (e.g. Gea et al., 2003; Gröcke et al., 1999; Grötsch et al., 1998; Jenkyns, 2003; Menegatti et al., 1998; Millán et al., 2009; Moreno-Bedmar et al., 2009; Weissert and Erba, 2004). Massive release of isotopically light CO_2 from volcanic sources or from oxidation of methane during dissociation of marine gas hydrates has been proposed to explain this negative excursion (Beerling et al., 2002; Gröcke, 2002; Jahren, 2002; Jahren et al., 2001; Jenkyns, 2003, Méhay et al., 2009). The negative excursion in $\delta^{13}C$ is followed by a shift toward positive values, which resulted from the increase of organic carbon burial during deposition of organic matter and black-shale formation (e.g. Bralower et al., 1994; Gröcke et al., 1999; Menegatti et al., 1998; Scholle and Arthur, 1980; Weissert et al., 1998). The negative spike at the onset of the OAE 1a is of much interest because it represents a brief interval (~27–44 kyr, according to Li et al.,

2008) of rapid environmental perturbation that activated the rest of the environmental events. However, some inaccuracies still exist with respect to its timing due to poor integration of the biostratigraphies used by different authors, and some differences in the zones and subzones used for the Tethyan and Boreal provinces (e.g. García-Mondéjar et al., 2009; Luciani et al., 2001; Moreno-Bedmar et al., 2009). Therefore, given its importance and implications, it is essential to constrain better the timing and nature of the negative excursion.

This paper presents an integration of stratigraphy, carbonate and total organic carbon (TOC) contents, and $\delta^{13}C_{carb}$ and $\delta^{13}C_{org}$ analyses, along with assemblages of ammonites, planktonic foraminifera, calcareous nannofossils and palynomorphs from two Lower Aptian sections (La Florida and Cuchía) located in the Basque Cantabrian Basin (northern Spain) (Fig. 1). Their excellent exposure exhibits a completely outcropping succession composed mostly of platform limestones that include a ~30–80 m thick marly unit (Patrocinio Formation) of Early Aptian age, the deposition of which occurred mostly at the onset of the OAE 1a. This marly unit provides a highly expanded record of this critical event allowing high-resolution sampling, in contrast to other better-known Tethyan sections that are more condensed, such as the Cismon APTICORE in Italy, which is considered as a reference section (Channell et al., 2000; Li et al., 2008; Menegatti et al., 1998). The multi-proxy data set compiled in this work aims to reconstruct processes and precise timing of the environmental changes occurring at the time of deposition of the marly unit, and permits to characterize the local expression of the OAE 1a in shallow platform carbonates of northern Spain. In addition, the abundance of climate-sensitive floral elements, particularly *Classopollis* sp. and bisaccate pollen, which are considered as consistent proxies for climate variations (Heimhofer et al., 2004; Vakhrameyev, 1982), supplies information that suggests palaeoclimatic changes from OAE 1a to post-OAE 1a conditions. The data set is discussed in the context of the current hypothesis on the nature of the global perturbations that occurred in the Early Aptian and is compared with other welldocumented Aptian C-isotope records from other Tethyan regions, particularly the classical reference sections of the southern Alps of northern Italy (Menegatti et al., 1998) and the Vocontian Basin of SE France (Herrle et al., 2004), and other more recent regional records reported from northern Spain (Millán et al., 2009; Moreno-Bedmar et al., 2009). Taken together, the data presented here provide an excellent case to investigate the onset of the OAE 1a, because the expanded records of this event in the

studied sections allow the acquisition of very high-resolution chemostratigraphic and biostratigraphic records within a detailed time frame.

GEOLOGICAL SETTING

The study area is located on the northwestern margin of the Basque Cantabrian Basin (BCB; Fig. 1), which formed during the Mesozoic–Early Cenozoic through several phases of continental rifting linked to the opening of the Bay of Biscay and the North Atlantic (e.g. Malod and Mauffret, 1990; Montadert et al., 1979; Olivet, 1996). During the Late Jurassic–Early Cretaceous rifting phase, this part of the BCB belonged to the northern margin of Iberia and was under "wet (sub-) tropical" climatic conditions in palaeo-latitude of about 30°N (e.g. Hay et al., 1999; Ziegler, 1988) (Fig. 1A). Due to the mentioned tectonic events, several extensional (intra-shelf) sub-basins developed during the Cretaceous in the northern margin of Iberia. These sub-basins were bounded by active synsedimentary faults producing thick accumulations of sediments that were subsequently folded and thrusted during the Cenozoic Alpine orogeny.

The two Lower Aptian successions studied here were deposited in the North Cantabrian (sub-) Basin (NCB; Figs. 1B, 2A). This was a relatively small (~20×80 km) E–W elongated sub-basin that developed as an independent structural unit, relatively less subsident than other areas of the BCB for most of the Cretaceous time (Martín-Chivelet et al., 2002; Najarro et al., 2010; Wilmsen, 2005). Palaeogeographically, the NCB was structured in a series of horsts and grabens limited by N–S, E–W and NE–SW trending faults, which controlled sedimentation at least during Barremian–Albian times (Fig. 2) (Najarro et al., 2007, 2009, 2010). From northeast to southwest three fault-bounded structural domains are differentiated: Cuchía, Santillana and La Florida areas respectively (Fig. 2B). The Cuchía and La Florida domains correspond to less-subsiding uplifted areas, whereas the Santillana domain represents a subsident trough between them and the main sedimentary depocentre of the region during the Early Cretaceous (Fig. 2B). This synsedimentary structural arrangement caused a complex basin topography, as indicated by distribution of facies and sedimentary thicknesses, which may reach less than 200 m for the Aptian–Albian in the marginal areas of La Florida and Cuchía, but may exceed 1000 m in the centre of the Santillana sink depression. The

two studied sections belong to the Cuchía and La Florida domains respectively, and are considered representative of these areas.

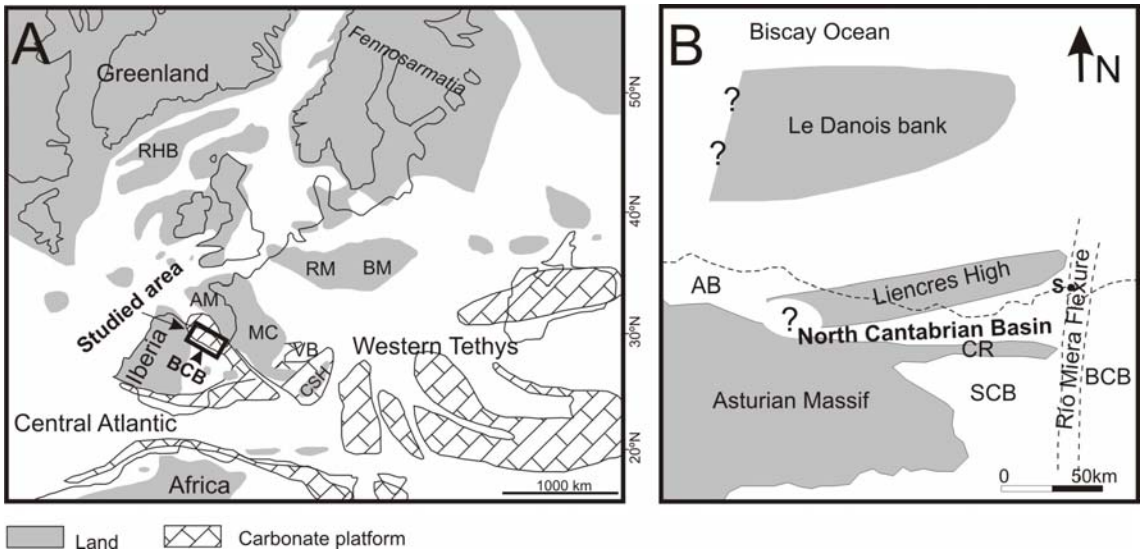

Figure 1.- (A) Palaeogeographical reconstruction of the Atlantic and western Tethys for the Aptian–Albian (taken from Herrle et al., 2003, modified after Ziegler, 1988; Hay et al., 1999). The studied sections are located in the Basque Cantabrian Basin (BCB = Basque Cantabrian Basin; AM = Armorican Massif; MC = Massif Central; VB = Vocontian Basin; RHB = Rockall–Hatton Bank; CSH=Corsica–Sardinia High; RM=Rhenish Massif; BM=Bohemian Massif). (B) Detailed palaeogeographical reconstruction of the North Cantabrian Basin (NCB) in the Early Cretaceous (modified after Wilmsen, 2000). The NCB was separated from the more strongly subsiding rest of the BCB to the east, by a N–S extensional structure (Río Miera Flexure after Feuillée and Rat, 1971). BCB=Basque Cantabrian Basin; CR=Cabuérniga Ridge; SCB=South Cantabrian (sub-) Basin; AB=Asturian Basin; S=Santander.

MATERIAL AND METHODOLOGY

Studied sections and sampling

The two Lower Aptian representative sections have been analysed along superbly exposed continuous outcrops (Fig. 3). The La Florida section is located about 20 km southwest of the village of San Vicente de la Barquera (Fig. 2A). This section is exposed close to the small village of Rábago, alongside the Puentenansa road. The Cuchía section (Figs. 2A, 3) is very well exposed in the coastal cliff of the Playa de los Caballos beach, 3 km NWof the small village of Cuchía. The two sections were logged and sampled at a metric scale, and the sedimentological features and fossil content were documented in detail in the field.

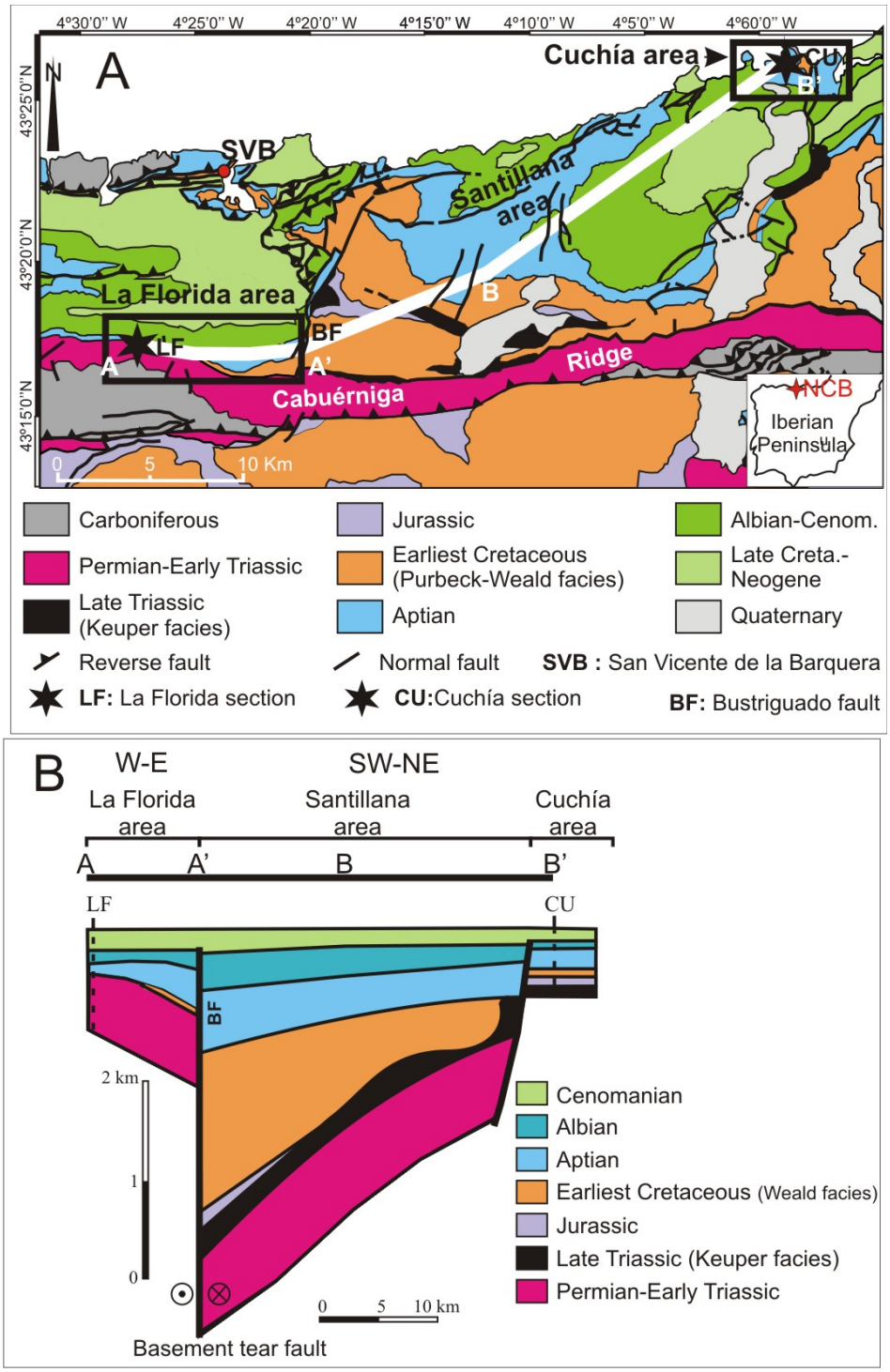

Figure 2.- (A) Geological map of the North Cantabrian Basin (NCB) with the location of the three principal depositional areas (La Florida, Santillana and Cuchía) and the two studied sections of La Florida and Cuchía. White line A–A′–B–B′ shows the location of the stratigraphic cross-section in B. (B) Cross-section showing the restored geometry of the NCB during the Early Cretaceous and the different sedimentary record in the three principal depositional areas.

A total of 235 rock samples were collected and processed for different geochemical and micropalaeontological studies. The $\delta^{13}C_{carb}$, $\delta^{13}C_{org}$, carbonate content and total organic carbon content (TOC) were measured on bulk rock samples from

limestones and marls drilled from fresh rock samples from the two sections. Previous works have proven the efficacy of bulk rock analysis on this type of rock successions (e.g. Ferreri et al., 1997; Scopelliti et al., 2008; Weissert et al., 1998). Powders were extracted with a micro drill mounted in a stereomicroscope. Potential problems associated with diagenetic resetting have been avoided as much as possible by carefully selecting micro samples of limestones and marls away from crack fillings, secondary products or matrix irregularities. Dolomitized samples were excluded and limestone samples with mudstone to wackestone textures were preferentially chosen. Samples derived from marls were systematically taken every 1–2 m, whereas for the limestones beds the sampling has been limited to those parts of the succession where the diagenetic features were minimal. Minor siliciclastic siltstones and sandstones interbedded in particular parts of the sections have not been analysed.

Geochemical analyses

Values of wt.% TOC and wt.% $CaCO_3$ contents were determined on 57 marly samples at Servizos de Apoio á Investigación of the University of A Coruña (Spain). Total carbon content of the samples (wt.% TC) was determined using a Carbo Erba elemental analyzer EA1108. For total organic carbon (TOC) determinations, the samples were previously digested in HCl at 80 °C to remove the carbonate material and then measured. The difference between the values of TC and TOC was used to calculate the carbonate carbon content (TIC) and then the calcium carbonate content, assuming that all carbonate is calcite.

To analyse the C-isotope composition of the bulk carbonate carbon ($\delta^{13}C_{carb}$), 72 powdered samples were treated with 100% orthophosphoric acid, using the conventional digestion method (McCrea, 1950). The $\delta^{13}C_{carb}$ composition of the evolving CO_2-gas was analysed with a SIRA-II mass spectrometer equipped with an "ISOCARB" automatic system at the University of Salamanca (Spain). The $\delta^{13}C$ composition of the organic matter fraction of the 72 rock samples ($\delta^{13}C_{org}$) was analysed in the Stable Isotope Laboratory of the University of East Anglia (UK). For this determination, all the carbonate material was previously removed from the samples by digesting them several times in a 10% hydrochloric acid solution until there was no evidence of fizzing, which indicates the removal of all inorganic carbon. The samples were then washed several times with de-ionised water to remove the HCl traces. The washed residues were dried in an oven between 50 and 80 °C and then analysed using a

Finnigan Delta Plus XP, on-line with a Costech elemental analyser. The results are expressed in the common δ-notation in per mil (‰) relative to VPDB-standard. The international carbonate standard NBS-19 (National Bureau of Standards; $\delta^{13}C$=1.95‰) and a laboratory internal standard (ISA; $\delta^{13}C$=−2.47‰) were used to calibrate the $\delta^{13}C_{carb}$ values, with an average precision of 0.01‰ (n=3). The pattern used for the $\delta^{13}C_{org}$ composition was a laboratory internal standard, with an average precision of 0.1‰ (n=12).

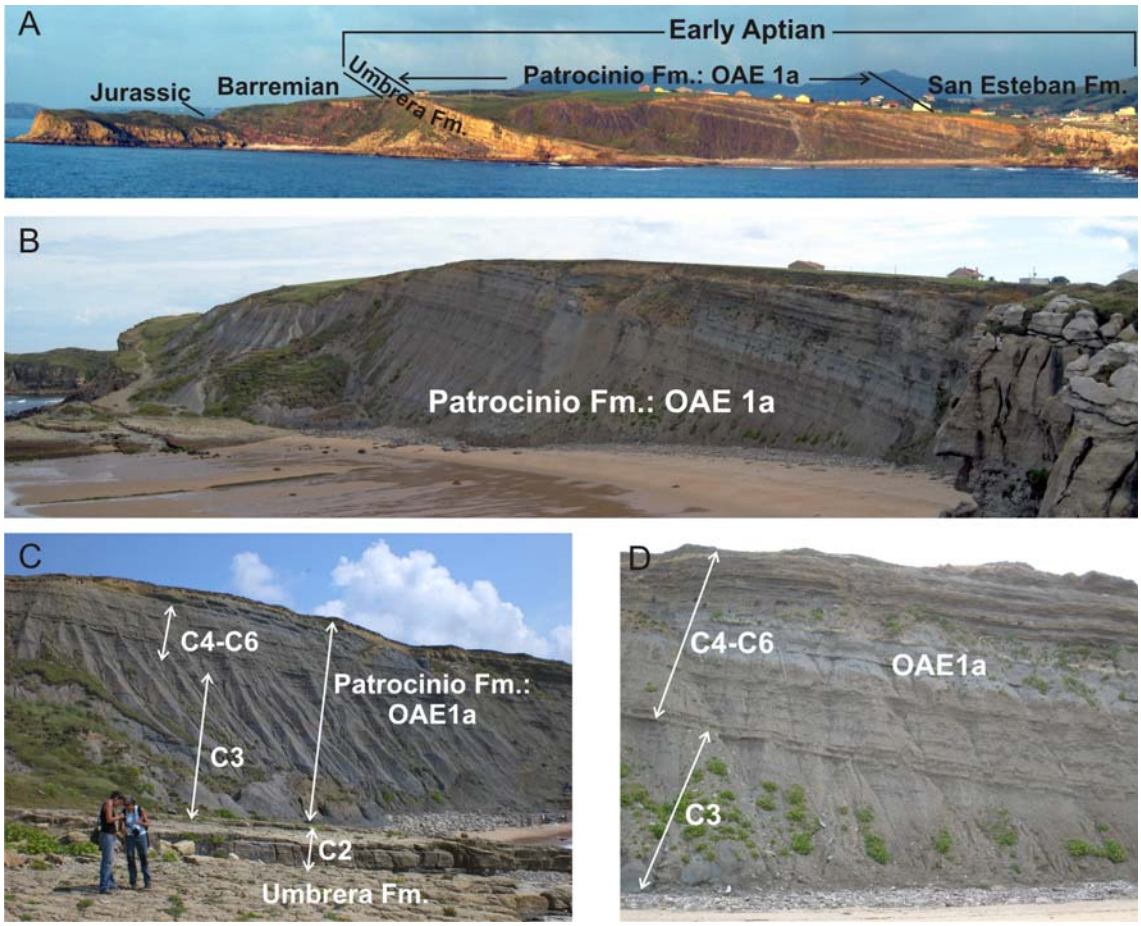

Figure. 3.- Field pictures of the Patrocinio Formation. (A) General view of continuous outcrop from Jurassic to Lower Aptian in the Cuchía area. (B) Field picture of the fully exposed Lower Aptian Patrocinio Formation in the coastal cliff of the Playa de Los Caballos beach. (C–D) Field position in the Cuchía outcrop of the Early Aptian $\delta^{13}C$ segments of the chemostratigraphic curve defined by Menegatti et al. (1998).

Palaeontological analyses

Regarding the study of nannofossils, a total of 55 marly samples from the Cuchía and La Florida sections were prepared and examined. The slides for nannofossil analysis were processed according to standard techniques and were studied under a magnification of 1250× using a light polarized microscope. The biostratigraphic events reported by Applegate and Bergen (1988) and Aguado et al. (1999) were used for the definition of biozones and zonal boundaries.

The planktonic foraminifera assemblages were studied in 40 marly samples only from the Cuchía section, because in the samples of La Florida the planktonic foraminifera were scarce and poorly preserved. The samples were disaggregated and washed through sieves, the residue being separated into three fractions (N200 μm, 100–200 μm, and 50–100 μm). Although the three fractions were studied, the richest planktonic foraminiferal assemblages were found in the 100–200 μm fractions. The planktonic foraminifers were studied using optical and electronic (SEM) observations.

Ammonites are scarce in the study area and appear only at discrete levels but with high occurrence within these levels. All the specimens studied here come from two ammonites-rich levels of the Cuchía section. The specimens were collected during fieldwork surveys, and are now deposited in the collections of the Colleccions de Paleontologia de la Universitat Autònoma in Barcelona (PUAB) and the Museo Geominero (IGME) of Madrid. Additional specimens were also supplied by the Museo Geológico del Seminario of Barcelona (MGSB) and by a particular collection (Manuel Díaz, Cantabria).

Six samples were prepared for palynological studies in the laboratory of ALICONTROL (Madrid, Spain). The rock samples were treated following the standard palynological preparation technique (Batten, 1999), which consists in an acid attack with HCl, HF and HNO_3 at high temperature. The residue was concentrated and sieved throughout sieves of different grid sizes (500, 250, 75, 50 and 12 μm). Then, the samples were mounted in glycerin jelly on glass slides for light microscope. The samples were studied with an Olympus BX51 optical microscopy. Only four samples yielded representative and well-preserved assemblages (i.e. Canales-Patrocinio, Sop-Patrocinio, Ru-Cuchía and Ru-Reocín, with 771, 430, 476, and 391 palynomorphs respectively).

STRATIGRAPHY

Previous work on the Lower Aptian succession of the NCB is relatively limited. Earlier stratigraphic and biostratigraphic frameworks had been established by Ramírez del Pozo (1972), Collignon et al. (1979), Hines (1985) and Wilmsen (2005), and have been recently revised and updated by Najarro et al. (2007, 2010). A simplified lithostratigraphy of the two studied areas is provided in Fig. 4.

In the area of La Florida, the Mesozoic sedimentary record starts with a thick (~600 m average) succession of Lower Triassic continental red mudstones, sandstones and conglomerates ("Buntsandstein" facies) resting unconformably on folded (Variscan deformation) Carboniferous basement (Fig. 4). The Upper Triassic, Jurassic and lowermost Cretaceous successions are absent in this sector (Fig. 4), most probably because during the Late Jurassic–Early Cretaceous rifting stage the area was subjected to erosion and non-deposition. In contrast, in the Cuchía area the oldest outcropping deposits correspond to the Upper Triassic (Keuper evaporitic mudstones and dolostones), and are overlain by Lower Jurassic (Hettangian–Pliensbachian) marine carbonates. These deposits are truncated by an angular unconformity and karstification surface that separates tilted marine Jurassic strata from overlying Lower Cretaceous continental red beds. As in the area of La Florida, Upper Jurassic and lowermost Cretaceous deposits are also absent and sedimentation restarted in the Hauterivian–Barremian with deposition of ~100 m of fluvial deposits ("Wealden" or Pas Group; Pujalte, 1982).

Rapid marine transgression occurred in the earliest Aptian, leaving deposits that in both areas unconformably overlie either the continental "Wealden" facies or the pre-Cretaceous substratum. The Aptian lithostratigraphy of the study area is organized into six stratigraphic units, named as follows from oldest to youngest (Fig. 4). 1) Rábago Formation (0–12 m thick; lower Bedoulian, lower *Palorbitolina lenticularis* zone), which is a shallow marine mixed carbonate– siliciclastic unit that represents the initial marine transgression. This unit is absent in the Cuchía area (Fig. 4). 2) Umbrera Formation (lower Bedoulian, *P. lenticularis* zone). This unit (0–52 mthick) consists mostly of cross-bedded skeletal-oolitic grainstones and rudstones, interpreted as shallow platform agitated shoal deposits (Najarro and Rosales, 2008a; Najarro et al., 2010). This unit thickens toward basin depocentres and pinches out toward marginal uplifted areas. 3) Patrocinio Formation (~30–80 m), the focus of this study, is made of open marine

marls, marly siltstones and locally sandstones. Previous biostratigraphic data from this marly unit give associations of benthic foraminifera and ammonite fauna indicative of an Early Aptian age (Collignon et al., 1979). 4) San Esteban Formation (0–40 m), is characterized by metre to decimetre bedded, shallow platform rudist and coral limestones with *P. lenticularis* (Blumenbach), *Choffatella decipiens* Schlumberger and *Iraquia simplex* Henson (Pascal, 1985), which indicate a late Early Aptian (upper Bedoulian) age. 5) Rodezas Formation (0–80 m; uppermost Bedoulian–lower Gargasian, according to Collignon et al., 1979) is characterized by marine sandstones, grainstones, marly limestones and marls with large oysters (*Exogyra*) and ammonites. It grades upwards and laterally to the Reocín Formation. 6) Reocín Formation (80–250 m; upper Gargasian–Clansayesian; *Orbitolina* (*Mesorbitolina*) *texana texana* and *Simplorbitolina manasi* benthic foraminiferal zones; Ramírez del Pozo, 1972) is composed of shallow water coral-rudist limestones and grainstones. The San Esteban and Rodezas formations are absent in the less-subsident basin margin of La Florida area located to the west. Thus, in the La Florida section, the Reocín Formation lies directly over the Patrocinio Formation (Fig. 4).

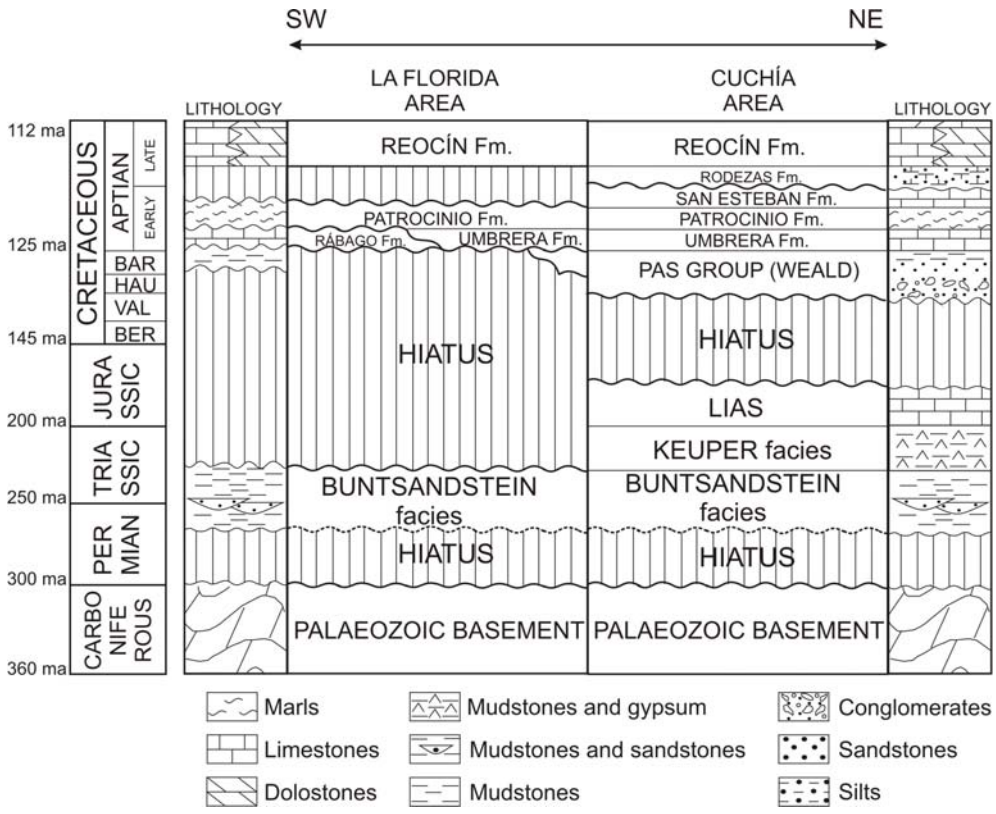

Figure 4. Lithostratigraphy of La Florida and Cuchía areas. Chronostratigraphy after Gradstein (2004). P.G. = Pas Group.

RESULTS

Lithostratigraphic and chemostratigraphic data

La Florida section

In La Florida section, the Patrocinio Formation comprises a 31 m thick succession of fully marine argillaceous marls overlying ~13 m of shallow marine limestones and orbitolinid siltstones of the Rábago and Umbrera formations (Fig. 5). The latter is represented here by less than 1 m of skeletal grainstones that pinch over an unconformity surface marked by dissolution and coated by iron oxides (Najarro and Rosales, 2008a; Najarro et al., 2010). This unconformity separates the Umbrera grainstones from the Rábago unit underneath; thus, a certain stratigraphic gap exists here between the two limestone units. Above, the facies of the Patrocinio Formation corresponds to homogeneous dark marls showing good lamination, pyrite framboids and rare belemnites. At the top of the unit, the content of siliciclastic silt and bioclastic remains increases, and evidence of activity of benthic fauna appears, represented by bioturbation and orbitolinids. This suggests rapid shallowing in the last few metres of the Patrocinio Formation before recovery of shallow water carbonate sedimentation (Reocín Formation).

The total organic carbon content (TOC) of the Patrocinio Formation in this section is relatively low, with values ranging from 0.1 to 0.5 wt.%. The results present three distinctive segments (Fig. 5). The first segment, at the base of the Patrocinio Formation (12–19 m, samples PN-1 to PN-4, Fig. 5), shows maximum TOC values at the bottom that progressively decrease from 0.5 to 0.3 wt.%. The second segment (19–22 m, samples PN-4 to PN-6, Fig. 5) displays a rapid spike to higher values up to 0.5 wt. %. The values decrease again in the third segment located at the upper part of the Patrocinio Formation (22–39 m, samples PN-6 to PN-14, Fig. 5), which exhibits values fluctuating around 0.3 wt.% and finally reaches a minimumof 0.1 wt.% at the top. Calcium carbonate content of these samples fluctuates between 0.1 and 27.6 wt.% (Fig. 5). There is no correlation between TOC and $CaCO_3$ contents, except for the middle part of the marly unit (19–27 m, samples PN-4 to PN-8, Fig. 5), which exhibits a roughly negative correlation of these two values. Thus, in this part of the succession, the highest concentration of calcium carbonate (27.6 wt.%, sample PN-8) correlates with a minimum of TOC, and the opposite. In the uppermost part of the Patrocinio unit, the

terrigenous input is important, as shown by a higher proportion of quartz silt and mica. This part of the section is characterized by the lowest $CaCO_3$ values, which stay below 1 wt.%.

Carbon isotope values of the carbonate and organic matter fractions of the samples record significant negative excursions across the Patrocinio Formation in La Florida section. The organic C-isotope values ($\delta^{13}C_{org}$ in Fig. 5) range between −21.2‰ and −25.2‰ and show three prominent negative spikes. From the bottom, the C-isotope curve starts with values of −22.2‰ and decrease sharply to −24.8‰ at 15 m, resulting in a first negative excursion of 2.6‰ in magnitude. This is followed by a return to more positive values (−21.6‰) similar to those observed before the spike. The following $\delta^{13}C_{org}$ values show a gradual decrease towards more negative values, reaching a minimum of −25.2‰ at 23 m (second negative spike of 3.5‰ in magnitude). Then, the values change progressively to more positive values and peak at values of −22.6‰ at 31 m. The negative trend of the $\delta^{13}C_{org}$ is resumed, and at 37 m the curve displays a third negative spike of −24.6‰ (~2‰ in magnitude). Finally, the upper part of the Patrocinio Formation records a rapid rise in the $\delta^{13}C_{org}$ values, showing the highest value (−21.2‰) at the top of the studied segment (Fig. 5).

The $\delta^{13}C_{carb}$ values measured in La Florida section range between −4.5‰ and +3.6‰. In their temporal record, three major segments can be recognized. In the first segment (0–12 m, samples LA-1 to LA- 13; Fig. 5), the carbonate carbon isotope curve presents relatively stable positive values of 1.6 to 2.7‰ (mean of +2.2‰). The second segment (12–39 m, samples PN-1 to PN-14; Fig. 5), which correlates with deposition of the Patrocinio Formation, is characterized by a remarkable negative excursion (~6‰ in magnitude) from values of +1.6‰ just beneath the base of the unit to −4.5‰ at its top. This negative shift occurs in three steps, each of which records progressively more negative peak values (−2.9‰, −4.1‰ and −4.5‰ respectively). Finally, a return to $\delta^{13}C_{carb}$ positive values occurs at the top of the section (39–64 m, samples PN-15 to LA-19, Fig. 5), coinciding with the recovery of the carbonate sedimentation and the installation of a shallow carbonate platform. In this segment, the $\delta^{13}C_{carb}$ values vary from +2.5‰ to +3.6‰, which are slightly higher than those obtained from the first segment.

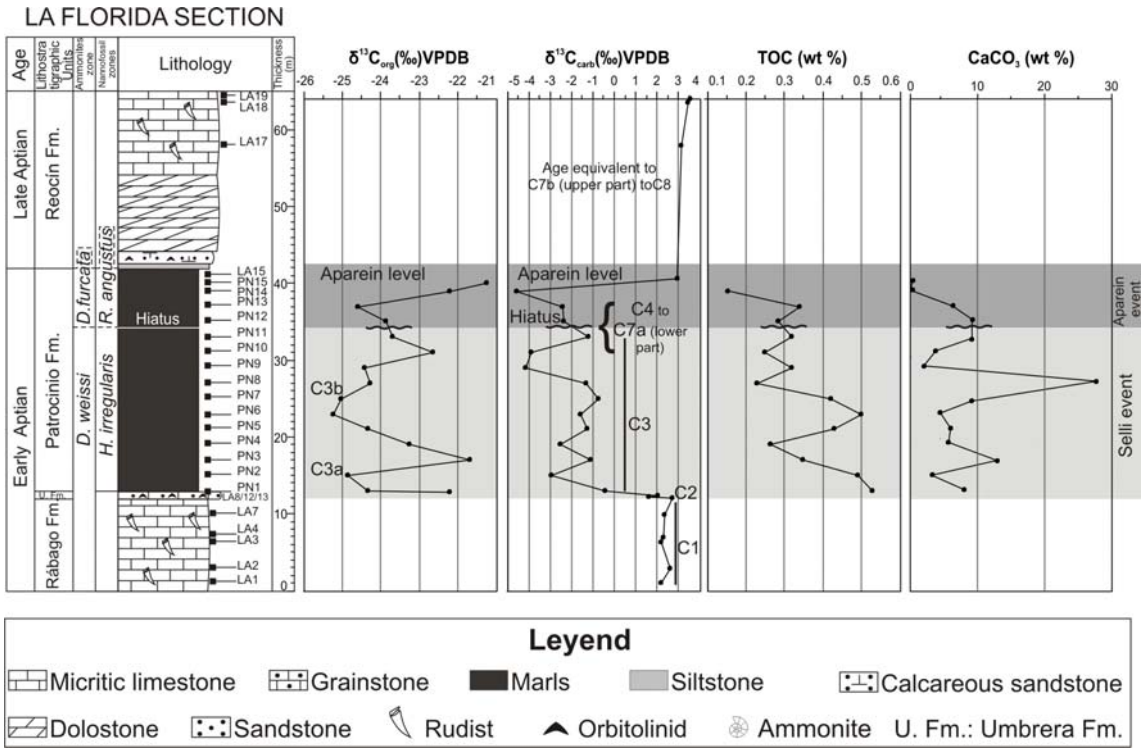

Figure 5.- La Florida section, showing the lithological log, $\delta^{13}C_{carb}$, $\delta^{13}C_{org}$, total organic carbon (TOC) and $CaCO_3$ data. Legend applies for Figs. 6, 7, and 10.

Cuchía section

The Lower Aptian succession exposed at the Playa de los Caballos beach can be subdivided into four parts (Figs. 3, 6): (1) a lower part (~24 m thick) of cross-bedded rudstones and grainstones of the Umbrera Formation. The contact with the continental Wealden facies underneath is sharp and erosional in places, and the Rábago Formation is absent here (Fig. 4). (2) A second part (from 24 to 75 m; Figs. 3B–C, 6), which here corresponds to the lower part of the Patrocinio Formation, is composed mainly of dark clayey marls with red ironstones nodules. Two levels (at 30 and 36 m respectively, Fig. 6) of nodular bioclastic limestones with ammonites and remains of brachiopods, echinoids, bivalves, orbitolinids, the mecochirid decapod *Meyeria magna* M'Coy, as well as wood debris are intercalated. These levels represent the two horizons with ammonites described by Collignon et al. (1979). (3) The third part of the succession corresponds to the upper part of the Patrocinio Formation, and is formed of ~30 m of heterolithic alternations of carbonaceous and mica-rich claystones, siltstones and cross-bedded quartz sandstones, organized in a coarsening- and thickening-upwards sequence (Fig. 3D). This part of the succession represents a local delta progradation at the top of

the Patrocinio Formation (Wilmsen, 2005). 4) Above, the shallow platform carbonate sedimentation recovered, and the sedimentary facies change gradually to orbitolinid rich sands and coral-rudist limestones (San Esteban Formation).

The TOC content of the Patrocinio Formation in the Cuchía section is low (Fig. 6), and although slightly higher than in the La Florida section, all values are below 1 wt.% (i.e. 0.1 to 0.8 wt.%). In general terms, four segments can be roughly differentiated. The first segment at the base of the Patrocinio Formation shows a decrease from 0.5 wt.% to 0.2 wt.%. The second segment (40.5–51.5 m; Fig. 6) displays an increase to TOC values up to 0.5 wt.%. The third segment (51.5–73 m; Fig. 6) exhibits a progressive decrease until reaching a minimum of 0.1 wt.%. Finally, maximum TOC values of 0.8 wt.% are obtained in the last segment at the top. The calcium carbonate content of the samples ranges between 0.8 and 47.5 wt.% (Fig. 6) and shows no correlation with the TOC content. The lower values are obtained in the upper part of the Patrocinio Formation, coinciding with the lithological change to siliciclastic deposits.

The carbon isotope composition of the bulk organic matter measured across the Patrocinio Formation in the Cuchía section varies from −21.3‰ to −26.1‰ (Fig. 6). In the lower part, the isotopic signal shows a significant negative shift in $\delta^{13}C_{org}$ of ~5‰ (26.5 m of the section), from values that fluctuate between −22.8‰ and −20.7‰ to values of −26.1‰. Values remain predominantly low (below−24‰) between 26.5 and 45 m (Fig. 6), with the exception of one sample at the base. Next, there is an increase in the $\delta^{13}C_{org}$ signal up to values of −21.4‰ at 48.5 m. The succeeding portion of the carbon isotope curve is defined by a gradual decrease of the $\delta^{13}C_{org}$ signature that peaks at values of −25.6‰ at 54 m, recording a second negative excursion of 4‰ in magnitude. This is followed by an increase toward values of ~−22.3‰ with small-scale fluctuations. The $\delta^{13}C_{org}$ values fall again to relatively constant values of ~−25.4‰ between 66–73 m (Fig. 6), which represent a third negative excursion of ~3‰. Finally, in the upper part of the section the $\delta^{13}C_{org}$ values show an increase to values of ~−22.8‰ coinciding with the more siliciclastic upper part of the Patrocinio Formation.

The carbonate carbon isotope composition measured in the Cuchía section varies significantly from +4.1‰ to −3.6‰, recording a prominent negative excursion during deposition of the marly lower part of the Patrocinio Formation (Fig. 6). The structure of the $\delta^{13}C_{carb}$ curve reproduces the three segments observed in La Florida section, but with some differences. The first of these, at the base of the section, starts with positive

values but with a clear decreasing trend upwards from +2.5‰ in the Umbrera Formation to −2.0‰ at the base of Patrocinio Formation. The second segment coincides with the marly lower part of the Patrocinio Formation, and records a notable negative excursion. The high-resolution quality of this segment of the curve allows recognition of two negative peaks within the overall negative excursion (Fig. 6). The first, at 29.5 m, reaches a minimum $\delta^{13}C_{carb}$ value of −3.6‰, implying a negative excursion of 3‰ in magnitude. The second peak ($\delta^{13}C_{carb}$=−3.1‰) appears at 70.5 m and shows a negative excursion of ~2‰. Between these two peaks (30.5–69.5 m), the carbonate carbon isotope composition is relatively constant with a mean value of −1‰ (Fig. 6). Finally, the third segment of the isotope curve is recorded across the limestone of the San Esteban Formation. This segment is characterized by a stepwise increase of $\delta^{13}C_{carb}$ to values as high as +4.5‰, with a mean of +3‰.

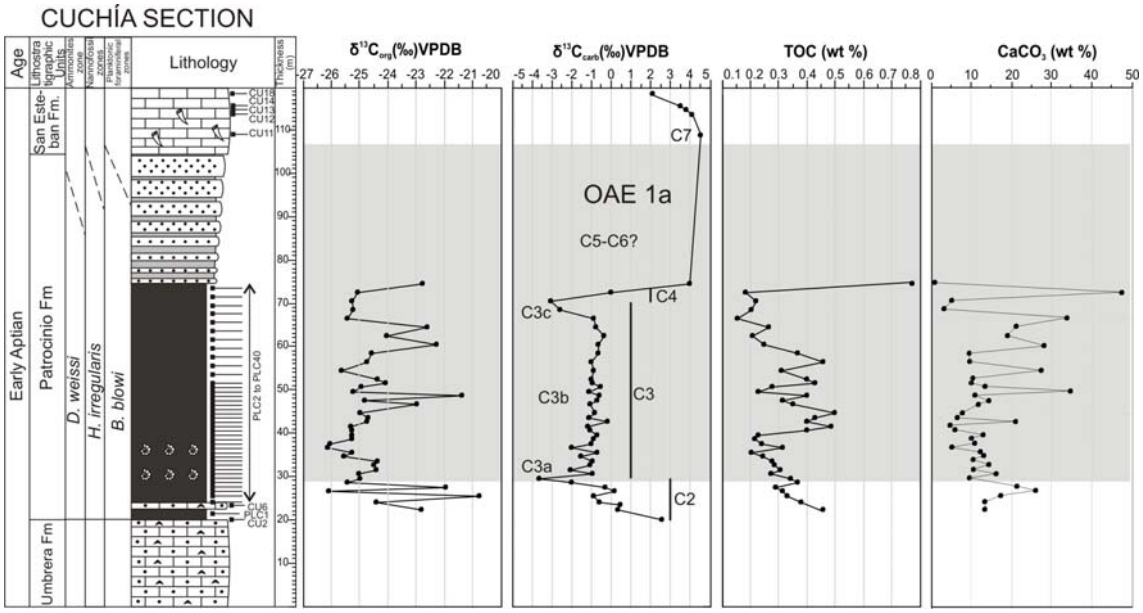

Figure 6.- Cuchía section, showing the lithological log, $\delta^{13}C_{carb}$, $\delta^{13}C_{org}$, total organic carbon (TOC) and $CaCO_3$ data. See Fig. 5 for lithological legend.

BIOSTRATIGRAPHIC DATA

To evaluate the impact of the OAE 1a event in the studied series and to correlate its geochemical record with coeval records in other regions, the age of the event must be adequately calibrated using biostratigraphic data. Ammonites may offer one of the highest resolution biostratigraphic frameworks for the position of the OAE 1a (e.g. García-Mondéjar et al., 2009; Moreno-Bedmar et al., 2009), although they are usually scarce. For this last reason, in recent years the biostratigraphic schemes of the OAE 1a have been essentially based upon planktonic foraminifera and calcareous nannofossils (e.g. Aguado et al., 1999; Ando et al., 2008; Bralower et al., 1994; Erba et al., 1999; Gea et al., 2003; Luciani et al., 2001). In this study, the biostratigraphic position of the Patrocinio Formation was constrained using four different fossil groups: ammonites, calcareous nannofossils, planktonic foraminifera and palynomorphs.

Ammonites

Only the Cuchía section has yielded ammonite fauna. Ammonoids from this section were previously studied by Collignon et al. (1979), who identified two horizons within their "Formation terrigène à Ammonites" (corresponding to the Patrocinio Formation). On the basis of their determinations, Collignon et al. (1979) attributed their lower horizon to the *Prodeshayesites fissicostatus* and *Deshayesites forbesi* Zones, and the upper one to the *Deshayesites deshayesi* and *Tropaeum bowerbanki* Zones of the zonal scheme proposed by Casey (1961). Therefore, according to Collignon et al. (1979), all the Lower Aptian ammonite zones would be represented within these two horizons. This stratigraphic interpretation was recently accepted as valid by Wilmsen (2005).

In this study, it has also been possible to recognize the two horizons identified by Collignon et al. (1979) at the lower part of the Patrocinio Formation, but the biostratigraphic attributions reported here are rather different (Fig. 7). The new ammonite assemblages yielded by this study from the two ammonite-rich levels are represented in Figs. 7 and 8. The lower level has yielded *Deshayesites cf. forbesi* Casey, *Deshayesites cf. callidiscus* Casey, *Roloboceras cf. hambrovi* (Forbes), *Pseudohaploceras liptoviense* (Zeuschner), *Pseudosaynella undulata* (Sarasin), and *Toxoceratoides sp. ind*. The upper horizon has provided *Deshayesites cf. consobrinus* (d'Orbigny), *Deshayesites planus* Casey, *D. cf. forbesi* Casey *R. hambrovi* (Forbes),

Roloboceras sp. ind., *Pseudosaynella bicurvata* (Michelin), *Toxoceratoides sp.* ind., and the *nautiloid Heminautilus saxbii* (Morris). The specimens from the Cuchía section deposited in the collections of the Museo Geológico del Seminario in Barcelona (MGSB) and the Museo Geominero (IGME) in Madrid, and in a particular collection, have been identified as *Deshayesites sp. callidiscus* Casey, *D. cf. forbesi* Casey, *D. planus* Casey, *R. hambrovi* (Forbes), *Roloboceras sp*. ind., *P. undulate* (Sarasin), and *Toxoceratoides royerianus* (d'Orbigny). All these assemblages can be attributable to the *Deshayesites weissi* Zone of the standard Mediterranean Zonation (Reboulet et al., 2009). In fact, all the mentioned deshayesitid species are characteristic of this biozone, equivalent to the *D. forbesi* Zone of Casey (1961). Furthermore, the occurrence of *Roloboceras* in both horizons suggests that the entire segment of the section correlates with the middle/upper part of the *D. weissi* Zone (Casey, 1961; Casey et al., 1998; Moreno-Bedmar et al., 2009). The striking differences with the conclusions of Collignon et al. (1979) can only be explained by divergences in the taxonomic interpretation of ammonites.

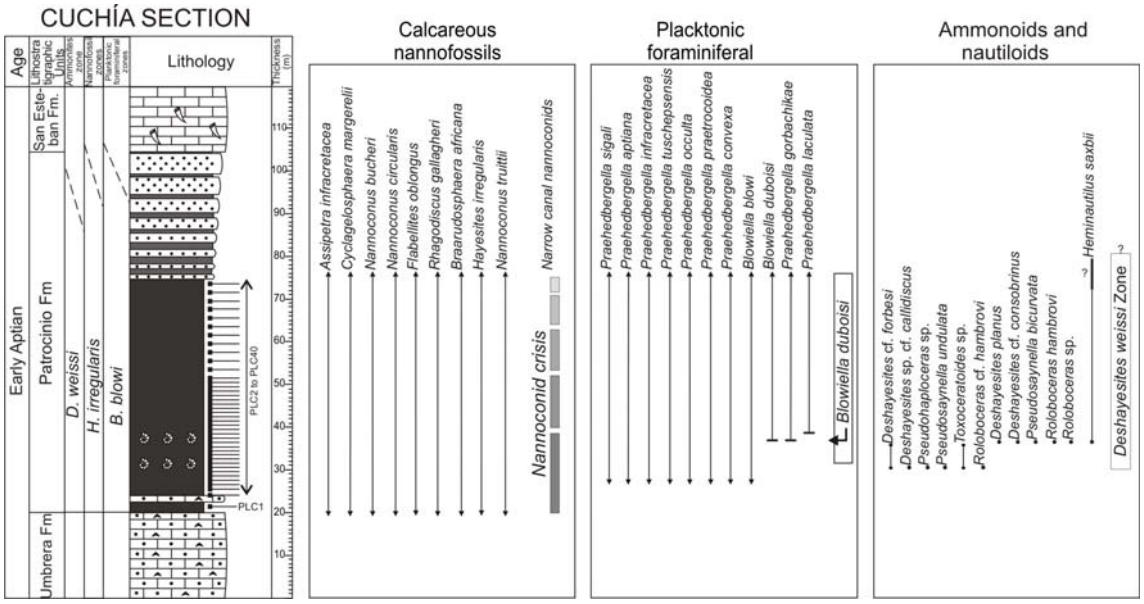

Figure 7.- Cuchía section, showing calcareous nannofossils, placktonic foraminifera and ammonites biostratigraphy. See Fig. 5 for lithological legend

Calcareous nannofossils

Nannofossils are not very abundant in the samples and present a moderate preservation and a scarce diversity. The assemblages (Figs. 7, 9 and 10), of marked Tethyan character, are dominated by the genera *Watznaueria, Rhagodiscus* and *Nannoconus*. Abundant species include *Assipetra terebrodentaria, Hayesites irregularis, Zeugrhabdotus noeliae, Lithraphidites carniolensis, Biscutum ellipticum, Discorhabdus ignotus, Diazomatolithus lehmanii and Micrantholithus obtusus*. Other characteristic but less abundant forms include *Cyclagelosphaera margerelii, Braarudosphaera africana, Flabellites oblongus, Assipetra infracretacea and Helenea chiastia*. As can be seen in Figs. 7, 9 and 10, most of the samples of the Patrocinio Formation in the two studied sections contain the association *H. irregularis, Nannoconus truittii, B. africana and Conusphaera rothii* typical of the middle/upper part of the *H. irregularis nannofossil* Zone, according to the zonation of Applegate and Bergen (1988) and Aguado (1994). This assemblage is correlated with the *Deshayesites weissi ammonite* Zone (Aguado et al., 1999). The quantitative analysis of the nannofossil abundance has revealed a widespread absence of narrow canal nannoconids (i.e. Nannoconus steinmannii), which can be identified with the "nannoconid crisis" inferred for the same time interval by Erba (1994). The "nannoconid crisis" is recorded in the upper half of the *H. irregularis* Zone (Aguado et al., 1999; Erba, 1994), and may be correlated with the middle/upper part of the *D. weissi* ammonite Zone.

These observations allow to conclude that, in the Cuchía section, the dark clayey marls of the lower part of the Patrocinio Formation (samples PCL-1 to PCL-40 in Fig. 7, and C3 segment in Fig. 3C) belong to the upper half of the *Hayesites irregularis* nannofossil Zone, being equivalent to the middle/upper part of the *Deshayesites weissi* ammonite Zone of the Lower Aptian. In La Florida section (Fig. 10), most of the Patrocinio Formation (up to sample PN-12) belongs also to the upper half of the *H. irregularis* nannofossil Zone. The first occurrence (FO) of *Eprolithus floralis* is registered from sample PN-12 onwards (Fig. 10). This biostratigraphic event enables the assignment of the uppermost part of the Patrocinio Formation in this section to the *Rhagodiscus angustus* nannofossil Zone (defined as the interval between the FO of *E. floralis* and the FO of *Praediscosphaera columnata*). According to Aguado et al. (1999) the base of the *R. angustus nannofossil* Zone falls within the upper part of the *Dufrenoyia furcata* ammonite Zone and is dated as latest Early Aptian. Therefore, in the La Florida section exists a stratigraphic gap affecting at least the upper part of the

Lower Aptian. This would comprise the uppermost part of the *D. weissi*, the whole *Deshayesites deshayesi* and the lower part of the *D. furcata* Zones of ammonites.

Planktonic foraminifera

Although in general planktonic foraminifera are scarce in the samples of the Cuchía section, only the lowermost part of the Patrocinio Formation has not yielded planktonic foraminifera (from samples PLC-1 to PLC-3, Fig. 7). The planktonic foraminiferal assemblages are characterized by forms with smooth microperforate wall having four or five rounded chambers (Fig. 11). The samples are characterized by forms assigned to the genera *Praehedbergella* (*Praehedbergella sigali*, 6–11 in Fig. 11; *Praehedbergella aptiana*, 20–23 in Fig. 11; *Praehedbergella infracretacea*, 14–19 in Fig. 11; *Praehedbergella occulta*, 3–4 in Fig. 11; *Praehedbergella convexa*, 5 in Fig. 11; *Praehedbergella praetrocoidea*, 1–2 in Fig. 11; *Praehedbergella gorbachikae*, 24–25 in Fig. 11; *Praehedbergella tuschepsensis*, 12–13 in Fig. 11; *Praehedbergella laculata*) and *Blowiella (Blowiella blowi*, 26–28 in Fig. 11; *Blowiella duboisi*, 29–31 in Fig. 11, *Blowiella maridalensis*). No typical forms of *Schackoina (Schackoina cabri*) were found in the studied samples of this section. The first occurrence (FO) of *B. duboisi* and *P. gorbachikae* was found in sample PLC-14 (Fig. 7). These bioevents have been shown to happen in the upper part of the *B. blowi* Zone, and precede the first occurrence of *S. cabri* at the lower part of the main anoxic event in south Spain (Aguado et al., 1999; Gea et al., 2003). According to these data (Fig. 7), the studied part of the section (at least up to sample PLC-40) is assigned to the upper part of the *B. blowi* planktonic foraminiferal Zone (Moullade, 1974; Moullade et al., 2002). In this section, this biozone is correlated with the upper half of the *Hayesites irregularis* nannofossil Zone and the middle/upper part of the *D. weissi* ammonite Zone.

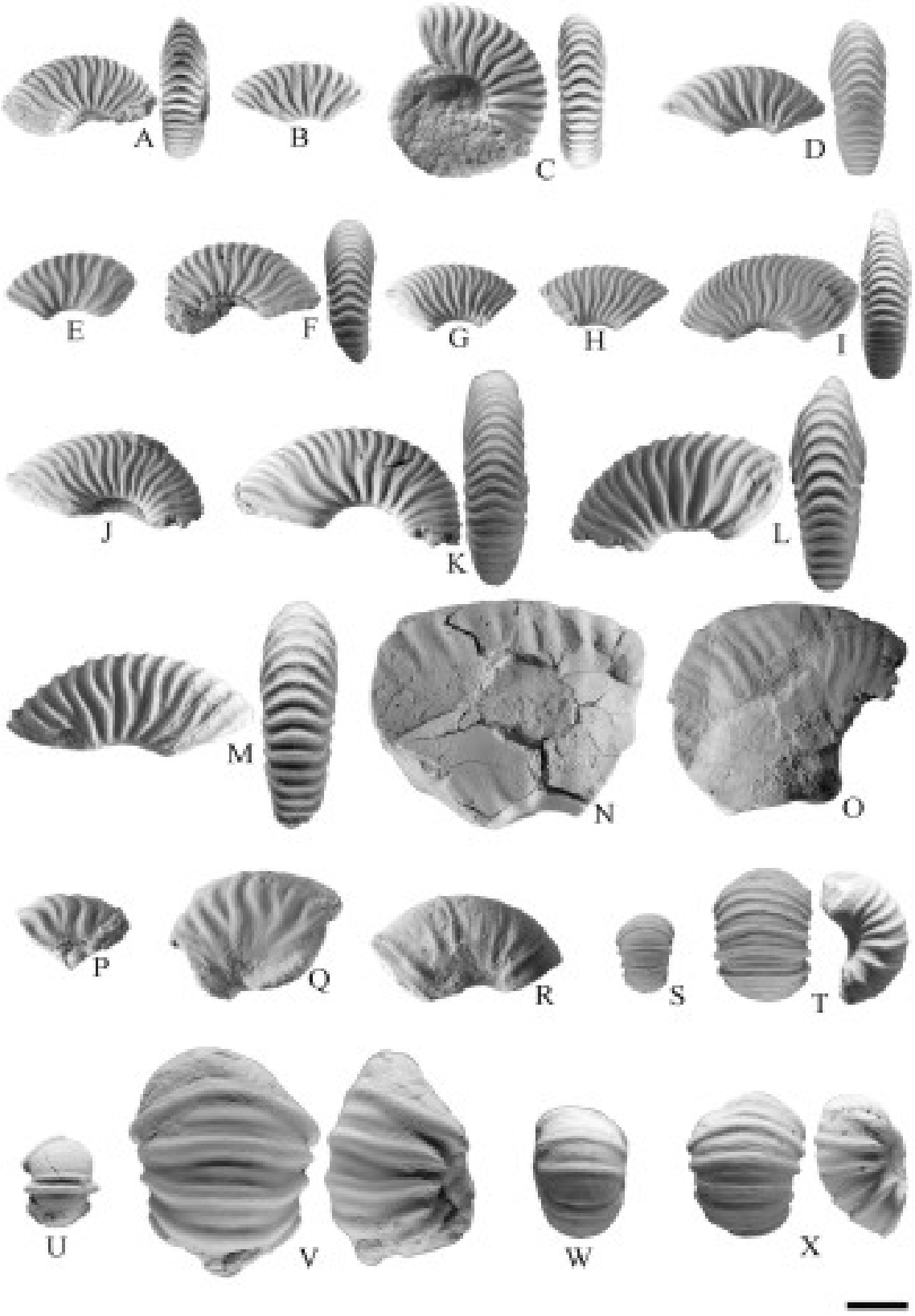

Figure 8.- Ammonites. A: *Deshayesites* cf. *forbesi*, lateral and ventral view of the specimen MGSB (Museo Geológico del Seminario de Barcelona) 18730-3. B: *Deshayesites* cf. *forbesi*, lateral view of the specimen MGSB 1870-2. C: *Deshayesites* cf. *forbesi*, lateral and ventral view of the specimen MGSB 18730-1. D: *Deshayesites* cf. *forbesi*, lateral and ventral view of the specimen PUAB (Colleccions de Paleontologia de la Universitat Autònoma de Barcelona) 68536, horizon 1. E: *Deshayesites* cf. *forbesi* lateral view of the specimen PUAB 68533, horizon 1. F: *Deshayesites* cf. *forbesi*, lateral and ventral view of the specimen PUAB 68545, horizon 1. G: *Deshayesites planus*, lateral view of the specimen PUAB

68554, horizon 2. H: *Deshayesites planus*, ventral view of the specimen PUAB 68555, horizon 2. I: *Deshayesites planus*, lateral and ventral view of the specimen PUAB 68557, horizon 2. J: *Deshayesites planus*, lateral view of the specimen PUAB 68559, horizon 2. K: *Deshayesites* cf. *forbesi*, lateral and ventral view of the specimen PUAB 68562, horizon 2. L: *Deshayesites* cf. *consobrinus*, lateral and ventral view of the specimen PUAB 68561, horizon 2. M: *Deshayesites* cf. *consobrinus*, lateral and ventral view of the specimen PUAB 68563, horizon 2. N: *Deshayesites* sp. cf. *callidiscus*, lateral view of the specimen MGSB 18730-4.O: *Pseudosaynella bicurvata*, lateral view of the specimen PUAB 68564, horizon 2. P: *Pseudosaynella undulata*, lateral view of the specimen PUAB 68538, horizon 1. Q: *Pseudosaynella undulata*, lateral view of the specimen MGSB 18730-5. R: *Pseudohaploceras liptoviense*, lateral view of the specimen PUAB 68534, horizon 1. S: *Roloboceras* sp., ventral view of the specimen PUAB 68542, horizon 1. T: *Roloboceras* sp., microconch, lateral and ventral view of the specimen PUAB 68552, horizon 2. U: *Roloboceras* sp., ventral view of the specimen PUAB 68532, horizon 1. V: *Roloboceras* sp., macroconch, lateral and ventral view of the specimen MGSB 78706. W: *Roloboceras* sp., microconch, ventral view of the specimen MGM (Museo Geominero, IGME) 10807C. X: *Roloboceras hambrovi*, macroconch, lateral and ventral view of the specimen MGM 10809C. Scale bar=1 cm.

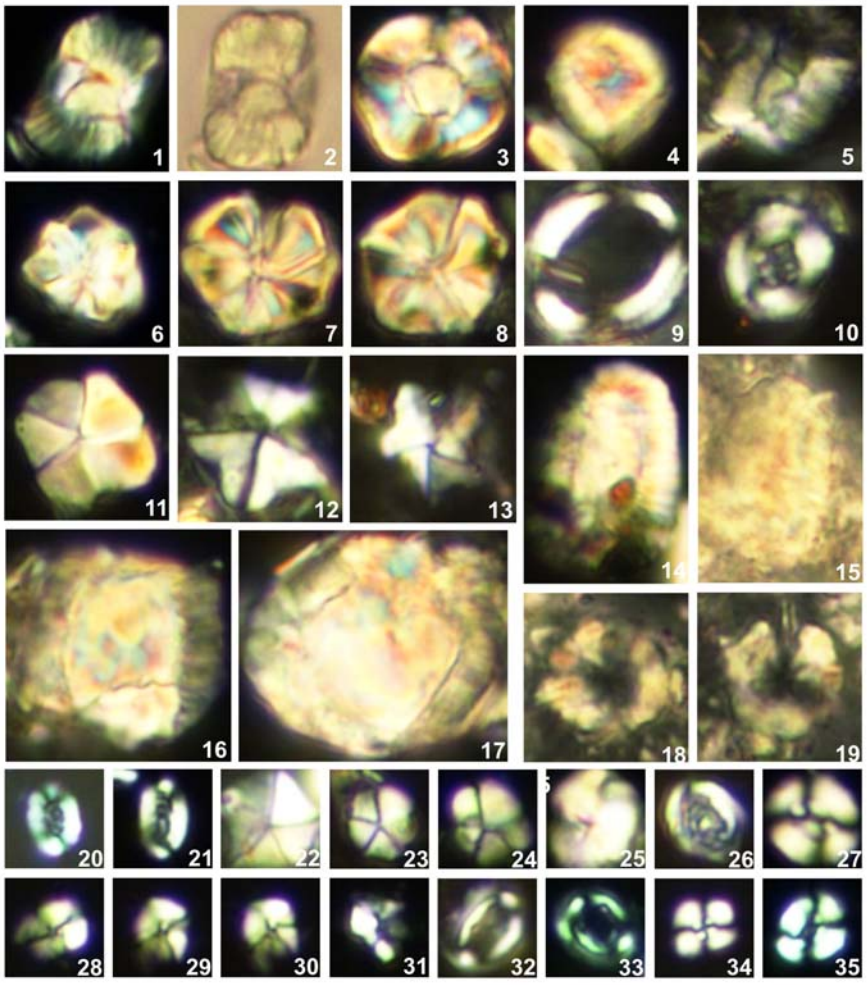

Figure 9.- Calcareous nannofossils. 1-5, *Nannoconus truittii* (picture 2 to parallels nicols). 6-8, *Assipetra terebrodentaria* (large specimens). 9, *Manivitella pemmatoidea*. 10, *Helenea chiastia*. 11, *Braarudosphaera africana*.12, *Micrantholithus obtusus*. 13, *Micrantholithus stellatus*. 14, *Nannoconus kamptneri*. 15, *Nannoconus steinmannii*. 16, *Nannoconus bucheri*. 17, *Nannoconus circularis*. 18, 19, *Eprolithus floralis*. 20, 21, *Rhagodicus gallagheri*. 22, *Micrantholithus hoschulzii*. 23, 24, *Braarudosphaera africana*. 25, *Assipetra infracretacea*. 26, *Rhagodiscus asper*. 27, *Watznaueria barnesae*. 28-31, *Hayesites irregularis*. 32, 33, *Flabellites oblongus*. 34, *Cyclagelosphaera margerelii*. 35, *Watznaueria britanica*. All Figures c. x3000. Scale bar for all pictures = 5μm

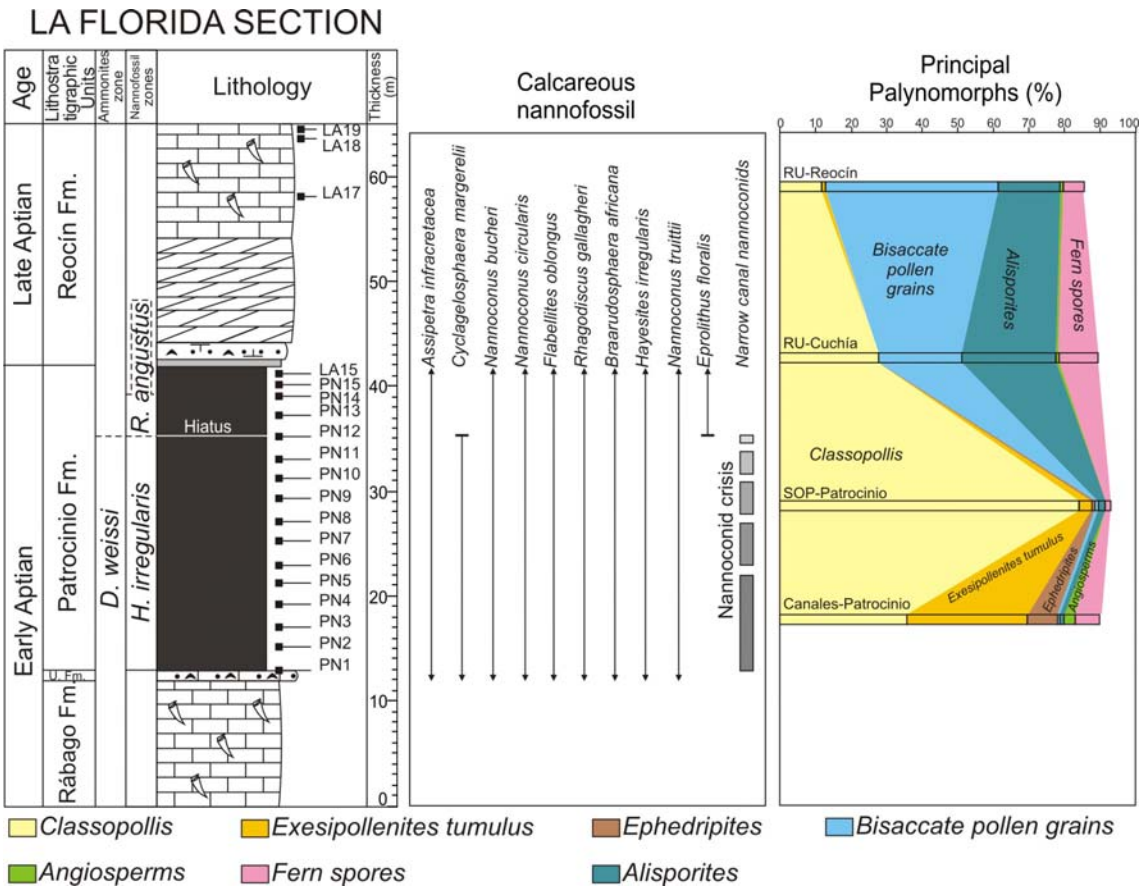

Figure 10.- La Florida section, showing calcareous nannofossil biostratigraphy and the principal palynomorphs content. See Fig. 5 for lithological legend.

Palynomorphs

An exploratory palynological study has been carried out in order to compare patterns of distribution of terrestrial floras during the onset of the OAE 1a (samples Canales-Patrocinio and Sop-Patrocinio, from marls of the Lower Aptian Patrocinio Formation, Table 1) and after the OAE 1a (samples Ru-Cuchía and Ru-Reocín from marls and carbonaceous shales of Upper Aptian formations, Table 1). In addition, the palynological analysis yielded some useful age information that can be used in combination with the other biostratigraphic data.

A total of 24 spores and 34 pollen types, and some poorly preserved dinoflagellate cysts were found (Fig. 12 and Table 1). Due to their predominance, pollen grains of gymnosperms characterized the assemblages of the four samples. The majority of the palynomorphs in the two Lower Aptian samples from the Patrocinio Formation are constituted by *Classopollis* (Fig. 12E).

In the Canales-Patrocinio sample both *Classopollis* (36.4%) and *Exesipollenites tumulus* (33.9%) numerically dominate. The genus *Classopollis* was produced by conifers of the extinct family *Cheirolepidiaceae* (Taylor and Alvin, 1984; Watson, 1988), while *E. tumulus* could be produced by plants of the order *Bennettitales* (Balme, 1995). The Canales-Patrocinio sample is also characterized by relatively high percentages of polyplicate pollen of the genus *Ephedripites* (8.6%) (Fig. 12F). This genus is related to the order *Ephedrales* (Azéma and Boltenhagen, 1974) and is considered as an influence of the Northern Gondwana floral province (Heimhofer et al., 2004). The calculated percentages of these latter pollen grains are unusually high for the Early Cretaceous of the Iberian Peninsula (Trincão, 1990), although they occur with similar values in the upper Barremian Calizas de Artoles Formation in the Eastern Iberian Ranges of NE Spain (Solé de Porta and Salas, 1994). In the Sop-Patrocinio sample *Classopollis* is the predominant pollen (84.9%), followed by scarce percentages of *E. tumulus* (4.4%). Fern spores in the samples of the Patrocinio Formation exhibit low percentages (1.6% and 6.9% respectively), being essentially represented by both the schizaeaceous *Cicatricosisporites spp*. and the *cyatheaceous Deltoidospora australis* (Fig. 12B).

The Late Aptian assemblages, represented by the samples Ru-Cuchía and Ru-Reocín, are distinguished from the Early Aptian assemblages by a decrease in *Classopollis* (28.5% and 12.1% respectively), the near disappearance of *Exesipollenites* (1% or absent), and a remarkable increase of poorly preserved bisaccate pollen grains related to conifers (54% and 67.6% respectively). In addition, a conspicuous percentage of *Alisporites* (27% and 17.8% respectively) has been recorded (Fig. 12G). This pollen is related to seed ferns of the order *Peltaspermales* (Balme, 1995). Also evident is the appearance of the species *Inaperturopollenites dubius* (up to 6.5%), which corresponds with inaperturate and psilate pollen grains related to the coniferous *Cupressaceae* family (Peyrot et al., 2007a). The occurrence of some scarce dinoflagellate cysts (*Tenua histrix Eisenak emend Sarjeant, Pseudoceratium polymorphum* (Eisenak) *Bint and Spiniferites sp*. in the sample Ru-Reocín, and *Callaiosphaeridium asymmetricum* (Deflandre and Courteville) Davey and Williams, *Hystrichosphaerina schindewolfii* Alberti and *aff. Criboperidinium sp*. In the sample Ru-Cuchía; (Fig. 12H) as well as organic test of foraminifera indicates a clear marine influence at these levels.

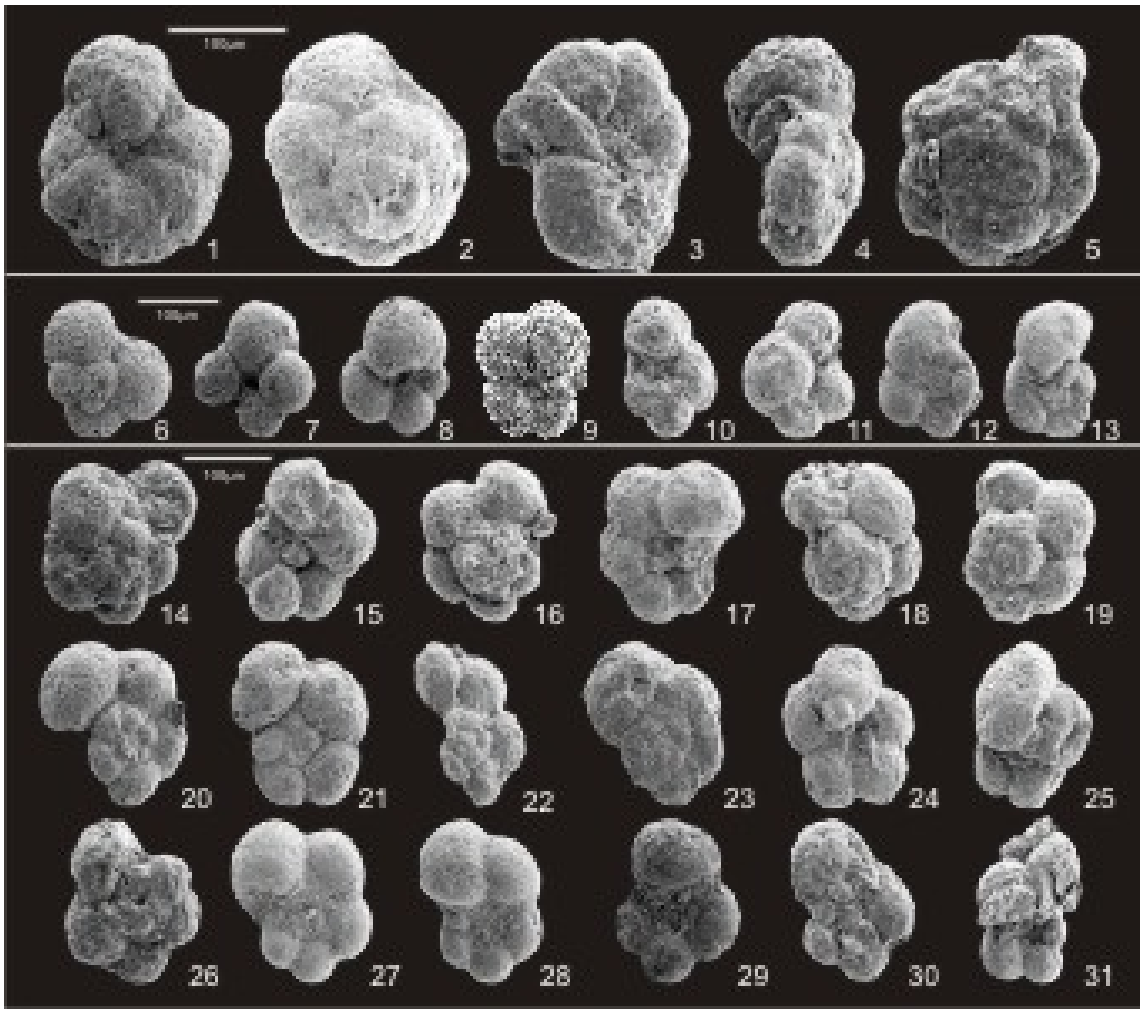

Figure 11.- Planktonic foraminifera. 1,2, *Praehedbergella praetrocoidea*. 3,4*, Praehedbergella oculta*. 5, *Praehedbergella convexa*. 6-11, *Praehedbergella sigali*. 12,13, *Praehedbergella tuschepsensis*. 14-19. *Praehedbergella infracretacea*. 20-23, *Praehedbergella aptiana.* 24,25, *Praehedbergella gorbachikae*. 26-28, *Blowiella blowi*. 29-31, *Blowiella duboisi.* Figures 1-5 c x 300. Figures 6-13 c x500. Figures 14-31 c x400.

Pollen grains of ancient angiosperms are very scarce in all the samples (maximum 2.6%). The presence of seven taxa, however, indicates that these plants had a relative importance in the plant communities of the region. The occurrence of a single grain of *Tricolpites* in one of the samples of the Patrocinio Formation (Fig. 12C) is remarkable because it is the oldest record of tricolpate pollen grains on the Iberian Peninsula. The encountered pollen grain morphologically resembles Albian specimens of the species *Tricolpites parvus* Stanley from Northwestern Alberta, Canada (Singh, 1971; pp. 187–188, pl. 32, Figs. 12–17). Although the first occurrence of tricolpate pollen grains in Europe is reported in mid-Barremian strata from the Isle of Wight (Hughes and McDougall, 1990), until now the oldest presence known in the Iberian Peninsula was found in upper Aptian–Albian deposits from the Basque Cantabrian

Basin (Álava province) and Oliete sub-basin (Teruel province) in Spain (Barrón et al., 2001; Peyrot et al., 2007a,b), and in lower Albian rocks from the Lusitanian and Algarve basins in Portugal (Heimhofer et al., 2007). Therefore, although the identified palynomorphs represent long stratigraphic ranges across the Early Cretaceous, the presence of *Tricolpites* sp. and the dinoflagellate cysts *Pseudoceratium polymorphumindicates*, however, an age not older than the mid-Barremian (Hughes and McDougall, 1990; Stover et al., 1996).

Palynomorphs	Canales-Patrocinio	(%)	Sop-Patrocinio	(%)	Ru-Cuchía	(%)	Ru-Reocín	(%)
Spores of pteridophytes								
Appendicisporites spp.	0	0	0	0,0	2	0,4	0	0
Cicatricosisporites venustus Deák 1963	0	0,0	0	0,0	0	0,0	1	0,3
Cicatricosisporites spp.	20	2,6	2	0,5	11	2,3	6	1,6
Cingutriletes sp.	2	0,3	0	0,0	0	0,0	0	0,0
Concavissimisporites verrucosus (Delcourt & Sprumont) Delcourt, Dettmann & Hughes	0	0,0	0	0,0	1	0,2	0	0,0
Converrucosisporites sp.	1	0,1	1	0,2	0	0,0	0	0,0
Costatoperforosporites spp.	0	0,0	0	0,0	0	0,0	1	0,3
Deltoidospora australis (Couper 1953) Srivastava 1975	0	0,0	1	0,2	4	0,8	5	1,3
Deltoidospora minor (Couper 1953) Pocock 1970	13	1,7	3	0,7	3	0,6	3	0,8
Deltoidospora sp.	1	0,1	0	0,0	22	4,6	4	1,0
Distaltriangulisporites sp.	0	0,0	0	0,0	4	0,8	0	0,0
Gleicheniidites senonicus Ross 1949	0	0,0	0	0,0	1	0,2	1	0,3
Ischyosporites sp.	0	0,0	0	0,0	3	0,6	1	0,3
Laevigatosporites sp.	1	0,1	0	0,0	0	0,0	0	0,0
Leptolepidites macroverrucosus Schulz 1967	1	0,1	0	0,0	0	0,0	1	0,3
Leptolepidites sp.	8	1,0	0	0,0	0	0,0	0	0,0
Maculatisporites sp.	0	0,0	0	0,0	1	0,2	0	0,0
Neoraistrickia truncata (Cookson 1953) Potonié 1956	1	0,1	0	0,0	0	0,0	0	0,0
Neoraistrickia sp.	0	0,0	0	0,0	1	0,2	0	0,0
Patellasporites tavaredensis Groot & Groot 1962	2	0,3	0	0,0	0	0,0	2	0,5
Punctatisporites sp.	0	0,0	0	0,0	1	0,2	0	0,0
Rubinella major (Couper 1958) Norris 1968	3	0,4	0	0,0	0	0,0	0	0,0
Todisporites major Couper 1958	0	0,0	0	0,0	1	0,2	0	0,0
Undulatisporites sp.	1	0,1	0	0,0	0	0,0	0	0,0
Pollen grains (gymnosperms)						0,0		
Alisporites bilateralis Rouse 1959	2	0,3	2	0,5	24	5,0	11	2,8
Alisporites grandis (Cookson 1947) Dettmann 1963	0	0,0	0	0,0	2	0,4	0	0,0
Alisporites spp.	8	1,0	5	1,2	103	21,6	58	15,0
Araucariacites australis Cookson 1947	3	0,4	1	0,2	6	1,3	5	1,3
Callialasporites dampieri Dev 1961	1	0,1	0	0,0	1	0,2	1	0,3
Cedripites sp.	0	0,0	0	0,0	0	0,0	1	0,3
Classopollis classoides Pflug 1953 emend. Pocock and Jansonius 1961	118	15,3	46	10,7	23	4,8	9	2,3
Classopollis spp.	163	21,1	319	74,2	113	23,7	38	9,8
Ephedripites zaklinskainae Azéma et Boltenhagen 1974	2	0,3	0	0,0	0	0,0	0	0,0
Ephedripites multicostatus Brenner 1963	3	0,4	0	0,0	0	0,0	0	0,0
Ephedripites spp.	61	7,9	2	0,5	0	0,0	0	0,0
Eucommiidites troedsonii Erdtman 1948	2	0,3	0	0,0	0	0,0	1	0,3
Eucommiidites minor Groot & Penny 1960	1	0,1	0	0,0	0	0,0	2	0,5
Exesipollenites tumulus Balme 1957	261	33,9	19	4,4	0	0,0	4	1,0
Ginkgocycadophytus nitididus (Balme 1957) de Jersey 1962	5	0,6	0	0,0	0	0,0	3	0,8
Inaperturopollenites dubius (Potonié et Venitz 1932) Thompson et Pflug 1953	0	0,0	14	3,3	5	1,1	25	6,5
Inaperturopollenites spp.	12	1,6	7	1,6	11	2,3	7	1,8
Monosulcites chaloneri Brenner 1963	1	0,1	0	0,0	0	0,0	0	0,0
Monosulcites minimus Cookson 1947 ex. Couper 1953	21	2,7	0	0,0	0	0,0	0	0,0
Monosulcites spp.	6	0,8	2	0,5	1	0,2	1	0,3
Perinopollenites elatoides Couper 1958	8	1,0	1	0,2	1	0,2	0	0,0
Pinuspollenites sp.	0	0,0	1	0,2	3	0,6	3	0,8
Podocarpidites sp.	0	0,0	0	0,0	3	0,6	1	0,3
Spheripollenites sp.	8	1,0	0	0,0	0	0,0	0	0,0
Vitreisporites pallidus (Reissinger 1950) Nilsson 1958	0	0,0	0	0,0	2	0,4	0	0,0
Undetermined bisaccate pollen grains of conifers	2	0,3	4	0,9	121	25,4	188	48,7
Pollen grains (angiosperms)								
Afropollis sp.	4	0,5	0	0,0	1	0,2	0	0,0
Clavatipollenites hughesii Couper 1958	4	0,5	0	0,0	0	0,0	1	0,3
Clavatipollenites minutus Brenner, 1963	3	0,4	0	0,0	0	0,0	0	0,0
Clavatipollenites sp. (Trichotomosulcate)	1	0,1	0	0,0	0	0,0	0	0,0
Clavatipollenites spp.	4	0,5	0	0,0	0	0,0	0	0,0
Retimonocolpites sp.	1	0,1	0	0,0	0	0,0	0	0,0
Tricolpites sp.	1	0,1	0	0,0	0	0,0	0	0,0
Undetermined angiospermous pollen grains	11	1,4	0	0,0	1	0,2	2	0,5
Total	771	100	430	100,0	476	100,0	386	100

Table 1.- Diagram of palynomorphs identified in the Aptian of the North Cantabrian Basin.

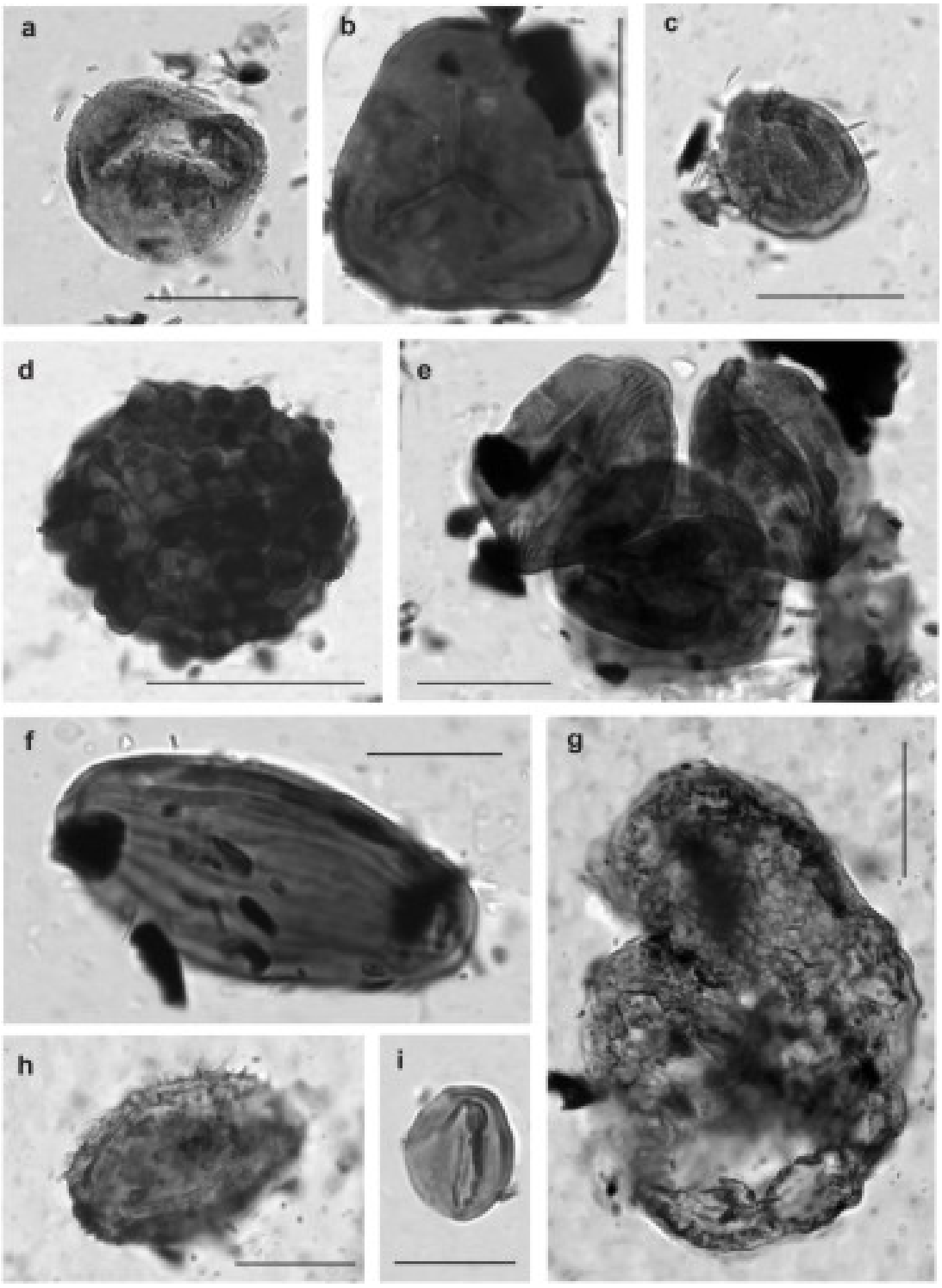

Figure 12.- Selected palynomorphs of the Aptian of the North Cantabrian Basin (NW margin of the Basque Cantabrian Basin): **A**. Trichotomo sulcate pollen grain of *Clavatipollenites* sp., Canales-Patrocinio sample; **B**. Trilete and psilte spore of the species *Deltoidospora australis* (Couper) Pocock, Canales-Patrocinio sample; **C**. Tricolpate pollen grain of *Tricolpites* sp. (*T.* aff. *parvus* Stanley), Canales-Patrocinio sample; **D**. Trilete and verrucate spore of *Rubinella major* (Couper) Norris, Canales-Patrocinio sample; **E**. Tetrade of *Classopollis classoides* Pflug emend. Pocock and Jansonius, Canales-Patrocinio sample; **F**. Polyplicate pollen grain of *Ephedripites multicostatus* Brenner; Canales-Patrocinio sample; **G**. Bad preserved bisaccate pollen grains of *Alisporites* sp., Ru-Reocín sample; **H**. Dinoflagellate cyst of aff. *Criboperidinium* sp., Ru-Cuchía sample; **I**. Monosulcate and psilate pollen grain of *Ginkgocycadophytus nitidus* (Balme) de Jersey Cookson ex. Couper, Canales-Patrocinio sample. Graphic scale: 20 μm, except for I: 10 μm.

DISCUSSION

Time-equivalent facies of the OAE 1a and comparison of $\delta^{13}C$ with other sections

The C-isotope curve of the Early Aptian is one of the best known of the Cretaceous. Menegatti et al. (1998) subdivided this part of the C-isotope record from the Cismon section (northern Italy) in a series of segments that they labelled C2 to C7, which have been accepted to be globally reproducible (e.g. Ando et al., 2008; Bellanca et al., 2002; Erba et al., 1999; Herrle et al., 2004; Moullade et al., 1998; Tejada et al., 2009). Recently, Herrle et al. (2004) reported a detailed carbon isotope stratigraphy of the Aptian for the Vocontian Basin (SE France) and have documented a series of segments for the Early Aptian (Ap1–Ap7) that are almost identical to those of Menegatti et al. (1998), allowing confirmation of the stratigraphic reproducibility of the structure of the curve. The curve is basically characterized by positive $\delta^{13}C$ values (around 2.5‰) at the base of the Early Aptian (C2 of Menegatti et al., 1998) followed by an abrupt and pronounced negative excursion (up to −4‰), labelled as C3, which coincides with the base of the OAE 1a. A stepwise return to positive values follows across the black-shale levels that represent the OAE 1a (Selli level in Italy or Niveau Goguel in France). This part of the isotopic curve, which corresponds to the segments C4–C5–C6, precedes the acme of the $\delta^{13}C$ positive excursion (up to 4.5‰) that occurred after the OAE 1a in the *S. cabri* foraminiferal Zone (C7 of Menegatti et al., 1998). According to the mentioned authors, the segment C1 is Barremian in age whereas segment C8 lies in the Upper Aptian (*G. ferreolensis* and *G. algerianus* foraminiferal Zones; *Rhagodiscus angustus* nannofossil Zone). Only the C2 to C7 segments of the carbon isotope curve of Menegatti et al. (1998) are Early Aptian in age, and only the C3 to C6 segments are time-equivalent to the OAE 1a, independently of organic facies development. These segments represent, therefore, a definition of the OAE 1a based on C-isotope stratigraphy, and their identification helps to correlate this event in other basins lacking organic facies with a higher temporal stratigraphic resolution than that provided by biostratigraphy. The regional value of these isotopic stages has been already verified in other localities of the Spanish basins (Gea et al., 2003; Millán et al., 2009; Moreno-Bedmar et al., 2009).

Correlation of the reference curve with the isotopic record obtained from the two sections reported herein, in combination with the integrated litho- and biostratigraphic data, allows recognition of the position of these segments, or their absence, in the

Aptian succession of the North Cantabrian Basin. The initial segment of positive carbonate C-isotope values (~2.5‰) with an upward decreasing trend, at the base of the Aptian succession in both sections (Cuchía and La Forida), can be assigned to stage C2 of the reference isotopic curve (Figs. 5–6). The significant negative excursion that both the $\delta^{13}C_{org}$ and $\delta^{13}C_{carb}$ curves present (Figs. 5–6) across the marly lower part of the Patrocinio Formation can be definitely assigned to the stage C3 of Menegatti et al. (1998). The almost identical structure of this excursion at two distant sections (Cuchía and La Florida) of the study area and in other sections of the Basque Cantabrian Basin (Millán et al., 2009), within different palaeogeographic domains, excludes major diagenetic overprinting. Accordingly, the negative values of this segment reflect a depositional feature and represent the beginning of the OAE 1a in the North Cantabrian Basin. In the Cuchía section, stage C4 may correspond to the upper 4 m of the marly lower part of the Patrocinio Formation (Fig. 6). This level shows a rapid positive shift in $\delta^{13}C_{carb}$ to values more positive than those of the pre- C3 stage. Stages C5+C6 cannot be correlated with confidence in this section because the corresponding time-equivalent facies are probably represented by the siliciclastic deltaic deposits of the upper part of the Patrocinio Formation. The positive $\delta^{13}C_{carb}$ values above the siliciclastic unit are correlated in age with stage C7 (Fig. 6), which is registered across the shallow platform limestones of the San Esteban Formation (late Early Aptian in age). In contrast, in La Florida section only stage C3 of the OAE 1a was recorded, because stages C4 to C7 are cut out within the sedimentary hiatus (Fig. 5).

The main difference of this isotopic record with other reported records is that the thickness of the stage C3 and the maximum amplitude of the negative δ13C excursion is much greater than those published previously for the Tethyan domain, including other sectors of the Basque Cantabrian Basin (i.e. Aralar sector; Millán et al., 2009). The most negative values (−3.1 to −4.1‰) are, however, similar to those published from the DSDP Site 463 (western Mid-Pacific) by Ando et al. (2008). According to Li et al. (2008), the stage C3 may have a duration of about 41 kyr. This suggests that the great sedimentary thickness of the stage C3 in the North Cantabrian Basin represents much higher sedimentation rates, and in consequence allows a higher resolution study for this stage, than other previous studies. In detail, in the Cuchía section where the sedimentary record is more complete, the C3 segment splits into three sub-segments (C3a–C3c, Fig. 6). Substages C3a and C3c are two peaks of minimum values (below −3‰) respectively at the base and top of the stage C3. They are separated by sub-stage C3b, a plateau with

a mean value of ~−1‰. The same isotopic sub-division and values are observed in the section of La Florida for stage C3 (Fig. 5), although the record is less extended due to lower sedimentation rates in this area. The third negative $\delta^{13}C$ shift observed in the La Florida section at the top of the Patrocinio Formation lies above the sedimentary hiatus and would correspond to a younger (post-C7 stage) negative isotopic shift. The $\delta^{13}C_{org}$ curves are roughly parallel with the $\delta^{13}C_{carb}$ curves, although the excursions are less defined and not exactly in phase, probably showing similar effects with respect to carbon sources and temperature-induced changes of fractionations to those discussed by Méhay et al. (2009).

Timing of anoxia

According to the biostratigraphic and chemostratigraphic data presented here, the Patrocinio Formation represents a time of global environmental perturbations that led to worldwide organic deposition, possibly as a result of anoxic conditions. This critical event is marked by a significant lithological change from limestone to dark marlstone and siltstone. Although the TOC values of the dark marls of the Patrocinio Formation are not very high (up to 0.8 wt.%), oxygen deficient conditions are inferred during their deposition from the presence of well-preserved lamination and pyrite framboids, and from the absence of evidence for benthic activity except at particular levels. Moreover, euxinic conditions in the water column during deposition of the Patrocinio Formation are suggested by preliminary data from biomarkers that point to the presence of specific compounds (i.e. gammacerane and high C29/C30 hopane; Quijano et al., 2010) indicative of oxygen deficits and reduced salinity, which may have promoted water stratification on these marginal sections (Erbacher et al., 2001). The low TOC values of the Patrocinio Formation could reflect dilution of organic matter by inorganic sediment. The low $CaCO_3$ values of the succession suggest high input of siliciclastic material. Thus, the TOC may be "diluted" by the high clay and silt content of this unit.

Study of the nannofossils in the Cantabrian sections reveals that the marls of the Patrocinio Formation were deposited during the biocalcification crisis, which occurred before and at the beginning of the OAE 1a in the upper part of the *B. blowi* or at the base of the *S. cabri* foraminiferal Zones (Aguado et al., 1999; Erba et al., 1999). According to other authors (i.e. Aguado et al., 1999; Bellanca et al., 2002; Bralower et al., 1994; Erba, 1994; Erba et al., 1999; Luciani et al., 2001; among others) the

beginning of the "nannoconid crisis" clearly preceded the peak intensity of the anoxic conditions and the maximum deposition of organic-rich shales of the "Selli Level" in other places. In the Tethyan regions, these black-shale levels are usually located above the C3 isotopic stage and below the FO of *Eprolithus floralis* (e.g. Bralower et al., 1994; Erba et al., 1999; Gea et al., 2003; Leckie et al., 2002; Menegatti et al., 1998). The dark marls of the Patrocinio Formation were deposited during the C-isotope stage C3, except for the part above sample PN-12 in the La Florida section. Therefore, the dark marls of the Patrocinio Formation are not exactly equivalent to the "Selli Level" but represent slightly older deposits. This suggests that the oxygen-poor conditions related to the Selli event occurred relatively earlier in the North Cantabrian Basin, just coinciding with the nannoconid crisis and the negative C3 isotopic stage. This study allows a precise assignment of these events to the middle/upper part of the *Deshayesites weissi* Zone and the upper part of the *B. blowi* Zone.

According to the chemostratigraphic and biostratigraphic data, another negative excursion of both $\delta^{13}C_{org}$ and $\delta^{13}C_{carb}$ post-dates the FO of *Eprolithus floralis* in the upper part of the Patrocinio Formation of La Florida section (above sample PN-12, Fig. 5). This new negative excursion is placed in the *Rhagodiscus angustus* nannofossils Zone. According to the zonation of Aguado et al. (1999), in the Spanish Tethys the base of *R. angustus* (and the FO of *E. floralis*) lies in the upper half of the *Dufrenoyia furcata* Zone of ammonites (Fig. 13). This implies that the last negative C-isotope shift could be as old as the upper part of the *D. furcata* Zone. García- Mondéjar et al. (2009) and Millán et al. (2009), who studied the Lower Aptian succession cropping out in Aralar (SE Basque Cantabrian Basin), recognized organic-rich shales at this stratigraphic position, which they called the "Aparein level". In their section, the Aparein level is registered as a negative excursion in $\delta^{13}C$ located above the main Early Aptian C-isotope positive excursion (C7 isotopic stage of the S. cabri Zone according to Menegatti et al., 1998; Fig. 14). Based on ammonites and their biostratigraphic attribution of the Aparein level to the *D. furcata* Zone, these authors concluded that this is a regional anoxic event older than the Niveau Noire black-shale horizon defined in France and Switzerland within the *G. ferreolensis* foraminiferal Zone (Herrle et al., 2004). However, the biozonation of Aguado et al. (1999) and a recently revised ammonite biostratigraphy (Moreno-Bedmar; personal observation) for south Spain place the base of the *G. ferreolensis* foraminiferal Zone in the uppermost *D. furcata* Zone (Fig. 13). In addition, according to Föllmi et al. (2006), the onset of the organic-

rich layers of the Niveau Noire in the Vocontian Basin occurs at least in part within the *D. furcata* ammonite Zone. Therefore, it is very likely that the Aparein level of Aralar and the upper part of the Patrocinio Formation in the La Florida section are equivalent (Fig. 14). The Niveau Noire may be in part equivalent or may represent slightly younger black-shale deposits that succeeded the negative C-isotopic anomaly of the *D. furcata* Zone, as it occurs with the Selli Level. In that case, the related negative excursion in $\delta^{13}C_{org}$ and $\delta^{13}C_{carb}$ recorded in La Florida and in Aralar would represent a supraregional C-isotope perturbation particularly observable on the most expanded series of northern Spain, as has been already suggested by Millán et al. (2009). The integrated biostratigraphy and chemostratigraphy of the studied sections from Cantabria allow a more precise location of this isotopic event between the C7 and C8 chemostratigraphic segments of the C isotope curve (Fig. 14).

Environmental changes

The Early Aptian was a time of severe environmental change, which resulted in the oceanic anoxic event. A generalized carbonate crisis also took place, characterized by a significant drop in carbonate production and by a biocalcification crisis with the near disappearance of narrow canal nannoconids (Erba, 1994; Erba and Tremolada, 2004). Quantitative analysis of nannofossil abundance across the Patrocinio Formation has demonstrated a scarcity of narrow canal nannoconids coinciding with the C-isotope negative excursion of the Cantabrian sections. This suggests that the major changes in nannofossil assemblages preceding the OAE 1a were extensive and that the so-called "nannoconid crisis" can be also recognized in northern Spain within the C3 stage of the C-isotope curve. This carbonate crisis was likely induced by oceanic water acidification due to an excess of dissolved CO_2 (Weissert and Erba, 2004). At the moment, the possible triggering mechanisms that have been considered for this massive emission of CO_2 to the ocean–atmosphere reservoir are methane release from gas hydrate dissociation (e.g. Beerling et al., 2002; Jahren et al., 2001) and intensive volcanic activity related to the Ontong Java large igneous province (e.g. Méhay et al., 2009; Tejada et al., 2009). New Os isotopic records of seawater preserved in marine sedimentary rocks from Italy seem to support better the latter hypothesis (Tejada et al., 2009). The rapid release of ^{13}C-depleted CO_2 from either a mantle source or gas hydrate dissociation would have initiated a major carbon cycle perturbation that resulted in the

negative and positive $\delta^{13}C$ excursions of the discussed Early Aptian chemostratigraphic curve (Ando et al., 2008; Herrle et al., 2004; Menegatti et al., 1998).

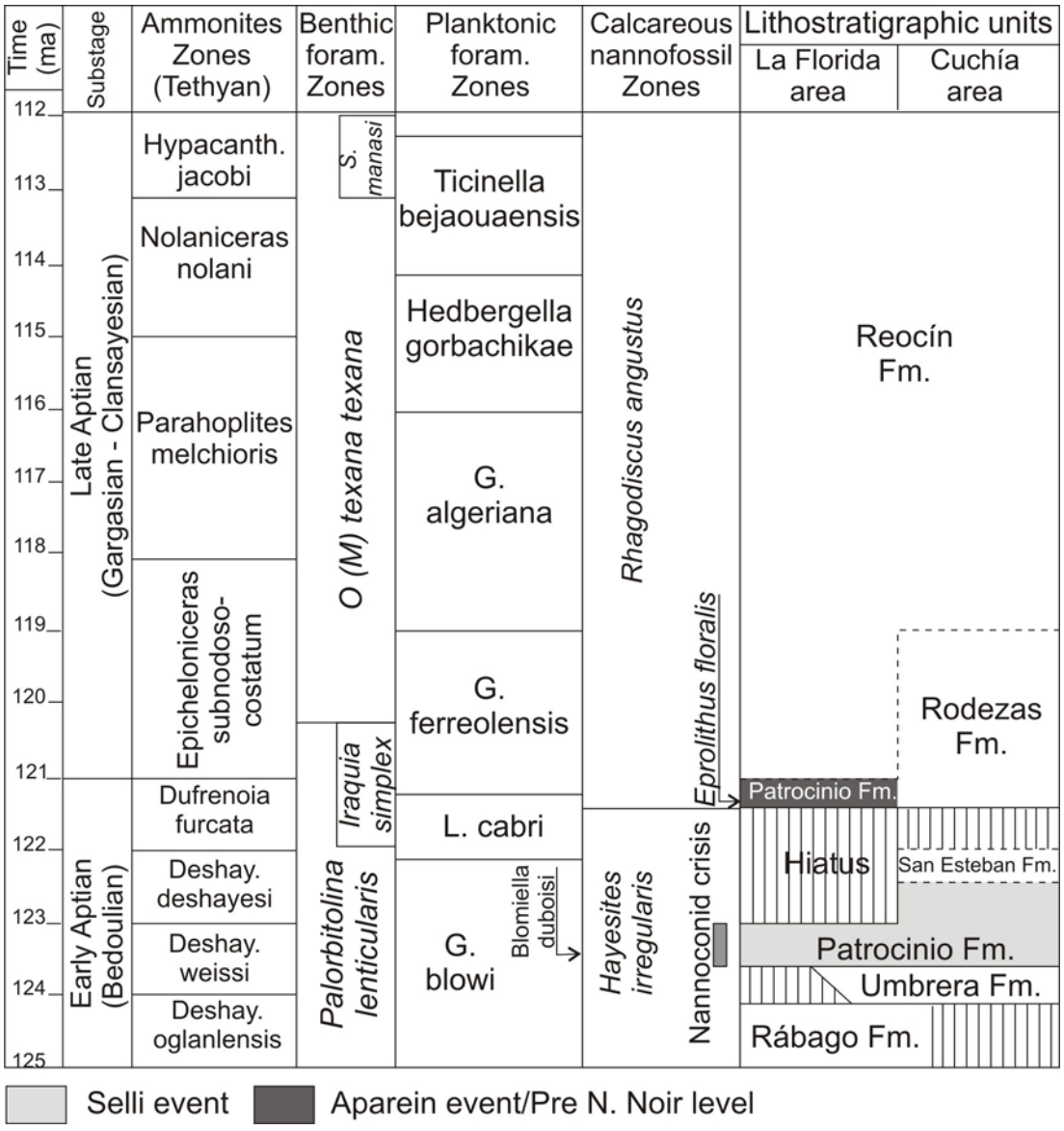

Figure 13.- Proposed integrated ammonite, benthic foraminifera (after Pascal, 1985), planktonic foraminifera and calcareous nannofossil biostratigraphic scheme of the Aptian lithostratigraphic units of La Florida and Cuchía areas. Note the equivalence between the Patrocinio Formation and the Selli event and the Aparein (after Millán et al., 2009) or pre- Niveau Noir event.

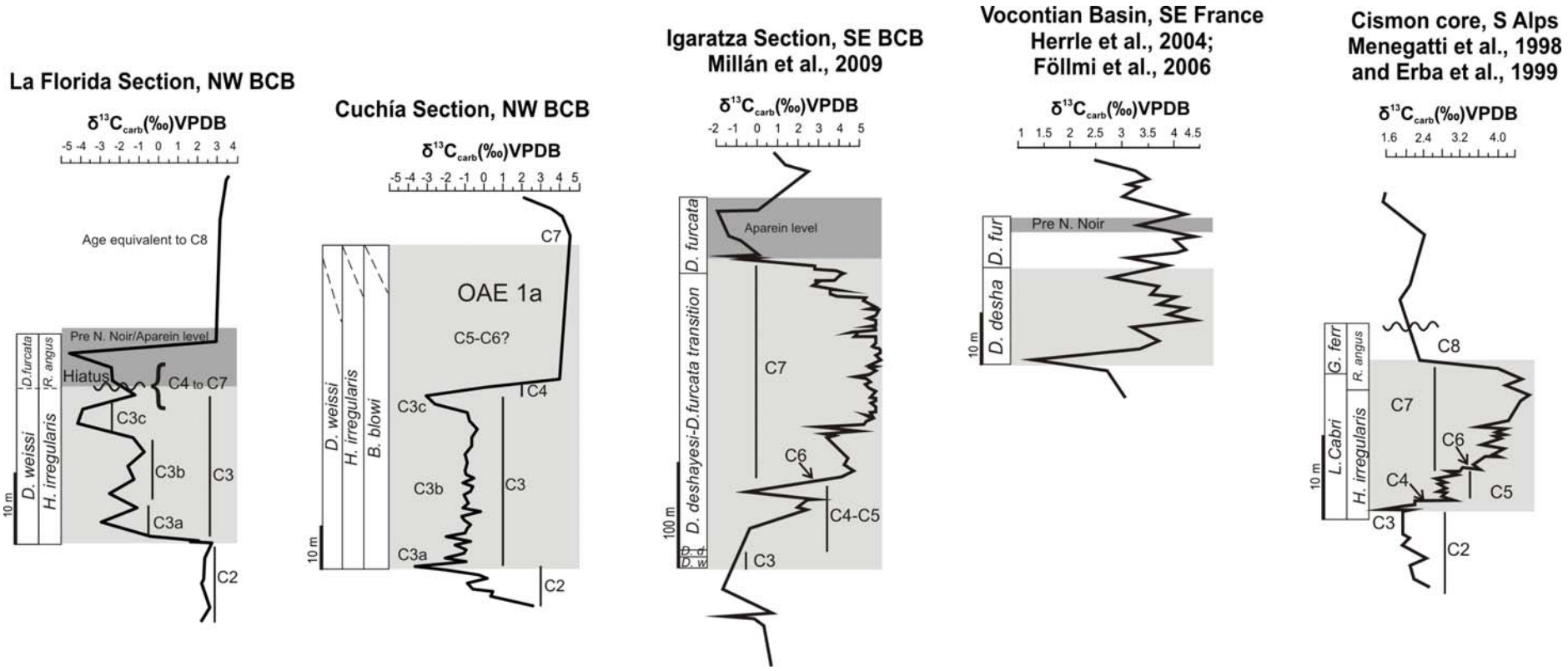

Figure 14. Proposed chemostratigraphic correlation of La Florida and Cuchía sections (this study, NW of the Basque Cantabrian Basin, BCB) with the SE of the Basque Cantabrian Basin (SE BCB), the Vocontian Basin (SE France) and the Cismon core (S Alps).

Besides perturbations in the carbon cycle, the OAE 1a was also accompanied by periods of global transgression and drowning of carbonate platforms (e.g. Föllmi and Gainon, 2008; Föllmi et al., 1994, 2006; Jenkyns, 1991; Weissert et al., 1998). In the North Cantabrian Basin two periods of maximum deepening occurred within the overall scenario of the Early Aptian transgression. Based on the biostratigraphic ages provided in this work, the first maximum deepening is dated at the middle–upper part of the *Deshayesites weissi* ammonite Zone and coincided with the onset of the OAE 1a. The sedimentary expression of this maximum flooding event across the basin is the series of dark marls of the lower part of the Patrocinio Formation. The carbonate stages that preceded this event (Rábago and Umbrera Formations; Fig. 13) exhibit a clear compositional change from inferred photozoan to heterozoan styles of carbonate production, (Najarro and Rosales, 2008b; Najarro et al., 2010). At this time the sea level rose very quickly and the transgressive facies were characterized by significant clastic inputs and deterioration of the neritic environments (Najarro et al., 2010). This, coupled with increased basin subsidence, resulted in the drowning of the carbonate platform just coinciding with the beginning of the OAE 1a (Najarro and Rosales, 2008b; Najarro et al., 2010). Platform environments were quickly re-established after this major transgressive pulse, with deposition of platform-top carbonate facies containing rudists and corals (San Esteban Formation), attributed to the *Deshayesites deshayesi* and lower part of the *Dufrenoyia furcata* ammonite zones (Fig. 13). These carbonate deposits represent regressive deposits between the two transgressive pulses. They are recorded only in the most complete section of Cuchía and in more subsiding basin sectors. In the uplifted block of La Florida these carbonate deposits are missing and only the two maximum transgressions are registered (Figs. 13, 14).

The second major transgressive pulse occurred in the lower part of the *Rhagodiscus angustus* nannofossil Zone, equivalent to the upper part of the *Dufrenoyia furcata* ammonite Zone. This flooding episode followed a period of subaerial exposure of the previous San Esteban Formation (Najarro et al., 2007; Wilmsen, 2005). The transgressive deposits of this stage, which correlate with the third negative spike in $\delta^{13}C_{carb}$ and $\delta^{13}C_{org}$, are represented in La Florida by the upper marls of the Patrocinio Formation directly overlying the sedimentary hiatus (Fig. 13). In Cuchía and other rapidly subsiding sectors, these transgressive deposits are represented by glauconite-rich marls and clastic deposits of the lower part of the Rodezas Formation (Fig. 13), which were deposited on top of the San Esteban platform. Based on ammonites and $\delta^{13}C$

records, this episode appears to be coeval with the onset of a major transgressive phase registered in other sites across the Basque Cantabrian Basin. It can be correlated with a drowning event associated with condensation and glauconitic deposits in the Castro Urdiales platform (central Basque Cantabrian Basin; Rosales, 1999). Biostratigraphic data based on ammonites demonstrated that the platform drowning and subsequent condensed deposits in Castro Urdiales are late Early Aptian–early Late Aptian in age (*D. furcata* to *Parahoplites nutfieldiensis* zones; Rosales, 1999). The onset of these condensed deposits correlates also with the drowning of the Sarastarri platform in Aralar (García-Mondéjar et al., 2009). In other regions, the onset of major drowning and demise of carbonate platforms have been reported at this time in the Helvetic Alps lasting until the Late Aptian (Föllmi and Gainon, 2008; Föllmi et al., 1994, 2006). All these events seems to be associated with the onset of the palaeoceanographic conditions that eventually may have led to deposition of the organic-rich layers of the Niveau Noir of the Vocontian Basin (Föllmi and Gainon, 2008).

Another environmental factor usually linked with OAEs is high global palaeotemperatures. Warm climate conditions accompanying the Selli Event have been previously inferred for the Cismon section from low $\delta^{18}O$ values and from the abundance of the thermophilic pollen *Classopollis* (Hochuli et al., 1999). Indeed, the relative abundance of climate-sensitive pollen groups, such as *Classopollis* and bisaccate pollen, maybe indicative of variations in vegetation distribution,which is controlled by palaeoclimatic variations (Vakhrameyev, 1982). Generally, bisaccate pollen, which typified the Boreal-influenced Southern Laurasian floral province, indicates relatively cool and humid conditions, whereas *Classopollis* constituted an abundant element of the Northern Gondwana floral province and its abundance indicates warmer and drier climates (Heimhofer et al., 2004; Vakhrameyev, 1982). In this study, the data obtained from the four analysed palynological samples must be considered with caution because their contents could not indicate a floral and vegetational trend but sporadic episodes. Nevertheless, the high predominance of *Classopollis, Exesipollenites* and *Ephedripites* (pollen grains produced by plants assumed to be drought resistant; Hughes, 1991; Thévenard et al., 2005), in the Lower Aptian samples from the Patrocinio Formation could be related with a phase of aridity and warmth, which began in western Europe during the Hauterivian–middle Barremian and dominated the climate of the region until the Early-Middle Aptian (Ruffell and Batten, 1990). In contrast, the drastic decrease of these pollen types and the increase of

bisaccate pollen grains in the two Upper Aptian samples analysed (Ru-Cuchían and Ru-Reocín; see Fig. 10) suggest important modifications in the vegetational patterns, and is interpreted as a change to wet and cooler climates commencing during the latest part of the OAE1a and lasting after it. These results are in strong agreement with the palynological studies of the Cismon section in Italy (Hochuli et al., 1999). A global cooling trend after the OAE 1a during the Late Aptian, lasting to the Early Albian, is well documented from oxygen isotopes derived from bulk carbonates (Ando et al., 2008; Hochuli et al., 1999) and belemnites (Pirrie et al., 2004), and correlates with an increase of glendonite and ice-rafting occurrences in high palaeolatitudes (De Lurio and Frakes, 1999; Frakes and Francis, 1988; Kemper, 1987; Price, 1999; Skelton, 2003a). Unfortunately, this cooling trend could not be corroborated in a palynological study of Early and Late Aptian assemblages from El Maestrazgo (NE Spain) (Solé de Porta and Salas, 1994). Cooler conditions could be the effect of inverse greenhouse conditions as a result of the drawdown of CO_2 from the system due to massive burial of organic matter in the oceanic basins during the OAE 1a (Jenkyns, 2003; Skelton, 2003b).

CONCLUSIONS

1. This study presents new chemostratigraphic and biostratigraphy records from two Lower Aptian sections (La Florida and Cuchía) of the North Cantabrian Basin, which include the signature of OAE 1a. This event is expressed by the interruption of shallow shelf carbonate sedimentation and deposition of a ~40 m thick marl unit (Patrocinio Formation). This marly unit records an abrupt negative C-isotope excursion in both bulk organic matter an carbonates, as has been already observed worldwide in the Earl Aptian at the onset of the OAE 1a, preceding the Selli Level. The negative anomaly is attributed to the C3 stage of the reference Aptian C-isotope curve.
2. The data set is well calibrated against a detailed biostratigraphy scheme based on the integration of new ammonite determination and micropalaeontological data (calcareous nannofossils and planktonic foraminifera). Combination of these biozonation refines the age of the C3 isotopic stage as middle–upper part of the *Deshayesites weissi* ammonite Zone, upper part of the *Blowiell blowi* foraminifera Zone, and upper part of the *Hayesites irregulari* nannofossil Zone. A major hiatus

in most marginal areas (La Florida) affecting the C4–C7 segments of the reference isotope curve has been identified from the calcareous nannofossils record. Another $\delta^{13}C_{carb}$ and $\delta^{13}C_{org}$ negative excursion post-dates the FO of *E. floralis* and is equivalent to the *Dufrenoyia furcata* ammonite Zone. This new C-isotope anomaly (pre-Niveau Noir or Aparei event) can be correlated with deposition of glauconitic marls and black shales in other parts of the basin, and just precedes the deposit of black shales in the northern Tethys (Niveau Noir). This pattern resembles the case of the negative carbon isotope anomaly of the onset of the OAE 1a preceding the Selli Level.

3. Quantitative analysis of nannofossil abundance shows a scarcity of narrow canal nannoconids coinciding with the negative excursion of the Patrocinio Formation. This corroborates former interpretation of a contemporaneous biocalcification crisis related to CO_2 induced changes in seawater chemistry in the stages that preceded the peak anoxic event.
4. Identification of a thermal maximum followed by a cooling phase is suggested by palynomorphs. This study supports the existence of *Classopollis* optimum during the OAE 1a, which is followed by decrease in *Classopollis* and an increase of bisaccate pollen after the event. Cooler conditions during the latest stage and after the OAE could be a reversal greenhouse effect resulting from the drawdown of CO_2 due to massive burial of organic matter in the oceanic basin during the OAE 1a.

ACKNOWLEDGEMENTS

This work is part of the Ph.D. Thesis of the first author (M.N.), who was supported by a scholarship from the Instituto Geológico y Minero de España (IGME). The study is a contribution of the DGI projects CGL2008-01237/BTE and CGL2008-00550/BTE funded by the MICINN, Spanish Government, and of the project UJA-07-16-41 funded by the University of Jaén (Spain). We thank Manuel Díaz (Cantabria, Spain) who has allowed the access to his particular collection of ammonites from Cantabria for this study. This paper benefited significantly from comprehensive reviews by Professors K. Föllmi, P. Skelton and F. Surlyk. We are further indebted to Professor

S. Robles (Universidad del País Vasco, Spain) for his help and instructive comments in the field.

APPENDIX

List of identified taxa of nannofossils, planktonic foraminifera, ammonoids and nautiloids with author attributions and dates.

Calcareous nannofossil

Assipetra infracretacea (Thierstein, 1973) Roth, 1973

Assipetra terebrodentaria (Applegate et al. in Covington & Wise, 1987) Rutledge & Bergen, 1994

Biscutum ellipticum (Gorka, 1957) Grün in Grün & Allemann, 1975

Braarudosphaera africana Stradner, 1961

Conusphaera rothii (Thierstein, 1971) Jakubowski, 1986

Cyclagelosphaera margerelii Noël, 1965

Diazomatolithus lehmanii Noël, 1965

Discorhabdus ignotus (Gorka, 1957) Perch-Nielsen, 1968

Eprolithus floralis (Stradner, 1962) Stover 1966

Flabellites oblongus (Bukry, 1969) Crux, 1982

Hayesites irregularis (Thierstein in Roth & Thierstein, 1972)

Covington & Wise, 1987

Helenea chiastia Worsley, 1971

Lithraphidites carniolensis Deflandre, 1963

Manivitella pemmatoidea (Deflandre ex Manivit, 1961) Thierstein, 1971

Micrantholithus hoschulzii (Reinhardt, 1966) Thierstein, 1971

Micrantholithus obtusus Stradner, 1963

Micrantholithus stellatus Aguado, 1997

Nannoconus bucheri Brönnimann, 1955

Nannoconus circularis Déres & Achériteguy, 1980

Nannoconus kamptneri kamptneri Brönnimann, 1955

Nannoconus steinmannii Kamptner, 1931 ssp. steinmannii

Nannoconus truittii Brönnimann, 1955

Prediscosphaera columnata (Stover, 1966) Manivit, 1971

Rhagodiscus angustus (Stradner, 1963) Reinhardt, 1971

Rhagodiscus asper (Stradner, 1963) Reinhardt, 1967

Rhagodiscus gallagheri Rutledge & Bown, 1996

Watznaueria barnesae (Black in Black & Barnes, 1959) Perch-Nielsen, 1968

Watznaueria britannica (Stradner, 1963) Reinhardt, 1964

Zeugrhabdotus noeliae Rood, Hay & Barnard, 1971

Planktonic foraminifera

Blowiella blowi (Bolli, 1959)

Blowiella duboisi (Chevalier, 1961)

Blowiella maridalensis (Bolli, 1959)

Praehedbergella aptiana (Bartenstein, 1965) s.s.

Praehedbergella convexa (Longoria, 1974)

Praehedbergella gorbachikae (Longoria, 1974)

Praehedbergella infracretacea (Glaessner, 1936)

Praehedbergella laculata Banner, Copestake & White, 1993

Praehedbergella occulta (Longoria, 1974)

Praehedbergella praetrocoidea (Krechmar & Gorbachik, 1986)

Praehedbergella sigali (Moullade, 1966)

Praehedbergella tuschepsensis (Antonova, 1964)

Schackoina cabri Sigal, 1952

Ammonites

Deshayesites cf. forbesi Casey, 1961

Deshayesites cf. callidiscus Casey, 1961

Roloboceras cf. hambrovi (Forbes, 1845)

Pseudohaploceras liptoviense (Zeuschner, 1856)

Pseudosaynella undulata (Sarasin, 1893)

Toxoceratoides sp.

Deshayesites cf. consobrinus (d'Orbigny, 1841)

Deshayesites planus Casey, 1964

Pseudosaynella bicurvata (Michelin, 1838)

Heminautilus saxbii (Morris, 1848)

Toxoceratoides royerianus (d'Orbigny, 1842)

REFERENCES

Aguado, R., 1994. Nannofósiles del Cretácico de la Cordillera Bética (sur de España). Bioestratigrafía. Ph.D. Thesis, Universidad de Granada, 413 pp.

Aguado, R., Castro, J.M., Company, M., Gea de, G.A., 1999. Aptian bio-events –an integrated biostratigraphic analysis of the Almadich Formation, Inner Prebetic Domain, SE Spain. Cretaceous Research 20, 663–683.

Ando, A., Kaiho, K., Kawahata, H., Kakegawa, T., 2008. Timing and magnitude of Early Aptian extreme warming: Unraveling primary $\delta^{18}O$ variation in indurated pelagic carbonates at Deep Sea Drilling Project Site 463, central Pacific Ocean. Palaeogeography, Palaeoclimatology, Palaeoecology 260, 463–476.

Applegate, J.L., Bergen, J.A., 1988. Cretaceous calcareous nannofossil biostratigraphy of sediments recovered from the Galicia Margin, ODP leg 103. In: Boillot, G., Winterer, E.L., et al. (Eds.), Proceedings of the Ocean Drilling Program, Scientific Results 103, 293–348.

Arthur, M.A., Brumsack, H.J., Jenkyns, H.C., Schlanger, S.O., 1990. Stratigraphy, geochemistry and paleoceanography of organic carbon-rich Cretaceous sequences. In: Ginsburg, R.N., Beaudoin, B. (Eds.), Cretaceous resources, events and rhythms-background and plans for research. Kluwer Academic Publications, Dordrecht, pp. 75–119.

Azéma, C., Boltenhagen, E., 1974. Pollen du Crétacé Moyen du Gabon attribué aux Ephedrales. Paléobiologie continentale 5, 1–37.

Balme, B.E., 1995. Fossil in situ spores and pollen grains: an annotated catalogue. Review of Palaeobotany and Palynology 87, 81–323.

Barrón, E., Comas-Rengifo, M.J., Elorza, L., 2001. Contribuciones al estudio palinológico del Cretácico Inferior de la Cuenca Vasco-Cantábrica: los afloramientos ambarígenos de Peñacerrada (España). Coloquios de Paleontología 52, 135–156.

Batten, D.J., 1999. Extraction techniques - Small palynomorphs. In: Jones, T.P., Rowe, N.P. (Eds.), Fossil plants and spores: modern techniques. The Geological Society, London, pp. 15–19.

Beerling, D.J., Lomas, M.R., Gröcke, D.R., 2002. On the nature of methane gas-hydrate dissociation during the Toarcian and Aptian oceanic anoxic events. American Journal of Science 302, 28–49.

Bellanca, A., Erba, E., Neri, R., Premoli Silva, I., Sprovieri, M., Tremolada, F., Verga, D., 2002. Palaeoceanographic significance of the Tethyan 'Livello Selli' (Early Aptian) from the Hybla Formation, northwestern Sicily: biostratigraphy and high-resolution chemostratigraphic records. Palaeogeography, Palaeoclimatology, Palaeoecology 185, 175–196.

Bralower, T.J., Arthur, M.A., Leckie, R.M., Sliter, W.V., Allard, D., Schlanger, S.O., 1994. Timing and paleoceanography of oceanic dysoxia/anoxia in the Late Barremian to Early Aptian (Early Cretaceous). Palaios 9, 335–369.

Casey, R., 1961. A monograph of the Ammonoidea of the Lower Greensand, part III. Monographs of the Palaeontographical Society, London 114, 119–216.

Casey, R., Bayliss, H.M., Simpson, M.I., 1998. Observations on the lithostratigraphy and ammonite succession of the Aptian (Lower Cretaceous) Lower Greensand of Chale Bay, Isle of Wight, UK. Cretaceous Research 19, 511–535.

Channell, J.E.T., Erba, E., Muttoni, G., Tremolada, F., 2000. Early Cretaceous magnetic stratigraphy in the APTICORE drill core adjacent outcrop at Cismon (Southern Alps, Italy), and correlation to the proposed Barremian-Aptian boundary stratotype. Geological Society of American Bulletin 112, 1430–1443.

Coccioni, R., Franchi, R., Nesci, O., Wezel, F.-C., Battistini, F., Pallecchi, P., 1989. Stratigraphy and mineralogy of the Selli Level (Early Aptian) at the base of the Marne a Fucoidi in the Umbria-Marche Apennines (Italy). In: Wiedmann, J. (Eds.), Cretaceous of the Western Tethys. Proceedings of the 3rd International Cretaceous Symposium. Tübingen, 563–584.

Collignon, M., Pascal., A., Peybernès, B., Rey J., 1979. Faunes d'ámmonites de l'Aptien de la Région de Santander (Espagne). Annales de Paléontologie 65, 139–156.

De Lurio, J.L., Frakes, L.A., 1999. Glendonite as a paleoenvironmental tool: Implications for Early Cretaceous high latitude climates in Australia. Geochimica et Cosmochimica Acta 63, 1039–1048.

Dumitrescu, M., Brassell, S.C., Schouten, S., Hopmans, E.C., Damsté, J.S.S., 2006. Instability in tropical Pacific sea-surface temperatures during the Early Aptian. Geology 34, 833–836.

Erba, E., 1994. Nannofossils and superplumes: the Early Aptian nannoconid crisis. Paleoceanography 9, 483–501.

Erba, E., 2004. Calcareous nannofossils and Mesozoic oceanic anoxic events. Marine Micropaleontology 52, 85–106.

Erba, E., Channell, J.E.T., Claps, M., Jones, C., Larson, R., Opdyke, B., Premoli Silva, I., Riva, A., Salvini, G., Torricelli, S., 1999. Integrated stratigraphy of the Cismon APTICORE (southern Alps, Italy): a "reference section" for the Barremian-Aptian interval at low latitudes. Journal of Foraminiferal Research 29, 371–392.

Erba, E., Tremolada, F., 2004. Nannofossil carbonate fluxes during the Early Cretaceous: Phytoplankton response to nutrification episodes, atmospheric CO_2, and anoxia. Paleoceanography 19, PA1008, doi: 10.1029/2003PA000884.

Erbacher, J., Huber, B.T., Norris, R.D., Markey, M., 2001. Increased thermohaline stratification as a possible cause for an ocean anoxic event in the Cretaceous period. Nature 409, 325–327.

Ferreri, V., Weissert, H., D'Argenio, B., Buonocunto, F.P., 1997. Carbon isotope stratigraphy: a tool for basin to carbonate platform correlation. Terra Nova 9, 57–61.

Feuillée, P., Rat, P., 1971. Structures et paléogéographies Pyrénéo-Cantabriques. In: Debyser, J., Le Pichon, X., Montardet, L. (Eds.), Histoire Structurale du Golfe de Gascogne. Publication de l'Institute Français du Pétrole. Collection Colloques et Séminaires, Technip, Paris, 22, pp. 1–48.

Föllmi, K.B., Gainon, F., 2008. Demise of the northern Tethyan Urgonian carbonate platform and subsequent transition towards pelagic conditions: The sedimentary record of the Col de la Plaine Morte area, central Switzerland. Sedimentary Geology 205, 142–159.

Föllmi, K.B., Godet, A., Bodin, S., Linder, P., 2006. Interactions between environmental change and shallow water carbonate builup along the northern Tethyan margin and their impact on the Early Cretaceous carbon isotope record. Paleoceanography 21, PA4211, doi: 10.1029/2006PA001313.

Föllmi, K.B., Weissert, H., Bisping, M., Funk, H., 1994. Phosphogenesis, carbon-isotope stratigraphy, and carbonate-platform evolution along the Lower Cretaceous northern Tethyan margin. Geological Society of American Bulletin 106, 729–746.

Frakes, L.A., 1979. Climates throughout geological time. Elsevier, Amsterdam, 310 pp.

Frakes, L.A., Francis, J.E., 1988. A guide to Phanerozoic cold polar climates from high lautitude ice-rafting in the Cretaceous. Nature 333, 547–449.

García-Mondéjar, J., Owen, H.G., Raisossadat, N., Millán M.I. and Fernández-Mendiola, P.A., 2009. The Early Aptian of Aralar (northern Spain): stratigraphy, sedimentology, ammonite biozonation, and OAE1. Cretaceous Research 30, 434–464.

Gradstein, F.M., 2004. A Geologic Time Scale 2004. Cambrige University Press.

Gea de, G.A., Castro, J.M., Aguado, R., Ruiz-Ortiz, P.A., Company, M., 2003. Lower Aptian carbon isotope stratigraphy from a distal carbonate shelf setting: the Cau section, Prebetic zone, SE Spain. Palaeogeography, Palaeoclimatology, Palaeoecology 200, 207–219.

Gröcke, D.R, 2002. The carbon isotope composition of ancient CO_2 based on higher-plant organic matter. Philosophical Transactions of the Royal Society of London A 360, 633–658.

Gröcke, D.R., Hesselbo, S.P., Jenkyns, H.C., 1999. Carbon isotope composition of Lower Cretaceous fossil wood: ocean-atmosphere chemistry and relation to sea-level change. Geology 27, 155–158.

Grötsch, J., Billing, I., Vahrenkamp, V., 1998. Carbon-isotope stratigraphy in shallow-water carbonates: implications for Cretaceous black-shale deposition. Sedimentology 45, 623–634.

Haq, B.U., Hardenbol, J., Vail, P.R., 1988. Mesozoic and Cenozoic chronostratigraphy and cycles of sea-level change. In: Wilgus, C., Hastings, B., Ross, C., Posamentier, H., Van Wagoner, J., Kendal, C.G.S.C. (Eds.), Sea-level change: An integrated approach. Society of Economic Paleontologists and Mineralogists, Special Publication 42, pp. 71–108.

Hay, W.W., De Conto, R.M., Wold, C.N., Wilson, K.M., Voigt, S., Schulz, M., Rossby-Wold, A., Dullo, W.-Chr., Ronov, A.B., Balukhovsky, A.N., Söding, E., 1999. An alternative global Cretaceous paleogeography. In: Barrera, E., Johnson, C.C. (Eds.), Evolution of Cretaceous Ocean/Climate System. Geological Society of America, Special Paper 332, pp. 1–47.

Heimhofer, U., Hochuli, P.A., Burla, S., Weissert, H., 2007. New records of Early Cretaceous angiosperm pollen from Portuguese coastal deposits: Implications

for the timing of the early angiosperm radiation. Review of Palaeobotany and Palynology 144, 39–76.

Heimhofer, U., Hochuli, P.A., Herrle, J.O., Andersen, N., Weissert, H., 2004. Absence of major vegetation and palaeoatmospheric ρCO_2 changes associated with oceanic anoxic event 1a (Early Aptian, SE France). Earth and Planetary Science Letters 223, 303–318.

Herman, A.B., Spicer, R.A., 1996. Palaeobotonical evidence for a warm Cretaceous Artic Ocean. Nature 380, 330–333.

Herrle, J.O., Köler, P., Friedrich, O., Erlenkeuser, H., Hemleben, Ch., 2004. High-resolution carbon isotope records of the Aptian to Lower Albian from SE France and the Mazagan Plateau (DSDP Site 545): a stratigraphic tool for paleoceanographic and paleobiologic reconstruction. Earth and Planetary Science Letters 218, 149–161.

Herrle, J.O., Pross, J., Friedrich, O., Hemleben, Ch., 2003. Short-term environmental changes in the Cretaceous Tethyan Ocean: Micropaleontological evidence from the Early Albian Oceanic Anoxic Event 1b. Terra Nova 15, 14–19.

Hines, F.M., 1985. Sedimentation and tectonics in north-west Santander. In: Milá, M.D., Rosell, J. (Eds.), 6th European Regional Meeting, Excursion Guidebook, International Association of Sedimentologists, pp. 371–398.

Hochuli, P.A., Menegatti, A.P., Weissert, H., Riva, A., Erba, E., Premoli Silva, I., 1999. Episodes of high productivity and cooling in the Early Aptian Alpine Tethys. Geology 27, 657–660.

Hughes, N.F., 1991. Mesozoic gymnosperms and period classifications. Current Science 61(9-10), 630–633.

Hughes, N.F., McDougall, A.B., 1990. Barremian-Aptian angiospermid pollen records from southern England. Review of Palaeobotany and Palynology 65, 145–151.

Jahren, A.H. 2002. The biogeochemical consequences of the mid-Cretaceous superplume. Journal of Geodynamics 34, 177–191.

Jahren, A.H., Arens, N.C., Sarmiento, G., Guerrero, J., Amundson, R., 2001. Terrestrial record of methane hydrate dissociation in the Early Cretaceous. Geology 29, 159–162.

Jenkyns, H.C., 1980. Cretaceous anoxic events: from continents to oceans. Journal of the Geological Society of London 137, 171–188.

Jenkyns, H.C., 1991. Impact of Cretaceous sea-level rise and anoxic events on the Mesozoic carbonate platform of Yugoslavia. Bulletin of the American Association of Petroleum Geologists 75, 1007–1017.

Jenkyns, H.C., 1999. Mesozoic anoxic events and palaeoclimate. Zentralblatt für Geologie und Paläontologie 1997, 943–949.

Jenkyns, H.C., 2003. Evidence for rapid climate change in the Mesozoic-Palaeogene greenhouse world. Philosophical Transactions of the Royal Society of London A 361, 1885–1961.

Kemper, E. 1987. Das Klima der Kreidezeit. Geologisches Jahrbuch, Reihe A 96, 5–185.

Larson, R.L., 1991. Geological consequences of superplumes. Geology 19, 963–966.

Larson, R.L., Erba, E., 1999. Onset of the Mid-Cretaceous greenhouse in the Barremian-Aptian: Igneous events and the biological, sedimentary and geochemical responses. Paleoceanography 14, 663–678.

Leckie, R.M., Bralower, T.J., Cashman, R., 2002. Oceanic anoxic events and plankton evolution: Biotic response to tectonic forcing during the mid-Cretaceous. Paleoceanography 17, 1–29.

Li, Y.-X., Bralower, T.J., Montañez, I.P., Osleger, D.A., Arthur, M.A., Bice, D.M., Herbert, T.D., Erba, E., Premoli Silva, I., 2008. Toward an orbital chronology for the Early Aptian Oceanic Anoxic Event (OAE1a, ~120 Ma). Earth and Planetary Science Letters 271, 88–100.

Luciani, V., Cobianchi, M., Jenkyns, H.C., 2001. Biotic and geochemical response to anoxic events: the Aptian pelagic succession of the Gargano Promontory (southern Italy). Geological Magazine 138, 277–298.

Malod, J.A., Mauffret, A., 1990. Iberian plate motions during the Mesozoic. Tectonophysics 184, 261–278.

Martín-Chivelet, J., Berasategui, X., Rosales, I., Vilas, L., Vera, J.A., Caus, E., Gráfe, K.U., Mas, R., Puig, C., Segura, M., Robles, S., Floquet, M., Quesada, S., Ruiz-Ortiz, P.A., Frenegal-Martínez, M.A., Salas, R., García, A., Martín-Algarra, A., Arias, C., Meléndez, M., Chacón, B., Molina, J.M., Sanz, J.L., Castro, J.M., García-Hernández, M., Carenas, B., García-Hidalgo, J., Gil, J., Ortega, F., 2002. Cretaceous. In: Gibbons, W. and Moreno, T. (Eds.), The Geology of Spain. The Geological Society, London, pp. 255–292.

McCrea, J.M., 1950. On the isotopic chemistry of carbonates and a paleotemperature scale. Journal of Chemical Physics 18, 849–857.

Méhay, S., Keller, C.E., Bernasconi, S.M., Weissert, H., Erba, E., Bottini, C., Hochuli, P.A., 2009. A volcanic CO_2 pulse triggered the Cretaceous Oceanic Anoxic Event 1a and a biocalcification crisis. Geology 37, 819–822.

Menegatti, A.P., Weissert, H., Brown, R.S., Tyson, R.V., Farrimond, P., Strasser, A., Caron, M., 1998. High-resolution $\delta^{13}C$ stratigraphy through the Early Aptian 'Livello Selli' of the Alpine Tethys. Paleoceanography 13, 530–545.

Millán, M.I., Weissert, H.J., Fernández-Mendiola, P.A., García-Mondéjar, J., 2009. Impact of Early Aptian carbon cycle perturbations on evolution of a marine shelf system in the Basque-Cantabrian Basin (Aralar, N Spain). Earth and Planetary Sciences Letters 287, 392–401.

Montadert, L., Roberts, D.G., de Charpal, O., Guennoc, P., 1979. Rifting and subsidence of the northern continental margin of the Bay of Biscay. In: Montadert, L., Roberts, L. (Eds.), Initial Reports of the Deep Sea Drilling Project 48, 1025–1059.

Moreno-Bedmar, J.A., Company, M., Bover-Arnal, T., Salas, R., Delanoy, G., Martínez, R., Grauges, A., 2009. Biostratigraphic characterization by means of ammonoids of the lower Aptian Oceanic Anoxic Event (OAE 1a) in the eastern Iberian Chain (Maestrat Basin, eastern Spain). Cretaceous Research 30, 864–872.

Moullade, M., 1974. Zones de foraminiféres du Crétacé Inférieur mésogéen. Comptes Rendus Hebdomadaires des Séances de l'Académie des Sciences de Paris, Serie D 278, 1813–1816.

Moullade, M., Bellier, J.P., Tronchetti, G., 2002. Hierarchy of criteria, evolutionary processes and taxonomic simplification in the classification of Lower Cretaceous planktonic foraminifera. Cretaceous Research 23, 111–148.

Moullade, M., Kuhnt, W., Bergen, J.A., Masse, J.P., Tronchetti, G., 1998. Correlation of biostratigraphic and stable isotope events in the Aptian historical stratotype of La Bédoule (SE France). Comptes Rendus de l'Académie des sciences Paris, IIA 327, 693–698.

Najarro, M., Peñalver, E., Rosales, I., Pérez-de la Fuente, R., Daviero-Gomez, V., Gomez, B., Delclòs, X., 2009. Unusual concentration of Early Albian arthropod-bearing amber in the Basque-Cantabrian Basin (El Soplao, Cantabria, Northern

Spain): Palaeoenvironmental and palaeobiological implications. Geologica Acta 7, 363–387.

Najarro, M., Rosales, I., 2008a. Disoluciones e incrustaciones ferruginosas asociadas al OAE 1a en la plataforma carbonatada de La Florida (NO de Cantabria). Geogaceta 44, 199–202.

Najarro, M., Rosales, I., 2008b. Evidencias sedimentológica, diagenética y quimioestratigráfica del Evento Anóxico Oceánico del Aptiense Inferior (OAE 1a) en la plataforma carbonatada de La Florida (NO de Cantabria). Geotemas 10, 163–166.

Najarro, M., Rosales, I., Martín-Chivelet, J., 2007. Evolución de la plataforma carbonatada de la Florida durante el rifting del Cretácico Inferior (Aptiense, NO de Cantabria). In: Bermúdez, D.D., Najarro, M., Quesada, C. (Eds.), Volumen Monográfico de la II Semana de Jóvenes Investigadores del IGME. Publicaciones del IGME, pp. 123–128.

Najarro, M., Rosales, I., Martín-Chivelet, J., 2010. Major palaeoenvironmental perturbation in an Early Aptian carbonate platform: Prelude of the Oceanic Anoxic Event 1a? Sedimentary Geology, doi: 10.1016/j.sedgeo.2010.03.011.

Olivet, J.M., 1996. La cinématique de la plaque Ibérique. Bulletin des Centres de Recherches Exploration-Production Elf-Aquitaine 20, 131–195.

Pascal, A., 1985. Les Systems biosédimentaires urgoniens (Aptien–Albien) sur la marge Nord Ibérique. Mémoires Géologiques de l'Úniversité de Dijon 10, 1–569.

Peyrot, D., Rodríguez-López, J.P., Lassaletta, L., Meléndez-Hevia, N., Barrón, E., 2007a. Contributions to the palaeoenvironmental knowledge of the Escucha Formation in the Lower Cretaceous Oliete Sub-basin, Teruel, Spain. Comptes Rendus Palevol 6, 469–481.

Peyrot, D., Rodríguez-López, J.P., Barrón, E., Meléndez-Hevia, N., 2007b. Palynology and biostratigraphy of the Escucha Formation in the Early Cretaceous Oliete Sub-basin, Teruel, Spain. Revista Española de Micropaleontología 39, 135–154.

Pirrie, D., Marshall, J.D., Doyle, P., Riccardi, A.C., 2004. Cool Early Albian climates; new data from Argentina. Cretaceous Research 25, 27–33.

Price, G.D., 1999. The evidence and implications of polar ice during the Mesozoic. Earth-Science Reviews 48, 183–210.

Pujalte, V., 1982. La evolución paleogeográfica de la cuenca "wealdense" de Cantabria. Cuadernos de Geología Ibérica 8, 65–83.

Quijano, M.L., Castro, J.M., Pancost, R.D., Gea de, G.A., Najarro, M., Aguado, R., Rosales. I., Martín-Chivelet, J., 2010. Biomarker characterization of the record of the OAE1a (Early Aptian) in Betic and Cantabrian basins (Spain)-Sedimentary implications. Geophysical Research Abstracts 12, EGU2010-6502-5.

Ramírez del Pozo, J., 1972. Algunos datos sobre la estratigrafía y micropaleontología del Aptense y Albense al oeste de Santander. Revista Española de Micropaleontología 15, 59–97.

Reboulet, S., Klein, J., Barragán, R., Company, M., González-Arreola, C., Lukeneder, A., Raisossadat, S.N., Sandoval, J., Szives, O., Tavera, J.M., Vasicek, Z., Vermeulen, J., 2009. Report on the 3rd International Meeting of the IUGS Lower Cretaceous Ammonite Working Group, the "Kilian Group" (Vienna, Austria, 15th April, 2008). Cretaceous Research 30, 496–502.

Rosales, I., 1999. Controls on carbonate-platform evolution on active fault-blocks: The Lower Cretaceous Castro Urdiales platform (Aptian–Albian, northern Spain). Journal of Sedimentary Research 69, 447–465.

Ruffell, A.H., Batten D.J., 1990. The Barremian-Aptian arid phase in western Europe. Palaeogeography, Palaeoclimatology, Palaeoecology 80, 197–212.

Schlanger, S.O., Jenkyns, H.C., 1976. Cretaceous oceanic anoxic events: causes and consequences. Geologie en Mijnbouw 55, 179–184.

Scholle, P.A., Arthur, M.A., 1980. Carbon-isotope fluctuations in Cretaceous pelagic limestones: potential stratigraphy and petroleum exploration tool. American Association of Petroleum Geologists Bulletin 64, 67–87.

Scopelliti, C., Bellanca, A., Erba, E., Jenkyns, H.C., Neri, R., Tamagnini, P., Luciani, V., Masetti, D., 2008. Cenomanian–Turonian carbonate and organic-carbon isotope records, biostratigraphy and provenance of a key section in NE Sicily, Italy: Palaeoceanographic and palaeoclimatic implications. Palaeogeography, Palaeoclimatology, Palaeoecology 265, 59–77.

Singh, C., 1971. Lower Cretaceous microfloras of the Peace River Area, Northwestern Alberta. Research Council of Alberta Bulletin 28, 1–299.

Skelton, P.W. 2003a. Rudists evolution and extinction- a North African perspective. In: Gili, E., Negra, H., Skelton, P.W. (Eds.) North African Cretaceous carbonate platform Systems, NATO Science Series, IV. Earth and Environmental Sciences, Kluwer Academic Publisher 28, pp. 215–227.

Skelton, P.W. 2003b. The Cretaceous World. Cambrige Univeristy Press and The Open University, 360 pp.

Solé de Porta, N., Salas, R., 1994. Conjuntos microflorísticos del Cretácico Inferior de la Cuenca del Maestrazgo. Cordillera Ibérica Oriental (NE de España). Cuadernos de Geología Ibérica 18, 355–368.

Stover, L.E., Brinkhuis, H., Damassa, S.P., de Verteuil, L., Helby, R.J., Monteil, E., Partridge, A.D., Powell, A.J., Riding, J.B., Smelror, M., Williams, G.L., 1996. Mesozoic-Tertiary dinoflagellates, acritarchs and prasinophytes. In: Jansonius, J., McGregor, D.C. (Eds.), Palynology, principles and applications. American Association of Stratigraphic Palynologists Foundation 2, Salt Lake City, Utah, pp. 641–750.

Taylor, T.N., Alvin, K.L., 1984. Ultrastructure and development of Mesozoic pollen: *Classopollis*. American Journal of Botany 71, 575–587.

Tejada, M.L.G., Suzuki, K., Kuroda, J., Coccioni, R., Mahoney, J.J., Ohkouchi, N., Sakamoto, T., Tatsumi, Y., 2009. Ontong Java Plateau eruption as a trigger for the Early Aptian oceanic anoxic event. Geology 37, 855−858.

Thévenard, F., Gomez, B., Daviero-Gomez, V., 2005. Xeromorphic adaptations of some Mesozoic gymnosperms. A review with palaeoclimatological implications. Comptes Rendus Palevol 4, 67−77.

Trincão, P.R., 1990. Esporos e granos de polen do Cretácico Inferior (Berriasiano-Aptiano) de Portugal: Paleontología e Biostratigrafia. Ph.D. Thesis, Universidade Nova, Lisboa, Portugal.

Vakhrameyev, V.A., 1982. *Classopollis* pollen as an indicator of Jurassic and Cretaceous climate. International Geological Review 24, 1190–1196.

Watson, J., 1988. The Cheirolepidiaceae. In: Beck, C.B. (Eds.), Origin and evolution of Gymnosperms. Columbia University Press, New York, pp. 382–447.

Weissert, H., Erba, E., 2004. Volcanism, CO_2 and palaeoclimate: a Late Jurassic–Early Cretaceous carbon and oxygen isotope record. Journal of the Geological Society, London 161, 695–702.

Weissert, H., Lini, A., Föllmi, K.B., Kuhn, O., 1998. Correlation of Early Cretaceous carbon isotope stratigraphy and platform drowning events: a possible link? Palaeogeography, Palaeoclimatology, Palaeoecology 137, 189–203.

Wilmsen, M., 2000. Evolution and demise of a Mid-Cretaceous carbonate shelf: the Altamira Limestones (Cenomanian) of northern Cantabria (Spain). Sedimentary Geology 133, 195−226.

Wilmsen, M., 2005. Stratigraphy and biofacies of the Lower Aptian of Cuchía (Cantabria, northern Spain). Journal of Iberian Geology 31, 253−275.

Ziegler, P.A., 1988. Evolution of the Arctic, North Atlantic and the Western Tethys. American Association of Petroleum Geologists Memoir 43, 198 pp.

4.3.- Unusual concentration of Early Albian arthropod-bearing amber in the Basque-Cantabrian Basin (El Soplao, Cantabria, Spain): Palaeoenvironmental and palaeobiological implications

M. NAJARRO[(1)] E. PEÑALVER[(1)] I. ROSALES[(1)] R. PÉREZ-DE LA FUENTE [(2)] V. DAVIERO-GOMEZ[(3)] B. GOMEZ[(3)] and X. DELCLÒS[(2)]

(1) Instituto Geológico y Minero de España.

(2) Departament d'Estratigrafia, Paleontologia i Geociències Marines, Universitat de Barcelona.

(3) UMR 5125 (PEPS) CNRS, Paléobotanique, Université Lyon-1 (Claude-Bernard).

Doi: 10.1344/105.000001443.

Geological Acta, 2009, Vol.7, Nº 3, p. 363-387.

RESUMEN

El yacimiento paleontológico del Albiense Inferior de El Soplao es un enclave descubierto recientemente en la cuenca Vasco-Cantábrica que ha proporcionado un gran número de piezas de ámbar con abundantes bioinclusiones. Los depósitos ambarígenos se incluyen en una unidad siliciclástica de ambiente continental a marino-transicional (Formación Las Peñosas) que está intercalada en una secuencia marina regresiva-transgresiva, principalmente carbonatada, de edad Aptiense Inferior-Albiense Superior. La Formación Las Peñosas corresponde con el pico regresivo e inicio de la fase transgresiva de esta secuencia, que internamente se subdivide en dos ciclos regresivos-transgresivos de menor rango. Los depósitos ricos en ámbar y carbones se depositaron en ambientes deltaico-estuarinos desarrollados durante los episodios de máxima regresión de los ciclos regresivo-transgresivo menores. El ámbar de El Soplao presenta un espectro de IRTF similar a otros ámbares del Cretácico Inferior de España, y está caracterizado por la profusión de piezas subaéreas de flujos tipo estalactítico o *chorreadura*. Los niveles asociados con el ámbar presentan abundantes cutículas de plantas perfectamente preservadas, asignadas a los géneros de coníferas *Frenelopsis* y *Mirovia* y en menor proporción hojas de ginkgoales de los géneros de *Nehvizdya* y *Pseudotorellia.* Las bioinclusiones están representadas principalmente por insectos fósiles de los órdenes Blattaria, Hemiptera, Thysanoptera, Raphidioptera, Neuroptera, Coleoptera, Hymenoptera y Diptera, aunque también se han observado algunas arañas y telas de araña. Algunos de los insectos encontrados pertenecen a grupos con una escasa representación en el registro fósil, tales como un nuevo morfotipo de la avispa *Archaeromma* (de la familia Mymarommatidae) y el pequeño jején *Lebanoculicoides* (de la subfamilia monogenérica *Lebanoculicoidinae*). Este nuevo yacimiento ambarígeno constituye un hallazago muy significativo que contribuirá a mejorar el conocimiento y entendimiento de la fauna no-marina de paleoartrópodos del Albiense.

ABSTRACT

The El Soplao site is a recently-discovered Early Albian locality of the Basque-Cantabrian Basin (northern Spain) that has yielded a number of amber pieces with abundant bioinclusions. The amber-bearing deposit occurs in a non-marine to transitional marine siliciclastic unit (Las Peñosas Formation) that is interleaved within a regressive-transgressive, carbonate-dominated Lower Aptian-Upper Albian marine sequence. The Las Peñosas Formation corresponds to the regressive stage of this sequence and in its turn it splits into two smaller regressive-transgressive cycles. The coal and amber-bearing deposits occur in deltaic-estuarine environments developed during the maximum regressive episodes of these smaller regressive-transgressive cycles. The El Soplao amber shows Fourier Transform Infrared Spectroscopy spectra similar to other Spanish Cretaceous ambers and it is characterized by the profusion of sub-aerial, stalactite-like flows. Well-preserved plant cuticles assigned to the conifer genera *Frenelopsis* and *Mirovia* are abundant in the beds associated with amber. Leaves of the ginkgoalean genera *Nehvizdya* and *Pseudotorellia* also occur occasionally. Bioinclusions mainly consist of fossil insects of the orders Blattaria, Hemiptera, Thysanoptera, Raphidioptera, Neuroptera, Coleoptera, Hymenoptera and Diptera, although some spiders and spider webs have been observed as well. Some insects belong to groups scarce in the fossil record, such as a new morphotype of the wasp *Archaeromma* (of the family Mymarommatidae) and the biting midge *Lebanoculicoides* (of the monogeneric subfamily Lebanoculicoidinae). This new amber locality constitutes a very significant finding that will contribute to improving the knowledge and comprehension of the Albian non-marine paleoarthropod fauna.

***Keywords*: Arthropod bioinclusions. Fossil resin. Plant cuticles. Lower Albian. Spain.**

INTRODUCTION

Oldest ambers with micro-bioinclusions are known from the Triassic of Italy (Schmidt et al., 2006), but it is not until the Barremian-Aptian of Lebanon that macro-bioinclusions occur more profusely (Azar, 2000; Poinar and Milki, 2001). During the Early Cretaceous amber-bearing deposits become especially common in the geological record. This was promoted possibly by the rise and spread of conifers, such as the Araucariaceae and Cheirolepidiaceae, and by a palaeoclimate warmer than today due to higher pCO_2 levels and significantly different oceanic circulation and geography (Crowley and North, 1991; Huber et al., 1995; Haywood et al., 2004). Coinciding with the initiation of the moist megathermal zone in the Northern Hemisphere, amber deposits developed between 29ºN–50ºN during the earliest Cretaceous and extended to 27ºN to near 70ºN during the Mid Cretaceous (Morley, 2000). During these periods the Iberian Peninsula was situated at low latitude, along the boundary between wet and warm tropical–"paratropical" climates where coal and other organic-rich rocks were deposited.

Early Cretaceous ambers bearing fossil inclusions are scarce, and such localities are of great scientific interest (Fig. 1). In Cantabria (northern Spain), amber is relatively widespread in the Cretaceous deposits, and previously has been found in minor amounts at least at 23 localities. However, to date none of these localities had provided amber with arthropod inclusions. An intensive geological survey in the Lower Cretaceous succession of northwest Cantabria recently resulted in the discovery of a new amber locality near Rábago village, within the El Soplao territory (Fig. 1B). This site shows a remarkable accumulation of amber with abundant biological inclusions. The so-called El Soplao amber site occurs within a Lower Albian siliciclastic unit (Las Peñosas Fm.; García-Mondéjar and Pujalte, 1982). Preliminary data for this new amber accumulation indicate that this is probably the largest site of amber with arthropod bioinclusions found in Spain so far.

This paper deals with i) documenting this new finding of arthropod bearing amber as an unusual concentration, as well as describing its related deposits in terms of major stratigraphic and sedimentological characteristics, description of the associated plant cuticles and bioinclusions, and preliminary study of the amber geochemistry; ii) discussing geological and depositional features that may help understanding the palaeoenvironmental implications of these deposits and their palaeogeographic context;

and iii) providing an appropriate introduction for future, more specific studies, on this exceptional new amber site.

Emphasis is given in providing a solid sedimentological, palaeoenvironmental and palaeogeographic framework of this palaeontologically significant deposit for its exceptional preservation and age.

METHODOLOGY AND TECHNIQUES

Sedimentological and palaeoenvironmental interpretations are based on field observations. Four laterally correlative stratigraphic sections (Puente Arrudo, Rábago, La Florida and Plaza del Monte), belonging to the Las Peñosas Fm., have been logged at a meter–centimetre scale. From these data a W–E cross-section has been established to display the principal depositional and palaeoenvironmental features and the stratigraphic distribution of the amber and coal-bearing unit. When possible, rock sampling and measurement of palaeocurrent orientations of selected structures were carried out to help in sedimentological interpretations.

Pieces of amber were acquired by surface collection during field work in the area. To characterize El Soplao amber, three Fourier Transform Infrared Spectroscopy (FTIR) spectra of three separate amber samples and one sample of recent kauri resin - *Agathis australis* (D. Don) Lindl. in Loud., 1829 - were obtained using an infrared Fourier Bomem DA3 spectrometer, in the Molecular Spectrometry Unit of the University of Barcelona (SCT-UB).

Palaeobotanical samples from plant cuticle-rich claystones were obtained by macerating the clayey sediment in hydrogen peroxide and air drying the organic residues. Resulting fossil plant fragments were sorted both with the naked eye and under the stereomicroscope.

The amber was kept wet during screening in order to improve visibility and to detect arthropod bioinclusions. Screening was done under a stereoscope, using transmitted and obliquely reflected light. The amber pieces were cut around the detected arthropods and then polished to permit optimal study. Drawings of some specimens were made with the aid of an image drawing tube, an Olympus V-DA mounted on an Olympus BX51 stereoscopic microscope. Photomicrographs were made with a digital camera mounted on the same microscope. The specimens are housed provisionally in

the Museo Geominero of the Instituto Geológico y Minero de España (IGME), in Madrid, Spain.

PALEOGEOGRAPHICAL DISTRIBUTION OF EARLY–MID CRETACEOUS AMBER

Early–Mid Cretaceous (Aptian to Cenomanian) amber occurrences have great scientific interest owing to their scarcity (Fig. 1). In fact, macrobioinclusion-bearing ambers of this age are basically restricted to four Eurasian areas: Northern Siberia (Taimyr Peninsula), southeastern Asia (Myanmar), western Middle-East (Lebanon and Jordan), and southwestern Europe (Spain and France). A review of amber localities in the literature was compiled by Martínez-Delclòs et al., 2004. The four areas were located within the warm temperate and tropical-paratropical palaeoclimatic regions (Fig. 1) *sensu* Scotese (2000), also referred as tropical and south-subtropical Cretaceous climate belts by Spicer et al. (1994).

In Spain, aside from the frequent occurrence of amber in Aptian to Cenomanian deposits, only a few localities show sufficient quantity to be identified as accumulations (Fig. 1B). In the past, only two of these deposits had yielded important amounts of bioinclusions in terms of quantity and quality, specifically the Álava deposits of Peñacerrada and Montoria (Alonso et al., 2000; Delclòs et al., 2007) and the San Just outcrop in Teruel (Delclòs et al., 2007; Peñalver et al., 2007b). In Asturias, although less significant, amber with bioinclusions has been described in El Caleyu and Pola de Siero (Arbizu et al., 1999) (Fig. 1). The identification of the new amber deposit of the El Soplao in Cantabria (Figs. 1 and 2) enlarges the still patchy record of these palaeontological deposits of exceptional preservation in Spain.

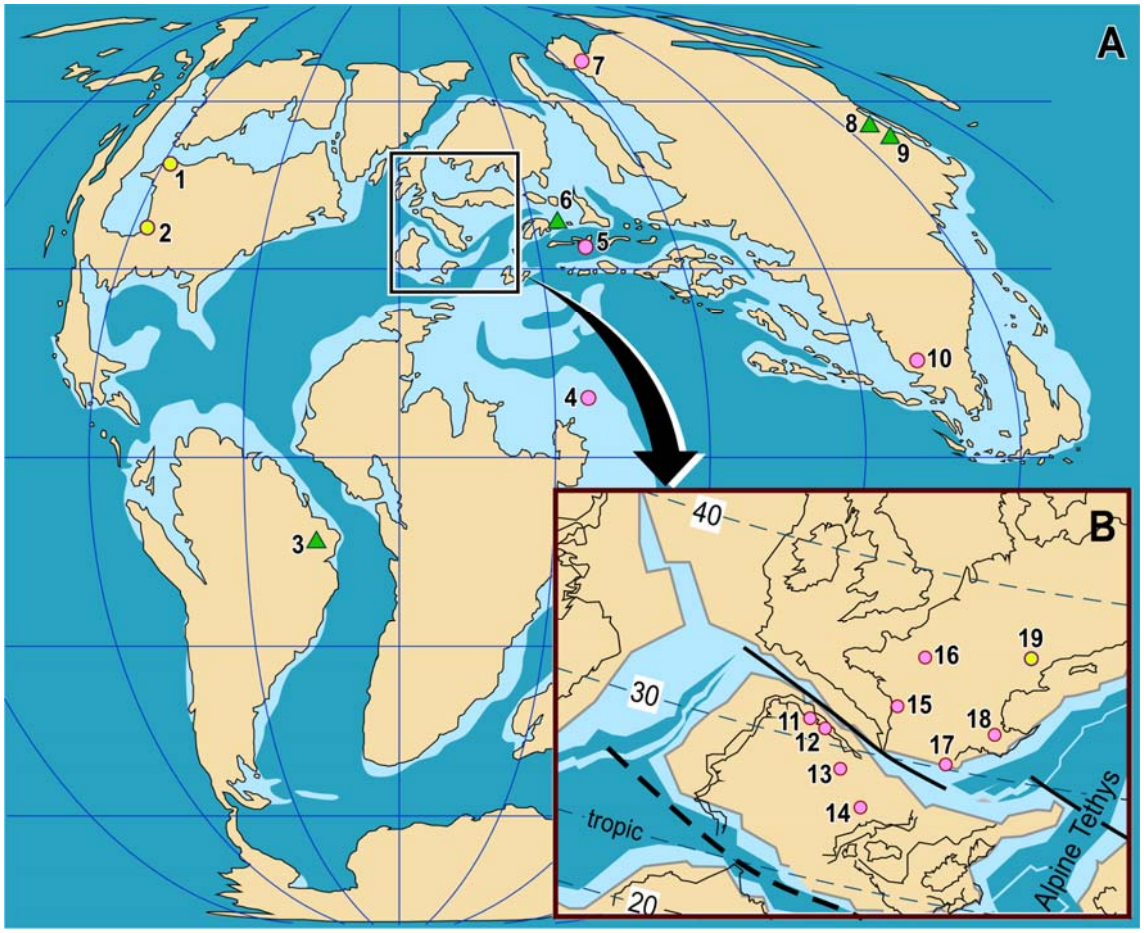

Figure 1.- **A)** Major Early-Mid Cretaceous (Aptian to Cenomanian) amber occurrences (Redrawn from Blakey, 2008). Amber localities with bioinclusions are symbolized with circles, otherwise green triangles are used. Moreover, yellow circles represent ambers that have only provided microbioinclusions (bacteria, protists, algae and/or fungi). Pink circles account for macrobioinclusion-bearing ambers (essentially arthropods), with the exception of El Soplao amber, which is designated out with a black star. Broken purple lines delimit palaeoclimatic regions sensu Scotese (2000). (1) Ruby Creek (Alberta, Canada; Medioli et al., 1990). (2) Ellsworth (Kansas, USA; Waggoner, 1996). (3) Nova Olinda-Santana (Ceará, Brazil; Martill et al., 2005). (4) Middle-East. Wadi Zerka (Amman, Jordan; Bandel et al., 1997; Kaddumi, 2005). Bcharreh, Hammana, and Jezzine, among others (Lebanon; Azar, 2000; Veltz, 2008). Mt. Hermon (North District, Israel; Greenblatt et al., 1999). (5) Yukhary Agdzhakend (Goranboy, Azerbaijan; Ratnitsyn and Quicke, 2002). Russia (Zherikhin and Eskov, 1999; Ratnitsyn and Quicke, 2002). (6) Stary Oskol (Belgorod). (7) Taimyr Peninsula (Northern Siberia). Baikura-Neru Bay in Lake Taimyr (Central Taimyr). Nizhnyaya Agapa River (West Taimyr). Begichev Fm. in the Khatanga River (Eastern Taimyr). (8) Khetana River in South of Okhotsk (Khabarovsk Krai). (9) Suyfun Coal Basin (Primorye). (10) Hukawng Valley (Kachin, Myanmar; Cruickshank and Ko, 2003). **B)** Amplified area squared at subfigure A, corresponding to SW Europe. Spain (Arbizu et al., 1999; Alonso et al., 2000; Peñalver et al., 2007b; Delclòs et al., 2007). (11) El Caleyu and Pola de Siero (Asturias). (12) El Soplao Territory, near Rábago village (Cantabria, in this paper). (13) Moraza and Peñacerrada-Montoria (Burgos and Álava respectively). (14) San Just (Teruel). France (Nel et al., 2004; Perrichot, 2004, 2005; Néraudeau et al., 2005; Perrichot et al., 2007; Néraudeau et al., 2008; Girard, 2008). (15) Archingeay-Les Nouillers, La Buzinie, Cadeuil, Fouras, l'Ile d'Aix, and Les Renardières (Les Charentes). (16) Ecommoy and Durtal (Sarthe and Maine-et-Loire respectively). (17) Fourtou (L'Aude). (18) Salignac and Sisteron (Alpes-de-Haute-Provence). (19) Schliersee (Bavaria, Germany; Schmidt et al., 2001).

GEOLOGICAL AND PALAEOGEOGRAPHIC SETTING

The recently discovered amber outcrop is located in the El Soplao territory in northwestern Cantabria (Fig. 2). This area, located immediately to the north of the Cabuérniga Ridge, constituted the northwestern margin of the Basque-Cantabrian Basin during the Cretaceous (Fig. 3). The evolution and current structure of the Basque-Cantabrian Basin are related to the kinematics between the European and Iberian plates (Malod and Mauffret, 1990; Olivet, 1996). The inception of the basin occurred during a Permo-Triassic rifting event. A second extensional phase was related to the opening of the Bay of Biscay during the Late Jurassic-Early Cretaceous (e.g., Rat, 1988; García-Mondéjar et al., 1996). Renewed extension and perhaps strike-slip faulting along a NW-SE trend occurred during the Aptian-Albian (e.g., García-Mondéjar et al., 1996; Martín-Chivelet et al., 2002; Soto et al., 2007). These tectonic events resulted in the development of several extensional sub-basins bounded by synsedimentary faults, in which great thicknesses of sediments accumulated. These sedimentary sub-basins underwent widespread contraction during the Pyrenean Orogeny in Late Eocene-Oligocene times (Hines, 1985; Fernández Viejo and Gallastegui, 2005). Consequently, the present structure of the study area is the result of the inversion of the previous Mesozoic extensional and strike-slip structures.

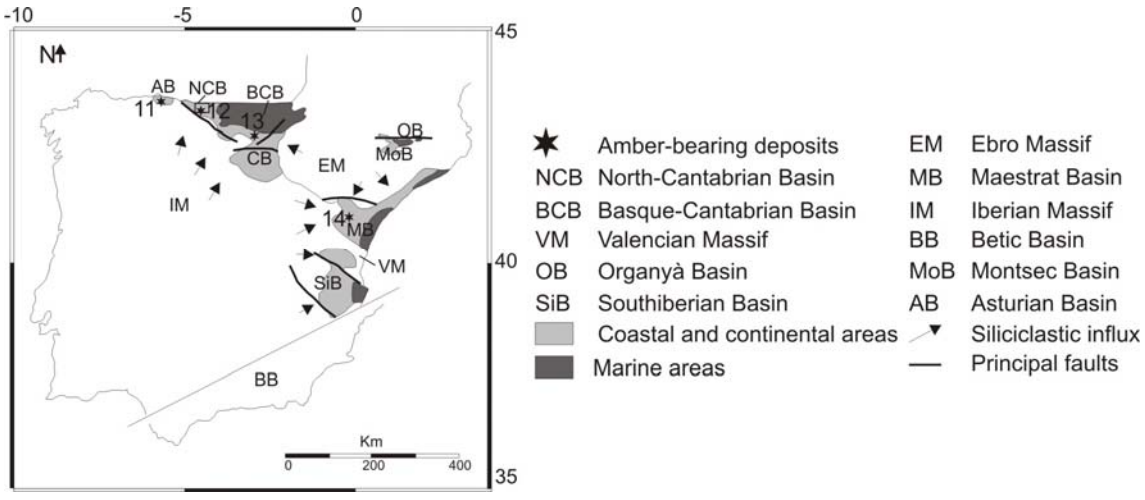

Figure 2.- Map of the Iberian Peninsula showing the location of the Lower Albian basins and the distribution of the Lower Cretaceous amber-bearing deposits (same nomenclature as in Figure 1). (11) El Caleyu and Pola de Siero deposits. (12) The El Soplao deposit. (13) Peñacerrada-Montoria deposits. (14) San Just deposit. (Modified from Salas et al., 2001).

The studied succession was deposited in the North Cantabrian sub-basin (NCB) (Fig. 3A), which subsided moderately for most of Cretaceous time (Martín-Chivelet et al., 2002; Wilmsen, 2005). The Cabuérgina Ridge (Fig. 3) is an E-W trending fault zone, which bounds this (sub) basin to the south. This palaeo-high represents a previous Variscan structure that was reactivated through extensional faulting during the Mesozoic (Rat, 1988; García-Espina, 1997).

Structurally, the studied succession was deposited during the Cretaceous on an eastward tilted block (Fig. 3B). The tilted block forms the footwall of the N-S Bustriguado Fault (BF, Figs. 3A and 3C) that bounds to the west the main Cretaceous depocenter (Figs. 3A and 3B). Recent geological mapping has shown that the BF branches at a corner point with the E-W trending North Cabuérniga Fault (NCF; Fig. 3A); (García-Senz "pers. comm."), forming an extensional-linked system, as in the examples described by Gibbs (1990). Because in the northern margin of the Iberian plate, the direction of extension during the Cretaceous is considered to be roughly orthogonal to the Cantabrian margin (Malod and Mauffret, 1990), the BF is interpreted as a left-lateral transfer fault, and the NCF as the corresponding frontal extensional ramp. The tilted block that contains the El Soplao territory dips and thickens towards the master BF (Fig. 3B), a feature commonly interpreted as the result of extensional fault propagation folding (Withjack et al., 1993). Models of such faults have been described in frontal ramps (Withjack et al., 1993) but few examples in transfer faults are known. This Cretaceous configuration was inverted during the Palaeogene folding and the faults reversed their movement. The NCF behaved as a frontal thrust ramp, and the BF as a right-lateral strike-slip fault. The latter passes northwards to an oblique thrust sheet that superposes the Cretaceous on the Cenozoic.

STRATIGRAPHY OF THE EL SOPLAO AREA

The bulk of the Mesozoic succession of the El Soplao area lies unconformably on folded (Variscan deformation) Carboniferous basement (Fig. 4). This succession was initiated with a thick sequence of Lower Triassic continental red sandstones and mudstones (Buntsandstein facies). Late Triassic, Jurassic and earliest Cretaceous sequences are absent in the studied area, probably because during the Late Jurassic-Early Cretaceous rifting stage, the area to the north of the Cabuérniga Ridge was

subjected to erosion and nondeposition. Subsidence renewed in the Early Aptian and was accompanied by gradual marine transgression. Thus, the Aptian-Albian succession of the El Soplao area, unconformably overlies Triassic strata and was dominated by shallow marine carbonate deposition (Fig. 4).

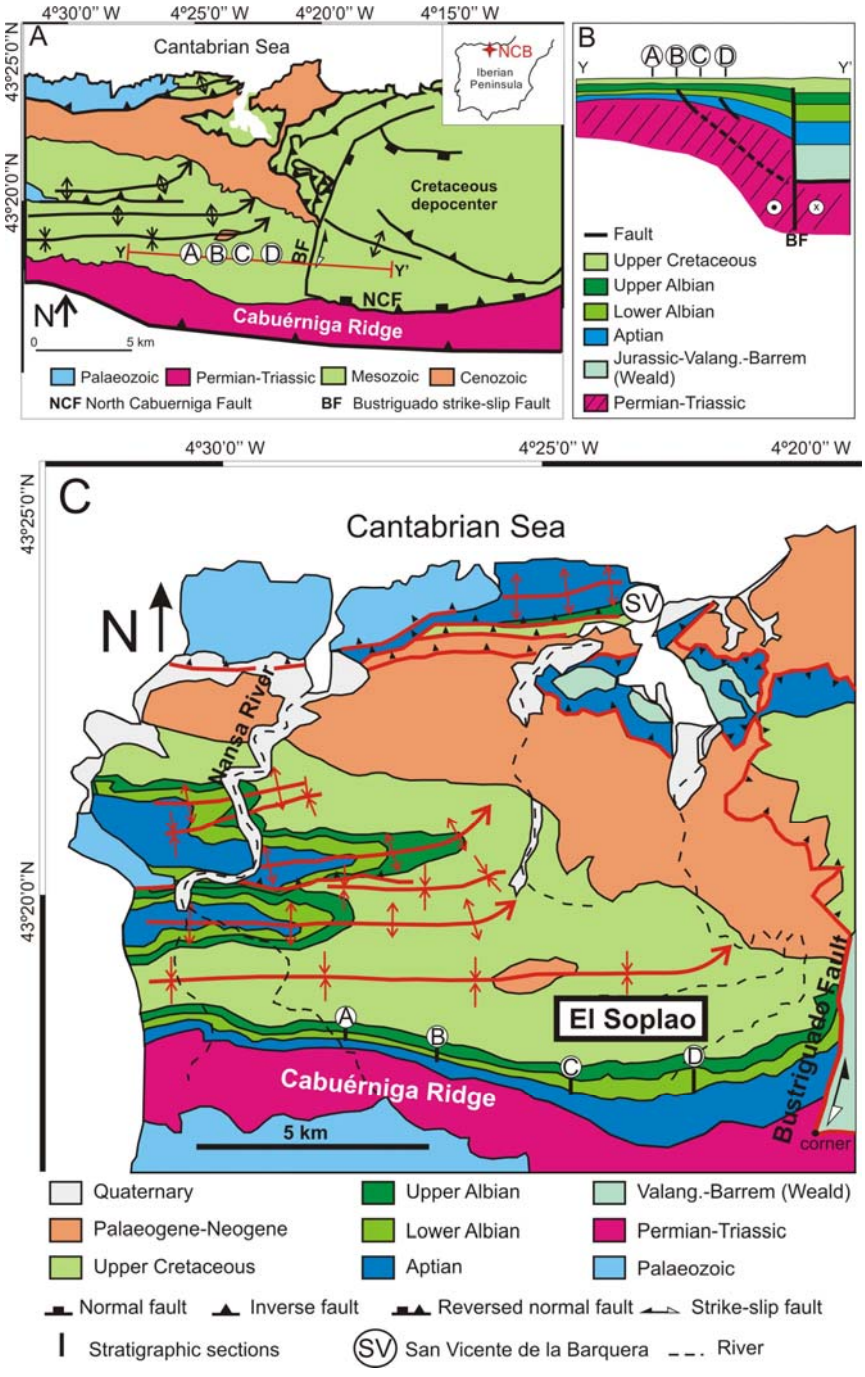

Figure 3.- **A)** Geological sketch with the main structural elements of the North Cantabrian sub-basin (NCB). The red line Y-Y' indicates the position of the cross-section of Fig. 3B. **B)** Schematic cross-section showing the restored geometry of the NCB in the El Soplao territory during the Cretaceous. Figure not to scale. **C)** Detailed geological map of the NCB Basin in the El Soplao area with location of the stratigraphic sections studied. (A) Puente Arrudo Section, (B) Rábago Section, (C) La Florida Section, (D) Plaza del Monte Section.

As a whole, the Aptian-Albian succession of the El Soplao territory constitutes an E-W elongated lithesome 9 km long with wedge-shaped geometry deepening and thickening eastward, on the slope of the tilted block active during this time (Najarro et al., 2007) (Fig. 3B). Thicknesses vary from about 600 m in the eastern part of the tilted block (Bustriguado area, Fig. 3) to less than 200 m toward the west (Puente Arrudo-Rábago Sections, Fig. 3C). The general stratigraphic and biostratigraphic framework of the Aptian-Albian lithological units has been established by Ramírez del Pozo (1972) and Hines (1985), but the main depositional systems and sequences have been revised recently (Najarro et al., 2007; Najarro and Rosales, 2008). A simplified stratigraphy of this interval is provided, adapted from the terminology by Hines (1985) for the major lithological units (Fig. 4).

The Early Aptian marine transgression led to deposition of shallow platform carbonates of the Lower Aptian Rábago Limestone Fm. and Umbrera Fm. that spread over the studied area. Continued transgression during the Early Aptian caused platform drowning, and resulted in deposition of relatively deep-water marls (Patrocinio Fm.) that covered the entire carbonate platform (Najarro and Rosales, 2008). Subsequent gradual regression led to deposition of shallow water carbonates of the Reocín Fm. during the Late Aptian, and finally delta-estuarine siliciclastics and carbonaceous lutites of the Las Peñosas Fm. during the Early Albian (Fig. 4). The vertical evolution from the Upper Aptian Reocín Fm. to the Lower Albian Las Peñosas Fm. is interpreted herein as a relative sealevel fall associated with a deltaic progradation. The Upper Albian succession follows with deposition of the Barcenaciones Fm. (Fig. 4), a shallow water carbonate bank that expands more than 50 km throughout the North Cantabrian sub-basin, as a result of a transgression following deposition of the Las Peñosas Fm. A subsequent regression during the Lower Cenomanian deposited the transitional marine siliciclastic Bielba Fm. Later, deeper water conditions were established during the Late Cretaceous, leading to deposition of open-platform carbonates for the remainder of the Cretaceous succession.

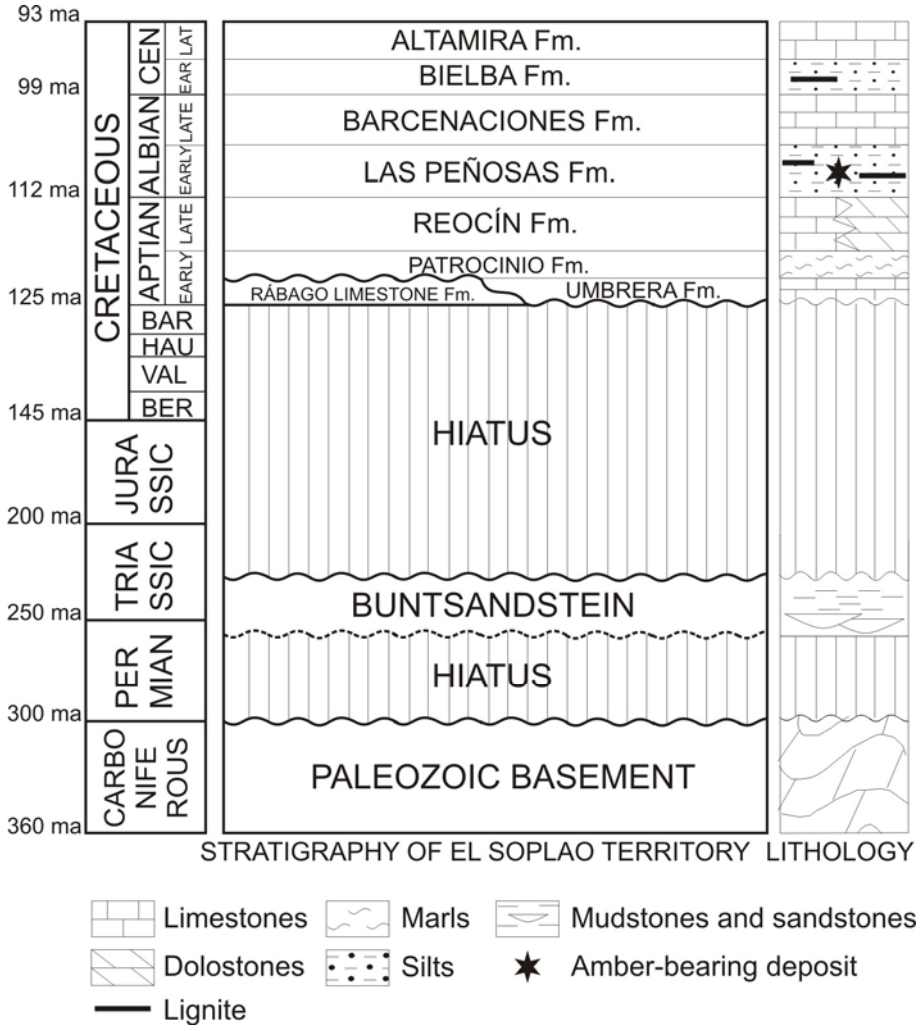

Figure 4.- Carboniferous to Upper Cretaceous lithostratigraphy of the El Soplao area (modified from Hines, 1985). Chronostratigraphy after Gradstein (2004).

LAS PEÑOSAS FORMATION

Primarily, this paper examines the Lower Albian heterolithic amber-bearing deposit that is included within the Las Peñosas Fm. Regional palaeogeographical and palaeoenvironmental reconstructions of the Basque-Cantabrian Basin during this time slice (García-Mondéjar, 1990) indicate that siliciclastic sediment was transported from highlands and continental areas located to the west and south towards the north during deposition of the Las Peñosas Fm. This amber-bearing unit is approximately equivalent in age and facies to the broadly extended Escucha Fm., deposited to the south of the Basque-Cantabrian Basin (Barrón et al., 2001; Martínez-Torres et al., 2003), as well as other Mesozoic basins of northeastern Spain, including the Maestrat Basin (e.g., Salas

and Martín-Closas, 1991; Salas et al., 1991; Querol et al., 1992; Salas et al., 2001; Rodríguez-López and Meléndez, 2004; Rodríguez-López et al., 2005, 2007; Peyrot et al., 2007; Moreno-Bedmar et al., 2008). These units basically represent littoral facies dominated by delta-estuarine deposits, which can be laterally correlated in a NW-SE direction for more than 500 km, from northeastern Cantabria, through the southeast Basque-Cantabrian Basin in the Álava region (Basque Country), and into the Maestrat Basin in Teruel to the Alicante Province (Fig. 2). These areas, which trace the approximate location of the coastline during the Early Albian, are characterized by the presence of coal-bearing deposits with common presence of amber (Delclòs et al., 2007).

Facies and sequence arrangement

The Las Peñosas Fm. previously has been described as a unit formed by a complex of fluvio-estuarine channel sandstones, overbank black carbonaceous mudstones, tidal channel bars and tidal flat facies, and minor intercalations of carbonate beds, exhibiting unclear internal organization (García-Mondéjar and Pujalte, 1982; Hines, 1985). However, detailed stratigraphic and sedimentological logging of four W-E correlative stratigraphic sections (the Puente Arrudo, Rábago, La Florida and Plaza del Monte sections; Fig. 3) in the El Soplao region has revealed the depositional architecture of the Las Peñosas Fm. and the stratigraphic distribution of the coal- and amber-bearing deposits (Fig. 5). A summary of the general facies associations, depositional environments and their sequential arrangement is given in this section and summarized in Fig. 5 and Table 1.

It is significant that the facies distribution within the Las Peñosas Fm. displays a clear tectonic control, as suggested in the study area by the strong lateral thickness variation in an E-W direction (Fig. 5), which, in the studied area, ranges from between 45 m to the west to more than 100 m to the east. In this way, the Rábago Section that contains the amber deposit represents the highest point of the flexured footwall block of the Bustriguado fault (Fig. 3B) at the time of deposition of the Las Peñosas Fm. This flexure seems to be accommodated by several minor synsedimentary faults that delineate the structure observed in the Rábago Section (Figs. 3B and 5).

The Las Peñosas Fm. can be informally split into three correlatable units, which are named in this paper, from base to top, Las Peñosas 1 to 3 (P1-P3; Figs. 5 and 6A). The lower Unit P1 overlies the Reocín Fm. It ranges from about 11 m (Rábago Section)

to 40 m (Plaza del Monte Section) and it is characterized by an alternation of bioclastic, oyster-rich limestones and bioturbated, nodular marly-silty limestones to siltstones with intervals of very fine sands. The overall succession presents an upward decrease of carbonate content and a progressive increase in the quartz silt and sand content of the marly intervals. This succession is interpreted as a transitional unit from a shallow carbonate platform to a siliciclastic estuary-delta bay, caused by rapid change in the sedimentary conditions resulting from deltaic progradation.

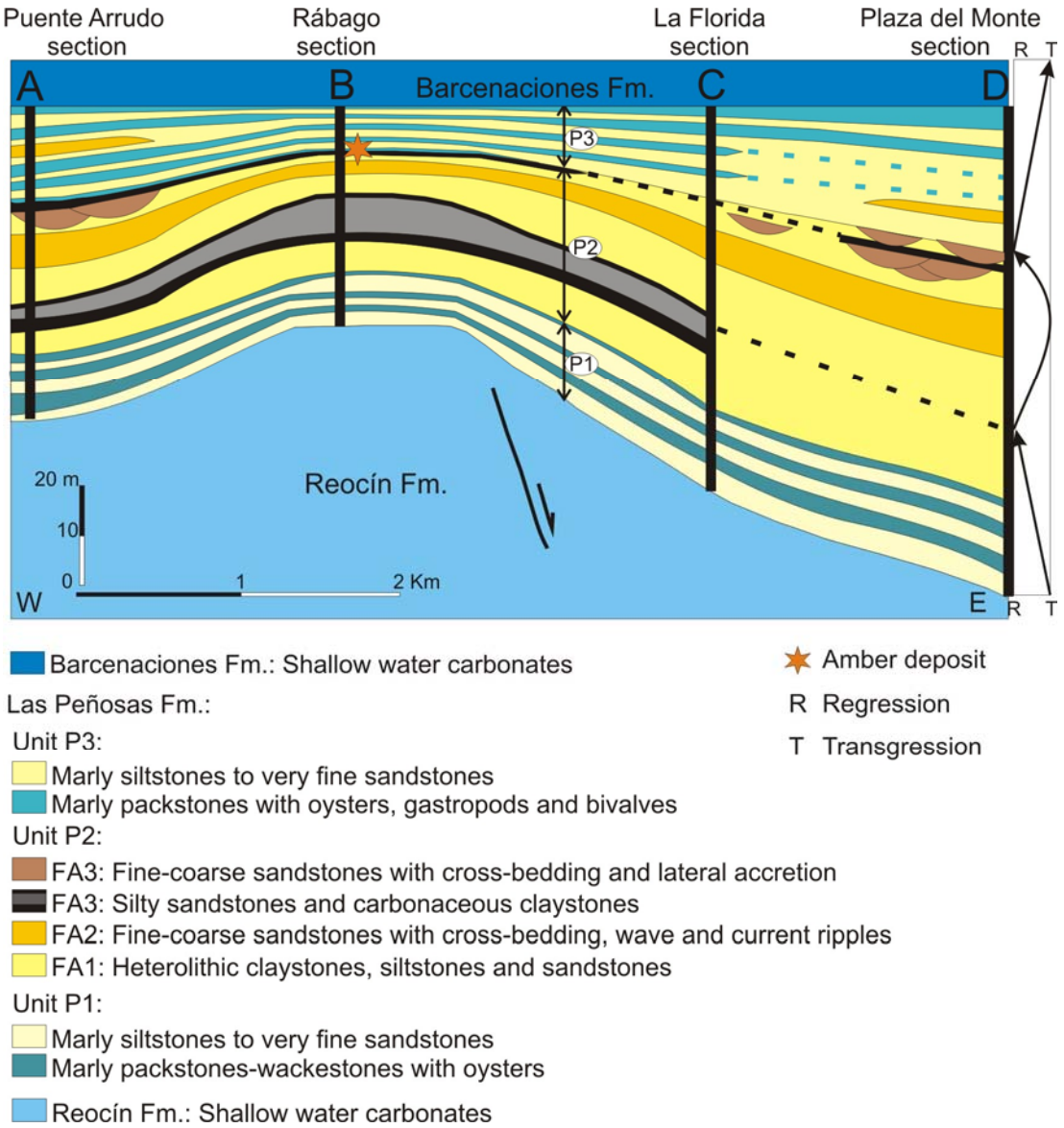

Figure 5.- Stratigraphic correlation of the four studied sections (A to D in Figure 3). Note the location of the amber deposit and the thickness variation of the Las Peñosas Fm. along the W-E cross section (see also Fig. 3). (P1-P3) Members of the Las Peñosas Fm. (see text for explanation). (FA1- FA3) Sedimentary facies associations studied in the Las Peñosas Fm. Amber accumulation usually occurs at the P2-P3 unit boundary.

Unit	FA	F	Lithology	Primary Structures	Vertical Stacking	Interpretation
P3			Alternation of nodular marly-packestones with bioclasts and heterolithic levels of mud- silt- and fine to medium grain-sized sandstones	Wavy, flaser and lenticular lamination	Progressive upward increase in carbonate content	Carbonate-siliciclastic mixed platform
P2	FA3	F6	Weakly cemented, moderate-well sorted, very fine- coarse to grained sandstones in erosionally-based, channalized units. Accretion surfaces with silty clay, plant remains, coal and mudclasts. Iron cemented ripples, pyritized trunk fragments and pyritized burrows at the top.	Large scale trough-, longitudinal-, low angle- and small-ripple-cross bedding; lateral accretion; horizontal-and sigmoidal-stratification; complex deformations	Fining upward	Delta plain: Distributary meandering channels
		F5	Dark organic, sulphide-rich mudstones with bivalves, gastropods, leaves, coal, trunks, sulphide nodules and amber	Wavy and lenticular lamination; current ripples	Rhythmic alternations	Delta plain: Interdistributary bay
		F4	Silty very fine sandstones with coal layers, sulphide nodules, trunks and amber		Rhythmic alternations	Delta plain: Interdistributary bay
	FA2	F3	Weakly cemented, moderated to well-sorted fine to coarse-grained sandstones with mud drapes and mudclasts	Large scale trough cross-bedding; planar cross-bedding; wave ripples	Coarsening and thickening upwards	Delta front: Distributary mouth-bars
	FA1	F2	Sulphide mudstone-siltstones with coal and trunk fragments. Minor to moderate bioturbation	Wavy and lenticular lamination	Fining upward	Wave- and tidal influenced estuarine-delta bay
		F1	Pale-yellow, very fine- to medium-grained, well-sorted sandstones. Mudclasts and coal fragments. Minor to abundant bioturbation dominated by *Skolithos* and track traces.	Low angle and horizontal lamination; planar cross-stratification; flaser and wavy lamination; wave and current-ripples		
P1			Alternation of bioclastic, oyster-rich limestones and bioturbated, nodular marly–silty limestones to siltstones with very fine sand levels	Wavy lamination	Upward decrease in carbonate content and progressive increase in siliciclastics	Transition from shallow carbonate platform to estuarine-delta bay

FA: Facies association. F: Facies

Table 1.- Characteristics of the facies associations in the Las Peñosas Fm.

The middle Unit P2 contains the amber-rich deposit that has been recently discovered in the Rábago Section (Figs. 6B-D and 7A). It lies on top of P1 and ranges in thickness from 25 m (Rábago Section) to 60 m (Plaza del Monte Section; Fig. 5). This unit consists predominantly of heterolithic sandstones-siltstones and carbonaceous mudstones deposited in broadly coastal estuarine and delta environments. Facies associations can be grouped into three main depositional environments. First is delta front facies association without evidence of emergence, interpreted largely as shallow marine. This environment includes distributary mouth-bar facies, deposited mostly, if not entirely, under marine conditions, as well as distal bar, nearshore to offshore deposits. Second are wave- and tide-influenced estuarine-delta bay deposits. Third is delta plain facies association, with sedimentary facies that reflect deposition in both distributary meandering channels (Fig. 7B and Table 1) and infilling of interdistributary bays (Figs. 6C and 7C), the latter with high accumulation of coal, plant cuticles (Fig. 7D) and amber pieces (Fig. 6D). Due to the sedimentological and palaeontological importance of this unit, more detailed stratigraphic characteristics and environmental interpretation is provided in the next section.

The Unit P3 superposed the Unit P2 by an erosive transgressive surface (a *ravinement*; Fig. 7C) and in turn is overlain by the Barcenaciones Fm. The thickness of the Unit P3 varies from 13 m to the west (Rábago Section) to 40 m to the east (Plaza del Monte Section; Fig. 5) and is characterized by the stacking of several meterscale mixed siliciclastic-carbonate sequences. Contrasting with P1, the vertical stacking pattern of P3 presents a progressive increase in the carbonate content toward the top of the unit. This unit is interpreted as a transition from estuarine bay deposits (Fig. 7E) to a shallow carbonate platform system. Thus, a carbonate-siliciclastic mixed platform is proposed. The contact with the overlaying Barcenaciones Fm. is taken at the base of a marly-nodular limestone bed with large bivalves that indicates the definitive abandonment of the siliciclastic system (Fig. 7F).

The amber-rich deposit in the Rábago Section

As noted above, the recently discovered site of amber accumulation is located at the top of Unit P2 in the Rábago Section, where this unit is comprised of three facies associations (Fig. 6 and Table 1).

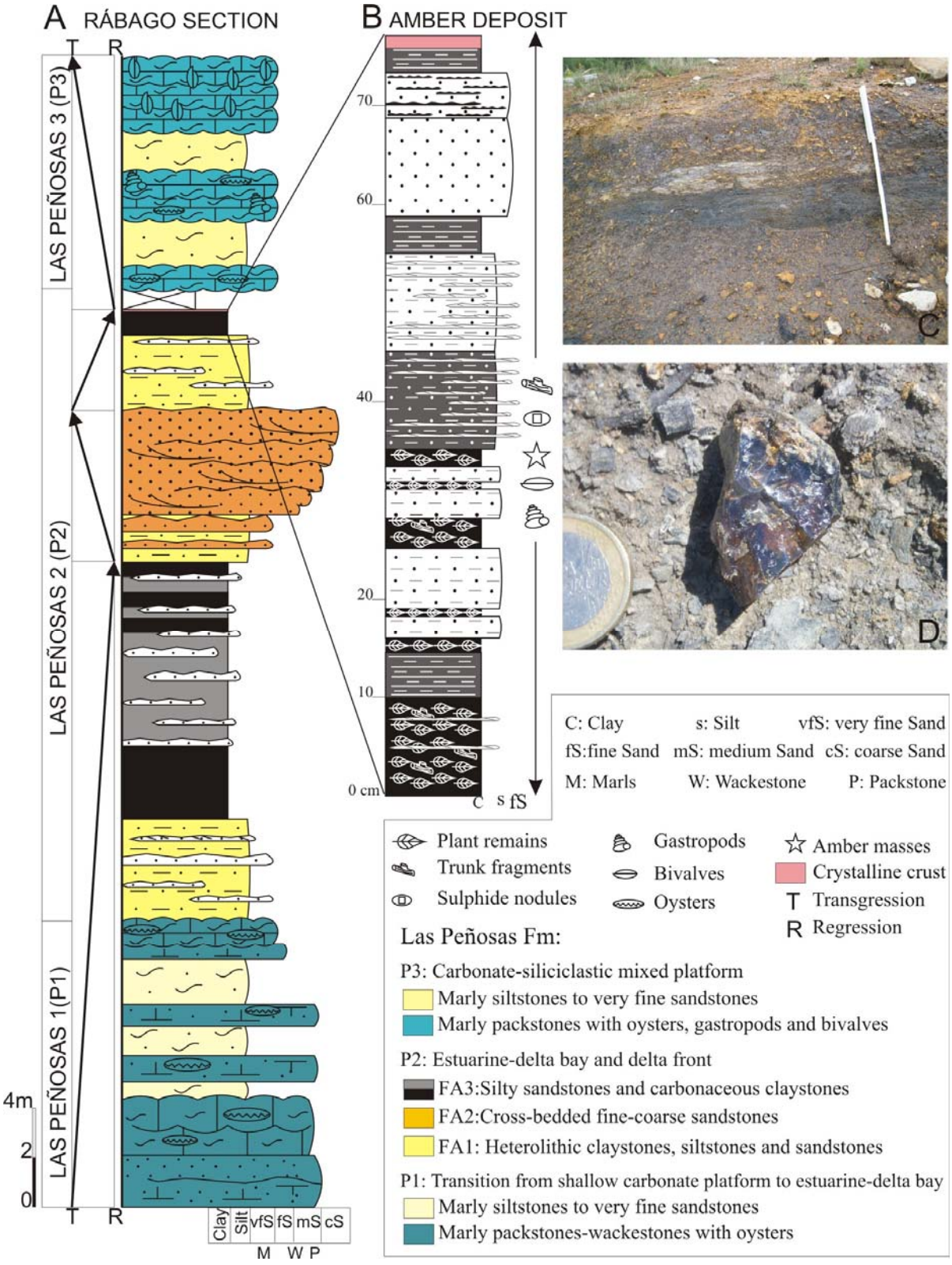

Figure 6.- **A)** Simplified stratigraphic log of the Rábago Section. Two regressive-transgressive cycles are defined. Note that the position of the amber deposit coincides with the maximum regression of the second cycle. **B)** High-resolution stratigraphy of the amber deposit. **C)** General view of the amber deposit (scale: 1m). **D)** Example of a blue amber piece in situ.

Figure 7.- Field pictures of the Las Peñosas Fm. **A)** General view of the new discovered amber-rich deposit in Rábago Section within the Unit P2. **B)** FA3: Distributary meandering channel with trough cross-bedding, sigmoidal and horizontal stratification and lateral accretion within the Unit P2 in La Florida Section. **C)** FA3: Interdistributary bay facies within the Unit P2, capped by an erosive transgressive surface (ravinement), and overlain by marine limestones (Unit P3) (Puente Arrudo Section). **D)** FA3: Exceptionally well-preserved plant cuticle compressions that appear associated with the amber-rich deposit in Rábago Section. **E)** Detail of FA1 constituted of interbedded mudstones-siltstones with wavy and lenticular lamination and fine-grained sandstones. Unit P2 in Plaza del Monte Section. **F)** Marly level with high concentration of bivalves at the top of the Unit P3 in Rábago Section.

Facies association 1 (FA 1): wave- and tide-influenced estuarine-delta bay

This facies association consists of heterolithic alternations of thinly bedded dark coloured mudstones, siltstones and sandstones, stacked vertically in meter-scale sequences with a general fining-upward trend. The sequences range in thickness from 3 to 4 m. This facies association displays two sedimentary facies. Facies 1 consists of 5 to 40 cm thick, pale-yellow, very fine- to medium-grained, well-sorted sandstones. The basal contacts are flat and sharp, while the contacts in the top are wavy due to ripples. This facies is characterized by low angle and horizontal lamination, planar cross-stratification, flaser and wavy lamination and wave and current ripples at the tops of the beds. Both current and wave ripples are associated with flaser bedding, and current ripples are seen as climbing in some places. Palaeocurrents have been measured in some crests of the wave ripples resulting in a shoreline direction with an overall E-W trend. Mud drapes occur frequently with thicknesses up to 0.5 cm. Mudclasts and coal fragments appear locally. Bioturbation ranges from sparse to elevated but is consistently characterized by a low diversity assemblage dominated by *Skolithos* and various track traces. Facies 2 consists of beds of mudstone to siltstone. These beds are relatively sulphide-rich and range from 0.5 to 2 m thick, which often combine with facies 1 to form wavy and lenticular bedding (heterolithic facies). Coal and pyritized trunk fragments up to 20 cm long are concentrated at the base of these beds. Minor to moderate bioturbation and sulphide nodules also are present.

The presence of wave and current ripples occurring both as lenticular and flaser bedding, along with the wavy lamination and wave ripples on some sandstone beds, suggests a tidal- and wave-influenced estuarine-delta bay environment (e.g., Reineck and Wunderlich, 1968; Reineck and Singh, 1975; Dalrymple, 1992; Willis, 1997; Kuecher et al., 1990; Folkestad and Satur, 2008). The suite of trace fossils described above may occur in such an environment (Pemberton et al., 1992). The common occurrence of mud drapes and rhythmic bedding of sandstones and mudstones suggests involvement of tidal processes in the formation of this facies (Visser, 1980), but the occurrence of wave-generated structures suggests that reworking also was controlled by waves. The climbing current ripples indicate rapid deposition of sand (Reineck and Singh, 1975). These deposits are interpreted to have originated in the intertidal part of an estuarine-delta bay.

Facies association 2 (FA 2): Delta front distributary mouth-bars

Facies 3 consists of weakly cemented, moderate to well-sorted, fine to coarse-grained sandstone, organized in a coarsening and thickening upwards sequence of about 6 m thick. Sedimentary structures grade vertically from large-scale trough cross-bedding to planar cross-bedding with wave ripples at the top. Mud drapes and mud pebbles are present in foresets. Although preservation at the outcrops prevents detailed sedimentological observations and measurements, in most instances, unidirectional, diffuse palaeocurrent features are observed.

The thickening and coarsening upward trend of this facies association suggests a progradational character. The upward transition from trough cross-bedding to wave ripples at the top suggests decreasing energy conditions. Moreover, the occurrence of mud drapes and mud clasts suggests fluctuating energy conditions likely produced by tidal processes occurring during deposition (Reineck and Singh, 1975; Dalrymple et al., 1990; Shanmugam et al., 2000; Kitazawa, 2007). The presence of wave-ripple lamination also indicates wave influence. As a whole, this facies association is interpreted as a progradation of distributary mouth-bar deposits and sand bars into a wave and tidal influenced estuarine-delta bay.

Facies Association 3 (FA 3): Interdistributary bay

This facies association is composed of a very thin intercalation of silty to very fine sandstones (facies 4) that contain dark organic- and sulphide-rich mudstones (facies 5), ranging in thickness from 0.7 to 2.5 m. Facies 4 is greyish-brown reaching a maximum thickness of 10 cm. It presents wavy and lenticular lamination with current ripples, coal layers (up to 3 cm), sulphide nodules, partially pyritized trunk fragments, minor bioturbation as pyritized burrows, and amber. Facies 5 is mostly composed of layers formed by the accumulation of leaves and other plant remains. These leaves are very well preserved, showing many original details and their venation patterns. When present, the matrix between the plant-bearing levels consists of clay. Also present in this facies are small pyritized moulds of marine gastropods and bivalves, sulphide nodules (up to 6 cm in size), coal, trunk fragments (up to 15 cm), and abundant pieces of amber. Although amber fragments have been found in all stratigraphic sections, the most abundant yield comes from the Rábago Section, where they consist of both stalactite-shaped and globular or kidney-shaped amber pieces. At the top of this facies association a 5 cm thick crystalline crust appears. The crust surface is colonized by serpulid worm

tubes and its genesis remains uncertain. A pale-yellow silty rooting level with associated white mottling occurs in the Plaza del Monte Section at a stratigraphic position laterally equivalent to this crystalline crust.

Dark organic-rich mudstone deposits are interpreted as extensive accumulations of plant remains with a relatively low input of clastic material followed by relatively rapid burial to prevent decomposition (Dalrymple, 1992; Folkestand and Satur, 2008). Mudstones were mostly deposited in interdistributary and coastal bays with a high supply of continental organic matter transported by fluvially associated floods that undoubtedly originated during rainstorm periods. The exceptional preservation of the leaves, along with the presence of pyrite, organic remains, and the low-diversity of fossil traces and benthic fauna, suggest suboxic conditions within the interphase water-sediment. Occasionally, the combined action of spring tides, storms and overbank floods was strong enough to deposit silty and very fine sand layers (Reineck and Singh, 1975; Noe-Nygaard and Surlyk, 1988; Dalrymple, 1992). This inference also is supported by the presence of thin shell remains. The root activity at the top of the infilling sequence implies eventual subaerial conditions, and the development of a horizon exposed to vegetative processes in a palaeosol (McCarthy and Plint, 2003; Folkestand and Satur, 2008). This event is coincident with the maximum regressive stage within the Las Peñosas Fm.

Deposicional sequences and facies model of the amber-bearing deposits

Within the Las Peñosas Fm., amber accumulation occurs principally towards the top of the Unit P2, in dark organic rich mudstones that deposited in interdistributary bays between meandering distributary channels (i.e., facies association 3; Fig. 8 and Table 1). The vertical stacking of the described facies association of the Unit P2 suggests that it internally displays two smaller transgressive-regressive cycles, with the coal-bearing deposits developing during the regressive phase of the cycles (Fig. 5). These deposits are underlain by shallow marine, siliciclastic and carbonate deposits formed under relatively higher sea-level conditions (Unit P1). The Unit P2 is capped by an erosive transgressive surface (*ravinement*), overlain by full-marine limestones (Fig. 7C). These deposits represent a marked landward shift in the siliciclastic coastal facies, displaying a retrogradational- aggradational stacking pattern (Unit P3). Therefore, deposition of the amber and coal rich levels was coincident with the maximum regressive episode of the estuary-delta progradation (Fig. 5), and represents a relative

sea-level fall. The same pattern in coal- and amber-rich deposits has also been described for the Escucha Fm., in the south of the Basque-Cantabrian Basin (Peñacerrada-Montoria outcrops; Martínez- Torres et al., 2003), in the Maestrat Basin (Rodríguez-López et al., 2005), and in the Oliete sub-basin along the San Just outcrop (Peñalver et al., 2007b), both in the Teruel Province. In all these areas amber deposits were related to the progradation of a delta-estuarine system. In Peñacerrada-Montoria, amber accumulated in interdistributary bays within lower delta plain environments (Martínez-Torres et al., 2003), whereas in San Just, amber was deposited in freshwater ponds both within the upper delta plain and in the lower delta plain (Querol et al., 1992). Despite of the similarities between the depositional environments of all the amber-rich deposits of the Lower Cretaceous of Spain, it is worth noting that the depositional environment of the El Soplao amber presents a slight marine influence, as it can be inferred from the presence of some small marine bivalves and gastropods within the amber deposit and bryozoans and serpulids incrusting the surface of some amber samples. In the amber from southwestern France, marine influence has been pointed out as well, but directly evidenced from marine microfossil inclusions like marine diatoms, radiolarians, sponge spicules, and foraminifers (Girard et al., 2008). On the contrary, amber deposits from Lebanon (Azar et al., 2003; Veltz, 2008) and the Isle of Wight (United Kingdom) (Jarzembowski et al., 2008) were accumulated in more proximal delta environments and fluviatile channel deposits with a larger continental influence.

Stratigraphic models for clastic deposition generally suggest that regressive wave-dominated shallow marine systems develop during sea-level falls, whereas tidally influenced paralic coal-rich deposits develop during the transgressive infilling of incised valleys (e.g., Allen and Posamentier, 1993). The majority of these case studies came from areas with relatively simple tectonic settings and subsidence patterns, such as the Cretaceous of the Western Interior Seaway in North America (Posamentier and Vail, 1988) and Quaternary successions along passive margins (e.g., Allen and Posamentier, 1993). In these studies, the tectonic influence on sequence arrangement is relatively minor and the eustatic fluctuation in sea level is the principal control on stratal succession. In contrast, the Las Peñosas Fm. was deposited in rifting setting during a period of major tectonic rearrangement across the entire Basque-Cantabrian Basin, with active faulting that resulted in uplift and marked subsidence changes over short distances (García-Mondéjar et al., 1996, 2003). It is in this context that local regression occurred with coeval progradation of siliciclastic coastal deposits.

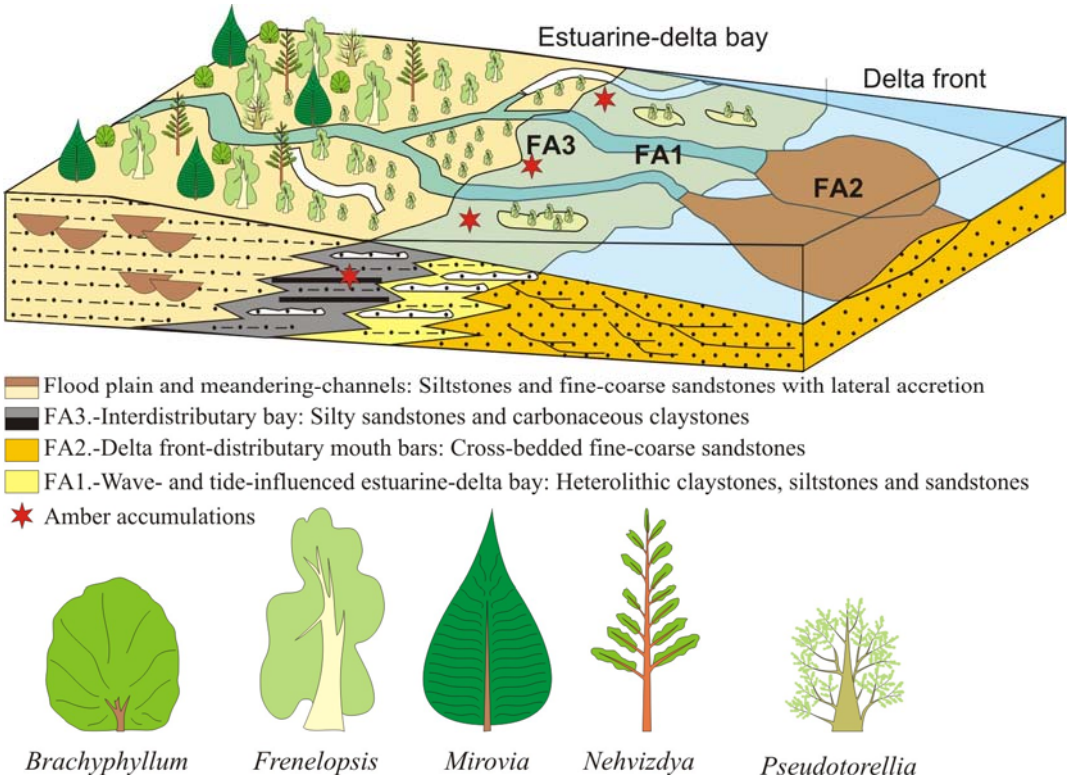

Figure 8.- Block diagram illustrating an idealized model of the depositional environments during sedimentation of the amber- and coal-rich levels. The accumulation of amber- and coal-rich sediments took place during the maximum regressive episode of the estuarine-delta progradation. FA: Facies association.

THE AMBER

General characteristics and morphological types

Trees can produce different kind of resins depending on what structural part is noted, such as roots, trunk, branches and leaves (Langenheim, 1995). It has long been known that resins are exuded outside the plant as defence from megaherbivores, insects, and pathogens, such as fungi (especially in the tropics), viruses, other microbes and bacteria. Presently, no methodology is available to differentiate what parts of the tree were involved in the origin of different amber types. Due to the relative abundance of amber at several outcrops, it is generally supposed that the exudation of the original resin occurred mainly in trunks. Our observations of *Agathis australis* in New Zealand

subtropical forest suggest that roots were probably significant producers of resin during the past, attributable to copious exudations of root-generated resin.

The new Albian deposit described herein is unusually rich in amber flows of different types formed under aerial conditions by liquid resin (containing flow structure). Normally, these flows are very rich in bioinclusions, especially small insects. The richest flows are stalactite-shaped amber pieces (Figs. 9A-9B). These cylindrical or subcylindrical pieces commonly contain very well preserved bioinclusions in clear yellow amber. The amber flows also include sub-spherical or elongated specimens with a pattern of striations and bulges and apparently an attached scar suggesting a bark pattern. This morphology indicates that the flows originated by viscous resin under aerial conditions. The viscous resin avoided capture of insects and plant debris due to the short time that these structures remained surficially sticky. Other specimens are plain or unelaborated in shape with several layers accumulating by different flows by less viscous resin with marks indicating aerial conditions (Fig. 9C). This last type usually contains abundant bioinclusions.

A different type are the kidney-shaped masses, normally very large in size (up to a decimetre in diameter) with an external surface slightly granulose that lacks evidence of aerial exposure (Fig. 9D). Some authors consider that this type of mass had formed by subterranean resin secretion from roots, probably explaining their lack of bioinclusions. These amber masses also are abundant in the El Soplao outcrop.

Of gemmological interest, abundant blue amber pieces (Fig. 6D) were found, similar to the noted blue amber from the Dominican Republic (Bellani et al., 2005). Both are the only well-known occurrences of this type of amber. A fluorescent blue glow appears in these pieces under normal sunlight, and under ultraviolet light it glows a bright milky-blue. In contrast, under artificial light these fragments show the typical honey-reddish colour of the Cretaceous amber.

Geochemistry

The Fourier Transform Infrared Spectroscopy (FTIR) is a solid-state spectroscopic technique usually used to characterize ambers (Langenheim and Beck, 1965). Nevertheless, the majority of fossil resins of the same geological range often show similar patterns preventing objective classification.

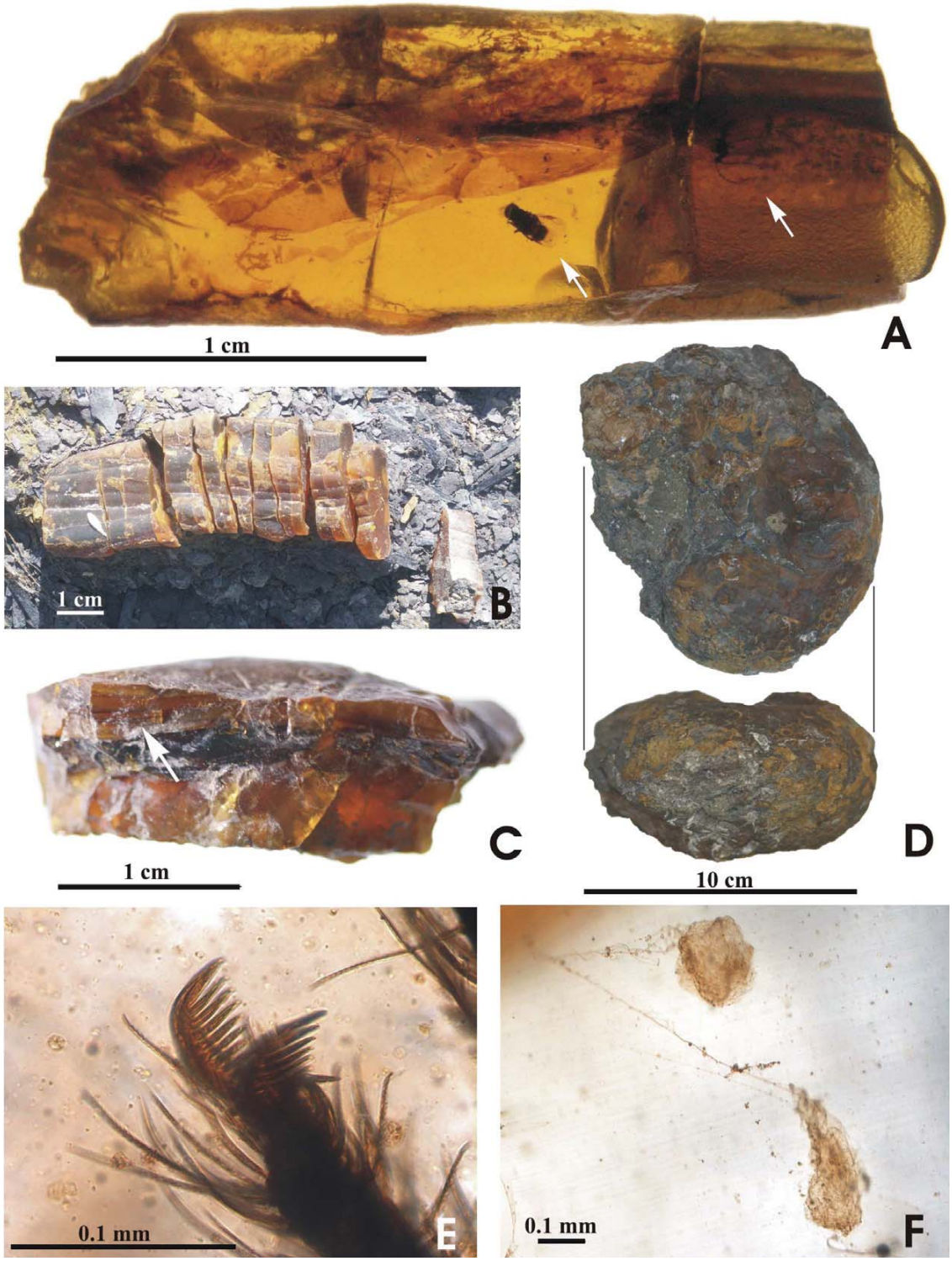

Figure 9.- Different types of amber pieces and amber bioinclusions related to spiders from El Soplao (Rábago, Cantabria). **A)** Stalactite-shaped amber flow with a wasp of the family Megaspilidae -left arrow- trapped on a spider web fragment (see detail of the spider web in 9F) and two insects shown in figure 12C -right arrow-. **B)** Stalactite-shaped amber flow exposed in situ which contained a scelionid wasp. **C)** Amber flow (crust); arrow indicates some flows that originated from liquid resin and cover a copious flow of dark amber. **D)** Big kidney-shaped mass in two views. **E)** Pectinate paired claws, adapted to efficient handling of silk and locomotion on an aerial web, present in an Araneoidea spider. **F)** Detail of the spider web fragment which trapped a megaspilid wasp. Images E and F were made with integrated consecutive pictures taken at successive focal planes.

Gas Chromatography-Mass Spectrometry (GC-MS) determines the individual non-volatile amber compounds and their molecular structure, and also suggests the plant producer (Grimalt et al., 1988; Chaler and Grimalt, 2005). Previous GC-MS studies on Cretaceous amber from Álava (southern Basque-Cantabrian Basin) indicate that some isolated compounds found may have originated from agathic acid, suggesting that the genus *Agathis*, or a close genus of Araucariaceae (Coniferales), was the amber producer (Alonso et al., 2000; Chaler and Grimalt, 2005). The palynological study supported this indication, because it revealed that a high percentage of pollen grains related to Araucariaceae (Barrón et al., 2001). Nevertheless, currently no araucariacean meso- or macro-remains have been found within the Álava amber or in the surrounding rock.

Here, we compare the FTIR of recent *Agathis australis* resin and amber samples from El Soplao (Fig. 10). The *Agathis* resin is a mixture of mono-, sesqui- and diterpenes, and each of its 13 species has a characteristic mixture of diterpenoid acids. Today this araucariacean genus produces large quantities of resin under natural conditions which polymerize rapidly, forming indurated masses. Recent studies from the Álava amber (Chaler and Grimalt, 2005) indicate that all samples show branched monoalkybenzenes, bicyclic sesquiterpenoids and tricyclic diterpenoids related to pimaric acid precursors, suggesting a distinctive palaeobotanic origin from *Agathis*-like species.

Three amber samples were analysed from the El Soplao amber: i) a fragment of a stalactite-like amber piece from an organic-rich clay level (AMB82); ii) a fragment of large kidney-shaped mass, red in colour, found in an organic-rich sand layer (AMB80), and iii) a fragment of orange kidney-shaped mass from an organic- rich clay level (AMB81). A fragment of stalactiteshaped dry resin from *Agathis australis* also was analysed for comparison (AMB83). The FTIR spectra obtained are shown in Fig. 10.

Structural changes in the organic components of the amber samples are due to maturation processes during rock diagenesis. In the evaluation of the maturity of the coal and organic matter from the Escucha Fm. and other Early Cretaceous Spanish basins, such as the Maestrat Basin and the Basque-Cantabrian Basin, the thermal analysis based on the vitrinite reflectance (%R) suggests around 52ºC as maximum temperature from modelling (Sangüesa and Arostegui, 2003; Permanyer, pers. comm.) The FTIR analyses (transmittance and absorbance) of the amber pieces of El Soplao show that all three spectra are practically identical. The IR spectra of all samples exhibited the same bands, but with different intensities (Fig. 10). In absorbance, all

spectra show similar relative intensity, but in the sample AMB80, which corresponds to a red amber fragment, the intensity decreases at wave-numbers 727 and 814 cm-1, and increases considerably at approximately wave-number group 1714 cm-1, a complex band associated with carboxyl groups (Fig. 10). In this sample we also observe broad absorption bands at ca. 3460 and 1635 cm-1, the signal due to water or possibly to weathering. The spectra coincide in the major features with the previous results obtained from other Spanish Cretaceous ambers (see FTIR spectra in Alonso et al., 2000; Chaler and Grimalt, 2005; Peñalver et al., 2007a, 2007b; Corchón et al., 2008). All the spectra are dominated by small C-H stretching bands near 2950 cm-1, C-H banding occurs between 1470 and 1380 cm-1, and the carbonyl bands are close to 1700 cm-1. The lack of exocyclic methylenic bands at 880, 1640 and 3070 cm-1 is consistent with the high maturity of the amber.

When the IR absorbance spectra is compared between the amber sample AMB82, an aerial stalactite, and the sample AMB83, a fragment of recent stalactite of the araucariacean *Agathis australis* (Fig. 10), numerous differences may be observed. However, without GC-MS studies, the origin of the variable intensity and the presence of several bands cannot be possibly known. The presence of the absorption maximum in the single-band around 3081 cm-1 is typical in *Agathis* resin; however, it is typically absent in amber due to the polymerization of the resin and increasing maturity. In addition, the spectra around range bands 1650-1700 cm-1, corresponding to the carboxyl groups, is very different between the amber and the resin. The intensity of absorption at wave-numbers 3400 and 1700 cm-1 decreases according to an increase in the maturity level of the samples. Other bands observed constitute an unresolved group near wave number 2930 cm-1 (C-H st), the most intens group band known for all Cretaceous spectra.

FOSSIL RECORD

Plant cuticle compressions

Exceptionally well preserved plant cuticle compressions are very abundant in the El Soplao amber deposit (Fig. 11), sometimes accumulating in levels up to 10 cm thick. The palaeobotanical samples taken from these levels also show amber and woody fragments, but at less percentage than plant-cuticle compressions (Figs. 11A-11D).

Amber pieces show various shapes and colours from yellow to red (Fig. 11A), whereas unidentified, small, dark, woody fragments are preserved as spheroidal, charcoalified masses or charcoals (Fig. 11B).

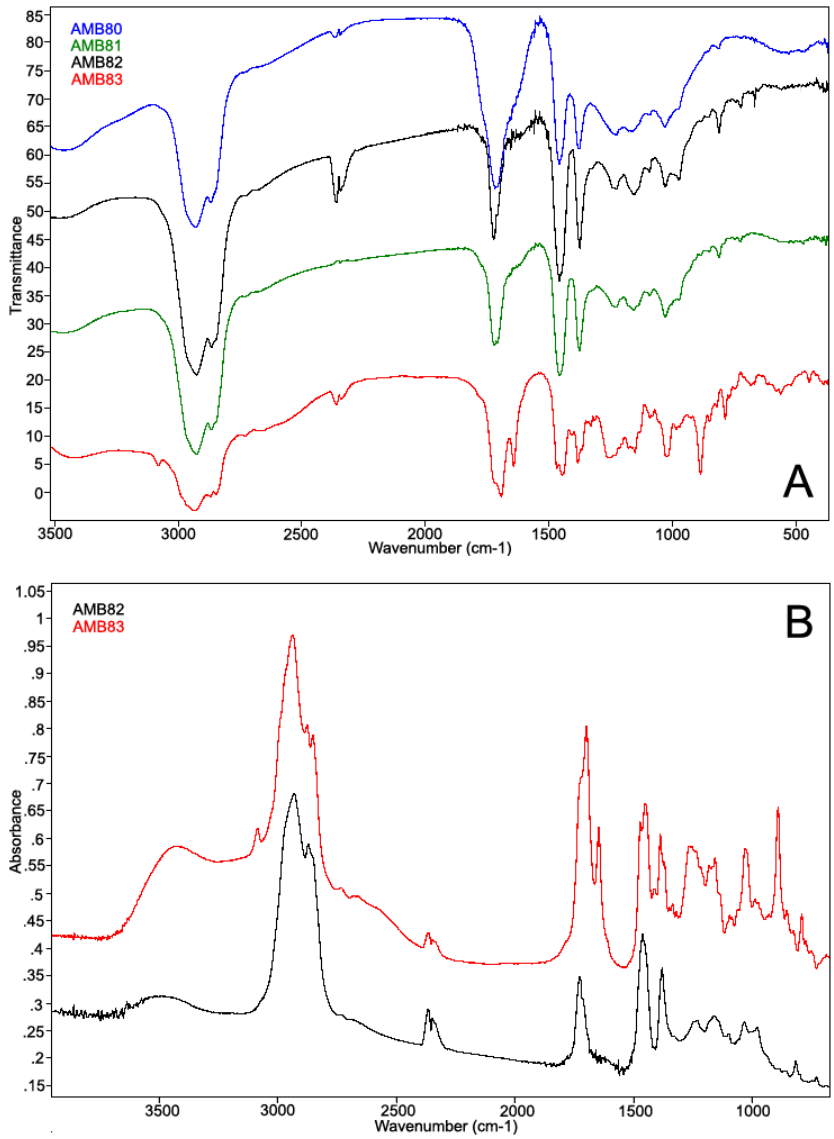

Figure 10.- **A)** Transmittance IR spectra of El Soplao amber: AMB80 red amber from a kidney-shaped mass found within sands; AMB81 orange amber from a kidney-shaped mass found within clays; AMB82 orange amber from a stalactite-shaped flow, found within clays; and AMB83 dry resin from an Agathis australis stalactite-like flow, New Zealand in origin. **B)** IR absorbance spectra from the El Soplao amber and dry resin of Agathis australis, both samples analysed came from stalactite-shaped flows.

Cuticle fragments of the conifer *Frenelopsis*, of the extinct family Cheirolepidiaceae (Gomez et al., 2002), are the most numerous plant-cuticle components (Fig. 11C). These coniferous axes typically constitute cylindrical internodes bearing apically a nodal whorl of three leaves (Fig. 11E). Some *Frenelopsis*

sp. cuticles also show a particular branching of axes borne in the internode (Fig. 11F) (see Daviero et al., 2001 for architectural details). A female cone scale formed by several layers of very thin cuticle (Fig. 11P) constitutes a doubtful record of the genus *Alvinia* Kva ˇcek (Kvaˇcek, 2000), associated with *Frenelopsis* vegetative material. Additionally, the conifer *Mirovia* sp. of the extinct family Miroviaceae (Gomez, 2002) shows about the same quantity of leaf cuticle fragments (Fig. 11D). The leaves clearly display a white central line on one side corresponding to the single middle stomatal-bearing groove, as well as a mucronate apex and suction-pad-shaped base (Figs. 11G-11H). Such leaves have been also described from the Albian of Pyrenees (Corça) and Teruel (Rubielos de Mora) (Gomez, 2002). Also present are two conifer leafy axes of *Brachyphyllum*-type with tiny, helicoidally arranged leaves (Figs. 11L-11M). In addition, two types of ginkgolean leaves also occur. *Nehvizdya* sp. shows obovate leaves with variable apex shapes (Fig. 11I) and attenuate base (Fig. 11J) (Gomez et al., 2000). The venation pattern showing several successive dichotomies and the presence of resin bodies between the veins are clearly seen in the most transparent leaves. In Spain, *Nehvizdya penalveri* has been reported only from the Albian of Rubielos de Mora in Teruel (Gomez et al., 2000). Other ginkgolean leaves are represented by *Pseudotorellia* sp. It has narrow leaves with three stomatal bands located on one side (Fig. 11K). This genus has also been described from the Albian of Rubielos de Mora in Teruel (Gomez, 2000). In addition, it has distinctive reproductive organs similar to the genus *Nehvizdyella* Kva ˇcek (Kva ˇcek et al., 2005), which probably are ovules associated with *Nehvizdya* (Figs. 11N-11O).

Arthropod inclusions

Until now, the arthropods found as inclusions in the El Soplao amber have been spiders and insects. All specimens are small in size, less than 1 cm long, and are well preserved, possessing slight deformation due to pressure. Apparently, the degree of maturation of the amber is slightly higher than the San Just and Álava ambers, because the external surface of the insects is dark, without a silvery gaseous film. That film produces silver-hued reflections under strong direct illumination and makes the appreciation of microsculptural details easier. Formal taxonomy of the new taxa of arthropods will be published elsewhere, principally by Paul Selden and one of us during the completion of a Doctoral Thesis (R.P.F.). Thus, only a brief overview of the most important specimens is presented below.

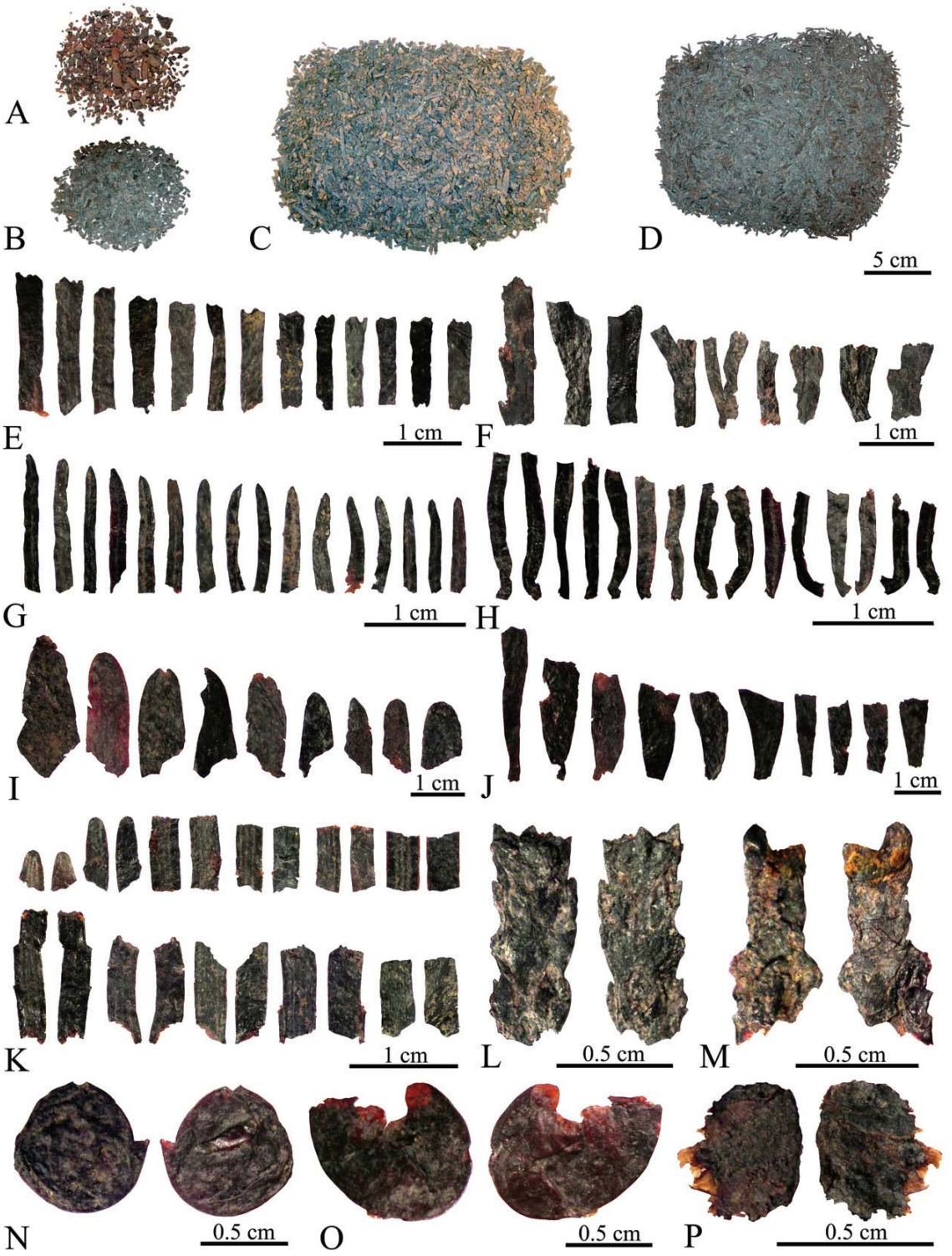

Figure 11.- **A, D)** Four major palaeobotanical components sorted out from a sediment sample (all to the same scale). **A)** Yellow to red amber pieces. **B)** Wood fragments. **C)** Frenelopsis sp. cuticles. **D)** Mirovia sp. cuticles. **E, F)** Internodes of Frenelopsis sp. **E)** Apical nodal whorl of three leaves. **F)** Intra-internodal branching of axes. **G, H)** Leaves of Mirovia sp. **G)** A single middle stomatal groove and a mucronate apex. **H)** Suction-pad-shaped base. **I, J)** Leaves of Nehvizdya sp. **I)** Variable shapes of apices. **J)** Attenuate bases. **K)** Leaves of Pseudotorellia sp., showing two apices and three or more stomatal bands on one side of the leaves. **L, M)** Two Brachyphyllum-type leafy axes, showing small, helicoidally arranged leaves. **N, O)** Ovules of cf. Nehvizdyella sp.,. **P)** cf. Alvinia sp., a multilayered female cone scale of Frenelopsis sp.

One of the most remarkable finds is a virtually complete spider specimen. The excellent preservation of the legs shows detailed structure of the tarsal claws (Fig. 9E). The tarsi have large, pectinate paired claws with one row of nine teeth and one small, non-pectinate median claw and numerous serrate bristles, similar to the Araneoidea specimen described by Selden (1989) from the Early Cretaceous limestones of El Montsec (Lleida Province, northeastern Spain). Subsequently, the Montsec specimen was described as *Cretaraneus vilaltae* by Selden (1990) and assigned to the orb-weaver family Tetragnathidae by Selden and Penney (2003). The characteristic claw morphology is structured for an efficient handling of silk and locomotion on an aerial web. Peñalver et al. (2006) published the oldest web with entrapped preys, most likely an orb web, from San Just amber. Penney and Ortuño (2006) described a spider from Álava amber, which displays three tarsal claws and accessory setae, as the oldest true orb-weaving spider, but without illustration and more detailed description of this crucial structure. Also, from the El Soplao amber, a portion of an aerial spider web was found (Fig. 9F), which trapped a small wasp of the family Megaspilidae. This new spider web has a different structure than the specimen from San Just amber. Both the spider specimen and aerial web found in the El Soplao amber shed light on and support the role of aerial webs in the palaeoecology of Cretaceous forests discussed by Peñalver et al. (2006, 2008).

The insect orders found to date in this new site also are the most abundant in other Cretaceous deposits (Fig. 12). These co-occurring orders are Thysanoptera (Fig. 12A), Hymenoptera (Fig. 12B), Blattaria (Fig. 12D), Hemiptera, Coleoptera, and Diptera; the last two are especially plentiful (Figs. 12C-12D). Raphidioptera and Neuroptera have a scarce record in El Soplao as is common in Cretaceous ambers.

Hymenopterans were represented previously by the families Scelionidae (Figs. 12B and 12D), Mymarommatidae, and Megaspilidae (Fig. 9A). The extinct family Mymarommatidae, or false fairy wasps, are among the smallest of Hymenoptera and constitute a very important record for the El Soplao amber, represented by a complete winged female of a new morphotype of the extinct genus *Archaeromma*. The family includes only five genera, three extant and two extinct genera (Gibson et al., 2007). The fossil record of this family is very scarce and is only preserved in amber. The genus *Archaeromma* contains eight species (Gibson et al., 2007; Engel and Grimaldi, 2007).

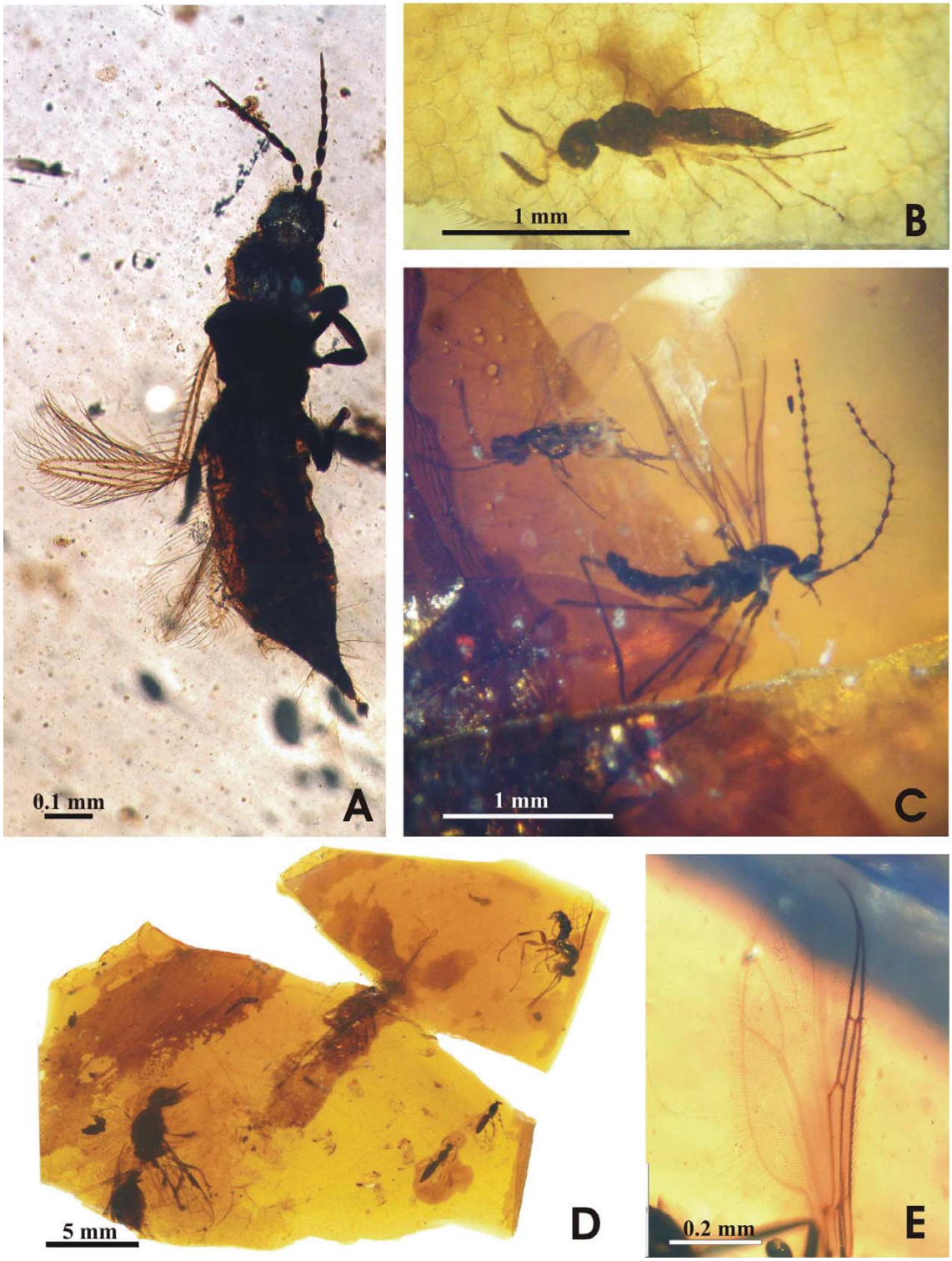

Figure 12.- Fossil insects as bioinclusions in El Soplao amber. **A)** Thysanopteran specimen. **B**) Female wasp of the family Scelionidae. **C)** Chalcidoidean wasp -top- and dipteran of the family Cecidomyiidae (gall midges). **D)** Amber fragment with seven wasps and one immature cockroach in the centre of the preparation. **E)** Wing of Archiaustroconops sp. Images A and E were made with integrated consecutive pictures taken at successive focal planes**.**

This group of minute wasps is characterized by having a head capsule with a hyperoccipital band of pleated membrane separating the frontal plate from the flat occipital plate; an occipital foramen originating at ventral margin of occipital plate; mandibles exodont; female antennae with 6 or 7 funicular segments and 3 or 4 larger distal segments which form a compact tube; and other characters (Gibson et al., 2007). Due to their small size and unusual morphological characters, they are suspected egg parasitoids. The new record from the El Soplao amber is the oldest for this genus.

Among the most interesting insect records in the El Soplao amber are biting midges (Diptera: Ceratopogonidae). The genus *Archiaustroconops*, of the subfamily Austroconopinae, is the only Cretaceous Ceratopogonidae with two well-developed radial cells, an oblique r-m vein (Fig. 12E), and a foreleg/hindleg tarsal ratio ≥ 1.4 (Borkent, 2000). The genus includes six species known only from Lower Cretaceous Lebanese and Álava ambers (Borkent, 2000). It is represented in the El Soplao amber by one new morphotype (Fig. 12E), clearly different from *A. alavensis* found in Álava amber. This new morphotype is characterized by having a strongly elongate first radial cell. Most interesting is the presence of a new taxon of the rare genus *Lebanoculicoides* (Fig. 13), which is only known by two specimens described as *L. mesozoicus* from Lebanese amber (Szadziewski, 1996). This genus is the only member of the Ceratopogonidae having a wing with fully developed R1, R3 and R4+5 veins. This character, among others, indicates that *L. mesozoicus* is the sister group of all other Ceratopogonidae and for that reason it had been included in its own subfamily, named Lebanoculicoidinae by Borkent (2000). The new morphotype differs mainly from the other known species by having ovoidal flagellomeres (not cylindrical) and R4+5 vein terminating in a basal position before reaching the wing apex.

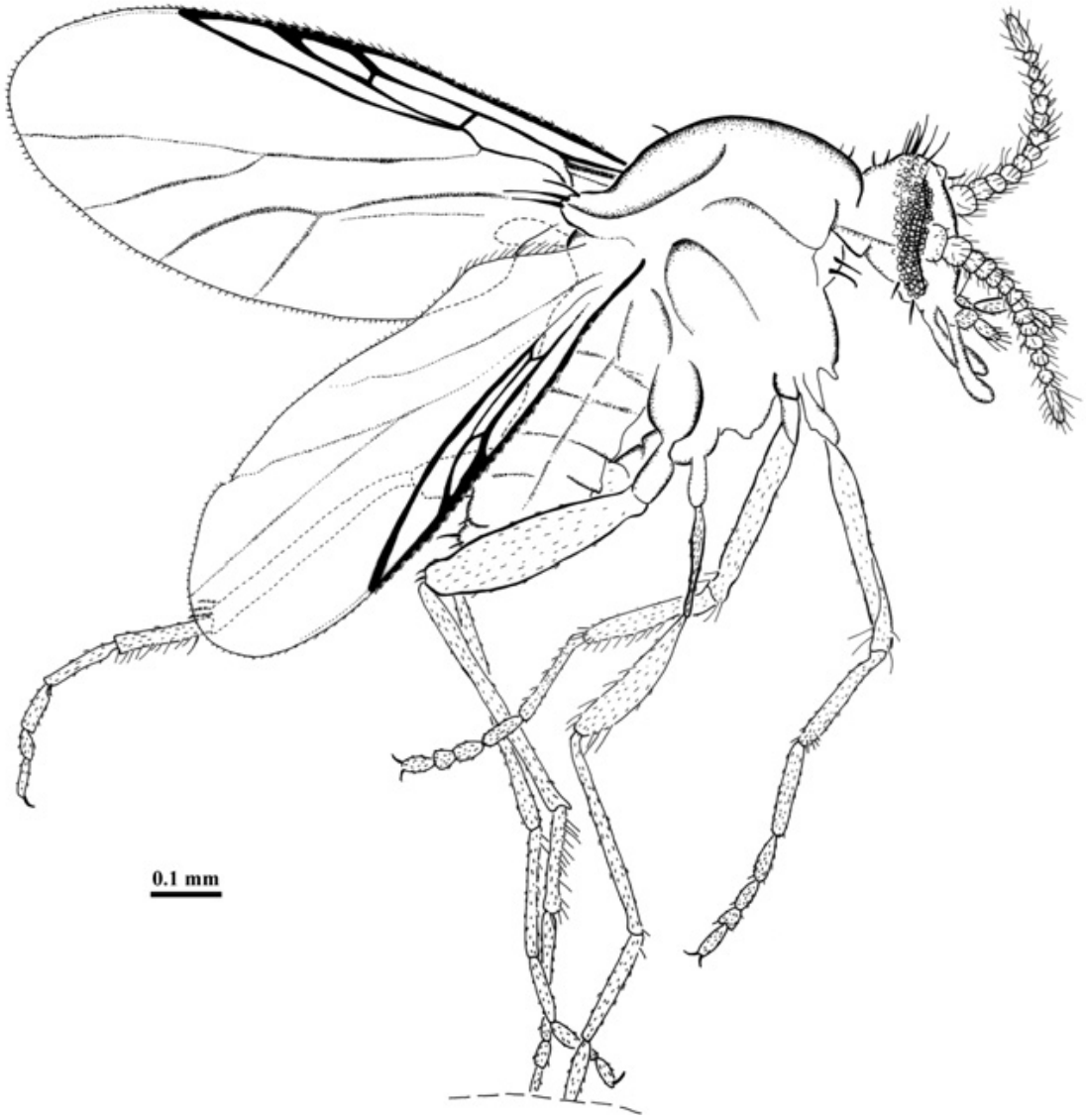

Figure 13.- Camera lucida drawing of Lebanoculicoides sp. (Ceratopogonidae: Lebanoculicoidinae) in lateral habitus, from the El Soplao amber**.**

DISCUSSION AND CONCLUDING REMARKS

Stratigraphic and sedimentologic analyses of the amber-bearing deposit of the Lower Albian Las Peñosas Fm. indicate that it was deposited on a regressive deltaic-estuarine environment. Facies associations are assigned to three different depositional units (P1 to P3). The stacking of these units and their internal vertical and lateral relationships resulted from an overall marine regressive phase followed by a transgressive marine phase, with the resin accumulation occurring at the most regressive part of the regressive-transgressive sequence (Unit P2). Sedimentological analysis of

this unit suggests that the amber deposit constitutes part of the infilling of interdistributary bays, which are laterally associated with distributary meandering channels. The amber-rich beds always contain abundant fragments of carbonaceous material, wood fragments and leaves that still preserve the vegetal textures. The amber-rich beds appear associated with laminated, organic clays, but also with discontinuous beds of massive to laminated sandstones and siltstones with disorganized fragments of woody material. These deposits also contain shells of marine and/or brackish-water molluscs, which suggest a littoral to coastal marsh environment of deposition. Therefore, the suggested depositional scenario for the amber-rich beds is an environment of low-energy coastal and interdistributary bays connected with the sea and affected episodically by higher-energy conditions. Floods during rain storms eroded and removed the amber and plant remains from their original place of accumulation at the soils of the coast-fringing forest. Then, the amber and plant fragments were transported by density flows that carried large amounts of these materials, mixed with mud and sand, to the coastal and interdistributary bays, where were rapidly accumulated and buried. Most of the amber pieces show their original form of subrounded and stalactite-shape suggesting little erosion during transport. A remarkable characteristic of this amber deposit is the unusual accumulation of aerial amber pieces that contain abundant arthropod and other bioinclusions.

The El Soplao deposit likely originated during a period of abundant production of fluid resin within the palaeoforests, possibly coinciding with a warmer episode. The plant-cuticle assemblage of the El Soplao deposit is quite reminiscent of that from the Albian of Rubielos de Mora (Teruel Province); (Gomez, 2000, 2002; Gomez et al., 2000, 2002). However, the latter deposit has poorly preserved amber and identification at the species level is tenuous, lacking the precision for any determination of amber production. Araucariacean trees are the suggested resin-producing plants during the Cretaceous (Alonso et al., 2000; Chaler and Grimalt, 2005), but leaf remains of this group of conifers are absent from the El Soplao assemblage, although they occur in other similar Spanish deposits. Future palynological studies will complete our understanding of the palaeobotanical context of this deposit.

The abundance of fossil insects in the Early Cretaceous amber of El Soplao is particularly important for further evolutionary studies and palaeoecological reconstructions. This abundance is a consequence of the unusual concentration of amber flows (stalactite-like amber flow pieces and crusts), which contain the most bioinclusions. The fidelity of the arthropod preservation in this amber allows for detailed studies of the ancient forest biota, similar to other Spanish ambers. The Albian age of the El Soplao amber also is of particular importance because during this period certain groups of insects were diversifying to become major pollinators of the first flowering plants. In this context, the presence of spiders and their entrapping aerial webs in El Soplao amber reinforces the hypothesis advocated by Peñalver et al. (2006, 2008) which associates the diversification of spiders to the radiation of winged (pterygote) insects.

Several insect specimens recorded from the El Soplao amber are very scarce in the fossil record, for instance wasps and dipterans. Such is the case for the wasp specimen that belongs to the extinct family Mymarommatidae. Discovery of a new form of the rare dipteran *Lebanoculicoides* in the El Soplao amber indicates that this basal genus had a much more extensive distribution than previously supposed during the Early Cretaceous. Consequently, any new findings of fossil representatives of these groups would be of particular interest.

The FTIR spectra of the El Soplao amber are quite similar to other previously studied Spanish Cretaceous ambers.

However, further investigations are necessary to complete the study of this new locality, including the taphonomic study of the deposit in order to know its origin, the palynological analysis of the amber-bearing stratigraphic sequence, determination of plant species represented as cuticles, and the taxonomic study of the arthropods included within the amber.

ACKNOWLEDGEMENTS

This work is part of the Ph.D. Thesis of the first author (M.N.), who is supported by a scholarship from the Instituto Geológico y Minero de España (IGME), and the Ph.D. Thesis of a co-author (R.P.F., palaeobiology), funded by an APIF grant of the University of Barcelona. This study is a contribution of the IGME projects 275-CANOA 35006 "Relación entre sedimentación tectónica y flujo de fluidos durante la extensión del Cretácico Inferior en la Cuenca de Santander"; 491-CANOA 35015 "Investigación científica y técnica de la Cueva de El Soplao y su entorno geológico", and the projects CGL2008- 00550/BTE and CGL2008-01237/BTE. The study is framed in a collaborative agreement among IGME, SIEC S.A. and the Cantabrian Government (Regional Cultural, Tourism and Sports Ministry). We are grateful to José Pedro Calvo Sorando (IGME) for his support and engagement. We also express our thanks to Francisco Javier López Marcano (Regional Minister of the Cantabrian Government) and Fermin Unzué (manager of the El Soplao Cave) for their efforts and promotion of the study of the new outcrop. One of the coauthors (E.P.) benefited from a "Ramón y Cajal" contract of the Spanish Ministry of Science and Innovation. B.G. also received support from the CNRS-UMR 5125 PEPS and the project ANR AMBRACE (No BLAN07-1-184190) of the French National Research Agency (L'Agence Nationale de la Recherche). The authors thank the editor for his patient and constructive reviews and Cynthia Voelker for the final review of the English writing. The manuscript benefited greatly from corrections and improvements by C. Labandeira and R. Salas.

REFERENCES

Allen, G.P., Posamentier, H.W., 1993. Sequence stratigraphy and facies model of an incised valley fill: the Gironde Estuary, France. Journal of Sedimentary Petrology, 63, 378–391.

Alonso, J., Arillo, A., Barrón, E., Corral, J.C., Grimalt, J., López, J.F., López, R., Martínez-Delclòs, X., Ortuño, V., Peñalver, E., Trincão, P.R., 2000. A new fossil resin with biological inclusions in Lower Cretaceous deposits from Álava (Northern Spain, Basque-Cantabrian Basin). Journal of Paleontology, 74, 158–178.

Arbizu, M., Bernárdez, E., Peñalver, E., Prieto, M.A., 1999. El ámbar de Asturias (España). Estudios del Museo de Ciencias Naturales de Álava, 14, 245–254.

Azar, D., 2000. Les Ambres Mésozoiques du Liban. Doctoral thesis. Université Paris XI Orsay, Paris, 165 pp.

Azar, D., Nel, A., Gèze. R., 2003. Use of Lebanese amber bioinclusions in paleoenvironmental reconstruction, dating and paleobiogeography. Acta Zoologica Cracoviensia, 46, 393–398.

Bandel, K., Shinaq, R., Weitschat, W., 1997. First insect inclusions from the amber of Jordan (Mid Cretaceous). Mitteilungen des Geologisch-Paläontologischen Institutes der Universität Hamburg, 80, 213–223.

Barrón, E., Comas-Rengifo, M.J., Elorza, L., 2001. Contribuciones al estudio palinológico del Cretácico Inferior de la Cuenca Vasco-Cantábrica: los afloramientos ambarígenos de Peñacerrada (España). Coloquios de Paleontología, 52, 135–156.

Bellani, V., Giulotto, E., Linati, L., Sacchi, D., 2005. Origin of the blue fluorescence in Dominican amber. Journal of Applied Physics, 97, 016101-1 – 016101-2.

Blakey, R.C., 2008. Global Paleogeographic Views of Earth History: Late Precambrian to Recent. http://jan.ucc.nau.edu/~rcb7/120moll.jpg.

Borkent, A., 2000. Biting midges (Ceratopogonidae: Diptera) from Lower Cretaceous Lebanese amber with a discussion of the diversity and patterns found in other ambers, In: Grimaldi, D. (eds.). Studies on Fossils in Amber, with Particular Reference to the Cretaceous of New Jersey, Backhuys Publishers Leiden, 355–451.

Chaler, R., Grimalt, J., 2005. Fingerprinting of Cretaceous Higher Plant Resins by Infrared Spectroscopy and Gas Chromatography Coupled to Mass Spectrometry. Phytochemical Analysis, 16, 446–450.

Corchón, M.S., Mateos, A., Álvarez-Fernández, E., Peñalver, E., Delclòs, X., Van der Made, J., 2008. Ressources complémentaires et mobilité dans le Magdalénien cantabrique. Nouvelles données sur les mammifères marins, les crustacés, les mollusques et les roches organogènes de la Grotte de Las Caldas (Asturies, Espagne). L'Anthropologie, 112, 284–327.

Crowley, T.J., North, G.R., 1991. Distribution of climatically sensitive deposits for the Mid-Cretaceous (Aptian–Albian–Cenomanian, 120–90 Ma.). Paleoclimatology-

Oxford Monographs on Geology and Geophysics ed. Oxford University Press, 18, 157 pp.

Cruickshank, R.D., Ko, K., 2003. Geology of an amber locality in the Hukawng Valley, northern Myanmar. Journal of Asian Earth Sciences, 21, 441–455.

Dalrymple, R.W., 1992. Tidal depositional systems. In: Walker, R.G., James, N.P. (eds.). Facies Models: Response to Sea Level Change. Geological Association of Canada, 195–218.

Dalrymple, R.W., Knight, R.J., Zaitlin, B.A., Middleton, G.V., 1990. Dynamics and facies model of a macrotidal sandbar complex, Cobequid Bay- Salmon river estuary (Bay of Fundy). Sedimentology, 37, 577–612.

Daviero, V., Gomez, B., Philippe, M., 2001. Uncommon branching pattern within conifers: *Frenelopsis turolensis*, a Spanish Lower Cretaceous Cheirolepidiaceae. Canadian Journal of Botany, 79, 1400–1408.

Delclòs, X., Arillo, A., Peñalver, E., Barrón, E., Soriano, C., López del Valle, R., Bernárdez, E., Corral, C., Ortuño, V.M., 2007. Fossiliferous amber deposits from the Cretaceous (Albian) of Spain. Comptes Rendus Palevol, 6, 135–149.

Engel, M.S., Grimaldi, D., 2007. New false fairy wasps in Cretaceous amber from New Jersey and Myanmar (Hymenoptera: Mymarommatoidea). Transactions of the Kansas Academy of Sciences, 110, 159–168.

Fernández Viejo, G., Gallastegui, J., 2005. The ESCI-N Project after a decade: a synthesis of the results and open questions. Trabajos de Geología, Universidad de Oviedo, 25, 9–25.

Folkestad, A., Satur, N., 2008. Regressive and transgressive cycles in a rift-basin: Depositional model and sedimentary partitioning of the Middle Jurassic Hugin Formation, southern Viking Graben, North Sea. Sedimentary Geology, 207, 1–21.

García-Espina, R., 1997. La estructura y evolución tectonoestratigráfica del borde occidental de la Cuenca Vasco-Cantábrica (Cordillera Cantábrica, NO de España). Doctoral thesis. Universidad de Oviedo, 230 pp.

García-Mondéjar, J., 1990. The Aptian–Albian carbonate episode of the Basque-Cantabrian Basin (northern Spain): General characteristics, controls and evolution. International Association of Sedimentologists, 9, 257–290.

García-Mondéjar, J., Aguirrezabala, L.M., Aranburu, A., Fernández-Mendiola, P.A., Gómez-Pérez, I., López-Horgue, M., Rosales, I., 1996. Aptian–Albian tectonic

pattern of the Basque-Cantabrian Basin (northern Spain). Geological Journal, 31, 13–45.

García-Mondéjar, J., López-Horgue, M.A., Aramburu, A., Fernández-Mendiola, P.A., 2003. Pulsating subsidence during a rift episode: stratigraphic and tectonic consequences (Aptian–Albian, northern Spain). Terra Nova, 17, 517–525.

García- Mondéjar, J., Pujalte, V., 1982. Región Vasco-Cantábrica y Pirineo Navarro. In: Universidad Complutense de Madrid (eds.). El Cretácico de España, 49–159.

Gibbs, A.D., 1990. Linked fault families in basin formation. Journal of Structural Geology, 12, 796–803.

Gibson, G.A., Read, J., Huber, J.T., 2007. Diversity, Classification and Higher Relationships of Mymarommatoidea (Hymenoptera). Journal of Hymenoptera Research, 16, 51–146.

Girard, V., 2008. Microcenoses des ambres medio - Crétacés français. Taphonomie, systématique, paléoécologie et reconstitution du paléoenvironnement. Doctoral thesis. Université Rennes, 310 pp.

Girard, V., Schmidt, A.R., Saint Martin, S., Struwe, S., Perrichot, V., Saint Martin, J.P., Grosheny, D., Breton, G., Néraudeau, D., 2008. Evidence for marine microfossils from amber. Proceedings of the National Academy of Sciences, 105, 17426-17429.

Gomez, B., 2000. Paléoenvironnements de la marge occidentale de la Téthys au Crétacé inférieur; apports taxonomiques et taphonomiques de gisements espagnols. Doctoral thesis. University Claude Bernard Lyon, 218 pp.

Gomez, B., 2002. A new species of *Mirovia* (Coniferales, Miroviaceae) from the Lower Cretaceous of the Iberian Ranges (Spain). Cretaceous Research, 23, 761–773.

Gomez, B., Martín-Closas, C., Barale, G., Solé de Porta, N., Thévenard, F., Guignard, G., 2002. *Frenelopsis* (Coniferales: Cheirolepidiaceae) and related male organ genera from the Lower Cretaceous of Spain. Palaeontology, 45, 997–1036.

Gomez, B., Martín-Closas, C., Barale, G., Thévenard, F., 2000. A new species of *Nehvizdya* (Ginkgoales) from the Lower Cretaceous of the Iberian Ranges (Spain). Review of Palaeobotany and Palynology, 111, 49–70.

Gradstein, F.M., 2004. A Geologic Time Scale 2004. Cambrige University Press.

Greenblatt, C.L., Davis, A., Clement, B.G., Kitts, C.L., Cox, T., Cano, R.J., 1999. Diversity of microorganisms isolated from amber. Microbial ecology, 38, 58–68.

Grimalt, J., Simoneit, B.R.T., Hatcher, P.G., Nissenbaum, A., 1988. The molecular composition of ambers. Organic Geochemistry, 13, 677–690.

Haywood, A.M., Valdes, P.J., Markwick, P.J., 2004. Cretaceous (Wealden) climates: a modelling perspectiva. Cretaceous Research, 25, 303–311.

Hines, F.M., 1985. Sedimentation and tectonics in north-west Santander. In: 6th European Regional Meeting, Excursion Guidebook. Milá, M.D. and Rosell, J. (eds.). International Association of Sedimentologists, 371–398.

Huber, B.T., Hodell, D.A., Hamilton, C.P., 1995. Middle–Late Cretaceous climate of the southern high latitudes; stable isotopic evidence for minimal equator-to-pole thermal gradients. Geological Society of American Bulletin, 107, 1164–1191.

Jarzembowski, E.A., Azar, D., Nel, A., 2008. A new chironomid (Insecta: Diptera) from Wealden amber (Lower Cretaceous) of the Isle of Wight (UK). Geologica Acta, 6, 285–291.

Kaddumi, H.F., 2005. Amber of Jordan: the Oldest Prehistoric Insects in Fossilized Resin. Amman, ed. Kaddumi, 168 pp.

Kitazawa, T., 2007. Pleistocen macrotidal tide-dominated estuary-delta succession, along the Dong Nai River, southern Vietnam. Sedimentary Geology, 194, 115–140.

Kuecher, G.J., Woodland, B. G., Broadhurst, F. M., 1990. Evidence of deposition from individual tides on a tidal cycles from the Francis Creek Shale (host rock to the Mazon Creek Biota) Westphalian D (Pennsylvanian), north-eastern Illinois. Sedimentary Geology, 68, 211–221.

Kvaček, J., 2000. *Frenelopsis alata* and its microsporangiate and ovuliferous reproductive structures from the Cenomanian of Bohemia (Czech Republic, Central Europe). Review of Palaeobotany and Palynology, 112, 51–78.

Kvaček, J., Falcon-Lang, H., Dašková, J., 2005. A new Late Cretaceous ginkgoalean reproductive structure *Nehvizdyella* gen. nov. from the Czech Republic and its whole-plant reconstruction. American Journal of Botany, 92, 1958–1969.

Langenheim, J.H., 1995. Biology of Amber-Producing Trees: Focus on Case Studies of *Hymenaea* and *Agathis*. In: Anderson, K.B., Crelling, J.C (eds.). Amber, Resinite, and Fossil Resins, Washington, ACS Symposium Series 617, 1–32.

Langenheim, J.H., Beck, C.W., 1965. Infrared Spectra as a Means of Determining Botanical Sources of Amber. Science 149 (3679), 52–54.

Lindl. in Laoud, 1829. In: Encyclp. Pl, Moore and Edgard (eds.). Fl. New Zealand, 2, 329 (1976).

Malod, J.A., Mauffret, A., 1990. Iberian plate motions during the Mesozoic. Tectonophysics, 184, 261–278.

Martill, D.M., Loveridge, R.F., de Andrade, J.A.F.G., Cardoso, A.H., 2005. An unusual ocurrence of amber in laminated limestones: the Crato Formation lagerstätte (Early Cretaceous) of Brazil. Paleontology, 48, 1339–1408.

Martín-Chivelet, J., Berasategui, X., Rosales, I., Vilas, L., Vera, J.A., Caus, E., Gráfe, K.U., Mas, R., Puig, C., Segura, M., Robles, S., Floquet, M., Quesada, S., Ruiz-Ortiz, P.A., Frenegal-Martínez, M.A., Salas, R., García, A., Martín-Algarra, A., Arias, C., Meléndez, M., Chacón, B., Molina, J.M., Sanz, J.L., Castro, J.M., García-Hernández, M., Carenas, B., García-Hidalgo, J., Gil J., Ortega, F., 2002. Cretaceous. In: Gibbons, W. and Moreno, T. (eds.). The Geology of Spain, The Geological Society, 255–292.

Martínez-Delclòs, X., Briggs, D.E.G., Peñalver, E., 2004. Taphonomy of insects in carbonates and amber. Palaeogeography, Palaeoclimatology, Palaeoecology, 203, 19–64.

Martínez-Torres, L., Pujalte, V., Robles, S., 2003. Los yacimientos de ámbar del Cretácico Inferior de Montoria-Peñacerrada (Álava, Cuenca Vasco-Cantábrica): Estratigrafía, reconstrucción paleogeográfica y estructura tectónica. Estudios del Museo de Ciencias Naturales de Álava, 18, 9–32.

McCarthy, P.J., Plint, A.G., 2003. Spatial variability of paleosols across Cretaceous interfluves in the Dunvegan Formation, NE British Columbia, Canada: palaeohydrological, palaeogeomorphological and stratigraphic implications. Sedimentology, 50, 1187–1220.

Medioli, F.S., Scott, D.B., Collins, E.S., Wall, J.H, 1990. Thecamoebians from the early Cretaceous deposits of Ruby Creek, Alberta (Canada). In: Hemleben, C., Kaminski, M.A., Kuhnt, W., Scott, D.B. (eds.), Paleoecology, Biostratigraphy, Paleoceanography and Taxonomy of Agglutinated Foraminifera, NATO Advanced Study Institute Series, Series C, Mathematical and Physical Sciences, 327, 793–812.

Moreno-Bedmar, J.A., Bulot, L., Latil, J.L., Martínez, R., Ferrer, O., Bover-Arnal, T., Salas, R., 2008. Precisiones sobre la edad de la base de la Formación Escucha,

mediante ammonoideos, en la subcuenca de la Salcedella, Cuenca del Maestrat (E Cordillera Ibérica). Geo-temas, 10, 159–162.

Morley, R.J., 2000. Origin and Evolution of Tropical Rain Forests. In: Chichester, J. (eds). Wiley and Sons Ltd., 362 pp.

Najarro, M., Rosales, I., 2008. Evidencias sedimentológica, diagenética y quimioestratigráficas del Evento Anóxico Oceánico del Aptiense Inferior (OAE 1a) en la plataforma carbonatada de la Florida (NO de Cantabria). Geo-temas, 10, 163–166.

Najarro, M., Rosales, I., Martín-Chivelet, J., 2007. Evolución de la plataforma carbonatada de la Florida durante el rifting del Cretácico Inferior (Aptiense, NO de Cantabria). Volumen Monográfico de la II Semana de Jóvenes Investigadores del IGME, 123–128.

Nel, A., de Ploëg, G., Millet, J., Menier, J.J., Waller, A., 2004. The Frech ambers: a general conspectus and the Lowermost Eocene amber deposit of Le Quesnoy in the Paris Basin.

Néraudeau, D., Perrichot, V., Colin, J.-P., Girard, V., Gomez, B., Guillocheau, F., Masure, E., Peyrot, D., Tostain, F., Videt, B., Vullo, R., 2008. A new amber deposit from the Cretaceous (uppermost Albian-lowermost Cenomanian) of southwestern France. Cretaceous Research, 29, 925–929.

Néraudeau, D., Vullo, R., Gomez, B., Perrichot, V., Videt, B., 2005. Stratigraphie et paléontologie (plantes, vertébrés) de la série paralique Albien terminal-Cénomanien basal de Tonnay-Charente (Charente-Maritime, France). Comptes Rendus Palevol, 4, 79–93.

Noe-Nygaard, N., Surlyk, F., 1988. Washover fan and brackish bay sedimentation in the Berriasian-Valanginian of Bornholkm, Denmark. Sedimentology, 35, 197–217.

Olivet, J.M., 1996. La cinématique de la plaque ibérique. Bulletin des centres de Recherches Exploration-Production Elf-Aquitaine, 20, 131–195.

Pemberton, S.G., MacEachern, J.A., Frey, R.W., 1992. Trace fossils/facies models: environmental and allostratigraphic significance. In: Walker, R.G., James, N.P. (eds.). Facies Models: Response to sea level change. Geological Association of Canada, 47–72.

Penney, D., Ortuño, V., 2006. Oldest true orb-weaving spider (Araneae: Araneidae). Biology Letters, 2, 447–450.

Peñalver, E., Álvarez-Fernández, E., Arias, P., Delclòs, X., Ontañón, R., 2007a. Local amber in a Palaeolithic context in Cantabrian Spain: the case of La Garma A. Journal of Archaeological Science, 34, 843–849.

Peñalver, E., Delclòs, X., Soriano, C., 2007b. A new rich amber outcrop with palaeobiological inclusions in the Lower Cretaceous of Spain. Cretaceous Research, 28, 791–802.

Peñalver, E., Grimaldi, D.A., Delclòs, X., 2006. Early Cretaceous spider web with its prey. Science, 312, 1761.

Peñalver, E., Grimaldi, D., Delclòs, X., 2008. Early spider web. In: MacGraw Hill (eds.). Yearbook of Science and Technology, 103–105.

Perrichot, V., 2004. Early Cretaceous amber from south-western France: insight into the Mesozoic litter fauna. Geologica Acta, 2, 9–22.

Perrichot, V., 2005. Environnements paraliques à ambre et à végétaux du Crétacé Nord-Aquitain (Charentes, Sud-Ouest de la France). Mémoires des Géosciences ed. Rennes 118, 213 pp.

Perrichot, V., Néraudeau, D., Nel, A., de Ploëg, G., 2007. A reassesment of the Cretaceous amber deposits from France and their palaeontological significance. African Invertebrates, 48, 213–227.

Peyrot, D., Rodríguez-López, J.P., Barrón, E., Meléndez, N., 2007. Palynology and biostratigraphy of the Escucha Formation in the Early Cretaceous Oliete Sub-basin, Teruel, Spain. Revista Española de Micropaleontología, 39, 135–154.

Poinar, G.O., Milki, R., 2001. The Oldest Insect Ecosystem in Fossilized Resin. In: Oregon State University Press (eds.). Lebanese Amber, 96 pp.

Posamentier, H.W., Vail, P.R., 1988. Eustatic controls on clastic deposition II-sequence and systems tract models. In: Wilgus, C.K., Hastings, B.S., Kendall, C.G.St.C., Posamentier, H.W., Ross, C.A. and Van Wagoner J.C. (eds.). Sea-level changes-An integrated approach. SEPM, 42, 125–154.

Querol, X., Salas, R., Pardo, G., Ardevol, L., 1992. Albian coal-bearing deposits of the Iberian Range in northeastern Spain. In: J. P. McCabe and J.T. Panish (eds.). Controls and distribution and quality of Cretaceous coals. Geological Society of America, 267, 193–208.

Ramírez del Pozo, J., 1972. Algunos datos sobre la estratigrafía y micropaleontología del Aptense y Albense al oeste de Santander. Revista Española de Micropaleontología, 15, 59–97.

Rat, P., 1988. The Basque-Cantabrian basin between the Iberian and European plates some facts but still many problems. Revista de la Sociedad geológica de España, 1, 327–348.

Ratnitsyn, A., Quicke, D.L.J. (eds.), 2002, History of insects. Kluwer Academic Publishers, United States, 517 pp.

Reineck, H.E., Singh, I.B., 1975. Tidal Flats. In: Reineck and Singh (eds.). Depositional Sedimentary Environments. Springer-Verlag, 355–372.

Reineck, H.E., Wunderlich, F., 1968. Classification and origin of flaser and lenticular bedding. Sedimentology, 11, 99–104.

Rodríguez-López, J.P., Meléndez, N., 2004. Sedimentología de la Fm Escucha (Albiense Inferior–Medio) entre Estercuel y Crivillén (Teruel) en la cubeta de Oliete (Cuenca Ibérica Central). Geo-temas, 6, 119–122.

Rodríguez-López, J.P., Meléndez, N., Soria, A.R., 2005. Arquitectura estratigráfica de la Fm. Escucha (Albiense) en el flanco sur del Sinclinal de Cueva Forada. Subcuenca de Oliete (Teruel), Cuenca Ibérica Central. Geo-temas, 8, 95–98.

Rodríguez-López, J.P., Meléndez, N., Soria, A.R., Lisea, C. L., 2007. Lateral variability of ancient seismites related to differences in sedimentary facies (the synrift Escucha Formation, Mid-Cretaceous, eastern Spain). Sedimentary Geology, 201, 461–484.

Salas, R., Guimerà, J., Mas, R., Martín-Closas, C., Meléndez, A., Alonso, A., 2001. Evolution of the Mesozoic Central Iberian rift system and its Cenozoic inversion (Iberian Chain). In: Cavazza W., Robertson, A.H.F.R., Ziegler, P. and Crasquin-Soleaun, S. (eds.). Peri-Tethyan Rift/Wrench Basins and Passive Margins. Mémoires du Musée National de Histoire Naturel, 186, 145–185.

Salas, R., Martín-Closas, C. (eds.), 1991. El Cretácico Inferior del nordeste de Iberia. Publicacions Universitat de Barcelona, 153 pp.

Salas, R., Martín-Closas, C., Querol, X., Guimerà, J., Roca, E., 1991. Evolución tectonosedimentaria de las cuencas del Maestrazgo y Aliaga-Penyagolosa durante el Cretácico Inferior. In: Salas, R., Martín-Closas, C. (eds.). El Cretácico Inferior del nordeste de Iberia, Publicacions Universitat de Barcelona, 15–47.

Sangüesa, F.J., Arostegui, J., 2003. Modelo subsidente y térmico de la Formación Escucha en la Zona de Montoria-Peñacerrada (Álava). Estudios del Museo de Ciencias Naturales de Álava, 18, 91–100.

Schmidt, A.R., Ragazzi, E., Coppellotti, O., Roghi, G., 2006. A microworld in Triassic amber. Nature, 444, 835.

Schmidt, A.R., von Eynatten, H., Wagreich, M., 2001. The Mesozoic amber of Schliersee (southern Germany) is Cretaceous in age. Cretaceous Research, 22, 423–428.

Scotese, C.R., 2000. Paleomap project. Climate History. www.scotes.com/climate.htm.

Selden, P.A., 1989. Orb-web weaving spiders in the early Cretaceous. Nature, 340, 711–713.

Selden, P. A., 1990. Lower Cretaceous spiders from the Sierra de Montsech, north–east Spain. Palaeontology, 33, 257–285.

Selden, P.A., Penney, D., 2003. Lower Cretaceous spiders (Arthropoda: Arachnida: Araneae) from Spain. Neues Jahrbuch für Geologie und Paläontologie–Abhandlungen, 3, 175–192.

Shanmugam, G., Poffenberger, M., Álava, J.T., 2000. Tide-dominated estuarine facies in the Hollin and Napo ("T" and "U") Formations (Cretaceous), Sacha Field, Oriente Basin, Ecuador. American Association of Petroleum Geologists Bulletin, 84, 652–682.

Soto, R., Casas-Sainz, A.M., Villalaín, J., Oliva-Urcía, B., 2007. Mesozoic extension in the Basque-Cantabrian Basin (N Spain): Contributions from AMS and brittle mesostructures. Tectonophysics, 445, 373–394.

Spicer, A.R., Rees, P.M., Chapmann, J.L., 1994. Cretaceous phytogeography and climate signals. In: Allen, J.R.L., Hoskins, B.J., Sellwood, B.W., Spicer, R.A., Valdes, P.J. (eds.). Palaeoclimates and their Modelling; with Special Reference to the Mesozoic Era. Chapman and Hall, London, 69–77.

Szadziewski, R., 1996. Biting midges from Lower Cretaceous amber of Lebanon and Upper Cretaceous Siberian amber of Taimyr (Diptera, Ceratopogonidae). Studia Dipterologica, 3, 23–86.

Veltz, I., 2008. Le passage Jurassique Crétacé au Liban. Doctoral thesis. Université de Reims Champagne-Ardenne, 255 pp.

Visser, M.J., 1980. Neap-spring cycles reflected in Holocene subtidal large-scale bedforms deposits: a preliminary note. Geology, 8, 543–546.

Waggoner, B.M., 1996. Bacteria and protists from Middle Cretaceous amber of Ellsworth County, Kansas. PaleoBios, 17, 20–26.

Willis, B.J., 1997. Architecture of fluvial-dominated valley-fill deposits in the Cretaceous Fall River Formation. Sedimentology, 44, 735–757.

Wilmsen, M., 2005. Stratigraphy and biofacies of the Lower Aptian of Cuchía (Cantabria, north Spain). Journal of Iberian Geology, 31, 253–275.

Withjack, M.O., Olson, J., Peterson, E., 1993. Experimental models of extensional forced folds. The American Association of Petroleum Geologists Bulletin, 74, 1038–1054.

Zherikhin, V.V., Eskov K.Y., 1999. Mesozoic and Lower Tertiary resins in former USSR. Estudios del Museo de Ciencias Naturales de Álava, 14, 119–131.

4.4.- Review of the El Soplao amber outcrop, Early Cretaceous of Cantabria (Spain)

M. NAJARRO[(1)], E. PEÑALVER[(1)], R. PÉREZ-DE LA FUENTE[(2)], J. ORTEGA-BLANCO[(2)], C. MENOR-SALVÁN[(3)], E. BARRÓN[(1)], C. SORIANO[(4)], I. ROSALES[(1)], R. LÓPEZ DEL VALLE[(5)], F. VELASCO[(6)], F. TORNOS[(1)], V. DAVIERO-GOMEZ[(7)], B. GOMEZ[(7)] and X. DELCLÒS[(2)]

(1) Instituto Geológico y Minero de España

(2) Departament d'Estratigrafia, Paleontologia i Geociències Marines, Facultat de Geologia, Universitat de Barcelona.

(3) Centro de Astrobiología (CSIC-INTA

(4) European Synchrotron Radiation Facilities.

(5) El Soplao S.L.

(6) Dpto. Mineralogía y Petrología, Universidad del País Vasco

(7) CNRS-UMR 5125 PEPS, Université Lyon.

Doi: 10.1111/j.1755-6724.2010.00258.x.

Acta Geologica Sinica (English edition), 2010, Vol. 84, Nº4, p. 801-840.

RESUMEN

El yacimiento de El Soplao, un depósito de ámbar del Cretácico Inferior descubierto recientemente en el Norte de España (Cantabria), está considerado como el mayor yacimiento de ámbar con bioinclusiones de artrópodos encontrado en España hasta la fecha. Los datos relevantes que se aportan en este artículo, correspondientes a los estudios biogeoquímico del ámbar, palinológico, tafonómico y de las bioinclusiones de artrópodos, complementan los trabajos previamente publicados. Los datos presentados sugieren la presencia de al menos dos orígenes o fuentes botánicas distintas para el ámbar de El Soplao. El primero (ámbar tipo A), con gran seguridad tendría un origen relacionado con la familia Cheirolepidiaceae, mientras que el segundo (ámbar tipo B) no muestra biomarcadores espécificos de coníferas. El estudio comparativo de la composición molecular del ámbar tipo A con hojas de *Frenelopsis* (Cheirolepidiaceae) indica una gran afinidad bioquímica entre ambos, sugiriendo un origen botánico común. El estudio palinológico preliminar de los depósitos del yacimiento revela una alta diversidad taxonómica regional, principalmente de esporas de pteridofitas y granos de polen de gimnospermas. Así, los datos palinológicos preliminaries sugieren que la región estuvo habitada por bosques de coníferas adaptados a estaciones secas en un clima subtropical. Por otro lado, la abundancia de madera carbonizada o de tipo charcoal que aparece junto al ámbar en los mismos niveles, indicaría que el área de estudio estuvo afectada por paleoincendios, que posiblemente desencadenaron la alta producción de resina y una intensa erosión del substrato, con la consecuente acumulación de abundantes masas de ámbar y cutículas de plantas en los sistemas litorales adyacentes. Además, por primera vez en el registro fósil, han sido identificadas bioinclusiones de fibras de plantas carbonizadas (*charcoal*). Otro dato tafonómico relevante es la presencia excepcional de serpúlidos y briozoos en la superficie de algunas piezas de ámbar, indicando una larga exposición de éstas a las aguas marinas y/o salobres, así como una mezcla de tipos de ámbar. Finalmente, se han identificado nuevas bioinclusiones de insectos, algunos de ellos poco comunes en el registro fósil y otros mostrando notables adaptaciones. En conclusión, con esta contribución se proporciona un escenario bien documentado del origen del yacimiento de ámbar de El Soplao.

ABSTRACT

El Soplao outcrop, an Early Cretaceous amber deposit recently discovered in northern Spain (Cantabria), has been shown to be the largest site of amber with arthropod inclusions that has been found in Spain so far. Relevant data provided herein for biogeochemistry of the amber, palynology, taphonomy and arthropod bioinclusions complement those previously published. This set of data suggests at least two botanical sources for the amber of El Soplao deposit. The first (type A amber) strongly supports a source related to Cheirolepidiaceae, and the second (type B amber) shows non-specific conifer biomarkers. Comparison of molecular composition of type A amber with Frenelopsis leaves (Cheirolepidiaceae) strongly suggests a biochemical affinity and a common botanical origin. A preliminary palynological study indicates a regional high taxonomical diversity, mainly of pteridophyte spores and gymnosperm pollen grains. According to the preliminary palynological data, the region was inhabited by conifer forests adapted to a dry season under a subtropical climate. The abundant charcoalified wood associated with the amber in the same beds is evidence of paleofires that most likely promoted both the resin production and an intensive erosion of the litter, and subsequent great accumulation of amber plus plant cuticles. In addition, for the first time in the fossil record, charcoalified plant fibers as bioinclusions are reported. Other relevant taphonomic data are the exceptional presence of serpulids and bryozoans on the surfaces of some amber pieces indicating both a long exposure on marine or brackish-water and a mixed assemblage of amber. Lastly, new findings of insect bioinclusions, some of them uncommon in the fossil record or showing remarkable adaptations, are reported. In conclusion, a documented scenario for the origin of the El Soplao amber outcrop is provided.

***Keywords*: fossil resin, chemotaxonomy, paleobotany, charcoal, arthropod bioinclusions, taphonomy, Early Albian.**

INTRODUCTION

Amber preserves delicate organic fossils, including microorganisms, cells and tissues, but the most abundant record is constituted by insects, sometimes showing interactions between them, such as mating interaction, commensalism and parasitism (e.g. Grimaldi, 1996; Martínez-Delclòs et al., 2004; Grimaldi and Engel, 2005). Early Cretaceous amber is remarkably important, because it was during this period that there occurred explosive radiations of the flowering plants and many modern families of insects (Grimaldi and Engel, 2005). During the last decade several new deposits of Cretaceous amber have been discovered in Spain and France (e.g. Delclòs et al., 2007; Perrichot and Néraudeau, 2009), and researches on various aspects of Cretaceous amber have increased greatly. However, most of the researches made concern the taxonomical descriptions of arthropods and microorganisms embedded in amber. Only a few studies have been conducted on the origin of both the amber and the deposits that contain it. One of the most important aspects concerning Cretaceous amber is the plant source, if there was only one, but this aspect has been shown to be very difficult to ascertain with confidence.

The first detailed description of Spanish amber was published by Casal (1762). Approximately 150 years later Boscá (1910) first indicated the possible presence of insects preserved in Spanish amber. After the discovery of two remarkable amber deposits rich in bioinclusions, Peñacerrada I in the north and San Just in the north-east of Spain, a third major amber deposit was discovered in 2008 in Cantabria, named El Soplao. Thus it was not included in the most recent review of Spanish amber outcrops by Delclòs et al. (2007). Najarro et al. (2009) described in detail the regional geology, the features of the amber pieces, including infrared spectroscopy analyses, and a first attempt of the bioinclusions and the plant cuticles associated with the amber. Subsequent papers deal with biogeochemistry of amber and descriptions of new arthropod taxa preserved as bioinclusions. Thus, Menor-Salván et al. (2009a, 2009b) investigated biomarkers from amber pieces and *Frenelopsis* leaves from the El Soplao outcrop, concluding that they share the same origin; in addition, they identified the chemical compound form that produces an intensive fluorescent blue glow when this amber is under normal sunlight. More recently, Menor-Salván et al. (2010) report some paleochemotaxonomical aspects of the biological diterpenes preserved in El Soplao amber. On the other hand, Pérez-de la Fuente et al. (2010) and Nel et al. (2010)

described the new insect taxa *Cantabroraphidia marcanoi* (Raphidioptera: Mesoraphidiidae) and *Tethysthrips hispanicus* (Thysanoptera: Thripidae), respectively. Lastly, Ortega-Blanco et al. (2010a) report the fauna of false fairy wasps (Mymarommatoidea) that has been recorded in Spanish Cretaceous amber, including a paratype specimen from El Soplao amber.

We report relevant new data about El Soplao amber deposit, such as new detail on stratigraphy of the amber-bearing levels, new geochemical and biogeochemical information of the amber and fossil leaves, palynological data, the presence of a great abundance of charcoal associated with the amber, the presence of marine invertebrates on the surface of some amber pieces and new discoveries about the bioinclusions. These new contributions permit us to portray a more documented scenario for the origin of the El Soplao amber outcrop.

GEOLOGY

The El Soplao outcrop belongs to the Cretaceous succession of the north-western margin of the Basque-Cantabrian Basin. During the Cretaceous, this basin was affected by extensional tectonics, and perhaps strike-slip, associated with the opening of the North Atlantic Ocean and the Bay of Biscay (e.g. Le Pichon and Sibuet, 1971; Rat, 1988; García-Mondéjar et al., 1996; Soto et al., 2007). During the Late Jurassic–Early Cretaceous a major rift phase developed that led to the formation of several narrow sub-basin controlled by E–W, NW–SE and SW–NW trending faults, in which variable thicknesses of continental to marine sediments accumulated (García-Mondéjar et al., 1996; Soto et al., 2007). The El Soplao area lies in the North Cantabrian sub-basin located immediately to the north of the Cabuérniga Ridge (Wilmsen, 2005), which is an E–W late-Variscan structure reactivated first as a paleo-high bounded by normal faults during the Early Cretaceous, and later as a reversal fault during widespread Tertiary (Pyrenean) compression (Fig. 1). The Lower Cretaceous (Aptian–Albian) deposits of the El Soplao area lie unconformably on lower Triassic (Buntsandstein facies) basement. They constitute a relatively thin (~300 m) sedimentary wedge weakly deformed and affected only by gently folding. The El Soplao amber outcrop is located

in the southern flank of the Bielva syncline (Fig. 1), where the average strike of the succession is E–W and the dip about 40º N.

Thermal maturity of the area based on vitrinite reflectance values (% *R*o) performed on vitrinite macerals from plant fragments have yield relatively low reflectance values that range between 0.50% and 0.61% (mean 0.56%) (Menor-Salván et al., 2010). These values suggest that the organic matter associated with the amber is only early mature, and the estimated temperatures from these indices of thermal maturation of organic matter are in the range of 60–70ºC (e.g. Sweeney & Burnham, 1989), which are the burial maximum temperatures suffered by the amber deposit. These low maturity levels may be responsible for the good conservation of the molecular composition of the amber and its biological inclusions.

A synthesis of the stratigraphy of the Soplao area is represented in Fig. 2 (after Najarro et al., 2009, 2010). The amber-bearing deposit of El Soplao is included within the Las Peñosas Formation (Fig. 2), which is a Lower Albian unit (~112–110 Ma) of continental to transitional marine siliciclastic deposits interbedded in a succession of shallow marine, rudist and coral carbonate platform deposits. General sedimentary descriptions, depositional environments and fossil content of the Las Peñosas Formation have been already discussed in Najarro et al. (2009). In the El Soplao outcrop, the amber-rich beds occur in the lower-middle part of the Las Peñosas Formation. There, this unit rests disconformably above a thin (1–2 m) bed of continental red clay with root traces, deposited at the top of shallow marine limestones of the Reocín Formation (Fig. 2). The El Soplao amber deposit is characterized by dark, carbonaceous, pyritiferous shales with subordinated siltstones and sandstones laminae and crosslaminated centimetric sandstone layers, forming wavy and lenticular bedding. They contain remarkable accumulations of plant remains and amber pieces of different sizes and forms, as well as some remains and small shells of marine gastropods and bivalves. The principal amber-bearing shale bed of the El Soplao outcrop forms a lenticular body with maximum thickness of 1.5– 2.0 m and a width of at least 10 m in N–S cross-section. In the strike of the bed, the amber-bearing shale extends more than 75 m. The base of this len-shaped shale bed is erosional and truncates highly bioturbated, medium to coarse-grained sandstones with cross-bedding. At its top, the amber-bearing shale bed is overlain by heterolithic carbonaceous sandstones and muddy siltstones to sandstones

with flaser bedding, which are also relatively rich in amber pieces. All of these deposits accumulated in a proximal estuarine bay system with small bayhead deltas (Najarro et al., 2009) and represent the transgressive inundation of a continental fluvial plain and an incised valley fill. Based on geometry and facies, we interpret the amber-bearing shale of the El Soplao outcrop to have accumulated in a restricted tidal channel with low circulation and anoxic bottom-water, as suggested by widespread early pyritization.

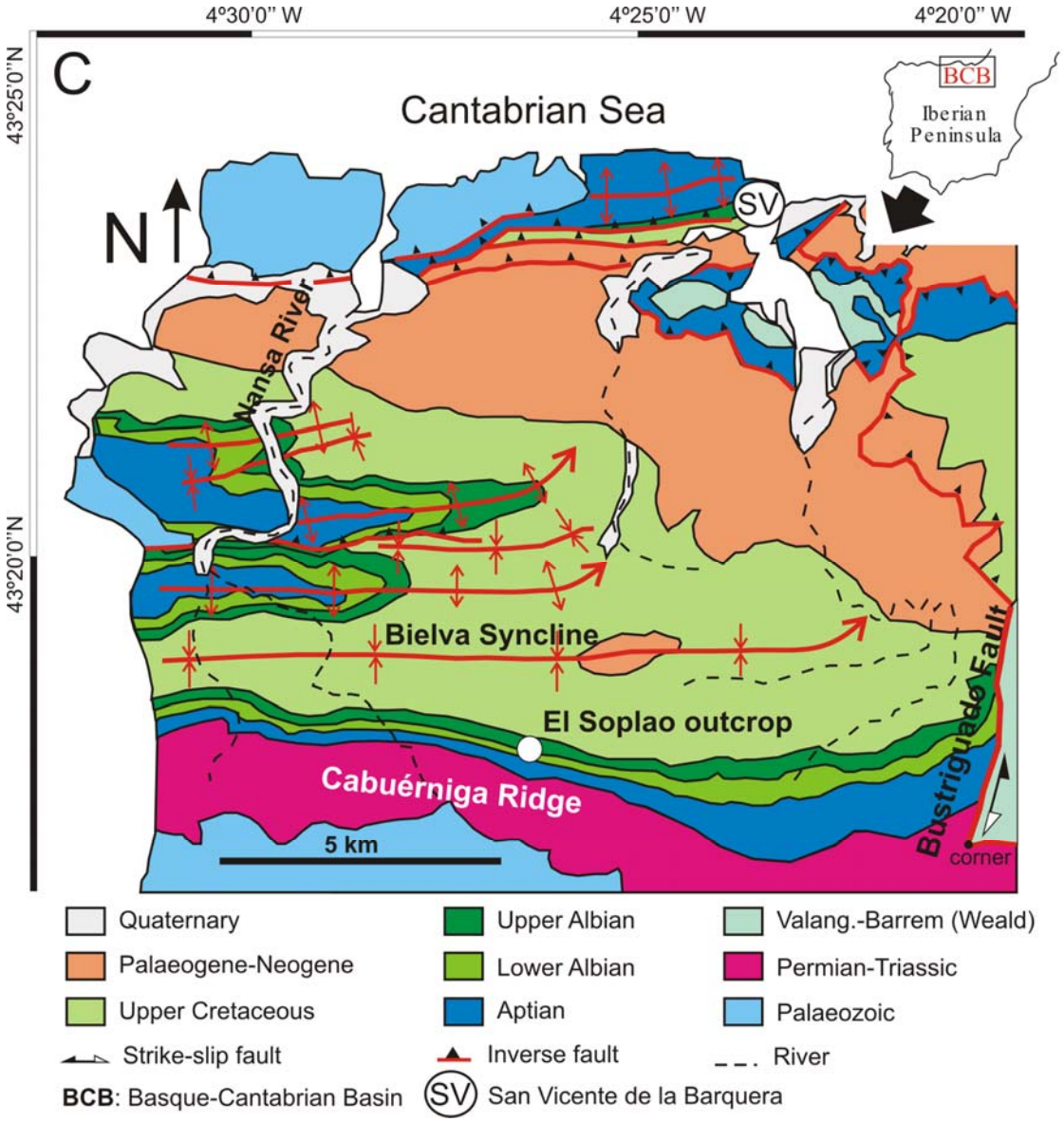

Figure 1.- Geological map of the study area showing the location of the El Soplao amber outcrop. Modified from Najarro et al. (2009).

METHODS

Paleontological excavations

Three paleontological excavations have been carried out in El Soplao amber outcrop. During the first one (October 2008) different extraction methods were applied to obtain amber pieces. Amber was obtained manually with small tools. In addition a large prospect hole, approximately 7 × 2.5 × 2 m in size, was dug in one of the amber-rich areas of the outcrop using a bulldozer. Several tons of amber-bearing sediment from the large prospect hole were transported to a washing area located in the same outcrop, where a cement mixer and a sieve were used to obtain all ranges of amber sizes as described in Corral et al. (1999) and Alonso et al. (2000). This permitted to obtain a sampling without taphonomic biases introduced by the extraction methods towards the large and medium sizes. During the last excavation (July 2009) additional small prospect holes were dug close to the limits of the outcrop to find lateral extensions of the amber deposit. This task showed a high abundance of amber and revealed that the amber bed is at least 75 m long laterally, supporting the assertion of Najarro et al. (2009), which is that the El Soplao is the largest site of amber with arthropod inclusions that has ever been found in Spain so far.

During the second paleontological excavation (March 2009) a new method was used to obtain abundant amber material increasing the collection of bioinclusions. The technique involves the use of high pressure water (Fig. 3.1 and 3.2) to extract entire large amber pieces that would be too fragile to resist conventional methods (Fig. 3.3). The water at high pressure disintegrated the sediment of the prospect hole and exposed the amber pieces, which were manually extracted to avoid fracturing. On the other hand, the small and medium pieces were retained using a large sieve where water and mud flowed (Fig. 3.2). The pieces from the mixture of mud, plant cuticles, coal and amber retained by the large sieve were separated in the washing area described above. This high pressure water method used for the first time to extract amber is already used in mining to fragment mineral seams, and to extract the useful parts from the waste rock. In conclusion, the new method was useful in obtaining numerous large amber pieces in a short period of time.

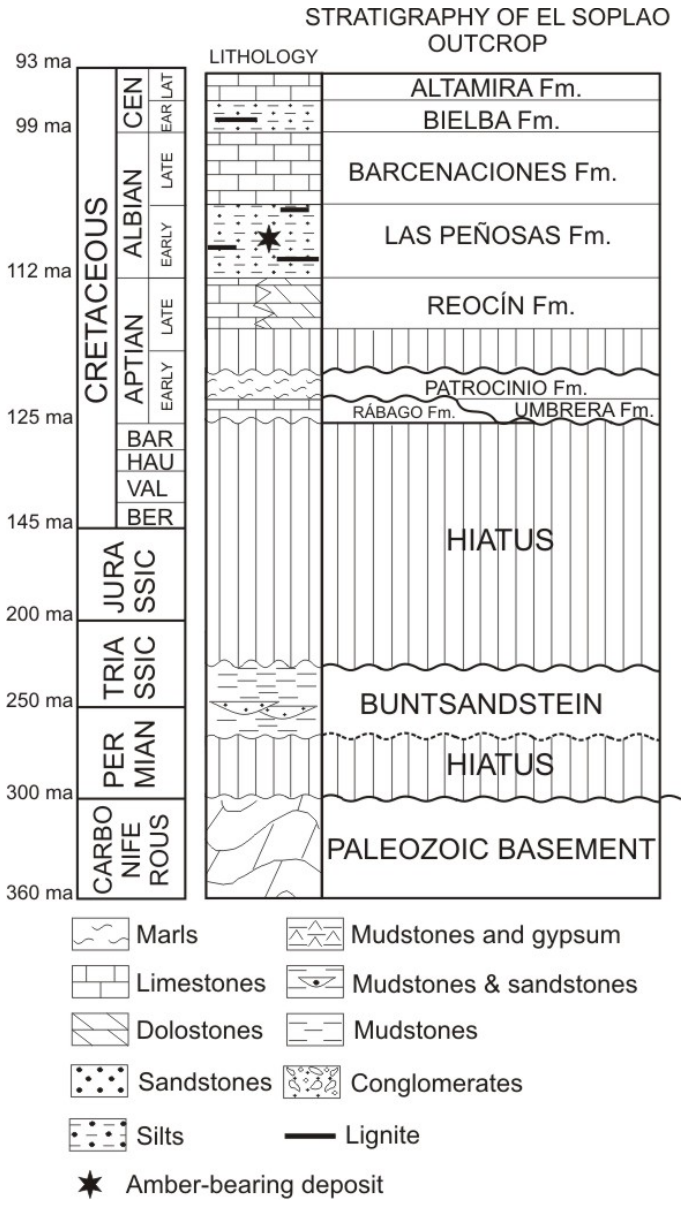

Figure 2.- Chrono- and lithostratigraphy of the El Soplao area. Modified from Hines (1985) and Najarro et al. (2010). Chronostratigraphy after Gradstein and Ogg (2009).

Biogeochemical analyses

For the biogeochemical analysis amber pieces, fossil wood, and sediments rich in plant cuticles were collected from the El Soplao deposit during the first excavation on October 2008. Two types of amber pieces were collected: type A, characterized by a strong blue purple color under natural light (Fig. 3.3 and 3.4), purple-reddish under artificial light, and type B, less abundant, yellow under artificial light and with a bluish tinge under natural light. Plant cuticles were

obtained from claystones by rinsing the plant-rich sediment in an ultrasonic bath of distilled water to remove all of the clay and silt sediment. The organic residue was air-dried. Plant fragments and leaves were distinguished and separated under a stereomicroscope. In addition, several resin and leaf samples from extant conifers of the families Cupressaceae and Araucariaceae (*Cupressus arizonica, Agathis australis* and *Araucaria angustifolia*) were collected from living trees at the Royal Botanic Garden of Madrid and in the kauri forests of New Zealand, in order to compare their compounds with those of the amber and fossil leaves and also to determine potential affinities of the amber with fossil taxa.

For the analytical characterization, several representative pieces of amber of the types A and B of about 50 g each, with the highest transparency available and free of major inclusions, crusts and debris, were selected from the El Soplao deposit. Following standard techniques, each piece was crushed and extracted for 4 h with dichloromethane:methanol (2:1) using a Büchi model B-811 automatic extractor. One aliquot of extract was injected directly into the injection port of the gas chromatograph. The bulk extract was concentrated to a volume of 20 mL and fractionated by use of flash chromatography on silica gel. The elution was carried out using hexane, dichloromethane, dichloromethane:methanol (1:1), and methanol, and subsequently 25 fractions were collected. Each fraction was concentrated by evaporation of the solvent under N2 and analyzed by gas chromatography/mass spectrometry (GC/ MS). The fractions with similar compositions were combined. The polar fraction (eluted with methanol) and the fractions containing ferruginol were recombined, further separated using a glass column (20 cm) filled with chromatographic-grade silica gel, and eluted sequentially with n-hexane:dichloromethane (1:1), pure dichloromethane, dichloromethane:methanol (1:1), and methanol. Four fractions were collected, designated A through D. All fractions were dried and the alcohols and acids converted to trimethylsilyl derivatives by reaction with N,O-bis-(trimethylsilyl)trifluoroacetamide (BSTFA) containing 1% trimethylchlorosilane (TMCS) at 65ºC for a period of 3 h. Finally, the derived fractions were diluted with n-hexane and injected into the port of the gas chromatograph.

To study the molecular composition of fossil *Frenelopsis* and *Arctopitys* leaves (genus name *Mirovia* changed to *Arctopitys*; see Nosova and Wcisło-

Luraniec, 2007), 5 g of leaves were extracted for 4 h with dichloromethane:methanol (2:1) using a Büchi model B-811 automated extractor. The bulk extract was filtered and analyzed directly by gas chromatography-mass spectrometry. After, extract was fractionated using silica gel chromatography in two fractions by elution with hexane:dichloromethane (3:1) and dichloromethane:methanol (4:1). The polar fraction was dried and derived using the method described above. For comparison, the chemotaxonomy of extant Cupressaceae and Araucariaceae was investigated using resin samples from *Cupressus arizonica*, *Agathis australis*, and *Araucaria angustifolia*. The resin was dissolved in dichloromethane:methanol (1:1) and fractionated by chromatography on silica gel in two fractions: the less-polar fraction being eluted with n-hexane:dichloromethane (1:4), and the second polar fraction being eluted with methanol. The polar fraction was dried under a nitrogen stream, yielding a white powder composed mainly of resin acids and highly polar compounds. The polar components were converted into trimethylsilyl derivatives by BSTFA and analyzed using GC-MS as described previously (Menor-Salván et al., 2010).

Palynological method

Two samples, Sop-Peñosas (this from the amber outcrop) and Peñosas-Cóbreces, both from Las Peñosas Formation, were prepared for palynological studies in the laboratory of ALICONTROL (Madrid, Spain). The rock samples were treated following the standard palynological preparation technique (Batten, 1999), which consists of an acid attack with HCl, HF and HNO3 at high temperature. The residue was concentrated and sieved throughout sieves of different grid sizes (500, 250, 75, 50 and 12 μm). Then, the samples were mounted in glycerin jelly on glass slides for light microscopy. The samples were studied with an Olympus BX51 optical microscope. Both samples yielded representative and well-preserved assemblages: Sop-Peñosas yielded 488 miospores and Peñosas-Cóbreces 681 miospores.

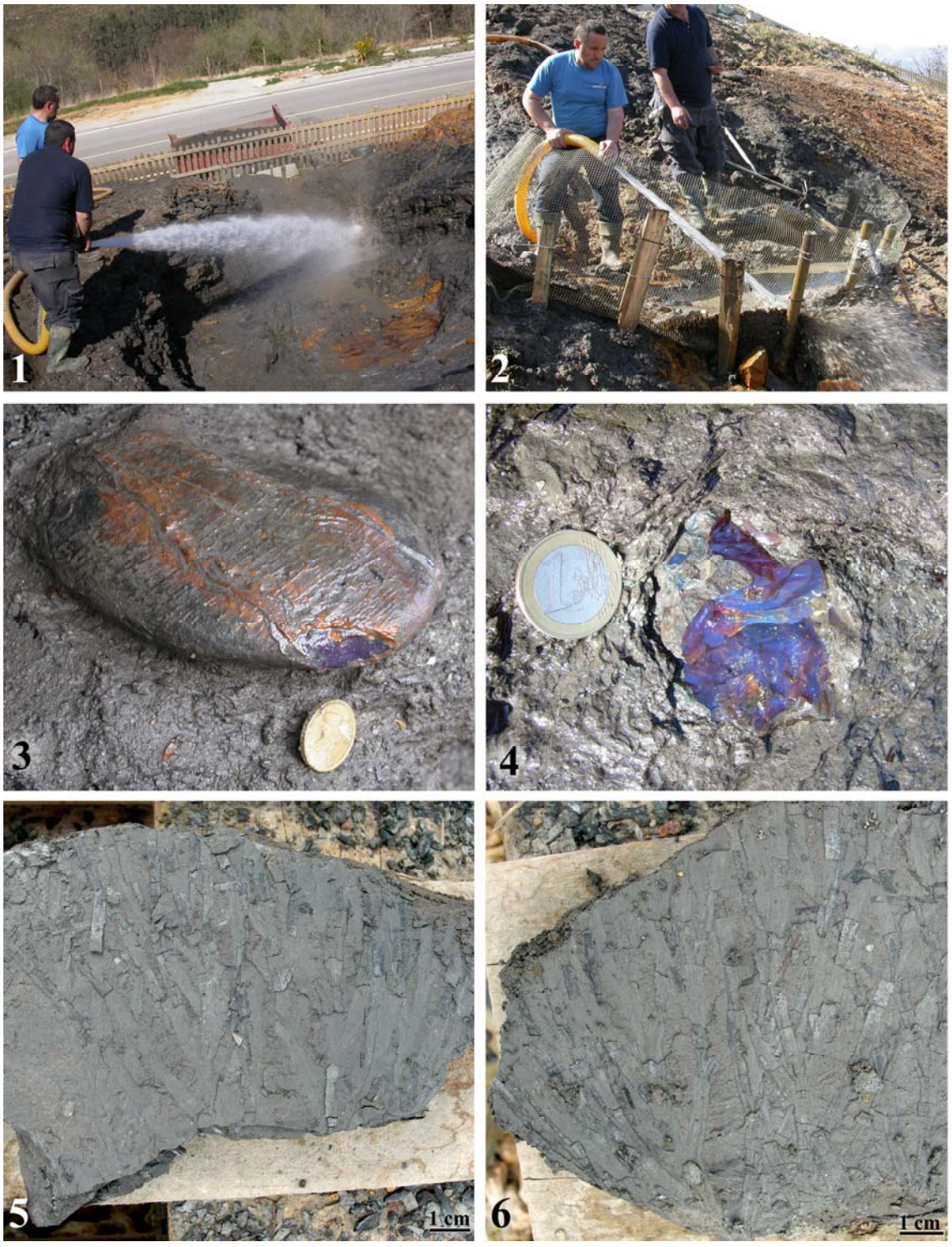

Figure 3.- Paleontological excavation in El Soplao amber outcrop (March 2009) with a new extractive method and some of the pieces obtained in situ. 1. High pressure water directed to the prospect hole; 2. large sieve to which water and mud flowed; 3. flattened amber piece virtually complete exposed *in situ* by high pressure water showing intensive fluorescent blue glow on its fracture (coin diameter 24 mm); 4. fragment of amber *in situ* showing intensive fluorescent blue glow (coin diameter 23 mm); 5–6. part and counterpart of four-time branched shoots of *Frenelopsis* sp. collected during the last excavation carried out (July 2009).

Microscopic photography

Scanning electron micrographs of the charcoal were taken using a HITACHI model S-2500 of the University of Valencia. Optical photography used both a digital camera attached to a microscope Olympus BX51 and a digital camera Leica DFC420 attached to a stereomicroscope Leica MS5.

BIOGEOCHEMESTRY OF THE AMBER

The overall aim of this part of the research was to identify the bioterpenoids preserved in the fossil resin and to determine their possible botanical source. Due to exceptional preservation, the amber-bearing deposit at El Soplao offers a unique opportunity to compare the molecular composition of the amber with that of the plant remains that appear in the same deposit.

The analysis of the polar terpenoids of the amber from El Soplao indicates that most likely at least two resin producers contributed to the amber record (Fig. 4). The main parent resin (type A; Fig. 4a) originally contained phenolic abietanes (dominated by ferruginol), totarol, dehydroabietane and pimarane/isopimarane acids. The dominant resin acids found were 13-dihydroagatholic and bisnordehydroabietic acids, as well as various other alteration products and minor quantities of callitrisic acid and hinokiol. The second parent resin (type B; Fig. 4b) shares some general compounds characteristic of conifers with type A amber, but shows remarkable differences in specific biomarkers. It contained pimarane/isopimarane acids as the only identifiable biological precursors preserved and shows absence of phenolic terpenoids (ferruginol, totarol, hinokiol) and other specific biomarkers that are present in type A amber (e.g. dehydroabietane, callitrisic acid).

The direct diagenetic products of the pimarane/abietane and labdane class terpenoids constitute the main geoterpenoids extractable from both types of El Soplao amber. The moderate degree of burial diagenesis of the studied material deduced from the low vitrinite reflectance values is consistent with the high level of preservation of the natural product diterpenoids and their direct diagenetic derivatives.

The preliminary molecular data obtained from the comparative study of the megafossil plant leaves, extant plant samples and the two amber types lead to the following results:

(a) There is absence of abietic and dehydroabietic acids in both types of amber samples. This allows us to reject a relationship between the amber and resin of Pinaceae species. Also, the absence of triterpenoids and labdatriene acids discards the contribution of angiosperms (Anderson et al., 1992; Yamamoto et al., 2006).

(b) In type A amber, the phenolic diterpenoids present in the analyzed samples and the absence of phyllocladane/kaurane type terpenoids discard the contribution of the family Araucariaceae. The presence of phenolic terpenoids (ferruginol, totarol and hinokiol) points to a relation with the extant conifer families Cupressaceae, Taxodiaceae and Podocarpaceae. However, the presence of dehydroabietane (also present in representatives of Pinaceae and Cupressaceae; Otto et al., 2007) points to a rather relationship with the family Cupressaceae. The presence of callitrisic acid in type A amber reinforces a biochemical relation between the parent resin of amber and modern Cupressaceae, because in modern conifer resins the synthesis of callitrisic acid seems to be restricted to certain genera of Cupressaceae (Anderson, 2006). The analysis of the molecular composition of fossil leaves from the same outcrop shows the presence of key terpenoids, such as ferruginol, in type A amber and the analyzed *Frenelopsis* fossil leaves, suggesting that this amber could be derived from the genus *Frenelopsis* (Cheirolepidiaceae). For the type A amber, a possible diagenetic route is suggested in Fig. 5 that connects the preserved biological precursors and the major geoterpenoids found in the sample (Otto and Simoneit, 2002; Stefanova et al., 2002; Hautevelle et al., 2006; Pereira et al., 2009). Morphological similarities between extinct Cheirolepidiaceae and extant Cupressaceae has been already described, but their phylogenetic relationship remains speculative, mainly due to the lack of molecular evidence (Seoane, 1998; Miller, 1999; Farjon, 2008); there are also paleobotanical data that support close affinities between Cheirolepidiaceae and Araucariaceae mainly based on female cone morphology. The chemotaxonomical affinity between type A amber and the analyzed leaves of *Frenelopsis* (Cheirolepidiaceae), and the affinity between type A amber and Cupressaceae as well, strongly suggests biochemical affinity between the extinct *Frenelopsis* and the modern representatives of the family Cupressaceae.

(c) The overall terpenoid composition of B samples (Fig. 4b) is represented by non-specific conifer biomarkers. Absence of phenolic terpenoids and 13-dihydroagatholic acid, together with a major presence of diagenetic products of pimarane type terpenoids, saturated and unsaturated norabietanes and alkyltetralines in B samples, points to a different biological origin. Paleobotanical source for this type of amber could not be identified on the basis of the biomarker composition found so far.

Although these results are preliminary and might change when more data become available from analyses of more samples, it is estimated that they already provide a good indication of the potential plant source that originated in the El Soplao amber. Future analyses could include fossil wood, leaf cuticle of *Nehvizdya*, more amber samples and conifer resin samples of other taxa.

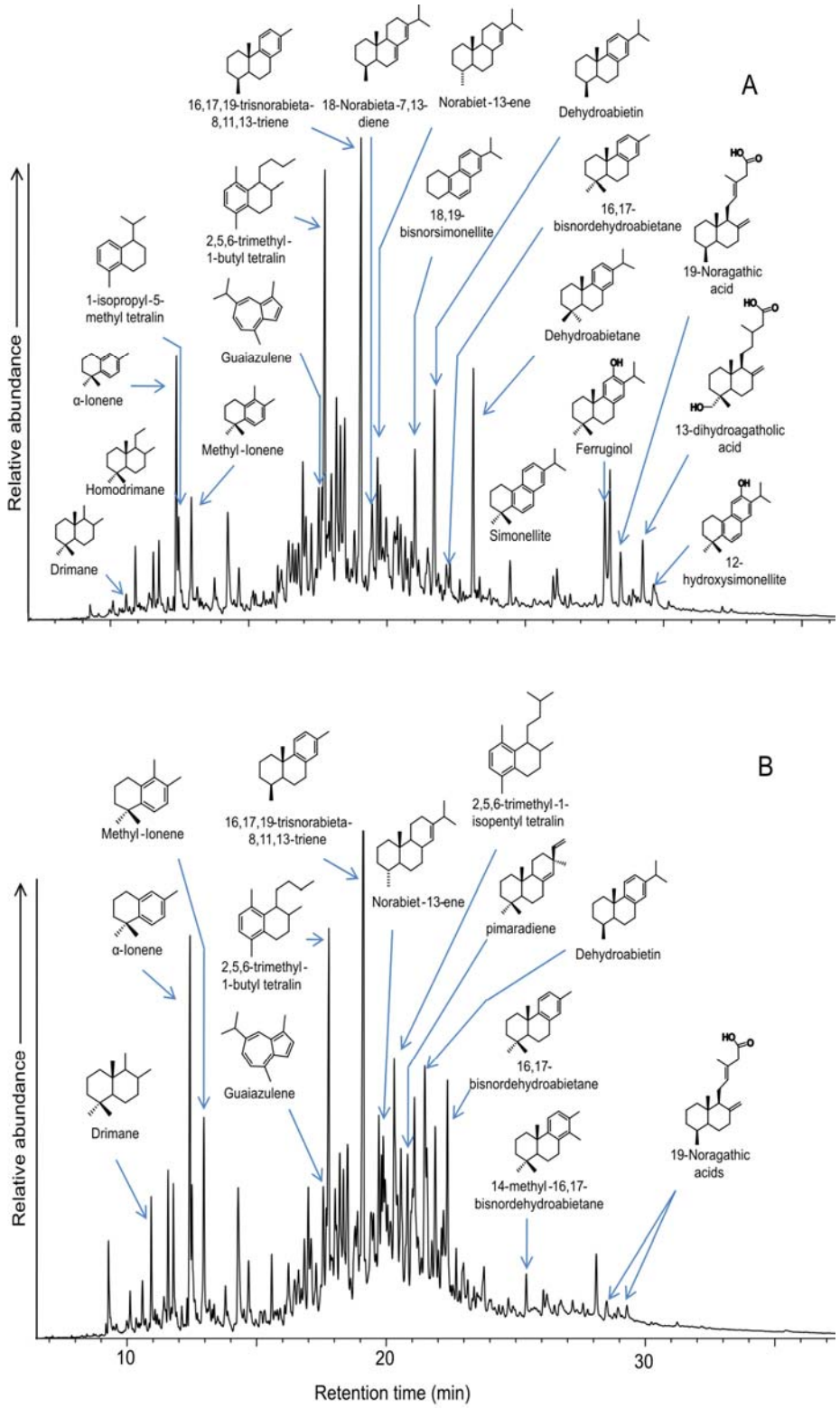

Figure 4.- Gas chromatography-mass spectrometry traces (TIC) analysis and main biomarkers identified in the two types of amber found at El Soplao deposit: type A (a) and type B (b). After Menor-Salván et al. (2010).

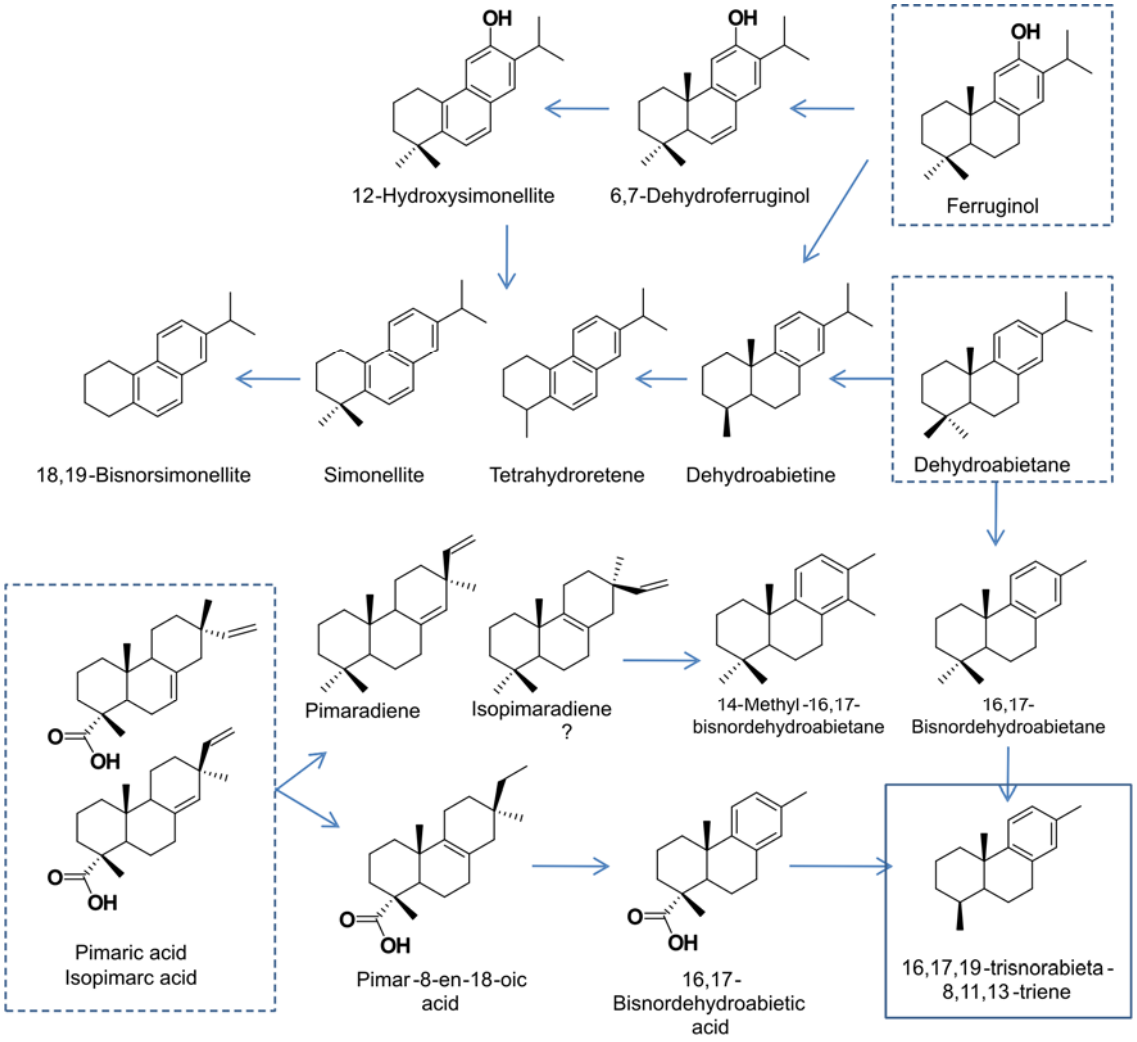

Figure 5.- Diagenetic pathways proposed for the El Soplao amber. Dotted box: biological precursors. After Menor-Salván et al. (2010).

PALINOLOGY

This preliminary palynological study complements that based on plant cuticles from the amber outcrop (see Najarro et al., 2009), revealing some additional aspects of the regional paleobotany. The studied samples from Las Peñosas Formation have yielded 32 spore and 29 pollen types (Fig. 6; see Table 1). In addition, undetermined bad-preserved dinoflagellate cysts and lining of foraminifera scarcely occurred. The Peñosas-Cóbreces sample presents more abundant taxa (52) than the Sop-Peñosas sample (44). It may be related to a lower palynological richness in the second sample. Both samples present high percentages of conifer pollen grains, especially those of *Classopollis* and *Inaperturopollenites dubius*. The spores of vascular cryptogams are

more diverse than pollen grains although they occur in lower amounts. The most usual spores belong to both the trilete and taeniate genus *Cicatricosisporites* and the trilete and psilate genus *Deltoidospora*. Pollen grains of ancient angiosperms occur scarcely in both samples. They are mainly represented by monosulcate and reticulate pollen grains of the genus *Clavatipollenites*.

The Peñosas-Cóbreces sample exhibits high amounts of pollen grains of *Classopollis* (~40%) and *I. dubius* (~30%). Other gymnospermous pollen grains such as *Alisporites* spp., *Araucariacites australis*, *Monosulcites chaloneri* and *Spheripollenites* sp. present lower but remarkable percentages. Spores also present low amounts being *Cicatricosisporites* spp. the best represented (~2%). The occurrence of a single tricolpate pollen grain of the genus *Tricolpites* is noteworthy, because up to the Middle Albian this taxon is not abundantly represented.

The Sop-Peñosas sample corresponds to the El Soplao amber outcrop. The palynological assemblage inferred in this sample is characterized by a conspicuous increase in *I. dubius* (~51%) and a marked decrease in *Classopollis* (~11%). The percentage of spores of the genus *Deltoidospora* also increases (~8%). *Cicatricosisporites* scarcely occurs at this sample. Angiosperm pollen grains are low represented in this sample compared to Peñosas-Cóbreces.

From a biostratigraphical point of view, the occurrence of *Appendicisporites robustus* and *Cicatricosisporites patapscoensis* (Fig. 6.2) indicates a Late Aptian–Middle Albian age. However, the occurrence of *Liliacidites dividuus* (Fig. 6.1) and the low presence of *Tricolpites* sp. indicate an Early Albian age for the Peñosas-Cóbreces sample (Doyle and Robbins, 1977).

The area could have been covered by mixed conifer forests of Cupressaceae and Cheirolepidiaceae that grew near the sea. Their understory was integrated by pteridophytes, cycads and/or Bennettitales. Ponds and swampy areas were mainly occupied by vascular cryptogams and early angiosperms, which could have aquatic habits. The predominance of *Classopollis* and the lower amount of spores observed in the Peñosas-Cóbreces sample could be related to a drier period. The more humid conditions of Sop-Peñosas are indicated by the higher percentages of *I. dubius* and *Deltoidospora* spp. as well as those of *Laevigatosporites* sp., *Alisporites* spp. and *Araucaricites australis*. Considering their composition, the assemblages are similar to those from the Upper Aptian–Lower Albian sediments of the Oliete sub-basin (Iberian Ranges) (Peyrot et al., 2007a, 2007b).

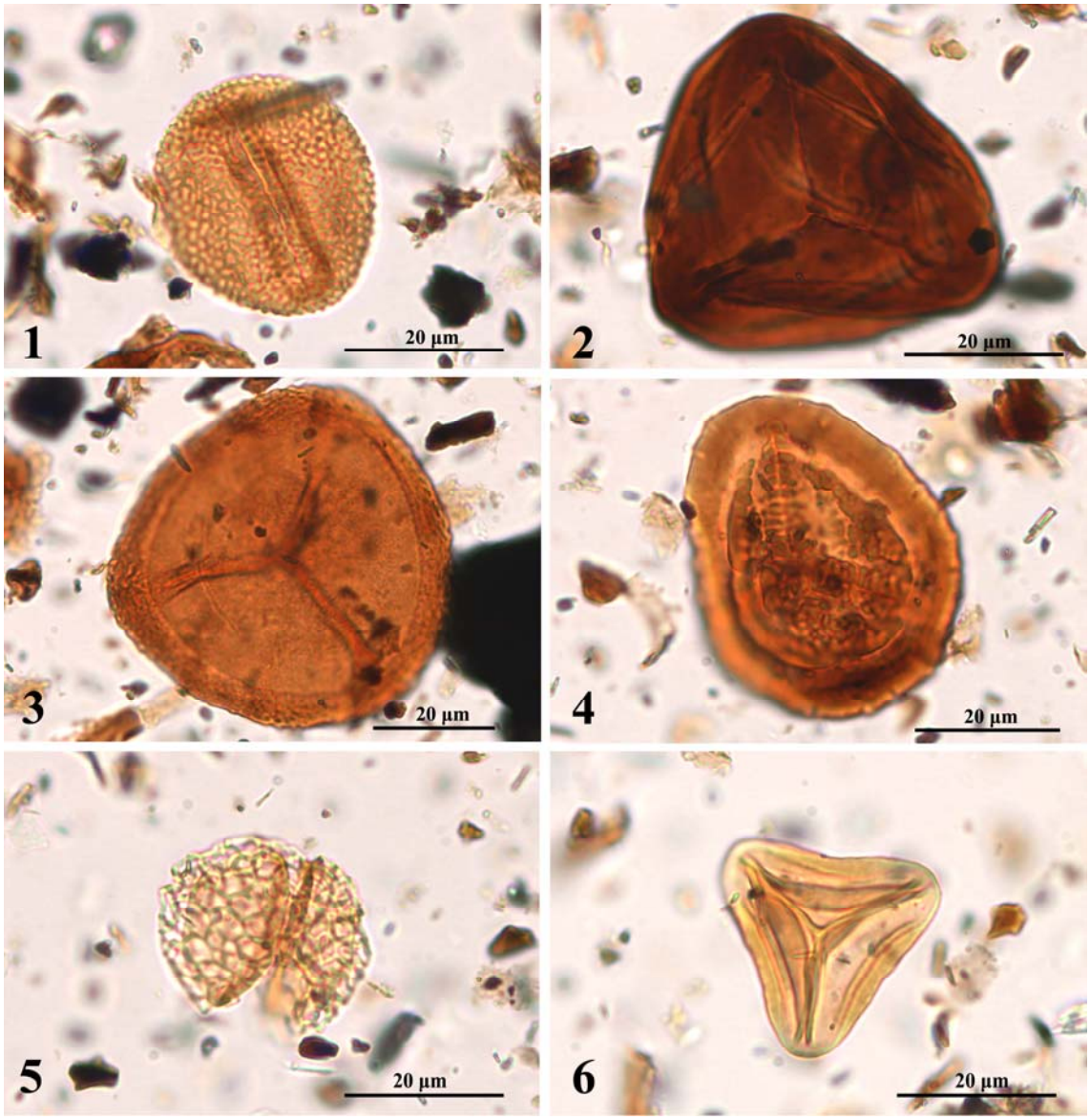

Figure 6.- Miospores from Peñosas-Cóbreces (1–5) and Sop-Peñosas (6) palynological samples. 1. *Liliacidites dividuus* (Pierce) Brenner; 2. *Cicatricosisporites patapscoensis* Brenner; 3. *Densoisporites velatus* Weyland & Krieger; 4. *Taurocosporites segmentatus* Stover; 5. *Pennipollis peroreticulatus* Brenner; 6. *Gleicheniidites senonicus* Ross.

	Peñosas-Cóbreces	%	Sop-Peñosas	%
Spores				
Appendicisporites robustus Kemp 1970	1	0.147	0	0
Appendicisporites dentimarginatus Brenner 1963	0	0	2	0.410
Appendicisporites tricornitatus Weyland & Greifeld 1953	1	0.147	0	0
Appendicisporites spp.	2	0.290	1	0.205
Baculatisporites sp.	0	0	1	0.205
Biretisporites potoniaei Delcourt & Sprumont 1955	3	0.440	3	0.615
Ceratosporites sp.	1	0.147	0	0
Cibotiumspora jurienensis (Balme 1957) Filatoff 1975	0	0	1	0.205
Cicatricosisporites apicanalis Phillips & Felix 1971	1	0.147	0	0
Cicatricosisporites apitereus Phillips & Felix 1971	1	0.147	0	0
Cicatricosisporites patapscoensis Brenner 1963	1	0.147	0	0
Cicatricosisporites recticicatricosus Döring 1965	1	0.147	0	0
Cicatricosisporites venustus Deák 1963	2	0.290	1	0.205
Cicatricosisporites spp.	13	1.908	6	1.230
Cingutriletes sp.	1	0.147	1	0.205
Contignisporites spp.	1	0.147	0	0
Crybelosporites sp.	0	0	1	0.205
Deltoidospora australis (Couper 1953) Srivastava 1975	4	0.587	13	2.664
Deltoidospora minor (Couper 1953) Pocock 1970	8	1.174	27	5.533
Deltoidospora sp.	4	0.587	8	1.640
Densoisporites velatus Weyland & Krieger 1953	1	0.147	1	0.205
Dictyophyllidites harrisii Couper 1958	2	0.290	1	0.205
Echinatisporis sp.	1	0.147	0	0
Gleicheniidites senonicus Ross 1949	0	0	4	0.819
Laevigatosporites sp.	0	0	7	1.434
Leptolepidites sp.	0	0	1	0.205
Patellasporites tavaredensis Groot & Groot 1962	1	0.147	0	0
Retitriletes sp.	0	0	1	0.205
Stereisporites sp.	0	0	1	0.205
Taurucosporites segmentatus Stover 1962	1	0.147	0	0
Trachysporites sp.	1	0.147	0	0
Triporoletes reticulatus (Pocock 1962) Playford 1971	1	0.147	1	0.205
Todisporites major Couper 1958	1	0.147	0	0
Pollen grains (gymnosperms)				
Alisporites bilateralis Rouse 1959	5	0.734	8	1.640
Alisporites spp.	20	2.937	12	2.460
Araucariacites australis Cookson 1947	12	1.762	25	5.123
Callialasporites dampieri Dev 1961	1	0.147	0	0
Cedripites sp.	1	0.147	0	0
Classopollis classoides Pflug 1953 emend. Pocock & Jansonius 1961	213	31.277	46	9.426
Classopollis spp.	58	8.517	9	1.844
Cycadopites spp.	8	1.174	2	0.410
Eucommiidites minor Groot & Penny 1960	4	0.587	2	0.410
Exesipollenites tumulus Balme 1957	6	0.881	3	0.615
Ginkgocycadophytus nitididus (Balme 1957) de Jersey 1962	1	0.147	3	0.615
Inaperturopollenites dubius (Potonié & Venitz 1932) Thompson & Pflug 1953	205	30.102	249	51.024
Inaperturopollenites spp.	21	3.084	9	1.844
Monosulcites chaloneri Brenner 1963	22	3.230	8	1.640
Monosulcites sp.	4	0.587	3	0.615
Pinuspollenites sp.	2	0.290	2	0.410
Podocarpidites sp.	0	0	2	0.410
Spheripollenites sp.	12	1.762	5	1.024
Vitreisporites pallidus (Reissinger 1950) Nilsson 1958	2	0.300	1	0.205
Undetermined bisaccate pollen grains	1	0.147	6	1.230
Pollen grains (angiosperms)				
Afropollis sp.	2	0.300	1	0.205
Clavatipollenites hughesii Couper 1958	2	0.300	3	0.615
Clavatipollenites minutus Brenner 1963	5	0.734	1	0.205
Clavatipollenites sp. (trichomosulcate)	4	0.587	0	0
Clavatipollenites spp.	5	0.734	4	0.819
Liliacidites dividus (Pierce 1961) Brenner 1963	3	0.440	0	0
Pennipollis peroreticulatus Brenner 1963	1	0.147	1	0.205
Tricolpites sp.	1	0.147	0	0
Undetermined angiospermous pollen grains	6	0.881	1	0.205
TOTAL miospores	681	100	488	100

Table 1.- List of spores and pollen grains recorded from the Early Albian sediments of Las Peñosas Fm.

PLANT CUTICLES

Najarro et al. (2009) reported abundant plant cuticles in the amber-bearing beds of El Soplao outcrop, sometimes as levels up to 10 cm thick. This plant assemblage comprises female cones of the genus *Alvinia*, leafy axes of *Brachyphyllum*-type, *Nehvizdya* sp. (and its reproductive organs classified into the genus *Nehvizdyella*), *Pseudotorellia* sp., and mainly *Frenelopsis* and *Arctopitys* (cited as *Mirovia* in that paper, but see Nosova & Wcisło-Luraniec, 2007).

Up to four-time branched shoots of the cheirolepidiaceous conifer *Frenelopsis* have been collected during the last excavation in July 2009 (Fig. 3.5 and 3.6), due to the large area exposed in the prospect hole excavated. The shoots show lateral branches with a single branch per node, a branching pattern similar to that described and discussed by Daviero et al. (2001). These new records are of taphonomic and paleoenvironmental relevance. From the taphonomic point of view, the stiff, articulated leafy internodes of *Frenelopsis* were probably very brittle and fragmented when transport occurred (Gomez et al., 2001, 2002; Riera et al., 2010). At least for some of the plants of the insect-bearing amber assemblage of El Soplao, such an organization suggests a parautochthonous deposition. The representatives of *Frenelopsis* occupied habitats from freshwater wetlands to saline, coastal or estuarine marshes (e.g. Gomez et al., 2001, 2002; Mendes et al., 2010). Such a wide range of habitats suggests possible mangrove-like ecology for the *Frenelopsis* of El Soplao. This paleoecological inference is also supported by the sedimentological context and the occurrence of marine or brackish-water invertebrates in the sediment and on amber surfaces.

CHARCOAL AND CHARCOALIFIED PLAN FIBERS

The first record of charcoalified (=fusainized) plant remains indicating paleofires is from the Silurian from Ludford Lane in the Welsh Borders in England (Glasspool et al., 2004). Scott (2000) provided a general view of the Pre-Quaternary history of fire based on charcoalified plant remains, which are especially important in sediments from the latest Jurassic and Early Cretaceous. Charcoalified plant remains are moderately common in a wide variety of facies, and some notable concentrations of considerable paleobotanical and paleoecological value can occur locally (Nichols et al., 2000).

In Spanish outcrops, amber and charcoal are very scarce except for a few levels in which both appear abundantly. This is the case of all the main outcrops for which this aspect has been explored: Peñacerrada (Suárez-Ruiz, 2003 and López del Valle, per. obs., 2008), La Hoya, San Just (Peñalver et al., 2007, 2008) and El Soplao. In these outcrops there are abundant cuboidal pieces of charcoal (=fusinite) of a few centimeters long (Fig. 7.2), and they are easily recognized with the naked eye even in the field by its silky luster, brittleness and friability. In addition, charcoal pieces are fibrous, black and opaque.

Features of the charcoal associated with amber in El Soplao outcrop using SEM are the undeformed structure and fabric of the tissue with open cell lumina, pits and homogenization of the cell walls (Fig. 7.3–7.5); see Sander and Gee (1990) and Scott (2000, 2010) for general description of charcoal. All of these features revealed by SEM examination are particularly characteristic of a pyrolysis origin. The most important feature is that different layers of the cell wall and adjacent cell walls cannot be distinguished from one to another due to the homogenization during burning. This homogenization of the wall takes place above 300ºC and the resulting charcoal is highly resistant to microbiological or chemical degradation during sedimentation and diagenesis (Cope and Chaloner, 1980). In San Just and El Soplao outcrops charcoal pieces with the cell lumina diagenetically filled with framboidal pyrite are found frequently (Fig. 7.6).

The levels of concentration of amber and charcoal in Spanish outcrops, including El Soplao, reveal paleofires in the resinous forests. Grimaldi et al. (2000) reported wood, insect remains and flowers, all charcoalified, and fire-damaged amber from the Upper Cretaceous (Turonian) of New Jersey, and Jarzembowski et al. (2008) reported a single piece of amber with similar features from the Lower Cretaceous of the Isle of Wight. Brasier et al. (2009) reported abundant examples of amber associated with charcoalified wood from the Early Cretaceous (140 Ma) amber deposit in Hastings (Sussex).

In addition to the frequent presence of charcoal associated with the amber in the same beds, a few amber pieces from El Soplao contain charcoalified plant fibers that appear dispersed inside the amber (Fig. 7.1). It is the first time in the fossil record that charcoalified fibers as bioinclusions have been reported. These fibers are small (around 0.7 mm long) and can be recognized as charcoalified fibers due to both their opaque black color and silky luster. This appearance is not due to the fossil diagenetic process

because they contrast to other plant fibers in the same amber pieces that have the common translucent clear brown color without silky luster. These small charcoalified plant fibers became included in resin during paleofires moved by convective currents or, after paleofires, transported by the wind to the exposed resin from the soil of burned areas. Scott et al. (2000) reported how abundant finer charcoal material was transported by wind from a charred area of the Frensham Common Country Park (England) several days after a wildfire.

The kauri forests (Araucariaceae) of New Zealand most likely are the best extant correlate to the Cretaceous resiniferous forests, except, perhaps, for the fact that the kauri forests do not have a fire ecology (Daniel J. Bickel, pers. comm., 2010). As it has been observed by us in the kauri forests, very large amounts of organic material occur due to the floor accumulation of litter, including resin pieces; Silvester and Orchard (1999) indicated that litter around a large kauri tree may reach 2 m or more in depth, with a mean residence time of 9–78 years due to a slow decomposition rate. Although resin burns easily, forest fires only affect the litter superficially, except for ground fires (Scott, 2000). Thus the main part of the accumulated resin usually remains intact. Scott et al. (2000) reported a surface fire in the Frensham Common Country Park that charred only a few millimeters of the organic litter, so the pine crown was practically not affected by the fire. As indicated by Grimaldi et al. (2000) and Martínez-Delclòs et al. (2004), forest fires traumatically induced copious production of resin and they might have been an important factor in the genesis of amber deposits. From this respect, Brasier et al. (2009) reported charcoalified conifer wood from Hastings deposit with cell lumina filled with resin after the paleofire. However, we consider that the joined occurrences of large accumulations of amber and charcoal in Spanish outcrops, and abundant plant cuticles as well, were mainly the consequence of an intensive erosion of the litter in burnt forests, possibly including mass wasting; at this respect, Scott & Stea (2002) reported evidences of post-fire soil erosion in Cretaceous charcoal horizons of Nova Scotia. As summarized by Nichols et al. (2000) from different sources, the removal of vegetation by modern fires can increase erosion rates by weathering and during rainstorms by up to 30 times compared with the sink of pre-fire levels, and single wildfire events may be recognizable as responsible for individual depositional units, for example on alluvial fans.

Nichols et al. (2000) conducted actualistic experiments and concluded that charcoal is an unusual sedimentary material because most fresh material floats, but after

prolonged immersion becomes waterlogged and sinks, mainly the small pieces. After the study of an area of heathland in SW England burned by an uncontrolled fire, Blackford (2000) concluded that large particles are not transported long distances and thus are indicative of local fires. The great abundances of centimetersized charcoal in amber-bearing beds of San Just and El Soplao outcrops suggest that paleofires in these cases were local or occurred close to the area of deposition. In the scenario we propose, intensive erosion by rivers and storm floods of a burned resinous forest area located close to the deltaic environments of deposition was promoted by the loss of vegetation, and resin plus charcoalified wood were transported together through water to coastal environments.

Another complementary factor that could contribute to the great amber accumulation in El Soplao outcrop was proposed by Najarro et al. (2009) based on sedimentological data: floods during rainstorms eroded and removed the resin and plant remains from the soils of coast-fringing forests. Pieces of resin and wood mixed with mud and sand then were transported by density flows to the coastal and interdistributary bays. Surely, more than one of these three factors might have occurred.

We can assume that wildfires had a great impact on environments and most likely they occurred mainly during the warm, drought season; lightning strike is the most important reported cause of naturally ignited fires today (Cope and Chaloner, 1980; Scott, 2010) and it was probably the same during the Cretaceous. Moreover, levels of atmospheric oxygen during the Cretaceous were among the highest during the Phanerozoic, close to 30% (vs. 20% today), leading to a much higher prevalence of fires (Robinson, 1989). Secondary evidence of the environmental impacts of wildfires can be obtained from plant and insect fossil records. The tree fern *Weichselia reticulata* has been recorded in some adjacent beds to the Spanish amber outcrops and this taxon can be related to environments disturbed by both floods and fires according to Coiffard et al. (2007) and Scott et al. (2000). More recently Ortega-Blanco et al. (2008) described a new species of anaxyelid woodwasp, *Eosyntexis parva*, from Peñacerrada I amber closely related to the extant anaxyelid taxa that lay eggs in burnt conifer trees shortly after the wildfires.

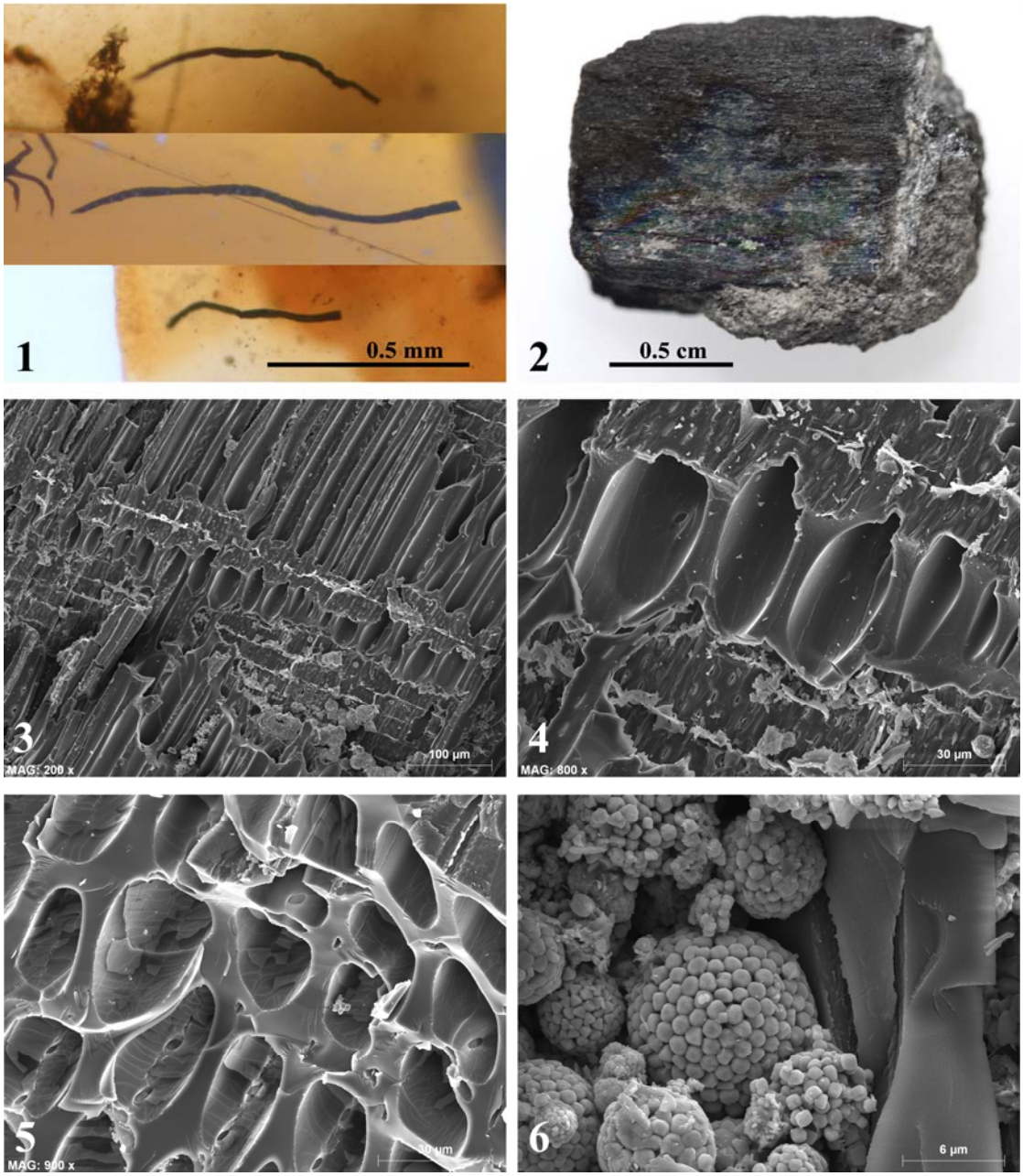

Figure 7.- Fossil carbonized woody tissues (charcoals) from El Soplao outcrop. 1: Three charcoalified plant fibers from the same small amber piece containing numerous of these remains (at the same scale); 2: Cuboidal piece of charcoal; 3–5: Scanning electron micrographs of charcoals show both pits and cell-wall homogenization in epidermis and peripheral tissues (micrograph 4 is a detail of 3); 6: Framboidal pyrite partially filling the cell lumina (micrographs 3–6 are from microsamples of the piece figured in picture 2).

MARINE OR BRACKISH-WATER INVERTEBRATES ON AMBER SURFACES

El Soplao amber deposit in some levels contains internal marcasite moulds of marine or brackish-water mollusks, and oyster shells that preserve the original calcium carbonate biomineralization. In addition, for the first time in the fossil record we report findings of large amber pieces that show their surfaces colonized by both serpulid worm tubes (Annelida: Polychaeta) (Fig. 8.1 and 8.2) and encrusting bryozoan colonies (Bryozoa: Cheilostomata) (Fig. 8.3); barnacles encrusting Baltic amber surfaces have been reported, but they are recent barnacles (see Grimaldi, 1996). Amber pieces with their entire surface colonized, or only with one side colonized, have been found.

Serpulid worm tubes exhibit four modes of fossilization that sometimes occur in the same amber piece, but in different parts: (1) as limonitic impressions of the tubes (Fig. 8.1); (2) as internal marcasite moulds (Fig. 8.2); (3) as amber tubes (internal fillings with resin during first fossildiagenetic phases); and (4) as original carbonate remains (Fig. 8.3). Serpulid tube remains are several millimeters long and internal tube fillings are approximately 0.35 mm diameter.

Bryozoan colonies left marks of the zooid exoskeletons on the amber surface and when original calcium carbonate remains are preserved (Fig. 8.3) they easily fade away during the washing of the pieces. Bryozoan colonies are multiserial and belong to the Order Cheilostomata; that group produces mineralized exoskeletons and form single-layered sheets that encrust over surfaces. Box-shaped, rectangular zooids are 0.34 × 0.29 mm in size.

Completeness of these large pieces suggests that they were constituted by polymerized resin when serpulids and bryozoans developed, not fossil resin from eroded strata (reworking process). Resin is comparatively less fragile than amber or copal and, in consequence, more commonly keeps its integrity during marine transport. In any case, this deposit contained a mixture of resin pieces from the litter, and fresh resin pieces directly transported from the trees, together with reworked resin pieces that remained a certain time in saline water. The presence of encrusting bryozoan colonies on the amber surfaces is not surprising because this type of organism is better adapted to shallow, high energy environments. In conclusion, this exceptional record indicates a littoral to coastal marsh environment of deposition for El Soplao outcrop.

Figure 8.- Marine or brackish-water invertebrates on the surfaces of El Soplao amber and insects as bioinclusions. 1: Detail of the serpulids preserved as limonitic impressions on the entire kidney-shaped amber piece 12 x 10 x 5 cm in size; 2: two serpulid worm tubes preserved as marcasite internal mould of the same amber piece; 3: bryozoan colony and several serpulids preserved as carbonate fossils on the surface of a large amber piece; 4: virtually complete specimen of the family Berothidae (Neuroptera); 5: specimen of Cucujoidea (Coleoptera). Photos 4 and 5 were made with integrated consecutive pictures taken at successive focal planes.

NEW DATA ON INSECT BIOINCLUSIONS

Najarro et al. (2009) reported a high abundance of arthropod specimens embedded in the Early Cretaceous amber of El Soplao outcrop, and explained it as a consequence of the unusual concentration of amber pieces indicative of resin flows (drops, crusts and runnels) in this deposit. A significant percentage of amber pieces of this type contains numerous bioinclusions because the original resin was exposed to the atmosphere, was less viscous (it was more easily penetrated by insects), and successive flows encapsulated the trapped insects (Martínez-Delclòs et al., 2004).

Recent paleontological excavations have provided new bioinclusions of significant paleoecological and taxonomical value. To date, El Soplao amber has provided more than 200 bioinclusions, including fungi, plants, and diverse arthropods. Among them, only systematic studies on insects have been already started. The insect inclusions found belong to 11 recognized orders: Blattaria, Isoptera, Psocoptera, Thysanoptera, Raphidioptera, Neuroptera, Hemiptera, Coleoptera, Trichoptera, Hymenoptera, and Diptera; last two groups are the most abundant.

Neuropterid fauna from El Soplao amber is composed so far of Raphidioptera and Neuroptera, including the new genus and species of mesoraphidiid described by Pérez-de la Fuente et al. (2010) that is currently being studied. Neuropterans are represented by two specimens of dustywings (Coniopterygidae) and two beaded lacewings (Berothidae), one of them very complete and interpreted as a new morphotype (Fig. 8.4). Surely, the most outstanding finding is a tentative green lacewing larva (Chrysopidae), which, if confirmed, would be the oldest representative of the family in amber and one of the very few fossil chrysopid larvae ever reported. Its morphology, to be described and discussed elsewhere, is similar to those of the extant trash-carrying chrysopid larvae, which cover their backs with animal or plant debris chiefly as a defense against predators (Eisner et al., 2002). In fact, the specimen is surrounded by a dense filamentous cloud corresponding to its protective cover, proving the antiquity of the trash-carrying behavior in these lacewings, as was hypothesized by Engel and Grimaldi (2007).

Coleopterans from El Soplao amber are represented only by members of the suborder Polyphaga, and all of them are up to now interpreted as herbivorous or saproxylic forms, most probably living under the bark of the trees. As in other Lower Cretaceous outcrops of surrounding areas in Spain and France, the most abundant forms

of beetles from El Soplao belong to superfamilies Elateroidea and Cucujoidea (Fig. 8.5), but there are also present forms of Curculionoidea (?Attelabidae, ? Nemonychidae) and possibly a member of Dascilloidea. The presence of two specimens of Curculionoidea in such small collection of beetles (approximately 10 specimens) is of paleoecological relevance, because this group of beetles is up to day closely related to hard parts of trees, in which larval stages developed, and the action damaging trees has also been pointed to as one of the possible causes for the increase in resin production in trees during the Early Cretaceous and its subsequent record as fossil resins.

Although the hymenopteran assemblage of El Soplao is scarce, it is providing interesting data. It is composed of parasitoid wasps of several superfamilies as Ceraphronoidea (parasitoids of numerous taxa, hyperparasitoids sometimes), Platygastroidea (insect and spider egg parasitoids), Evanioidea (cockroach egg consumers during larval stage), Ichneumonoidea (commonly hyperparasitoids) and Mymarommatoidea (tiny egg parasitoids). Although ceraphronoids are currently under study, a first approximation allows us to recognize members of a recently described new family of Ceraphronoidea (Ortega-Blanco et al., 2010b). Ceraphronoids were exclusive from the Peñacerrada amber until date; venation and some antennae aspects of the El Soplao morphotype indicate that it belongs to the same genus that is present in Peñacerrada amber. Platygastroids are the most common hymenopteran insects in El Soplao amber, as in all other Spanish ambers, and the study of this group is in progress. Apparently platygastroids belong to a new species with large, 14-articled antennae. A new parasitoid wasp species of the genus *Archaeromma* (Mymarommatoidea) has been recorded in El Soplao, as it was in Peñacerrada I. Recording the same insect species supports the hypothesis that the age of these ambers was equivalent or at least very close, and suggests that both outcrops had similar paleoecological characteristics.

Dipterans from El Soplao amber are represented by Brachycera and Nematocera forms. One specimen of *Litolepti* sp. (Spaniidae) has been identified within the Brachycera, similar to one specimen described from San Just amber (Arillo et al., 2009). Other dipteran families present include Hybotidae (Brachycera), as well as Cecidomyiidae and Psychodoidea. The current paleodiversity of biting midges (Ceratopogonidae) has been evaluated, leading to the discovery of five species, including three new species (Najarro et al., 2009). The new species belong to the genera *Archiaustroconops*, Szadziewski, 1996, *Atriculicoides* Remm, 1976, and *Lebanoculicoides* Szadziewski, 1996. All these ancient biting midges would have

shown a hematophagous diet which is considered plesiotypic within the family (Borkent, 1995).

CONCLUSIONS

We present herein data that suggest that amber pieces from El Soplao have at least two botanical sources. Part of these data strongly supports a source related to Cheirolepidiaceae and also suggests a molecular relationship of Frenelopsis with extant Cupressaceae. This relationship is based on the chemotaxonomic comparison of biological diterpenes found in amber and plant megafossils and extant Cupressaceae.

The taphonomic significance of wildfires in the origin of the Cretaceous amber accumulations has received little attention and has been clearly underestimated. The potential presence of charcoal, fire-damaged amber pieces and charcoalified plant fibers embedded inside the amber must be considered when studying the origin of the Cretaceous amber deposits. In fact, the occurrence of large accumulations of amber and charcoal in Spanish outcrops were consequence of intensive erosion of the litter in burnt forests, possibly including mass wasting. This scenario has been well documented in the case of the El Soplao deposit, but similar studies on other Spanish amber deposits should be conducted.

The new data on the biological inclusions from El Soplao amber show a highly diversified entomofauna, mainly represented by dipterans and hymenopterans, with the presence of very specialized groups such as chrysopids or weevils, which may help to better understand the early evolution of some insect groups.

The data previously published and new data herein provided suggest a taphonomic history for the El Soplao amber that may have run approximately as follows: resin was exuded by conifers (perhaps by two different conifers, including Cheirolepidiaceae) closely to the deltaic environments of deposition. Conifer forests were well-present in the region, with understory integrated by pteridophytes, cycads and/or Bennettitales; ponds and swampy areas were mainly occupied by vascular cryptogams and early angiosperms, which could have aquatic habits. A diversified insect fauna, mainly represented by hymenopterans and dipterans, developed around the conifer trees and was abundantly embedded in resin. Coleopterans, which probably lived under the bark

or in close contact with the wood of the conifer trees, were abundantly embedded as well. Wildfires in the resinous forests promoted both the resin production and an intensive erosion of the partially burned litter. Resin, fresh leaves, wood and charcoal were shortly transported together through water and accumulated alongside marine or brackish-water mollusks in a restricted tidal channel with low circulation and anoxic bottom-water. The conifer Frenelopsis, a potential source of resin as suggested by the biogeochemical analyses, grew close to the deposition area, where articulated branched shoots accumulated (parautochthonous deposition). Resin pieces differed in their biostratinomic histories because some of them remained a certain time in shallow, high energy saline waters where serpulids and bryozoans grew on the resin surfaces, resulting in a mixed assemblage. Low circulation and anoxic bottom-water promoted an early pyritization of the marine mollusks, charcoal and amber surfaces, including the fixed serpulid tubes. The assemblage was lastly buried by siltstones and sandstones. The maximum temperatures suffered by the amber deposit during diagenesis were in the range of 60–70ºC. The inferred low maturity levels were maybe responsible for the good preservation of amber molecular composition and its biological inclusions.

ACKNOWLEDGEMENTS

This work is part of the Ph.D. Thesis of three of the authors (M.N. -geology-, R.P.F. and J.O.B. -paleobiology-), which are supported by a scholarship from the Instituto Geológico y Minero de España (IGME), an APIF grant of the University of Barcelona, and a FPI grant from the Spanish Ministry of Science and Technology, respectively. This study is a contribution of the IGME Project 491-CANOA 35015 "Investigación científica y técnica de la Cueva de El Soplao y su entorno geológico", the projects CGL2008-/01237BTE from the MICINN, CGL2008- 00550/BTE: "Amber of the Cretaceous of Spain: A multidisciplinary study", and the ANR Project AMBRACE BLAN07-1-184190. The contribution is framed in a collaborative agreement among the Cantabrian Government (Regional Cultural, Tourism and Sports Ministry), IGME and SIEC S.A. We thank Gonzalo Nieto and the staff of the Royal Botanic Garden of Madrid for permission and assistance in the sampling of extant conifers. We also express our thanks to Francisco Javier López Marcano (Regional

Minister of the Cantabrian Government), José Pedro Calvo Sorando (IGME) and Fermin Unzué (manager of the El Soplao Cave) for their efforts and promotion of the study of the outcrop. We are grateful to Dr Daniel J. Bickel (Australian Museum, Sydney), Dr Vladimir Blagoderov (Natural History Museum, London) and an anonymous reviewer for careful reviews of the manuscript. Thanks are due to all people that participated in the paleontological excavations.

REFERENCES

Alonso, J., Arillo, A., Barrón, E., Corral, J.C., Grimalt, J., López, J.F., López, R., Martínez-Delclòs, X., Ortuño, V., Peñalver, E., and Trincão, P.R., 2000. A new fossil resin with biological inclusions in Lower Cretaceous deposits from Álava (Northern Spain, Basque-Cantabrian Basin). *Journal of Paleontology*, 74(1): 158–178.

Anderson, K.B., 2006. The nature and fate of natural resins in the geosphere. XII. Investigation of C-ring aromatic diterpenoids in Raritan amber by pyrolysis-GC-matrix isolation FTIR-MS. *Geochemical Transactions*, 7: 2.

Anderson, K.B., Winans, R.E., and Botto, R.E., 1992. The nature and fate of natural resins in the geosphere-II. Identification, classification and nomenclature of resinites. *Organic Geochemistry*, 18(6): 829–841.

Arillo, A., Peñalver, E., and García-Gimeno, V., 2009. First fossil *Litoleptis* (Diptera: Spaniidae) from the Lower Cretaceous amber of San Just (Teruel Province, Spain). *Zootaxa*, 2026: 33–39.

Batten, D.J., 1999. Extraction techniques - Small palynomorphs. In: Jones, T.P., Rowe, N.P. (eds.), *Fossil plants and spores: modern techniques*. The Geological Society, London, 15–19.

Blackford, J.J., 2000. Charcoal fragments in surface samples following a fire and the implications for interpretation of subfossil charcoal data. *Palaeogeography, Palaeoclimatology, Palaeoecology*, 164: 33–42.

Borkent, A., 1995. *Biting midges in the Cretaceous amber of North America (Diptera: Ceratopogonidae)*. Backhuys Publishers, Leiden, The Netherlands, 237 p.

Boscá, A., 1910. Cuenca calaminífera de Linares de Aragón. *Asociación Española para el Progreso de las Ciencias*, 4(1ª part): 171–181.

Brasier, M., Cotton, L., and Yenney, I., 2009. First report of amber with spider webs and microbial inclusions from the earliest Cretaceous (*c*. 140 Ma) of Hastings, Sussex. *Journal of the Geological Society*, London, 166: 989–997.

Casal, G., 1762. Succini Asturici, à Doctore Gafpar Cafal, Almae Eclefiae Cathedralis Ovetenfis Medico, reperti, folertique ejufdem cura probati, & examinati, Hiftoria. *Historia Natural y Médica del Principado de Asturias*, Facsimile ED. 1998. Servicio de Publicaciones. Principado de Asturias, Oviedo: 480.

Coiffard, C., Gomez, B., and Thevenard, F., 2007. Early Cretaceous Angiosperm Invasion of Western Europe and Major Environmental Changes. *Annals of Botany*, 100: 545–553.

Cope, M.J., and Chaloner, W.G., 1980. Fossil charcoal as evidence of past atmospheric composition. *Nature*, 283: 647–649.

Corral J.C., López Del Valle R., and Alonso J., 1999. El ámbar cretácico de Álava (Cuenca Vasco-Cantábrica, norte de España). Su colecta y preparación. *Estudios del Museo de Ciencias Naturales de Álava*, 14(special volume): 7–21.

Daviero, V., Gomez, B., and Philippe, M., 2001. Uncommon branching pattern within conifers: *Frenelopsis turolensis*, a Spanish Lower Cretaceous Cheirolepidiaceae. *Canadian Journal of Botany*, 79: 1400–1408.

Delclòs, X., Arillo, A., Peñalver, E., Barrón, E., Soriano, C., López del Valle, R., Bernárdez, E., Corral, C., and Ortuño, V. M., 2007. Fossiliferous amber deposits from the Cretaceous (Albian) of Spain. *Comptes Rendus Palevol*, 6: 135–149.

Doyle, J.A., and Robbins, E.I., 1977. Angiosperm pollen zonation of the Continental Cretaceous of the Atlantic coastal plain and its application to deep wells in the Salisbury embayment. *Palynology*, 1: 43–78.

Eisner, T., Carrel, J.E., Van Tassel, E., Hoebeke, E.R., and Eisner, M., 2002. Construction of a defensive trash packet from sycamore leaf trichomes by a chrysopid larva (Neuroptera: Chrysopidae). *Proceedings of the Entomological Society of Washington*, 104(2): 437–446.

Engel, M. S., and Grimaldi, D. A., 2007. The neuropterid fauna of Dominican and Mexican amber (Neuropterida: Megaloptera, Neuroptera). *American Museum Novitates*, 3587: 58 pp.

Farjon, A., 2008. *The natural history of Conifers*. Timber Press, New York, 304.

García-Mondéjar, J., Aguirrezabala, L.M., Aranburu, A., Fernández-Mendiola, P.A., Gómez-Pérez, I., López-Horgue, M., and Rosales, I., 1996. Aptian-Albian

tectonic pattern of the Basque-Cantabrian Basin (northern Spain). *Geological Journal*, 31: 13–45.

Glasspool, I.J., Edwards, D., and Axe, L., 2004. Charcoal in the Silurian as evidence for the earliest wildfire. *Geology*, 32(5): 381–383.

Gomez, B., Martín-Closas, C., Barale, G., Solé de Porta, N., Thévenard, F., and Guignard, G., 2002. *Frenelopsis* (Coniferales: Cheirolepidiaceae) and related male organ genera from the Lower Cretaceous of Spain. *Palaeontology*, 45: 997–1036.

Gomez, B., Martín-Closas, C., Méon, H., Thévenard, F., and Barale, G., 2001. Plant taphonomy and palaeoecology in the lacustrine delta of Uña (Upper Barremian, Iberian Ranges, Spain). *Palaeogeography, Palaeoclimatology, Palaeoecology*, 170: 133–148.

Gradstein, F.M., and Ogg, J.G., 2009. The geologic time scale. In: Hedges, S.B., and Kumar, S. (eds.), *The Timetree of Life*, Oxford University Press, 26–34.

Grimaldi, D.A., 1996. *Amber: window to the past*. American Museum of Natural History Ed., New York, 215.

Grimaldi, D.A., and Engel, M.S., 2005. *Evolution of the insects*. Cambridge University Press, New York, 755 p.

Grimaldi, D.A., Shedrinsky, A., and Wampler, P., 2000. A remarkable deposit of fossiliferous amber from the Upper Cretaceous (Turonian) of New Jersey. In: Grimaldi, D.A. (ed.), *Studies on Fossils in Amber, with Particular Reference to the Cretaceous of New Jersey*. Backhuys Publishers Leiden, Leiden, 1–76.

Hautevelle, Y., Michels, R., Malartre, F., and Trouiller, A., 2006. Vascular plant biomarkers as proxies for palaeoflora and palaeoclimatic changes at the Dogger/Malm transition of the Paris Basin (France). *Organic Geochemistry*, 23: 610–625.

Hines, F.M., 1985. Sedimentation and tectonics in north-west Santander. In: Milá, M.D., and Rosell, J. (eds.), 6th European Regional Meeting, Excursion Guidebook. International Association of Sedimentologists, 371–398.

Jarzembowski, E.A., Azar, D., and Nel, A., 2008. A new chironomid (Insecta: Diptera) from Wealden amber (Lower Cretaceous) of the Isle of Wight (UK). *Geologica Acta*, 6(3): 285–291.

Le Pichon, X., and Sibuet, J.C., 1971. Western extension of boundary between European and Iberian plates during the Pyrenean orogeny. *Earth and Planetary Science Letters*, 12: 83–88.

Martínez-Delclòs, X., Briggs, D.E.G., and Peñalver, E., 2004. Taphonomy of insects in carbonates and amber. *Palaeogeography, Palaeoclimatology, Palaeoecology*, 203: 19–64.

Mendes, M.M., Dinis, J.L., Gomez, B., and Pais, J., 2010. The cheirolepidiaceous conifer *Frenelopsis teixeirae* Alvin et Pais from the lower Hauterivian of Vale Cortiço (Torres Vedras, western Portugal). *Review of Palaeobotany and Palynology*, doi: 10.1016/j.revpalbo.2010.03.002.

Menor-Salván, C., Najarro, M., Rosales, I., Velasco, F., and Tornos, F., 2009a. Quimiotaxonomía y origen botánico del ámbar de El Soplao (Cantabria, España). *Macla*, 11: 123–124.

Menor-Salván, C., Najarro, M., Rosales, I., Velasco, F., Tornos, F., and Simoneit, B.R.T., 2010. Biological diterpenes preserved in lower Cretaceous amber from Basque Cantabrian Basin (El Soplao, Cantabria, Spain). Paleochemotaxonomical aspects. *Organic Geochemistry*. Accepted.

Menor-Salván, C, Najarro, M., Velasco, F., Tornos, F., and Rosales, I., 2009b. A new Lower Cretaceous fossil resin from El Soplao, Cantabria (Spain): Biomarkers and chemotaxonomy. *Geochimica et Cosmochimica Acta*, 73(13S), A870.

Miller, C.N., 1999. Implications of Fossil Conifers for the Phylogenetic Relationships of Living Families. *Botanical Reviews*, 65: 239–277.

Najarro, M., Peñalver, E., Rosales, I., Pérez-de la Fuente, R., Daviero-Gomez, V., Gomez, B., and Delclòs, X., 2009. Unusual concentration of Early Albian arthropod-bearing amber in the Basque-Cantabrian Basin (El Soplao, Cantabria, Northern Spain): Palaeoenvironmental and palaeobiological implications. *Geologica Acta*, 7(3): 363–387.

Najarro, M., Rosales, I., and Martín-Chivelet, J., 2010. Major palaeoenvironmental perturbation in an Early Aptian carbonate platform: Prelude of the Oceanic Anoxic Event 1a?. *Sedimentary Geology*, doi: 10.1016/j.sedgeo.2010.03.011.

Nel, P., Peñalver, E., Azar, D., Hodebert, G., and Nel, A., 2010. Modern thrips families Thripidae and Phlaeothripidae in the Early Cretaceous amber (Insecta: Thysanoptera). *Annales de la Société entomologique de France*, 46(1). In press.

Nichols, G., Cripps, J.A., Collinson, M.E., and Scott, A.C., 2000. Experiments in waterlogging and sedimentology of charcoal: results and implications. *Palaeogeography, Palaeoclimatology, Palaeoecology*, 164: 43–56.

Nosova, N., and Wcisło-Luraniec, E., 2007. A reinterpretation of *Mirovia* Reymanówna (Coniferales) based on the reconsideration of the type species *Mirovia szaferi* Reymanówna from the Polish Jurassic. *Acta Palaeobotanica,* 47: 359–377.

Ortega-Blanco, J., Peñalver, E., Delclòs, X., and Engel, M.S., 2010a. False fairy wasps in Early Cretaceous amber from Spain (Hymenoptera: Mymarommatoidea). *Palaeontology*. In press.

Ortega-Blanco, J., Rasnitsyn, A.P., and Delclòs, X., 2008. First record of anaxyelid woodwasps (Hymenoptera: Anaxyelidae) in Lower Cretaceous Spanish amber. *Zootaxa*, 1937: 39–50.

Ortega-Blanco, J., Rasnitsyn, A.P., and Delclòs, X., 2010b. A new family of ceraphronoid wasps from Early Cretaceous Álava Amber, Spain. *Acta Paleontologica Polonica*. In press.

Otto, A., and Simoneit, B.R.T., 2002. Biomarkers of Holocene buried conifer logs from Bella Coola and north Vancouver, British Columbia, Canada. *Organic Geochemistry*, 33: 124–1251.

Otto, A., Simoneit, B.R.T., and Wilde, V., 2007. Terpenoids as chemosystematic markers in selected fossil and extant species of Pine (*Pinus*, Pinaceae). *Botanical Journal of the Linnean Society*, 154: 129–140.

Peñalver, E., Delclòs, X., and Soriano, C., 2007. A new rich amber outcrop with palaeobiological inclusions in the Lower Cretaceous of Spain. *Cretaceous Research*, 28: 791–802.

Peñalver, E., Grimaldi, D., and Delclòs, X., 2008. *Early spider web*. Yearbook of Science and Technology 2008. MacGraw Hill: 103–105.

Pereira, R., de Souza Carvalho, I., Simoneit, B.R.T., and de Almeida Azevedo, D., 2009. Molecular composition and chemosystematic aspects of Cretaceous amber from the Amazonas, Araripe and Recôncavo basins, Brasil. *Organic Geochemistry*, 40: 863–875.

Pérez-de la Fuente, R., Nel, A., Peñalver, E., and Delclòs, X., 2010. A new Early Cretaceous snakefly (Raphidioptera: Mesoraphidiidae) from El Soplao amber (Spain). *Annales de la Société entomologique de France*, 46(1). In press.

Perrichot, V., and Néraudeau, D., 2009. Foreword. Cretaceous ambers from southwestern France: geology, taphonomy and palaeontology. *Geodiversitas*, 31(1): 7–12.

Peyrot, D., Rodríguez-López, J.P., Barrón, E., and Meléndez, N., 2007a. Palynology and biostratigraphy of the Escucha Formation in the Early Cretaceous Oliete Sub-basin, Teruel, Spain. *Revista Española de Micropaleontología*, 39(1–2): 135–154.

Peyrot, D., Rodríguez-López, J.P., Lassaletta, L., Meléndez-Hevia, N., and Barrón, E., 2007b. Contributions to the palaeoenvironmental knowledge of the Escucha Formation in the Lower Cretaceous Oliete Sub-basin, Teruel, Spain. *Comptes Rendus Palevol*, 6: 469–481.

Rat, P., 1988. The Basque-Cantabrian basin between the Iberian and European plates some facts but still many problems. *Revista de la Sociedad Geológica de España*, 1: 327–348.

Riera, V., Marmi, J., Oms, O., and Gomez, B., 2010. Orientated plant fragments revealing tidal palaeocurrents in the Fumanya mudflat (Maastrichtian, southern Pyrenees): insights in palaeogeographic reconstructions. *Palaeogeography, Palaeoclimatology, Palaeoecology*, 288: 82–92.

Robinson, J.M., 1989. Phanerozoic O_2 variation, fire, and terrestrial ecology. *Palaeogeography, Palaeoclimatology, Palaeoecology*, 75: 223–240.

Sander, P.M., and Gee, C.T., 1990. Fossil charcoal: techniques and applications. *Review of Palaeobotany and Palynology*, 63: 269–279.

Scott, A.C., 2000. The Pre-Quaternary history of fire. *Palaeogeography, Palaeoclimatology, Palaeoecology*, 164: 281–329.

Scott, A.C., 2010. Charcoal recognition, taphonomy and uses in palaeoenvironmental analysis. *Palaeogeography, Palaeoclimatology, Palaeoecology*, doi: 10.1016/j.palaeo.2009.12.012

Scott, A.C., and Stea, R., 2002. Fires sweep across the Mid-Cretaceous landscape of Nova Scotia. *Geoscientist*, 12 (1): 4–6.

Scott, A.C., Cripps, J.A., Collinson, M.E., and Nichols, G.J., 2000. The taphonomy of charcoal following a recent heathland fire and some implications for the interpretation of fossil charcoal deposits. *Palaeogeography, Palaeoclimatology, Palaeoecology*, 164(1–4): 1–31.

Seoane, L.V., 1998. Comparative study of extant and fossil conifer leaves from the Baqueró Formation (Lower Cretaceous), Santa Cruz Province, Argentina. *Review of Palaeobotany and Palynology*, 99: 247–263.

Silvester, W.B., and Orchard, T.A., 1999. The biology of kauri (*Agathis australis*) in New Zealand. I. Production, biomass, carbon storage, and litter fall in four forest remnants. *New Zealand Journal of Botany*, 37: 553–571.

Soto, R., Casas-Sainz, A.M., Villalaín, J., and Oliva-Urcía, B., 2007. Mesozoic extension in the Basque Cantabrian basin (N Spain): Contributions from AMS and brittle mesostructures. *Tectonophysics*, 445: 373–394.

Stefanova, M., Oros, D.R., Otto, A., and Simoneit, B.R.T., 2002. Polar aromatic biomarkers in the Miocene Maritza-East lignite, Bulgaria. *Organic Geochemistry*, 33: 1076–1091.

Suárez-Ruiz, I., 2003. Caracterización y estudio petrográfico del ámbar y de los sedimentos carbonosos a él asociados en el Cretácico de Álava (País Vasco). *Estudios del Museo de Ciencias Naturales de Álava*, 18(special volume): 63–89.

Sweeney, J.J., and Burnham, A.K., 1989. A chemical kinetic model of vitrinite maturation and reflection. *Geochimica et Cosmochimica Acta*, 53: 2649–2657.

Wilmsen, M., 2005. Stratigraphy and biofacies of the Lower Aptian of Cuchía (Cantabria, northern Spain). *Journal of Iberian Geology*, 31: 253–275.

Yamamoto, S., Otto, A., Krumbiegel, G., and Simoneit, B.R.T., 2006. The natural product biomarkers in succinite, glessite and stantienite ambers from Bitterfield, Germany. *Review of Palaeobotany and Palynology*, 140: 27–49.

CAPÍTULO 5:

CONCLUSIONES

CAPÍTULO 5

CONCLUSIONES

En este capítulo final se destacan los resultados más relevantes aportados por esta Tesis Doctoral en los capítulos de tectónica, litoestratigrafía y bioestratigrafía, así como las conclusiones sacadas de los artículos científicos (capítulo 4).

5.1.- TECTÓNICA

Los datos e interpretaciones aportados en este estudio han incrementado el conocimiento de la estructura de la Cuenca Nor-Cantábrica en los siguientes puntos:

1) La estructura de los sectores estudiados de la Banda del Nansa y del Bloque Costero de Santander se ha descrito en planta y en diversos cortes geológicos. La Banda del Nansa constituye un imbricado alpino de pliegues de propagación de falla E-O y vergencia sur que se atenúa hacia el este por disminución del gradiente de acortamiento. La estructura del Bloque Costero de Santander está configurada por fallas normales e inversas con orientaciones variables N060, N017 y N097, pliegues asociados y alineaciones de diapiros que en conjunto definen una distribución poco simétrica.
2) Las anteriores diferencias se explican mecánicamente considerando que la Banda del Nansa representa el estilo de deformación del basamento donde la geometría de las fallas causativas es heredada de los cabalgamientos variscos y la cobertera delgada mesozoica se adapta pasivamente. En contraste, la estructura del Bloque Costero de Santander representa un estilo de deformación de cobertera muy segmentado, parcialmente desvinculado del basamento por el horizonte dúctil del Keuper.
3) Se han identificado las principales estructuras extensionales que producen cambios de espesor en los sedimentos del Aptiense-Albiense Inferior. En la Banda del Nansa (área de La Florida) la restitución de las capas de la Fm. Reocín a su estado pre-alpino permite concluir que existe una flexión del

basamento hacia N117 en el bloque inferior de la falla de Bustriguado, que es la falla principal que separa la Banda del Nansa y el Bloque Costero de Santander. En el Bloque Costero de Santander la forma de la cuenca extensional se ha reconstruido mediante el contorneo del relleno sinextensivo usando como discontinuidades las fallas reconocidas en el mapa y en los cortes geológicos, para concluir que existen dos subcuencas individuales (Treceño y Santander), separadas por un alto transverso NNO-SSE (Reocín) situado en la zona de solape de los segmentos de falla. La subsidencia dentro de estas subcuencas refleja la variación del desplazamiento de las fallas a lo largo de su dirección, la transferencia del desplazamiento a otras fallas y en gran medida también la movilidad de la sal del Keuper.

4) Finalmente se ha elaborado un modelo extensional para explicar la forma en planta de este sector de la cuenca Nor-Cantábrica. Así, la extensión dentro del Bloque Costero de Santander ocurre en los bloques de fallas N060 con relevos en escalera destrales a 30º respecto a los límites externos del basamento orientados E-O, lo que es característico de zonas de *rift* de baja oblicuidad. Con este patrón, la dirección de extensión más propicia es N330 pero existe un rango de variación compatible de unos 45º hacia el norte.

5.2.- LITOESTRATIGRAFÍA Y BIOESTRATIGRAFÍA

1) Se han levantado 15 columnas estratigráficas a lo largo de los tres sectores de estudio (áreas de La Florida, sinclinal de Santillana y Cuchía), que en conjunto acumulan más de 3.100 metros de serie estratigráfica medida. Estas secciones han servido de base para caracterizar los tipos de facies y sus cambios laterales, con especial atención en la geometría de los depósitos, litología, textura, contenido fósil y presencia de estructuras sedimentarias. Constituyen también la base para el reconocimiento de las secuencias deposicionales y ayudan a establecer la geometría de la cuenca extensiva y los rasgos paleogeográficos principales.

2) Con respecto a la litoestratigrafía, se ha erigido un armazón más preciso que el existente, mejorando la caracterización de las unidades incluyendo las series

tipo (estratotipo e hipoestratotipo) y proponiendo la definición de una nueva unidad estratigráfica, la Formación Rábago, de edad Aptiense Inferior (Bedouliense inferior), en las áreas de La Florida y del sinclinal de Santillana.

3) Como resultado bioestratigráfico, este trabajo aporta nuevas dataciones en base a ammonites, foraminíferos planctónicos y bentónicos, nanofósiles calcáreos y palinomorfos. Mediante datos bioestratigráficos y litoestratigráficos se ha podido determinar la existencia de una laguna estratigráfica que abarca al menos la parte alta del Aptiense Inferior y la base del Aptiense Superior en el área de La Florida, de lagunas estratigráficas que abarcan la parte más basal del Aptiense (Fm. Rábago) y gran parte del Albiense Inferior y Medio en el área de Cuchía (Fm. Las Peñosas), y se ha afinado la edad de varias unidades en el área de Cuchía y La Florida (ej. Fm. Patrocinio).

4) Las facies reconocidas en las secciones estratigráficas del Aptiense y Albiense Inferior han permitido establecer la siguiente evolución de ambientes sedimentarios:

    a. Plataforma mixta terrígeno-carbonatada (Fm. Rábago, Aptiense Inferior, Bedouliense inferior, parte baja de la Zona *D. oglanlensis*): presenta facies siliciclásticas someras de plataforma submareal a intermareal; facies de plataforma abierta mixta terrígeno-carbonatada con orbitolinas y facies de plataforma carbonatada interna somera restringida, de corales, rudistas y miliólidos.
    b. Rampa interna-media energética con bajíos o *shoals* (Fm. Umbrera, Aptiense Inferior, Bedouliense inferior, parte alta de la Zona *D. oglanlensis*): presenta facies energéticas de calcarenitas *grainstone-packstone* oolítico-bioclásticas con estratificación cruzada, interpretadas como bajíos o *shoals* de rampa interna-media.
    c. Cuenca marina abierta, prodelta y frente deltaico (Fm. Patrocinio, Aptiense Inferior, Bedouliense inferior, Zona *D. forbesi*): presenta lutitas margosas oscuras de ambiente de cuenca y facies heterolíticas de lutitas y areniscas de prodelta a frente deltaico.

d. Plataforma carbonatada somera (Fm. San Esteban, Aptiense Inferior, Bedouliense superior, zonas *D. deshayesi* y *D. furcata*): compuesta principalmente por alternancia de bancos de margocalizas con orbitolinas, calizas con miliólidos y calizas con requiénidos, corales y *L. aggregatum-B. irregularis*.
e. Plataforma carbonatada externa-media y plataforma siliciclástica (Fm. Rodezas, Gargasiense inferior, parte baja del Aptiense Superior): formada por calizas margosas con corales; *packstone* con bioclastos y orbitolinas; lutitas, limos y areniscas de *offshore* y *shoreface*; y calizas margosas con braquiópodos y ostreidos (aislados o formando bancos monoespecíficos de *Exogyra latissima* o *Plicatula placunea*).
f. Plataforma carbonara somera interna a externa (Fm. Reocín, Aptiense Superior–parte basal del Albiense Inferior): formada por alternancia de bancos de caliza rica en foraminíferos bentónicos y rudistas y bancos de caliza micrítica con *B. irregularis-L. aggregatum*, que lateralmente gradan a margas y calizas nodulosas con orbitolinas, esponjas y corales, y calizas *grainstone* y *packstone* bioclásticas.
g. Sistema deltaico-estuarino (Fm. Las Peñosas, Albiense Inferior): constituida por facies mixta terrígeno-carbonatada de relleno de bahía/*lagoon* influenciado por marea y oleaje, de llanura deltaica y relleno de canal, de relleno de bahía interdistributaria y de frente deltaico con barras distributarias.

5) Se han identificado 5 secuencias de depósito transgresivas-regresivas (T-R) principales limitadas por discontinuidades. Estas secuencias son: 1) SD1, Bedouliense basal. Comprende la Fm. Rábago. No tiene representación en el área de Cuchía (por laguna estratigráfica). Límite inferior: superficie de transgresión rápida sobre materiales continentales del Cretácico inferior (facies Weald) o del Triásico (facies Buntsandstein). Límite superior: superficie de truncamiento erosivo (área del sinclinal de Santillana) y superficie de exposición subaérea (área de la Florida); 2) SD2, Bedouliense inferior-superior. Comprende a las Fms. Umbrera, Patrocinio y San Esteban. Límite inferior: erosión y transgresión rápida sobre materiales continentales del Cretácico inferior (facies

Weald; área de Cuchía), superficie de exposición subaérea (área de la Florida) y truncamiento erosivo (área del sinclinal de Santillana). Límite superior: diastema (área del sinclinal de Santillana), superficie de exposición subaérea (área de Cuchía) y laguna estratigráfica a techo de la Fm. Patrocinio (área de La Florida); 3) SD3, Gargasiense inferior. Comprende a la Fm. Rodezas y parte inferior de la Fm. Reocín. Límite superior: exposición subaérea y posterior retrabajamiento erosivo durante la siguiente transgresión marina (área de La Florida), superficie erosiva y de regresión forzada (área Suances-Cuchía) y máximo regresivo de facies (área del sinclinal de Santillana; 4) SD4, Gargasiense–base del Albiense Inferior. Comprende la parte superior de la Fm. Reocín. Límite superior: superficie de exposición subaérea a techo de la Fm. Reocín; 5) SD5, Albiense Inferior. Comprende la Fm. Las Peñosas. No tiene representación en el área de Cuchía (por laguna estratigráfica). Se interpreta esta secuencia como el relleno transgresivo de valles incisos de escala kilométrica controlados por tectónica. Límite superior: nivel transgresivo bioturbado y noduloso, con bivalvos megalodontos, sobre el cual se recupera la sedimentación carbonatada de la Formación Barcenaciones del Albiense Superior en todas las zonas de estudio. El origen de estas secuencias se atribuye a la acción conjunta de la actividad local sinsedimentaria de las fallas distensivas, junto a los cambios eustáticos y paleoambientales que tuvieron lugar durante el Aptiense-Albiense Inferior.

6) Como resultado del análisis quimioestratigráfico ($\delta^{13}C$, $\delta^{18}O$, TOC, $CaCO_3$) de alta resolución realizado sobre las margas de la Fm. Patrocinio se han identificado sendas excursiones en la relación isotópica de $^{13}C/^{12}C$ del carbono tanto orgánico como inorgánico del sedimento, y que se relacionan con el evento anóxico OAE 1a. Estas conclusiones serán tratadas con mayor detalle en el siguiente apartado dedicado a las conclusiones de los artículos científicos.

5.3.- ARTÍCULOS CIENTÍFICOS

Las conclusiones principales de los artículos científicos que se aportan en esta Tesis son las siguientes:

Major palaeoenvironmental perturbation in an Early Aptian carbonate platform: prelude of the Oceanic Anoxic Event 1a?

1) Este trabajo muestra el impacto regional y los efectos que tuvo el Evento Anóxico Oceánico del Aptiense Inferior (OAE 1a) en carbonatos de plataforma de aguas someras depositados durante el Aptiense Inferior en la cuenca Nor-Cantábrica, a partir de un análisis sedimentológico, diagenético y quimioestratigráfico de dichos depósitos carbonatados.
2) Para el Aptiense Inferior del área de estudio se han reconocido cuatro estadios evolutivos de producción carbonatada: 1) plataforma mixta terrígeno-carbonatada a plataforma carbonatada con corales y rudistas, que culmina con exposición subaérea (Fm. Rábago), 2) plataforma transgresiva calcarenítica con bioclástos (grandes foraminíferos aglutinantes, briozoos, equinodermos, algas rojas, ostreidos, bivalvos, gasterópodos) y oolitos ferruginosos (Fm. Umbrera), 3) margas y lutitas margosas oscuras que culminan con arenas (Fm. Patrocinio), y 4) calizas de plataforma somera con rudistas y corales (Fm. San Esteban) que culminan con exposición subaérea. El estadio 3 corresponde con la expresión local del Evento Anóxico Oceánico del Aptiense Inferior (OAE1a).
3) Los estadios carbonatados que preceden el OAE1a, muestran un cambio composicional de comunidades *fotozoan* (estadio 1) a *heterozoan* (estadio 2). Estos dos estadios de producción carbonatada están separados por una discontinuidad. Esta discontinuidad presenta evidencias de erosión, disolución kárstica y diagénesis meteórica. Sobre ella se generó, en un ambiente submarino, una costra marina ferruginosa con incrustación de serpúlidos y foraminíferos aglutinantes (nubeculáridos) durante el siguiente episodio transgresivo.
4) Los cambios composicionales en la fábrica de carbonato estuvieron acompañados de una mayor actividad tectónica junto con una aceleración del ciclo hidrogeológico, lo que favoreció el aporte de partículas terrígenas desde zonas

emergidas y un incremento del aporte de agua dulce y de nutrientes a la plataforma, causando el cambio de condiciones oligotróficas a mesotróficas.

5) La acción conjunta del incremento en el aporte de agua dulce, eutrofización de las aguas por el aumento en el aporte de nutrientes, la actividad tectónica, y la subida del nivel del mar, debieron producir la desestabilización en el ambiente marino y el cambio a factorías de producción de carbonatos menos efectivas (comunidades *heterozoan*) justo antes del OAE1a.
6) Finalmente, la integración de los análisis sedimentológicos, diagenéticos y quimioestratigráficos ha resultado ser de gran utilidad a la hora de identificar y caracterizar las perturbaciones paleoclimáticas globales en ambientes de plataforma carbonatada somera.

High-resolution chemo- and biostratigraphic records of the Early Aptian Oceanic Anoxic Event in Cantabria (N Spain): Palaeoceanographic and palaeoclimatic implications

1) Este estudio presenta nuevos registros quimioestratigráficos ($\delta^{13}C$, TOC, $CaCO_3$) y bioestratigráficos (ammonites, foraminíferos plantónicos, nanofósiles calcáreos, palinomorfos) de dos secciones del Aptiense Inferior (La Florida y Cuchía) de la cuenca Nor-Cantábrica, habiéndose identificado en ambas secciones la señal del Evento Anóxico Oceánico del Aptiense Inferior (OAE1a o evento *Selli*). Este evento se caracterizó en el área de estudio por el cese de la sedimentación carbonatada de plataforma somera y el depósito de unos 40 m de espesor de una unidad margosa relativamente rica en materia orgánica (Formación Patrocinio).
2) El estudio quimioestratigráfico de isótopos de carbono, tanto en la fracción de carbonato como de materia orgánica ($\delta^{13}C_{car}$, $\delta^{13}C_{org}$) de la Fm. Patrocinio en las áreas de La Florida y Cuchía, ha revelado que esta unidad margosa registra una excursión negativa del $\delta^{13}C$ en ambos reservorios de C, tal y como ha sido observado en otras cuencas durante el Aptiense Inferior al inicio del OAE 1a, justo precediendo al nivel *Selli*. Esta anomalía negativa se atribuye al segmento C3 de la curva de referencia del isótopo de C durante el Aptiense.

3) Estos datos quimioestratigráficos han sido calibrados con nuevos datos bioestratigráficos basados en biozonas de ammonites, nanofósiles calcáreos y foraminíferos planctónicos. La combinación de estas biozonas acota la edad del segmento C3 del OAE 1a en el área de estudio a la parte media-alta de la zona *Deshayesites forbesi* (antes denominada *D. weissi*) de ammonites, la parte alta de la zona *Blowiella blowi* de foraminíferos planctónicos, y la parte alta de la zona *Hayesites irregularis* de nanofósiles calcáreos.
4) A partir del registro de nanofósiles calcáreos se ha identificado una laguna estratigráfica en el área de La Florida, que afecta a los segmentos C4–C7 de la curva isotópica de referencia. Estos segmentos C4–C7 si han sido identificados en la curva de isótopos de C obtenida para el área de Cuchía. Además, se ha identificado otra excursión negativa del $\delta^{13}C_{carb}$ y $\delta^{13}C_{org}$ que postdata la primera aparición de *Eprolithus floralis*, lo que es equivalente a la zona *Dufrenoyia furcata* de ammonites. Esta nueva anomalía en la curva del isótopos de C, que equivaldría al pre-Nivel *Noir* definido en Francia o al evento *Aparein* de otras secciones de la cuenca Vascocantábrica (según Millán et al. 2009), se correlaciona aquí con el depósito de margas con glauconita y *black shales*, mientras que en otras parte de la cuenca y en el norte del Tetis (Nivel *Noir*) justo precede el depósito de *black shales*. Este patrón se asemeja a la excursión negativa del isótopo de C al comienzo del OAE 1a, antes del nivel *Selli*.
5) El análisis cuantitativo de nanofósiles muestra la escasez de nanocoides de canal estrecho coincidiendo con la excursión negativa de la Formación Patrocinio. Esto corrobora la interpretación de una crisis contemporánea de biocalcificación relacionada con los cambios de CO_2 inducidos en el quimismo del océano en los estadios que preceden el pico del OAE 1a.
6) El análisis de palinomorfos ha permitido identificar un máximo térmico, seguido de un enfriamiento en los ecosistemas terrestres. Así, se ha identificado un máximo de *Classopollis* (polen procedente de árboles de la familia Cheirolepidiaceae, que se asocia a climas más calurosos) durante el OAE 1a, al cual le sigue un descenso de *Classopollis* y un incremento de polen bisacado después del evento. Las condiciones más frías justo antes y después del OAE deducidas por el contenido polínico pudieron deberse a un efecto invernadero

reverso, producido por la disminución de CO_2 debido al enterramiento masivo de materia orgánica en las cuencas oceánicas durante el OAE 1a.

Unusual concentration of Early Albian arthropod-bearing amber in the Basque-Cantabrian Basin (El Soplao, Cantabria, Northern Spain): Palaeoenvironmental and palaeobiological implications

1) Este trabajo presenta un estudio paleoambiental y paleobotánico preliminar del yacimiento de ámbar de El Soplao, de edad Albiense Inferior.
2) El yacimiento se incluye en una unidad siliciclástica de ambiente continental a marino-transicional (Formación Las Peñosas), que está intercalada en una sucesión de depósitos marinos, principalmente carbonatados, de edad Aptiense Inferior-Albiense Superior. La Formación Las Peñosas internamente se subdivide en dos ciclos regresivos-transgresivos de bajo rango. Los depósitos ricos en ámbar y carbones se depositaron en ambientes deltaico-estuarinos desarrollados durante los episodios de máxima regresión e inicio de la transgresión, de los ciclos regresivo-transgresivo menores. El estudio sedimentológico de esta unidad indica que el yacimiento de ámbar constituye parte del relleno de una bahía interdistributaria que lateralmente se asocia con canales fluvio-deltaicos meandriformes. Los niveles ricos en ámbar también presentan abundantes fragmentos de carbón, madera, y hojas con excelente preservación de sus texturas vegetales. Estos niveles aparecen tanto en lutitas oscuras, laminadas, con abundante materia orgánica, como en niveles discontinuos de areniscas y limos masivos o laminados con fragmentos de madera. Estos depósitos también contienen conchas de moluscos marinos y/o de agua salobre, lo que sugiere un ambiente de depósito litoral o de marisma costera. De esta manera, los sedimentos ricos en ámbar se depositaron en un ambiente costero de bahía interdistributaria de baja energía, conectado con el mar y afectado ocasionalmente por condiciones energéticas mayores. Las inundaciones producidas durante tormentas tropicales pudieron erosionar y arrastrar el ámbar y los restos de plantas desde los bosques que bordeaban la costa, siendo transportados por flujos de densidad, que llevaban además arcilla y arenas, hacia la costa y bahías interdistributarias, donde se acumularon y enterraron rápidamente. La mayoría de

las masas de ámbar muestran su forma original subredondeada o de estalactita, lo que sugiere una baja erosión durante el transporte.

3) El yacimiento de El Soplao, muy probablemente se originó durante un periodo de abundante producción de resina en los paleo-bosques, posiblemente coincidiendo con un episodio de clima más cálido. Los niveles asociados con el ámbar presentan abundantes cutículas de plantas perfectamente preservadas, asignadas principalmente a los géneros de coníferas *Frenelopsis* y *Arctopitys* (citado como *Mirovia* en este artículo pero renombrado con posterioridad) y en menor proporción hojas de ginkgoales de los géneros de *Nehvizdya* y *Pseudotorellia*.
4) El ámbar de El Soplao está caracterizado por la profusión de piezas de ámbar subaéreas de flujos tipo estalactítico o *chorreadura*.
5) Las bioinclusiones están representadas principalmente por insectos fósiles de los órdenes Blattaria, Hemiptera, Thysanoptera, Raphidioptera, Neuroptera, Coleoptera, Hymenoptera y Diptera.
6) Algunos de los insectos encontrados pertenecen a grupos con una escasa representación en el registro fósil, tales como un nuevo morfotipo de la avispa *Archaeromma* (de la familia Mymarommatidae) y el pequeño jején *Lebanoculicoides* (de la subfamilia monogenérica Lebanoculicoidinae).
7) El espectro FTIR del ámbar de El Soplao es muy similar al que muestra el ámbar de otros yacimientos del Cretácico de España.

Review of the El Soplao amber outcrop, Early Cretaceous of Cantabria, Spain.

1) Los datos más relevantes que se aportan en este artículo corresponden a los estudios biogeoquímico, palinológico, tafonómico y de bioinclusiones de artrópodos del ámbar de El Soplao, los cuales complementan los trabajos previamente publicados.
2) Los datos biogeoquímicos presentados en este trabajo sugieren la presencia de al menos dos orígenes o fuentes botánicas distintas para el ámbar de El Soplao. El primero (ámbar tipo A), tendría un origen relacionado con la familia Cheirolepidiaceae, mientras que el segundo (ámbar tipo B) no muestra biomarcadores específicos de coníferas. El estudio comparativo de la composición molecular del ámbar tipo A con hojas de *Frenelopsis* (Cheirolepidiaceae) indica una gran afinidad bioquímica entre ambos, sugiriendo un origen botánico común.

3) El estudio palinológico de los depósitos del yacimiento revela una alta diversidad taxonómica regional, principalmente de esporas de pteridofitas y granos de polen de gimnospermas. Así, los datos palinológicos aportados sugieren que la región estuvo habitada por bosques de coníferas adaptados a estaciones secas en un clima subtropical.
4) Los nuevos datos de las inclusiones biológicas del ámbar de El Soplao muestran una alta diversidad de la entomofauna, principalmente representada por los órdenes dipteráno y himenopteráno, con la presencia de grupos muy especializados como los crisópidos o gorgojos, lo cual puede ayudar a una mejor compresión en el inicio de la evolución de algunos grupos de insectos.
5) La presencia de restos vegetales carbonizados (*charcoal*), piezas de ámbar dañadas por fuego y fibras de plantas carbonizadas encontradas en el interior del ámbar, sugieren que el origen del ámbar de El Soplao pudo estar asociado por grandes paleo-incendios.
6) Los nuevos de datos aportados en este trabajo junto con los resultados previamente publicados sugieren el siguiente escenario como origen del yacimiento de ámbar de El Soplao: la resina fue exudada por coníferas (posiblemente por dos tipos de coníferas, incluyendo las de la familia Cheirolepidiaceae), en bosques cercanos a ambientes deltaicos. Estos bosques de coníferas estaban ampliamente extendidos en la región, presentando pteridofitas, cicadáceas y Bennettitales; las charcas y áreas pantanosas estaban ocupadas por criptógamas vasculares y angiospermas primitivas, las cuales podían habitar en hábitats acuáticos. Una gran diversidad de insectos, representados principalmente por dípteros e himenópteros, se desarrolló alrededor de las plantas coníferas, siendo atrapados en su resina. Los coleópteros, que probablemente vivieron debajo de la corteza o en contacto con la madera de las coníferas, fueron también incluidos en la resina. El desarrollo de grandes incendios en los bosques pudo fomentar la producción de resina, así como favorecer la intensa erosión del lecho del bosque parcialmente quemado. La resina, hojas, madera y plantas quemadas fueron transportados como flujos de derrubios por los cursos de agua y fueron acumulados junto con moluscos de agua marina o salobre en lagunas y canales de marea restringidos con escasa circulación y condiciones anóxicas en el fondo. Las coníferas *Frenelopsis*, potencial fuente de la resina, tal y como sugieren los análisis biogeoquímicos, crecieron cerca del área de depósito, donde se

depositaron ramas articuladas (depósito parautóctono). Las piezas de resina difieren en su historia bioestratinómica, debido a que alguna de ellas permanecieron cierto tiempo expuestas a las aguas marinas someras, donde fueron colonizadas por serpúlidos y briozoos que crecieron en la superficie de la resina. La baja circulación y las condiciones anóxicas del fondo produjeron una piritización temprana en la concha de los moluscos marinos, así como en las plantas quemadas y en la superficie de las masas de ámbar, incluyendo los tubos de serpúlidos. Todo ello fue posteriormente enterrado por limos y arenas. Las máximas temperaturas alcanzadas durante la diagénesis en el yacimiento de El Soplao fueron del rango de 60-70ºC. Estos bajos niveles de maduración, pudieron ser los responsables de la excelente preservación de la composición molecular del ámbar y de sus bioinclusiones.

APÉNDICE

Sedimentary Geology 235 (2011) 50–71

Contents lists available at ScienceDirect

Sedimentary Geology

journal homepage: www.elsevier.com/locate/sedgeo

Major palaeoenvironmental perturbation in an Early Aptian carbonate platform: Prelude of the Oceanic Anoxic Event 1a?

María Najarro [a,*], Idoia Rosales [a], Javier Martín-Chivelet [b]

[a] Departamento de Investigación y Prospectiva Geocientífica, Instituto Geológico y Minero de España, IGME, Ríos Rosas 23, 28003 Madrid, Spain
[b] Departamento de Estratigrafía, Instituto de Geología Económica (CSIC-UCM), Facultad de Ciencias Geológicas. Universidad Complutense, 28040 Madrid, Spain

ARTICLE INFO

Article history:
Received 21 September 2009
Received in revised form 6 March 2010
Accepted 19 March 2010
Available online 29 March 2010

Keywords:
Carbonate platform
OAE 1a
Heterozoan facies
Meteoric diagenesis
Early Aptian
Cantabria

ABSTRACT

The Early Aptian Oceanic Anoxic Event (OAE 1a) was characterized by intensified greenhouse climate conditions, widespread accumulation of organic deposits in open-marine settings, major perturbations in the C cycle and a generalized increase in terrestrial runoff. Sedimentological, diagenetic and chemostratigraphic analyses of Lower Aptian platform carbonates from the North Cantabrian basin (N Spain) illustrate the regional impact and effects of those global conditions on shallow marine environments.

The studied interval outlines four stages of platform evolution. Stage 1 (earliest Bedoulian) is defined by an initial rapid marine transgression that led to deposition of shallow water oligotrophic photozoan skeletal assemblages, and by a later interval of subaerial exposure. Stage 2 (early Bedoulian) starts with a rapid transgression followed by deposition of grainstones that yield heterozoan assemblages, more typical of mesotrophic conditions, along with ferruginized oolites. Stage 3 (early Bedoulian) is defined by the drowning of the carbonate platform and subsequent deposition of open-marine marls, which are thought to represent the local expression of the OAE 1a. Finally, stage 4 shows the return of shallow water photozoan carbonate sedimentation. The carbonate O and C stable isotope records have revealed prominent negative excursions during deposition of the marly interval of the stage 3, which may be associated with the important global changes that occurred at the onset of the OAE 1a. The change in skeletal assemblages that preceded the isotopic excursions and the platform drowning documents conditions of environmental stress caused by a combination of local and global factors. The global change, coupled with increased basin subsidence, triggered the drowning of the platform by progressive reduction of the growth potential of the carbonate factory.

1. Introduction

The Cretaceous shallow carbonate platforms of the northern Tethys domain are typically characterized by rudist-dominated facies with corals and green algae, which are considered as an oligotrophic, photozoan style of carbonate production (e.g. Carannante et al., 1995; James, 1997; Philip and Gari, 2005; Föllmi et al., 2006; Burla et al., 2008). Their evolution is however punctuated by some stages of dominance of heterozoan communities as well as several phases of platform demise (e.g. Föllmi et al., 1994, 2006; Philip and Gari, 2005; Weissert et al., 1998). One of the best known stage of platform growth crisis occurred during the Early Aptian linked to a global oceanic anoxic event, the so-called OAE 1a. This event was characterized by widespread distribution of organic-rich deposits, and was associated to extreme greenhouse conditions and significant changes in the ocean-climate system (Schlanger and Jenkyns, 1976; Spicer and Corfield, 1992; Jenkyns, 2003). During this time, widespread drowning of shallow water carbonate platforms appears to have been synchronous at a global scale, defining a correlation between the OAE 1a and these drowning incidents (e.g. Arnaud-Vanneau and Arnaud, 1990; Hunt and Tucker, 1993; Jansa, 1993; Masse, 1993; Scott, 1993; Föllmi et al., 1994; Lehmann et al., 1998; Ruiz-Ortiz and Castro, 1998; Weissert et al., 1998; Bosellini et al., 1999; Wissler et al., 2003). One indicator of the influence upon the platform carbonates of environmental change associated to this event is the occurrence of significant variations in styles of carbonate production and diagenesis. In fact, the anoxic event is not other than the effect of a battery of interrelated palaeoclimatic and palaeoceanographic changes that converge at this time and whose triggering mechanisms are still poorly understood. Under such situation of environmental collapse, carbonate sedimentation is expected to suffer strong modifications. One important consequence is that heterozoan associations become dominant in the platforms (Simone and Carannante, 1988; James, 1997). However, there are still few references to heterozoan style of carbonate production during this

* Corresponding author. Tel.: +34 91 7287288; fax: +34 91 7287202.
E-mail addresses: m.najarro@igme.es (M. Najarro), i.rosales@igme.es (I. Rosales), j.m.chivelet@geo.ucm.es (J. Martín-Chivelet).

0037-0738/$ – see front matter © 2010 Elsevier B.V. All rights reserved.
doi:10.1016/j.sedgeo.2010.03.011

period, and a timing correspondence between rising of heterozoan facies and the anoxic episode has not yet been clearly established.

This study examines the effects of the OAE 1a on the style of carbonate sedimentation and early diagenesis of a Lower Aptian carbonate platform from northwest Cantabria, in northern Spain. The area exhibits a well-exposed and continuous succession of Aptian shallow water platform carbonates that include a Lower Aptian open-marine marly unit (Patrocinio Formation). The latter is thought to represent a short-lived episode of platform drowning and the local expression of the OAE 1a (Wilmsen, 2005; Najarro and Rosales, 2008a,b). The carbonate platform turned from photozoan to heterozoan biogenic assemblages before experiencing platform drowning. In attempts to explain the change of carbonate production and the drowning event, several questions arise: (I) which factors determined the carbonate factory shutdown and the drowning of the Cantabrian platform?, (II) to which extent all those changes could be induced or enhanced by regional mechanisms (e.g., local tectonics) rather than global forcings? Sedimentological, geochemical, and diagenetic data are evaluated here in order to address those questions and to discriminate the effects of the OAE 1a on shallow carbonate deposition.

2. Geological setting

The studied area is located in the northwestern margin of the Basque-Cantabrian Basin (BCB; Fig. 1). During the Cretaceous, this part of the BCB belonged to the northern margin of the Iberian plate and was subjected to extension. The BCB evolution and its current structure are the result of a complex kinematics between the European and Iberian plates (Malod and Mauffret, 1990; Olivet, 1996). After a first extensional phase during the Permian–Triassic, a second rifting phase linked to the opening of the Bay of Biscay and North Atlantic ocean took place during the Late Jurassic–Early Cretaceous (e.g. Le Pichon and Sibuet, 1971; Rat, 1988; García-Mondéjar et al., 1996; Martín-Chivelet et al., 2002). Renewed extension and perhaps left-lateral strike slip movement along NW–SE faults occurred in the Aptian–Cenomanian, during the last rifting phases (e.g. Malod and Mauffret, 1990; García-Mondéjar et al., 1996; Soto et al., 2007). Due to these tectonic events, numerous extensional basins and sub-basins bounded by active synsedimentary faults developed in the North Iberian plate margin (Fig. 1A).

The studied succession was deposited in one of these sub-basins, the North Cantabrian basin (NCB; Fig. 1B). This area developed as a

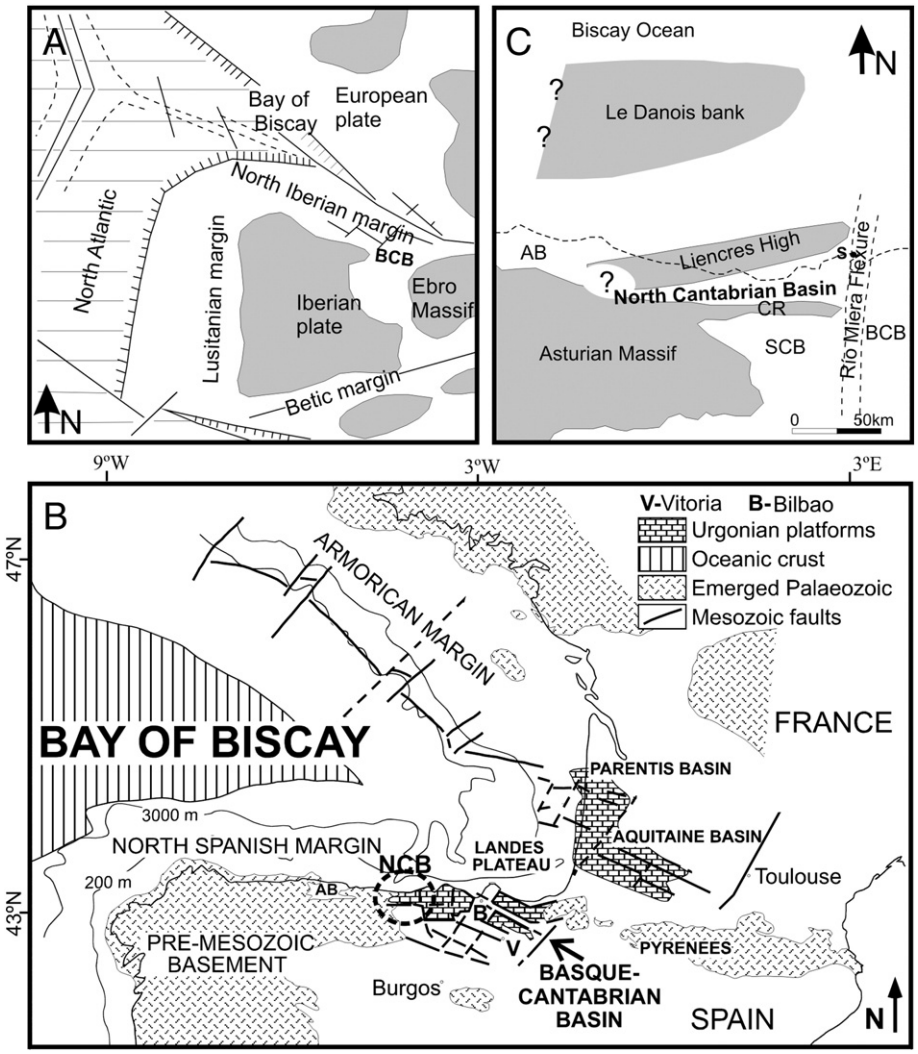

Fig. 1. (A) Palaeogeography and plate tectonics setting of Iberia during the Early Cretaceous (modified from Wilmsen, 2000). (B) Palaeotectonic map during the Early Cretaceous of the Bay of Biscay, showing the location of the North Cantabrian sub-basin (NCB) and major palaeotectonic features (modified from García-Mondéjar and Fernández-Mendiola, 1993). (C) Palaeogeography of the NCB in the Lower Cretaceous (modified from Wilmsen, 2000). BCB: Basque-Cantabrian basin; CR: Cabuérniga Ridge; SCB: South Cantabrian sub-basin; AB: Asturian basin.

relatively small (~20×80 km), E–W elongated sub-basin, that behaved independently for most of the Cretaceous time (Fig. 1C). The NCB was separated from the more strongly subsiding rest of the BCB to the east, by a N–S extensional structure (Río Miera Flexure; Feuillée and Rat, 1971) (Fig. 1C). To the south it was limited by the Cabuérniga Ridge (Figs. 1C and 2), an E–W trending palaeo-high which represents a previous Variscan tectonic structure reactivated as extensional faults during the Mesozoic (Rat, 1988; García-Espina, 1997). To the west, the NCB was bounded by the Asturian Massif and, to the north, by the Liencres High, an ENE–WSW trending swell now situated mostly offshore in the Bay of Biscay (Wilmsen, 2000) (Fig. 1C). Internally, the NCB was configured into swells and troughs controlled by the presence of N–S and E–W oriented synsedimentary faults and secondarily by NE–SW oriented faults (Najarro et al., 2009). Among the principal synsedimentary faults, it is worth mentioning the important role that played the North Cabuérniga and Bustriguado faults (Fig. 2A), which controlled subsidence patterns during the Early Cretaceous and determined strong local changes in sedimentary accumulation (Fig. 2B) (Najarro et al., 2007, 2009). As shown in the SW–NE cross-section of Fig. 2, the NCB can be divided into three main

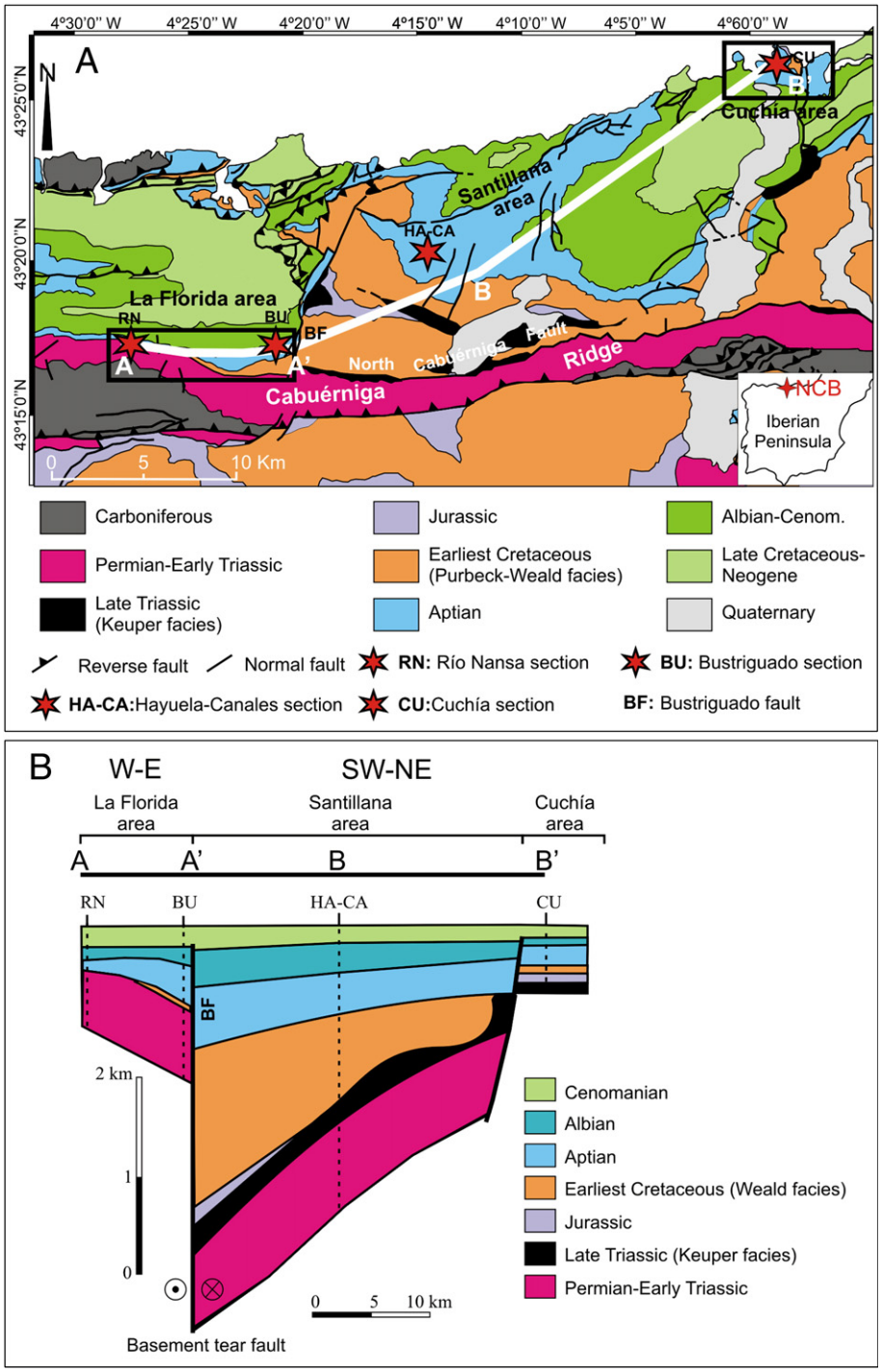

Fig. 2. (A) Geological map of the NCB. White line A–A′–B–B′ shows the location of the stratigraphic cross-section in B. (B) Cross-section showing the restored geometry of the NCB during the Cretaceous and the sedimentary record in the three principal areas (La Florida, Santillana and Cuchía).

areas according to their tectonic evolution and stratigraphy, from SW to NE: La Florida, Santillana, and Cuchía. The areas of La Florida and Cuchía represent respectively two low-subsiding blocks. Between them, the Santillana area formed a sedimentary trough and the main depocentre of the NCB during the Early Cretaceous (Fig. 2).

3. Stratigraphy

The general stratigraphic and biostratigraphic frameworks of the Aptian successions of the NCB were established by Ramírez del Pozo (1972), Collignon et al. (1979) and Hines (1985). More recently, the main depositional systems and sequences have been revised, establishing a new lithostratigraphic unit (Rábago Formation) and updating the stratigraphic and biostratigraphic schemes (Figs. 3 and 4) (Najarro and Rosales, 2008c; Najarro et al., 2009; Rosales et al., 2009). The Aptian lithostratigraphy of the NCB is composed of six formations, named from oldest to youngest (Fig. 3): 1) Rábago Formation (early Bedoulian, *Palorbitolina lenticularis* zone), which consists of shallow platform sandstones, orbitolinid marls and rudists limestones. 2) Umbrera Formation (early Bedoulian, *P. lenticularis* zone), composed of shallow platform cross-bedded grainstones. 3) Patrocinio Formation (mostly early Bedoulian, *Deshayesites weissi* ammonite zone and middle upper part of the *Hayesites irregularis* nannofossil zone; Rosales et al., 2009), made of open-marine marls. 4) San Esteban Formation (late Bedoulian), characterized by shallow platform rudist-bearing limestones, with *Iraquia simplex* (Pascal, 1985). 5) Rodezas Formation (latest Bedoulian–early Gargasian, according to Collignon et al., 1979), made of shallow marine sandstones, marly limestones and marls; and finally 6) Reocín Formation (Gargasian–Clansayesian, *Orbitolina* (*Mesorbitolina*) *texana texana* and *Simplorbitolina manasi* zones; Ramírez del Pozo, 1972), composed of shallow water coral and rudist-bearing limestones.

In the La Florida area, the Aptian succession consists of an E–W elongate lithosome, 9 km long, with wedge-shaped geometry deepening and thickening eastward, on the slope of a tilted block active during this time (Najarro et al., 2007) (Fig. 2B). In this area, the initial Early Aptian marine transgression led to deposition of the Rábago and Umbrera formations (Figs. 3 and 4). Continued transgression during the early Bedoulian caused platform drowning and resulted in deposition of the Patrocinio Formation, which completely covered the former carbonate platform. Subsequent regression during the Late Aptian originated the deposition of the Reocín Formation (Figs. 3 and 4). New biostratigraphic data based on calcareous nannofossils (Rosales et al., 2009) reveal the existence of a stratigraphic gap (paraconformity) in this area that comprises at least the late Early Aptian (late Bedoulian). This stratigraphic gap is time-equivalent to the San Esteban Formation, which is missed in this area (Fig. 4). In contrast, in the Santillana area the Aptian succession is essentially complete without major hiatuses and the lithological units show their largest thicknesses (Fig. 3).

Finally, in the Cuchía area, the first recorded Aptian unit is the Umbrera Formation, which rests unconformably on continental Wealdean facies (Fig. 3). Remarkably, the Rábago unit is missing here (Figs. 3 and 4), probably because it was eroded before the deposition of Umbrera Formation, or alternatively because it pinched out in this area. Subsequent transgression produced deposition of the marly Patrocinio Formation. The upper part of this unit shows in this area an upward increase in the content of siliciclastic siltstones and sandstones which resulted of a local delta progradation (Wilmsen, 2005). The siliciclastic deltaic deposits grade upwards to the San Esteban Formation. Like in the previous area, the Late Aptian stratigraphy is represented by the Rodezas and Reocín Formations, except in the Suances section where these two units are absent; indicative of a depositional and/or erosive hiatus that comprises at least the entire Late Aptian (Fig. 3).

4. Methodology and studied sections

A total of eight laterally correlative stratigraphic sections were measured and analyzed through the NCB for this work (Fig. 5). Six of them belong to the La Florida area (from W to E: Río Nansa, Rábago,

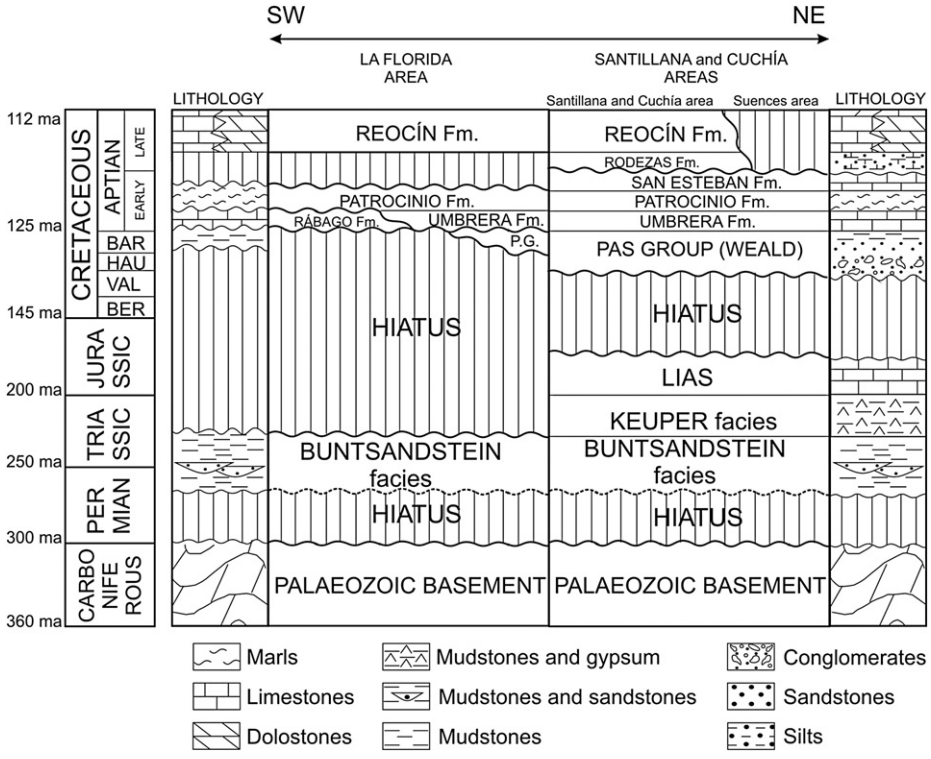

Fig. 3. Lithostratigraphy of the La Florida, Santillana and Cuchía areas. P.G. is Pass Group (Weald). Chronostratigraphy after Gradstein (2004).

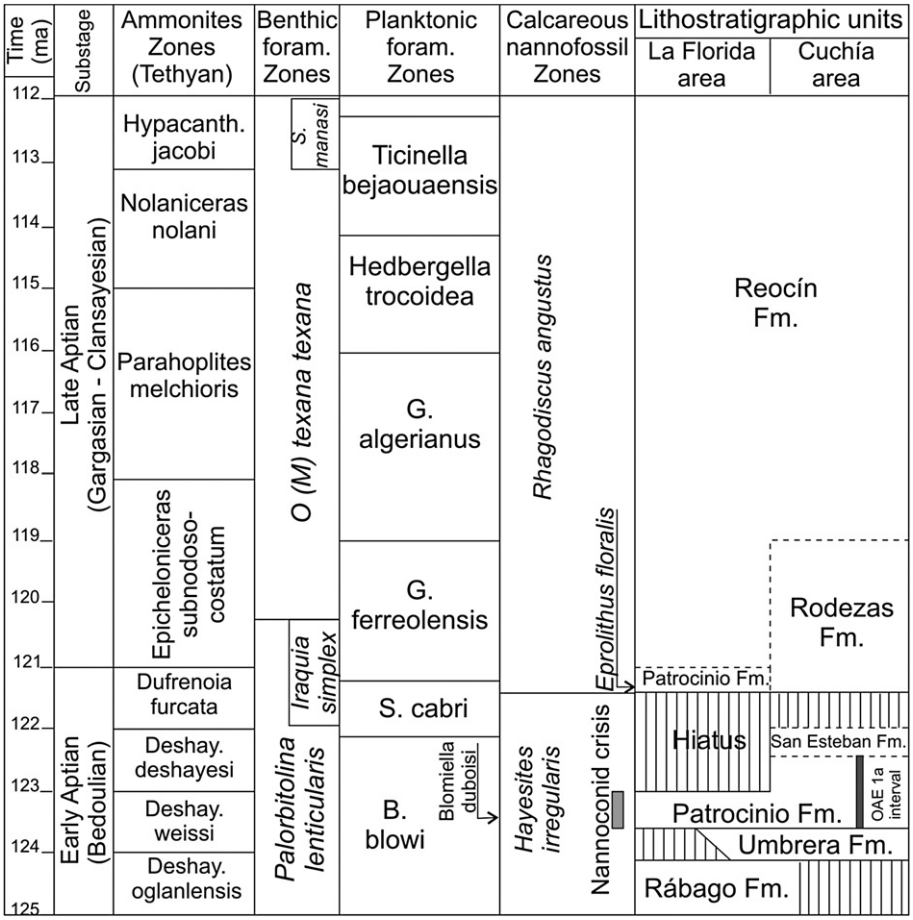

Fig. 4. Chrono-biostratigraphic scheme for the Aptian succession of the NCB. Ammonoid data based on Collignon et al. (1979), Rosales et al. (2009), and Moreno-Bedmar (pers. com.). Benthic foraminifera data based on Ramírez del Pozo (1972), Pascal (1985), and Castro (pers. com.). Planktonic foraminifera and nannofossil data based on Rosales et al. (2009), and de Gea (pers. com.). The OAE 1a interval is equivalent to the "Selli level" defined by Menegatti et al. (1998). Chronostratigraphy after Gradstein (2004).

El Soplao, La Florida, Corona de Arnero, and Bustriguado, Fig. 6). The other two are considered to be representative of the Santillana and Cuchía areas respectively: the first one logged between the villages of Hayuela and Canales, and the second at the Los Caballos beach near the village of Cuchía (Fig. 2A).

When outcrop conditions were favourable, sedimentological features and macrofossil content were documented in detail in the field and sampling for microfacies analysis was conducted systematically (at least 1 sample per 2 m, often at a smaller scale). Uncovered and polished thin sections were investigated with an optical microscope and cold cathodoluminescence (CL), and then classified according to microfabrics and mineral composition. Thin sections were stained with a mixture of Alizarin Red S and potassium ferricyanide (Dickson, 1966) to aid in the identification of ferroan and non-ferroan phases of calcite and dolomite. Cathodoluminescence (CL) analyses were obtained from a Technosyn cold cathodoluminescence operator model CL8200 MK5, operating at ~15 kV with a current of 500–600 μA. Oxygen and carbon stable isotope analyses were performed on limestone and marl samples throughout two selected stratigraphic sections (Río Nansa and Rábago), which may be easily correlated and combined to conform a composite complete section. Powders for isotope analyses were retrieved by using a microdrill on micrites and marls, and avoiding diagenetic calcite and dolomite from crack fillings, replaced fossils or matrix irregularities, especially in limestone samples. The sample material was treated with 100% orthophosphoric acid using the conventional digestion method (McCrea, 1950) and the $\delta^{13}C$ and $\delta^{18}O$ composition of the evolving CO_2 gas was analyzed in a SIRA-II doted with an "ISOCARB" automatic system at the University of Salamanca (Spain). The results are expressed in the common δ-notation in per mil (‰) relative to VPDB-standard. The international carbonate standard NBS-19 (National Bureau of Standards; $\delta^{13}C = 1.95‰$ and $\delta^{18}O = -2.20‰$) was used to calibrate the PDB, with an average precision of 0.01‰ for $\delta^{13}C$ and 0.05‰ for $\delta^{18}O$.

5. Stages of platform evolution

During the Early Aptian, the shallow water carbonate succession of the NCB presents four distinctive stages of platform evolution, which have been differentiated on the basis of facies and stratal patterns, with special emphasis in vertical changes in facies, skeletal composition and particle associations, and correlation of particular sedimentary surfaces (Figs. 5 and 6). Lithological description and interpretation of the four stages are summarized in Table 1, which show the following principal aspects from base to top:

5.1. Stage 1: Initial transgression and carbonate platform development

5.1.1. Description

It corresponds to the Rábago Formation. In the studied sections it presents a maximum thickness of 12–17 m. Its basal part is predominantly siliciclastic or mixed carbonate–siliciclastic, whereas the upper part is mostly carbonate alternating with some orbitolinid-rich marls (Fig. 7). Vertical stacking patterns of facies show three main facies associations, which from base to top are: i) siliciclastic platform, ii) mixed carbonate–siliciclastic platform, and iii) carbonate platform (Fig. 7 and Table 1).

Siliciclastic platform facies are present at the base of Río Nansa and Rábago sections (Fig. 7). They consist of a 5 to 7 m thick interval of

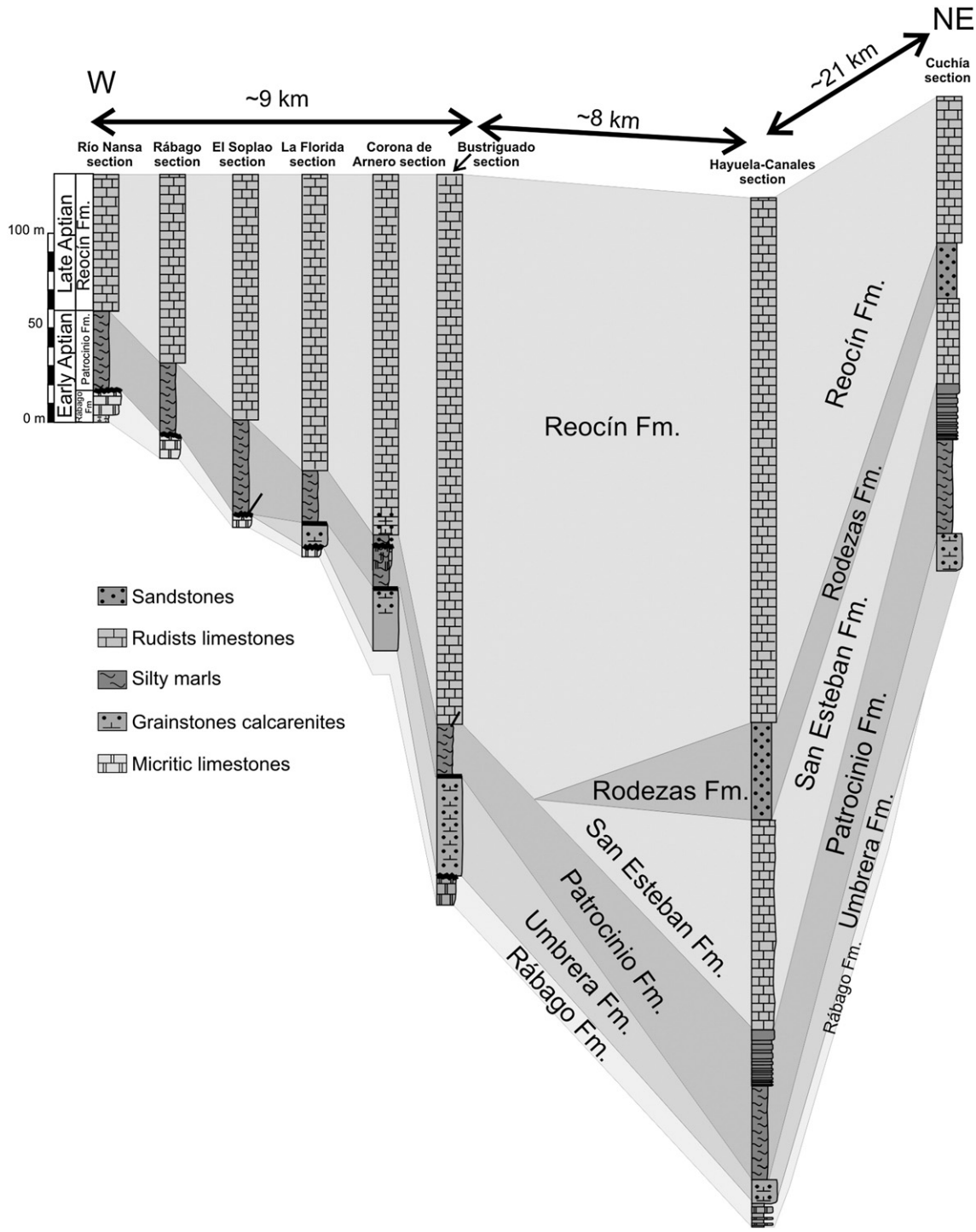

Fig. 5. Lithostratigraphic correlation of logged sections through the NCB, showing the main units, depositional facies and lateral thickness variation.

interbedded, carbonaceous and laminated claystones, siltstones and fine- to medium-grained micaceous sandstones, typically with lenticular and flaser bedding, and current ripples at the tops of the sandstones beds.

Mixed carbonate–siliciclastic platform facies mainly consist of sandy limestones with variable amount of quartz sand and other terrigenous grains. They are organized in tabular beds 20 cm to 1 m thick (Fig. 8A), which often show wavy lamination and occasionally wave ripples at the bed tops. These sandy limestones are interbedded with claystones–siltstones, packstone–grainstones, and orbitolinid-rich marls (Fig. 7).

Carbonate platform facies consist of alternations of orbitolinid-rich marls and nodular marly limestones, grainstones, packstones, wackestones and mudstones with corals and rudists of small size (Figs. 7 and 8B). They are organized in planar to nodular, massive beds ranging from 0.3 to 1 m thick. These facies are arranged in a fining-upward succession. Hence, packstone and grainstone are the most frequent textures in the lower terms of the succession, whereas coral-rudist wackestone and microbialite mudstone with fenestral fabrics developed on the upper part (Fig. 7 and Table 1).

In the La Florida area, the succession culminates with a dissolution surface displaying irregular cavities of decimetre size, fissures and macro and micro topographic relief with corrosive surfaces and indents. Interestingly, a thin Fe-rich crust appears in places coating the

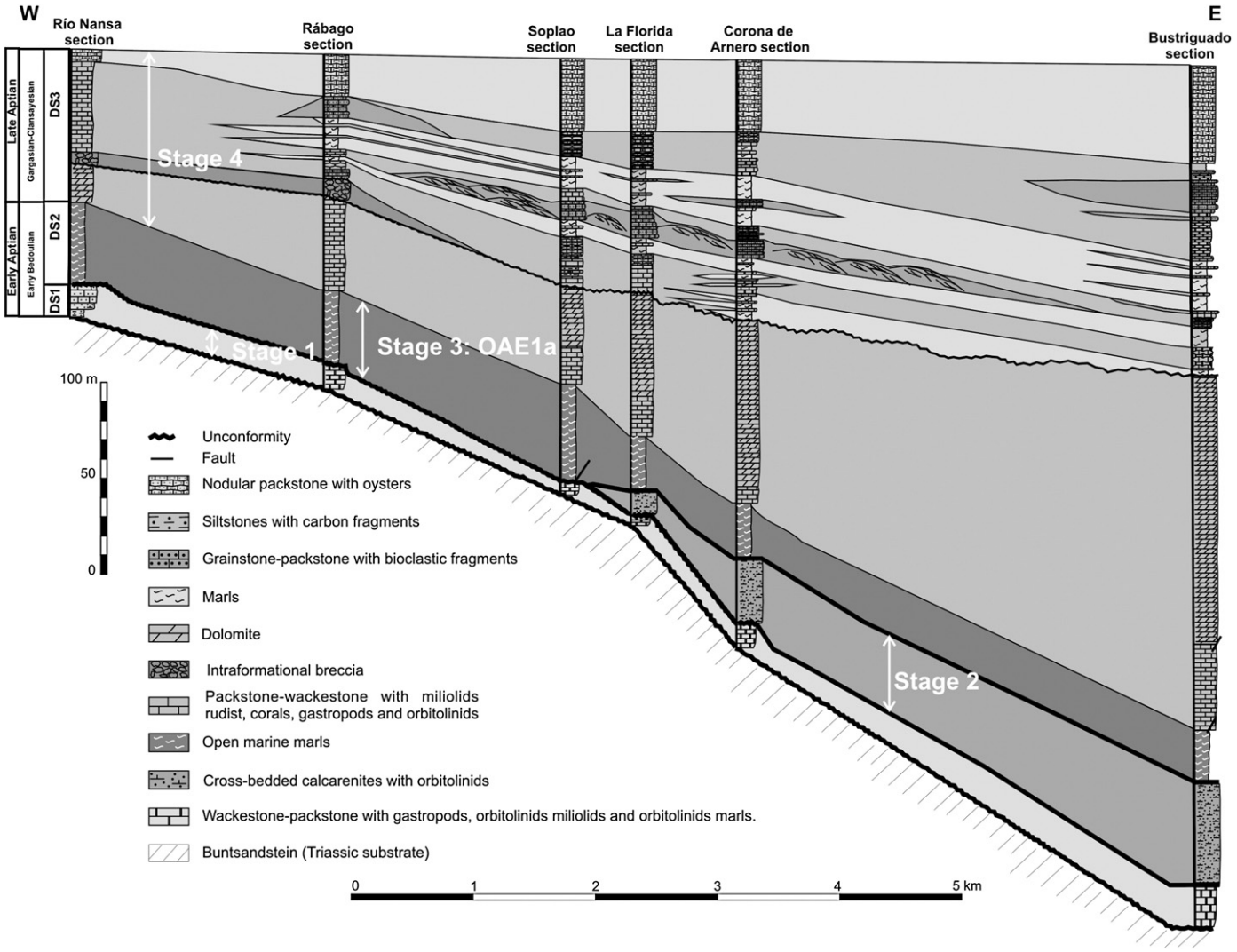

Fig. 6. Detailed stratigraphic correlation of the sections logged in La Florida area, showing the main stages of carbonate production and changes in sedimentary thickness and facies. Note the lateral thickness variation from west to east.

dissolution surface (Fig. 8D). This crust is several millimetres thick and is made of very thin films (biofilms) of iron oxides with encrustations of agglutinated foraminifera, serpulids and microborings. Above this surface, the depressed zones of the palaeorelief and the cavities are filled with carbonate breccias made of centimetre- to decimetre-size sub-angular clasts of the underlying limestone (Fig. 8E) and small broken (reworked) pieces of the Fe-crust. The matrix of the breccia consists of red-stained crinoid-rich calcarenite infiltrated of the overlaying stage 2.

In the Santillana area, the end of the stage 1 is recorded as an erosive surface that truncates strata below (Fig. 9A). In the Cuchía area, the stage 1 is not recorded.

5.1.2. Interpretation

As a whole, the stage 1 reflects an initial transgressive event followed by a shallowing-upward succession with gradual upward decrease in siliciclastic content in conjunction with increment of carbonate production. The platform evolves from a siliciclastic or mixed carbonate–siliciclastic platform to a restricted inner fossiliferous carbonate platform under low-energy and photic zone conditions, and finally to peritidal facies. The dissolution surface at the top suggests emersion with small-scale karst morphologies (*kamenitzas*, as described in Di Stefano and Mindszenty, 2000) (Fig. 8C). The presence of the marine Fe-rich crust (hardground) coating the dissolution surface is interpreted to form during the following transgression at the onset of the stage 2.

5.2. Stage 2: Carbonate production — deepening phase

5.2.1. Description

Stage 2 is represented by the Umbrera Formation (Fig. 9), which consists mostly of cross-bedded bioclastic grainstone and packstone, rarely rudstone, arranged in a thinning- and fining-upward succession. Coarser bioclastic sands are concentrated in the lower part of the succession in beds up to 1–2 m thick. Red to tan coloured ferruginized oolitic grainstones with trough cross-bedding characterize the base of the succession. The lower–middle part of the succession is made of bioclastic–oolitic grainstones organized in massive and metre- to decimetre-thick cross-bedded sets (Fig. 9C). The upper part of the succession is made of packstones and fine-grained grainstones that alternate with orbitolinid-rich marls. The top of the limestone beds is frequently bioturbated by *Thalassinoides* burrows (Fig. 9D), which are filled with the overlying orbitolinid marls.

The maximum thickness of the calcarenite deposits of stage 2 is 52 m in the eastern part of La Florida area (Bustriguado section; Fig. 6). Here, these deposits pinch out and disappear westward (Río Nansa section, Fig. 6), onlapping progressively on the underlying dissolution surface

Table 1
Main characteristics of the different stages of the carbonate platform.

Characteristics		Stage 1		Stage 2	Stage 3		Stage 4
Lithology	Interbedded, carbonaceous and laminated claystones, siltstones and micaceous sandstones	Sandy limestone with quartz sand	Marls, marly limestones, grainstones, packstones, wackestones, and mudstones	Grainstones and packstones, rarely rudstones. Orbitolinid marls upsection	Silty marls to dark-grey, soft clayed marls	Siltstones and mica-rich sandstones	Wackestones, packstones and many limestones
Primary structures, vertical stacking and bioturbation	Lenticular and flaser bedding; current ripples	Wavy lamination; current ripples	Planar to nodular massive beds. Fining-upward	High-amplitude wavy lamination; planar-oblique and high-angle cross-stratification; internal erosive surfaces, bi-directional and sigmoidal cross-stratification. Thinning- and fining-upward. *Thalassinoides* up section.	–	Ripple trough cross-bedding flaser and lenticular bedding. Coarsening-upward and *Ophiomorpha nodosa*	Fining-upward
Particle composition	Wood fragments, fine- to medium-grained quartz, clay minerals and mica	Orbitolinids, echinoderm plates and thin shelled bivalves. Clay minerals (<5%)	Protozoan: Rudist and coral lithosomes, *L. aggregatum–B. irregularis*, miliolids, nerineid gastropods, *Chondrodonta*, dasycladacean green algae, orbitolinids, peloids, intraclasts and micritized grains	Heterozoan: Large agglutinated benthic foraminifera, bryozoans, plates and spines, of echinoderms, crinoid ossicles, red algae, oysters, bivalves, gastropods, quartz grains, glauconite, calcite ooids, ferruginized ooids and coated grains, extraclasts, and plant fragments	Ammonites, belemnites, planktonic foraminifera nannofossils, glauconite, and Fe-nodules	Bivalves, brachiopods, echinoids, orbitolinids, and wood fragments	Protozoan: Rudists and corals lithosomes, miliolids, orbitolinids, calcareous algae, *L. aggregatum–B. irregularis*, peloids, and bioclasts
Depositional environment	Siliciclastic platform	Mixed carbonate–siliciclastic platform	Restricted inner carbonate platform. Low energy and shallow water conditions. Shallowing upward and emersion at the top	Inner to mid carbonate shelf. High-energy shallow bars and shoals	Open marine	Delta progradation	Restricted inner carbonate platform. Low energy and shallow water conditions
Nutrient levels	–	–	Oligotrophic	Meso-eutrophic	–	–	Oligotrophic
Cement C1	–	–	Scarce	High	–	–	Scarce
Cement C2	–	–	High	Only in reworked bioclasts	–	–	–
Glauconite	–	–	–	High	High	–	–
Ferruginization	–	–	–	High	–	–	–
$\delta^{13}C$ values	–	–	Stable and positive values. Mean: 2.2‰	Progressive decrease of ~1‰. Positive values. Mean: 1.1‰	Negative excursion from −0.41% to −4.53‰		Positive excursion. Mean 2.8‰

coated by the Fe-rich crust. The end of the carbonate stage 2 is marked by a discontinuity on top of a bioturbated and reddish calcarenite bed, which is covered by marls of the Patrocinio Formation (Fig. 10A).

5.2.2. Interpretation

Sedimentary lithofacies and structures suggest that high-energy tidal and coastal currents controlled deposition of these carbonate sands (sand waves). They represent high-energy shallow bars and shoals deposited in an open-marine, inner to midcarbonate shelf environment. At the upper part of the succession, abandoned bars were rapidly colonized by burrowing organisms (*Thalassinoides*) and then buried by marls. This suggests an overall deepening trend of the succession linked to a transgressive episode.

5.3. Stage 3: Carbonate platform drowning at the onset of OAE 1a

5.3.1. Description

The stage is represented by the Patrocinio Formation (Fig. 10A). Open-marine marls of this unit abruptly overlie the shallow water carbonates of stage 2. Lithofacies are formed by silty marls to dark-grey, soft clayed marls with glauconite and ironstone nodules. These yield ammonites, belemnites, and microfossils including planktonic foraminifera and nannoplankton. Up-section, the silt content of the marls increases and appear bioclastic beds with erosional surfaces, and debris of bivalves, brachiopods, echinoids and orbitolinids as well as wood fragments. Bioturbation also becomes intense upwards. In the Cuchía area (Fig. 10A), the upper part of the stage 3 records an upward increase in the content of siltstones and mica-rich, bioturbated sandstones with *Ophiomorpha nodosa*, ripple trough cross-bedded sandstones, and heterolithic facies with flaser and lenticular bedding, organized in a thickening and coarsening-upward sequence.

5.3.2. Interpretation

These deposits reflect the shutdown of the shallow water carbonate factory in the area and the drowning of carbonate platform stage 2, likely as the result of a combined action of a relative sea-level rise and poisoning by siliciclastic particles. The lower marly interval is interpreted as formed by fall of fine carbonate particles mixed with fine-grained terrigenous material, under low-energy conditions below storm wave base. Up-section, the increment of silt content suggests input of coarser siliciclastic material from continent. The bioclastic erosive layers suggest storm beds deposited above the storm wave base, and finally, the sandstone lithofacies at the top represents progradation of deltaic facies (Wilmsen, 2005). This whole succession indicates a net shallowing-upward trend and rapid regression towards the end of the stage.

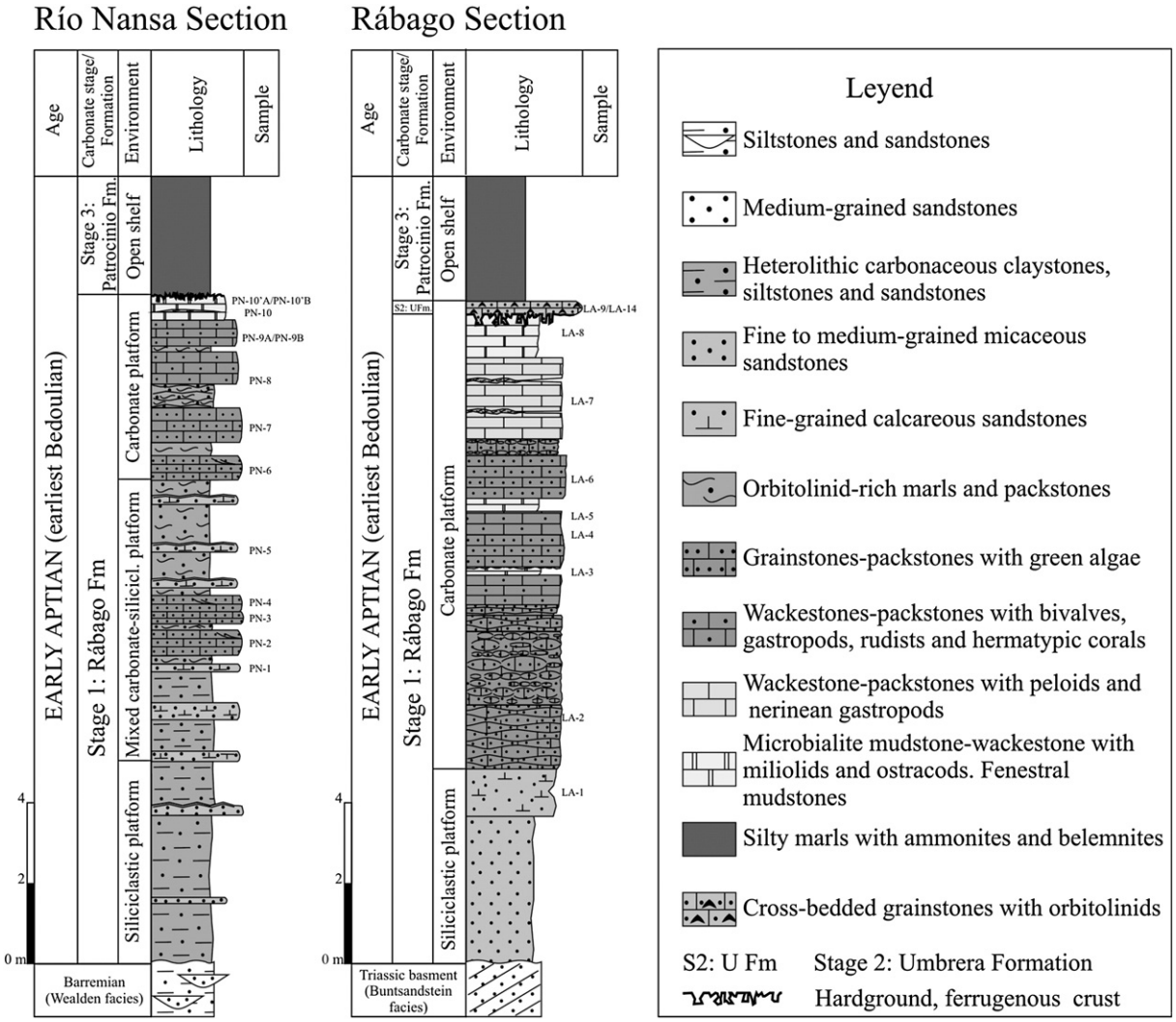

Fig. 7. Stratigraphic sections of stage 1 (Rábago Formation) at Río Nansa and Rábago localities, showing the main depositional environments and facies associations.

5.4. Stage 4: Carbonate platform recovering

5.4.1. Description

The shallow water carbonate production and deposition recovered during the late Early Aptian (late Bedoulian) and dominated until the Late Aptian. The interval is represented by decimetre- to metre-scale beds of wackestones and packstones with rudist–coral assemblages and *L. aggregatum–B. irregularis* oncoids. The succession starts with up to 4 m of orbitolinid-rich, marly to nodular limestone beds (Fig. 10B–D), that are usually followed by marly limestones with orbitolinids, bioclasts, sponges and corals; these grading upward to well-bedded limestones with abundant requieniid rudists (*Toucasia* and *Requienia*) (Fig. 10C).

5.4.2. Interpretation

The instauration of stage 4 indicates the recovery in the effectiveness of the carbonate factory, favoured by the progressive shallowing of the depositional system and by the decontamination of terrigenous particles. When the carbonate sedimentation was re-established, the orbitolinids were the first colonizers, due to their higher tolerance to adverse conditions such as water turbidity, terrigenous poisoning and limited light (as described in a similar case by Vilas et al., 1995). The vertical evolution from marly orbitolinid facies to micrite rudist facies may indicate a gradual environmental change to more favourable ecological conditions for carbonate secretion and biodiversity. The micritic limestones with miliolids, rudists and benthic foraminifera indicate a shallow water, restricted lagoonal environment with low terrigenous influence.

6. Particle composition

6.1. Skeletal carbonate components of stages 1 and 4

Carbonate platform lithofacies of stages 1 and 4 display comparable assemblages of skeletal components. In grainstone and packstone lithofacies, well-rounded fragments of green algae (dasycladacean, codiacean), coralline sponges, lumps of cyanobacteria, benthic arenaceous foraminifera, orbitolinids, and fragments of rudists and other bivalves are the most common carbonate components, with a minor contribution of plates and spines of echinoderms, gastropods, and fragments of branching corals, brachiopods and oysters. Microfacies of wackestone beds are dominated by intact and fragmented skeletons of rudists (mostly requieniids and monopleurids), nerineid gastropods, branching and colonial corals, dasycladacean green algae and thin shelled bivalves, with variable contributions of *L. aggregatum–B. irregularis* oncoids, *Chondrodonta*, miliolids, orbitolinids and benthic agglutinated foraminifera (Fig. 11A–C). In minor proportion, coralline algae, brachiopods, echinoderm plates, oysters and ostracods are also found.

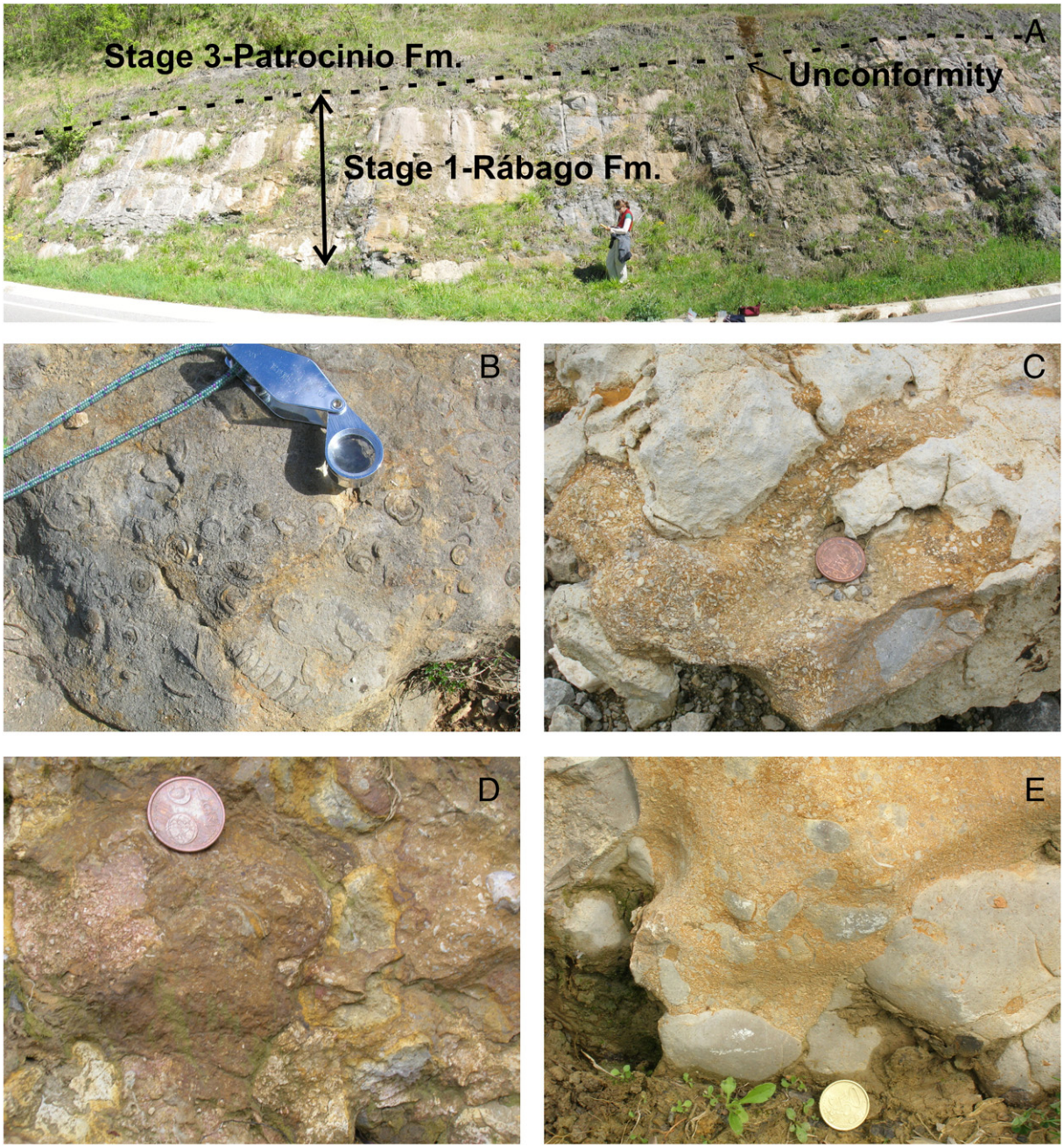

Fig. 8. Field pictures of the stage 1 (Rábago Formation) at La Florida area. (A) Field view of the stage 1 at Río Nansa section. (B) Detailed picture of a wackestone–packstone with gastropods and corals at Río Nansa section. (C) Detail of the dissolution surface at the top of stage 1, showing irregular cavities and fissures filled by red-stained bioclastic grainstones of the stage 2 at Rábago section. (D) Fe-rich crust coating the dissolution surface of the stage 1 at Rábago section. (E) Irregular cavity filled by carbonate breccia made of cm-size sub-angular clasts and a matrix of red-stained bioclastic calcarenite from the stage 2 at Rábago section.

6.2. Non-skeletal components of stages 1 and 4

Intraclasts, peloids and micritized grains represent the most common non-skeletal particles in the carbonate platform lithofacies of stages 1 and 4. Intraclasts (<5%) are small and well rounded, and derived from facies of micrite matrix with foraminifera and bioclasts (Fig. 11D). Peloids are small in size, subspherical to ovoidal in shape, conspicuously rounded, and well sorted. They don't exhibit any evident structure or organization such as gradation or lamination. Silt-size grains of quartz (<1%) and opaque minerals are also present.

6.3. Skeletal carbonate components of stage 2

During the carbonate stage 2, the principal skeletal components of the microfacies are large agglutinated benthic foraminifera (orbitolinids and large lituolids), bryozoans, plates and spines of echinoderms, crinoid ossicles, red algae and mollusc debris (bivalves, gastropods, and oysters) (Fig. 12A). No intact rudist shells, corals and green algae have been observed. These appear as minor components preferentially concentrated in the basal beds of the calcarenite interval, immediately above the basal unconformity, and correspond to well-rounded to subrounded, abraded fragments, generally about 1 mm in size or less

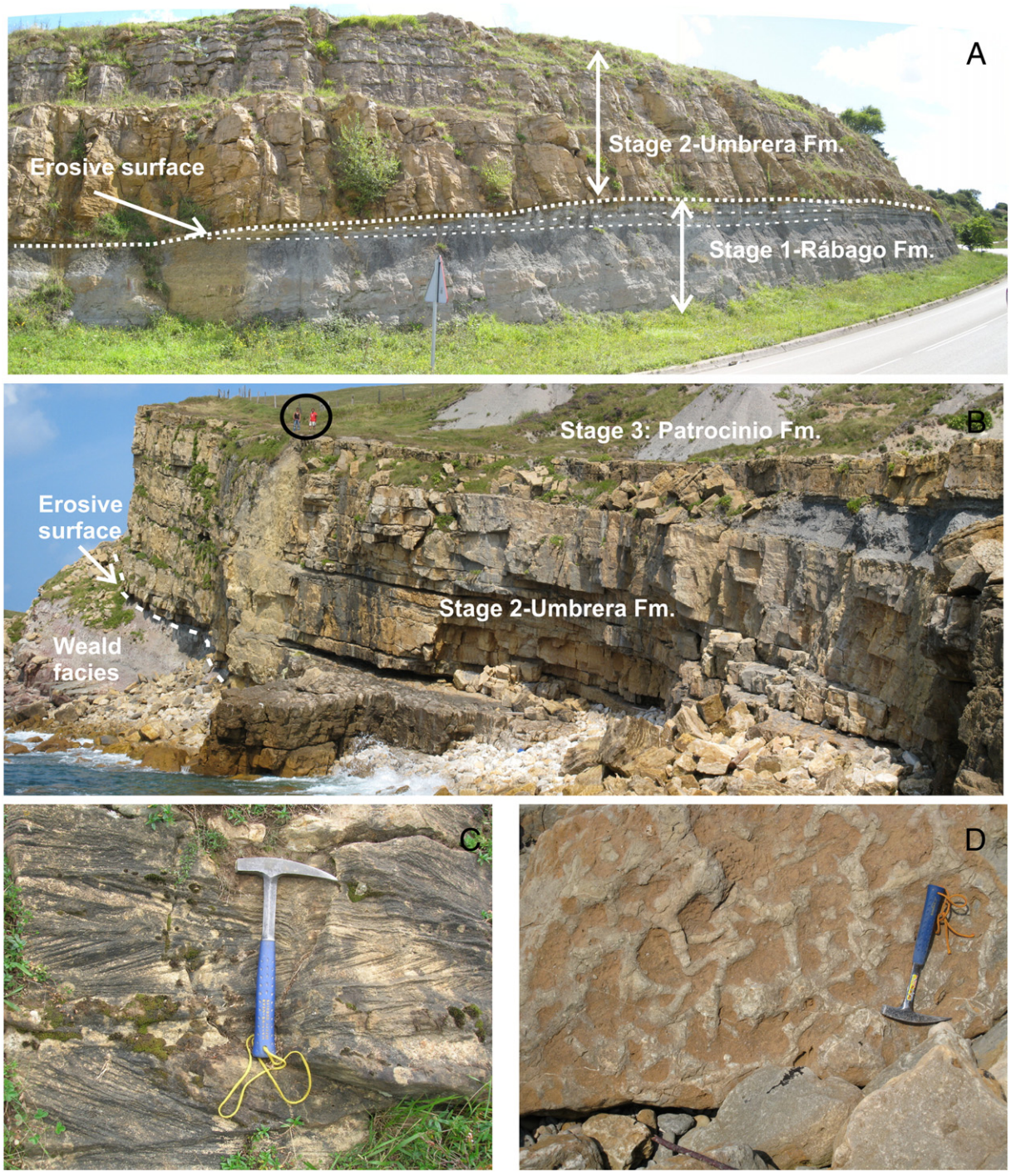

Fig. 9. Field pictures of the stage 2 (Umbrera Formation). (A) Contact between the stage 1 (orbitolinid marls and marly limestones) and the stage 2 (cross-bedded grainstones) at Santillana area. An erosive surface truncates the top of stage 1; traffic sign for scale is 2 m. (B) Cross-bedded bioclastic grainstone of the stage 2 at Cuchía. In this area the stage 1 is not recorded and the stage 2 rests directly on Wealden facies. The end of stage 2 is marked by deposition of the dark marls of the Patrocinio Formation; people for scale. (C) Detail of cross-bedding of bioclastic–oolitic grainstones at the lower part of the Umbrera Formation (Corona de Arnero section, La Florida area). (D) Large *Thalassinoides* burrows at the top of the Umbrera Formation in the Cuchía area.

(Fig. 12B). These reworked fragments of rudists and corals are recrystallized and commonly constitute the nucleus of ooids (Fig. 12C). Occasionally miliolids are present and may appear broken as well (Fig. 12B).

6.4. Non-skeletal components of stage 2

Non-skeletal components of stage 2 are represented by fine to medium sand-sized quartz grains, glauconite grains, calcite ooids, ferruginized ooids and coated grains, and extraclasts (reworked fragments of previously lithified rocks). The latter include rock fragments derived from the underlying Fe-rich crust, from limestones deposited during the stage 1, and from older sandstone units. Quartz grains may represent 5 to 30% of the whole components, are sub-angular to subrounded in shape, and show moderate sorting. Plant fragments are a minor but ubiquitous component.

Ooids and coated grains are fine to medium-grained, moderately to poorly sorted and well-rounded (Fig. 12C–E). The nuclei consist of quartz grains, chert, extraclasts, echinoid plates, and abraded

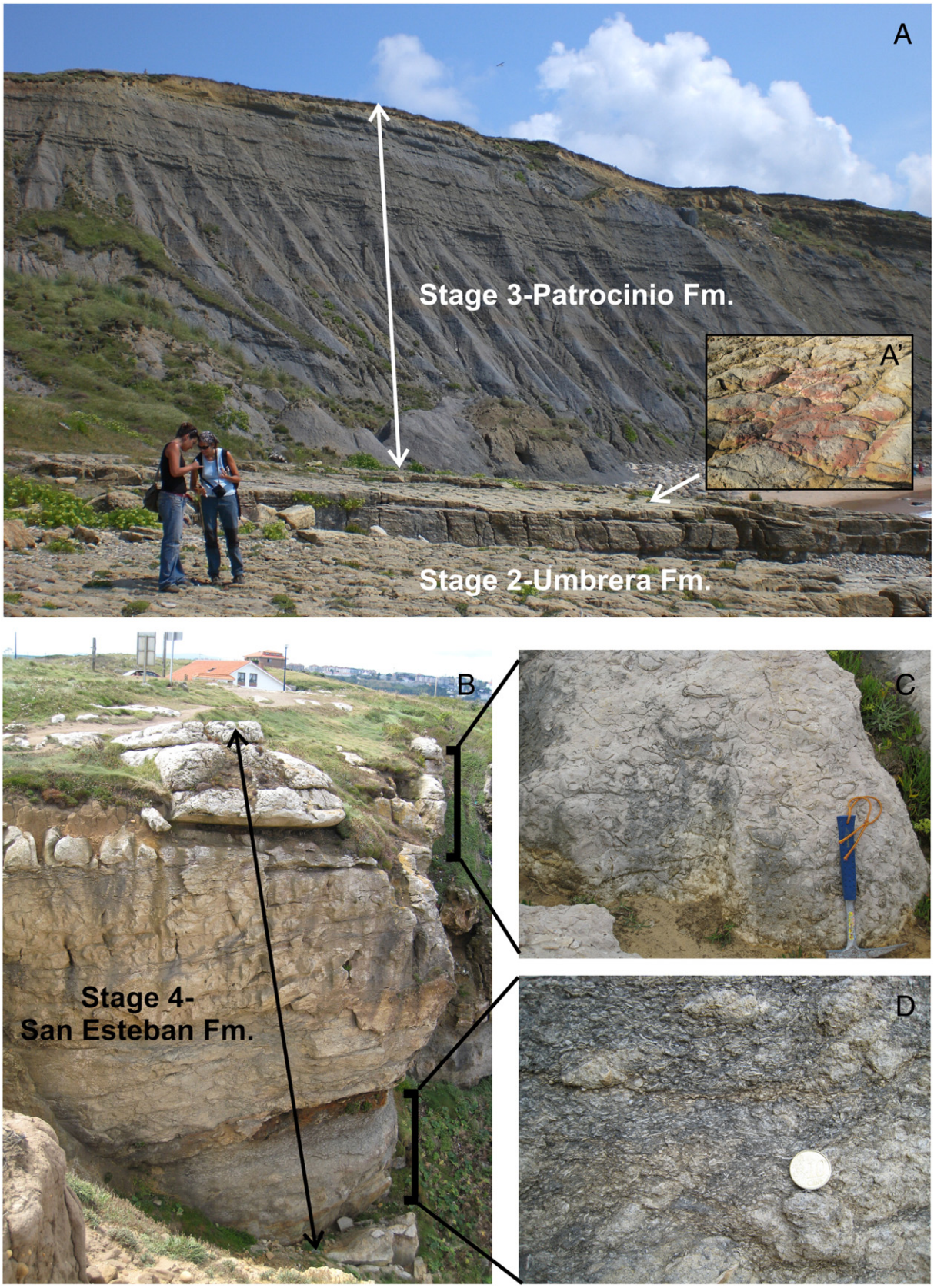

Fig. 10. Field aspects of the stage 3 (Patrocinio Formation) and the stage 4 (San Esteban Formation) at Cuchía area. (A–A′) Bioturbated and reddish surface at the top of stage 2 covered by dark marls of the Patrocinio Formation. (B) General view of shallow water limestones of the stage 4 (San Esteban Formation). (C) Limestones with requiniid rudists at the upper part of the unit. (D) Orbitolinid marls at the lower part of the unit.

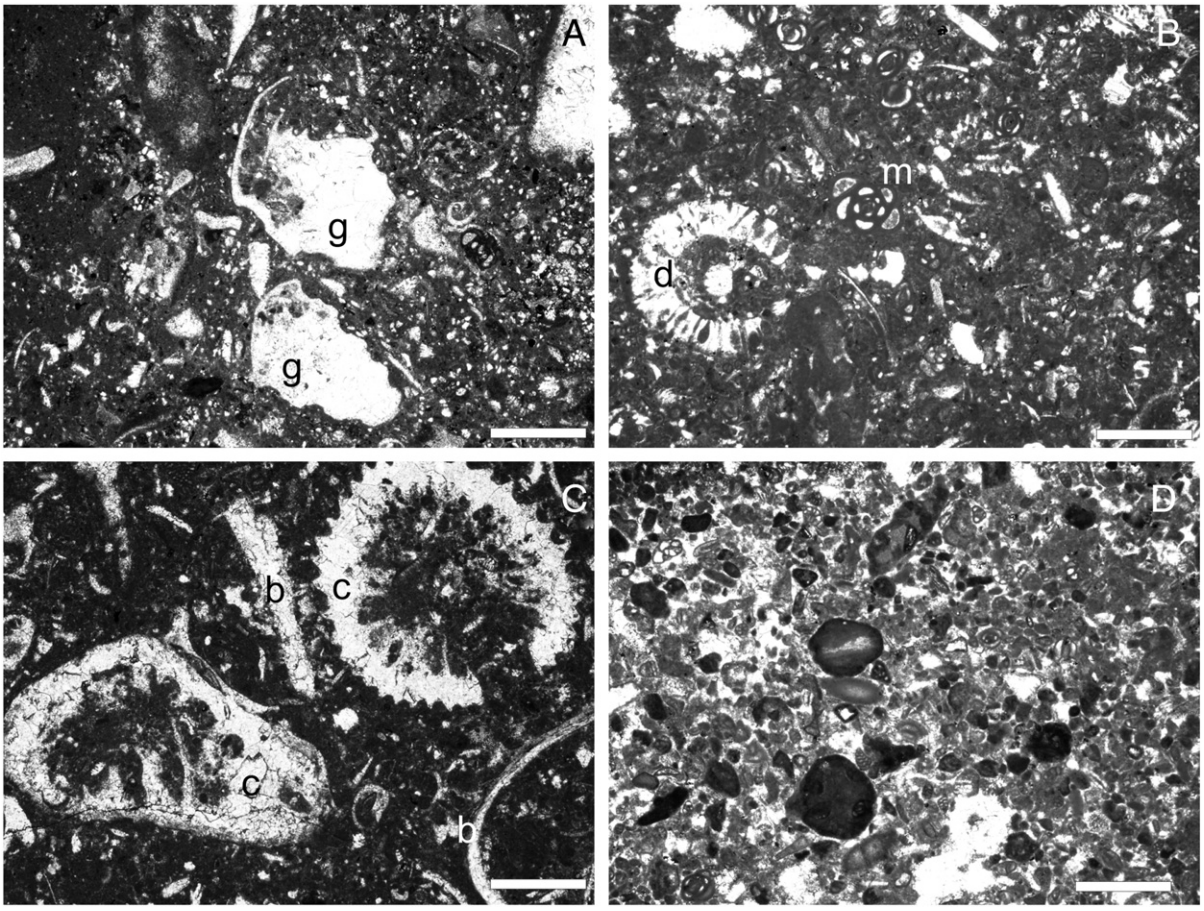

Fig. 11. Microfacies of the stages 1 and 4; scale bar for all plane-light photomicrographs is 1 mm. (A) Packstone with dissolved gastropods (g), bioclasts and miliolids. Sample PN-9, Río Nansa section, La Florida area, Rábago Formation. (B) Packstone–wackestone with micritized grains, miliolids (m) and dasycladacean green algae (d); Bustriguado section, La Florida area, Rábago Formation. (C) Wackestone with hermatypic corals (c) and thin shelled bivalves (b); Rábago section, La Florida area, Reocín Formation. (D) Peloidal packstone with intraclasts formed by micritic limestones, foraminiferans and bioclasts. Sample LA-7, Rábago section, La Florida area, Rábago Formation.

fragments of corals and bioclasts that generally appear dissolved and replaced by calcite (Fig. 12C). It has been distinguished both superficial and well-developed (normal) ooids with thick mixed cortices. Irregular concentric cortices of one or two layers form superficial ooids. Mixed ooids are common and result from the superposition of cortices made of both tangential calcite and micrite layers (Fig. 12E). In addition, ooids formed entirely by layers of tangential arrangement of tightly packed radial calcite crystals, and micritic ooids made of concentric micrite layered structures have been observed. Some composed ooids with two or more nuclei also occur. Some ooid cortices appear broken and separated from the nucleus or other cortices by thin calcite cement (Fig. 12C). Cracked ooids also occur, which may develop new cortices in discordance with the broken ones.

Glauconite beds occur in the upper part of the calcarenite succession, appearing as detrital grains, filling pore spaces, or replacing skeletal particles (Fig. 12F).

7. Early diagenesis

The study of thin sections under optical and CL microscopy allows differentiation of a series of diagenetic features which reveal essential aspects of early diagenesis. These notably complete the environmental information given by facies and fossils, and contribute to reconstruct the evolution of the platform, especially during the stages 1 and 2, that preceded the OAE 1a.

7.1. Micritization

During the stage 1, bioclasts commonly present micrite rims or appear completely micritized. Both destructive and constructive micrite envelops are observed. Micrite envelops and micritization also occurred during the stage 2 affecting to skeletal particles and ooids.

Destructive micrite envelopes are formed by microboring produced by microendolithic organism and infilling of the tiny little voids by microcrystalline Mg calcite or aragonite cements (Bathurst, 1966; Perry, 1999). Constructive micrite envelopes may result from the growth of externally calcified filamentous algae on the surface of the carbonate grains (e.g. Calvet, 1982). Both modes are interpreted to be connected with the activity of microbes, algae and fungi (Perry, 1999; Flügel, 2004; Chacón et al., 2006) and represent microbial development on the bioclastic debris. The micritized ooids are considered as the result of intense micritization of radial calcite ooids, caused by microboring by algae or fungi (Margolis and Rex, 1971).

7.2. Ferruginization

Concentration of iron oxide occurred on the ferruginous crust that coated the palaeokarst surface on top of the stage 1. It is made by serpulid worm tubes and encrusting agglutinated foraminifera (nubeculariids) embedded in a matrix of iron-oxide films (Fig. 13A). In addition, red to brown grainstone beds with abundant iron-stained components occurred in the first metres above this surface. Iron staining affects to echinoderm fragments, foraminifera and bryozoan chambers

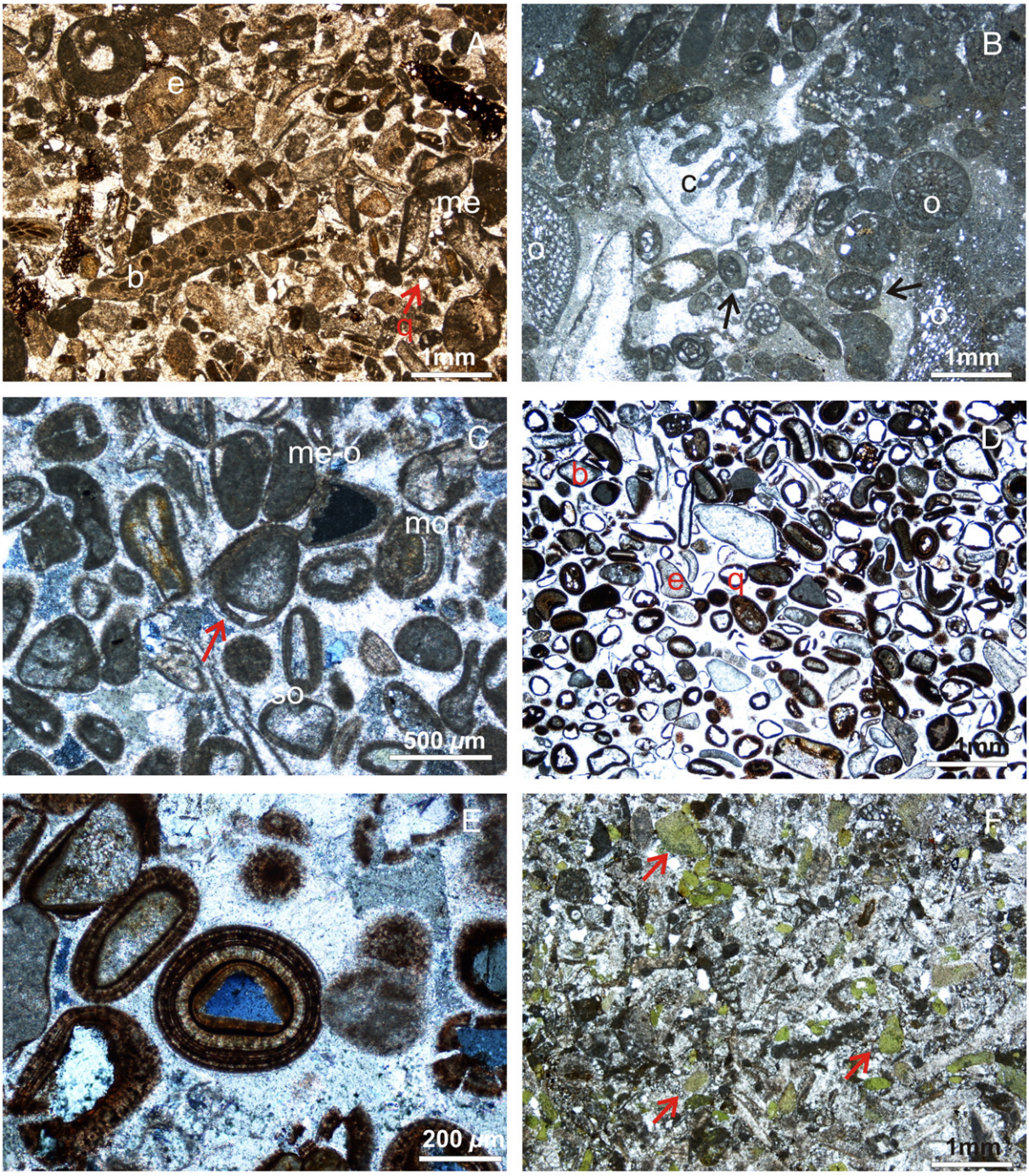

Fig. 12. Photomicrographs showing microfacies of the stage 2 (Umbrera Formation.). (A) Bioclastic grainstone with bryozoans (b), plates of echinoderms (e), micritized bioclasts (me) and quartz grains (q); Bustriguado section, La Florida area. (B) Packstone with orbitolinids (o) and abraded fragments of corals (c) and miliolids (arrows); Cuchía section, Cuchía area. (C) Oolitic grainstone with mixed ooids (mo), superficial ooids (so) and micritized ooids (me-o). Note the broken ooid cortex separated from the nucleus by thin calcite cement (arrow); crossed polarized-light; La Florida section, La Florida area. (D) Ferruginized oolites with different types of nucleus such as quartz grains (q), echinoderm (e) and dissolved bioclast (b), and iron oxide or iron-stained cortices; Bustriguado section, La Florida area. (E) Detail of a mixed ooid whose nucleus is composed by a quartz-grain and the cortex by layers of iron oxides and calcite; Bustriguado section, La Florida area; crossed polarized-light. (F) Glauconite-rich grainstone with quartz grains and bioclasts. Glauconite appears as detrital grains and replacing echinoderm plates (arrow); Cuchía section, Cuchía area.

and ooids. In these reddish beds, the cortex and nucleus of the majority of the ooids are strongly ferruginized and present abundant microborings and microfilaments (Fig. 13B–D), which may have destroyed completely the original textural patterns. The iron oxides may replace the external calcite cortices only or may form mixed ooids. Mixed ooids are formed by tangential calcite or fine micrite layers that alternate with thin Fe-rich coatings (Fig. 13B, C).

Ferruginized ooids and crusts similar to those described above are frequent in Jurassic hardgrounds and condensed sections of the Tethyan basins (e.g. Di Stefano and Mindszenty, 2000; Préat et al., 2000; Ramajo et al., 2002; Gradzinski et al., 2004; Mamet and Préat, 2006; Reolid et al., 2008), but are identified throughout the whole stratigraphic record since the Proterozoic. Their genesis has been interpreted in diverse ways that include subaerial and submarine environments, with the iron being supplied from volcanic to hydrothermal, lateritic or continental sources (e.g. Jenkyns, 1970; Nahon et al., 1980; Kearsley, 1989; Aurell et al., 1994; Sturesson et al., 2000). In this study, the presence of serpulids and encrusting foraminifera in the iron films and the marine nature of most

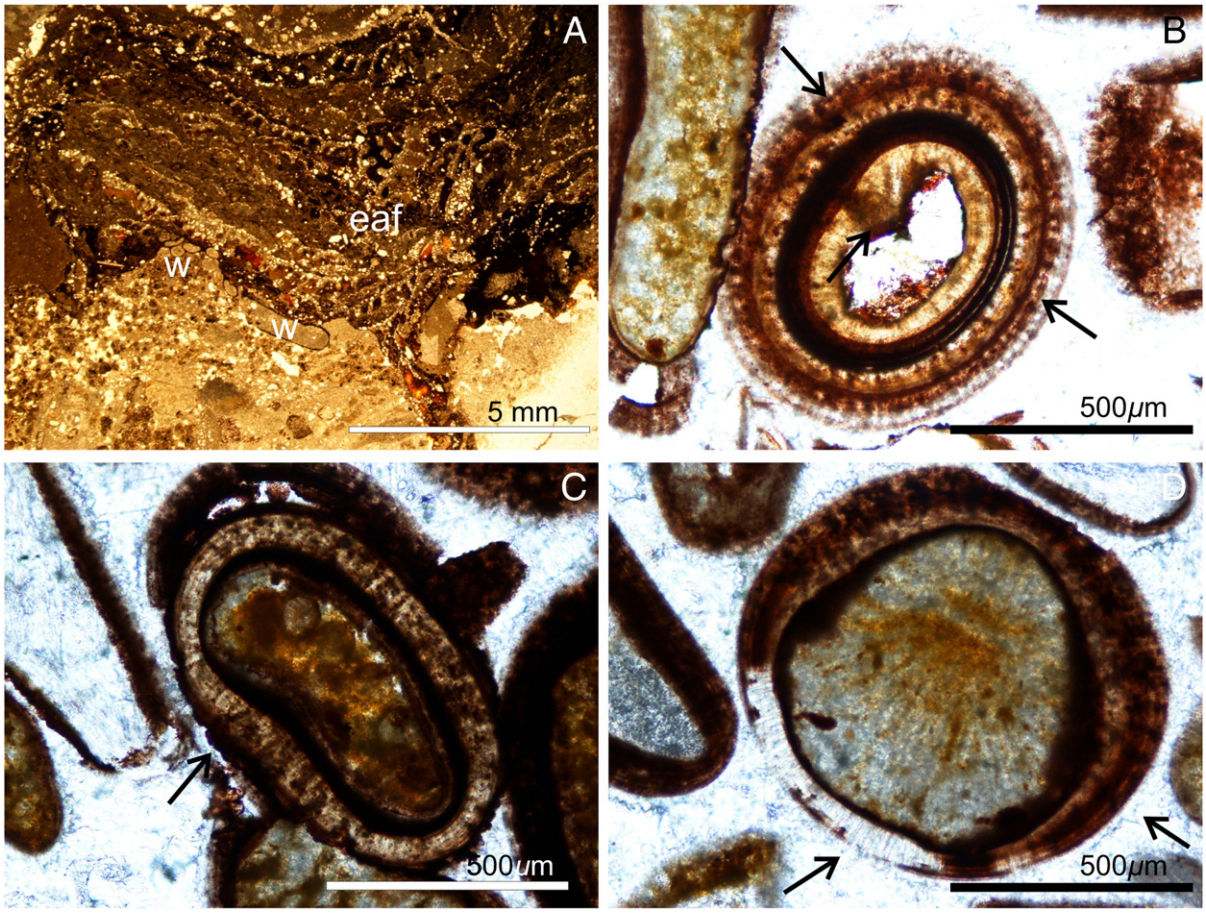

Fig. 13. Detailed plane-light photomicrographs of the hardground that appears coating the palaeokarst surface of the stage 1, and of the ferruginized oolites at the first metres above this surface. (A) Fe-rich crust composed by worm tubes (w), encrusting agglutinated foraminifera (eaf) embedded in a matrix of iron-oxide films. Sample LA-12, Rábago section, La Florida area. (B) Detail of mixed iron ooid with microborings (arrow); Bustriguado section, La Florida area. (C) Mixed iron ooid with microborings (arrow) resulted from reworking of previously deposited ooid and formation of new carbonate cortex on previous ferruginous layers; Bustriguado section, La Florida area. (D) Fine-radial calcite cortex is replaced by submicrometre-scale iron oxides. Note the isopachous, fibrous-to-bladed calcite cement (C1) around the ferruginized ooid (arrows).

ooid nuclei indicate a definitive marine origin for the iron crust and ooids. The fact that the iron staining is related to bioclast and ooid portions which have lost the original texture suggests the presence of microbes that oxidized the ferrous iron. This may have occurred at the sediment–water interface (Préat et al., 2000), but implies that water energy at the sea bottom varied intermittently. Once the calcite ooids were formed, they rested on the sea-floor during a time interval long enough to allow that the original calcite surfaces of the ooids provide substratum for colonization of iron-oxidizing bacteria and fungi, forming colonies within the carbonate cortex. The microbial activity led to precipitation and replacement of the carbonate support by submicrometric iron oxides, and the ooids became reddish (Fig. 13D). This is an early marine diagenetic process that occurred at slow rates and that requires a relatively large exposition of the ooids near the sediment–water interface. After that, the ferruginized ooids may be reworked during subsequent episodes of high energy, or may be latterly transported to the high-energy depositional settings of stage 2. Mixed ooids may result from reworking of previously deposited and ferruginized ooids affected by later formation of a new carbonate cortex on old ferruginous layers (Fig. 13C).

7.3. Glauconite authigenesis

Glauconite cement has been observed in the stage 2, filling primary intraparticle voids, particularly within echinoderms and orbitolinids.

This authigenic glauconite is considered to have been precipitated from marine pore waters during early marine diagenesis, under low sedimentary rates and partially reducing conditions (Odin and Matter, 1981), and indicates primary mineralization in condensed marine sediments (Odin, 1988; Glenn et al., 1994).

7.4. Carbonate cementation

Carbonate cementation affects all the analyzed samples from a variety of diagenetic processes extending from early marine diagenesis on the sea-floor to meteoric and burial environments. Only the sea-floor and meteoric diagenetic stages are discussed in this paper. These carbonate cements appear as pore-lining and pore-filling cements in primary cavities, intergranular pore space, and in secondary mouldic porosity.

7.4.1. Early marine cement

Isopachous, fibrous-to-bladed calcite cement (C1) appears around ferruginized ooids, skeletal grains, quartz particles and extraclasts, associated preferably to the grainstone of the stage 2 of carbonate production. Isopachous fringing cement is also observed on samples from the stages 1 and 4, although it occurs more scarcely. This cement stains pink (non-ferroan) and fills primary intergranular porosity. Under cathodoluminescence (CL), it is bright to dull orange (Fig. 14A–B).

This calcite cement appears to have formed early, in the marine phreatic or near sea-floor environment as high-Mg calcite or fibrous aragonite, and later transformed to low-Mg calcite (Moore, 1989;

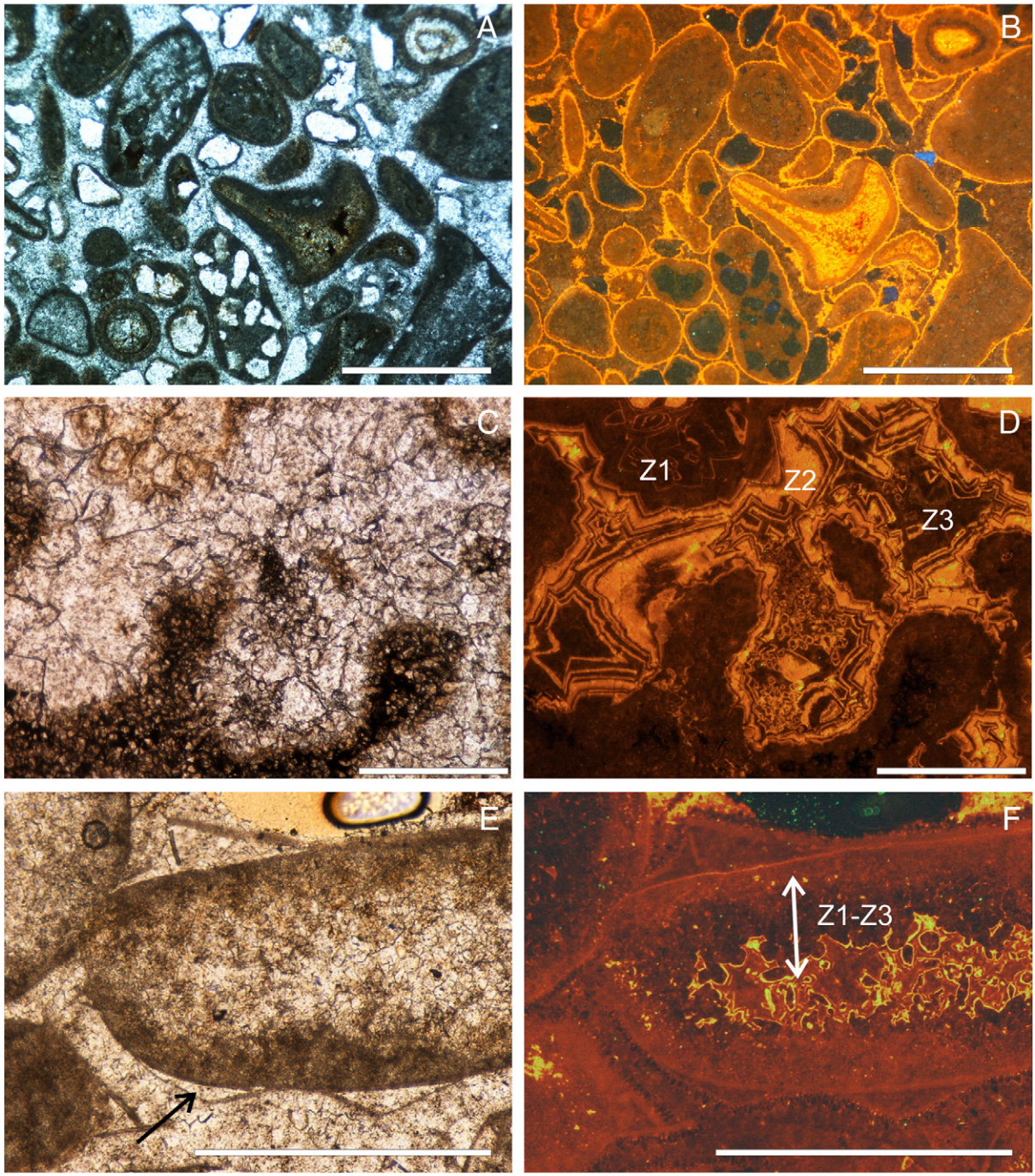

Fig. 14. Photomicrographs of paired plane-light (left) and CL (right) images; scale bar in each case is 500 μm. (A–B) Isopachous, fibrous-to-bladed calcite cement (C1) fringing primary intergranular porosity in grainstones of the stage 2. Under CL the fringing cement is bright orange; Hayuela-Canales section, Santillana area. (C–D) Pore filling, low-Mg, non-ferroan calcite cement (C2) precipitated in the mould porosity of a dissolved coral of the stage 1. In CL, C2 presents three cements zones (Z1–Z3). Z1 is non-luminescent. Z2 is mainly multizoned non-luminescent and orange bright luminescent and Z3 is dark-dull luminescent; sample LA-6, Rábago section, La Florida area. (E–F) Reworked bioclast of stage 2 replaced by equant calcite cement (C2) that in CL shows the Z1–Z3 cement zones. Note the micrite envelope separated from the bioclast due to early mechanical compaction (arrow); Sample LA-12, Rábago section, La Florida area.

James and Choquette, 1990). The luminescence bright-dull orange suggests recrystallization or primary precipitation under slightly reducing conditions (Barbin, 2000). However, the regular pattern and homogeneous intensity of luminescence point to a rather primary precipitation.

7.4.2. Shallow burial meteoric cement

Blocky equant calcite spar (C2) occurs as pore-lining and pore-filling cement in primary inter- and intraparticle pores as well as in secondary mouldic porosity. This cement commonly occurs as scalenohedral (dogtooth) spar around pores or as drusy to equant calcite when occluding pore spaces. It is non-ferroan and probably low-Mg, and is rich in Fe-oxide solid inclusions. In CL this cement presents three cements zones (Z1 to Z3; Fig. 14C–D). Z1 is non-luminescent. Z2 is mainly orange- to yellow bright luminescent, and may occur as one single bright zone or as several bright luminescent/non-luminescent multizones (Fig. 14D). Z3 zone is dark-dull luminescent.

Spar crystals of calcite C2 have been observed in all the carbonate stages. However, there is a significant difference in how calcite C2

appears through the succession, especially through the stages 1 and 2. Beneath the unconformity at the top of stage 1, this calcite spar occurs extensively in intergranular, shelter, intraskeletal and mouldic pores, the later generated after leaching of aragonite skeletons. In contrast, above the unconformity, C2 calcite does not cement grainstones of the stage 2 (Fig. 14E–F). In this case, it is observed only in some abraded skeletal grains, eroded and reworked from the previous stage 1 (Fig. 14E–F).

Calcite spar C2 is considered to indicate freshwater shallow burial (meteoric) cementation from oxidizing (non-luminescent) to moderate reducing (bright luminescent) pore fluids (Moore, 1989; Muchez et al., 1998; Dickson and Saller, 1995; Mutti, 1995). This process is well documented in modern aquifers (Champ et al., 1979). Leaching of the aragonite skeletons and subsequent replacement by calcite spar C2 occurred during emersion at the end of stage 1. During the following transgression, with erosion of the previous stage, they were eroded and recycled in the grainstones of the stage 2.

8. Stable isotopes

Stable carbon isotopic composition ($\delta^{13}C$) throughout the studied succession in La Florida area (Fig. 15), varies from +3.6‰ to −4.5‰, recording a noticeable range of variability, which exceeds 8‰. In that succession, the $\delta^{13}C$ record can be subdivided into three successive intervals (Fig. 15). The basal interval matches with stages 1 and 2 of carbonate production. It shows relatively homogeneous and positive $\delta^{13}C$ values during the stage 1 (mean of +2.2‰), and a significant and progressive decrease (of about 1‰) in the record of the stage 2 (but still within positive values). The second interval of the $\delta^{13}C$ curve correlates with the Patrocinio Formation (stage 3). This interval is characterized by a notable negative excursion from values of −0.4‰ at the base of the interval to −4.5‰ at the top. The decrease in the values is not gradual but shows three negative peaks (−2.9‰, −4.1‰ and −4.5‰ respectively; Fig. 15). Finally, the third interval in the $\delta^{13}C$ record shows the return to positive values. This change occurs during the re-instauration of carbonate production in the stage 4. During this interval the $\delta^{13}C$ values range from +2.5‰ to +3.6‰, and are, in average, more positive than those of the first interval.

The oxygen-isotope record ($\delta^{18}O$) also shows a remarkable variability, with values varying from −2.7‰ to −13.8‰ (Fig. 15). It reveals comparable patterns to those of the carbon-isotope curve, and three main intervals can be also differentiated along the section. The first interval coincides with the stages 1 and 2, and presents relatively constant values (mean of −3.5‰). A sharp negative excursion is recorded during deposition of the marly Patrocinio Formation. Here the values range from −5.7‰ to −13.8‰. The third interval of the $\delta^{18}O$ curve shows a return to less negative values (mean of −4.3‰), which are correlated with deposition of the stage 4 (Fig. 15).

9. Discussion

Understanding the effects of the OAEs in the deep oceans has become a major objective of a large number of works in the last years. However, little is still known about the effects of these events on shallow marine platform carbonates and the interaction of their effects with local tectonic factors. The studied shallow platform succession was affected during the Aptian by the OAE 1a and by extensional tectonics. During the Aptian and immediately preceding

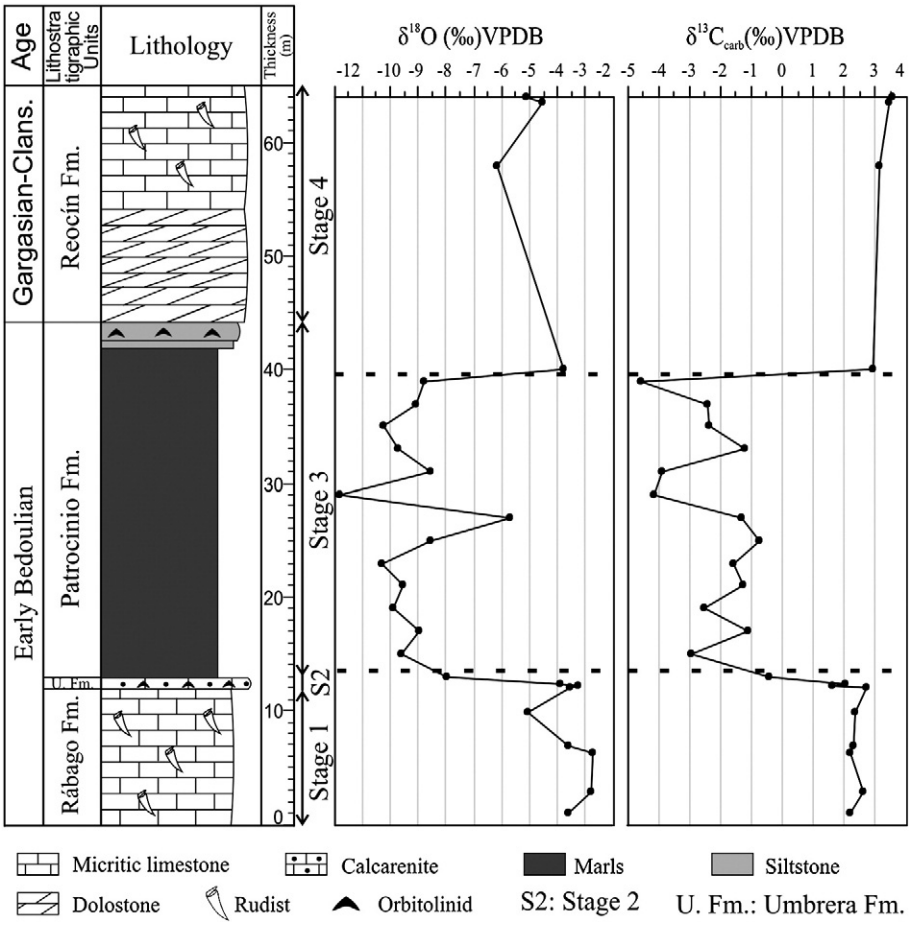

Fig. 15. Carbonate carbon and oxygen stable isotope records of the Aptian carbonate succession from La Florida area. The isotopic records are plotted against stratigraphic thickness, lithology and stratigraphic units. Dotted lines mark isotopic intervals.

the anoxic event, the platform evolved from stage 1 (photozoan assemblages) to stage 2 (heterozoan assemblages) of carbonate production. Later, a rapid drowning of the platform and deposition of open-marine shales (stage 3) occurred at the onset of the OAE 1a. Finally, the recovering of shallow water carbonate deposition with photozoan assemblages took place during the stage 4, at the end and after the anoxic event. The data indicate that the stratigraphic, sedimentological, diagenetic and chemostratigraphic shifts that affected the platform carbonates during this time were abrupt, and all of them point to rapid environmental changes accompanying the platform evolution.

9.1. Photozoan versus heterozoan styles of carbonate production

The predominance during the carbonate stages 1 and 4 of light-dependent benthic organisms and skeletal grain types (corals, dasycladacean algae, etc.) indicates a photozoan style of carbonate production (Table 1). Comparing with modern carbonate sediments, this photozoan assemblage reflects favourable platform growth conditions in seawaters that are shallow, transparent, warm, euhaline, and oligotrophic (Hallock, 1988; Föllmi et al., 1994; James, 1997). The photozoan textures (wackestone and packstone) of stages 1 and 4 suggest that the depositional energy was predominantly low. The presence of miliolids, monopleurid and requieniid rudist banks, *L. aggregatum–B. irregularis*, and fenestral microbialites suggests shallow water with stable bottom conditions and deposition in protected lagoons with weak bottom currents (e.g. Ross and Skelton, 1993; Gómez-Pérez et al., 1998), only occasionally affected by high-energy episodes. The low amount of non-skeletal grains and the minor contribution of siliciclastic particles, except for the mixed carbonate–siliciclastic facies at the transgressive bases of the carbonate stages, suggest low contribution of terrigenous runoff during these stages of carbonate growth.

In contrast, during the stage 2, the platform sedimentation was dominated by a heterozoan style of carbonate production, with predominance of calcite components, absence of organic build-ups, and abundance of suspension feedings such as crinoids and bryozoans. The substantial amount of orbitolinids indicates conditions of high nutrient input, since these asexually reproducing benthic foraminifera thrive in such conditions (Birkeland, 1988; Vilas et al., 1995). The heterozoan skeletal grains of the stage 2 (e.g. echinoids, coralline algae and molluscs) are ubiquitous elements present in a wide range of shallow marine systems and latitudes, although they became predominant only when other organisms are inhibited by environmental conditions such as light availability, temperature, salinity and nutrients (Hallock, 1988). In modern platform analogues, this heterozoan association typifies sedimentation in cool waters, or alternatively, sedimentation below the photic zone (James, 1997). However, nutrient poisoning (excess) can produce enough environmental stress to radically alter the platform benthos and eventually led to platform drowning (Hallock and Schlager, 1986; Hallock, 1988; Jenkyns, 1995). During the Aptian, sedimentation in the Basque-Cantabrian basin occurred in warm, sub-tropical climatic regions (e.g. Scotese et al., 1998), and the data indicate that both the photozoan and heterozoan stages of carbonate deposition took place in shallow water conditions. The presence of light-dependent organisms in the photozoan stages implies deposition within the photic zone. In the heterozoan stage 2, the overall lack of carbonate mud, the common high-energy traction current structures, and the presence of oolites suggest deposition under agitated bottom waters, likely within the photic zone as well. Therefore, depth seems not to have played a major role in the compositional shifting to heterozoan carbonate sedimentation during the stage 2. The presence of substantial amounts of sand-sized siliciclastic particles accompanying the heterozoan stage 2 may be considered as an indicator of higher nutrient influx levels accompanying the import of detrital particles in this stage that preceded the OAE 1a (Föllmi et al., 1994; Burla et al., 2008).

Recently, there is an open debate about a possible causal relationship between the presence of *Lithocodium–Bacinella* communities in shallow epicontinental seas and the OAE 1a (Immenhauser et al., 2005). According to these authors, the *Lithocodium–Bacinella* consortium may represent an out-of-balance facies, flourished under rising nutrient levels, which are time-equivalent in shallow water platforms to the black shales deposited in hemipelagic and pelagic environments during the OAE 1a (Immenhauser et al., 2005). However, in this study the presence of *Lithocodium–Bacinella* communities is not related with the OAE 1a. In fact, this facies appears indistinctly before and after the OAE 1a, (stages 1 and 4) with the maximum bloom taking place during the Late Aptian (Reocín Formation), which is not time-equivalent with the OAE 1a. On the contrary, the time-equivalent facies at the onset of the OAE 1a are represented by the black marls of the stage 3 (Patrocinio Formation) deposited during transgression and drowning of the platform.

9.2. Ferruginization, glauconite, and environmental stress

The shifting from the photozoan stage 1 to the heterozoan stage 2 was marked by a subaerial exposure surface coated by a later submarine iron crust; and the heterozoan skeletal association of stage 2 was accompanied by formation of ferruginized oolites. The ferruginous crust indicates early sea-floor cementation resulting in a hardground-capped unconformity, likely related to iron bacteria and microbe activity. This is suggested by the existence of microborings filled with iron oxides. The presence of nubeculariid foraminifers may suggest relatively shallow warm waters (Gradzinski et al., 2004).

Ferruginization of previous calcite oolites resulting in the formation of ferruginized oolites took place also under the influence of iron-oxidizing bacteria. This process can be produced by a variety of both phototrophic and non-phototrophic microorganisms. Due to the lack of light dependence of these organisms, they probably formed under dim conditions and required slow sedimentation rates, the presence of low-oxygen water masses and a source of iron (Mamet and Préat, 2006; Préat et al., 2008). Such conditions were likely associated with dysaerobic sediment–water interfaces (Mamet and Préat, 2006). Under such conditions the stability of the soluble reduced state of iron is higher and the metabolic activity of Fe-oxidizing bacteria can induce ferric oxide and hydroxide precipitation as a secondary by-product (Konhauser, 1998; Mamet and Préat, 2006). Therefore, these ferruginized oolites suggest the existence of long periods with dysaerobic bottom conditions that would alternate with high-energy conditions where the cross-stratified grainstones were formed. As indicated by the presence of some oolites with mixed layers of iron oxides and calcite, iron precipitation occurred probably very early, just after formation of oolite calcite cortices and fragmentation of skeletons and their immediate deposition, although they were still susceptible of periodic reworking. The source of the iron mineral can be explained by a terrigenous origin, with the iron derived from enhanced continental weathering during sedimentation.

The formation of both hardground surfaces coated with iron oxide and glauconite-bearing sediments is frequent in the geological record related to condensed series and submarine hiatuses, and their genesis appear to be directly related to rapid sea-level rises, carbonate platform destruction and eutrophication (Hallock and Schlager, 1986; Hallock, 1988; Föllmi et al., 1994). The data suggest that enhanced terrestrial runoff during the stage 2 of carbonate production probably brought iron and nutrients to the North Cantabrian platform, resulting in water-column eutrophication and environmental stress. These particular trophic conditions may explain the proliferation of heterotrophic Fe-oxidizing bacteria and suspension-feeding benthic organisms, such as crinoids and other heterozoan skeletal components of the stage 2 (James, 1997; Föllmi et al., 2006).

9.3. Early calcite cements and environmental conditions of stages 1 and 2

The analysis of diagenetic features in the carbonates has been of great value to recognize meteoric alteration of the platform carbonates and to provide an additional record of changes in relative sea-level and environmental conditions. The occurrence of pre-compaction, calcite spar C2 is interpreted to precipitate from oxidized to slightly reduced meteoric waters in the phreatic zone (e.g. Benito et al., 2005; Bishop et al., 2009). Early meteoric cements have been exclusively observed on samples from the stage 1, accompanying medium-scale karstic features that occur at the top of this stage. The meteoric fluids entered the platform as a result of a combination of both subaerial exposure and acceleration of the hydrological cycle, which induced increased rainfall, fluvial discharge, and continental runoff. The interaction of meteoric waters with exposed marine carbonates during platform emersion caused dissolution and favoured the circulation of freshwater lenses through the carbonate mass, which acted as an unconfined aquifer. This resulted in further dissolution and precipitation of the non-luminescent to bright luminescent (Z1–Z2) blocky spar, filling all available porosity (primary cavities and secondary mouldic porosity). It should be noted that the occurrence of these type of cements recognized in some of the basal samples of the stage 2 is only apparent, as they are always found in recycled and reworked lithoclasts from the previous stage.

Primary intergranular porosity in grainstones from the stage 2 was filled with rinds of marine isopachous calcite cements, which precipitated primary most likely as luminescent cements. Manganese is the most common activator of the luminescence in natural calcites (Marshall, 1988) and its incorporation in marine cements may suggest changes in the trace element concentration of the seawater or changes in the redox environmental conditions of precipitation (Barbin, 2000). Besides, the influx of freshwater may increase the Mn content of seawater and, therefore, of the calcite precipitated under such environmental conditions. For example, cathodoluminescence studies carried out on recent biogenic calcites have revealed an increase of luminescence and Mn contents of the shell calcites with decreasing salinity (Barbin et al., 1991).

9.4. Platform drowning and negative C and O isotope excursions of stage 3

The platform drowned during the evolutionary stage 3. The age of the drowning episode is well constrained with ammonites, planktonic foraminifers and nannofossils (Fig. 4), confirming that the marly interval (Patrocinio Formation) corresponds unequivocally to the OAE 1a (Gea et al., 2003; Rosales et al., 2009; Moreno-Bedmar et al., 2009). The chemostratigraphic analyses have revealed a prominent negative shift (~6‰) in the carbon-isotope record during deposition of these open-marine black marls. This negative shift is very similar to those reported from other coeval sections from adjacent basins (e.g. Moreno-Bedmar et al., 2009) and other basins from Europe, North America, Japan and the Pacific Ocean (Menegatti et al., 1998; Erba et al., 1999; Gröcke et al., 1999; Jenkyns and Wilson, 1999; Luciani et al., 2001; Ando et al., 2002; Bellanca et al., 2002; Jenkyns, 2003; Weissert and Erba, 2004, Burla et al., 2008), and is defined as a distinctive feature of the onset of the OAE 1a. Although the possible causal mechanisms of this carbon-isotope negative excursion are under a controversial debate (Jahren et al., 2001; Beerling et al., 2002; Jenkyns, 2003; Milkov, 2004), the massive release of isotopically light carbon to the atmosphere/hydrosphere reservoirs from methane hydrate dissociation is regarded as the most plausible hypothesis. This release was probably triggered by intensive volcanism and formation of large igneous provinces (Larson and Erba, 1999).

There is a good correlation between the $\delta^{13}C$ record of the studied Aptian carbonates and the main changes occurring in the evolution of the platform. The photozoan stages 1 and 4 are characterized by $\delta^{13}C$ values typical of micritic limestones from carbonate platforms of this period (Menegatti et al., 1998; Burla et al., 2008). The installation of the heterozoan stage 2 is correlated with a slight shift to more negative $\delta^{13}C$ values before the sharp negative spike that characterize the stage 3 of platform drowning and the onset of the OAE 1a. Similar correlations of $\delta^{13}C$ negative shifts and phases of heterozoan carbonate growth have been also described for other Early Cretaceous Tethyan platforms (Föllmi et al., 2006). The cause of this correlation is unclear but may be influenced in some degree by the input to the basin of continental water rich in dissolved isotopically light carbon derived from soil erosion.

The oxygen-isotope record during the stage 3 of platform drowning shows also a prominent shift (up to 11‰) to more negative values accompanying the C-isotope negative spike. Generally, relative low $\delta^{18}O$ values in pristine marine calcites are explained as reflecting elevated seawater temperatures (e.g. Marshall, 1992). However, the negative $\delta^{18}O$ values registered during the stage 3 are incompatible with any reasonable palaeotemperature reconstruction since, if interpreted only in terms of palaeotemperature, would give unrealistic extremely high seawater temperatures. New $\delta^{18}O$ data on pelagic carbonates from ODP survey in the central Pacific (Ando et al., 2008) has revealed extreme warming at the onset of the OAE 1a, with $\delta^{18}O$ pelagic values as low as −4.5‰ departing from background values of about −2‰. By comparison, only a small portion (~2–3‰) of the isotopic shift recorded in the samples across the marly interval of stage 3 may have been caused by this warming episode.

Other possible mechanism to explain isotopically light values of both $\delta^{18}O$ and $\delta^{13}C$ records in shallow platform carbonates can be found in early diagenetic processes associated with platform exposure (Immenhauser et al., 2002, 2003, 2008). These authors propose that low C and O isotope values in platforms tops are usually related to the combination of two processes. One is the influence of ^{18}O-depleted early meteoric fluids and the other is the influence of ^{13}C-depleted soil-zone CO_2 during carbonate recrystallization. However, in this study the negative shifts in C and O isotopes are not recorded in the shallow platform carbonates but in the open-marine marls of the Patrocinio Formation, which deposited during widespread transgression under water-depth conditions far from subaerial exposure.

More plausible, secondary changes in the isotope ratios could occur with carbonate recrystallization during burial diagenesis, and could explain at least the anomalous low $\delta^{18}O$ values. Early precipitation of diagenetic isotopically light calcite in the marly interval as a consequence of bacterial organic matter decomposition in the sulphate-reducing zone is likely a mechanism that operated in many organic-rich rocks (Sass et al., 1991). However, the scarcity of organic matter present in our samples (0.5% or less; Rosales et al., 2009) may compromise this interpretation. Alternatively, depletion in the $\delta^{18}O$ and $\delta^{13}C$ composition of the seawater may have been caused by an influx of terrestrial runoff into the platform during the stage 3 as a consequence of acceleration of the hydrological cycle (e.g. as described in the Early Toarcian OAE by Sælen et al., 1996). The change in the isotope composition of the platform seawater during this stage may have acted in combination with the warming episode (Ando et al., 2008) to cause the low $\delta^{18}O$ values detected in the samples.

9.5. Climate (global) versus tectonic (local) controls on the platform evolution

Beyond the influence of the OAE 1a, the described patterns of platform evolution in the NCB are also influenced by regional factors such as local tectonics and differential subsidence or runoff changes. Eustacy also should play a significant role in the evolution of the platform.

Regionally, rift tectonism occurred during the Tithonian–Cenomanian (e.g. Martín-Chivelet et al., 2002). The syn-rift nature of the carbonate succession deposited during the Aptian in the NCB is indicated by the fact that strata thicken and fan out into hangingwall areas and thin onto

footwall areas (Figs. 2B and 5). Therefore, it can be assumed that the accommodation space for platform growth was created from a combination of sea-level change, local block movements, and regional subsidence from crustal thinning and sediment loading.

The contact between the carbonate platform stage 1 and the next stage 2, which is marked by an unconformity with evidence of erosion, dissolution and meteoric diagenesis on footwall crests, points to local uplift and a brief period of subaerial exposure. The stage 2 was a carbonate sequence developed initially only on the more subsiding parts of the basin. The unit shows pronounced onlap at the base and is interpreted as the passive fill of a wedge-shape accommodation space during a phase of relative sea-level rise. This stratigraphic pattern closely resembles the depositional architecture predicted by the models of Bosence (2005) and Gardner et al. (2009) for fault-block carbonate platforms, and suggests that local tectonics was the major cause of this unconformity that produced hangingwall subsidence and footwall uplift. The flooding and onlapping on this surface were accompanied by the change to a heterozoan style of carbonate production with influx of siliciclastic particles. The predominance of such type of grains, and the rest of evidences presented in this study, all suggest environmental perturbation by continental waters charged in siliciclastic particles and nutrients, resulting in a mesotrophic habitat in the stage that preceded the OAE 1a. The carbonate factory changed to a less-effective mode of sedimentation that occurred at slow rates, as indicated by the presence of glauconite, and the high rates of microbial activity and ferruginization. This sedimentary response may have been induced by the tectonic uplift and fluvial erosion of the southern and western margins of the NCB. However, deterioration of the shallow water carbonate systems occurred almost simultaneously worldwide, such in the Pacific (Jenkyns, 1995), France (Masse et al., 1999), Switzerland (Wissler et al., 2003), Helvetic Alps (Föllmi et al., 2006), and Portugal (Burla et al., 2008) among others, suggesting that this was an inter-regional phenomenon.

The shallow water carbonate platform deterioration took place during a rapid rise in relative sea-level. The weakened production rate of the carbonate stage 2 could not keep-up with the rising sea-level, with the consequent drowning of the platform and deposition of open-marine marls of the stage 3. Although this event was influenced by tectonic subsidence, the early Aptian flooding should be considered as a major eustatic transgressive event. It is well recorded in other rifted-basins of both the Tethys and the North Atlantic, and remarkably, it has been also reported from cratonic areas, such as the East African craton, which are considered as geologically more stable (Bosellini et al., 1999). Because this transgression correlates well with similar events around the world and within different tectonostratigraphic settings (Somalia, Arabian Peninsula, Ethiopia, southern Italy, France, Spain, Portugal, north-eastern Mexico, Pacific realm, etc.) (e.g. Lehmann et al., 1999; Bosellini et al., 1999; Rosales, 1999; Burla et al., 2008; Föllmi, 2008), it is considered as a global phenomenon linked to the OAE 1a. Therefore, and in summary, in the NCB, the proximity of emerged land areas to the south of the Cabuérniga Ridge and in the Asturian Massif (see Fig. 1C for location) along with a combination of tectonic movements and more humid climate conditions, would have increased continental erosion, river drainage and runoff, which ultimately would have been responsible for the local/regional platform eutrophication and the subsequent drowning that accompany the OAE 1a.

10. Conclusions

The following conclusions from the study of the Early Aptian carbonate succession of the North Cantabrian basin can be drawn:

1) Four successive stages of carbonate production (1 to 4) outline the evolution of the platform, from which stage 3 corresponds to the local expression of the OAE 1a.
2) The carbonate stages that preceded the OAE 1a exhibit a compositional shifting from photozoan (stage 1) to heterozoan (stage 2) skeletal grains. These two stages of carbonate production are separated by an unconformity. This surface exhibits evidence of erosion, karstic dissolution and meteoric diagenesis, and is capped by a submarine ferruginous crust during the following transgressive event.
3) Tectonic activity favoured the influx of terrigenous particles from terrestrial runoff that accompanied the observed biotic changes. Besides, an accelerated hydrological cycle increased the input of freshwater and nutrients into the platform, causing the change from oligotrophic (stage 1) to mesotrophic (stage 2) conditions.
4) This event in the evolution of the carbonate platform correlates well with worldwide environmental deterioration of benthic environments. The combination of water freshening, nutrient poisoning, tectonic activity and rising eustatic sea-level may have acted together resulting in the progressive destabilisation of the marine environments and the change to less-effective carbonate factories (heterozoan), which may be the cause of the demise of many carbonate platforms worldwide previous to the instauration of the OAE.
5) Finally, the integration of sedimentological, diagenetic and chemostratigraphic analysis has been proven as a useful tool to identify and characterize global palaeoclimatic perturbations in shallow water carbonate platform environments.

Acknowledgements

This work is part of the Ph.D. Thesis of the first author (M.N.), who is supported by a scholarship from the Instituto Geológico y Minero de España (IGME). The study is a contribution to the DGI project CGL2008-01237/BTE (MICINN, Spanish Government), and to the UJA-07-16-41 project (Jaén University, Spain). Many thanks are due to A. Immenhauser and D. Sanders for valuable scientific comments and suggestions to improve the original manuscript.

References

Ando, A., Kakegawa, T., Takashima, R., Saito, T., 2002. New perspective on Aptian carbon isotope stratigraphy: data from $\delta^{13}C$ records of terrestrial organic matter. Geology 30, 227–230.

Ando, A., Kaiho, K., Kawahata, H., Kakegawa, T., 2008. Timing and magnitude of Early Aptian extreme warming: unraveling primary $\delta^{18}O$ variation in indurated pelagic carbonates at Deep Sea Drilling Project Site 463, central Pacific Ocean. Palaeogeography, Palaeoclimatology, Palaeoecology 260, 463–476.

Arnaud-Vanneau, A., Arnaud, H., 1990. Hauterivian to Lower Aptian carbonate shelf sedimentation and sequence stratigraphy in the Jura and northern subalpine chains (southeastern France and Swiss Jura). In: Tucker, M.E., Wilson, J.L., Crevello, P.D., Sarg, J.R., Read, J.F. (Eds.), Carbonate Platforms: Facies, Sequences, and Evolution: IAS Special Publication, 9, pp. 203–233.

Aurell, M., Fernández-López, S., Meléndez, G., 1994. The Middle–Upper Jurassic oolitic ironstone bed in the Iberian Range (Spain). Eustatic implications. Geobios Mémoire Spéciale 17, 549–561.

Barbin, V., 2000. Cathodoluminescence of carbonate shells: biochemical vs diagenetic process. In: Pagel, M., Barbin, V., Blanc, Ph., Ohnenstetter, D. (Eds.), Cathodoluminescence in Geosciences, 12. Springer Verlag, pp. 303–329.

Barbin, V., Ramseyer, K., Debena, J.P., Schein, E., Roux, M., Decrouez, D., 1991. Cathodoluminescence of recent biogenic carbonates: an environmental and ontogenetic fingerprint. Geological Magazine 128, 19–26.

Bathurst, R.G.G., 1966. Boring algae, micrite envelops and lithification of molluscan biosparites. Geological Journal 5, 15–32.

Beerling, D.J., Lomas, M.R., Gröcke, D., 2002. On the nature of methane gas-hydrate dissociation during the Toarcian and Aptian oceanic anoxic events. American Journal of Sciences 302, 28–49.

Bellanca, A., Erba, E., Neri, R., Premoli-Silva, I., Sprovieri, M., Tremolada, F., Verga, D., 2002. Palaeoceanographic significance of the Tethyan 'Livello Selli' (Early Aptian) from the Hybla Formation, northwestern Sicily: biostratigraphy and high-resolution chemostratigraphic records. Palaeogeography, Palaeoclimatology, Palaeoecology 185, 175–196.

Benito, M.I., Lohmann, K.C., Mas, R., 2005. Late Jurassic palaeogeography and palaeoclimate in the Northern Iberian Basin of Spain: constraints from diagenetic records in reefal and continental carbonates. Journal of Sedimentary Research 75, 82–96.

Birkeland, C., 1988. Second-order ecological effects of nutrient input into coral communities. Galaxea 7, 91–100.

Bishop, J.W., Montañez, I.P., Gulbranson, E.L., Brenkle, P.L., 2009. The onset of mid-Carboniferous glacio-eustasy: sedimentologic and diagenetic constrains, Arrow Canyon, Nevada. Palaeogeography, Palaeoclimatology, Palaeoecology 276, 217–243.
Bosence, D., 2005. A genetic classification of carbonate platforms based on their basinal and tectonic setting in the Cenozoic. Sedimentary Geology 175, 49–72.
Bosellini, A., Russo, A., Schroeder, R., 1999. Stratigraphic evidence for an Early Aptian sea-level fluctuation: the Graua Limestone of south-eastern Ethiopia. Cretaceous Research 20, 783–791.
Burla, S., Heimhofer, U., Hochuli, P.A., Weissert, H., Skelton, P., 2008. Changes in sedimentary patterns of coastal and deep-sea successions from the North Atlantic (Portugal) linked to Early Cretaceous environmental change. Palaeogeography, Palaeoclimatology, Palaeoecology 257, 38–57.
Calvet, F., 1982. Constructive micrite envelope developed in vadose continental environment in Pleistocene eolianites of Mallorca (Spain). Acta Geológica Hispánica 17, 169–178.
Carannante, G., Cherchi, A., Simone, L., 1995. Chlorozoan versus foramol lithofacies in Upper Cretaceous rudist limestones. Palaeogeography, Palaeoclimatology, Palaeoecology 119, 137–154.
Chacón, E., Barrendero, E., García-Pichel, F., 2006. Biogeological signatures of microboring cyanobacterial communities in marine carbonates from Cabo Rojo, Puerto Rico. Sedimentary Geology 185, 215–228.
Champ, D.R., Gulens, J., Jackson, R.E., 1979. Oxidation–reduction sequences in ground water flow systems. Canadian Journal of Earth Sciences 16, 12–23.
Collignon, M., Pascal, A., Peybernès, B., Rey, J., 1979. Faunes d'ámmonites de l'Aptien de la Région de Santander (Espagne). Annales de Paléontologie 65, 139–156.
Di Stefano, P., Mindszenty, A., 2000. Fe–Mn-encrusted "Kamenitza" and associated features in the Jurassic of Monte Kumeta (Sicily): subaerial and/or submarine dissolution? Sedimentary Geology 132, 37–68.
Dickson, J.A.D., 1966. Carbonate identification and genesis as revealed by staining. Journal of Sedimentary Petrology 36, 491–505.
Dickson, J.A.D., Saller, A.H., 1995. Identification of subaerial exposure surfaces and porosity preservation in Pennylvanian and Lower Permian shelf limestones, eastern Central basin Platform, Texas. In: Budd, D.A., Saller, A.H., Harris, P.M. (Eds.), Unconformities and Porosity in Carbonate Strata: American Association of Petroleum Geologists, Memory, 63, pp. 239–257.
Erba, E., Channell, J.E.T., Claps, M., Jones, C., Larson, R., Opdyke, B., Premoli-Silva, I., Riva, A., Salvini, G., Torricelli, S., 1999. Integrated stratigraphy of the Cismon APTICORE (Southern Alps, Italy): a 'reference section' for the Barremian–Aptian interval at low latitudes. Journal of Foraminiferal Research 29, 371–391.
Feuillée, P., Rat, P., 1971. Structures et paléogéographies Pyrénéo-Cantabriques. In: Debyser, J., Le Pichon, X., Montadert, L. (Eds.), Histoire Structurale du Golfe de Gascogne. Publication de l'Institute Français du Pétrole: Collection Colloque et Séminaires, Technip, Paris, 22, pp. 1–48.
Flügel, E., 2004. Microfacies of Carbonate Rocks: Analysis, Interpretation and Application. Springer-Verlag, Berlin Heidelberg. 976 pp.
Föllmi, K.B., 2008. A synchronous, middle Early Aptian age for the demise of the Helvetic Urgonian platform related to the unfolding oceanic anoxic event 1a ("Selli event"). Revue de Paléobiologie 27, 461–468.
Föllmi, K.B., Weissert, H., Bisping, M., Funk, H., 1994. Phosphogenesis, carbon-isotope stratigraphy and carbonate platform evolution along the Lower Cretaceous northern Tethyan margin. Geological Society of American Bulletin 106, 729–746.
Föllmi, K.B., Godet, A., Bodin, S., Linder, P., 2006. Interactions between environmental change and shallow water carbonate buildup along the northern Tethyan margin and their impact on the early Cretaceous carbon isotope record. Paleoceanography 21, PA4211.
García-Espina, R., 1997. La estructura y evolución tectonoestratigráfica del borde occidental de la Cuenca Vasco-Cantábrica (Cordillera Cantábrica, NO de España). Ph. D. Thesis, Oviedo University, Spain.
García-Mondéjar, J., Fernández-Mendiola, P.A., 1993. Sequence stratigraphy and systems tracts of a mixed carbonate and siliciclastic platform-basin setting: the Albian of Lunada and Soba, Northern Spain. American Association of Petroleum Geologists Bulletin 77, 245–275.
García-Mondéjar, J., Agirrezabala, L.M., Aranburu, A., Fernández-Mendiola, P.A., Gómez-Pérez, I., López-Horgue, M., Rosales, I., 1996. Aptian–Albian tectonic pattern of the Basque-Cantabrian Basin (northern Spain). Geological Journal 31, 13–45.
Gardner, J.A., Bosence, D., Burgess, P.M., Waltham, D., 2009. Tectono-stratigraphic models for Phanerozoic platforms. AAPG Search and Discovery Article #90090. AAPG Annual Convention and Exhibition, Denver, Colorado, June 2009.
Gea, G.A., de, Castro, J.M., Aguado, R., Ruiz-Ortiz, P.A., Company, M., 2003. Lower Aptian carbon isotope stratigraphy from a distal carbonate shelf setting: the Cau section, Prebetic Zone SE Spain. Palaeogeography, Palaeoclimatology, Palaeoecology 200, 207–219.
Glenn, C.R., Föllmi, K.B., Riggs, S.R., Baturin, G.N., Grim, K.A., Trappe, J., Abed, A.M., Galli-Olivier, C., Garrison, R.E., Ilyin, A.V., Jehl, C., Rorhlich, V., Sadaqah, R.M.Y., Schidlowski, M., Sheldon, R.E., Siegmund, H., 1994. Phosphorous and phosphorites: sedimentology and environments of formation. Eclogae Geologicae Helvetiae 87, 747–788.
Gómez-Pérez, I., Fernández-Mendiola, P.A., García-Mondéjar, J., 1998. Constructional dynamics for a Lower Cretaceous carbonate ramp (Gorbea Massif, north Iberia). In: Wright, V.P., Burchette, T.P. (Eds.), Carbonate Ramps: Geological Society, London, Special Publications, 149, pp. 229–252.
Gradstein, F.M., 2004. A Geologic Time Scale 2004. Cambrige University Press.
Gradzinski, M., Tyszka, J., Uchman, A., Jach, R., 2004. Large microbial–foraminiferal oncoids from condensed Lower-Middle Jurassic deposits: a case study from the Tatra Mountains, Polan. Palaeogeography, Palaeoclimatology, Palaeoecology 213, 133–151.
Gröcke, D., Hesselbo, S.P., Jenkyns, H.C., 1999. Carbon-isotope composition of Lower Cretaceous fossil wood: ocean–atmosphere chemistry and relation to sea level change. Geology 27, 155–158.
Hallock, P., 1988. The role of nutrient availability in bioerosion: consequences to carbonate buildups. Palaeogeography, Palaeoclimatology, Palaeoecology 63, 275–291.
Hallock, P., Schlager, W., 1986. Nutrient excess and the demise of coral reefs and carbonate platforms. Palaios 1, 389–398.
Hines, F.M., 1985. Sedimentation and tectonics in north-west Santander. In: Milá, M.D., Rosell, J. (Eds.), 6th European Regional Meeting, Excursion Guidebook. International Association of Sedimentologists, Lleida, Spain, pp. 371–398.
Hunt, D., Tucker, M.E., 1993. The Middle Cretaceous urgonian platform of southeastern France. In: Simo, J.A.T., Scott, R.W., Masse, J.P. (Eds.), Cretaceous Carbonate Platforms: American Association of Petroleum Geologists Memory, 56, pp. 409–453.
Immenhauser, A., Kenter, J.A.M., Ganssen, G., Bahamonde, J.R., van Vliet, A., Saher, M.H., 2002. Origin and significance of isotope shifts in Penssylvanian carbonates (Asturias, NW Spain). Journal of Sedimentary Research 72, 82–94.
Immenhauser, A., Della Porta, G., Kenter, J.A.M., Bahamonde, J.R., 2003. An alternative model for positives shifts in shallow marine carbonate $\delta^{13}C$ and $\delta^{18}O$. Sedimentology 50, 953–959.
Immenhauser, A., Hillgartner, H., van Bentum, E., 2005. Microbial foraminiferal episodes in the Early Aptian of the southern Tethyan margin: ecological significance and possible relation to Oceanic Anoxic Event 1a. Sedimentology 52, 77–99.
Immenhauser, A., Holmden, C., Patterson, W.P., 2008. Interpreting the carbon-isotope record of ancient shallow epeiric seas: lessons from the Recent. In: Pratt, B.R., Holmden, C. (Eds.), Dynamics of Epeiric Seas: Geological Association of Canada, Special Paper, 48, pp. 137–174.
Jahren, A.H., Arens, N.C., Sarmiento, G., Guerrero, J., Amundson, R., 2001. Terrestrial record of methane hydrate dissociation in the Early Cretaceous. Geology 29, 159–162.
James, N.P., 1997. The cool-water carbonate depositional realm. In: James, N.P., Clarke, J.A.D. (Eds.), Cool-water Carbonates: SEPM Special Publication, 56, pp. 1–20.
James, N.P., Choquette, P.W., 1990. Limestones: the meteoric diagenetic environment. In: Macillreath, I.A., Morrow, D.W. (Eds.), Diagenesis. Geosciences Canada, pp. 161–194.
Jansa, L.F., 1993. Early Cretaceous carbonate platforms of the northeastern North American margin. In: Simo, J.A.T., Scott, R.W., Masse, J.P. (Eds.), Cretaceous Carbonate Platforms: American Association of Petroleum Geologists Memory, 56, pp. 111–126.
Jenkyns, H.C., 1970. Submarine volcanism and the Toarcian iron pisolites of western Sicily. Eclogae Geologicae Helvetiae 63, 741–774.
Jenkyns, H.C., 1995. Carbon isotope stratigraphy and paleoceanographic significance of the Lower Cretaceous shallow-water carbonates of Resolution Guyot, Mid Pacific Mountains. In: Winterer, E.L., Sager, W.W., Firth, Sinton, J.M. (Eds.), Proceedings of the Ocean Drilling Program. Scientific Results.: Ocean Drilling Program, Collage Station, Texas, United States, 143, pp. 99–104.
Jenkyns, H.C., 2003. Evidence for rapid climate change in the Mesozoic–Palaeogene greenhouse world. Philosophical Transactions of the Royal Society A 361, 1885–1916.
Jenkyns, H.C., Wilson, P.A., 1999. Stratigraphy, paleoceanography, and evolution of Cretaceous Pacific guyots: relics from a greenhouse Earth. American Journal of Science 299, 341–392.
Kearsley, A.T., 1989. Iron-rich ooids, their mineralogy and microfabrics: clues to their origin and evolution. In: Young, T.P., Taylor, W.E.G. (Eds.), Geological Society, London, Special Publication, 46, pp. 141–163.
Konhauser, K.O., 1998. Diversity of bacterial iron mineralization. Earth Science Reviews 43, 91–121.
Larson, R.L., Erba, E., 1999. Onset of the Mid-Cretaceous greenhouse in the Barremian–Aptian: igneous events and the biological, sedimentary and geochemical response. Paleoceanography 14, 663–678.
Le Pichon, X., Sibuet, J.C., 1971. Western extension of the boundary between European and Iberian plates during the Pyrenean orogeny. Earth and Planetary Science Letters 12, 83–88.
Lehmann, Ch., Osleger, D.A., Montañez, I.P., 1998. Controls on cyclostratigraphy of Lower Cretaceous carbonates and evaporites, Cupido and Coahuila platforms, northeastern Mexico. Journal of Sedimentary Research 68, 1109–1130.
Lehmann, Ch., Osleger, D.A., Montañez, I.P., Sliter, W., Arnaud-Vanneau, A., Banner, J., 1999. Evolution of Cupido and Coahuila carbonate platforms, Early Cretaceous, north-eastern Mexico. Geological Society of America Bulletin 111, 1010–1029.
Luciani, V., Cobianchi, M., Jenkyns, H.C., 2001. Biotic and geochemical response to anoxic events: the Aptian pelagic succession of the Gargano promontory (southern Italy). Geological Magazine 138, 277–298.
Malod, J.A., Mauffret, A., 1990. Iberian plate motions during the Mesozoic. Tectonophysics 184, 261–278.
Mamet, B., Préat, A., 2006. Iron-bacterial mediation in Phanerozoic red limestones: state of the art. Sedimentary Geology 185, 147–157.
Margolis, S., Rex, R.W., 1971. Endolithic algae and micritic envelope formation in Bahamian oolites as revealed by scanning electron microscopy. Geological Society of American Bulletin 82, 843–852.
Marshall, D.J., 1988. Cathodoluminescence of Geological Materials. Unwin Hyman, Boston. 149 pp.
Marshall, D.J., 1992. Climatic and oceanographic isotopic signals from the carbonate rock record and their preservation. Geological Magazine 129, 143–160.
Martín-Chivelet, J., Berástegui, X., Rosales, I., Vilas, L., Vera, J.A., Caus, E., Gräfe, K.U., Mas, R., Puig, C., Segura, M., Robles, S., Floquet, M., Quesada, S., Ruiz-Ortiz, P.A., Frenegal-Martínez, M.A., Salas, R., Arias, C., García, A., Martín-Algarra, A., Meléndez, M.N., Chacón, B., Molina, J.M., Sanz, J.L., Castro, J.M., García-Hernández, M., Carenas, B.,

García-Hidalgo, J., Gil, J., Ortega, F., 2002. Cretaceous. In: Gibbons, W., Moreno, T. (Eds.), The Geology of Spain. The Geological Society, London, pp. 255–292.
Masse, J.P., 1993. Valanginian–Early Aptian carbonate platforms from Provence, southeastern France. In: Simo, J.A.T., Scott, R.W., Masse, J.P. (Eds.), Cretaceous Carbonate Platforms: American Association of Petroleum Geologists Memory, 56, pp. 363–374.
Masse, J.P., El Albani, A., Erlenkeuser, H., 1999. Stratigraphie isotopique ($\delta^{13}C$) de l'Aptien inférieur de Provence (SE France); application aux corrélations plateforme/bassin. Eclogae Geologicae Helvetiae 92, 259–263.
McCrea, J.M., 1950. On the isotopic chemistry of carbonates and a paleotemperature scale. Journal of Chemical Physics 18, 849–857.
Menegatti, A.P., Weissert, H., Brown, R.S., Tyson, R.V., Farrimond, P., Strasser, A., Caron, M., 1998. High-resolution $\delta^{13}C$ stratigraphy through the Early Aptian 'Livello Selli' of the Alpine Tethys. Paleoceanography 13, 530–545.
Milkov, A.V., 2004. Global estimates of hydrate-bound gas in marine sediments: how much is really out there? Earth Sciences Reviews 66, 183–197.
Moore, C.H., 1989. Carbonate Diagenesis and Porosity. Developments in Sedimentology. Elsevier, Amsterdam, 338 pp.
Moreno-Bedmar, J.A., Company, M., Bover-Arnal, T., Salas, R., Delanoy, G., Martínez, R., Grauges, A., 2009. Biostratigraphic characterization by means of ammonoids of the Lower Aptian Oceanic Anoxic Event (OAE1a) in the eastern Iberian Chain (Maestrat Basin, eastern Spain). Cretaceous Research 30, 864–872.
Muchez, P., Nielsen, P., Sintubin, M., Lagrou, D., 1998. Conditions of meteoric calcite formation along a Variscan fault and their possible relation to climatic evolution during the Jurassic–Cretaceous. Sedimentology 45, 845–854.
Mutti, M., 1995. Porosity development and diagenesis in the Orfento Supersequence and its bounding unconformities (upper Cretaceous, Montagna Della Maiella, Italy). In: Budd, D.A., Saller, A.H., Harris, P.M. (Eds.), Unconformities and Porosity in Carbonate Strata: American Association of Petroleum Geologists, Memory, 63, pp. 141–158.
Nahon, D., Carozzi, A.V., Parron, C., 1980. Lateritic weathering as a mechanism for the generation of ferruginous ooids. Journal of Sedimentary Petrology 50, 1287–1298.
Najarro, M., Rosales, I., 2008a. Disoluciones e incrustaciones ferruginosas asociadas al OAE 1a en la plataforma carbonatada de La Florida (NO de Cantabria). Geogaceta 44, 199–202.
Najarro, M., Rosales, I., 2008b. Evidencias sedimentológica, diagenética y quimioestratigráfica del Evento Anóxico Oceánico del Aptiense Inferior (OAE 1a) en la plataforma carbonatada de La Florida (NO de Cantabria). Geotemas 10, 163–166.
Najarro, M., Rosales, I., 2008c. Facies evolution, diagenesis and isotope analyses in a carbonate platform related to the Lower Cretaceous Anoxic Event 1a. SDGG 58. Abstract Volume of the 26th Regional Meeting of the International Association of Sedimentologists. Bochum, Germany, pp. 194.
Najarro, M., Rosales, I., Martín-Chivelet, J., 2007. Evolución de la plataforma carbonatada de la Florida durante el rifting del Cretácico Inferior (Aptiense, NO de Cantabria). In: Bermúdez, D.D., Najarro, M., Quesada, C. (Eds.), Volumen Monográfico de la II Semana de Jóvenes Investigadores del IGME. Publicaciones del IGME, pp. 123–128.
Najarro, M., Peñalver, E., Rosales, I., Pérez-de la Fuente, R., Daviero-Gomez, V., Gomez, B., Delclòs, X., 2009. Unusual concentration of Early Albian arthropod-bearing amber in the Basque-Cantabrian Basin (El Soplao, Cantabria, Northern Spain): Palaeoenvironmental and palaeobiological implications. Geologica Acta 7, 363–387.
Odin, G.S., 1988. Green Marine Clays. Developments in Sedimentology 45. Elsevier, Amsterdam, 445 pp.
Odin, G.S., Matter, A., 1981. De glauconiarum origine. Sedimentology 28, 611–641.
Olivet, J.L., 1996. La cinématique de la plaque Ibérique. Bulletin des Centres de Recherches Exploration-Production Elf-Aquitaine 20, 131–195.
Pascal, A., 1985. Les systèmes biosédimentaires urgoniens (Aptien-Albien) sur la marge Nord Ibérique. Mémoires Géologiques de l'Úniversité de Dijon 10, 1–569.
Perry, C.T., 1999. Biofilm-related calcification, sediment trapping and constructive micrite envelopes: a criterion for the recognition of ancient grass-bed environments? Sedimentology 46, 33–45.
Philip, J.M., Gari, J., 2005. Late Cretaceous heterozoan carbonates: palaeoenvironmental setting, relationship with rudist carbonates (Provence, south-east France). Sedimentary Geology 175, 315–337.
Préat, A., Mamet, B., De Ridder, C., Boulvain, F., Gillan, D., 2000. Iron bacterial and fungal mats, Bajocian stratotype (Mid-Jurassic, northern Normandy, France). Sedimentary Geology 137, 107–126.
Préat, A., El Hassani, A., Mamet, B., 2008. Iron bacteria in Devonian carbonates (Tafilat, Anti-Atlas, Marocco). Facies 54, 107–120.
Ramajo, J., Aurell, M., Cepría, J., 2002. Facies analysis of the Arroyofrío ferruginous oolitic bed in Sierra de Arcos (Jurassic, northern Iberian Chain). Journal of Iberian Geology 28, 45–64.
Ramírez del Pozo, J., 1972. Algunos datos sobre la estratigrafía y micropaleontología del Aptense y Albense al oeste de Santander. Revista Española de Micropaleontología 15, 59–97.
Rat, P., 1988. The Basque-Cantabrian basin between the Iberian and European plates some facts but still many problems. Revista de la Sociedad Geológica de España 1, 327–348.
Reolid, M., Abad, I., Martín-García, J.M., 2008. Palaeoenvironmental implications of ferruginous deposits related to a Middle-Late Jurassic discontinuity (Prebetic Zone, Betic Cordillera, Southern Spain). Sedimentary Geology 203, 1–16.
Rosales, I., 1999. Controls on carbonate-platform evolution on active fault blocks: the Lower Cretaceous Castro Urdiales platform (Aptian-Albian, northern Spain). Journal of Sedimentary Research 69, 447–465.
Rosales, I., Najarro, M., Moreno-Bedmar, J.A., Gea, G.A. de, Company, M., 2009. High resolution chemo and biostratigraphy records of the Early Aptian Oceanic Anoxic Event in Cantabria (northern Spain). Geochimica et Cosmochimica Acta, 73 (13S), A1118.
Ross, D.J., Skelton, P.W., 1993. Rudists formations of the Cretaceous: a palaeoecological, sedimentological and stratigraphical review. In: Wright, V.P. (Ed.), Sedimentology Review. Blackwell Scientific publications, pp. 73–91.
Ruiz-Ortiz, P.A., Castro, J.M., 1998. Carbonate depositional sequences in shallow to hemipelagic platform deposits; Aptian, Prebetic of Alicante (SE Spain). Bulletin de la Société Géologique de France 169, 21–33.
Sass, E., Bein, A., Almogi-Labin, A., 1991. Oxygen-isotope composition of diagenetic calcite in organic-rich rocks: Evidence for ^{18}O depletion in marine anaerobic pore water. Geology 19, 839–842.
Sælen, G., Doyle, P., Talbot, M.R., 1996. Stable-isotope analyses of belemnite rostra from the Whitby Mudstone Formation, England: surface water conditions during deposition of a marine black shale. Palaios 11, 97–117.
Schlanger, S.O., Jenkyns, H.C., 1976. Cretaceous oceanic anoxic events: causes and consequences. Geologie en Mijnbouw 55, 179–184.
Scotesse, C.R., Gahagan, L.M., Larson, R.L., 1998. Plate tectonic reconstructions of the Cretaceous and Cenozoic ocean basins. Tectonophysics 155, 27–48.
Scott, R.W., 1993. Cretaceous carbonate platform, U.S. Gulf Coast. In: Simo, J.A.T., Scott, R.W., Masse, J.P. (Eds.), Cretaceous Carbonate Platforms: American Association of Petroleum Geologists Memory, 56, pp. 97–109.
Simone, L., Carannante, G., 1988. The fate of foramol ('temperate-type') carbonate platforms. Sedimentary Geology 60, 347–354.
Soto, R., Casas-Sainz, A.M., Villalaín, J.J., Oliva-Urcia, B., 2007. Mesozoic extension in the Basque-Cantabrian basin (N Spain): contributions from AMS and brittle mesostructures. Tectonophysics 445, 373–394.
Spicer, R.A., Corfield, R.M., 1992. A review of terrestrial and marine climates in the Cretaceous with implications for modelling the "Greenhouse Earth". Geological Magazine 129, 169–180.
Sturesson, U., Heikoop, J.M., Risk, M.J., 2000. Modern and Palaeozoic iron ooids: a similar volcanic origin. Sedimentary Geology 136, 137–146.
Vilas, L., Masse, J.P., Arias, C., 1995. Orbitolina episodes in carbonate platform evolution: the Early Aptian model from SE Spain. Palaeogeography, Palaeoclimatology, Palaeoecology 119, 35–45.
Weissert, H., Erba, E., 2004. Volcanism, CO2 and palaeoclimate: a Late Jurassic–Early Cretaceous carbon and oxygen isotope record. Journal of the Geological Society, London, 161, 995–702.
Weissert, H., Lini, A., Föllmi, K.B., Kuhn, O., 1998. Correlation of Early Cretaceous carbon isotope stratigraphy and platform drowning events: a possible link? Palaeogeography, Palaeoclimatology, Palaeoecology 137, 189–203.
Wilmsen, M., 2000. Evolution and demise of a Mid-Cretaceous carbonate shelf: the Altamira Limestones (Cenomanian) of northern Cantabria (Spain). Sedimentary Geology 133, 195–226.
Wilmsen, M., 2005. Stratigraphy and biofacies of the Lower Aptian of Cuchía (Cantabria, northern Spain). Journal of Iberian Geology 31, 253–275.
Wissler, L., Funk, H., Weissert, H., 2003. Response of Early Cretaceous carbonate platforms to changes in atmospheric carbon dioxide levels. Palaeogeography, Palaeoclimatology, Palaeoecology 200, 187–205.

Palaeogeography, Palaeoclimatology, Palaeoecology 299 (2011) 137–158

Contents lists available at ScienceDirect

Palaeogeography, Palaeoclimatology, Palaeoecology

journal homepage: www.elsevier.com/locate/palaeo

High-resolution chemo- and biostratigraphic records of the Early Aptian oceanic anoxic event in Cantabria (N Spain): Palaeoceanographic and palaeoclimatic implications

María Najarro [a,*], Idoia Rosales [a], Josep A. Moreno-Bedmar [b], Ginés A. de Gea [c], Eduardo Barrón [a], Miguel Company [d], Gérard Delanoy [e]

[a] Instituto Geológico y Minero de España, IGME, Ríos Rosas 23, 28003 Madrid, Spain
[b] Departament de Geoquímica, Petrología i Prospecció Geológica, Facultat de Geologia, Universitat de Barcelona, Martí i Franquès s/n, 08028 Barcelona, Spain
[c] Departamento de Geología, Facultad de Ciencias Experimentales, Universidad de Jaén, Campus Las Lagunillas, 23071 Jaén, Spain
[d] Departamento de Estratigrafía y Paleontología, Universidad de Granada, Avenida Fuentenueva s/n, 18002 Granada, Spain
[e] Département des Sciences de la Terre, Université de Nice-Sophia Antipolis, 28 Avenue Valrose, F-06100 Nice, France

ARTICLE INFO

Article history:
Received 27 February 2010
Received in revised form 19 August 2010
Accepted 29 October 2010
Available online 5 November 2010

Keywords:
Early Aptian
OAE 1a
C-isotopes
High-resolution biostratigraphy
Biocalcification crisis
Basque Cantabrian Basin

ABSTRACT

During the Early Aptian, major palaeoenvironmental changes occurred leading to an oceanic anoxic event (OAE 1a) and a perturbation of the global carbon cycle. New detailed litho-, bio-, and chemostratigraphic (TOC, $\delta^{13}C_{carb}$, $\delta^{13}C_{org}$) records of two superbly exposed and expanded Lower Aptian sections in Cantabria (La Florida and Cuchía) allow to recognize the expression of the OAE 1a in shallow shelf environments of northern Spain. The succession consists of shallow platform limestones that include a marly unit (Patrocinio Formation), the deposition of which occurred mostly at the onset of the OAE 1a (~120.5 Ma). This study presents a new integrated biostratigraphy based on ammonites, planktonic foraminifera, calcareous nannofossils and palynomorphs that allows an accurate age resolution of the succession. The marly unit records an abrupt negative $\delta^{13}C$ excursion in both bulk organic matter (up to 5‰) and carbonate (up to 6‰, mean 3‰), as has been already observed at the onset of the OAE 1a in other Lower Aptian deposits worldwide. In detail, however, the negative excursion presents two minima in the studied sections. This negative spike is confidently attributed to the upper half of the *Hayesites irregularis* nannofossil Zone, to the upper part of the *Blowiella blowi* foraminiferal Zone, and to the middle–upper part of the *Deshayesites weissi* ammonite Zone. A third negative excursion occurs at the base of the *Rhagodiscus angustus* nannofossil Zone, which may be correlatable with the *Dufrenoyia furcata* ammonite Zone. This data set refines the age of the OAE 1a and reveals the existence of a stratigraphic gap in the westernmost margin of the Basque Cantabrian Basin that covers at least a portion of the upper part of the Early Aptian. Sedimentary facies and quantitative analysis of palynomorphs and nannofossils document significant environmental changes associated with the OAE 1a: compositional changes of neritic carbonates and calcareous nannofossils data indicate the occurrence of a biocalcification crisis inferred to have been related to CO_2-induced changes in seawater chemistry, and palynomorphs identify a thermal maximum followed by a cooling phase. The latter show a *Classopollis* maximum during the OAE 1a, which is followed by a decrease in *Classopollis* and an increase of bisaccate pollen after the event.

1. Introduction

The Early Aptian is recognised as an interval of significant, widespread environmental change generated by a battery of interrelated palaeogeographic and palaeoceanographic events. It is marked by a geologically brief (≤1 Myr; Bralower et al., 1994) episode known as the oceanic anoxic event 1a (OAE 1a) (Arthur et al., 1990; Jenkyns, 1980, 1999; Schlanger and Jenkyns, 1976), which is characterized by global rise in sea level (Haq et al., 1988), extreme greenhouse conditions (Dumitrescu et al., 2006; Frakes, 1979; Herman and Spicer, 1996; Larson, 1991; Vakhrameyev, 1982), global distribution of organic-rich deposits (so-called "Selli Event"; Coccioni et al., 1989; Jenkyns, 2003; Schlanger and Jenkyns, 1976), increase in continental weathering and runoff (Erba, 1994; Föllmi et al., 1994; Najarro et al., 2010), a biocalcification crisis with strong impact on planktonic microfauna and nannoflora (Erba, 1994, 2004; Erba and Tremolada, 2004; Gea et al., 2003; Larson and Erba, 1999; Weissert and Erba, 2004), and major perturbations in global carbon cycling (e.g.

* Corresponding author. Tel.: +34 91 7287288; fax: +34 91 7287202.
E-mail address: m.najarro@igme.es (M. Najarro).

0031-0182/$ – see front matter © 2010 Elsevier B.V. All rights reserved.
doi:10.1016/j.palaeo.2010.10.042

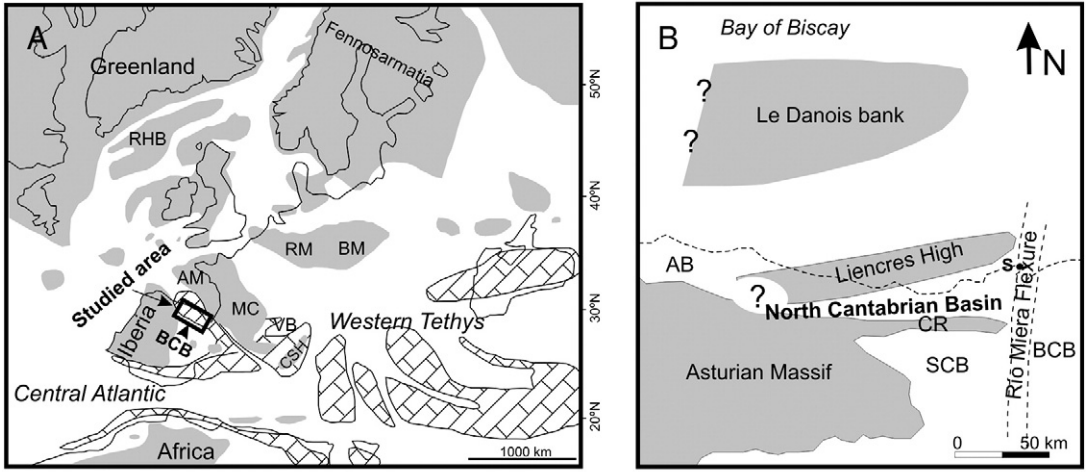
A
Greenland
Fennosarmatia
RHB
RM
BM
AM
MC
VB
CSH
Studied area
Iberia
BCB
Western Tethys
Central Atlantic
Africa
1000 km
50°N
40°N
30°N
20°N
B
Bay of Biscay
N
Le Danois bank
?
?
AB
Liencres High
?
North Cantabrian Basin
CR
SCB
BCB
Asturian Massif
Río Miera Flexure
0
50 km
Land
Carbonate platforms

sub-basins were bounded by active synsedimentary faults producing thick accumulations of sediments that were subsequently folded and thrusted during the Cenozoic Alpine orogeny.

The two Lower Aptian successions studied here were deposited in the North Cantabrian (sub-)Basin (NCB; Figs. 1B, 2A). This was a relatively small (~20×80 km) E–W elongated sub-basin that developed as an independent structural unit, relatively less subsident than other areas of the BCB for most of the Cretaceous time (Martín-Chivelet et al., 2002; Najarro et al., 2010; Wilmsen, 2005). Palaeogeographically, the NCB was structured in a series of horsts and grabens limited by N–S, E–W and NE–SW trending faults, which controlled sedimentation at least during Barremian–Albian times (Fig. 2) (Najarro et al., 2007, 2009, 2010). From northeast to southwest three fault-bounded structural domains are differentiated: Cuchía, Santillana and La Florida areas respectively (Fig. 2B). The Cuchía and La Florida domains correspond to less-subsiding uplifted areas, whereas the Santillana domain represents a subsident trough between them and the main sedimentary depocentre of the region during the Early Cretaceous (Fig. 2B). This synsedimentary structural arrangement caused a complex basin topography, as indicated by distribution of facies and sedimentary thicknesses, which may reach less than 200 m for the Aptian–Albian in the marginal areas of La Florida and Cuchía, but may exceed 1000 m in the centre of the Santillana sink depression. The two studied sections belong to the

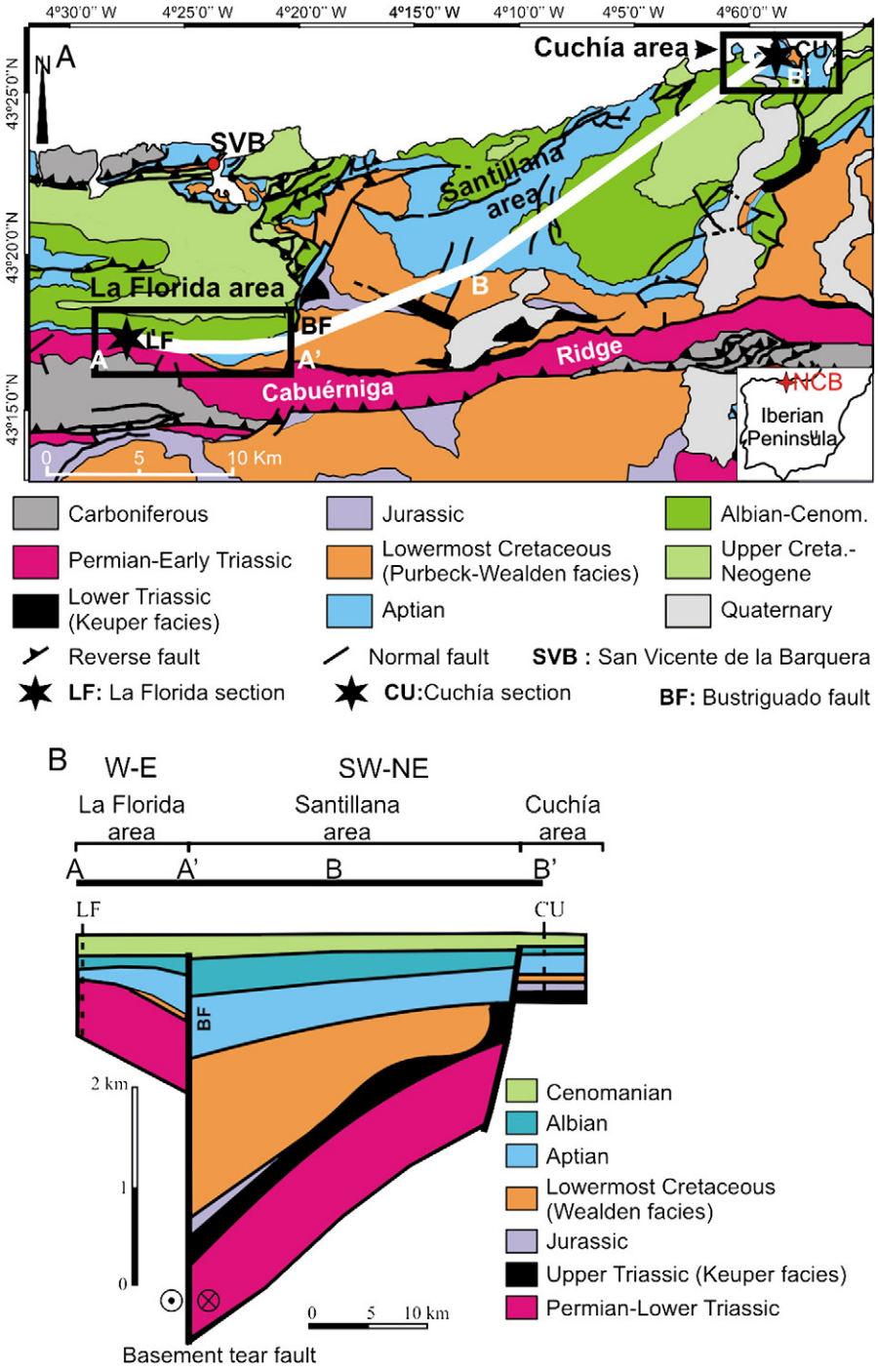

Fig. 2. (A) Geological map of the North Cantabrian Basin (NCB) with the location of the three principal depositional areas (La Florida, Santillana and Cuchía) and the two studied sections of La Florida and Cuchía. White line A–A′–B–B′ shows the location of the stratigraphic cross-section in B. (B) Cross-section showing the restored geometry of the NCB during the Early Cretaceous and the different sedimentary record in the three principal depositional areas.

Cuchía and La Florida domains respectively, and are considered representative of these areas.

3. Material and methodology

3.1. Studied sections and sampling

The two Lower Aptian representative sections have been analysed along superbly exposed continuous outcrops (Fig. 3). The La Florida section is located about 20 km southwest of the village of San Vicente de la Barquera (Fig. 2A). This section is exposed close to the small village of Rábago, alongside the Puentenansa road. The Cuchía section (Figs. 2A, 3) is very well exposed in the coastal cliff of the Playa de los Caballos beach, 3 km NW of the small village of Cuchía. The two sections were logged and sampled at a metric scale, and the sedimentological features and fossil content were documented in detail in the field.

A total of 235 rock samples were collected and processed for different geochemical and micropalaeontological studies. The $\delta^{13}C_{carb}$, $\delta^{13}C_{org}$, carbonate content and total organic carbon content (TOC) were measured on bulk rock samples from limestones and marls drilled from fresh rock samples from the two sections. Previous works have proven the efficacy of bulk rock analysis on this type of rock successions (e.g. Ferreri et al., 1997; Scopelliti et al., 2008; Weissert et al., 1998). Powders were extracted with a micro drill mounted in a stereomicroscope. Potential problems associated with diagenetic resetting have been avoided as much as possible by carefully selecting micro samples of limestones and marls away from crack fillings, secondary products or matrix irregularities. Dolomitized samples were excluded and limestone samples with mudstone to wackestone textures were preferentially chosen. Samples derived from marls were systematically taken every 1–2 m, whereas for the limestones beds the sampling has been limited to those parts of the succession where the diagenetic features were minimal. Minor siliciclastic siltstones and sandstones interbedded in particular parts of the sections have not been analysed.

3.2. Geochemical analyses

Values of wt.% TOC and wt.% $CaCO_3$ contents were determined on 57 marly samples at Servizos de Apoio á Investigación of the University of A Coruña (Spain). Total carbon content of the samples (wt.% TC) was determined using a Carbo Erba elemental analyzer EA1108. For total organic carbon (TOC) determinations, the samples were previously digested in HCl at 80 °C to remove the carbonate material and then measured. The difference between the values of TC and TOC was used to calculate the carbonate carbon content (TIC) and then the calcium carbonate content, assuming that all carbonate is calcite.

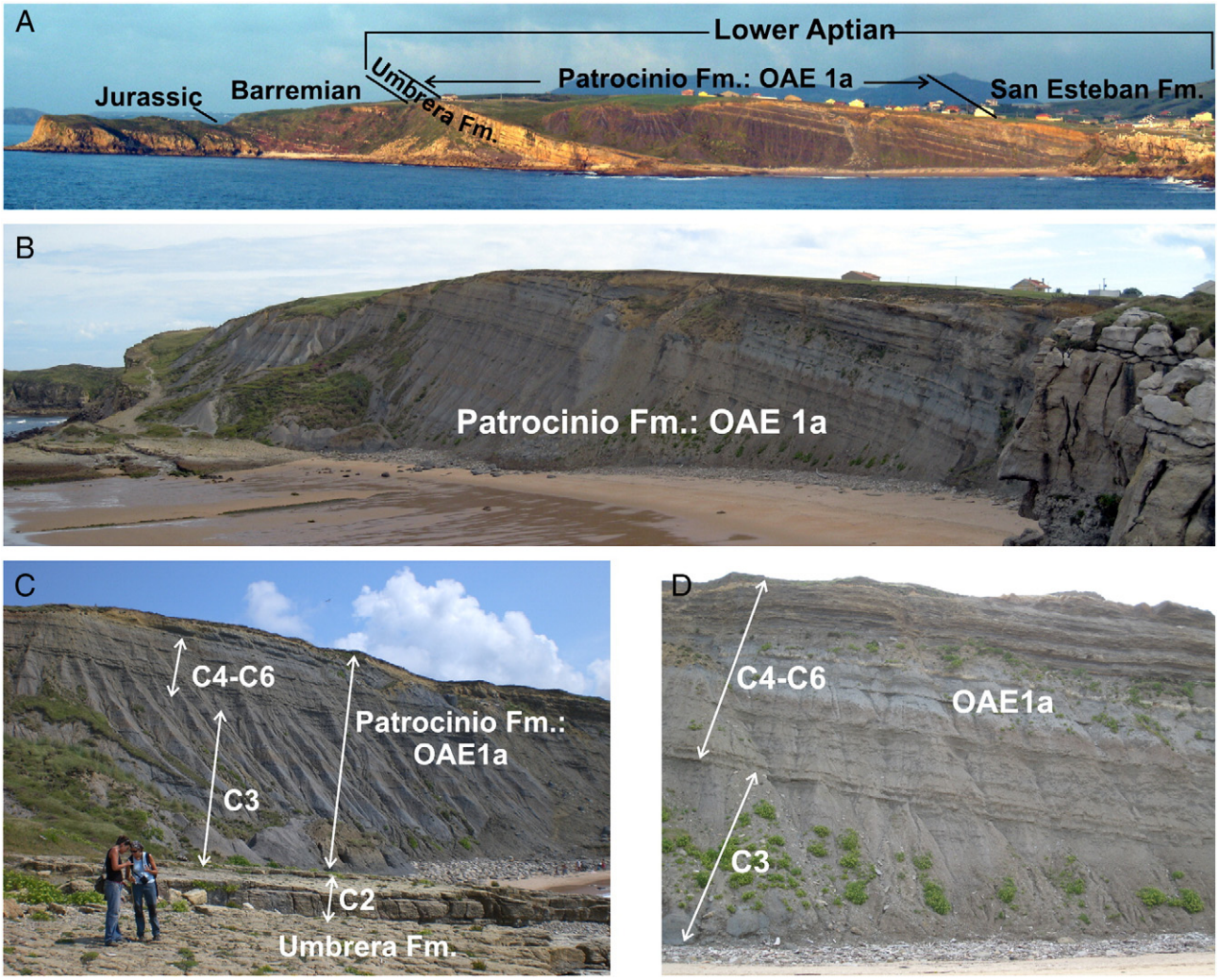

Fig. 3. Field pictures of the Patrocinio Formation. (A) General view of continuous outcrop from Jurassic to Lower Aptian in the Cuchía area. (B) Field picture of the fully exposed Lower Aptian Patrocinio Formation in the coastal cliff of the Playa de Los Caballos beach. (C–D) Field position in the Cuchía outcrop of the Early Aptian $\delta^{13}C$ segments of the chemostratigraphic curve defined by Menegatti et al. (1998).

To analyse the C-isotope composition of the bulk carbonate carbon ($\delta^{13}C_{carb}$), 72 powdered samples were treated with 100% orthophosphoric acid, using the conventional digestion method (McCrea, 1950). The $\delta^{13}C_{carb}$ composition of the evolving CO_2-gas was analysed with a SIRA-II mass spectrometer equipped with an "ISOCARB" automatic system at the University of Salamanca (Spain). The $\delta^{13}C$ composition of the organic matter fraction of the 72 rock samples ($\delta^{13}C_{org}$) was analysed in the Stable Isotope Laboratory of the University of East Anglia (UK). For this determination, all the carbonate material was previously removed from the samples by digesting them several times in a 10% hydrochloric acid solution until there was no evidence of fizzing, which indicates the removal of all inorganic carbon. The samples were then washed several times with de-ionised water to remove the HCl traces. The washed residues were dried in an oven between 50 and 80 °C and then analysed using a Finnigan Delta Plus XP, on-line with a Costech elemental analyser. The results are expressed in the common δ-notation in per mil (‰) relative to VPDB-standard. The international carbonate standard NBS-19 (National Bureau of Standards; $\delta^{13}C = 1.95‰$) and a laboratory internal standard (ISA; $\delta^{13}C = -2.47‰$) were used to calibrate the $\delta^{13}C_{carb}$ values, with an average precision of 0.01‰ ($n = 3$). The pattern used for the $\delta^{13}C_{org}$ composition was a laboratory internal standard, with an average precision of 0.1‰ ($n = 12$).

3.3. Palaeontological analyses

Regarding the study of nannofossils, a total of 55 marly samples from the Cuchía and La Florida sections were prepared and examined. The slides for nannofossil analysis were processed according to standard techniques and were studied under a magnification of 1250× using a light polarized microscope. The biostratigraphic events reported by Applegate and Bergen (1988) and Aguado et al. (1999) were used for the definition of biozones and zonal boundaries.

The planktonic foraminifera assemblages were studied in 40 marly samples only from the Cuchía section, because in the samples of La Florida the planktonic foraminifera were scarce and poorly preserved. The samples were disaggregated and washed through sieves, the residue being separated into three fractions (>200 μm, 100–200 μm, and 50–100 μm). Although the three fractions were studied, the richest planktonic foraminiferal assemblages were found in the 100–200 μm fraction. The planktonic foraminifers were studied using optical and electronic (SEM) observations.

Ammonites are scarce in the study area and appear only at discrete levels but with high occurrence within these levels. All the specimens studied here come from two ammonites-rich levels of the Cuchía section. The specimens were collected during fieldwork surveys, and are now deposited in the collections of the Colleccions de Paleontologia de la Universitat Autònoma in Barcelona (PUAB) and the Museo Geominero (IGME) of Madrid. Additional specimens were also supplied by the Museo Geológico del Seminario of Barcelona (MGSB) and by a particular collection (Manuel Díaz, Cantabria).

Six samples were prepared for palynological studies in the laboratory of ALICONTROL (Madrid, Spain). The rock samples were treated following the standard palynological preparation technique (Batten, 1999), which consists in an acid attack with HCl, HF and HNO_3 at high temperature. The residue was concentrated and sieved throughout sieves of different grid sizes (500, 250, 75, 50 and 12 μm). Then, the samples were mounted in glycerin jelly on glass slides for light microscope. The samples were studied with an Olympus BX51 optical microscopy. Only four samples yielded representative and well-preserved assemblages (i.e. Canales-Patrocinio, Sop-Patrocinio, Ru-Cuchía and Ru-Reocín, with 771, 430, 476, and 391 palynomorphs respectively).

4. Stratigraphy

Previous work on the Lower Aptian succession of the NCB is relatively limited. Earlier stratigraphic and biostratigraphic frameworks had been established by Ramírez del Pozo (1972), Collignon et al. (1979), Hines (1985) and Wilmsen (2005), and have been recently revised and updated by Najarro et al. (2007, 2010). A simplified lithostratigraphy of the two studied areas is provided in Fig. 4.

In the area of La Florida, the Mesozoic sedimentary record starts with a thick (~600 m average) succession of Lower Triassic continental red mudstones, sandstones and conglomerates ("Buntsandstein" facies) resting unconformably on folded (Variscan deformation) Carboniferous basement (Fig. 4). The Upper Triassic, Jurassic and lowermost Cretaceous successions are absent in this sector (Fig. 4), most probably because during the Late Jurassic–Early Cretaceous rifting stage the area was subjected to erosion and non-deposition. In contrast, in the Cuchía area the oldest outcropping deposits correspond to the Upper Triassic (Keuper evaporitic mudstones and dolostones), and are overlain by Lower Jurassic (Hettangian–Pliensbachian) marine carbonates. These deposits are truncated by an angular unconformity and karstification surface that separates tilted marine Jurassic strata from overlying Lower Cretaceous continental red beds. As in the area of La Florida, Upper Jurassic and lowermost Cretaceous deposits are also absent and sedimentation restarted in the Hauterivian–Barremian with deposition of ~100 m of fluvial deposits ("Wealden" or Pas Group; Pujalte, 1982).

Rapid marine transgression occurred in the earliest Aptian, leaving deposits that in both areas unconformably overlie either the continental "Wealden" facies or the pre-Cretaceous substratum. The Aptian lithostratigraphy of the study area is organized into six stratigraphic units, named as follows from oldest to youngest (Fig. 4). 1) Rábago Formation (0–12 m thick; lower Bedoulian, lower *Palorbitolina lenticularis* zone), which is a shallow marine mixed carbonate–siliciclastic unit that represents the initial marine transgression. This unit is absent in the Cuchía area (Fig. 4). 2) Umbrera Formation (lower Bedoulian, *P. lenticularis* zone). This unit (0–52 m thick) consists mostly of cross-bedded skeletal-oolitic grainstones and rudstones, interpreted as shallow platform agitated shoal deposits (Najarro and Rosales, 2008a; Najarro et al., 2010). This unit thickens toward basin depocentres and pinches out toward marginal uplifted areas. 3) Patrocinio Formation (~30–80 m), the focus of this study, is made of open marine marls, marly siltstones and locally sandstones. Previous biostratigraphic data from this marly unit give associations of benthic foraminifera and ammonite fauna indicative of an Early Aptian age (Collignon et al., 1979). 4) San Esteban Formation (0–40 m), is characterized by metre to decimetre bedded, shallow platform rudist and coral limestones with *P. lenticularis* (Blumenbach), *Choffatella decipiens* Schlumberger and *Iraquia simplex* Henson (Pascal, 1985), which indicate a late Early Aptian (upper Bedoulian) age. 5) Rodezas Formation (0–80 m; uppermost Bedoulian–lower Gargasian, according to Collignon et al., 1979) is characterized by marine sandstones, grainstones, marly limestones and marls with large oysters (*Exogyra*) and ammonites. It grades upwards and laterally to the Reocín Formation. 6) Reocín Formation (80–250 m; upper Gargasian–Clansayesian; *Orbitolina* (*Mesorbitolina*) *texana texana* and *Simplorbitolina manasi* benthic foraminiferal zones; Ramírez del Pozo, 1972) is composed of shallow water coral-rudist limestones and grainstones. The San Esteban and Rodezas formations are absent in the less-subsident basin margin of La Florida area located to the west. Thus, in the La Florida section, the Reocín Formation lies directly over the Patrocinio Formation (Fig. 4).

5. Results

5.1. Lithostratigraphic and chemostratigraphic data

5.1.1. La Florida section

In La Florida section, the Patrocinio Formation comprises a 31 m thick succession of fully marine argillaceous marls overlying ~13 m of shallow marine limestones and orbitolinid siltstones of the Rábago and Umbrera formations (Fig. 5). The latter is represented here by less

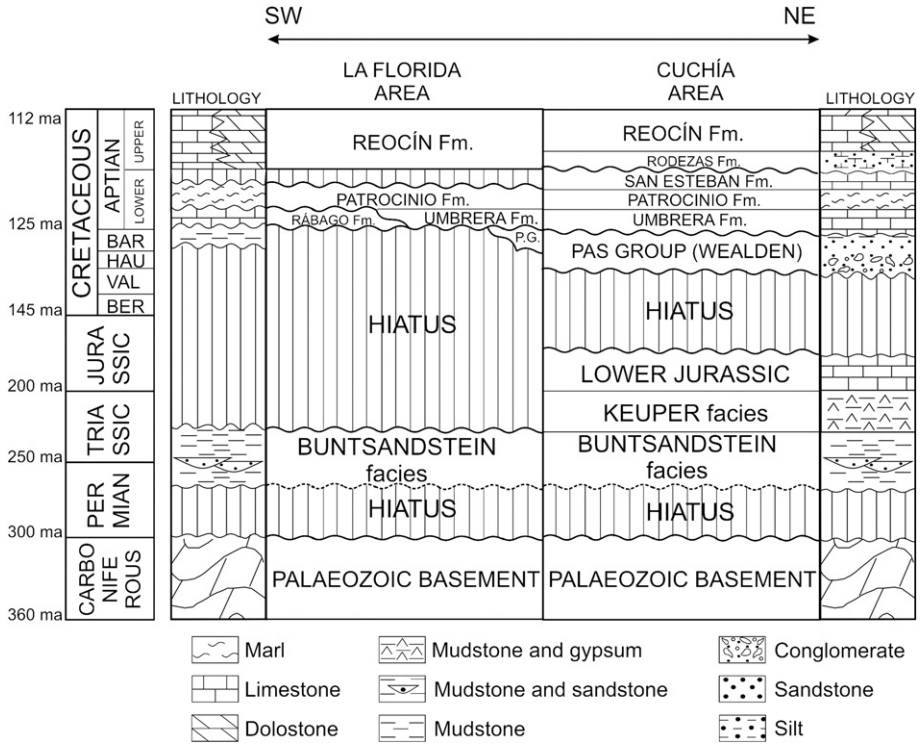

Fig. 4. Lithostratigraphy of La Florida and Cuchía areas. Chronostratigraphy after Gradstein (2004). P.G. = Pas Group.

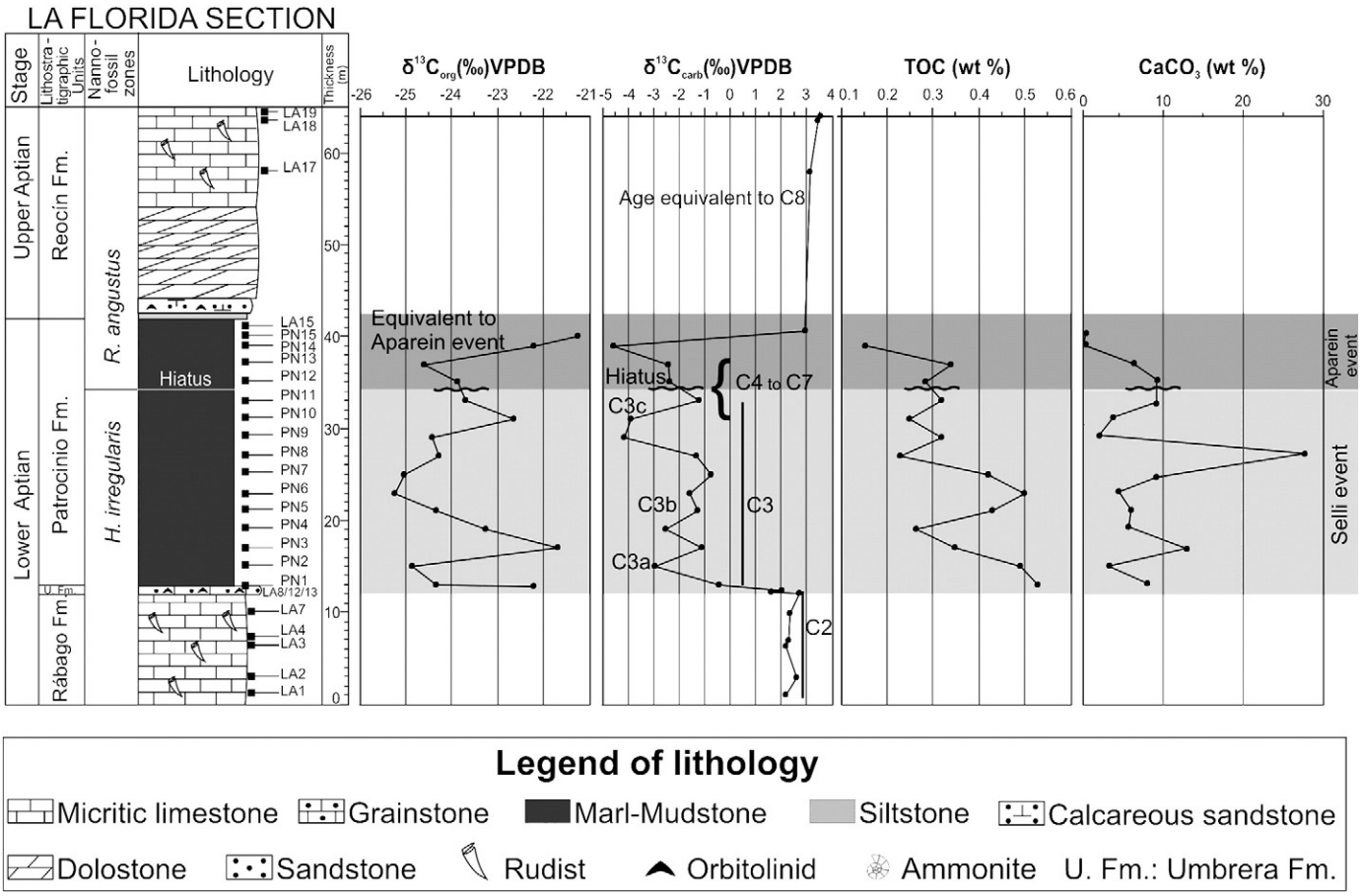

Fig. 5. La Florida section, showing the lithological log, $\delta^{13}C_{carb}$, $\delta^{13}C_{org}$, total organic carbon (TOC) and $CaCO_3$ data. Legend applies for Figs. 6, 7, and 10.

than 1 m of skeletal grainstones that pinch over an unconformity surface marked by dissolution and coated by iron oxides (Najarro and Rosales, 2008a; Najarro et al., 2010). This unconformity separates the Umbrera grainstones from the Rábago unit underneath; thus, a certain stratigraphic gap exists here between the two limestone units. Above, the facies of the Patrocinio Formation corresponds to homogeneous dark marls showing good lamination, pyrite framboids and rare belemnites. At the top of the unit, the content of siliciclastic silt and bioclastic remains increases, and evidence of activity of benthic fauna appears, represented by bioturbation and orbitolinids. This suggests rapid shallowing in the last few metres of the Patrocinio Formation before recovery of shallow water carbonate sedimentation (Reocín Formation).

The total organic carbon content (TOC) of the Patrocinio Formation in this section is relatively low, with values ranging from 0.1 to 0.5 wt.%. The results present three distinctive segments (Fig. 5). The first segment, at the base of the Patrocinio Formation (12–19 m, samples PN-1 to PN-4, Fig. 5), shows maximum TOC values at the bottom that progressively decrease from 0.5 to 0.3 wt.%. The second segment (19–22 m, samples PN-4 to PN-6, Fig. 5) displays a rapid spike to higher values up to 0.5 wt. %. The values decrease again in the third segment located at the upper part of the Patrocinio Formation (22–39 m, samples PN-6 to PN-14, Fig. 5), which exhibits values fluctuating around 0.3 wt.% and finally reaches a minimum of 0.1 wt.% at the top. Calcium carbonate content of these samples fluctuates between 0.1 and 27.6 wt.% (Fig. 5). There is no correlation between TOC and $CaCO_3$ contents, except for the middle part of the marly unit (19–27 m, samples PN-4 to PN-8, Fig. 5), which exhibits a roughly negative correlation of these two values. Thus, in this part of the succession, the highest concentration of calcium carbonate (27.6 wt.%, sample PN-8) correlates with a minimum of TOC, and the opposite. In the uppermost part of the Patrocinio unit, the terrigenous input is important, as shown by a higher proportion of quartz silt and mica. This part of the section is characterized by the lowest $CaCO_3$ values, which stay below 1 wt.%.

Carbon isotope values of the carbonate and organic matter fractions of the samples record significant negative excursions across the Patrocinio Formation in La Florida section. The organic C-isotope values ($\delta^{13}C_{org}$ in Fig. 5) range between −21.2‰ and −25.2‰ and show three prominent negative spikes. From the bottom, the C-isotope curve starts with values of −22.2‰ and decrease sharply to −24.8‰ at 15 m, resulting in a first negative excursion of 2.6‰ in magnitude. This is followed by a return to more positive values (−21.6‰) similar to those observed before the spike. The following $\delta^{13}C_{org}$ values show a gradual decrease towards more negative values, reaching a minimum of −25.2‰ at 23 m (second negative spike of 3.5‰ in magnitude). Then, the values change progressively to more positive values and peak at values of −22.6‰ at 31 m. The negative trend of the $\delta^{13}C_{org}$ is resumed, and at 37 m the curve displays a third negative spike of −24.6‰ (~2‰ in magnitude). Finally, the upper part of the Patrocinio Formation records a rapid rise in the $\delta^{13}C_{org}$ values, showing the highest value (−21.2‰) at the top of the studied segment (Fig. 5).

The $\delta^{13}C_{carb}$ values measured in La Florida section range between −4.5‰ and +3.6‰. In their temporal record, three major segments can be recognized. In the first segment (0–12 m, samples LA-1 to LA-13; Fig. 5), the carbonate carbon isotope curve presents relatively stable positive values of 1.6 to 2.7‰ (mean of +2.2‰). The second segment (12–39 m, samples PN-1 to PN-14; Fig. 5), which correlates with deposition of the Patrocinio Formation, is characterized by a remarkable negative excursion (~6‰ in magnitude) from values of +1.6‰ just beneath the base of the unit to −4.5‰ at its top. This negative shift occurs in three steps, each of which records progressively more negative peak values (−2.9‰, −4.1‰ and −4.5‰ respectively). Finally, a return to $\delta^{13}C_{carb}$ positive values occurs at the top of the section (39–64 m, samples PN-15 to LA-19, Fig. 5), coinciding with the recovery of the carbonate sedimentation and the installation of a shallow carbonate platform. In this segment, the $\delta^{13}C_{carb}$ values vary from +2.5‰ to +3.6‰, which are slightly higher than those obtained from the first segment.

5.1.2. Cuchía section

The Lower Aptian succession exposed at the Playa de los Caballos beach can be subdivided into four parts (Figs. 3, 6): (1) a lower part (~24 m thick) of cross-bedded rudstones and grainstones of the Umbrera Formation. The contact with the continental Wealden facies underneath is sharp and erosional in places, and the Rábago Formation is absent here (Fig. 4). (2) A second part (from 24 to 75 m; Figs. 3B–C, 6), which here corresponds to the lower part of the Patrocinio Formation, is composed mainly of dark clayey marls with red ironstones nodules. Two levels (at 30 and 36 m respectively, Fig. 6) of nodular bioclastic limestones with ammonites and remains of brachiopods, echinoids, bivalves, orbitolinids, the mecochirid decapod *Meyeria magna* M'Coy, as well as wood debris are intercalated. These levels represent the two horizons with ammonites described by Collignon et al. (1979). (3) The third part of the succession corresponds to the upper part of the Patrocinio Formation, and is formed of ~30 m of heterolithic alternations of carbonaceous and mica-rich claystones, siltstones and cross-bedded quartz sandstones, organized in a coarsening- and thickening-upwards sequence (Fig. 3D). This part of the succession represents a local delta progradation at the top of the Patrocinio Formation (Wilmsen, 2005). 4) Above, the shallow platform carbonate sedimentation recovered, and the sedimentary facies change gradually to orbitolinid-rich sands and coral-rudist limestones (San Esteban Formation).

The TOC content of the Patrocinio Formation in the Cuchía section is low (Fig. 6), and although slightly higher than in the La Florida section, all values are below 1 wt.% (i.e. 0.1 to 0.8 wt.%). In general terms, four segments can be roughly differentiated. The first segment at the base of the Patrocinio Formation shows a decrease from 0.5 wt.% to 0.2 wt.%. The second segment (40.5–51.5 m; Fig. 6) displays an increase to TOC values up to 0.5 wt.%. The third segment (51.5–73 m; Fig. 6) exhibits a progressive decrease until reaching a minimum of 0.1 wt.%. Finally, maximum TOC values of 0.8 wt.% are obtained in the last segment at the top. The calcium carbonate content of the samples ranges between 0.8 and 47.5 wt.% (Fig. 6) and shows no correlation with the TOC content. The lower values are obtained in the upper part of the Patrocinio Formation, coinciding with the lithological change to siliciclastic deposits.

The carbon isotope composition of the bulk organic matter measured across the Patrocinio Formation in the Cuchía section varies from −21.3‰ to −26.1‰ (Fig. 6). In the lower part, the isotopic signal shows a significant negative shift in $\delta^{13}C_{org}$ of ~5‰ (26.5 m of the section), from values that fluctuate between −22.8‰ and −20.7‰ to values of −26.1‰. Values remain predominantly low (below −24‰) between 26.5 and 45 m (Fig. 6), with the exception of one sample at the base. Next, there is an increase in the $\delta^{13}C_{org}$ signal up to values of −21.4‰ at 48.5 m. The succeeding portion of the carbon isotope curve is defined by a gradual decrease of the $\delta^{13}C_{org}$ signature that peaks at values of −25.6‰ at 54 m, recording a second negative excursion of 4‰ in magnitude. This is followed by an increase toward values of ~−22.3‰ with small-scale fluctuations. The $\delta^{13}C_{org}$ values fall again to relatively constant values of ~−25.4‰ between 66–73 m (Fig. 6), which represent a third negative excursion of ~3‰. Finally, in the upper part of the section the $\delta^{13}C_{org}$ values show an increase to values of ~−22.8‰ coinciding with the more siliciclastic upper part of the Patrocinio Formation.

The carbonate carbon isotope composition measured in the Cuchía section varies significantly from +4.1‰ to −3.6‰, recording a prominent negative excursion during deposition of the marly lower part of the Patrocinio Formation (Fig. 6). The structure of the $\delta^{13}C_{carb}$ curve reproduces the three segments observed in La Florida section, but with some differences. The first of these, at the base of the section, starts with positive values but with a clear decreasing trend upwards

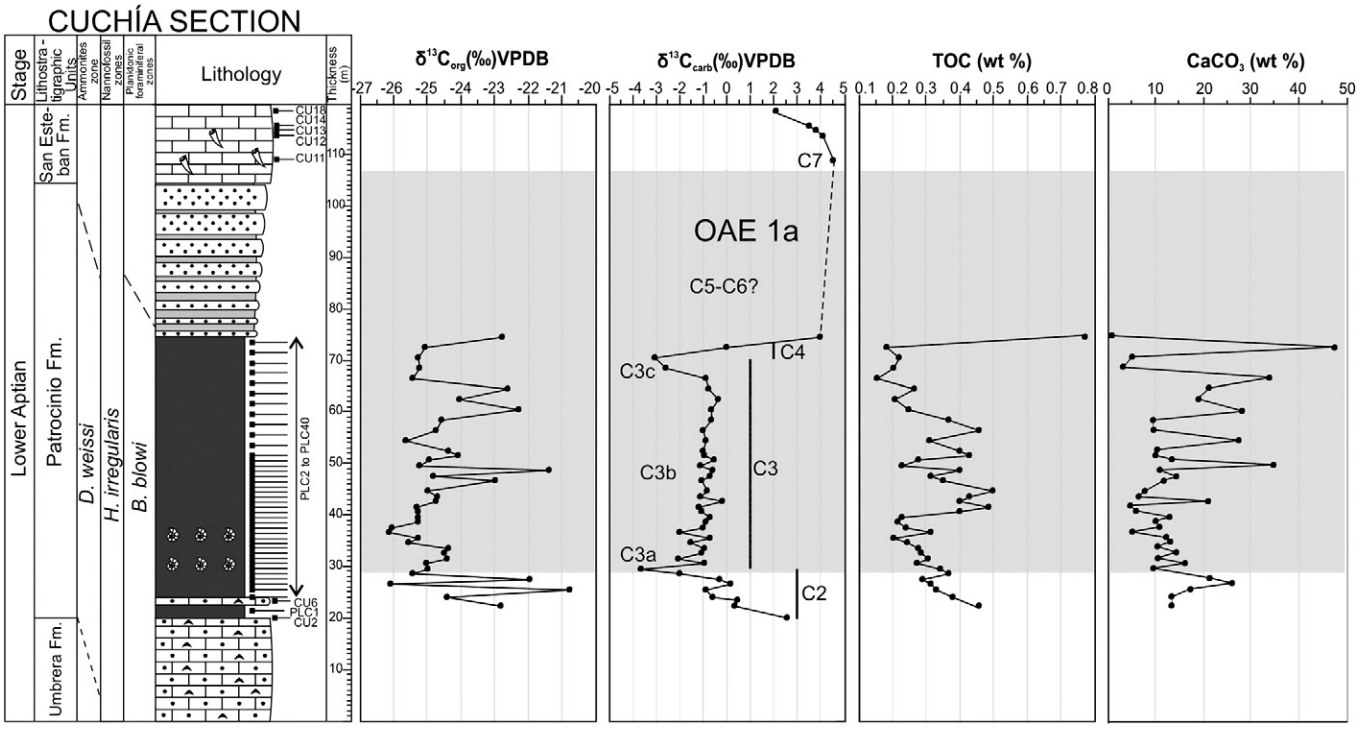

Fig. 6. Cuchía section, showing the lithological log, $\delta^{13}C_{carb}$, $\delta^{13}C_{org}$, total organic carbon (TOC) and $CaCO_3$ data. See Fig. 5 for lithological legend.

from +2.5‰ in the Umbrera Formation to −2.0‰ at the base of Patrocinio Formation. The second segment coincides with the marly lower part of the Patrocinio Formation, and records a notable negative excursion. The high-resolution quality of this segment of the curve allows recognition of two negative peaks within the overall negative excursion (Fig. 6). The first, at 29.5 m, reaches a minimum $\delta^{13}C_{carb}$ value of −3.6‰, implying a negative excursion of 3‰ in magnitude. The second peak ($\delta^{13}C_{carb}$ = −3.1‰) appears at 70.5 m and shows a negative excursion of ~2‰. Between these two peaks (30.5–69.5 m), the carbonate carbon isotope composition is relatively constant with a mean value of −1‰ (Fig. 6). Finally, the third segment of the isotope curve is recorded across the limestone of the San Esteban Formation. This segment is characterized by a stepwise increase of $\delta^{13}C_{carb}$ to values as high as +4.5‰, with a mean of +3‰.

5.2. Biostratigraphic data

To evaluate the impact of the OAE 1a event in the studied series and to correlate its geochemical record with coeval records in other regions, the age of the event must be adequately calibrated using biostratigraphic data. Ammonites may offer one of the highest-resolution biostratigraphic frameworks for the position of the OAE 1a (e.g. García-Mondéjar et al., 2009; Moreno-Bedmar et al., 2009), although they are usually scarce. For this last reason, in recent years the biostratigraphic schemes of the OAE 1a have been essentially based upon planktonic foraminifera and calcareous nannofossils (e.g. Aguado et al., 1999; Ando et al., 2008; Bralower et al., 1994; Erba et al., 1999; Gea et al., 2003; Luciani et al., 2001). In this study, the biostratigraphic position of the Patrocinio Formation was constrained using four different fossil groups: ammonites, calcareous nannofossils, planktonic foraminifera and palynomorphs.

5.2.1. Ammonites

Only the Cuchía section has yielded ammonite fauna. Ammonoids from this section were previously studied by Collignon et al. (1979), who identified two horizons within their "Formation terrigène à Ammonites" (corresponding to the Patrocinio Formation). On the basis of their determinations, Collignon et al. (1979) attributed their lower horizon to the *Prodeshayesites fissicostatus* and *Deshayesites forbesi* Zones, and the upper one to the *Deshayesites deshayesi* and *Tropaeum bowerbanki* Zones of the zonal scheme proposed by Casey (1961). Therefore, according to Collignon et al. (1979), all the Lower Aptian ammonite zones would be represented within these two horizons. This stratigraphic interpretation was recently accepted as valid by Wilmsen (2005).

In this study, it has also been possible to recognize the two horizons identified by Collignon et al. (1979) at the lower part of the Patrocinio Formation, but the biostratigraphic attributions reported here are rather different (Fig. 7). The new ammonite assemblages yielded by this study from the two ammonite-rich levels are represented in Figs. 7 and 8. The lower level has yielded *Deshayesites* cf. *forbesi* Casey, *Deshayesites* cf. *callidiscus* Casey, *Roloboceras* cf. *hambrovi* (Forbes), *Pseudohaploceras liptoviense* (Zeuschner), *Pseudosaynella undulata* (Sarasin), and *Toxoceratoides* sp. ind. The upper horizon has provided *Deshayesites* cf. *consobrinus* (d'Orbigny), *Deshayesites planus* Casey, *D.* cf. *forbesi* Casey *R. hambrovi* (Forbes), *Roloboceras* sp. ind., *Pseudosaynella bicurvata* (Michelin), *Toxoceratoides* sp. ind., and the nautiloid *Heminautilus saxbii* (Morris). The specimens from the Cuchía section deposited in the collections of the Museo Geológico del Seminario in Barcelona (MGSB) and the Museo Geominero (IGME) in Madrid, and in a particular collection, have been identified as *Deshayesites* sp. *callidiscus* Casey, *D.* cf. *forbesi* Casey, *D. planus* Casey, *R. hambrovi* (Forbes), *Roloboceras* sp. ind., *P. undulata* (Sarasin), and *Toxoceratoides royerianus* (d'Orbigny). All these assemblages can be attributable to the *Deshayesites weissi* Zone of the standard Mediterranean Zonation (Reboulet et al., 2009). In fact, all the mentioned deshayesitid species are characteristic of this biozone, equivalent to the *D. forbesi* Zone of Casey (1961). Furthermore, the occurrence of *Roloboceras* in both horizons suggests that the entire segment of the section correlates with the middle/upper part of the *D. weissi* Zone (Casey, 1961; Casey et al., 1998; Moreno-Bedmar et al., 2009). The striking differences with the conclusions of Collignon et al. (1979) can only be explained by divergences in the taxonomic interpretation of ammonites.

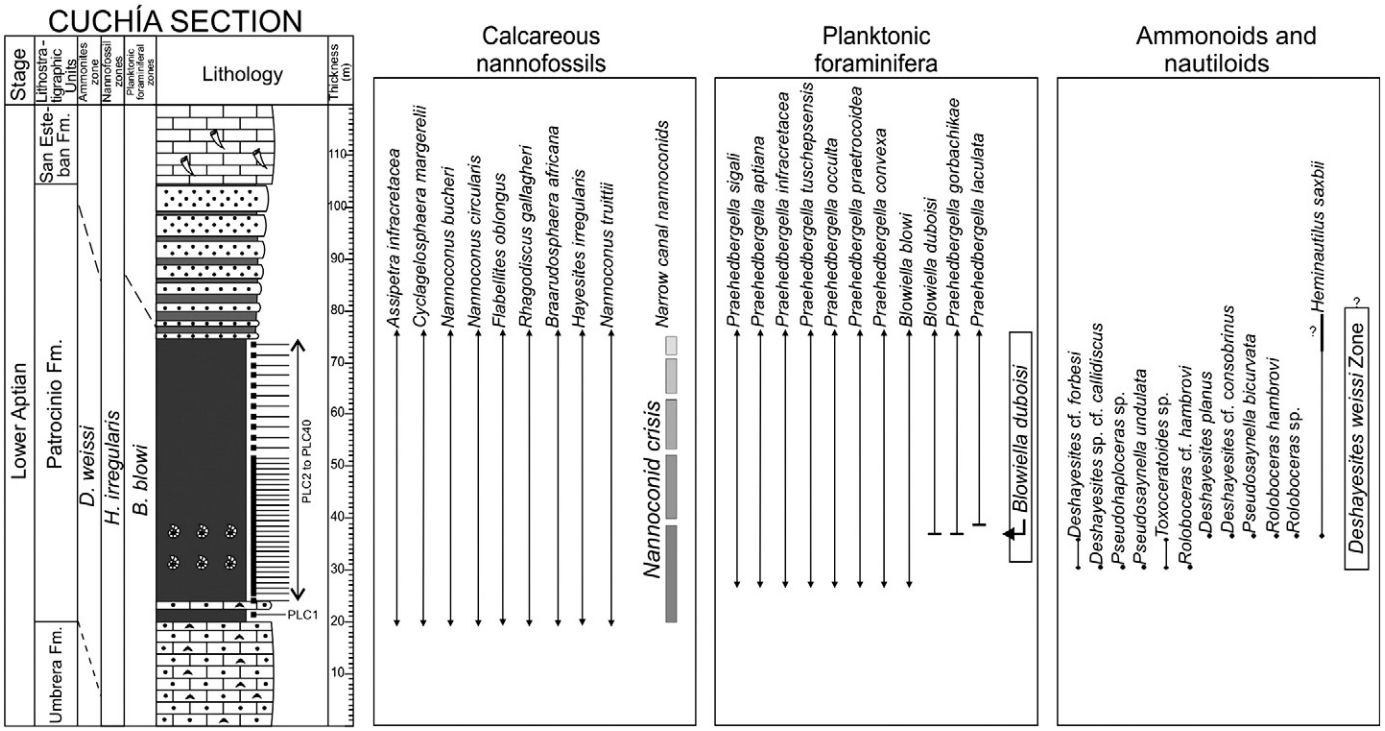

Fig. 7. Cuchía section, showing calcareous nannofossils, placktonic foraminifera and ammonites biostratigraphy. See Fig. 5 for lithological legend.

5.2.2. Calcareous nannofossils

Nannofossils are not very abundant in the samples and present a moderate preservation and a scarce diversity. The assemblages (Figs. 7, 9 and 10), of marked Tethyan character, are dominated by the genera *Watznaueria*, *Rhagodiscus* and *Nannoconus*. Abundant species include *Assipetra terebrodentaria*, *Hayesites irregularis*, *Zeugrhabdotus noeliae*, *Lithraphidites carniolensis*, *Biscutum ellipticum*, *Discorhabdus ignotus*, *Diazomatolithus lehmanii* and *Micrantholithus obtusus*. Other characteristic but less abundant forms include *Cyclagelosphaera margerelii*, *Braarudosphaera africana*, *Flabellites oblongus*, *Assipetra infracretacea* and *Helenea chiastia*. As can be seen in Figs. 7, 9 and 10, most of the samples of the Patrocinio Formation in the two studied sections contain the association *H. irregularis*, *Nannoconus truittii*, *B. africana* and *Conusphaera rothii* typical of the middle/upper part of the *H. irregularis* nannofossil Zone, according to the zonation of Applegate and Bergen (1988) and Aguado (1994). This assemblage is correlated with the *Deshayesites weissi* ammonite Zone (Aguado et al., 1999). The quantitative analysis of the nannofossil abundance has revealed a widespread absence of narrow canal nannoconids (i.e., *Nannoconus steinmannii*), which can be identified with the "nannoconid crisis" inferred for the same time interval by Erba (1994). The "nannoconid crisis" is recorded in the upper half of the *H. irregularis* Zone (Aguado et al., 1999; Erba, 1994), and may be correlated with the middle/upper part of the *D. weissi* ammonite Zone.

These observations allow to conclude that, in the Cuchía section, the dark clayey marls of the lower part of the Patrocinio Formation (samples PCL-1 to PCL-40 in Fig. 7, and C3 segment in Fig. 3C) belong to the upper half of the *Hayesites irregularis* nannofossil Zone, being equivalent to the middle/upper part of the *Deshayesites weissi* ammonite Zone of the Lower Aptian. In La Florida section (Fig. 10), most of the Patrocinio Formation (up to sample PN-12) belongs also to the upper half of the *H. irregularis* nannofossil Zone. The first occurrence (FO) of *Eprolithus floralis* is registered from sample PN-12 onwards (Fig. 10). This biostratigraphic event enables the assignment of the uppermost part of the Patrocinio Formation in this section to the *Rhagodiscus angustus* nannofossil Zone (defined as the interval between the FO of *E. floralis* and the FO of *Praediscosphaera columnata*). According to Aguado et al. (1999) the base of the *R. angustus* nannofossil Zone falls within the upper part of the *Dufrenoyia furcata* ammonite Zone and is dated as latest Early Aptian. Therefore, in the La Florida section there exists a stratigraphic gap affecting at least the upper part of the Lower Aptian. This would comprise the uppermost part of the *D. weissi*, the whole *Deshayesites deshayesi* and the lower part of the *D. furcata* Zones of ammonites.

5.2.3. Planktonic foraminifera

Although in general planktonic foraminifera are scarce in the samples of the Cuchía section, only the lowermost part of the Patrocinio Formation has not yielded planktonic foraminifera (from samples PLC-1 to PLC-3, Fig. 7). The planktonic foraminiferal assemblages are characterized by forms with smooth microperforate wall having four or five rounded chambers (Fig. 11). The samples are characterized by forms assigned to the genera *Praehedbergella* (*Praehedbergella sigali*, 6–11 in Fig. 11; *Praehedbergella aptiana*, 20–23 in Fig. 11; *Praehedbergella infracretacea*, 14–19 in Fig. 11; *Praehedbergella occulta*, 3–4 in Fig. 11; *Praehedbergella convexa*, 5 in Fig. 11; *Praehedbergella praetrocoidea*, 1–2 in Fig. 11; *Praehedbergella gorbachikae*, 24–25 in Fig. 11; *Praehedbergella tuschepsensis*, 12–13 in Fig. 11; *Praehedbergella laculata*) and *Blowiella* (*Blowiella blowi*, 26–28 in Fig. 11; *Blowiella duboisi*, 29–31 in Fig. 11, *Blowiella maridalensis*). No typical forms of *Schackoina* (*Schackoina cabri*) were found in the studied samples of this section. The first occurrence (FO) of *B. duboisi* and *P. gorbachikae* was found in sample PLC-14 (Fig. 7). These bioevents have been shown to happen in the upper part of the *B. blowi* Zone, and precede the first occurrence of *S. cabri* at the lower part of the main anoxic event in south Spain (Aguado et al., 1999; Gea et al., 2003). According to these data (Fig. 7), the studied part of the section (at least up to sample PLC-40) is assigned to the upper part of the *B. blowi* planktonic foraminiferal Zone (Moullade, 1974; Moullade et al., 2002). In this section, this biozone is correlated with the upper half of the *Hayesites irregularis* nannofossil Zone and the middle/upper part of the *D. weissi* ammonite Zone.

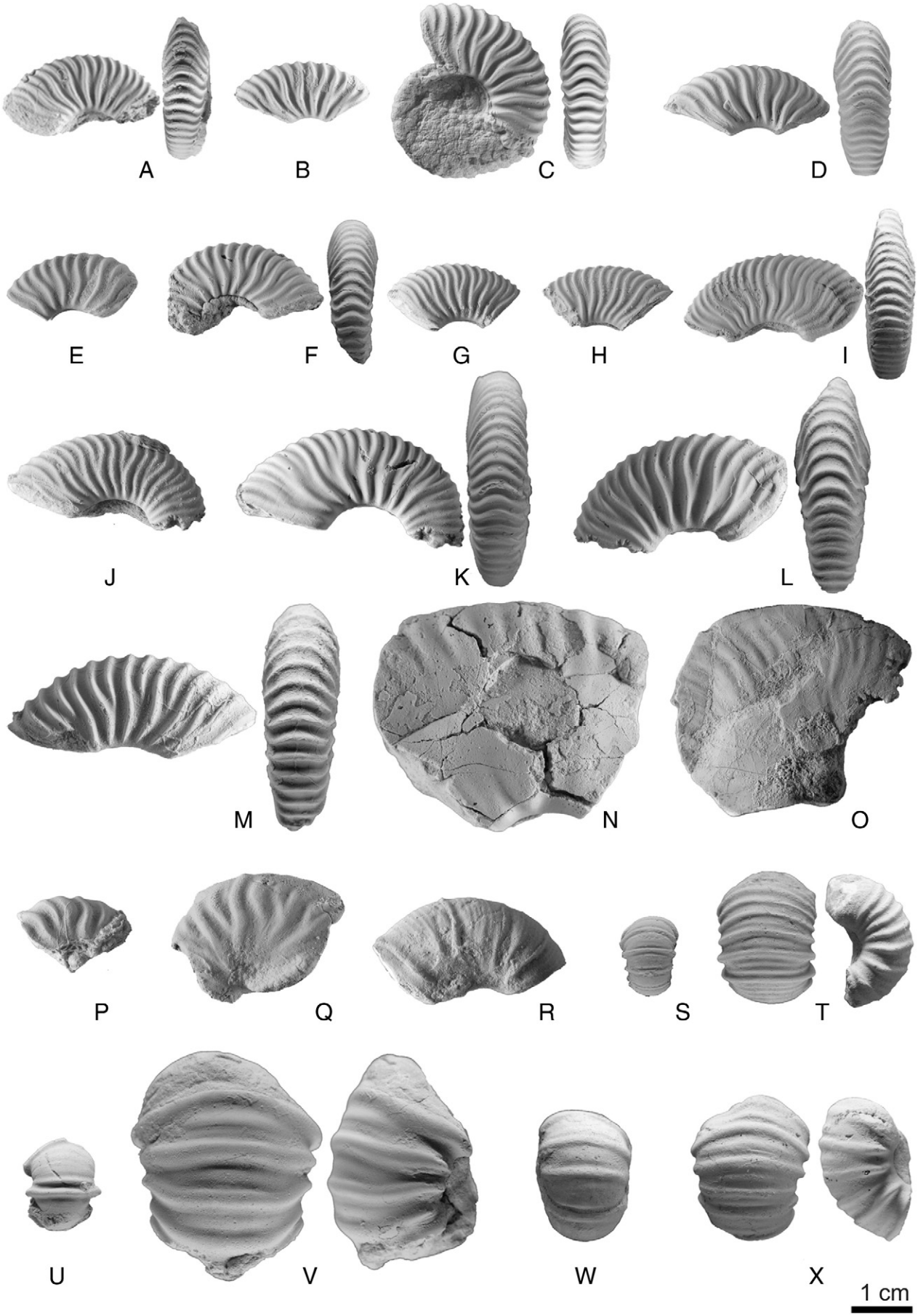
A
B
C
D
E
F
G
H
I
J
K
L
M
N
O
P
Q
R
S
T
U
V
W
X
1 cm

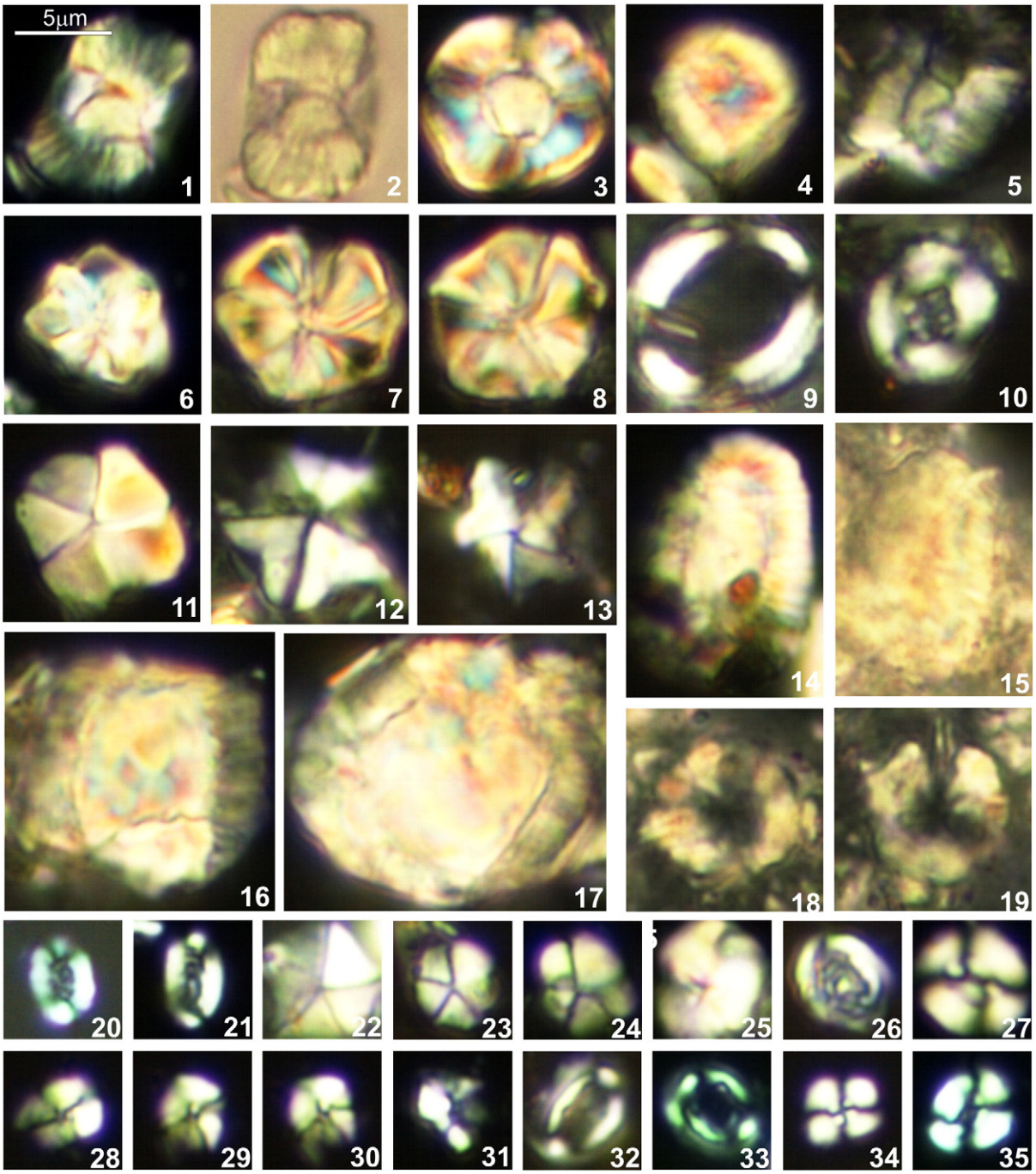

Fig. 9. Calcareous nannofossils. 1–5, *Nannoconus truittii* (picture 2 to parallels nicols). 6–8, *Assipetra terebrodentaria* (large specimens). 9, *Manivitella pemmatoidea*. 10, *Helenea chiastia*. 11, *Braarudosphaera africana*.12, *Micrantholithus obtusus*. 13, *Micrantholithus stellatus*. 14, *Nannoconus kamptneri*. 15, *Nannoconus steinmannii*. 16, *Nannoconus bucheri*. 17, *Nannoconus circularis*. 18, 19, *Eprolithus floralis*. 20, 21, *Rhagodicus gallagheri*. 22, *Micrantholithus hoschulzii*. 23, 24, *Braarudosphaera africana*. 25, *Assipetra infracretacea*. 26, *Rhagodiscus asper*. 27, *Watznaueria barnesae*. 28–31, *Hayesites irregularis*. 32, 33, *Flabellites oblongus*. 34, *Cyclagelosphaera margerelii*. 35, *Watznaueria britanica*. All Figures c. ×3000. Scale bar for all pictures = 5 µm.

Fig. 8. Ammonites. A: *Deshayesites* cf. *forbesi*, lateral and ventral view of the specimen MGSB (Museo Geológico del Seminario de Barcelona) 18730-3. B: *Deshayesites* cf. *forbesi*, lateral view of the specimen MGSB 1870-2. C: *Deshayesites* cf. *forbesi*, lateral and ventral view of the specimen MGSB 18730-1. D: *Deshayesites* cf. *forbesi*, lateral and ventral view of the specimen PUAB (Colleccions de Paleontologia de la Universitat Autònoma de Barcelona) 68536, horizon 1. E: *Deshayesites* cf. *forbesi* lateral view of the specimen PUAB 68533, horizon 1. F: *Deshayesites* cf. *forbesi*, lateral and ventral view of the specimen PUAB 68545, horizon 1. G: *Deshayesites planus*, lateral view of the specimen PUAB 68554, horizon 2. H: *Deshayesites planus*, ventral view of the specimen PUAB 68555, horizon 2. I: *Deshayesites planus*, lateral and ventral view of the specimen PUAB 68557, horizon 2. J: *Deshayesites planus*, lateral view of the specimen PUAB 68559, horizon 2. K: *Deshayesites* cf. *forbesi*, lateral and ventral view of the specimen PUAB 68562, horizon 2. L: *Deshayesites* cf. *consobrinus*, lateral and ventral view of the specimen PUAB 68561, horizon 2. M: *Deshayesites* cf. *consobrinus*, lateral and ventral view of the specimen PUAB 68563, horizon 2. N: *Deshayesites* sp. cf. *callidiscus*, lateral view of the specimen MGSB 18730-4.O: *Pseudosaynella bicurvata*, lateral view of the specimen PUAB 68564, horizon 2. P: *Pseudosaynella undulata*, lateral view of the specimen PUAB 68538, horizon 1. Q: *Pseudosaynella undulata*, lateral view of the specimen MGSB 18730-5. R: *Pseudohaploceras liptoviense*, lateral view of the specimen PUAB 68534, horizon 1. S: *Roloboceras* sp., ventral view of the specimen PUAB 68542, horizon 1. T: *Roloboceras* sp., microconch, lateral and ventral view of the specimen PUAB 68552, horizon 2. U: *Roloboceras* sp., ventral view of the specimen PUAB 68532, horizon 1. V: *Roloboceras* sp., macroconch, lateral and ventral view of the specimen MGSB 78706. W: *Roloboceras* sp., microconch, ventral view of the specimen MGM (Museo Geominero, IGME) 10807C. X: *Roloboceras hambrovi*, macroconch, lateral and ventral view of the specimen MGM 10809C. Scale bar=1 cm.

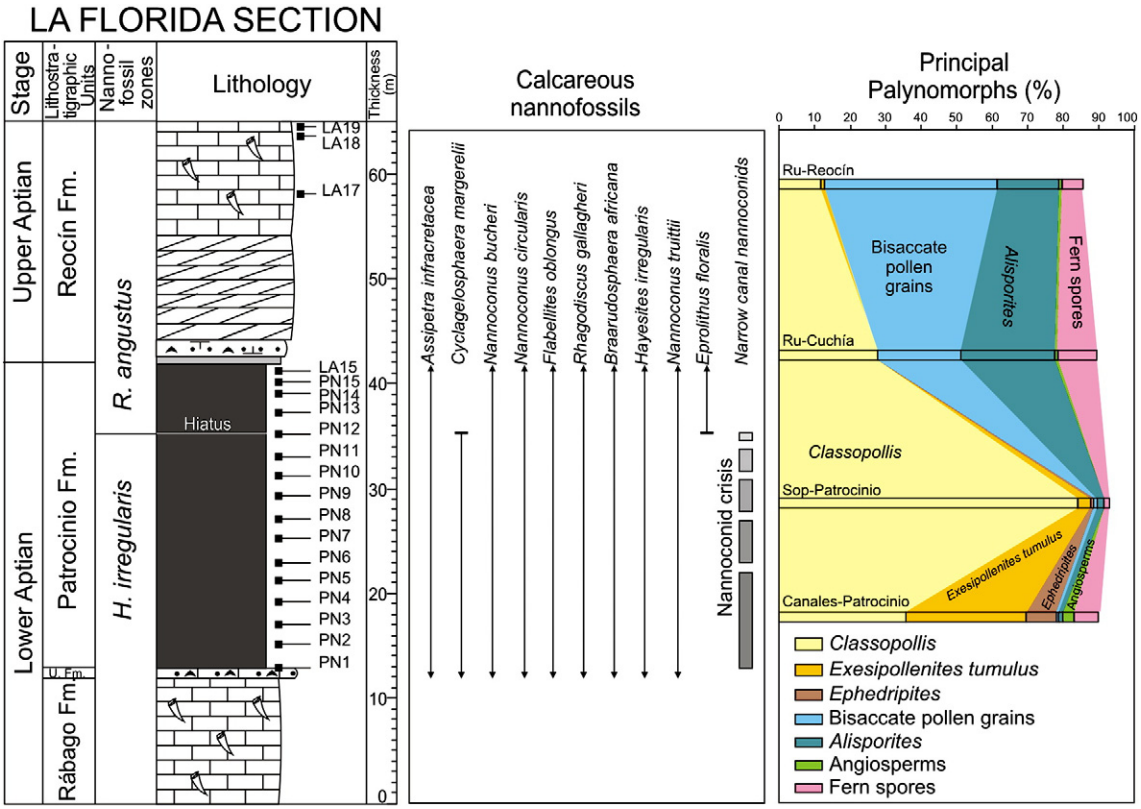

Fig. 10. La Florida section, showing calcareous nannofossil biostratigraphy and the principal palynomorphs content. See Fig. 5 for lithological legend.

5.3. Palynomorphs

An exploratory palynological study has been carried out in order to compare patterns of distribution of terrestrial floras during the onset of the OAE 1a (samples Canales-Patrocinio and Sop-Patrocinio, from marls of the Lower Aptian Patrocinio Formation, Table 1) and after the OAE 1a (samples Ru-Cuchía and Ru-Reocín from marls and carbonaceous shales of Upper Aptian formations, Table 1). In addition, the palynological analysis yielded some useful age information that can be used in combination with the other biostratigraphic data.

A total of 24 spores and 34 pollen types, and some poorly preserved dinoflagellate cysts were found (Fig. 12 and Table 1). Due to their predominance, pollen grains of gymnosperms characterized the assemblages of the four samples. The majority of the palynomorphs in the two Lower Aptian samples from the Patrocinio Formation are constituted by *Classopollis* (Fig. 12E).

In the Canales-Patrocinio sample both *Classopollis* (36.4%) and *Exesipollenites tumulus* (33.9%) numerically dominate. The genus *Classopollis* was produced by conifers of the extinct family Cheirolepidiaceae (Taylor and Alvin, 1984; Watson, 1988), while *E. tumulus* could be produced by plants of the order Bennettitales (Balme, 1995). The Canales-Patrocinio sample is also characterized by relatively high percentages of polyplicate pollen of the genus *Ephedripites* (8.6%) (Fig. 12F). This genus is related to the order Ephedrales (Azéma and Boltenhagen, 1974) and is considered as an influence of the Northern Gondwana floral province (Heimhofer et al., 2004). The calculated percentages of these latter pollen grains are unusually high for the Early Cretaceous of the Iberian Peninsula (Trincão, 1990), although they occur with similar values in the upper Barremian Calizas de Artoles Formation in the Eastern Iberian Ranges of NE Spain (Solé de Porta and Salas, 1994). In the Sop-Patrocinio sample *Classopollis* is the predominant pollen (84.9%), followed by scarce percentages of *E. tumulus* (4.4%). Fern spores in the samples of the Patrocinio Formation exhibit low percentages (1.6% and 6.9% respectively), being essentially represented by both the schizaeaceous *Cicatricosisporites* spp. and the cyatheaceous *Deltoidospora australis* (Fig. 12B).

The Late Aptian assemblages, represented by the samples Ru-Cuchía and Ru-Reocín, are distinguished from the Early Aptian assemblages by a decrease in *Classopollis* (28.5% and 12.1% respectively), the near disappearance of *Exesipollenites* (1% or absent), and a remarkable increase of poorly preserved bisaccate pollen grains related to conifers (54% and 67.6% respectively). In addition, a conspicuous percentage of *Alisporites* (27% and 17.8% respectively) has been recorded (Fig. 12G). This pollen is related to seed ferns of the order Peltaspermales (Balme, 1995). Also evident is the appearance of the species *Inaperturopollenites dubius* (up to 6.5%), which corresponds with inaperturate and psilate pollen grains related to the coniferous Cupressaceae family (Peyrot et al., 2007a). The occurrence of some scarce dinoflagellate cysts (*Tenua histrix* Eisenak emend Sarjeant, *Pseudoceratium polymorphum* (Eisenak) Bint and *Spiniferites* sp. in the sample Ru-Reocín, and *Callaiosphaeridium asymmetricum* (Deflandre and Courteville) Davey and Williams, *Hystrichosphaerina schindewolfii* Alberti and aff. *Criboperidinium* sp. in the sample Ru-Cuchía; Fig. 12H) as well as organic test of foraminifera indicates a clear marine influence at these levels.

Pollen grains of ancient angiosperms are very scarce in all the samples (maximum 2.6%). The presence of seven taxa, however, indicates that these plants had a relative importance in the plant communities of the region. The occurrence of a single grain of *Tricolpites* in one of the samples of the Patrocinio Formation (Fig. 12C) is remarkable because it is the oldest record of tricolpate pollen grains on the Iberian Peninsula. The encountered pollen grain morphologically resembles Albian specimens of the species *Tricolpites parvus* Stanley from Northwestern Alberta, Canada (Singh, 1971; pp. 187–188, pl. 32, Figs. 12–17). Although the first occurrence of tricolpate pollen grains in Europe is reported in mid-Barremian strata from the Isle of Wight (Hughes and McDougall, 1990), until now the oldest presence known in the Iberian Peninsula was found in upper Aptian–Albian deposits from the Basque Cantabrian Basin (Álava province) and Oliete sub-basin

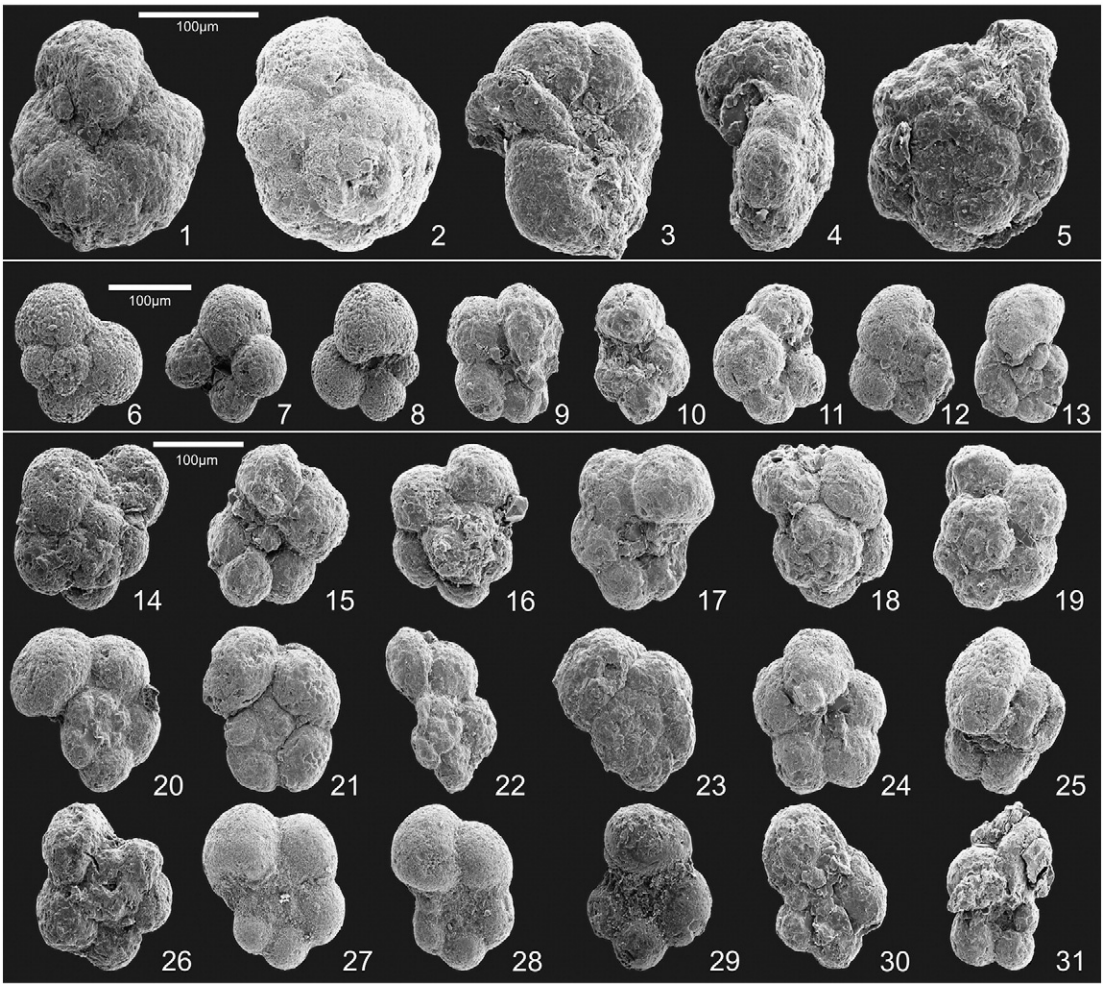

Fig. 11. Planktonic foraminifera. 1,2, *Praehedbergella praetrocoidea*. 3,4, *Praehedbergella oculta*. 5, *Praehedbergella convexa*. 6–11, *Praehedbergella sigali*. 12,13, *Praehedbergella tuschepsensis*. 14–19. *Praehedbergella infracretacea*. 20–23, *Praehedbergella aptiana*. 24,25, *Praehedbergella gorbachikae*. 26–28, *Blowiella blowi*. 29–31, *Blowiella duboisi*. Figs. 1–5 c ×300. Figs. 6–13 c ×500. Figs. 14-31 c ×400.

(Teruel province) in Spain (Barrón et al., 2001; Peyrot et al., 2007a,b), and in lower Albian rocks from the Lusitanian and Algarve basins in Portugal (Heimhofer et al., 2007). Therefore, although the identified palynomorphs represent long stratigraphic ranges across the Early Cretaceous, the presence of *Tricolpites* sp. and the dinoflagellate cysts *Pseudoceratium polymorphum* indicates, however, an age not older than the mid-Barremian (Hughes and McDougall, 1990; Stover et al., 1996).

6. Discussion

6.1. Time-equivalent facies of the OAE 1a and comparison of $\delta^{13}C$ with other sections

The C-isotope curve of the Early Aptian is one of the best known of the Cretaceous. Menegatti et al. (1998) subdivided this part of the C-isotope record from the Cismon section (northern Italy) in a series of segments that they labelled C2 to C7, which have been accepted to be globally reproducible (e.g. Ando et al., 2008; Bellanca et al., 2002; Erba et al., 1999; Herrle et al., 2004; Moullade et al., 1998; Tejada et al., 2009). Recently, Herrle et al. (2004) reported a detailed carbon isotope stratigraphy of the Aptian for the Vocontian Basin (SE France) and have documented a series of segments for the Early Aptian (Ap1–Ap7) that are almost identical to those of Menegatti et al. (1998), allowing confirmation of the stratigraphic reproducibility of the structure of the curve. The curve is basically characterized by positive $\delta^{13}C$ values (around 2.5‰) at the base of the Early Aptian (C2 of Menegatti et al., 1998) followed by an abrupt and pronounced negative excursion (up to −4‰), labelled as C3, which coincides with the base of the OAE 1a. A stepwise return to positive values follows across the black-shale levels that represent the OAE 1a (Selli level in Italy or Niveau Goguel in France). This part of the isotopic curve, which corresponds to the segments C4–C5–C6, precedes the acme of the $\delta^{13}C$ positive excursion (up to 4.5‰) that occurred after the OAE 1a in the *S. cabri* foraminiferal Zone (C7 of Menegatti et al., 1998). According to the mentioned authors, the segment C1 is Barremian in age whereas segment C8 lies in the Upper Aptian (*G. ferreolensis* and *G. algerianus* foraminiferal Zones; *Rhagodiscus angustus* nannofossil Zone). Only the C2 to C7 segments of the carbon isotope curve of Menegatti et al. (1998) are Early Aptian in age, and only the C3 to C6 segments are time-equivalent to the OAE 1a, independently of organic facies development. These segments represent, therefore, a definition of the OAE 1a based on C-isotope stratigraphy, and their identification helps to correlate this event in other basins lacking organic facies with a higher temporal stratigraphic resolution than that provided by biostratigraphy. The regional value of these isotopic stages has been already verified in other localities of the Spanish basins (Gea et al., 2003; Millán et al., 2009; Moreno-Bedmar et al., 2009).

Correlation of the reference curve with the isotopic record obtained from the two sections reported herein, in combination with the integrated litho- and biostratigraphic data, allows recognition of the position of these segments, or their absence, in the Aptian succession of the North Cantabrian Basin. The initial segment of

Table 1
Diagram of palynomorphs identified in the Aptian of the North Cantabrian Basin.

Palynomorphs	Canales-Patrocinio		Sop-Patrocinio		Ru-Cuchla		Ru-Reocin	
	(%)		(%)		(%)		(%)	
Spores of pteridophytes								
Appendicisporites spp.	0	0.0	0	0.0	2	0.4	0	0.0
Cicatricosisporites venustus Deák 1963	0	0.0	0	0.0	0	0.0	1	0.3
Cicatricosisporites spp.	20	2.6	2	0.5	11	2.3	6	1.6
Cingutriletes sp.	2	0.3	0	0.0	0	0.0	0	0.0
Concavissimisporites verrucosus (Delcourt & Sprumont) Delcourt, Dettmann & Hughes	0	0.0	0	0.0	1	0.2	0	0.0
Converrucosisporites sp.	1	0.1	1	0.2	0	0.0	0	0.0
Costatoperforosporites spp.	0	0.0	0	0.0	0	0.0	1	0.3
Deltoidospora australis (Couper 1953) Srivastava 1975	0	0.0	1	0.2	4	0.8	5	1.3
Deltoidospora minor (Couper 1953) Pocock 1970	13	1.7	3	0.7	3	0.6	3	0.8
Deltoidospora sp.	1	0.1	0	0.0	22	4.6	4	1.0
Distaltriangulisporites sp.	0	0.0	0	0.0	4	0.8	0	0.0
Gleicheniidites senonicus Ross 1949	0	0.0	0	0.0	1	0.2	1	0.3
Ischyosporites sp.	0	0.0	0	0.0	3	0.6	1	0.3
Laevigatosporites sp.	1	0.1	0	0.0	0	0.0	0	0.0
Leptolepidites macroverrucosus Schulz 1967	1	0.1	0	0.0	0	0.0	1	0.3
Leptolepidites sp.	8	1.0	0	0.0	0	0.0	0	0.0
Maculatisporites sp.	0	0.0	0	0.0	1	0.2	0	0.0
Neoraistrickia truncata (Cookson 1953) Potonié 1956	1	0.1	0	0.0	0	0.0	0	0.0
Neoraistrickia sp.	0	0.0	0	0.0	1	0.2	0	0.0
Patellasporites tavaredensis Groot & Groot 1962	2	0.3	0	0.0	0	0.0	2	0.5
Punctatisporites sp.	0	0.0	0	0.0	1	0.2	0	0.0
Rubinella major (Couper 1958) Norris 1968	3	0.4	0	0.0	0	0.0	0	0.0
Todisporites major Couper 1958	0	0.0	0	0.0	1	0.2	0	0.0
Undulatisporites sp.	1	0.1	0	0.0	0	0.0	0	0.0
Pollen grains (gymnosperms)						0.0		
Alisporites bilateralis Rouse 1959	2	0.3	2	0.5	24	5.0	11	2.8
Alisporites grandis (Cookson 1947) Dettmann 1963	0	0.0	0	0.0	2	0.4	0	0.0
Alisporites spp.	8	1.0	5	1.2	103	21.6	58	15.0
Araucariacites australis Cookson 1947	3	0.4	1	0.2	6	1.3	5	1.3
Callialasporites dampieri Dev 1961	1	0.1	0	0.0	1	0.2	1	0.3
Cedripites sp.	0	0.0	0	0.0	0	0.0	1	0.3
Classopollis classoides Pflug 1953 emend. Pocock and Jansonius 1961	118	15.3	46	10.7	23	4.8	9	2.3
Classopollis spp.	163	21.1	319	74.2	113	23.7	38	9.8
Ephedripites zaklinskainae Azema et Boltenhagen *1974*	2	0.3	0	0.0	0	0.0	0	0.0
Ephedripites multicostatus Brenner 1963	3	0.4	0	0.0	0	0.0	0	0.0
Ephedripites spp.	61	7.9	2	0.5	0	0.0	0	0.0
Eucommiidites troedsonil Erdtman 1948	2	0.3	0	0.0	0	0.0	1	0.3
Eucommildites minor Groot & Penny 1960	1	0.1	0	0.0	0	0.0	2	0.5
Exesipollenites tumulus Balme 1957	261	33.9	19	4.4	0	0.0	4	1.0
Ginkgocycadophytus nitididus (Balme 1957) de Jersey 1962	5	0.6	0	0.0	0	0.0	3	0.8
Inaperturopollenites dubius (Potonie et Venitz 1932) Thompson et Pflug 1953	0	0.0	14	3.3	5	1.1	25	6.5
Inaperturopollenites spp.	12	1.6	7	1.6	11	2.3	7	1.8
Monosulcites chaloneri Brenner 1963	1	0.1	0	0.0	0	0.0	0	0.0
Monosulcites minimus Cookson 1947 ex. Couper 1953	21	2.7	0	0.0	0	0.0	0	0.0
Monosulcites spp.	6	0.8	2	0.5	1	0.2	1	0.3
Perinopollenites elatoides Couper 1958	8	1.0	1	0.2	1	0.2	0	0.0
Pinuspollenites sp.	0	0.0	1	0.2	3	0.6	3	0.8
Podocarpidites sp.	0	0.0	0	0.0	3	0.6	1	0.3
Spheripollenites sp.	8	1.0	0	0.0	0	0.0	0	0.0
Vitreisporites pallidus (Reissinger 1950) Nilsson 1958	0	0.0	0	0.0	2	0.4	0	0.0
Undetermined bisaccate pollen grains of conifers	2	0.3	4	0.9	121	25.4	188	48.7
Pollen grains (angiosperms)								
Afropollis sp.	4	0.5	0	0.0	1	0.2	0	0.0
Clavatipollenites hughesii Couper 1958	4	0.5	0	0.0	0	0.0	1	0.3
Clavatipollenites minutus Brenner. 1963	3	0.4	0	0.0	0	0.0	0	0.0
Clavatipollenites sp. (Trichotomosulcate)	1	0.1	0	0.0	0	0.0	0	0.0
Clavatipollenites spp.	4	0.5	0	0.0	0	0.0	0	0.0
Retimonocolpites sp.	1	0.1	0	0.0	0	0.0	0	0.0
Tricolpites sp.	1	0.1	0	0.0	0	0.0	0	0.0
Undetermined angiospermous pollen grains	11	1.4	0	0.0	1	0.2	2	0.5
Total	771	100.0	430	100.0	476	100.0	386	100.0

positive carbonate C-isotope values (~2.5‰) with an upward decreasing trend, at the base of the Aptian succession in both sections (Cuchía and La Forida), can be assigned to stage C2 of the reference isotopic curve (Figs. 5–6). The significant negative excursion that both the $\delta^{13}C_{org}$ and $\delta^{13}C_{carb}$ curves present (Figs. 5–6) across the marly lower part of the Patrocinio Formation can be definitely assigned to the stage C3 of Menegatti et al. (1998). The almost identical structure of this excursion at two distant sections (Cuchía and La Florida) of the study area and in other sections of the Basque Cantabrian Basin (Millán et al., 2009), within different palaeogeographic domains, excludes major diagenetic overprinting. Accordingly, the negative values of this segment reflect a depositional feature and represent the beginning of the OAE 1a in the North Cantabrian Basin. In the Cuchía section, stage C4 may correspond to the upper 4 m of the marly lower part of the Patrocinio Formation (Fig. 6). This level shows a rapid positive shift in $\delta^{13}C_{carb}$ to values more positive than those of the pre-

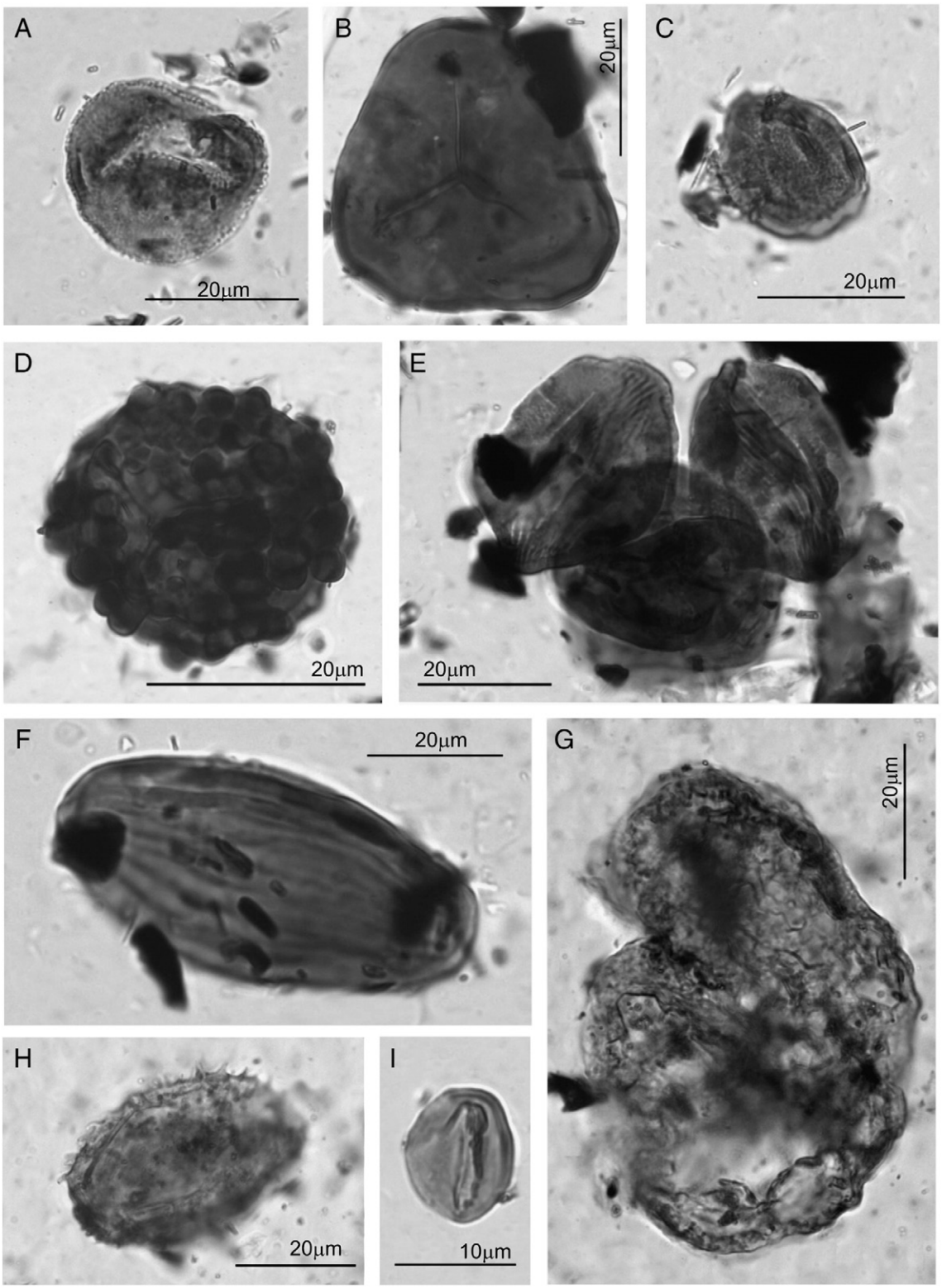

Fig. 12. Selected palynomorphs of the Aptian of the North Cantabrian Basin (NW margin of the Basque Cantabrian Basin): A. Trichotomo sulcate pollen grain of *Clavatipollenites* sp., Canales-Patrocinio sample; B. Trilete and psilate spore of the species *Deltoidospora australis* (Couper) Pocock, Canales-Patrocinio sample; C. Tricolpate pollen grain of *Tricolpites* sp. (*T.* aff. *parvus* Stanley), Canales-Patrocinio sample; D. Trilete and verrucate spore of *Rubinella major* (Couper) Norris, Canales-Patrocinio sample; E. Tetrade of *Classopollis classoides* Pflug emend. Pocock and Jansonius, Canales-Patrocinio sample; F. Polyplicate pollen grain of *Ephedripites multicostatus* Brenner; Canales-Patrocinio sample; G. Bad preserved bisaccate pollen grains of *Alisporites* sp., Ru-Reocín sample; H. Dinoflagellate cyst of aff. *Criboperidinium* sp., Ru-Cuchía sample; I. Monosulcate and psilate pollen grain of *Ginkgocycadophytus nitidus* (Balme) de Jersey Cookson ex. Couper, Canales-Patrocinio sample. Graphic scale: 20 μm, except for I: 10 μm.

C3 stage. Stages C5 + C6 cannot be correlated with confidence in this section because the corresponding time-equivalent facies are probably represented by the siliciclastic deltaic deposits of the upper part of the Patrocinio Formation. The positive $\delta^{13}C_{carb}$ values above the siliciclastic unit are correlated in age with stage C7 (Fig. 6), which is registered across the shallow platform limestones of the San Esteban

Formation (late Early Aptian in age). In contrast, in La Florida section only stage C3 of the OAE 1a was recorded, because stages C4 to C7 are cut out within the sedimentary hiatus (Fig. 5).

The main difference of this isotopic record with other reported records is that the thickness of the stage C3 and the maximum amplitude of the negative $\delta^{13}C$ excursion is much greater than those published previously for the Tethyan domain, including other sectors of the Basque Cantabrian Basin (i.e. Aralar sector; Millán et al., 2009). The most negative values (−3.1 to −4.1‰) are, however, similar to those published from the DSDP Site 463 (western Mid-Pacific) by Ando et al. (2008). According to Li et al. (2008), the stage C3 may have a duration of about 41 kyr. This suggests that the great sedimentary thickness of the stage C3 in the North Cantabrian Basin represents much higher sedimentation rates, and in consequence allows a higher resolution study for this stage, than other previous studies. In detail, in the Cuchía section where the sedimentary record is more complete, the C3 segment splits into three sub-segments (C3a–C3c, Fig. 6). Sub-stages C3a and C3c are two peaks of minimum values (below −3‰) respectively at the base and top of the stage C3. They are separated by sub-stage C3b, a plateau with a mean value of ~−1‰. The same isotopic sub-division and values are observed in the section of La Florida for stage C3 (Fig. 5), although the record is less extended due to lower sedimentation rates in this area. The third negative $\delta^{13}C$ shift observed in the La Florida section at the top of the Patrocinio Formation lies above the sedimentary hiatus and would correspond to a younger (post-C7 stage) negative isotopic shift. The $\delta^{13}C_{org}$ curves are roughly parallel with the $\delta^{13}C_{carb}$ curves, although the excursions are less defined and not exactly in phase, probably showing similar effects with respect to carbon sources and temperature-induced changes of fractionations to those discussed by Méhay et al. (2009).

6.2. Timing of anoxia

According to the biostratigraphic and chemostratigraphic data presented here, the Patrocinio Formation represents a time of global environmental perturbations that led to worldwide organic deposition, possibly as a result of anoxic conditions. This critical event is marked by a significant lithological change from limestone to dark marlstone and siltstone. Although the TOC values of the dark marls of the Patrocinio Formation are not very high (up to 0.8 wt.%), oxygen-deficient conditions are inferred during their deposition from the presence of well-preserved lamination and pyrite framboids, and from the absence of evidence for benthic activity except at particular levels. Moreover, euxinic conditions in the water column during deposition of the Patrocinio Formation are suggested by preliminary data from biomarkers that point to the presence of specific compounds (i.e. gammacerane and high C29/C30 hopane; Quijano et al., 2010) indicative of oxygen deficits and reduced salinity, which may have promoted water stratification on these marginal sections (Erbacher et al., 2001). The low TOC values of the Patrocinio Formation could reflect dilution of organic matter by inorganic sediment. The low $CaCO_3$ values of the succession suggest high input of siliciclastic material. Thus, the TOC may be "diluted" by the high clay and silt content of this unit.

Study of the nannofossils in the Cantabrian sections reveals that the marls of the Patrocinio Formation were deposited during the biocalcification crisis, which occurred before and at the beginning of the OAE 1a in the upper part of the *B. blowi* or at the base of the *S. cabri* foraminiferal Zones (Aguado et al., 1999; Erba et al., 1999). According to other authors (i.e. Aguado et al., 1999; Bellanca et al., 2002; Bralower et al., 1994; Erba, 1994; Erba et al., 1999; Luciani et al., 2001; among others) the beginning of the "nannoconid crisis" clearly preceded the peak intensity of the anoxic conditions and the maximum deposition of organic-rich shales of the "Selli Level" in other places. In the Tethyan regions, these black-shale levels are usually located above the C3 isotopic stage and below the FO of *Eprolithus floralis* (e.g. Bralower et al., 1994; Erba et al., 1999; Gea et al., 2003; Leckie et al., 2002; Menegatti et al., 1998). The dark marls of the Patrocinio Formation were deposited during the C-isotope stage C3, except for the part above sample PN-12 in the La Florida section. Therefore, the dark marls of the Patrocinio Formation are not exactly equivalent to the "Selli Level" but represent slightly older deposits. This suggests that the oxygen-poor conditions related to the Selli event occurred relatively earlier in the North Cantabrian Basin, just coinciding with the nannoconid crisis and the negative C3 isotopic stage. This study allows a precise assignment of these events to the middle/upper part of the *Deshayesites weissi* Zone and the upper part of the *B. blowi* Zone.

According to the chemostratigraphic and biostratigraphic data, another negative excursion of both $\delta^{13}C_{org}$ and $\delta^{13}C_{carb}$ post-dates the FO of *Eprolithus floralis* in the upper part of the Patrocinio Formation of La Florida section (above sample PN-12, Fig. 5). This new negative excursion is placed in the *Rhagodiscus angustus* nannofossils Zone. According to the zonation of Aguado et al. (1999), in the Spanish Tethys the base of *R. angustus* (and the FO of *E. floralis*) lies in the upper half of the *Dufrenoyia furcata* Zone of ammonites (Fig. 13). This implies that the last negative C-isotope shift could be as old as the upper part of the *D. furcata* Zone. García-Mondéjar et al. (2009) and Millán et al. (2009), who studied the Lower Aptian succession cropping out in Aralar (SE Basque Cantabrian Basin), recognized organic-rich shales at this stratigraphic position, which they called the "Aparein level". In their section, the Aparein level is registered as a negative excursion in $\delta^{13}C$ located above the main Early Aptian C-isotope positive excursion (C7 isotopic stage of the *S. cabri* Zone according to Menegatti et al., 1998; Fig. 14). Based on ammonites and their biostratigraphic attribution of the Aparein level to the *D. furcata* Zone, these authors concluded that this is a regional anoxic event older than the Niveau Noire black-shale horizon defined in France and Switzerland within the *G. ferreolensis* foraminiferal Zone (Herrle et al., 2004). However, the biozonation of Aguado et al. (1999) and a recently revised ammonite biostratigraphy (Moreno-Bedmar; personal observation) for south Spain place the base of the *G. ferreolensis* foraminiferal Zone in the uppermost *D. furcata* Zone (Fig. 13). In addition, according to Föllmi et al. (2006), the onset of the organic-rich layers of the Niveau Noire in the Vocontian Basin occurs at least in part within the *D. furcata* ammonite Zone. Therefore, it is very likely that the Aparein level of Aralar and the upper part of the Patrocinio Formation in the La Florida section are equivalent (Fig. 14). The Niveau Noire may be in part equivalent or may represent slightly younger black-shale deposits that succeeded the negative C-isotopic anomaly of the *D. furcata* Zone, as it occurs with the Selli Level. In that case, the related negative excursion in $\delta^{13}C_{org}$ and $\delta^{13}C_{carb}$ recorded in La Florida and in Aralar would represent a supraregional C-isotope perturbation particularly observable on the most expanded series of northern Spain, as has been already suggested by Millán et al. (2009). The integrated biostratigraphy and chemostratigraphy of the studied sections from Cantabria allow a more precise location of this isotopic event between the C7 and C8 chemostratigraphic segments of the C-isotope curve (Fig. 14).

6.3. Environmental changes

The Early Aptian was a time of severe environmental change, which resulted in the oceanic anoxic event. A generalized carbonate crisis also took place, characterized by a significant drop in carbonate production and by a biocalcification crisis with the near disappearance of narrow canal nannoconids (Erba, 1994; Erba and Tremolada, 2004). Quantitative analysis of nannofossil abundance across the Patrocinio Formation has demonstrated a scarcity of narrow canal nannoconids coinciding with the C-isotope negative excursion of the Cantabrian sections. This suggests that the major changes in nannofossil assemblages preceding the OAE 1a were extensive and that the so-called "nannoconid crisis" can be also recognized in

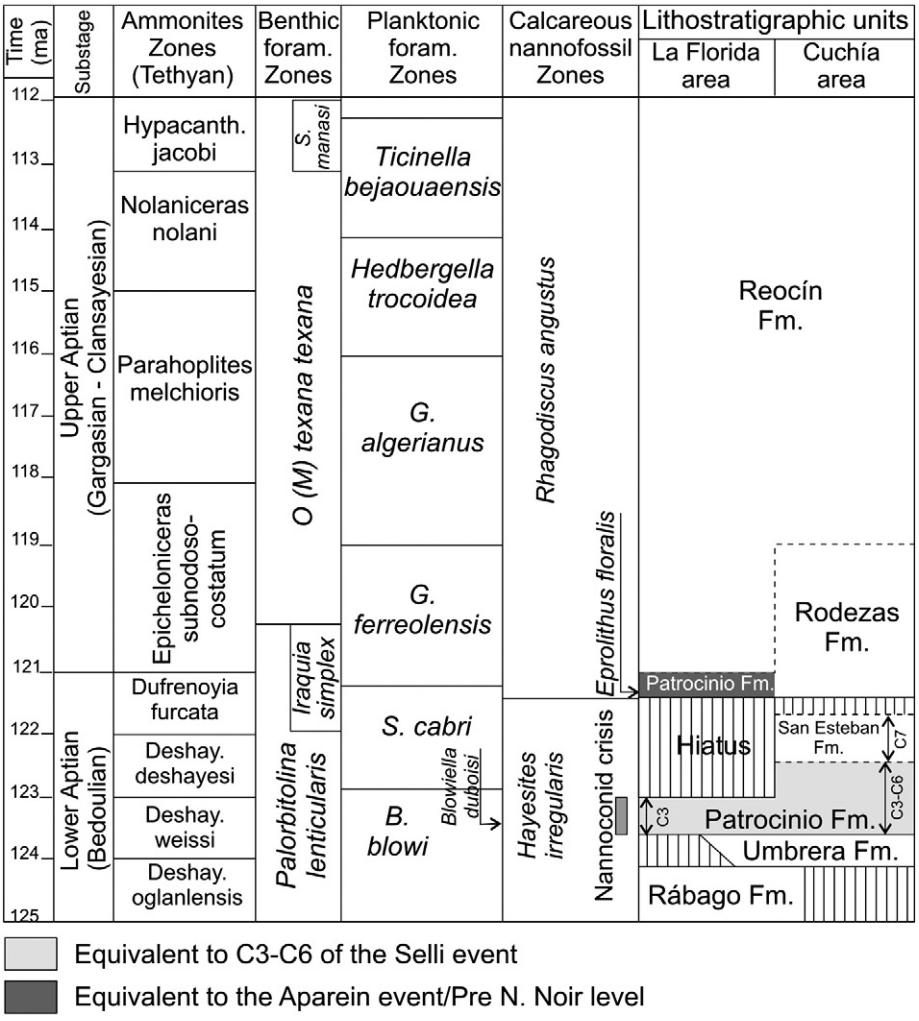

Fig. 13. Proposed integrated ammonite, benthic foraminifera (after Pascal, 1985), planktonic foraminifera and calcareous nannofossil biostratigraphic scheme of the Aptian lithostratigraphic units of La Florida and Cuchía areas. Note the equivalence between the Patrocinio Formation and the Selli event and the Aparein (after Millán et al., 2009) or pre-Niveau Noir event.

northern Spain within the C3 stage of the C-isotope curve. This carbonate crisis was likely induced by oceanic water acidification due to an excess of dissolved CO_2 (Weissert and Erba, 2004). At the moment, the possible triggering mechanisms that have been considered for this massive emission of CO_2 to the ocean–atmosphere reservoir are methane release from gas hydrate dissociation (e.g. Beerling et al., 2002; Jahren et al., 2001) and intensive volcanic activity related to the Ontong Java large igneous province (e.g. Méhay et al., 2009; Tejada et al., 2009). New Os isotopic records of seawater preserved in marine sedimentary rocks from Italy seem to support better the latter hypothesis (Tejada et al., 2009). The rapid release of ^{13}C-depleted CO_2 from either a mantle source or gas hydrate dissociation would have initiated a major carbon cycle perturbation that resulted in the negative and positive $\delta^{13}C$ excursions of the discussed Early Aptian chemostratigraphic curve (Ando et al., 2008; Herrle et al., 2004; Menegatti et al., 1998).

Besides perturbations in the carbon cycle, the OAE 1a was also accompanied by periods of global transgression and drowning of carbonate platforms (e.g. Föllmi and Gainon, 2008; Föllmi et al., 1994, 2006; Jenkyns, 1991; Weissert et al., 1998). In the North Cantabrian Basin two periods of maximum deepening occurred within the overall scenario of the Early Aptian transgression. Based on the biostratigraphic ages provided in this work, the first maximum deepening is dated at the middle–upper part of the *Deshayesites weissi* ammonite Zone and coincided with the onset of the OAE 1a. The sedimentary expression of this maximum flooding event across the basin is the series of dark marls of the lower part of the Patrocinio Formation. The carbonate stages that preceded this event (Rábago and Umbrera Formations; Fig. 13) exhibit a clear compositional change from inferred photozoan to heterozoan styles of carbonate production, (Najarro and Rosales, 2008b; Najarro et al., 2010). At this time the sea level rose very quickly and the transgressive facies were characterized by significant clastic inputs and deterioration of the neritic environments (Najarro et al., 2010). This, coupled with increased basin subsidence, resulted in the drowning of the carbonate platform just coinciding with the beginning of the OAE 1a (Najarro and Rosales, 2008b; Najarro et al., 2010). Platform environments were quickly re-established after this major transgressive pulse, with deposition of platform-top carbonate facies containing rudists and corals (San Esteban Formation), attributed to the *Deshayesites deshayesi* and lower part of the *Dufrenoyia furcata* ammonite zones (Fig. 13). These carbonate deposits represent regressive deposits between the two transgressive pulses. They are recorded only in the most complete section of Cuchía and in more subsiding basin sectors. In the uplifted block of La Florida these carbonate deposits are missing and only the two maximum transgressions are registered (Figs. 13, 14).

The second major transgressive pulse occurred in the lower part of the *Rhagodiscus angustus* nannofossil Zone, equivalent to the upper part of the *Dufrenoyia furcata* ammonite Zone. This flooding episode followed a period of subaerial exposure of the previous San Esteban

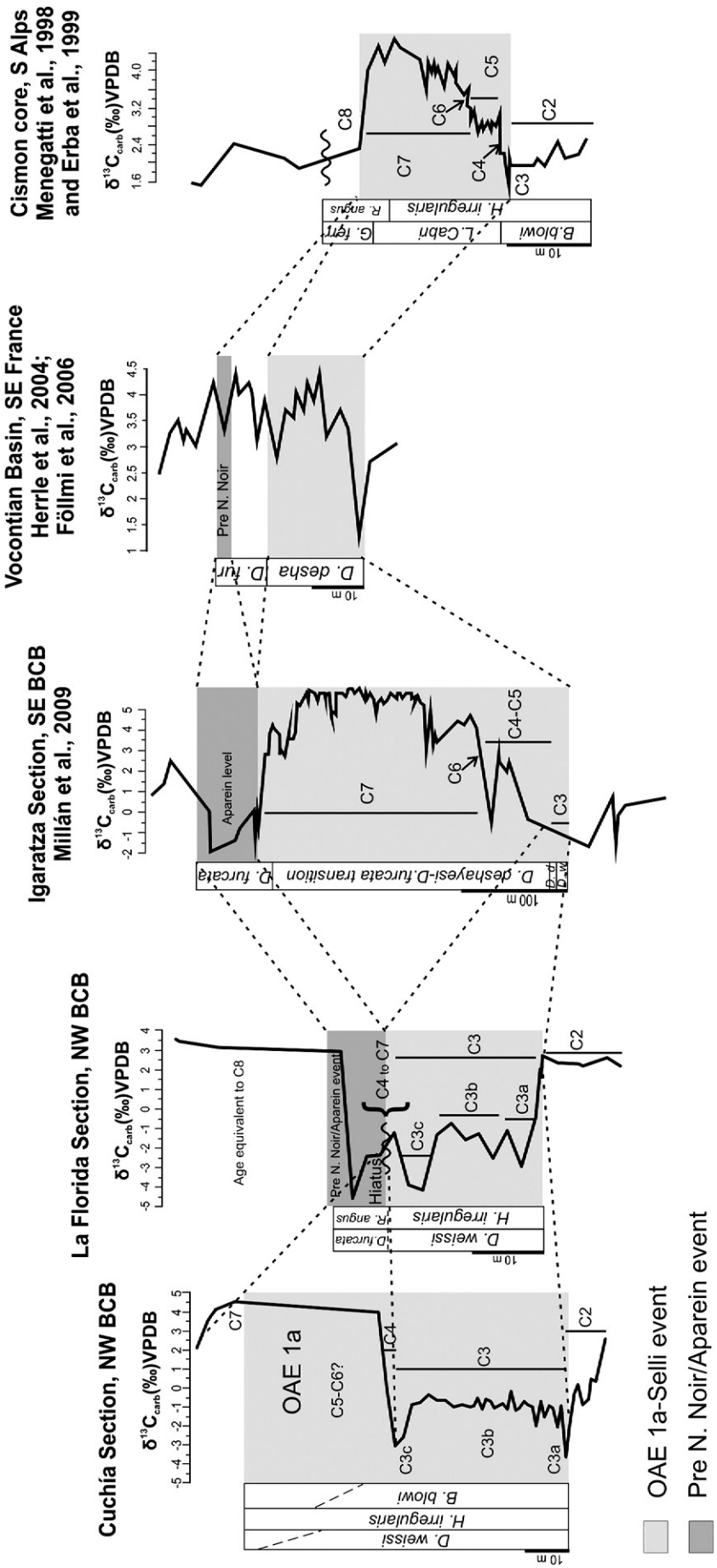

Fig. 14. Proposed chemostratigraphic correlation of La Florida and Cuchía sections (this study, NW of the Basque Cantabrian Basin, BCB) with the SE of the Basque Cantabrian Basin (SE BCB), the Vocontian Basin (SE France) and the Cismon core (S Alps).

Formation (Najarro et al., 2007; Wilmsen, 2005). The transgressive deposits of this stage, which correlate with the third negative spike in $\delta^{13}C_{carb}$ and $\delta^{13}C_{org}$, are represented in La Florida by the upper marls of the Patrocinio Formation directly overlying the sedimentary hiatus (Fig. 13). In Cuchía and other rapidly subsiding sectors, these transgressive deposits are represented by glauconite-rich marls and clastic deposits of the lower part of the Rodezas Formation (Fig. 13), which were deposited on top of the San Esteban platform. Based on ammonites and $\delta^{13}C$ records, this episode appears to be coeval with the onset of a major transgressive phase registered in other sites across the Basque Cantabrian Basin. It can be correlated with a drowning event associated with condensation and glauconitic deposits in the Castro Urdiales platform (central Basque Cantabrian Basin; Rosales, 1999). Biostratigraphic data based on ammonites demonstrated that the platform drowning and subsequent condensed deposits in Castro Urdiales are late Early Aptian–early Late Aptian in age (*D. furcata* to *Parahoplites nutfieldiensis* zones; Rosales, 1999). The onset of these condensed deposits correlates also with the drowning of the Sarastarri platform in Aralar (García-Mondéjar et al., 2009). In other regions, the onset of major drowning and demise of carbonate platforms have been reported at this time in the Helvetic Alps lasting until the Late Aptian (Föllmi and Gainon, 2008; Föllmi et al., 1994, 2006). All these events seems to be associated with the onset of the palaeoceanographic conditions that eventually may have led to deposition of the organic-rich layers of the Niveau Noir of the Vocontian Basin (Föllmi and Gainon, 2008).

Another environmental factor usually linked with OAEs is high global palaeotemperatures. Warm climate conditions accompanying the Selli Event have been previously inferred for the Cismon section from low $\delta^{18}O$ values and from the abundance of the thermophilic pollen *Classopollis* (Hochuli et al., 1999). Indeed, the relative abundance of climate-sensitive pollen groups, such as *Classopollis* and bisaccate pollen, may be indicative of variations in vegetation distribution, which is controlled by palaeoclimatic variations (Vakhrameyev, 1982). Generally, bisaccate pollen, which typified the Boreal-influenced Southern Laurasian floral province, indicates relatively cool and humid conditions, whereas *Classopollis* constituted an abundant element of the Northern Gondwana floral province and its abundance indicates warmer and drier climates (Heimhofer et al., 2004; Vakhrameyev, 1982). In this study, the data obtained from the four analysed palynological samples must be considered with caution because their contents could not indicate a floral and vegetational trend but sporadic episodes. Nevertheless, the high predominance of *Classopollis*, *Exesipollenites* and *Ephedripites* (pollen grains produced by plants assumed to be drought resistant; Hughes, 1991; Thévenard et al., 2005), in the Lower Aptian samples from the Patrocinio Formation could be related with a phase of aridity and warmth, which began in western Europe during the Hauterivian–middle Barremian and dominated the climate of the region until the Early-Middle Aptian (Ruffell and Batten, 1990). In contrast, the drastic decrease of these pollen types and the increase of bisaccate pollen grains in the two Upper Aptian samples analysed (Ru-Cuchían and Ru-Reocín; see Fig. 10) suggest important modifications in the vegetational patterns, and is interpreted as a change to wet and cooler climates commencing during the latest part of the OAE1a and lasting after it. These results are in strong agreement with the palynological studies of the Cismon section in Italy (Hochuli et al., 1999). A global cooling trend after the OAE 1a during the Late Aptian, lasting to the Early Albian, is well documented from oxygen isotopes derived from bulk carbonates (Ando et al., 2008; Hochuli et al., 1999) and belemnites (Pirrie et al., 2004), and correlates with an increase of glendonite and ice-rafting occurrences in high palaeolatitudes (De Lurio and Frakes, 1999; Frakes and Francis, 1988; Kemper, 1987; Price, 1999; Skelton, 2003a). Unfortunately, this cooling trend could not be corroborated in a palynological study of Early and Late Aptian assemblages from El Maestrazgo (NE Spain) (Solé de Porta and Salas, 1994). Cooler conditions could be the effect of inverse greenhouse conditions as a result of the drawdown of CO_2 from the system due to massive burial of organic matter in the oceanic basins during the OAE 1a (Jenkyns, 2003; Skelton, 2003b).

7. Conclusions

1. This study presents new chemostratigraphic and biostratigraphic records from two Lower Aptian sections (La Florida and Cuchía) of the North Cantabrian Basin, which include the signature of OAE 1a. This event is expressed by the interruption of shallow shelf carbonate sedimentation and deposition of a ~40 m thick marly unit (Patrocinio Formation). This marly unit records an abrupt negative C-isotope excursion in both bulk organic matter and carbonates, as has been already observed worldwide in the Early Aptian at the onset of the OAE 1a, preceding the Selli Level. The negative anomaly is attributed to the C3 stage of the reference Aptian C-isotope curve.
2. The data set is well calibrated against a detailed biostratigraphic scheme based on the integration of new ammonite determinations and micropalaeontological data (calcareous nannofossils and planktonic foraminifera). Combination of these biozonations refines the age of the C3 isotopic stage as middle–upper part of the *Deshayesites weissi* ammonite Zone, upper part of the *Blowiella blowi* foraminifera Zone, and upper part of the *Hayesites irregularis* nannofossil Zone. A major hiatus in most marginal areas (La Florida) affecting the C4–C7 segments of the reference isotope curve has been identified from the calcareous nannofossils record. Another $\delta^{13}C_{carb}$ and $\delta^{13}C_{org}$ negative excursion post-dates the FO of *E. floralis* and is equivalent to the *Dufrenoyia furcata* ammonite Zone. This new C-isotope anomaly (pre-Niveau Noir or Aparein event) can be correlated with deposition of glauconitic marls and black shales in other parts of the basin, and just precedes the deposit of black shales in the northern Tethys (Niveau Noir). This pattern resembles the case of the negative carbon isotope anomaly of the onset of the OAE 1a preceding the Selli Level.
3. Quantitative analysis of nannofossil abundance shows a scarcity of narrow canal nannoconids coinciding with the negative excursion of the Patrocinio Formation. This corroborates former interpretations of a contemporaneous biocalcification crisis related to CO_2-induced changes in seawater chemistry in the stages that preceded the peak anoxic event.
4. Identification of a thermal maximum followed by a cooling phase is suggested by palynomorphs. This study supports the existence of a *Classopollis* optimum during the OAE 1a, which is followed by a decrease in *Classopollis* and an increase of bisaccate pollen after the event. Cooler conditions during the latest stage and after the OAE could be a reversal greenhouse effect resulting from the drawdown of CO_2 due to massive burial of organic matter in the oceanic basins during the OAE 1a.

Acknowledgements

This work is part of the Ph.D. Thesis of the first author (M.N.), who was supported by a scholarship from the Instituto Geológico y Minero de España (IGME). The study is a contribution of the DGI projects CGL2008-01237/BTE and CGL2008-00550/BTE funded by the MICINN, Spanish Government, and of the project UJA-07-16-41 funded by the University of Jaén (Spain). We thank Manuel Díaz (Cantabria, Spain) who has allowed the access to his particular collection of ammonites from Cantabria for this study. This paper benefited significantly from comprehensive reviews by Professors K. Föllmi, P. Skelton and F. Surlyk. We are further indebted to Professor S. Robles (Universidad del País Vasco, Spain) for his help and instructive comments in the field.

Appendix

List of identified taxa of nannofossils, planktonic foraminifera, ammonoids and nautiloids with author attributions and dates.

Calcareous nannofossil

Assipetra infracretacea (Thierstein, 1973) Roth, 1973
Assipetra terebrodentaria (Applegate *et al.* in Covington & Wise, 1987) Rutledge & Bergen, 1994
Biscutum ellipticum (Gorka, 1957) Grün in Grün & Allemann, 1975
Braarudosphaera africana Stradner, 1961
Conusphaera rothii (Thierstein, 1971) Jakubowski, 1986
Cyclagelosphaera margerelii Noël, 1965
Diazomatolithus lehmanii Noël, 1965
Discorhabdus ignotus (Gorka, 1957) Perch-Nielsen, 1968
Eprolithus floralis (Stradner, 1962) Stover 1966
Flabellites oblongus (Bukry, 1969) Crux, 1982
Hayesites irregularis (Thierstein in Roth & Thierstein, 1972) Covington & Wise, 1987
Helenea chiastia Worsley, 1971
Lithraphidites carniolensis Deflandre, 1963
Manivitella pemmatoidea (Deflandre ex Manivit, 1961) Thierstein, 1971
Micrantholithus hoschulzii (Reinhardt, 1966) Thierstein, 1971
Micrantholithus obtusus Stradner, 1963
Micrantholithus stellatus Aguado, 1997
Nannoconus bucheri Brönnimann, 1955
Nannoconus circularis Déres & Achériteguy, 1980
Nannoconus kamptneri kamptneri Brönnimann, 1955
Nannoconus steinmannii Kamptner, 1931 ssp. *steinmannii*
Nannoconus truittii Brönnimann, 1955
Prediscosphaera columnata (Stover, 1966) Manivit, 1971
Rhagodiscus angustus (Stradner, 1963) Reinhardt, 1971
Rhagodiscus asper (Stradner, 1963) Reinhardt, 1967
Rhagodiscus gallagheri Rutledge & Bown, 1996
Watznaueria barnesae (Black in Black & Barnes, 1959) Perch-Nielsen, 1968
Watznaueria britannica (Stradner, 1963) Reinhardt, 1964
Zeugrhabdotus noeliae Rood, Hay & Barnard, 1971

Planktonic foraminifera

Blowiella blowi (Bolli, 1959)
Blowiella duboisi (Chevalier, 1961)
Blowiella maridalensis (Bolli, 1959)
Praehedbergella aptiana (Bartenstein, 1965) *s.s.*
Praehedbergella convexa (Longoria, 1974)
Praehedbergella gorbachikae (Longoria, 1974)
Praehedbergella infracretacea (Glaessner, 1936)
Praehedbergella laculata Banner, Copestake & White, 1993
Praehedbergella occulta (Longoria, 1974)
Praehedbergella praetrocoidea (Krechmar & Gorbachik, 1986)
Praehedbergella sigali (Moullade, 1966)
Praehedbergella tuschepsensis (Antonova, 1964)
Schackoina cabri Sigal, 1952

Ammonites

Deshayesites cf. *forbesi* Casey, 1961
Deshayesites cf. *callidiscus* Casey, 1961
Roloboceras cf. *hambrovi* (Forbes, 1845)
Pseudohaploceras liptoviense (Zeuschner, 1856)
Pseudosaynella undulata (Sarasin, 1893)
Toxoceratoides sp.
Deshayesites cf. *consobrinus* (d'Orbigny, 1841)
Deshayesites planus Casey, 1964
Pseudosaynella bicurvata (Michelin, 1838)
Heminautilus saxbii (Morris, 1848)
Toxoceratoides royerianus (d'Orbigny, 1842)

References

Aguado, R., 1994. Nannofósiles del Cretácico de la Cordillera Bética (sur de España). Bioestratigrafía. Ph.D. Thesis, Universidad de Granada, 413 pp.
Aguado, R., Castro, J.M., Company, M., Gea de, G.A., 1999. Aptian bio-events—an integrated biostratigraphic analysis of the Almadich Formation, Inner Prebetic Domain, SE Spain. Cretaceous Research 20, 663–683.
Ando, A., Kaiho, K., Kawahata, H., Kakegawa, T., 2008. Timing and magnitude of Early Aptian extreme warming: unraveling primary $\delta^{18}O$ variation in indurated pelagic carbonates at Deep Sea Drilling Project Site 463, central Pacific Ocean. Palaeogeography, Palaeoclimatology, Palaeoecology 260, 463–476.
Applegate, J.L., Bergen, J.A., 1988. Cretaceous calcareous nannofossil biostratigraphy of sediments recovered from the Galicia Margin, ODP leg 103. In: Boillot, G., Winterer, E.L., et al. (Eds.), Proceedings of the Ocean Drilling Program, Scientific Results, 103, pp. 293–348.
Arthur, M.A., Brumsack, H.J., Jenkyns, H.C., Schlanger, S.O., 1990. Stratigraphy, geochemistry and paleoceanography of organic carbon-rich Cretaceous sequences. In: Ginsburg, R.N., Beaudoin, B. (Eds.), Cretaceous Resources, Events and Rhythms-background and Plans for Research. Kluwer Academic Publications, Dordrecht, pp. 75–119.
Azéma, C., Boltenhagen, E., 1974. Pollen du Crétacé Moyen du Gabon attribué aux Ephedrales. Paléobiologie continentale 5, 1–37.
Balme, B.E., 1995. Fossil in situ spores and pollen grains: an annotated catalogue. Review of Palaeobotany and Palynology 87, 81–323.
Barrón, E., Comas-Rengifo, M.J., Elorza, L., 2001. Contribuciones al estudio palinológico del Cretácico Inferior de la Cuenca Vasco-Cantábrica: los afloramientos ambarígenos de Peñacerrada (España). Coloquios de Paleontología 52, 135–156.
Batten, D.J., 1999. Extraction techniques—small palynomorphs. In: Jones, T.P., Rowe, N.P. (Eds.), Fossil Plants and Spores: Modern Techniques. The Geological Society, London, pp. 15–19.
Beerling, D.J., Lomas, M.R., Gröcke, D.R., 2002. On the nature of methane gas-hydrate dissociation during the Toarcian and Aptian oceanic anoxic events. American Journal of Science 302, 28–49.
Bellanca, A., Erba, E., Neri, R., Premoli Silva, I., Sprovieri, M., Tremolada, F., Verga, D., 2002. Palaeoceanographic significance of the Tethyan 'Livello Selli' (Early Aptian) from the Hybla Formation, northwestern Sicily: biostratigraphy and high-resolution chemostratigraphic records. Palaeogeography, Palaeoclimatology, Palaeoecology 185, 175–196.
Bralower, T.J., Arthur, M.A., Leckie, R.M., Sliter, W.V., Allard, D., Schlanger, S.O., 1994. Timing and paleoceanography of oceanic dysoxia/anoxia in the Late Barremian to Early Aptian (Early Cretaceous). Palaios 9, 335–369.
Casey, R., 1961. A monograph of the Ammonoidea of the Lower Greensand, part III. Monographs of the Palaeontographical Society, London 114, 119–216.
Casey, R., Bayliss, H.M., Simpson, M.I., 1998. Observations on the lithostratigraphy and ammonite succession of the Aptian (Lower Cretaceous) Lower Greensand of Chale Bay, Isle of Wight, UK. Cretaceous Research 19, 511–535.
Channell, J.E.T., Erba, E., Muttoni, G., Tremolada, F., 2000. Early Cretaceous magnetic stratigraphy in the APTICORE drill core adjacent outcrop at Cismon (Southern Alps, Italy), and correlation to the proposed Barremian–Aptian boundary stratotype. Geological Society of American Bulletin 112, 1430–1443.
Coccioni, R., Franchi, R., Nesci, O., Wezel, F.-C., Battistini, F., Pallecchi, P., 1989. Stratigraphy and mineralogy of the Selli Level (Early Aptian) at the base of the Marne a Fucoidi in the Umbria-Marche Apennines (Italy). In: Wiedmann, J. (Ed.), Cretaceous of the Western Tethys. Proceedings of the 3rd International Cretaceous Symposium. Tübingen, pp. 563–584.
Collignon, M., Pascal, A., Peybernès, B., Rey, J., 1979. Faunes d'ámmonites de l'Aptien de la Région de Santander (Espagne). Annales de Paleontologie 65, 139–156.
De Lurio, J.L., Frakes, L.A., 1999. Glendonite as a paleoenvironmental tool: implications for Early Cretaceous high latitude climates in Australia. Geochimica et Cosmochimica Acta 63, 1039–1048.
Dumitrescu, M., Brassell, S.C., Schouten, S., Hopmans, E.C., Damsté, J.S.S., 2006. Instability in tropical Pacific sea-surface temperatures during the Early Aptian. Geology 34, 833–836.
Erba, E., 1994. Nannofossils and superplumes: the Early Aptian nannoconid crisis. Paleoceanography 9, 483–501.
Erba, E., 2004. Calcareous nannofossils and Mesozoic oceanic anoxic events. Marine Micropaleontology 52, 85–106.
Erba, E., Channell, J.E.T., Claps, M., Jones, C., Larson, R., Opdyke, B., Premoli Silva, I., Riva, A., Salvini, G., Torricelli, S., 1999. Integrated stratigraphy of the Cismon APTICORE (southern Alps, Italy): a "reference section" for the Barremian–Aptian interval at low latitudes. Journal of Foraminiferal Research 29, 371–392.
Erba, E., Tremolada, F., 2004. Nannofossil carbonate fluxes during the Early Cretaceous: phytoplankton response to nutrification episodes, atmospheric CO_2, and anoxia. Paleoceanography 19, PA1008 doi:10.1029/2003PA000884.
Erbacher, J., Huber, B.T., Norris, R.D., Markey, M., 2001. Increased thermohaline stratification as a possible cause for an ocean anoxic event in the Cretaceous period. Nature 409, 325–327.

Ferreri, V., Weissert, H., D'Argenio, B., Buonocunto, F.P., 1997. Carbon isotope stratigraphy: a tool for basin to carbonate platform correlation. Terra Nova 9, 57–61.
Feuillée, P., Rat, P., 1971. Structures et paléogéographies Pyrénéo-Cantabriques. In: Debyser, J., Le Pichon, X., Montardet, L. (Eds.), Histoire Structurale du Golfe de Gascogne. : Collection Colloques et Séminaires, 22. Publication de l'Institute Français du Pétrole, Technip, Paris, pp. 1–48.
Föllmi, K.B., Gainon, F., 2008. Demise of the northern Tethyan Urgonian carbonate platform and subsequent transition towards pelagic conditions: the sedimentary record of the Col de la Plaine Morte area, central Switzerland. Sedimentary Geology 205, 142–159.
Föllmi, K.B., Godet, A., Bodin, S., Linder, P., 2006. Interactions between environmental change and shallow water carbonate builup along the northern Tethyan margin and their impact on the Early Cretaceous carbon isotope record. Paleoceanography 21, PA4211 doi:10.1029/2006PA001313.
Föllmi, K.B., Weissert, H., Bisping, M., Funk, H., 1994. Phosphogenesis, carbon-isotope stratigraphy, and carbonate-platform evolution along the Lower Cretaceous northern Tethyan margin. Geological Society of American Bulletin 106, 729–746.
Frakes, L.A., 1979. Climates Throughout Geological Time. Elsevier, Amsterdam. 310 pp.
Frakes, L.A., Francis, J.E., 1988. A guide to Phanerozoic cold polar climates from high latitude ice-rafting in the Cretaceous. Nature 333, 547–549.
García-Mondéjar, J., Owen, H.G., Raisossadat, N., Millán, M.I., Fernández-Mendiola, P.A., 2009. The Early Aptian of Aralar (northern Spain): stratigraphy, sedimentology, ammonite biozonation, and OAE1. Cretaceous Research 30, 434–464.
Gradstein, F.M., 2004. A Geologic Time Scale 2004. Cambrige University Press.
Gea de, G.A., Castro, J.M., Aguado, R., Ruiz-Ortiz, P.A., Company, M., 2003. Lower Aptian carbon isotope stratigraphy from a distal carbonate shelf setting: the Cau section, Prebetic zone, SE Spain. Palaeogeography, Palaeoclimatology, Palaeoecology 200, 207–219.
Gröcke, D.R., 2002. The carbon isotope composition of ancient CO_2 based on higher-plant organic matter. Philosophical Transactions of the Royal Society of London. Series A 360, 633–658.
Gröcke, D.R., Hesselbo, S.P., Jenkyns, H.C., 1999. Carbon isotope composition of Lower Cretaceous fossil wood: ocean–atmosphere chemistry and relation to sea-level change. Geology 27, 155–158.
Grötsch, J., Billing, I., Vahrenkamp, V., 1998. Carbon-isotope stratigraphy in shallow-water carbonates: implications for Cretaceous black-shale deposition. Sedimentology 45, 623–634.
Haq, B.U., Hardenbol, J., Vail, P.R., 1988. Mesozoic and Cenozoic chronostratigraphy and cycles of sea-level change. In: Wilgus, C., Hastings, B., Ross, C., Posamentier, H., Van Wagoner, J., Kendal, C.G.S.C. (Eds.), Sea-level Change: An Integrated Approach: Society of Economic Paleontologists and Mineralogists, Special Publication, 42, pp. 71–108.
Hay, W.W., De Conto, R.M., Wold, C.N., Wilson, K.M., Voigt, S., Schulz, M., Rossby-Wold, A., Dullo, W.-Chr., Ronov, A.B., Balukhovsky, A.N., Söding, E., 1999. An alternative global Cretaceous paleogeography. In: Barrera, E., Johnson, C.C. (Eds.), Evolution of Cretaceous Ocean/Climate System: Geological Society of America, Special Paper, 332, pp. 1–47.
Heimhofer, U., Hochuli, P.A., Burla, S., Weissert, H., 2007. New records of Early Cretaceous angiosperm pollen from Portuguese coastal deposits: implications for the timing of the early angiosperm radiation. Review of Palaeobotany and Palynology 144, 39–76.
Heimhofer, U., Hochuli, P.A., Herrle, J.O., Andersen, N., Weissert, H., 2004. Absence of major vegetation and palaeoatmospheric ρCO_2 changes associated with oceanic anoxic event 1a (Early Aptian, SE France). Earth and Planetary Science Letters 223, 303–318.
Herman, A.B., Spicer, R.A., 1996. Palaeobotonical evidence for a warm Cretaceous Artic Ocean. Nature 380, 330–333.
Herrle, J.O., Köβler, P., Friedrich, O., Erlenkeuser, H., Hemleben, Ch., 2004. High-resolution carbon isotope records of the Aptian to Lower Albian from SE France and the Mazagan Plateau (DSDP Site 545): a stratigraphic tool for paleoceanographic and paleobiologic reconstruction. Earth and Planetary Science Letters 218, 149–161.
Herrle, J.O., Pross, J., Friedrich, O., Hemleben, Ch., 2003. Short-term environmental changes in the Cretaceous Tethyan Ocean: Micropaleontological evidence from the Early Albian Oceanic Anoxic Event 1b. Terra Nova 15, 14–19.
Hines, F.M., 1985. Sedimentation and tectonics in north-west Santander. In: Milá, M.D., Rosell, J. (Eds.), 6th European Regional Meeting, Excursion Guidebook. International Association of Sedimentologists, pp. 371–398.
Hochuli, P.A., Menegatti, A.P., Weissert, H., Riva, A., Erba, E., Premoli Silva, I., 1999. Episodes of high productivity and cooling in the Early Aptian Alpine Tethys. Geology 27, 657–660.
Hughes, N.F., 1991. Mesozoic gymnosperms and period classifications. Current Science 61 (9–10), 630–633.
Hughes, N.F., McDougall, A.B., 1990. Barremian–Aptian angiospermid pollen records from southern England. Review of Palaeobotany and Palynology 65, 145–151.
Jahren, A.H., 2002. The biogeochemical consequences of the mid-Cretaceous super-plume. Journal of Geodynamics 34, 177–191.
Jahren, A.H., Arens, N.C., Sarmiento, G., Guerrero, J., Amundson, R., 2001. Terrestrial record of methane hydrate dissociation in the Early Cretaceous. Geology 29, 159–162.
Jenkyns, H.C., 1980. Cretaceous anoxic events: from continents to oceans. Journal of the Geological Society of London 137, 171–188.
Jenkyns, H.C., 1991. Impact of Cretaceous sea-level rise and anoxic events on the Mesozoic carbonate platform of Yugoslavia. Bulletin of the American Association of Petroleum Geologists 75, 1007–1017.
Jenkyns, H.C., 1999. Mesozoic anoxic events and palaeoclimate. Zentralblatt für Geologie und Paläontologie 1997, 943–949.
Jenkyns, H.C., 2003. Evidence for rapid climate change in the Mesozoic–Palaeogene greenhouse world. Philosophical Transactions of the Royal Society of London. Series A 361, 1885–1961.
Kemper, E., 1987. Das Klima der Kreidezeit. Geologisches Jahrbuch, Reihe A 96, 5–185.
Larson, R.L., 1991. Geological consequences of superplumes. Geology 19, 963–966.
Larson, R.L., Erba, E., 1999. Onset of the Mid-Cretaceous greenhouse in the Barremian–Aptian: igneous events and the biological, sedimentary and geochemical responses. Paleoceanography 14, 663–678.
Leckie, R.M., Bralower, T.J., Cashman, R., 2002. Oceanic anoxic events and plankton evolution: biotic response to tectonic forcing during the mid-Cretaceous. Paleoceanography 17, 1–29.
Li, Y.-X., Bralower, T.J., Montañez, I.P., Osleger, D.A., Arthur, M.A., Bice, D.M., Herbert, T.D., Erba, E., Premoli Silva, I., 2008. Toward an orbital chronology for the Early Aptian Oceanic Anoxic Event (OAE1a, 120 Ma). Earth and Planetary Science Letters 271, 88–100.
Luciani, V., Cobianchi, M., Jenkyns, H.C., 2001. Biotic and geochemical response to anoxic events: the Aptian pelagic succession of the Gargano Promontory (southern Italy). Geological Magazine 138, 277–298.
Malod, J.A., Mauffret, A., 1990. Iberian plate motions during the Mesozoic. Tectonophysics 184, 261–278.
Martín-Chivelet, J., Berasategui, X., Rosales, I., Vilas, L., Vera, J.A., Caus, E., Gráfe, K.U., Mas, R., Puig, C., Segura, M., Robles, S., Floquet, M., Quesada, S., Ruiz-Ortiz, P.A., Frenegal-Martínez, M.A., Salas, R., García, A., Martín-Algarra, A., Arias, C., Meléndez, M., Chacón, B., Molina, J.M., Sanz, J.L., Castro, J.M., García-Hernández, M., Carenas, B., García-Hidalgo, J., Gil, J., Ortega, F., 2002. Cretaceous. In: Gibbons, W., Moreno, T. (Eds.), The Geology of Spain. The Geological Society, London, pp. 255–292.
McCrea, J.M., 1950. On the isotopic chemistry of carbonates and a paleotemperature scale. The Journal of Chemical Physics 18, 849–857.
Méhay, S., Keller, C.E., Bernasconi, S.M., Weissert, H., Erba, E., Bottini, C., Hochuli, P.A., 2009. A volcanic CO_2 pulse triggered the Cretaceous Oceanic Anoxic Event 1a and a biocalcification crisis. Geology 37, 819–822.
Menegatti, A.P., Weissert, H., Brown, R.S., Tyson, R.V., Farrimond, P., Strasser, A., Caron, M., 1998. High-resolution $\delta^{13}C$ stratigraphy through the Early Aptian 'Livello Selli' of the Alpine Tethys. Paleoceanography 13, 530–545.
Millán, M.I., Weissert, H.J., Fernández-Mendiola, P.A., García-Mondéjar, J., 2009. Impact of Early Aptian carbon cycle perturbations on evolution of a marine shelf system in the Basque-Cantabrian Basin (Aralar, N Spain). Earth and Planetary Sciences Letters 287, 392–401.
Montadert, L., Roberts, D.G., de Charpal, O., Guennoc, P., 1979. Rifting and subsidence of the northern continental margin of the Bay of Biscay. In: Montadert, L., Roberts, L. (Eds.), Initial Reports of the Deep Sea Drilling Project, 48, pp. 1025–1059.
Moreno-Bedmar, J.A., Company, M., Bover-Arnal, T., Salas, R., Delanoy, G., Martínez, R., Grauges, A., 2009. Biostratigraphic characterization by means of ammonoids of the lower Aptian Oceanic Anoxic Event (OAE 1a) in the eastern Iberian Chain (Maestrat Basin, eastern Spain). Cretaceous Research 30, 864–872.
Moullade, M., 1974. Zones de foraminiféres du Crétacé Inférieur mésogéen. Comptes Rendus Hebdomadaires des Séances de l'Académie des Sciences de Paris, Serie D 278, 1813–1816.
Moullade, M., Bellier, J.P., Tronchetti, G., 2002. Hierarchy of criteria, evolutionary processes and taxonomic simplification in the classification of Lower Cretaceous planktonic foraminifera. Cretaceous Research 23, 111–148.
Moullade, M., Kuhnt, W., Bergen, J.A., Masse, J.P., Tronchetti, G., 1998. Correlation of biostratigraphic and stable isotope events in the Aptian historical stratotype of La Bédoule (SE France). Comptes Rendus de l'Académie des sciences Paris, IIA 327, 693–698.
Najarro, M., Peñalver, E., Rosales, I., Pérez-de la Fuente, R., Daviero-Gomez, V., Gomez, B., Delclòs, X., 2009. Unusual concentration of Early Albian arthropod-bearing amber in the Basque-Cantabrian Basin (El Soplao, Cantabria, Northern Spain): palaeoenvironmental and palaeobiological implications. Geologica Acta 7, 363–387.
Najarro, M., Rosales, I., 2008a. Disoluciones e incrustaciones ferruginosas asociadas al OAE 1a en la plataforma carbonatada de La Florida (NO de Cantabria). Geogaceta 44, 199–202.
Najarro, M., Rosales, I., 2008b. Evidencias sedimentológica, diagenética y quimioestratigráfica del Evento Anóxico Oceánico del Aptiense Inferior (OAE 1a) en la plataforma carbonatada de La Florida (NO de Cantabria). Geotemas 10, 163–166.
Najarro, M., Rosales, I., Martín-Chivelet, J., 2007. Evolución de la plataforma carbonatada de la Florida durante el rifting del Cretácico Inferior (Aptiense, NO de Cantabria). In: Bermúdez, D.D., Najarro, M., Quesada, C. (Eds.), Volumen Monográfico de la II Semana de Jóvenes Investigadores del IGME. Publicaciones del IGME, pp. 123–128.
Najarro, M., Rosales, I., Martín-Chivelet, J., 2010. Major palaeoenvironmental perturbation in an Early Aptian carbonate platform: prelude of the Oceanic Anoxic Event 1a? Sedimentary Geology doi:10.1016/j.sedgeo.2010.03.011.
Olivet, J.M., 1996. La cinématique de la plaque Ibérique. Bulletin. Centres de Recherches Exploration-Production Elf-Aquitaine 20, 131–195.
Pascal, A., 1985. Les Systems biosédimentaires urgoniens (Aptien–Albien) sur la marge Nord Ibérique. Mémoires Géologiques de l'Úniversité de Dijon 10, 1–569.
Peyrot, D., Rodríguez-López, J.P., Lassaletta, L., Meléndez-Hevia, N., Barrón, E., 2007a. Contributions to the palaeoenvironmental knowledge of the Escucha Formation in the Lower Cretaceous Oliete Sub-basin, Teruel, Spain. Comptes Rendus Palevol 6, 469–481.
Peyrot, D., Rodríguez-López, J.P., Barrón, E., Meléndez-Hevia, N., 2007b. Palynology and biostratigraphy of the Escucha Formation in the Early Cretaceous Oliete Sub-basin, Teruel, Spain. Revista Española de Micropaleontología 39, 135–154.

Pirrie, D., Marshall, J.D., Doyle, P., Riccardi, A.C., 2004. Cool Early Albian climates; new data from Argentina. Cretaceous Research 25, 27–33.
Price, G.D., 1999. The evidence and implications of polar ice during the Mesozoic. Earth Science Reviews 48, 183–210.
Pujalte, V., 1982. La evolución paleogeográfica de la cuenca "wealdense" de Cantabria. Cuadernos de Geología Ibérica 8, 65–83.
Quijano, M.L., Castro, J.M., Pancost, R.D., Gea de, G.A., Najarro, M., Aguado, R., Rosales, I., Martín-Chivelet, J., 2010. Biomarker characterization of the record of the OAE1a (Early Aptian) in Betic and Cantabrian basins (Spain)—sedimentary implications. Geophysical Research Abstracts 12 EGU2010-6502-5.
Ramírez del Pozo, J., 1972. Algunos datos sobre la estratigrafía y micropaleontología del Aptense y Albense al oeste de Santander. Revista Española de Micropaleontología 15, 59–97.
Reboulet, S., Klein, J., Barragán, R., Company, M., González-Arreola, C., Lukeneder, A., Raisossadat, S.N., Sandoval, J., Szives, O., Tavera, J.M., Vasicek, Z., Vermeulen, J., 2009. Report on the 3rd International Meeting of the IUGS Lower Cretaceous Ammonite Working Group, the "Kilian Group" (Vienna, Austria, 15th April, 2008). Cretaceous Research 30, 496–502.
Rosales, I., 1999. Controls on carbonate-platform evolution on active fault-blocks: the Lower Cretaceous Castro Urdiales platform (Aptian–Albian, northern Spain). Journal of Sedimentary Research 69, 447–465.
Ruffell, A.H., Batten, D.J., 1990. The Barremian–Aptian arid phase in western Europe. Palaeogeography, Palaeoclimatology, Palaeoecology 80, 197–212.
Schlanger, S.O., Jenkyns, H.C., 1976. Cretaceous oceanic anoxic events: causes and consequences. Geologie en Mijnbouw 55, 179–184.
Scholle, P.A., Arthur, M.A., 1980. Carbon-isotope fluctuations in Cretaceous pelagic limestones: potential stratigraphy and petroleum exploration tool. American Association of Petroleum Geologists Bulletin 64, 67–87.
Scopelliti, C., Bellanca, A., Erba, E., Jenkyns, H.C., Neri, R., Tamagnini, P., Luciani, V., Masetti, D., 2008. Cenomanian–Turonian carbonate and organic-carbon isotope records, biostratigraphy and provenance of a key section in NE Sicily, Italy: palaeoceanographic and palaeoclimatic implications. Palaeogeography, Palaeoclimatology, Palaeoecology 265, 59–77.
Singh, C., 1971. Lower Cretaceous microfloras of the Peace River Area, Northwestern Alberta. Research Council of Alberta Bulletin 28, 1–299.
Skelton, P.W., 2003a. Rudists evolution and extinction—a North African perspective. In: Gili, E., Negra, H., Skelton, P.W. (Eds.), North African Cretaceous Carbonate Platform Systems, NATO Science Series, IV. : Earth and Environmental Sciences, 28. Kluwer Academic Publisher, pp. 215–227.
Skelton, P.W., 2003b. The Cretaceous World. Cambrige Univeristy Press and The Open University. 360 pp.
Solé de Porta, N., Salas, R., 1994. Conjuntos microflorísticos del Cretácico Inferior de la Cuenca del Maestrazgo. Cordillera Ibérica Oriental (NE de España). Cuadernos de Geología Ibérica 18, 355–368.
Stover, L.E., Brinkhuis, H., Damassa, S.P., de Verteuil, L., Helby, R.J., Monteil, E., Partridge, A.D., Powell, A.J., Riding, J.B., Smelror, M., Williams, G.L., 1996. Mesozoic–Tertiary dinoflagellates, acritarchs and prasinophytes. In: Jansonius, J., McGregor, D.C. (Eds.), Palynology, Principles and Applications, 2. American Association of Stratigraphic Palynologists Foundation, Salt Lake City, Utah, pp. 641–750.
Taylor, T.N., Alvin, K.L., 1984. Ultrastructure and development of Mesozoic pollen: *Classopollis*. American Journal of Botany 71, 575–587.
Tejada, M.L.G., Suzuki, K., Kuroda, J., Coccioni, R., Mahoney, J.J., Ohkouchi, N., Sakamoto, T., Tatsumi, Y., 2009. Ontong Java Plateau eruption as a trigger for the Early Aptian oceanic anoxic event. Geology 37, 855–858.
Thévenard, F., Gomez, B., Daviero-Gomez, V., 2005. Xeromorphic adaptations of some Mesozoic gymnosperms. A review with palaeoclimatological implications. Comptes Rendus Palevol 4, 67–77.
Trincão, P.R., 1990. Esporos e granos de polen do Cretácico Inferior (Berriasiano-Aptiano) de Portugal: Paleontología e Biostratigrafia. Ph.D. Thesis, Universidade Nova, Lisboa, Portugal.
Vakhrameyev, V.A., 1982. *Classopollis* pollen as an indicator of Jurassic and Cretaceous climate. International Geological Review 24, 1190–1196.
Watson, J., 1988. The Cheirolepidiaceae. In: Beck, C.B. (Ed.), Origin and Evolution of Gymnosperms. Columbia University Press, New York, pp. 382–447.
Weissert, H., Erba, E., 2004. Volcanism, CO_2 and palaeoclimate: a Late Jurassic–Early Cretaceous carbon and oxygen isotope record. Journal of the Geological Society of London 161, 695–702.
Weissert, H., Lini, A., Föllmi, K.B., Kuhn, O., 1998. Correlation of Early Cretaceous carbon isotope stratigraphy and platform drowning events: a possible link? Palaeogeography, Palaeoclimatology, Palaeoecology 137, 189–203.
Wilmsen, M., 2000. Evolution and demise of a Mid-Cretaceous carbonate shelf: the Altamira Limestones (Cenomanian) of northern Cantabria (Spain). Sedimentary Geology 133, 195–226.
Wilmsen, M., 2005. Stratigraphy and biofacies of the Lower Aptian of Cuchía (Cantabria, northern Spain). Journal of Iberian Geology 31, 253–275.
Ziegler, P.A., 1988. Evolution of the Arctic, North Atlantic and the Western Tethys. American Association of Petroleum Geologists Memoir 43, 198 pp.

Geologica Acta, Vol.7, Nº 3, September 2009, 363-387
DOI: 10.1344/105.000001443
Available online at www.geologica-acta.com

geologica acta

Unusual concentration of Early Albian arthropod-bearing amber in the Basque-Cantabrian Basin (El Soplao, Cantabria, Northern Spain): Palaeoenvironmental and palaeobiological implications

M. NAJARRO [1] **E. PEÑALVER** [1] **I. ROSALES** [1] **R. PÉREZ-DE LA FUENTE** [2] **V. DAVIERO-GOMEZ** [3] **B. GOMEZ** [3] **and X. DELCLÒS** [2]

[1] **Instituto Geológico y Minero de España**
Ríos Rosas 23, 28003 Madrid, Spain. Najarro E-mail: m.najarro@igme.es
Peñalver E-mail: e.penalver@igme.es Rosales E-mail: i.rosales@igme.es

[2] **Departament d'Estratigrafia, Paleontologia i Geociències Marines, Universitat de Barcelona**
Campus de Pedralbes, 08071 Barcelona, Spain. Pérez-de la Fuente E-mail: perezdelafuente@ub.edu
Delclòs E-mail: xdelclos@ub.edu

[3] **UMR 5125 (PEPS) CNRS, Paléobotanique, Université Lyon-1 (Claude-Bernard)**
Campus de la Doua, F-69622 Villeurbanne, France. Daviero-Gomez E-mail: daviero@univ-lyon1.fr
Gomez E-mail: bernard.gomez@univ-lyon1.fr

ABSTRACT

The El Soplao site is a recently-discovered Early Albian locality of the Basque-Cantabrian Basin (northern Spain) that has yielded a number of amber pieces with abundant bioinclusions. The amber-bearing deposit occurs in a non-marine to transitional marine siliciclastic unit (Las Peñosas Formation) that is interleaved within a regressive-transgressive, carbonate-dominated Lower Aptian-Upper Albian marine sequence. The Las Peñosas Formation corresponds to the regressive stage of this sequence and in its turn it splits into two smaller regressive-transgressive cycles. The coal and amber-bearing deposits occur in deltaic-estuarine environments developed during the maximum regressive episodes of these smaller regressive-transgressive cycles. The El Soplao amber shows Fourier Transform Infrared Spectroscopy spectra similar to other Spanish Cretaceous ambers and it is characterized by the profusion of sub-aerial, stalactite-like flows. Well-preserved plant cuticles assigned to the conifer genera *Frenelopsis* and *Mirovia* are abundant in the beds associated with amber. Leaves of the ginkgoalean genera *Nehvizdya* and *Pseudotorellia* also occur occasionally. Bioinclusions mainly consist of fossil insects of the orders Blattaria, Hemiptera, Thysanoptera, Raphidioptera, Neuroptera, Coleoptera, Hymenoptera and Diptera, although some spiders and spider webs have been observed as well. Some insects belong to groups scarce in the fossil record, such as a new morphotype of the wasp *Archaeromma* (of the family Mymarommatidae) and the biting midge *Lebanoculicoides* (of the monogeneric subfamily Lebanoculicoidinae). This new amber locality constitutes a very significant finding that will contribute to improving the knowledge and comprehension of the Albian non-marine paleoarthropod fauna.

KEYWORDS | **Arthropod bioinclusions. Fossil resin. Plant cuticles. Lower Albian. Spain.**

INTRODUCTION

Oldest ambers with micro-bioinclusions are known from the Triassic of Italy (Schmidt et al., 2006), but it is not until the Barremian-Aptian of Lebanon that macro-bioinclusions occur more profusely (Azar, 2000; Poinar and Milki, 2001). During the Early Cretaceous, amber-bearing deposits become especially common in the geological record. This was promoted possibly by the rise and spread of conifers, such as the Araucariaceae and Cheirolepidiaceae, and by a palaeoclimate warmer than today due to higher pCO_2 levels and significantly different oceanic circulation and geography (Crowley and North, 1991; Huber et al., 1995; Haywood et al., 2004). Coinciding with the initiation of the moist megathermal zone in the Northern Hemisphere, amber deposits developed between 29ºN-50ºN during the earliest Cretaceous and extended to 27ºN to near 70ºN during the Mid Cretaceous (Morley, 2000). During these periods the Iberian Peninsula was situated at low latitude, along the boundary between wet and warm tropical-"paratropical" climates where coal and other organic-rich rocks were deposited.

Early Cretaceous ambers bearing fossil inclusions are scarce, and such localities are of great scientific interest (Fig. 1). In Cantabria (northern Spain), amber is relatively widespread in the Cretaceous deposits, and has been found previously in minor amounts at least at 23 localities. However, in the past none of these localities had provided amber with arthropod inclusions. An intensive geological survey in the Lower Cretaceous succession of northwest Cantabria recently resulted in the discovery of a new amber locality near Rábago village, within the El Soplao territory (Fig. 1B). This site shows a remarkable accumulation of amber with abundant biological inclusions. The El Soplao amber site occurs within a Lower Albian siliciclastic unit (Las Peñosas Formation [Fm.]; García-Mondéjar and Pujalte, 1982). Preliminary data for this new amber accumulation indicate that this is probably the largest site of amber with arthropod bioinclusions that has ever been found in Spain so far.

This paper deals with i) documenting this new finding of arthropod bearing amber as an unusual concentration, as well as describing its related deposits in terms of major stratigraphic and sedimentological characteristics, description of the associated plant cuticles and bioinclusions, and preliminary study of the amber geochemistry; ii) discussing geological and depositional features that may help in understanding the palaeoenvironmental implications of these deposits and their palaeogeographic context; and iii) providing an appropriate introduction for future, more specific studies, on this exceptional new amber site.

Emphasis is given in providing a solid sedimentological, palaeoenvironmental and palaeogeographic framework of this palaeontologically significant deposit for its exceptional preservation and age.

METHODOLOGY AND TECHNIQUES

Sedimentological and palaeoenvironmental interpretations are based on field observations. Four laterally correlative stratigraphic sections (Puente Arrudo, Rábago, La Florida and Plaza del Monte), belonging to the Las Peñosas Fm., have been logged at a meter-centimetre scale. From these data a W-E cross-section has been established to display the principal depositional and palaeoenvironmental features and the stratigraphic distribution of the amber and coal-bearing unit. Whenever possible, rock sampling and measurement of palaeocurrent orientations of selected structures were carried out to help in sedimentological interpretations.

Pieces of amber were acquired by surface collection during field work in the area. To characterize the El Soplao amber, three Fourier Transform Infrared Spectroscopy (FTIR) spectra of three separate amber samples and one sample of recent kauri resin -*Agathis australis* (D. Don) Lindl. in Loud., 1829- were obtained using an infrared Fourier Bomem DA3 spectrometer, in the Molecular Spectrometry Unit of the University of Barcelona (SCT-UB).

Palaeobotanical samples from plant cuticle-rich claystones were obtained by macerating the clayey sediment in hydrogen peroxide and air-drying the organic residues. Resulting fossil plant fragments were sorted using both the naked eye and the stereomicroscope.

The amber was kept wet during screening in order to improve visibility and to detect arthropod bioinclusions. Screening was done under a stereoscope, using transmitted and obliquely reflected light. The amber pieces were cut around the detected arthropods and then polished to permit optimal study. Drawings of some specimens were made with the aid of an image drawing tube, an Olympus V-DA mounted on an Olympus BX51 stereoscopic microscope. Photomicrographs were made with a digital camera mounted on the same microscope. The specimens are housed provisionally in the "Museo Geominero of the Instituto Geológico y Minero de España" (IGME), in Madrid, Spain.

PALEOGEOGRAPHICAL DISTRIBUTION OF EARLY-MID CRETACEOUS AMBER

Early-Mid Cretaceous (Aptian to Cenomanian) amber occurrences have great scientific interest owing to their scarcity (Fig. 1). In fact, macrobioinclusion-bearing ambers of this age are basically restricted to four Eurasian areas: Northern Siberia (Taimyr Peninsula), southeastern Asia (Myanmar), western Middle-East (Lebanon and Jordan), and southwestern Europe (Spain and France). A review of amber localities in the literature was compiled by Martínez-Delclòs et al. (2004). The four areas were located within the warm temperate and tropical-paratropical palaeoclimatic regions (Fig. 1) *sensu* Scotese (2000), also referred to as tropical and south-subtropical Cretaceous climate belts by Spicer et al. (1994).

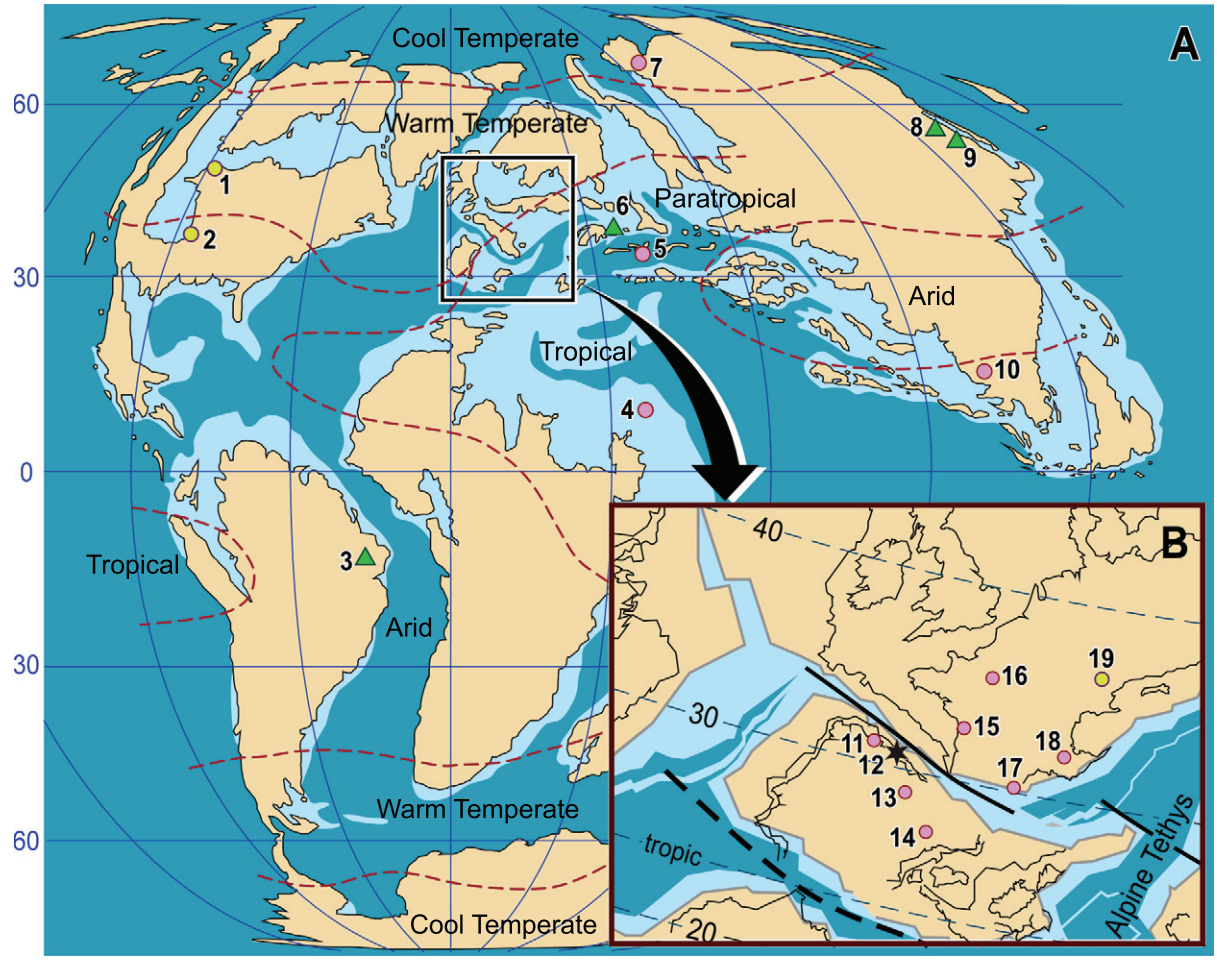

FIGURE 1 | **A) Major Early-Mid Cretaceous (Aptian to Cenomanian) amber occurrences (Redrawn from Blakey, 2008). Amber localities with bioinclusions are symbolized with circles, otherwise green triangles are used. Moreover, yellow circles represent ambers that have only provided microbioinclusions (bacteria, protists, algae and/or fungi). Pink circles account for macrobioinclusion-bearing ambers (essentially arthropods), with the exception of El Soplao amber, which is designated out with a black star. Broken purple lines delimit palaeoclimatic regions *sensu* Scotese (2000). (1) Ruby Creek (Alberta, Canada; Medioli et al., 1990). (2) Ellsworth (Kansas, USA; Waggoner, 1996). (3) Nova Olinda-Santana (Ceará, Brazil; Martill et al., 2005). (4) Middle-East. Wadi Zerka (Amman, Jordan; Bandel et al., 1997; Kaddumi, 2005). Bcharreh, Hammana, and Jezzine, among others (Lebanon; Azar, 2000; Veltz, 2008). Mt. Hermon (North District, Israel; Greenblatt et al., 1999). (5) Yukhary Agdzhakend (Goranboy, Azerbaijan; Ratnitsyn and Quicke, 2002). Russia (Zherikhin and Eskov, 1999; Ratnitsyn and Quicke, 2002). (6) Stary Oskol (Belgorod). (7) Taimyr Peninsula (Northern Siberia). Baikura-Neru Bay in Lake Taimyr (Central Taimyr). Nizhnyaya Agapa River (West Taimyr). Begichev Fm. in the Khatanga River (Eastern Taimyr). (8) Khetana River in South of Okhotsk (Khabarovsk Krai). (9) Suyfun Coal Basin (Primorye). (10) Hukawng Valley (Kachin, Myanmar; Cruickshank and Ko, 2003). B) Amplified area squared at subfigure A, corresponding to SW Europe. Spain (Arbizu et al., 1999; Alonso et al., 2000; Peñalver et al., 2007b; Delclòs et al., 2007). (11) El Caleyu and Pola de Siero (Asturias). (12) El Soplao Territory, near Rábago village (Cantabria, in this paper). (13) Moraza and Peñacerrada-Montoria (Burgos and Álava respectively). (14) San Just (Teruel). France (Nel et al., 2004; Perrichot, 2004, 2005; Néraudeau et al., 2005; Perrichot et al., 2007; Néraudeau et al., 2008; Girard, 2008). (15) Archingeay-Les Nouillers, La Buzinie, Cadeuil, Fouras, l'Ile d'Aix, and Les Renardières (Les Charentes). (16) Ecommoy and Durtal (Sarthe and Maine-et-Loire respectively). (17) Fourtou (L'Aude). (18) Salignac and Sisteron (Alpes-de-Haute-Provence). (19) Schliersee (Bavaria, Germany; Schmidt et al., 2001).**

In Spain, aside from the frequent occurrence of amber in Aptian to Cenomanian deposits, only a few localities show sufficient quantity to be identified as accumulations (Fig. 1B). In the past, only two of these deposits had yielded important amounts of bioinclusions in terms of quantity and quality, specifically the Álava deposits of Peñacerrada and Montoria (Alonso et al., 2000; Delclòs et al., 2007) and the San Just outcrop in Teruel (Delclòs et al., 2007; Peñalver et al., 2007b). In Asturias, although less significant, amber with bioinclusions has been described in El Caleyu and Pola de Siero (Arbizu et al., 1999) (Fig. 1). The identification of the new amber deposit of the El Soplao in Cantabria (Figs. 1 and 2) enlarges the still patchy record of these palaeontological deposits of exceptional preservation in Spain.

GEOLOGICAL AND PALAEOGEOGRAPHIC SETTING

The recently discovered amber outcrop is located in the El Soplao territory in northwestern Cantabria (Fig. 2).

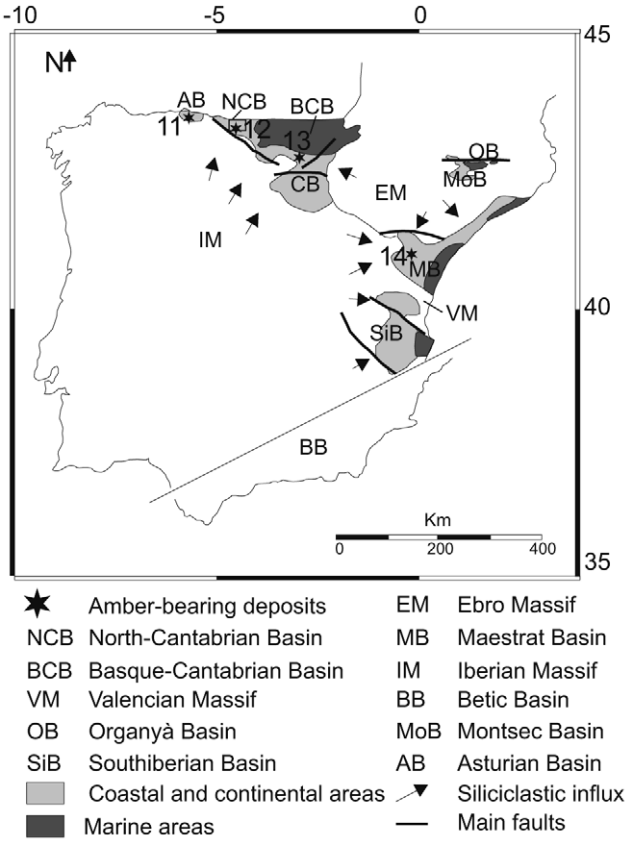

FIGURE 2 | **Map of the Iberian Peninsula showing the location of the Lower Albian basins and the distribution of the Lower Cretaceous amber-bearing deposits (same nomenclature as in Figure 1). (11) El Caleyu and Pola de Siero deposits. (12) The El Soplao deposit. (13) Peñacerrada-Montoria deposits. (14) San Just deposit. (Modified from Salas et al., 2001).**

This area, located immediately to the north of the Cabuérniga Ridge, constituted the northwestern margin of the Basque-Cantabrian Basin during the Cretaceous (Fig. 3). The evolution and current structure of the Basque-Cantabrian Basin are related to the kinematics between the European and Iberian plates (Malod and Mauffret, 1990; Olivet, 1996). The inception of the basin occurred during a Permo-Triassic rifting event. A second extensional phase was related to the opening of the Bay of Biscay during the Late Jurassic-Early Cretaceous (e.g., Rat, 1988; García-Mondéjar et al., 1996). Renewed extension and perhaps strike-slip faulting along a NW-SE trend occurred during the Aptian-Albian (e.g., García-Mondéjar et al., 1996; Martín-Chivelet et al., 2002; Soto et al., 2007). These tectonic events resulted in the development of several extensional sub-basins bounded by synsedimentary faults, in which great thicknesses of sediments accumulated. These sedimentary sub-basins underwent widespread contraction during the Pyrenean Orogeny in Late Eocene-Oligocene times (Hines, 1985; Fernández Viejo and Gallastegui, 2005). Consequently, the present structure of the study area is the result of the inversion of the previous Mesozoic extensional and strike-slip structures.

The studied succession was deposited in the North Cantabrian sub-basin (NCB) (Fig. 3A), which subsided moderately for most of Cretaceous time (Martín-Chivelet et al., 2002; Wilmsen, 2005). The Cabuérgina Ridge (Fig. 3) is an E-W trending fault zone, which bounds this sub-basin to the south. This palaeo-high represents a previous Variscan structure that was reactivated through extensional faulting during the Mesozoic (Rat, 1988; García-Espina, 1997).

Structurally, the studied succession was deposited during the Cretaceous on an eastward tilted block (Fig. 3B). The tilted block forms the footwall of the N-S Bustriguado Fault (BF, Figs. 3A and 3C) that bounds to the west the main Cretaceous depocenter (Figs. 3A and 3B). Recent geological mapping has shown that the BF branches at a corner point with the E-W trending North Cabuérniga Fault (NCF; Fig. 3A); (García-Senz "pers. comm."), forming an extensional-linked system, as in the examples described by Gibbs (1990). Because in the northern margin of the Iberian plate, the direction of extension during the Cretaceous is considered to be roughly orthogonal to the Cantabrian margin (Malod and Mauffret, 1990), the BF is interpreted as a left-lateral transfer fault, and the NCF as the corresponding frontal extensional ramp. The tilted block that contains the El Soplao territory dips and thickens towards the master BF (Fig. 3B), a feature commonly interpreted as the result of extensional fault propagation folding (Withjack et al., 1993). Models of such faults have been described in

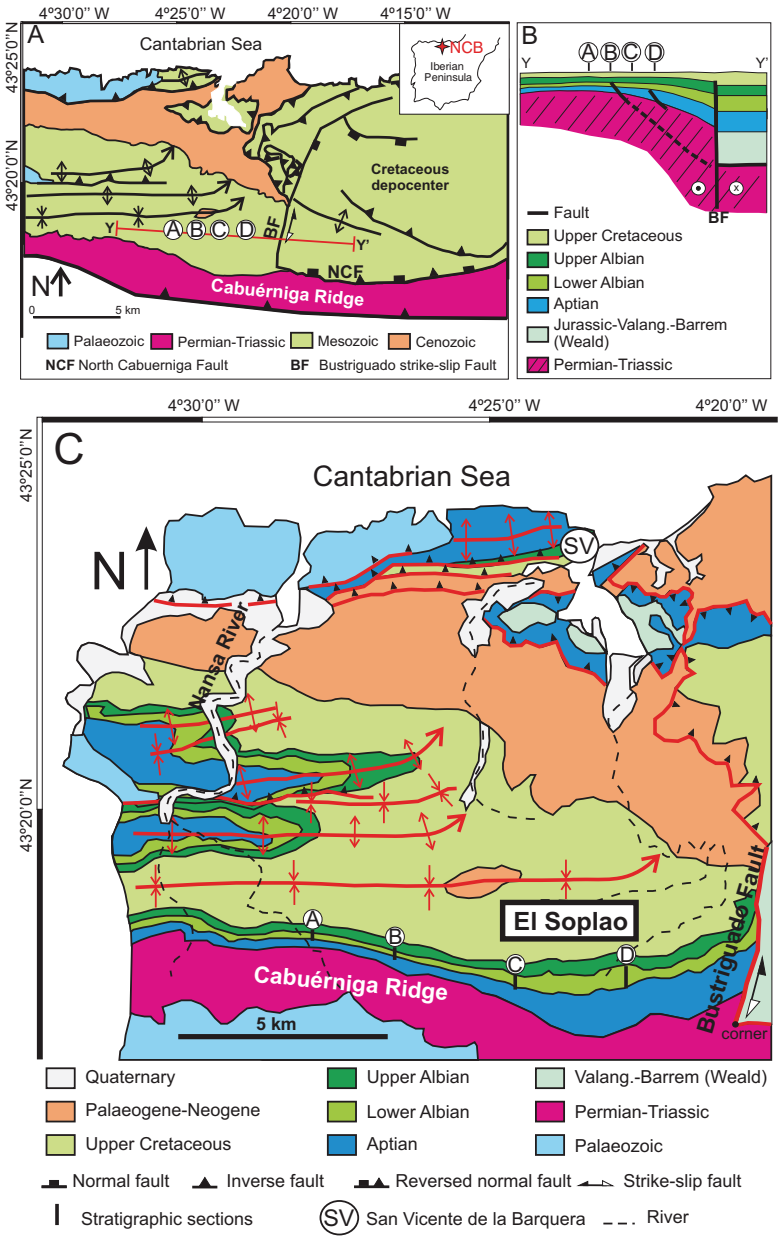

FIGURE 3 | **A) Geological sketch with the main structural elements of the North Cantabrian sub-basin (NCB). The red line Y-Y' indicates the position of the cross-section of Fig. 3B. B) Schematic cross-section showing the restored geometry of the NCB in the El Soplao territory during the Cretaceous. Figure not to scale. C) Detailed geological map of the NCB Basin in the El Soplao area with location of the stratigraphic sections studied. (A) Puente Arrudo Section, (B) Rábago Section, (C) La Florida Section, (D) Plaza del Monte Section.**

frontal ramps (Withjack et al., 1993) but few examples in transfer faults are known. This Cretaceous configuration was inverted during the Palaeogene folding and the faults reversed their movement. The NCF behaved as a frontal thrust ramp, and the BF as a right-lateral strike-slip fault. The latter passes northwards to an oblique thrust sheet that superposes the Cretaceous on the Cenozoic.

STRATIGRAPHY OF THE EL SOPLAO AREA

The bulk of the Mesozoic succession of the El Soplao area lies unconformably on folded (Variscan deformation) Carboniferous basement (Fig. 4). This succession was initiated with a thick sequence of Lower Triassic continental red sandstones and mudstones (Buntsandstein facies). Late Triassic, Jurassic and earliest Cretaceous sequences are absent in the studied area, probably because during the Late Jurassic-Early Cretaceous rifting stage, the area to the north of the Cabuérniga Ridge was subjected to erosion and nondeposition. Subsidence renewed in the Early Aptian and was accompanied by gradual marine transgression. Thus, the Aptian-Albian succession of the El Soplao area, unconformably overlies Triassic strata and was dominated by shallow marine carbonate deposition (Fig. 4).

As a whole, the Aptian-Albian succession of the El Soplao territory constitutes an E-W elongated lithosome

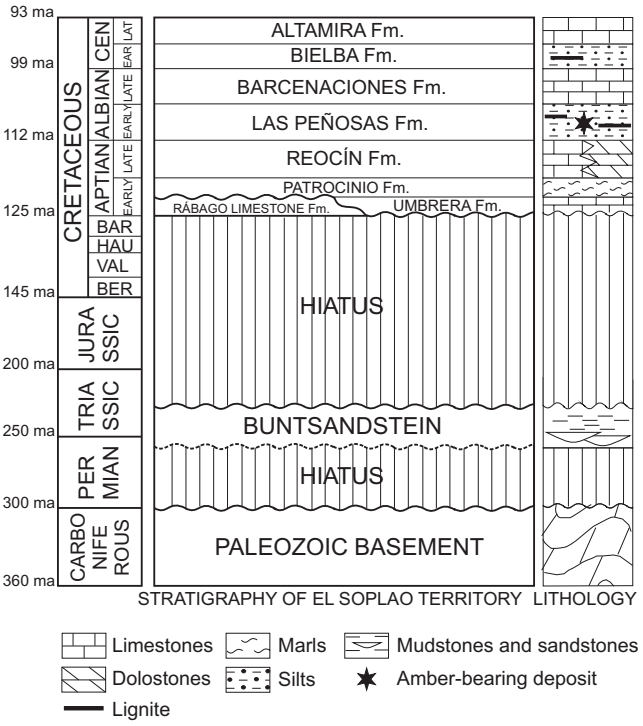

FIGURE 4 | **Carboniferous to Upper Cretaceous lithostratigraphy of the El Soplao area (modified from Hines, 1985). Chronostratigraphy after Gradstein (2004).**

9 km long with wedge-shaped geometry deepening and thickening eastward, on the slope of the tilted block active during this time (Najarro et al., 2007) (Fig. 3B). Thicknesses vary from about 600 m in the eastern part of the tilted block (Bustriguado area, Fig. 3) to less than 200 m toward the west (Puente Arrudo-Rábago Sections, Fig. 3C). The general stratigraphic and biostratigraphic framework of the Aptian-Albian lithological units has been established by Ramírez del Pozo (1972) and Hines (1985), but the main depositional systems and sequences have been revised recently (Najarro et al., 2007; Najarro and Rosales, 2008). A simplified stratigraphy of this interval is provided, adapted from the terminology by Hines (1985) for the major lithological units (Fig. 4).

The Early Aptian marine transgression led to deposition of shallow platform carbonates of the Lower Aptian Rábago Limestone Fm. and Umbrera Fm. that spread over the studied area. Continued transgression during the Early Aptian caused platform drowning, and resulted in deposition of relatively deep-water marls (Patrocinio Fm.) that covered the entire carbonate platform (Najarro and Rosales, 2008). Subsequent gradual regression led to deposition of shallow water carbonates of the Reocín Fm. during the Late Aptian, and finally delta-estuarine siliciclastics and carbonaceous lutites of the Las Peñosas Fm. during the Early Albian (Fig. 4). The vertical evolution from the Upper Aptian Reocín Fm. to the Lower Albian Las Peñosas Fm. is interpreted herein as a relative sea-level fall associated with a deltaic progradation. The Upper Albian succession follows with deposition of the Barcenaciones Fm. (Fig. 4), a shallow water carbonate bank that expands more than 50 km throughout the North Cantabrian sub-basin, as a result of a transgression following deposition of the Las Peñosas Fm. A subsequent regression during the Lower Cenomanian deposited the transitional marine siliciclastic Bielba Fm. Later, deeper water conditions were established during the Late Cretaceous, leading to deposition of open-platform carbonates for the remainder of the Cretaceous succession.

LAS PEÑOSAS FORMATION

Primarily, this paper examines the Lower Albian heterolithic amber-bearing deposit that is included within the Las Peñosas Fm. Regional palaeogeographical and palaeoenvironmental reconstructions of the Basque-Cantabrian Basin during this time slice (García-Mondéjar, 1990) indicate that siliciclastic sediment was transported from highlands and continental areas located to the west and south towards the north during deposition of the Las Peñosas Fm. This amber-bearing unit is approximately equivalent in age and facies to the broadly extended Escucha Fm., deposited to the south of the Basque-Cantabrian Basin (Barrón et al., 2001; Martínez-Torres et al., 2003), as well as other Mesozoic basins of northeastern Spain, including the Maestrat Basin (e.g., Salas and Martín-Closas, 1991; Salas et al., 1991; Querol et al., 1992; Salas et al., 2001; Rodríguez-López and Meléndez, 2004; Rodríguez-López et al., 2005, 2007; Peyrot et al., 2007; Moreno-Bedmar et al., 2008). These units basically represent littoral facies dominated by delta-estuarine deposits, which can be laterally correlated in a NW-SE direction for more than 500 km, from northeastern Cantabria, through the southeast Basque-Cantabrian Basin in the Álava region (Basque Country), and into the Maestrat Basin in Teruel to the Alicante Province (Fig. 2). These areas, which trace the approximate location of the coastline during the Early Albian, are characterized by the presence of coal-bearing deposits with common presence of amber (Delclòs et al., 2007).

Facies and sequence arrangement

The Las Peñosas Fm. previously has been described as a unit formed by a complex of fluvio-estuarine channel sandstones, overbank black carbonaceous mudstones, tidal channel bars and tidal flat facies, and minor intercalations of carbonate beds, exhibiting unclear internal organization (García-Mondéjar and Pujalte, 1982; Hines, 1985). However, detailed stratigraphic and sedimentologi-

cal logging of four W-E correlative stratigraphic sections (the Puente Arrudo, Rábago, La Florida and Plaza del Monte sections; Fig. 3) in the El Soplao region has revealed the depositional architecture of the Las Peñosas Fm. and the stratigraphic distribution of the coal- and amber-bearing deposits (Fig. 5). A summary of the general facies associations, depositional environments and their sequential arrangement is given in this section and summarized in Fig. 5 and Table 1.

It is significant that the facies distribution within the Las Peñosas Fm. displays a clear tectonic control, as suggested in the study area by the strong lateral thickness variation in an E-W direction (Fig. 5), which, in the studied area, ranges from between 45 m to the west to more than 100 m to the east. In this way, the Rábago Section that contains the amber deposit represents the highest point of the flexured footwall block of the Bustriguado fault (Fig. 3B) at the time of deposition of the Las Peñosas Fm. This flexure seems to be accommodated by several minor synsedimentary faults that delineate the structure observed in the Rábago Section (Figs. 3B and 5).

The Las Peñosas Fm. can be informally split into three correlatable units, which are named in this paper, from base to top, Las Peñosas 1 to 3 (P1-P3; Figs. 5 and 6A).

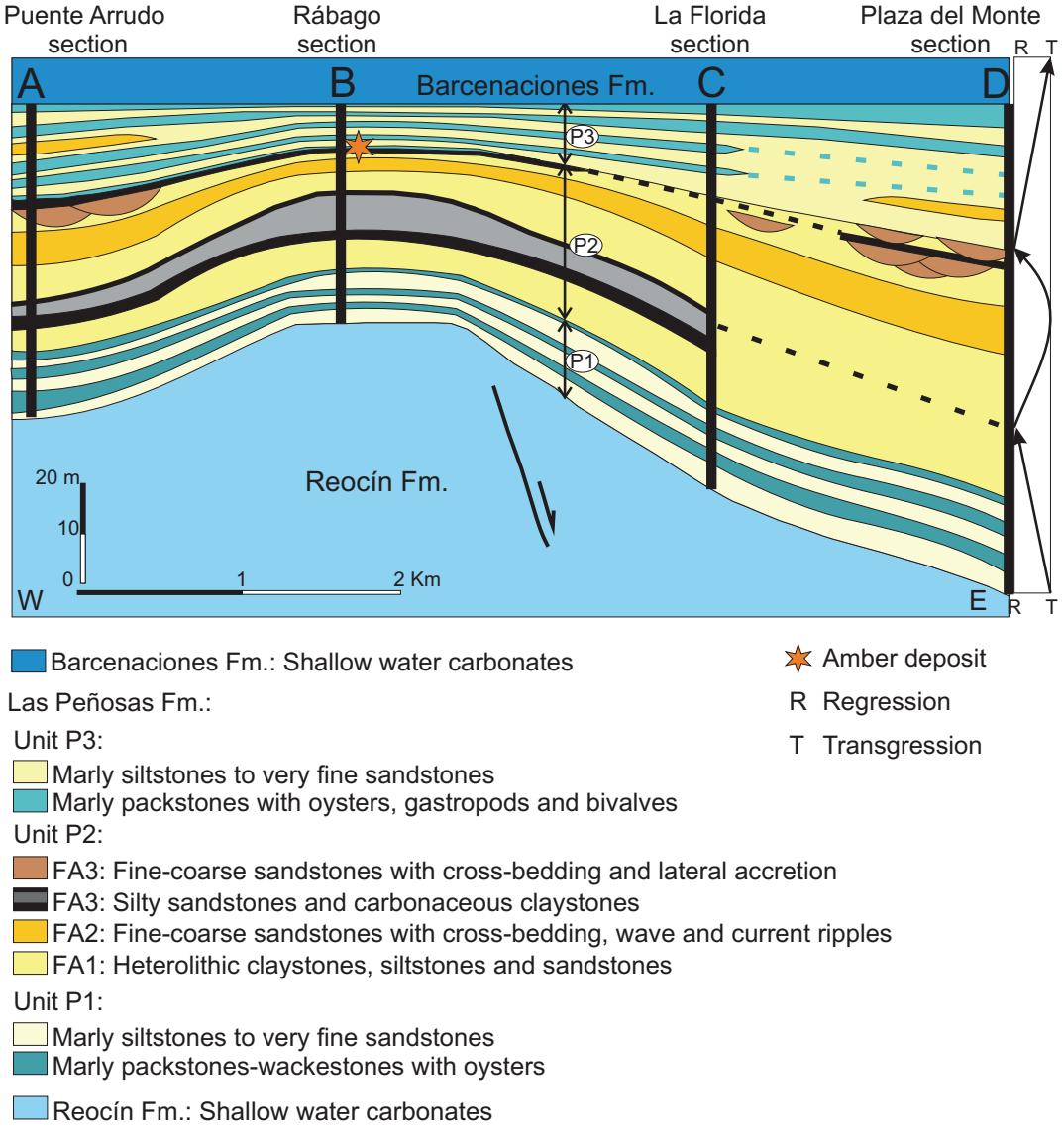

FIGURE 5 | **Stratigraphic correlation of the four studied sections (A to D in Figure 3). Note the location of the amber deposit and the thickness variation of the Las Peñosas Fm. along the W-E cross section (see also Fig. 3). (P1-P3) Members of the Las Peñosas Fm. (see text for explanation). (FA1-FA3) Sedimentary facies associations studied in the Las Peñosas Fm. Amber accumulation usually occurs at the P2-P3 unit boundary.**

TABLE 1 | **Characteristics of the facies associations in the Las Peñosas Fm.**

Unit	FA	F	Lithology	Primary Structures	Vertical Stacking	Interpretation
P3			Alternation of nodular marly-packestones with bioclasts and heterolithic levels of mud- silt- and fine to medium grain-sized sandstones	Wavy, flaser and lenticular lamination	Progressive upward increase in carbonate content	Carbonate-siliciclastic mixed platform
P2	FA3	F6	Weakly cemented, moderate-well sorted, very fine- coarse to grained sandstones in erosionally-based, channalized units. Accretion surfaces with silty clay, plant remains, coal and mudclasts. Iron cemented ripples, pyritized trunk fragments and pyritized burrows at the top.	Large scale trough-, longitudinal-, low angle- and small-ripple-cross bedding; lateral accretion; horizontal-and sigmoidal-stratification; complex deformations	Fining upward	Delta plain: Distributary meandering channels
		F5	Dark organic, sulphide-rich mudstones with bivalves, gastropods, leaves, coal, trunks, sulphide nodules and amber	Wavy and lenticular lamination; current ripples	Rhythmic alternations	Delta plain: Interdistributary bay
		F4	Silty very fine sandstones with coal layers, sulphide nodules, trunks and amber		Rhythmic alternations	Delta plain: Interdistributary bay
	FA2	F3	Weakly cemented, moderated to well-sorted fine to coarse-grained sandstones with mud drapes and mudclasts	Large scale trough cross-bedding; planar cross-bedding; wave ripples	Coarsening and thickening upwards	Delta front: Distributary mouth-bars
	FA1	F2	Sulphide mudstone-siltstones with coal and trunk fragments. Minor to moderate bioturbation	Wavy and lenticular lamination	Fining upward	Wave- and tidal influenced estuarine-delta bay
		F1	Pale-yellow, very fine- to medium-grained, well-sorted sandstones. Mudclasts and coal fragments. Minor to abundant bioturbation dominated by *Skolithos* and track traces.	Low angle and horizontal lamination; planar cross-stratification; flaser and wavy lamination; wave and current-ripples		
P1			Alternation of bioclastic, oyster-rich limestones and bioturbated, nodular marly–silty limestones to siltstones with very fine sand levels	Wavy lamination	Upward decrease in carbonate content and progressive increase in siliciclastics	Transition from shallow carbonate platform to estuarine-delta bay

FA: Facies association. F: Facies

The lower Unit P1 overlies the Reocín Fm. It ranges from about 11 m (Rábago Section) to 40 m (Plaza del Monte Section) and it is characterized by an alternation of bioclastic, oyster-rich limestones and bioturbated, nodular marly-silty limestones to siltstones with intervals of very fine sands. The overall succession presents an upward decrease of carbonate content and a progressive increase in the quartz silt and sand content of the marly intervals. This succession is interpreted as a transitional unit from a shallow carbonate platform to a siliciclastic estuary-delta bay, caused by rapid change in the sedimentary conditions resulting from deltaic progradation.

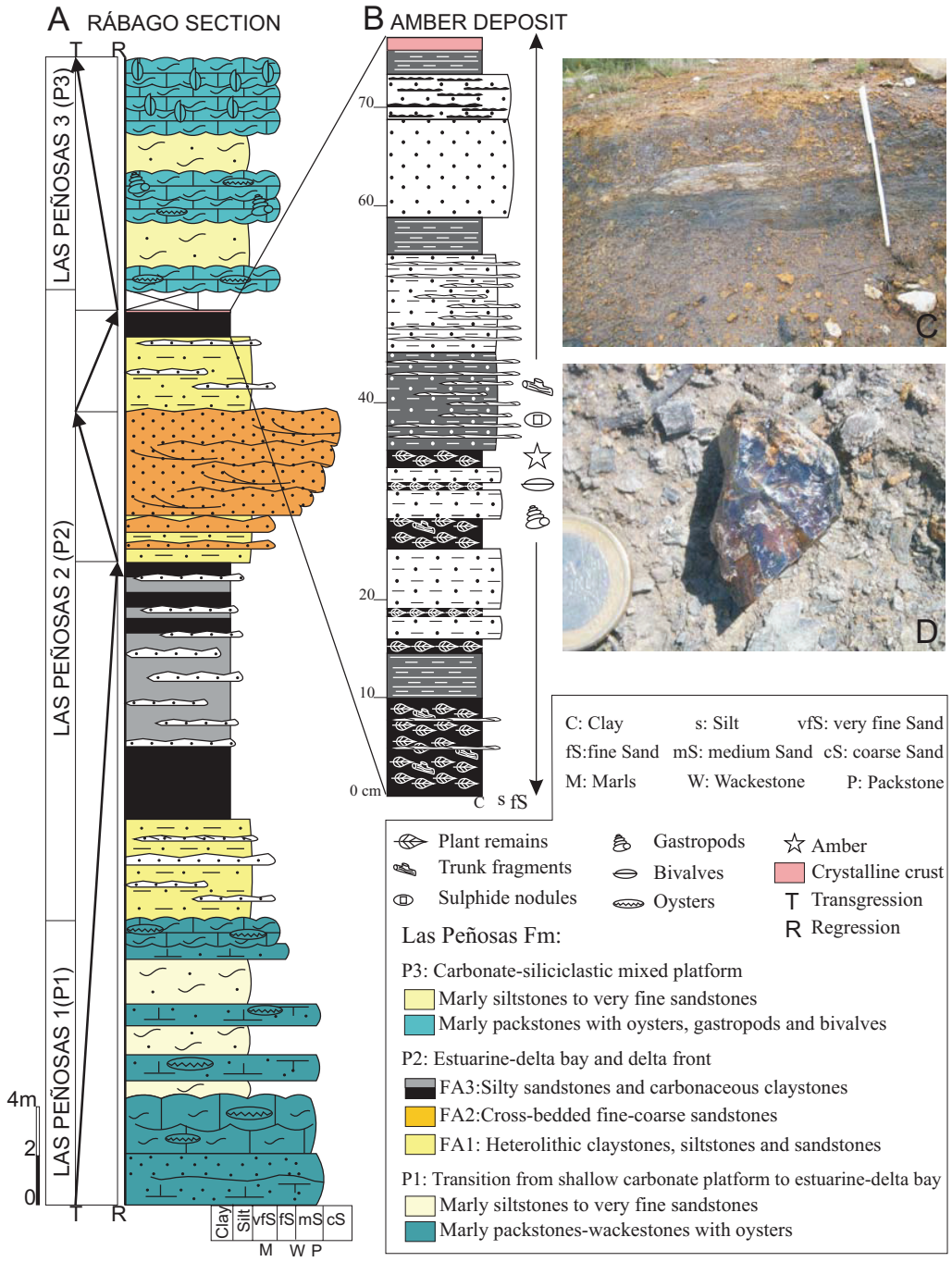

FIGURE 6 | **A) Simplified stratigraphic log of the Rábago Section. Two regressive-transgressive cycles are defined. Note that the position of the amber deposit coincides with the maximum regression of the second cycle. B) High-resolution stratigraphy of the amber deposit. C) General view of the amber deposit (scale: 1m). D) Example of a blue amber piece in situ.**

The middle Unit P2 contains the amber-rich deposit that has been recently discovered in the Rábago Section (Figs. 6B-D and 7A). It lies on top of P1 and ranges in thickness from 25 m (Rábago Section) to 60 m (Plaza del Monte Section; Fig. 5). This unit consists predominantly of heterolithic sandstones-siltstones and carbonaceous mudstones deposited in broadly coastal estuarine and delta environments. Facies associations can be grouped into three main depositional environments. First is delta front facies association without evidence of emergence, interpreted largely as shallow marine. This environment includes distributary mouth-bar facies, deposited mostly, if not entirely, under marine conditions, as well as distal bar, nearshore to offshore deposits. Second are wave- and tide-influenced estuarine-delta bay deposits. Third is delta plain facies association, with sedimentary facies that reflect deposition in both distributary meandering channels (Fig. 7B and Table 1) and infilling of interdistributary bays (Figs. 6C and 7C), the latter with high accumulation of coal, plant cuticles (Fig. 7D) and amber pieces

FIGURE 7 | **Field pictures of the Las Peñosas Fm. A) General view of the new discovered amber-rich deposit in Rábago Section within the Unit P2. B) FA3: Distributary meandering channel with trough cross-bedding, sigmoidal and horizontal stratification and lateral accretion within the Unit P2 in La Florida Section. C) FA3: Interdistributary bay facies within the Unit P2, capped by an erosive transgressive surface (ravinement), and overlain by marine limestones (Unit P3) (Puente Arrudo Section). D) FA3: Exceptionally well-preserved plant cuticle compressions that appear associated with the amber-rich deposit in Rábago Section. E) Detail of FA1 constituted of interbedded mudstones-siltstones with wavy and lenticular lamination and fine-grained sandstones. Unit P2 in Plaza del Monte Section. F) Marly level with high concentration of bivalves at the top of the Unit P3 in Rábago Section.**

(Fig. 6D). Due to the sedimentological and palaeontological importance of this unit, more detailed stratigraphic characteristics and environmental interpretation is provided in the next section.

The Unit P3 superposed the Unit P2 by an erosive transgressive surface (a *ravinement*; Fig. 7C) and in turn is overlain by the Barcenaciones Fm. The thickness of the Unit P3 varies from 13 m to the west (Rábago Section) to 40 m to the east (Plaza del Monte Section; Fig. 5) and is characterized by the stacking of several meter-scale mixed siliciclastic-carbonate sequences. Contrasting with P1, the vertical stacking pattern of P3 presents a progressive increase in the carbonate content toward the top of the unit. This unit is interpreted as a transition from estuarine bay deposits (Fig. 7E) to a shallow carbonate platform system. Thus, a carbonate-siliciclastic mixed platform is proposed. The contact with the overlaying Barcenaciones Fm. is taken at the base of a marly-nodular limestone bed with large bivalves that indicates the definitive abandonment of the siliciclastic system (Fig. 7F).

The amber-rich deposit in the Rábago Section

As noted above, the recently discovered site of amber accumulation is located at the top of Unit P2 in the Rábago Section, where this unit is comprised of three facies associations (Fig. 6 and Table 1).

Facies association 1 (FA 1): wave- and tide-influenced estuarine-delta bay

This facies association consists of heterolithic alternations of thinly bedded dark coloured mudstones, siltstones and sandstones, stacked vertically in meter-scale sequences with a general fining-upward trend. The sequences range in thickness from 3 to 4 m. This facies association displays two sedimentary facies. Facies 1 consists of 5 to 40 cm thick, pale-yellow, very fine- to medium-grained, well-sorted sandstones. The basal contacts are flat and sharp, while the contacts in the top are wavy due to ripples. This facies is characterized by low angle and horizontal lamination, planar cross-stratification, flaser and wavy lamination and wave and current ripples at the tops of the beds. Both current and wave ripples are associated with flaser bedding, and current ripples are seen as climbing in some places. Palaeocurrents have been measured in some crests of the wave ripples resulting in a shoreline direction with an overall E-W trend. Mud drapes occur frequently with thicknesses up to 0.5 cm. Mudclasts and coal fragments appear locally. Bioturbation ranges from sparse to elevated but is consistently characterized by a low diversity assemblage dominated by *Skolithos* and various track traces. Facies 2 consists of beds of mudstone to siltstone. These beds are relatively sulphide-rich and range from 0.5 to 2 m thick, which often combine with facies 1 to form wavy and lenticular bedding (heterolithic facies). Coal and pyritized trunk fragments up to 20 cm long are concentrated at the base of these beds. Minor to moderate bioturbation and sulphide nodules also are present.

The presence of wave and current ripples occurring both as lenticular and flaser bedding, along with the wavy lamination and wave ripples on some sandstone beds, suggests a tidal- and wave-influenced estuarine-delta bay environment (e.g., Reineck and Wunderlich, 1968; Reineck and Singh, 1975; Dalrymple, 1992; Willis, 1997; Kuecher et al., 1990; Folkestad and Satur, 2008). The suite of trace fossils described above may occur in such an environment (Pemberton et al., 1992). The common occurrence of mud drapes and rhythmic bedding of sandstones and mudstones suggests involvement of tidal processes in the formation of this facies (Visser, 1980), but the occurrence of wave-generated structures suggests that reworking also was controlled by waves. The climbing current ripples indicate rapid deposition of sand (Reineck and Singh, 1975). These deposits are interpreted to have originated in the intertidal part of an estuarine-delta bay.

Facies association 2 (FA 2): Delta front distributary mouth-bars

Facies 3 consists of weakly cemented, moderate to well-sorted, fine to coarse-grained sandstone, organized in a coarsening and thickening upwards sequence of about 6 m thick. Sedimentary structures grade vertically from large-scale trough cross-bedding to planar cross-bedding with wave ripples at the top. Mud drapes and mud pebbles are present in foresets. Although preservation at the outcrops prevents detailed sedimentological observations and measurements, in most instances, unidirectional, diffuse palaeocurrent features are observed.

The thickening and coarsening upward trend of this facies association suggests a progradational character. The upward transition from trough cross-bedding to wave ripples at the top suggests decreasing energy conditions. Moreover, the occurrence of mud drapes and mud clasts suggests fluctuating energy conditions likely produced by tidal processes occurring during deposition (Reineck and Singh, 1975; Dalrymple et al., 1990; Shanmugam et al., 2000; Kitazawa, 2007). The presence of wave-ripple lamination also indicates wave influence. As a whole, this facies association is interpreted as a progradation of distributary mouth-bar deposits and sand bars into a wave and tidal influenced estuarine-delta bay.

Facies Association 3 (FA 3): Interdistributary bay

This facies association is composed of a very thin intercalation of silty to very fine sandstones (facies 4) that contain dark organic- and sulphide-rich mudstones (facies 5), ranging in thickness from 0.7 to 2.5 m. Facies 4 is greyish-brown reaching a maximum thickness of 10 cm. It presents wavy and lenticular lamination with current ripples, coal layers (up to 3 cm), sulphide nodules, partially pyritized trunk fragments, minor bioturbation as pyritized burrows, and amber. Facies 5 is mostly composed of layers formed by the accumulation of leaves and other plant remains. These leaves are very well preserved, showing many original details and their venation patterns. When present, the matrix between the plant-bearing levels consists of clay. Also present in this facies are small pyritized moulds of marine gastropods and bivalves, sulphide-nodules (up to 6 cm in size), coal, trunk fragments (up to 15 cm), and abundant pieces of amber. Although amber fragments have been found in all stratigraphic sections, the most abundant yield comes from the Rábago Section, where they consist of both stalactite-shaped and globular or kidney-shaped amber pieces. At the top of this facies association a 5 cm thick crystalline crust appears. The crust surface is colonized by serpulid worm tubes and its genesis remains uncertain. A pale-yellow silty rooting level with associated white mottling occurs in the Plaza del Monte Section at a stratigraphic position laterally equivalent to this crystalline crust.

Dark organic-rich mudstone deposits are interpreted as extensive accumulations of plant remains with a relatively low input of clastic material followed by relatively rapid burial to prevent decomposition (Dalrymple, 1992; Folkestand and Satur, 2008). Mudstones were mostly deposited in interdistributary and coastal bays with a high supply of continental organic matter transported by fluvially associated floods that undoubtedly originated during rainstorm periods. The exceptional preservation of the leaves, along with the presence of pyrite, organic remains, and the low-diversity of fossil traces and benthic fauna, suggest suboxic conditions within the interphase water-sediment. Occasionally, the combined action of spring tides, storms and overbank floods was strong enough to deposit silty and very fine sand layers (Reineck and Singh, 1975; Noe-Nygaard and Surlyk, 1988; Dalrymple, 1992). This inference also is supported by the presence of thin shell remains. The root activity at the top of the infilling sequence implies eventual subaerial conditions, and the development of a horizon exposed to vegetative processes in a palaeosol (McCarthy and Plint, 2003; Folkestand and Satur, 2008). This event is coincident with the maximum regressive stage within the Las Peñosas Fm.

Deposicional sequences and facies model of the amber-bearing deposits

Within the Las Peñosas Fm., amber accumulation occurs principally towards the top of the Unit P2, in dark organic-rich mudstones that deposited in interdistributary bays between meandering distributary channels (i.e., facies association 3; Fig. 8 and Table 1). The vertical stacking of the described facies association of the Unit P2 suggests that it internally displays two smaller transgressive-regressive cycles, with the coal-bearing deposits developing during the regressive phase of the cycles (Fig. 5). These deposits are underlain by shallow marine, siliciclastic and carbonate deposits formed under relatively higher sea-level conditions (Unit P1). The Unit P2 is capped by an erosive transgressive surface (*ravinement*), overlain by full-marine limestones (Fig. 7C). These deposits represent a marked landward shift in the siliciclastic coastal facies, displaying a retrogradational-aggradational stacking pattern (Unit P3). Therefore, deposition of the amber and coal rich levels was coincident with the maximum regressive episode of the estuary-delta progradation (Fig. 5), and represents a relative sea-level fall. The same pattern in coal- and amber-rich deposits has also been described for the Escucha Fm., in the south of the Basque-Cantabrian Basin (Peñacerrada-Montoria outcrops; Martínez- Torres et al., 2003), in the Maestrat Basin (Rodríguez-López et al., 2005), and in the Oliete sub-basin along the San Just outcrop (Peñalver et al., 2007b), both in the Teruel Province. In all these areas amber deposits were related to the progradation of a delta-estuarine system. In Peñacerrada-Montoria, amber accumulated in interdistributary bays within lower delta plain environments (Martínez-Torres et al., 2003), whereas in San Just, amber was deposited in freshwater ponds both within the upper delta plain and in the lower delta plain (Querol et al., 1992). Despite of the similarities between the depositional environments of all the amber-rich deposits of the Lower Cretaceous of Spain, it is worth noting that the depositional environment of the El Soplao amber presents a slight marine influence, as it can be inferred from the presence of some small marine bivalves and gastropods within the amber deposit and bryozoans and serpulids incrusting the surface of some amber samples. In the amber from southwestern France, marine influence has been pointed out as well, but directly evidenced from marine microfossil inclusions like marine diatoms, radiolarians, sponge spicules, and foraminifers (Girard et al., 2008). On the contrary, amber deposits from Lebanon (Azar et al., 2003; Veltz, 2008) and the Isle of Wight (United Kingdom) (Jarzembowski et al., 2008) were accumulated in more proximal delta environments and fluviatile channel deposits with a larger continental influence.

Stratigraphic models for clastic deposition generally suggest that regressive wave-dominated shallow marine systems develop during sea-level falls, whereas tidally

influenced paralic coal-rich deposits develop during the transgressive infilling of incised valleys (e.g., Allen and Posamentier, 1993). The majority of these case studies came from areas with relatively simple tectonic settings and subsidence patterns, such as the Cretaceous of the Western Interior Seaway in North America (Posamentier and Vail, 1988) and Quaternary successions along passive margins (e.g., Allen and Posamentier, 1993). In these studies, the tectonic influence on sequence arrangement is relatively minor and the eustatic fluctuation in sea level is the principal control on stratal succession. In contrast, the Las Peñosas Fm. was deposited in rifting setting during a period of major tectonic rearrangement across the entire Basque-Cantabrian Basin, with active faulting that resulted in uplift and marked subsidence changes over short distances (García-Mondéjar et al., 1996, 2003). It is in this context that local regression occurred with coeval progradation of siliciclastic coastal deposits.

THE AMBER

General characteristics and morphological types

Trees can produce different kind of resins depending on what structural part is noted, such as roots, trunk, branches and leaves (Langenheim, 1995). It has long been known that resins are exuded outside the plant as defence from megaherbivores, insects, and pathogens, such as fungi (especially in the tropics), viruses, other microbes and bacteria. Presently, no methodology is available to differentiate what parts of the tree were involved in the origin of different amber types. Due to the relative abundance of amber at several outcrops, it is generally supposed that the exudation of the original resin occurred mainly in trunks. Our observations of *Agathis australis* in New Zealand subtropical forest suggest that roots were probably significant producers of resin during the past, attributable to copious exudations of root-generated resin.

The new Albian deposit described herein is unusually rich in amber flows of different types formed under aerial conditions by liquid resin (containing flow structure). Normally, these flows are very rich in bioinclusions, especially small insects. The richest flows are stalactite-shaped amber pieces (Figs. 9A-9B). These cylindrical or subcylindrical pieces commonly contain very well preserved bioinclusions in clear yellow amber. The amber flows also include sub-spherical or elongated specimens with a pattern of striations and bulges and apparently an attached scar suggesting a bark pattern. This morphology indicates that the flows

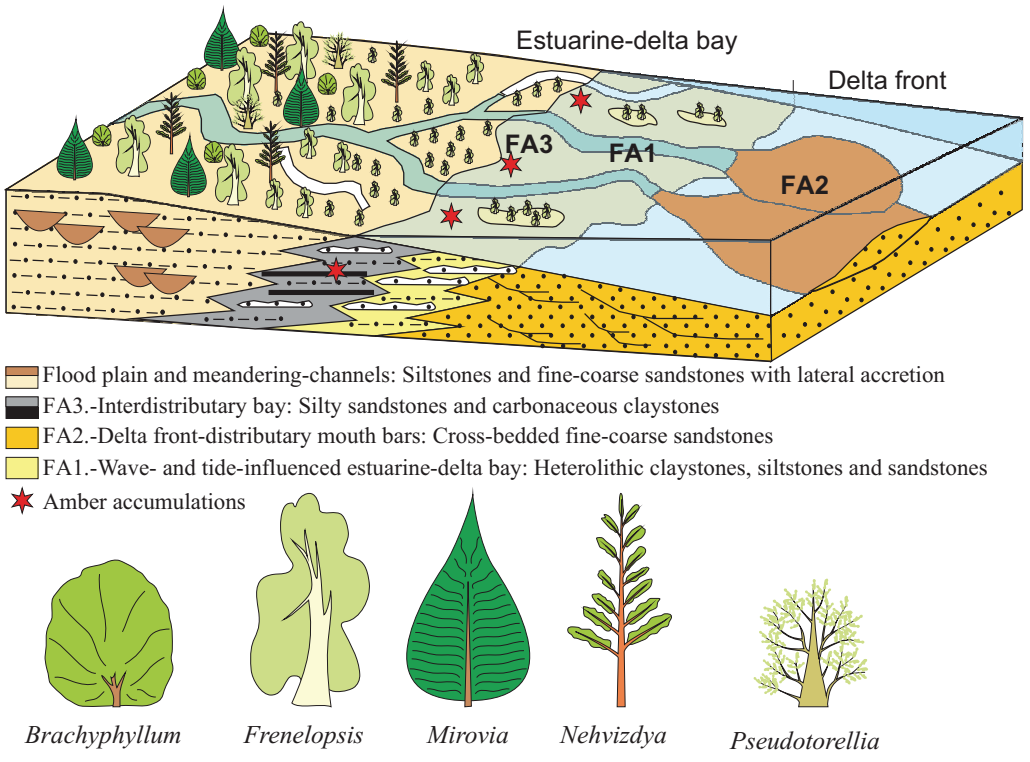

FIGURE 8 | **Block diagram illustrating an idealized model of the depositional environments during sedimentation of the amber- and coal-rich levels. The accumulation of amber- and coal-rich sediments took place during the maximum regressive episode of the estuarine-delta progradation. FA: Facies association.**

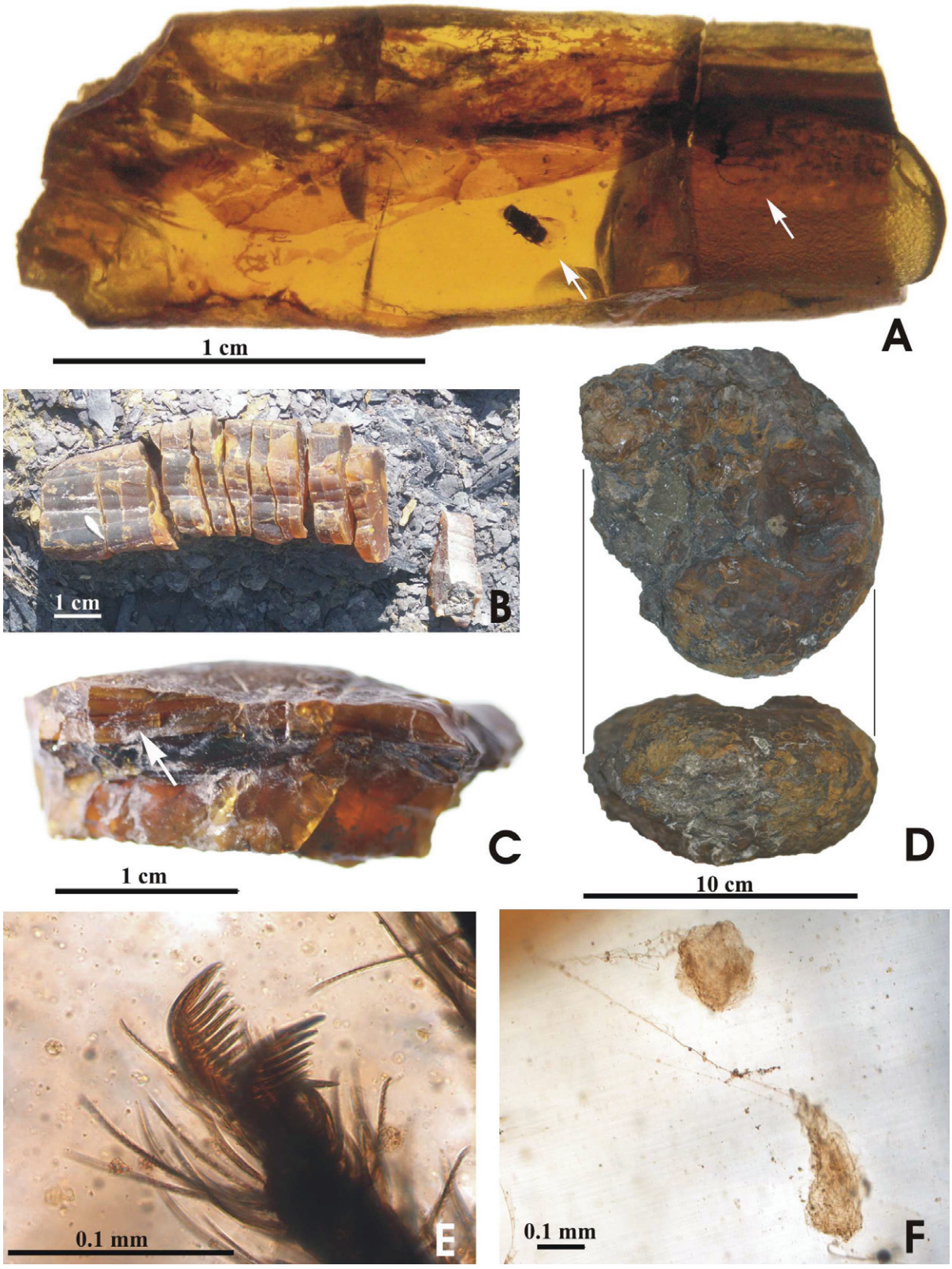

FIGURE 9 | **Different types of amber pieces and amber bioinclusions related to spiders from El Soplao (Rábago, Cantabria). A) Stalactite-shaped amber flow with a wasp of the family Megaspilidae -left arrow- trapped on a spider web fragment (see detail of the spider web in 9F) and two insects shown in figure 12C -right arrow-. B) Stalactite-shaped amber flow exposed in situ which contained a scelionid wasp. C) Amber flow (crust); arrow indicates some flows that originated from liquid resin and cover a copious flow of dark amber. D) Big kidney-shaped mass in two views. E) Pectinate paired claws, adapted to efficient handling of silk and locomotion on an aerial web, present in an Araneoidea spider. F) Detail of the spider web fragment which trapped a megaspilid wasp. Images E and F were made with integrated consecutive pictures taken at successive focal planes.**

originated by viscous resin under aerial conditions. The viscous resin avoided capture of insects and plant debris due to the short time that these structures remained surficially sticky. Other specimens are plain or unelaborated in shape with several layers accumulating by different flows by less viscous resin with marks indicating aerial conditions (Fig. 9C). This last type usually contains abundant bioinclusions.

A different type are the kidney-shaped masses, normally very large in size (up to a decimetre in diameter) with an external surface slightly granulose that lacks evidence of aerial exposure (Fig. 9D). Some authors consider that this type of mass had formed by subterranean resin secretion from roots, probably explaining their lack of bioinclusions. These amber masses also are abundant in the El Soplao outcrop.

Of gemmological interest, abundant blue amber pieces (Fig. 6D) were found, similar to the noted blue amber from the Dominican Republic (Bellani et al., 2005). Both are the only well-known occurrences of this type of amber. A fluorescent blue glow appears in these pieces under normal sunlight, and under ultraviolet light it glows a bright milky-blue. In contrast, under artificial light these fragments show the typical honey-reddish colour of the Cretaceous amber.

Geochemistry

The Fourier Transform Infrared Spectroscopy (FTIR) is a solid-state spectroscopic technique usually used to characterize ambers (Langenheim and Beck, 1965). Nevertheless, the majority of fossil resins of the same geological range often show similar patterns preventing objective classification. Gas Chromatography-Mass Spectrometry (GC-MS) determines the individual non-volatile amber compounds and their molecular structure, and also suggests the plant producer (Grimalt et al., 1988; Chaler and Grimalt, 2005). Previous GC-MS studies on Cretaceous amber from Álava (southern Basque-Cantabrian Basin) indicate that some isolated compounds found may have originated from agathic acid, suggesting that the genus *Agathis*, or a close genus of Araucariaceae (Coniferales), was the amber producer (Alonso et al., 2000; Chaler and Grimalt, 2005). The palynological study supported this indication, because it revealed that a high percentage of pollen grains related to Araucariaceae (Barrón et al., 2001). Nevertheless, currently no araucariacean meso- or macro-remains have been found within the Álava amber or in the surrounding rock.

Here, we compare the FTIR of recent *Agathis australis* resin and amber samples from El Soplao (Fig. 10). The *Agathis* resin is a mixture of mono-, sesqui- and diterpenes, and each of its 13 species has a characteristic mixture of diterpenoid acids. Today this araucariacean genus produces large quantities of resin under natural conditions which polymerize rapidly, forming indurated masses. Recent studies from the Álava amber (Chaler and Grimalt, 2005) indicate that all samples show branched monoalkybenzenes, bicyclic sesquiterpenoids and tricyclic diterpenoids related to pimaric acid precursors, suggesting a distinctive palaeobotanic origin from *Agathis*-like species.

Three amber samples were analysed from the El Soplao amber: i) a fragment of a stalactite-like amber piece from an organic-rich clay level (AMB82); ii) a fragment of large kidney-shaped mass, red in colour, found in an organic-rich sand layer (AMB80), and iii) a fragment of orange kidney-shaped mass from an organic-rich clay level (AMB81). A fragment of stalactite-shaped dry resin from *Agathis australis* also was analysed for comparison (AMB83). The FTIR spectra obtained are shown in Fig. 10.

Structural changes in the organic components of the amber samples are due to maturation processes during rock diagenesis. In the evaluation of the maturity of the coal and organic matter from the Escucha Fm. and other Early Cretaceous Spanish basins, such as the Maestrat Basin and the Basque-Cantabrian Basin, the thermal analysis based on the vitrinite reflectance (%R) suggests around 52ºC as maximum temperature from modelling (Sangüesa and Arostegui, 2003; Permanyer, pers. comm.) The FTIR analyses (transmittance and absorbance) of the amber pieces of El Soplao show that all three spectra are practically identical. The IR spectra of all samples exhibited the same bands, but with different intensities (Fig. 10). In absorbance, all spectra show similar relative intensity, but in the sample AMB80, which corresponds to a red amber fragment, the intensity decreases at wave-numbers 727 and 814 cm^{-1}, and increases considerably at approximately wave-number group 1714 cm^{-1}, a complex band associated with carboxyl groups (Fig. 10). In this sample we also observe broad absorption bands at ca. 3460 and 1635 cm^{-1}, the signal due to water or possibly to weathering. The spectra coincide in the major features with the previous results obtained from other Spanish Cretaceous ambers (see FTIR spectra in Alonso et al., 2000; Chaler and Grimalt, 2005; Peñalver et al., 2007a, 2007b; Corchón et al., 2008). All the spectra are dominated by small C-H stretching bands near 2950 cm^{-1}, C-H banding occurs between 1470 and 1380 cm^{-1}, and the carbonyl bands are close to 1700 cm^{-1}. The lack of exocyclic methylenic bands at 880, 1640 and 3070 cm^{-1} is consistent with the high maturity of the amber.

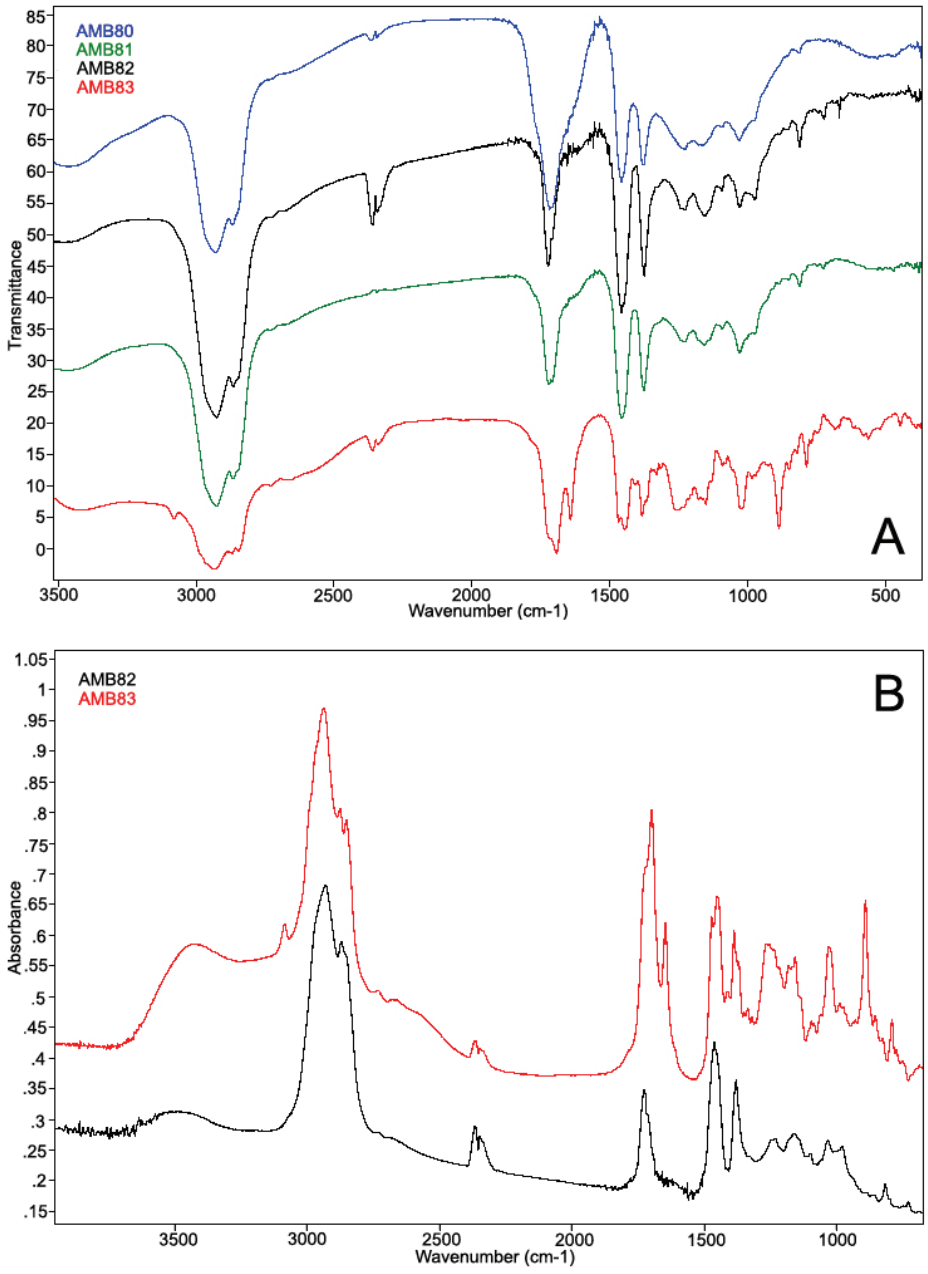

FIGURE 10 | **A) Transmittance IR spectra of El Soplao amber: AMB80 red amber from a kidney-shaped mass found within sands; AMB81 orange amber from a kidney-shaped mass found within clays; AMB82 orange amber from a stalactite-shaped flow, found within clays; and AMB83 dry resin from an *Agathis australis* stalactite-like flow, New Zealand in origin. B) IR absorbance spectra from the El Soplao amber and dry resin of *Agathis australis*, both samples analysed came from stalactite-shaped flows.**

When the IR absorbance spectra is compared between the amber sample AMB82, an aerial stalactite, and the sample AMB83, a fragment of recent stalactite of the araucariacean *Agathis australis* (Fig. 10), numerous differences may be observed. However, without GC-MS studies, the origin of the variable intensity and the presence of several bands cannot be possibly known. The presence of the absorption maximum in the single-band around 3081 cm^{-1} is typical in *Agathis* resin; however, it is typically absent in amber due to the polymerization of the resin and increasing maturity. In addition, the spectra around range bands 1650-1700 cm^{-1}, corresponding to the carboxyl groups, is very different between the amber and the resin. The intensity of absorption at wave-numbers 3400 and 1700 cm^{-1} decreases according to an increase in the maturity level of the samples. Other bands observed constitute an unresolved group near wave number 2930 cm^{-1} (C-H st), the most intense group band known for all Cretaceous spectra.

FOSSIL RECORD

Plant cuticle compressions

Exceptionally well preserved plant cuticle compressions are very abundant in the El Soplao amber deposit (Fig. 11), sometimes accumulating in levels up to 10 cm thick. The palaeobotanical samples taken from these levels also show amber and woody fragments, but at less percentage than plant-cuticle compressions (Figs. 11A-11D). Amber pieces show various shapes and colours from yellow to red (Fig. 11A), whereas unidentified, small, dark, woody fragments are preserved as spheroidal, charcoalified masses or charcoals (Fig. 11B). Cuticle fragments of the conifer *Frenelopsis*, of the extinct family Cheirolepidiaceae (Gomez et al., 2002), are the most numerous plant-cuticle components (Fig. 11C). These coniferous axes typically constitute cylindrical internodes bearing apically a nodal whorl of three leaves (Fig. 11E). Some *Frenelopsis* sp. cuticles also show a particular branching of axes borne in the internode (Fig. 11F) (see Daviero et al., 2001 for architectural details). A female cone scale formed by several layers of very thin cuticle (Fig. 11P) constitutes a doubtful record of the genus *Alvinia* Kvaček (Kvaček, 2000), associated with *Frenelopsis* vegetative material. Additionally, the conifer *Mirovia* sp. of the extinct family Miroviaceae (Gomez, 2002) shows about the same quantity of leaf cuticle fragments (Fig. 11D). The leaves clearly display a white central line on one side corresponding to the single middle stomatal-bearing groove, as well as a mucronate apex and suction-pad-shaped base (Figs. 11G-11H). Such leaves have been also described from the Albian of Pyrenees (Corça) and Teruel (Rubielos de Mora) (Gomez, 2002). Also present are two conifer leafy axes of *Brachyphyllum*-type with tiny, helicoidally arranged leaves (Figs. 11L-11M). In addition, two types of ginkgolean leaves also occur. *Nehvizdya* sp. shows obovate leaves with variable apex shapes (Fig. 11I) and attenuate base (Fig. 11J) (Gomez et al., 2000). The venation pattern showing several successive dichotomies and the presence of resin bodies between the veins are clearly seen in the most transparent leaves. In Spain, *Nehvizdya penalveri* has been reported only from the Albian of Rubielos de Mora in Teruel (Gomez et al., 2000). Other ginkgolean leaves are represented by *Pseudotorellia* sp. It has narrow leaves with three stomatal bands located on one side (Fig. 11K). This genus has also been described from the Albian of Rubielos de Mora in Teruel (Gomez, 2000). In addition, it has distinctive reproductive organs similar to the genus *Nehvizdyella* Kvaček (Kvaček et al., 2005), which probably are ovules associated with *Nehvizdya* (Figs. 11N-11O).

Arthropod inclusions

Until now, the arthropods found as inclusions in the El Soplao amber have been spiders and insects. All specimens are small in size, less than 1 cm long, and are well preserved, possessing slight deformation due to pressure. Apparently, the degree of maturation of the amber is slightly higher than the San Just and Álava ambers, because the external surface of the insects is dark, without a silvery gaseous film. That film produces silver-hued reflections under strong direct illumination and makes the appreciation of microsculptural details easier. Formal taxonomy of the new taxa of arthropods will be published elsewhere, principally by Paul Selden and one of us during the completion of a Doctoral Thesis (R.P.F.). Thus, only a brief overview of the most important specimens is presented below.

One of the most remarkable finds is a virtually complete spider specimen. The excellent preservation of the legs shows detailed structure of the tarsal claws (Fig. 9E). The tarsi have large, pectinate paired claws with one row of nine teeth and one small, non-pectinate median claw and numerous serrate bristles, similar to the Araneoidea specimen described by Selden (1989) from the Early Cretaceous limestones of El Montsec (Lleida Province, northeastern Spain). Subsequently, the Montsec specimen was described as *Cretaraneus vilaltae* by Selden (1990) and assigned to the orb-weaver family Tetragnathidae by Selden and Penney (2003). The characteristic claw morphology is structured for an efficient handling of silk and locomotion on an aerial web. Peñalver et al. (2006) published the oldest web with entrapped preys, most likely an orb web, from San Just amber. Penney and Ortuño (2006) described a spider from Álava amber, which displays three tarsal claws and accessory setae, as the oldest true orb-weaving spider, but without illustration and more detailed description of this crucial structure. Also, from the El Soplao amber, a portion of an aerial spider web was found (Fig. 9F), which trapped a small wasp of the family Megaspilidae. This new spider web has a different structure than the specimen from San Just amber. Both the spider specimen and aerial web found in the El Soplao amber shed light on and support the role of aerial webs in the palaeoecology of Cretaceous forests discussed by Peñalver et al. (2006, 2008).

The insect orders found to date in this new site also are the most abundant in other Cretaceous deposits (Fig. 12). These co-occurring orders are Thysanoptera (Fig. 12A), Hymenoptera (Fig. 12B), Blattaria (Fig. 12D), Hemiptera, Coleoptera, and Diptera; the last two are especially plentiful (Figs. 12C-12D). Raphidioptera and Neuroptera have a scarce record in El Soplao as is common in Cretaceous ambers.

Hymenopterans were represented previously by the families Scelionidae (Figs. 12B and 12D), Mymarommatidae, and Megaspilidae (Fig. 9A). The extinct family

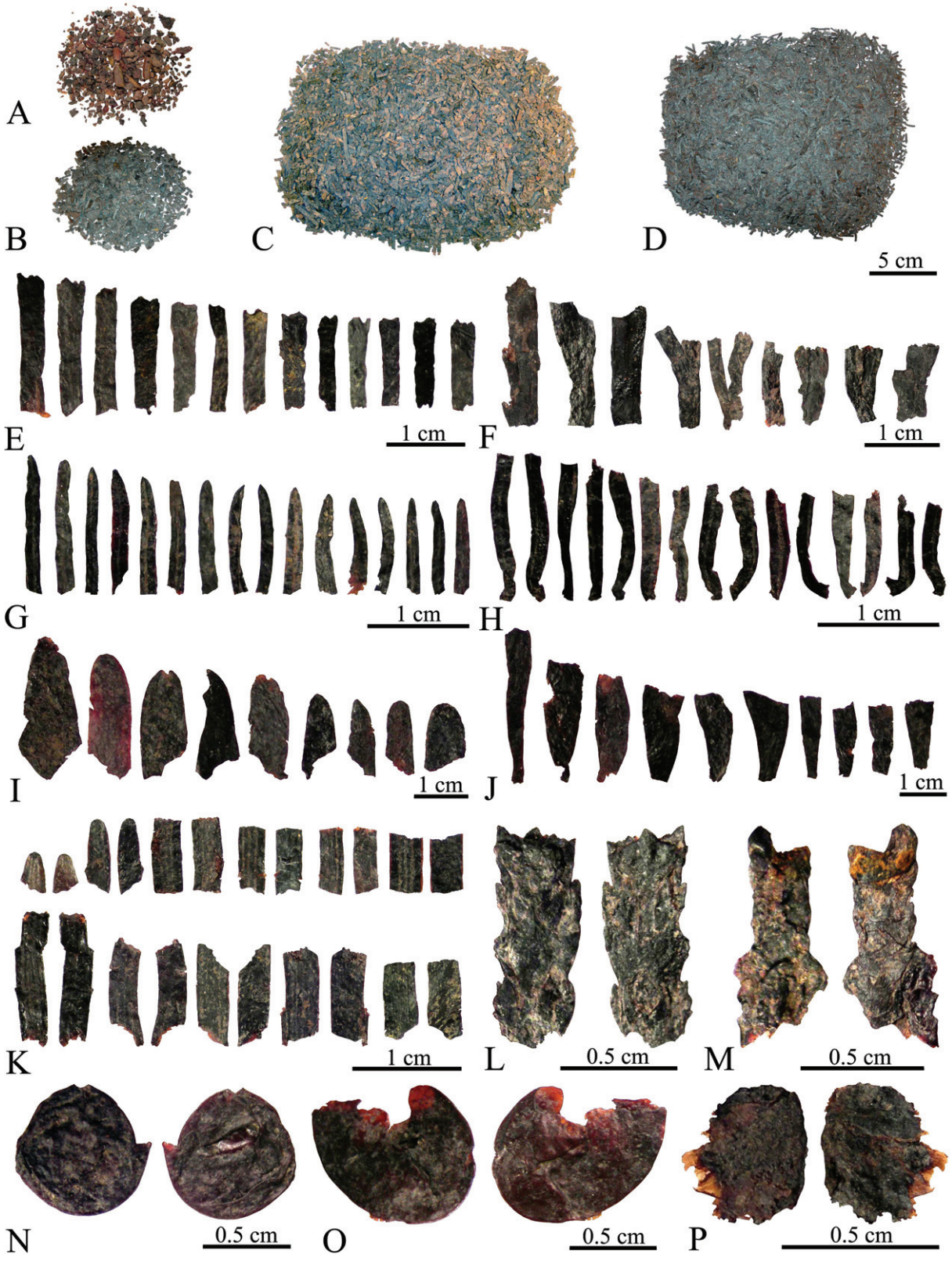

FIGURE 11 | **A, D) Four major palaeobotanical components sorted out from a sediment sample (all to the same scale). A) Yellow to red amber pieces. B) Wood fragments. C) *Frenelopsis* sp. cuticles. D) *Mirovia* sp. cuticles. E, F) Internodes of *Frenelopsis* sp. E) Apical nodal whorl of three leaves. F) Intra-internodal branching of axes. G, H) Leaves of *Mirovia* sp. G) A single middle stomatal groove and a mucronate apex. H) Suction-pad-shaped base. I, J) Leaves of *Nehvizdya* sp. I) Variable shapes of apices. J) Attenuate bases. K) Leaves of *Pseudotorellia* sp., showing two apices and three or more stomatal bands on one side of the leaves. L, M) Two *Brachyphyllum*-type leafy axes, showing small, helicoidally arranged leaves. N, O) Ovules of cf. *Nehvizdyella* sp., P) cf. *Alvinia* sp., a multilayered female cone scale of *Frenelopsis* sp.**

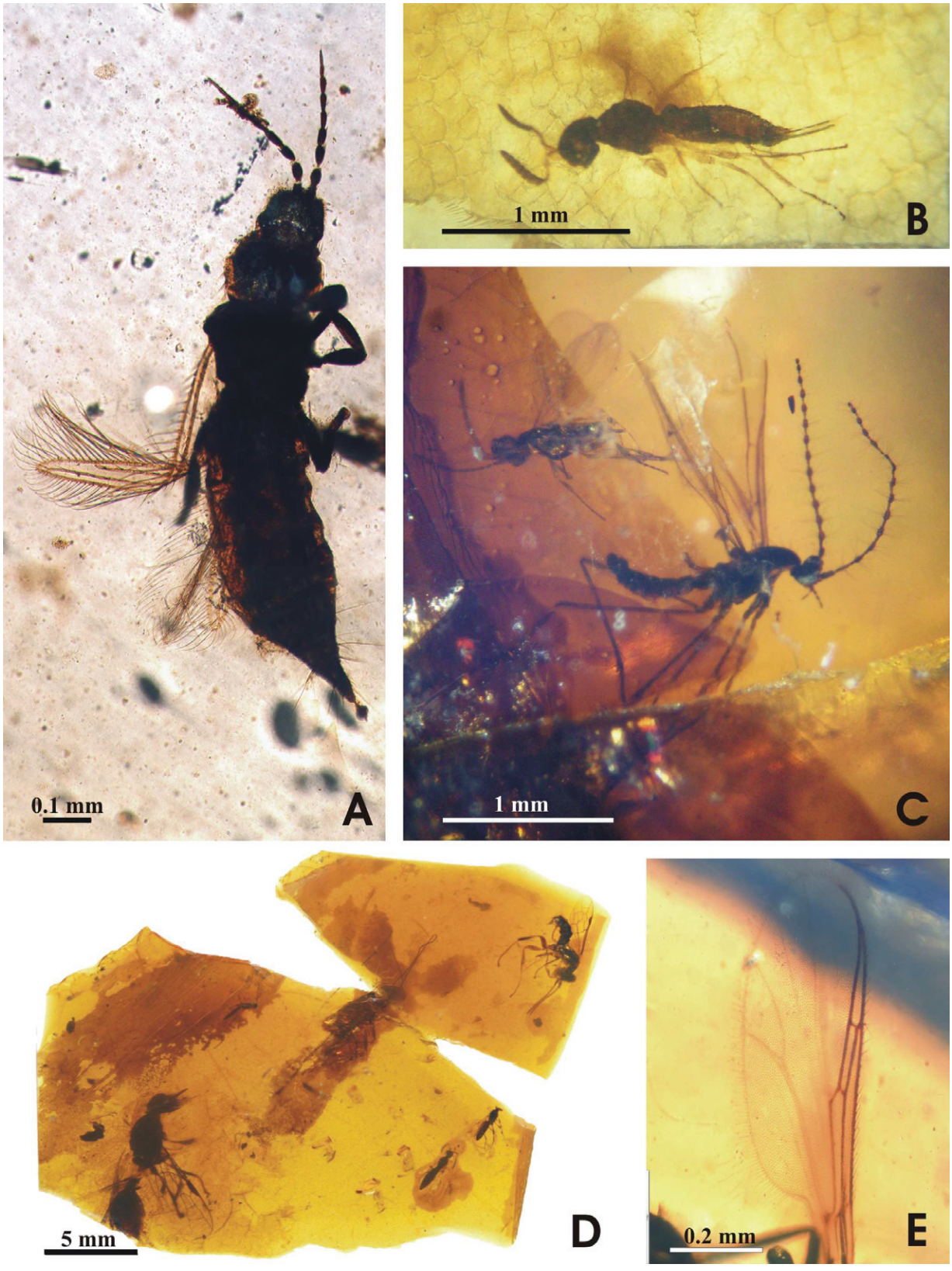

FIGURE 12 | **Fossil insects as bioinclusions in El Soplao amber. A) Thysanopteran specimen. B) Female wasp of the family Scelionidae. C) Chalcidoidean wasp -top- and dipteran of the family Cecidomyiidae (gall midges). D) Amber fragment with seven wasps and one immature cockroach in the centre of the preparation. E) Wing of *Archiaustroconops* sp. Images A and E were made with integrated consecutive pictures taken at successive focal planes.**

Mymarommatidae, or false fairy wasps, are among the smallest of Hymenoptera and constitute a very important record for the El Soplao amber, represented by a complete winged female of a new morphotype of the extinct genus *Archaeromma*. The family includes only five genera, three extant and two extinct genera (Gibson et al., 2007). The fossil record of this family is very scarce and is only preserved in amber. The genus *Archaeromma* contains eight species (Gibson et al., 2007; Engel and Grimaldi, 2007). This group of minute wasps is characterized by having a head capsule with a hyperoccipital band of pleated membrane separating the frontal plate from the flat occipital plate; an occipital foramen originating at ventral margin of occipital plate; mandibles exodont; female antennae with 6 or 7 funicular segments and 3 or 4 larger distal segments which form a compact tube; and other characters (Gibson et al., 2007). Due to their small size and unusual morphological characters, they are suspected egg parasitoids. The new record from the El Soplao amber is the oldest for this genus.

Among the most interesting insect records in the El Soplao amber are biting midges (Diptera: Ceratopogonidae). The genus *Archiaustroconops*, of the subfamily Austroconopinae, is the only Cretaceous Ceratopogonidae with two well-developed radial cells, an oblique r-m vein (Fig. 12E), and a foreleg/hindleg tarsal ratio ≥ 1.4 (Borkent, 2000). The genus includes six species known only from Lower Cretaceous Lebanese and Álava ambers (Borkent, 2000). It is represented in the El Soplao amber by one new morphotype (Fig. 12E), clearly different from *A. alavensis* found in Álava amber. This new morphotype is characterized by having a strongly elongate first radial cell. Most interesting is the presence of a new taxon of the rare genus *Lebanoculicoides* (Fig. 13), which is only known by two specimens described as *L. mesozoicus* from Lebanese amber (Szadziewski, 1996). This genus is the only member of the Ceratopogonidae having a wing with fully developed R1, R3 and R4+5 veins. This character, among others, indicates that *L. mesozoicus* is the sister group of all other Ceratopogonidae and for that reason it had been included in its own subfamily, named Lebanoculicoidinae by Borkent (2000). The new morphotype differs mainly from the other known species by having ovoidal flagellomeres (not cylindrical) and R4+5 vein terminating in a basal position before reaching the wing apex.

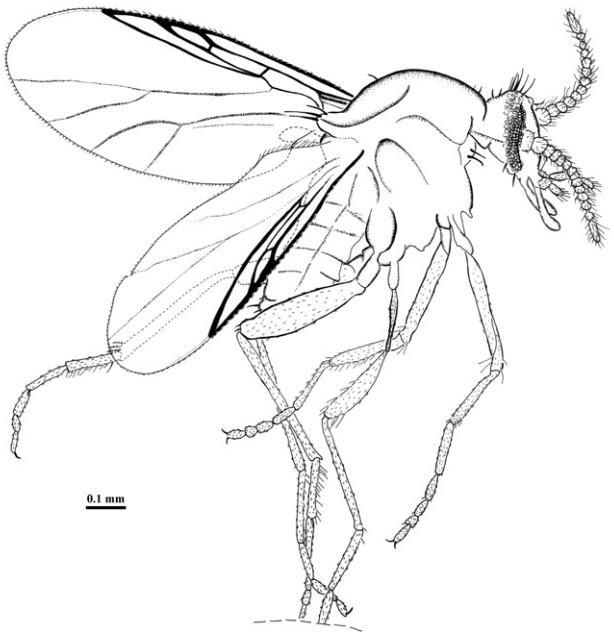

FIGURE 13 | **Camera lucida drawing of *Lebanoculicoides* sp. (Ceratopogonidae: Lebanoculicoidinae) in lateral habitus, from the El Soplao amber.**

DISCUSSION AND CONCLUDING REMARKS

Stratigraphic and sedimentologic analyses of the amber-bearing deposit of the Lower Albian Las Peñosas Fm. indicate that it was deposited on a regressive deltaic-estuarine environment. Facies associations are assigned to three different depositional units (P1 to P3). The stacking of these units and their internal vertical and lateral relationships resulted from an overall marine regressive phase followed by a transgressive marine phase, with the resin accumulation occurring at the most regressive part of the regressive-transgressive sequence (Unit P2). Sedimentological analysis of this unit suggests that the amber deposit constitutes part of the infilling of interdistributary bays, which are laterally associated with distributary meandering channels. The amber-rich beds always contain abundant fragments of carbonaceous material, wood fragments and leaves that still preserve the vegetal textures. The amber-rich beds appear associated with laminated, organic clays, but also with discontinuous beds of massive to laminated sandstones and siltstones with disorganized fragments of woody material. These deposits also contain shells of marine and/or brackish-water molluscs, which suggest a littoral to coastal marsh environment of deposition. Therefore, the suggested depositional scenario for the amber-rich beds is an environment of low-energy coastal and interdistributary bays connected with the sea and affected episodically by higher-energy conditions. Floods during rainstorms eroded and removed the amber and plant remains from their original place of accumulation at the soils of the coast-fringing forest. Then, the amber and plant fragments were transported by density flows that carried large amounts of these materials, mixed with mud and sand, to the coastal and interdistributary bays, where were rapidly accumulated and buried. Most

of the amber pieces show their original form of subrounded and stalactite-shape suggesting little erosion during transport. A remarkable characteristic of this amber deposit is the unusual accumulation of aerial amber pieces that contain abundant arthropod and other bioinclusions.

The El Soplao deposit likely originated during a period of abundant production of fluid resin within the palaeoforests, possibly coinciding with a warmer episode. The plant-cuticle assemblage of the El Soplao deposit is quite reminiscent of that from the Albian of Rubielos de Mora (Teruel Province); (Gomez, 2000, 2002; Gomez et al., 2000, 2002). However, the latter deposit has poorly preserved amber and identification at the species level is tenuous, lacking the precision for any determination of amber production. Araucariacean trees are the suggested resin-producing plants during the Cretaceous (Alonso et al., 2000; Chaler and Grimalt, 2005), but leaf remains of this group of conifers are absent from the El Soplao assemblage, although they occur in other similar Spanish deposits. Future palynological studies will complete our understanding of the palaeobotanical context of this deposit.

The abundance of fossil insects in the Early Cretaceous amber of El Soplao is particularly important for further evolutionary studies and palaeoecological reconstructions. This abundance is a consequence of the unusual concentration of amber flows (stalactite-like amber flow pieces and crusts), which contain the most bioinclusions. The fidelity of the arthropod preservation in this amber allows for detailed studies of the ancient forest biota, similar to other Spanish ambers. The Albian age of the El Soplao amber also is of particular importance because during this period certain groups of insects were diversifying to become major pollinators of the first flowering plants. In this context, the presence of spiders and their entrapping aerial webs in El Soplao amber reinforces the hypothesis advocated by Peñalver et al. (2006, 2008) which associates the diversification of spiders to the radiation of winged (pterygote) insects.

Several insect specimens recorded from the El Soplao amber are very scarce in the fossil record, for instance wasps and dipterans. Such is the case for the wasp specimen that belongs to the extinct family Mymarommatidae. Discovery of a new form of the rare dipteran *Lebanoculicoides* in the El Soplao amber indicates that this basal genus had a much more extensive distribution than previously supposed during the Early Cretaceous. Consequently, any new findings of fossil representatives of these groups would be of particular interest.

The FTIR spectra of the El Soplao amber are quite similar to other previously studied Spanish Cretaceous ambers. However, further investigations are necessary to complete the study of this new locality, including the taphonomic study of the deposit in order to know its origin, the palynological analysis of the amber-bearing stratigraphic sequence, determination of plant species represented as cuticles, and the taxonomic study of the arthropods included within the amber.

ACKNOWLEDGMENTS

This work is part of the Ph.D. Thesis of the first author (M.N.), who is supported by a scholarship from the Instituto Geológico y Minero de España (IGME), and the Ph.D. Thesis of a co-author (R.P.F., palaeobiology), funded by an APIF grant of the University of Barcelona. This study is a contribution of the IGME projects 275-CANOA 35006 "Relación entre sedimentación tectónica y flujo de fluidos durante la extensión del Cretácico Inferior en la Cuenca de Santander"; 491-CANOA 35015 "Investigación científica y técnica de la Cueva de El Soplao y su entorno geológico", and the projects CGL2008-00550/BTE and CGL2008-01237/BTE. The study is framed in a collaborative agreement among IGME, SIEC S.A. and the Cantabrian Government (Regional Cultural, Tourism and Sports Ministry). We are grateful to José Pedro Calvo Sorando (IGME) for his support and engagement. We also express our thanks to Francisco Javier López Marcano (Regional Minister of the Cantabrian Government) and Fermin Unzué (manager of the El Soplao Cave) for their efforts and promotion of the study of the new outcrop. One of the coauthors (E.P.) benefited from a "Ramón y Cajal" contract of the Spanish Ministry of Science and Innovation. B.G. also received support from the CNRS-UMR 5125 PEPS and the project ANR AMBRACE (No BLAN07-1-184190) of the French National Research Agency (L'Agence Nationale de la Recherche). The authors thank the editor for his patient and constructive reviews and Cynthia Voelker for the final review of the English writing. The manuscript benefited greatly from corrections and improvements by C. Labandeira and R. Salas.

REFERENCES

Allen, G.P., Posamentier, H.W., 1993. Sequence stratigraphy and facies model of an incised valley fill: the Gironde Estuary, France. Journal of Sedimentary Petrology, 63, 378-391.

Alonso, J., Arillo, A., Barrón, E., Corral, J.C., Grimalt, J., López, J.F., López, R., Martínez-Delclòs, X., Ortuño, V., Peñalver, E., Trincão, P.R., 2000. A new fossil resin with biological inclusions in Lower Cretaceous deposits from Álava (Northern Spain, Basque-Cantabrian Basin). Journal of Paleontology, 74, 158-178.

Arbizu, M., Bernárdez, E., Peñalver, E., Prieto, M.A., 1999. El ámbar de Asturias (España). Estudios del Museo de Ciencias Naturales de Álava, 14, 245-254.

Azar, D., 2000. Les Ambres Mésozoiques du Liban. Doctoral thesis. Paris, Université Paris XI Orsay, 165 pp.

Azar, D., Nel, A., Gèze. R., 2003. Use of Lebanese amber bioinclusions in paleoenvironmental reconstruction, dating and paleobiogeography. Acta Zoologica Cracoviensia, 46, 393-398.

Bandel, K., Shinaq, R., Weitschat, W., 1997. First insect inclusions from the amber of Jordan (Mid Cretaceous). Mitteilungen des Geologisch-Paläontologischen Institutes der Universität Hamburg, 80, 213-223.

Barrón, E., Comas-Rengifo, M.J., Elorza, L., 2001. Contribuciones al estudio palinológico del Cretácico Inferior de la Cuenca Vasco-Cantábrica: los afloramientos ambarígenos de Peñacerrada (España). Coloquios de Paleontología, 52, 135-156.

Bellani, V., Giulotto, E., Linati, L., Sacchi, D., 2005. Origin of the blue fluorescence in Dominican amber. Journal of Applied Physics, 97(1), 016101-1 - 016101-2.

Blakey, R.C., 2008. Global Paleogeographic Views of Earth History: Late Precambrian to Recent. http://jan.ucc.nau.edu/~rcb7/105moll.jpg.

Borkent, A., 2000. Biting midges (Ceratopogonidae: Diptera) from Lower Cretaceous Lebanese amber with a discussion of the diversity and patterns found in other ambers, In: Grimaldi, D. (eds.). Studies on Fossils in Amber, with Particular Reference to the Cretaceous of New Jersey. Leiden (The Netherlands), Backhuys Publishers, 355-451.

Chaler, R., Grimalt, J., 2005. Fingerprinting of Cretaceous Higher Plant Resins by Infrared Spectroscopy and Gas Chromatography Coupled to Mass Spectrometry. Phytochemical Analysis, 16, 446-450.

Corchón, M.S., Mateos, A., Álvarez-Fernández, E., Peñalver, E., Delclòs, X., Van der Made, J., 2008. Ressources complémentaires et mobilité dans le Magdalénien cantabrique. Nouvelles données sur les mammifères marins, les crustacés, les mollusques et les roches organogènes de la Grotte de Las Caldas (Asturies, Espagne). L'Anthropologie, 112, 284-327.

Crowley, T.J., North, G.R., 1991. Distribution of climatically sensitive deposits for the Mid-Cretaceous (Aptian-Albian-Cenomanian, 120-90 Ma.). Paleoclimatology-Oxford Monographs on Geology and Geophysics ed. Oxford University Press, 18, 157 pp.

Cruickshank, R.D., Ko, K., 2003. Geology of an amber locality in the Hukawng Valley, northern Myanmar. Journal of Asian Earth Sciences, 21, 441-455.

Dalrymple, R.W., 1992. Tidal depositional systems. In: Walker, R.G., James, N.P. (eds.). Facies Models: Response to Sea Level Change. Geological Association of Canada, 195-218.

Dalrymple, R.W., Knight, R.J., Zaitlin, B.A., Middleton, G.V., 1990. Dynamics and facies model of a macrotidal sandbar complex, Cobequid Bay- Salmon river estuary (Bay of Fundy). Sedimentology, 37, 577-612.

Daviero, V., Gomez, B., Philippe, M., 2001. Uncommon branching pattern within conifers: *Frenelopsis turolensis*, a Spanish Lower Cretaceous Cheirolepidiaceae. Canadian Journal of Botany, 79, 1400-1408.

Delclòs, X., Arillo, A., Peñalver, E., Barrón, E., Soriano, C., López del Valle, R., Bernárdez, E., Corral, C., Ortuño, V.M., 2007. Fossiliferous amber deposits from the Cretaceous (Albian) of Spain. Comptes Rendus Palevol, 6, 135-149.

Engel, M.S., Grimaldi, D., 2007. New false fairy wasps in Cretaceous amber from New Jersey and Myanmar (Hymenoptera: Mymarommatoidea). Transactions of the Kansas Academy of Sciences, 110, 159-168.

Fernández Viejo, G., Gallastegui, J., 2005. The ESCI-N Project after a decade: a synthesis of the results and open questions. Trabajos de Geología, Universidad de Oviedo, 25, 9-25.

Folkestad, A., Satur, N., 2008. Regressive and transgressive cycles in a rift-basin: Depositional model and sedimentary partitioning of the Middle Jurassic Hugin Formation, southern Viking Graben, North Sea. Sedimentary Geology, 207, 1-21.

García-Espina, R., 1997. La estructura y evolución tectonoestratigráfica del borde occidental de la Cuenca Vasco-Cantábrica (Cordillera Cantábrica, NO de España). Doctoral thesis. Universidad de Oviedo, 230 pp.

García-Mondéjar, J., 1990. The Aptian-Albian carbonate episode of the Basque-Cantabrian Basin (northern Spain): General characteristics, controls and evolution. International Association of Sedimentologists, 9, 257-290.

García-Mondéjar, J., Aguirrezabala, L.M., Aranburu, A., Fernández-Mendiola, P.A., Gómez-Pérez, I., López-Horgue, M., Rosales, I., 1996. Aptian-Albian tectonic pattern of the Basque-Cantabrian Basin (northern Spain). Geological Journal, 31, 13-45.

García-Mondéjar, J., López-Horgue, M.A., Aramburu, A., Fernández-Mendiola, P.A., 2003. Pulsating subsidence during a rift episode: stratigraphic and tectonic consequences (Aptian-Albian, northern Spain). Terra Nova, 17, 517-525.

García-Mondéjar, J., Pujalte, V., 1982. Región Vasco-Cantábrica y Pirineo Navarro. In: Universidad Complutense de Madrid (eds.). El Cretácico de España. Universidad Complutense de Madrid, 49-159.

Gibbs, A.D., 1990. Linked fault families in basin formation. Journal of Structural Geology, 12, 796-803.

Gibson, G.A., Read, J., Huber, J.T., 2007. Diversity, Classification and Higher Relationships of Mymarommatoidea (Hymenoptera). Journal of Hymenoptera Research, 16, 51-146.

Girard, V., 2008. Microcenoses des ambres medio - Crétacés français. Taphonomie, systématique, paléoécologie et reconstitution du paléoenvironnement. Doctoral thesis. Université Rennes, 310 pp.

Girard, V., Schmidt, A.R., Saint Martin, S., Struwe, S., Perrichot, V., Saint Martin, J.P., Grosheny, D., Breton, G., Néraudeau, D., 2008. Evidence for marine microfossils from amber. Proceedings of the National Academy of Sciences, 105, 17426-17429.

Gomez, B., 2000. Paléoenvironnements de la marge occidentale de la Téthys au Crétacé inférieur; apports taxonomiques et taphonomiques de gisements espagnols. Doctoral thesis. University Claude Bernard Lyon, 218 pp.

Gomez, B., 2002. A new species of *Mirovia* (Coniferales, Miroviaceae) from the Lower Cretaceous of the Iberian Ranges (Spain). Cretaceous Research, 23, 761-773.

Gomez, B., Martín-Closas, C., Barale, G., Solé de Porta, N., Thévenard, F., Guignard, G., 2002. *Frenelopsis* (Coniferales: Cheirolepidiaceae) and related male organ genera from the Lower Cretaceous of Spain. Palaeontology, 45, 997-1036.

Gomez, B., Martín-Closas, C., Barale, G., Thévenard, F., 2000. A new species of *Nehvizdya* (Ginkgoales) from the Lower Cretaceous of the Iberian Ranges (Spain). Review of Palaeobotany and Palynology, 111, 49-70.

Gradstein, F.M., 2004. A Geologic Time Scale 2004. Cambrige University Press.

Greenblatt, C.L., Davis, A., Clement, B.G., Kitts, C.L., Cox, T., Cano, R.J., 1999. Diversity of microorganisms isolated from amber. Microbial ecology, 38, 58-68.

Grimalt, J., Simoneit, B.R.T., Hatcher, P.G., Nissenbaum, A., 1988. The molecular composition of ambers. Organic Geochemistry, 13, 677-690.

Haywood, A.M., Valdes, P.J., Markwick, P.J., 2004. Cretaceous (Wealden) climates: a modelling perspectiva. Cretaceous Research, 25(3), 303-311.

Hines, F.M., 1985. Sedimentation and tectonics in north-west Santander. In: Milá, M.D., Rosell, J. (eds.). 6th European Regional Meeting, Excursion Guidebook. International Association of Sedimentologists, 371-398.

Huber, B.T., Hodell, D.A., Hamilton, C.P., 1995. Middle-Late Cretaceous climate of the southern high latitudes; stable isotopic evidence for minimal equator-to-pole thermal gradients. Geological Society of American Bulletin, 107, 1164-1191.

Jarzembowski, E.A., Azar, D., Nel, A., 2008. A new chironomid (Insecta: Diptera) from Wealden amber (Lower Cretaceous) of the Isle of Wight (UK). Geologica Acta, 6, 285-291.

Kaddumi, H.F., 2005. Amber of Jordan: the Oldest Prehistoric Insects in Fossilized Resin. Published by the author, Amman, 168 pp.

Kitazawa, T., 2007. Pleistocen macrotidal tide-dominated estuary-delta succession, along the Dong Nai River, southern Vietnam. Sedimentary Geology, 194, 115-140.

Kuecher, G.J., Woodland, B.G., Broadhurst, F.M., 1990. Evidence of deposition from individual tides on a tidal cycles from the Francis Creek Shale (host rock to the Mazon Creek Biota) Westphalian D (Pennsylvanian), north-eastern Illinois. Sedimentary Geology, 68, 211-221.

Kvaček, J., 2000. *Frenelopsis alata* and its microsporangiate and ovuliferous reproductive structures from the Cenomanian of Bohemia (Czech Republic, Central Europe). Review of Palaeobotany and Palynology, 112, 51-78.

Kvaček, J., Falcon-Lang, H., Dašková, J., 2005. A new Late Cretaceous ginkgoalean reproductive structure *Nehvizdyella* gen. nov. from the Czech Republic and its whole-plant reconstruction. American Journal of Botany, 92, 1958-1969.

Langenheim, J.H., 1995. Biology of Amber-Producing Trees: Focus on Case Studies of *Hymenaea* and *Agathis*. In: Anderson, K.B., Crelling, J.C (eds.). Amber, Resinite, and Fossil Resins. Washington, Proceedings of the American Chemical Society, Symposium Series, 617, 1-32.

Langenheim, J.H., Beck, C.W., 1965. Infrared Spectra as a Means of Determining Botanical Sources of Amber. Science, 149 (3679), 52-54.

London, J.C., 1829. An Encyclopedia of Plants. In: Moore, L.B., Edgar, E. (eds.). 1970. Flora of New Zealand, 2, Wellington, Government Printer, 359 pp.

Malod, J.A., Mauffret, A., 1990. Iberian plate motions during the Mesozoic. Tectonophysics, 184, 261-278.

Martill, D.M., Loveridge, R.F., Ferreira Gomes de Andrade, J.A., Herzog Cardoso, A., 2005. An unusual ocurrence of amber in laminated limestones: the Crato Formation lagerstätte (Early Cretaceous) of Brazil. Paleontology, 48, 1339-1408.

Martín-Chivelet, J., Berasategui, X., Rosales, I., Vilas, L., Vera, J.A., Caus, E., Gráfe, K.U., Mas, R., Puig, C., Segura, M., Robles, S., Floquet, M., Quesada, S., Ruiz-Ortiz, P.A., Frenegal-Martínez, M.A., Salas, R., García, A., Martín-Algarra, A., Arias, C., Meléndez, M., Chacón, B., Molina, J.M., Sanz, J.L., Castro, J.M., García-Hernández, M., Carenas, B., García-Hidalgo, J., Gil J., Ortega, F., 2002. Cretaceous. In: Gibbons, W., Moreno, T. (eds.). The Geology of Spain. London, The Geological Society, 255-292.

Martínez-Delclòs, X., Briggs, D.E.G., Peñalver, E., 2004. Taphonomy of insects in carbonates and amber. Palaeogeography, Palaeoclimatology, Palaeoecology, 203, 19-64.

Martínez-Torres, L., Pujalte, V., Robles, S., 2003. Los yacimientos de ámbar del Cretácico Inferior de Montoria-Peñacerrada (Álava, Cuenca Vasco-Cantábrica): Estratigrafía, reconstrucción paleogeográfica y estructura tectónica. Estudios del Museo de Ciencias Naturales de Álava, 18, 9-32.

McCarthy, P.J., Plint, A.G., 2003. Spatial variability of paleosols across Cretaceous interfluves in the Dunvegan Formation, NE British Columbia, Canada: palaeohydrological, palaeogeomorphological and stratigraphic implications. Sedimentology, 50, 1187-1220.

Medioli, F.S., Scott, D.B., Collins, E.S., Wall, J.H, 1990. Thecamoebians from the early Cretaceous deposits of Ruby Creek, Alberta (Canada). In: Hemleben, C., Kaminski, M.A., Kuhnt, W., Scott, D.B. (eds.), Paleoecology, Biostratigraphy, Paleoceanography and Taxonomy of Agglutinated Foraminifera, NATO Advanced Study Institute Series, Series C, Mathematical and Physical Sciences, 327, 793-812.

Moreno-Bedmar, J.A., Bulot, L., Latil, J.L., Martínez, R., Ferrer, O., Bover-Arnal, T., Salas, R., 2008. Precisiones sobre la edad de la base de la Formación Escucha, mediante ammonoideos, en la subcuenca de la Salcedella, Cuenca del Maestrat (E Cordillera Ibérica). Geo-temas, 10, 159-162.

Morley, R.J., 2000. Origin and Evolution of Tropical Rain Forests. In: Chichester, J. (eds). John Wiley and Sons Ltd., 362 pp.

Najarro, M., Rosales, I., 2008. Evidencias sedimentológica, diagenética y quimioestratigráfica del Evento Anóxico Oceáni-

co del Aptiense Inferior (OAE 1a) en la plataforma carbonatada de la Florida (NO de Cantabria). Geo-temas, 10, 163-166.

Najarro, M., Rosales, I., Martín-Chivelet, J., 2007. Evolución de la plataforma carbonatada de la Florida durante el rifting del Cretácico Inferior (Aptiense, NO de Cantabria). Volumen Monográfico de la II Semana de Jóvenes Investigadores del IGME, 123-128.

Nel, A., de Ploëg, G., Millet, J., Menier, J.J., Waller, A., 2004. The Frech ambers: a general conspectus and the Lowermost Eocene amber deposit of Le Quesnoy in the Paris Basin. Geologica acta, 2(1), 3-8.

Néraudeau, D., Perrichot, V., Colin, J.-P., Girard, V., Gomez, B., Guillocheau, F., Masure, E., Peyrot, D., Tostain, F., Videt, B., Vullo, R., 2008. A new amber deposit from the Cretaceous (uppermost Albian-lowermost Cenomanian) of southwestern France. Cretaceous Research, 29, 925-929.

Néraudeau, D., Vullo, R., Gomez, B., Perrichot, V., Videt, B., 2005. Stratigraphie et paléontologie (plantes, vertébrés) de la série paralique Albien terminal-Cénomanien basal de Tonnay-Charente (Charente-Maritime, France). Comptes Rendus Palevol, 4, 79-93.

Noe-Nygaard, N., Surlyk, F., 1988. Washover fan and brackish bay sedimentation in the Berriasian-Valanginian of Bornholkm, Denmark. Sedimentology, 35, 197-217.

Olivet, J.M., 1996. La cinématique de la plaque ibérique. Bulletin des centres de Recherches Exploration-Production Elf-Aquitaine, 20, 131-195.

Pemberton, S.G., MacEachern, J.A., Frey, R.W., 1992. Trace fossils/facies models: environmental and allostratigraphic significance. In: Walker, R.G., James, N.P. (eds.). Facies Models: Response to sea level change. Geological Association of Canada, 47-72.

Penney, D., Ortuño, V., 2006. Oldest true orb-weaving spider (Araneae: Araneidae). Biology Letters, 2, 447-450.

Peñalver, E., Álvarez-Fernández, E., Arias, P., Delclòs, X., Ontañón, R., 2007a. Local amber in a Palaeolithic context in Cantabrian Spain: the case of La Garma A. Journal of Archaeological Science, 34, 843-849.

Peñalver, E., Delclòs, X., Soriano, C., 2007b. A new rich amber outcrop with palaeobiological inclusions in the Lower Cretaceous of Spain. Cretaceous Research, 28, 791-802.

Peñalver, E., Grimaldi, D.A., Delclòs, X., 2006. Early Cretaceous spider web with its prey. Science, 312, 1761.

Peñalver, E., Grimaldi, D., Delclòs, X., 2008. Early spider web. In: MacGraw Hill (eds.). Yearbook of Science and Technology. The McGraw-Hill Companies, 103-105.

Perrichot, V., 2004. Early Cretaceous amber from south-western France: insight into the Mesozoic litter fauna. Geologica Acta, 2, 9-22.

Perrichot, V., 2005. Environnements paraliques à ambre et à végétaux du Crétacé Nord-Aquitain (Charentes, Sud-Ouest de la France). Mémoires des Géosciences Rennes, 118, 1-310.

Perrichot, V., Néraudeau, D., Nel, A., de Ploëg, G., 2007. A reassesment of the Cretaceous amber deposits from France and their palaeontological significance. African Invertebrates, 48, 213-227.

Peyrot, D., Rodríguez-López, J.P., Barrón, E., Meléndez, N., 2007. Palynology and biostratigraphy of the Escucha Formation in the Early Cretaceous Oliete Sub-basin, Teruel, Spain. Revista Española de Micropaleontología, 39, 135-154.

Poinar, G.O., Milki, R., 2001. The Oldest Insect Ecosystem in Fossilized Resin. In: Oregon State University Press (eds.). Lebanese Amber. Oregon State University Press, 96 pp.

Posamentier, H.W., Vail, P.R., 1988. Eustatic controls on clastic deposition II-sequence and systems tract models. In: Wilgus, C.K., Hastings, B.S., Kendall, C.G.St.C., Posamentier, H.W., Ross, C.A., Van Wagoner J.C. (eds.). Sea-level changes-An integrated approach. Society of Economic Paleontologist and Mineralogist, 42, 125-154.

Querol, X., Salas, R., Pardo, G., Ardevol, L., 1992. Albian coal-bearing deposits of the Iberian Range in northeastern Spain. In: McCabe, J.P., Panish, J.T. (eds.). Controls and distribution and quality of Cretaceous coals. Geological Society of America, 267, 193-208.

Ramírez del Pozo, J., 1972. Algunos datos sobre la estratigrafía y micropaleontología del Aptense y Albense al oeste de Santander. Revista Española de Micropaleontología, 15, 59-97.

Rat, P., 1988. The Basque-Cantabrian basin between the Iberian and European plates some facts but still many problems. Revista de la Sociedad geológica de España, 1, 327-348.

Ratnitsyn, A., Quicke, D.L.J. (eds.), 2002, History of insects. United States, Kluwer Academic Publishers, 517 pp.

Reineck, H.E., Singh, I.B., 1975. Tidal Flats. In: Reineck, H.E., Singh, I.B. (eds.). Depositional Sedimentary Environments. Springer-Verlag, 355-372.

Reineck, H.E., Wunderlich, F., 1968. Classification and origin of flaser and lenticular bedding. Sedimentology, 11, 99-104.

Rodríguez-López, J.P., Meléndez, N., 2004. Sedimentología de la Fm. Escucha (Albiense Inferior-Medio) entre Estercuel y Crivillén (Teruel) en la cubeta de Oliete (Cuenca Ibérica Central). Geo-temas, 6, 119-122.

Rodríguez-López, J.P., Meléndez, N., Soria, A.R., 2005. Arquitectura estratigráfica de la Fm. Escucha (Albiense) en el flanco sur del Sinclinal de Cueva Forada. Subcuenca de Oliete (Teruel), Cuenca Ibérica Central. Geo-temas, 8, 95-98.

Rodríguez-López, J.P., Meléndez, N., Soria, A.R., Lisea, C.L., 2007. Lateral variability of ancient seismites related to differences in sedimentary facies (the synrift Escucha Formation, Mid-Cretaceous, eastern Spain). Sedimentary Geology, 201, 461-484.

Salas, R., Guimerà, J., Mas, R., Martín-Closas, C., Meléndez, A., Alonso, A., 2001. Evolution of the Mesozoic Central Iberian rift system and its Cenozoic inversion (Iberian Chain). In: Cavazza W., Robertson, A.H.F.R., Ziegler, P., Crasquin-Soleaun, S. (eds.). Peri-Tethyan Rift/Wrench Basins and Passive Margins. Mémoires du Musée National de Histoire Naturel, 186, 145-185.

Salas, R., Martín-Closas, C. (eds.), 1991. El Cretácico Inferior del nordeste de Iberia. Barcelona, Publicacions Universitat de Barcelona, 153 pp.

Salas, R., Martín-Closas, C., Querol, X., Guimerà, J., Roca, E., 1991. Evolución tectonosedimentaria de las cuencas del Maestrazgo y Aliaga-Penyagolosa durante el Cretácico Inferior. In: Salas, R., Martín-Closas, C. (eds.). El Cretácico Inferior del nordeste de Iberia. Publicacions Universitat de Barcelona, 15-47.

Sangüesa, F.J., Arostegui, J., 2003. Modelo subsidente y térmico de la Formación Escucha en la Zona de Montoria-Peñacerrada (Álava). Estudios del Museo de Ciencias Naturales de Álava, 18, 91-100.

Schmidt, A.R., Ragazzi, E., Coppellotti, O., Roghi, G., 2006. A microworld in Triassic amber. Nature, 444, 835.

Schmidt, A.R., von Eynatten, H., Wagreich, M., 2001. The Mesozoic amber of Schliersee (southern Germany) is Cretaceous in age. Cretaceous Research, 22, 423-428.

Scotese, C.R., 2000. Paleomap project. Climate History. www.scotese.com/climate.htm.

Selden, P.A., 1989. Orb-web weaving spiders in the early Cretaceous. Nature, 340, 711-713.

Selden, P.A., 1990. Lower Cretaceous spiders from the Sierra de Montsech, north-east Spain. Palaeontology, 33, 257-285.

Selden, P.A., Penney, D., 2003. Lower Cretaceous spiders (Arthropoda: Arachnida: Araneae) from Spain. Neues Jahrbuch für Geologie und Paläontologie- Abhandlungen, 3, 175-192.

Shanmugam, G., Poffenberger, M., Álava, J.T., 2000. Tide-dominated estuarine facies in the Hollin and Napo ("T" and "U") Formations (Cretaceous), Sacha Field, Oriente Basin, Ecuador. American Association of Petroleum Geologists Bulletin, 84, 652-682.

Soto, R., Casas-Sainz, A.M., Villalaín, J., Oliva-Urcía, B., 2007. Mesozoic extension in the Basque-Cantabrian Basin (N Spain): Contributions from AMS and brittle mesostructures. Tectonophysics, 445, 373-394.

Spicer, A.R., Rees, P.M., Chapmann, J.L., 1994. Cretaceous phytogeography and climate signals. In: Allen, J.R.L., Hoskins, B.J., Sellwood, B.W., Spicer, R.A., Valdes, P.J. (eds.). Palaeoclimates and their Modelling; with Special Reference to the Mesozoic Era. Chapman and Hall, London, 69-77.

Szadziewski, R., 1996. Biting midges from Lower Cretaceous amber of Lebanon and Upper Cretaceous Siberian amber of Taimyr (Diptera, Ceratopogonidae). Studia Dipterologica, 3, 23-86.

Veltz, I., 2008. Le passage Jurassique Crétacé au Liban. Doctoral thesis. Université de Reims Champagne-Ardenne, 255 pp.

Visser, M.J., 1980. Neap-spring cycles reflected in Holocene subtidal large-scale bedforms deposits: a preliminary note. Geology, 8, 543-546.

Waggoner, B.M., 1996. Bacteria and protists from Middle Cretaceous amber of Ellsworth County, Kansas. PaleoBios, 17, 20-26.

Willis, B.J., 1997. Architecture of fluvial-dominated valley-fill deposits in the Cretaceous Fall River Formation. Sedimentology, 44, 735-757.

Wilmsen, M., 2005. Stratigraphy and biofacies of the Lower Aptian of Cuchía (Cantabria, north Spain). Journal of Iberian Geology, 31, 253-275.

Withjack, M.O., Olson, J., Peterson, E., 1993. Experimental models of extensional forced folds. The American Association of Petroleum Geologists Bulletin, 74, 1038-1054.

Zherikhin, V.V., Eskov, K.Y., 1999. Mesozoic and Lower Tertiary resins in former USSR. Estudios del Museo de Ciencias Naturales de Álava, 14, 119-131

Manuscript received September 2008;
revision accepted March 2009;
published Online April 2009.

Vol. 84 No. 4 pp. 801–840 ACTA GEOLOGICA SINICA (English Edition) Aug. 2010

Review of the El Soplao Amber Outcrop, Early Cretaceous of Cantabria, Spain

María NAJARRO[1, *], Enrique PEÑALVER[1], Ricardo PÉREZ-DE LA FUENTE[2], Jaime ORTEGA-BLANCO[2], Cesar MENOR-SALVÁN[3], Eduardo BARRÓN[1], Carmen SORIANO[4], Idoia ROSALES[1], Rafael LÓPEZ DEL VALLE[5], Francisco VELASCO[6], Fernando TORNOS[1], Véronique DAVIERO-GOMEZ[7], Bernard GOMEZ[7] and Xavier DELCLÒS[2]

1 *Instituto Geológico y Minero de España, E-28003, Madrid, Spain*
2 *Departament d'Estratigrafia, Paleontologia i Geociències Marines, Facultat de Geologia, Universitat de Barcelona, E-08071, Barcelona, Spain*
3 *Centro de Astrobiología (CSIC-INTA), E-28850, Torrejón de Ardoz, Spain*
4 *European Synchrotron Radiation Facilities, F-38000 Grenoble, France/Géosciences Rennes - Université de Rennes 1, F-35042 Rennes, France*
5 *El Soplao S.L., Prao El Collao, E-39553, Cantabria, Spain*
6 *Universidad del País Vasco, Dpto. Mineralogía y Petrología, E-48080 Bilbao, Spain*
7 *CNRS-UMR 5125 PEPS, Université Lyon 1, Géode, F-69622 Villeurbanne, France*

Abstract: El Soplao outcrop, an Early Cretaceous amber deposit recently discovered in northern Spain (Cantabria), has been shown to be the largest site of amber with arthropod inclusions that has been found in Spain so far. Relevant data provided herein for biogeochemistry of the amber, palynology, taphonomy and arthropod bioinclusions complement those previously published. This set of data suggests at least two botanical sources for the amber of El Soplao deposit. The first (type A amber) strongly supports a source related to Cheirolepidiaceae, and the second (type B amber) shows non-specific conifer biomarkers. Comparison of molecular composition of type A amber with *Frenelopsis* leaves (Cheirolepidiaceae) strongly suggests a biochemical affinity and a common botanical origin. A preliminary palynological study indicates a regional high taxonomical diversity, mainly of pteridophyte spores and gymnosperm pollen grains. According to the preliminary palynological data, the region was inhabited by conifer forests adapted to a dry season under a subtropical climate. The abundant charcoalified wood associated with the amber in the same beds is evidence of paleofires that most likely promoted both the resin production and an intensive erosion of the litter, and subsequent great accumulation of amber plus plant cuticles. In addition, for the first time in the fossil record, charcoalified plant fibers as bioinclusions are reported. Other relevant taphonomic data are the exceptional presence of serpulids and bryozoans on the surfaces of some amber pieces indicating both a long exposure on marine or brackish-water and a mixed assemblage of amber. Lastly, new findings of insect bioinclusions, some of them uncommon in the fossil record or showing remarkable adaptations, are reported. In conclusion, a documented scenario for the origin of the El Soplao amber outcrop is provided.

Key words: fossil resin, chemotaxonomy, paleobotany, charcoal, arthropod bioinclusions, taphonomy, Early Albian

1 Introduction

Amber preserves delicate organic fossils, including microorganisms, cells and tissues, but the most abundant record is constituted by insects, sometimes showing interactions between them, such as mating interaction, commensalism and parasitism (e.g. Grimaldi, 1996; Martínez-Delclòs et al., 2004; Grimaldi and Engel, 2005). Early Cretaceous amber is remarkably important, because it was during this period that there occurred explosive radiations of the flowering plants and many modern families of insects (Grimaldi and Engel, 2005). During the last decade several new deposits of Cretaceous amber have been discovered in Spain and France (e.g. Delclòs et al., 2007; Perrichot and Néraudeau, 2009), and researches on various aspects of Cretaceous amber have increased greatly. However, most of the researches made concern the taxonomical descriptions of arthropods and microorganisms embedded in amber. Only a few studies have been conducted on the origin of both the amber and the deposits that contain it. One of the most important aspects concerning Cretaceous amber is the plant source, if there was only one, but this aspect has been shown to be very difficult to ascertain with confidence.

* Corresponding author. E-mail: m.najarro@igme.es

The first detailed description of Spanish amber was published by Casal (1762). Approximately 150 years later Boscá (1910) first indicated the possible presence of insects preserved in Spanish amber. After the discovery of two remarkable amber deposits rich in bioinclusions, Peñacerrada I in the north and San Just in the north-east of Spain, a third major amber deposit was discovered in 2008 in Cantabria, named El Soplao. Thus it was not included in the most recent review of Spanish amber outcrops by Delclòs et al. (2007). Najarro et al. (2009) described in detail the regional geology, the features of the amber pieces, including infrared spectroscopy analyses, and a first attempt of the bioinclusions and the plant cuticles associated with the amber. Subsequent papers deal with biogeochemistry of amber and descriptions of new arthropod taxa preserved as bioinclusions. Thus, Menor-Salván et al. (2009a, 2009b) investigated biomarkers from amber pieces and *Frenelopsis* leaves from the El Soplao outcrop, concluding that they share the same origin; in addition, they identified the chemical compound form that produces an intensive fluorescent blue glow when this amber is under normal sunlight. More recently, Menor-Salván et al. (2010) report some paleochemotaxonomical aspects of the biological diterpenes preserved in El Soplao amber. On the other hand, Pérez-de la Fuente et al. (2010) and Nel et al. (2010) described the new insect taxa *Cantabroraphidia marcanoi* (Raphidioptera: Mesoraphidiidae) and *Tethysthrips hispanicus* (Thysanoptera: Thripidae), respectively. Lastly, Ortega-Blanco et al. (2010a) report the fauna of false fairy wasps (Mymarommatoidea) that has been recorded in Spanish Cretaceous amber, including a paratype specimen from El Soplao amber.

We report relevant new data about El Soplao amber deposit, such as new detail on stratigraphy of the amber-bearing levels, new geochemical and biogeochemical information of the amber and fossil leaves, palynological data, the presence of a great abundance of charcoal associated with the amber, the presence of marine invertebrates on the surface of some amber pieces and new discoveries about the bioinclusions. These new contributions permit us to portray a more documented scenario for the origin of the El Soplao amber outcrop.

2 Geology

The El Soplao outcrop belongs to the Cretaceous succession of the north-western margin of the Basque-Cantabrian Basin. During the Cretaceous, this basin was affected by extensional tectonics, and perhaps strike-slip, associated with the opening of the North Atlantic Ocean and the Bay of Biscay (e.g. Le Pichon and Sibuet, 1971; Rat, 1988; García-Mondéjar et al., 1996; Soto et al., 2007). During the Late Jurassic–Early Cretaceous a major rift phase developed that led to the formation of several narrow sub-basin controlled by E–W, NW–SE and SW–NW trending faults, in which variable thicknesses of continental to marine sediments accumulated (García-Mondéjar et al., 1996; Soto et al., 2007). The El Soplao area lies in the North Cantabrian sub-basin located immediately to the north of the Cabuérniga Ridge (Wilmsen, 2005), which is an E–W late-Variscan structure reactivated first as a paleo-high bounded by normal faults during the Early Cretaceous, and later as a reversal fault during widespread Tertiary (Pyrenean) compression (Fig. 1). The Lower Cretaceous (Aptian–Albian) deposits of the El Soplao area lie unconformably on lower Triassic (Buntsandstein facies) basement. They constitute a relatively thin (~300 m) sedimentary wedge weakly deformed and affected only by gently folding. The El Soplao amber outcrop is located in the southern flank of the Bielva syncline (Fig. 1), where the average strike of the succession is E–W and the dip about 40º N.

Thermal maturity of the area based on vitrinite reflectance values (% *R*o) performed on vitrinite macerals from plant fragments have yield relatively low reflectance values that range between 0.50% and 0.61% (mean 0.56%) (Menor-Salván et al., 2010). These values suggest that the organic matter associated with the amber is only early mature, and the estimated temperatures from these indices of thermal maturation of organic matter are in the range of 60–70ºC (e.g. Sweeney & Burnham, 1989), which are the burial maximum temperatures suffered by the amber deposit. These low maturity levels may be responsible for the good conservation of the molecular composition of the amber and its biological inclusions.

A synthesis of the stratigraphy of the Soplao area is represented in Fig. 2 (after Najarro et al., 2009, 2010). The amber-bearing deposit of El Soplao is included within the Las Peñosas Formation (Fig. 2), which is a Lower Albian unit (~112–110 Ma) of continental to transitional marine siliciclastic deposits interbedded in a succession of shallow marine, rudist and coral carbonate platform deposits. General sedimentary descriptions, depositional environments and fossil content of the Las Peñosas Formation have been already discussed in Najarro et al. (2009). In the El Soplao outcrop, the amber-rich beds occur in the lower-middle part of the Las Peñosas Formation. There, this unit rests disconformably above a thin (1–2 m) bed of continental red clay with root traces, deposited at the top of shallow marine limestones of the Reocín Formation (Fig. 2). The El Soplao amber deposit is characterized by dark, carbonaceous, pyritiferous shales with subordinated siltstones and sandstones laminae and cross-laminated centimetric sandstone layers, forming wavy and lenticular bedding. They contain remarkable accumulations of plant remains and amber pieces of different sizes and forms, as well as some remains and small shells of marine gastropods and bivalves. The principal amber-bearing shale bed of the El Soplao outcrop forms a lenticular body with maximum thickness of 1.5–2.0 m and a width of at least 10 m in N–S cross-section. In the strike of the bed, the amber-bearing shale extends more than 75 m. The base of this len-shaped shale bed is erosional and truncates highly bioturbated, medium to coarse-grained sandstones with cross-bedding. At its top, the amber-bearing shale bed is overlain by heterolithic carbonaceous sandstones and muddy siltstones to sandstones with flaser bedding, which are also relatively rich in amber pieces. All of these deposits accumulated in a proximal estuarine bay system with small bayhead deltas (Najarro et al., 2009) and represent the transgressive inundation of a continental fluvial plain and an incised valley fill. Based on geometry and facies, we interpret the amber-bearing shale of the El Soplao

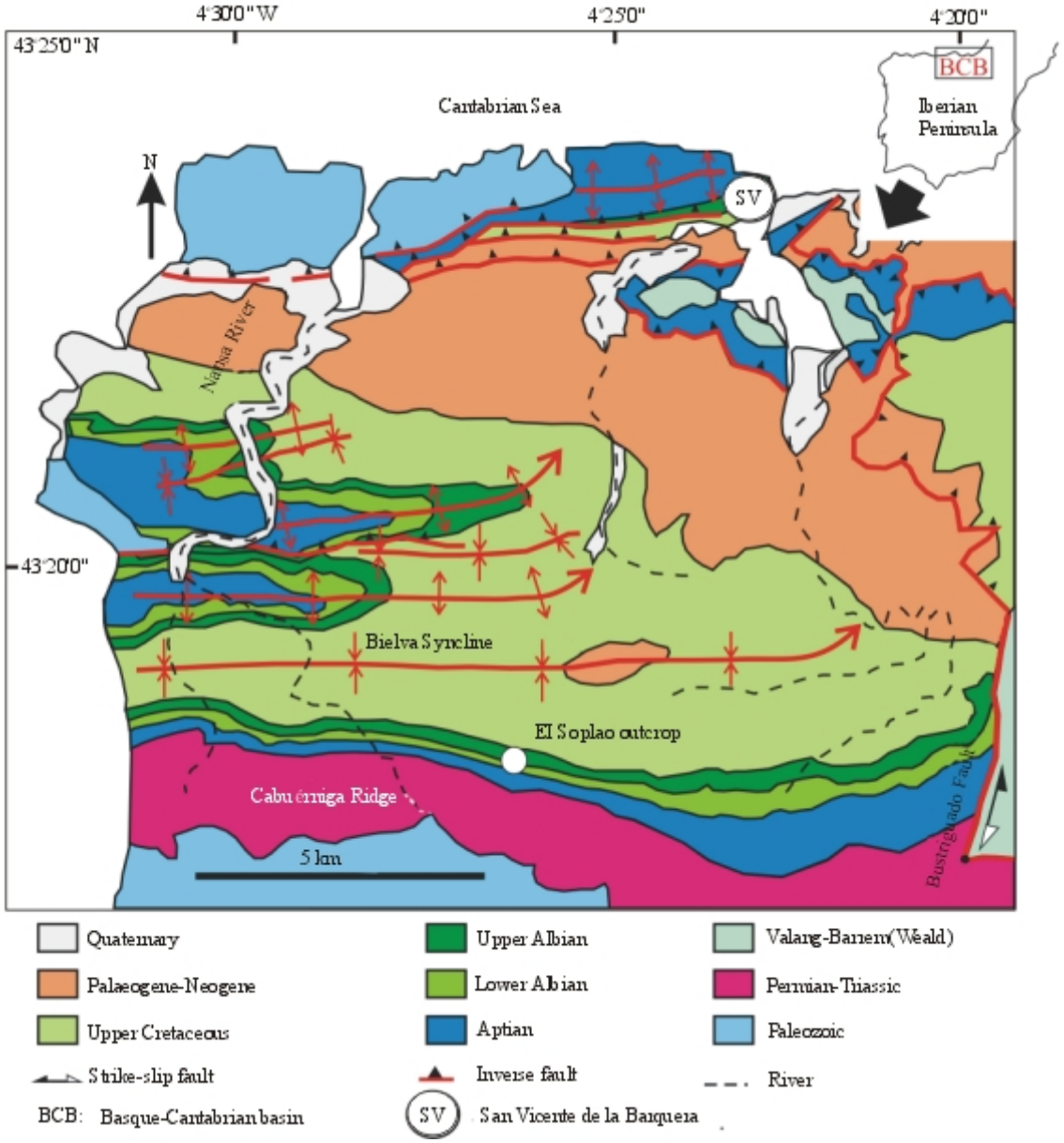

Fig. 1. Geological map of the study area showing the location of the El Soplao amber outcrop.
Modified from Najarro et al. (2009).

outcrop to have accumulated in a restricted tidal channel with low circulation and anoxic bottom-water, as suggested by widespread early pyritization.

3 Methods

3.1 Paleontological excavations

Three paleontological excavations have been carried out in El Soplao amber outcrop. During the first one (October 2008) different extraction methods were applied to obtain amber pieces. Amber was obtained manually with small tools. In addition a large prospect hole, approximately 7 × 2.5 × 2 m in size, was dug in one of the amber-rich areas of the outcrop using a bulldozer. Several tons of amber-bearing sediment from the large prospect hole were transported to a washing area located in the same outcrop, where a cement mixer and a sieve were used to obtain all ranges of amber sizes as described in Corral et al. (1999) and Alonso et al. (2000). This permitted to obtain a sampling without taphonomic biases introduced by the extraction methods towards the large and medium sizes. During the last excavation (July 2009) additional small prospect holes were dug close to the limits of the outcrop to find lateral extensions of the amber deposit. This task showed a high abundance of amber and revealed that the amber bed is at least 75 m long laterally, supporting the assertion of Najarro et al. (2009), which is that the El Soplao is the largest site of amber with arthropod inclusions that has ever been found in Spain so far.

During the second paleontological excavation (March 2009) a new method was used to obtain abundant amber material increasing the collection of bioinclusions. The technique

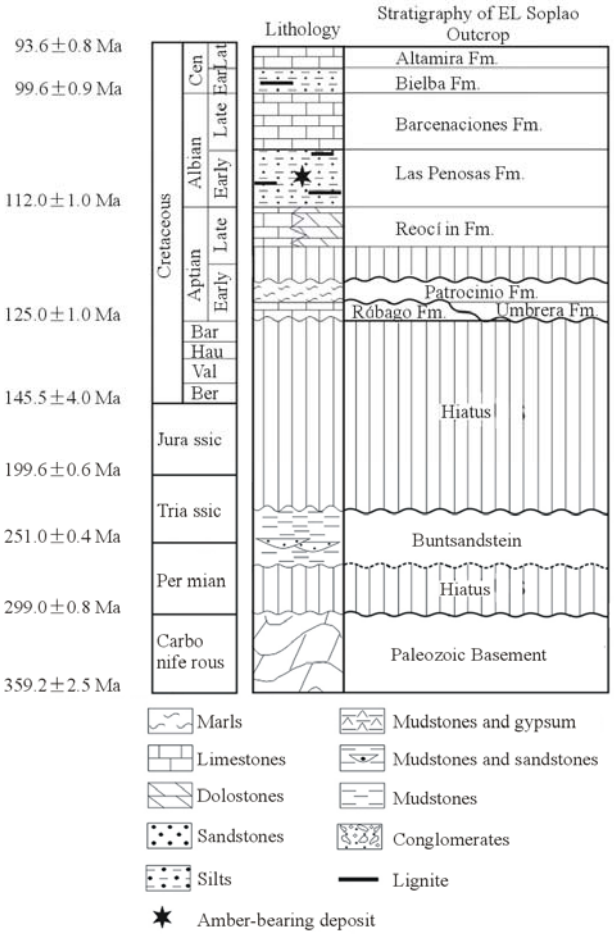

Fig. 2. Chrono- and lithostratigraphy of the El Soplao area.
Modified from Hines (1985) and Najarro et al. (2010). Chronostratigraphy after Gradstein and Ogg (2009).

involves the use of high pressure water (Fig. 3.1 and 3.2) to extract entire large amber pieces that would be too fragile to resist conventional methods (Fig. 3.3). The water at high pressure disintegrated the sediment of the prospect hole and exposed the amber pieces, which were manually extracted to avoid fracturing. On the other hand, the small and medium pieces were retained using a large sieve where water and mud flowed (Fig. 3.2). The pieces from the mixture of mud, plant cuticles, coal and amber retained by the large sieve were separated in the washing area described above. This high pressure water method used for the first time to extract amber is already used in mining to fragment mineral seams, and to extract the useful parts from the waste rock. In conclusion, the new method was useful in obtaining numerous large amber pieces in a short period of time.

3.2 Biogeochemical analyses

For the biogeochemical analysis amber pieces, fossil wood, and sediments rich in plant cuticles were collected from the El Soplao deposit during the first excavation on October 2008. Two types of amber pieces were collected: type A, characterized by a strong blue purple color under natural light (Fig. 3.3 and 3.4), purple-reddish under artificial light, and type B, less abundant, yellow under artificial light and with a bluish tinge under natural light. Plant cuticles were obtained from claystones by rinsing the plant-rich sediment in an ultrasonic bath of distilled water to remove all of the clay and silt sediment. The organic residue was air-dried. Plant fragments and leaves were distinguished and separated under a stereomicroscope. In addition, several resin and leaf samples from extant conifers of the families Cupressaceae and Araucariaceae (*Cupressus arizonica, Agathis australis* and *Araucaria angustifolia*) were collected from living trees at the Royal Botanic Garden of Madrid and in the kauri forests of New Zealand, in order to compare their compounds with those of the amber and fossil leaves and also to determine potential affinities of the amber with fossil taxa.

For the analytical characterization, several representative pieces of amber of the types A and B of about 50 g each, with the highest transparency available and free of major inclusions, crusts and debris, were selected from the El Soplao deposit. Following standard techniques, each piece was crushed and extracted for 4 h with dichloromethane:methanol (2:1) using a Büchi model B-811 automatic extractor. One aliquot of extract was injected directly into the injection port of the gas chromatograph. The bulk extract was concentrated to a volume of 20 mL and fractionated by use of flash chromatography on silica gel. The elution was carried out using hexane, dichloromethane, dichloromethane:methanol (1:1), and methanol, and subsequently 25 fractions were collected. Each fraction was concentrated by evaporation of the solvent under N_2 and analyzed by gas chromatography/mass spectrometry (GC/MS). The fractions with similar compositions were combined. The polar fraction (eluted with methanol) and the fractions containing ferruginol were recombined, further separated using a glass column (20 cm) filled with chromatographic-grade silica gel, and eluted sequentially with n-hexane:dichloromethane (1:1), pure dichloromethane, dichloromethane:methanol (1:1), and methanol. Four fractions were collected, designated A through D. All fractions were dried and the alcohols and acids converted to trimethylsilyl derivatives by reaction with N,O-bis-(trimethylsilyl)trifluoroacetamide (BSTFA) containing 1% trimethylchlorosilane (TMCS) at 65ºC for a period of 3 h. Finally, the derived fractions were diluted with n-hexane and injected into the port of the gas chromatograph.

To study the molecular composition of fossil *Frenelopsis* and *Arctopitys* leaves (genus name *Mirovia* changed to *Arctopitys*; see Nosova and Wcisło-Luraniec, 2007), 5 g of leaves were extracted for 4 h with dichloromethane:methanol (2:1) using a Büchi model B-811 automated extractor. The bulk extract was filtered and analyzed directly by gas chromatography-mass spectrometry. After, extract was fractionated using silica gel chromatography in two fractions by elution with hexane:dichloromethane (3:1) and dichloromethane:methanol (4:1). The polar fraction was dried and derived using the method described above. For comparison, the chemotaxonomy of extant Cupressaceae and Araucariaceae was investigated using resin samples from *Cupressus arizonica*, *Agathis australis*, and *Araucaria angustifolia*. The resin was dissolved in dichloromethane:methanol (1:1) and fractionated by

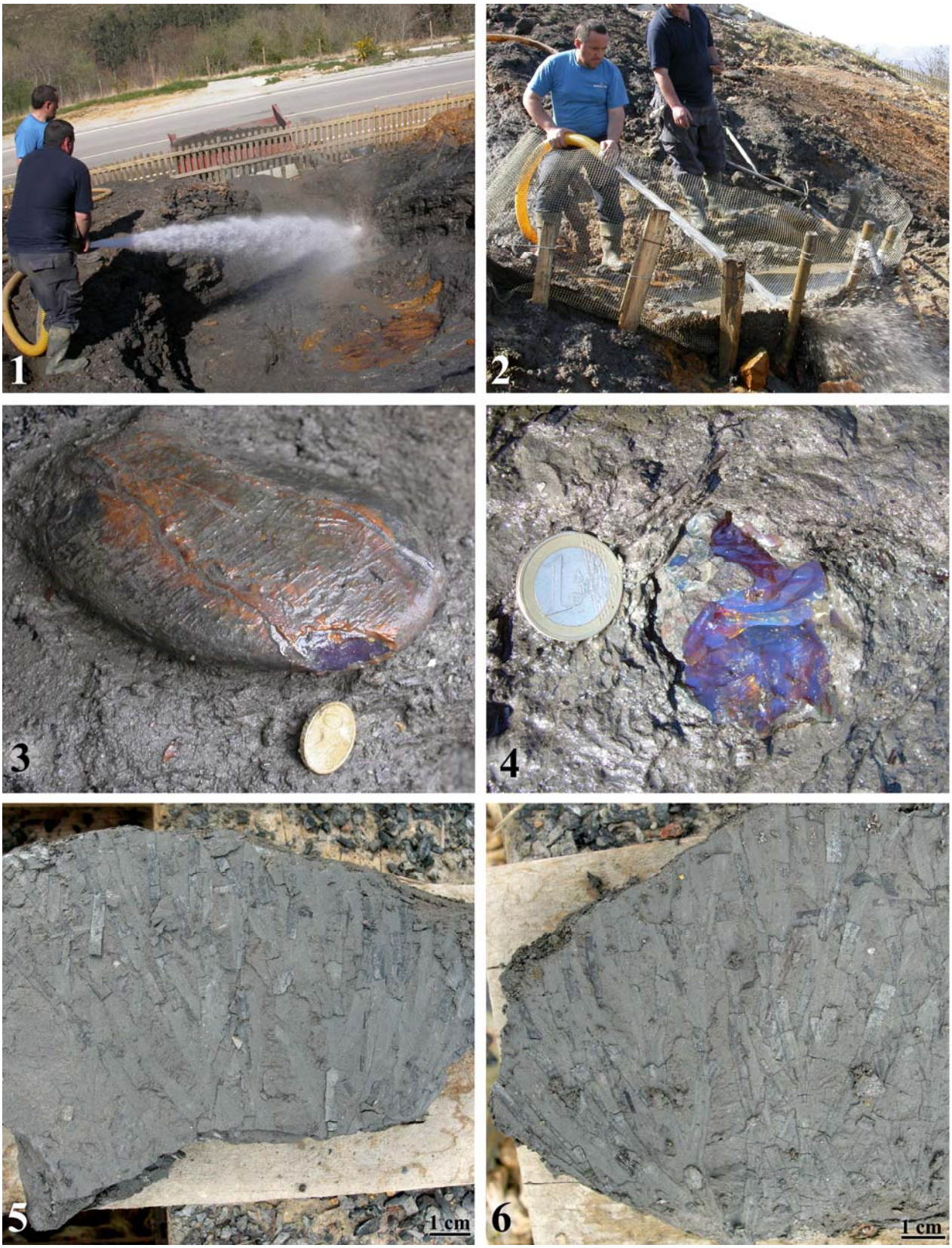

Fig. 3. Paleontological excavation in El Soplao amber outcrop (March 2009) with a new extractive method and some of the pieces obtained *in situ*.

1: High pressure water directed to the prospect hole; 2: large sieve to which water and mud flowed; 3: flattened amber piece virtually complete exposed *in situ* by high pressure water showing intensive fluorescent blue glow on its fracture (coin diameter 24 mm); 4: fragment of amber *in situ* showing intensive fluorescent blue glow (coin diameter 23 mm); 5–6: part and counterpart of four-time branched shoots of *Frenelopsis* sp. collected during the last excavation carried out (July 2009).

chromatography on silica gel in two fractions: the less-polar fraction being eluted with n-hexane:dichloromethane (1:4), and the second polar fraction being eluted with methanol. The polar fraction was dried under a nitrogen stream, yielding a white powder composed mainly of resin acids and highly polar compounds. The polar components were converted into trimethylsilyl derivatives by BSTFA and analyzed using GC-MS as described previously (Menor-Salván et al., 2010).

3.3 Palynological method

Two samples, Sop-Peñosas (this from the amber outcrop) and Peñosas-Cóbreces, both from Las Peñosas Formation, were prepared for palynological studies in the laboratory of ALICONTROL (Madrid, Spain). The rock samples were treated following the standard palynological preparation technique (Batten, 1999), which consists of an acid attack with HCl, HF and HNO_3 at high temperature. The residue was concentrated and sieved throughout sieves of different grid sizes (500, 250, 75, 50 and 12 μm). Then, the samples were mounted in glycerin jelly on glass slides for light microscopy. The samples were studied with an Olympus BX51 optical microscope. Both samples yielded representative and well-preserved assemblages: Sop-Peñosas yielded 488 miospores and Peñosas-Cóbreces 681 miospores.

3.4 Microscopic photography

Scanning electron micrographs of the charcoal were taken using a HITACHI model S-2500 of the University of Valencia. Optical photography used both a digital camera attached to a microscope Olympus BX51 and a digital camera Leica DFC420 attached to a stereomicroscope Leica MS5.

4 Biogeochemistry of the Amber

The overall aim of this part of the research was to identify the bioterpenoids preserved in the fossil resin and to determine their possible botanical source. Due to exceptional preservation, the amber-bearing deposit at El Soplao offers a unique opportunity to compare the molecular composition of the amber with that of the plant remains that appear in the same deposit.

The analysis of the polar terpenoids of the amber from El Soplao indicates that most likely at least two resin producers contributed to the amber record (Fig. 4). The main parent resin (type A; Fig. 4a) originally contained phenolic abietanes (dominated by ferruginol), totarol, dehydroabietane and pimarane/isopimarane acids. The dominant resin acids found were 13-dihydroagatholic and bisnordehydroabietic acids, as well as various other alteration products and minor quantities of callitrisic acid and hinokiol. The second parent resin (type B; Fig. 4b) shares some general compounds characteristic of conifers with type A amber, but shows remarkable differences in specific biomarkers. It contained pimarane/isopimarane acids as the only identifiable biological precursors preserved and shows absence of phenolic terpenoids (ferruginol, totarol, hinokiol) and other specific biomarkers that are present in type A amber (e.g. dehydroabietane, callitrisic acid).

The direct diagenetic products of the pimarane/abietane and labdane class terpenoids constitute the main geoterpenoids extractable from both types of El Soplao amber. The moderate degree of burial diagenesis of the studied material deduced from the low vitrinite reflectance values is consistent with the high level of preservation of the natural product diterpenoids and their direct diagenetic derivatives.

The preliminary molecular data obtained from the comparative study of the megafossil plant leaves, extant plant samples and the two amber types lead to the following results:

(a) There is absence of abietic and dehydroabietic acids in both types of amber samples. This allows us to reject a relationship between the amber and resin of Pinaceae species. Also, the absence of triterpenoids and labdatriene acids discards the contribution of angiosperms (Anderson et al., 1992; Yamamoto et al., 2006).

(b) In type A amber, the phenolic diterpenoids present in the analyzed samples and the absence of phyllocladane/kaurane type terpenoids discard the contribution of the family Araucariaceae. The presence of phenolic terpenoids (ferruginol, totarol and hinokiol) points to a relation with the extant conifer families Cupressaceae, Taxodiaceae and Podocarpaceae. However, the presence of dehydroabietane (also present in representatives of Pinaceae and Cupressaceae; Otto et al., 2007) points to a rather relationship with the family Cupressaceae. The presence of callitrisic acid in type A amber reinforces a biochemical relation between the parent resin of amber and modern Cupressaceae, because in modern conifer resins the synthesis of callitrisic acid seems to be restricted to certain genera of Cupressaceae (Anderson, 2006). The analysis of the molecular composition of fossil leaves from the same outcrop shows the presence of key terpenoids, such as ferruginol, in type A amber and the analyzed *Frenelopsis* fossil leaves, suggesting that this amber could be derived from the genus *Frenelopsis* (Cheirolepidiaceae). For the type A amber, a possible diagenetic route is suggested in Fig. 5 that connects the preserved biological precursors and the major geoterpenoids found in the sample (Otto and Simoneit, 2002; Stefanova et al., 2002; Hautevelle et al., 2006; Pereira et al., 2009). Morphological similarities between extinct Cheirolepidiaceae and extant Cupressaceae has been already described, but their phylogenetic relationship remains speculative, mainly due to the lack of molecular evidence (Seoane, 1998; Miller, 1999; Farjon, 2008); there are also paleobotanical data that support close affinities between Cheirolepidiaceae and Araucariaceae mainly based on female cone morphology. The chemotaxonomical affinity between type A amber and the analyzed leaves of *Frenelopsis* (Cheirolepidiaceae), and the affinity between type A amber and Cupressaceae as well, strongly suggests biochemical affinity between the extinct *Frenelopsis* and the modern representatives of the family Cupressaceae.

(c) The overall terpenoid composition of B samples (Fig. 4b) is represented by non-specific conifer biomarkers. Absence of phenolic terpenoids and 13-dihydroagatholic acid, together with a major presence of diagenetic products of pimarane type terpenoids, saturated and unsaturated norabietanes and

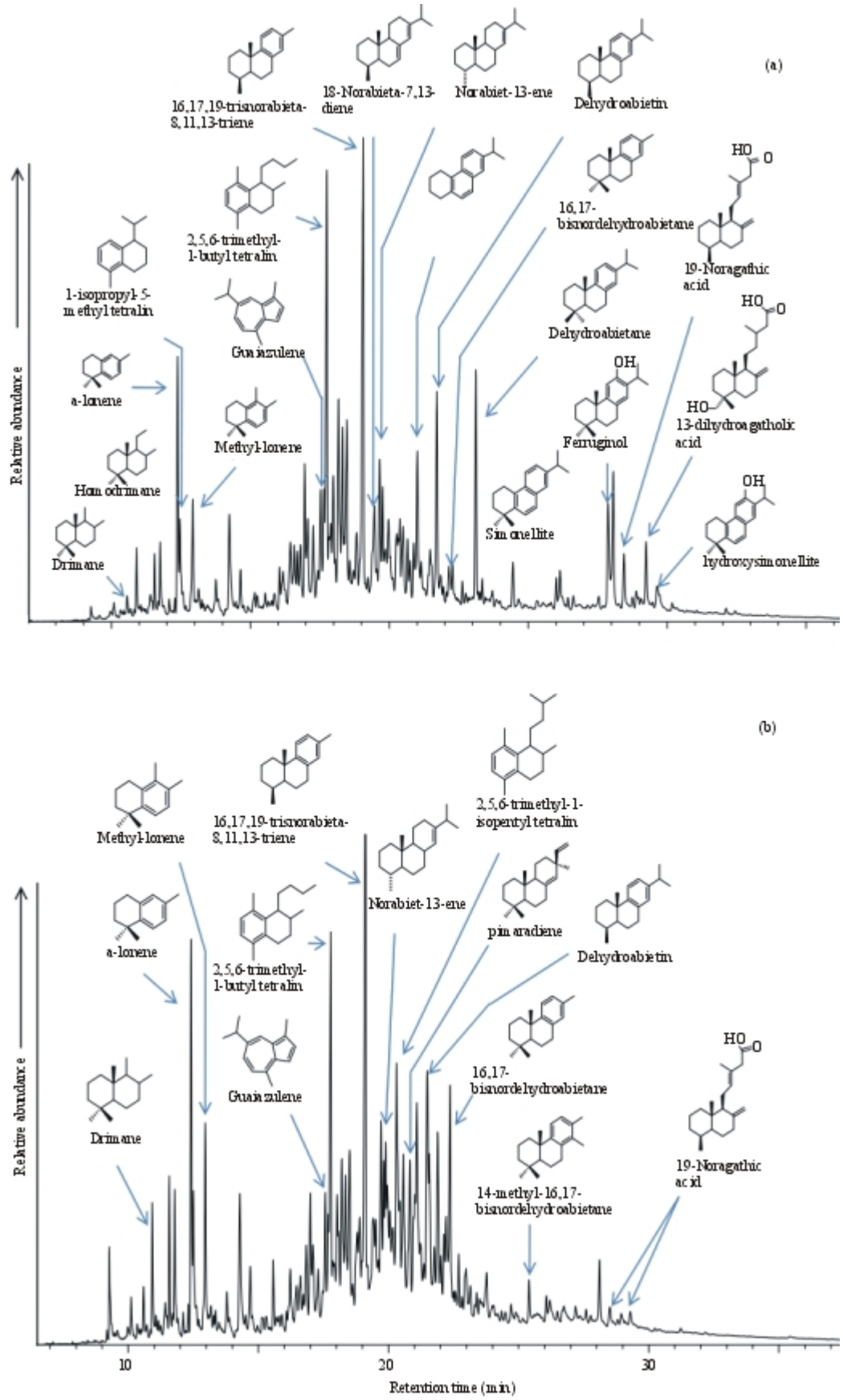

Fig. 4. Gas chromatography-mass spectrometry traces (TIC) analysis and main biomarkers identified in the two types of amber found at El Soplao deposit: type A (a) and type B (b). After Menor-Salván et al. (2010).

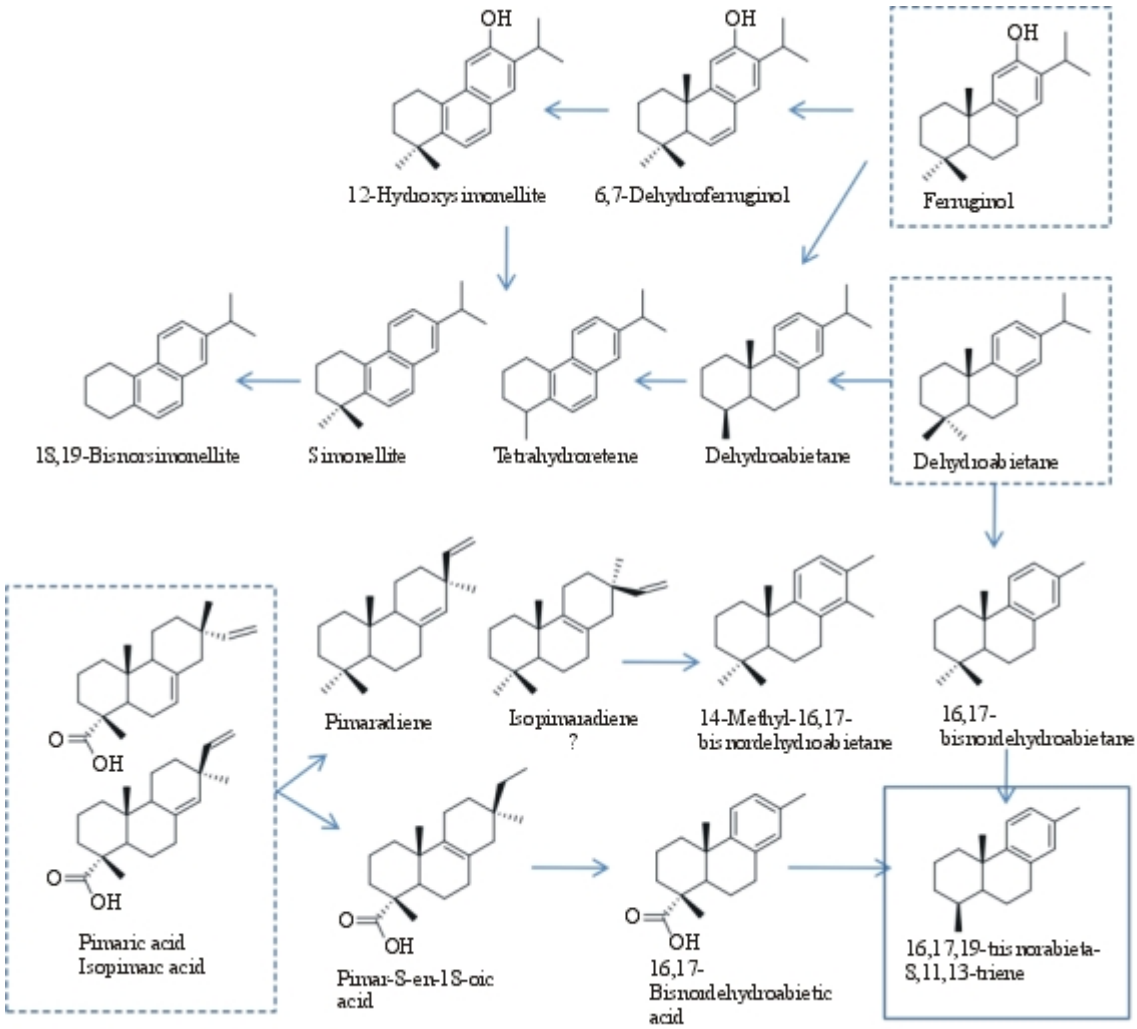

Fig. 5. Diagenetic pathways proposed for the El Soplao amber.

alkyltetralines in B samples, points to a different biological origin. Paleobotanical source for this type of amber could not be identified on the basis of the biomarker composition found so far.

Although these results are preliminary and might change when more data become available from analyses of more samples, it is estimated that they already provide a good indication of the potential plant source that originated in the El Soplao amber. Future analyses could include fossil wood, leaf cuticle of *Nehvizdya*, more amber samples and conifer resin samples of other taxa.

5 Palynology

This preliminary palynological study complements that based on plant cuticles from the amber outcrop (see Najarro et al., 2009), revealing some additional aspects of the regional paleobotany. The studied samples from Las Peñosas Formation have yielded 32 spore and 29 pollen types (Fig. 6; see Table 1). In addition, undetermined bad-preserved dinoflagellate cysts and lining of foraminifera scarcely occurred. The Peñosas-Cóbreces sample presents more abundant taxa (52) than the Sop-Peñosas sample (44). It may be related to a lower palynological richness in the second sample. Both samples present high percentages of conifer pollen grains, especially those of *Classopollis* and *Inaperturopollenites dubius*. The spores of vascular cryptogams are more diverse than pollen grains although they occur in lower amounts. The most usual spores belong to both the trilete and taeniate genus *Cicatricosisporites* and the trilete and psilate genus *Deltoidospora*. Pollen grains of ancient angiosperms occur scarcely in both samples. They are mainly represented by monosulcate and reticulate pollen grains of the genus *Clavatipollenites*.

The Peñosas-Cóbreces sample exhibits high amounts of pollen grains of *Classopollis* (~40%) and *I. dubius* (~30%). Other gymnospermous pollen grains such as *Alisporites* spp., *Araucariacites australis*, *Monosulcites chaloneri* and *Spheripollenites* sp. present lower but remarkable percentages. Spores also present low amounts being *Cicatricosisporites* spp. the best represented (~2%). The occurrence of a single tricolpate

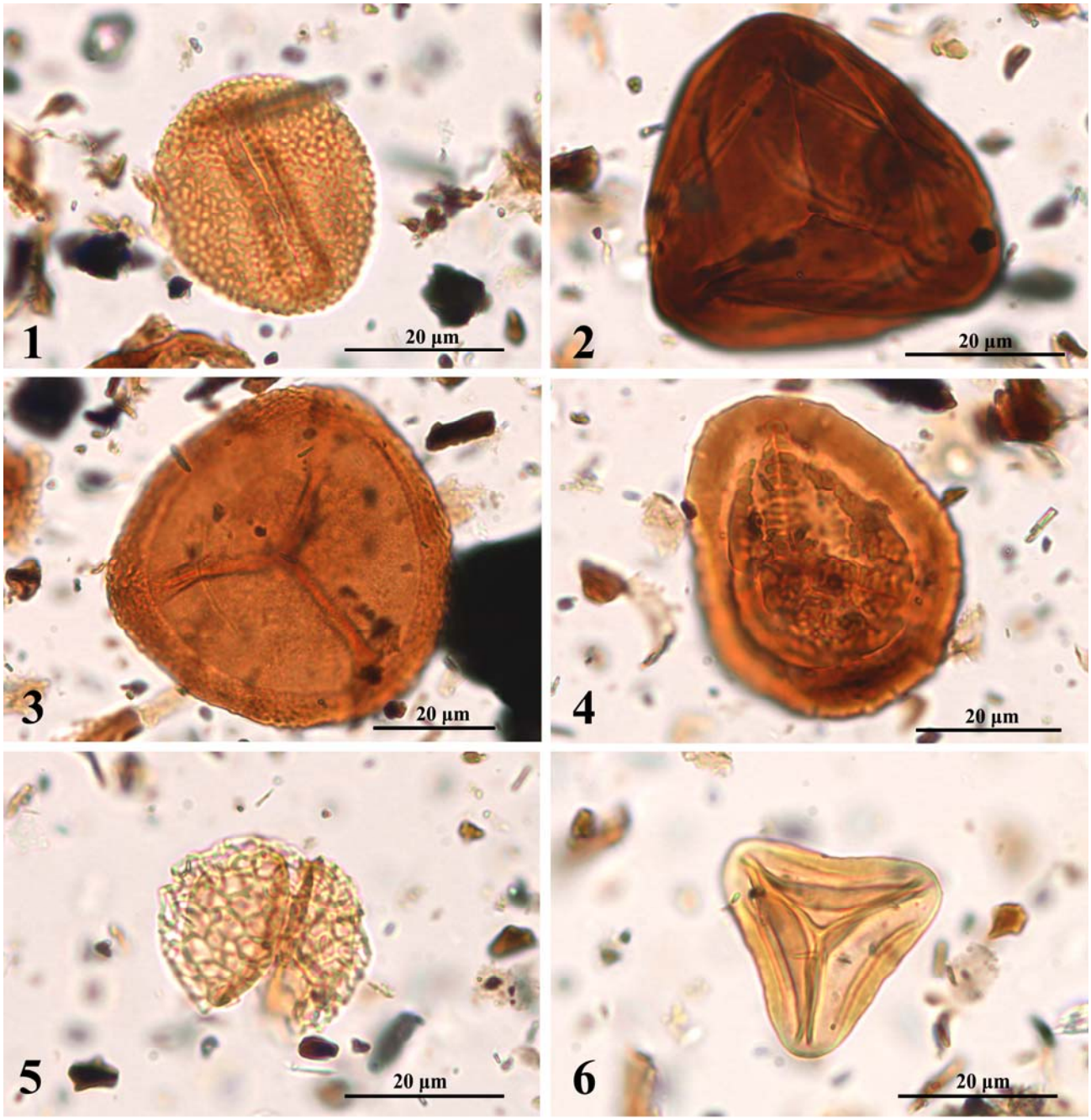

Fig. 6. Miospores from Peñosas-Cóbreces (1–5) and Sop-Peñosas (6) palynological samples.
1: *Liliacidites dividuus* (Pierce) Brenner; 2: *Cicatricosisporites patapscoensis* Brenner; 3: *Densoisporites velatus* Weyland & Krieger; 4: *Taurocosporites segmentatus* Stover; 5: *Pennipollis peroreticulatus* Brenner; 6: *Gleicheniidites senonicus* Ross.

pollen grain of the genus *Tricolpites* is noteworthy, because up to the Middle Albian this taxon is not abundantly represented.

The Sop-Peñosas sample corresponds to the El Soplao amber outcrop. The palynological assemblage inferred in this sample is characterized by a conspicuous increase in *I. dubius* (~51%) and a marked decrease in *Classopollis* (~11%). The percentage of spores of the genus *Deltoidospora* also increases (~8%). *Cicatricosisporites* scarcely occurs at this sample. Angiosperm pollen grains are low represented in this sample compared to Peñosas-Cóbreces.

From a biostratigraphical point of view, the occurrence of *Appendicisporites robustus* and *Cicatricosisporites patapscoensis* (Fig. 6.2) indicates a Late Aptian–Middle Albian age. However, the occurrence of *Liliacidites dividuus* (Fig. 6.1) and the low presence of *Tricolpites* sp. indicate an Early Albian age for the Peñosas-Cóbreces sample (Doyle and Robbins, 1977).

The area could have been covered by mixed conifer forests of Cupressaceae and Cheirolepidiaceae that grew near the sea. Their understory was integrated by pteridophytes, cycads and/or

Table 1 List of spores and pollen grains recorded from the Early Albian sediments of Las Peñosas Formation

	Peñosas-Cóbreces	%	Sop-Peñosas	%
Spores				
Appendicisporites robustus Kemp 1970	1	0.147	0	0
Appendicisporites dentimarginatus Brenner 1963	0	0	2	0.41
Appendicisporites tricornitatus Weyland & Greifeld 1953	1	0.147	0	0
Appendicisporites spp.	2	0.290	1	0.205
Baculatisporites sp.	0	0	1	0.205
Biretisporites potoniaei Delcourt & Sprumont 1955	3	0.440	3	0.615
Ceratosporites sp.	1	0.147	0	0
Cibotiumspora jurienensis (Balme 1957) Filatoff 1975	0	0	1	0.205
Cicatricosisporites apicanalis Phillips & Felix 1971	1	0.147	0	0
Cicatricosisporites apitereus Phillips & Felix 1971	1	0.147	0	0
Cicatricosisporites patapscoensis Brenner 1963	1	0.147	0	0
Cicatricosisporites recticicatricosus Döring 1965	1	0.147	0	0
Cicatricosisporites venustus Deák 1963	2	0.290	1	0.205
Cicatricosisporites spp.	13	1,908	6	1,230
Cingutriletes sp.	1	0.147	1	0.205
Contignisporites spp.	1	0.147	0	0
Crybelosporites sp.	0	0	1	0.205
Deltoidospora australis (Couper 1953) Srivastava 1975	4	0.587	13	2,664
Deltoidospora minor (Couper 1953) Pocock 1970	8	1,174	27	5,533
Deltoidospora sp.	4	0.587	8	1,640
Densoisporites velatus Weyland & Krieger 1953	1	0.147	1	0.205
Dictyophyllidites harrisii Couper 1958	2	0.290	1	0.205
Echinatisporis sp.	1	0.147	0	0
Gleicheniidites senonicus Ross 1949	0	0	4	0.819
Laevigatosporites sp.	0	0	7	1,434
Leptolepidites sp.	0	0	1	0.205
Patellasporites tavaredensis Groot & Groot 1962	1	0.147	0	0
Retitriletes sp.	0	0	1	0.205
Stereisporites sp.	0	0	1	0.205
Taurucosporites segmentatus Stover 1962	1	0.147	0	0
Trachysporites sp.	1	0.147	0	0
Triporoletes reticulatus (Pocock 1962) Playford 1971	1	0.147	1	0.205
Todisporites major Couper 1958	1	0.147	0	0
Pollen grains (gymnosperms)				
Alisporites bilateralis Rouse 1959	5	0.734	8	1,640
Alisporites spp.	20	2,937	12	2,460
Araucariacites australis Cookson 1947	12	1,762	25	5,123
Callialasporites dampieri Dev 1961	1	0.147	0	0
Cedripites sp.	1	0.147	0	0
Classopollis classoides Pflug 1953 emend. Pocock & Jansonius 1961	213	31,277	46	9,426
Classopollis spp.	58	8,517	9	1,844
Cycadopites spp.	8	1,174	2	0.410
Eucommiidites minor Groot & Penny 1960	4	0.587	2	0.410
Exesipollenites tumulus Balme 1957	6	0.881	3	0.615
Ginkgocycadophytus nitididus (Balme 1957) de Jersey 1962	1	0.147	3	0.615
Inaperturopollenites dubius (Potonié & Venitz 1932) Thompson & Pflug 1953	205	30,102	249	51,024
Inaperturopollenites spp.	21	3,084	9	1,844
Monosulcites chaloneri Brenner 1963	22	3,230	8	1,640
Monosulcites sp.	4	0.587	3	0.615
Pinuspollenites sp.	2	0.290	2	0.410
Podocarpidites sp.	0	0	2	0.410
Spheripollenites sp.	12	1,762	5	1,024
Vitreisporites pallidus (Reissinger 1950) Nilsson 1958	2	0.300	1	0.205
Undetermined bisaccate pollen grains	1	0.147	6	1,230
Pollen grains (angiosperms)				
Afropollis sp.	2	0.300	1	0.205
Clavatipollenites hughesii Couper 1958	2	0.300	3	0.615
Clavatipollenites minutus Brenner 1963	5	0.734	1	0.205
Clavatipollenites sp. (trichomosulcate)	4	0.587	0	0
Clavatipollenites spp.	5	0.734	4	0.819
Liliacidites dividus (Pierce 1961) Brenner 1963	3	0.440	0	0
Pennipollis peroreticulatus Brenner 1963	1	0.147	1	0.205
Tricolpites sp.	1	0.147	0	0
Undetermined angiospermous pollen grains	6	0.881	1	0.205
TOTAL miospores	681	100	488	100

Bennettitales. Ponds and swampy areas were mainly occupied by vascular cryptogams and early angiosperms, which could have aquatic habits. The predominance of *Classopollis* and the lower amount of spores observed in the Peñosas-Cóbreces sample could be related to a drier period. The more humid conditions of Sop-Peñosas are indicated by the higher percentages of *I. dubius* and *Deltoidospora* spp. as well as those of *Laevigatosporites* sp., *Alisporites* spp. and *Araucaricites australis*. Considering their composition, the assemblages are similar to those from the Upper Aptian–Lower Albian sediments of the Oliete sub-basin (Iberian Ranges) (Peyrot et al., 2007a, 2007b).

6 Plant Cuticles

Najarro et al. (2009) reported abundant plant cuticles in the amber-bearing beds of El Soplao outcrop, sometimes as levels up to 10 cm thick. This plant assemblage comprises female cones of the genus *Alvinia*, leafy axes of *Brachyphyllum*-type, *Nehvizdya* sp. (and its reproductive organs classified into the genus *Nehvizdyella*), *Pseudotorellia* sp., and mainly *Frenelopsis* and *Arctopitys* (cited as *Mirovia* in that paper, but see Nosova & Wcisło-Luraniec, 2007).

Up to four-time branched shoots of the cheirolepidiaceous conifer *Frenelopsis* have been collected during the last excavation in July 2009 (Fig. 3.5 and 3.6), due to the large area exposed in the prospect hole excavated. The shoots show lateral branches with a single branch per node, a branching pattern similar to that described and discussed by Daviero et al. (2001). These new records are of taphonomic and paleoenvironmental relevance. From the taphonomic point of view, the stiff, articulated leafy internodes of *Frenelopsis* were probably very brittle and fragmented when transport occurred (Gomez et al., 2001, 2002; Riera et al., 2010). At least for some of the plants of the insect-bearing amber assemblage of El Soplao, such an organization suggests a parautochthonous deposition. The representatives of *Frenelopsis* occupied habitats from freshwater wetlands to saline, coastal or estuarine marshes (e.g. Gomez et al., 2001, 2002; Mendes et al., 2010). Such a wide range of habitats suggests possible mangrove-like ecology for the *Frenelopsis* of El Soplao. This paleoecological inference is also supported by the sedimentological context and the occurrence of marine or brackish-water invertebrates in the sediment and on amber surfaces.

7 Charcoal and Charcoalified Plant Fibers

The first record of charcoalified (=fusainized) plant remains indicating paleofires is from the Silurian from Ludford Lane in the Welsh Borders in England (Glasspool et al., 2004). Scott (2000) provided a general view of the Pre-Quaternary history of fire based on charcoalified plant remains, which are especially important in sediments from the latest Jurassic and Early Cretaceous. Charcoalified plant remains are moderately common in a wide variety of facies, and some notable concentrations of considerable paleobotanical and paleoecological value can occur locally (Nichols et al., 2000).

In Spanish outcrops, amber and charcoal are very scarce except for a few levels in which both appear abundantly. This is the case of all the main outcrops for which this aspect has been explored: Peñacerrada (Suárez-Ruiz, 2003 and López del Valle, per. obs., 2008), La Hoya, San Just (Peñalver et al., 2007, 2008) and El Soplao. In these outcrops there are abundant cuboidal pieces of charcoal (=fusinite) of a few centimeters long (Fig. 7.2), and they are easily recognized with the naked eye even in the field by its silky luster, brittleness and friability. In addition, charcoal pieces are fibrous, black and opaque.

Features of the charcoal associated with amber in El Soplao outcrop using SEM are the undeformed structure and fabric of the tissue with open cell lumina, pits and homogenization of the cell walls (Fig. 7.3–7.5); see Sander and Gee (1990) and Scott (2000, 2010) for general description of charcoal. All of these features revealed by SEM examination are particularly characteristic of a pyrolysis origin. The most important feature is that different layers of the cell wall and adjacent cell walls cannot be distinguished from one to another due to the homogenization during burning. This homogenization of the wall takes place above 300ºC and the resulting charcoal is highly resistant to microbiological or chemical degradation during sedimentation and diagenesis (Cope and Chaloner, 1980). In San Just and El Soplao outcrops charcoal pieces with the cell lumina diagenetically filled with framboidal pyrite are found frequently (Fig. 7.6).

The levels of concentration of amber and charcoal in Spanish outcrops, including El Soplao, reveal paleofires in the resinous forests. Grimaldi et al. (2000) reported wood, insect remains and flowers, all charcoalified, and fire-damaged amber from the Upper Cretaceous (Turonian) of New Jersey, and Jarzembowski et al. (2008) reported a single piece of amber with similar features from the Lower Cretaceous of the Isle of Wight. Brasier et al. (2009) reported abundant examples of amber associated with charcoalified wood from the Early Cretaceous (140 Ma) amber deposit in Hastings (Sussex).

In addition to the frequent presence of charcoal associated with the amber in the same beds, a few amber pieces from El Soplao contain charcoalified plant fibers that appear dispersed inside the amber (Fig. 7.1). It is the first time in the fossil record that charcoalified fibers as bioinclusions have been reported. These fibers are small (around 0.7 mm long) and can be recognized as charcoalified fibers due to both their opaque black color and silky luster. This appearance is not due to the fossildiagenetic process because they contrast to other plant fibers in the same amber pieces that have the common translucent clear brown color without silky luster. These small charcoalified plant fibers became included in resin during paleofires moved by convective currents or, after paleofires, transported by the wind to the exposed resin from the soil of burned areas. Scott et al. (2000) reported how abundant finer charcoal material was transported by wind from a charred area of the Frensham Common Country Park (England) several days after a wildfire.

The kauri forests (Araucariaceae) of New Zealand most likely are the best extant correlate to the Cretaceous resiniferous

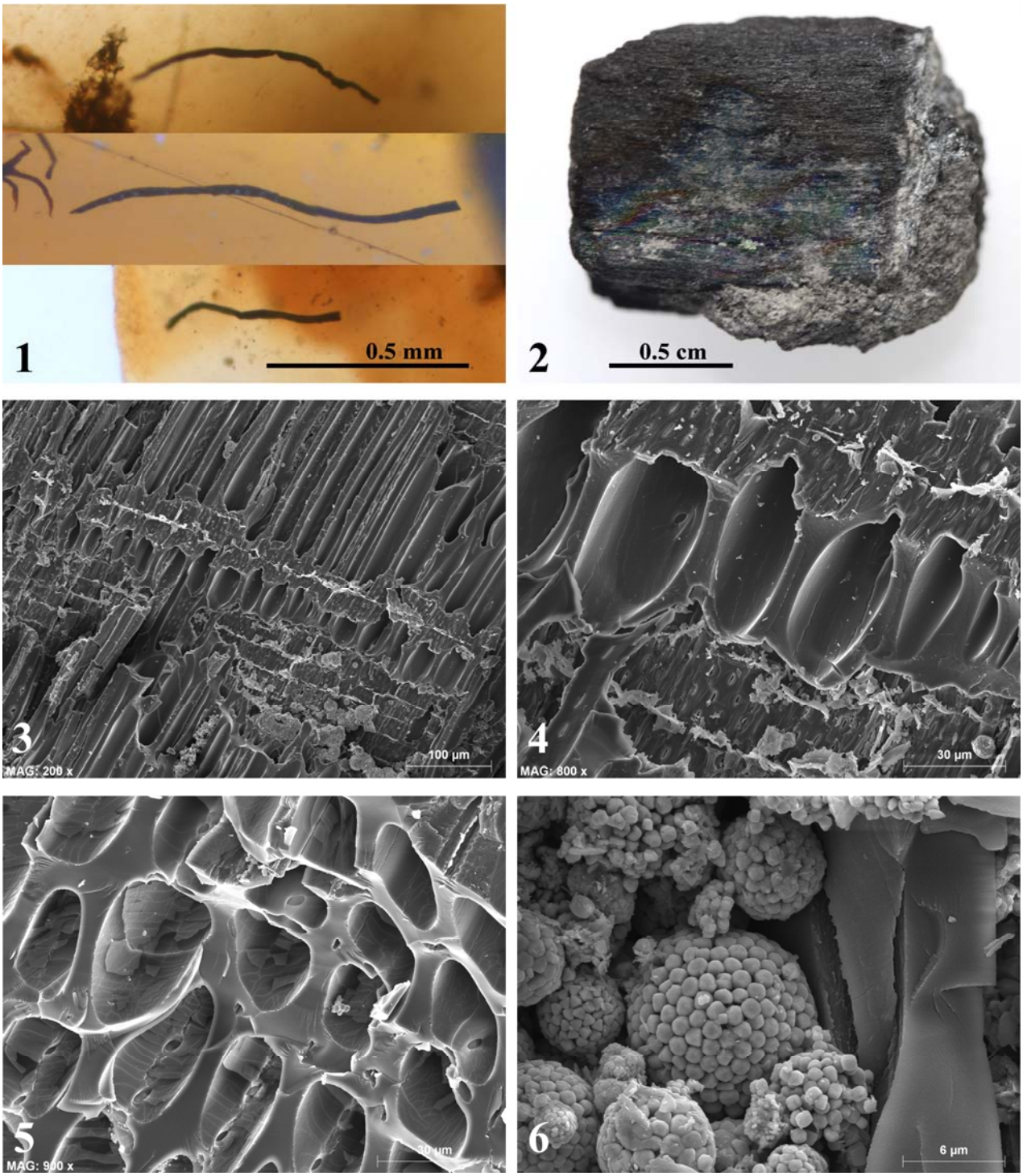

Fig. 7. Fossil carbonized woody tissues (charcoals) from El Soplao outcrop.
1: Three charcoalified plant fibers from the same small amber piece containing numerous of these remains (at the same scale); 2: cuboidal piece of charcoal; 3–5: scanning electron micrographs of charcoals show both pits and cell-wall homogenization in epidermis and peripheral tissues (micrograph 4 is a detail of 3); 6: framboidal pyrite partially filling the cell lumina (micrographs 3–6 are from microsamples of the piece figured in picture 2).

forests, except, perhaps, for the fact that the kauri forests do not have a fire ecology (Daniel J. Bickel, pers. comm., 2010). As it has been observed by us in the kauri forests, very large amounts of organic material occur due to the floor accumulation of litter, including resin pieces; Silvester and Orchard (1999) indicated that litter around a large kauri tree may reach 2 m or more in depth, with a mean residence time of 9–78 years due to a slow decomposition rate. Although resin burns easily, forest fires only

affect the litter superficially, except for ground fires (Scott, 2000). Thus the main part of the accumulated resin usually remains intact. Scott et al. (2000) reported a surface fire in the Frensham Common Country Park that charred only a few millimeters of the organic litter, so the pine crown was practically not affected by the fire. As indicated by Grimaldi et al. (2000) and Martínez-Delclòs et al. (2004), forest fires traumatically induced copious production of resin and they might have been an important factor in the genesis of amber deposits. From this respect, Brasier et al. (2009) reported charcoalified conifer wood from Hastings deposit with cell lumina filled with resin after the paleofire. However, we consider that the joined occurrences of large accumulations of amber and charcoal in Spanish outcrops, and abundant plant cuticles as well, were mainly the consequence of an intensive erosion of the litter in burnt forests, possibly including mass wasting; at this respect, Scott & Stea (2002) reported evidences of post-fire soil erosion in Cretaceous charcoal horizons of Nova Scotia. As summarized by Nichols et al. (2000) from different sources, the removal of vegetation by modern fires can increase erosion rates by weathering and during rainstorms by up to 30 times compared with the sink of pre-fire levels, and single wildfire events may be recognizable as responsible for individual depositional units, for example on alluvial fans.

Nichols et al. (2000) conducted actualistic experiments and concluded that charcoal is an unusual sedimentary material because most fresh material floats, but after prolonged immersion becomes waterlogged and sinks, mainly the small pieces. After the study of an area of heathland in SW England burned by an uncontrolled fire, Blackford (2000) concluded that large particles are not transported long distances and thus are indicative of local fires. The great abundances of centimeter-sized charcoal in amber-bearing beds of San Just and El Soplao outcrops suggest that paleofires in these cases were local or occurred close to the area of deposition. In the scenario we propose, intensive erosion by rivers and storm floods of a burned resinous forest area located close to the deltaic environments of deposition was promoted by the loss of vegetation, and resin plus charcoalified wood were transported together through water to coastal environments.

Another complementary factor that could contribute to the great amber accumulation in El Soplao outcrop was proposed by Najarro et al. (2009) based on sedimentological data: floods during rainstorms eroded and removed the resin and plant remains from the soils of coast-fringing forests. Pieces of resin and wood mixed with mud and sand then were transported by density flows to the coastal and interdistributary bays. Surely, more than one of these three factors might have occurred.

We can assume that wildfires had a great impact on environments and most likely they occurred mainly during the warm, drought season; lightning strike is the most important reported cause of naturally ignited fires today (Cope and Chaloner, 1980; Scott, 2010) and it was probably the same during the Cretaceous. Moreover, levels of atmospheric oxygen during the Cretaceous were among the highest during the Phanerozoic, close to 30% (vs. 20% today), leading to a much higher prevalence of fires (Robinson, 1989). Secondary evidence of the environmental impacts of wildfires can be obtained from plant and insect fossil records. The tree fern *Weichselia reticulata* has been recorded in some adjacent beds to the Spanish amber outcrops and this taxon can be related to environments disturbed by both floods and fires according to Coiffard et al. (2007) and Scott et al. (2000). More recently Ortega-Blanco et al. (2008) described a new species of anaxyelid woodwasp, *Eosyntexis parva*, from Peñacerrada I amber closely related to the extant anaxyelid taxa that lay eggs in burnt conifer trees shortly after the wildfires.

8 Marine or Brackish-water Invertebrates on Amber Surfaces

El Soplao amber deposit in some levels contains internal marcasite moulds of marine or brackish-water mollusks, and oyster shells that preserve the original calcium carbonate biomineralization. In addition, for the first time in the fossil record we report findings of large amber pieces that show their surfaces colonized by both serpulid worm tubes (Annelida: Polychaeta) (Fig. 8.1 and 8.2) and encrusting bryozoan colonies (Bryozoa: Cheilostomata) (Fig. 8.3); barnacles encrusting Baltic amber surfaces have been reported, but they are recent barnacles (see Grimaldi, 1996). Amber pieces with their entire surface colonized, or only with one side colonized, have been found.

Serpulid worm tubes exhibit four modes of fossilization that sometimes occur in the same amber piece, but in different parts: (1) as limonitic impressions of the tubes (Fig. 8.1); (2) as internal marcasite moulds (Fig. 8.2); (3) as amber tubes (internal fillings with resin during first fossildiagenetic phases); and (4) as original carbonate remains (Fig. 8.3). Serpulid tube remains are several millimeters long and internal tube fillings are approximately 0.35 mm diameter.

Bryozoan colonies left marks of the zooid exoskeletons on the amber surface and when original calcium carbonate remains are preserved (Fig. 8.3) they easily fade away during the washing of the pieces. Bryozoan colonies are multiserial and belong to the Order Cheilostomata; that group produces mineralized exoskeletons and form single-layered sheets that encrust over surfaces. Box-shaped, rectangular zooids are 0.34 × 0.29 mm in size.

Completeness of these large pieces suggests that they were constituted by polymerized resin when serpulids and bryozoans developed, not fossil resin from eroded strata (reworking process). Resin is comparatively less fragile than amber or copal and, in consequence, more commonly keeps its integrity during marine transport. In any case, this deposit contained a mixture of resin pieces from the litter, and fresh resin pieces directly transported from the trees, together with reworked resin pieces that remained a certain time in saline water. The presence of encrusting bryozoan colonies on the amber surfaces is not surprising because this type of organism is better adapted to shallow, high energy environments. In conclusion, this exceptional record indicates a littoral to coastal marsh environment of deposition for El Soplao outcrop.

Fig. 8. Marine or brackish-water invertebrates on the surfaces of El Soplao amber and insects as bioinclusions.
1: Detail of the serpulids preserved as limonitic impressions on the entire kidney-shaped amber piece 12 × 10 × 5 cm in size; 2: two serpulid worm tubes preserved as marcasite internal mould of the same amber piece; 3: bryozoan colony and several serpulids preserved as carbonate fossils on the surface of a large amber piece; 4: virtually complete specimen of the family Berothidae (Neuroptera); 5: specimen of Cucujoidea (Coleoptera). Photos 4 and 5 were made with integrated consecutive pictures taken at successive focal planes.

9 New Data on Insect Bioinclusions

Najarro et al. (2009) reported a high abundance of arthropod specimens embedded in the Early Cretaceous amber of El Soplao outcrop, and explained it as a consequence of the unusual concentration of amber pieces indicative of resin flows (drops, crusts and runnels) in this deposit. A significant percentage of amber pieces of this type contains numerous bioinclusions because the original resin was exposed to the atmosphere, was less viscous (it was more easily penetrated by insects), and successive flows encapsulated the trapped insects (Martínez-Delclòs et al., 2004).

Recent paleontological excavations have provided new bioinclusions of significant paleoecological and taxonomical value. To date, El Soplao amber has provided more than 200 bioinclusions, including fungi, plants, and diverse arthropods. Among them, only systematic studies on insects have been already started. The insect inclusions found belong to 11 recognized orders: Blattaria, Isoptera, Psocoptera, Thysanoptera, Raphidioptera, Neuroptera, Hemiptera, Coleoptera, Trichoptera, Hymenoptera, and Diptera; last two groups are the most abundant.

Neuropterid fauna from El Soplao amber is composed so far of Raphidioptera and Neuroptera, including the new genus and species of mesoraphidiid described by Pérez-de la Fuente et al. (2010) that is currently being studied. Neuropterans are represented by two specimens of dustywings (Coniopterygidae) and two beaded lacewings (Berothidae), one of them very complete and interpreted as a new morphotype (Fig. 8.4). Surely, the most outstanding finding is a tentative green lacewing larva (Chrysopidae), which, if confirmed, would be the oldest representative of the family in amber and one of the very few fossil chrysopid larvae ever reported. Its morphology, to be described and discussed elsewhere, is similar to those of the extant trash-carrying chrysopid larvae, which cover their backs with animal or plant debris chiefly as a defense against predators (Eisner et al., 2002). In fact, the specimen is surrounded by a dense filamentous cloud corresponding to its protective cover, proving the antiquity of the trash-carrying behavior in these lacewings, as was hypothesized by Engel and Grimaldi (2007).

Coleopterans from El Soplao amber are represented only by members of the suborder Polyphaga, and all of them are up to now interpreted as herbivorous or saproxylic forms, most probably living under the bark of the trees. As in other Lower Cretaceous outcrops of surrounding areas in Spain and France, the most abundant forms of beetles from El Soplao belong to superfamilies Elateroidea and Cucujoidea (Fig. 8.5), but there are also present forms of Curculionoidea (?Attelabidae, ? Nemonychidae) and possibly a member of Dascilloidea. The presence of two specimens of Curculionoidea in such small collection of beetles (approximately 10 specimens) is of paleoecological relevance, because this group of beetles is up to day closely related to hard parts of trees, in which larval stages developed, and the action damaging trees has also been pointed to as one of the possible causes for the increase in resin-production in trees during the Early Cretaceous and its subsequent record as fossil resins.

Although the hymenopteran assemblage of El Soplao is scarce, it is providing interesting data. It is composed of parasitoid wasps of several superfamilies as Ceraphronoidea (parasitoids of numerous taxa, hyperparasitoids sometimes), Platygastroidea (insect and spider egg parasitoids), Evanioidea (cockroach egg consumers during larval stage), Ichneumonoidea (commonly hyperparasitoids) and Mymarommatoidea (tiny egg parasitoids). Although ceraphronoids are currently under study, a first approximation allows us to recognize members of a recently described new family of Ceraphronoidea (Ortega-Blanco et al., 2010b). Ceraphronoids were exclusive from the Peñacerrada amber until date ; venation and some antennae aspects of the El Soplao morphotype indicate that it belongs to the same genus that is present in Peñacerrada amber. Platygastroids are the most common hymenopteran insects in El Soplao amber, as in all other Spanish ambers, and the study of this group is in progress. Apparently platygastroids belong to a new species with large, 14-articled antennae. A new parasitoid wasp species of the genus *Archaeromma* (Mymarommatoidea) has been recorded in El Soplao, as it was in Peñacerrada I. Recording the same insect species supports the hypothesis that the age of these ambers was equivalent or at least very close, and suggests that both outcrops had similar paleoecological characteristics.

Dipterans from El Soplao amber are represented by Brachycera and Nematocera forms. One specimen of *Litoleptis* sp. (Spaniidae) has been identified within the Brachycera, similar to one specimen described from San Just amber (Arillo et al., 2009). Other dipteran families present include Hybotidae (Brachycera), as well as Cecidomyiidae and Psychodoidea. The current paleodiversity of biting midges (Ceratopogonidae) has been evaluated, leading to the discovery of five species, including three new species (Najarro et al., 2009). The new species belong to the genera *Archiaustroconops*, Szadziewski, 1996, *Atriculicoides* Remm, 1976, and *Lebanoculicoides* Szadziewski, 1996. All these ancient biting midges would have shown a hematophagous diet which is considered plesiotypic within the family (Borkent, 1995).

10 Conclusions

We present herein data that suggest that amber pieces from El Soplao have at least two botanical sources. Part of these data strongly supports a source related to Cheirolepidiaceae and also suggests a molecular relationship of *Frenelopsis* with extant Cupressaceae. This relationship is based on the chemotaxonomic comparison of biological diterpenes found in amber and plant megafossils and extant Cupressaceae.

The taphonomic significance of wildfires in the origin of the Cretaceous amber accumulations has received little attention and has been clearly underestimated. The potential presence of charcoal, fire-damaged amber pieces and charcoalified plant fibers embedded inside the amber must be considered when studying the origin of the Cretaceous amber deposits. In fact, the occurrence of large accumulations of amber and charcoal in Spanish outcrops were consequence of intensive erosion of the

litter in burnt forests, possibly including mass wasting. This scenario has been well documented in the case of the El Soplao deposit, but similar studies on other Spanish amber deposits should be conducted.

The new data on the biological inclusions from El Soplao amber show a highly diversified entomofauna, mainly represented by dipterans and hymenopterans, with the presence of very specialized groups such as chrysopids or weevils, which may help to better understand the early evolution of some insect groups.

The data previously published and new data herein provided suggest a taphonomic history for the El Soplao amber that may have run approximately as follows: resin was exuded by conifers (perhaps by two different conifers, including Cheirolepidiaceae) closely to the deltaic environments of deposition. Conifer forests were well-present in the region, with understory integrated by pteridophytes, cycads and/or Bennettitales; ponds and swampy areas were mainly occupied by vascular cryptogams and early angiosperms, which could have aquatic habits. A diversified insect fauna, mainly represented by hymenopterans and dipterans, developed around the conifer trees and was abundantly embedded in resin. Coleopterans, which probably lived under the bark or in close contact with the wood of the conifer trees, were abundantly embedded as well. Wildfires in the resinous forests promoted both the resin production and an intensive erosion of the partially burned litter. Resin, fresh leaves, wood and charcoal were shortly transported together through water and accumulated alongside marine or brackish-water mollusks in a restricted tidal channel with low circulation and anoxic bottom-water. The conifer *Frenelopsis*, a potential source of resin as suggested by the biogeochemical analyses, grew close to the deposition area, where articulated branched shoots accumulated (parautochthonous deposition). Resin pieces differed in their biostratinomic histories because some of them remained a certain time in shallow, high energy saline waters where serpulids and bryozoans grew on the resin surfaces, resulting in a mixed assemblage. Low circulation and anoxic bottom-water promoted an early pyritization of the marine mollusks, charcoal and amber surfaces, including the fixed serpulid tubes. The assemblage was lastly buried by siltstones and sandstones. The maximum temperatures suffered by the amber deposit during diagenesis were in the range of 60–70ºC. The inferred low maturity levels were maybe responsible for the good preservation of amber molecular composition and its biological inclusions.

Acknowledgements

This work is part of the Ph.D. Thesis of three of the authors (M.N. -geology-, R.P.F. and J.O.B. -paleobiology-), which are supported by a scholarship from the Instituto Geológico y Minero de España (IGME), an APIF grant of the University of Barcelona, and a FPI grant from the Spanish Ministry of Science and Technology, respectively. This study is a contribution of the IGME Project 491-CANOA 35015 “Investigación científica y técnica de la Cueva de El Soplao y su entorno geológico”, the projects CGL2008-/01237BTE from the MICINN, CGL2008-00550/BTE: “Amber of the Cretaceous of Spain: A multidisciplinary study”, and the ANR Project AMBRACE BLAN07-1-184190. The contribution is framed in a collaborative agreement among the Cantabrian Government (Regional Cultural, Tourism and Sports Ministry), IGME and SIEC S.A. We thank Gonzalo Nieto and the staff of the Royal Botanic Garden of Madrid for permission and assistance in the sampling of extant conifers. We also express our thanks to Francisco Javier López Marcano (Regional Minister of the Cantabrian Government), José Pedro Calvo Sorando (IGME) and Fermin Unzué (manager of the El Soplao Cave) for their efforts and promotion of the study of the outcrop. We are grateful to Dr Daniel J. Bickel (Australian Museum, Sydney), Dr Vladimir Blagoderov (Natural History Museum, London) and an anonymous reviewer for careful reviews of the manuscript. Thanks are due to all people that participated in the paleontological excavations.

Manuscript received
accepted
edited by Fei Hongcai

References

Alonso, J., Arillo, A., Barrón, E., Corral, J.C., Grimalt, J., López, J.F., López, R., Martínez-Delclòs, X., Ortuño, V., Peñalver, E., and Trincão, P.R., 2000. A new fossil resin with biological inclusions in Lower Cretaceous deposits from Álava (Northern Spain, Basque-Cantabrian Basin). *Journal of Paleontology*, 74(1): 158–178.

Anderson, K.B., 2006. The nature and fate of natural resins in the geosphere. XII. Investigation of C-ring aromatic diterpenoids in Raritan amber by pyrolysis-GC-matrix isolation FTIR-MS. *Geochemical Transactions*, 7: 2.

Anderson, K.B., Winans, R.E., and Botto, R.E., 1992. The nature and fate of natural resins in the geosphere-II. Identification, classification and nomenclature of resinites. *Organic Geochemistry*, 18(6): 829–841.

Arillo, A., Peñalver, E., and García-Gimeno, V., 2009. First fossil *Litoleptis* (Diptera: Spaniidae) from the Lower Cretaceous amber of San Just (Teruel Province, Spain). *Zootaxa*, 2026: 33–39.

Batten, D.J., 1999. Extraction techniques - Small palynomorphs. In: Jones, T.P., Rowe, N.P. (eds.), *Fossil plants and spores: modern techniques*. The Geological Society, London, 15–19.

Blackford, J.J., 2000. Charcoal fragments in surface samples following a fire and the implications for interpretation of subfossil charcoal data. *Palaeogeography, Palaeoclimatology, Palaeoecology*, 164: 33–42.

Borkent, A., 1995. *Biting midges in the Cretaceous amber of North America (Diptera: Ceratopogonidae)*. Backhuys Publishers, Leiden, The Netherlands, 237 p.

Boscá, A., 1910. Cuenca calaminífera de Linares de Aragón. *Asociación Española para el Progreso de las Ciencias*, 4(1ª part): 171–181.

Brasier, M., Cotton, L., and Yenney, I., 2009. First report of amber with spider webs and microbial inclusions from the earliest Cretaceous (*c.* 140 Ma) of Hastings, Sussex. *Journal of the Geological Society*, London, 166: 989–997.

Casal, G., 1762. Succini Asturici, à Doctore Gafpar Cafal, Almae Eclefiae Cathedralis Ovetenfis Medico, reperti, folertique ejufdem cura probati, & examinati, Hiftoria. *Historia Natural y Médica del Principado de Asturias*, Facsimile ED. 1998. Servicio de Publicaciones. Principado de Asturias, Oviedo: 480.

Coiffard, C., Gomez, B., and Thevenard, F., 2007. Early Cretaceous Angiosperm Invasion of Western Europe and Major Environmental Changes. *Annals of Botany*, 100: 545–553.

Cope, M.J., and Chaloner, W.G., 1980. Fossil charcoal as evidence of past atmospheric composition. *Nature*, 283: 647–649.

Corral J.C., López Del Valle R., and Alonso J., 1999. El ámbar cretácico de Álava (Cuenca Vasco-Cantábrica, norte de España). Su colecta y preparación. *Estudios del Museo de Ciencias Naturales de Álava*, 14(special volume): 7–21.

Daviero, V., Gomez, B., and Philippe, M., 2001. Uncommon branching pattern within conifers: *Frenelopsis turolensis*, a Spanish Lower Cretaceous Cheirolepidiaceae. *Canadian Journal of Botany*, 79: 1400–1408.

Delclòs, X., Arillo, A., Peñalver, E., Barrón, E., Soriano, C., López del Valle, R., Bernárdez, E., Corral, C., and Ortuño, V. M., 2007. Fossiliferous amber deposits from the Cretaceous (Albian) of Spain. *Comptes Rendus Palevol*, 6: 135–149.

Doyle, J.A., and Robbins, E.I., 1977. Angiosperm pollen zonation of the Continental Cretaceous of the Atlantic coastal plain and its application to deep wells in the Salisbury embayment. *Palynology*, 1: 43–78.

Eisner, T., Carrel, J.E., Van Tassel, E., Hoebeke, E.R., and Eisner, M., 2002. Construction of a defensive trash packet from sycamore leaf trichomes by a chrysopid larva (Neuroptera: Chrysopidae). *Proceedings of the Entomological Society of Washington*, 104(2): 437–446.

Engel, M. S., and Grimaldi, D. A., 2007. The neuropterid fauna of Dominican and Mexican amber (Neuropterida: Megaloptera, Neuroptera). *American Museum Novitates*, 3587: 58 pp.

Farjon, A., 2008. *The natural history of Conifers*. Timber Press, New York, 304.

García-Mondéjar, J., Aguirrezabala, L.M., Aranburu, A., Fernández-Mendiola, P.A., Gómez-Pérez, I., López-Horgue, M., and Rosales, I., 1996. Aptian-Albian tectonic pattern of the Basque-Cantabrian Basin (northern Spain). *Geological Journal*, 31: 13–45.

Glasspool, I.J., Edwards, D., and Axe, L., 2004. Charcoal in the Silurian as evidence for the earliest wildfire. *Geology*, 32(5): 381–383.

Gomez, B., Martín-Closas, C., Barale, G., Solé de Porta, N., Thévenard, F., and Guignard, G., 2002. *Frenelopsis* (Coniferales: Cheirolepidiaceae) and related male organ genera from the Lower Cretaceous of Spain. *Palaeontology*, 45: 997–1036.

Gomez, B., Martín-Closas, C., Méon, H., Thévenard, F., and Barale, G., 2001. Plant taphonomy and palaeoecology in the lacustrine delta of Uña (Upper Barremian, Iberian Ranges, Spain). *Palaeogeography, Palaeoclimatology, Palaeoecology*, 170: 133–148.

Gradstein, F.M., and Ogg, J.G., 2009. The geologic time scale. In: Hedges, S.B., and Kumar, S. (eds.), *The Timetree of Life*, Oxford University Press, 26–34.

Grimaldi, D.A., 1996. *Amber: window to the past*. American Museum of Natural History Ed., New York, 215.

Grimaldi, D.A., and Engel, M.S., 2005. *Evolution of the insects*. Cambridge University Press, New York, 755 p.

Grimaldi, D.A., Shedrinsky, A., and Wampler, P., 2000. A remarkable deposit of fossiliferous amber from the Upper Cretaceous (Turonian) of New Jersey. In: Grimaldi, D.A. (ed.), *Studies on Fossils in Amber, with Particular Reference to the Cretaceous of New Jersey*. Backhuys Publishers Leiden, Leiden, 1–76.

Hautevelle, Y., Michels, R., Malartre, F., and Trouiller, A., 2006. Vascular plant biomarkers as proxies for palaeoflora and palaeoclimatic changes at the Dogger/Malm transition of the Paris Basin (France). *Organic Geochemistry*, 23: 610–625.

Hines, F.M., 1985. Sedimentation and tectonics in north-west Santander. In: Milá, M.D., and Rosell, J. (eds.), 6th European Regional Meeting, Excursion Guidebook. International Association of Sedimentologists, 371–398.

Jarzembowski, E.A., Azar, D., and Nel, A., 2008. A new chironomid (Insecta: Diptera) from Wealden amber (Lower Cretaceous) of the Isle of Wight (UK). *Geologica Acta*, 6(3): 285–291.

Le Pichon, X., and Sibuet, J.C., 1971. Western extension of boundary between European and Iberian plates during the Pyrenean orogeny. *Earth and Planetary Science Letters*, 12: 83–88.

Martínez-Delclòs, X., Briggs, D.E.G., and Peñalver, E., 2004. Taphonomy of insects in carbonates and amber. *Palaeogeography, Palaeoclimatology, Palaeoecology*, 203: 19–64.

Mendes, M.M., Dinis, J.L., Gomez, B., and Pais, J., 2010. The cheirolepidiaceous conifer *Frenelopsis teixeirae* Alvin et Pais from the lower Hauterivian of Vale Cortiço (Torres Vedras, western Portugal). *Review of Palaeobotany and Palynology*, doi: 10.1016/j.revpalbo.2010.03.002.

Menor-Salván, C., Najarro, M., Rosales, I., Velasco, F., and Tornos, F., 2009a. Quimiotaxonomía y origen botánico del ámbar de El Soplao (Cantabria, España). *Macla*, 11: 123–124.

Menor-Salván, C., Najarro, M., Rosales, I., Velasco, F., Tornos, F., and Simoneit, B.R.T., 2010. Biological diterpenes preserved in lower Cretaceous amber from Basque Cantabrian Basin (El Soplao, Cantabria, Spain). Paleochemotaxonomical aspects. *Organic Geochemistry*. Accepted.

Menor-Salván, C, Najarro, M., Velasco, F., Tornos, F., and Rosales, I., 2009b. A new Lower Cretaceous fossil resin from El Soplao, Cantabria (Spain): Biomarkers and chemotaxonomy. *Geochimica et Cosmochimica Acta*, 73 (13S), A870.

Miller, C.N., 1999. Implications of Fossil Conifers for the Phylogenetic Relationships of Living Families. *Botanical Reviews*, 65: 239–277.

Najarro, M., Peñalver, E., Rosales, I., Pérez-de la Fuente, R., Daviero-Gomez, V., Gomez, B., and Delclòs, X., 2009. Unusual concentration of Early Albian arthropod-bearing amber in the Basque-Cantabrian Basin (El Soplao, Cantabria, Northern Spain): Palaeoenvironmental and palaeobiological implications. *Geologica Acta*, 7(3): 363–387.

Najarro, M., Rosales, I., and Martín-Chivelet, J., 2010. Major palaeoenvironmental perturbation in an Early Aptian carbonate platform: Prelude of the Oceanic Anoxic Event 1a?. *Sedimentary Geology*, doi: 10.1016/j.sedgeo.2010.03.011.

Nel, P., Peñalver, E., Azar, D., Hodebert, G., and Nel, A., 2010. Modern thrips families Thripidae and Phlaeothripidae in the Early Cretaceous amber (Insecta: Thysanoptera). *Annales de la Société entomologique de France*, 46(1). In press.

Nichols, G., Cripps, J.A., Collinson, M.E., and Scott, A.C., 2000. Experiments in waterlogging and sedimentology of charcoal: results and implications. *Palaeogeography, Palaeoclimatology, Palaeoecology*, 164: 43–56.

Nosova, N., and Wcisło-Luraniec, E., 2007. A reinterpretation of *Mirovia* Reymanówna (Coniferales) based on the reconsideration of the type species *Mirovia szaferi* Reymanówna from the Polish Jurassic. *Acta Palaeobotanica,* 47: 359–377.

Ortega-Blanco, J., Peñalver, E., Delclòs, X., and Engel, M.S., 2010a. False fairy wasps in Early Cretaceous amber from Spain (Hymenoptera: Mymarommatoidea). *Palaeontology*. In press.

Ortega-Blanco, J., Rasnitsyn, A.P., and Delclòs, X., 2008. First record of anaxyelid woodwasps (Hymenoptera: Anaxyelidae) in Lower Cretaceous Spanish amber. *Zootaxa*, 1937: 39–50.

Ortega-Blanco, J., Rasnitsyn, A.P., and Delclòs, X., 2010b. A new family of ceraphronoid wasps from Early Cretaceous Álava Amber, Spain. *Acta Paleontologica Polonica*. In press.

Otto, A., and Simoneit, B.R.T., 2002. Biomarkers of Holocene buried conifer logs from Bella Coola and north Vancouver, British Columbia, Canada. *Organic Geochemistry*, 33: 124–1251.

Otto, A., Simoneit, B.R.T., and Wilde, V., 2007. Terpenoids as chemosystematic markers in selected fossil and extant species of Pine (*Pinus*, Pinaceae). *Botanical Journal of the Linnean Society*, 154: 129–140.

Peñalver, E., Delclòs, X., and Soriano, C., 2007. A new rich amber outcrop with palaeobiological inclusions in the Lower Cretaceous of Spain. *Cretaceous Research*, 28: 791–802.

Peñalver, E., Grimaldi, D., and Delclòs, X., 2008. *Early spider web*. Yearbook of Science and Technology 2008. MacGraw Hill: 103–105.

Pereira, R., de Souza Carvalho, I., Simoneit, B.R.T., and de Almeida Azevedo, D., 2009. Molecular composition and chemosystematic aspects of Cretaceous amber from the Amazonas, Araripe and Recôncavo basins, Brasil. *Organic Geochemistry*, 40: 863–875.

Pérez-de la Fuente, R., Nel, A., Peñalver, E., and Delclòs, X., 2010. A new Early Cretaceous snakefly (Raphidioptera: Mesoraphidiidae) from El Soplao amber (Spain). *Annales de la Société entomologique de France*, 46(1). In press.

Perrichot, V., and Néraudeau, D., 2009. Foreword. Cretaceous ambers from southwestern France: geology, taphonomy and palaeontology. *Geodiversitas*, 31(1): 7–12.

Peyrot, D., Rodríguez-López, J.P., Barrón, E., and Meléndez, N., 2007a. Palynology and biostratigraphy of the Escucha Formation in the Early Cretaceous Oliete Sub-basin, Teruel, Spain. *Revista Española de Micropaleontología*, 39(1–2): 135–154.

Peyrot, D., Rodríguez-López, J.P., Lassaletta, L., Meléndez-Hevia, N., and Barrón, E., 2007b. Contributions to the palaeoenvironmental knowledge of the Escucha Formation in the Lower Cretaceous Oliete Sub-basin, Teruel, Spain. *Comptes Rendus Palevol*, 6: 469–481.

Rat, P., 1988. The Basque-Cantabrian basin between the Iberian and European plates some facts but still many problems. *Revista de la Sociedad Geológica de España*, 1: 327–348.

Riera, V., Marmi, J., Oms, O., and Gomez, B., 2010. Orientated plant fragments revealing tidal palaeocurrents in the Fumanya mudflat (Maastrichtian, southern Pyrenees): insights in palaeogeographic reconstructions. *Palaeogeography, Palaeoclimatology, Palaeoecology*, 288: 82–92.

Robinson, J.M., 1989. Phanerozoic O_2 variation, fire, and terrestrial ecology. *Palaeogeography, Palaeoclimatology, Palaeoecology*, 75: 223–240.

Sander, P.M., and Gee, C.T., 1990. Fossil charcoal: techniques and applications. *Review of Palaeobotany and Palynology*, 63: 269–279.

Scott, A.C., 2000. The Pre-Quaternary history of fire. *Palaeogeography, Palaeoclimatology, Palaeoecology*, 164: 281–329.

Scott, A.C., 2010. Charcoal recognition, taphonomy and uses in palaeoenvironmental analysis. *Palaeogeography, Palaeoclimatology, Palaeoecology*, doi: 10.1016/ j.palaeo.2009.12.012

Scott, A.C., and Stea, R., 2002. Fires sweep across the Mid-Cretaceous landscape of Nova Scotia. *Geoscientist*, 12 (1): 4–6.

Scott, A.C., Cripps, J.A., Collinson, M.E., and Nichols, G.J., 2000. The taphonomy of charcoal following a recent heathland fire and some implications for the interpretation of fossil charcoal deposits. *Palaeogeography, Palaeoclimatology, Palaeoecology*, 164(1–4): 1–31.

Seoane, L.V., 1998. Comparative study of extant and fossil conifer leaves from the Baqueró Formation (Lower Cretaceous), Santa Cruz Province, Argentina. *Review of Palaeobotany and Palynology*, 99: 247–263.

Silvester, W.B., and Orchard, T.A., 1999. The biology of kauri (*Agathis australis*) in New Zealand. I. Production, biomass, carbon storage, and litter fall in four forest remnants. *New Zealand Journal of Botany*, 37: 553–571.

Soto, R., Casas-Sainz, A.M., Villalaín, J., and Oliva-Urcía, B., 2007. Mesozoic extension in the Basque Cantabrian basin (N Spain): Contributions from AMS and brittle mesostructures. *Tectonophysics*, 445: 373–394.

Stefanova, M., Oros, D.R., Otto, A., and Simoneit, B.R.T., 2002. Polar aromatic biomarkers in the Miocene Maritza-East lignite, Bulgaria. *Organic Geochemistry*, 33: 1076–1091.

Suárez-Ruiz, I., 2003. Caracterización y estudio petrográfico del ámbar y de los sedimentos carbonosos a él asociados en el Cretácico de Álava (País Vasco). *Estudios del Museo de Ciencias Naturales de Álava*, 18(special volume): 63–89.

Sweeney, J.J., and Burnham, A.K., 1989. A chemical kinetic model of vitrinite maturation and reflection. *Geochimica et Cosmochimica Acta*, 53: 2649–2657.

Wilmsen, M., 2005. Stratigraphy and biofacies of the Lower Aptian of Cuchía (Cantabria, northern Spain). *Journal of Iberian Geology*, 31: 253–275.

Yamamoto, S., Otto, A., Krumbiegel, G., and Simoneit, B.R.T., 2006. The natural product biomarkers in succinite, glessite and stantienite ambers from Bitterfield, Germany. *Review of Palaeobotany and Palynology*, 140: 27–49.

Organic Geochemistry 41 (2010) 1089–1103

Contents lists available at ScienceDirect

Organic Geochemistry

journal homepage: www.elsevier.com/locate/orggeochem

Terpenoids in extracts of Lower Cretaceous ambers from the Basque-Cantabrian Basin (El Soplao, Cantabria, Spain): Paleochemotaxonomic aspects

César Menor-Salván [a,*], Maria Najarro [b], Francisco Velasco [c], Idoia Rosales [b], Fernando Tornos [b], Bernd R.T. Simoneit [d,e]

[a] Centro de Astrobiología (CSIC-INTA), 28850 Torrejón de Ardoz, Spain
[b] Instituto Geológico y Minero de España (IGME), Rios Rosas 23, 28003 Madrid, Spain
[c] Universidad del País Vasco, Departamento Mineralogía y Petrología, Apdo. 644, 48080 Bilbao, Spain
[d] COGER, King Saud University, Riyadh 11451, Saudi Arabia
[e] Department of Chemistry, Oregon State University, Corvallis, OR 97331, USA

ARTICLE INFO

Article history:
Received 22 June 2010
Accepted 30 June 2010
Available online 3 July 2010

ABSTRACT

The composition of terpenoids from well preserved Cretaceous fossil resins and plant tissues from the amber bearing deposits of El Soplao and Reocín in Cantabria (northern Spain) have been analyzed using gas chromatography–mass spectrometry and the results are discussed using the terpenoid composition of extant conifers as a reference. Amber is present at many horizons within two units of coastal to shallow marine siliciclastics of Albian and Cenomanian age. The fossil resins are associated with black amber (jet) and abundant, well preserved plant cuticle compressions, especially those of the extinct conifer genus *Frenelopsis* (Cheirolepidiaceae).

We report the molecular characterization of two types of amber with different botanical origins. One of them is characterized by the significant presence of phenolic terpenoids (ferruginol, totarol and hinokiol) and pimaric/isopimaric acids, as well as their diagenetic products. The presence of phenolic diterpenoids together with the lack of abietic and dehydroabietic acids excludes both Pinaceae and Araucariaceae as sources for this type of amber. The biological diterpenoid composition is similar to that observed for extant Cupressaceae. The second type of amber is characterized by the absence of phenolic terpenoids and other specific biomarkers. Some terpenoids with uncertain structure were detected, as well as the azulene derivative guaiazulene. Our results suggest that the amber from Cantabria could be fossilized resin from *Frenelopsis* and other undetermined botanical sources. The biological terpenoid assemblage confirms a chemosystematic relationship between *Frenelopsis* and modern Cupressaceae.

1. Introduction

Amber is fossilized resin produced from the exudates of conifers and certain angiosperms and is considered to be one of the few fossil deposits of exceptional preservation (*Konservat Lagerstätten*), because it permits the conservation of fossil organisms with all their delicate anatomical details. Fossil resins not only preserve the anatomy of fossil life forms that were trapped as biological inclusions, but also constitute a valuable source of information about their own botanical origin, ancient terrigenous ecosystems and climatic change by means of their chemical composition (Anderson and Crelling, 1995).

Analysis of the chemical composition of fossil resins is not straightforward, because the original biochemical fingerprints of the resins are usually modified during diagenesis, with the bioterpenoids (unmodified biosynthetic natural products) being transformed into geoterpenoids (diagenetic products of degraded bioterpenoids that are found in amber and fossil plant tissues; Otto et al., 2007). Despite these diagenetic alterations, geoterpenoids retain the basic skeletal structures of their biological precursors and can be used as molecular markers (biomarkers; Peters et al., 2005; Marynowski et al., 2007). Conifers synthesize mainly diterpenoids, which are, along with sesquiterpenoids, the compounds that provide the best results as diagnostic biomarkers of conifers and their resins (Otto and Wilde, 2001). Among the diterpenoids preserved in amber, labdane derivatives and non-phenolic abietane diagenetic derivatives have the most limited chemotaxonomic value, as they occur in all conifer families. On the other hand, phenolic terpenoids, such as ferruginol and totarol, are produced only by

* Corresponding author. Tel.: +34 91 520 6402 6458; fax: +34 91 520 1621.
E-mail addresses: cmenor@amyp.es, menorsc@inta.es (C. Menor-Salván), m.najarro@igme.es (M. Najarro), francisco.velasco@ehu.es (F. Velasco), i.rosales@igme.es (I. Rosales), f.tornos@igme.es (F. Tornos).

0146-6380/$ - see front matter © 2010 Elsevier Ltd. All rights reserved.
doi:10.1016/j.orggeochem.2010.06.013

the members of the families Cupressaceae and Podocarpaceae (Cox et al., 2007). Therefore, the chemotaxonomic value of these compounds is very high and their presence in amber provides very useful palaeobotanical information. Although the preservation potential of polar biomarkers is considered to be low (Otto et al., 2007), the oldest polar diterpenoids have been identified in extracts of Middle Jurassic fossil conifer wood from Poland (Marynowski et al., 2007), and diterpenoid derivatives could also be liberated from a Carboniferous amber by pyrolysis (Bray and Anderson, 2009).

Recently, a new Cretaceous amber deposit with exquisite, well preserved fossil organisms, mostly insects, has been discovered in northern Spain (Rábago village in El Soplao territory, Cantabria; Menor-Salván et al., 2009; Najarro et al., 2009). Based on preliminary infrared spectroscopy of the El Soplao amber (Najarro et al., 2009) and previous gas chromatography–mass spectrometry (GC–MS) studies on amber from a neighboring site in Álava (Alonso et al., 2000; Chaler and Grimalt, 2005), it has been suggested that exudate from *Agathis* (a conifer of the family Araucariaceae) was the most likely source of this amber, as has also been proposed for other Cretaceous ambers (e.g. Lambert et al., 1996; Alonso et al., 2000; Poinar et al., 2004; Chaler and Grimalt, 2005; Delclòs et al., 2007). This speculation was largely based on the presence of some geoterpenoids that may have been derived from agathic and pimaric acids. However, although those compounds and their diagenetic derivatives are characteristic of Araucariaceae, they are not diagnostic, because they can also be found in other extant conifer families (Otto et al., 2007). Moreover, Alonso et al. (2000) have reported the presence of the phenolic abietane ferruginol in the Álava amber samples, indicating that more extensive study of the chemotaxonomic information contained in the amber is necessary to establish its definite botanical origin.

In addition, meso- and macrofossil plant remains of Araucariaceae are absent in these amber bearing deposits, although there are plenty of cuticles and remains of other vascular plants, especially the genera *Frenelopsis* sp. and *Mirovia* sp., of the extinct conifer families Cheirolepidiaceae and Miroviaceae, respectively (Gomez et al., 2002a; Najarro et al., 2009). This is also the case in many other amber deposits from the Cretaceous of Spain and France (e.g. Delclòs et al., 2007; Néraudeau et al., 2008). Thus, the recurrent association of amber with cuticles of Cheirolepidiaceae and Miroviaceae, along with the lack of Araucariaceae remains (except for a small amount of pollen grains in the sediments) (Barrón et al., 2001), challenges the proposed origin of the amber. Since chemical evidence has not yet given a definitive answer, more convincing proof is necessary to accept Araucariaceae as the source of the resin.

In this study, amber pieces and associated fossil leaves from the Cretaceous amber bearing deposit of El Soplao (Cantabria; Fig. 1) were systematically analyzed using complementary techniques such as infrared spectroscopy (FTIR) and GC–MS. The overall aim was to identify the terpenoids preserved and their diagenetic transformation products in the fossil resin and to determine their possible botanical sources. Due to exceptional preservation, the amber bearing deposit at El Soplao offers a unique opportunity to compare the molecular composition of the amber with that of plant remains from the family Cheirolepidiaceae and Miroviaceae, which appear in the same deposit. A morphological similarity between extinct Cheirolepidiaceae and extant Cupressaceae has been described, but their relationship remains speculative due mainly to the lack of molecular evidence (Broutin and Pons, 1975; Alvin and Hluštík, 1979; Seoane, 1998; Miller, 1999; Farjon, 2008). As Cheirolepidiaceae is an extinct family, the connection between the two families could aid in the chemotaxonomical study of amber and in the confirmation of the botanical origin. We present data of two separate types of amber found in the El Soplao deposit and discuss their botanical origin using comparative chemotaxonomy based on modern resin compositions and related terpenoids found in amber associated fossils.

2. Samples and methods

2.1. Geological background

The analyzed samples belong to the Cretaceous succession at the northwestern margin of the Basque-Cantabria Basin in northern Spain. During the Cretaceous, the evolution of this basin was controlled by extensional, and perhaps strike-slip, deformation associated with the opening of the North Atlantic Ocean and the Bay of Biscay (e.g. Le Pichon and Sibuet, 1971; Rat, 1988; García-Mondéjar et al., 1996; Soto et al., 2007). Rifting during the Late Jurassic–Early Cretaceous led to the formation of several narrow sub-basins controlled by E–W, NW–SE and SW–NW trending faults; these basins host both continental and marine sediments of variable thickness (García-Mondéjar et al., 1996; Soto et al., 2007).

The study area lies in the Cantabria region immediately to the north of the Cabuérniga Ridge (Fig. S1; supplementary material), an E–W fault zone that represents a Late-Variscan structure reactivated first as a paleo-high bounded by normal faults during the Early Cretaceous, and later as reversal faults during the widespread Cenozoic (Pyrenean) compression. The Lower–Middle Cretaceous (Barremian–Early Cenomanian) deposits in the study area are weakly deformed and affected only by gentle folding. They are composed of a relatively thin (~200–800 m) syn-rift sequence that lies unconformably on Carboniferous to Lower Jurassic basement (Fig. S1).

A simplified synthesis of the stratigraphy in the El Soplao and Reocín areas is shown in Fig. 1, with formation names according to Hines (1985) and revised by Najarro et al. (2009). The amber bearing deposit at El Soplao is included within the Las Peñosas Formation (Fig. 1), a Lower Albian unit (~112–110 Ma) of continental to transitional marine siliciclastics. Detailed descriptions of field sections, depositional environments and fossil content of this unit are given in Najarro et al. (2009). Within the outcrop, the El Soplao amber deposit is characterized by about 1.5–2 m of dark, carbonaceous lutites, siltstones and sandstones with interbedded, centimeter to decimeter layers with remarkable accumulations of plant remains and amber pieces of different sizes and forms (Fig. 2A and B). Most amber pieces show a blue-purple color under normal sunlight and bright milky blue fluorescence under ultraviolet light. Plant cuticles are very abundant in the levels associated with amber (Fig. 2C). They are mainly assigned to the conifer genera *Frenelopsis* and *Mirovia*, along with other more occasional leaves of the ginkgoalean genera *Nehvizdya* and *Pseudotorellia* (Najarro et al., 2009). In most of the amber beds, leaves of the genus *Frenelopsis* of the extinct conifer family Cheirolepidiaceae are the dominant macro-botanical remains. *Frenelopsis* were xeromorphic plants adapted to coastal habitats and probably grew mainly in brackish coastal marshes and mangroves, but were adapted to a wider range of habitats (Gomez et al., 2002a, 2003).

The amber deposit at Reocín (Fig. S1; supplementary material) is slightly younger than the El Soplao amber deposit. It is included within the Bielva Formation (Fig. 1), a Latest Albian–Early Cenomanian (~102–99 Ma) unit composed of about 250 m of tidal dominated, estuarine siliciclastic deposits in the study area (Hines, 1985). Within this unit, the amber accumulations are associated with carbonaceous claystones and tidal channel sandstones developed in estuarine mouth subtidal areas (López-Horgue et al., 2001). Despite the differences in age, the Reocín amber shows the same composition as the El Soplao amber. Thermal maturity indicators (vitrinite reflectance) of macerals in the El Soplao deposit reveal minor changes in the organic matter of the resins during their diagenetic history and maximum thermal conditions during burial of

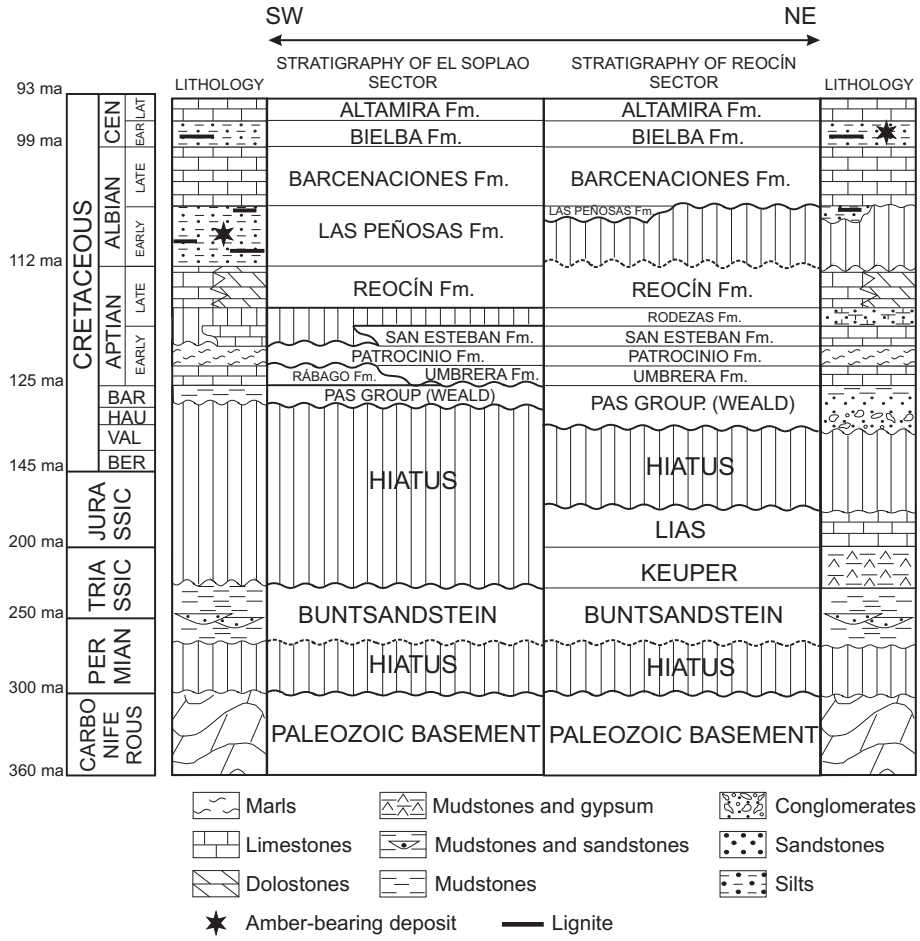

Fig. 1. Chrono- and lithostratigraphy of the El Soplao and Reocín areas (modified from Hines, 1985). Chronostratigraphy after Gradstein et al. (2004).

~60–70 °C (Supplementary material). Consequently and due to its higher transparency and lack of inclusions and interferences, the El Soplao amber was used preferentially for the chemosystematic study.

2.2. Sampling

Amber pieces, jet (black amber), fossil wood and sediments rich in plant cuticles were collected from the El Soplao deposit during a recent excavation in October 2008. Two types of amber pieces were found at the deposit in the same sedimentological and taphonomical context: *A* type, characterized by a strong blue-purple color under natural light, purple-reddish under artificial light and less abundant *B* type, yellow-honey under artificial light and honey with a bluish tinge under natural light. We collected the two types of amber present and the black amber associated with amber of type *A* and fossil plant tissue. Plant cuticles were obtained from claystones by rinsing the plant rich sediment in an ultrasonic bath of distilled water to remove all the clay and silt sediment. The organic residue (Fig. 2C) was air dried. Plant fragments and leaves from different families were distinguished and separated under a stereomicroscope.

2.3. Analytical methods

2.3.1. Infrared spectroscopy (FTIR)

IR spectra of pulverized solid amber were obtained using a Nexus Nicolet FTIR spectrometer in the 4000–400 cm^{-1} range.

2.3.2. Extraction and fractionation

For the analytical characterization, two representative single pieces (*A* and *B*; Table 1) of amber of about 50 g, with the highest transparency available and free of major inclusions, crusts and debris, were collected from the El Soplao deposit. Each piece was crushed and extracted for 4 h with dichloromethane:methanol (2:1 v:v) using a Büchi model B-811 automatic extractor. The extractable material constitutes 16% of the total amber weight on average. One aliquot of extract was injected directly into the port of the gas chromatograph.

The bulk extract was then processed in order to purify the phenolic terpenoid fraction and the acidic fraction and to identify unambiguously the minor components with higher chemosystematic value. The aim was to establish a complete descriptive composition of the amber sample. The extract was concentrated to a volume of 20 ml and fractionated by flash chromatography on silica gel. The elution was performed using *n*-hexane, dichloromethane, dichloromethane:methanol (1:1 v:v), and methanol as eluents and 25 fractions of 1.5 ml were collected using an automatic fraction collector. Each fraction was concentrated by evaporation of the solvent under N_2 and analyzed by GC–MS. The fractions with similar compositions were combined. The polar fraction (eluted with methanol) and the fractions containing ferruginol were recombined, further separated using a glass column (20 cm) filled with chromatographic grade silica gel, and eluted sequentially with *n*-hexane:dichloromethane (1:1 v:v), pure dichloromethane, dichloromethane:methanol (1:1 v:v) and methanol. Four fractions of 20 ml were collected, designated A to D. All fractions were dried and the alcohols and acids converted to trimethylsilyl derivatives

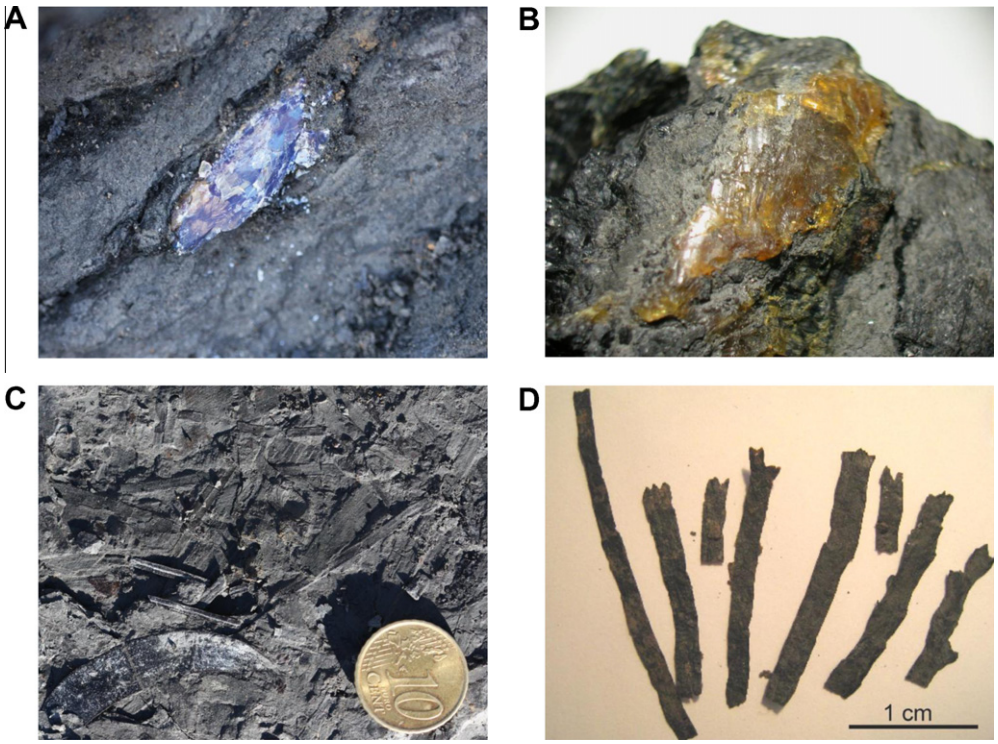

Fig. 2. Photographs of amber and palaeobotanical components used in this study. (A) In situ amber piece of type *A* (6 cm) from the El Soplao deposit, showing blue-purple color under sunlight. (B) Amber piece of type *B* (3 cm) on fossil wood under sunlight. (C) In situ sediments showing their palaeobotanical components: fossil leaves of *Mirovia* and *Frenelopsis* and one leaf of Ginkgoaceae. (D) Selected leaves of *Frenelopsis* sp. were used for biomarker analysis. (For interpretation of the references to color in this figure legend, the reader is referred to the web version of this article.)

by reaction with N,O-bis-(trimethylsilyl)trifluoroacetamide (BSTFA) containing 1% trimethylchlorosilane (TMCS) at 65 °C for a period of 3 h. Finally, the derivatized fractions were diluted with *n*-hexane and injected into the port of the gas chromatograph.

To study the molecular content of fossil *Frenelopsis* and *Mirovia* leaves (Fig. 2), 5 g of leaves were extracted for 4 h with dichloromethane:methanol (2:1 v:v) using a Büchi model B-811 automated extractor. The bulk extract was filtered and analyzed directly by GC–MS. The extract was then fractionated using silica gel chromatography in two fractions by elution with *n*-hexane:dichloromethane (3:1 v:v) and dichloromethane:methanol (4:1 v:v). The polar fraction was dried and derivatized using the method described above. The samples of jet (black amber) were extracted using the same protocol. Due to the lesser availability of leaves and jet and the lower percentage of extractable organic matter, we used the simplified fractionation described above in order to compare their biomarker composition with that of amber.

2.3.3. GC–MS

The analyses were performed on an Agilent 6850 GC coupled to an Agilent 5975C quadrupole mass spectrometer. Separation was achieved on a HP-5MS column coated with (5%-phenyl)-methylpolysiloxane (30 m × 0.25 mm, 0.25 μm film thickness). The operating conditions were as follows: 8 psi carrier pressure, initial temperature held at 40 °C for 1.5 min, increased from 40 °C to 150 °C at a rate of 15 °C/min, held for 2 min, increased from 150 °C to 255 °C at a rate of 5 °C/min, held constant for 20 min and finally increased to 300 °C at a rate of 5 °C/min. The sample was injected in the splitless mode with the injector temperature at 290 °C. The mass spectrometer was operated in the electron impact mode at 70 eV ionization energy and scanned from 40 to 700 Da. The temperature of the ion source was 230 °C and the quadrupole temperature was 150 °C. Data were acquired and processed using Chemstation software. Individual compounds were identified by comparing their mass spectra with those of authentic standards and with published data (see Section 3.2).

3. Results and discussion

3.1. Infrared spectroscopy

The application of IR to the study of amber is well documented and constitutes a basic technique for the characterization of fossil resins (Langenheim, 1969; Grimalt et al., 1988; Alonso et al., 2000). Because of the inclination of all ambers and resins (even non-fossil resins) to show similar bulk infrared spectra (due to their common chemical functional groups), IR spectroscopy has strong limitations for the determination of their botanical origin (Yamamoto et al., 2006). The IR spectrum of the Cantabrian amber is consistent with those observed for other amber samples (Fig. S2; supplementary material) and could indicate that it is composed of a mixture of terpenoids and labdatriene copolymers. The band pattern is similar to the IR spectrum expected for the labdatrienes communic acid and biformene and their polymers, consistent with the stated macromolecular structure of amber (Villanueva-García et al., 2005) and with the terpenoid composition found (see Section 3.2). The weak band at 882 cm^{-1} (Fig. S2, supplementary material) is characteristic of the exocyclic methylene moiety supporting the labdatriene input. The two types of amber samples found in the deposit show similar IR spectra.

3.2. Terpenoid composition of Cantabrian amber

The total extracts of the amber contain methylated naphthalenes (di-, tri- and tetramethylnaphthalenes) and di- and trimethyltetralins, sesquiterpenoids and bi- and tricyclic diterpenoids (Table 1). GC analysis of the bulk extract shows three different zones in the gas chromatogram (Fig. 3). The dominant compounds in the early

Table 1
Terpenoids and their diagenetic derivatives identified in bulk and chromatographic fractions of extracts from the ambers (types *A* and *B*) of the El Soplao deposit.

No[a]	Compound	Composition	MW	Relative abundance[b]	
				A	*B*
Abietanes and Podocarpanes					
1 (**XVI**)	16,17-Bisnorsimonellite	$C_{17}H_{20}$	224	38.2	–
2 (**XXII**)	16,17,18-Trisnorabieta-8,11,13-triene	$C_{17}H_{24}$	228	100	100
3	16,17,19-Trisnorabieta-8,11,13-triene	$C_{17}H_{24}$	228	23.4	20.9
4 (**XVII**)	Retene	$C_{18}H_{18}$	234	1.0	–
5	16,17-Bisnordehydroabietane	$C_{18}H_{26}$	242	4.6	42.5
6	Simonellite	$C_{19}H_{24}$	252	9.3	1.5
7 (**XXVII**)	14-Methyl-16,17-bisnordehydroabietane	$C_{19}H_{28}$	256	2.5	6.9
8	1-Methyl-10,18-bisnorabieta-8,11,13-triene	$C_{19}H_{28}$	256	–	6.6
9 (**I**)	18-Norabietatriene (Dehydroabietin)	$C_{19}H_{28}$	256	45.8	14.0
10 (**I**)	19-Norabietatriene	$C_{19}H_{28}$	256	3.6	4.1
11 (**IV**)	18-Norabieta-7,13-diene	$C_{19}H_{30}$	258	9.7	–
12 (**V**)	Norabiet-13-ene	$C_{19}H_{32}$	260	57.0	23.0
13 (**III**)	Fichtelite	$C_{19}H_{34}$	262	5.8	d
14 (**X**)	12-Hydroxysimonellite	$C_{19}H_{24}O$	268	11.8	–
15 (**II**)	Dehydroabietane	$C_{20}H_{30}$	270	40.3	–
16 (**XXV**)	16,17-Bisnordehydroabietic acid[c]	$C_{18}H_{24}O_2$	272	d	d
17 (**VIII**)	Ferruginol	$C_{20}H_{30}O$	286	24.3	–
18 (**XIII**)	Callitrisic acid[c]	$C_{20}H_{28}O_2$	300	d	–
19 (**XII**)	Hinokiol[c]	$C_{20}H_{30}O_2$	302	d	–
Pimaranes and Isopimaranes					
20 (**XXI**)	Pimaric acid[c]	$C_{20}H_{30}O_2$	302	d	d
21 (**XXII**)	Isopimaric acid[c]	$C_{20}H_{30}O_2$	302	d	d
22 (**XXVI**)	Pimar-8-en-18-oic acid[c]	$C_{20}H_{32}O_2$	304	d	d
23	Pimaradiene	$C_{20}H_{32}$	272	–	4.5
Labdanes					
24	14,15-Bisnorlabda-8,12-dien-18-oic acid[c]	$C_{18}H_{28}O_2$	276	d	d
25 (**XXXIV**)	E-19-Noragathic acid	$C_{19}H_{30}O_2$	290	10.6	3.1
26 (**XXXIII**)	Z-19-Noragathic acid	$C_{19}H_{30}O_2$	290	3.7	1.5
27 (**XXIX**)	13-Dihydro-19-noragathic acid[c]	$C_{19}H_{32}O_2$	290	d	–
28 (**XXVIII**)	13-Dihydroagatholic acid	$C_{20}H_{34}O_3$	322	11.8	–
Other compounds					
29	Ionene	$C_{13}H_{18}$	174	37.2	48.4
30	Methylionene	$C_{14}H_{20}$	188	13.0	34.2
31	Tetrahydroeudalene	$C_{14}H_{20}$	188	16.0	8.3
32 (**XXXVII**)	Guaiazulene	$C_{15}H_{18}$	198	7.6	1.5
33 (**XXXVIII**)	Cadalene	$C_{15}H_{18}$	198	8.2	7.5
34	Drimane	$C_{15}H_{28}$	208	3.6	14.8
35	Homodrimane	$C_{16}H_{30}$	222	3.3	3.9
36 (**XXXI**)	2,5,8-Trimethyl-1-butyltetralin	$C_{17}H_{26}$	230	79.1	57.3
37 (**XXXII**)	2,5,8-Trimethyl-1-isopentyltetralin	$C_{18}H_{28}$	244	d	10.8
38 (**XX**)	Diaromatic totarane	$C_{19}H_{24}$	252	1.0	–
39 (**XI**)	Totarol[c]	$C_{20}H_{30}O$	286	d	–

[a] Roman numerals in parentheses refer to structures shown in Appendix A.
[b] Abundance relative to the major peak (100%) in the bulk extracts (GC–MS TIC). Occurrence is tabulated on compounds detected only after fractionation and derivatization (d: detected; –: not detected).
[c] Also analyzed as the TMS derivative.

elution range are α-ionene, methylionene, trimethylnaphthalene isomers, tetrahydroeudalene, calamenene isomers, drimane and homodrimane (identified after Dzou et al., 1999 and Sonibare and Ekweozor, 2004). The α-ionene, methylionene and drimanes may be derived from labdanes in the resin through degradation processes (Yamamoto et al., 2006; Pereira et al., 2009). Overall, these components are highly degraded diagenetic products that have no chemotaxonomic value due to their unrecognizable parent structures. The second section of the gas chromatogram is dominated by non-oxygenated bi- and tricyclic diterpenoids and the third section contains polar bi- and tricyclic diterpenoids. We did not find aliphatic lipids, hopanoids, fungal terpenoids or plant triterpenoids in the amber samples, discarding an angiosperm contribution and major contamination.

3.2.1. Abietane diterpenoids

The diterpenoids identified in the extracts belong to the abietane, pimarane/isopimarane and labdane structural classes (Fig. 3). These diterpenoids are typical of conifers (Otto and Wilde, 2001; Yamamoto et al., 2006), confirming such an origin for the Cantabrian ambers. The abietane class terpenoids were identified by comparison of their mass spectra with those of standards or published in the literature (Czechowski et al., 1996; Otto and Simoneit, 2002; Otto et al., 2002; Hautevelle et al., 2006; Cox et al., 2007), and comprised 18- and 19-norabieta-8,11,13-triene (**I**; chemical structures cited are shown in Appendix A), dehydroabietane (**II**), fichtelite (**III**), 18-norabieta-7,13-diene (**IV**) and norabiet-13-ene (**V**). The latter compound was tentatively identified by match with a mass spectrum in the literature (Hautevelle et al., 2006), characterized by a molecular ion at *m/z* 260 and loss of an isopropyl group (*m/z* 217). 18-Norabieta-7,13-diene (**IV**) was identified only in sample *A* by a match with the published mass spectrum (Otto and Simoneit, 2002). This compound has been described as a decarboxylation product of abietic acid during diagenesis (Otto and Simoneit, 2002). In this case, the precursor molecule has not been found. The lack of a clear biological precursor for norabieta-7,13-diene (**IV**) suggests an alternative origin, possibly by double bond isomerization of unsaturated abietanes. This composition is consistent with the dominance of dehydroabietane and abietane geoterpenoids in the type *A* amber. The norabietatrienes (dehydroabietins) found in both amber

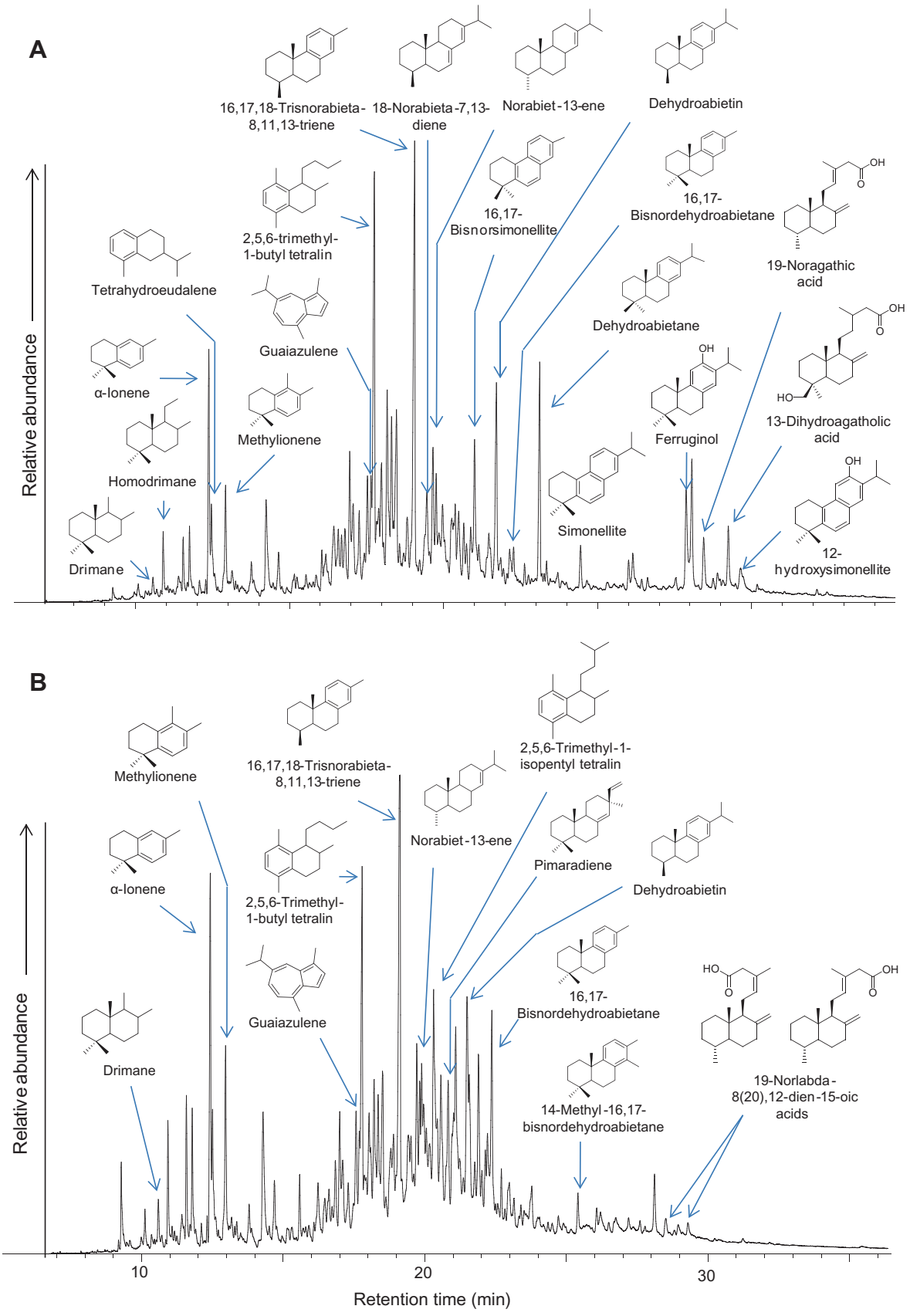

Fig. 3. GC–MS total ion current (TIC) traces of the underivatized total extracts of: (A) El Soplao blue amber, type *A*, (B) El Soplao yellow-blue amber, type *B*, with the main terpenoid compounds identified. Peaks not annotated are unidentified, tentatively identified or known compounds with little chemotaxonomic value. (For interpretation of the references to color in this figure legend, the reader is referred to the web version of this article.)

samples could be derived from all abietane precursors by diagenetic alteration (Simoneit, 1986; Hautevelle et al., 2006).

Dehydroabietane (**II**) is a natural product of many Pinaceae resins (Otto et al., 2007) as well as some Cupressaceae resins. In these samples, dehydroabietane is a significant component in amber type *A*, whereas it is not detectable in amber type *B*, suggesting a different paleobotanical origin for both types of amber samples. The absence of abietic (**VI**) or dehydroabietic acids (**VII**) eliminates a Pinaceae contribution to the amber, because abietic acid is a major component of such resins and dehydroabietic acid, its major diagenetic derivative, is present in ambers derived from Pinaceae (Yamamoto et al., 2006).

Phenolic diterpenoids occur in polar fraction B of the type *A* amber (Fig. 4), with a dominance of ferruginol (**VIII**) and its oxidation products 6,7-dehydroferruginol (**IX**) and 12-hydroxysimonellite (**X**) and totarol (**XI**) (Otto and Simoneit, 2001; Otto et al., 2002). Ferruginol and 12-hydroxysimonellite are also identifiable (underivatized) in the bulk extract as part of the main components of the amber (Fig. 3). The presence of these phenolic diterpenoids is of significant chemosystematic value, as ferruginol is an abundant natural product in extant conifers of the families Cupressaceae and Podocarpaceae and can be used as a characteristic biomarker of these families (Otto and Simoneit, 2001; Marynowski et al., 2007). A minor amount of hinokiol (3-hydroxyferruginol, **XII**; Fig. 5A) was also found in the type *A* amber. Hinokiol has been described from Cupressaceae (Otto et al., 2002; Cox et al., 2007). There is no reported presence of phenolic diterpenoids in modern Araucariaceae (Cox et al., 2007), but Otto and Wilde (2001) cited the occurrence of ferruginol in *Araucaria*. To avoid this ambiguity and to test this finding under our experimental conditions, resins of *Agathis sp*. and *Araucaria sp*. were analyzed and ferruginol was not detected in any Araucariaceae resins. Hence, these results, coupled with the absence of kaurane or phyllocladane diterpenoids, the presence of totarol (see below) and the fossil record of the deposit, suggest that Araucariaceae did not contribute to the main type of amber found at the studied deposit (type *A*). On the other hand, we did not find phenolic abietanes in the type *B* amber sample. This fact, taken together with the presence of dehydroabietane in sample *A* and its absence in sample *B*, constitutes the main chemotaxonomic difference between the two types of samples. A significant relationship between amber type *A* and modern Cupressaceae is the presence of a low quantity of callitrisic acid (**XIII**) which is an epimer of dehydroabietic acid (**VII**, Fig. 5). The difference in retention time with dehydroabietic acid and the higher relative intensity of the ion at *m/z* 357 (M-CH_3) versus the molecular ion in callitrisic acid are distinctive features between the two epimers used here for the identification of the acid (Van den Berg et al., 2000; Cox et al., 2007). Callitrisic acid has a higher chemotaxonomical value than dehydroabietic acid due to its scarcity. In modern conifer resins, the synthesis of callitrisic acid seems to be restricted to certain genera of the Cupressaceae family and it was also found in Cenomanian amber from the Raritan Formation (New Jersey, USA), suggesting a relationship with Cupressaceae (Anderson, 2006).

Degradation of phenolic diterpenoids could lead to the abietane geoterpenoids found in the type *A* amber (Otto et al., 1997; Otto and Simoneit, 2001; Stefanova et al., 2002). Hautevelle et al. (2006) and Yamamoto et al. (2006) discussed the diagenetic pathways of abietane class bioterpenoids, suggesting that 18-norferruginol (**XIV**) could be the precursor of dehydroabietin, and ferruginol (**VIII**) could lead to 12-hydroxysimonellite (**X**), simonellite (**XV**), 16,17-bisnorsimonellite (**XVI**) and retene (**XVII**), all found in the type *A* amber. Under the anaerobic depositional conditions of the amber (Najarro et al., 2009), we could not disregard redox reactions that lead to the actual composition found (Pereira et al., 2009). If, as in some modern Cupressaceae genera (i.e. *Cupressus*; Fig. S3, supplementary material), the original proportion of ferruginol (**VIII**) was high, its

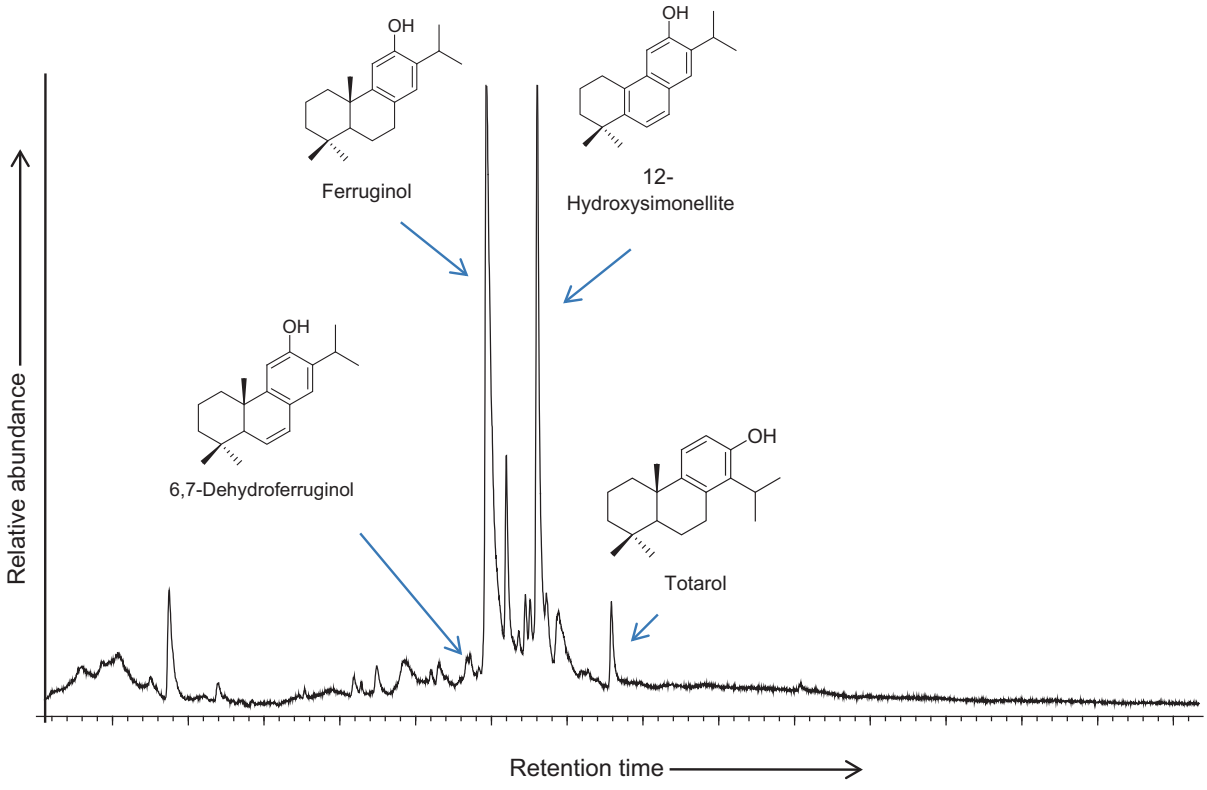

Fig. 4. GC–MS TIC trace of fraction B resulting from the column separation of the polar fraction of amber *A*. This fraction contains the partially purified phenolic terpenoids. Compounds are analyzed as the TMS derivatives.

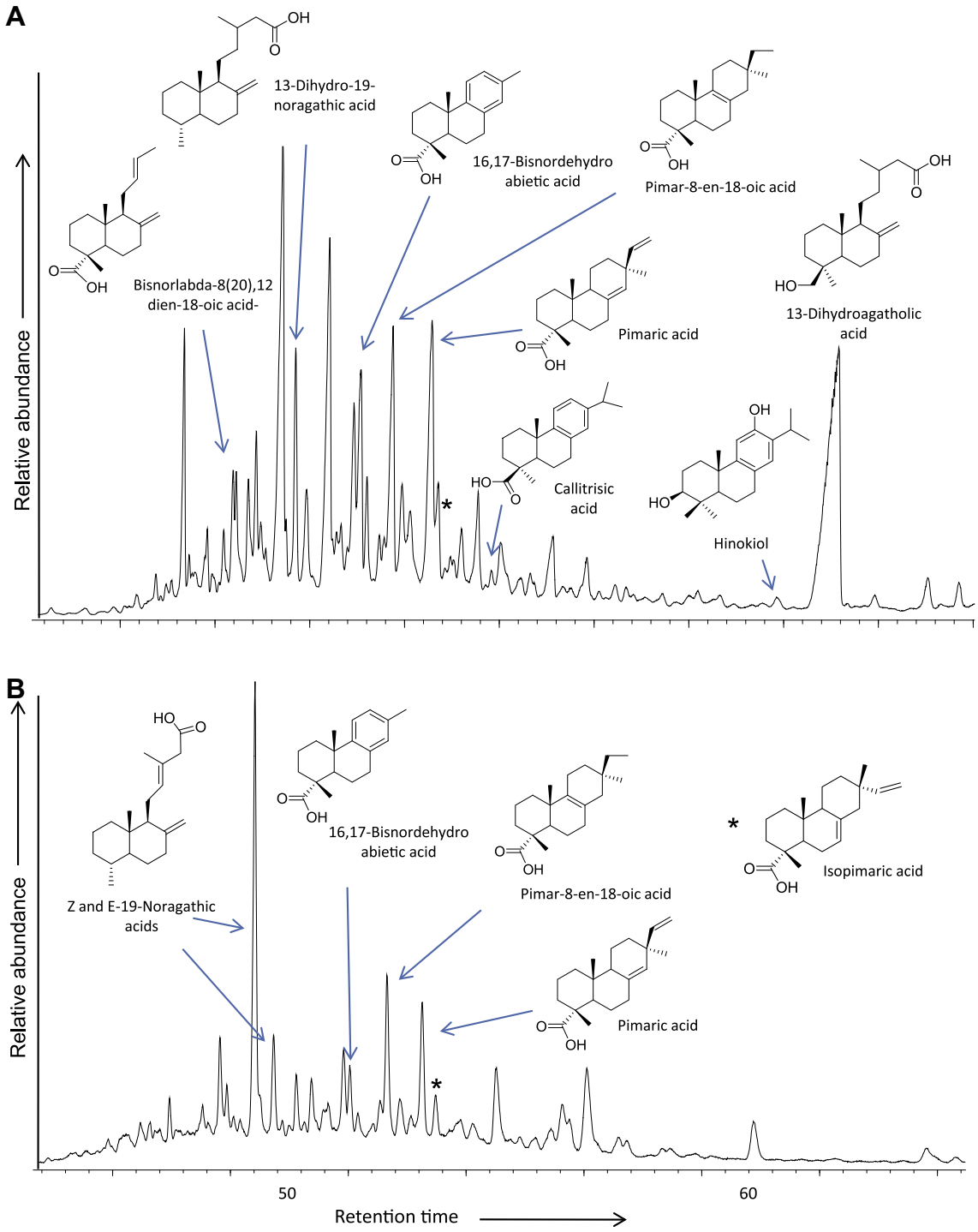

Fig. 5. GC–MS TIC traces of the polar fractions C of: (A) amber *A* and (B) amber *B*. This fraction contains mainly pimaric and labdenoic acids. The figure shows the identified compounds in the fraction. Unlabelled peaks are considered as unidentified due to the lack of standards and published references or databases with details of their mass spectra. Compounds are analyzed as the TMS derivatives.

diagenesis could ultimately have generated dehydroabietane (**II**) and simonellite (**XV**), both significant in the type *A* amber.

3.2.2. Totarol

Totarol (**XI**), a tricyclic diterpenoid phenol, is considered as a confirmatory chemotaxonomic marker for Cupressaceae and Podocarpaceae, even at low concentrations (Le Métayer et al., 2008; Stefanova and Simoneit, 2008). Totarol is detectable in the bulk extract using the characteristic mass fragments of *m/z* 271 and 286. The identification is unambiguous in amber sample *A* after purification of the phenolic fraction of the bulk extract and analysis as trimethylsilyl derivatives (Fig. 4). Due to the similarities between the mass spectra of phenolic diterpenoids, the retention time and mass spectrum of totarol (**XI**) were determined using a standard (Sigma–Aldrich). The presence of totarol suggests a relationship between the palaeobotanic origin of the amber and extant Cupressaceae or Podocarpaceae. To test this possibility, the phenolic diterpenoids of the amber were compared with those from a modern Cupressaceae (*Cupressus* arizonica; Fig. S3, supplementary material). Both extracts contain ferruginol (**VIII**), totarol (**XI**) and hinokiol (**XII**) as the main phenolic

diterpenoids, but sempervirol (**XVIII**) has not been observed. A difference between the assemblage of polar terpenoids from *C. arizonica* and the amber is the presence of sugiol (**XIX**) and the lack of callitrisic acid (**XIII**) in the former. We identified a diaromatic totarane (**XX**) as a possible diagenetic product of totarol (**XI**), which may be derived by a parallel diagenetic pathway as simonellite (**XV**) from ferruginol (**VIII**) (Otto et al., 1997). In accord with the phenolic abietane composition, totarol is not detectable in the type *B* amber, confirming that both amber types found in the Cantabria deposits differ in their biological origins.

3.2.3. Pimarane/isopimarane diterpenoids

Polar fraction C of amber contains low amounts of pimaric (**XXI**) and isopimaric (**XXII**) acids (Fig. 6). Diagenesis of pimarane

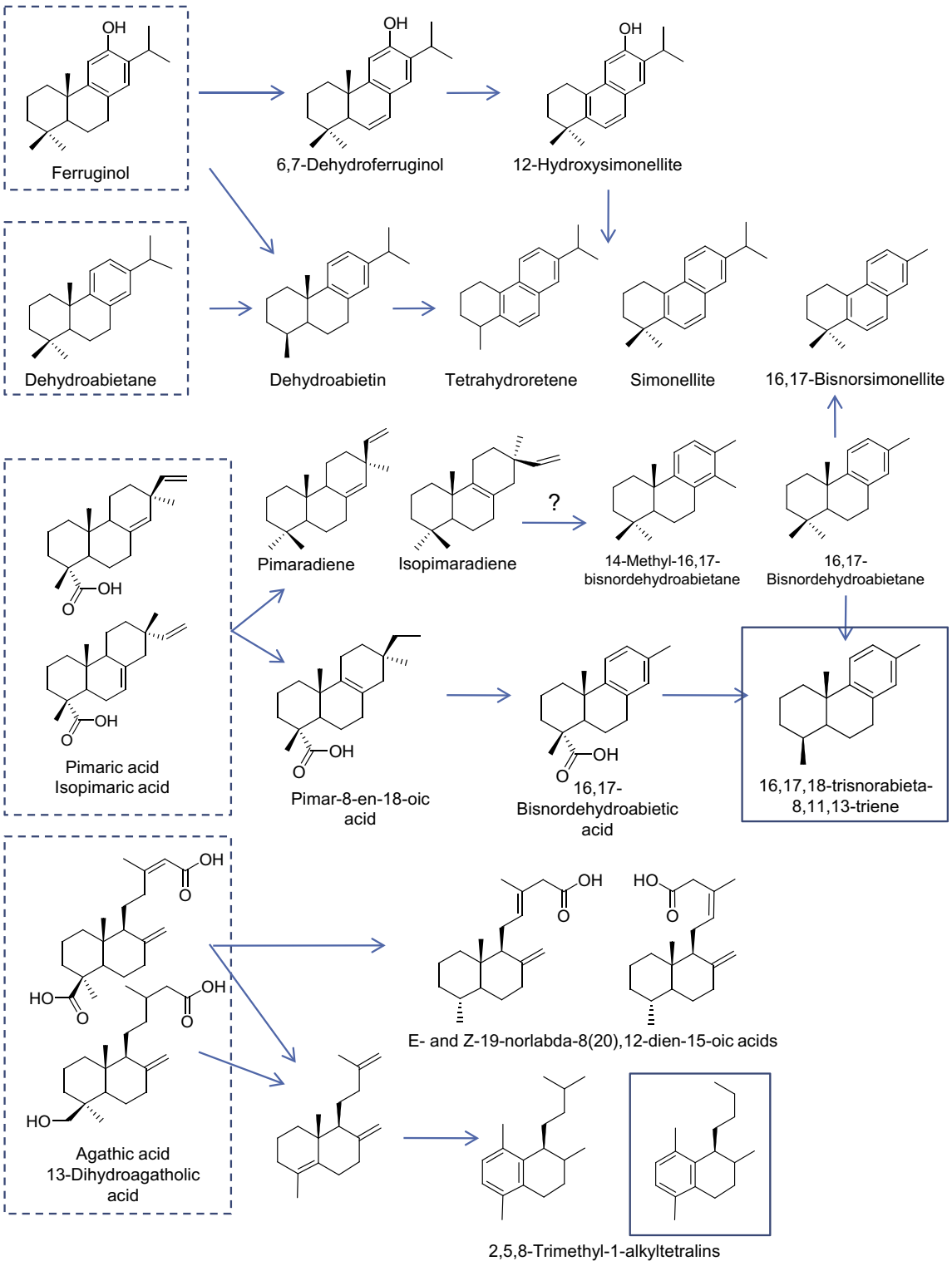

Fig. 6. Proposed diagenetic pathways for the diterpenoid precursors from the Cantabrian ambers (based on Otto and Simoneit (2002), Stefanova et al. (2002), Hautevelle et al. (2006), and Pereira et al. (2009)). Dotted box: biological precursors; solid box: major terpenoid found in the samples.

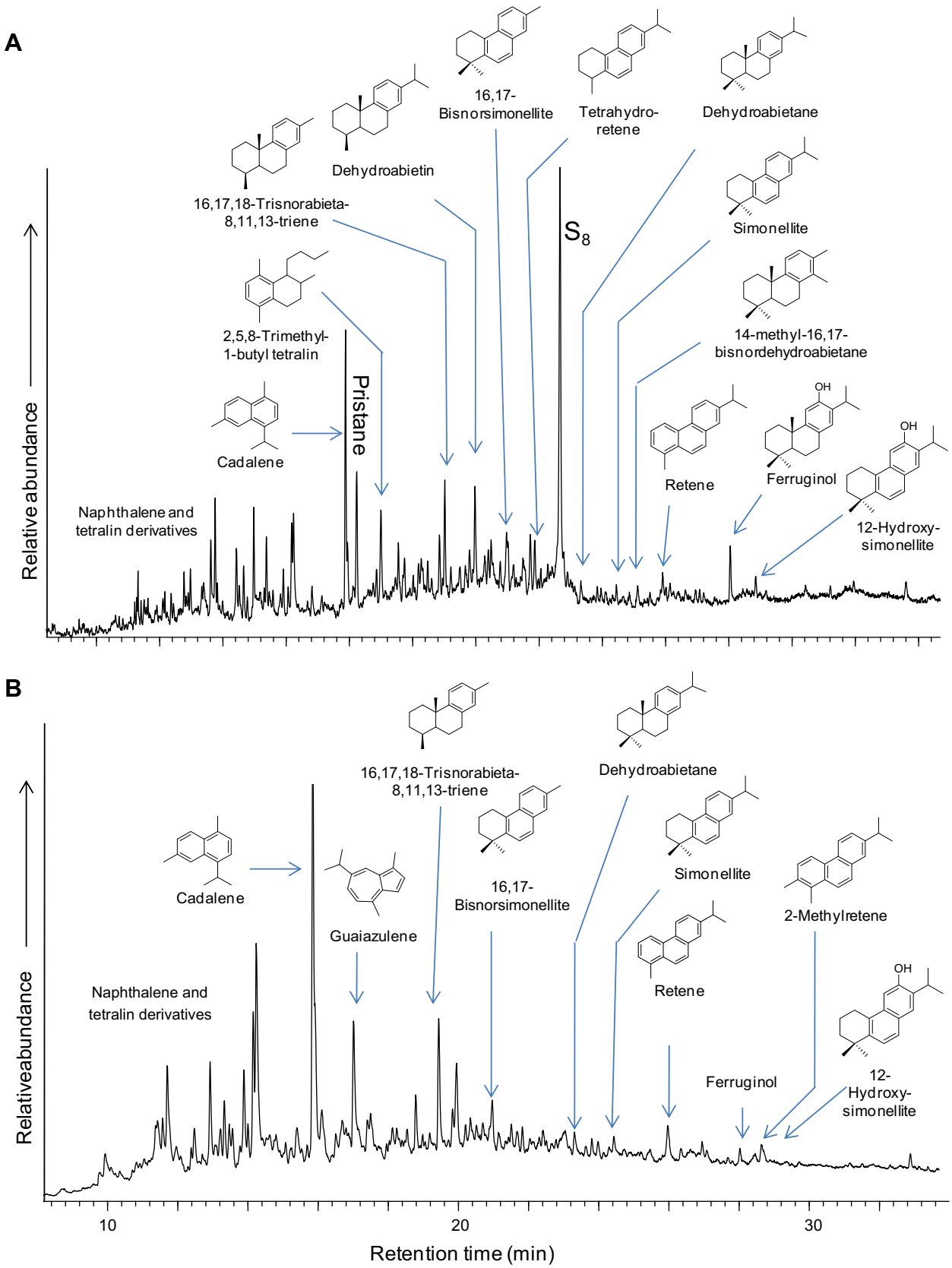

Fig. 7. GC–MS TIC traces of the total extracts from: (A) *Frenelopsis* leaves and (B) jet (black amber), showing the identified biomarkers.

diterpenoids could be one of the possible origins of 16,17,19-trisnorabieta-8,11,13-triene (**XXIII**), a major compound identified in the amber samples. Another possible origin for this compound is by diagenesis of dehydroabietane and other abietane related terpenoids (Fig. 6; Otto et al., 2002; Pereira et al., 2009). Due to the widespread distribution of the pimaric/isopimaric acids, the chemotaxonomical interpretation of their presence in the Cantabrian ambers must be taken with caution and comparisons with

other markers and samples should be made. Continuing the comparison with extant conifers, pimaric and isopimaric acids constitute the main tricyclic resin acids present in the conifer families Cupressaceae, Araucariaceae and Podocarpaceae (Otto and Wilde, 2001). Taking into account a possible molecular relationship between the botanical source of Cantabrian amber *A* and modern Cupressaceae, if pimaric acid (**XXI**) and isopimaric acid (**XXII**) were the main resin acids in the precursor resin of these ambers, diagenetic degradation to 16,17,18-trisnorabieta-8,11,13-triene (**XXIII**) is consistent with the dominance of the pimarane resin acid compounds in the extract, as loss of the vinyl moiety at C-13, with concomitant aromatization and decarboxylation at C-4 generates this predominant isomer. Following this pathway, the presence of a related molecule to 16,17,18-trisnorabieta-8,11,13-triene with a C-13 ethyl group (i.e. 16,18-bisnorabieta-8,11,13-triene, **XXIV**) should be expected as well, but we failed to detect such a compound. Otto et al. (2002) reported a significant presence of that geoterpenoid (**XXIV**) in fossil resin of the Lower Cretaceous *Tritaenia linkii* (Miroviaceae), but due to the absence of precursor bioterpenoids, the assignment to a specific taxon was unclear. Recent work of Pereira et al. (2009) on Cretaceous amber from Brazil, inferred some intermediates of this diagenetic route (Fig. 6), namely 16,17-bisnordehydroabietic acid (**XXV**), pimar-8-en-18-oic acid (**XXVI**) and 14-methyl-16,17-bisnordehydroabietane (**XXVII**), that are also present in the type *A* amber (Figs. 3–5). Work is in progress in our laboratory in order to confirm this hypothetical pathway, as the formation of 14-methyl-16,17-bisnordehydroabietane by rearrangement of a pimaradiene or abietane precursor has not been demonstrated to date.

3.2.4. Labdane diterpenoids

Labdanoic acids and other labdane derivatives are common components in all conifers and are therefore non-specific biomarkers (Otto and Wilde, 2001). 13-Dihydroagatholic acid (**XXVIII**) is the predominant labdenoic acid present in the polar fraction of amber *A* (Fig. 5). This acid could be a precursor molecule preserved that constitutes the chemotaxonomic difference between the two paleobotanical resin producers, as it is not detectable in the extract of amber *B*. 13-Dihydro-19-noragathic acid (**XXIX**), found in sample *A*, could be formed from the 13-dihydroagatholic acid (**XXVIII**) precursor by loss of the C-19 hydroxymethyl group at C-4 or from the agathic acid (**XXX**) precursor by C-19 decarboxylation at C-4, respectively. The diagenetic transformation of the major labdanoic acids may be the source of the 2,5,8-trimethyl-1-alkyltetralins, ionenes and drimanes found in the samples (Fig. 3). The MS fragmentation pattern of the major compound of this family, i.e. 2,5,8-trimethyl-1-butyltetralin (**XXXI**) with a molecular ion at *m/z* 230, shows a butyl loss (57 da) from the saturated ring to form an *m/z* 173 fragment (see Fig. S4, supplementary material). Another homologue of this compound group is 2,5,8-trimethyl-1-isopentyltetralin (**XXXII**), which is significant in amber type *B* but only occurs in trace amounts in amber *A*. The degradation pathway leading to **XXXII** could be decarboxylation at C-4 of a labdanoic acid precursor (i.e. agathic acid, **XXX**), followed by aromatization of ring A with methyl migration from C-10 to C-1 and decarboxylation of C-15 (Fig. 6). These compounds were also reported from Brazilian ambers (Pereira et al., 2009). The difference found between the ambers could be indicative of differential labdanoic acid compositions in the original resins. Another source of these molecules may be the degradation of the labdane macromolecular structure of amber due to particular conditions that prevailed in the Cantabrian deposits (see below). Other diagenetic degradation products of labdanoic acids found in both amber samples are *Z*- and *E*-19-norlabda-8(20),12-dien-15-oic acids (**XXXIII** and **XXXIV**, respectively) and bisnorlabda-8(20),12-dien-18-oic acid (**XXXV**) (Otto and Simoneit, 2002). It is not possible to identify all peaks found in the polar fractions of the amber extracts due to the lack of references and possible precursors.

During burial, the El Soplao and Reocín amber deposits suffered the influence of hydrothermal fluids related to the La Florida-Reocín Pb–Zn mine mineralization. As a consequence, we cannot discard the possibility of alternative transformation routes leading to the unusual compounds found in the amber. These alternative transformations must be added to the lack of information about the possible chemotaxonomy of extinct Cheirolepidiaceae. Despite these uncertainties, which result in the presence of some unidentified compounds, the low maturation (cf. vitrinite reflectance data, supplementary material) and excellent preservation of the organic compounds in the amber allows us to use the components of the extract to obtain chemotaxonomic information. We suggest that the tricyclic diterpenes originally biosynthesized by the main botanical precursor of amber *A* were dominated by phenolic abietanes, pimarane resin acids and totarol. The bicyclic diterpenes probably contained a high proportion of labdanoic acids, in particular 13-dihydroagatholic acid (**XXVIII**) and communic acid (**XXXVI**), whose polymerization leads to the typical macromolecular structure of ambers.

3.3. Terpenoid composition of co-occurring fossil leaves and paleochemotaxonomic aspects

Due to the lack of Cupressaceae representatives in all the outcrops of Las Peñosas Formation (Fig. 1) and the excellent preservation and dominance of *Frenelopsis* material, the comparison of the terpenoid assemblage of these plant remains with those found in the amber may help to confirm the botanical origin of the fossil resin and to understand the chemosystematics of the extinct family Cheirolepidiaceae. Since no amber associated with this family has been documented to date (Bray and Anderson, 2008; Pereira et al., 2009), the inclusion of *Frenelopsis* genera as a possible source of one of the amber types found in the El Soplao deposit has to be considered. Previous reports relating a possible botanical origin of ambers to Cheirolepidiaceae should be mentioned (Gomez et al., 2002b; Roghi et al., 2006). Macrofossil evidence of two potential conifer resin producers was found by Najarro et al. (2009) in the study zone: *Frenelopsis* (Cheirolepidiaceae family) and *Mirovia* (Miroviaceae). Also, the palynological record shows a contribution from the Araucariaceae family, but no meso- or macrofossils of this family have been recognized yet. As Anderson (2006) pointed out, the correlation between plant fossil evidence and co-deposited amber should be taken with caution since the major resin producer could be a minor species in the ecosystem. As we find two different potential palaeobotanical contributors for the ambers of the El Soplao deposit, all the types of plant macrofossil remains identified in the deposit were examined separately in order to establish possible chemosystematic relationships.

Overall, despite the increase of aromatized derivatives such as retene, the diterpene speciation in the *Frenelopsis* leaves shows that all the main components are shared with the type *A* ambers from El Soplao (Fig. 7A). Cadalene (**XXXVII**) and 16,17,18-trisnorabieta-8,11,13-triene (**XXIII**) are among the biomarkers detected in the fossil leaves of *Frenelopsis*. The diagenetic processes undergone by terpenoids from the fossil leaves are consistent with those observed in sediments, as the leaves are not protected by the polymeric structure of the amber. The formation of aromatic derivatives may be governed by clay catalysis or other abiotic processes in soils and sediments (Otto et al., 2007). Also, the aromatic abietanes may be generated under aerobic conditions, consistent with the major presence of pristane and the lack of phytane (Peters et al., 2005). The presence of norabietanes is consistent with the diagenetic processes for terpenoids described by Frenkel and Heller-Kallai (1977). 14-Methyl-16,17-bisnordehydroabietane (**XXVII**)

and 2,4,8-trimethylalkyltetralins (e.g. **XXXI**), described above, are also present in the *Frenelopsis* leaves. The phenolic abietane ferruginol (**VIII**) and its derivative 12-hydroxysimonellite (**X**) are key biomarkers also found in the *Frenelopsis* leaves. This result is consistent with the presence of ferruginol in Cenomanian *Frenelopsis alata* (Nguyen Tu et al., 2000a). This evidence, together with the absence of ferruginol in *Mirovia* leaves (Fig. 8), suggests that *Frenelopsis* could be one of the botanical origins for the Cantabrian amber. The terpenoid composition found in *Mirovia* leaves is dominated by oxidized non-specific abietane terpenoids (mainly simonellite and retene).

The *Frenelopsis* leaves and the amber of the El Soplao deposit are largely associated with jet (black amber). The analysis of jet extract shows a composition dominated by cadalene and alkyl derivatives of naphthalene and tetralin. The identifiable terpenoids include aromatized abietanes and ferruginol. Fractionation and derivatization and GC–MS of jet extract showed the presence of ferruginol and totarol, suggesting that jet has the same botanical origin as the main type *A* amber in the deposit.

The azulene hydrocarbon derivative guaiazulene (**XXXVIII**), an isomer of cadalene (**XXXVII**), with a strong blue color and purple-blue fluorescence, is found in low amounts in all type *A* ambers, *Frenelopsis* leaves and jet, suggesting a common origin from sesquiterpenoids synthesized by Cheirolepidiaceae. Guaiazulene is a common compound with low chemosystematic value, but the presence of this hydrocarbon in amber has not been reported to date. The significant quantity of this compound in the El Soplao samples could be at the cause for the characteristic blue-purple tinge of these ambers. Although the relationships between Cheirolepidiaceae and extant conifers are unclear (Bray and Anderson, 2008; Pereira et al., 2009), a morphological and histological correlation between Cheirolepidiaceae and Cupressaceae has been established (Daviero et al., 2001; Farjon, 2008). Moreover, Nguyen Tu et al. (2000b) have observed a resemblance between the lipid composition of *Frenelopsis alata* and *Tetraclinis articulata*, a representative of Cupressaceae. The presence of ferruginol in *Frenelopsis* (Nguyen Tu et al., 2000b and the present data) confirms the hypothesis of a possible relationship between *Frenelopsis* and the Cupressaceae family. Moreover, the presence of 13-dihydroagatholic acid (**XXVIII**) in the amber and the overall biomarker assemblage show a similarity to extant *Cupressus* genera (see Fig. S4, supplementary material). The resemblance in the chemical composition between *Frenelopsis* and Cupressaceae representatives may be due to convergence, as it has been demonstrated that the physical similarities between these taxa resulted from convergence rather than phylogenetic connection (Broutin and Pons, 1975; Alvin, 1982). The evolutionary changes in the biochemistry of terpenoids since the synthesis of the parent resin of amber to the modern conifers are unknown. Consequently, we should consider that the lack or presence of certain compounds in a correlation with extant conifers is informative, and that detailed biomarker compositions of extinct conifer fossils, complemented by morphological and histological relationships, are necessary to establish a definite evolutionary relationship. Keeping this in mind, the paleobotanical considerations suggested by our data obtained on macrofossil plant samples and amber types can be summarized as follows:

a. The absence of abietic and dehydroabietic acid in both types of amber samples excludes an origin from resin of the Pinaceae family. Also, the absence of plant triterpenoids and labdenoic acids eliminates a contribution from angiosperms (Anderson et al., 1992; Yamamoto et al., 2006).
b. The presence of phenolic terpenoids (ferruginol, totarol and hinokiol) in the type *A* amber indicates the conifer families Cupressaceae and Podocarpaceae as possible biological precursors, and rejects the Araucariaceae family. The presence of callitrisic acid (**XIII**) reinforces the biochemical relationship between the parent resin of amber and modern Cupressaceae. The plant macrofossil record in the deposit shows that there are no representatives of Cupressaceae or Podocarpaceae among the possible resin producers (Najarro et al., 2009). The co-occurrence of key terpenoids (e.g. ferruginol), between amber *A* and fossil tissue of *Frenelopsis* suggests that this amber could be derived from *Frenelopsis* (Cheirolepidiaceae).

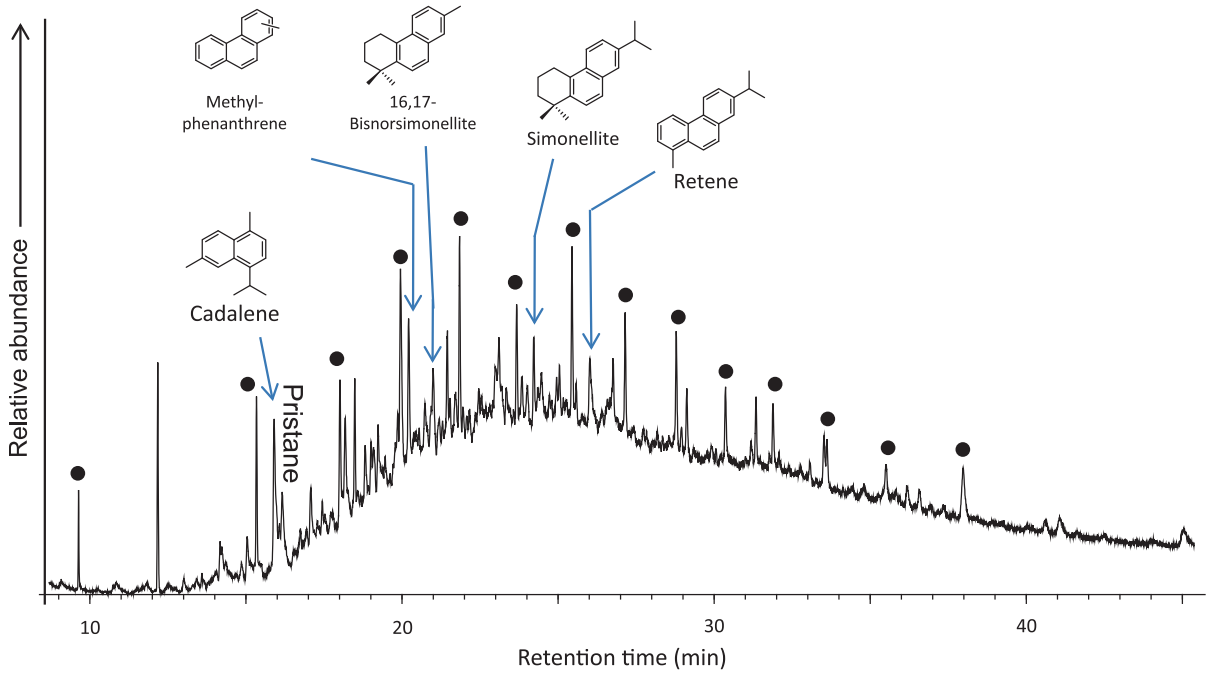

Fig. 8. GC–MS TIC trace of the total extract of *Mirovia sp.* leaves found in the amber deposit at El Soplao showing the identified biomarkers. Solid dots: *n*-alkanes (last dot: C_{30}).

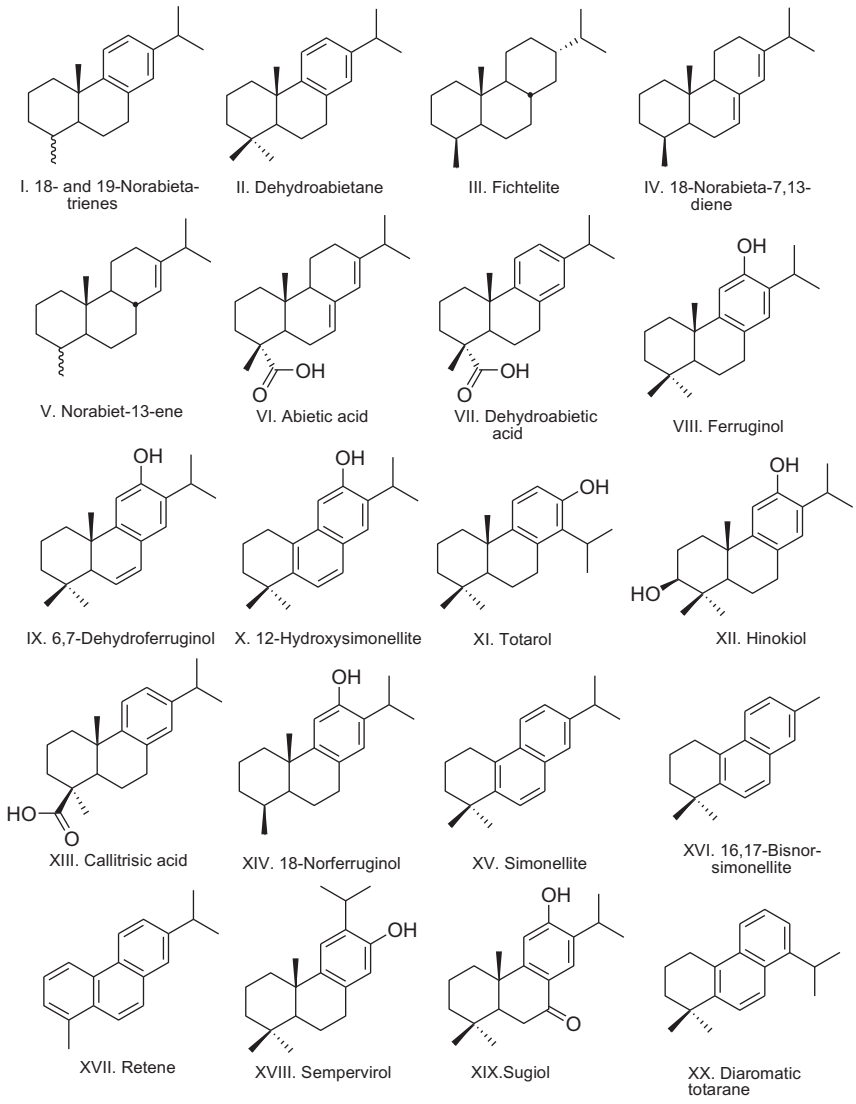

Fig. A1. Chemical structures cited in the text.

c. The overall terpenoid composition of the type *B* amber is comprised of non-specific conifer biomarkers. The absence of phenolic terpenoids and of 13-dihydroagatholic acid (**XXVIII**), together with the presence of major amounts of diagenetic products of pimarane-type diterpenoids, saturated and unsaturated norabietanes, and alkyltetralins point to a different biological origin. A paleobotanical source for this type of amber could not be determined on the basis of its biomarker composition.

4. Conclusions

Analysis of the polar diterpenoids of Cretaceous ambers from El Soplao (Cantabria, Spain) indicates that two resin producers contributed to the amber record. The main parent resin (type *A*) originally contained phenolic abietanes (dominated by ferruginol), totarol, dehydroabietane and pimaric/isopimaric acids. The dominant resin acids found are 13-dihydroagatholic and bisnordehydroabietic acids, with various other alteration products and a minor quantity of callitrisic acid. This composition suggests a biochemical relation with the resin of extant Cupressaceae. The second parent resin (type *B*) contains pimaric/isopimaric acids as the only identifiable biological precursors preserved. The phenolic diterpenoids present in the samples (type *A*), the lack of phyllocladane/kaurane-type terpenoids and the absence of macrofossil plant remains exclude a significant contribution of Araucariaceae to the amber. Diagenetic products of the pimarane/abietane and labdane class terpenoids constitute the main geoterpenoids extractable from the amber of El Soplao. Insights from petrographic characterization of coal macerals provide a correlation between temperature, time and level of organic diagenesis, indicating only a moderate degree of diagenetic alteration during burial. This is consistent with the high level of preservation of the natural product diterpenoids and their direct diagenetic derivatives. The sedimentological relationships and chemotaxonomical observations suggest that one source of the amber may be the extinct *Frenelopsis* (Cheirolepidiaceae).

Acknowledgments

We thank Drs. Philippe Schaeffer, Thanh Thuy Nguyen Tu and Débora de Almeida Azevedo for their thorough and constructive comments, aiding our revision of the manuscript. We thank the staff of the Royal Botanic Garden of Madrid for permission and assistance to sample several of their living conifer species. We also thank the Consejería de Cultura, Turismo y Deportes (Gobierno de Cantabria) and in particular F.J. López Marcano

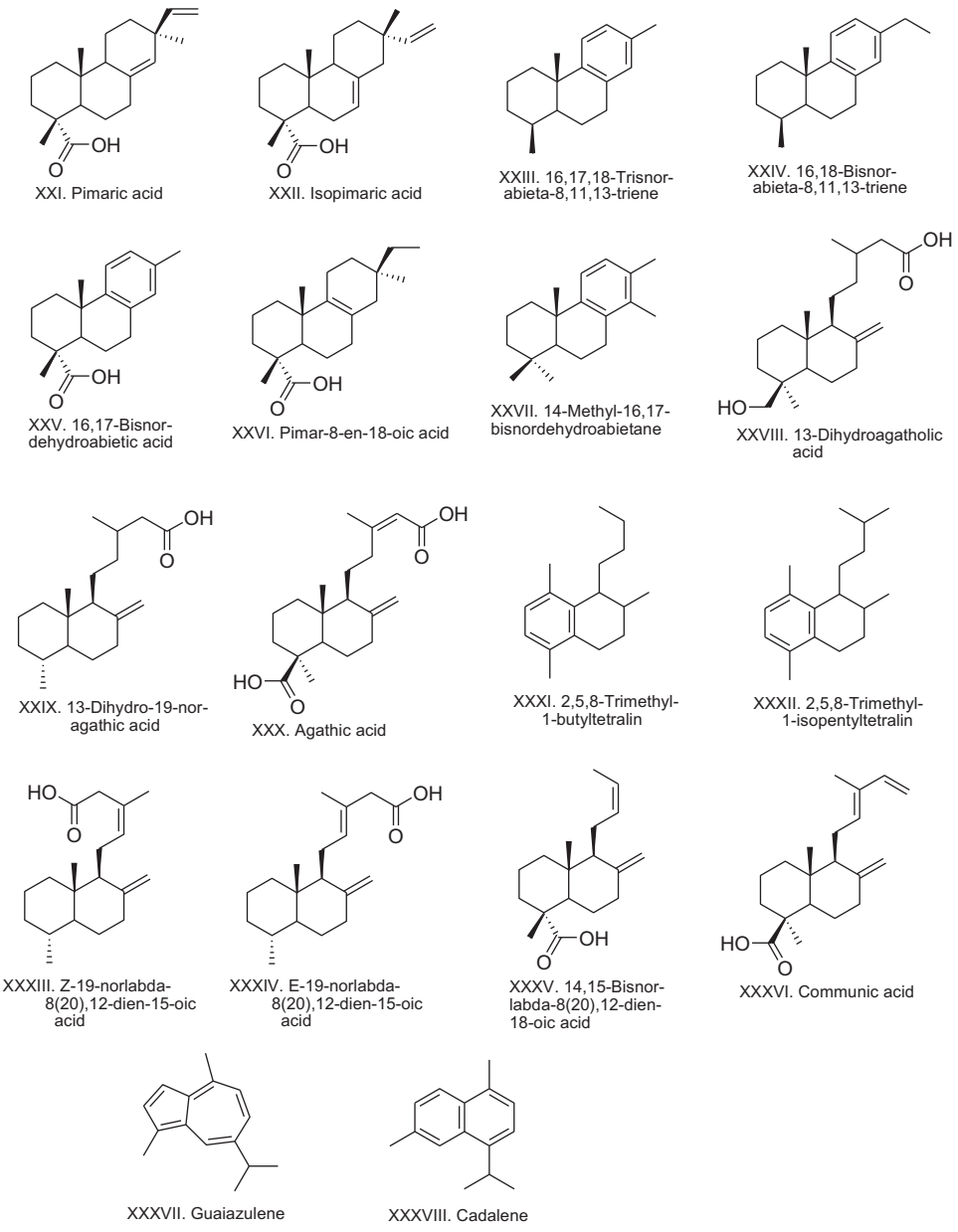

Fig. A1 (*continued*)

(Regional Minister of the Cantabria Government) and F. Unzué (manager of El Soplao Cave and Territory) for their support and promotion of the study of the new amber deposit at El Soplao. Thanks should go to Antonino Bueno Yanes for providing Reocín amber samples. We thank the Centro de Astrobiología (CSIC-INTA) and Instituto de Tecnica Aerospacial "Esteban Terradas", where all chemical analyses were performed. This study is framed in a collaborative agreement among IGME, SIEC S.A. and the Cantabria Government (Consejería de Cultura, Turismo y Deportes), and is a contribution to IGME project 491-CANOA 53.6.00.12.00: "Investigación científica y técnica de la Cueva de El Soplao y su entorno geológico", and DGI project CGL2008-01237/BTE (MICINN, Spanish Government).

Appendix A

See Fig. A1.

Appendix B. Supplementary material

Supplementary data associated with this article can be found, in the online version, at doi:10.1016/j.orggeochem.2010.06.013.

Associate Editor—**Philippe Schaeffer**

References

Alonso, J., Arillo, A., Barron, E., Carmelo-Corral, J., Grimalt, J., Lopez, J.F., Lopez, R., Martinez-Delclós, X., Ortuño, V., Peñalver, E., Trincao, P.R., 2000. A new fossil resin with biological inclusions in Lower Cretaceous deposits from Alava (Northern Spain, Basque-Cantabrian Basin). Journal of Paleontology 74, 158–178.

Alvin, K.L., 1982. Cheirolepidiaceae: biology, structure and paleoecology. Reviews in Palaeobotany and Palynology 37, 71–98.

Alvin, K.L., Hluštík, A., 1979. Modified axillary branching in species of the fossil genus *Frenelopsis*: a new phenomenon among conifers. Botanical Journal of the Linnean Society 79, 231–241.

Anderson, K.B., 2006. The nature and fate of natural resins in the geosphere. XII. Investigation of C-ring aromatic diterpenoids in Raritan amber by pyrolysis–GC–matrix isolation FTIR–MS. Geochemical Transactions 7, 2–7.

Anderson, K.B., Crelling, J.C., 1995. Amber, Resinite and Fossil Resins. ACS Symposium Series 617. American Chemical Society, Washington, DC, USA.

Anderson, K.B., Winans, R.E., Botto, R.E., 1992. The nature and fate of natural resins in the geosphere – II. Identification, classification and nomenclature of resinites. Organic Geochemistry 18, 829–841.

Barrón, E., Comas-Rengifo, M.J., Elorza, L., 2001. Contribuciones al estudio palinológico del Cretácico Inferior de la Cuenca Vasco-Cantábrica: los afloramientos ambarígenos de Peñacerrada (España). Coloquios de Paleontología 52, 135–156.

Bray, P.S., Anderson, K.B., 2008. The nature and fate of natural resins in the geosphere XIII: a probable pinaceous resin from the early Cretaceous (Barremian), Isle of Wight. Geochemical Transactions 9, 3–9.

Bray, P.S., Anderson, K.B., 2009. Identification of Carboniferous (320 million year old) Class Ic amber. Science 326, 132–134.

Broutin, J., Pons, D., 1975. Nouvelles précisions sur la morphologie et la phytodermologie de quelques rameaux du genre *Frenelopsis Schenk*. In: Comptes Rendus du 100ème Congrès National des Sociétés Savantes, Paris, vol. II, 1975, pp. 29–46.

Chaler, R., Grimalt, J.O., 2005. Fingerprinting of Cretaceous higher plant resins by infrared spectroscopy and gas chromatography coupled to mass spectrometry. Phytochemical Analysis 16, 446–450.

Cox, R.E., Yamamoto, S., Otto, A., Simoneit, B.R.T., 2007. Oxygenated di- and tricyclic diterpenoids of southern hemisphere conifers. Biochemical Systematics and Ecology 35, 342–362.

Czechowski, F., Simoneit, B.R.T., Sachanbinski, M., Chojcan, J., Wolowiec, S., 1996. Physicochemical structural characterization of ambers from deposits in Poland. Applied Geochemistry 11, 811–834.

Daviero, V., Gomez, B., Philippe, M., 2001. Uncommon branching pattern within conifers: *Frenelopsis turolensis*, a Spanish Early Cretaceous Cheirolepidiaceae. Canadian Journal of Botanics 79, 1400–1408.

Delclòs, X., Arillo, A., Peñalver, E., Barrón, E., Soriano, C., López del Valle, R., Bernárdez, E., Corral, C., Ortuño, V.M., 2007. Fossiliferous amber deposits from the Cretaceous (Albian) of Spain. Comptes Rendus Palevol 6, 135–149.

Dzou, L.I., Holba, A.G., Ramon, J.C., Moldowan, J.M., Zinniker, D., 1999. Application of new diterpane biomarkers to source, biodegradation and mixing effects on Central Llanos Basin oils, Colombia. Organic Geochemistry 30, 515–534.

Farjon, A., 2008. The Natural History of Conifers. Timber Press, New York.

Frenkel, M., Heller-Kallai, L., 1977. Aromatization of limonene – a geochemical model. Organic Geochemistry 1, 3–5.

García-Mondéjar, J., Aguirrezabala, L.M., Aranburu, A., Fernández-Mendiola, P.A., Gómez-Pérez, I., López-Horgue, M., Rosales, I., 1996. Aptian–Albian tectonic pattern of the Basque-Cantabrian Basin (northern Spain). Geological Journal 31, 13–45.

Gomez, B., Martín-Closas, C., Barale, G., Solé de Porta, N., Thévenard, F., Guignard, G., 2002a. *Frenelopsis* (Coniferales: Cheirolepidiaceae) and related male organ genera from the Lower Cretaceous of Spain. Palaeontology 45, 997–1036.

Gomez, B., Bamford, M., Martinez-Delclós, X., 2002b. Lower Cretaceous plant cuticles and amber (Kikwood Formation, South Africa). Comptes Rendus Palevol 1, 83–87.

Gomez, B., Thévenard, F., Fantin, M., Giusberti, L., 2003. Late Cretaceous plants from the Bonarelli Level of the Venetian Alps, northeastern Italy. Cretaceous Research 23, 671–685.

Gradstein, F.M., Ogg, J.G., Smith, A.G., 2004. A Geologic Time Scale 2004. Cambridge University Press.

Grimalt, J.O., Simoneit, B.R.T., Hatcher, P.G., Nissenbaum, A., 1988. The molecular composition of ambers. Organic Geochemistry 13, 677–690.

Hautevelle, Y., Michels, R., Malartre, F., Trouiller, A., 2006. Vascular plant biomarkers as proxies for palaeoflora and palaeoclimatic changes at the Dogger/Malm transition of the Paris Basin (France). Organic Geochemistry 37, 610–625.

Hines, F.M., 1985. Sedimentation and tectonics in north-west Santander. In: Milá, M.D., Rosell, J. (Eds.), 6th European Regional Meeting, Excursion Guidebook. International Association of Sedimentologists, pp. 371–398.

Lambert, J.B., Johnson, S.C., Poinar Jr., G.O., 1996. Nuclear magnetic resonance characterization of Cretaceous amber. Archaeometry 38, 325–335.

Langenheim, R.H., 1969. Amber: a botanical inquiry. Science 163, 1157–1169.

Le Métayer, P., Schaeffer, P., Adam, P., Albrecht, P., Roussé, S., Duringer, P., 2008. An unprecedented condensation pathway leading to the formation of phenolic C_{40} bis-diterpenoids in sediments from the Lower Oligocene of the Rhine Rift Valley. Organic Geochemistry 39, 658–675.

Le Pichon, X., Sibuet, J.C., 1971. Western extension of boundary between European and Iberian plates during the Pyrenean orogeny. Earth and Planetary Science Letters 12, 83–88.

López-Horgue, M.A., Aranburu, A., Fernández-Mendiola, P.A., García-Mondéjar, J., 2001. Facies estuarinas en el Albiense superior de Cabo Quintres (Cantabria, región Vasco-Cantábrica occidental). Geogaceta 30, 75–78.

Marynowski, L., Otto, A., Zaton, M., Philippe, M., Simoneit, B.R.T., 2007. Biomolecules preserved in ca. 168 million year old fossil conifer wood. Naturwissenschaften 94, 228–236.

Menor-Salván, C., Najarro, M., Rosales, I., Velasco, F., Tornos, F., 2009. Quimiotaxonomia y Origen Botánico del Ámbar de El Soplao (Cantabria, España). Macla 11, 123–124.

Miller, C.N., 1999. Implications of fossil conifers for the phylogenetic relationships of living families. The Botanical Review 65, 239–277.

Najarro, M., Peñalver, E., Rosales, I., Pérez de la Fuente, R., Daviero-Gomez, V., Gomez, B., Delclòs, X., 2009. Unusual concentration of Early Albian arthropod-bearing amber in the Basque-Cantabrian Basin (El Soplao, Cantabria, Spain): palaeoenvironmental and palaeobiological implications. Geologica Acta 7, 363–387.

Néraudeau, D., Perrichot, V., Colin, J.-P., Girard, V., Gomez, B., Guillocheau, F., Masure, E., Peyrot, D., Tostain, F., Videt, B., Vullo, R., 2008. A new amber deposit from the Cretaceous (uppermost Albian–lowermost Cenomanian) of southwestern France. Cretaceous Research 29, 925–929.

Nguyen Tu, T.T., Derenne, S., Largeau, C., Pons, D., Broutin, J., Mariotti, A., Bocherens, H., 2000a. Lipids from fossil plants and their relation to modern plants. Examples of Cenomanian flora from Anjou and Bohemia. Journal de la Societé Biologique 194, 57–64.

NguyenTu, T.T., Derenne, S., Largeau, C., Mariotti, A., Bocherens, H., Pons, D., 2000b. Effects of fungal infection on lipid extract composition of higher plant remains: comparison of shoots of a Cenomanian conifer, uninfected and infected by extinct fungi. Organic Geochemistry 31, 1743–1754.

Otto, A., Simoneit, B.R.T., 2001. Chemosystematics and diagenesis of terpenoids in fossil conifer species and sediment from the Eocene Zeitz Formation, Saxony, Germany. Geochimica et Cosmochimica Acta 65, 3505–3527.

Otto, A., Simoneit, B.R.T., 2002. Biomarkers of Holocene buried conifer logs from Bella Coola and north Vancouver, British Columbia, Canada. Organic Geochemistry 33, 124–1251.

Otto, A., Wilde, V., 2001. Sesqui-, di- and triterpenoids as chemosystematic markers in extant conifers – a review. The Botanical Review 67, 141–238.

Otto, A., Walther, H., Püttmann, W., 1997. Sesqui- and diterpenoid biomarkers preserved in Taxodium-rich Oligocene lake clays, Weisselster basin, Germany. Organic Geochemistry 26, 105–115.

Otto, A., Simoneit, B.R.T., Wilde, V., Kunzmann, L., Püttmann, W., 2002. Terpenoid composition of three fossil resins from Cretaceous and Tertiary conifers. Reviews on Palaeobotany and Palynology 120, 203–215.

Otto, A., Simoneit, B.R.T., Wilde, V., 2007. Terpenoids as chemosystematic markers in selected fossil and extant species of pine (*Pinus*, Pinaceae). Botanical Journal of the Linnean Society 154, 129–140.

Pereira, R., Carvalho, I.S., Simoneit, B.R.T., Azevedo, D.A., 2009. Molecular composition and chemosystematic aspects of Cretaceous amber from the Amazonas, Araripe and Recôncavo basins, Brazil. Organic Geochemistry 40, 863–875.

Peters, K.E., Walters, C.C., Moldowan, J.M., 2005. The Biomarker Guide. Biomarkers and Isotopes in Petroleum Exploration and Earth History, second ed.. vol. 2 Cambridge University Press, Cambridge.

Poinar Jr., G., Lambert, J.B., Wu, Y., 2004. NMR analysis of amber in the Zubair Formation, Khafji oilfield (Saudi Arabia-Kuwait): Coals as an oil source rock? Journal of Petroleum Geology 27, 207–209.

Rat, P., 1988. The Basque-Cantabrian basin between the Iberian and European plates: some facts but still many problems. Revista de la Sociedad Geologica de España 1, 327–348.

Roghi, G., Ragazzi, E., Gianolla, P., 2006. Triassic amber from Southern Alps (Italy). Palaios 21, 143–154.

Seoane, L.V., 1998. Comparative study of extant and fossil conifer leaves from the Baqueró Formation (Lower Cretaceous), Santa Cruz Province, Argentina. Review of Palaeobotany and Palynology 99, 247–263.

Simoneit, B.R.T., 1986. Cyclic terpenoids of the geosphere. In: Johns, R.B. (Ed.), Biological Markers in the Sedimentary Record. Elsevier Science Publishers, Amsterdam, pp. 43–99.

Sonibare, O.O., Ekweozor, C.M., 2004. Identification of bicyclic sesquiterpanes in oils from the Niger delta, Nigeria. Journal of Applied Sciences 4, 508–512.

Soto, R., Casas-Sainz, A.M., Villalaín, J., Oliva-Urcía, B., 2007. Mesozoic extension in the Basque Cantabrian basin (N Spain): Contributions from AMS and brittle mesostructures. Tectonophysics 445, 373–394.

Stefanova, M., Simoneit, B.R.T., 2008. Polar aromatic biomarkers of Miocene-aged Churukovo resinite and correlation with a progenitor macrofossil. International Journal of Coal Geology 75, 166–174.

Stefanova, M., Oros, D.R., Otto, A., Simoneit, B.R.T., 2002. Polar aromatic biomarkers in the Miocene Maritza-East lignite, Bulgaria. Organic Geochemistry 33, 1079–1091.

Van den Berg, K.J., Boon, J.J., Pastorova, I., Spetter, L.F.M., 2000. Mass spectrometric methodology for the analysis of highly oxidized diterpenoid acids in Old Master paintings. Journal of Mass Spectrometry 35, 512–533.

Villanueva-García, M., Martínez-Richa, A., Robles, J., 2005. Assignment of vibrational spectra of labdatriene derivatives and ambers: a combined experimental and density functional theoretical study. Arkivoc 2005 (iv), 449–458.

Yamamoto, S., Otto, A., Krumbiegel, G., Simoneit, B.R.T., 2006. The natural product biomarkers in succinite, glessite and stantienite ambers from Bitterfield, Germany. Review of Palaeobotany and Palynology 140, 27–49.

Palaeogeography, Palaeoclimatology, Palaeoecology 365–366 (2012) 276–293

Contents lists available at SciVerse ScienceDirect

Palaeogeography, Palaeoclimatology, Palaeoecology

journal homepage: www.elsevier.com/locate/palaeo

Organic geochemistry, stable isotopes, and facies analysis of the Early Aptian OAE—New records from Spain (Western Tethys)

María Luisa Quijano [a,*], José Manuel Castro [b], Richard D. Pancost [c], Ginés A. de Gea [b], María Najarro [d], Roque Aguado [b], Idoia Rosales [d], Javier Martín-Chivelet [e]

[a] Departamento de Química Inorgánica y Orgánica, Universidad de Jaén, Campus Las Lagunillas, E-23071 Jaén, Spain
[b] Departamento de Geología, Universidad de Jaén, Campus Las Lagunillas, 23071 Jaén, Spain
[c] Organic Geochemistry Unit, Bristol Biogeochemistry Research Centre, The Cabot Institute, School of Chemistry, University of Bristol, BS8 1TS, UK
[d] Instituto Geológico y Minero de España, IGME, Ríos Rosas 23, 28003 Madrid, Spain
[e] Departamento de Estratigrafía-IGEO (CSIC-UCM), Universidad Complutense, 28040 Madrid, Spain

ARTICLE INFO

Article history:
Received 10 March 2011
Received in revised form 30 July 2012
Accepted 12 September 2012
Available online 8 October 2012

Keywords:
Early Aptian
Oceanic Anoxic Event 1a
Biomarkers
C-isotopes
Spain

ABSTRACT

The Early Aptian Oceanic Anoxic Event (OAE1a) is a time interval characterized by increased organic carbon accumulation in marine sediments, notable sedimentary and biotic changes, and abrupt carbon-isotope excursions indicative of significant major palaeoenvironmental changes linked to a perturbation in the global carbon cycle. Here we present the study of four sections recording the OAE1a (Early Aptian) in Spain, which are located in two broad basins respectively located in the South and the North of Iberia: the Southern Iberian Palaeomargin (Carbonero, La Frontera and Cau sections) and the Basque–Cantabrian Basin (Puentenansa section), which represent depositional settings ranging from shallow marine (distal ramp -Cau- and drowned platform -Puentenansa-) to pelagic environments (Carbonero, La Frontera). Biomarker compositions, C-isotope profiles, biostratigraphic data and facies analysis from the four sections are correlated and integrated. The C-isotope curves all present a clear negative excursion followed by a positive shift. The integration of the C-isotope curves with the biostratigraphic data has been used to correlate the studied sections and to tentatively identify the eight segments formerly proposed from the Alpine domain, and subsequently identified in sections worldwide. Four main groups of compounds are present in all sections: *n*-alkanes, isoprenoids, hopanes and steranes. *n*-Alkanes and acyclic isoprenoids (pristane and phytane) are dominant in most samples. The hopanes are represented by a range of C_{27} to C_{35} components, with the specific isomers varying amongst the sections due to differences in thermal maturity. Steranes occur as a range of C_{27}, C_{28} and C_{29} isomers, whereas diasteranes only occur in the most thermally mature section (Carbonero). Other compounds of interest include gammacerane and dinosterane. Differences in thermal maturity appear to be the first order control on different biomarker assemblages amongst the studied sections. The Carbonero section is thermally mature, whereas the nearby La Frontera and Cau sections are immature. Puentenansa has intermediate values. Organic matter is derived from a range of terrestrial, marine and bacterial sources. The dominance of the C_{29} sterane isomers in all sections suggests a strong contribution from higher plants. The presence of gammacerane indicates water column stratification, and high C_{29}/C_{30} hopane ratios suggest anoxia at the water/sediment interface, respectively. Sedimentologic analysis also suggests anoxic conditions during sedimentation, but evidence for strong and persistent water column anoxia is equivocal. The correlation of the sections reveals that sedimentation of organic-rich facies started earlier in pelagic and later in the shallow marine settings, which can be related to an expansion of the favorable conditions for organic matter accumulation and preservation from deep marine waters to shallower platform environments during the development of OAE1a.

1. Introduction

The Cretaceous was generally characterized by a greenhouse climate state (Hallam, 1985; Wilson and Norris, 2001), with a reduced latitudinal temperature gradient (Huber et al., 1995; Hay, 2008), elevated pCO_2 levels (Beerling and Royer, 2002, and references therein), and high sea level (e.g. Jenkyns, 1980; Skelton, 2003). In this context, significant short-term changes took place in the ocean-climate

* Corresponding author. Tel.: +34 953212741; fax: +34 953211876.
E-mail addresses: lquijano@ujaen.es (M.L. Quijano), jmcastro@ujaen.es (J.M. Castro), R.D.Pancost@bristol.ac.uk (R.D. Pancost), gadegea@ujaen.es (G.A. de Gea), m.najarro@igme.es (M. Najarro), raguado@ujaen.es (R. Aguado), i.rosales@igme.es (I. Rosales), j.m.chivelet@geo.ucm.es (J. Martín-Chivelet).

0031-0182/$ – see front matter © 2012 Elsevier B.V. All rights reserved.
http://dx.doi.org/10.1016/j.palaeo.2012.09.033

system, primarily reflected in the widespread deposition of organic carbon-rich marine sediments, whose relation to anoxic marine conditions led to the definition of Oceanic Anoxic Events (Schlanger and Jenkyns, 1976; Jenkyns, 1980). Subsequent research on OAEs have revealed that they represent notable perturbations in the global carbon cycle, which have been related to massive submarine volcanism, formation of oceanic plateaus, and increased rates of seafloor spreading (Leckie et al., 2002). These perturbations were reflected in rapid climate and environmental changes (Jenkyns, 2003; Dumitrescu et al., 2006; Hermoso et al., 2009) affecting both the marine and continental realms (e.g. Skelton, 2003).

Among the OAEs that punctuated the Cretaceous Period, the one that occurred during the Early Aptian (so called OAE1a) was one of the first identified and remains one of the most widely studied. It had a global extent (Arthur et al., 1990; Leckie et al., 2002) and a duration of 1.0 to 1.3 Myr (Li et al., 2008). Sediments recording this event have been recognized in the Tethys domain ("Selli level", Menegatti et al., 1998; Hochuli et al., 1999; Luciani et al., 2001; de Gea et al., 2003; Erba and Tremolada, 2004; Heimhofer et al., 2004; Aguado et al., 2008; de Gea et al., 2008b; Najarro and Rosales, 2008b; Rosales et al., 2009; Mehay et al., 2009; Millán et al., 2009; Najarro et al., 2011a, b; Stein et al., 2011, among others), in the Boreal domain (Gröcke et al., 1999; Föllmi et al., 2006), in the Pacific (Jenkyns, 1995; Ando et al., 2002; Price, 2003; Dumitrescu and Brassell, 2005), and Mexico (Bralower et al., 1999). Dramatic environmental changes occurred in association with OAE1a in settings ranging from continental to pelagic, and particularly in shallow marine carbonate platforms. Among the most striking time-related phenomena were the "nannoconid crisis" (Erba, 1994; Aguado et al., 1999; Erba et al., 2010), profound changes in the marine biota (e.g. Bralower et al., 1994; Erbacher et al., 2001; Leckie et al., 2002), and drastic perturbations in land vegetation and in continental weathering (Föllmi et al., 2006). Nevertheless, other studies suggest that major pCO_2 and vegetation changes did not occur during OAE1a (Heimhofer et al., 2004).

The impact of OAE1a on shallow carbonate platform environments has been analyzed in several studies. One major environmental perturbation is the widespread drowning event recorded at multiple sites (i.e. Weissert et al., 1998; Föllmi et al., 2006; Castro et al., 2008; Najarro et al., 2011a; Castro et al., 2012). In addition, notable faunal and facies changes in carbonate platforms have been related to the OAE1a (i.e. Huck et al., 2012), including the remarkable widespread development of Lithocodium–Bacinella episodes in the Tethys domain (Immenhauser et al., 2005; Bover-Arnal, 2010; Rameil et al., 2010).

A pervasive feature of OAE1a stratigraphic successions is the series of pronounced isotopic excursions, first negative and then positive, that occur in both δ^{13}Ccarb and δ^{13}Corg (e.g. Menegatti et al., 1998; Leckie et al., 2002; de Gea et al., 2003; Herrle et al., 2004, among others). The widespread documentation of these features of the carbon isotope profile in numerous successions of marine carbonate and pelagic sediments from the aforementioned Tethys, Boreal and Pacific regions enables their use as a tool for stratigraphic correlation and as a record of the global perturbations of the carbon cycle. Although there is general agreement that the positive excursion in sedimentary δ^{13}C values arises from increased burial of organic matter during the OAE, multiple explanations have been proposed to explain the negative carbon isotope excursion at the onset of OAE1a and, by extension, the causal mechanism. One explanation is that emplacement of large igneous provinces (LIPs; e.g. Ontong-Java and Manihiki Plateaus: Larson, 1991; Larson and Erba, 1999; Tejada et al., 2009; Mehay et al., 2009) raised atmospheric pCO_2 and enhanced nutrient fluxes to the ocean. Other potential triggers include dissociation of gas hydrates releasing methane in continental margin sediments (Beerling and Royer, 2002; Jahren et al., 2005), or increased recycling rates of ^{12}C and nutrient-rich intermediate waters linked to changes in ocean productivity (Menegatti et al., 1998; Larson and Erba, 1999; Erba and Tremolada, 2004; Weissert and Erba, 2004).

This paper presents the study of four sections recording the OAE1a in Spain, from two different basins (Southern Iberian Palaeomargin and North Cantabrian Basin, Fig. 1), and also representing different palaeogeographic settings (shallow marine and pelagic settings). The sections have been characterized using a combination of isotopic, elemental and biomarker approaches. The latter have been widely used in the investigation of OAEs, including the assessment of marine productivity, terrestrial vs. marine sources of organic matter, and the redox state of the ocean (Meyers, 1997; Pancost et al., 2004). The timing of C-rich sediment deposition is interpreted with respect to the local carbon isotope stratigraphy, with biomarker and elemental analyses being used to further constrain changes in organic carbon inputs and differences in thermal maturity among the four sections. Overall, the integration of stratigraphy and geochemistry, and the correlation with reference sections, has led to present a sedimentary model which assess mechanisms for the spread of anoxia, taking into consideration global and regional effects.

2. Geological setting

2.1. Palaeogeographic framework

During Aptian times the sedimentary basins of Iberia were strongly influenced by the relative motions of the contiguous Eurasian and African plates (Fig. 1). The initiation of the seafloor spreading in the North Atlantic, which started very early in the Cretaceous, led to a decrease in the sinistral movement between Iberia and Africa that had prevailed during part of the Jurassic (Ziegler, 1988), and to a phase of rapid anticlockwise rotation of Iberia relative to Europe that would culminate in seafloor spreading in the Bay of Biscay from middle Aptian times onwards (Olivet, 1996; Vergès and García-Senz, 2001). In that geodynamic framework, extensional tectonics prevailed in the main sedimentary basins, including the two considered in this paper: the North Cantabrian Basin (NCB), which belonged to the northern margin of the Iberian plate, and the Southern Iberian Palaeomargin (SIPM) (Fig. 1). That extensional tectonism experienced a strong phase during the latest Jurassic to the Hauterivian, followed, during the Barremian–Aptian, by an interval of smaller tectonic movements but larger subsidence rates, that favored the development of wide and thick carbonate platforms (including the Urgonian facies) in the shallow areas of the basins (e.g., Martín-Chivelet et al., 2002; Vera, 2004).

The Lower Cretaceous sequence of the SIPM includes thick successions (>3000 m) of carbonates and siliciclastics that were deposited in shallow platforms (mostly in the so-called Prebetic Zone, Fig. 2A) and hemipelagic/pelagic settings (dominant in the Subbetic Zone, Fig. 2A) (e.g. Ruiz-Ortiz, 1980; Martín-Chivelet et al., 2002; Vera, 2004). The configuration of the SIPM was defined by a series of basin-scale troughs and swells, bounded by large extensional faults roughly parallel to the continental margin, that were initiated in the Middle Jurassic (e.g., Azéma et al., 1979; García Hernández et al., 1980; Vera, 1988; Ruiz-Ortiz et al., 2001). This tectonic pattern controlled strong differential subsidence and deposition rates. The stratigraphic sections herein considered correspond to depocentral areas in both the Prebetic (Cau section), and the Subbetic (Carbonero and La Frontera sections) (Fig. 2A).

The North Cantabrian Basin (NCB) was a relatively small ($\approx 20 \times 80$ km), E–W elongated sub-basin, which belonged during the Mesozoic to the larger Basque–Cantabrian Basin (BCB). Located in the northwestern margin of the BCB, this sub-basin behaved independently for most of the Cretaceous, and was relatively less subsident than other areas of the BCB. It was separated from the rest of the basin to the east by a N–S complex fault structure (Río Miera Flexure; Feuillée and Rat, 1971). The NBC was generated by rifting tectonics linked to the opening of the Bay of Biscay and

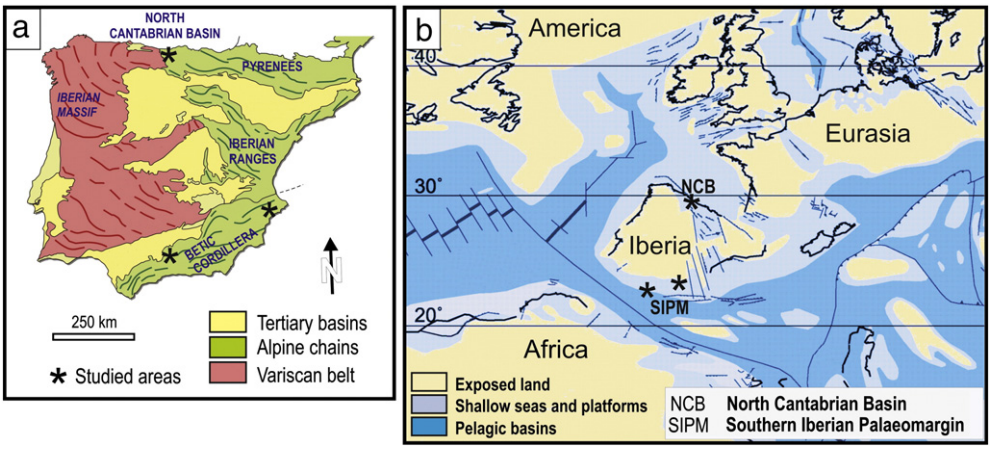

Fig 1. a. Schematic geological map of the Iberian Peninsula showing the main geological units and the location of the studied sections (see Fig. 2 for details). b. Paleogeographic reconstruction of Iberia and its surroundings during the Aptian (simplified from Masse et al., 2000) showing the palaeogeographic location of the studied basins: the Southern Iberian Palaeomargin and the North Cantabrian Basin, respectively located in the southern and the northern margins of Iberia. Note that these basins were inverted and deformed in the Alpine Orogeny during the Tertiary, and are now respectively incorporated into the External Zones of the Betic Cordillera and the Western Pyrenees.

North Atlantic during the Late Jurassic and the Early Cretaceous. This tectonism structured a series of horsts and grabens, mainly outlined by the presence of N–S, NE–SW, and E–W oriented faults, which controlled differential subsidence and sedimentation patterns at least during Barremian–Albian times (Najarro et al., 2007, 2011a). The Lower Cretaceous sediment infill includes relatively thick successions (up to 2000 m thick) of siliciclastics and carbonates, deposited in environments that ranged from fluvial/estuarine to open marine. The studied section corresponds to the Puentenansa road outcrop, near the village of Rábago (Fig. 2B). This area, characterized by moderate subsidence during sedimentation, corresponded to the footwall block of the N–S Bustriguado synsedimentary fault, which is considered as a Cretaceous left–lateral transfer fault (García-Senz and Robador, 2009; Najarro et al., 2009).

Interestingly, the studied successions in the SIPM and the NCB, despite their proximity from a global perspective, were isolated from each other during deposition because of the palaeogeography of Iberia and the palaeoceanography of the surrounding seas. The SIPM belongs to the westernmost part of the northern margin of the Tethys, whereas the NCB belongs to the North Atlantic realm. That relative isolation favored, for example, the development of separate faunal (sub)bioprovinces during Cretaceous times (e.g., Caus and Hottinger, 1986; Caus et al., 2009). Beyond regional tectonics and palaeogeography, the sedimentation in the basins of Iberia should be also influenced in Aptian times by eustatic changes (e.g., Immenhauser et al., 1999; Immenhauser, 2005) and regional climate. At that time Iberia was located approximately between 23° and 33° North latitude, with a tropical to subtropical climate (e.g., Masse et al., 2000).

2.2. Previous stratigraphic data of the studied sections

2.2.1. Southern Iberian Palaeomargin (SIPM)

Three sections have been previously studied, two from the pelagic Subbetic domain (La Frontera and Carbonero), and one other from the Prebetic domain (Cau section), which represents shallow marine settings.

2.2.1.1. La Frontera section. This section is located in the South of the Jaén province (Fig. 2A) and was deposited in a pelagic environment, in a rapidly subsiding area bounded by extensional faults. In this area of the Subbetic Zone, the Barremian is represented by a pelagic rhythmite of the Carretero Formation, whereas the Aptian is represented by the Carbonero Formation, comprising dark marls with an interval of black shales in the Early Aptian, interpreted as the local record of OAE1a (Fig. 3). Here, the presence of calcareous nannofossils has led to the identification of the *Hayesites irregularis* and lower *Rhagodiscus angustus* biozones (Fig. 3). A detailed biostratigraphic characterization of this section, based on planktonic foraminifers, radiolarians and ammonites, can be found in Aguado et al. (1992a) and de Gea (2004).

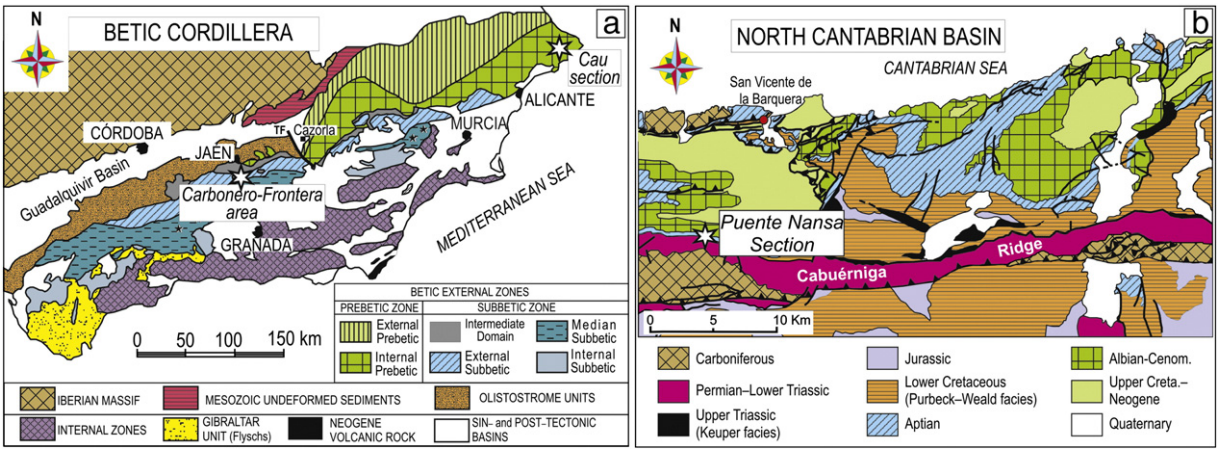

Fig. 2. Location of the studied sections. A.—Betic Cordillera: Cau section belongs to the Prebetic Zone, and Carbonero and La Frontera sections are located in the Subbetic Zone. B.—North Cantabrian Basin: Puentenansa section is located in La Florida area, which formed in the south- western margin of the Basin.

2.2.1.2. Carbonero section. This section is located in the South of the Jaén province, fifteen kilometres westward of the La Frontera section. In spite of the proximity, the Carbonero Formation here has strong differences to the La Frontera section and occurs as a rich association of facies, including marls and marlstones, black shales, radiolarian marls, siliceous shales, calcareous turbidites, cinerites, and concretions of barite and carbonate. de Gea et al. (2008a) provided a detailed study of several sections within the area of Carbonero section. They proposed a model of a small subsiding pelagic sub-basin bounded by active faults leading to scarps feeding the turbidite levels, associated with volcanic activity. This small sub-basin has a more complete stratigraphic record than the surrounding areas, with a locally restricted environment leading to high contents of organic matter, along with the development of barite concretions, interpreted to reflect anoxic conditions (Molina and Hernández-Molina, 1993; Bréheret and Brumsack, 2000; de Gea et al., 2008a). Characterization of nannofossil assemblages has led to the recognition of the *Micrantholitus hoschulzi*, *H. irregularis* and lower part of *R. angustus* biozones (Aguado et al., 1992b; Molina et al., 2001; Fig. 3).

2.2.1.3. Cau section. This section is located in the NE of the Alicante province (Fig. 2A) and represents the distal parts of a shallow carbonate ramp. In this setting, hemipelagic sedimentation took place during the late Barremian to late Aptian, when a progradational episode led to the deposition of shallow platform carbonates during the latest Aptian–Albian. The late Barremian to late Aptian is represented by the Almadich Formation, comprising hemipelagic marls and marlstones with ammonites, planktonic foraminifers and calcareous nannofossils. This formation includes a horizon of black marls corresponding to the Early Aptian OAE1a (Fig. 4). This black marl interval occurs in the lower part of the *Schackoina cabri* planktonic foraminifer biozone, *H. irregularis* nannofossil biozone, and corresponds also to the ´nannoconid crisis´ (Aguado et al., 1999; de Gea et al., 2003). The high organic matter content along with the planktonic foraminifers association (with elongation of the chambers) have been proposed to be related to anoxic–dysoxic conditions in the water column during sedimentation (Aguado et al., 1999; de Gea et al., 2003). The stratigraphy, biostratigraphy and isotope chemostratigraphy of the Cau section have been presented in detail in previous publications (Aguado et al., 1999; de Gea et al., 2003; Castro et al., 2008).

2.2.2. North Cantabrian Basin (NCB)

The Puentenansa section is located to the West of Cantabria, in the eastern edge of the North Cantabrian Basin. It is well exposed alongside the Puentenansa road. In this outcrop, the Aptian succession lies unconformably on the Permian to Early Triassic sedimentary rocks. The Early Aptian lithostratigraphy in this area is complex, including four formations: the Rábago and Umbrera Formations (lower Bedoulian), which consist of shallow platform limestones, marls and sandstones; the Patrocinio Formation (mostly early Bedoulian, *Deshayesites weissi* ammonite biozone and middle upper part of the *H. irregularis* nannofossil biozone; Rosales et al., 2009; Najarro et al., 2011b), comprising open marine, black marls and marly siltstones. These deposits, which represent the local record of the OAE1a, reflect the shutdown of the shallow water carbonate factory, as the result of a combined

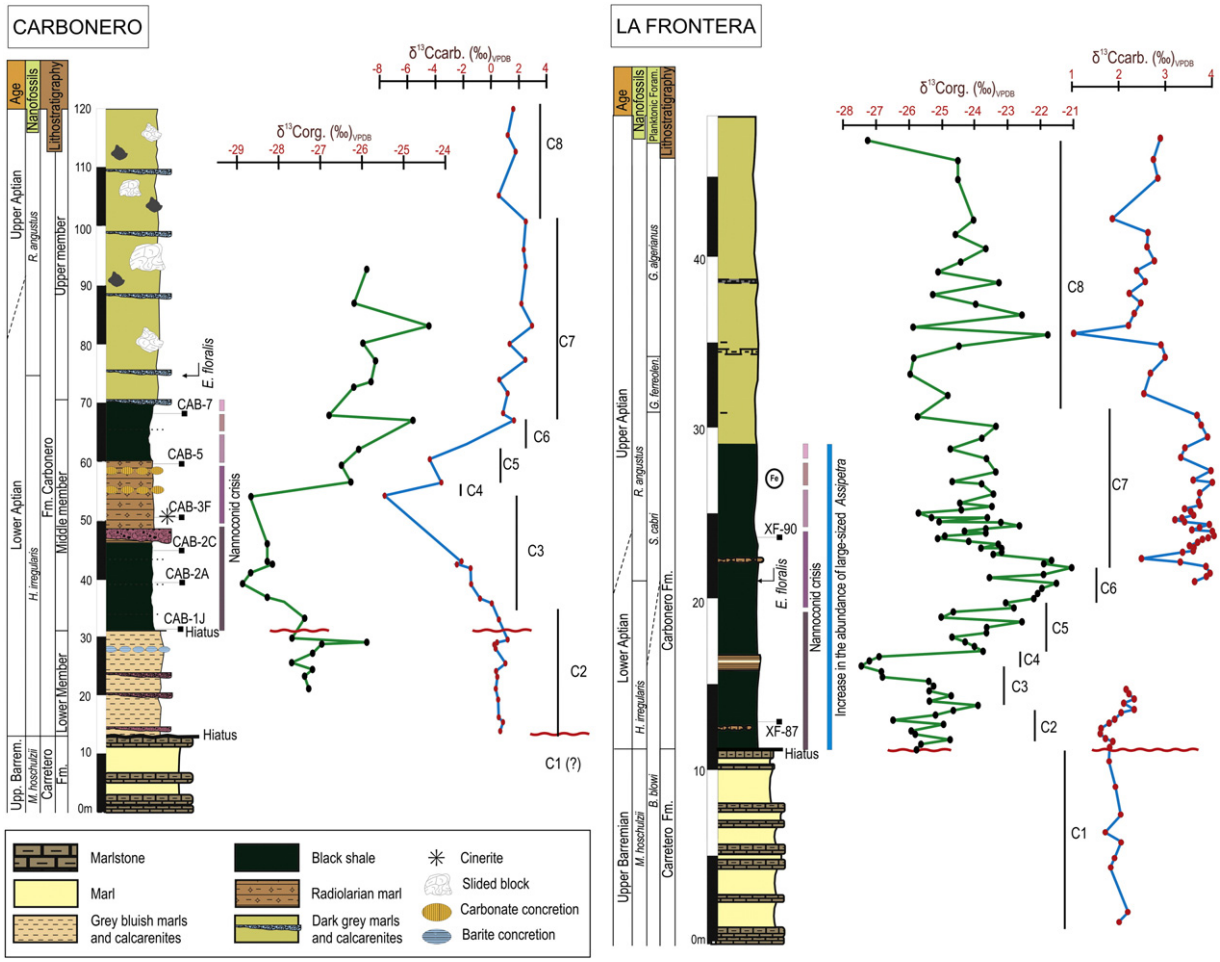

Fig. 3. Carbonero and La Frontera sections. Lithostratigraphy, biostratigraphy, and C-isotope curves. C1 to C8 refers to C-isotope stratigraphy proposed by Menegatti et al., 1998. Samples referred in sections are those selected for biomarker analysis.

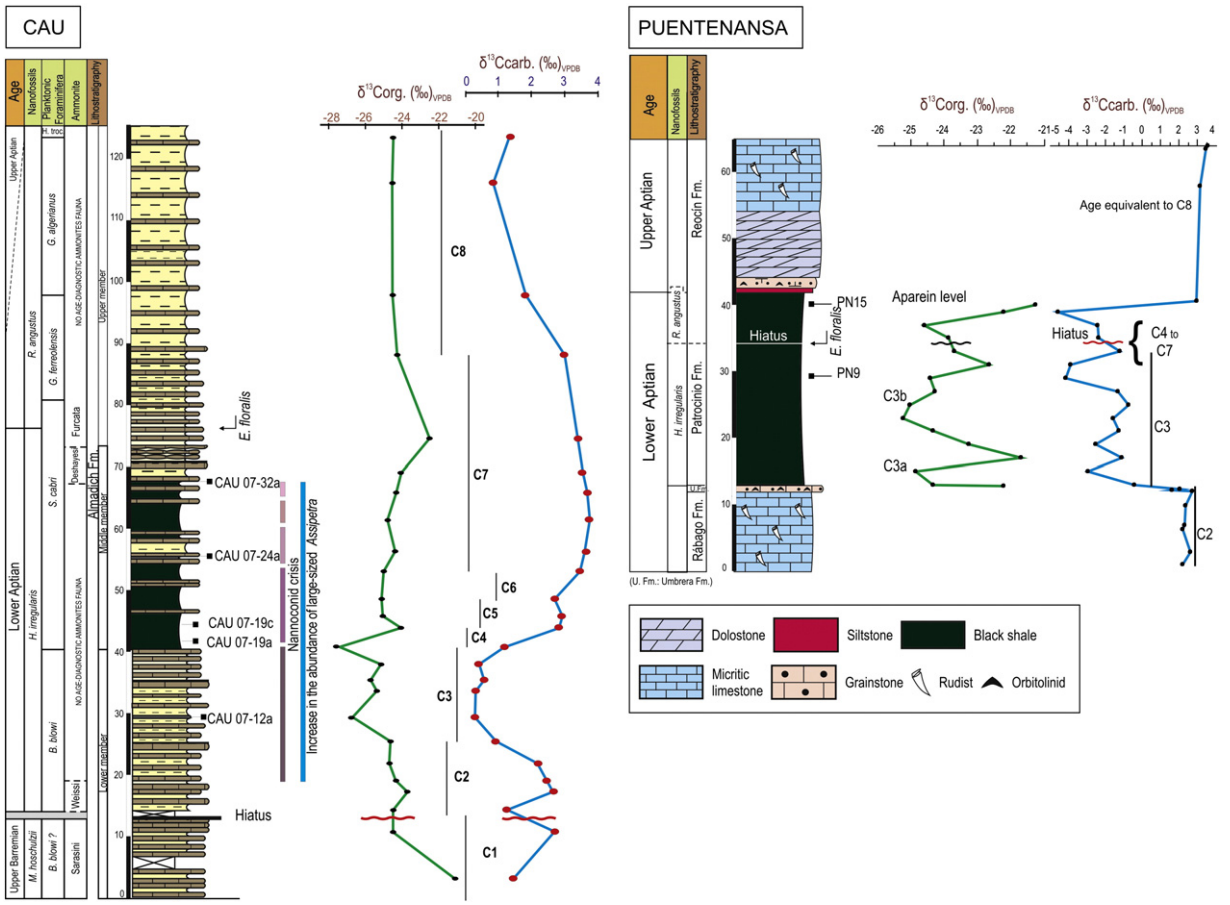

Fig. 4. Cau and Puentenansa sections. Modified from de Gea et al. (2003) and Najarro et al. (2011a). Samples named in sections refer to those selected for biomarker analysis.

action of a relative sea-level rise and environmental stress, and record a net deepening-upward trend leading to a drowned platform (Najarro et al., 2011a). Nannofossil assemblages from the Patrocinio Formation allow the recognition of the *H. irregularis* and lower *R. angustus* biozones (Fig. 4), showing the presence of a stratigraphic gap in the Patrocinio Formation of this area that lasts until the lower Gargasian and which affects the record of OAE1a (Najarro et al., 2011b). Finally, in this section the Reocín Formation (Gargasian), comprising shallow platform limestones, overlies the Patrocinio Formation.

3. Methods

3.1. Stratigraphy and biostratigraphy

Through previous extensive field work, the selected sections have been intensively investigated. As a result, the lithology, biostratigraphy and sedimentology of each section has been previously described in detail and finally integrated in a regional stratigraphic context (Aguado et al., 1992a,b, 1999; Castro, 1998; Molina et al., 2001; de Gea et al., 2003; de Gea, 2004; de Gea et al., 2005, 2008b, 2008c; Najarro et al., 2007; Najarro and Rosales, 2008a,b; Najarro et al., 2011a,b).

To allow further and integrated analyses, and to refine the dating and correlation between the different sections, all four were resampled for geochemical analyses and calcareous nannofossil and planktonic foraminiferal characterisation. The marly lithotypes were preferred for sampling in order to obtain the best preserved assemblages. In the Carbonero section, about 33 samples were collected at irregularly spaced intervals (50 cm–5 m) along a 120 m thick sucession of marls, marly limestones, black shales and radiolarian marls (Carbonero Formation), spanning the Lower Aptian–lower part of the Upper Aptian interval. The La Frontera section was sampled at a higher resolution, also at irregularly spaced intervals (15–250 cm), in order to characterize biostratigraphically and sedimentologically the small changes in facies and/or lithology. A total of 100 samples were collected from the marls, marly limestones and black shales of the Carretero and Carbonero Formations spanning the uppermost Barremian–lower part of the Upper Aptian interval. The Cau section was re-sampled for more detailed dating and for geochemical analyses. Finally, in the Puentenansa section, 15 samples of marls and marly siltstones were collected across the Lower Aptian Patrocinio Formation at approximately regular intervals of 2 m, and another 10 limestones were collected from the platform units below and above the Patrocinio Formation.

For calcareous nannofossil characterization, simple smear slides were prepared following standard procedures (Bown and Young, 1998). No physical concentration or separation was applied in order to retain the original assemblage composition. A polarizing light microscope at 1250× magnification was used to investigate the nannofossil assemblages through, at least, a longitudinal traverse of the smear slide (200 fields of view). Also, a fraction of each sample was disaggregated and washed through sieves, the residue being separated into three fractions (>200 μm, 100–200 μm and 50–100 μm). For each sample, the two great sized residues were investigated for planktonic foraminiferal content, although the richest assemblages were found in the 100–200 μm residues. A portion of the selected samples was separated for geochemical analyses, including carbon isotope, elemental and biomarker characterization.

3.2. Oxygen and Carbon isotopes

Oxygen and carbon stable isotope analyses were performed on marls collected from the four sections, and also on carbonates from

the Puentenansa section. Carbonero and La Frontera samples were powdered using an agate mill. The $\delta^{13}C$ values of carbonates were determined by treatment with 103% orthophosphoric acid using a VG Isocarb system thermostatized at 90 °C. The produced CO_2 was analyzed with an IRMS (Isotope Ratio Mass Spectrometer) VG Prism II. For analysis of organic matter $\delta^{13}C$ values, samples were treated with 3% HCL for 24 h to remove carbonates and then analyzed with an elemental analyzer Carlo Erba 1108 coupled to a IRMS VG Isochrom in continuous flow mode. These analyses were performed at the Stable Isotope Laboratory (SIDI) of the Universidad Autónoma of Madrid and Servicio General de Isótopos Estables of the University of Salamanca (Spain). The results are expressed in the common δ-notation in per mil (‰) relative to the VPDB-standard. The international carbonate standard NBS-19 (National Bureau of Standards; $\delta^{13}C = 1.95‰$ and $\delta^{18}O = -2.20‰$) was used to calibrate to V-PDB, with an average precision of 0.1‰ for δ^{13}Ccarb and 0.15‰ for δ^{13}Corg analyses. A description of the method used for the Puentenansa and Cau sections has been published in Najarro et al. (2011b) and de Gea et al. (2003), respectively.

3.3. Elemental analyses and total organic carbon

A total of 33 samples from the studied sections were analyzed for total organic carbon (TOC) concentrations and elemental composition (CNHSO and XRF). The CNHSO and X-ray fluorescence analyses were performed in the Centro de Instrumentación Científica of the Universidad de Jaén, with a Thermo Finnigan FlashEA1112 CHNS-O Elemental Analyzer, and an X-Ray expectrometer Bruker AXS model Pioner S4 explorer, respectively. The TOC analyses were performed in the Centre of Atomic Spectrometry of the Universidad Complutense (Madrid) with a SHIMADZU TOC-V device that performs the 680 °C combustion catalytic oxidation method. The TOC concentration was determined by subtracting the inorganic carbon (IC) concentration from the total carbon (TC) in each sample.

3.4. Biomarkers

A collection of 15 samples, with an emphasis on the OAE1a intervals, were selected from the studied sections (Figs. 3 and 4), in order to characterize the thermal maturity and organic source inputs. The samples were externally washed with dichloromethane (DCM) to remove contamination from handling and then crushed using a Pulverissete 5 agate mill. The crushed samples were Soxhlet extracted for 48 h with 500 ml DCM/MeOH (80:20). Activated copper turnings were added to the solvent flask to remove elemental sulphur from the Carbonero samples. After extraction, the turnings were removed, and the solvent volume was reduced under reduced pressure. The extracts were separated into three fractions by column chromatography using activated alumina and sequential elution with hexane (saturated hydrocarbons), hexane:dichloromethane (9:1) (aromatic compounds), and methanol (polar compounds).

The saturated hydrocarbon fractions were analyzed with gas chromatography–mass spectrometry (GC–MS). GC–MS was carried out on a Thermo DSQ II gas chromatograph connected to a Thermo Trace Ultra mass spectrometer in the Centro de Instrumentación Científica of the Universidad de Jaén, and a ThermoQuest Trace GC–MS housed in the Organic Geochemistry Unit (School of Chemistry) of the University of Bristol. The GC was fitted with a fused silica capillary column (Supelco Equity–5; 30 m x 0.25 mm x0.25 μm) and was operated with helium as carrier gas. The samples (in hexane) were injected at 70 °C and the oven was subsequently programmed to 130 °C at 20 °C/min and then at 4 °C/min to 300 °C where it was held for 25 min. Biomarkers were identified by comparison of mass spectra and retention time with those reported in the literature (i.e. Peters et al., 2005); for the identification of gammacerane an authentic standard purchased by Chiron was co–injected.

4. Results

4.1. Chemo- and biostratigraphy

The carbonate (C_{carb}) and bulk organic carbon (C_{org}) isotopic profiles are shown for each of the four sections (Figs. 3 and 4). Part of the data included in the curves comes from previous papers dealing with single sections (see de Gea et al., 2003 for the Cau section, and Najarro et al., 2011b for the Puentenansa section). The biostratigraphy of these successions is mostly based on the references cited and also on new data from this study. The reference curve used here for correlation is that published by Menegatti et al. (1998), because is the more widely used (i.e. Immenhauser et al., 2005; Föllmi et al., 2006; Dumitrescu and Brassell, 2006; Stein et al., 2011; Jenkyns et al., 2012), and it is focused on the same time interval studied here. Other more recent proposals of subdivision of the Barremian–Aptian C-isotope curve have also been considered (Bralower et al., 1999; Wissler et al., 2003; Herrle et al., 2004).

4.1.1. La Frontera section

The $\delta^{13}C_{carb}$ values of the La Frontera section range between 1.0‰ and 4.0‰ (Fig. 3). The lowest 9 samples in the section, corresponding to the latest Barremian marls and marly limestones of the Carretero Formation (*Micrantholithus hoschulzi* nannofossil biozone, Aguado et al., 1992a), show little isotopic variation, with values of $\delta^{13}C_{carb}$ ranging from 1.8‰ to 2.1‰ (Fig. 3). A stratigraphic gap, including probably part of the uppermost Barremian and the lowermost Aptian, has been interpreted to exist at the top of this lower portion of the section, because the marker species *Hayesites irregularis* is not recorded in the uppermost part (uppermost Barremian) of the Carretero Formation and the overlying black facies of the Carbonero Formation are within the 'nannoconid crisis' interval (Fig. 3). This stratigraphic gap affects the complete lower member of the Carbonero Formation (lowermost Aptian), which is not represented in this section. A minor 0.5‰ positive excursion in carbonate, with a maximum value of 2.3‰ occurs within the middle member of the Carbonero Formation, in layers belonging to the *H. irregularis* nannofossil biozone and located within the interval corresponding to the 'nannoconid crisis' (Fig. 3). This excursion is followed by 10 m of largely carbonate-free black-shales, after which the positive excursion apparently continues to a maximum value of 4.0‰. *Eprolithus floralis* was recorded in the first sample above the carbonate-free rocks. Within the following 8 m interval, corresponding to the lowermost part of the *R. angustus* nannofossil biozone and *S. cabri* planktonic foraminiferal biozone, the $\delta^{13}C_{carb}$ values remain relatively high (minimum 3.2‰; average 3.6‰). High abundances of *Assipetra*, (*A. infracretacea* and *A. terebrodentaria*), including large-sized specimens (*A. infracretacea* ssp. *larsonii* and *A. terebrodentaria* ssp. *youngii*; Tremolada and Erba, 2002), characterize this interval from the base of the middle member of the Carbonero Formation (Fig. 3). The next 5 m of the isotopic profile display an overall negative trend reaching a minimum of 1.0‰, coinciding with the *Globigerinelloides ferreolensis* and lower part of *G. algerianus* planktonic foraminiferal biozones (Lower–Upper Aptian transition). Finally, $\delta^{13}C_{carb}$ values in the uppermost 12 m of the investigated interval are characterized by a slight increasing trend (maximum 2.8‰ but also a marked minimum value of 1.9‰). This last interval is Late Aptian in age, and is characterized biostratigraphically by the upper part of *G. algerianus* planktonic foraminifer biozone.

The $\delta^{13}C_{org}$ values of the La Frontera section range between −21.0‰ and −27.4‰, and present a continuous record of C-isotope data. Generally, the $\delta^{13}C_{org}$ values parallel the $\delta^{13}C_{carb}$ curve. In detail, a large negative excursion, from −23.9‰ to −27.4‰, occurs in the interval lacking a $\delta^{13}C_{carb}$ record. The subsequent positive excursion is characterized by an increase in $\delta^{13}C_{org}$ values to −23.8‰ and this does parallel the $\delta^{13}C_{carb}$ profile. However, also present in the upper part of the

$\delta^{13}C_{org}$ profile are several high frequency and high amplitude variations, with maximum shifts of 4.0‰ (Fig. 3).

4.1.2. Carbonero section

The samples from the Carbonero section were taken in the type area of the Carbonero Formation (de Gea et al., 2008a). In this section, a stratigraphic gap has been interpreted to exist between the uppermost Barremian marls and marly limestones of the Carretero Formation and the overlying bluish-grey marls with intercalations of calcareous turbidites comprising the lower member of the Carbonero Formation (Lower Aptian). This gap, with a lower extent than that observed in the La Frontera section, has been deduced on the basis of the absence of the nannofossil *H. irregularis* in the Carretero Formation. The bluish-grey marls of the lower member of the Carbonero Formation, containing moderate to high proportions of nannoconids and *H. irregularis*, predate the 'nannoconid crisis' event (de Gea et al., 2008a). The base of the overlying black shales and radiolarian marls of the middle member of the Carbonero Formation (local expression of the OAE 1a), coincides with the onset of the 'nannoconid crisis'. For this reason, a new stratigraphic gap has been interpreted to exist in this section between the lower and middle members of the Carbonero Formation (de Gea et al., 2008a). Finally, the FO of the nannofosil *E. floralis*, has been recorded near the base of the alternation of greenish-grey marls and calcarenites of the upper member of the Carbonero Formation.

The Carbonero section has been analyzed at a lower resolution than the La Frontera section, but both the $\delta^{13}C_{carb}$ and $\delta^{13}C_{org}$ profiles are complete and largely parallel each other. Overall, they exhibit the same general trends as observed in the La Frontera Section (Fig. 3). $\delta^{13}C_{carb}$ values vary between 3.1‰ and −7.9‰. The lower 20 m of the section (lower member of the Carbonero Formation), have constant values around 0.8‰ but then increase slightly up to 1.2‰. The following 28 m is characterized by a dramatic negative trend to values of approximately −7.9‰ in the radiolarian marls of the middle member of the Carbonero Formation. The next 15 m record a positive trend, up to 1.5‰, and the upper 80 m are characterized by generally elevated values (from 1 to 3‰).

The $\delta^{13}C_{org}$ profile reproduces some of the major trends recorded by $\delta^{13}C_{carb}$ values, albeit at a reduced amplitude. Values range from −28.9‰ to −24.4‰, although only a 2‰ decrease occurs from 30 to 40 m, such that the magnitude of the negative carbon isotope excursion is much smaller than that recorded by carbonates.

4.1.3. Cau section

The studied interval of the Cau section belongs to the Almadich Formation. The lower member of the Almadich Formation in the Cau section encompass the Upper Barremian to lowermost Aptian interval and consists of a rhythmic alternation of marly limestones and light grey marls. The FO of *H. irregularis* has been recorded immediately above a ferruginous surface located within this lower member. As the levels below the ferruginous surface were assigned to the *M. hoschulzii* nannofossil biozone, a stratigraphic gap, probably affecting the uppermost Barremian and the lowermost Aptian, was interpreted to exist within this lower member (Aguado et al., 1999). The onset of the 'nannoconid crisis' event and an increase in the abundance of large-sized morphotypes of the nannofossil genus *Assipetra* (*A. infracretacea* ssp. *larsonii* and *A. terebrodentaria* ssp. *youngii*; Tremolada and Erba, 2002) were observed within this lower member about 15 m above the ferruginous surface (Aguado et al., 1999). The middle member of the Almadich Formation is mainly composed of black shales and marls and its base coincides with the FO of the planktonic foraminifer *Schackoina cabri*. The FO of *E. floralis* has been recorded near the base of the marly limestones and grey marls characterizing the upper member of the Almadich Formation.

The $\delta^{13}C_{carb}$ profile shows a clear pattern, with the same general trends observed in the La Frontera and Carbonero sections, with two prominent positive excursions separated by a negative shift. The lowest part of the curve is poorly documented, as it is represented by only two analyses, with a lowest value of 1.4‰, and is capped by a discontinuity at the Barremian–Aptian boundary. The first positive excursion, with a maximum value of 2.7‰, is recorded within the *Deshayesites weissi* ammonite biozone (Fig. 4), predating the onset of the 'nannoconid crisis'. The subsequent negative excursion attains a minimum value of 0.4‰ in the uppermost part of the *H. irregularis* calcareous nannofossil biozone (equivalent to *G. blowi* planktonic foraminiferal biozone). The upper positive excursion, occurring in the *Deshayesites deshayesi* and *Dufrenoyia furcata* ammonite biozones, spans over 50 m and achieves a maximum value of 3.7‰ (Fig. 4). The $\delta^{13}C_{org}$ record parallels that of the $\delta^{13}C_{carb}$, but with a lower sharpness (Fig. 4). de Gea et al. (2003) proposed a C-isotope stratigraphy, correlated with biostratigraphy published in Aguado et al. (1999), in which they recognized the eight segments first proposed by Menegatti et al. (1998) (Fig. 4). Although the C-isotope curve does not have a high-resolution, and some uncertainty in the segment boundaries can be acknowledged, the C3–C4 boundary, in the uppermost part of *B. blowi* biozone, is located at the base of the organic-rich interval, which records the main positive excursion.

4.1.4. Puentenansa section

The studied interval in the Puentenansa section corresponds to the Patrocinio Formation, which consists, in this section, of a 31 m thick succession of open marine argillaceous and silty marls overlying a 13 m thick unit of rudist, gastropod and coral limestones and orbitolinid marls. The contact between the two units is an unconformity represented by a dissolution surface coated by a thin ferruginous crust, suggesting a brief episode of emersion at the top of the limestone followed by a flooding surface. Above this surface, deposition of the marls of the Patrocinio Formation occurred as consequence of platform drowning as the result of a combined action of a relative sea-level rise and poisoning by siliciclastic (Najarro et al., 2011a). According to the study of nannofossil assemblages in the studied section, the first 22 m of the Patrocinio Formation belong to the upper half of the *H. irregularis* Zone, and the absence of narrow canal nannoconids has allowed the identification of the "nannoconid crisis" within this interval (Najarro et al., 2011b). The FO of *E. floralis* is registered 5 m above the sample PN-9 (Fig. 4). This biostratigraphic event allows the assignment of the upper part of the Patrocinio Formation in the Puentenansa section to the *R. angustus* Zone, suggesting the existence of a stratigraphic gap affecting to the upper part of the Lower Aptian (Najarro et al., 2011b).

In this section the $\delta^{13}C_{carb}$ record can be subdivided into three successive intervals (Najarro et al., 2011a), (Fig. 4). The basal interval coincides with the Rábago and Umbrera Formations. It shows relatively homogeneous and positive $\delta^{13}C$ values in the Rábago Formation (mean of +2.2‰), and a significant and progressive decrease of about 1‰ through the Umbrera Formation (but still with positive values). The second interval of the $\delta^{13}C$ curve correlates with the Patrocinio Formation. This interval is characterized by a notable negative excursion from values of −0.4‰ at the base of the interval to −4.5‰ at the top. This negative excursion is not gradual but punctuated by three negative peaks (−2.9‰, −4.1‰ and −4.5‰ respectively; Fig. 4). Finally, the third interval in the $\delta^{13}C_{carb}$ record shows the return to positive values, corresponding to the Reocín Formation. The carbon isotope composition of the bulk organic matter measured across the Patrocinio Formation in the Puentenansa section ($\delta^{13}C_{org}$ in Fig. 4) ranges between −21.2‰ and −25.2‰, and shows three prominent negative spikes. From the bottom, the C-isotope curve starts with values of −22.2‰ and decreases sharply to −24.8‰, resulting in a first negative excursion of 2.6‰ in magnitude. This is followed by a return to more positive values (−21.6‰). The subsequent $\delta^{13}C_{org}$ values show a gradual decrease towards lower values, reaching a minimum of −25.2‰ (second negative spike of 3.5‰ in

magnitude). Then, the values become progressively higher up to values of −22.6‰. Finally, at the top of the Patrocinio Formation, the profile displays a third negative spike of −24.6‰ (~2‰ in magnitude) above the hiatal unconformity (Fig. 4).

The $\delta^{13}C_{carb}$ and $\delta^{13}C_{org}$ profiles lack the C4 to C7 isotopic segments of Menegatti et al. (1998), due to a discontinuity (Fig. 4) (Najarro et al., 2011b). Therefore, in the Puentenansa section only segment C3 of the OAE1a was recorded (Fig. 4). This section differs from the sections studied in the SIPM mainly due to the presence of shallow water carbonates at the base of the Aptian and in the Upper Aptian (Fig. 4).

4.2. Elemental geochemistry

The TOC contents across all four sections vary between 0.5% and 5.6% (Table 1). Higher TOC contents occur in Carbonero and La Frontera sediments (average TOC = 3.8% and 1.9%, respectively), whereas Cau and Puentenansa sediments have lower TOC contents (average TOC = 1.0% and 0.6% respectively). Sulphur is absent or present in only trace concentrations in La Frontera and Cau, whereas it is present in low concentrations in the other sections (Puentenansa average S = 0.1% and Carbonero average S = 0.22%). Major element distributions (Table 1) clearly differentiate the four sections: Cau samples are marls and Puentenansa are mudstones, whereas Carbonero and La Frontera samples present a higher variability related to the facies differentiation between marls, mudstones and radiolarian marls.

4.3. Distributions of hydrocarbon biomarkers

The extractable hydrocarbons are dominated primarily by *n*-alkanes, acyclic isoprenoids, steranes and hopanes (Fig. 5), although some sections also contain strong low-molecular-weight (Cau) or high-molecular-weight (Carbonero) unresolved complex mixtures (UCM). *n*-Alkanes are saturated straight-chain compounds (Fig. 5), mainly derived from vascular plants, both from aquatic (short-chain) and terrestrial (long-chain) environments (e.g. Meyers, 1997); however, attributing a specific source to any *n*-alkanes in the more thermally mature settings (see below) is problematic due to catagenetic alterations. Acyclic isoprenoids are composed of polymerized isoprene units, and the dominant compounds identified here, pristane and phytane, are typically considered to be derived from chlorophyll (e.g. Powell and McKirdy, 1973; but see ten Haven et al., 1987). Hopanes are C_{27}–C_{35} pentacyclic triterpenoids and originate from bacterial bacteriohopanepolyols (Ourisson et al., 1982). Steranes are tetracyclic triterpanes arising from diagenetic alteration of sterols and consequently almost exclusively derive from eukaryotic organisms (e.g. Moldovan et al., 1985). In most samples, the *n*-alkanes, acyclic isoprenoids and hopanes dominate, with variable ratios of *n*-alkanes/hopanes, and steroids represent a lower contribution (Fig. 5).

4.3.1. n-Alkanes

The *n*-alkanes are present and typically the dominant compounds in most chromatograms. Short and long-chain *n*-alkanes are present, ranging from *n*-C_{13} up to *n*-C_{35} (Fig. 5), in all samples, but the distribution varies significantly among the samples studied, both between different sections and stratigraphically. In the Puentenansa and La Frontera sections there is a clear and strong bimodal distribution, represented by low-molecular-weight (LMW; $<C_{22}$) components with no carbon preference and high-molecular-weight-components (HMW; $>C_{24}$) that have an odd-over-even carbon number predominance (OEP) at La Frontera but not at Puentenansa (Fig. 6). In contrast, all of the Carbonero rocks samples are dominated by short-chain compounds and the HMW components have no carbon number preference. Somewhat intermediate distributions occur in the Cau samples.

Table 1
TOC, and elemental composition of selected samples.

Sample	Thickness (m)	TOC %	N%	C%	S%	Al_2O_3%	SiO_2%	CaO%
La Frontera								
XF-103.1	43.25	1.1	0.0467	3.9193	0			
XF-96.2	26.90	1.4	0.0478	3.8031	0			
XF-1-33	25.7	0.7	0.0612	0.5714	0			
XF-1-27	24.5	0.8	0.063	0.6515	0			
XF-1-23	23.4	1.7	0.0945	1.3781	0.0397			
XF-1-20						13.89	59.19	0.78
XF-1-13						13.26	58.35	1.04
XF-1-1						9.47	29.8	23.98
XF-90.16	22.20	4.5	0.0296	6.7333	0	6.05	26.35	29.83
XF-90.5	20.00	0.7	0.0318	6.0533	0	7.49	27.24	27.61
XF-79	13.50	4.1	0.0418	5.517	0			
XF-72	9.30	4.8	0.0683	7.2018	0			
Puentenansa								
PN-14	29	0.5	0.0513	0.1489	0.0014	20.89	46.66	0.33
PN-13	27	0.8	0.0439	0.3525	0.0112	20.02	46.83	0.84
PN-10	21	0.6	0.0473	0.6973	0.0092	19.81	48.54	1.81
PN-7	15	0.6	0.0431	0.5447	0.2433			
PN-5	11	0.9	0.0418	1.1211	0.1706			
PN-4	9	0.7	0.0443	0.7718	0.1178			
PN-3	7	0.4	0.0275	3.7348	0.0123			
PN-2	5	0.6	0.0425	1.216	0.2702			
PN-1	3	0.5	0.0436	1.4614	0.292			
Cau								
Cau-32a	88.3	0.9				8.14	16.55	37.12
Cau28a	60.6	0.7	0.0225	9.8446	0	5.57	11.3	42.69
Cau23a	52.5	1.9	0.0338	9.3192	0.006	7.09	14.24	39.12
Cau20a	46	1	0.0305	9.4636	0.0071			
Cau19a	42	0.9	0.0279	9.2777	0.01	5.48	12.5	41.06
Cau16a	37.1	1	0.0337	8.6089	0.0369	6.98	16.84	36.76
Cau13a	33.6	0.8	0.0213	8.2714	0.0138	7.57	17.99	35.94
Cau12a	29.5	1.1	0.1051	0.9445	0.0846			
Cau10a	25.1	0.9	0.0192	9.2012	0			
Carbonero								
CAB-7	63.6	4.2	0.15	5.8234	0.1344			
CAB-6	53	5.6	0.18	5.3984	0.1254			
CAB-5	51	4.8	0.14	5.3118	0.7261	9.8	52.16	8.66
CAB-4	51	1.1	0.08	0.9067	0.2114	13.46	58.56	2.5
CAB-2C	40	3.7	0.1	6.6046	0.2951	10.3	35.05	19.71
CAB-2A	30.3	4.2	0.09	3.5869	0.0303	12.4	42.06	12.13
CAB-1J	25	3	0.0579	4.8499	0.0514	10.2	33.96	20.63

To facilitate interpretation of these *n*-alkane distributions, we have calculated two different ratios (Fig. 6): the HMW/LMW ratio ([*n*-C_{25} + *n*-C_{26} + *n*-C_{27} + *n*-C_{28} + *n*-C_{29}]/[*n*-C_{17} + *n*-C_{18} + *n*-C_{19} + *n*-C_{20} + *n*-C_{21}]) in order to constrain the relationship between long and short-chain compounds, and also the odd-over-even predominance ratio (OEP1 = $C_{21} + (6\times C_{23}) + C_{25}/(4\times C_{22}) + (4\times C_{24})$, and OEP2 = $C_{25} + (6\times C_{27}) + C_{29}/(4\times C_{26}) + (4\times C_{28})$), defined by Scalan and Smith (1970). We note that the HMW/LMW ratio has also been presented as the Terrestrial to Aquatic Ratio (TAR; Bourbonniere and Meyers, 1996), but the TAR terminology is not used in this context because of the prominent control of thermal maturity on calculated ratios (see below). There is a clear OEP (Table 2 and Fig. 6) in all of the La Frontera and Cau samples (OEP1 = 1.07–1.73; OEP2 = 1.75–3.49), but it is low or absent in the Puentenansa and Carbonero samples (PN: OEP1 = 1.37–1.53; OEP2 = 0.60–1.59; CAB: OEP1 = 0.71–1.35; OEP2 = 0.84–1.41; Table 2). Similarly, all Carbonero samples are characterized by a dominance of short-chain *n*-alkanes (average HMW/LMW ratios of 0.62 ± 0.36). HMW/LMW ratios at Puentenansa are similar to those at Carbonero (0.69 ± 0.47), but the distribution is different, as it is bimodal (see Fig. 5). In the other sections, the HMW *n*-alkanes are proportionally more abundant (HMW/LMW ratios at La Frontera = 0.83 ± 0.61 and Cau = 1.33 ± 0.17). With respect to vertical trends, we acknowledge that we have limited data from each section; nonetheless, the CAB and CAU sections, with

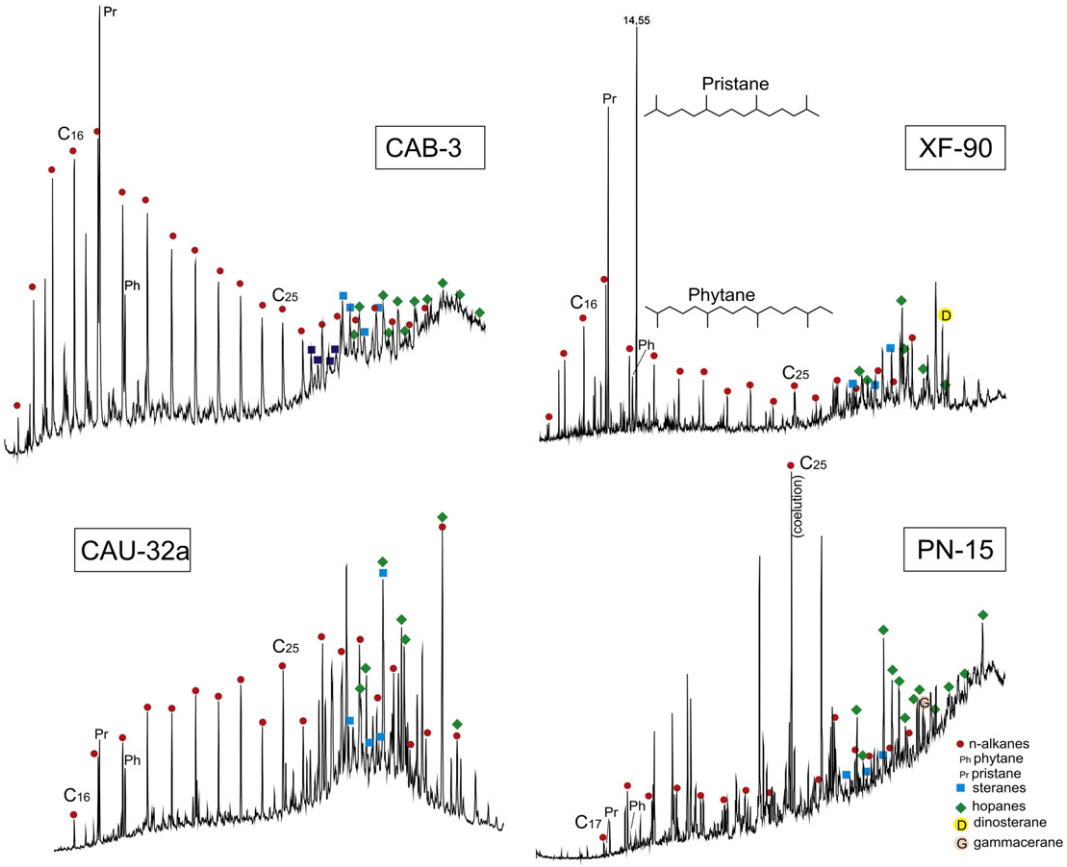

Fig. 5. Selected total ion chromatograms of samples from the studied sections. Numbers refer to *n*-alkanes.

greater sample resolution, show a clear variability trough the section in the HMW/LMW ratio (Fig. 6).

4.3.2. Isoprenoids

Pristane and phytane are abundant in all samples and exhibit high variability in their relative abundances. The Pr/Ph and isoprenoid/*n*-alkane ratios vary strongly, both between different sections and stratigraphically (Table 2 and Fig. 6). Pr/Ph ratios are highest in the Carbonero (Pr/Ph = 2–4.65, average = 2.98) and La Frontera samples (Pr/Ph = 2.08–4.6, average = 3.4), have intermediate values in the Cau samples (0.67–3.15, average = 1.64) and have the lowest values in the Puentenansa samples (0.6–0.68). At the Cau and Carbonero sections where a more complete suite of samples has been analyzed, Pr/Ph ratios generally decrease upsection, with highest values coinciding with pre-negative $\delta^{13}C$ excursion levels. The isoprenoid/*n*-alkane ratios (Fig. 6) are also highly variable, with generally higher Pr/*n*-C_{17} ratios and lower Ph/*n*-C_{18} ratios in the Carbonero Section than at Cau (Table 2 and Fig. 6).

4.3.3. Hopanes

Hopanes are present in all of the samples studied, ranging in carbon number from C_{27} to C_{35}. The C_{30} component is dominant in the Carbonero and La Frontera samples, C_{31} is dominant or equivalent to C_{30} in Cau samples, and the C_{29} hopane is dominant in the Puentenansa section (Fig. 7). The C_{31}–C_{35} extended hopanes (homohopanes) are present in CAB and PN samples, whereas in CAU and XF samples only C_{31}–C_{32} compounds are present. The commonly observed decrease in hopane concentration from C_{31} to C_{35} occurs in all samples, except for PN-15, where the C_{35} component is somewhat more abundant than the C_{34}. Crucially, the distribution of hopane stereoisomers differs dramatically among the four sections (Fig. 7 and Table 3). The 22S/(22S + 22R) homohopane ratio is 0.5 in the Carbonero and Puentenansa samples, whereas in La Frontera and Cau this ratio is 0.13–0.37. Similarly, the 17α,21β(H) isomers are dominant in the Carbonero and PN sections, with subordinate abundances of the 17β,21α(H) diastereomers (moretanes), whereas the Cau samples are characterized by a dominance of hopane diastereomers with the 17β,21β(H) configuration, although 17α,21β(H) and 17β,21α(H) diasteromers are also present. The Ts and Tm C_{27} hopane diastereomers are present in all samples, with a Tm/Ts ratio ≥1 in the Carbonero, La Frontera and Cau samples and a Tm/Ts ratio <0.4 in Puentenansa samples.

Gammacerane is present only in the Puentenansa samples (confirmed with standard co-injection), where this compound has a relatively high abundance in comparison with hopanes (G/C_{30} = 0.58).

4.3.4. Steranes

A range of C_{27} to C_{30} steranes occur in all of the sections studied (Fig. 8); in a broad sense, the relative distributions are similar, with C_{29} always being dominant (48%–70%), C_{27} intermediate (19%–28%), and C_{28} minor (9%–31%), but considerable variability within that framework is present. Further variability is reflected by the abundance of a C_{30} 4-methylsterane, tentatively interpreted to be dinosterane on the basis of its mass spectrum and retention time (Summons et al., 1987), which is present in some XF and CAU samples but is absent or occurs in only trace abundances in the PN and Carbonero samples. In fact, in one sample (Cau–24, see Fig. 8), it is one of the dominant compounds in the apolar fraction and certainly the most abundant sterane.

The sections also differ with respect to the relative abundances of sterane diastereomers. The CAU and XF samples are represented almost exclusively by the 5α(H),14α (H),17α(H),20R epimer. On the other hand, in CAB and PN samples, 5α(H),14β(H),17β(H) diastereomers and 22S steranes are also relatively abundant, with similar

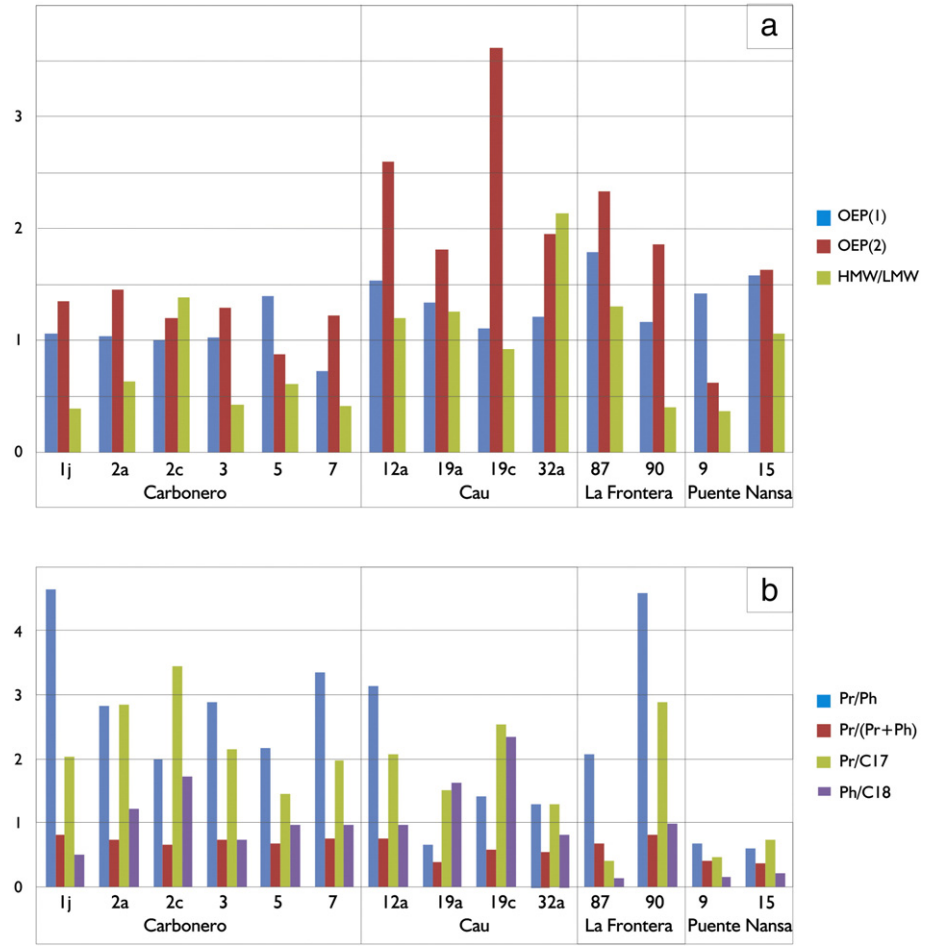

Fig. 6. Biomarker ratios derived from relative *n*-alkane (a) and isoprenoid (b) abundances. Ratio definitions and interpretations are provided in the text. Location of the samples shown in Figs. 3 and 4.

relative distributions in both sections (Fig. 8). Furthermore, the ratios of the 20S and 20R epimers differ between the latter two sections, with the 20S/20R ratio being around 1 for the 5α(H),14α(H), 17α(H) diastereomer in CAB samples, whereas in PN samples the 20R stereochemistry is dominant. Similarly, 13β,17α steranes (diasteranes) are relatively abundant compared to regular steranes in all of the Carbonero samples but absent in the other sections.

Table 2
n-Alkanes and isoprenoids ratios.

Sample	Pr/Ph	Pr/(Pr + Ph)	Pr/C17	Ph/C18	OEP (1)	OEP (2)	HMW/LMW
Carbonero							
CAB-1J	4.65	0.82	2.05	0.51	1.02	1.30	0.38
CAB-2A	2.84	0.74	2.86	1.23	1.00	1.41	0.62
CAB-2C	2.00	0.67	3.46	1.73	0.98	1.17	1.34
CAB-3	2.89	0.74	2.15	0.75	0.99	1.25	0.42
CAB-5	2.18	0.69	1.45	0.97	1.35	0.84	0.60
CAB-7	3.36	0.77	1.98	0.98	0.71	1.18	0.34
Cau							
CAU-12a	3.15	0.76	2.07	0.97	1.49	2.51	1.16
CAU-19a	0.67	0.40	1.52	1.63	1.29	1.75	1.22
CAU-19C	1.42	0.59	2.54	2.34	1.07	3.49	0.90
CAU- 32 a	1.32	0.57	1.30	0.84	1.17	1.88	2.06
La Frontera							
XF-87	2.08	0.68	0.41	0.14	1.73	2.25	1.26
XF-90	4.60	0.82	2.90	0.99	1.12	1.80	0.39
Puentenansa							
PN-9	0.68	0.41	0.46	0.16	1.37	0.60	0.36
PN-15	0.60	0.38	0.75	0.22	1.53	3.00	1.02

5. Discussion

5.1. Correlation of C-isotope curves and integration with biostratigraphic data and distribution of organic-rich facies

To correlate the four sections, we have used the biostratigraphic data and also attempted to identify the eight segments proposed by Menegatti et al. (1998) for the Aptian C-isotope profile from the "Selli level" in the Alps. Those authors proposed a subdivision of the Aptian C-isotopic record in 8 segments based on changes observed in two different sections in the Alpine domain and attempted to correlate those carbon isotopic temporal variations with nannofossils and planktonic foraminifers biozonations (Fig. 9). The Cau and La Frontera sections both contain the eight segments described by Menegatti et al. (1998), whereas in the Carbonero section there are no isotope data for the C1 segment, although biostratigraphic data suggest it is present. In Puentenansa, the succession starts within the C2 segment, and there is a discontinuity affecting the C4 to C7 segments (see Figs. 3, 4 and 9).

The sections exhibit the expected correlations between the biostratigraphic data and the C-isotope curves (i.e. segments proposed by Menegatti et al., 1998), and consistent relationships are observed in all four Iberian sections studied with the exception of the FO of *E. floralis*. This datum was recorded within the C6 segment in La

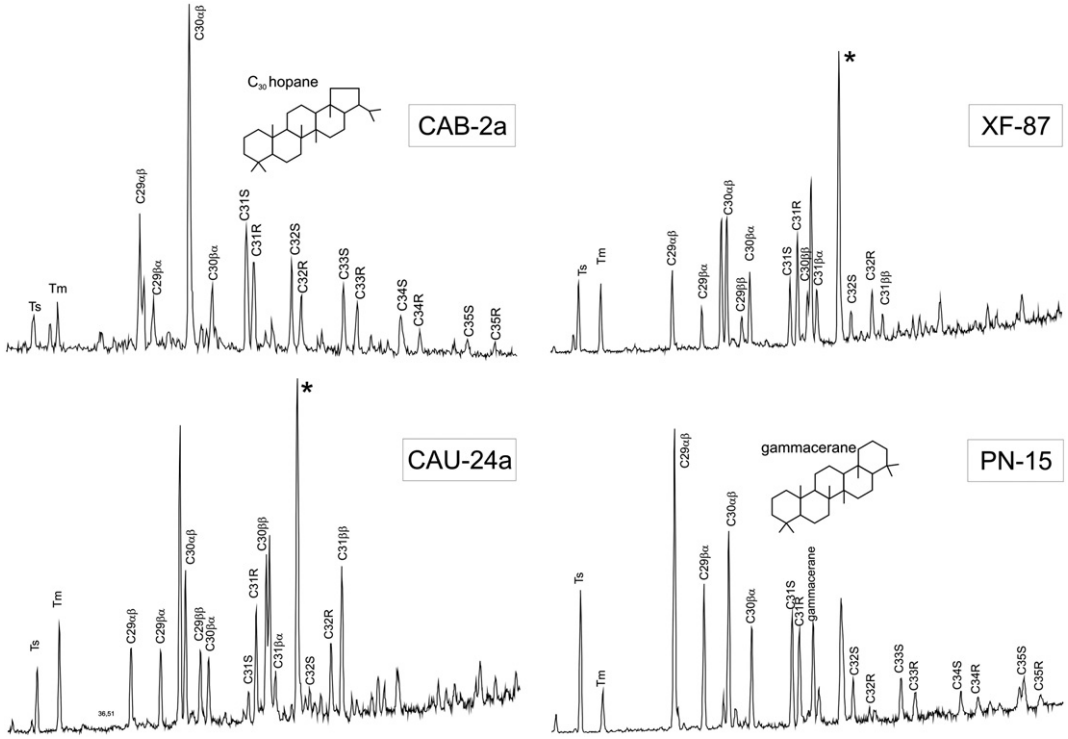

Fig. 7. Selected partial mass ($m/z = 191$) chromatograms of samples from the studied sections, showing hopanes and gammacerane (* unknown compound, probable ketone or diahopane).

Frontera section, and within the C7 segment in Carbonero and Cau sections. We suspect that the diachronism in the record of the FO of *E. floralis* in Carbonero section is related to the poor preservation of the nannofossil assemblages in the middle member and lowest part of the upper member of the Carbonero Formation. In most of the samples from this middle member, nannofossils were not found or were very poorly preserved.

In the Cau section, however, the cause of this diachronism cannot be attributed to preservation, as nannofossil assemblages are diverse and moderately well preserved in this interval, and we suspect that it is probably related to palaeoecological factors. The palaeoceanographic setting of the Cau section was more proximal and shallower (outer platform) than that of the La Frontera section (pelagic). In addition, the nannofossil assemblages from this interval in the Cau section contain higher proportions of nannoconids and pentaliths (*Braarudosphaera*, *Micrantholithus*) than those of the La Frontera section. Nannoconids are well-documented Cretaceous taxa predominantly associated to low-latitude carbonate-shelfal and epicontinental basins likely with stratified waters (Thierstein, 1976; Roth and Bowdler, 1981; Roth and Krumbach, 1986; Busson and Noël, 1991; Mutterlose, 1992; Street and Bown, 2000; Bown, 2005). They are also related to oligotrophic surface waters in which salinity may also have played a significant control (Lees et al., 2005). Erba (1994) suggested that nannoconids were analogous to the extant genus *Florisphaera*, which proliferates in the deep photic zone of modern oceans at a deep nutricline. This author suggested that the OAE1a-related nannoconid crisis was the result of nutrification of surface-waters, triggering blooms of surface waters coccolithophorids and depletion of deeper-dwelling nannoconids. Pentaliths (*Micrantholithus* and *Braarudosphaera*) appear to be similarly neritic to nannoconids in distribution. Its ecology is also probably related to neritic factors such as reduced salinity and enhanced nutrient content (Roth and Bowdler, 1981; Parker et al., 1985; Siesser et al., 1992; Street and Bown, 2000; Bown, 2005). *Micrantholithus* was replaced by *Braarudosphaera* in the Aptian, which appears to have retained a similar ecology from Aptian to recent times, being most common in neritic environments (Gran and Braarud, 1935). Other anomalous occurrences of *Braarudosphaera* blooms, linked to post-extinction assemblages (Cretaceous–Tertiary boundary) or to subtropical open-ocean sites (Parker et al., 1985; Scarparo-Cunha and Shimabukuro, 1997) suggest an opportunistic behavior for this taxon (Siesser et al., 1992). Given the paleoceanographic setting of the Cau section (distal part of a platform) and the above-mentioned higher abundances of ecologically significant nannoconids and pentaliths through the C6 and C7 carbon-isotope intervals, we suggest that a shallower, more restricted environment, with lower salinity, could be related with the delay in the first record of *E. floralis* in this section. Similar diachronisms in the FOs and LOs of several micro- and nannofossil indicators with respect to the carbon-isotope stratigraphy have been also detected for sections in the Mazagan Plateau and the Vocontian Trough (Herrle et al., 2004), and

Table 3
Maturity-related biomarker parameters (ratios of hopanes and steranes).

Sample	Hopanes		Sample	Steranes	
	22S/(22S + 22R) (C31)	C30βα/(βα + αβ)		ββ/ββ + αα	20S/(20S + 20R)
Carbonero			Carbonero		
CAB-7	0.53213368	0.14231738	CAB-7	0.302463054	0.516723549
CAB6a	0.54291845	0.11111111	CAB-5	0.34566787	0.4665195
CAB-5	0.54736842	0.13127413	CAB-3	0.44603033	0.432876712
CAB-3a	0.54174397	0.13378685	CAB-2C	0.399749373	0.505675955
CAB-2a	0.56915739	0.172322023	CAB-2A	0.371191136	0.512352309
CAB-1J	0.54363636	0.18592297	CAB-1J	0.331963001	0.492583919
La Frontera			Puentenansa		
XF-90	0.22988506	0,33174603	PN-15	0.466313763	0.434472208
XF-87	0.37260274	0,38235294			
Cau					
CAU-32A	0.131528046	0.581020591			
CAU-24a	0.21507761	0.32028986			
CAU-19a	0.225	0.32484076			
Puentenansa					
PN-15	0.52012384	0.32767402			
PN-9	0.50875146	0.42937063			

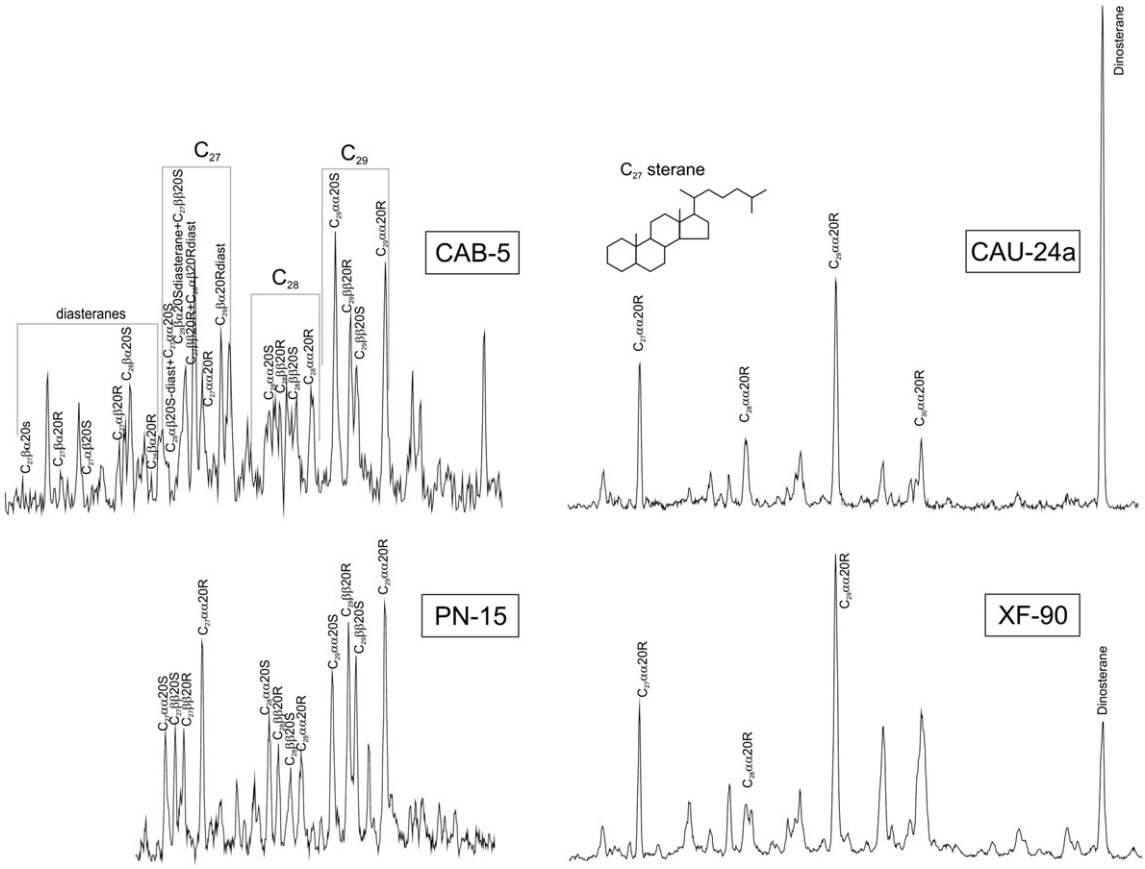

Fig. 8. Selected partial $m/z=217$ mass chromatograms of samples from the studied sections, showing steranes. Note that diasteranes are only present in CAB samples. Dinosterane, although present in these $m/z=217$ chromatograms, has a mass spectrum with a dominant 231 fragment and a minor 217 fragment.

interpreted in terms of regional differences in palaeoenvironmental conditions.

Taking this into account, the data presented in this study reveal several relationships, shown in Figs. 3 and 4: (1) The C1–C2 boundary is affected by a discontinuity, at the Barremian–Aptian boundary, in all four sections; (2) the C3–C4 boundary corresponds to the base of *S. cabri* foraminifer biozone; (3) the base of the *R. angustus* nannofossil biozone is diachronic, and its first occurrence lies within the C6 segment; and (4) the base of the *G. ferreolensis* foraminifer biozone occurs within the C7 segment.

Correlation of biostratigraphy, C-isotope stratigraphy and facies among the four sections reveals a variety of spatial and temporal relationships (Fig. 10). Although C-isotope stratigraphy is correlatable around the world, the timing of deposition of organic-rich sediments is not coeval (i.e. Jenkyns, 2010), and that is apparent in the Iberian region of the Tethys. Organic-rich facies are first deposited in pelagic environments (La Frontera and Carbonero sections), at the base of the Aptian and corresponding to the C2 segment of the carbon isotope profile, whereas organic-rich black shales or marls are deposited during the C3 or C4 segments in platform settings (Puentenansa and Cau

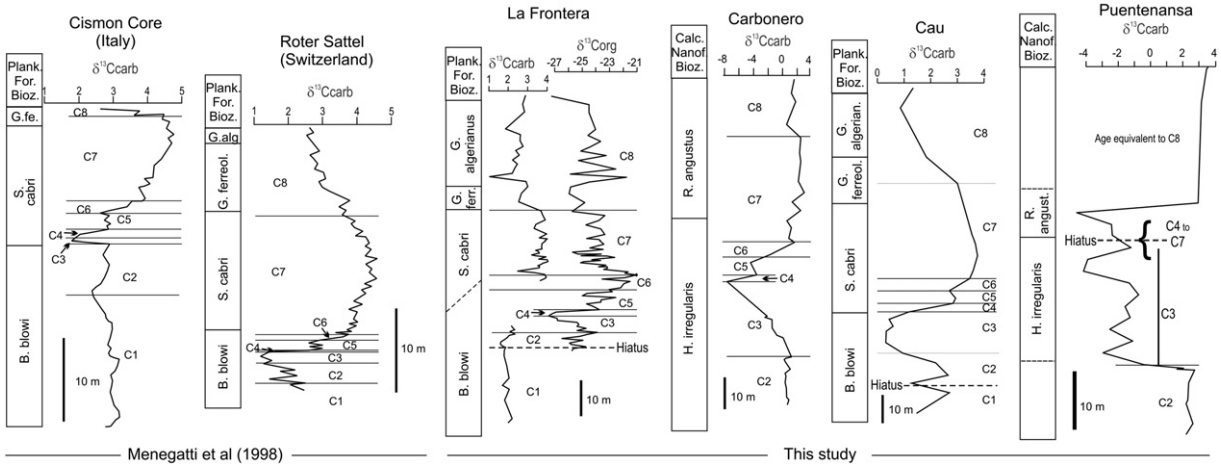

Fig. 9. Correlation of the studied sections with the reference curves of Menegatti et al., 1998.

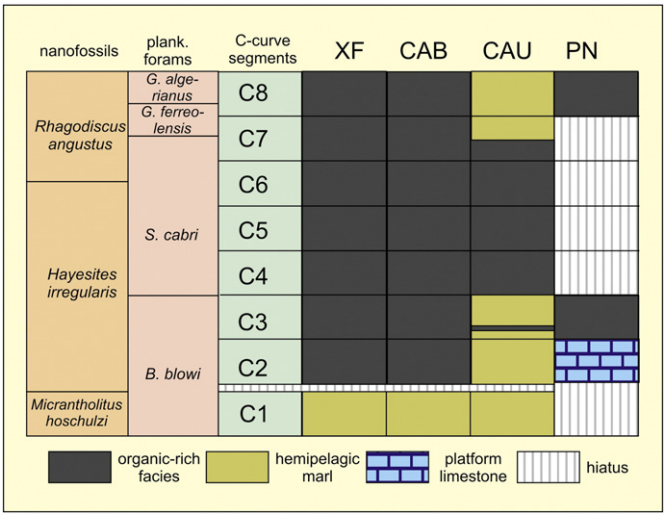

Fig. 10. Correlation between C-isotope stratigraphy (segments from Menegatti et al., 1998), biostratigraphy and facies.

sections, respectively). Also, the interval of deposition of black shales is longer in pelagic sections (up to the C8 segment) than in the platform sections (C7) in the SIPM. When comparing the palaeogeographically distinct platform settings (SIPM, Cau, and NCB, Puentenansa), the deposition of organic-rich facies starts earlier and persists longer in the North Cantabrian basin (C2 to C8) than in the South Iberian (C3 to "early" C7).

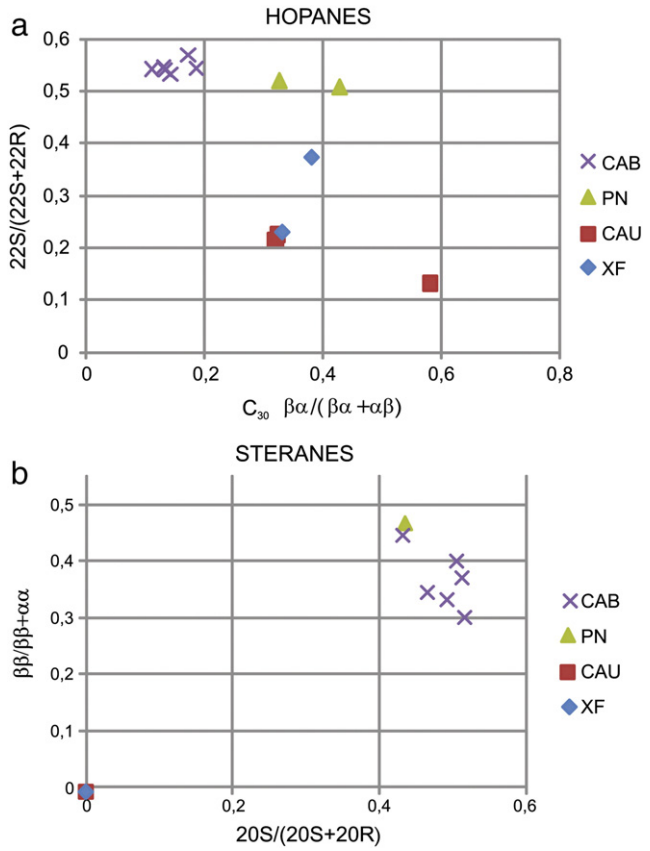

Fig. 11. Maturity-related biomarker parameters. a: 22S/(22S + 22R) homohopane ratios versus βα/(βα + αβ) hopane ratios. b: ββ/(ββ + αα) sterane ratios versus 20S/(20S + 20R) sterane ratios.

5.2. Organic geochemistry

5.2.1. Thermal maturity

The use of biomarker distributions to assess the thermal maturity of organic matter in sediments and rocks is well established (e.g. Peters et al., 2005). The most powerful tools at low to moderate maturity (with respect to oil generation) are those based on the relative distribution of sterane and hopane isomers, and that is the focus here. However, thermal maturity also affects *n*-alkane distributions and, therefore, informs our interpretation of between-section differences in those parameters.

The Carbonero section has 22S/(22S + 22R) homohopane ratios of ca 0.55, C30 βα/(βα + αβ) hopane ratios of ca 0.15 (Fig. 11a), ββ/(ββ + αα) sterane ratios of 0.37, and 20S/(20S + 20R) sterane ratios of 0.49 (Table 3, Fig. 11b), and abundant diasteranes. All of these data indicate that OM from the Carbonero section is thermally mature with respect to oil generation (Mackenzie et al., 1980; Seifert and Moldowan, 1980; Waples and Machihara, 1991). Although the homohopane ratios are at a maximum and cannot put an upper limit on the section's thermal maturity, the persistence of these biomarkers—and especially the moretanes—suggests that the section has not exited the oil generation window. Sterane distributions also indicate that the section is near the peak stage of oil generation, equivalent to a vitrinite reflectance between 0.65 and 0.85 (according to Peters et al., 2005). The elevated thermal maturity accounts for the low HMW/LMW *n*-alkane ratios and the lack of an odd-over-even predominance.

The Cau and La Frontera sections, in contrast, are characterized by distributions consistent with low thermal maturity, including a dominance of 22R homohopanes (i.e. 22S/(22S + 22R) homohopane ratios of 0.13–0.37), the persistence of hopanes with the biological and thermally unstable 17β,21β(H) configuration, steranes represented only by the ααα20R isomers, and an absence of diasteranes (Table 3, Figs. 7 and 8). These data indicate that Cau and La Frontera have very low maturity and explain why higher plant wax *n*-alkane distributions, including the high OEP and HMW/LMW ratios, have persisted. Puentenansa samples have hopane and sterane ratios indicating that the OM is thermally mature (within the peak stage of oil generation) but not to the same degree as the Carbonero samples; for example, diasteranes are not present in Puentenansa. Thus, differences in thermal maturity are a main driver of organic geochemical differences among the studied sections. Specifically, Carbonero and Puentenansa OM is thermally mature, whereas Cau and La Frontera OM is thermally immature, probably with an equivalent vitrinite reflectance lower than 0.4 (according to Peters et al., 2005). Particularly interesting are the important differences observed between Carbonero and La Frontera OM, taking into account that they were deposited in nearby areas. The higher degree of maturation showed in Carbonero samples could be related to the Cretaceous tectonic and volcanic activity occurred in the Carbonero area, related to the extensional tectonics (Molina et al., 1998; de Gea et al., 2008a, 2008b) which could have resulted in a heating of the sediments, whereas the nearby La Frontera area, not affected by these processes, records immature OM; however, a different burial history cannot be dismissed. The low thermal maturity in Cau and La Frontera sections suggests that functionalized biological compounds, including alcohols and carboxylic acids, will be preserved in these sections (which we have confirmed but will be discussed in subsequent papers). This will affect interpretation of OM sources and sedimentary environments and is an important caveat to subsequent sections.

5.2.2. OM sources and environmental conditions

Lipid biomarkers can be used to infer sources of organic matter (e.g. terrestrial vs marine) and depositional conditions (e.g. oxic vs. anoxic). Overall, all of the OM present in the studied samples is interpreted to derive from significant terrestrial inputs as well as

marine and bacterial sources. The differences in thermal maturity complicate comparison of biomarker parameters among the sections. Moreover, the high level of maturity in several samples prevents an accurate interpretation in terms of source. Nevertheless, biomarker data from this study do reveal some systematic relationships, allowing tentative comparisons.

5.2.2.1. OM sources. The predominance of high molecular weight *n*-alkanes (C_{25}–C_{35}) with an odd-over-even carbon number in the La Frontera and Cau sections indicate a terrestrial contribution from wax lipids of higher plants (Eglinton and Hamilton, 1967). The low molecular weight C_{14}–C_{24} *n*-alkanes, as well as pristane and phytane, from the same sections likely derive from marine contributions. Puentenansa samples have a slight OEP, but still contain a strong HMW *n*-alkane (C_{25}–C_{35}) signal, which would also indicate a terrestrial contribution. The predominance of LMW *n*-alkanes in CAB samples reflects their thermal maturity rather than OM sources.

The steranes show a rather constant distribution with a dominance of C_{29} compounds in all samples. This feature could also indicate a strong terrestrial contribution (Huang and Meinschein, 1979), but caution is essential as many algae synthesize C_{29} sterols (Peters et al., 2005 and references therein). Further evidence that the high $\%C_{29}$ steranes should be interpreted cautiously comes from the fact that there are no systematic differences between the platform and pelagic sections, even when comparing sections with similar thermal maturity. Marine inputs are clearly significant at all sites, despite the relatively low $\%C_{27}$ and $\%C_{28}$ values, indicated in particular by the occurrence of dinosterane derived from dinoflagellates (Withers, 1983). Dinosterane occurs in several samples in concentrations comparable to those of steranes (XF samples), is absent in others (CAB and PN samples, CAU-12, CAU-19a and CAU-19c), and is one of the most abundant hydrocarbons in CAU-24. Although the sample resolution is limited, there is strong variation in dinosterane concentrations within a given section, indicating that dinoflagellate production varied, perhaps reflecting changes in nutrient status. Moreover, the particularly high concentration in the CAU-24 sample suggests that these conditions arose when either upwelling or runoff delivered nutrients to the shallow marine environment. However, insufficient data prevent us from further interpretation of either temporal trends or differences between sections.

Bacterial sources of OM are demonstrated by the presence of hopanes in all samples. Also, although it is not a bacterial compound, gammacerane typically occurs when bacteria are present in the water column (Sinninghé-Damsté et al., 1995; Peters et al., 2005). Intriguingly, the abundance of hopanes relative to *n*-alkanes is particularly high in samples CAB-5, XF-90, and CAU-19a, all corresponding to the interval located above the negative carbon isotope excursion. Previous work has shown that other times of global anoxia are associated with major changes in the bacterial population, and in particular the proportional contributions of cyanobacteria (e.g. Kuypers et al., 2004 -OAE2-, Xie et al., 2007 -Permian–Triassic Boundary), and future work will focus on similar changes in the Iberian region during OAE1a.

5.2.2.2. Environmental conditions. One of the main questions related to anoxic events is the geographical extent of reducing conditions in the water column. Gammacerane is present in the Puentenansa samples, and its principal source appears to be bacteriovorous ciliates, which occur at the interface between oxic and anoxic zones in stratified water columns (Sinninghé-Damsté et al., 1995; Peters et al., 2005), such that its presence is often associated with anoxia induced by water column stratification. Intriguingly, we did not detect gammacerane in the Carbonero section, even though it is characterized by the highest TOC contents, and has sedimentologic evidence of anoxia (i.e. barite concretions, Molina and Hernández-Molina, 1993; de Gea et al., 2008a).

A range of other biomarker distribution based redox proxies have been developed (e.g. Peters et al., 2005), but these are based on empirical observations of petroleum and corresponding source rocks rather than thermally immature sediments; thus, in our samples they can only be applied to the CAB and PN samples. The Pr/Ph ratio has been used to infer redox conditions, but is also governed by thermal maturity, source inputs and lithology (Didyck et al., 1978; Ten Haven et al., 1987; Hughes et al., 1995). Carbonero samples have a relatively high Pr/Ph ratio, between 2.3 and 5.5, whereas PN samples have very low values (0.4 and 0.5), with the latter being typical for anoxic conditions (<0.8; Hughes et al., 1995). Other aspects of the PN biomarker profile are consistent with this, including the elevated concentrations of the C_{35}-homohopane (Peters and Moldowan, 1991) and the high gammacerane/hopane ratios. Collectively, all of the biomarker data suggest that CAB samples, despite being more organic-rich, reflect more oxygenated conditions than PN samples (Fig. 12). By extension, this suggests that more reducing environments prevailed in the North Cantabrian Basin than the SIPM.

5.3. Sedimentary model: integration of stratigraphy, geochemistry, palaeogeography and palaeoceanography

The differences observed in the timing of deposition of the organic-rich facies between sections can be explained in relation to the different palaeogeographic settings and the palaeoceanography (Fig. 13). During Menegatti's C2 interval, the organic-rich deposition only occurs in the deep pelagic sections of the SIPM (Carbonero and La Frontera), located in fault-bounded high-subsident areas, probably with reduced water circulation, whereas in the shallow marine settings normal hemipelagic sedimentation took place (Cau) or shallow carbonate deposits (Puentenansa) were recorded (Fig. 13). This distribution could correspond to a model of deep stagnant oxygen-depleted waters (i.e. Jenkyns, 1980; Pedersen and Calvert, 1990). During the C3 interval, an episode of environmental change affected the northern, more restricted NCB, leading to the drowning of the Puentenansa carbonate platform and deposition of organic-rich facies (Najarro et al., 2011a), under oxygen-depleted, probably stratified, waters. Contemporaneously in the SIPM environments, a short episode of organic-rich sediment deposition took place in the shallower Cau sector, whereas in shallow carbonate platforms of the SIPM a drowning event took place (i.e. Castro et al., 2008; Castro et al., 2012). An interesting question is the temporal relationship between platform drowning and the onset of the OAE1a (i.e. Weissert et al., 1998). The data from Puentenansa indicate that the platform drowning predates the C4 segment, which is in agreement with previous

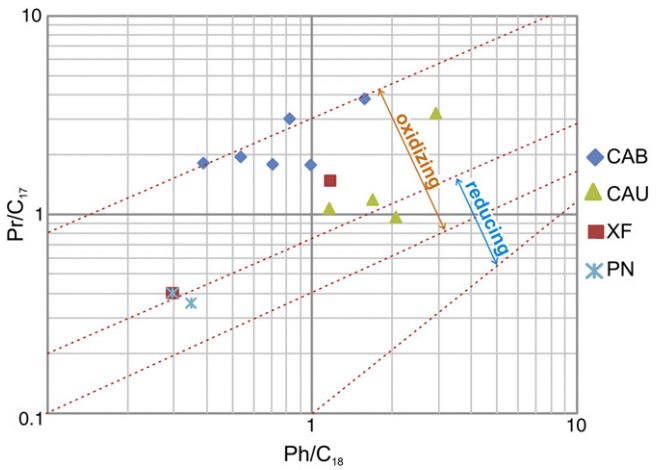

Fig. 12. Pr/C_{17} vs. Ph/C_{18} plot. The reference lines are from Didyck et al., 1978, but should not be interpreted against the data from less thermally mature sections (CAU and XF) as they have been empirically derived from oils and source rocks.

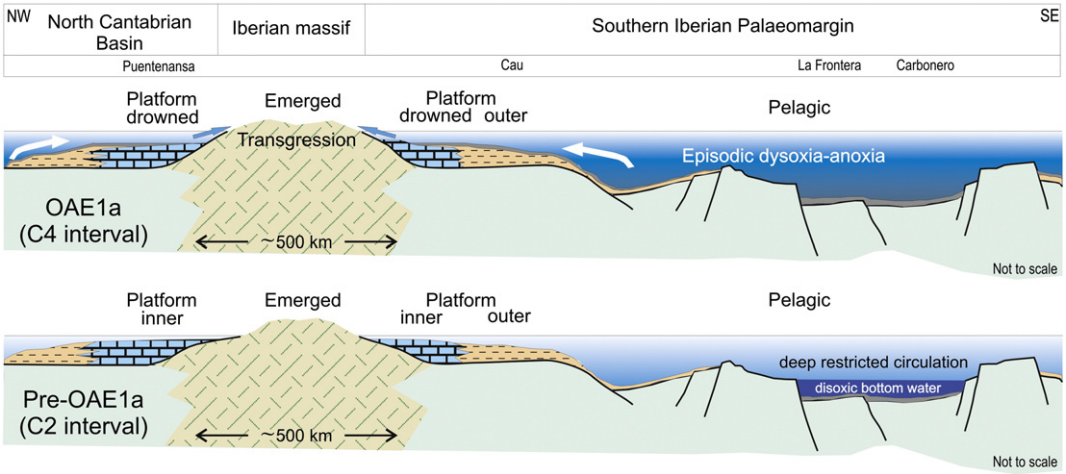

Fig. 13. Sedimentary model. See text for explanation.

studies from the Betic Cordillera (Castro et al., 2012), and also from the Subalpine Chains (Huck et al., 2011).

During the C4–C5 intervals, which corresponds to the global widespread deposition of organic matter of the OAE1a (i.e. Menegatti et al., 1998; Dumitrescu and Brassell, 2006) organic-rich sedimentation characterized all four sections. This persisted until the C8 interval, except at Cau, where organic rich sedimentation ended during C7 interval. This distribution could reflect an expansion of the OMZ, reaching shallower areas on the margins, coincident with a major transgression, which could favor increased continental runoff and an increase in nutrient inputs (i.e. Burla et al., 2008; Castro et al., 2008; Blattler et al., 2011; Najarro et al., 2011a). Similar models of expansion of the OMZ have been proposed for the OAE2 (i.e. Pancost et al., 2004; Li et al., 2006).

The main factors leading to deposition of organic-rich marine sediments are anoxia and productivity (e.g. Pedersen and Calvert, 1990). Marine organic-rich sediments related to OAEs have been extensively interpreted as being deposited under anoxic or dysoxic conditions (e.g. Jenkyns, 1980). In the Iberian sections studied here, evidence for anoxia has been found, both from sedimentology (high TOC contents, barite concretions, laminations, lack of bioturbation, planktonic associations…), and biomarkers (presence of gammacerane, distribution of homohopanes, Pr/Ph ratios, isoprenoids/*n*-alkane ratios). However, the signature for anoxia is neither unambiguous nor widespread. Differences among sections are interesting: Carbonero section shows a stronger sedimentologic signal of anoxia (i.e. highest TOC contents), whereas the biomarker proxies of these conditions are weak. Although deeper studies are needed about redox proxies for the Carbonero section, a high productivity environment should be also considered; this is consistent with the presence of Ba, which has been proposed as a powerful proxy for productivity in marine environments (Paytan and Griffith, 2007), although more detailed investigation on this element are necessary to avoid misinterpretations. The other SIPM sections (La Frontera and Cau) show both sedimentary and biomarker evidence of anoxia, as stated before. On the other hand, the NCB section (Puentenansa) shows stronger biomarker evidence for anoxia (presence of gammacerane, homohopane distributions, Pr/Ph ratios), which can be related to the palaeogeographic setting in the Bay of Biscay, probably with a more restricted communication of the waters to the open ocean.

Finally, although the sections studied represent different sedimentary environments (platform and pelagic), there are no systematic biomarker differences related to this, for example, there is no evidence for greater terrigenous OM inputs to the platform settings. Instead, the main differences in biomarker distributions are associated with thermal maturity and vertical variability.

6. Conclusions

Four sections recording the Early Aptian OAE1a in Spain have been characterized by biostratigraphy, C-isotope stratigraphy, elemental geochemistry, biomarker distribution, and sedimentology; the sections represent different palaeogeographic (North Cantabrian Basin and Southern Iberian Palaeomargin) and geotectonic settings (pelagic and shallow marine). The C-isotope curves allowed the recognition of the eight segments proposed by Menegatti et al. (1998) and subsequently identified in sections from around the world, and the integration of biostratigraphic and C-stratigraphic data was used to develop an integrated stratigraphic framework, allowing correlation of the Iberian OAE1a. Biomarker distributions revealed significant variations in thermal maturity, which was very low in the Cau and La Frontera sections, moderate in the Puentenansa samples, but relatively high for the Carbonero section, which is within the oil window. The strong lateral variations in maturity over short distances were interpreted as probably due to volcanic activity or burial history. Overall, all of the OM present in the studied samples is interpreted to derive from significant terrestrial inputs as well as marine and bacterial sources, and dinosterane was particularly abundant in several samples. Environmental proxies indicatives of anoxia–dysoxia occur in all the sections, but evidence for strong and persistent water column anoxia is equivocal. Crucially, however, the correlation of the sections reveals that deposition of organic-rich facies started earlier in pelagic settings and later in the platform settings, which can be related to an expansion of the oxygen minimum zone from deep marine waters to shallower marine environments during the development of the OAE1a.

Acknowledgments

We would like to specially thank Prof. Pedro A. Ruiz-Ortiz for his support and encouragement with this research. This work is a contribution of the research projects UJA-07-16-41 (University of Jaen), CGL2011-24546 and CGL2009-10329 (Spanish Ministry of Science and Technology), IEG617028019 (Instituto de Estudios Giennenses) and RNM-200 (Junta de Andalucía). Authors wish to thank Marina Sánchez Royo for her help in the laboratory work. We thank Adrian Immenhauser, Finn Surlyk and an anonymous reviewer for their helpful comments and critical reviews.

References

Aguado, R., Castro, J.M., Company, M., de Gea, G.A., 1999. Aptian bioevents—an integrated biostratigraphic analysis of the Almadich Formation, Inner Prebetic Domain, SE Spain. Cretaceous Research 20, 663–683.

Aguado, R., Company, M., O'Dogherty, L., Sandoval, J., Tavera, J.M., 1992a. Biostratigraphic analysis of the pelagic Barremian/Aptian in the Betic Cordillera (Southern Spain). Prelimiary data. Cretaceous Research 13, 445–452.

Aguado, R., Molina, J.M., O'Dogherty, L., 1992b. Bioestratigrafía y litoestratigrafía de la Formación Carbonero (Barremiense–Albiense?) en la transición Subbético Externo-Subbético Medio (Sur de Jaén). Cuadernos de Geologia Iberica 17, 325–344.

Aguado, R., O'Dogherty, L., Sandoval, J., 2008. Fertility changes in surface waters during the Aalenian (mid Jurassic) of the Western Tethys as revealed by calcareous nannofossils and carbon-cycle perturbations. Marine Micropaleontology 68, 268–285.

Ando, A., Kakegawa, T., Takashima, R., Saito, T., 2002. New perspective on Aptian carbon isotope stratigraphy: data from $\delta^{13}C$ records of terrestrial organic matter. Geology 30, 227–230.

Arthur, M.A., Jenkyns, H.C., Brumsack, H., Schlanger, S.O., 1990. Stratigraphy, geochemistry, and paleoceanography of organic carbon-rich Cretaceous sequences. In: Ginsburg, R.N., Beaudoin, B. (Eds.), Cretaceous Resources, Events and Rhythms. NATO AS1 Series C, 304. Kluwer Academic, Dordrecht, pp. 75–119.

Azéma, J., Foucault, A., Fourcade, E., García Hernández, M., González Donoso, J.M., Linares, A., Linares, D., López Garrido, A.C., Rivas, P., Vera, J.A., 1979. Las microfacies del Jurásico y Cretácico de las Zonas Externas de las Cordilleras Béticas. Universidad de Granada (83 pp.).

Beerling, D.J., Royer, D.L., 2002. Fossil plants as indicators of the Phanerozoic global carbon cycle. Annual Review of Earth and Planetary Sciences 30, 527–556.

Blattler, C.L., Jenkyns, H.C., Reynard, L.M., Henderson, G., 2011. Significant increases in global weathering during Oceanic Anoxic Events 1a and 2 indicated by calcium isotopes. Earth and Planetary Science Letters 309, 77–88.

Bourbonniere, R.A., Meyers, P.A., 1996. Sedimentary geolipid records of historical changes in the watersheds and productivities of Lakes Ontario and Erie. Limmology and Oceanography 41, 352–359.

Bover-Arnal, T., 2010. The Aptian evolution of the Galve sub-basin (Maestrat Basin; E Iberia). Ph.D. Thesis. Universität Bayreuth, 209 pp.

Bown, P., 2005. Selective calcareous nannoplankton survivorship at the Cretaceous-Tertiary boundary. Geology 33, 653–656.

Bown, P.R., Young, J.R., 1998. Techniques. In: Bown, P.R. (Ed.), Calcareous Nannofossil Biostratigraphy. Chapman & Hall, London, pp. 16–28.

Bralower, T.J., Arthur, M.A., Leckie, R.M., Sliter, W.V., Allard, D.J., Schlanger, S.O., 1994. Timing and paleoceanography of oceanic dysoxia/anoxia in the Late Barremian to Early Aptian (Early Cretaceous). Palaios 9, 335–369.

Bralower, T.J., CoBabe, E., Clement, B., Sliter, W.V., Osburn, C.L., Longoria, J., 1999. The record of global change in Mid-Cretaceous (Barremian–Albian) sections from the Sierra Madre, northeastern Mexico. Journal of Foraminiferal Research 29, 418–437.

Bréheret, J.G., Brumsack, H.J., 2000. Barite concretions as evidence of pauses in sedimentation in the Marnes Bleues Formation of the Vocontian Basin (SE France). Sedimentary Geology 130, 205–228.

Burla, S., Heimhofer, U., Hochuli, P.A., Weissert, H., Skelton, P., 2008. Changes in sedimentary patterns of coastal and deep-sea successions from the North Atlantic (Portugal) linked to Early Cretaceous environmental change. Palaeogeography, Palaeoclimatology, Palaeoecology 257, 38–57.

Busson, G., Noël, D., 1991. Les nannoconidés, indicateurs environmentaux des océans et mers épicontinentales du Jurassique terminal et du Crétacé inférieur. Oceanologica Acta 14, 333–356.

Castro, J.M. 1998. Las plataformas del Valanginiense superior–Albiense superior en el Prebético de Alicante. Ph.D. Thesis. University of Granada, 464 pp.

Castro, J.M., de Gea, G.A., Ruiz-Ortiz, P.A., Nieto, L.M., 2008. Development of carbonate platforms on an extensional (rifted) margin. The Valanginian–Albian record of the Prebetic of Alicante (SE Spain). Cretaceous Research 29, 848–860.

Castro, J.M., de Gea, G.A., Ruiz-Ortiz, P.A., Quijano, M.L., Pancost, R.D., Jimenez de Cisneros, C., Caballero, E., 2012. Stratigraphy and geochemistry of an early Aptian carbonate platform: interactions between relative sea level and environmental changes (Prebetic Zone, Spain). Geophysical Research Abstracts 14 (EGU2012–6217–1).

Caus, E., Bernaus, J.M., Calonge, E., Martín-Chivelet, J., 2009. Mid-Cenomanian separation of Atlantic and Tethyan domains in Iberia by a land-bridge: the origin of larger foraminifera provinces? Palaeogeography, Palaeoclimatology, Palaeoecology 283, 172–181.

Caus, E., Hottinger, L., 1986. Particularidades de la fauna (foraminíferos) del Cretácico superior pirenaico. Paleontologia i Evolució 20, 115–123.

Didyck, B.M., Simoneit, B.R.T., Brassel, S.C., Eglinton, G., 1978. Organic geochemical indicators of palaeoenvironmental conditions of sedimentation. Nature 272, 216–222.

Dumitrescu, M., Brassell, S.C., 2005. Biogeochemical assessment of sources of organic matter and paleoproductivity during the Early Aptian Oceanic Anoxic Event at Shatsky Rise, ODP Leg 198. Organic Geochemistry 36, 1002–1022.

Dumitrescu, M., Brassell, S.C., 2006. Compositional and isotopic characteristics of organic matter for the Early Aptian Oceanic Anoxic Event at Shatsky Rise, ODP Leg 198. Palaeogeography, Palaeoclimatology, Palaeoecology 235, 168–191.

Dumitrescu, M., Brassell, S.C., Schouten, S., Hopmans, E.C., Sinninghe-Damste, J.S., 2006. Instability in tropical Pacific sea-surface temperatures during the early Aptian. Geology 34 (10), 833–836.

Eglinton, G., Hamilton, R.J., 1967. Leaf epicuticular waxes. Science 156, 1322–1335.

Erba, E., 1994. Nannofossils and superplumes: the early Aptian "nannoconid crisis". Paleoceanography 9, 483–501.

Erba, E., Tremolada, F., 2004. Nannofossil carbonate fluxes during the Early Cretaceous: phytoplankton response to nutrification episodes, atmospheric CO2, and anoxia. Paleoceanography 19 http://dx.doi.org/10.1029/2003PA00084.

Erba, E., Bottini, C., Weissert, H., Keller, C.E., 2010. Calcareous nannoplankton response to surface-water acidification around Oceanic Anoxic Event 1a. Science 329, 428 http://dx.doi.org/10.1126/science.1188886.

Erbacher, J., Huber, B.T., Norris, R.D., Markey, M., 2001. Increased thermohaline stratification as a possible cause for an ocean anoxic event in the cretaceous period. Nature 409, 325–327.

Feuillée, P., Rat, P., 1971. Structures et paléogéographies Pyrénéo-Cantabriques. Histoire Structurale du Golfe de Gascogne. Publication de l'Institute Français du Pétrole: Collection Colloque et Séminaires, Technip, Paris, 22, pp. 1–48.

Föllmi, K.B., Godet, A., Bodin, S., Linder, P., 2006. Interactions between environmental change and shallow water carbonate buildup along the northern Tethyan margin and their impact on the Early Cretaceous carbon isotope record. Paleoceanography 21, PA4211 http://dx.doi.org/10.1029/2006PA001313.

García Hernández, M., López Garrido, A.C., Sanz de Galdeano, C., Vera, J.A., Rivas, P., 1980. Mesozoic paleogeographic evolution in the External Zones of the Betic Cordillera (Spain). Geologie en Mijnbouw 59, 155–168.

García-Senz, J., Robador, A., 2009. Variation in structural style at a lateral termination of a basement-involved wedge: the margin of the West Cantabrian basin. 6th Symposium on the Atlantic Iberian Margin, Oviedo, Spain, pp. 61–64.

de Gea, G.A., Aguado, R., Castro, J.M., Molina, J.M., Ruiz Ortiz, P.A., 2005. Subbetic anoxic Lower Aptian facies (Carbonero Fm., External Zones of the Betic Cordillera, S Jaén, Spain) and the OAE1a. 7th International Symposium on the Cretaceous, Scientific Program and Abstracts, pp. 65–66 (Neuchâtel).

de Gea, G.A., Aguado, R., Castro, J.M., Molina, J.M., Ruiz Ortiz, P.A., 2008a. Registro del evento anóxico del Aptiense inferior en la cuenca subbética (Sur de Jaén): La Formación Carbonero. VII Congreso Geológico de España. Las Palmas de Gran Canaria, 14–18 Julio.

de Gea, G.A., 2004. Bioestratigrafía y eventos del Cretácico Inferior en las Zonas Externas de la Cordillera Bética. Servicio de Publicaciones de la Universidad de Jaén, Jaén . (658 pp.).

de Gea, G.A., Aguado, R., Castro, J.M., 2008b. Variaciones en el registro isotópico del carbono en dos secciones de edad Aptiense inferior en la zona de transición entre el Subbético Externo y el Subbético Medio (Cordilleras Béticas, Provincia de Jaén). Geogaceta 44, 191–194.

de Gea, G.A., Aguado, R., Castro, J.M., Molina, J.M., O'Dogherty, L., Ruiz-Ortiz, P.A., 2008c. Early Aptian Subbetic organic-rich facies, radiolarites and associated deposits. The local expression of the Oceanic Anoxic Event 1a (Carbonero Formation, Southern Spain). Cretaceous Research 29, 861–870.

de Gea, G.A., Castro, J.M., Aguado, R., Company, M., Ruiz-Ortiz, P.A., 2003. Lower Aptian carbon-isotope stratigraphy from a distal carbonate shelf setting. The Cau section, Prebetic Zone, SE of Spain. Palaeogeography, Palaeoclimatology, Palaeoecology 200, 207–219.

Gran, H.H., Braarud, T., 1935. A quantitative study of the phytoplankton in the Bay of Fundy and the Gulf of Maine (including observations of the hydrogeology, chemistry and turbidity). Journal of the Biological Board of Canada 1, 279–467.

Gröcke, D.R., Hesselbo, S.P., Jenkyns, H.C., 1999. Carbon-isotope composition of Lower Cretaceous fossil wood: ocean–atmosphere chemistry and relation to sea-level change. Geology 27, 155–158.

Hallam, A., 1985. A review of Mesozoic climate. Journal of the Geological Society of London 142, 433–445.

Hay, W.W., 2008. Evolving ideas about the Cretaceous climate and ocean circulation. Cretaceous Research 29, 725–753.

Heimhofer, U., Hochuli, P.A., Herrle, J.O., Andersen, N., Weissert, H., 2004. Absence of major vegetation and palaeoatmospheric pCO2 changes associated with oceanic anoxic event 1a (Early Aptian, SE France). Earth and Planetary Science Letters 223, 303–318.

Hermoso, M., Le Callonnec, L., Minoletti, F., Renard, M., Hesselbo, S.P., 2009. Expression of the Early Toarcian negative carbon-isotope excursion in separated carbonate microfractions (Jurassic, Paris Basin). Earth and Planetary Science Letters 277, 194–203.

Herrle, J.O., Köβler, P., Friedrich, O., Erlenkeuser, H., Hemleben, C., 2004. High-resolution carbon isotope records of the Aptian to Lower Albian from SE France and the Mazgan Plateau (DSDP Site 545): a stratigraphic tool for paleoceanographic and paleobiologic reconstruction. Earth and Planetary Science Letters 218, 149–161.

Hochuli, P.A., Menegatti, A.P., Weissert, H., Riva, A., Erba, E., Premoli Silva, I., 1999. Episodes of high productivity and cooling in the early Aptian Alpine Tethys. Geology 27, 657–660.

Huang, W.Y., Meinschein, W.G., 1979. Sterols as ecological indicators. Geochimica et Cosmochimica Acta 43, 739–745.

Huber, B.T., Hodell, D.A., Hamilton, C.P., 1995. Middle–Late Cretaceous climate of the southern high latitudes: stable isotopic evidence for minimal equator-to-pole thermal gradients. Geological Society of America Bulletin 107, 1164–1191.

Huck, S., Heimhofer, U., Rameil, N., Bodin, S., Immenhauser, A., 2011. Strontium and carbon-isotope chronostratigraphy of Barremian–Aptian shoal-water carbonates: Northern Tethyan platform drowning predates OAE 1a. Earth and Planetary Science Letters 304, 547–558.

Huck, S., Rameil, N., Korbar, T., Heimhofer, U., Wieczorek, T.D., Immenhauser, A., 2012. Latitudinally different responses of Tethyan shoal-water carbonate systems to the Early Aptian oceanic anoxic event (OAE 1a). Sedimentology 57, 1585–1614.

Hughes, W.B., Albert, T., Holba, G., Dzou, L., 1995. The ratios of dibenzothiophene to phenanthrene and pristane to phytane as indicators of depositional environment and lithology of petroleum source rocks. Geochimica et Cosmochimica Acta 59, 3581–3598.

Immenhauser, A., Hillgärtner, H., van Bentum, E., 2005. Microbial–foraminiferal episodes in the Early Aptian of the southern Tethyan margin: ecological significance and possible relation to Oceanic Anoxic Event 1a. Sedimentology 52, 77–99.
Immenhauser, A., Schlager, W., Burns, S.J., Scott, R.W., Geel, T., Lehmann, J., et al., 1999. Late Aptian to Late Albian sea-level fluctuations constrained by geochemical and biological evidence (Nahr Umr Fm Oman). Journal of Sedimentary Research 69, 434–446.
Immenhauser, A., 2005. High-rate sea-level change during the Mesozoic: new approaches to an old problem. Sedimentary Geology 175, 277–296.
Jahren, A.H., Conrad, C.P., Crystal Arens, N., Mora, G., Lithgow-Bertelloni, C., 2005. A plate tectonic mechanism for methane hydrate release along subduction zones. Earth and Planetary Science Letters 236, 691–704.
Jenkyns, H.C., 1980. Cretaceous anoxic events: from continents to oceans. Journal of the Geological Society of London 137, 171–188.
Jenkyns, H.C., 1995. Carbon isotope stratigraphy and paleoceanographic significance of the Lower Cretaceous shallow water carbonates of Resolution Guyot, mid-Pacific Mountains. In: Winterer, E.L., Sager, W.W., Firth, V.J., Sinton, M. (Eds.), Proceedings of the Ocean Drilling Program, Scientific Results, 143. College Station, Texas, pp. 89–97.
Jenkyns, H.C., 2010. Geochemistry of oceanic anoxic events. Geochemistry Geophysics Geosystem 11, Q03004 http://dx.doi.org/10.1029/2009GC002788.
Jenkyns, H.C., 2003. Evidence for rapid climate change in the Mesozoic–Palaeogene greenhouse world. Philosophical Transactions of the Royal Society of London. Series A 361, 1885–1916.
Jenkyns, H.C., Schouten-Huibers, L., Schouten, S., Sinninghe-Damsté, J.S., 2012. Warm Middle Jurassic-Early Cretaceous high-latitude sea-surface temperatures from the Southern Ocean. Climate of the Past 8, 215–226.
Kuypers, M.M.M., Lourens, L., Rijpstra, W.I.C., Pancost, R.D., Nijenhuis, I.A., Sinninghe Damsté, J.S., 2004. Orbital forcing of organic carbon burial in the proto-North Atlantic during Oceanic Anoxic Event 2. Earth and Planetary Science Letters 228, 465–482.
Larson, R.L., 1991. Latest pulse of the Earth: evidence for a mid-Cretaceous super plume. Geology 19, 547–550.
Larson, R.L., Erba, E., 1999. Onset of the mid-Cretaceous greenhouse in the Barremian–Aptian: igneous events and the biological, sedimentary and geochemical responses. Paleoceanography 14, 663–678.
Leckie, R.M., Bralower, T.J., Cashman, R., 2002. Oceanic anoxic events and plankton evolution: biotic response to tectonic forcing during the mid-Cretaceous. Paleoceanography 17 http://dx.doi.org/10.1029/2001PA000623.
Lees, J.A., Bown, P.R., Mattioli, E., 2005. Problems with proxies? Cautionary tales of calcareous nannofossil paleoenvironmental indicators. Micropaleontology 51, 333–343.
Mutterlose, J., 1992. Biostratigraphy and palaeobiogeography of Early Cretaceous calcareous nannofossils. Cretaceous Research 13, 167–189.
Li, Y.-X., Bralower, T.J., Montañez, I.P., Osleger, D.A., Arthur, M.A., Bice, D.M., Herbert, T.D., Erba, E., Premoli Silva, I., 2008. Toward an orbital chronology for the early Aptian Oceanic Anoxic Event (OAE1a, 120 Ma). Earth and Planetary Science Letters 271, 88–100.
Li, X., Jenkyns, H.C., Wang, C., Hu, X., Chen, X., Wei, Y., Huang, Y., Cui, J., 2006. Upper Cretaceous carbon- and oxygen-isotope stratigraphy of hemipelagic carbonate facies from southern Tibet, China. Journal of the Geological Society of London 163, 375–382.
Luciani, V., Cobianchi, M., Jenkyns, H.C., 2001. Biotic and geochemical response to anoxic events: the Aptian pelagic succession of the Gargano Promontory (southern Italy). Geological Magazine 138, 277–298.
Mackenzie, A.S., Patience, R.L., Maxwell, J.R., Vandenbroucke, M., Durand, B., 1980. Molecular parameters of maturation in the Toarcian shales, Paris Basin, France—I. Changes in the configurations of acyclic isoprenoid alkanes, steranes and triterpanes. Geochimica et Cosmochimica Acta 44, 1709–1721.
Martín-Chivelet, J., Berasategui, X., Rosales, I., Vilas, L., Vera, J.A., Caus, E., Gráfe, K.U., Mas, R., Puig, C., Segura, M., Robles, S., Floquet, M., Quesada, S., Ruiz-Ortiz, P.A., Frenegal-Martínez, M.A., Salas, R., García, A., Martín-Algarra, A., Arias, C., Meléndez, M., Chacón, B., Molina, J.M., Sanz, J.L., Castro, J.M., García-Hernández, M., Carenas, B., García-Hidalgo, J., Gil, J., Ortega, F., 2002. Cretaceous. In: Gibbons, W., Moreno, T. (Eds.), The Geology of Spain. The Geological Society, London, pp. 255–292.
Masse, J.P., Bouaziz, S., Amon, E.O., et al., 2000. Early Aptian. (94.7–93.5 Ma). In: Dercourt, J., Gaetani, M., Vrielynck, B., Barrier, E., Biju-Duval, B., Brunet, M.F., Cadet, J.P., Crasquin, S., Sandulescu, M. (Eds.), Peri-Tethys Palaeogeographical Atlas. CCGM/CGMW, Paris (Map 13).
Mehay, S., Keller, C.E., Bernasconi, S., Weissert, H., Erba, E., Bottini, C., Hochuli, P.A., 2009. A volcanic CO_2 pulse triggered the Cretaceous Oceanic Anoxic Event 1a and a biocalcification crisis. Geology 37, 819–822 http://dx.doi.org/10.1130/G30100A.
Menegatti, A.P., Weissert, H., Brown, R.S., Tyson, R.V., Farrimond, P., Strasser, A., Caron, M., 1998. High-resolution $\delta^{13}C$ stratigraphy through the early Aptian "Livello Selli" of the Alpine Tethys. Paleoceanography 13, 530–545.
Meyers, P.A., 1997. Organic geochemical proxies of paleoceanographic, paleolimnologic, and paleoclimatic processes. Organic Geochemistry 27, 213–250.
Millán, M.I., Weissert, H.J., Fernández-Mendiola, P.A., García-Mondéjar, J., 2009. Impact of Early Aptian carbon cycle perturbations on evolution of a marine shelf system in the Basque–Cantabrian Basin (Aralar, N Spain). Earth and Planetary Sciences Letters 287, 392–401.
Moldovan, J.M., Seifert, W.K., Gallegos, E.J., 1985. Relationship between petroleum composition and depositional environment of petroleum source rocks. American Association of Petroleum Geologists Bulletin 69, 1255–1268.
Molina, J.M., de Gea, G.A., Aguado, R., 2001. Facies anóxicas, radiolaríticas y turbidíticas en el Cretácico de la Zona Subbética: la Formación Carbonero. In: Ruiz-Ortiz, P.A., Molina, J.M., Nieto, L.M., Castro, J.M., Gea, G.A. (Eds.), Itinerarios geológicos por el Mesozoico de la provincia de Jaén. Departamento de Geología. Universidad de Jaén, pp. 41–60.
Molina, J.M., Hernández-Molina, F.J., 1993. Concreciones de barita en el Cretácico (Aptiense–Albiense) del Subbético (Cordilleras Béticas). Boletín Geológico y Minero 104, 548–573.
Molina, J.M., Vera, J.A., de Gea, G.A., 1998. Vulcanismo submarino del Santoniense en el Subbético: Datación con nannofósiles e Interpretación (Formación Capas Rojas, Alamedilla, Provincia de Granada). Estudios Geológicos 54, 191–197.
Najarro, M., Rosales, I., 2008a. Disoluciones e incrustaciones ferruginosas asociadas al OAE 1a en la plataforma carbonatada de La Florida (NO de Cantabria). Geogaceta 44, 199–202.
Najarro, M., Rosales, I., 2008b. Evidencias sedimentológica, diagenética y quimioestratigráfica del Evento Anóxico Oceánico del Aptiense Inferior (OAE 1a) en la plataforma carbonatada de La Florida (NO de Cantabria). Geo-Temas 10, 163–166.
Najarro, M., Peñalver, E., Rosales, I., Pérez-de la Fuente, R., Daviero-Gomez, V., Gomez, B., Delclòs, X., 2009. Unusual concentration of Early Albian arthropod-bearing amber in the Basque–Cantabrian Basin (El Soplao, Cantabria, Northern Spain): palaeoenvironmental and palaeobiological implications. Geologica Acta 7, 363–387.
Najarro, M., Rosales, I., Martín-Chivelet, J., 2011a. Major palaeoenvironmental perturbation in an Early Aptian carbonate platform: prelude of the Oceanic Anoxic Event 1a? Sedimentary Geology 235, 50–71.
Najarro, M., Rosales, I., Martín-Chivelet, J., 2007. Evolución de la plataforma carbonatada de la Florida durante el rifting del Cretácico Inferior (Aptiense, NO de Cantabria). In: Bermúdez, D.D., Najarro, M., Quesada, C. (Eds.), Volumen Monográfico de la II Semana de Jóvenes Investigadores del IGME. Publicaciones del IGME, pp. 123–128.
Najarro, M., Rosales, I., Moreno-Bedmar, J.A., de Gea, G., Barrón, E., Company, M., Delanoy, G., 2011b. High-resolution chemo- and biostratigraphic records of the Early Aptian oceanic anoxic event in Cantabria (N Spain): palaeoceanographic and palaeoclimatic implications. Palaeogeography, Palaeoclimatology, Palaeoecology 299, 137–158 http://dx.doi.org/10.1016/j.palaeo.2010.10.042.
Olivet, J.M., 1996. La cinématique de la plaque ibérique. Bulletin des Centres de Recherches Exploration-Production Elf-Aquitaine 20, 131–195.
Ourisson, G., Albrecht, P., Rohmer, M., 1982. Predictive microbial biochemistry from molecular fossils to prokaryotic membranes. Trends in Biochemical Sciences 7, 236–239.
Pancost, R.D., Crawford, N., Magness, S., Turner, A., Jenkyns, H.C., Maxwell, J.R., 2004. Further evidence for the development of photic-zone euxinic conditions during Mesozoic oceanic anoxic events. Journal of the Geological Society of London 161, 353–364.
Parker, M.E., Clark, M., Wise, S.W., 1985. Calcareous nannofossils of Deep Sea Drilling Project Sites 558 and 563, North Atlantic Ocean: biostratigraphy and the distribution of Oligocene braarudosphaerids. Initial Reports of the Deep Sea Drilling Project 82, 559–589.
Paytan, A., Griffith, E.M., 2007. Marine barite: recorder of variations in ocean export productivity. Deep-Sea Research II 54, 687–705.
Pedersen, T.F., Calvert, S.E., 1990. Anoxia vs. productivity: what controls the formation of organic-carbon-rich sediments and sedimentary rocks. American Association of Petroleum Geologists Bulletin 74, 454–466.
Peters, K.E., Moldowan, J.M., 1991. Effects of source, thermal maturity, and biodegradation on the distribution and isomerization of homohopanes in petroleum. Organic Geochemistry 17, 47–51.
Peters, K.E., Walters, C.C., Moldowan, J.M., 2005. 2nd ed. The Biomarker Guide, vol. 2. Cambridge University Press (1155pp.).
Powell, T.G., McKirdy, D.M., 1973. Relationship between ratio of pristane to phytane, crude oil composition and geological environment in Australia. Nature 243, 37–39.
Price, G.D., 2003. New constraints upon isotope variation during the early Cretaceous (Barremian–Cenomanian) from the Pacific Ocean. Geological Magazine 140, 513–522.
Rameil, N., Immenhauser, A., Warrlich, G., Hillgärtner, H., Droste, H.J., 2010. Morphological patterns of Aptian Lithocodium–Bacinella geobodies: relation to environment and scale. Sedimentology 57, 883–911.
Rosales, I., Najarro, M., Moreno-Bedmar, J.A., de Gea, G.A., Company, M., 2009. High resolution chemo- and biostratigraphic records of the Early Aptian Oceanic Anoxic Event in Cantabria (northern Spain). Geochimica et Cosmochimica Acta 73 (13S), A1118.
Roth, P.H., Bowdler, J.L., 1981. Middle Cretaceous nannoplankton biogeography of the Atlantic Ocean. The Society of Economic Paleontologists and Mineralogists Special Publication 32, 517–546.
Roth, P.H., Krumbach, K.R., 1986. Middle Cretaceous calcareous nannofossil biogeography and presevation in the Atlantic and Indian oceans: implications for paleoceanography. Marine Micropaleontology 10, 235–266.
Ruiz-Ortiz, P.A., 1980. Análisis de facies del Mesozoico de las Unidades Intermedias (entre Castril—provincia de Granada—y Jaén). Ph.D. Thesis. University of Granada, 372 pp.
Ruiz-Ortiz, P.A., Molina, J.M., Nieto, L.M., Castro, J.M., de Gea, G., 2001. Itinerarios geológicos por el Mesozoico de la provincia de Jaén. 1. Introducción al Mesozoico de la parte externa del paleomargen sudibérico. Cordillera Bética: IV Coloquio del Cretácico de España, University of Jaén, pp. 11–24.
Scalan, R.S., Smith, J.E., 1970. An improved measure of the odd-even predominance in the normal alkanes of sediment extracts and petroleum. Geochimica et Cosmochimica Acta 34, 611–620.
Scarparo-Cunha, A.A., Shimabukuro, S., 1997. Braarudosphaera blooms and anomalous enrichments of Nannoconus: evidence from the Turonian South Atlantic, Santos Basin, Brazil. Journal of Nannoplankton Research 19, 51–55.
Schlanger, S.O., Jenkyns, H.C., 1976. Cretaceous oceanic anoxic events: causes and consequences. Geologie en Mijnbouw 55, 179–184.
Seifert, W.K., Moldowan, J.M., 1980. The effect of thermal stress on source-rock quality as measured by hopane stereochemistry. Physics and Chemistry of the Earth 12, 229–237.

Siesser, W.G., Bralower, T.J., De Carlo, E.H., 1992. Mid-Tertiary Braarudosphaera-rich sediments on the Exmouth Plateau. Proceedings of the Ocean Drilling Program, Scientific Results 122, 653–663.
Sinninghé-Damsté, J.P., Kenig, F., Koopmans, M.P., Koster, J.G., Schouten, S., Hayes, J.M., De Leeljw, J.W., 1995. Evidence for gammacerane as an indicator of water column stratification. Geochimica et Cosmochimica Acta 59, 1895–1900.
Skelton, P.W. (Ed.), 2003. The Cretaceous World. The Open University, Milton Keynes, and Cambridge University Press, Cambridge (360pp.).
Stein, M., Föllmi, K.B., Westermann, S., Godet, S., Adatte, T., Matera, V., Fleitmann, D., Berner, Z., 2011. Progressive palaeoenvironmental change during the Late Barremian–Early Aptian as prelude to Oceanic Anoxic Event 1a: evidence from the Gorgo a Cerbara section (Umbria-Marche basin, central Italy). Palaeogeography, Palaeoclimatology, Palaeoecology http://dx.doi.org/10.1016/j.palaeo.2011.01.025.
Street, C., Bown, P.R., 2000. Palaeobiogeography of Early Cretaceous (Berriasian–Barremian) calcareous nannoplankton. Marine Micropaleontology 39, 265–291.
Summons, R.E., Volkman, J.K., Boreham, C.J., 1987. Dinosterane and other steroidal hydrocarbons of dinollagellate origin in sediments and petroleum. Geochimica et Cosmochimica Acta 51, 3075–3082.
Tejada, M.L., Suzuki, K., Kuroda, J., Coccioni, R., Mahoney, J.J., Ohkouchi, N., Sakamoto, N., Tatsumi, Y., 2009. Ontong Java Plateau eruption as a trigger for the early Aptian oceanic anoxic event. Geology 37, 855–858 http://dx.doi.org/10.1130/G25763A.
Ten Haven, H.L., de Leeuw, J.W., Rullköter, J., Sinninghe Damsté, J.S., 1987. Restricted utility of the pristane/phytane ratio as a palaeoenvironmental indicator. Nature 330, 641–643.
Thierstein, H.R., 1976. Mesozoic calcareous nannoplankton biostratigraphy of marine sediments. Marine Micropaleontology 1, 325–362.
Tremolada, F., Erba, E., 2002. Morphometric analyses of Aptian Assipetra infracretacea and Rucinolithus terebrodentarius nannoliths: implications for taxonomy, biostratigraphy and palaeoceanography. Marine Micropaleontology 44, 77–92.
Vera, J.A., (Coord.), 2004. Cordillera Bética y Baleares. In: Vera, J.A. (Ed.), Geología de España. SGE-IGME, Madrid, 347–464.
Vera, J.A., 1988. Evolución de los sistemas de depósito en el margen ibérico de la Cordillera Bética. Revista Sociedad Geológica España 1, 373–391.
Vergès, J., García-Senz, J., 2001. Mesozoic evolution and Cainozoic inversion of the Pyrenean Rift. In: Ziegler, P.A., Cavazza, W., Robertson, A.H.F., Crasquin-Soleau, J. (Eds.), Peri-Tethys Memoir 6: Peri-Tethyan Rift/Wrench Basins and Passive Margins: Mémoires du Muséum National d'Historie Naturelle, Paris, 186, pp. 187–212.
Waples, D.W., Machihara, T., 1991. Biomarkers for geologists. American Association of Petroleum Geologists—Methods in Exploration Series, 9 (91pp.).
Weissert, H., Erba, E., 2004. Volcanism, CO2 and palaeoclimate: a Late Jurassic–Early Cretaceous carbon and oxygen isotope record. Journal of the Geological Society of London 161, 695–702.
Weissert, H., Lini, A., Föllmi, K.B., Kuhn, O., 1998. Correlation of Early Cretaceous carbon isotope stratigraphy and platform drowning events: a possible link? Palaeogeography, Palaeoclimatology, Palaeoecology 137, 189–203.
Wilson, P.A., Norris, R.D., 2001. Warm tropical ocean surface and global anoxia during the mid-Cretaceous period. Nature 412, 425–428.
Wissler, L., Funk, H.P., Weissert, H., 2003. Response of Early Cretaceous carbonate platforms to changes in atmospheric carbon dioxide levels. Palaeogeography, Palaeoclimatology, Palaeoecology 200, 187–205.
Withers, N., 1983. Dinoflagellatesterols. In: Scheuer, P.J. (Ed.), Marine Natural Products, 5. Academic Press, New York, pp. 87–130.
Xie, S., Pancost, R.D., Huang, X., Jiao, D., Lu, L., Huang, J., Yang, F., Evershed, R.P., 2007. Molecular and isotopic evidence for episodic environmental change across the Permo/Triassic boundary at Meishan in South China. Global and Planetary Change 55, 56–65.
Ziegler, P.A., 1988. Evolution of the Artic–North Atlantic and the Western Tethys, publ. Int. lithos. Program, 0144. AAPG Memoir 43 (193pp.).